ELEMENTAL, ISOTOPIC AND MOLECULAR SIGNATURES OF EARLY CAMBRIAN MARINE SEDIMENTS AND A PHANTOM PETROLEUM SYSTEM IN SOUTH AUSTRALIA

By

Philip Anthony Hall

M.Phil. Environmental and Geographical Sciences, Manchester Metropolitan University, U.K.
B.Sc. Hons. Geology and Petroleum Geology, University of Aberdeen, U.K.

Thesis submitted for the degree of

Doctor of Philosophy

Geology and Geophysics
School of Earth and Environmental Science
Faculty of Science
University of Adelaide

2012

This work contains no material which has been accepted for the award of any other degree or diploma in any university or other tertiary institution to Philip Anthony Hall and, to the best of my knowledge and belief, contains no material previously published or written by another person, except where due reference has been made in the text.

I give consent to this copy of my thesis when deposited in the University Library, being made available for loan and photocopying, subject to the provisions of the Copyright Act 1968.

The author acknowledges that copyright of published works contained within this thesis (as listed below) resides with the copyright holder(s) of those works. I also give permission for the digital version of my thesis to be made available on the web, via the University's digital research repository, the Library catalogue, and also through web search engines, unless permission has been granted by the University to restrict access for a period of time

Palaeoredox status and thermal alteration of the lower Cambrian (Series 2) Emu Bay Shale Lagerstätte, South Australia. Australian Journal of Earth Sciences 58 (2011) 259-272. doi: 10.1080/08120099.2011.557439

Biomarker and isotopic signatures of an early Cambrian Lagerstätte in the Stansbury Basin, South Australia. Organic Geochemistry 42 (2011) 1324-1330. doi:10.1016/j.orggeochem.2011.09.003

Signed..... Date.....

ABSTRACT

The aim of the research study is to apply mass spectrometric geochemical techniques to the investigation of palaeoenvironmental, chemostratigraphic and provenance questions from several South Australian Phanerozoic basins.

Results of a multi-pronged palaeoenvironmental investigation of Early Cambrian marine sediments, employing trace and REE abundances, TOC and stable isotopes (C, S) are reported from three formations in the Stansbury Basins; Heatherdale Shale, Emu Bay Shale and Talisker Formation. The multiproxy approach in conjunction with sedimentological information provides a powerful tool for interpreting palaeoenvironmental conditions. Prevalent palaeoredox conditions of the Heatherdale Shale and Talisker Formation were dysoxic, evolving progressively more reducing natures up section. The Emu Bay Shale conversely demonstrates consistently aerobic interpretations for the redox proxies. Comparison of trace element and REE distributions to similar sequences of the Yangtze platform, South China shows striking similarities, Analogous basinal environments and common provenance may have lead to the seawater trace element chemistry of the Palaeo Pacific & Asian oceans exhibiting a homogenous nature.

The Emu Bay Shale biota is the richest Burgess Shale-type (BST) fauna in the southern hemisphere. The implied oxic water column during accumulation appears difficult to reconcile with the exceptional preservation exhibited. Micro-scale sealed vessel (MSSV) pyrolysis of isolated kerogen and $\delta^{13}C_{org}$ values provided confirmation of its redox status and implicate cyanobacteria in the preservation mechanism. Molecular signatures diagnostic of *Gloeocapsomorpha prisca* were identified, the first indication that microbial mats were involved in the taphonomy of a BST deposit.

The biostratigraphic definition of GSSP horizons though the use of cosmopolitan taxa biohorizons is problematical for sections such as lower Cambrian deposits where few candidate fossils exist. Instead, an integrated approach comprising chemostratigraphy and/or sequence stratigraphy with the known biostratigraphy greatly increases our ability to make high-resolution correlations., $\delta\ ^{13}C_{carb}$ profiles from three South Australian basins; the Stansbury, the Arrowie and the Officer are correlated regionally with the existing data from the Flinders Ranges. Globally identified excursions such as the negative ROECE and AECE event and the positive CARE and MICE events, are recognised in the profiles. This chemostratigraphic interpretation appears to support the biostratigraphic assignment of the sections.

Asphaltic bitumens are long known to strand along coastlines of southern Australia and as far afield as New Zealand and Macquarie Island. Widely regarded as artefacts of an unidentified submarine oil seepages, a common source is interpreted from remarkably uniform compositions. An important consideration when attempting to locate their point of origin is the degree of weathering exhibited, which will reflect the residence time in the marine environment and proximity of the seep to the stranding site. Biomarker signatures and *n*-alkane C-isotopic profiles from interior and weathered exterior sub-samples of asphaltum from four localities in South Australia and New Zealand were compared. No distinction could be made between strandings despite their widely separated localities. The degree of degradation and isotopic variance suggest an origin from low intensity seeps in the western Otway Basin as strandings on the Limestone Coast and Kangaroo Island appear less weathered than those from Eyre Peninsula and New Zealand.

ACKNOWLEDGEMENTS

I would like to express my gratitude to my supervisors; Alan Collins, David McKirdy, Galen Halverson and Kliti Grice without who's advice and guidance I would never have achieved this goal.

I would also like to thank Jim Jago (University of South Australia) for his continual support and insightful comment throughout my research.

My thanks goes to Elinor Alexander & Tony Hill of PIRSA for providing financial support for this research project and Evelyn Krull and Thomas Kuhn from CSIRO for allowing access to their facilities and technical help in conducting CSIA analyses.

My deepest thanks goes to all my family and friends who have supported and encouraged me through this project, from both sides of the world.

Special thanks goes to my Mam & Dad, Keith & Margaret, who have helped in every way they could, organising analyses, parts for our instrumentation and always wanting to lend a hand.

Finally I'd like to express by heartfelt thanks, love and indebtedness to my wife, Pauline who's support and encouragement has been unwavering and to my sons Jude & Zion for making every day special.

.....and I'd like to thanks the late Douglas Adams for two little words inscribed in large friendly letters on the front cover of the Hitchhiker's Guide to the Galaxy:

DON'T PANIC

CONTENTS

Introduction

1.1. Research Aims and Outline

The aim of the research study is to apply mass spectrometric geochemical techniques to the investigation a variety of palaeoenvironmental, chemostratigraphic and provenance questions from South Australian Phanerozoic basin geology.

South Australia hosts a comprehensive succession of early Cambrian strata from the upper sections of the Nemakit-Daldynian, through the Tommotian, Atdabanian and Botoman, which also generally extends into the lower sections of the middle Cambrian and in places the Ordovician. Deposited at the culmination of an extensive period of deposition in two distinct basins: the Adelaide Rift-basin (Stansbury Basin and Arrowie Basin) and the Centralian Superbasin (Officer Basin and Warburton Basin). These strata host both mineral and petroleum resources with current and likely future prospectively. Understanding the nature of the sediments, depositional environments and relationships regionally is a key aspect in assessing the viability of these prospects, in addition to increasing the academic knowledge base. As such a major focus of this study is on the early Cambrian strata, especially those of the Stansbury basin.

Palaeoenvironmental investigations are undertaken on its' black shale deposits; the Heatherdale Shale (Fleurieu Peninsula and Mt Lofty Ranges), Talisker Formation (Mt Lofty Ranges) and the globally renowned Emu Bay Shale Lagerstätte (Kangaroo Island) (Fig.1), where biogeochemical analysis using MSSV pyrolysis - GC-MS is also undertaken. The significance of black shale deposits, a characteristic feature of warm intervals in Earth history, in reconstructing palaeoenvironments and basin redox are widely accepted. It has long been assumed that deep ocean anoxia was a prerequisite for the deposition of marine black shales, which are commonly rich

petroleum source rocks. However, the presence of abundant benthic animals and trace fossil evidence in exposed shale sections, points to oxic or dysoxic living conditions beneath bottom waters in apparent contradiction to geochemical interpretations. Investigations from the archetypal lower Cambrian Burgess Shale Lagerstätten, Canada have suggested oxic conditions may have been prevalent at the ocean floor during its' deposition. To address this questions we use ICP-MS analysis to assess trace and rare earth element distributions in conjunction with TOCs and bulk organic carbon and sulphur isotopic ratios to interpret the prevailing palaeoredox conditions during deposition of the South Australian shales.

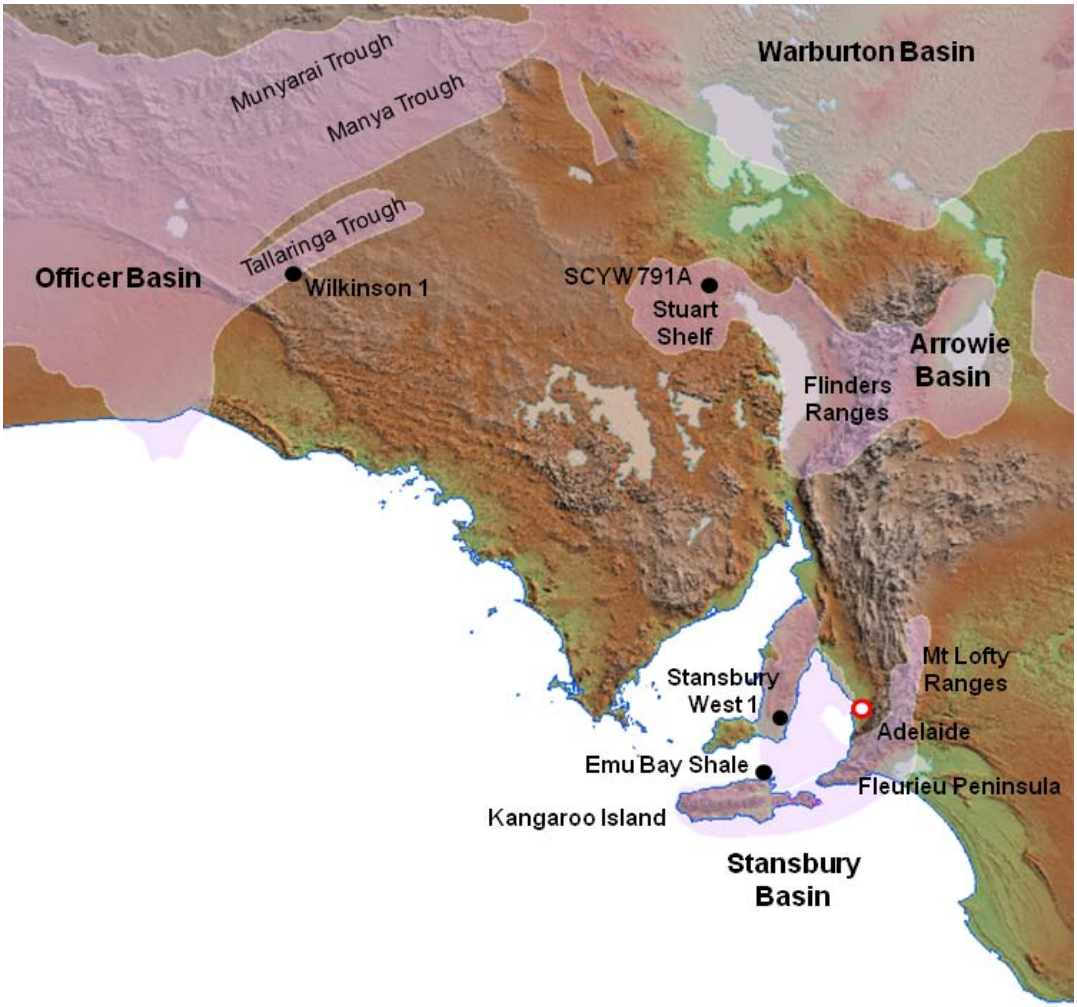

Fig. 1. Location map of the South Australian basin from study highlighting general sample areas and drill core sites.

Carbon isotope signatures from well cuttings of the Stansbury Basin are also explored in conjunction with core samples from the Arrowie and Officer Basins using IR-MS to assess chemostratigraphic relationships, both locally within South Australia and globally. This also addresses the fact the early Cambrian isotopic profile from Australia is extremely limited in comparison to the extensively studied Neoproterozoic sequences and those of the middle to late Cambrian.

The final area of study applies organic geochemistry techniques; GC-MS and GC-IR-MS, to investigate provenance of the enigmatic asphaltitic bitumen strandings common to the southern margin of Australia. These heavy oils are interpreted as being sourced from OAE related early Cretaceous calcareous marine shales, which a number of the late Mesozoic basins formed during the rifting of Antarctica and Australia may contain. Most commonly distributed on the shores of the Otway Basin and Kangaroo Island strandings range all along the southern margin from the Cape Leeuwin coast in Western Australia to Tasmania and as far afield as Macquarie Island and New Zealand (Fig.2). Generally accepted as an expression of a submarine oil seep, the origin and thus the petroleum system associated with the seep, is unknown. Samples taken from the Eyre Peninsula, Kangaroo Island, Limestone Coast and New Zealand (Fig.2) are correlated and used to compare weathering patterns. Organic geochemical analysis is conducted on the extracted and isolated saturate and aromatic hydrocarbon fractions to assess degradation due to environmental exposure, which will be expressed as differences between outer surface distributions and those of inner, less weathered portions of the asphaltum with the aim of refining the possible source location.

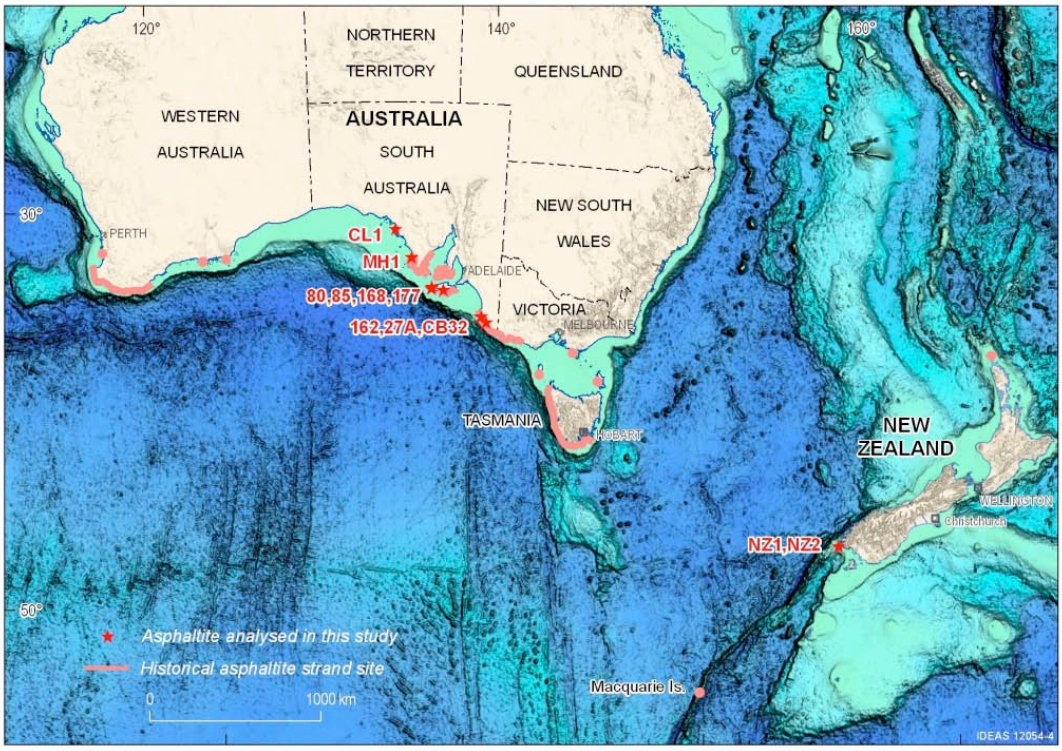

Fig. 2. Location of historically documented asphaltite strandings and samples from this study.

1.2. Early Cambrian.

The Precambrian–Cambrian transition is well documented as a time of intense change in the Earth system coinciding with the tectonic upheaval involved in the final breakup of Rodinia and assembly of Gondwana, (Collins & Pisarevsky, 2005; Meert & Lieberman, 2008). The profound reorganisation of the biosphere with the rapid diversification of metazoans and increased oxygenation of the atmosphere and oceans to roughly modern levels (Brazier & Hewitt 1979, Seilacher 1998, Canfield, 2005; Hurtgen et al., 2005; Fike et al., 2006; Halverson et. al 2009; Saltzman et al., 2011) was punctuated by episodes of ocean anoxia (Saltzman et al., 2000; Kimura and Watanabe, 2001; Schröder & Grotzinger, 2007, Wotte et al., 2007; Guo et al., 2010, Och et al., 2012).

Early Cambrian sedimentology, geochemistry and plate reconstructions suggest that global warming of the climate occurred during this interval and allowed for development of widespread shallow-water carbonate reef systems, even in high latitudes (Brasier, 1992a; Riding, 1994; Gravestock, 1995; Brock et al., 2000; Maloof et al., 2005, 2010a) along with numerous examples of black shale deposits including North and South China, Canada, Siberia, India, Oman and Australia (e.g., Brasier, 1992b; Nedin, 1995a,b; Powell et al., 2003; Gou et al., 2007; Lehmann et al., 2007; Piper & Calvert, 2009; Powell, 2009; Yu et al., 2009; Zhou & Jiang, 2009; McKirdy et al., 2011; Och & Shields-Zhou, 2012). These Cambrian black shale deposits play host to an extraordinary number of fossil assemblages of soft-bodied organisms (Lagerstätten) around the world (Allison & Briggs 1993; Powell et al., 2003; Zhu et al., 2006; Powell, 2009; Gehling et al., 2011; McKirdy et al., 2011)

The proliferation of metazoan fauna, or ‘Cambrian Explosion’ (Brasier, 1992a), is well documented, but the origin and its link to environmental change is still a matter of debate. Prevalent hypotheses include eustatic sea level changes, alterations in oceanic chemistry though increased weathering or hydrothermal sources, an increase in oceanic and atmospheric oxygen over the Proterozoic and early Cambrian transition, developmental adaptations to predation, and even cosmic radiation (Braiser & Hewitt, 1979; Derry et al., 1992; Brasier, 1992a; Canfield, 1998; Babcock et al., 2003; Fike et al., 2006; Squire et al., 2006; Canfield et al., 2007; Goldberg et al., 2007, Muruyama & Santosh, 2008; Scott et al., 2008; Halverson et al., 2009; Erwin et al., 2011). However, because early animals inhabited the oceans, improving our understanding of the marine environment is central to testing and refining hypotheses for early animal evolution.

1.2.1 Early Cambrian of South Australia

The early Cambrian successions of South Australia were accumulated at end of an extended period of virtually continuous Neoproterozoic–Cambrian deposition, from approximately 830 Ma to 500 Ma. Cambrian sedimentation occurred in two distinct, but possibly interconnected marine basins: the Centralian Superbasin (Officer & Warburton Basins) to the north and west and the Adelaide Fold Beltrift-basin (Stansbury & Arrowie Basins) to the south and east (Fig.2) (Gravestock, 1995; Preiss, 2000). Continental reorganisation culminated with the final assembly of the Gondwanan supercontinent from the remnants of Rodinia during the Cambrian, with both depositional systems linked to this breakup and the amalgamation (Powell et al., 1994; Gravestock, 1995; Preiss, 2000; Lindsay, 2002; Collins & Pisarevsky, 2005). Deposition was strongly influenced by regional tectonism, which started with rifting related to the ~550 Ma Petermann Ranges Orogeny and terminated by the Delamerian Orogeny at ~500 Ma (Gravestock, 1995; Preiss, 2000; Jago et al., 2006).

Both basins sat in humid, tropical climate at low northern palaeolatitudes on, or connected to, the western margin of the palaeo-Pacific Ocean during the Early Cambrian (Gravestock, 1995; Brock et al., 2000; Li et al., 2008). They provide a near continuous sequence of deposits from the upper sections of the Nemakit-Daldynian, through the Early Cambrian Tommotian, Atdabanian and Botoman stages, and generally extend into the lower sections of the middle Cambrian and in places to the Ordovician. The southern basins are renowned for their thick fossiliferous limestones which include peritidal archaeocyathid reefs spanning much of the Early Cambrian (James & Gravestock, 1990, Jago et al., 2006) and also host the Emu Bay Shale lagerstätte (Gehling et al., 2011).

1.2.2. Sequence Stratigraphy.

The South Australian Cambrian was divided into four supersequence sets; Є1, Є2 (both Early Cambrian), Є3 (Middle Cambrian) and Є4 (Late Cambrian to Ordovician) by Gravestock (1995). These have been revised further with subdivision into 3rd order sequences Є1.0, Є1.1, Є1.2 & Є1.3 and Є2.1 & Є2.2 within the Early Cambrian supersequences (Fig.3) (Gravestock, 1995; Jago et al., 2002b, 2006; Zang et al., 2004). The stratotype are recognised across the basin boundaries and are used as the basis for much of the South Australian correlation (Fig 3).

NOTE:
This figure/table/image has been removed to comply with copyright regulations.
It is included in the print copy of the thesis held by the University of Adelaide Library.

Fig. 3. Early to Middle Cambrian stratigraphy of the Officer, Arrowie & Stansbury basins (modified after Jago et al., 2012).

1.2.3. Biostratigraphy

The increase of biomineralising metazoans through the Cambrian period (Porter, 2007; Kouchinsky et al., 2012) has allowed robust biostratigraphic correlation regionally, globally and the definition of Global boundary Stratotype Section and Point (GSSP) horizons through the use of cosmopolitan taxa biohorizons (Babcock & Peng, 2007; Babcock et al., 2007; Peng et al., 2009). The use of archaeocyatha, trilobites, chonodonts and shelly fossils, as well as acritarchs, has been used to define assemblage zones allowing these correlations (e.g., Gravestock, 1984; Zhuravlev & Gravestock, 1994, Brasier et al., 1996; Brock et al., 2000; Babcock et al., 2004; Jago et al., 2006; Peng et al., 2006, 2009; Zang et al., 2007; Bagnoli et al., 2008).

Jago et al. (2006) reviewed South Australian biostratigraphy, with particular reference to trilobite occurrences and Zang et al (2007) conducted a reviewed acritarchs assemblages. In summary, trilobites from the Stansbury and Arrowie Basins are largely Atdabanian–Botoman with4 zones are recognized: Abadiella huoi (latest Atdabanian–earliest Botoman), Pararaia tatei, Pararaia bunyerooensis and Pararaia janeae Zones (all Botoman). Higher in the succession the sparse Toyonian specimens are correlated with the upper Lower Cambrian Lungwangmiaoan Stage of China and Pagetia sp. of early Middle Cambrian age have been reported in the Coobowie Formation of the Stansbury Basin. Few trilobite occurrences are described from the Officer Basin with Abadiella officerensis, of Atdabanian age the most reliable from the Ouldburra Formation (Jago et al., 2002a). The Cambrian faunas of the Warburton Basin range in age from early Middle Cambrian to very Late Cambrian. Conodonts, including Cordylodus proavus, occur in a Datsonian fauna. The archaeocyath successions of the Arrowie Basin include the Warriootacyathus wilkawillensis,

Spirillicyathus tenuis and Jugalicyathus tardus Zones from the lower Wilkawillina Limestone (Arrowie Basin) and equivalents which are correlated with the Atdabanian in Siberia (Gravestock, 1984) whilst Botoman archaeocyathids occur higher in the Wilkawillina Limestone. The Wirrealpa Limestone (Arrowie Basin) contains Toyonian archaeocyatha, the youngest in Australia (Gravestock, 1984). Brachiopods and molluscs of the Arrowie and Stansbury Basins can be divided into four biostratigraphic assemblages and informal Early Cambrian SSF biostratigraphic assemblages are recognized. Seven informal acritarch assemblages are recognised from the lowest Cambrian to Toyonian in the Stansbury and Arrowie Basins with zones 4 & 5 correlated to the Eastern European Platform and Qiongzhusi Formation in southern China.

On the northern coast of Kangaroo Island the Emu Bay Shale lagerstätte exhibits a diverse range of fauna, with exceptional preservation including gut remains and other soft parts common, comprising at least 30 taxa. The Emu Bay Shale biota is of lower Cambrian age and is suggested to be correlative of the Pararaia janeae Zone of mainland South Australia, the early-mid Canglangpuan Stage of China and the mid-late Botoman of Siberia; equivalent to undefined Cambrian Series 2, Stage 4 (Jago et al., 2006; Paterson et al., 2008).

1.2.4. Chemostratigraphy

The observed carbon isotope composition of unaltered marine carbonates ($\delta^{13}C_{carb}$) precipitated in equilibrium with seawater closely approximate the composition of the dissolved inorganic carbon (DIC) pool of that seawater. These values show secular variation, resulting from a combination of factors including continental weathering, initial isotopic composition of carbon entering the ocean-atmosphere system, primary

productivity, efficiency of organic carbon burial and ocean circulation. Even though the reliability of the carbon isotope proxy applied to ancient carbonate strata has been challenged by a series of recent studies (e.g., Melchin and Holmden, 2006; Swart & Kennedy, 2012), it has been widely applied to investigations palaeoenvironmental changes and biological events (Tucker, 1989; Brasier, 1992b; Brasier et al., 1994, 1996; Montanez et al., 2000; Buggisch et al., 2003; Zhu et al., 2004; Guo et al., 2005; Maloof et al., 2005; Saltzman et al., 2005, 2011). The potential of applying secular variations in carbon isotope composition as a tool for both intercontinental stratigraphic correlation and explaining biospheric perturnbations has been highlighted by numerous authors (e.g., Tucker, 1986; Magaritz et al., 1986; Brasier, 1992b; Brasier & Sukhov, 1998; Halverson et al., 2002, 2005) and has been implemented with a fair degree of success in the Cambrian (e.g., Saltzman et al., 1998, 2000; Peng et al 2004; Kouchinshy et al., 2001, 2005, 2010; Lindsay et al 2005; Maloof et al., 2005; Wotte et al., 2007; Guo et al., 2007b, 2010). The Cambrian displays $\delta^{13}C$ patterns that appear transitional between the Neoproterozoic, marked by long duration and large amplitude fluctuations, and the Phanerozoic, distinguished by shorter duration and less extreme anomalies (Halverson et al., 2009; Maloof et al., 2010b). Potential explanations for the relatively high frequency fluctuations in the Cambrian $\delta^{13}C$ record include extreme chemical weathering of Gondwana, palaeogeographical configuration, or ecosystem simplicity could have had a significant role in making this interval of geological time more prone to perturbations of the carbon cycle (Woods et al., 2011).

The implementation of isotopic variations through chemostratigraphy is problematic, a number of diagenetic factors may alter or obscure primary signatures; cementation, recrystallisation and late dolomitization as well as alterations through metamorphism

(Tucker, 1989; Machel, 1997, 2005; Glumac & Walker, 1998; Railsback et al., 2003; Swart & Kennedy, 2012). Excursions and shifts in the carbon isotope curve have been shown to correspond with events in sequence stratigraphy, interpreted as indicating the interdependence of sea level and the partition between C_{org} and C_{carb} (Buggisch et al., 2003, Halverson et al., 2009). This interpretation has been questioned because isotopic fluctuations of similar magnitude as those observed in the ancient geological record have been documented in recent Quaternary carbonate platform sediments (Swart, 2008). These are ascribed to the effects of meteoric influences on carbonate shelf environments resulting from eustatic sea level fluctuations rather than secular variation of the global carbon cycle (Swart & Kennedy, 2012; Oehlert et al., 2012) although the application of this model to ancient carbonate platforms is controversial. The Late Cambrian SPICE $\delta^{13}C$ excursion, which is preserved in a remarkably wide range of depositional and diagenetic settings in a number of sections from North America, Australia, China, and Kazakhstan (Saltzman et al., 2000), argues for the robustness of the method.

The global reproducibility of Cambrian $\delta^{13}C$ excursions has led to the identification and naming of many of these isotopic stages (analogous to the oxygen isotope stages of the Quaternary) such as the Steptoean Positive Carbon Isotope Excursion (SPICE) and Drumian Carbon Isotope Excursion (DICE) (Saltzman et al., 1998, 2000; Babcock et al., 2007; Howley & Jiang, 2010). Following the Fourth International Symposium on the Cambrian System, Zhu et al. (2006), produced a composite $\delta^{13}C$ profile for the Cambrian from available published data (Fig.4). These authors also expanded the existing nomenclature by defining additional acronyms for the previously unnamed isotopic excursions, linked the chronological position of various Lagerstätten, and highlighted the importance of the $\delta^{13}C$ profile for intra- and inter-

continental correlation. The currently defined GSSPs for the Cambrian have all been associated with carbon isotope excursions: the Terreneuvian (Series 1) Fortunian (Stage I) is associated with the BASE negative excursion (Landing et al., 2007), the Series 3 Drumian (Stage VI) is tied to the negative DICE event (Babcock et al 2007); the Furongian (Series IV), Paibian (Series VIII) is linked to the positive SPICE excursion (Peng et al., 2004); and the Series 3 Guzhangian (Stage VII) correlates with an undefined low amplitude negative excursion (Peng et al., 2009). Other prominent biostratigraphical events through the Cambrian are also related to isotopic events; AECE (Archaeocyathid Extinction Carbon isotope Excursion); ROECE excursion (Redlichiid-Olenellid Extinction Carbon isotope Excursion), SHICE (SHIyantou Carbon isotope Excursion corresponding in position to the extinction of many SSF secreting organisms); MICE (MIngxinsi Carbon Isotope Excursion corresponding in position to the radiation of archaeocyathids), ZHUCE (ZHUjiaqing Carbon isotope Excursion corresponding in position to SSF zone 3 on the Yangtze Platform) and CARE (Cambrian Arthropod Radiation isotope Excursion).

Previous studies of the δ13C profile of Cambrian sequences in Australia are limited. As a consequence of the limited chemostratigraphic and radiometric data, Australian Cambrian strata are poorly correlated with other continents. Lindsay et al. (2005) compiled a comprehensive data set of 996 samples from Middle Cambrian to Ordovician sections in several northern and eastern Australian basins. This study highlighted 3 positive excursions (497.5-495 Ma, 506-503 Ma and 509-506 Ma), between the middle and late Cambrian the youngest of which was correlated with the SPICE event. Tucker (1989) reported 37 $\delta^{13}C_{carb}$ values across the Tommotian and Atdabanian stages in outcrop samples from the Flinders Ranges, South Australia.

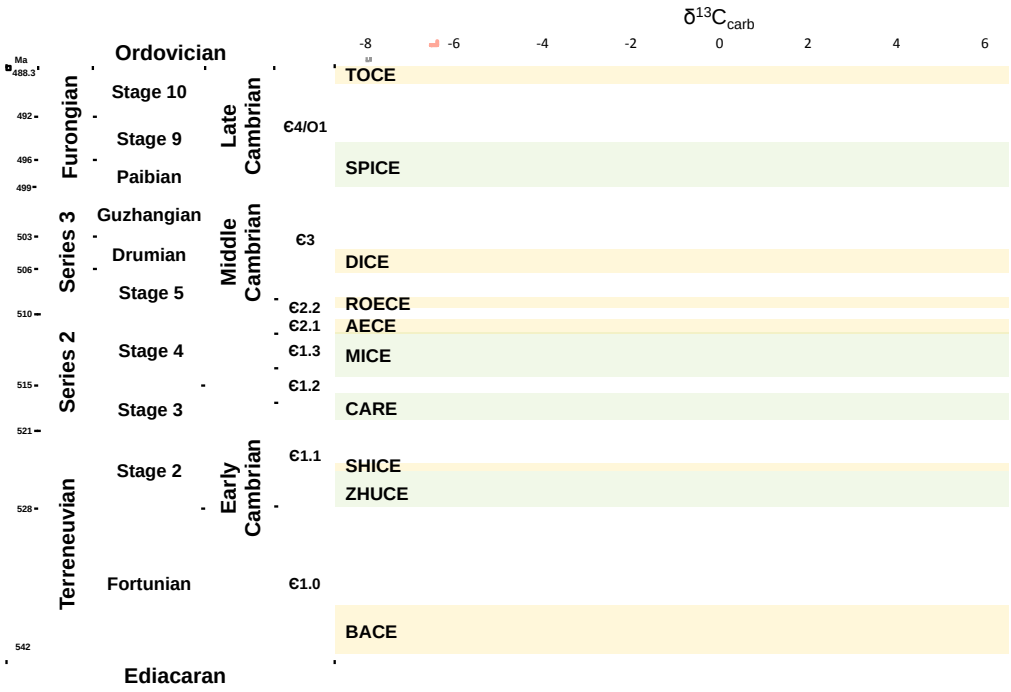

Fig. 4. Global carbon isotope composite and excursion events, after Zhu et al. (2006)

1.2.5. Geochronology

Radiometric dating techniques based on mass spectrometric evaluation of radioactive decay products are widely accepted and applied to geological investigations. The majority of the Phanerozoic is well defined (Gradstein et al., 2004) though dating of the Cambrian is the exception. Uranium-lead (U-Pb) dating techniques, conducted upon zircons contained within rocks such as tuffs or gneiss, allow accurate calculation of the age. The most accurate technique is isotope dilution thermal ionization mass spectrometry (ID-TIMS), whilst in-situ ‘microbeam’ techniques Secondary Ion Mass Spectrometry (SIMS); e.g., Sensitive High Mass Resolution Ion Microprobe (SHRIMP), and Laser Ablation Inductively Coupled Plasma Mass Spectrometry (LA-ICP-MS) provide less accurate (~1 order of magnitude) though valid age constraints.

The base of the Cambrian, or the Terreneuvian Stage, has been infered to be at 542.0±1.0Ma (Bowring et al., 2003; Amthor et al., 2003) whilst the upper limit is defined at the base of the Tremadocian, assigned to be 488.3±1.7Ma (Gradstein et al., 2004). The base of the Middle Cambrian is constrained by ID-TIMS U-Pb dating at 511±1Ma (Landing et al., 1998; Bowring and Erwin, 1998) and Landing et al. (1998) also report a 517±1.5Ma date close to the Atdabanian-Botoman boundary. Additional biostratigraphically controlled data points are infrequent within the Cambrian, though Maloof et al. (2010b) have constrained the Nemakit-Daldynian–Tommotian (ND-T) boundary at 524.84 ± 0.09 Ma using ID-TIMS and report further dates within the Tommotian at 523.2±0.16Ma and 520.9±0.14Ma.

Geochronological constraints for the Cambrian of South Australia is sparse. Two felsic tuffs in the Early Cambrian have been dated by SHRIP U-Pb: (i) 522.0±2.1 Ma from the Heatherdale Shale of the Stansbury Basin, about 400m above latest Atdabanian archaeocyathids (Jenkins et al, 2002) and (ii) 522.0±1.8 Ma from the lower Billy Creek Formation in the Arrowie Basin (Gravestock & Shergold, 2001). The reliability of both dates have been queried (Paterson, 2005; Jago et al., 2006, 2012). Other, much less reliable dates include Rb–Sr ages of 524±68Ma and 660±60 Ma were obtained from the Observatory Hill Formation in Byilkaoora 1 and Cadney Park Member in Byilkaoora 3 (Webb, 1978; Henry and Brewer, 1984, both references from Gravestock et al, 2002) although strontium concentrations may be too high for reliable age determination by the Rb–Sr method (Gravestock et al, 2002). A syn-post kinematic igneous intrusions within the Є2 Kanmantoo Group was dated at 514 ± 3 Ma, using both 207Pb-206Pb single zircon evaporation and SHRIMP U-Pb secondary ion mass spectrometry (Foden et al., 2006), providing some constraint of the upper sequences of the Early Cambrian.

1.3. Geological Setting of Cambrian Basins of South Australia

1.3.1. Stansbury Basin

The Stansbury Basin is situated at the southern end of the Adelaide fold belt and crops out in a roughly triangular region bound by the Yorke and Fleurieu Peninsulas and Kangaroo Island, and extending in the subsurface beneath Gulf St Vincent and the Murray Basin across to at least the Victorian border (Gravestock, 1995, Gravestock & Gatehouse, 1995; Flöttmann et al., 1998, Haines et al., 2009). Stable platformal environments are recorded throughout the lowermost parts of the Stansbury Basin in the first of these sequences. Here Є1 comprises predominantly passive margin carbonate shelf-ramp sediments deposited on the Palaeo-Pacific passive margin along the trailing edge of Gondwana (Gravestock & Gatehouse, 1995; Preiss, 2000; Jago et al., 2003). On the western shelf (Yorke Peninsula) thick successions of carbonates were deposited whilst further to the east (Fleurieu Peninsula) lower carbonate sequences passed into thick shales.

A final period of extensional tectonism within the Adelaide Fold Belt (Preiss, 2000; Foden et al., 2006) during Є2 and Є3 saw the formation of the Kanmantoo Trough, prior to the evolution of an active margin setting and development of a foreland basin by the encroaching Ross-Delamerian Orogen (Haines & Flöttmann, 1998; Flöttmann et al., 1998; Jago et al., 2003; Foden et al., 2006).

The Kanmantoo Trough was an isolated arcuate basin filled with 7-8 km of coarse and fine grained, almost entirely clastic, sediments, the upper two-thirds of which have a distinctly different provenance to the Є1 sediments (Turner et al., 1993; Flöttmann et al., 1998; Haines et al., 1996, 2001, 2009; Preiss, 2000; Jago et al., 2003). North and west of the Kanmantoo Trough, probably coeval sediments of the Kangaroo Island

Group accumulated along the tectonically active southern margin of the Gawler Craton (Gehling et al., 2011), whilst on the western shelf a an attenuated section (~400m) of alternating carbonate and siliciclastic units accumulated ranging up to the middle Cambrian.

Cessation of sedimentation in the Stansbury Basin occurred following the deposition of the Є3 sequence set with the shift from an extensional (or transtensional) setting to contraction during the Delamerian Orogeny culminating in significant uplift and up to 50% shortening of the Kanmantoo Group (Haines & Flöttmann, 1998; Flöttmann et al., 1998; Preiss, 2000). Zircon geochronology of the syn-post kinematic igneous intrusions within the Delamerian Orogen, using both ^{207}Pb-^{206}Pb single zircon evaporation and U-Pb secondary ion mass spectrometry, suggest that contractional orogenesis commenced at 514 ± 5 Ma (Foden et al., 1999) and continued until at least 490 ± 3 Ma. It was terminated by rapid uplift, cooling and extension in association with post-tectonic magmatism (Foden et al., 2006). However, the timing of the onset of uplift and deformation associated with this event is controversial, Turner (2009) arguing that it may have begun some 40-25 million years earlier, synchronous with the Antarctic Ross Orogeny.

1.3.1.2. Fleurieu Peninsula & Mount Lofty

1.3.1.2.1. The Normanville Group

The Normanville Group, observed in section on the Fleurieu Peninsula and in the eastern Mount Lofty Ranges, comprises the basal Mount Terrible Formation, the Wangkonda Formation, the Sellick Hill Formation, the Fork Tree Limestone, and the Heatherdale Shale (Fig. 2). These units comprise the Є1 supersequence set deposits of the eastern Stansbury Basin. The succession has a clastic base and passes upward into shelf and marginal slope/ramp carbonates, overlain by deeper water siliciclastics of the Heatherdale Shale (Gravestock, 1995; Jago et al., 2002b). The Heatherdale Shale is unconformably overlain by the Carrickalinga Head Formation of the Kanmantoo Group on the Fleurieu Peninsula. This unconformity represents a Type 1 sequence boundary, the erosional surface of which may be up to 300 m in relief (Jago et al., 1994, Carson 1994). The laterally equivalent section in the eastern Mount Lofty Ranges appears to show a conformable transition into the Kanmantoo Group (Gatehouse et al., 1993, Jago et al., 2003). The Heatherdale Shale comprises flat-laminated black calcareous shale and siltstone, in part pyritic and phosphatic (Carson, 1994; Turner, 1994; Gravestock and Gatehouse, 1995). Zircon geochronological data show a wide range of detrital ages; both late Mesoproterozoic and older Proterozoic components are well represented, suggesting a westerly provenance (Ireland et al., 1998; Preiss, 2000). The presence of younger detrital grains (800–540 Ma) suggests a transition from the typical provenance of the underlying Neoproterozoic and lower Normanville Group units to that exhibited in the Kanmantoo Group (Ireland et al., 1998, Haines et al., 2009; Turner et al., 2009). Largely unmetamorphosed outcrops are confined to the west coast of the Fleurieu Peninsula (Sellick Hill – Carrickalinga

Head) whilst the lateral equivalents in the Karinya Syncline are metamorphosed to biotite grade (Mancktelow, 1990; Preiss, 1995). Carson (1994) has suggested that the Heatherdale Shale may be split into lower and upper units, reflecting the transition from ramp to basinal facies at the end of a transgressive cycle. The upper facies is only observed in the southern sections at Sellick Hill as it either wasn't deposited, or has been eroded or faulted out in the other Fleurieu Peninsula outcrops. It is likely the Mount Lofty section, which shows a conformable boundary to the overlying units, incorporate both this upper unit and some of the lower unit though the base is faulted out. Interbedded tuff horizons have been reported throughout the Heatherdale Shale; crystal tuffs and pillow lavas were described by Gatehouse et al. (1993) at Red Creek in the Karinya Syncline. These are usually associated with the eruptive phases of the Truro Volcanics (Jenkins and Hasenohr, 1989, Foden et al., 1990, Gravestock and Gatehouse, 1995), though Gatehouse et al. (1993) suggest they may be a similar, but stratigraphically separate, suite in the Red Creek area. Jenkins et al. (2002) dated one such tuff from the upper section of Heatherdale Shale at Sellick Hill at 522 ± 2.1 Ma, recalculated from the 526 ± 4 Ma date of Cooper et al. (1992). However, whilst Cambrian SHRIMP ages are not as accurate as TIMS ages, or used by Shergold and Cooper (2004) and Ogg et al. (2008) and are generally discounted by the IUGS Cambrian Subcommission, these data show good precision and are consistent with the age constraints of the IUGS . Biostratigraphic evidence is limited within the Heatherdale Shale with rare trilobites, hyoliths sponges, brachiopods, molluscs and trace fossils (Jago et al., 1984, Jenkins & Hasenohr, 1989, Jago et al., 2003; Jago et al., 2006). The only reliable biostratigraphic age in the Sellick Hill succession is that of the Fork Tree Limestone from which Debrenne & Gravestock (1990) described late

Atdabanian to Botoman archaeocyatha. This suggests that the Heatherdale Shale has a Botoman age.

1.3.1.2.2. The Kangaroo Island Group

The Kangaroo Island Group, on the north coast of Kangaroo Island, includes the Emu Bay Shale, host to the most important Burgess Shale-type fossil assemblage (or Lagerstätte) in Australia. Gehling et al. (2011) gave a detailed review of the geology of these and adjacent stratigraphic units (Fig. 2) that form part of an essentially unmetamorphosed Cambrian platform succession north of the Kangaroo Island shear zone (Flöttmann and James, 1997). Syndepositional faulting and features such as folding and slumping within the Kangaroo Island Group suggest that it was deposited in a series of localised, deep-water sub-basins in an area of tectonic activity, sourced locally from the Yorke Peninsula (Nedin, 1995a; Flöttmann et al., 1998; Gehling et al., 2011) and possibly displaced northwards by thrusting (Flöttmann et al., 1995).

The Emu Bay Shale unconformably overlies the Marsden Sandstone, their contact forming a major sequence boundary. The Lagerstätte occurs within a basal dark grey to black laminated micaceous mudstone facies, in places pyritic, deposited below the wave base (Paterson et al., 2008). The Emu Bay Shale crops out east of the mouth of Big Gully, Kangaroo Island where it is about 78 m thick (Daily et al., 1979). A new fossil excavation site located inland at Buck Quarry has revealed a far greater diversity of the biota in the Emu Bay Shale (Paterson et al., 2008). The mudstone beds that contain the lagerstätte thin southwards and disappear 500-600 m south of the coast. The Emu Bay Shale coarsens upwards and in coastal sections the sandstone facies of the Boxing Bay Formation rest conformably on the Emu Bay Shale.

Correlation of the Kangaroo Island Group to Cambrian sequences on the Yorke and Fleurieu Peninsulas is tenuous, as little evidence exists to tie its formations to the mainland. However, tentative correlations with the Minlaton Formation on Yorke Peninsula and the Billy Creek Formation of the Flinders Ranges have recently been proposed (Gehling et al., 2011; Jago et al., 2012 in press).

1.3.1.2.3. The Kanmantoo Group

The Kanmantoo Group was deposited within a tectonically active zone of the southern Stansbury Basin. Originally described in its type section on the south coast of the Fleurieu Peninsula as an essentially non-faulted homoclinal structure with conformable successions (Daily & Milnes, 1971, 1973), the structural complexity of the section has subsequently been recognised (Gravestock & Gatehouse, 1995; Haines et al., 1996; Jago et al., 2003 and references therein). Jago et al. (2003) subdivided the Kanmantoo Group into the Keynes and Bollaparudda Subgroups, representing the Є2 and Є3 transgressive to highstand sequence sets, and revised the existing nomenclature of the sequence sets (Fig. 2), which is followed in this paper. The Kanmantoo Group comprises predominantly fine to medium grained siliciclastic rocks (Haines et al., 2001) that have all undergone metamorphism, ranging from chlorite grade at Carrickalinga Head to upper amphibolite grade on the south coast of Kangaroo Island and in the eastern Mount Lofty Ranges (Jago et al., 2003), though the metasediments are herein referred as their unmetamorphosed precursors. The Karinya Shale of Thomson (1969), the equivalent of the Talisker Formation calc-siltstones of the southern Fleurieu Peninsula, was incorporated into the Talisker Formation of Jago et al. (2003). It comprises a calcareous basal unit of interbedded carbonate and siltstone overlain by fining-upward shale beds and was interpreted as a

transgressive sequence (Turner, 1994). The Kanmantoo Group was deposited in predominantly deep-water settings, but thick shallow-water formations occur in the upper sections of both subgroups (Preiss, 2000; Haines et al., 2001; Jago et al., 2003, Jago & Gatehouse, 2009). Deposition of the estimated 7-8 km thickness of the Kanmantoo Group has been constrained to as little as 8 million years (Foden et al., 1999; Jenkins et al., 2002). Preiss (2000) and Haines et al. (2001, 2009) note a south to north proximal to distal trend to all facies suggesting the source to be a delta-fan complex of high-load-capacity rivers situated at the southern margin of the basin, perhaps a westerly extension of the Kanmantoo Trough in the tectonic zone along which Australia and Antarctica later separated. This could explain the high rate of deposition, ≥150cm/Ka , and is supported by palaeocurrent measurements in turbiditic facies indicating flow from the south or southwest (Flöttmann et al., 1998; Haines et al., 2001). Jago & Gatehouse (2009) report opposite current directions in shallower water facies, invoking tidal redistribution as the cause of the variation. Detrital zircon studies indicate a distinct change in the provenance of the Kanmantoo Group sediments from those of the underlying Neoproterozoic rocks and the early Cambrian Normanville Group, with dominant contributions from 0.7-0.5 Ga (dominant) and 1.2-1.0 Ga (secondary) sources being observed (Ireland, 1998; Suto, 2011). These source ages are common for Palaeozoic sedimentary rocks throughout much of Gondwana (Squire et al., 2006; Veevers et al., 2006; Haines et al., 2009; Myrow et al., 2010). This observation has led to an extraordinary interpretation of a ‘Gondwana Super-fan System’ that covered much of eastern Gondwana and was sourced from a huge mountain range at the site of the East African Orogen (Squire et al., 2006). However, the south-to-north palaeocurrent directions and presence of potential source rocks of the required ages in the Prydz-Leeuwin Belt (Collins et al., 2003) and exposed or

thinly covered parts of eastern Antarctica (Kelsey et al., 2008; Veevers et al., 2006) suggest that a more proximal part of Antarctica is a more likely source area for these sediments (Haines et al., 2009; Suto, 2011).

1.3.1.3. Yorke Peninsula

The shelf sequences of the Yorke Peninsula lie unconformably on crystalline basement of the Gawler Craton. The basal Є1.0 Winulta conglomeratic arkose is overlain by stromatolitic and fenestral micritic limestones of the Є1.1 lowstand Kulpara Formation. This is the conformably succeeded by the Parara Limestone, which encompasses the three transgressive sequences of Є1.1, Є1.2 to Є1.3 and includes the Є1.2 Koolywurtie Member. These thick (~400m in the Stansbury West 1 well) carbonates contain numerous fossil assemblages including archaeocyatha, brachiopods and trilobites that range in age from the Atdabanian through the late Botoman (Zhuravlev & Gravestock, 1993; Gravestock & Gatehouse, 1995; Jago et al 2006). The Є1 carbonates are succeeded unconformably by the Minlaton Formation, whose basal conglomerate contains clasts of the underlying limestones. The richly fossiliferous and predominantly nodular lime mudstone of the Ramsay Limestone conformably follows, the base of which forms the boundary between Є2.1 and Є2.2 (Gravestock & Cowley, 1995; Jago et al 2006). Over the transgressive Ramsay Limestone the calcareous sandstones of the Corrodgery Formation and oolitic grainstone/lime mudstone of the Stansbury Limestone show gradual transitions before a sharp contact with the basal Moonan Formation. This non-calcareous shale is conformably overlain by the oolitic Coobowie Limestone. The Ramsay-Coobowie section is interpreted as a transgressive–regressive cycle by Gravestock and Cowley (1995). The intertidal to alluvial stream, feldspathic sandstone and siltstone deposits

of the Є3 Yuruga Formation form the top section of Cambrian sediments this westerly section of the Stansbury basin.

1.3.2. Arrowie Basin.

The Arrowie Basin is situated at the northern end of the fold belt with the Flinders Ranges in the central zone flanked to the west by the Stuart Shelf and east by the Curnamona Province. The Arrowie Basin was subjected to similar tectonic influences as the southerly Stansbury Basin. Є1 carbonate shelf-ramp sediments were deposited on the passive margin of the Palaeo-Pacific Ocean, though no pronounced shelf slope break has been interpreted and deeper water deposits are inferred to the northeast and southeast (Gravestock & Cowley, 1995; Zang, 2002). Regional uplift at the boundary of Є1.1 & Є1.2 during the Atdabanian is expressed by the Flinders Unconformity whilst fault reactivation of the Torrens Hinge Zone with the Kangaroonian Movements (Daily & Forbes, 1969) are associated with volcanic activity and a period of uplift during the upper sequence Є1.3. A continuation of the southeasterly palaeoslope of the rapidly subsiding Kanmantoo trough is suggested for Є2 deposits though by Є3 uplift of the southern Arrowie Basin is evident, likely due to the encroaching Delamerian Orogen, which separated the depocenters (Gravestock & Cowley, 1995). Sedimentation ceased following the deposition of the Є3, at the onset of the Delamerian Orogeny (Preiss, 1995, 2000).

1.3.2.1. Flinders Ranges

In the Flinders Ranges a near complete succession of carbonates spans from the Tommotian through to the Botoman (Є1.1 to Є1.3). Above the basal Uratanna Formation, the Parachilna Formation comprises interbedded sandstones and dolomitized oolites, whilst the overlying Woodendinna Dolomite and lower

Wilkawillina Limestone consist of mostly shallow water shelf carbonates with oolites, stromatolites, archaeocyathid bioherms and bioclastic limestones (Gravestock & Cowley, 1995). These units are interpreted as having been deposited during a transgressive to highstand system during Є1.1 on the passive margin of the palaeo-Pacific Ocean. (Tucker, 1989, Gravestock & Cowley, 1995). The overlying Є1.2 sequences, bound at the base by the Flinders unconformity, consist of shelf carbonate (e.g., middle Wilkawillina Limestone) and redeposited slope sedimentation (e.g., Mernmerna Formation). Sequence Є1.3 comprises mixed siliciclastics and carbonates: the Bunkers Sandstone, Oraparinna Shale and upper Wilkawillina Limestone (Zang et al., 2007).

The Є2.1 siliciclastic Billy Creek Formation unconformably follows with the subsequent, conformable Є2.2 Wirrealpa Limestone containing the youngest archaeocyathid fauna described in Australia (Gravestock, 1984; Jago et al., 2006). These sequences pass on into the late Є2.2 to Є3 Lake Frome Group sediments (Gravestock and Cowley, 1995).

1.3.2.2. Stuart Shelf

The Andamooka Limestone, deposited on the Stuart Shelf is a northwestern lateral equivalent of the Wilkawillina Limestone (Fig. 2), comprising predominantly shallow marine carbonate. The lower part of the section consists of peritidal oolite, stromatolites and subtidal boundstone with karst surfaces indicating periods of subaerial exposure. These lower beds are interpreted as regressive to lowstand deposits but also coincide with a period of regional uplift associated with the Flinders unconformity (Zang, 2002). The lower unit passes up into burrowed fossil wackestones in the transgressive to highstand middle part of the section and fenestral

spiculitic wackestones in the upper part of the formation rich in archaeocyaths and calcareous sponge-like organisms. Regressive deposits are again observed with peritidal siltstones with mudcracked, fenestral, bioclastic limestone and evaporitic breccia. The lowstand deposits are overlain by prograding bioherm limestones and dolomitised stromatolites evident of an renewed period of transgression (James & Gravestock, 1990, Gravestock & Cowley, 1995). The Andamooka Limestone is abruptly overlain by the Є2.1 Yarrawurta Shale, a succession of red beds observed across the Arrowie Basin (Gravestock & Cowley, 1995; Jago et al., 2006).

1.3.3 Officer Basin

Situated to the north and west of the Adelaide Fold Belt, the Officer basin sediments were part of the Centralian Superbasin and were deposited in what was initially an intracratonic sag basin during the Neoproterozoic (Lindsay, 2002). Later north-south compression (~560 to 550 Ma) during the Petermann Ranges Orogeny resulted in the uplift of the Musgrave Block (Gravestock, 2002), which segmented the Centralian Superbasin and resulted in folding and thrusting over the northern margin of the Officer Basin and flexural subsidence within the basin (Tingate & Duddy 2002). The Delamerian Orogeny (~515 to 490 Ma) resulted in uplift and halted the Cambrian deposition (Preiss, 1995). This epeiric Cambrian basin was bound to the west by the Yilgarn Block and connected eastward to the open ocean through a series of throughs between the Musgrove Block (north) and Gawler Craton (south). In the northeast the Munyarai and Manya troughs show significant Neoproterozoic to Cambrian sediment fill (up to 10km). The southerly Tallaringa Trough (Fig.2), a 200 km long, 40 km wide depocentre, bound to the northwest by the Nawa Ridge and to the southeast by the Gawler craton, was not part of the ocean seaway but contains the richest oil-prone

source rocks in the Officer Basin (Kamali, 1995; Gravestock & Morton, 2002). The trough contains up to 600 m of Cambrian strata and possibly 1600 m of underlying Neoproterozoic sedimentary rocks above magnetic basement (Gravestock, 2002).

The earliest Cambrian sediments were terrestrial throughout the basin, represented by the basal aeolian Relief Sandstone, a formation that continued deposition in the western section of the basin until the end of sequence Є1.3 in the mid-Botoman. Evolution of coastal sabkha to shallow marine successions in the eastern section of the basin is demonstrated by the Relief Sandstone being conformably overlain by the evaporitic lower units of the Ouldburra Formation (Gravestock et al., 1995, Morton, 2002). The lower Ouldburra Formation comprise a suite of halite-carbonate-siliciclastic cycles unique in the Cambrian of South Australia, and probably representing the lowstand to early transgressive Є1.1 depositional phases (Gravestock et al., 1995). Deposition of thick transgressive laminated silty carbonate mudstones of sequence Є1.2 ensued. These grade upward into an intercalated laminated carbonate mudstone and red siltstone, with a carbonate breccia marking subaerial exposure representing the top of sequence Є1.2 (Mason, 2001; Morton, 2002). The Є1.3 successions of the upper Ouldburra Formation are characteristically shoaling upwards cycles of red-beds and sabkha carbonates with repeated exposure surfaces in the upper section marking the terminal Є1.3 regression (Gravestock et al., 1995). The Ouldburra Formation is sparsely fossiliferous, with the identified examples being Atdabanian, although trilobites observed in the Manya 3 drill core have been suggest a Botomian age (Morton, 2002). Following this major regression at the end of the Relief–Ouldburra deposition the succeeding Є2 and Є3 units (Observatory Hills Formation to Trainor Hill Sandstone) were formed in non marine environments with alluvial fan to alluvial plain deposits and playa lakes (Morton, 2002).

1.4. Palaeoenvironment; Redox, Isotopes and Trace Elements.

The significance of black shale deposits in reconstructing palaeoenvironments and basin redox are widely accepted (e.g., Braiser, 1992a; Powell et al., 2003; Guo et al., 2007a; Pi et al., in press). Black shales are a characteristic feature of warm intervals in Earth history, notably the early Cambrian, late Devonian–Carboniferous, mid-late Permian and Cretaceous periods (Guo et al., 2007a). Numerous studies across the globe have focussed on lower Cambrian black shale geochemistry, including North and South China, Canada, Siberia, India, Oman and Australia (e.g., Brasier, 1992a; Nedin, 1995a,b; Powell et al., 2003; Gou et al., 2007a; Lehmann et al., 2007; Piper & Calvert, 2009; Powell, 2009; Yu et al., 2009; Zhou & Jiang, 2009; Och & Shields-Zhou, 2012; Pi et al., in press). The early Cambrian successions of the Adelaide Fold Belt are renowned for their thick fossiliferous limestones (including archaeocyathid reefs) and shales, the latter commonly black, pyritic and phosphatic. These marine sediments were deposited in a humid tropical climate at low northern palaeolatitudes on the western margin of the Palaeo-Pacific Ocean (Gravestock, 1995, Brock et al. 2000).

It has long been assumed that deep ocean anoxia was a prerequisite for the deposition of marine black shales (e.g., Calvert & Pederson, 1993; Kimura & Watanabee, 2001; Tribovillard et al., 2006; Guo et al., 2007a; Jiang et al., 2007). However, the presence of abundant benthic animals and trace fossil evidence, points to oxic or dysoxic living conditions beneath bottom waters in several cases, in apparent contradiction to geochemical interpretations (Carson, 1994; Gehling et al., 2011; Pi et al., in press). Studies such as Powell et al., (2003), Powell (2009) and McKirdy et al., (2011) from lower Cambrian Lagerstätten have suggested oxic conditions may have been prevalent

at the ocean floor, although a sharp redox boundary probably existed at the water-sediment interface.

1.4.1 Trace Elements

Trace element distributions can provide an insight into the palaeoenvironment during deposition of the original sediments, as depending on their solubility under oxidising or reducing conditions within the water column certain elements may become enriched or depleted during deposition. Trace metals, specifically, are commonly enriched in black shales. Concentrations of trace element are commonly normalised against 'standard' shale values (e.g., Post Archean Australian Shale [PAAS] of Taylor & McLennan, 1985) and/or a detrital element (e.g., Al), highlighting relative depletions and enrichments thus simplifying palaeoenvironmental interpretations (e.g., Nedin, 1995a, b, Yan et al., 2000; Tribovillard et al., 2006; Guo et al., 2007a). Molybdenum (Mo) has often been cited as showing enrichment under reducing conditions (e.g., Nedin, 1995; Tribovillard et al., 2004; Guo et al., 2007a; Scott et al., 2008; Halverson et al., 2009; Och & Shield-Zhou, 2012), as have vanadium (V), uranium (U) and other organometallic complex-forming elements such as nickel (Ni) and copper (Cu) (Tribovillard et al., 2006). Some elements, such as scandium (Sc), cobalt (Co) and thorium (Th) are insensitive to palaeoredox conditions and hence are useful determinants for normalizations and in determining sedimentary provenance. Numerous trace metal proxies have been applied to reconstructing palaeoredox conditions, including V/(V+Ni), V/Sc, Th/U (or U/Th) and Ni/Co (e.g., Hatch & Leventhal, 1992; Kimura & Watanabe, 2001; Jones & Manning, 1994; Powell et al., 2003).

1.4.2 Rare Earth Elements

Rare earth element (REE) distributions and enrichment factors are less commonly used as proxies for depositional environments due to their predominantly detrital nature. Most frequently utilised in authigenic precipitates that best retain primary seawater signatures, Ce and Eu anomalies can still prove helpful in determining redox conditions and hydrothermal activity respectively in shale deposits (Taylor & Mclennan, 1985; Shields & Still, 2001; Guo et al., 2007a; Jiang et al., 2007; Yu et al., 2009; Pi et al., in press), providing support for more robust proxies when covariance is exhibited. These anomalies are calculated relative to their neighbouring elements in the transition series following normalisation to standards such as chondrite or PAAS.

In addition to their palaeoenvironmental application, trace elements can prove valuable in the assessment of provenance. Elements such as Th, Sc, light rare earth elements (LREE) and heavy rare earth elements (HREE) are relatively immobile, have low residence times in seawater, and display a geochemically distinct behaviour (Wombacher & Monker, 2000). These characteristics makes them ideal tracers of provenance, especially as REE distributions in fine-grained terrigenous sedimentary rocks, even when derived from a reasonably widespread and complex provenance, reflect the average REE composition of exposed continental crust (McLennan & Taylor, 1987). Thus, the relationships between elements including La, Th, Sc and Co have been applied to the determination of provenance and tectonic setting of a variety of sedimentary rocks (e.g., Bhatia and Crook, 1986; McLennan, 1989; Naqvi et al., 2002; Yan et al., 2007; Xie et al., 2011).

1.4.3 Trace and Rare Earth Element Mobility

Mobility of redox-sensitive elements is also a consideration when assessing palaeoenvironments as diagenesis can significantly alter sedimentary goechemistry. For example, REE + Y in sedimentary carbonates and organic-rich sediments, such as black shales, can be affected by fluid mobilization during diagenesis and metamorphism (Abanda & Hannigan, 2006; Zhao et al., 2009). Kidder et al. (2003) showed significant effects on trace element chemistry for black shales with >5% P_2O_5, though no effect was observed for concentrations <0.5%. REE enrichment in shales is also associated with the presence of phosphate minerals such as monazite and apatite (Yan et al., 2000). Thomson et al. (1998) also observed mobilisation of Cu, Co, Ni and Zn during early diagenesis within recently deposited turbidites, although other elements, namely V, appeared immobile. In sedimentary carbonates the early diagenetic reduction of porosity and permeability through cementation and low concentrations of REE in diagenetic fluids are believed to reduce secondary alteration (Banner & Hanson, 1990; Zhao et al., 2009). Microbial carbonates have been shown to be the most faithful archives of primary seawater REE signatures (Webb and Kamber, 2000). The low porosity and permeability of black shale facies is believed to promote retention of their primary seawater trace element and REE signatures, but their utilisation is fraught with difficulties as diagenetic alterations can obscure or fundamentally change these distributions (Powell et al., 2003).

1.4.4 Total Organic Carbon

Palaeoenvironmental indications may also be provided from parameters such as organic carbon content and isotopic signatures. The quantity of organic carbon available for sequestration is dependent upon carbon availability for fixation,

commonly the dissolved inorganic carbon (DIC) content of seawater and nutrient supply. McKirdy (1994) argued that total organic carbon (TOC) concentrations are also a reasonable indicator of depositional environment as organic matter is not preserved well under oxic conditions. However, the processes of carbon sequestration are still poorly understood and the interaction between mineral surfaces and organic carbon compounds is likely to play a critical role (Kennedy et al., 2002, Kennedy & Wagner, 2011). Hence, the relationship between anoxia and TOC may well be complex, but the general observation persists that TOC and enrichment of redox sensitive elements such as Mo, V, Ni, Cu and U are coupled. Good linear correlations are evident in anoxic environments, which indicates that metal scavenging is likely to be linked to organic productivity and decay, though this decouples towards higher enrichment under euxinic conditions (Wilde et al., 2004; Tribovillard et al., 2006; Guo et al., 2007a).

1.4.5 Carbon Isotopes

Bulk $\delta^{13}C_{org}$ isotopic signatures may reflect fluctuations in the isotopic composition of the DIC pool, analogous to $\delta^{13}C_{carb}$ signatures. Multiple studies (e.g., Knoll et al., 1986; Hayes et al., 1999; McKirdy et al., 2001) have demonstrated a broad correlation with contemporaneous $\delta^{13}C_{carb}$ and $\delta^{13}C_{org}$ and a $\Delta^{13}C$ (=$\delta^{13}C_{carb}$ - $\delta^{13}C_{org}$) of ~30‰. It has been suggested that $\delta^{13}C_{org}$ could even be used in parallel with, or in place of, inorganic carbon data where primary carbonates are unavailable as a proxy for seawater dissolved inorganic carbon (DIC) compositions, although the net fractionation between the original DIC reservoir and extracted kerogen is inherently variable (Halverson et al., 2010). Thermal alteration of organic matter must also be considered because kinetic fractionation during kerogen maturation resulting in

enrichment of ^{13}C (Peters et al 2005). The degree of thermal alteration can be inferred by measuring H/C ratios; the rule of thumb is that thermal maturation begins to alter the isotopic composition of organic matter where H/C <0.2 (McKirdy & Powell 1974; Hayes et al., 1983).

1.4.6 Sulphur Isotopes

Sulphur isotopes are commonly measured from minerals containing sulphates ($\delta^{34}S_{sulf}$), which are presumed to represent seawater sulphate compositions or sulphides ($\delta^{34}S_{pyr}$), which represent fractionation due to bacterial sulphate reduction (BSR) plus the effects of oxidative recycling (Halverson et al., 2010). The biogeochemical processes impose significant and predictable isotopic fractionations on sulphur species and consequently, the isotopic composition of sedimentary sulphides and sulphates are sensitive indicators of environmental change (Hurtgen et al., 2002). The difference between $\delta^{34}S_{sulf}$ and $\delta^{34}S_{pyr}$, $\Delta^{34}S$, is broadly connected to the oxidation state of the ocean (Canfield et al., 1996). Therefore, an observed increase in average $\Delta^{34}S$ values in the late Neoproterozoic is cited as indirect evidence of an end-Proterozoic oxygenation event (e.g. Hurtgen et al., 2005; Fike et al., 2006; Halverson and Hurtgen, 2007). However, other factors may also have contributed to the increasing $\Delta^{34}S$ documented in the Ediacaran, such as increased irrigation of marine sediments by bioturbating animals and more complicated controls on the isotopic fractionation by bacterial sulphate reducers (Canfield et al., 2006, Johnson et al., 2007; Canfield and Farquhar, 2009; Wu et al., 2010). $\delta^{34}S_{sulf}$ values peaked +40‰ across the PCB, whereas reported $\delta^{34}S_{pyr}$ values show significant variability throughout the period: −30‰ to +53‰ (e.g. Shields et al., 1999; Hurtgen et al., 2002; Strauss, 2002; Gorjan et al., 2003; Shields et al., 2004; Fike & Grotzinger, 2008).

1.5 Southern Margin Coastal Asphaltic Bitumen Strandings

1.5.1. History of Southern Margin Bitumen Strandings.

Bitumen strandings along the coastal sections of South Australia, Victoria, Tasmania and Western Australia have been documented since the early 19th Century (Sprigg & Woolley, 1963; Volkman et al 1992; McKirdy et al 1994; Padley, 1996; Edwards et al 1998 and references there in). Their location along the shorelines of the southern margin (Fig.1), and particularly around the Otway Basin and southern Tasmania, fuelled early petroleum exploration in the region on the assumption they were sourced from local submarine seepages (Sprigg, 1986, Volkman et al 1992; McKirdy et al., 1994). Accounts describe a variety of oily substances and these hydrocarbons can be assigned to three categories with differing origins; oils (crude and refined), waxy bitumens & asphaltites (Edwards et al., 1998). Historically, reports that asphaltum was strandings were predominantly described, though since the 1960s waxy bitumen strandings have become more prevalent (Padley, 1996).

The oils, mainly observed as liquid droplets, are likely derived from anthropogenic input due to local maritime traffic (Padley 1993, Padley, 1996). The waxy bitumens comprise a number of genetic families, categorised through subtle differences in their geochemical composition (e.g., sulphur content, biomarker and isotopic signatures). Typically observed as small tar balls (5-120mm) with APIs ~13-38° they are paraffinic to aromatic-intermediate crude oils. McKirdy (1984a, 1984b) initially identified three families, whilst further investigations by Padley (1996) sub-divide these waxy bitumens into 5 families; Families 1-3 exhibit molecular signals rich tropical angiosperms, dinoflagellates and botryococcus derived components, whilst Families 4-5 show ambiguous biomarker profiles but lack the botryococcanes. The

geochemical evidence suggests these have an Indonesian origin (McKirdy et al 1994; Padley 1996), supported by distributions of similar material along the northern and western margins of Australia, with long distance transportation on the Southern Equatorial and Leeuwin Currents accounting for their widespread dispersal (McKirdy & Horvath, 1976; Currie et al., 1992; Summons et al 1993; McGowran et al., 1997; Summons et al 2001).

1.5.2. Asphaltite Characteristics

The asphaltic bitumens (Family 4 of McKirdy 1984a; 1984b; McKirdy et al 1994) which are geochemically distinct from the waxy bitumens. These are sulphur rich aromatic-asphaltic crudes (S ~4%, 57-84% asphaltenes) and commonly strand as large jet black ovoid lumps (upto 670mm & 7kg) of material at the high water mark on medium to high energy, gently sloping sandy beaches (McKirdy et al., 1994). Slightly more dense than water (4-18° API, SG~1.02), the fresh strandings have a strong petroliferous smell (Volkman et al., 1992; Padley, 1996; Edwards et al., 1998). The upper surface is characteristically traversed by shrinkage cracks, and though the interior is pliable when fresh they become brittle upon storage and often show a conchoidal fracture pattern (Fig.2). The asphaltite strandings show a unique, remarkably uniform molecular & isotopic composition, rich in metallo-porphyrins (McKirdy et al., 1986, 1994; Currie et al., 1992; Volkman et al., 1992; Dowling et al., 1995; Padley, 1996; Edwards et al., 1998; Boreham et al., 2001; Boult et al., 2005; Totterdell et al., 2008). These characteristics correlate between samples collected both recently and historically (>100yrs) as well as samples collected in Western Australia, South Australia, Victoria and Tasmania and even from as far afield as New Zealand

and Macquarie Island (Fig.1), suggesting they all originate from the same offshore petroleum system (Padley, 1996; Edwards et al., 1998).

Asphaltic mats, or volcanos, observed by remote sensing vehicle at Chapopote in the Gulf of Mexico (Brüning et al., 2010) from low intensity seeps of heavily biodegraded viscous oil, exhibit analogous physical properties to the southern margin strandings. Surface cracking due to the loss of volatiles and subsequent fragmentation of older more brittle deposits, which both occur in situ, are described in conjunction with flow structures and lamination. Additionally benthic colonies of bivalves and tubular worms were evident and allowed estimation of flow ages with surface fissures believed to occur in about a decade. These flow asphaltites are also generally negatively buoyant, however, a freshly-deposited asphalt was unexpectedly positively buoyant when sampled.

Boult et al. (2005) proposed it is likely the source for the southern margin strandings is a similar seafloor flow seepage of a tar mat. Alternatively, Logan et al. (2010) expanding upon one of the hypotheses of Edwards et al. (1998) forwarded the idea that the asphaltites were the result of oil slick mousse formation which stabilise at the ocean surface prior to stranding.

1.5.3. Asphaltite Geochemistry

Geochemically the asphaltites show a homologous series of normal alkanes extending beyond nC_{35} with depletion of $<nC_9$ hydrocarbons which generally maximise at nC_{15}, display no odd or even preference and have a uniformly low Pr/Ph ratio (1.1 – 1.3). Terpane biomarker profiles feature dominant C_{30} αβ hopanes, Ts/Tm ratio <1, include both 29,30 & 28,30 bisnorhopnes, exhibit $C_{19\text{-}26}$ tricyclic profile with a predominant

C_{24} tetracyclic component and lack both 25-norhopanes and land-plant biomarkers (e.g. oleanane, bicadinanes). Sterane biomarker profiles feature regular sterane abundance: $C_{27} \geq C_{29} > C_{28}$, abundant diasteranes and the presence of C_{30} steranes including dinosterane. Bulk $\delta^{13}C$ compositions are light (mean $\delta^{13}C_{sat}$ = -30.1‰) whilst normal alkane $\delta^{13}C$ vs carbon number plots show arcuate pattern with C_{12-18} & C_{26-32} generally less depleted. They also exhibit a high V:Ni alkylporphyrin ratio ≈22:1.

Source & age-specific biomarkers indicate origin from Cretaceous marine calcareous shale deposited under anoxic/sulphidic conditions, probably during an oceanic anoxic event (OAE) (Mckirdy et al., 1994, Edwards et al., 1998, Boreham et al., 2001). OAEs record profound changes in the climatic and paleoceanographic state of the planet and represent major disturbances in the global carbon cycle. They correspond to periods of warmer, wetter climate thought to be induced by rapid influx of CO2 to the atmosphere causing greenhouse conditions. Increased continental weathering lead to high nutrient flow and subsequent high primary productivity in the warmer waters. Intense oxygen demand in the water column meant conditions could readily evolve from poorly oxygenated to anoxic and ultimately euxinic, particularly in those restricted oceans and seaways where density stratification was favoured by palaeogeography and significant fluvial input (Jenkyns, 2010). Whether anoxia was prevalent in the whole global oceanic system or confined to these restricted environments is still a matter for conjecture, however, examples such as the Tethyan and Atlantic Oceans of Northern Hemisphere are renowned for their extensive organic-rich muds deposited during mid-Cretaceous OAEs. In the Southern Hemisphere the Indian Ocean, Toolebuc and Blue Whale Seaways exhibited these restricted characteristics and Cretaceous sediments associated with anoxic and euxinic

conditions have been identified in the associated Australian basins, possibly correlating to the Cenomanian–Turonian boundary OAE2 (Bonarelli Event) and shorter-lived late Albian oceanic anoxic subevents (OAE 1d; Breistrofffer Event) (Edwards et al., 1999; Boreham et al., 2001; Struckmeyer et al., 2001; Pancost et al., 2005; Totterdell et al., 2008; Jenkyns, 2010).

All the asphaltites lack 25-norhopanes, implying little in-reservoir alteration & hence may be characterised as at Level 4 on the degredation scale of Peters & Moldawan (1993) (Edwards et al., 1998). This level of biodegradation also suggests that if the origin is a natural seepage it would be of a low intensity (Wenger & Isaksen, 2002) which fits well with the pattern described for the Australian continental shelf (Logan et al., 2010), ascribed to low recent burial rates.

1.5.4. Possible Origins of Asphaltites.

The origin of the asphaltic bitumens is unknown to date and no reliable correlation has been made to a source rock or oil family either locally on the southern margin of Australia or globally which may source these enigmatic hydrocarbons.

The close proximity of common stranding sites to historical whaling stations has raised the possibility of an anthropogenic origin for the material. Investigation of the pine and coal tars, identified as being the common caulking materials brought into the region, recovered from 17th, 18th and 19th century shipwreck sites differ significantly from asphaltites geochemically thus excluding industrially transported materials as a source (Smart, 1999).

In the Stansbury Basin, South Australia potential source rocks are Cambrian in age and the Kulpara Formation was suggested as a possible source early in provenance

investigations due to sterane biomarker signatures from show striking similarities (McKirdy et al, 1996). The late Mesozoic age constraints of the molecular fossil distributions of the asphaltites discounts this (Edwards et al., 1998).

A number of basins with sedimentary fill of the required late Mesozoic age extend along the southern margin related to the Australian Southern Rift System. As Australia separated in a west to east direction from Antarctica a series of extensional basins were formed; Mentelle, Bight (Denmark, Bremer, Recherche, Eyre, Ceduna & Duntroon sub-basins), Otway, Sorell, Bass and Gippsland Basins. For the late Cretaceous period shelf & open marine, non-calcareous deposits are predominant in the westerly Mentelle Basin and the Denmark, Bremer and Recherche sub-basins of the Bight Basin (Bradshaw et al 2003, Blevin & Cathro, 2008). No geochemical data is currently available but it is unlikely these formations could provide a suitable source pod. The stratigraphy of the Sorell, Bass and Gippsland basins are terrestrially dominated during the period (Ozimic et al 1987; Blevin & Cathro, 2008). Hydrocarbons recovered from these basins reflect the terrestrial influence and have biomarker profiles dissimilar to those of the asphaltites (Edwards et al 1998; Edwards et al 1999).

The late Albian Toolebuc Formation of the on-shore Eromanga Basin has been shown to have striking geochemical similarities to the biomarker and isotopic signatures of the asphaltum (Boreham et al, 2001). Co-eval sediments deposited in the Blue Whale Seaway may well provide the enigmatic source rocks. These successions are the post-rift sag phase deposits of the Blue Whale Supersequence in the Bight Basin and the Crayfish Group in the Otway Basin (Boreham et al., 2001, Struckmeyer, 2001;

Bradshaw et al., 2003, Totterdell & Struckmeyer, 2003, Boult et al., 2005, Totterdell et al., 2008, Blevin & Cathro, 2008, Boreham, 2008).

1.5.4.1. Bight Basin

In the Bight Basin both the Eyre and Duntroon sub-basins (Fig. 5A) are perched rift basins and consist of Middle Jurassic-Early Cretaceous half graben overlain by comparatively thin sag phase sediments (Espurt et al., 2009). The Eyre sub-basin has been quite well characterised and though Blue Whale sediments are evident they are geochemically distinct from the coastal bitumens (Edwards et al., 1999). The main potential source rocks are thought to be the earlier syn-rift terrestrial and lacustrine deposits of the Sea Lion and Minke supersequences (Blevin & Cathro, 2008). The Duntroon sub-basin appears to have a significant proportion of the Cretaceous sequences removed, including the Blue Whale Supersequence (Blevin & Cathro, 2008), Geochemical analysis of oil shows within the basin have identified evidence for anoxic marine source rocks, though they also exhibited terrestrial biomarkers not observed in the asphaltites (Edwards et al., 1999).

The Ceduna sub-basin (Fig. 5A) has been proposed as a likely source area for the asphaltic strandings with numerous stranding sites to both east and west (Boreham et al., 2001; Totterdell et al., 2008). A Cretaceous depositional system covering over 155000 km^2 it comprises two stacked, though tectonically independent, prograding delta systems with up to 16km depth of sediment. (Blevin et al., 2000; Totterdell et al., 2000;Totterdell & Struckmeyer, 2003; Totterdell et al., 2008; Espurt et al., 2009). The lower White Pointer delta is of late Albian to Santonian age and overlies late Albian shales of the Blue Whale Supersequence having formed under accelerated subsidence rates as Australia and Antarctic separated at horizontal stretching rates

estimated between 2 and 5 km Ma^{-1} (Espurt et al., 2009). The upper Hammerhead delta is of late Santonian-Maastrichtian age.and formed during initial, slow seafloor spreading and sag basin evolution on the Australian margin following lithospheric failure (Espurt et al., 2009).

Initial studies of onshore wells highlighted the Blue Whale Supersequence from Eyre-1 drill hole as similar to the asphaltum, suggest a deeper water lateral equivalent to the shallow water end-member analysed as a possible correlative (Boreham et al., 2001). The subsequent Bight Basin Sampling and Seepage Survey SS01/2007 identified a number of potential areas for natural seepage and collected 259 dredge, core & grab samples from the Ceduna sub-basin (Fig. 5B). Geochemical investigation of these immature samples identified them as excellent potential source rocks (up to 6.2% TOC & 479 mg HC/g TOC) with biomarkers consistent with a late Cenomanian–early Turonian age of the organic rich samples (Totterdell et al., 2008). Analyses of 30 high-grade samples from the Blue Whale, White Pointer & Tiger supersequences show good correlation of biomarker distributions with asphaltites. However subtle differences to the asphaltites, with alkylporphyrins showing Ni>V rather than V>Ni and an absence of isorenieratane in the Bight samples, exclude them as the asphaltite source. These compositional differences are possibly due to local depositional environments within same system and local ‘sweet spots’ as suggested in seismic mapping down dip from sampling sites may be the enigmatic source zone (Totterdell et al., 2008). The major proportion of these potential source rocks in the western Ceduna sub-basin are in the gas window or over-mature, except along the outer edge, with modelling (Fig. 5C) suggesting Blue Whale derived hydrocarbons are likely to be gas accumulations (Totterdell et al., 2008).

Fig.5. A) Structural elements map of the eastern Bight Basin; B) Bight Basin Sampling and Seepage Survey SS01/2007: survey areas and location of sampling sites; C) Modelled present-day maturity zones (% R_o) for the northern transect as mark in yellow on map B (all after Totterdell et al. 2008).

In the eastern section of the basin the sequences are still within the oil generation window and an active petroleum system has been identified based on information from the Greenly-1 well (Edwards et al., 1999; Boult, 2012). Geochemical analysis has indicated anoxic marine conditions and calcareous mudstone sourced hydrocarbons though significantly a terrestrially derived component to the oil suggests a mixture of algal and land plant organic matter is preserved in the facies. These significant oil and gas shows in Greenly 1 in the Wigunda Formation are presumed to have been sourced from coaly intervals of the Borda Formation (Edwards et al., 1999). Evidence of hydrocarbon seeps along the margins of the depocentre from sniffer, Synthetic Aperture Radar (SAR) and Airborne Laser Fluorescence (ALF) data is strong whilst 2D seismic data appears to show pocks, sea floor mounds, upturned reflectors at depth and depressed shallow reflectors within the Tertiary sediments that represent recent or currently active fluid escape features (Hillis & Reynolds, 2003; Totterdell et al., 2008; Boult, 2012).

1.5.4.2. Otway Basin

The Otway Basin also exhibits good potential to host the asphaltite source. The long history and high concentration of asphaltum along the shores of the basin, as well as the generally larger size of strandings than more distant homologues, have been cited as possible evidence for a local origin (Sprigg & Wooley, 1963; Sprigg, 1986; McKirdy et al 1994). The apparent temporary increase in occurrences following local earthquake activity and large quantities collected after severe storm event such as in 1961 when Sprigg collected ‘almost half a ton’ south of Kingston also provide indirect evidence for the proximity of the provenance (Sprigg & Wooley, 1963; McKirdy et al 1994; Boult et al., 2005).

NOTE:
This figure/table/image has been removed to comply with copyright regulations.
It is included in the print copy of the thesis held by the University of Adelaide Library.

Fig. 6. A) Outline of Otway Basin with inferred sediment thickness and sub-basin, seismic section 137-03 and Crayfish-A1 well locations; and B) Interpretation of seismic section 137-03, showing the location of the possible upper Albian OAE source pod (after Boult et al., 2005).

Situated adjoining the south eastern boundary of the Bight Basin, the Otway Basin shows great similarity to the Bight. A series of separate grabens and half grabens filled with Jurassic to Early Cretaceous rift sequence are interpreted to exist across most of the basin (Boult & Hibburt, 2002). The rate of rifting slowed during the Barremian to Albian but rapidly increased before the end of the Albian in the northern part of the basin, with extension rate studies suggesting deposition of marine sediments in the Morum Sub-basin age equivalent to the prolific Albian OAE (Palmowski et al., 2004; Boult et al., 2005).

Over 4 km of late Albian to Late Cretaceous sediments occur within the Morum Sub-basin offshore (Fig. 5A), and the widespread Cenomanian unconformity observed in Otway Basin deposits is predicted not to occur with these northern sections (Boult & Hibburt, 2002). A potential Albian OAE source pod has been interpreted from seismic data (Fig. 5B) where amplitude anomalies, diapiric structures and possible gas chimneys are observed (Boult et al., 2005). A Cretaceous marine OAE derived oil show identified as a migrated oil in Crayfish-1 well at edge of depo-centre exhibits the potential of the region, though this does not correlate with the asphaltum (Edwards et al., 1999; Boult et al., 2005).

These potential source beds appear to be incised by canyons on the continental slope, which cut as deeply as 1.6km into the stratigraphic section and coincide with Synthetic Aperture Radar (SAR) anomalies possibly indicative of light hydrocarbon escape to the sea surface (Boult et al., 2005). It has been postulated by Boult et al. (2005) that oil seepage within these canyons or nearby slope may form asphaltic mats, which are periodically dislodged and transported up the canyons onto the shelf by the summertime Bonney upwelling of the east-west travelling, cold deep water Flinders

current (Fig. 7) or local earthquake activity. Subsequent interaction with the warmer, west-east travelling surface Coastal Current could explain the concentration of strandings on the western shores of Kangaroo Island and more distantly westward.

Fig. 7. Bathymetry with an overlay of surface temperature contours of 3rd March 1995, showing the location of the deep-water Flinders Current, Bonney Upwelling, asphaltite strandings and SAR anomalies (Boult et al., 2005).

The biogeochemical status of the Palaeo-Pacific Ocean: clues from the early Cambrian of South Australia

P.A. Hall[1*], D.M. McKirdy[1], G.P. Halverson[1,3],J.B. Jago[2], A.S. Collins[1] and M.W. Carson[1,4]

Submitted Manuscript GR-D-12-00258
Gondwana Research
Elsevier B.V.

1. School of Earth and Environmental Sciences, University of Adelaide, SA 5005
2. School of Natural and Built Environments, University of South Australia, Mawson Lakes, SA 5005
3. Present address: Department of Earth & Planetary Sciences, McGill University, Montreal, Canada H3A 2A7
4. Present address: BHP Billiton Iron Ore, 225 St Georges Terrace, Perth, WA 6000.

STATEMENT OF AUTHORSHIP

The biogeochemical status of the Palaeo-Pacific Ocean: clues from the early Cambrian of South Australia

Philip Anthony Hall (Candidate)

Performed preparation and analysis or oversaw the analysis on all samples, interpreted data, wrote manuscript and acted as corresponding author

I hereby certify that the statement of contribution is accurate

Signed …….Date……

David M. McKirdy

The biogeochemical status of the Palaeo-Pacific Ocean: clues from the early Cambrian of South Australia

Statement of contribution (in terms of the conceptualization of the work, its realization and its documentation)

Contributed to planning of article and provided critical evaluation

Certification that the statement of contribution is accurate and permission is given for the inclusion of the paper in the thesis

Signed …….Date…15/06/2012…

Galen P. Halverson

The biogeochemical status of the Palaeo-Pacific Ocean: clues from the early Cambrian of South Australia

Statement of contribution (in terms of the conceptualization of the work, its realization and its documentation)

Contributed to sample analysis, planning of article and provided critical evaluation

Certification that the statement of contribution is accurate and permission is given for the inclusion of the paper in the thesis

Signed …….Date…19/06/2012…

James B. Jago

The biogeochemical status of the Palaeo-Pacific Ocean: clues from the early Cambrian of South Australia

Statement of contribution (in terms of the conceptualization of the work, its realization and its documentation)

Contributed to sample collection and provided critical evaluation

Certification that the statement of contribution is accurate and permission is given for the inclusion of the paper in the thesis

Signed …….Date…20/06/2012…

Alan S. Collins

The biogeochemical status of the Palaeo-Pacific Ocean: clues from the early Cambrian of South Australia

Statement of contribution (in terms of the conceptualization of the work, its realization and its documentation)

Contributed to planning of article and provided critical evaluation

Certification that the statement of contribution is accurate and permission is given for the inclusion of the paper in the thesis

Signed …….Date…19-06-2012

Matthew W. Carson

The biogeochemical status of the Palaeo-Pacific Ocean: clues from the early Cambrian of South Australia

Statement of contribution (in terms of the conceptualization of the work, its realization and its documentation)

Contributed to sample collection, analysis and provided critical evaluation

Certification that the statement of contribution is accurate and permission is given for the inclusion of the paper in the thesis

Signed …….Date…20/06/2012…

Abstract

The Ediacaran-Cambrian transition was a time of profound reorganisation of the biosphere, coinciding with the final breakup of Rodinia, assembly of Gondwana and increasing atmospheric and oceanic oxygenation. The early Cambrian marine sediments of the Stansbury Basin, South Australia, were deposited at low northern palaeolatitudes on the western margin of the emerging Pacific Ocean. Here we report results of a multi-pronged investigation employing trace and rare earth element (REE) abundances, total organic carbon (TOC) contents and stable isotopic compositions (C_{org}, S_{pyr}) in carbonaceous shales from three formations within the Normanville and Kanmantoo Groups (sequences Є1.2 to Є2.2).

TOC ranges from ≤0.5% in the Emu Bay Shale, through 0.4–1.9% in the Talisker Formation, to 0.2–2.6% in the Heatherdale Shale. Covariance is demonstrated between trace elements and organic matter, with comparative uranium enrichment in the Heatherdale Shale likely linked to increased primary productivity. Light REEs are typically enriched, while heavy REEs and yttrium are depleted. Provenance appears to evolve through the late Normanville sediments into the Kanmantoo Group, corroborating published detrital zircon interpretations.

A multiproxy approach, in conjunction with sedimentological information, provides a powerful tool for interpreting palaeoenvironmental conditions. The prevailing palaeoredox regime for the Heatherdale Shale and the Talisker Formation was dysoxic, evolving into progressively more reducing conditions up section, the latter exhibiting a secular decline in $\delta^{34}S_{pyr}$ (from +10 to –11‰). Conversely, redox proxies concur in demonstrating that the basal fossiliferous Emu Bay Shale accumulated beneath an oxic water column. Comparison of trace element and REE distributions

with those of similar sequences on the Yangtze Platform, South China reveals striking similarities, implying that the trace element chemistry of the Palaeo-Pacific and Asian oceans was homogenous.

2.1. Introduction

The Ediacaran-Cambrian transition was a time of profound reorganisation of the biosphere, coinciding with the tectonic upheaval involved in the final breakup of Rodinia and assembly of Gondwana, and the increased oxygenation of the atmosphere and oceans (Collins and Pisarevsky, 2005; Canfield et al., 2007; Meert and Lieberman, 2008; Halverson et al. 2009). The proliferation of metazoan fauna, or 'Cambrian Explosion' (Brasier, 1992), is well documented, but their origin and its link to environmental change is still a matter of debate. Prevalent hypotheses include eustatic sea level changes, alterations in oceanic chemistry though increased weathering or hydrothermal sources, an increase in oceanic and atmospheric oxygen over the Proterozoic and early Cambrian transition, developmental adaptations to predation, and even cosmic radiation (Braiser and Hewitt, 1979; Derry et al., 1992; Brasier, 1992; Canfield et al., 1998; Babcock et al., 2003; Fike et al., 2006; Squire et al., 2006; Canfield et al., 2007; Goldberg et al., 2007, Muruyama and Santosh, 2008; Scott et al., 2008; Halverson et al., 2009; Erwin et al., 2011). However, because early animals inhabited the oceans, improving our understanding of the marine environment is central to testing and refining hypotheses for early animal evolution.

The significance of black shale deposits in reconstructing palaeoenvironments and basin redox are widely accepted (Brasier, 1992; Powell et al., 2003; Guo et al., 2007; Pi et al., in press). Black shales are a characteristic feature of warm intervals in Earth history, notably the early Cambrian, late Devonian–Carboniferous, mid-late Permian

and Cretaceous periods (Guo et al., 2007). Numerous studies have focussed on lower Cambrian black shale geochemistry across the globe, including in North and South China, Canada, Siberia, India, Oman and Australia (Brasier, 1992; Nedin, 1995; Powell et al., 2003; Gou et al., 2007; Lehmann et al., 2007; Piper and Calvert, 2009; Powell, 2009; Yu et al., 2009; Zhou & Jiang, 2009; Och and Shields-Zhou, 2012; Pi et al., in press). The early Cambrian successions of the Adelaide Fold Belt are renowned for their thick fossiliferous limestones (including archaeocyathid reefs) and shales, the latter commonly black, pyritic and phosphatic. These marine sediments were deposited in a humid tropical climate at low northern palaeolatitudes on the western margin of the emerging Pacific Ocean (Gravestock, 1995; Brock et al., 2000).

It has long been assumed that deep ocean anoxia was a prerequisite for the deposition of marine black shales (Calvert and Pederson, 1993; Kimura and Watanabe, 2001; Tribovillard et al., 2006; Guo et al., 2007; Jiang et al., 2007). However, the occurrence of abundant benthic animal and trace fossils, points to oxic or dysoxic conditions in some bottom waters, in apparent contradiction of the prevailing geochemical wisdom (Carson, 1994; Gehling et al., 2011; Pi et al., in press). Indeed, geochemical studies of lower Cambrian Lagerstätten by Powell et al. (2003), Powell (2009) and McKirdy et al. (2011) suggest that oxic conditions may have been common on the ocean floor, although a sharp redox boundary probably existed at the water-sediment interface.

Trace element distributions of sedimentary rocks can provide an insight into the palaeoenvironment of the original sediments. This is because, depending on their solubility under oxidising or reducing conditions within the water column, certain elements may become enriched or depleted during deposition. Trace metals,

specifically, are commonly enriched in black shales. Concentrations of trace element are commonly normalised against 'standard' shale values (e.g. the post-Archean Australian shale [PAAS] of Taylor and McLennan, 1985) and/or a detrital element (e.g. Al), highlighting relative depletions and enrichments and thereby simplifying palaeoenvironmental interpretations (Yan et al., 2000; Tribovillard et al., 2006). Molybdenum (Mo) has often been cited as showing enrichment under reducing conditions (e.g. Nedin, 1995; Tribovillard et al., 2004; Guo et al., 2007; Scott et al., 2008; Halverson et al., 2009; Och and Shields-Zhou, 2012), as have vanadium (V), uranium (U) and other organometallic complex-forming elements such as nickel (Ni) and copper (Cu) (Tribovillard et al., 2006). Some elements, such as scandium (Sc), cobalt (Co) and thorium (Th), are insensitive to palaeoredox conditions and hence are useful for the aforementioned normalization and in determining sedimentary provenance. Among the trace metal proxies found to be most helpful in reconstructing palaeoredox conditions are V/(V+Ni), V/Sc, Th/U (or U/Th) and Ni/Co (Hatch and Leventhal, 1992; Kimura and Watanabe, 2001; Jones and Manning, 1994; Powell et al., 2003).

Rare earth element (REE) distributions and enrichment factors are less commonly employed as environmental proxies due to the predominantly detrital nature of their host minerals. They are most useful in circumstances where shales contain authigenic precipitates (notably phosphate) capable of retaining primary seawater signatures. Thus, for example, Ce and Eu anomalies can prove helpful in determining redox conditions and hydrothermal activity, respectively, in marine shales (Taylor and McLennan, 1985; Shields and Still, 2001; Guo et al., 2007; Jiang et al., 2007; Yu et al., 2009; Pi et al., in press), particularly when used in conjunction with other proxies.

These anomalies are calculated relative to their neighbouring elements in the transition series, after normalisation to standards such as chondrite or PAAS.

In addition to their palaeoenvironmental implications, trace elements also can prove valuable in the assessment of provenance. Th and Sc, the light rare earth elements (LREE) and the heavy rare earth elements (HREE) are relatively immobile and have low residence times in seawater (Wombacher and Münker, 2000). These characteristics make them ideal tracers of provenance, especially as REE distributions in fine-grained terrigenous sedimentary rocks, even those derived from a reasonably broad and complex hinterland, reflect the average REE composition of the exposed continental crust (McLennan and Taylor, 1987). Thus, the interrelationships of La, Th, Sc and Co have been applied to the determination of provenance and tectonic setting for a variety of sedimentary rocks (Bhatia and Crook, 1986; McLennan, 1989; Naqvi et al., 2002; Yan et al., 2007; Xie et al., 2011).

Palaeoenvironmental information may also be obtained from parameters such as total organic carbon (TOC) content and its isotopic composition ($\delta^{13}C_{org}$). The quantity of organic matter preserved in a marine mudstone is dependent upon carbon availability for fixation, commonly the dissolved inorganic carbon (DIC) content of seawater, and nutrient supply. McKirdy (1994) argued that TOC concentrations in Cambrian sediments are a reasonable indicator of palaeoredox as organic matter is not well preserved under oxic conditions. However, the processes of organic carbon sequestration are still poorly understood and the interaction between mineral surfaces and natural organic matter is likely to play a critical role (Kennedy et al., 2002; Kennedy and Wagner, 2011). While the relationship between anoxia and TOC may well be complex, the general observation that TOC and redox-sensitive elements such

as Mo, V, Ni, Cu and U are coupled remains valid. Good linear correlations between these variables are evident in anoxic marine settings, which indicates that metal scavenging is likely to be linked to organic productivity and decay, although these variables tend to become decoupled during higher metal enrichment under euxinic conditions (Wilde et al., 2004; Tribovillard et al., 2006; Guo et al., 2007).

Bulk $\delta^{13}C_{org}$ isotopic signatures may reflect fluctuations in the isotopic composition of the DIC pool, analogous to $\delta^{13}C_{carb}$ signatures. Numerous studies of Neoproterozoic sediments (e.g. Knoll et al., 1986; Hayes et al., 1999; McKirdy et al., 2001) have demonstrated a broad correlation between coexisting $\delta^{13}C_{carb}$ and $\delta^{13}C_{org}$ in which $\Delta^{13}C$ (= $\delta^{13}C_{carb}$ - $\delta^{13}C_{org}$) is ~30‰. It has been suggested that $\delta^{13}C_{org}$ could even be used in parallel with, or in place of, inorganic carbon data where primary carbonates are unavailable as a proxy for seawater DIC, although the net fractionation between the original DIC reservoir and extracted kerogen is inherently variable (Halverson et al., 2010). Thermal alteration of organic matter must also be taken into account because kinetic fractionation during kerogen maturation results in its enrichment in ^{13}C (Peters et al., 2005). The degree of thermal alteration can be inferred by measuring atomic H/C ratios; the rule of thumb is that thermal maturation begins to alter the isotopic composition of the residual organic matter where H/C <0.2 (McKirdy and Powell, 1974; Hayes et al., 1983).

Sulfur isotopes are commonly measured from minerals containing sulphates (δ34Ssulf), which are presumed to represent seawater sulphate compositions, or from sulphides (δ34Spyr), which represent fractionation due to bacterial sulphate reduction (BSR) plus the effects of oxidative recycling (Halverson et al., 2010). Biogeochemical processes impose significant and predictable isotopic fractionations on sulfur species

and, consequently, the isotopic composition of sedimentary sulphides and sulphates are sensitive indicators of environmental change (Hurtgen et al., 2002). The difference between δ34Ssulf and δ34Spyr, Δ34S, is broadly connected to the oxidation state of the ocean (Canfield et al., 1996). Therefore, an observed increase in average D34S values in the late Neoproterozoic is cited as indirect evidence of an end-Proterozoic oxygenation event (e.g. Hurtgen et al., 2005; Fike et al., 2006; Halverson and Hurtgen, 2007). However, other factors may also have contributed to the secular increase in D34S during the Ediacaran, such as irrigation of marine sediments by bioturbating animals and more complicated controls on the isotopic fractionation attributable to bacterial sulphate reducers (Canfield et al., 2006; Johnson et al., 2007; Canfield and Farquhar, 2009; Wu et al., 2010). δ34Ssulf peaked +40‰ across the Proterozoic-Cambrian boundary, whereas δ34Spyr values show significant variability throughout the Cambrian period: −30‰ to +53‰ (e.g. Shields et al., 1999; Hurtgen et al., 2002; Strauss, 2002; Gorjan et al., 2003; Shields et al., 2004; Fike and Grotzinger, 2008).

The post-depositional mobility of redox-sensitive elements is also a consideration when assessing palaeoenvironments. For example, REE + Y in sedimentary carbonates and organic-rich sediments, such as black shales, can be affected by fluid mobilization during diagenesis and metamorphism (Abanda and Hannigan, 2006; Zhou et al., 2009). Kidder et al. (2003) reported significant effects on the trace element chemistry of black shales with >5% P_2O_5 arising from the growth of phosphate concretions, though no effect was observed for concentrations <0.5%. REE enrichment in shales is associated with the presence of phosphate minerals such as monazite and apatite (Yan et al., 2000). Thomson et al. (1998) also observed mobilisation of Cu, Co, Ni and Zn during early diagenesis within recently deposited

turbidites, although other elements, notably V, appeared immobile. In sedimentary carbonates the early diagenetic reduction of porosity and permeability through cementation and low concentrations of REE in diagenetic fluids are believed to reduce such secondary alteration (Banner and Hanson, 1990; Zhou et al., 2009). Microbial carbonates have been shown to be the most faithful archives of primary seawater REE signatures (Webb and Kamber, 2000). The low porosity and permeability of black shale facies is believed to promote retention of their primary seawater trace element and REE signatures.

In this paper we present trace element, RRE, TOC and isotopic (C,S) data on the early Cambrian Heatherdale Shale, Emu Bay Shale and Talisker Formation (sequences Є1.2 to Є2.2) from four sections in the Stansbury Basin, South Australia: Carrickalinga Head and Sellick Hill on the southern Fleurieu Peninsula; Emu Bay, northeastern Kangaroo Island; and the Karinya Syncline in the northeastern Mt Lofty Ranges (Fig.1). The objective of the study is to provide elemental and isotopic signatures of the developing Palaeo-Pacific Ocean and clues to its redox and nutrient status.

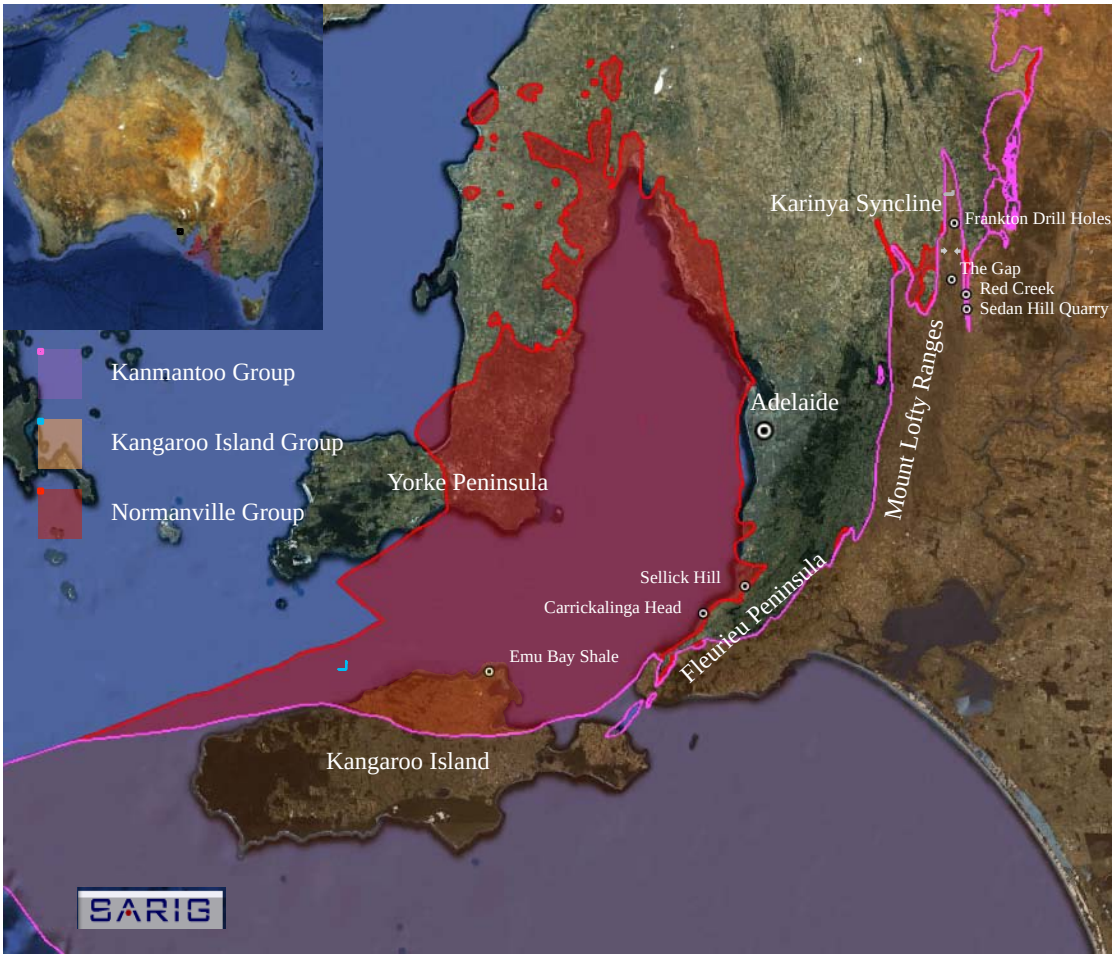

Fig. 1. Location map of early Cambrian deposits of the Normanville, Kangaroo Island and Kanmantoo Groups, South Australia, with sample localities highlighted. The four northeastern localities all lie within the Karinya Syncline.

2.2. Geological setting and stratigraphy

2.2.1. Stansbury Basin overview

The Cambrian successions of South Australia conclude an extended period of deposition that begin with early extension related to the break-up of Rodinia ca. 830 Ma and ended with the assembly of Gondwana at 500 Ma (Powell et al., 1994; Gravestock, 1995; Preiss, 2000; Lindsay et al., 2002). Thick Cambrian sequences are preserved in two distinct provinces: the Adelaide Fold Belt (Stansbury Basin and Arrowie Basin) and the Centralian Superbasin (Officer Basin and Warburton Basin).

The Stansbury Basin is situated at the southern end of the fold belt, cropping out in a roughly triangular region bound by the Yorke and Fleurieu Peninsulas and Kangaroo Island, and extending in the subsurface beneath Gulf St Vincent and the Murray Basin across to at least the Victorian border (Gravestock, 1995; Gravestock and Gatehouse, 1995; Flöttmann et al., 1998, Haines et al., 2009). The South Australian Cambrian was divided into four sequence sets, Є1, Є2, Є3 and Є4 by Gravestock (1995). Stable platformal environments are recorded throughout the lowermost parts of the Stansbury Basin in the first of these sequence sets. Here Є1 comprises predominantly carbonate shelf-ramp sediments that were deposited on the Palaeo-Pacific passive margin along the trailing edge of Gondwana (Preiss, 2000; Jago et al., 2003). By mid early Cambrian times the eastern and southern parts of the Stansbury Basin were sites of renewed extensional subsidence, resulting in the deposition of two further sequence sets, Є2 and Є3, the latter ranging up to the middle Cambrian (Gatehouse et al., 1990; Jago et al., 1994; Carson, 1994; Gravestock, 1995; Jago et al., 2002) (Fig. 2). This final period of extensional tectonism within the Adelaide Fold Belt (Preiss, 2000; Foden et al., 2006) saw the formation of the Kanmantoo Trough, prior to the

evolution of an active margin setting and development of a foreland basin by the encroaching Ross-Delamerian Orogen (Flöttmann et al., 1998; Jago et al., 2003; Foden et al., 2006).

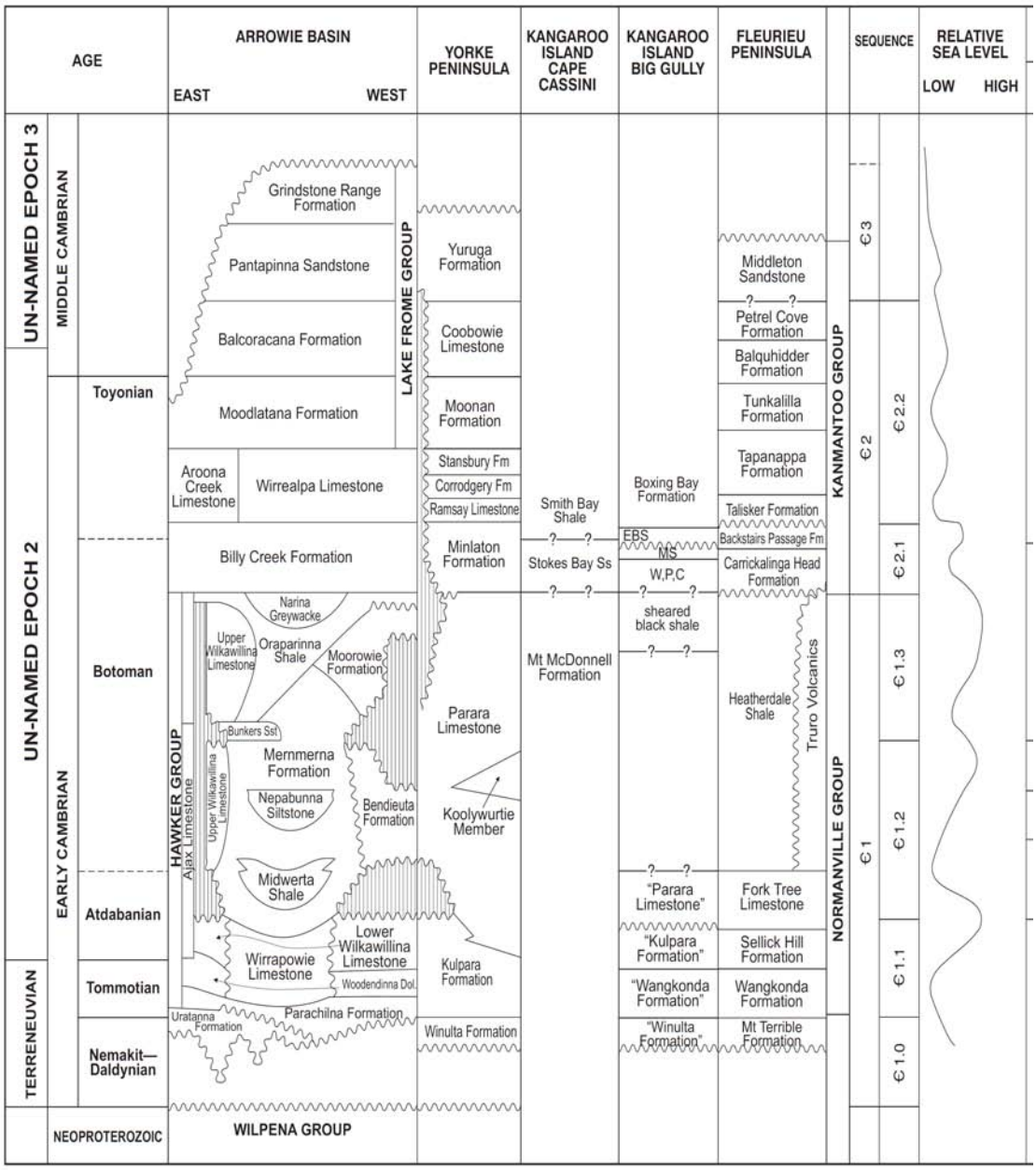

Fig.2. Stratigraphic chart of early to mid Cambrian sediments of the Adelaide Fold Belt, South Australia.

The Kanmantoo Trough is an isolated arcuate basin filled with 7–8 km of coarse and fine grained, almost entirely siliciclastic, sediments (the Kanmantoo Group: Fig. 2), the upper two-thirds of which have a distinctly different provenance to the Є1 sediments (Turner et al., 1993; Flöttmann et al., 1998; Haines et al., 1996, 2001, 2009; Preiss, 2000; Jago et al., 2003). North and west of the Kanmantoo Trough, probably coeval sediments of the Kangaroo Island Group accumulated along the tectonically active southern margin of the Gawler Craton (Gehling et al., 2011).

Cessation of sedimentation in the Stansbury Basin occurred following the deposition of the Є3 sequence set with the shift from an extensional (or transtensional) setting to contraction during the Delamerian Orogeny, culminating in significant uplift and up to 50% shortening of the Kanmantoo Group (Flöttmann et al., 1998; Preiss, 2000). Zircon geochronology of the syn-post kinematic igneous intrusions within the Delamerian Orogen, using both ^{207}Pb-^{206}Pb single zircon evaporation and U-Pb secondary ion mass spectrometry, suggest that contractional orogenesis commenced at 514 ± 5 Ma (Foden et al., 1999) and continued until at least 490 ± 3 Ma. It was terminated by rapid uplift, cooling and extension in association with post-tectonic magmatism (Foden et al., 2006). However, the timing of the onset of uplift and deformation associated with this event is controversial, Turner (2009) arguing that it may have begun some 40–25 million years earlier, synchronous with the Antarctic Ross Orogeny.

2.2.2. The Normanville Group

The Normanville Group, observed in section on the Fleurieu Peninsula and in the eastern Mount Lofty Ranges, comprises the basal Mount Terrible Formation, the Wangkonda Formation, the Sellick Hill Formation, the Fork Tree Limestone, and the Heatherdale Shale (Fig. 2). This succession has a clastic base and passes upward into shelf and marginal slope/ramp carbonates, overlain by deeper water siliciclastics of the Heatherdale Shale (Gravestock, 1995; Jago et al., 2002). The Heatherdale Shale is unconformably overlain by the Carrickalinga Head Formation of the Kanmantoo Group on the Fleurieu Peninsula. This unconformity represents a Type 1 sequence boundary, the erosional surface of which may be up to 300 m in relief (Carson 1994; Jago et al., 1994). The laterally equivalent section in the eastern Mount Lofty Ranges appears to show a conformable transition into the Kanmantoo Group (Gatehouse et al., 1993; Jago et al., 2003). The Heatherdale Shale comprises flat-laminated black calcareous shale and siltstone, in part pyritic and phosphatic (Carson, 1994; Turner, 1994; Gravestock, 1995). Zircon geochronological data show a wide range of detrital ages; both late Mesoproterozoic and older Proterozoic components are well represented, suggesting a westerly provenance (Ireland et al., 1998; Preiss, 2000). The presence of younger detrital grains (800–540 Ma) suggests a transition from the typical provenance of the underlying Neoproterozoic and lower Normanville Group units to that exhibited in the Kanmantoo Group (Ireland et al., 1998; Haines et al., 2009; Turner et al., 2009). Largely unmetamorphosed outcrops are confined to the west coast of the Fleurieu Peninsula (Sellick Hill to Carrickalinga Head: Fig. 1) whilst the lateral equivalents in the Karinya Syncline are metamorphosed to biotite grade (Mancktelow, 1990; Preiss, 1995). Carson (1994) has suggested that the Heatherdale Shale may be split into lower and upper units, reflecting the transition from ramp to

basinal facies at the end of a transgressive cycle. The upper facies is only observed in the southern sections at Sellick Hill as it either wasn't deposited, or has been eroded or faulted out in the other Fleurieu Peninsula outcrops. It is likely that the Mount Lofty section, which shows a conformable boundary to the overlying units, incorporates both this upper unit and some of the lower unit although the base is faulted out. Interbedded tuff horizons have been reported throughout the Heatherdale Shale; crystal tuffs and pillow lavas were described by Gatehouse et al. (1993) at Red Creek in the Karinya Syncline. These are usually associated with the eruptive phases of the Truro Volcanics (Jenkins and Hasenohr, 1989, Foden et al., 1990, Gravestock, 1995), though Gatehouse et al. (1993) suggest they may be a similar, but stratigraphically separate, suite in the Red Creek area. Jenkins et al. (2002) dated one such tuff from the upper section of Heatherdale Shale at Sellick Hill at 522 ± 2.1 Ma, recalculated from the 526 ± 4 Ma date of Cooper et al. (1992). Cambrian SHRIMP ages generally lack the precision of TIMS ages; they are not used by Shergold and Cooper (2004) and Ogg et al. (2008), and are discounted by the IUGS Cambrian Subcommission. Nevertheless, these Heatherdale dates are very precise and, moreover, consistent with the age constraints of the IUGS. Biostratigraphic evidence is limited within the Heatherdale Shale with rare trilobites, hyoliths sponges, brachiopods, molluscs and trace fossils (Jago et al., 1984, Jenkins and Hasenohr, 1989, Jago et al., 2003; Jago et al., 2006). The only reliable biostratigraphic age in the Sellick Hill succession is that of the Fork Tree Limestone from which Debrenne and Gravestock (1990) described late Atdabanian to Botoman archaeocyatha. This suggests that the Heatherdale Shale has a Botoman age.

2.2.3. The Kangaroo Island Group

The Kangaroo Island Group, on the north coast of Kangaroo Island, includes the Emu Bay Shale, host to the most important Burgess Shale-type fossil assemblage (or Lagerstätte) in Australia. Gehling et al. (2011) gave a detailed review of the geology of these and adjacent stratigraphic units (Fig. 2) that form part of an essentially unmetamorphosed Cambrian platform succession north of the Kangaroo Island shear zone (Flöttmann et al., 1997). Syndepositional faulting and features such as folding and slumping within the Kangaroo Island Group suggest that it was deposited in a series of localised, deep-water sub-basins in an area of tectonic activity, sourced locally from the Yorke Peninsula (Nedin, 1995; Flöttmann et al., 1998; Gehling et al., 2011) and possibly displaced northwards by thrusting (Flöttmann et al., 1995). The Emu Bay Shale unconformably overlies the Marsden Sandstone, their contact forming a major sequence boundary. The Lagerstätte occurs within a basal dark grey to black laminated micaceous mudstone facies, in places pyritic, deposited below the wave base (Paterson et al., 2008). The Emu Bay Shale crops out east of the mouth of Big Gully, Kangaroo Island where it is about 78 m thick (Daily et al., 1979). A new fossil excavation site located inland at Buck Quarry has revealed a far more diverse Emu Bay fauna (Paterson et al., 2009). The mudstone beds that contain the lagerstätte thin southwards and disappear 500–600 m south of the coast. The formation coarsens upwards and in coastal sections is conformably overlain by the sandstone facies of the Boxing Bay Formation. Correlation of the Kangaroo Island Group with Cambrian sequences on the Yorke and Fleurieu Peninsulas is tenuous, as little evidence exists to tie its formations to those on the mainland. However, tentative correlations with the

Minlaton Formation on Yorke Peninsula and the Billy Creek Formation of the Flinders Ranges have recently been proposed (Gehling et al., 2011; Jago et al., 2012).

2.2.4. The Kanmantoo Group

The Kanmantoo Group was deposited within a tectonically active zone of the southern Stansbury Basin. Originally described in its type section on the south coast of the Fleurieu Peninsula as an essentially non-faulted homoclinal structure with conformable successions (Daily and Milnes, 1971, 1973), the structural complexity of the section has subsequently been recognised (Gravestock and Gatehouse, 1995; Haines et al., 1996; Jago et al., 2003 and references therein). Jago et al. (2003) subdivided the Kanmantoo Group into the Keynes and Bollaparudda Subgroups, representing the Є2 and Є3 transgressive to highstand sequence sets, and revised the existing nomenclature of the sequence sets to that which is followed in this paper (Fig. 2). The Kanmantoo Group comprises predominantly fine to medium grained siliciclastic rocks (Haines et al., 2001) that have all undergone metamorphism, ranging from chlorite grade at Carrickalinga Head to upper amphibolite grade on the south coast of Kangaroo Island and in the eastern Mount Lofty Ranges (Jago et al., 2003), though the metasediments are herein referred as their unmetamorphosed precursors. The Karinya Shale of Thomson (1969), the equivalent of the Talisker Formation calc-siltstones of the southern Fleurieu Peninsula, was incorporated into the Talisker Formation of Jago et al. (2003). It comprises a calcareous basal unit of interbedded carbonate and siltstone overlain by fining-upward shale beds and is interpreted as a transgressive sequence (Turner, 1994). The Kanmantoo Group was deposited in predominantly deep-water settings, but thick shallow-water formations occur in the upper sections of both subgroups (Preiss, 2000; Haines et al., 2001; Jago

et al., 2003, Jago and Gatehouse, 2009). Deposition of the estimated 7–8 km thickness of the Kanmantoo Group has been constrained to as little as 8 million years (Foden et al., 1999; Jenkins et al., 2002). Preiss (2000) and Haines et al. (2001, 2009) note a south to north proximal to distal trend within all facies, suggesting the source to be a delta-fan complex of high-load-capacity rivers situated at the southern margin of the basin, perhaps a westerly extension of the Kanmantoo Trough in the tectonic zone along which Australia and Antarctica later separated. This could explain the high rate of deposition, ≥150cm/Kyr , and is supported by palaeocurrent measurements in turbiditic facies indicating flow from the south or southwest (Flöttmann et al., 1998; Haines et al., 2001). Jago and Gatehouse (2009) report opposite current directions in shallower water facies, invoking tidal redistribution as the cause of the variation. Detrital zircon studies indicate a distinct change in the provenance of the Kanmantoo Group sediments from those of the underlying Neoproterozoic rocks and the early Cambrian Normanville Group, with contributions from 0.7–0.5 Ga (dominant) and 1.2–1.0 Ga (secondary) sources being observed (Ireland, 1998; Suto, 2011). These source ages are common for Palaeozoic sedimentary rocks throughout much of Gondwana (Squire et al., 2006; Veevers et al., 2008; Haines et al., 2009; Myrow et al., 2010). This observation has led to an extraordinary interpretation of a ‘Gondwana Super-fan System’ that covered much of eastern Gondwana and was sourced from a huge mountain range at the site of the East African Orogen (Squire et al., 2006). However, the south-to-north palaeocurrent directions and presence of potential source rocks of the required ages in the Prydz-Leeuwin Belt (Collins, 2003) and exposed or thinly covered parts of eastern Antarctica (Kelsey et al., 2008; Veevers et al., 2008) suggest that a more proximal part of Antarctica is a more likely source area for these sediments (Haines et al., 2009; Suto, 2011).

2.3. Methodology

2.3.1. Sample sets

This study is based on a suite of 104 samples of the Heatherdale Shale, Emu Bay Shale and Talisker Formation assembled from various localities in the Stansbury Basin, South Australia: Carrickalinga Head and Sellicks Hill on the southern Fleurieu Peninsula; Emu Bay, northeastern Kangaroo Island; and the Karinya Syncline in the northeastern Mt Lofty Ranges (Fig.1, Table 1).

Specimens of the Heatherdale Shale and Talisker Formation were gathered in the field from eight sites on the Fleurieu Peninsula and in Mt Lofty Ranges. Additional samples of the Talisker Formation were taken from the cuttings recovered by drill holes Frankton-l (34° 18' N, 139° 11.1'E) and Frankton-2 (34° 18' N, 139° II.7'E). All were collected as part of two BSc Honours research projects (Carson, 1994; Turner 1994). Portion of each outcrop sample was reduced to gravel size with a hammer and steel plate, care being taken to avoid weathered surfaces and contact of the chips with extraneous material. The crushed samples were then ground to a very fine powder using a Seibtechnik chrome-steel mill and the resultant powders were stored in glass jars.

Outcrop samples of the Emu Bay Shale were collected during 2009 from two sites at Big Gully, Kangaroo Island. Representative portions (5 g) were removed from freshly exposed interior surfaces of ~2 kg-sized specimens. These were then crushed using a pre-cleaned mortar and pestle and the resultant powders stored in glass jars in preparation for analysis.

Table 1 Shale units and locations sampled for this study

Location	Formation	n
Fleurieu Peninsula		
Carrickalinga Head Creek	Heatherdale Shale (lower)	9
Carrickalinga Head Cove	Heatherdale Shale (lower)	13
Myponga Beach	Heatherdale Shale (lower)	1
Sellick Hill	Heatherdale Shale (upper)	19
	Total	42
Mt Lofty Ranges		
Red Creek, north fork	Heatherdale Shale	7
Red Creek, south fork	Heatherdale Shale	11
Sedan Hill Quarry	Heatherdale Shale	3
	Total	21
The Gap	Talisker (Karinya Shale)	9
Frankton-1 drill hole	Talisker (Karinya Shale)	10
Frankton-2 drill hole	Talisker (Karinya Shale)	10
	Total	29
Kangaroo Island		
Big Gully, shoreline	Emu Bay Shale	10
Big Gully, Buck Quarry	Emu Bay Shale	2
	Total	12

2.3.2. Analytical techniques

Unless otherwise indicated, all analyses were carried out in the Mawson Laboratories of the School of Earth and Environmental Sciences, University of Adelaide.

2.3.2.1 Trace and rare earth element determination

Aliquots of powdered shale (~15 mg) were weighed into Teflon beakers and digested in a mixture of concentrated HCl, HNO_3 and HF, according to an established in-house protocol. Following digestion and evaporation to dryness, the samples were treated with 1% ultrapure H_2O_2 to remove organic residues, dried, and then redissolved in 1 mL 6M HCl. From this solution, 100 µl was then transferred to 5 ml Teflon autosampler vials, dried and redissolved in 1.5 ml of 2% HNO_3 for elemental analysis. A total of 44 trace elements (including rare earth elements) were measured on an Agilent 7500cx solution ICP-MS at Adelaide Microscopy (University of Adelaide). Calibration was achieved using a suite of 10 ppb to 500 ppb standard reference solutions (Choice Analytical) with a co-aspirated solution of 200 ppb indium mixed online via a T-junction to correct for instrument drift and matrix effects.

2.3.2.2 Organic carbon isotope ratio determination

Two procedures were used to acquire $\delta^{13}C_{org}$ data. Powdered aliquots (~0.2 g) from the Mt Lofty Ranges and Kangaroo Island sample sets were digested three times in 10% HCl to remove carbonate, then rinsed in deionised water and dried. The residues were transferred to pre-cleaned 6 x 4 mm tin capsules for combustion in a Carlo Erba EA1500 Series II elemental analyser and the produced CO_2 analysed in continuous flow mode on a tandem Fisons Optima IRMS. The acquired raw data were calibrated against glycine and glutamic acid in-house standards ($\delta^{13}C_{V\text{-}PDB}$ = –31.2‰, –17.1‰,

respectively). Precision and accuracy were monitored by regular analyses of an in-house sucrose standard (–25.8‰), with all in-house standards calibrated against the Certified Reference Material NBS-19. Over the course of the analyses, the reproducibility (1σ) was ±0.2‰. The resulting $\delta^{13}C_{org}$ measurements are reported relative to the V-PDB standard.

Powered samples (~5g) of Heatherdale Shale from the Fleurieu Peninsula were submitted to GHGeochem Ltd, Wirral, UK. Serial acid digestion in HCl and HF yielded kerogen concentrates that were then combusted in sealed quartz tubes, following the method of Sofer (1980). The produced CO_2 was then purified cryogenically before being transferred to a SIRA 10 dual inlet mass spectrometer. All values are reported against V-PDB, with the primary laboratory standard being Certified Reference Material NBS-22 ($\delta^{13}C_{org}$ = –30.0‰).

2.3.2.3 Sulfur isotope ratio determination

Powdered samples (~0.2g) from the Mt Lofty Ranges and Fleurieu Peninsula sample in which pyrite was described (Carson, 1994; Turner, 1994) were weighed into pre-cleaned 6 x 4 mm tin capsules for combustion in a Carlo Erba EA1500 series II elemental analyser. The resulting SO_2 was analysed in continuous flow mode on a tandem Fisons Optima IRMS against an in-house reference gas with an isotopic composition of 0‰ $_{VCDT}$. Sample data were calibrated against IAEA S1, S2 & S3 silver sulphide standards ($\delta^{34}S$ = –0.30‰, +22.7‰ and –32.3‰, respectively) and precision and accuracy monitored by regular analyses of in-house barium sulphate standards (+31.2‰ and +22.9‰, respectively). Over the course of the analyses, the reproducibility (1σ) was ±1‰. The resulting $\delta^{34}S_{py}$ measurements are reported relative to the VCDT standard.

2.3.2.4 Total organic carbon

Whole-rock samples (~2 g) were submitted to Amdel Limited, Thebarton, South Australia, for determination of TOC on a Leco Carbon/Sulfur Analyser.

2.3.3 Calculation of REE distributions and anomalies

REE+Y distributions and individual element anomalies were calculated using the protocol of Guo et al. (2007), as follows:

LREE = Σ La;Ce;Pr;Nd;Sm;Eu

HREE = Σ Gd;Tb;Dy;Ho;Er;Tm;Yb;Lu;Y

For calculation of anomalies, the concentration of each element was normalised to the REE chondrite concentrations of Taylor and McLennan (1985) (see Table 3) prior to use in the equations:

$Eu/Eu^* = Eu_{PAAS} / (½Sm_{PAAS} + ½Gd_{PAAS})$

$Ce/Ce^* = Eu_{PAAS} / (½La_{PAAS} + ½Pr_{PAAS})$

$Y/Y^* = Y_{PAAS} / (½Dy_{PAAS} + ½Ho_{PAAS})$

$Pr/Pr^* = Eu_{PAAS} / (½Ce_{PAAS} + ½Nd_{PAAS})$

2.4. Results

Analytical results for TOC, $\delta^{13}C_{org}$, $\delta^{34}{}_{Spy}$, selected trace and REE concentrations and associated proxies are presented in Tables 2 and 3. Where concentrations have been normalised, the Post-Archean Australian Shale (PAAS) and REE chondrite data of Taylor and McLennan (1985) have been used. A full data set is available in an on-line appendix.

The TOC content of the Heatherdale and Talisker shales exhibits significant stratigraphic variation (0.2–2.6%), whereas that of the basal Emu Bay Shale is uniformly low (0.25–0.55%). The Heatherdale Shale on the Fleurieu Peninsula and the Emu Bay Shale have relatively consistent $\delta^{13}C_{org}$ signatures (average –31.2 and –30.0‰, respectively). Further north, in the Karinya Syncline, both the Heatherdale Shale and the Talisker Formation this signature is highly variable, ranging from –26.4 to –10.0‰. Only a limited number of $\delta^{34}S_{py}$ measurements were obtained (n = 22) due to generally low pyrite contents. Most of these are from the Talisker Formation at Frankton-1 and 2 where $\delta^{34}S_{py}$ = –11.5 to +9.9‰.

The Heatherdale Shale (n = 63) displays general PAAS normalised enrichment of Mo>U>V>Pb and depletion of Zn>Th>Co>Sc>Ni>Co. The Emu Bay Shale (n = 12) is enriched in Zn>Pb>Th>U>Mo>Cu and depleted in Sc>V>Ni>Co, while the Talisker Formation (n = 29) is enriched in Mo>Pb>V>Zn>U>Th and depleted in Cu>Sc>Ni>Co.

All three formations typically exhibit LREE enrichment and HREE and yttrium depletion with respect to PAAS. Notable exceptions are the lower Heatherdale Shale at Carrickalinga Head and samples from The Gap (n = 9) and Sedan Hill Quarry (n = 3)

(Fig. 1), where all elements are depleted. Across the data set significant anomalies are evident in chondrite/PAAS normalised Eu/Eu^*_{PAAS} and Y/Y^*_{PAAS} distributions (±0.80 and ±0.56, respectively), while Ce/Ce^*_{PAAS} & Pr/Pr^*_{PAAS} exhibit less variation (±0.21 and ±0.13, respectively).

The Heatherdale Shale at Sedan Hill Quarry and the Talisker Formation at The Gap, both structurally complex sections (Turner, 1994), yield anomalous results. Severe Co depletion (normalised average = 0.02) and significant Ni depletion (normalised averages = 0.26 and 0.28) are observed at both sites, along with Zn depletion (normalised average = 0.21) at The Gap. Considerable enrichment of Zn and Pb in the basal metre of the Emu Bay Shale is evident (Zn = 3.3% and Pb = 0.5% at 0.1 m) though general enrichment for both elements is shown over the whole section (average = 3.34 and 1.61%, respectively, excluding basal metre).

Table 2 TOC, $\delta^{13}C_{org}$, $\delta^{34}S_{pyr}$ and trace element concentrations and proxies for the Heatherdale Shale, Talisker Formation and Emu Bay Shale.

Sample	Formation	Height (m)	TOC (%)	$\delta^{13}C_{org}$ (‰)	$\delta^{34}S_{py}$ (‰)	Sc (ppm)	V (ppm)	Co (ppm)	Ni (ppm)	Cu (ppm)	Zn (ppm)	Mo (ppm)	Pb (ppm)	Th (ppm)	U (ppm)	V/Sc	Ni/Co	U/Th	Th/U	V/(V+Ni)
Carrickalinga Head Creek																				
C3	HS (lower)	1	1.66	-31.0		8.38	250	5.47	24.4	26.8	71.3	6.66	17.5	9.79	6.22	29.9	4.47	0.64	1.57	0.91
C5	HS (lower)	5	0.63	-30.9		6.57	109	2.90	13.5	22.4	75.9	6.04	21.0	8.24	7.39	16.6	4.66	0.90	1.11	0.89
C6	HS (lower)	9.5	0.55	-31.3		2.82	55.1	2.73	4.57	9.35	48.0	2.39	11.6	3.08	4.45	19.5	1.67	1.45	0.69	0.92
C7	HS (lower)	10	0.77	-31.2		15.2	120	3.66	19.1	54.5	66.7	1.90	24.0	21.4	6.93	7.87	5.23	0.32	3.09	0.86
C8	HS (lower)	10.5	0.55	-32.0		2.69	56.8	2.89	4.21	8.80	38.1	2.42	14.8	3.02	4.49	21.1	1.46	1.49	0.67	0.93
C9	HS (lower)	12	0.77	-31.7		3.11	65.4	2.76	5.75	10.7	39.0	3.73	11.1	3.72	5.10	21.0	2.08	1.37	0.73	0.92
C10	HS (lower)	13.5	0.47	-31.7		2.92	52.5	2.28	3.50	7.64	33.8	1.02	8.7	3.35	3.04	18.0	1.53	0.91	1.10	0.94
C10A	HS (lower)	13.5	0.52	-31.4		8.06	220	6.50	25.5	29.2	80.7	7.50	23.2	9.58	7.63	27.3	3.92	0.80	1.26	0.90
C11	HS (lower)	17	0.40	-31.8		2.49	34.7	3.02	4.21	10.8	57.2	3.25	12.7	3.09	3.57	13.9	1.39	1.16	0.86	0.89
Carrickalinga Head Cove																				
C15	HS (lower)	59.5	0.46	-32.7		3.24	45.8	2.71	6.75	14.2	93.7	0.64	6.50	3.99	2.59	14.1	2.49	0.65	1.54	0.87
C16	HS (lower)	59	1.07	-29.3		9.51	143	12.4	44.9	29.2	344	2.72	18.3	12.6	4.21	15.0	3.62	0.33	2.99	0.76
C17	HS (lower)	57.5	1.75	-27.3		12.0	324	6.86	30.7	55.8	80.8	4.10	18.8	15.7	5.89	26.9	4.47	0.37	2.67	0.91
C18A	HS (lower)	57	1.16	-31.6		8.71	107	5.64	19.1	43.1	63.1	1.70	12.0	12.4	3.83	12.3	3.39	0.31	3.23	0.85
C18C	HS (lower)	57	0.56	-32.4		3.75	42.0	3.17	6.55	41.6	31.1	1.78	10.8	3.65	5.01	11.2	2.07	1.37	0.73	0.87
C19A	HS (lower)	55	0.72	-32.0	10.1	4.21	65.3	2.38	4.30	10.5	53.8	4.20	9.33	4.48	20.3	15.5	1.81	4.52	0.22	0.94
C19B	HS (lower)	55	2.14	-32.3		10.7	697	6.88	44.6	54.1	105	15.9	26.7	14.1	8.29	65.2	6.49	0.59	1.70	0.94
C20	HS (lower)	50	0.25	-32.4		3.42	43.3	1.56	3.37	13.1	48.1	0.41	9.88	3.72	2.98	12.7	2.17	0.80	1.25	0.93
C23	HS (lower)	41	0.24	-31.3		3.23	50.0	5.56	11.2	7.50	84.6	1.22	11.3	2.96	3.26	15.5	2.02	1.10	0.91	0.82
C27	HS (lower)	25	1.05	-30.9		6.95	77.5	2.45	10.0	11.6	40.7	2.11	10.6	8.51	5.21	11.1	4.11	0.61	1.63	0.89
C28	HS (lower)	24	0.19	-29.6		3.24	22.2	1.69		9.07	55.1	1.72	10.7	3.71	1.72	6.86	0.00	0.46	2.16	1.00
C29	HS (lower)	22	1.16	-30.4		9.01	68.8	4.30	15.4	16.3	51.1	1.82	12.8	10.4	3.39	7.64	3.57	0.33	3.06	0.82
C31	HS (lower)	9	0.21	-30.5		3.25	18.6	2.39		12.8	15.4	0.06	4.96	3.26	1.41	5.73	0.00	0.43	2.32	1.00
Myponga Beach																				
M3	HS (lower)		0.37	-30.5		12.8	159	4.11	24.2	50.5	74.1	1.89	21.9	15.6	6.41	12.5	5.89	0.41	2.44	0.87
Sellick Hill				-31.7		8.14	280	3.98	27.7	31.6	97.5	3.47	21.5	11.8	5.94	34.4	6.97	0.50	1.99	0.91
S12	HS (upper)		0.83	-31.2		13.4	176	4.38	32.3	66.9	105	2.47	23.7	17.5	6.11	13.1	7.37	0.35	2.86	0.85
S13	HS (upper)		1.09	-31.0	7.79	11.2	304	7.90	21.8	46.7	79.7	5.04	19.8	14.0	5.86	27.2	2.76	0.42	2.38	0.93
S14	HS (upper)		0.73	-31.0	11.2	12.9	209	8.94	32.6	60.3	120	4.00	21.5	15.8	6.72	16.2	3.65	0.42	2.36	0.86
S17	HS (upper)	3	1.62	-31.2	-2.68	12.8	1034	13.9	70.8	125	127	24.4	43.4	15.9	10.6	80.7	5.08	0.66	1.50	0.94
S18	HS (upper)	3.5	1.60	-30.9	-3.00	12.2	144	6.43	11.7	50.4	119	44.3	76.1	16.8	12.1	11.8	1.82	0.72	1.39	0.92
S20	HS (upper)	5.5	1.85	-30.9		15.2	828	4.34	19.0	28.5	105	15.6	39.1	20.5	9.34	54.3	4.36	0.45	2.20	0.98
S21	HS (upper)	7	2.03	-31.2		12.4	728	3.80	28.2	65.4	120	16.6	31.3	16.9	8.11	58.8	7.43	0.48	2.09	0.96
S22	HS (upper)	8	1.99	-31.4		14.6	705	4.03	25.8	38.8	98.9	15.8	38.2	19.8	8.03	48.3	6.41	0.41	2.47	0.96
S23	HS (upper)	10.5	2.03	-31.3		13.7	880	3.81	27.3	47.5	103	18.9	37.6	18.3	11.0	64.1	7.18	0.60	1.66	0.97
S24	HS (upper)	12.5	2.22	-30.8		14.1	280	2.19	12.2	44.3	63.9	3.53	24.8	17.7	6.41	19.9	5.56	0.36	2.76	0.96
S25	HS (upper)	16	1.94	-31.3		15.3	284	4.63	17.7	55.7	74.8	20.0	48.9	20.9	11.5	18.5	3.81	0.55	1.82	0.94
S27	HS (upper)	22	1.57	-31.2	6.36	14.6	352	8.79	24.3	60.8	74.0	19.8	47.4	18.7	14.0	24.2	2.77	0.75	1.34	0.94
S28	HS (upper)	25.5	2.28	-31.1		8.46	79.7	9.07	30.2	47.5	84.1	1.96	13.5	11.5	3.52	9.42	3.33	0.30	3.28	0.73
S30	HS (upper)	27.5	2.57	-31.1		14.5	493	4.53	19.6	50.6	92.7	12.8	43.9	19.5	11.1	34.1	4.34	0.57	1.76	0.96
S32	HS (upper)	30	0.91	-31.5		14.5	476	6.43	28.9	37.2	81.6	11.4	38.8	18.5	7.63	32.7	4.50	0.41	2.43	0.94
S33	HS (upper)	41	2.11	-31.7		5.25	254	5.16	13.4	17.2	64.4	5.46	18.8	6.32	5.81	48.5	2.61	0.92	1.09	0.95
S35	HS (upper)	44.5	2.05	-31.2		15.7	424	1.13	4.04	48.3	40.6	5.17	33.1	19.5	8.74	27.0	3.59	0.45	2.23	0.99
S37	HS (upper)	48.5	1.18	-30.5		12.8	159	4.11	24.2	50.5	74.1	1.89	21.9	15.6	6.41	12.5	5.89	0.41	2.44	0.87
S39	HS (upper)	55.5	2.33	-31.7		8.14	280	3.98	27.7	31.6	97.5	3.47	21.5	11.8	5.94	34.4	6.97	0.50	1.99	0.91
Red Creek, north fork																				
N22	HS	84	0.65	-13.0		9.10	84.8	4.42	24.5	32.7	39.9	2.03	15.0	12.0	3.54	9.31	5.54	0.29	3.39	0.78
N28	HS	125	0.81	-16.6		12.6	200	4.72	22.5	47.0	41.0	5.56	14.0	14.2	3.58	15.9	4.78	0.25	3.95	0.90
N44	HS	268	0.44	-15.9		13.7	120	4.73	22.5	21.6	102	1.18	12.8	14.1	2.63	8.75	4.76	0.19	5.36	0.84
N46	HS	272	0.73	-15.4		18.8	185	11.7	33.9	44.9	93.7	2.19	13.5	20.3	3.66	9.81	2.91	0.18	5.54	0.84
N47	HS	274	0.69	-16.0		20.0	179	9.01	29.0	51.1	108	0.85	40.4	18.1	3.97	8.97	3.22	0.22	4.56	0.86
N48	HS	278	0.57	-15.9		10.9	141	10.8	50.8	36.8	122	1.36	18.8	5.58	2.75	12.9	4.69	0.49	2.03	0.73
N49	HS	284	0.82	-15.9		14.0	158	10.2	35.2	49.6	58.0	3.31	12.2	15.9	4.07	11.2	3.47	0.26	3.91	0.82
Red Creek, south fork																				
S5	HS	125	0.55	-11.1		9.54	166	21.6	35.5	72.8	20.0	6.61	8.02	9.94	5.86	17.36	1.64	0.59	1.70	0.82
S16	HS	165	0.74	-12.2		9.64	204	11.8	36.0	62.9	117	5.21	16.8	6.62	3.41	21.13	3.04	0.52	1.94	0.85
S17	HS	172	0.59	-11.2		11.9	114	6.27	17.8	31.5	39.5	1.68	7.56	11.9	2.77	9.53	2.84	0.23	4.29	0.86
S23	HS	208	0.42	-11.0		12.1	102	13.4	40.9	39.6	23.8	1.49	4.35	11.1	2.52	8.40	3.05	0.23	4.42	0.71
S26	HS	232	1.12	-14.9		13.5	368	15.3	66.3	110	49.1	14.6	11.6	14.5	7.60	27.26	4.34	0.52	1.91	0.85
S30	HS	250	0.23	-11.5		23.3	169	27.2	56.7	17.6	141	0.25	24.9	21.0	3.53	7.27	2.09	0.17	5.94	0.75
S31	HS	256	0.21	-15.5		23.7	180	18.2	57.3	26.0	125	0.24	18.0	20.7	3.04	7.59	3.15	0.15	6.79	0.76
S32	HS	258	0.25	-19.5		23.9	189	13.2	40.2	1.48	74.1	0.22	7.91	20.8	3.29	7.91	3.06	0.16	6.32	0.82
S37	HS	288	0.57	-10.0		15.1	110	11.1	21.7	23.9	101	0.46	13.8	20.3	5.27	7.32	1.95	0.26	3.86	0.84
S38	HS	295	1.06	-11.9		15.0	182	11.5	62.0	67.2	63.2	5.03	11.8	18.0	6.13	12.2	5.40	0.34	2.94	0.75
S39	HS	297	0.32	-15.0		22.4	173	24.6	48.7	39.3	114	0.26	7.27	21.0	3.95	7.71	1.98	0.19	5.32	0.78
Sedan Hill Quarry																				
SQ2	HS		1.56	-19.0		16.6	669	0.48	13.2	23.3	52.4	11.2	4.51	13.3	3.78	40.2	27.6	0.29	3.51	0.98
SQ3	HS		1.24	-18.5		15.0	531	0.47	11.9	23.1	42.7	13.1	22.6	12.4	5.68	35.3	25.3	0.46	2.18	0.98
SQ5	HS		0.92	-18.8		13.5	222	1.13	18.6	38.5	47.1	14.6	31.0	12.4	9.52	16.4	16.5	0.77	1.30	0.92
The Gap																				
K1	T		1.06	-24.7		15.6	365	0.31	4.30	12.0	16.0	9.68	82.1	11.4	3.17	23.3	13.8	0.28	3.59	0.99
K2	T		0.79	-24.3		17.3	395	0.60	17.7	49.0	19.9	19.5	154	20.2	2.91	22.9	29.5	0.14	6.94	0.96
K3	T		0.9	-24.5		19.7	456	0.58	6.56	29.8	14.3	42.5	186	17.9	3.84	23.1	11.3	0.22	4.65	0.99
K4	T		1.28	-14.8		16.8	389	0.53	23.1	18.8	31.1	29.3	160	14.0	4.55	23.1	43.8	0.33	3.07	0.94
K5	T		1.18	-24.6		13.8	419	0.55	18.6	18.2	45.3	17.4	181	16.4	4.58	30.4	33.5	0.28	3.58	0.96
K6	T		1.24	-24.5		13.9	289	0.32	14.5	8.52	20.8	6.76	170	12.5	6.49	20.8	44.9	0.52	1.93	0.95
K7	T		1.44	-26.4		16.8	397	0.77	6.43	134	21.9	41.6	56.0	16.3	3.22	23.6	8.31	0.20	5.05	0.98
K8	T		1.04	-24.7		13.5	489	0.28	2.60	9.95	18.1	9.61	67.1	11.4	2.80	36.2	9.37	0.25	4.07	0.99
K9	T		1.18	-24.2		15.3	435	0.34	8.14	18.1	29.7	18.8	90.6	13.3	1.80	28.4	24.2	0.14	7.40	0.98
Frankton-1 drill hole																				
F1 (1)	T	125	1.9	-21.4	-9.56	14.9	358	21.0	87.3	64.8	175	32.7	99.5	18.3	7.98	24.1	4.15	0.44	2.29	0.80
F1 (2)	T	121	1.28	-19.2	-11.0	15.2	180	30.5	87.5	73.7	181	14.0	82.4	24.3	4.22	11.9	2.87	0.17	5.75	0.67
F1 (3)	T	118	0.92	-17.1	-11.0	14.3	240	43.1	83.1	39.1	522	18.4	41.3	16.0	4.52	16.8	1.93	0.28	3.55	0.74
F1 (4)	T	85	1.09	-15.2	-11.5	14.6	486	19.5	83.9	56.7	242	10.3	15.1	20.0	7.19	33.3	4.31	0.36	2.78	0.85
F1 (5)	T	80	0.93	-13.7	-7.26	15.3	270	32.0	60.4	76.4	131	14.7	63.9	19.8	6.69	17.7	1.89	0.34	2.95	0.82
F1 (6)	T	75	0.96	-14.3	-7.83	11.9	217	27.4	52.4	29.7	38.6	20.6	28.7	13.5	7.70	18.2	1.91	0.57	1.75	0.81
F1 (7)	T	68	1.15	-14.6	-8.97	14.7	140	26.3	42.8	45.5	165	7.96	63.6	20.1	7.35	9.49	1.63	0.37	2.74	0.77
F1 (8)	T	60	0.94	-12.8		4.43	97.6	23.2	58.5	94.3	112	3.14	32.0	3.39	9.49	22.0	2.53	2.80	0.36	0.63
F1 (9)	T	16	0.36	-16.5		8.64	85.7	13.1	35.5	2.26	72.7	0.99	13.3	11.5	3.45	9.92	2.71	0.30	3.34	0.71
F1 (10)	T	5	0.41	-18.5		12.3	108	17.9	48.8	6.25	113	1.06	22.2	17.9	4.26	8.79	2.73	0.24	4.19	0.69
Frankton-2 drill hole																				
F2 (1)	T	103	1.39	-23.1	-2.18	13.3	460	39.0	85.0	87.8	94.2	14.2	80.2	16.7	4.74	34.6	2.18	0.28	3.52	0.84
F2 (2)	T	96	1.33	-23.3	-0.98	14.7	490	42.4	98.9	116	140	19.2	55.6	21.5	5.98	33.4	2.33	0.28	3.60	0.83
F2 (3)	T	85	1.24	-19.4	-2.22	15.0	272	22.6	65.0	48.5	78.2	8.41	33.3	19.9	4.99	18.1	2.87	0.25	3.99	0.81
F2 (4)	T	78	1.12	-15.9	2.02	13.3	218	21.0	40.9	37.2	71.3	4.30	34.8	15.2	3.53	16.3	1.95	0.23	4.30	0.84
F2 (5)	T	75	1.18	-16.3	1.33	15.8	182	27.7	50.9	53.8	95.7	13.9	42.0	18.8	4.95	11.5	1.84	0.26	3.81	0.78
F2 (6)	T	72	0.93	-15.9	1.57	14.9	129	19.6	44.5	56.4	113	1.19	20.9	17.3	4.14	8.66	2.27	0.24	4.18	0.74
F2 (7)	T	52	1.36	-16.3	8.41	10.6	148	26.3	41.9	40.8	340	5.59	91.0	10.1	4.95	13.9	1.59	0.49	2.03	0.78
F2 (8)	T	45	1.03	-17.1	0.26	12.5	202	26.1	52.4	46.6	517	14.6	96.1	13.3	4.71	16.2	2.01	0.35	2.83	0.79
F2 (9)	T	42	1.11	-16.6	9.79	8.44	205	15.1	38.1	47.6	739	8.96	87.5	7.94	4.60	24.3	2.52	0.58	1.72	0.84
F2 (10)	T	32	1.03	-16.0		11.3	148	12.3	35.0	34.7	439	1.26	51.6	11.9	3.62	13.2	2.84	0.31	3.27	0.81
Big Gully, shoreline																				
EB09S0.1	EBS	0.1	0.35	-29.2		17.6	142	11.6	29.7	79.9	32927	2.27	4973	21.1	4.51	8.06	2.56	0.21	4.68	0.83
EB09S0.9	EBS	0.9	0.30	-30.7		15.8	105	10.0	31.5	40.6	2225	0.41	366	19.0	3.31	6.64	3.14	0.17	5.74	0.77
EB09S2.8	EBS	2.8	0.25	-29.7		17.1	119	14.0	33.9	42.5	740	3.17	36.3	20.5	4.10	6.92	2.42	0.20	5.01	0.78
EB09S4	EBS	4	0.30	-27.8		13.7	60.6	10.3	23.6	33.9	60.1	0.58	35.5	16.8	3.50	6.64	2.28	0.21	4.80	0.79
EB09S5	EBS	5	0.50	-29.8		14.9	99.5	10.9	28.3	38.6	112	0.45	36.4	17.8	3.49	6.69	2.59	0.20	5.09	0.78
EB09S6	EBS	6	0.45	-29.8		15.6	111	13.2	32.9	54.1	110	0.90	38.9	19.0	3.89	7.09	2.49	0.20	4.90	0.77
EB09S7	EBS	7	0.40	-30.2		17.7	119	13.1	37.9	54.5	111	2.06	21.2	19.7	3.95	6.76	2.89	0.20	4.99	0.76
EB09S7.1	EBS	7.1	0.35	-28.3		9.65	109	8.51	16.7	31.5	115	0.18		11.3	2.45	11.3	1.97	0.22	4.60	0.87
EB09S7.6	EBS	7.6	0.30	-29.9		16.5	109	17.1	37.3	34.3	72.5	0.58	36.4	17.4	3.94	6.56	2.18	0.23	4.41	0.74
EB09S	EBS		0.30	-30.3		15.7	113	10.4	33.7	74.6	78.4	0.29	38.1	17.4	3.79	7.19	3.25	0.22	4.58	0.77
Big Gully, Buck Quarry																				
EBQ1	EBS	5-6	0.45	-31.8		16.2	133	9.53	32.3	81.9	868	1.35	26.2	17.4	3.02	8.22	3.39	0.17	5.78	0.81
EBQ2	EBS	5-6	0.55	-31.8		15.3	114	10.5	30.7	75.2	569	0.62	21.5	16.8	2.63	7.43	2.94	0.16	6.38	0.79
PAAS						16	150	23	55	50	85	1	20	15	3	9.38	2.39	0.20	5.00	0.73
Average $_{PAAS}$	T					0.86	1.90	0.77	0.81	0.93	1.86	14.2	3.80	1.04	1.64					
Average $_{PAAS}$	HS					0.70	1.62	0.31	0.46	0.75	0.95	6.38	1.02	0.85	1.96					
Average $_{PAAS}$	EBS					0.97	0.76	0.50	0.56	1.07	37.2	1.07	25.6	1.19	1.18					

T = Talisker Formation; HS = Heatherdale Shale; EBS = Emu Bay Shale
Height datum = base of formation PAAS = Post-Archean Australian shale, Taylor & McLennan (1985)

Table 3 Rare earth element concentrations and proxies for the Heatherdale Shale, Talisker Formation and Emu Bay Shale.

Sample	Formation	La (ppm)	Ce (ppm)	Pr (ppm)	Nd (ppm)	Sm (ppm)	Eu (ppm)	Gd (ppm)	Tb (ppm)	Dy (ppm)	Ho (ppm)	Er (ppm)	Tm (ppm)	Yb (ppm)	Lu (ppm)	Y (ppm)	ΣREE+Y (ppm)	ΣLREE/ΣHREE	ΣLREE/ΣHREE to PAAS	Eu/Eu*$_{PAAS}$	Ce/Ce*$_{PAAS}$	Y/Y*$_{PAAS}$	Pr/Pr*$_{PAAS}$
Carrickalinga Head Creek																							
C3	HS (lower)	30.3	62.8	7.18	26.6	4.90	0.97	4.48	0.63	3.90	0.76	2.27	0.28	2.05	0.27	25.3	173	3.32	0.89	0.97	0.98	1.17	1.03
C5	HS (lower)	25.3	49.0	5.87	21.7	4.28	1.01	4.12	0.65	3.55	0.74	2.00	0.29	1.69	0.28	23.0	144	2.95	0.79	1.12	0.93	1.14	1.06
C6	HS (lower)	16.4	29.7	3.77	13.8	3.04	1.18	3.09	0.47	2.77	0.57	1.61	0.22	1.33	0.20	20.1	98.2	2.24	0.60	1.80	0.87	1.28	1.09
C7	HS (lower)	57.8	116	12.6	44.6	8.01	1.75	7.09	0.98	5.32	1.09	3.13	0.46	3.00	0.46	31.3	294	4.56	1.22	1.08	1.00	1.04	1.03
C8	HS (lower)	16.6	30.3	3.82	14.6	2.94	0.91	3.00	0.47	2.75	0.57	1.62	0.21	1.34	0.19	20.7	100	2.24	0.60	1.43	0.88	1.32	1.07
C9	HS (lower)	29.5	43.8	4.82	17.9	3.36	1.01	3.69	0.53	3.19	0.67	1.95	0.26	1.57	0.24	28.6	141	2.47	0.66	1.34	0.85	1.56	1.01
C10	HS (lower)	16.3	28.9	3.69	13.6	2.80	0.90	2.85	0.42	2.36	0.49	1.32	0.18	1.10	0.16	18.4	93.6	2.42	0.65	1.49	0.86	1.37	1.10
C10A	HS (lower)	34.8	71.0	8.13	29.7	5.83	1.19	5.63	0.84	5.04	1.03	2.93	0.42	2.51	0.38	33.2	203	2.90	0.78	0.97	0.97	1.16	1.04
C11	HS (lower)	13.5	24.3	2.87	10.9	2.16	0.76	2.05	0.31	1.73	0.34	0.94	0.13	0.78	0.12	12.5	73.4	2.88	0.77	1.70	0.90	1.30	1.04
Carrickalinga Head Cove																							
C15	HS (lower)	15.6	26.1	3.15	11.4	2.29	0.83	2.45	0.38	2.31	0.50	1.37	0.21	1.21	0.19	18.4	86.3	2.19	0.59	1.63	0.86	1.37	1.08
C16	HS (lower)	31.2	63.5	6.65	23.7	4.40	0.91	4.00	0.60	3.50	0.76	2.22	0.33	2.21	0.32	23.1	168	3.52	0.94	1.01	1.02	1.13	1.01
C17	HS (lower)	37.4	74.3	7.83	27.7	5.19	1.06	4.52	0.67	4.00	0.85	2.52	0.39	2.52	0.38	26.5	196	3.62	0.97	1.02	1.00	1.15	1.02
C18A	HS (lower)	30.6	59.5	6.59	23.3	4.45	0.88	4.08	0.60	3.60	0.76	2.34	0.33	2.16	0.32	24.7	164	3.22	0.86	0.96	0.97	1.19	1.04
C18C	HS (lower)	35.1	57.9	6.97	26.3	5.25	1.45	6.03	0.90	5.57	1.19	3.46	0.44	2.75	0.41	47.5	201	1.95	0.52	1.21	0.85	1.47	1.05
C19A	HS (lower)	22.5	41.0	4.72	17.5	3.48	0.83	3.46	0.54	3.33	0.71	2.08	0.30	1.84	0.26	25.7	128	2.35	0.63	1.12	0.92	1.34	1.04
C19B	HS (lower)	36.0	75.8	8.33	30.0	5.77	1.10	5.04	0.72	4.22	0.87	2.50	0.38	2.34	0.33	26.9	200	3.62	0.97	0.95	1.01	1.12	1.03
C20	HS (lower)	29.8	46.5	5.17	18.9	3.67	1.07	3.97	0.63	3.80	0.85	2.50	0.35	2.15	0.33	32.0	152	2.26	0.60	1.31	0.86	1.42	1.03
C23	HS (lower)	16.3	30.4	3.99	15.6	3.22	0.98	3.33	0.48	2.77	0.58	1.56	0.22	1.28	0.19	21.4	102	2.22	0.59	1.39	0.87	1.35	1.08
C27	HS (lower)	35.5	76.8	8.62	32.3	6.33	1.12	5.77	0.84	4.69	0.92	2.54	0.34	2.06	0.28	31.0	209	3.32	0.89	0.86	1.01	1.19	1.02
C28	HS (lower)	18.2	30.3	3.61	12.9	2.47	0.67	2.24	0.33	1.88	0.39	1.07	0.15	0.93	0.13	13.6	88.9	3.28	0.88	1.33	0.86	1.27	1.07
C29	HS (lower)	28.1	54.0	6.49	23.2	4.55	0.87	4.08	0.58	3.38	0.66	1.89	0.27	1.74	0.26	21.2	151	3.44	0.92	0.95	0.92	1.13	1.08
C31	HS (lower)	17.2	29.1	3.80	13.6	2.73	0.60	2.42	0.38	2.09	0.42	1.12	0.15	0.96	0.14	14.1	88.9	3.08	0.82	1.09	0.83	1.19	1.12
Myponga Beach																							
M3	HS (lower)	30.8	59.2	7.01	25.2	4.76	0.93	4.14	0.63	3.89	0.82	2.46	0.36	2.33	0.34	25.4	168	3.17	0.85	0.98	0.93	1.14	1.07
Sellick Hill																							
S12	HS (upper)	43.2	86.4	9.14	32.2	5.79	1.38	4.74	0.66	3.77	0.79	2.42	0.37	2.40	0.37	24.7	218	4.43	1.19	1.23	1.00	1.14	1.02
S13	HS (upper)	29.7	62.7	6.39	22.4	4.14	0.84	3.53	0.48	2.85	0.61	1.88	0.29	1.97	0.29	19.3	157	4.04	1.08	1.03	1.05	1.17	1.00
S14	HS (upper)	49.3	99.6	10.4	36.4	6.89	1.52	5.90	0.80	4.59	0.92	2.66	0.38	2.55	0.37	29.9	252	4.24	1.14	1.11	1.02	1.16	1.02
S17	HS (upper)	38.0	79.8	8.42	30.0	5.51	0.97	4.57	0.61	3.46	0.70	2.00	0.31	1.94	0.29	21.3	198	4.63	1.24	0.90	1.03	1.09	1.01
S18	HS (upper)	42.3	90.5	9.38	33.0	5.87	1.12	5.09	0.69	3.89	0.81	2.35	0.35	2.29	0.34	24.2	222	4.56	1.22	0.96	1.05	1.09	1.01
S20	HS (upper)	39.1	84.8	9.35	33.1	6.04	1.07	5.03	0.71	3.99	0.79	2.41	0.35	2.27	0.36	22.8	212	4.48	1.20	0.91	1.02	1.03	1.04
S21	HS (upper)	41.6	86.6	9.18	31.9	5.73	0.92	4.40	0.62	3.60	0.75	2.39	0.38	2.54	0.41	21.4	212	4.82	1.29	0.86	1.02	1.04	1.03
S22	HS (upper)	52.0	107	11.2	38.7	6.76	1.38	5.36	0.72	4.19	0.89	2.73	0.42	2.80	0.42	26.4	261	4.93	1.32	1.07	1.02	1.09	1.03
S23	HS (upper)	39.9	82.1	8.75	30.4	5.47	1.17	4.51	0.62	3.67	0.75	2.22	0.33	2.19	0.35	21.7	204	4.62	1.24	1.10	1.01	1.04	1.03
S24	HS (upper)	49.3	101	10.7	36.3	6.22	1.26	4.90	0.65	3.71	0.77	2.33	0.37	2.45	0.39	22.4	243	5.40	1.45	1.06	1.02	1.06	1.03
S25	HS (upper)	47.1	97.6	10.4	35.9	6.47	1.32	5.34	0.72	4.07	0.84	2.52	0.38	2.50	0.37	24.9	240	4.78	1.28	1.05	1.02	1.07	1.03
S27	HS (upper)	46.6	94.6	9.85	33.9	6.28	1.44	5.09	0.70	4.04	0.84	2.47	0.39	2.50	0.39	26.3	235	4.51	1.21	1.19	1.02	1.14	1.02
S28	HS (upper)	54.7	118	12.4	42.7	7.49	1.28	5.72	0.75	4.20	0.86	2.61	0.39	2.77	0.42	26.4	280	5.36	1.44	0.91	1.04	1.11	1.03
S30	HS (upper)	48.6	102	10.9	38.4	6.95	1.18	5.67	0.78	4.46	0.92	2.75	0.42	2.81	0.43	26.9	253	4.60	1.23	0.87	1.02	1.06	1.03
S32	HS (upper)	33.6	68.2	7.73	28.4	5.67	1.59	5.33	0.79	4.48	0.96	2.66	0.38	2.30	0.36	33.1	195	2.88	0.77	1.35	0.98	1.27	1.03
S33	HS (upper)	56.3	126	13.9	51.2	9.89	2.07	8.72	1.16	6.38	1.22	3.44	0.48	3.02	0.44	37.7	322	4.15	1.11	1.04	1.04	1.08	1.01
S35	HS (upper)	49.7	105	11.3	40.0	7.53	1.49	6.28	0.88	4.82	0.95	2.77	0.41	2.71	0.39	27.9	263	4.58	1.23	1.01	1.03	1.04	1.02
S37	HS (upper)	21.9	40.5	4.92	18.3	3.60	0.84	3.55	0.53	3.02	0.63	1.75	0.25	1.46	0.22	22.1	124	2.69	0.72	1.10	0.90	1.28	1.06
S39	HS (upper)	57.0	118	12.6	44.7	8.64	1.74	7.10	0.93	5.16	1.02	2.87	0.44	2.87	0.43	30.6	295	4.72	1.27	1.04	1.02	1.06	1.02
Red Creek, north fork																							
N22	HS	36.8	65.1	7.32	27.1	4.99	1.04	4.69	0.60	3.16	0.60	1.71	0.25	1.83	0.26	15.9	171	4.90	1.31	1.00	0.91	0.93	1.02
N28	HS	45.4	84.9	9.48	35.3	6.41	1.31	5.49	0.63	2.87	0.49	1.45	0.22	1.65	0.24	12.1	208	7.26	1.95	1.03	0.94	0.81	1.02
N44	HS	51.1	102	11.7	45.3	8.92	1.42	7.41	0.86	4.02	0.72	2.03	0.30	2.19	0.34	17.8	256	6.19	1.66	0.82	0.97	0.83	1.01
N46	HS	41.0	78.6	8.79	32.8	5.99	1.08	5.13	0.64	3.03	0.53	1.48	0.22	1.65	0.24	13.4	194	6.39	1.71	0.91	0.96	0.84	1.02
N47	HS	28.0	65.9	8.15	30.5	5.88	1.12	5.26	0.67	3.31	0.56	1.57	0.24	1.74	0.26	13.7	167	5.11	1.37	0.94	1.01	0.81	1.07
N48	HS	18.3	34.5	4.63	17.8	3.40	0.75	2.91	0.37	1.88	0.33	0.95	0.15	1.04	0.16	5.09	92.3	6.16	1.65	1.11	0.86	0.51	1.10
N49	HS	46.8	86.6	9.68	35.9	6.46	1.19	5.82	0.69	3.18	0.55	1.52	0.22	1.55	0.23	13.8	214	6.76	1.81	0.90	0.94	0.84	1.02
Red Creek, south fork																							
S5	HS	31.1	63.5	7.04	26.4	4.77	1.44	4.48	0.54	2.68	0.48	1.41	0.21	1.50	0.23	11.8	157	5.76	1.54	1.45	0.99	0.83	1.01
S16	HS	18.5	39.3	4.73	18.4	3.58	0.81	3.46	0.48	2.55	0.46	1.32	0.19	1.42	0.23	10.1	106	4.22	1.13	1.07	0.97	0.75	1.03
S17	HS	13.6	28.0	3.17	12.2	2.44	0.62	2.48	0.35	2.07	0.41	1.22	0.19	1.41	0.20	10.5	79.0	3.18	0.85	1.18	0.98	0.91	1.01
S23	HS	26.8	56.1	6.30	24.5	4.78	1.20	4.34	0.53	2.69	0.49	1.43	0.20	1.48	0.22	13.1	144	4.89	1.31	1.22	1.00	0.91	1.00
S26	HS	40.1	80.3	8.81	33.4	6.13	1.16	5.20	0.63	2.98	0.50	1.37	0.20	1.38	0.20	12.8	195	6.74	1.81	0.96	0.99	0.84	1.00
S30	HS	57.0	112	12.5	46.5	8.21	1.50	7.06	0.84	3.93	0.67	1.86	0.27	1.86	0.27	16.4	271	7.18	1.92	0.92	0.97	0.81	1.01
S31	HS	54.9	107	11.8	44.1	7.76	1.52	6.60	0.77	3.73	0.67	1.80	0.26	1.89	0.27	15.8	259	7.14	1.92	0.99	0.97	0.80	1.01
S32	HS	56.5	113	12.5	45.6	7.67	1.33	6.43	0.74	3.45	0.58	1.61	0.23	1.61	0.24	13.8	265	8.24	2.21	0.89	0.98	0.78	1.03
S37	HS	37.7	80.5	8.63	31.2	5.89	1.13	4.59	0.63	3.18	0.60	1.73	0.27	1.87	0.30	16.5	195	5.55	1.49	1.02	1.03	0.95	1.01
S38	HS	42.6	84.3	9.16	33.9	6.13	1.06	5.20	0.65	3.20	0.56	1.51	0.21	1.49	0.23	13.3	203	6.71	1.80	0.88	0.98	0.80	1.01
S39	HS	50.4	98.9	10.9	40.8	7.19	1.32	6.18	0.74	3.48	0.62	1.77	0.26	1.85	0.28	15.1	240	6.93	1.86	0.92	0.97	0.82	1.01
Sedan Hill Quarry																							
SQ2	HS	10.2	17.4	1.73	6.18	1.32	0.32	1.49	0.27	1.97	0.41	1.26	0.21	1.55	0.23	11.2	55.7	2.00	0.53	1.07	0.95	1.00	0.98
SQ3	HS	24.8	52.7	5.79	22.4	4.24	0.90	4.07	0.48	2.28	0.40	1.19	0.18	1.39	0.21	11.4	132	5.14	1.38	1.01	1.01	0.95	0.99
SQ5	HS	24.1	43.6	4.16	15.3	3.14	0.70	3.27	0.46	2.66	0.53	1.55	0.24	1.68	0.24	13.6	115	3.75	1.01	1.02	1.01	0.92	0.95
The Gap																							
K1	T	21.3	37.5	3.62	12.2	2.50	0.60	2.63	0.38	2.25	0.42	1.24	0.18	1.35	0.19	9.92	96.3	4.19	1.12	1.09	0.99	0.82	1.00
K2	T	30.9	47.7	4.28	13.7	2.53	0.60	2.68	0.38	2.21	0.40	1.19	0.18	1.32	0.19	9.63	118	5.48	1.47	1.08	0.96	0.81	0.98
K3	T	34.6	58.0	4.95	15.3	2.88	0.69	2.92	0.43	2.49	0.47	1.33	0.20	1.49	0.22	10.6	137	5.80	1.55	1.11	1.02	0.78	0.98
K4	T	38.3	58.7	5.94	20.2	3.60	0.84	3.64	0.48	2.66	0.47	1.32	0.20	1.34	0.19	10.7	149	6.07	1.63	1.08	0.90	0.77	1.02
K5	T	36.0	58.7	5.85	19.8	3.41	0.76	3.37	0.45	2.53	0.44	1.29	0.19	1.35	0.19	9.37	144	6.49	1.74	1.05	0.93	0.71	1.01
K6	T	28.2	53.5	4.60	15.7	3.10	0.68	3.15	0.44	2.48	0.46	1.29	0.18	1.36	0.19	10.4	126	5.31	1.42	1.01	1.08	0.78	0.93
K7	T	19.5	36.8	3.22	11.1	2.35	0.62	2.62	0.40	2.34	0.42	1.20	0.18	1.34	0.19	9.49	91.7	4.04	1.08	1.16	1.07	0.76	0.94
K8	T	10.3	22.9	1.85	6.30	1.46	0.50	1.80	0.29	1.86	0.36	1.07	0.18	1.40	0.21	7.22	57.7	3.01	0.81	1.44	1.21	0.70	0.91
K9	T	19.5	27.7	2.43	7.91	1.64	0.47	1.89	0.31	1.84	0.35	1.05	0.17	1.22	0.18	8.52	75.2	3.84	1.03	1.23	0.93	0.84	0.96
Frankton-1 drill hole																							
F1 (1)	T	39.6	81.0	8.97	33.5	6.56	1.46	5.87	0.85	3.83	0.79	1.95	0.38	2.01	0.41	16.1	203	5.32	1.43	1.09	0.99	0.74	1.01
F1 (2)	T	61.0	119	13.0	48.1	8.54	1.65	7.11	0.81	3.67	0.62	1.70	0.24	1.68	0.25	14.4	282	8.24	2.21	0.99	0.97	0.76	1.02
F1 (3)	T	30.7	65.1	7.08	26.5	5.13	1.06	4.65	0.59	3.02	0.55	1.53	0.23	1.54	0.24	13.2	161	5.31	1.42	1.01	1.02	0.81	1.00
F1 (4)	T	45.4	89.6	9.85	37.5	6.88	1.25	6.02	0.72	3.40	0.58	1.56	0.23	1.63	0.27	13.2	218	6.89	1.85	0.90	0.98	0.75	1.00
F1 (5)	T	49.1	95.8	10.4	38.6	6.98	1.28	6.15	0.75	3.66	0.62	1.63	0.23	1.73	0.28	14.6	232	6.83	1.83	0.91	0.98	0.77	1.01
F1 (6)	T	37.1	76.9	8.49	32.1	6.07	1.17	5.43	0.68	3.56	0.63	1.71	0.26	1.77	0.26	13.3	189	5.87	1.58	0.95	1.00	0.71	1.00
F1 (7)	T	47.9	95.5	10.2	38.0	6.98	1.29	6.15	0.74	3.68	0.64	1.77	0.25	1.82	0.27	15.3	231	6.53	1.75	0.92	0.99	0.80	1.00
F1 (8)	T	26.4	62.0	7.09	28.2	6.24	1.52	6.94	1.11	6.88	1.33	3.59	0.48	2.95	0.39	24.7	180	2.72	0.73	1.08	1.04	0.65	1.00
F1 (9)	T	34.7	70.4	7.87	29.9	5.57	1.16	4.85	0.58	2.77	0.46	1.17	0.16	1.06	0.16	10.1	171	7.01	1.88	1.04	0.98	0.72	1.01
F1 (10)	T	52.0	104	11.2	41.5	7.06	1.41	5.60	0.60	2.61	0.41	1.09	0.15	1.05	0.15	9.91	239	10.08	2.70	1.05	1.00	0.76	1.00
Frankton-1 drill hole																							
F2 (1)	T	39.2	78.8	8.45	31.7	5.93	1.09	5.37	0.67	3.19	0.59	1.67	0.25	1.79	0.28	14.2	193	5.90	1.58	0.90	1.00	0.83	0.99
F2 (2)	T	51.0	102	10.7	40.1	7.39	1.33	6.67	0.80	4.06	0.73	2.11	0.32	2.28	0.34	18.0	248	6.01	1.61	0.88	1.01	0.84	0.98
F2 (3)	T	46.6	90.9	9.86	37.0	6.90	1.19	6.09	0.75	3.75	0.65	1.74	0.26	1.86	0.27	15.3	223	6.27	1.68	0.85	0.98	0.79	1.00
F2 (4)	T	42.3	83.7	8.95	33.5	6.23	1.12	5.87	0.76	4.04	0.75	2.12	0.32	2.34	0.34	18.9	211	4.96	1.33	0.87	0.99	0.86	0.99
F2 (5)	T	49.3	96.5	10.6	39.9	7.24	1.31	6.61	0.81	4.13	0.74	2.06	0.30	2.05	0.30	18.1	240	5.83	1.56	0.88	0.98	0.83	1.00
F2 (6)	T	42.8	82.7	8.93	33.2	6.02	1.16	5.49	0.68	3.55	0.65	1.75	0.26	1.87	0.28	16.5	206	5.64	1.51	0.94	0.98	0.86	1.00
F2 (7)	T	31.8	69.7	7.59	28.7	5.43	1.05	4.97	0.65	3.39	0.62	1.71	0.25	1.69	0.26	12.5	170	5.54	1.49	0.94	1.03	0.69	1.00
F2 (8)	T	39.4	79.9	8.79	33.1	6.05	1.07	5.32	0.65	3.39	0.59	1.71	0.25	1.76	0.27	13.5	196	6.13	1.64	0.88	0.99	0.76	1.01
F2 (9)	T	26.9	59.7	6.31	24.1	4.42	0.85	4.00	0.55	2.83	0.55	1.50	0.22	1.56	0.23	11.8	146	5.26	1.41	0.94	1.06	0.76	0.98
F2 (10)	T	32.7	64.5	6.93	26.1	4.85	0.92	4.44	0.57	2.90	0.52	1.44	0.22	1.57	0.24	13.9	162	5.28	1.42	0.93	0.99	0.90	0.99
Big Gully, shoreline																							
EB09S0.1	EBS	53.3	117	13.5	51.1	10.4	2.18	10.1	1.40	7.69	1.41	3.73	0.48	3.17	0.43	41.1	317	3.56	0.96	0.99	1.01	1.00	1.03
EB09S0.9	EBS	45.6	88.6	10.3	37.4	6.78	1.26	6.21	0.87	5.11	0.99	2.90	0.39	2.72	0.38	28.4	238	3.96	1.06	0.91	0.94	1.01	1.05
EB09S2.8	EBS	42.2	89.2	10.1	36.8	6.95	1.21	5.88	0.83	4.89	0.93	2.74	0.36	2.51	0.35	25.5	230	4.23	1.14	0.88	1.00	0.96	1.03
EB09S4	EBS	38.9	82.1	8.86	31.7	5.96	1.12	5.38	0.73	4.58	0.87	2.59	0.34	2.44	0.33	24.9	211	4.00	1.07	0.92	1.02	0.99	1.02
EB09S5	EBS	39.7	81.5	9.42	34.2	6.43	1.16	5.75	0.77	4.62	0.90	2.63	0.35	2.45	0.34	25.4	216	3.99	1.07	0.89	0.97	0.99	1.05
EB09S6	EBS	40.0	85.5	9.22	33.4	6.17	1.16	5.51	0.78	4.62	0.86	2.59	0.34	2.43	0.33	25.1	218	4.12	1.11	0.93	1.03	1.01	1.01
EB09S7	EBS	42.4	90.2	10.1	37.1	6.78	1.25	6.22	0.84	4.91	0.94	2.71	0.36	2.58	0.36	26.8	234	4.11	1.10	0.90	1.00	0.99	1.03
EB09S7.1	EBS	23.9	50.1	5.50	19.6	3.78	0.68	3.40	0.44	2.75	0.51	1.53	0.18	1.50	0.18	15.2	129	4.03	1.08	0.89	1.01	1.02	1.03
EB09S7.6	EBS	36.0	72.3	8.32	30.3	5.77	1.12	5.07	0.67	4.20	0.79	2.26	0.30	2.11	0.29	22.6	192	4.02	1.08	0.97	0.96	0.99	1.05
EB09S	EBS	38.2	65.1	8.43	29.8	5.37	1.03	4.69	0.63	4.00	0.77	2.28	0.30	2.21	0.31	22.4	186	3.93	1.05	0.95	0.84	1.02	1.13
Big Gully, Buck Quarry																							
EBQ1	EBS	36.4	68.9	8.64	31.1	5.89	1.19	5.43	0.75	4.65	0.90	2.61	0.34	2.49	0.35	26.3	196	3.48	0.93	0.98	0.90	1.03	1.10
EBQ2	EBS	33.6	70.3	8.90	33.6	6.54	1.21	5.70	0.75	4.48	0.81	2.37	0.31	2.06	0.28	24.3	195	3.75	1.01	0.93	0.94	1.02	1.08
PAAS		38.0	80.0	8.90	32.0	5.60	1.10	4.70	0.77	4.40	1.00	2.90	0.40	2.80	0.43	27.0	210	3.73					
Chondrite		0.367	0.957	0.137	0.711	0.231	0.087	0.306	0.058	0.381	0.0851	0.249	0.0356	0.248	0.0381	2.100							
Average $_{PAAS}$	T	0.97	1.04	1.02	1.06	1.13	1.11	1.21	0.93	0.82	0.65	0.61	0.66	0.64	0.64	0.55	0.98		1.53	1.01	1.00	0.78	0.99
Average $_{PAAS}$	HS (KT)	0.95	0.89	0.89	0.93	0.98	0.99	1.03	0.78	0.67	0.53	0.52	0.56	0.58	0.56	0.49	0.84		1.53	1.01	0.97	0.84	1.02
Average $_{PAAS}$	HS (lower)	0.71	0.64	0.66	0.67	0.74	0.91	0.85	0.77	0.79	0.72	0.71	0.73	0.65	0.62	0.91	0.71		0.78	1.20	0.92	1.25	1.05
Average $_{PAAS}$	HS (upper)	1.16	1.15	1.11	1.08	1.14	1.18	1.13	0.94	0.94	0.84	0.86	0.93	0.87	0.86	0.96	1.10		1.19	1.04	1.02	1.11	1.03
Average $_{PAAS}$	EBS	1.03	1.00	1.04	1.06	1.14	1.11	1.23	1.03	1.07	0.89	0.89	0.85	0.85	0.76	0.95	1.02		1.05	0.93	0.97	1.00	1.05

T = Talisker Formation; HS = Heatherdale Shale; EBS = Emu Bay Shale; KT = Kanmantoo Trough
PAAS = Post-Archean Australian shale, Taylor & McLennan (1985); Chondrite, Taylor & McLennan (1985)

2.2.5. Discussion

2.2.5.1 Total organic carbon

The organic richness of the Heatherdale Shale and Talisker Formation varies from low to moderate, whereas throughout the fossiliferous lower Emu Bay Shale it remains uniformly low (Table 2). These shales have all undergone thermal maturation to well beyond the oil window. The resulting generation and expulsion of petroleum hydrocarbons (plus some associated thermogenic CO_2) means that their present TOC values are appreciably less than those of their precursor mudstones. Based on its kerogen atomic H/C ratio and Weaver index of illite crystallinity (0.48 and 3.8, respectively), the Emu Bay Shale at Big Gully (average TOC = 0.38%) has a rank equivalent to ~1.5% vitrinite reflectance, suggesting an initial organic carbon content no higher than 1% (McKirdy et al., 2011).

The Heatherdale Shale on the Fleurieu Penisula (TOC = 0.19–2.57%, mean = 1.20%) yielded kerogen with atomic H/C ratios of 0.22 to 0.36 (n = 5). These, in conjunction with a methylphenanthrene index (MPI-1) of 0.90, are indicative of a rank equivalent to ~2.5% vitrinite reflectance (Carson, 1994). Therefore, the original TOC content of the host shales could have been as high as ~8.5% given that a typical marine Type II kerogen will generate hydrocarbons equivalent to 70% of its TOC (Tissot and Welte, 1984). Further north in the Karinya Syncline the same formation is less organic-rich (TOC = 0.21–1.56%, mean = 0.69%), consistent with its higher metamorphic grade. Here the overlying Talisker Formation (TOC = 0.36–1.90%, mean = 1.10%) contains kerogen with H/C ratios of <0.02 to 0.12 (Turner, 1994). Again, allowing for catagenic and metagenic loss of hydrocarbons, the initial TOC values of the host rock may have been as high as ~6.5%.

These concentrations of organic carbon in the Heatherdale and Talisker shales are not exceptionally high in comparison to those black shales described by Kennedy and Wagner (2011) as 'supersource rocks', wherein TOC exceeds 15% (e.g. the Alum Shale: Bharati et al., 1995). Nevertheless, they do indicate high primary productivity and effective preservation of the resulting marine organic detritus. Moreover, the measured TOC concentrations and their degree of stratigraphic variability fit the patterns observed from oscillating oxic-anoxic settings.

2.5.2 Stable isotopes

2.5.2.1 Organic carbon isotopes

Early Cambrian shales from the Fleurieu Peninsula and Kangaroo Island have relatively consistent $\delta^{13}C_{org}$ signatures, ranging from –32.7 to –27.3‰ (average –31.2‰) in the Heatherdale Shale and from –31.8 to –27.8‰ (average –30.0‰) in the Emu Bay Shale. Further north in the Karinya Syncline, the organic carbon in shales of this age is significantly but variably richer in ^{13}C. In the Heatherdale Shale the signatures range from –19.5 to –10.0‰ (average –14.7‰), and in the Talisker Formation from –26.4 to –12.8‰ ‰ (average –19.2‰). These heavier signatures are typical of metamorphosed sediments where $^{13}C/^{12}C$ ratios become altered from their primary value. The onset of alteration correlates with kerogen atomic H/C ratios falling below 0.2 (McKirdy and Powell, 1974; Hayes et al., 1983). Turner (1994) obtained values of <0.02, 0.03, 0.06 and 0.13 from a subset of Karinya Syncline samples, supporting the conclusion that these data are thermally altered. Elsewhere, the signatures are likely to be original. Carson (1994) reported H/C ratios of 0.22–0.36 for a subset of five samples of Heatherdale Shale from the Fleurieu Peninsula, whilst McKirdy (1971) reported a H/C ratio of 0.48 for the Emu Bay Shale. No

definitive correlation is evident between the unaltered $\delta^{13}C_{org}$ data and TOC. A positive anomaly in $\delta^{13}C_{org}$ is observed in the upper section of the Heatherdale Shale at Carrickalinga Head Cove where a +4‰ shift coincides with a sharp rise in TOC (to 1.75%). However, another spike in TOC (to 2.14%) just 2.5 m lower in the section exhibits no isotopic anomaly. Given the small sample sets for each location and the relatively sparse $\delta^{13}C_{org}$ record they provide, any chemostratigraphic comparison would be at best tenuous, other than to say that these values closely match the signatures obtained from other organic-rich early Cambrian (Stage 2 and 3) successions (e.g. Goldberg et al., 2007; Maloof et al., 2010; Ishikawa et al., 2011; Cremonese et al., 2012).

2.5.2.2 Pyrite sulfur isotopes

Recorded within the correlated Frankton-1 and 2 drill hole sections of the Talisker Formation (Karinya Shale Member) is a striking secular decline in the ^{34}S content of pyrite, wherein $\delta^{34}S_{pyr}$ decreases from +10‰ to –11‰ (Fig.3). The pyrite in question is considered to be syngenetic, although it has subsequently been realigned and redistributed along cleavage planes (Morris, 1991). Gum (1998) compiled a suite of $\delta^{34}S_{pyr}$ data from the Kanmantoo Trough, concluding that the values could be assigned to discrete families of biogenic, seawater and metamorphosed sulfur, or combinations thereof. It appears from the new higher resolution data set presented here that the gradual depletion up section may represent a change in the palaeoenvironmental conditions under which the pyrite formed, rather than a diagenetic or metamorphic overprint. The majority of the redox proxies seem to suggest the water column became more reducing over time (see section 5.5). Thus, the high initial δ34S values could indicate that the bottom waters were more oxic, and that BSR occurred

primarily within the sediment where sulphate limitation was soon established (Goldberg et al., 2007). As conditions became more reducing and sulphate became more available to bacteria, so the resulting pyrite would become more depleted in 34S. Alternatively, the secular decline could represent a change in the primary isotopic signature of seawater sulphate from which the sulphide was derived. The Ediacaran to early Cambrian Atdabanian stage is thought to have had a stable seawater sulphate isotopic value of around 33‰ (Claypool et al., 1980; Shields et al., 2004), an argument consistent with a long marine sulphate residence time similar to that of the modern ocean (~14 to 22 million years: Holser and Kaplan, 1966; Walker, 1986). However, short-term, high magnitude variations are reported in a number of studies with deviations of −30‰ to +53‰ worldwide (e.g., Shen et al., 2000; Strauss, 2002; Gorjan et al., 2003; Zhang et al., 2003; Shields et al., 2004; Halverson and Hurtgen, 2007; Lehmann et al., 2007; Fike and Grotzinger, 2008). These may be attributed to extreme climatic conditions or perhaps to a much more restricted sulphate budget in the early Cambrian, ~8 mM as opposed to a modern value of 28 mM (Brennan et al., 2004). Hence, with a smaller sulphate reservoir, flux imbalances will trigger more pronounced isotope variations in marine sulphate (Goldberg et al., 2005).

NOTE:
This figure/table/image has been removed to comply with copyright regulations.
It is included in the print copy of the thesis held by the University of Adelaide Library.

Fig.3. $\delta^{34}S_{pyr}$ profile of the Talisker Formation (Karinya Shale Member) in the Frankton-1 and 2 drill holes. Stratigraphic logs and correlation after Turner (1994).

2.5.3 Redox-sensitive trace elements and palaeoenvironmental proxies

2.5.3.1 Molybdenum

The positive correlation observed between concentrations of C_{org} and Mo in many black shales and sediments of modern, oxygen-deficient marine basins is well known (Wilde et al., 2004; Algeo and Lyons, 2006) and commonly ascribed to anoxic and euxinic depositional conditions. The high solubility of the unreactive molybdate oxyanion (MoO_4^{2-}) under oxic conditions makes it the most common transition metal in seawater (Algeo and Lyons, 2006). However, under reducing conditions, Mo is rapidly sequestered into sediments. Hence, enrichment of Mo when normalised to average shale may be used as a redox proxy for anoxic environments. A number of mechanisms have been proposed to explain the mechanism for this enrichment . These include authigenic formation in the presence of pore water sulphide (Zheng et al., 2000); adsorption onto Mn oxyhydroxides and subsequent recycling and sulphide fixation (Calvert and Pederson, 1993; Adelson et al., 2001), or fixation via Fe-Mo-S cluster complexes (Helz et al., 1996); scavenging by sulphidized (S-rich) organic material or Fe–S phases to form thiomolybdates (Tribovillard et al., 2004); and adsorption onto humic substances (Algeo and Lyons, 2006). However, sequestration of Mo has also been observed in dysoxic environments (Zheng et al., 2000) and Tribovillard et al. (2008) interpreted Mo enrichment in the Jurassic Bancs Jumeaux Formation in northern France to have occurred under dysoxic-oxic conditions.

Mo concentrations in the shales reported here exhibit general enrichment normalised to PAAS, with all samples containing >0.7% TOC being enriched. The high levels of

Mo common in black shales deposited under euxinic conditions, such as those from the early Cambrian of South China (Lehmann et al., 2007; Zhou and Ziang, 2009; Gill et al., 2011) are not typical of our South Australian data, although some intervals of both the upper Heatherdale Shale and Talisker Formation do exhibit PAAS normalised enrichment factors of >30. In the majority of the Talisker and the upper Heatherdale samples (79 and 68%, respectively), the factor is >5. The lower Heatherdale Shale shows significantly more variation (>5 in 27% and <1 in 20% of the samples) whilst in the Emu Bay Shale the enrichment factor is consistently <3.

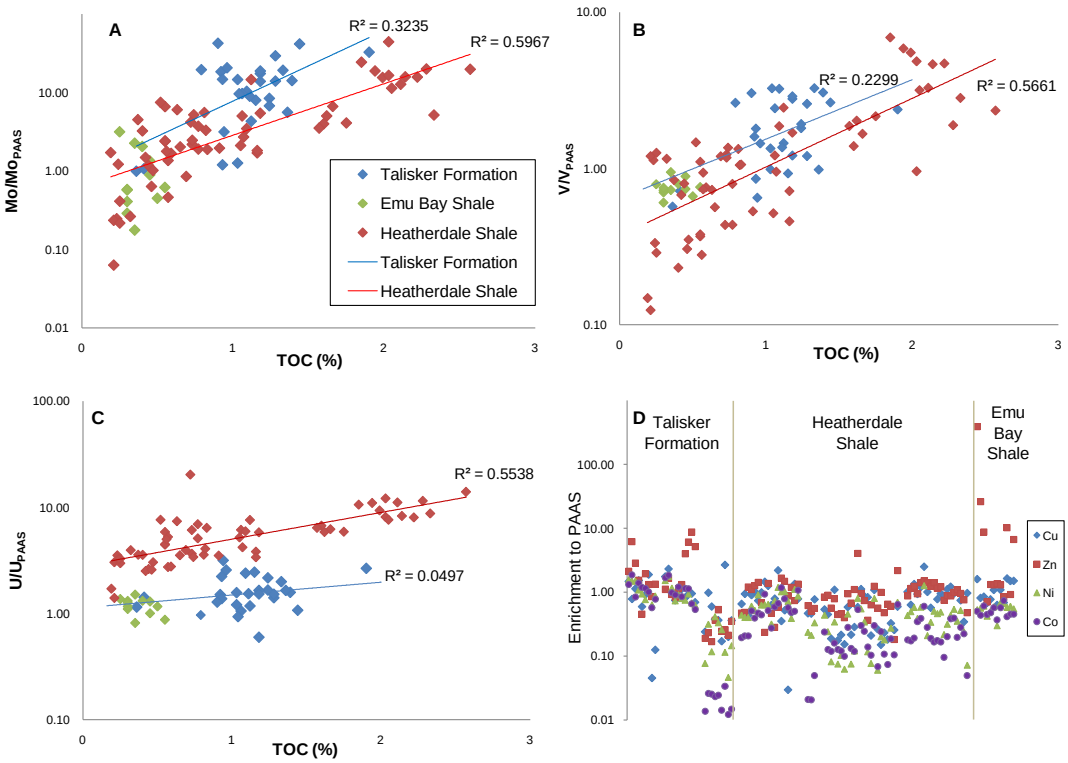

Fig. 4 Normalised abundances of selected redox-sensitive trace elements and their variation with TOC: (A) Mo_{PAAS} vs TOC; (B) V_{PAAS} vs TOC; (C) U_{PAAS} vs TOC; (D) shows distributions of Cu_{PAAS}, Zn_{PAAS}, Ni_{PAAS} & Co_{PAAS} from each formation with increasing stratigraphic height from left to right.

These data suggest that both the upper Heatherdale Shale and Talisker Formation were deposited in predominantly anoxic settings, with rare periods of short-lived euxinia, whereas those of the lower Heatherdale Shale and lower Emu Bay Shale were generally less oxygen depleted. The covariance between Mo and TOC in the Heatherdale Shale and Talisker Formation (Fig. 4A) supports the interpretation that these units were deposited under generally oxygen-depleted conditions. The more pronounced gradient shown by the Talisker Formation implies more depleted and/or sulphidic conditions.

2.5.3.2 Vanadium

Vanadium, which occurs in seawater as vanadate oxyanions (HVO_4^{2-} and $H_2VO_4^-$), behaves similarly to Mo in oxic and reducing environments, although the valency pathways for reduction from the stable V (V) are more complex than those of Mo (IV). Reduction of V(V) to V(IV) occurs under non-sulphidic anoxic conditions and is facilitated by humic and fulvic acids, whereas reduction of V(IV) to V(III) takes place under sulphidic conditions (Tribovillard et al., 2006). The initial reduction product, V (IV), usually correlates well with TOC, but V (III) abundances display no such correlation (Pi et al., in press). Our V data (Fig. 4B) follow a similar pattern to Mo, but with a higher proportion of depleted samples. All Emu Bay Shales are depleted in V relative to PAAS. Of the remaining samples exhibiting depletion most are from the lower Heatherdale Shale. Again the data suggest that both the upper Heatherdale Shale and Talisker Formation were deposited in predominantly anoxic environments.

2.5.3.3 Uranium

Uranium differs from Mo and V in the manner by which it is enriched from the water column. It is believed to exist as U(VI) in the form of uranyl ions bound to carbonate ions ($UO_2(CO_3)_3^{4-}$), which is reduced to U(IV) uranium oxides (UO_2, U_3O_7, U_3O_8) during early diagenesis, a process probably mediated by BSR and independent of Fe and Mn redox cycling (Tribovillard et al., 2006; Pi et al., in press). Thus one of the main factors controlling U enrichment is the availability of organic matter for BSR, leading to a covariance with TOC in anoxic non-sulphidic environments. The majority of our samples exhibit U enrichment (Fig. 4C), but obvious distinctions in this pattern exist between each formation. The Heatherdale Shale is more enriched and lies on separate trend of co-variation with TOC from the Talisker and Emu Bay samples. This distinction likely resulted from higher productivity during the deposition of the Heatherdale Shale, consistent with the occurrence of phosphate nodules indicative of nutrient-rich upwelling (e.g. Carson, 1994). The covariance of U, Mo, and V with TOC also suggests that oxygenated fluids have not affected these sediments since deposition (Tribovillard et al., 2006).

2.5.3.4 Nickel, cobalt, copper and zinc

Interestingly, other redox-sensitive group 4 trace elements, notably Ni, Co, Cu and to a lesser extent Zn, are generally depleted in all three formations (Fig. 4D). In comparison to Mo and V these elements are less sensitive to pyritization (Morse and Luther, 1999; Tribovillard et al., 2006). Co concentration is thought to require an appropriate clastic source (Tribovillard et al., 2006) implying that provenance may be the cause of the depletion here. Ni, Cu and Zn are concentrated through incorporation in organic matter and, while generally enriched in sulphidic settings, they are recycled

back into the water column under mildly reducing conditions (Tribovillard et al., 2006). Their depletion in the black shale lithofacies of the Stansbury Basin implies that the appropriate reducing conditions to allow fixation were generally not realized. This interpretation does not hold for the Talisker Formation and upper Heatherdale Shale where the observed concentrations of pyrite indicate that BSR was well established. However, these metals are known to be mobile during early diagenesis, even if migration is only localised, whereas V (and presumably the more immobile Mo) shows no evidence of migration (Thompson et al., 1998).

Our data reveal that some trace elements were remobilized. For example, Zn and Pb are anomalously concentrated in the basal metre of the Emu Bay Shale and Ni, Cu, Co and Zn are depleted in structurally complex zones of the Karinya Syncline (Table 2). The Emu Bay Shale pattern of enrichment is likely connected to the same metalliferous fluid migration event that triggered Ag, Pb and Zn mineralisation in the Kanmantoo Trough and south of the Snelling Fault on Kangaroo Island (McKirdy et al., 2011 and references therein). Ni, Cu, Co and Zn depletion in the structurally complex zone at Sedan Hill Quarry and The Gap probably resulted from scavenging of these elements by fluid flow within the shear zone. Gum (1998) also noted that units of the Kanmantoo Group underlying the Talisker Formation (viz. Carrickalinga Head Formation and Backstairs Passage Formation) appear to be significantly depleted, suggesting that these sediments were leached of some of their metal content during diagenesis. The resulting metal-rich formation waters subsequently migrated out of these formations to form sedimentary exhalative (SedEx) deposits elsewhere in the basin. From the data compiled in the present study, this explanation for Ni and Co depletion may be extended into the Heatherdale Shale, which unconformably underlies the Kanmantoo Group. The nature of mineralized veins observed in the

Talisker and Tapanappa Formations (sub-parallel to bedding, highly strained and boudinaged) indicates their emplacement prior to the end of the Delamerian Orogeny, thereby supporting the suggestion that mineralising fluids within the Kanmantoo Trough were mobilised during early diagenesis. In addition, later fluid movement associated with the Delamarian orogenic event, although not strong enough to form significant ore bodies, did locally enrich pyritic schists of the Talisker and Tapanappa formations resulting in base metal concentrations of up to several thousand ppm (Gum, 1998).

2.5.3.5 General overview of trace metal redox proxies

Excluding the samples from Sedan Hill Quarry and The Gap, which display clear evidence of remobilisation of certain trace elements (see section 5.1.4), a complex picture emerges from our redox proxy data for the Stansbury Basin. The majority of the samples are assigned to either oxic or dysoxic depositional environments (Tables 4 and 5, Fig. 5). Ni/Co, U/Th and Th/U (Figs. 5A, F and D) attribute oxic settings to the majority of samples (87, 85 and 68%, respectively). The V/Sc proxy (Fig. 5B) indicates that 73% of these early Cambrian shales were deposited under dysoxic regimes, with normalised Mo (Fig. 5E) similarly assigning 80% of the samples to anoxic settings. In marked contrast, V/(V+Ni) (Fig. 5C) designates every sample as either anoxic (53%) or euxinic (47%), an interpretation which differs sharply from that based on most other proxies.

Table 4 Selected redox proxies based on trace metal abundances.

	Euxinic	Anoxic	Dysoxic/Sub-oxic	Oxic	Reference
V/(V+Ni)	>0.84	0.54–0.84	0.46–0.60	<0.46	Hatch & Leventhal, 1992
V/Sc			>9.1	<9.1	Kimura & Watanabe, 2001
Ni / Co		>7	5–7	<5	Jones & Manning, 1994
U/Th		>1.25	0.75–1.25	<0.75	Powell et al., 2003
Th/U		<2		>2	Wignell & Twitchett, 1996
Mo_{PAAS}		>1		<1	Nedin, 1995

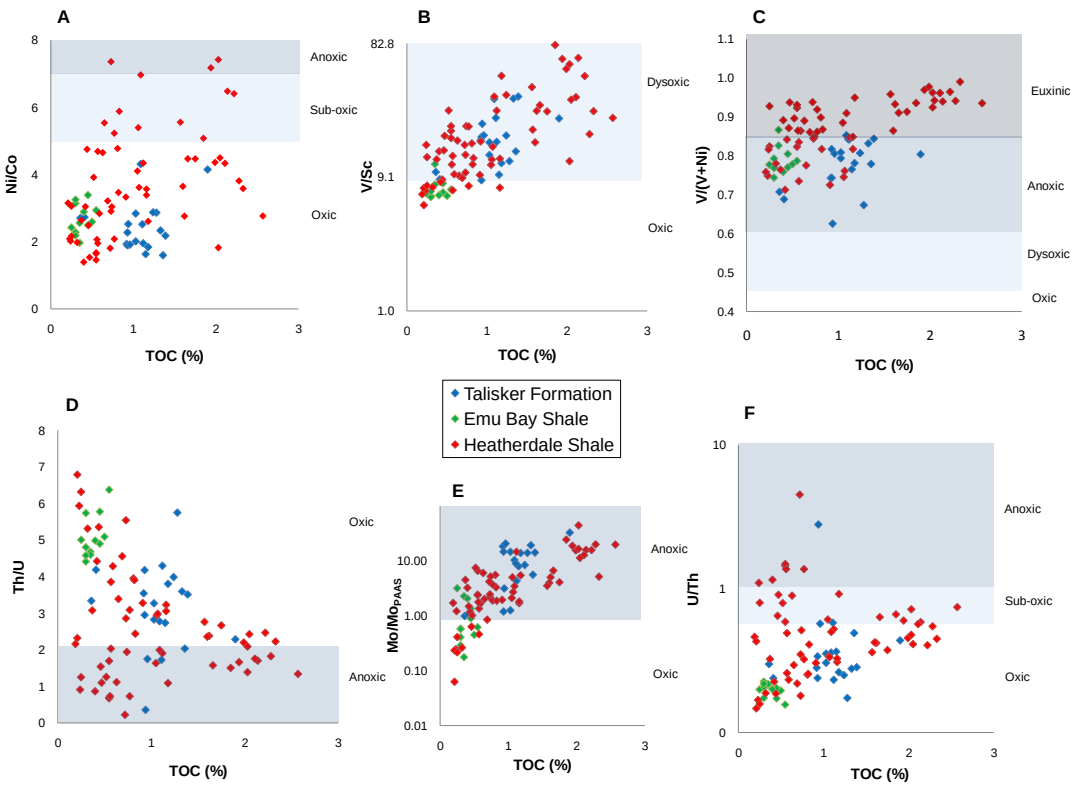

Fig. 5 Palaeoredox proxy distributions and their variance with TOC: (A) Ni/Co; (B) V/Sc; (C) V/(V+Ni); (D) Th/U; (E) Mo_{PAAS}; and (F) U/Th.

Depressed Ni values appear to have skewed the V/(V+Ni) redox interpretations, reflecting instead the diagenetic metal scavenging of this and other metals from the Talisker Formation and the underlying Heatherdale Shale (see section 5.3.5). This discrepancy has been noted in other basins (e.g. Rimmer et al., 2004; Racka et al., 2010), where the V/(V+Ni) ratio is known to indicate consistently more oxygen-restricted regimes with little correspondence between it and other redox proxies. Och and Shields (2012) also concluded that V/(V+Ni) was particularly inappropriate when used to infer sulphidic conditions, citing several reasons, including the transitory character of marine trace-metal geochemistry during the late Neoproterozoic and early Cambrian. Consequently, V/(V+Ni) is deemed unsuitable as a palaeoredox proxy and will not be used in the interpretation of data presented herein.

Co also is likewise depleted, possibly to the same degree as Ni. If so, the Ni/Co proxy may still be beneficial if interpreted in conjunction with other proxies and sedimentological evidence.

Table 5 Palaeoenvironmental assignments for Stansbury Basin shales (n = 92, excluding samples from Sedan Hill Quarry and The Gap).

	Mo_{PAAS}	Ni/Co	U/Th	Th/U	V/Sc	V/(V+Ni)
Euxinic	-	-	-	-	-	47%
Anoxic	80%	3%	7%	32%	-	53%
Sob-oxic or Dysoxic	-	10%	9%	-	73%	-
Oxic	20%	87%	85%	68%	27%	-

2.5.4 REE distributions: implications for palaeoredox and provenance

2.5.4.1 Cerium anomalies (Ce/Ce*)

The REE distributions of black shales are largely inherited from their primary detrital minerals. This limits the capacity of such elements to be a source of useful palaeoenvironmental information. On the other hand they are generally immobile in the sediments in which they have accumulated, hence preserving their primary distributions. Cerium (Ce) is the key REE in this regard as it is both biologically and abiotically oxidized to its relatively insoluble 4^{+}-valence state under ambient conditions (Sholkovitz et al., 1994; Guo et al., 2007). This process may lead to Ce recycling back into the water column under reducing conditions and its consequent depletion relative to other REE in the host sediment (as seen in Ce/Ce*: Wilde et al., 1996). This relationship is the inverse of that preserved in authigenic precipitates, where a negative anomaly indicates oxic conditions due to preferential removal of Ce(IV) from seawater (Guo et al., 2007). A Ce/Ce* anomaly should be interpreted with caution since several additional factors may influence Ce depletion (as outlined in Och and Shields-Zhou, 2012). Nevertheless, Ce still has some potential as an indicator of palaeoredox. In general our Ce/Ce* data have a variance of ±0.05, with occasional deviation beyond this range. The lower Heatherdale Shale displays the highest incidence of depletion (82%: see also Fig. 6), with 43% of the samples having values <0.95, suggesting predominantly reducing conditions during its deposition. Variable redox conditions may be ascribed to the other formations, which accumulated under generally oxic-dysoxic conditions interrupted by occasional periods of anoxia.

It has also been noted that praseodymium (Pr) enrichment commonly coincides with Ce depletion and can be used to corroborate the primary origin of this palaeoredox signature (Shields and Stille, 2001; Guo et al., 2007). Our data show a consistent antithetical covariance between normalised Ce and Pr (Fig. 7) confirming the validity of the suggested redox interpretation. Again, samples from the lower Heatherdale Shale offer the clearest example of this phenomenon (Fig. 7A), exhibiting general Ce depletion (0.83–1.02; mean = 0.92) with Pr enrichment (1.01–1.12; mean = 1.05) mirroring the depletion.

2.5.4.2 Europium anomalies (Eu/Eu*)

Europium (Eu) anomalies are normally associated with hydrothermal sources because of the high Eu(II) concentrations in plagioclase. Eu exists in seawater as Eu (III), but may be reduced to Eu (II) under anoxic conditions. Temperatures greater than 200°C are normally required for Eu (II) to be stable. Consequently, high-temperature, highly reducing hydrothermal brines are commonly enriched in Eu (Shields and Stille, 2001). Sediments deposited in seawater influenced by hydrothermal influx can record this Eu enrichment. The Stansbury Basin shales host moderate Eu/Eu* anomalies with a maximum of 1.80 in the lower Heatherdale Shale where 36% of the samples showing enrichment of >1.1. The upper Heatherdale Shale commonly exhibits slight enrichment (mean = 1.04), whilst the Talisker Formation is enriched at The Gap (mean = 1.14) but otherwise exhibits minor depletion in samples from the Frankton drill holes (mean = 0.95). The Emu Bay Shale shows only minor depletion in all samples (average = 0.93).

Within the Heatherdale Shale of the Karinya Syncline there appears to be a correlation between local volcanic activity and Eu enrichment. Stratigraphic logs

(available in Appendix) show that tuffaceous horizons and a pillow lava in the lower section of both the north and south fork outcrops at Red Creek correspond to levels of Eu enrichment. Additional examples of tuffs are described in the southern sections of the lower Heatherdale Shale on the Fleurieu Peninsula where general enrichment is also observed. This suggests that hydrothermal activity associated with these volcanic events was enriching Eu in the coeval sediments of the Stansbury Basin. However, the moderate levels of this enrichment would suggest seawater dilution prior to inclusion in the sediment, rather than direct authigenic incorporation. There is evidence from the Yangtze Platform, South China, that hydrothermal systems were widespread and active during the early Cambrian, which may have had a global influence on ocean chemistry (Chen et al., 2009) and been an additional source for the generalised minor Eu enrichment of the Heatherdale Shale.

2.5.4.3 REE as indicators of provenance

Marine black shales are commonly rich in REE + Y, probably related to their high concentrations of sedimentary organic matter (Filitsyn and Morad, 2002). There is a fractionation stemming from the preferential adsorption of LREE on particulate surface coatings (organics and Mn oxides), leaving seawater enriched in HREE and Y (Sholkovitz et al., 1994). The fact that the bulk normalised REE + Y distributions of black shales have flat profiles is typical of terrestrial detritus when the authigenic component is low (Pi et al., 2012) and the organic fraction is isolated. Variation in the proportion of light to heavy REE may then highlight differences in provenance, as the total REE pattern reflects the average distribution of the source area (Taylor and McLennan, 1997). The averaged data from the Stansbury Basin (Fig. 6) reveal a stratigraphic contrast between the lower and upper Heatherdale Shale on Fleurieu

Peninsula, both of which differ from the lower half of the formation in the Kanmantoo Trough. All three Heatherdale populations exhibit relatively flat profiles when normalised to PAAS, with the latter showing the greatest HREE depletion and being very similar to that of the Talisker Formation. The Emu Bay Shale and the upper Heatherdale Shale likewise are almost identical. Depletion of LREE is greatest in the lower Heatherdale Shale on Fleurieu Peninsula, although its HREE distribution lies within the range of the other profiles. The general correlation of Ce and Eu anomalies, independent of ΣREE, and the declining abundance of HREE from Gd to Lu together imply the occurrence of only minor diagenetic REE + Y scavenging, except in the aforementioned shear zone of the Karinya Syncline.

Applying the provenance indicators La/Sc and Th/Sc (Naqvi et al., 2002) to the South Australian data (Fig. 6), again we observe a close correspondence between the Emu Bay Shale and the upper Heatherdale Shale, Fleurieu Peninsula. Although less tightly clustered, data points from the Talisker Formation and Heatherdale Shale in the Karinya Syncline, Kanmantoo Trough, overlap those of the aforementioned units. The lower Heatherdale Shale on the Fleurieu Peninsula exhibits an aberrant pattern wherein the majority of samples are offset towards higher La/Sc values. The similarity of distribution observed between the lateral equivalents in the Heatherdale Shale being much closer between that of the Karinya Syncline sediments and upper unit of the Fleurieu Peninsula suggest these units correlates rather than the lower. The minor differences observed may be influences of locally derived clastic input or the aforementioned hydrothermal activity.

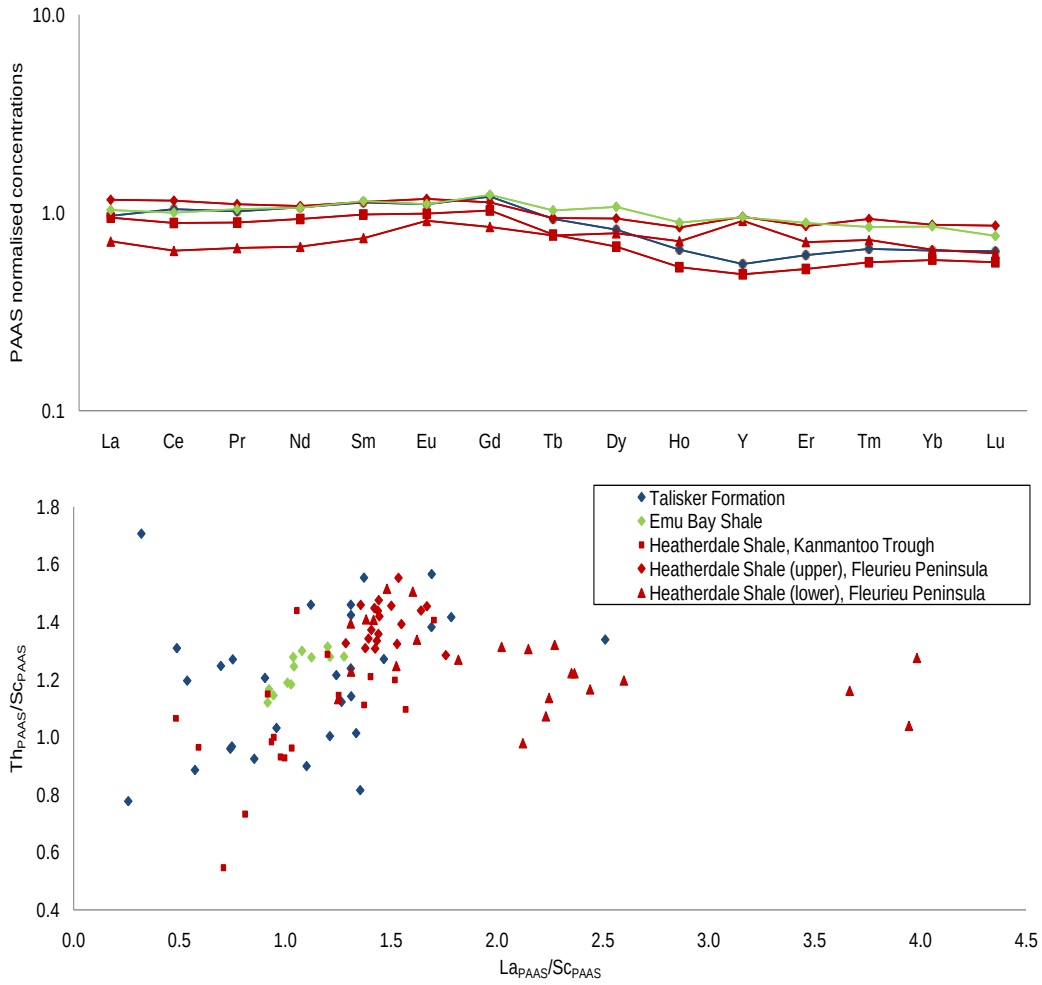

Fig. 6 Averaged REE + Y_{PAAS} distributions (above) and crossplot of Th_{PAAS}/Sc_{PAAS} versus La_{PAAS}/Sc_{PAAS} (below) for the Heatherdale Shale, Emu Bay Shale and Talisker Formation

An upward shift in detrital zircon age distributions has been demonstrated through the Normanville Group and into the Kanmantoo Group (Ireland et al., 1998; Haines et al., 2009; Turner et al., 2011). This transition is possibly being recorded in the aforementioned trace element data with the primary provenance changing progressively through the lower Heatherdale Shale, the upper Heatherdale Shale, the Emu Bay Shale and the Talisker Formation. The resemblance of the Emu Bay Shale to the upper Heatherdale Shale suggests a common input of proximal detrital material from the Gawler Craton,. This supports the opinion that the Emu Bay Shale was sourced locally from the Yorke Peninsula as deposits in a series of localised, deep-water sub-basins in an area of tectonic activity (Nedin, 1995; Flöttmann et al., 1998; Gehling et al., 2011), though the influence of distally sourced detrital material is apparent. The upper Heatherdale Shale units on the Fleurieu Peninsula and in the Karinya Syncline, and the Emu Bay Shale all lie within the range of distribution the Talisker Formation, suggesting a greater influence of the newly developing distal region which was subsequently the primary source of the Kanmantoo Group.

2.5.5 Palaeoenvironmental reconstruction

Plotting the multiple redox proxies against stratigraphic height for each of the three formations sampled (Fig.7) generally reveals internally consistent patterns of variation. Thus, despite individual proxies not assigning the sediment to the same redox state, secular shifts towards oxic or anoxic conditions become more readily apparent.

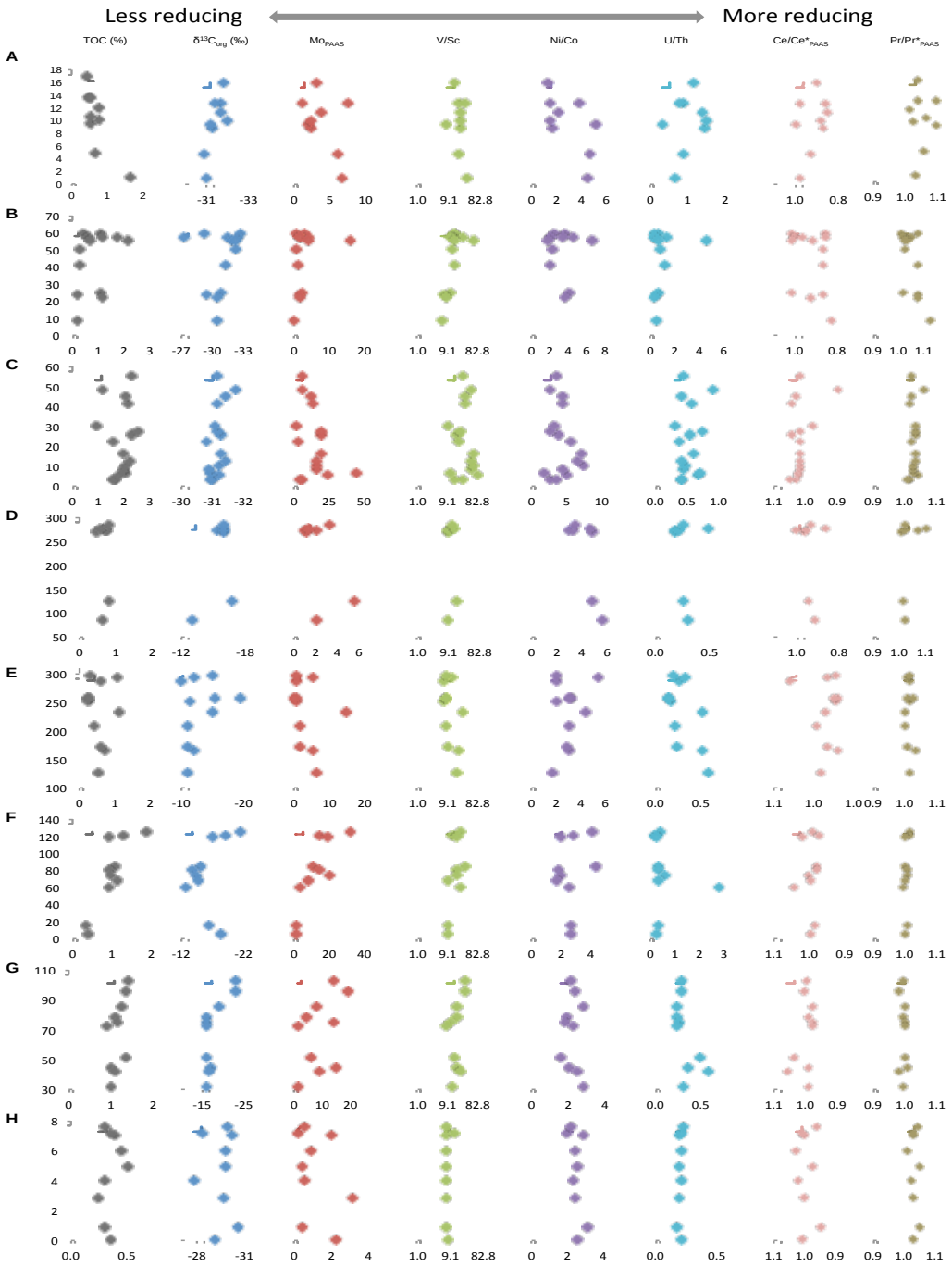

Fig. 7 Multiproxy approach to the assessment of palaeoredox variation within early Cambrian shales of the Stansbury Basin: (A) lower Heatherdale Shale, Carrickalinga Head Creek; (B) lower Heatherdale Shale, Carrickalinga Head Cove; (C) upper Heatherdale Shale, Sellick Hill; (D) Heatherdale Shale, Red Creek north fork; (E)

Heatherdale Shale, Red Creek south fork; (F) Emu Bay Shale, Big Gully; (G) Talisker Formation, Frankton-1 drill hole; (H) Talisker Formation, Frankton-2 drill hole.

2.5.5.1 Heatherdale Shale

The lower Heatherdale Shale sections (Figs. 7A and B) all display a good degree of correlation between the various proxies. There are numerous instances where pronounced excursions highlight short-lived changes to the prevailing suboxic regime. For example, in the Carrickalinga Head Creek section (Fig. 7A) stable dysoxic conditions were interrupted by an oxic event at ~10 m as indicated by decreases in U/Th, Ce/Ce*, V/Sc and Mo_{PAAS} (but seemingly contraindicated by a spike in Ni/Co). At ~57 m height in the Carrickalinga Head Cove section (Fig. 7B), sharp rises in TOC, Mo enrichment, V/Sc, Ni/Co, U/Th and a decrease in Ce/Ce* signal the development of anoxia. This was followed by a rapid change to oxic conditions at ~57.5 m, which coincides with a shift to heavier $\delta^{13}C_{org}$, and a return to dysoxia by ~59 m. The anoxic interval coincides with the presence of phosphate nodules (Carson, 1994), which in turn imply the upwelling of deep, nutrient-rich waters on to the shelf.

In the upper Heatherdale Shale at Sellick Hill (Fig. 7C) the proxies suggest redox conditions fluctuating between dysoxic and anoxic, with evidence of a sustained anoxic event within the lower 20 m of the section and another shorter event at ~25 m. Notwithstanding two periods of somewhat less reducing conditions at ~30 and ~50 m, the high concentrations of pyrite and phosphate (as nodules and stringers) throughout this upper unit, together with its finely laminated or “varved” texture (Carson, 1994), reflect a change towards a generally more stable oxygen-depleted outer shelf setting. Analogous deposits on some modern continental margins (e.g. Namibia, Peru and India) are characterised by a dysoxic seafloor rich in organic detritus derived from

phytoplankton blooms triggered by upwelling currents delivering a rich supply of nutrients to the photic zone (Helly and Levin, 2004; Naqvi et al., 2006; Strauss, 2006). Such conditions are consistent with the increased TOC, lighter $\delta^{13}C_{org}$ and greater enrichment of OM-associated trace metals (e.g. V, Ni, U) shown in Fig. 7C. In the modern analogues, such dysoxia precludes benthic fauna and the attendant bioturbation, while periodic storms or turbidity currents erode the phosphorites into "hiatus concretions" and conglomerates, aerating the waters and allow temporary colonization (Brasier, 1979). Similar episodes would explain the concoryphid trilobites and well-preserved arthropod trails in a tuff layer found within the upper Heatherdale Shale (Jago et al., 1984; Jenkins and Hasenohr, 1989).

Similar patterns of secular variation are observed in the northernmost sections of the Heatherdale Shale at Red Creek in the Karinya Syncline (Figs. 7D and E). Here the higher metamorphic grade of the formation accounts for both the anomalously heavy isotopic composition of its OM ($\delta^{13}C_{org} > -20‰$) and, in part, its lower organic richness (TOC <1%). The greater sampling frequency of the south fork section (Fig. 7E) reveals three excursions towards more reducing conditions (viz. at ~165, ~230 and ~295 m from a generally suboxic regime. The higher detrital input and lack of carbonate and phosphate nodules observed at this locality (Turner, 1994) suggests an inner shelf environment with the basin shallowing up section towards the contact with the Kanmantoo Group (Fig. 2). This is consistent with the correlation of the Red Creek section to the upper Heatherdale Shale on Fleurieu Peninsula, as more oxic conditions would be expected in the shallower shelfal environment.

2.5.5.2 Emu Bay Shale

The redox status of the richly fossiliferous basal Emu Bay Shale (Fig. 7F) remained relatively constant during its deposition. Its uniformly low TOC values are consistent with the V/Sc, Ni/Co and U/Th proxies in indicating oxic conditions and Mo enrichment,where exhibited, is only slight. Additional data acquired by Nedin (1995) confirm these oxic signatures, which seem to be at odds with the exceptional preservation of the fauna within this Lagerstätte. Features of the latter include intact gut and muscle tissues and eyes (Garcia-Bellido et al., 2009; Lee et al., 2011). In addition, the fossils show little evidence of predation or scavenging, whilst their host shale lacks burrows or other signs of bioturbation, a scenario commonly ascribed to prevailing anoxia at the sea floor. However, using the same trace element proxies, Powell et al. (2003) interpreted the depositional environments of two other Cambrian Lagerstätten, the Burgess Shale Formation of British Columbia and the Kinzers Formtion of Pennsylvania, to have been oxic, with localised ponds of anoxic bottom water and bacterial mats maintaining a sharp redox boundary at the sediment-water interface. The latter provided the ‘ex-aerobic’ conditions necessary for the observed authigenic replication of soft tissues and organs. The basal Emu Bay Shale emulates these characteristics and thus is interpreted as having been deposited under an oxic water column. Geochemical evidence for the presence of a coccoid cyanobacterium (Hall et al., 2011), together with the observation in thin section of irregular laminae of organic matter interpreted as remnant cyanobacterial mats, supports this conclusion (see McKirdy et al., 2011 for a comprehensive review of the palaeoredox status of the Emu Bay Shale Lagerstätte).

2.5.5.3 Talisker Formation

The two sections of the Talisker Formation (Fig. 3) show strong covariance of TOC, $\delta^{13}C_{org}$, Mo_{PAAS}, V/Sc and Ni/Co (Figs. 7G and H) . Calcareous siltstone and shale at the base of the formation passes upward into pyritic shale, reflecting the transgressive nature of the formation (Turner, 1994; Gum, 1998). Accordingly, at both sites there is an overall trend towards more reducing conditions up section. At Frankton-1 this trend is capped by a rapid shift towards higher Eh. Similar excursions are exhibited by Mo_{PAAS} at 43 and 72 m height in the Frankton-2 section. The consensus of the redox proxies is that the Talisker shales were deposited beneath suboxic bottom waters; the high value of U/Th at 62 m in Frankton-1 is clearly anomalous. The high concentrations of pyrite in these shales might reasonably be regarded as implying euxinic conditions at the sea floor. However, high concentrations of dissolved sulfide in anoxic pore waters commonly occur at or within a few millimetres of the sediment–water interface in many shallow sea-floor environments, above which fully oxic conditions prevail (Piper and Calvert, 2009). Moreover, the hydrothermal fluids which sourced the local SedEx mineralisation (Gum, 1998) could have supplied sufficient hydrogen sulfide to create localised euxinic conditions, as is believed to have happened on the Yangtze Platform, South China (Och et al., 2012).

2.5.5.4 Global paleogeographic context

During the early Cambrian, South Australia was situated in a northerly low latitude position (Brock et al., 2000). The juxtaposition of eastern Antarctica to the current southern margin of Australia is also well substantiated. Together they are thought to have formed the eastern margin of Gondwana. Unfortunately, geochemical studies of the siliciclastic sequences from the lower Palaeozoic Byrd Group in Antarctica have

focused on detrital zircons; no trace element and REE data are available for comparison with the data presented herein. In fact, there is a notable scarcity of such data from coeval sequences globally. Nevertheless, the trace element and REE distributions of slightly older sequences in South China (Jiang et al., 2006; Guo et al., 2007) are very similar to those of the South Australian units; the similarity of the upper Guojiaba Formation and the Heatherdale Shale being especially striking (Fig. 8). The Niutitang, Jiumenchong and Guojiaba Formations are of Tommotian and Atdabanian age (Steiner et al., 2007, Wang et al., 2012), with the upper Guojiaba Formation equivalent to the Fork Tree Limestone that is overlain by the Heatherdale Shale (Fig. 2). This implies that the same (or similar) oceanic seawater chemistry is recorded in the black shales of the Stansbury Basin and South China. Palaeomagnetic studies show that the South China Block (SCB) was on a similar northern tropical palaeolatitude to South Australia during the early Cambrian (Rui and Piper, 1997; Yang et al., 2004). Li et al. (2008) proposed that the SCB lay to the east of Australia in the paleo-Pacific Ocean, though the conventional interpretation locates it in the paleo-Asian Ocean to the west of Australia (Meert and Lieberman, 2006). If the SCB did lie to the east of Australia, this could explain the geochemical similarity of the aforementioned Chinese and South Australian shales, though much more rigorous testing would be required to substantiate this link. Recent provenance studies (Dong et al., 2011; Hofmann et al., 2011; Clark et al., 2012) and reviews of biostratigraphy (Steiner et al., 2007; McKenzie et al., 2011) all strongly correlate the SCB with Indian Gondwana, thus favouring the conventional paleogeographical positioning alongside Western Australia. If this is correct, our comparable data signify that the same source area fed detrital material into the Stansbury Basin and the Yagtze Platform. If the provenance of the South Australian deposits is to the west along the Prydz-Leeuwin

Belt and across eastern Antarctica, detrital material shedding from the other side of the orogenic belt would provide similar distributions of rare earth elements to both regions. The analogous basinal environments with oceanic upwelling, hydrothermal activity and a common source of siliciclastic sediment appear to have led to the homogeneous seawater trace and rare earth element chemistry of the Palaeo-Pacific and Asian Oceans.

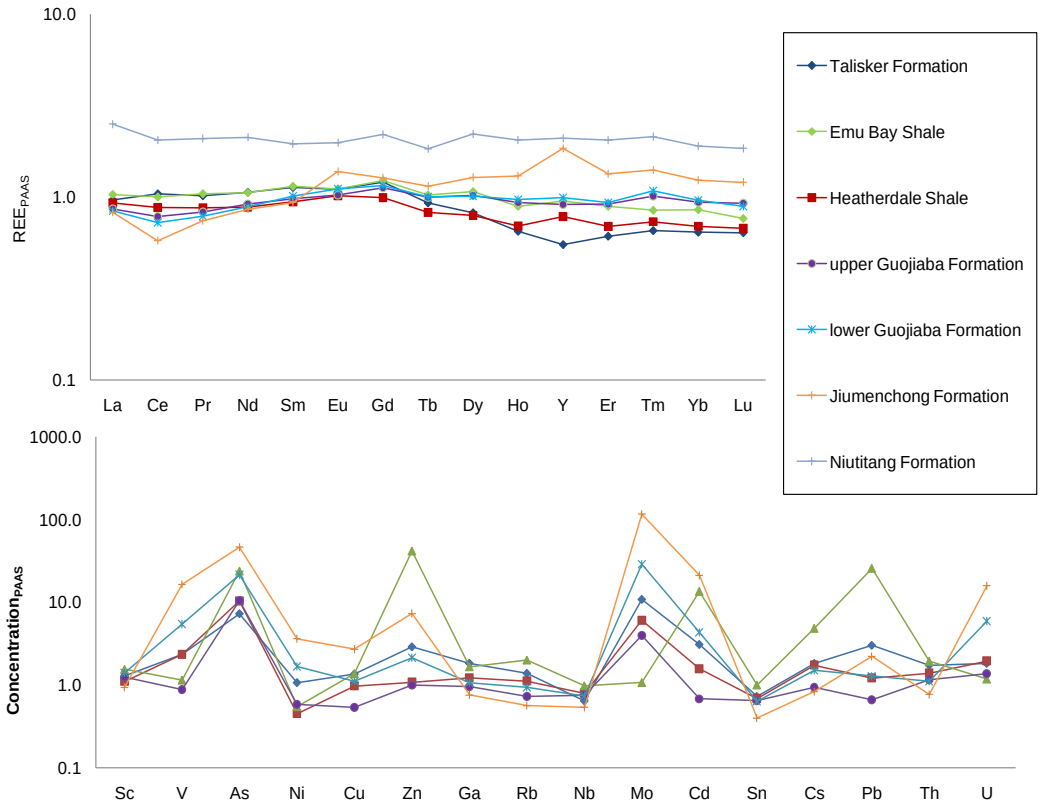

Fig. 8 Comparison of South Australian REE+Y (above) and trace element (below) distributions with those of the Niutitang, Jiumenchong and Guijiaba Formations, Yangtze Platform, South China (after Jiang et al., 2006; Guo et al., 2007).

2.6. Conclusions

A multiproxy approach employing trace element and REE distributions, TOC, bulk isotopic signatures and stratigraphic records, in conjunction with sedimentological information, provides a powerful tool for interpreting marine palaeoenvironmental conditions. Individual proxies, considered in isolation, may give rise to conflicting interpretations of depositional history. However, with multiple proxies in play, patterns emerge from the data allowing changes in factors such as primary productivity, ocean circulation, redox state and sediment source to be inferred more reliably. This was the rationale of the present investigation of carbonaceous shales from three early Cambrian formations in the Stansbury Basin, South Australia.

Deposition of the oldest formation, the variously phosphatic and pyritic Heatherdale Shale, occurred in an outer shelf setting subject to oceanic upwelling where the prevailing redox state of the bottom water was dysoxic, with periodic fluctuations into both fully oxic and anoxic conditions. Over time, the depocentre became progressively more reducing. Further south, the Emu Bay Shale lägerstatte was deposited in a restricted marine embayment beneath a fully oxic water column, with microbial mats providing a sharp redox boundary at the sediment-water interface. Like the Heatherdale Shale, the pyritic Talisker Formation (the youngest unit studied) displays evidence of increasing oxygen depletion up-section, with indications of possible euxinia in its uppermost portion. The observed secular decline in $\delta^{34}S_{pyr}$ is entirely consistent with this change in palaeoceanographic conditions, rather than the diagenetic or metamorphic overprint suggested by previous low-resolution studies. These interpretations of palaeoredox status correspond well with the documented sedimentology of the formations.

The strong covariance between TOC and normalised Mo, V and U in the black shales of all three formations reflects the evolving bioproductivity and oxygenation of the early Cambrian ocean. The Talisker Formation displays a Mo/TOC gradient steeper than those of the Heatherdale and Emu Bay shales, suggesting that it was deposited under more oxygen-depleted conditions. The Heatherdale Shale exhibits a comparatively pronounced enrichment in U, a propable indication of increased primary productivity.

The trace element and REE distributions of the three formations suggest that the transition from the late Normanville Group into the Kanmantoo Group was accompanied by a major change in sediment provenance. This finding is corroborated by previously published detrital zircon dates. Of even greater significance is the fact these elemental distributions closely match those of early Cambrian black shales on the Yangtze Platform . That essentially the same seawater trace element chemistry is recorded in South Australia and South China may have important implications for the early Cambrian palaeogeography of Gondwana.

2.7. Acknowledgements

This study forms part of a project on the Cambrian hydrocarbon potential of the Stansbury and Officer Basins, funded by Primary Industries and Resources South Australia (PIRSA). PAH is in receipt of an Australian Postgraduate Award, while JBJ acknowledges funding from an Australian Research Council Linkage Grant (LP0774959), and additional financial support from Beach Energy Ltd and the South Australian Museum. Paul and Carmen Buck are thanked for allowing access to the Emu Bay Shale. Gareth Harriman (GHGeochem Ltd) and Keith Hall (Hall Analytical Laboratories Ltd) are thanked for their support with the isotopic analyses. The contributions of PAH, DMMcK, GPH and AC to this paper form TRaX Record ###.

2.8. References

Abanda, P.A., Hannigan, R.E., 2006. Effect of diagenesis on trace element partitioning in shales. Chemical Geology 230, 42–59.

Adelson, J.M., Helz, G.R., Miller, C.V., 2001. Reconstructing the rise of recent coastal anoxia; molybdenum in Chesapeake Bay sediments. Geochimica et Cosmochimica Acta 65, 237–252.

Alexander, E.M., Gravestock, D.I., 1990. Sedimentary facies in the Sellick Hill formation, Fleurieu Peninsula, South Australia. In: Jago, J.B., Moore, P.S., (Eds.), The Evolution of a Late Precambrian-Early Palaeozoic Rift Complex: The Adelaide Geosyncline. Geological Society of Australia, Special Publication 16, 269–289.

Algeo, T.J., Lyons, T.W., 2006. Mo–total organic carbon covariation in modern anoxic marine environments: Implications for analysis of paleoredox and paleohydrographic conditions. Paleoceanography 21, 1016.

Alvaro J.J. & Debrenne F., 2010. The great atlasian reef complex: An early Cambrian subtropical fringing belt that bordered West Gondwana. Palaeogeography, Palaeoclimatology, Palaeoecology 294, 120–132.

Anbar, A.D., Knoll, A.H., 2002. Proterozoic ocean chemistry and evolution: A bioinorganic bridge? Science 297, 1137–1142.

Andersson, P.O.D., Johansson, A., Kumpulainen, R.A., 2003. Sm–Nd isotope evidence for the provenance of the Skoorsteenberg Formation, Karoo Supergroup, South Africa. Journal of African Earth Sciences 36, 173–183.

Babcock, L.E., 2003. Trilobites in Paleozoic predator–prey systems, and their role in reorganization of early Paleozoic ecosystems. In: Kelley, P.H., Kowalewski, M., Hansen, T.A. (Eds.), Predator–Prey Interactions in the Fossil Record. Kluwer Academic/Plenum Publishers, New York, pp. 55–92.

Banner, J.L., Hanson, G.N., 1990. Calculation of simultaneous isotopic and trace-element variations during water–rock interaction and with applications to carbonate diagenesis. Geochimica et Cosmochimica Acta 54, 3123–3137.

Bhatia, M.R., Crook, K.A.W., 1986. Trace element characteristics of greywackes and tectonic setting discrimination of sedimentarynbasins. Contributions to Mineralogy and Petrology 92, 181–193.

Brasier M.D., 1992. Towards a carbon isotope stratigraphy of the Cambrian System: potential of the Great Basin succession. In: Hailwood, E.A., Kidd, R.B. (Eds.), High Resolution Stratigraphy. Geological Society Special Publication, 70, 341–350.

Brasier, M.D., 1992. Background to the Cambrian explosion. Journal of Geological Society London 149, 585–587.

Brasier, M.D., Hewitt, R.A., 1979. Environmental setting of fossiliferous rocks from the uppermost Proterozoic - lower Cambrian of central England. Palaeogeography, Palaeoclimatology, Palaeoecology 27, 35–57.

Brennan, S.T., Lowenstein, T.K., Horita, J., 2004. Seawater chemistry and the advent of biocalcification. Geology 32, 473–476.

Brock, G. A., Engelbretsen, M.J., Jago, J.B., Kruse, P.D., Laurie, J.R., Shergold, J.H., Shi, G.R., Sorauf, J.E., 2000. Palaeobiogeographic affinities of Australian Cambrian faunas. Memoir of the Association of Australasian Palaeontologists 23, 1–61.

Burrett, C., Richardson, R., 1980. Trilobite biogeography and Cambrian tectonic models. Tectonophysics 63, 155–192.

Calvert, D.E., Pedersen, T.F., 1993. Geochemistry of recent oxic and anoxic marine sediments: implications for the geological record. Marine Geology 113, 67–88.

Canfield, D. E., Farquhar, J., 2009. Animal evolution, bioturbation, and the sulfate concentration of the oceans. Proceedings of the National Academy of Sciences of the United States of America 106, 8123–8127.

Canfield, D. E., Poulton, S. W., Narbonne, G. M., 2007. Late-Neoproterozoic deep-ocean oxygenation and the rise of animal life. Science 315, 92–95.

Canfield, D.E., 1998. A new model for Proterozoic ocean chemistry. Nature 396, 450–453.

Canfield, D.E., 2005. The early history of atmospheric oxygen. Annual Reviews of Earth and Planetary Sciences 33, 1–36.

Canfield, D.E., Olesen, C.A., Raymond, P.C., 2006. Temperature and its control of isotope fractionation by a sulphate-reducing bacterium. Geochimica et Cosmochimica Acta 70, 548–561.

Canfield, D.E., Teske, A., 1996. Late Proterozoic rise in atmospheric oxygen concentration inferred from phylogenetic and sulfur-isotope studies. Nature 382, 127–132.

Carson M., 1994. The stratigraphy, sedimentology and thermal history of the Early Cambrian Heatherdale Shale, Fleurieu Peninsula. Unpublished Hons thesis, University of Adelaide.

Chen, D., Wang, J., Qing, H., Yan, D., Li, R., 2009. Hydrothermal venting activities in the Early Cambrian, South China: petrological, geochronological and stable isotopic constraints. Chemical Geology 258, 168–181.

Clark, C., Kinny, P.D., Harley, S.L., 2012. Sedimentary provenance and age of metamorphism of the Vestfold Hills, East Antarctica: Evidence for a piece of Chinese Antarctica? Precambrian Research 196-197, 23-45.

Claypool, G.E., Holster, W.T., Kaplan, I.R., Sakai, H., Zak, I., 1980. Age curves of sulfur and oxygen isotopes in marine sulphate and their mutual interpretation. Chemical Geology 28, 199–206.

Collins A.S., Pivarevsky S.A., 2005. Amalgamating Eastern Gondwana: The Evolution Of The Circum-Indian Orogens. Earth-Science Reviews 71, 229–270.

Collins, A.S., Kröner, A., Fitzsimons, I.C.W., Razakamanana, T., 2003. Detrital footprint of the Mozambique ocean: U–Pb SHRIMP and Pb evaporation zircon geochronology of metasedimentary gneisses in eastern Madagascar. Tectonophysics 375, 77–99.

Condie, K.C., Des Marais, D.J., Abbott, D., 2001. Precambrian superplumes and supercontinents: a record in black shales, carbon isotopes, and paleoclimates? Precambrian Research 106, 239–260.

Cooper, J.A., Jenkins, R.J, Compston, W., Williams, I.S., 1992. Ion-probe zircon dating of amid-Early Cambrian tuff in South Australia. Journal of the Geological Society of London 149, 185–192.

Cooper, R.A., Sadler, P.M., 2004. The Ordovician Period. In Gradstein, F., Ogg, J., Smith, A. (Eds.), A Geologic Time Scale 2004. Cambridge University Press, Cambridge, pp. 165–187.

Cremonese, L., Shields-Zhou, G., Struck, U., Ling, H.-F., Och, L., Chen, X., Li, D., 2012. Marine biogeochemical cycling during the early Cambrian constrained by a nitrogen and organic carbon isotope study of the Xiaotan section, South China. Precambrian Research., doi:10.1016/j.precamres.2011.12.004

Daily, B., Milnes A.R., 1971. Stratigraphic notes on Lower Cambrian fossiliferous metasediments between Campbell Creek and Tunkalilla Beach in the type section of the Kanmantoo Group, Fleurieu Peninsula, South Australia. Transactions of the Royal Society of South Australia 95, 199–214.

Daily, B., Milnes A.R., 1973. Stratigraphy, structure and metamorphism of the Kanmantoo Group (Cambrian) in its type section east of Tunkalilla Beach, South Australia. Transactions of the Royal Society of South Australia 97, 199–214.

Daily, B., Milnes, A.R., Twidale, C.R., Bourne, J.A., 1979. Geology and Geomorphology. In: Tyler, M.J., Ling, J.K., Twidale, C.R. (Eds.), Natural History of Kangaroo Island. Royal Society of South Australia, Adelaide, pp. 1–38.

Debrenne F., Gravestock D., 1990. Archaeocyatha from the Sellick Hill Formation and Fork Tree Limestone on Fleurieu Peninsula, South Australia. In: Jago J.B., Moore P.J. (Eds), The evolution of a late Precambrian-early Palaeozoic rift complex: The Adelaide Geosyncline. Geological Society of. Australia, Special. Publication 16, 290–309.

Derry, L.A., Kaufman, A.J., Jacobsen, S., 1992. Sedimentary cycling and environmental change in the Late Proterozoic: evidence from stable and radiogenic isotopes. Geochimica et Cosmochimica Acta 56, 1317–1329.

Dong, X., Zhang, Z., Santosh, M., Wang, W., Yu, F., Liu, F., 2011. Late Neoproterozoic thermal events in the northern Lhasa terrane, south Tibet: Zircon chronology and tectonic implications. Journal of Geodynamics 52, 389–405.

Dyson I. A., Gatehouse C. G., Jago J. B., 1996. Sequence stratigraphy of the Talisker

Calc-siltstone and lateral equivalents in the Cambrian Kanmantoo Group. Geological Survey of South Australia Quarterly Geological Notes 129, 27–41.

Erwin, D.H., Laflamme, M., Tweedt, S.M., Sperling, E.A., Pisani, D., Peterson, K.J., 2011. The Cambrian conundrum: early divergence and later ecological success in the early history of animals. Science 334, 1091–1097.

Felitsyn, S., Morad, S., 2002. REE patterns in latest Neoproterozoic–early Cambrian phosphate concretions and associated organic matter. Chemical Geology 187, 257–265.

Fike D.A., Grotzinger J.P., Pratt L.M., Summons R.E., 2006. Oxidation of the Ediacaran Ocean. Nature 444, 744–747.

Fike, D.A., Grotzinger, J.P., 2008. A paired sulfate-pyrite $\delta^{34}S$ approach to understanding the evolution of the Ediacaran–Cambrian sulfur cycle. Geochimica et Cosmochimica Acta 72, 2636–2648.

Flöttmann, T., Haines, P.W., Cockshell C.D., Preiss, W. V., 1998. Reassessment of the seismic stratigraphy of the Early Palaeozoic Stansbury Basin, Gulf St Vincent, South Australia. Australian Journal of Earth Sciences 45, 547–557.

Flöttmann, T., James, P., 1997. Influence of basin architecture on the style of inversion and fold-thrust belt tectonics - the southern Adelaide Fold-Thrust Belt. South Australia by Journal Of Structural Geology 19, 1093–1110.

Flöttmann, T., James, P.R., Menpes, R., Cesare, P., Twining, M., Fairclough, M., Randabell, J., Marshak, S., 1995. The structure of Kangaroo Island (South Australia): strain and kinematic partitioning during Delamerian basin and platform reactivation. Australian Journal of Earth Sciences 42, 35-49.

Foden, J.D., Elburg, M. A., Dougherty-Page, J., Burtt, A., 2006. The timing and duration of the Delamerian Orogeny: correlation with the Ross Orogen and implications for Gondwana assembly. Journal of Geology 114, 189–210.

Foden, J.D., Sandiford, M., Dougherty-Page, J., Williams, I., 1999. The geochemistry and geochronology of the Rathjen Gneiss: implications for the early techtonic evolution of the Delamerian Orogen. Australian Journal of Earth Sciences 46, 377–389.

Foden, J.D., Turner, S.P., Morrison, R., 1990. The tectonic implications of the Delamerian magmatism in South Australia and western Victoria. In: Jago J. B., Moore, P.S., (Eds.), The evolution of a Late Precambrian–Early Palaeozoic Rift Complex: The Adelaide Geosyncline. Geological Society of Australia Special Publication 16, 483–495.

García-Bellido, D.C., Paterson, J.R., Edgecombe, G.D., Jago, J.B., Gehling, J.G., Lee, M.S.Y., 2009. The bivalved arthropods Isoxys and Tuzoia with soft-part preservation from the Lower Cambrian Emu Bay Shale Lagerstätte (Kangaroo Island, Australia). Palaeontology 52, 1221–1241.

Gatehouse, C.G., Jago, J.B., Cooper, B.J., 1990. Sedimentology and stratigraphy of the Carrickalinga Head Formation (low stand fan to high stand systems tract), Kanmantoo Group, South Australia. Geological Society of Australia Special Publication 16, 351–368.

Gatehouse, C.J., Jago, J.B., Clough, B.J., McCulloch, A.J., 1993. The Early Cambrian volcanics from Red Creek, Eastern Mt Lofty Ranges, South Australia. Transactions of the Royal Society of South Australia 117, 57–66.

Gehling J.G., Jago J.B., Paterson J.R., García-Bellido D.C., Edgecombe G.D., 2011. The geological context of the lower Cambrian (Series 2) Emu Bay Shale Lagerstätte and adjacent stratigraphic units, Kangaroo Island, South Australia. Australian Journal of Earth Sciences 58, 243–257.

Gill, B.C., Lyons, T.W., Young, S.A., Kump, L.R., Knoll, A.H., Saltzman, M.R., 2011. Geochemical evidence for widespread euxinia in the Late Cambrian ocean. Nature 69, 80–83.

Goldberg, T., Poulton, S.W., Strauss, H., 2005. Sulfur and oxygen isotope signatures of late Neoproterozoic to early Cambrian sulphate, Yangtze Platform, China: diagenetic constraints and seawater evolution. Precambrian Research 137, 223–241.

Goldberg, T., Strauss, H., Guo, Q., Liu, C., 2007. Reconstructing marine redox conditions for the early Cambrian Yangtze Platform: Evidence from biogenic sulfur and organic carbon isotopes. Palaeogeography, Palaeoclimatology, Palaeoecology 254, 175–193.

Goodge, J.W., Williams, I.S., Myrow, P., 2004. Provenance of Neoproterozoic and lower Paleozoic siliciclastic rocks of the central Ross Orogen, Antarctica: detrital record of rift-, passive- and active-margin sedimentation. Geological Society of America Bulletin 116, 1253–1279.

Gorjan, P., Walter, M.R., Swart, R., 2003. Global Neoproterozoic (Sturtian) post-glacial sulfide-sulfur isotope anomaly recognised in Namibia. Journal of African Earth Sciences 36, 89–98

Gravestock, D.I., 1995. Early and Middle Palaeozoic. The Geology of South Australia, Vol. 2: The Phanerozoic. Geological Survey of South Australia Bulletin 54, 3–61.

Gravestock, D.I., Gatehouse, C.G., 1995. Stansbury Basin. In: Drexel J. F., Preiss W. V. (Eds.), The Geology of South Australia, Vol. 2: The Phanerozoic. Geological Survey of South Australia Bulletin 54, 5–19.

Gum, J.C., 1998. The sedimentology, sequence stratigraphy and mineralisation of the Silverton Subgroup, South Australia. PhD thesis, University of South Australia, Adelaide (unpublished).

Guo, Q., Shields, G.A., Liu, C., Strauss, H., Zhu, M., Pi, D., Goldberg, T., Yang, X., 2007. Trace element chemostratigraphy of two Ediacaran–Cambrian successions in South China: Implications for organosedimentary metal enrichment and silicification in the Early Cambrian. Palaeogeography, Palaeoclimatology, Palaeoecology 254, 194–216.

Guo, Q., Strauss, H., Liu, C., Zhao, Y., Yang, X., Peng, J. Yang, H., 2010. A negative carbon isotope excursion defines the boundary from Cambrian Series 2 to Cambrian Series 3 on the Yangtze Platform, South China. Palaeogeography, Palaeoclimatology, Palaeoecology 285, 143-151.

Haines, P.W., Flöttmann, T., Gum, J.C., Jago, J.B., Gatehouse, C.G., 1996. Integrated approach to the reinterpretation of the Cambrian Kanmantoo Group type section, South Australia. Geological Society of Australia Abstracts 41, 77.

Haines, P.W., Jago, J.B., Gum, J.C., 2001. Turbidite deposition in the Cambrian Kanmantoo Group, South Australia. Australian Journal of Earth Sciences 48, 465–478.

Haines,P.W., Turner, S.P., Foden, J., Jago, J., 2009. Isotopic and geochemical characterization of the Cambrian Kanmantoo Group, South Australia: implications for stratigraphy and provenance. Australian Journal of Earth Sciences 56, 1095–1110.

Hall, P.A., McKirdy, D.M., Halverson, G.P., Jago, J.B., Gehling, J.G., 2011. Biomarker and isotopic signatures of an early Cambrian Lagerstätte in the Stansbury Basin, South Australia. Organic Geochemistry 42, 1324–1330.

Halverson, G. P. and Hurtgen, M. T., 2007. Ediacaran growth of the marine sulfate reservoir. Earth and Planetary Science Letters 263, 32–44.

Halverson, G.P., Hurtgen, M.T., Porter, S.M., Collins, A.S., 2009. Neoproterozoic-Cambrian biogeochemical evolution. In: Gaucher C., Sial A.N., Halverson G.P., Frimmel H.E. (Eds.), Developments in Precambrian Geology 16, 351–365.

Halverson, G.P., Wade, B.P., Hurtgen, M.T., Barovich, K.M., 2010. Neoproterozoic chemostratigraphy. Precambrian Research 182, 4, 337–350.

Hatch, J.R., Leventhal, J.S., 1992. Relationship between inferred redox potential of the depositional environment and geochemistry of the Upper Pennsylvanian (Missourian) Stark Shale Member of the Dennis Limestone, Wabaunsee County, Kansas, U.S.A. Chemical Geology 99,,65–82.

Hayes J.M., Kaplan I.R., Wedeking K.W., 1983. Precambrian organic geochemistry - preservation of the record. In: Schopf J.W. (Ed.), Earth's Earliest Biosphere, Its Origin and Evolution. Princeton University Press, New Jersey, pp. 93–134.

Hayes, J.M., Strauss, H., Kaufman, A.J., 1999. The abundance of C in marine organic carbon and isotopic fractionation in the global biogeochemical cycle of carbon during the past 800 ma, Chemical Geology 161, 103–125.

Helly J.J., Levin L.A., 2004. Global distribution of naturally occurring marine hypoxia on continental margins. Deep-Sea Research Part 1: Oceanographic Research Papers 51, 1159-1168.

Helz, G.R., Miller, C.V., Charnock, J.M., Mosselmans, J.L.W., Pattrick, R.A.D., Garner, C.D., Vaughan, D.J., 1996. Mechanisms of molybdenum removal from the sea and its concentration in black shales: EXAFS evidences. Geochimica et Cosmochimica Acta 60, 3631–3642

Hofmann, M., Linnemann, U., Rai, V., Becker, S., Gärtner, A., Sagawe, A., 2011. The India and South China cratons at the margin of Rodinia - Synchronous Neoproterozoic magmatism revealed by LA-ICP-MS zircon analyses. Lithos 123, 176–187.

Holser, W., Kaplan, I., 1966. Isotope geochemistry of sedimentary sulfates. Chemical Geology 1, 93–135.

Hurtgen, M.T., Arthur, M.A., Suits, N.S., Kaufman, A.J., 2002. The sulfur isotopic composition of Neoproterozoic seawater sulfate: implications for a snowball Earth? Earth and Planetary Science Letters 203, 413–430.

Ireland, T.R., Flöttmann T., Fanning, C.M., Gibson, G.M., Preiss, W.V., 1998. Development of the Early Paleozoic Pacific margin of Gondwana from detrital zircon ages across the Delamerian Orogen. Geology 26, 243–246.

Ishikawa, T., Ueno, Y., Shu, D., Li, Y., Han, J., Guo, J., Yoshida, N., Komiya, T., 2011. Irreversible change of the oceanic carbon cycle in the earliest Cambrian: High-resolution organic and inorganic carbon chemostratigraphy in the Three Gorges area, South China. Precambrian Research, doi:10.1016/j.precamres.2011.10.004

Jago J.B., Sun X., Zang W., 2002. Correlation within early Palaeozoic basins of eastern South Australia. PIRSA Report Book 2002/033.

Jago, J.B., Daily, B., von der Borch, C.C., Cernovskis, A., Saunders, N., 1984. First reported trilobites from the Lower Cambrian Normanville Group, Fleurieu Peninsula, South Australia. Royal Society of South Australia. Transactions 108, 207–211.

Jago, J.B., Dyson, I.A., Gatehouse, C.G., 1994. The nature of the sequence boundary between the Normanville and Kanmantoo Groups on Fleurieu Peninsula, South Australia. Australian Journal of Earth Sciences 41, 445–453.

Jago, J.B., Gatehouse C.G., 2009. The type section of the Cambrian Backstairs Passage Formation, Kanmantoo Group, South Australia. Transactions of the Royal Society of South Australia 133, 150–163.

Jago, J.B., Gehling, J.G., Paterson, J.R., Brock, G.A., Zang, W.L., 2012. Cambrian stratigraphy and biostratigraphy of the Flinders Ranges and the north coast of Kangaroo Island, South Australia. Episodes 35, 247-255.

Jago, J.B., Gum, J.C., Burtt, A.C., Haines, P.W., 2003. Stratigraphy of the Kanmantoo Group: a critical element of the Adelaide Fold Belt and the Palaeo-Pacific plate margin, Eastern Gondwana. Australian Journal of Earth Sciences 50, 343–363.

Jago, J.B., Zang, W., Sun, X., Brock, G.A., Paterson, G.A., Skovsted, C., 2006. A review of the Cambrian biostratigraphy of South Australia. Palaeoworld 15, 69–88.

James N.P., Gravestock D.I., 1990. Lower Cambrian shelf and shelf margin buildups, Flinders Ranges, South Australia. Sedimentology 37, 455–480.

Jenkins, R. J.; Cooper, J. C.; and Compston, W. 2002. Age and biostratigraphy of Early Cambrian tuffs from SE Australia and southern China. Journal of the Geological Society of London 159, 645–658.

Jenkins, R.J.F., Hasenohr, P., 1989. Trilobites and their trails in a black shale: Early Cambrian of the Fleurieu Peninsula, South Australia. Transactions of the Royal Society of South Australia 113, 195–203.

Jiang, S.Y., Zhao, H.X., Chen, Y.Q., Yang, T., Yang, J.H., Ling, H.F., 2007. Trace and rare earth element geochemistry of phosphate nodules from the lower Cambrian black shale sequence in the Mufu Mountain of Nanjing, Jiangsu province, China. Chemical Geology 244, 584–604.

Johnston, D.T., Farquhar, J., Canfield, D.E., 2007. Sulfur isotope insight into microbial sulphate reduction: When microbes meet models. Geochimica et Cosmochimica Acta 71, 3929–3947.

Jones, B., Manning, D.A.C., 1994. Comparison of geochemical indices used for the interpretation of palaeoredox conditions in ancient mudstones. Chemical Geology 111, 111–129.

Kampschulte, A., Strauss, H., 2004. The sulfur isotopic evolution of Phanerozoic seawater based on the analysis of structurally substituted sulfate in carbonates. Chemical Geology 204, 255–286.

Kelsey, D.E., Wade, B.P., Collins, A.S., Hand, M., Sealing, C.R., Netting, A. 2008. Discovery of a Neoproterozoic basin in the Prydz belt in East Antarctica and its implications for Gondwana assembly and ultrahigh temperature metamorphism. Precambrian Research 161, 3-4, 355–388

Kennedy, M.J., Droser, M., Mayer, L.M., Pevear, D.R., Mrofka, D., 2008. Late Precambrian Oxygenation; Inception of the Clay Mineral Factory. Science 311, 1446-1449.

Kennedy, M.J., Pevear, D.R., Hill, R.J., 2002. Mineral surface control of organic carbon in black shale. Science 295, 657–660.

Kennedy, M.J., Wagner, T., 2011. Clay mineral continental amplifier for marine carbon sequestration in a greenhouse ocean. Proceedings of the National Academy of Sciences of the United States of America 108, 9776–9781.

Kidder, D.L., Krishnaswamy, R., Mapes, R.H., 2003. Elemental mobility in phosphatic shales during concretion growth and implications for provenance analysis. Chemical Geology 198, 335–353.

Kimura, H., Watanabe, Y., 2001. Oceanic anoxia at the Precambrian-cambrian boundary. Geology 29, 11, 995–998.

Knoll, A., Hayes, J., Kaufman, A., Swett, K., Lambert, I., 1986. Secular variation in carbon isotope ratios from upper Proterozoic successions of Svalbard and east Greenland. Nature 321, 832–837.

Lee, M.S.Y., Jago, J.B., García-Bellido, D.C., Edgecombe, G.D., Gehling, J.G., Paterson, J.R., 2011. Modern optics in exceptionally preserved eyes of Early Cambrian arthropods from Australia. Nature 474, 631–634.

Lehmann, B., Nägler, T.F., Holland, H.D., Wille, M., Mao, J., Pan, J., Dulski, P., 2007. Highly metalliferous carbonaceous shale and early Cambrian seawater. Geology 35, 403–406.

Li, Z.X., Bogdanova, S.V., Collins, A.S., Davidson, A., De Waele, B., Ernst, R.E., Fitzsimons, I.C.W., Fuck, R.A., Gladkochub, D.P., Jacobs, J., Karlstrom K.E., Lu, S., Natapovm, L.M., Pease, V., Pisarevsky, S.A., Thrane, K., Vernikovsky, V., 2008. Assembly, configuration, and break-up history of Rodinia: A synthesis. Precambrian Research 160, 179–210.

Lindsay, J.F., 2002. Supersequences, superbasins, supercontinents - evidence from the Neoproterozoic basins of Central Australia. Basin Research 14, 204–223.

Lindsay, J.F., Kruse, P.D., Green, O.R., Hawkins, E., Brasier, M.D., Cartlidge, J., Corfield R.M., 2005. The Neoproterozoic–Cambrian record in Australia: A stable isotope study. Precambrian Research 15, 113–133.

Maloof, A.C., Halverson, G.P., Kirschvink, J.L., Schrag, D.P., Weiss, B., Hoffman, P.F., 2006. Combined paleomagnetic, isotopic and stratigraphic evidence for true polar wander from the Neoproterozoic Akademikerbreen Group, Svalbard, Geological Society of America Bulletin 118, 1099–1124.

Maloof, A.C., Porter, S.M., Moore, J.L., Dudas, F.O., Bowring, S.A., Higgins, J.A., Fike, D.A., Eddy, M.P., 2010. The earliest Cambrian record of animals and ocean geochemical change. Geological Society of America Bulletin 122, 1731–1774.

Maloof, A.C., Schrag, D.P., Crowley, J.L., Bowring, S.A., 2005. An expanded record of Early Cambrian carbon cycling from the Anti-Atlas Margin, Morocco. Canadian Journal of Earth Sciences 42, 2195–2216.

Mancktelow, N.S., 1990. The structure of the southern Adelaide Fold Belt, South Australia. In: Jago, J.B., Moore, P.S. (Eds.), The Evolution of a late Precambrian-Early Palaeozoic Rift Complex: The Adelaide Geosyncline, Geological Society of Australia Special Publication 16, 369–395

McKenzie, N.R., Hughes, N.C., Myrow, P.M., Choi, D.K., Park, T., 2011. Trilobites and zircons link north China with the eastern Himalaya during the Cambrian. Geology 39, 591–594.

McKirdy D.M., Powell T.G., 1974. Metamorphic alteration of carbon isotopic composition in ancient sedimentary organic matter: new evidence from Australia and South Africa. Geology 2, 591–595.

McKirdy, D.M., 1994. Biomarker geochemistry of the Early Cambrian oil show in Wilkatana-1: implications for oil generation in the Arrowie and Stansbury Basins. PESA Journal 22, 3–17.

McKirdy, D.M., Burgess, J.M., Lemon, N.M., Yu, X., Cooper, A.M., Gostin, V.A., Jenkins, R.J.F., Both, R.A., 2001. A chemostratigraphic overview of the late Cryogenian interglacial sequence in the Adelaide Fold-Thrust Belt, South Australia. Precambrian Research 106, 149–186.

McKirdy, D.M., Hall, P.A., Nedin C., Halverson, G.P., Michaelsen, B.H., Jago, J.B., Gehling, J.G., Jenkins, R.J.F., 2011. Palaeoredox status and thermal alteration of the lower Cambrian (Series 2) Emu Bay Shale Lagerstätte, South Australia. Australian Journal of Earth Sciences 58, 259–272.

McLennan S. M., Taylor S. R., 1987. Crustal evolution: Comments on ‘The Archean-Proterozoic transition: Evidence from the geochemistry of metasedimentary rocks from Guyana And Montana” By A.K. Gibbs, C.W. Montgomery, P.A. O’day and E.A. Erslev. Geochimica et Cosmochimica Acta 52, 785–787.

Mclennan, S.M., 1989. Rare earth elements in sedimentary rocks: Influence of provenance and sedimentary processes. Reviews in Mineralogy and Geochemistry 21, 169–200.

Meert J.G., Lieberman B.S., 2008. The Neoproterozoic assembly of Gondwana and its relationship to the Ediacaran–Cambrian radiation. Gondwana Research 14, 5–21.

Morris, B.J., 1991. Kanmantoo Trough geological investigations Karinya Syncline drilling report. South Australian Department of Mines and Energy, Report Book, 91/20.

Morse, J.W., Luther III, G.W., 1999. Chemical influences on trace metal–sulfide interactions in anoxic sediments. Geochimica et Cosmochimica Acta 63, 3373–3378.

Muruyama, S., Santosh, M., 2008. Models on Snowball Earth and Cambrian explosion: a synopsis. Gondwana Research 14, 22–32.

Myrow, P.M., Hughes, N.C., Goodge, J.W., Fanning, C.M., Williams I.S., Peng, S., Bhargava, O.N., Parcha, S.K., Pogue, K.R., 2010. Extraordinary transport and mixing of sediment across Himalayan central Gondwana during the Cambrian–Ordovician. Geological Society of America Bulletin 122, 1660–1670.

Naqvi, S.M., Uday Raj, B., Subba Rao, D.V., Manikyamba, C., Nirmal Charan, S., Balaram, V., Srinivasa Sarma, D., 2002. Geology and geochemistry of arenite–quartzwacke from the Late Archaean Sandur schist belt - implications for provenance and accretion processes. Precambrian research 114, 177–197

Naqvi, S.W.A., Naik, H., Jayakumar, D.A., Shailaja, M.S., Narvekar, P.V., 2006. Seasonal oxygen deficiency over the western continental shelf of India. in Neretin, L.N. (ed.) Past and present water column anoxia. NATO Science Series: IV: Earth and Environmental Sciences 64, 195-224.

Nedin C., 1995. The palaeontology and palaeoenvironment of the Early Cambrian Emu Bay Shale, Kangaroo Island,. South Australia. Unpublished PhD thesis, University of Adelaide.

Och, L.M., Shields-Zhou, G.A., 2012. The Neoproterozoic oxygenation event: Environmental perturbations and biogeochemical cycling. Earth-Science Reviews 110, 26–57.

Och, L.M., Shields-Zhou, G.A., Poulton, S.W., Manning, C., Thirlwall, M.F., Li, D., Chen, X., Ling, H., Osborn, T., Cremonese, L., 2011. Redox changes in Early Cambrian black shales at Xiaotan section, Yunnan Province, South China. Precambrian Research doi:10.1016/j.precamres.2011.10.005

Ogg, J.G., Ogg, G. & Gradstein, F.M., 2008. The concise Geologic Time Scale. Cambridge University Press, Cambridge, 177 p.

Paterson, J.R., Jago, J.B., Gehling, J.G., García-Bellido, D.C., Edgecombe, G.D., Lee, M.S.Y., 2008. Early Cambrian arthropods from the Emu Bay Shale Lagerstätte, South Australia. 319-325. In: Rábano, I., Gozalo, R., García-Bellido, D. (Eds), Advances in Trilobite Research. Instituto Geológico y Minero de España, Madrid.

Pi, D.H., Liub, C.Q., Shields-Zhou, G.A., Jianga, S.Y., 2011. Trace and rare earth element geochemistry of black shale and kerogen in the early Cambrian Niutitang Formation in Guizhou province, South China: Constraints for redox environments and origin of metal enrichments. Precambrian Research. doi:10.1016/j.precamres.2011.07.004

Popp, B.N., Trull, T., Kenig, F., Wakeham, S.G., Rust, T. M., Tilbrook, B., Griffiths, F.B., Wright, S.W., Marchant, H.J., Bidigare R.R., Laws, E.A., 1999. Controls on the carbon isotopic composition of Southern Ocean phytoplankton. Global Biogeochemistry Cycles 13, 827–843.

Powell W.G., 2009. Comparison of geochemical and distinctive mineralogical features associated with the Kinzers and Burgess Shale formations and their associated units. Palaeogeography, Palaeoclimatology, Palaeoecology 277, 127–140.

Powell W.G., Johnston P.A., Collom C.J., 2003. Geochemical evidence for oxygenated bottom waters during deposition of fossiliferous strata of the Burgess Shale Formation. Palaeogeography, Palaeoclimatology, Palaeoecology 201, 249–268.

Powell, C.M., Pisarevsky, S.A., 2002. Late Neoproterozoic assembly of East Gondwana. Geology 30, 3–6.

Powell, C.M., Preiss, W.V., Gatehouse, C.G., Krapez, B., Li, Z.X., 1994. South Australian record of a Rodinian epi-continental basin and its mid-Neoproterozoic breakup (~700Ma) to form the Palaeo-pacific Ocean. Tectonophysics 237, 113–140.

Preiss W.V., Forbes B.G., 1981. Stratigraphy, Correlation And Sedimentary History Of Adelaidean (Late Proterozoic) Basins In Australia. Department of Mines and Energy, Adelaide, S.A. Incomplete reference?

Preiss, W,V, Walter, M.R., Coats, R.P., Wells, A.T., 1978. Lithological correlations of Adelaidean glaciogenic rocks in parts of the Amadeus, Ngalia aand Georgina Basins. Journal of the Australian Bureau of Mineral Resorces, Geology and Geophysics 3, 43–53

Preiss, W.V., 1995. Delamerian Orogeny. In: Drexel J. F., Preiss W. V. (Eds.), The Geology of South Australia, Vol. 2: The Phanerozoic. Geological Survey of South Australia Bulletin 54, 45–60.

Preiss, W.V., 2000. The Adelaide Geosyncline of South Australia and its significance in Neoproterozoic continental reconstructions. Precambrian Research 100, 21–63.

Racka, M., Marynowski, L., Filipiak, P., Sobstel, M., Pisarzowska, A., Bond, D.P.G., 2010. Anoxic annulata events in the late Famennian of the Holy Cross Mountains (Southern Poland): geochemical and palaeontological record. *Palaeogeography, Palaeoclimatology, Palaeoecology* 297, 549–575.

Rimmer, S.M., 2004. Geochemical paleoredox indicators in Devonian–Mississipian black shales, Central Appalachian Basin (USA). Chemical Geology 206, 373–391.

Rutland, R.W.R., Parker, A.J., Pitt, G.M., Preiss, W.V., Murrell, B., 1981. Precambrian of South Australia. Developments in Precambrian Geology 2, 309–360

Saltzman M.R., Ripperdan R.L., Brasier M.D., Lohmann K.C., Robinson R.A., Chang W.T., Peng S., Ergaliev E.K., Runnegar B.R., 2000. A global carbon isotope excursion (SPICE) during the Late Cambrian: relation to trilobite extinctions, organic-matter burial and sea level. Palaeogeography, Palaeoclimatology, Palaeoecology 160, 211–223.

Scott, C., Lyons, T.W., Bekker, A., Shen, Y., Poulton, S.W., Chu, X., Anbar, A.D., 2008. Tracing the stepwise oxygenation of the Proterozoic ocean. Nature 452, 456–459.

Sepkoski, J.J., Schopf, J.W., 1992. Biotic Diversity and rates of evolution during Proterozoic and earliest Phanerozoic time. In: Schopf, J.W., Klein, C. (Eds.), The Proterozoic Biosphere. Cambridge University Press, pp. 521–566.

Shen, Y., Schidlowski, M., Chu, X., 2000. Biogeochemical approach to understanding phosphogenic events of the terminal Proterozoic to Cambrian. Palaeogeography, Palaeoclimatology. Palaeoecology 158, 99–108.

Shergold, J.H., Cooper, R.A., 2004. The Cambrian Period. In: Gradstein, F., Ogg, J., Smith, A. (Eds.), A Geologic Time Scale 2004. Cambridge University Press, Cambridge, pp. 147–164.

Shields, G., Kimura, H., Yang, J., Gammon, P., 2004. Sulfur isotopic evolution of Neoproterozoic–Cambrian seawater: new francolite-bound sulphate $\delta^{34}S$ data and critical appraisal of the existing record. Chemical Geology 204, 163–182.

Shields, G., Stille, P., 2001. Diagenetic constrains on the use of cerium anomalies as palaeoseawater proxies: an isotopic and REE study of Cambrian phosphorites. Chemical Geology 175, 29–48.

Shields, G., Strauss, H., Howe, S.S., Siegmund, H., 1999. Sulfur isotope compositions of sedimentary phosphorites from the basal Cambrian of China: implications for Neoproterozoic-Cambrian biogeochemical cycling. Journal of the Geological Society 156, 943–955.

Sholkovitz, E., Landing, W.M., Lewis, B.L., 1994. Ocean particle chemistry: the fractionation of the rare earth elements between suspended particles and seawater. Geochimica et Cosmochimica Acta 58, 1567–1580.

Shu, D., 2008. Cambrian expolsion: Birth of tree of life. Gondwana Research 14, 219–240.

Sofer, Z., 1980. Preparation of carbon dioxide for stable carbon isotope analysis of petroleum fractions. Analytical Chemistry 52, 1389–1391.

Squire, R.J., Campbell, I.H., Allen, C.M., Wilson, C.J.L., 2006. Did the Transgondwanan Supermountain trigger the explosive radiation of animals on Earth? Earth and Planetary Science Letters 250, 116–113.

Steiner, M., Li, G., Qian, Y., Zhu, M., Erdtmann, B., 2007. Neoproterozoic to Early Cambrian small shelly fossil assemblages and a revised biostratigraphic correlation of the Yangtze Platform (China), Palaeogeography, Palaeoclimatology, Palaeoecology 254, 67–99.

Strauss, H., 2002. The isotopic composition of Precambrian sulphides-seawater chemistry and biological evolution. Special Publications International Association of Sedimentologists 33, 67–105.

Strauss, H., 2006. Anoxia through time. in Neretin, L.N. (ed.) Past and present water column anoxia. NATO Science Series: IV: Earth and Environmental Sciences 64, 3-19.

Suto, A., 2011. Structure of the Kangaroo Island Fleurieu Peninsula Shear Zone and the provenance of its host sediments - The Kanmantoo Group - South Eastern Australia. Unpublished Honours thesis, University of Adelaide.

Taylor, S.R., McLennan, S.M., 1985. The Continental Crust: its Composition and Evolution. Blackwell Scientific Publications, ???p.

Thomson, B. P., 1969. The Kanmantoo Group and Early Palaeozoic Tectonics. In: Parkin L. W. (Ed.), Handbook of South Australian Geology, Geological Survey of South Australia, pp. 97–108

Thomson, J., Jarvis, I., Green, D.R.H., Green, D., Clayton, T., 1998. Mobility and immobility of redox-sensitive elements in deep-sea turbidites during shallow burial. Geochimica et Cosmochimica Acta 62, 643–656.

Tissot, B.P., Welte, D.H., 1984. Petroleum Formatíon and Occurrence, 2nd, edition. Springer-Verlag, Berlin, 699 p.

Tribovillard, N., Algeo, T.J., Lyons, T., Riboulleau, A., 2006. Trace metals as paleoredox and paleoproductivity proxies: an update. Chemical Geology 232, 12–32.

Tribovillard, N., Bout-Roumazeilles, V., Algeo, T.J., Lyons, T.W., Sionneau, T., Montero-Serrano, J.C., Riboulleau, A., Baudin, F., 2008. Paleodepositional conditions in the Orca Basin as inferred from organic matter and trace metal contents. Marine Geology 254, 62–72.

Tribovillard, N., Riboulleau, A., Lyons, T., Baudin, F., 2004. Enhanced trapping of molybdenum by sulfurized organic matter of marine origin as recorded by various Mesozoic formations. Chemical Geology 213, 385–401.

Tucker M.E., 1989. Carbon isotope and Precambrian-Cambrian boundary geology, South Australia: ocean basin formation, seawater chemistry and organic evolution. Terra Nova 1, 573–582.

Turner B.L., 1994. Cambrian black shales in the Karinya Syncline: stratigraphic distribution, sedimentology and kerogen composition. Unpublished Honours thesis,

University of Adelaide.

Turner, S.P., Adams, C.J., Flöttmann, T., Foden, J.D., 1993. Geochemical and geochronological constraints on the Glenelg River Complex, Western Victoria. Austrailian Journal of Earth Sciences 40, 275–292.

Turner, S.P., Haines, P.W., Foster, D., Powell, R., Sandiford, M., Offler, R., 2009. Did the Delamerian Orogeny Start in the Neoproterozoic? The Journal of Geology 117, 575–583.

Veevers, J.J., Belousova, E.A., Saeed, A., Sircombe, K., Cooper, A.F., Read, S.R., 2006. Pan-Gondwanaland detrital zircons from Australia analysed for Hf-isotopes and trace elements reflect an ice-covered Antarctic provenance of 700–500 Ma age, TDM of 2.0–1.0 Ga, and alkaline affinity. Earth-Science Reviews 76, 135–174.

Walker, J.C.G., 1986. Global geochemical cycles of carbon, sulfur and oxygen. Marine Geology 70, 159–174.

Walter, M.R., Veevers, J.J., Calver, C.R., Grey, K., 1995. Neoproterozoic stratigraphy of the Centralian Superbasin, Australia. Precambrian Research 73, 173–195.

Wang, X., Shi, X., Jiang, G., Zhang, W., 2012. New U–Pb age from the basal Niutitang Formation in South China: Implications for diachronous development and condensation of stratigraphic units across the Yangtze Platform at the Ediacaran–Cambrian transition. Journal of Asian Earth Sciences 48, 1–8.

Webb, G.E., Kamber, B.S., 2000. Rare earth elements in Holocene reefal microbialites: a new shallow seawater proxy. Geochimica et Cosmochimica Acta, 64, 1557–1565.

Wignall, P.B., Twitchett, R.J., 1996. Oceanic anoxia and the end Permian mass extinction. Science 272, 1155–1158.

Wilde, P., Lyons, T.W., Quinby-Hunt, M.S., 2004. Organic carbon proxies in black shales: molybdenum. Chemical Geology 206, 167–176.

Wilde, P., Quinby-Hunt, M.S., Erdtmann, B.D., 1996. The whole-rock cerium anomaly: a potential indicator of eustatic sea-level changes in shales of the anoxic facies. Sedimentary Geology 101, 43–53.

Wombacher, F., Munker, C., 2000. Pb, Nd, and Sr isotopes and REE systematic of Cambrian sediments from New Zealand: implications for the reconstruction of the Early Palaeozoic Gondwana margin along Australia and Antarctica. Journal of Geology 108, 663–686.

Wu, N., Farquhar, J., Strauss, H., Kim, S., Canfield, D.E., 2010. Evaluating the S-isotope fractionation associated with Phanerozoic pyrite burial. Geochimica et Cosmochimica Acta 74, 2053–2071.

Xie, S., Wu, Y., Gao, S., Liu, X., Zhou, L., Zhao, L., Hu, Z., 2011. Sr–Nd isotopic and geochemical constraints on provenance of late Paleozoic to early cretaceous sedimentary rocks in the Western Hills of Beijing, North China: Implications for the uplift of the northern North China Craton. Sedimentary Geology, doi:10.1016/j.sedgeo.2011.12.005

Yan X., Kerrich R., Hendry M.J., 2000. Trace element geochemistry of a thick till and clay-rich aquitard sequence, Saskatchewan, Canada. Chemical Geology 164, 930–120.

Yan, Y., Xia, B., Lin, G., Carter, A., Hu, X., Cui, X., Liu, B., Yan, P., Song, Z., 2007. Geochemical and Nd isotope composition of detrital sediments on the north margin of the South China Sea: provenance and tectonic implications. Sedimentology 54, 1–17.

Yang, J.H., Jiang, S.Y., Ling, H.F., Feng, H.Z., Chen, Y.Q., Chen, J.F., 2004. Paleoceangraphic significance of redox-sensitive metals of black shales in the basal Lower Cambrian Niutitang Formation in Guizhou Province, South China. Progress in Natural Science 14, 152–157.

Yu, B., Dong, H., Widom, E., Chen, J., Lin, C., 2009. Geochemistry of basal Cambrian black shales and cherts from the Northern Tarim Basin, Northwest China: Implications for depositional setting and tectonic history. Journal of Asian Earth Sciences 34, 418–436.

Yu, B.S., Wang, L.D., Chen, J.Q., Chen, X.L., Liang, S.Y., Liu, Z.B., Lin, C.S., 2003. The suboxic depositional setting of black shales in Lower Cambrian from northern Tarim Basin. Earth Sciences Frontiers 10, 547–550.

Zhang, Q.R., Piper, J.D.A., 1997. Palaeomagnetic study of Neoproterozoic glacial rocks of the Yangzi Block: Palaeolatitude and configuration of South China in the late Proterozoic Supercontinent. Precambrian Research 85, 173–199.

Zhang, T., Chu, X., Zhang, Q., Feng, L., Huo,W., 2003. Variations of sulfur and carbon isotopes in seawater during the Doushantuo stage in late Neoproterozoic. Chinese Science Bulletin 48, 1375–1380.

Zhao, Y., Zheng, Y., Chen, F., 2009. Trace element and strontium isotope constraints on sedimentary environment of Ediacaran carbonates in southern Anhui, South China. Chemical Geology 265, 345–362.

Zheng, Y., Anderson, R.F., van Geen, A., Kuwabara, J., 2000. Authigenic molybdenum formation in marine sediments: a link to pore water sulfide in the Santa Barbara Basin. Geochimica et Cosmochimica Acta 64, 4165–4178.

Zhou, C.M., Jiang, S.Y., 2009. Palaeoceanographic redox environments for the lower Cambrian Hetang Formation in South China: Evidence from pyrite framboids, redox-sensitive trace elements, and sponge biota occurrence. Palaeogeography, Palaeoclimatology, Palaeoecology 271, 279–286.

Zhu M., Babcock L.E., Peng S., 2006. Advances in Cambrian stratigraphy and palaeontology: integrating correlation techniques, palaeobiology, taphonomy and palaeoenvironmental reconstruction. Palaeoworld 15, 217–222.

PALAEOREDOX STATUS AND THERMAL ALTERATION OF THE LOWER CAMBRIAN (SERIES 2) EMU BAY SHALE LAGERSTÄTTE, SOUTH AUSTRALIA

D.M. Mckirdy[1], P.A. Hall[1], C. Nedin[2], G.P. Halverson[1,6], B.H. Michaelsen[3], J.B. Jago[4], J.G. Gehling[5] and R.J.F. Jenkins[5]

Australian Journal of Earth Sciences 58 (2011) 259-272

1. Organic Geochemistry in Basin Analysis Group and Centre for Tectonics, Resources & Exploration (TRaX), School of Earth & Environmental Sciences, University of Adelaide, SA 5095, Australia
2. Department of Innovation, Industry, Science & Research, Canberra, ACT 2601, Australia
3. Geological Survey of South Australia, Primary Industries & Resources SA, Adelaide, SA 5000, Australia
4. School of Natural & Built Environments, University of South Australia, Mawson Lakes, SA 5095, Australia
5. Science Centre, South Australian Museum, Adelaide, SA 5000, Australia
6. Present address: Department of Earth & Planetary Sciences, McGill University, Montreal, Quebec H3A 2A7, Canada

STATEMENT OF AUTHORSHIP

Palaeoredox status and thermal alteration of the lower Cambrian (Series 2) Emu Bay Shale Lagerstätte, South Australia

Philip Anthony Hall (Candidate)
Performed preparation and analysis (or oversaw the analysis of) the previously unreported third suite of samples, interpreted data, wrote original manuscript, provided critical evaluation

I hereby certify that the statement of contribution is accurate

Signed …….Date……

David M. McKirdy

Palaeoredox status and thermal alteration of the lower Cambrian (Series 2) Emu Bay Shale Lagerstätte, South Australia

Statement of contribution (in terms of the conceptualization of the work, its realization and its documentation)

Contributed to planning of article, provided critical evaluation, redrafted original manuscript and acted as corresponding author.

Certification that the statement of contribution is accurate and permission is given for the inclusion of the paper in the thesis

Signed: *Date:* 20/06/2012

Christopher Nedin

Palaeoredox status and thermal alteration of the lower Cambrian (Series 2) Emu Bay Shale Lagerstätte, South Australia

Statement of contribution (in terms of the conceptualization of the work, its realization and its documentation)

Contributed to sample collection, analyses and provided critical evaluation

Certification that the statement of contribution is accurate and permission is given for the inclusion of the paper in the thesis

Signed …… …….Date…02/07/2012…

Galen P. Halverson

Palaeoredox status and thermal alteration of the lower Cambrian (Series 2) Emu Bay Shale Lagerstätte, South Australia

Statement of contribution (in terms of the conceptualization of the work, its realization and its documentation)

Contributed to planning of article and provided critical evaluation.

Certification that the statement of contribution is accurate and permission is given for the inclusion of the paper in the thesis

Signed ……. Date…19/06/2012…

Bernd H. Michaelsen

Palaeoredox status and thermal alteration of the lower Cambrian (Series 2) Emu Bay Shale Lagerstätte, South Australia

Statement of contribution (in terms of the conceptualization of the work, its realization and its documentation)

Contributed to sample microscopy and provided critical evaluation

Certification that the statement of contribution is accurate and permission is given for the inclusion of the paper in the thesis

Signed …… …….Date…21st June 2012

James B. Jago

Palaeoredox status and thermal alteration of the lower Cambrian (Series 2) Emu Bay Shale Lagerstätte, South Australia

Statement of contribution (in terms of the conceptualization of the work, its realization and its documentation)

Contributed to sample collection and provided critical evaluation

Certification that the statement of contribution is accurate and permission is given for the inclusion of the paper in the thesis

Signed …….Date…20/06/2012…

James G. Gehling

Palaeoredox status and thermal alteration of the lower Cambrian (Series 2) Emu Bay Shale Lagerstätte, South Australia

Statement of contribution (in terms of the conceptualization of the work, its realization and its documentation)

Contributed to sample collection, field mapping and provided critical evaluation

Certification that the statement of contribution is accurate and permission is given for the inclusion of the paper in the thesis

Signed ……..…….Date…20/06/2012……

Richard J.F. Jenkins

Palaeoredox status and thermal alteration of the lower Cambrian (Series 2) Emu Bay Shale Lagerstätte, South Australia

Statement of contribution (in terms of the conceptualization of the work, its realization and its documentation)

Contributed to sample collection and provided critical evaluation

Certification that the statement of contribution is accurate and permission is given for the inclusion of the paper in the thesis

Signed …….Date…18/07/2012

Abstract

While exceptionally diverse fossil assemblages of soft-bodied organisms (Lagerstätten) are rare, they are unusually common in marine sedimentary sequences of early and mid-Cambrian age. Their mode of preservation has been the subject of much debate. The lower Cambrian (Series 2) Emu Bay Shale biota, found at Big Gully on the north coast of Kangaroo Island, is by far the best Burgess Shale-type fauna known in the southern hemisphere. Such fauna are preserved characteristically as two-dimensional compression fossils, comprising both carbonaceous and mineralised films on bedding surfaces of the host marine mudstones. The biotic diversity of the Big Gully assemblage suggests a habitat very favourable for life. Its preservation is exceptional, with gut remains and other soft parts quite common. Evidence of predation and scavenging is minimal and the finely laminated texture of the host mudstone attests to a lack of burrowing and bioturbation. Recent studies indicate that conservation of organic tissues, rather than authigenic mineralisation of their more labile components, is the principal taphonomic pathway responsible for BST deposits. Insofar as such preservation requires suppression of the early diagenetic processes that normally result in the rapid decay of organic matter at or near the sea floor, the oxicity of the bottom waters, below which the Emu Bay Shale accumulated, becomes critically important. Here we determine the palaeo-redox status of the fossiliferous basal portion of the formation using selected trace element proxies, in combination with total organic carbon (TOC) concentrations and isotopic signatures ($\delta^{13}C_{org}$). We also establish its degree of thermal alteration as a datum for use in taphonomic comparisons with other Cambrian Lagerstätten. The Emu Bay Shale contains insufficient organic matter (TOC = 0.25–0.55%) to have accumulated under stable anoxic conditions. Even allowing for the inevitable loss of organic

carbon during the oil- and gas-generation phases of thermal maturation, to a present rank equivalent to ~1.5% vitrinite reflectance, its original TOC content was <1%. Measurement of a series of redox-sensitive elemental ratios (viz. U/Th, V/Cr, Ni/Co and V/Sc) across the lower 8 m thick fossiliferous section of the Emu Bay Shale confirms that it was deposited beneath an oxic water column. In this respect it is similar to the archetypical Burgess Shale. In the absence of an exaerobic zone, benthic cyanobacterial mats are likely to have mantled recently dead fauna and helped maintain the integrity of a sharp redox boundary at the sediment-water interface.

3.1. Introduction

The Ediacaran-Cambrian transition was a time of profound reorganisation of the biosphere (Knoll & Walter, 1992; Halverson et al., 2009), coinciding with the tectonic upheaval involved in the final breakup of Rodinia and the assembly of Gondwana (Collins & Pisarevsky, 2005) and the full oxygenation of the atmosphere and oceans (Fike et al., 2006; Canfield et al., 2007). Unique aspects of the fossil record of this transition in South Australia are the exceptionally well-preserved faunas of the upper Ediacaran Rawnsley Quartzite (e.g. Glaessner & Wade, 1966; Jenkins, 1992; Gehling, 1999; Jenkins & Nedin, 2007) and the lower Cambrian (Cambrian Series 2, Stage 4) Emu Bay Shale (e.g. Glaessner, 1979; Nedin, 1995, 1997; Paterson & Jago, 2006; Paterson et al., 2008, 2010; García-Bellido et al., 2009). Like their time equivalents on other continents, such Lagerstätten collectively provide the foundation for our present understanding of the emergence and early evolution of the Metazoa (Knoll & Carroll, 1999; Briggs & Fortey, 2005; Narbonne, 2005).

While fossil assemblages of non-biomineralised organisms are rare in the geological record (Briggs, 2003), they are unusually common in marine sedimentary sequences

of early and mid-Cambrian age (Allison & Briggs, 1993; Conway Morris, 1998). Not surprisingly, their mode of preservation has been the subject of much debate. It is now clear that various taphonomic pathways may lead to the preservation (or replication) of soft-tissue entities such as embryos, eyes, digestive glands and muscles.

Studies dating back to the initial work of the late Brian Daily in the mid-1950s (Jago & Cooper, 2011) have established the Emu Bay Shale Lagerstätte at Big Gully on the north coast of Kangaroo Island, South Australia (Figure 1) as the richest Burgess Shale-type (BST) deposit in the southern hemisphere. In such deposits the fauna are characteristically preserved as two-dimensional compression fossils, comprising carbonaceous or mineralized compressions on bedding surfaces of the host marine mudstones (Butterfield, 1995). The Big Gully fauna is diverse, comprising at least 45 taxa, and thus suggesting a habitat very favourable for life. Its preservation is exceptional, with gut remains and other soft parts common. The Emu Bay Shale Lagerstätte is of Cambrian Epoch 2 age, equivalent to the *Pararaia janeae* Zone of mainland South Australia (Jago et al., 2006a, b; Paterson et al., 2008).

Many BST assemblages were deposited in deep water, outer shelf to basin-slope environments (Conway Morris, 1989; Hagadorn, 2002; Ivantsov et al., 2005; Zhang et al., 2008), the majority in North America and Greenland seaward of carbonate ramps or platforms (e.g. Stewart et al., 1993; Skinner, 2005; Babcock & Peel, 2007; Powell, 2009). Others were deposited on the landward side of the carbonate platform (Hagadorn, 2002), while the sediments containing the Chengjiang biota of China record deposition on a tidally influenced marine shelf (Babcock et al., 2001). The Emu Bay assemblage appears to be unique in that it was deposited in a more proximal inner shelf setting, perhaps semi-enclosed (Nedin, 1995), adjacent to an active

tectonic margin (Gehling et al., 2011). Moreover, the host mudstone is enriched in phosphate, resulting in replication of muscle tissue by authigenic calcium phosphate in Myoscolex, one of its common non-trilobite taxa (Briggs & Nedin, 1997). Another distinguishing aspect of this Lagerstätte, as highlighted by Ivantsov et al. (2005), is its apparent lack of algae, a characteristic it shares with the Sirius Passet site in Greenland.

NOTE:
This figure/table/image has been removed to comply with copyright regulations.
It is included in the print copy of the thesis held by the University of Adelaide Library.

Figure 1 Map of northeastern coast of Kangaroo Island, South Australia, showing (A) Cambrian outcrop and (B) detail of Big Gully and the locations of its shoreline and Buck Quarry lagerstätte sites within the Emu Bay Shale (after García-Bellido et al., 2009).

Notwithstanding earlier studies (e.g. Conway Morris, 1986; Orr et al., 1998; Briggs, 2003 and references therein), which suggested otherwise, Gaines et al. (2008) concluded that conservation of organic tissues, rather than authigenic mineralisation of their more labile components, is the principal taphonomic pathway responsible for BST deposits. Insofar as such preservation requires suppression of degenerative

biological processes that normally result in the rapid decay of organic matter at or near the sea floor, the redox status of the bottom waters, below which the Emu Bay Shale accumulated, becomes critically important. Hitherto (e.g. Daily et al., 1979, Nedin, 1995, Paterson et al., 2008) anoxic to suboxic conditions, possibly seasonal, at the seafloor have been invoked to explain various aspects of its basal Lagerstätte, viz. the dominance of complete, dorsum-down specimens of its two most common trilobite species *Estaingia bilobata* and *Redlichia takooensis*, both probably bottom dwellers (Gehling et al., 2011); a low proportion of moult ensembles; the presence of benthic dysaerobes such as paleoscolecid worms, hyoliths, leptomitid demosponges and non-trilobite lamellipedian arthropods; and, finally, the paucity of brachiopods and other fixosessile taxa (Pocock, 1964; Nedin, 1995; Gehling et al., 2011). Evidence of predation and scavenging is uncommon (Conway Morris & Jenkins, 1985; Nedin, 1999) and the finely laminated texture of the host mudstone attests to a lack of burrowing and bioturbation. Collectively the aforementioned characteristics appear consistent with the presence of oxygen-depleted bottom water, but not an exaerobic zone (*sensu* Savrda & Bottjer, 1987) at the low-oxygen end of the suboxic spectrum.

While benthic oxygen depletion has commonly been assumed to be a universal prerequisite for BST fossil deposits, there are few instances where the paleoredox status of the host sediments has been established using geochemical techniques. Notable exceptions include the middle Cambrian deposits of the Burgess Shale, southeastern British Columbia and part of the Kinzers Formation in southeastern Pennsylvannia (Cambrian Series 3 & 2, respectively: Powell et al., 2003; Powell, 2009). These studies revealed that the fossiliferous beds were deposited beneath

oxygenated bottom waters, while those beds deposited under anoxic conditions notably lack fossils of soft-bodied biota.

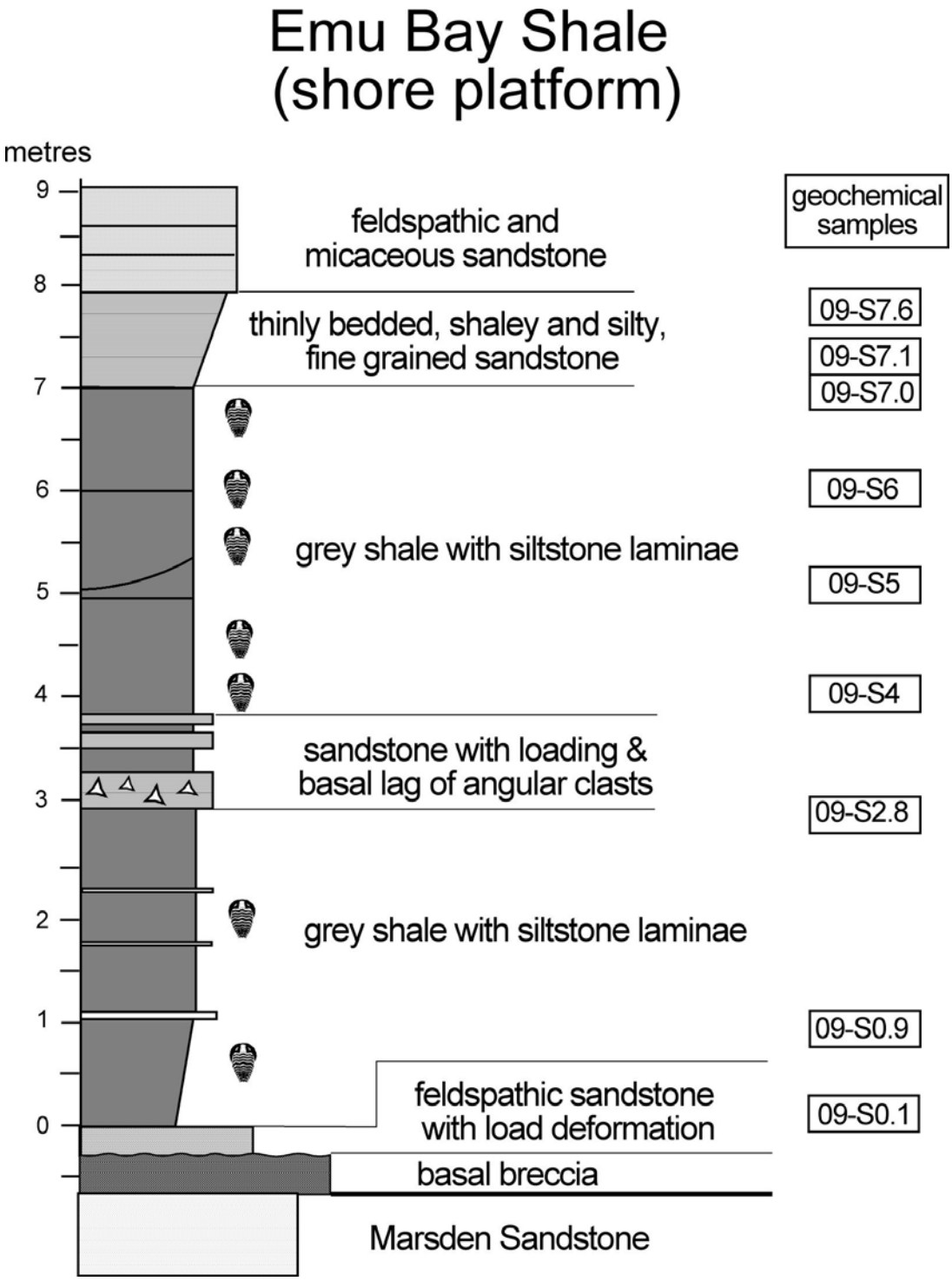

Figure 2 Lithostratigraphic section of basal Emu Bay Shale where exposed on the shore platform at the mouth of Big Gully.

The geological context of the Emu Bay Shale Lagerstätte, elaborated in a companion paper (Gehling et al., 2011), may be briefly summarised as follows. In the vicinity of Big Gully (Figure 1) the lower Cambrian succession comprises the White Point Conglomerate, Marsden Sandstone, Emu Bay Shale and Boxing Bay Formation. In coastal exposures the White Point Conglomerate (560+ m thick) is mainly a cobble to boulder conglomerate. However, clast size (maximum 1.5 m) decreases rapidly to the south where this massive lithofacies passes laterally into arkose with discrete lenses of polymict conglomerate. The clasts include archaeocyathid limestone and other carbonates (predominant), granite, gneiss, quartzite, vein quartz and sandstone. Their likely source area was the up-thrown northern flank of the E–W trending Cassini Fault Zone located just offshore in Investigator Strait. The Marsden Sandstone (newly defined by Gehling et al., 2011) is 43 m thick in its type section and conformably overlies the White Point Conglomerate. At its base is a 3 m-thick bioturbated calcareous mudstone (Rouge Mudstone Member) containing the emuellid trilobite *Balcoracania dailyi*. The remainder of the formation comprises coarsening-upward, slightly calcareous, feldspathic sandstone with subordinate mudstone and a gravel conglomerate near the top, consistent with deposition in a shallow subtidal to shoreface setting. A sedimentary hiatus separates the Marsden Sandstone from the succeeding formation. The basal lithofacies of the Emu Bay Shale on the present shore platform (Figure 2) is a cross-bedded breccia characterised by angular clasts of green shale and siltstone, along with some of granite and the underlying sandstone. Further inland, along Big Gully, the breccia appears thickest (up to 2 m thick) where syndepositional faulting produced a stepped topography in the Marsden Sandstone prior to deposition of the Emu Bay Shale. Accordingly, Gehling et al. (2011) interpret the base of this breccia as a sequence boundary. The breccia is overlain by feldspathic

sandstone, which in turn passes upward into richly fossiliferous grey shale, in part pyritic and silty, with subordinate sandstone beds. Although the Emu Bay Shale is up to 78 m thick (Daily et al., 1979), its Lagerstätte appears to be confined to the lowermost 10 m of the formation (Figure 2). The explanation for its remarkable preservation proposed by earlier workers (*viz.* rapid burial in a stagnant offshore setting) is too simplistic and no longer tenable. The Boxing Bay Formation, the final unit in the local Cambrian succession, conformably overlies the Emu Bay Shale. At least 510 m in thickness, it comprises red-brown feldspathic sandstone and arkose, with abundant trace fossils and evidence of soft-sediment slumping, suggestive of rapid sub-tidal deposition.

Here we re-examine the redox status of the fossiliferous basal portion of the Emu Bay Shale using established proxies based on trace element abundances (Jones & Manning, 1994; Kimura & Watanabe, 2001), in combination with total organic carbon (TOC) concentrations and isotopic signatures ($\delta^{13}C_{org}$). We also establish its degree of thermal alteration as a datum for use in taphonomic comparisons with other Cambrian Lagerstätten. This study forms part of a wider investigation of the biogeochemical status of the palaeo-Pacific Ocean, as recorded in minor and trace element abundances and stable isotopic signatures (C, S) of Cambrian fossiliferous shales and limestones from the Stansbury and Arrowie Basins, South Australia (Hall et al., 2010).

3.2. Samples And Methods

3.2.1. Sample suites

This study is based on outcrop specimens of the Emu Bay Shale acquired specifically for geochemical analysis during three generations of sampling. All are from Big Gully, Kangaroo Island (Figure 1) and typically comprise dark grey silty shale, in places pyritic. The initial sample (A320/11: Table 1) was collected from the wave-cut platform in 1967 and formed part of a pioneering organic geochemical survey of Australian Cambrian and Precambrian sedimentary rocks (McKirdy, 1971). A second suite of samples (n = 24: Table 2), from the shoreline cliffs, provided data for the first detailed minor and trace element profiles of the Emu Bay Lagerstätte (Nedin, 1995). The third suite (n = 12: Table 1) was collected in 2009 from two sites in Big Gully (Figure 1B). Representative portions (5 g) were removed from freshly exposed interior surfaces of ~2 kg-sized specimens. These were powdered using a pre-cleaned mortar and pestle in preparation for analysis.

3.2.2. Analytical methods

Unless otherwise indicated, all analyses were carried out in the Mawson Laboratories of the School of Earth and Environmental Sciences, University of Adelaide.

Whole-rock samples (~2 g) were submitted to Amdel Limited, Adelaide, for determination of TOC using a Leco Carbon/Sulphur Analyser.

Powdered samples (0.2 g) were digested three times in 10% HCl to remove carbonate, rinsed in deionised water, and dried. The residues were transferred to pre-cleaned 6 x 4 mm tin capsules for combustion in a Carlo Erba EA1500 series II elemental

analyser and the produced CO_2 analysed in continuous flow mode on a tandem Fisons Optima IRMS. Sample data were calibrated against glycine and glutamic acid house standards ($\delta^{13}C_{V\text{-}PDB}$ = -31.2, -17.1‰, respectively) and precision and accuracy monitored by regular analyses of a house sucrose standard (-25.8‰). Over the course of the analyses, the reproducibility (1σ) was ±0.2‰. In-house standards have been calibrated against the international standard NBS-19. The resulting $\delta^{13}C_{org}$ measurements are reported relative to the V-PDB standard.

Further aliquots of powdered shale (~15 mg) were accurately weighed into Teflon beakers for serial acid digestion in concentrated HCl, HNO_3 and HF, according to an established in-house protocol. Following digestion and evaporation to dryness, the samples were treated with 1% ultrapure H_2O_2 to remove organic residues, dried, then redissolved in 1 mL 6M HCl. From this solution, 100 µl of solution was then transferred to 5 ml Teflon autosampler vials, dried and redissolved in 1.5 ml of 0.5M HNO_3 ready for elemental analysis. Analyses for a suite of 44 trace and rare earth elements were conducted on an Agilent 7500cx solution ICP-MS at Adelaide Microscopy. Calibration was achieved using a suite of 10 ppb to 500 ppb standard reference solutions (Choice Analytical) with a co-aspirated solution of 200 ppb indium mixed online via a T-junction to correct for instrument drift and matrix effects.

The trace element data reported in Table 2 were acquired using a Philips PW 1480 X-ray fluorescence spectrometer, calibrated against a suite of 27 international standards. Typical detection limits (ppm in brackets) were: Sc (2), V (2), Cr (1.5), Co (2), Ni (3), Cu (4), Zn (3), Mo (1.5), Th (1.5) and U (1.5). Precision was ±5% at 100x detection limit.

Thin sections were examined and photographed using an Olympus BX 41 microscope fitted with an Olympus DP 20 digital camera. Polished sections were examined in white incident light and in fluorescence-mode (ultra-violet excitation) using a Leitz Ortholux II microscope fitted with a 32x oil immersion objective. For fluorescence-mode photography, a 100 Watt (Osram HBO100W/2) mercury burner was used: the light was filtered with a K 510 nm barrier filter, an N (diffusion) filter, in conjunction with a BG12 (blue) and a BG38 (green) excitation filter. The microscope incorporated a Berek prism and beam splitter (dichroic mirror). For photography in white incident light, only an N (diffusion) filter and a BG12 filter were used. Photographs were taken with a Wild Photoautomat MPS Spot camera using Fujifilm *Superior Reala* (100 ASA) colour negative film. The exposure times were 22 seconds for white light, and 162 seconds for fluorescence-mode.

Table 1 Elemental and isotopic data on the Emu Bay Shale from two fossil sites at Big Gully, Kangaroo Island

Height m	TOC %	$\delta^{13}C_{org}$ ‰	Sc ppm	V ppm	Co ppm	Ni ppm	Cu ppm	Zn ppm	Pb ppm	Mo ppm	Th ppm	U ppm	U/Th	Ni/Co	V/Sc
Shore platform (sample A320/11) [a]															
nd	0.37	-28.4	18	85	11	44	65	nd	nd	<10	nd	nd	nd	4.0	4.7
Buck Quarry [b]															
5-6	0.55	-31.8	15	114	10	31	75	569	22	0.6	17	2.6	0.16	2.9	7.4
5-6	0.45	-31.8	16	133	10	32	82	868	26	1.4	17	3.0	0.17	3.4	8.2
Shore platform [c]															
nd	0.30	-30.3	16	113	10	34	75	78	37	0.3	17	3.8	0.22	3.3	7.2
7.6	0.30	-29.9	17	109	17	37	34	73	36	0.6	17	3.9	0.23	2.2	6.6
7.1	0.35	-28.3	9.7	109	8.5	17	31	115	nd	0.2	11	2.5	0.22	2.0	11.3
7.0	0.40	-30.2	18	119	13	38	54	111	21	2.1	20	3.9	0.20	2.9	6.8
6.0	0.45	-29.8	16	111	13	33	54	110	38	0.9	19	3.9	0.20	2.5	7.1
5.0	0.50	-29.8	15	99	11	28	39	112	36	0.5	18	3.5	0.20	2.6	6.7
4.0	0.30	-27.8	14	91	10	24	34	60	35	0.6	17	3.5	0.21	2.3	6.6
2.8	0.25	-29.7	17	91	14	34	42	740	36	3.2	21	4.1	0.20	2.4	6.9
0.9	0.30	-30.7	16	105	10	31	41	2225	364	0.4	19	3.3	0.17	3.1	6.6
0.1	0.35	-29.2	18	142	12	30	80	32927	4906	2.3	21	4.5	0.21	2.6	8.1

[a] Data sources: McKirdy (1971); McKirdy & Powell (1984)

[b] Datum = base of Emu Bay Shale

[c] Datum = base of mudstone facies as shown in Fig. 2

nd = not determined

Table 2 Trace element data on the basal Emu Bay Shale at the Big Gully shoreline, Kangaroo Island

Height m[a]	Sc ppm	V ppm	Cr ppm	Co ppm	Ni ppm	Cu ppm	Zn ppm	Pb ppm	Mo ppm	Th ppm	U ppm	U/Th	V/Cr	Ni/Co	V/Sc
7.10	14	111	90	18	47	53	71	44	1.0	12	3.9	0.32	1.2	2.7	8.2
6.80	14	107	88	9	43	60	61	33	1.1	13	4.6	0.36	1.2	4.8	7.6
6.50	13	91	75	13	46	59	81	47	2.1	14	3.4	0.24	1.2	3.6	7.0
6.35	15	94	76	16	37	31	62	46	1.3	17	3.5	0.21	1.2	2.3	6.3
6.25	15	111	88	11	44	50	61	27	1.6	13	4.5	0.35	1.3	4.1	7.4
6.11	15	100	86	10	42	38	61	26	0.7	16	2.7	0.17	1.2	4.3	6.9
5.90	14	108	89	11	41	62	62	34	1.8	13	3.3	0.26	1.2	3.7	7.5
5.68	14	109	84	8	40	41	61	48	2.1	15	5.5	0.37	1.3	4.8	7.7
5.50	15	103	85	10	43	41	146	27	1.5	16	2.9	0.18	1.2	4.5	6.9
5.16	14	113	89	18	48	59	70	45	1.7	16	3.7	0.23	1.3	2.6	8.0
4.93	14	113	90	14	48	61	65	34	0.6	18	1.9	0.11	1.3	3.6	8.2
4.81	14	95	79	14	45	31	89	44	2.0	16	3.4	0.21	1.2	3.2	6.7
4.65	16	114	91	11	50	51	123	38	1.2	16	3.5	0.22	1.3	4.4	7.3
4.35	14	111	89	11	46	43	99	42	1.3	12	4.7	0.38	1.2	4.3	8.2
4.10	14	108	93	11	46	66	70	39	1.3	13	2.8	0.22	1.2	4.1	7.6
3.79	13	91	75	13	46	59	81	47	2.1	14	3.4	0.24	1.2	3.6	7.0
3.62	13	110	96	10	43	64	69	34	1.4	13	4.1	0.31	1.1	4.3	8.2
3.55	14	106	86	15	42	52	65	36	1.0	13	4.3	0.34	1.2	2.8	7.6
3.00	13	99	92	10	42	31	63	27	1.3	13	4.6	0.37	1.1	4.1	7.5
2.50	14	98	83	15	46	49	81	44	1.3	13	5.0	0.37	1.2	3.2	7.0
2.00	14	107	88	9	43	60	61	33	1.1	13	4.6	0.36	1.2	4.8	7.6
1.50	14	104	88	9	40	37	141	53	1.6	12	3.6	0.30	1.2	4.3	7.2
1.00	14	102	78	13	42	70	2162	498	2.7	17	3.4	0.21	1.3	3.3	7.4
0.50	15	105	91	11	41	37	2651	525	2.6	16	3.2	0.20	1.2	3.8	7.0
PAAS[b]	16	150	110	23	55	50	85	20	1	15	3	0.20	1.4	2.4	9.4

[a] Datum = base of formation

[b] Post-Archean Australian shale (Taylor & McLennan 1985)

Data source: Nedin (1995)

3.3. Redox status

One of the first attempts to reconstruct the palaeoredox status of the Emu Bay Lagerstatte was that of Pocock (1964). While perhaps overstating the darkness of the fossiliferous zone of the Emu Bay Shale at the shoreline locality in Big Gully ("dark-grey to black"), he noted that these finely laminated silty shales have "a relatively high iron content, in the form of limonite secondarily replacing pyrite, and a high percentage of organic matter". Moreover, whereas their "trilobites are preserved as tests replaced by calcite", they also seem to have been loci for the diagenetic formation of pyrite (subsequently altered to cryptocrystalline haematite). He concluded that these lithological aspects indicate "restricted circulation and oxygen-poor conditions" (p. 461).

A detailed geochemical investigation by Nedin (1995) confirmed the unusually ferruginous nature of these shales; the samples in Table 2 have an average Fe_2O_3 content of 6.5% (range 5.9–7.3%). With only two exceptions, these samples are enriched in molybdenum (relative to the average post-Archean Australian shale, PAAS: Table 2) but also depleted in manganese (Mn_{EBS} / Mn_{PAAS} = 0.56–0.89). Given the different redox sensitivity of these two elements (Calvert & Pedersen, 1993), Nedin (1995) interpreted their antithetical relationship in the basal Emu Bay Shale to imply its deposition under suboxic conditions, with the suboxic/anoxic boundary located at or close to the sediment/water interface.

Oxygen-depleted bottom waters favour the preservation of sedimentary organic matter. The greater the depletion, the higher the TOC content of the underlying sediment (Demaison & Moore, 1980; Demaison et al., 1984), although enhanced productivity in the photic zone can also lead to the same outcome (Calvert, 1987).

Assuming a normal level of primary planktonic productivity across its depocentre, the Emu Bay Shale appears to contain insufficient organic matter (TOC = 0.25–0.55%, mean = 0.38%: Table 1) to have accumulated under stable anoxic or suboxic conditions.

Even allowing for the inevitable loss of organic carbon during the oil- and gas-generation phases of thermal maturation (Raiswell & Berner, 1987), to a present rank equivalent to ~1.5% vitrinite reflectance (see Table 4 & below), its original TOC content is likely to have been <1%. A similar conclusion is reached using the fractional carbon loss calculation of Strauss et al. (1992) for a normal marine protokerogen of Type II composition that matures to one with an atomic H/C ratio of 0.48 (Table 1). In modern marine sediments, especially those lacking allochthonous vascular plant detritus, such a low level of organic enrichment is more typical of an oxic benthic regime (Tyson, 1995).

The mean TOC content of the fossiliferous Burgess Shale ranges from 0.11% (Butterfield, 1990) to 0.42% (after Kelafant, 1987, as cited by Powell et al., 2003). More recently, Powell (2009) reported TOC values of 0.17–0.32% (mean = 0.24%, n = 10) for the Burgess Shale and 0.11–2.42% (mean = 0.54%, n = 15) for the Kinzers Formation. Allowing for losses sustained during thermal alteration of the Burgess Shale to its present metamorphic grade (lower greenschist facies), Powell (2003) estimated that the average value of the four samples he studied (0.28%) represents a primary TOC value of ~1.5%. Thus, the pre-lithification organic richness of the Emu Bay Shale was somewhat less than that of the Burgess Shale, and considerably less than that of the upper Kinzers Formation (Longs Park Member: Figure 5).

Two additional factors are likely to have influenced the organic richness of the basal fossiliferous Emu Bay Shale at Big Gully. Its lack of horizons containing disarticulated moults implies a very high sedimentation rate (Gehling et al. 2011). If the rate was >5 cm/ka (as seems likely), this will have resulted in dilution of the organic input by siliciclastic mineral matter, further lowering the TOC content of the parent mud (Tyson, 2001). The enrichment of the shale in phosphate ($P_2O_{5\ EBS}$ / $P_2O_{5\ PAAS}$ = 1.4–7.4: Nedin 1995) suggests that its depocentre may have been impacted by marine upwelling and hence been a site of enhanced phytoplanktonic productivity. However, any resulting increase in the flux of organic matter to the seafloor clearly did not lead to the degree of organic enrichment evident in the partly contemporaneous Heatherdale Shale (TOC up to 2.6%: Hall et al., 2010). The latter unit comprises a 335 m thick succession of dark grey calcareous shale and siltstone, variously pyritic and rich in nodular phosphate, which was deposited in a more distal, outer ramp setting along the eastern flank of the Stansbury Basin (Gravestock & Gatehouse, 1995). By comparison with the Emu Bay Shale, its known arthropod fauna is highly impoverished, comprising three specimens of a single conocoryphid trilobite species, one specimen of the bivalved arthropod *Isoxys*, and some arthropod fragments, plus associated trails on bedding plane surfaces of black shale (Jago et al., 1984, 2006a, b; Jenkins & Hasenohr, 1989).

Like organic matter, certain trace metals also are commonly enriched (relative to their abundances in the PAAS) in modern muds and ancient black shales that were deposited in anoxic marine settings (Vine & Tourtelot, 1970; Calvert & Pedersen, 1993; Tribovillard et al., 2006). These metals include molybdenum, zinc, nickel, copper, uranium, vanadium and rare earth elements such as cerium. For example, Guo et al. (2007a) reported the following scenario of relative enrichment in the early

Cambrian (Terreneuvian Series) black shales of South China: Mo >Cd >V >U >Ni >Ag >Zn >Cu >Pb. Molybdenum is widely regarded as a sensitive and reliable paleoredox proxy (e.g. see above). As a result of oxidative weathering on the continents, Mo is delivered to the oceans in the form of the molybdate anion (MoO_4^{2-}), which is unreactive in oxygenated waters. In contrast, in anoxic bottom waters, reduced Mo(IV) reacts with dissolved sulphide to form insoluble MoS_2 that therefore precipitates and accumulates in the bottom sediment (Calvert & Pedersen, 1993). The concentrations of Mo and other selected trace elements in the Emu Bay Shale are shown in Tables 1 & 2. That they exhibit no obvious co-variation with organic matter (Figure 3) may be largely due to the narrow spread of TOC values.

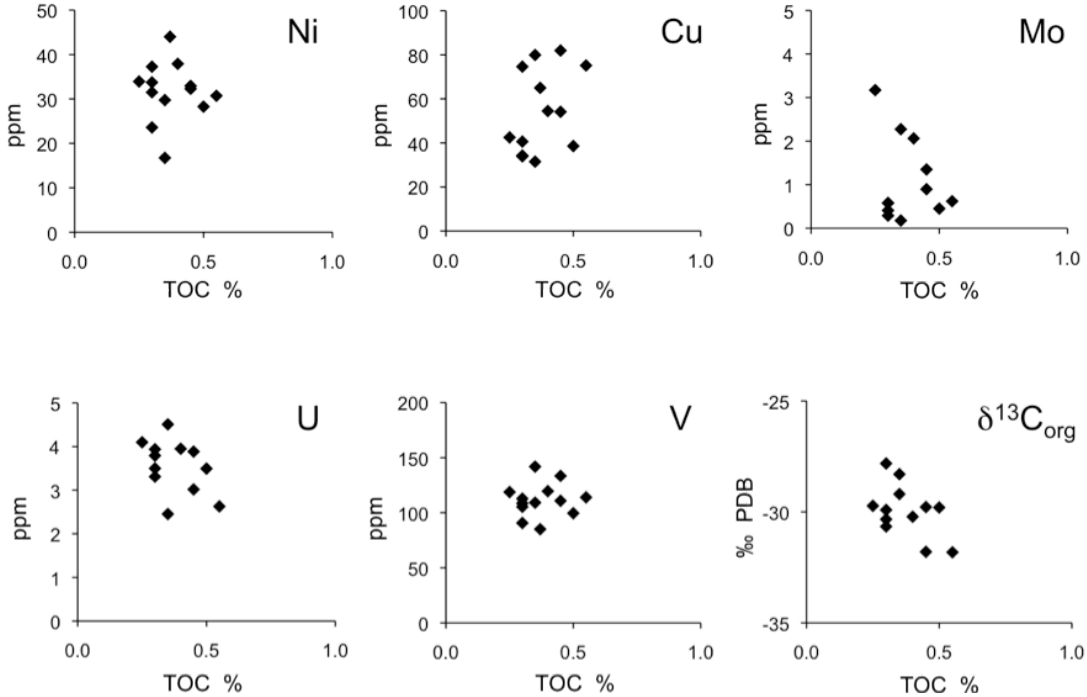

Figure 3 Relationship of total organic carbon content to the abundance of selected redox-sensitive trace elements in the Emu Bay Shale.

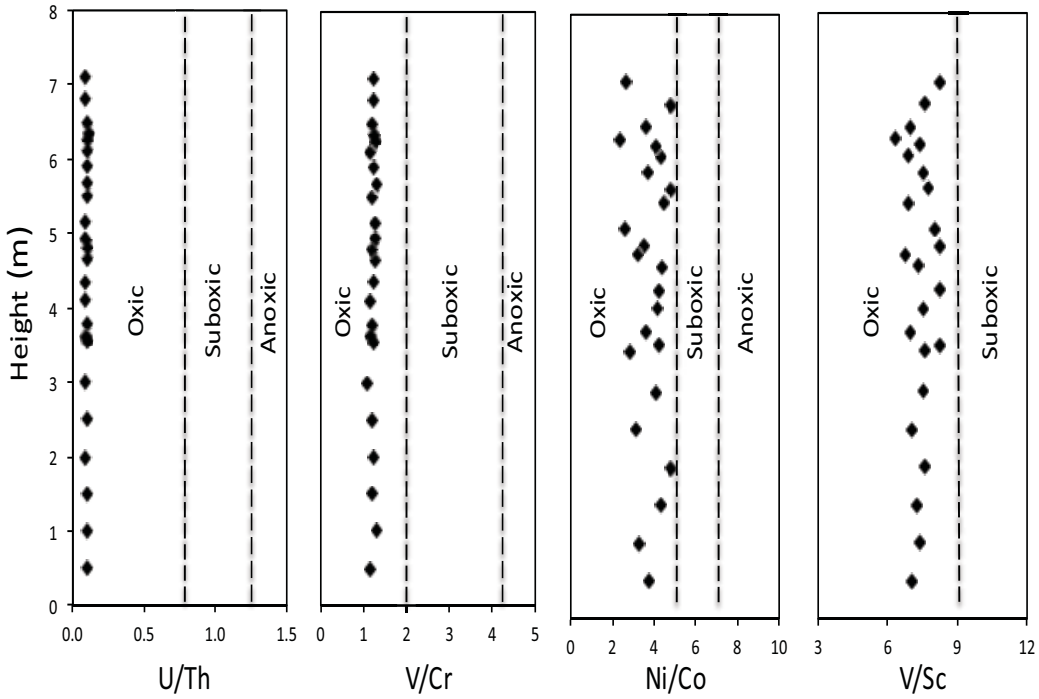

Figure 4 Chemostratigraphic profiles of redox-sensitive trace element ratios for the Emu Bay Shale at the Big Gully shoreline. Vertical subdivisions represent the redox zones of Jones & Manning (1994) and Kimura & Watanabe (2001).

The comparison of these absolute trace element abundances to those in average shales, with a view to inferring palaeo-redox conditions (e.g. Nedin, 1995), is fraught with difficulties (Powell et al., 2003). For example, detrital grains rich in one or more of these metals could distort or obscure the signal created by their redox-controlled precipitation within the sediment or immediately overlying water column. In the present instance, anomalous concentrations of Zn and Pb are present at several levels low in the Emu Bay Shale at both the shoreface and Buck Quarry sites (Tables 1 & 2). The fact that these anomalies occur close to breccias, erosional lags or sandstone interbeds (Fig. 2) suggests that they are the product of metalliferous fluids migrating during the Delamerian Orogeny, such as those that gave rise to Ag, Pb and Zn mineralisation south of the Snelling Fault on Kangaroo Island and elsewhere in the nearby Kanmantoo Trough (Parker, 1986). Alternatively these mineralising fluids

may have been mobilised much earlier, as part of the diagenetic processes accompanying deposition in the Kanmantoo Trough (Seccombe et al., 1985; Gum et al., 1994; Dyson et al., 1994; Gum, 1998). In order to obviate such problems, a series of elemental ratios have been devised in which one metal (the numerator) is redox-sensitive, while the other (denominator) is essentially independent of Eh.

Having reviewed the effectiveness of various proxy indicators employed by previous researchers, Powell et al. (2003) selected several of the more reliable elemental ratios to evaluate the paleoredox status of four North American BST deposits. Of these ratios U/Th, V/Cr and Ni/Co (after Jones & Manning, 1994) and V/Sc (after Kimura & Watanabe, 2001) were calculated for the Emu Bay Shale (Tables 1 & 2). All four parameters are consistent in revealing that the fossiliferous mudstones within the basal 7 m of the formation were deposited beneath an oxic water column (Figure 4). Moreover, in terms of their paleoredox status, these siliciclastic mudstones (with few exceptions) are essentially indistinguishable from those of the Burgess Shale and the Emigsville Member of the Kinzers Formation (middle Cambrian, Pennsylvania: Figure 5). On the other hand, the seafloor on which the BST fauna of the Longs Park Member of the Kinzers Formation accumulated was appreciably less oxygenated.

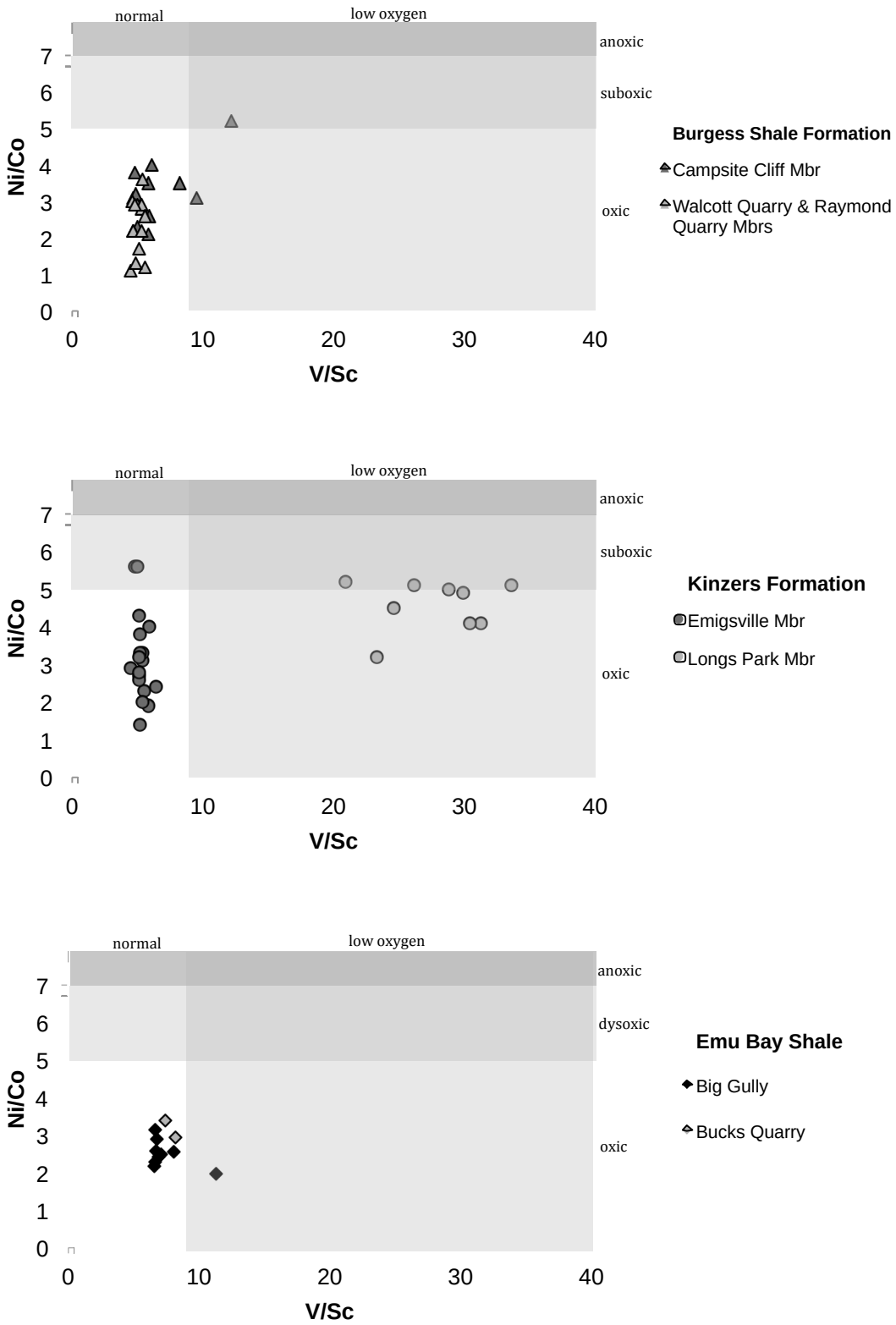

Figure 5 Comparison of the palaeoredox status of three Cambrian Lagerstätten: Emu Bay Shale, South Australia (this study), Burgess Shale Formation, British Columbia and Kinzers Formation, Pennsylvania (after Powell 2009).

3.4. Carbon isotopic signatures of organic matter

Organic carbon preserved in the Emu Bay Shale Lagerstätte has a bulk isotopic composition ($\delta^{13}C_{org}$ = -28 to -32‰, mean = -30‰: Table 1, Fig. 6) almost identical to that of marine kerogen in other unmetamorphosed lower Cambrian (Series 2) formations from elsewhere in South Australia (Table 3). These comprise the lower Wilkawillina Limestone and Andamooka Limestone in the Arrowie Basin and the Ouldburra Formation in the eastern Officer Basin, all shallow-water marine carbonate deposits. The samples of Wilkawillina Limestone were taken from stromatolitic bioherms (McKirdy, 1994a), implicating cyanobacteria as the principal sources of their dispersed organic matter. Stromatolites also are common throughout the Andamooka Limestone (James & Gravestock, 1990). Biomarker and compound-specific isotopic studies of the Ouldburra Formation (McKirdy et al., 1984; Logan et al., 1997) likewise confirm the prominence of benthic cyanobacteria in its marine sabkha palaeoenvironment.

Table 3 Bulk isotopic composition of organic carbon in unmetamorphosed early Cambrian marine sedimentary rocks, South Australia

Basin	Formation	$\delta^{13}C$ ‰ range	mean	n	Data sources
Stansbury	Emu Bay Shale	-31.8 to -27.8	-30.0	13	Table 1
	Parara Lst	-28.7	-28.7	1	McKirdy & Powell (1974)
Arrowie	Andamooka Lst	-30.2 to -28.8	-29.4	3	McKirdy (1994)
	Wilkawillina Lst	-31.3 to -28.6	-30.2	7	McKirdy (1994)
Officer	Ouldburra Fm	-31.8 to -26.7	-30.0	16	McKirdy *et al*. (1984) Logan *et al*. (1997)

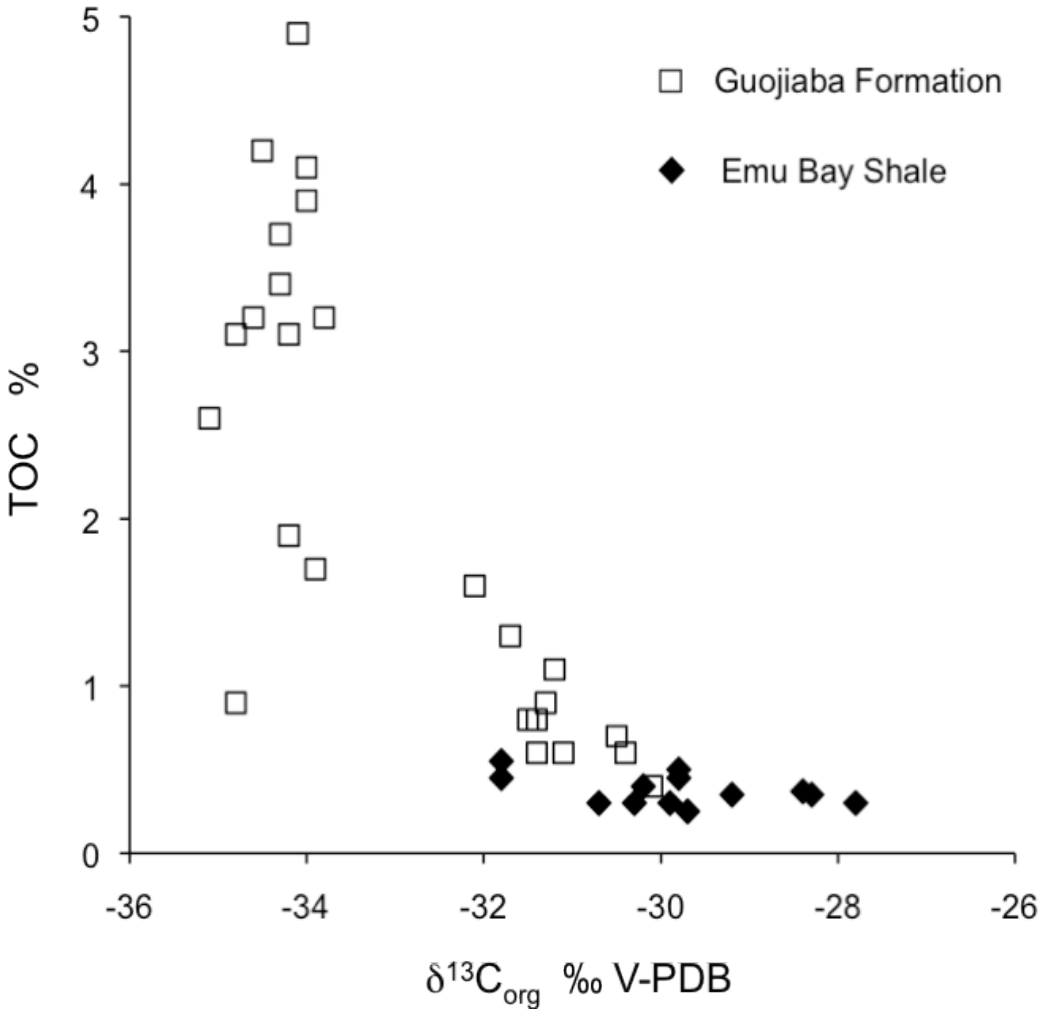

Figure 6 Relationship between bulk isotopic composition and concentration of organic carbon in shales from two unmetamorphosed lower Cambrian (Series 2) units: Emu Bay Shale, Stansbury Basin, South Australia (this study) and Guojiaba Formation, Shatan, Yangtze Platform, South China (Guo et al., 2007b).

Further clues to the likely source affinity of the organic carbon in the Emu Bay Shale may be obtained from its comparison with the black shale lithofacies of the Guojiaba Formation, South China (Figure 6). The latter unit is one of several argillaceous formations across the Yangtze Platform that are time equivalents of the Cambrian (Terreneuvian Series) Niutitang sponge-bearing Lagerstätte. Its lowermost section contains abundant small shelly fossils (Steiner et al., 2004). However, while likewise deposited in a shallow-water inner shelf setting, its high organic carbon content (up to

5% TOC), Mo enrichment and high Th/U and V/Sc ratios indicate that its bottom waters were anoxic and, at times, euxinic (Guo et al., 2007). Accordingly, its unmetamorphosed organic matter (kerogen H/C >0.3) is extremely depleted in ^{13}C ($\delta^{13}C_{org}$ = -36 to -30‰), indicating the dominant contribution of bacteria (including chemoautotrophs and sulphate reducers) to its residual biomass. The lower concentration and less ^{13}C-depleted isotopic composition of organic carbon in the Emu Bay Shale (Figure 6) are more compatible with a photoautotrophic cyanobacterial origin.

3.5. Post-depositional alteration

3.5.1. Thermal maturation

Determination of the post-depositional history of the Emu Bay Shale is an essential prerequisite for an informed understanding of the processes that led to the exceptional preservation of its soft-bodied fauna. Any metamorphic overprint is likely to have affected the mineralogy and texture of the host rock and fossils alike, as well as the concentration and composition of the dispersed organic matter (Powell, 2003).

Table 4 Degree of thermal alteration of the Emu Bay Shale at Big Gully, Kangaroo Island

Sample	Kerogen			Clay mineralogy		Illite crystallinity	
	H/C atomic	d_{002} Å	Subgraphite class [a]	Illite %	Chlorite %	Weaver Index [b]	Level of alteration [c]
A320/11 [d]	0.48	3.35, 3.44	$d_1 + d_{1a}$	53	47	3.8	Late catagenesis

[a] After Landis (1971)

[b] Sharpness of illite 10Å peak in X-ray diffractogram = $H_{10Å}$ / $H_{10.5Å}$ (Weaver 1961)

[c] Weaver Index <5, catagenesis; 5–15, anchizone; >15, epizone (Blenkinsop 1988)

[d] Porosity: vertical = 15.0%, horizontal = 14.4%. Permeability: vertical = 0.01 md, horizontal = 0.11 md.

Data source: McKirdy (1971)

Data acquired by McKirdy (1971) on the first specimen of Emu Bay Shale collected specifically for organic geochemical analysis provides several independent measures of its level of metamorphic alteration (Table 4). These include 1) kerogen with an atomic H/C ratio of 0.48 and a sub-graphitic structure (comprising a mixture of the d_1 and d_{1a} classes of Landais 1971); and 2) a phyllosilicate assemblage comprising illite and chlorite, the former with a crystallinity of 3.8 as expressed by the Weaver Index (WI: Weaver 1961). Considered together, these parameters indicate thermal alteration to the level of late catagenesis. According to Blenkinsop (1988), a WI of 5.1 marks the threshold of anchimetamorphism (or the anchizone: Kubler, 1968), which in turn corresponds to a vitrinite reflectance of 2.0%.

Although this assessment of thermal maturity is based on a single sample, the internal consistency of the kerogen and clay mineralogical parameters, and the limited areal extent of the known Lagerstätte (Figure 1), mean that it can be taken as representative of the entire deposit. Added weight is given to this interpretation by the low thermal maturity of an older Cambrian (Series 2) unit, the Mount McDonnell Formation, ~30 km further west along the northern coast of Kangaroo Island near Hummocky Point (calculated vitrinite reflectance = 0.9–1.1%, measured from di- and triaromatic hydrocarbon distributions in drill core samples: McKirdy, 1994b). The fact that the H/C ratio of the Emu Bay Shale kerogen is well above 0.2, the threshold at which its C-isotopic composition ($\delta^{13}C$) undergoes metamorphic alteration (McKirdy & Powell, 1974; Hayes et al., 1983), means that the $\delta^{13}C_{org}$ values obtained from the formation (Table 1, Figure 3) are near-primary signatures of the precursor biomass. Notwithstanding the preservation of soft animal tissue in the Lagerstätte (at least until permineralised), the bulk of its surviving dispersed organic matter is likely to have been of algal and bacterial origin.

In marked contrast to the Burgess Shale, which has undergone anchi- to early greenschist facies metamorphism (WI = 7–58: Powell 2003), the Emu Bay Shale has no detectable metamorphic overprint. It also lacks the bedding plane foliation and crenulation cleavage that characterise the Burgess Shale. Arguably, therefore, the Emu Bay Lagerstätte is better placed than the more intensely altered Burgess Shale (Powell, 2003, 2009) to provide a window on the taphonomy that is common to BST Lagerstätten (Gaines et al., 2008).

3.5.2. Weathering

Weathering is another factor that impacts negatively on BST fossil preservation. For example, the Chengjiang biota in Yunnan Province, South China, appear as orange films of Fe minerals and phosphate in highly weathered, light tan to yellow shale (Zhu et al., 2005; Dornbos & Chen, 2008). Where unweathered, the host Maotianshan Shale is grey to dark grey in colour.

The fossiliferous mudstone facies of the Emu Bay Shale crops out as a flaggy purple shale (Fairclough, 2008) which, when freshly broken open (as during the excavation of Buck Quarry), has a pale grey colour. The low porosity (≤15%) and permeability (≤0.1 md) of a typical specimen (sample A320/11 in Table 4; McKirdy 1971) reflect the absence of significant weathering and hence its suitability for further organic geochemical investigation. The timing of the oxidation of its primary pyrite to limonite and haematite, whether early (i.e authigenic) or late (following uplift and erosion), remains uncertain. The low initial permeability of its mixed carbonate-clay lithofacies was regarded by Gaines et al. (2005) to be a key factor contributing to the preservation of kerogenised tissue in the Lagerstätte of the middle Cambrian (Series 3, Drumian Stage) Wheeler Formation, Utah.

3.6. Taphonomic implications

Having established that oxygen-deficient bottom water was not, as previously assumed, a ubiquitous attribute of the Emu Bay Shale depocentre, one then has to explain 1) the exceptional preservation of gut and muscle tissue in some of its fossil taxa; 2) a near absence of evidence of the activities of scavengers and predators; 3) a lack of bioturbation in the host siliciclastic mudstone; and 4) the original presence of pyrite (now largely replaced by limonite). The coincidence of these paleontological and sedimentological aspects signifies the likely existence of a sharp and robust redox boundary at or just above the sediment-water interface. Beneath it the pore waters of the mud were anoxic, slowing the post-mortem decay of non-biomineralised tissue in arthropods; while above it the level of oxygenation of the shelf waters, for the most part, was normal. This oxic scenario accords with the relatively low concentration of dispersed organic matter (TOC <1%) and hence the lack of enrichment in redox sensitive elements such as Mo, V, U, Ni and Cu (Figures 3 & 4). It also indicates the likely participation of benthic microbial mats in maintaining the integrity of the redox boundary. Such mats have been implicated in the preservation of Ediacaran Lagerstätten (Gehling, 1999; Callow & Brasier, 2009) and shown to play a similar role in the taphonomy of the Burgess Shale deposits (Powell et al., 2003). In the latter deposits, they comprise calcareous bacterial filaments (possibly cyanobacteria), although estimates of the palaeo-bathymetry of the Burgess Shale (minimum depth ~100 m) favour an origin from chemosynthetic sulphur-oxidising bacteria.

Modern sulphur oxidisers (e.g. *Beggiatoa*) typically occupy deep marine settings, whereas in modern shallow-water mats the dominant filamentous microbiota are cyanophytes (Williams & Reimers, 1983). The interpreted inner shelf location of the

Emu Bay Shale Lagerstätte means that it almost certainly accumulated at a much shallower depth than did the Burgess Shale. Hence, the shelf floor is more likely to have been within the photic zone, with cyanobacteria the major benthic microbiota. Inspection of several petrographic thin and polished sections of the Emu Bay Shale from each site (Fig. 1) confirmed the presence of finely disseminated pyrite, evidence of *in situ* anaerobic bacterial sulphate reduction during diagenesis. Of particular interest are concentrations of pyrite (now limonite pseudomorphs) within or immediately beneath individual arthropod carapaces (Fig. 7) and what appear to be remnant microbial (probably cyanobacterial) mats comprising micrinitised lamalginite (Fig. 8). Sponge spicules commonly occupy the same bedding plane as lamalginite. This association is preserved in muddy intervals lacking coarser siliciclastic input and perhaps records periods of lower sedimentation rate. The sporadic preservation of such mats therefore is entirely consistent with the inferred overall high sedimentation rate of this Lagerstätte (Gehling et al., 2011). While the widespread occurrence of cyanobacterial mats throughout the Emu Bay Shale deposit is yet to be demonstrated, preliminary biomarker analyses confirm the cyanobacterial affinity of at least part of this organic matter (McKirdy et al., 2010).

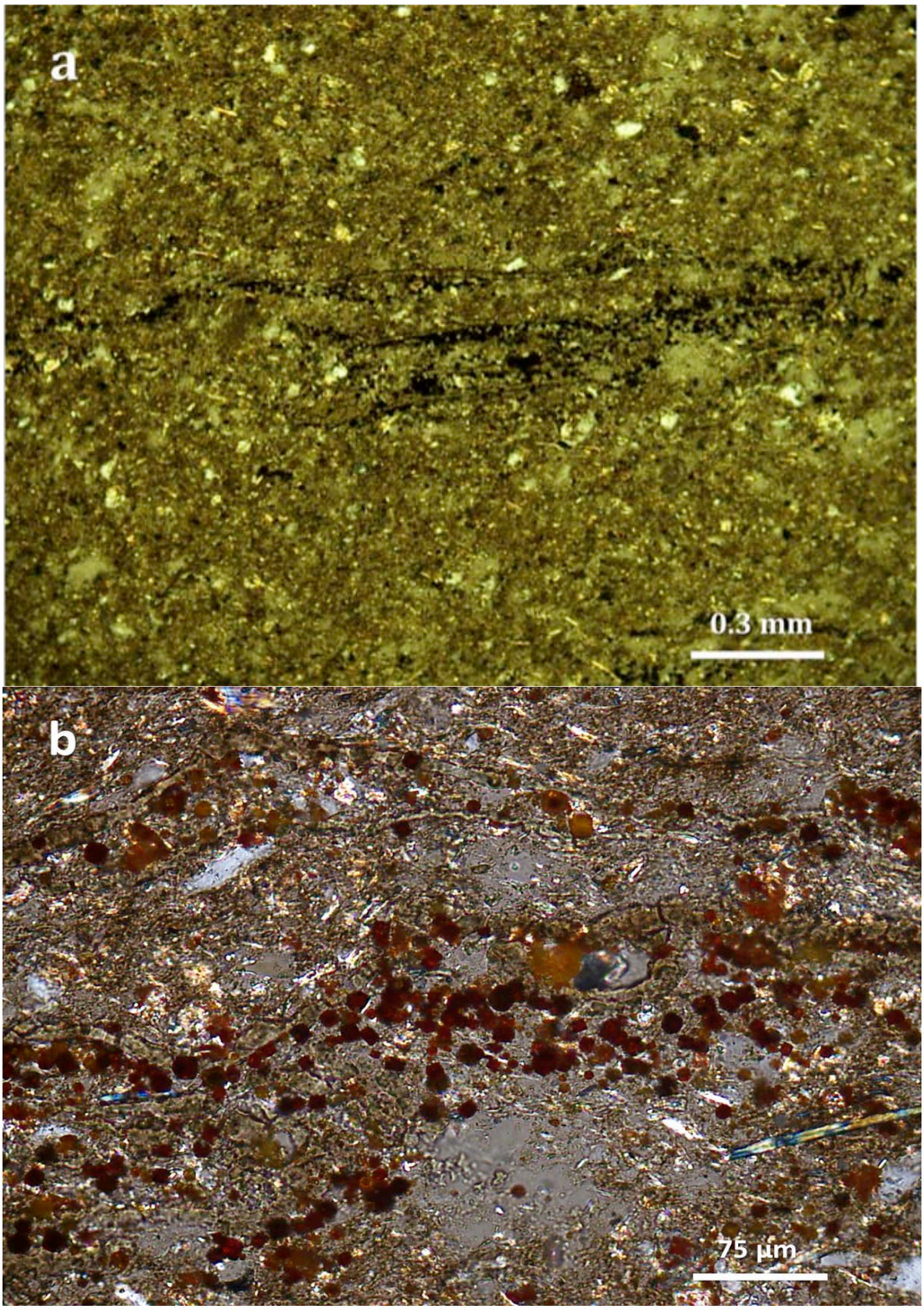

Figure 7 Photomicrographs of Emu Bay Shale in bedding-perpendicular thin section showing (a) limonite pseudomorphs of microcrystalline pyrite concentrated beneath and between thin (non-trilobite) arthropod carapaces; and (b) same entities at higher magnification, with a sponge spicule visible at bottom left. Plane polarised light.

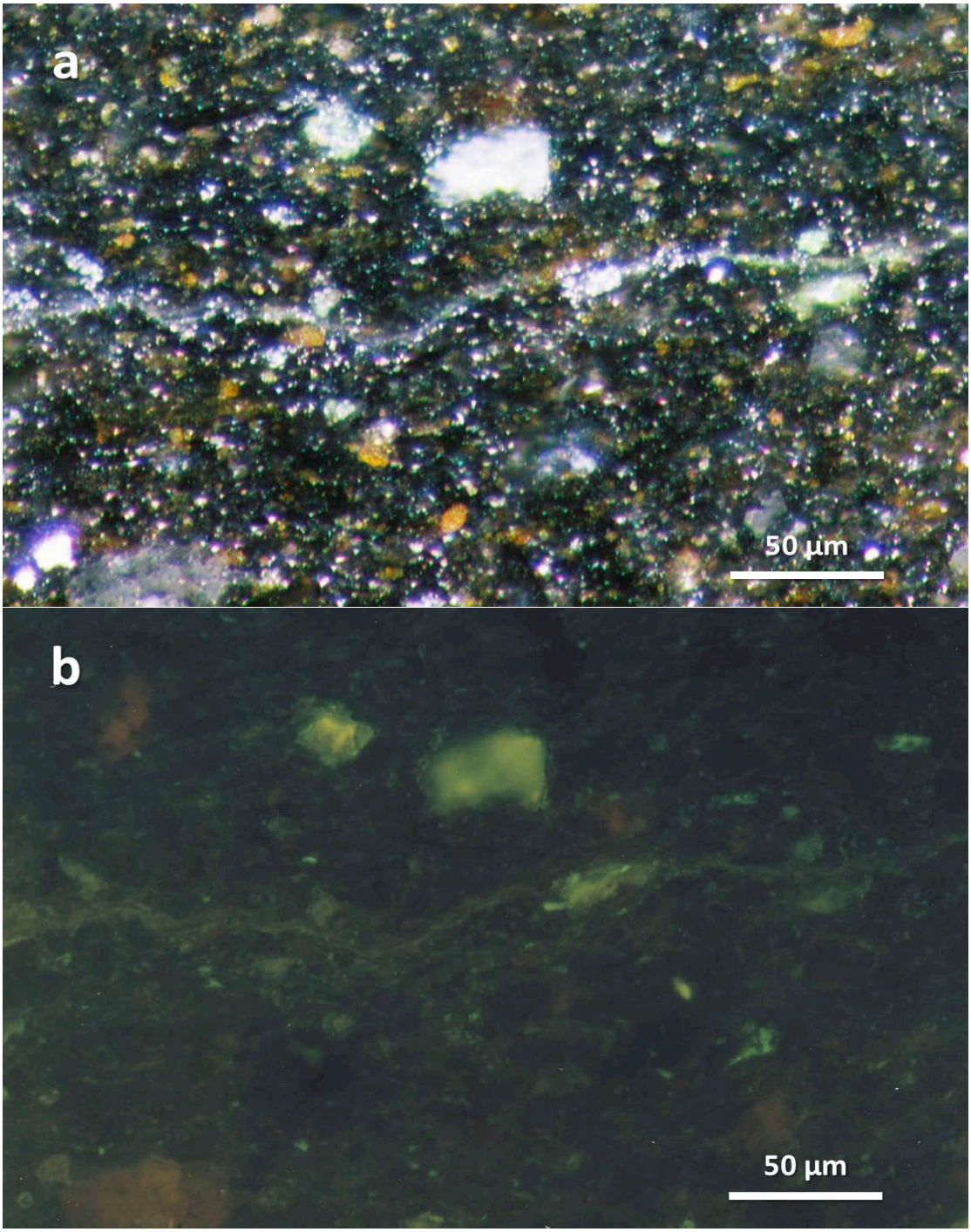

Figure 8 Photomicrographs of Emu Bay Shale in bedding-perpendicular polished section showing an irregular lamina of organic matter (interpreted as a remnant cyanobacterial mat) in silty mudstone containing finely disseminated authigenic pyrite. (a) Incident white light. (b) Same field of view in fluorescence mode.

The generally oxic paleoenvironment of the fossiliferous Emu Bay Shale does not rule out the possible existence of localised pockets of suboxic or anoxic bottom water into which benthic arthropods were swept by episodic slumping and associated turbidity currents. Such stagnant depressions on a pronounced depositional slope could have been created by the small-scale syndepositional faults that are evident at the base of the formation (Gehling et al., 2011). Of course, if and where it occurred, the smothering and rapid burial of bottom-dwelling fauna by slumped sediment would have precluded the need for anoxia in preserving soft tissue. Short-lived (seasonal?) anoxic or suboxic events may have provided an alternative trigger for the accumulation and preservation of the Emu Bay Shale biota. However, when evaluating the merits of either scenario, it is important to stress that none of the mudstone samples analysed in this study records any geochemical evidence of oxygen-depleted bottom water. The evidence for rapid sedimentation below wave base on an unstable slope within an actively faulted micro-basin is clear (as detailed in Gehling et al. 2011). Arthropods are preferentially preserved within siliciclastic muds rather than mass-flow sands. The possibility that salinity flux in the host sediments may have contributed to the exclusion of predators and bioturbators (cf. Babcock et al., 2001) has yet to be evaluated.

Further evaluation of the alternative modes of preservation of non-biomineralised tissue (via carbonaceous films) or replication (via aluminosilicate, siliceous, phosphatic and pyritic permineralisation) that may have operated in the Emu Bay Shale Lagerstätte requires elemental mapping of individual fossils, such as undertaken by Gaines et al., (2008). However, this is beyond the scope of the present study. The concentration of P in the host mudstone was higher than normal, making possible phosphatisation of some muscle tissue (Briggs & Nedin, 1997), although such

authigenic replication of non-biomineralised parts is by no means universal throughout the deposit. While also rich in Fe, the low organic carbon content of the host sediment may have inhibited sulphate reduction (Briggs, 2003), thereby limiting the extent of pyritisation. Finally, given the likely involvement of microbial mats in the preservation of the Emu Bay fauna, careful examination of additional petrographic thin sections (cut at a low angle to bedding) for the presence of carbonised filamentous or sphaeromorph microfossils (cf. Peat, 1984; Callow & Brasier, 2009) is warranted.

3.7. Conclusions

Measurement of the redox-sensitive trace element ratios U/Th, V/Cr, Ni/Co and V/Sc across the basal 8 m of the Emu Bay Shale confirms that it was deposited beneath an oxic water column. Thus oxygen-deficient bottom water was not a pre-requisite for the preservation of its Lagerstätte. In this respect it is similar to the archetypical Burgess Shale Formation in British Columbia.

The absence of burrowing and bioturbation implies the existence of a sharp redox boundary at the sediment-water interface, likely maintained by cyanobacterial mats that also mantled the tests of recently dead fauna. Below the boundary, anoxic pore water facilitated the preservation of soft tissue, while oxic conditions in the overlying water column diminished the flux of phytoplanktonic remains to the sea floor, as reflected in the low TOC content of the original sediment.

The Emu Bay Shale is less thermally altered than the Burgess Shale (which has undergone greenschist facies metamorphism) and less extensively weathered than the Maotianshan Shale (which hosts the Chenjiang biota of South China). Therefore,

potentially, it is a more useful source of information on BST preservation than these two classic deposits.

3.8. Acknowledgements

This study was undertaken as part of a project on the Cambrian hydrocarbon potential of the Stansbury and Officer Basins, for which PIRSA kindly provided funding. PAH also receives support from an Australian Postgraduate Award. JBJ and JGG acknowledge funding from an Australian Research Council Linkage Grant (LP0774959) to the University of Adelaide, additional financial support from Beach Petroleum Ltd and the South Australian Museum, and logistic support from SeaLink and the University of South Australia. We sincerely thank the Buck family for access to the field area. We thank Ben Wade (Adelaide Microscopy) for help with the ICP-MS analyses; John Stanley for general laboratory support; and Vic Gostin and Andreas Schmidt-Mumm for petrographic advice. Peter Haines and Loren Babcock are thanked for their constructive comments on the manuscript. The contributions of DMMcK, PAH and GPH to this paper form TRaX Record #117. Finally, DMMcK acknowledges the guidance and foresight of the late Professor M.F. Glaessner who, by suggesting the Emu Bay Shale to be worthy of organic geochemical investigation, launched his scientific career.

3.9. References

Allison, P.A., Briggs, D.E.G., 1993. Exceptional fossil record: Distribution of soft-tissue preservation through the Phanerozoic. Geology 21, 527–530.

Babcock L. E., Zhang W. T. & Leslie S. A. 2001. The Chengjiang Biota: record of the early Cambrian diversification of life and clues to exceptional preservation. GSA Today 11(2), 4–9.

Babcock, L.E., Peel, J.S., 2007. Palaeobiology, taphonomy and stratigraphic significance of the trilobite Buenellus from the Sirius Passet biota, Cambrian of North Greenland. Memoirs of the Association of Australasian Palaeontologists 34, 401–418.

Blenkinsop, T.G., 1988. Definition of low-grade metamorphic zones using illite crystallinity. Journal of Metamorphic Geology 6, 623–636.

Briggs, D.E.G., 2003. The role of decay and mineralization in the preservation of soft-bodied fossils. Annual Reviews of Earth and Planetary Sciences 31, 275–301.

Briggs, D.E.G., Fortey, R.A., 2005. Wonderful strife: Systematics, stem groups and the early phylogenetic signal of the Cambrian radiation. Paleobiology 31, 94–112.

Briggs, D.E.G., Nedin, C., 1997. The taphonomy and affinities of the problematic fossil Myoscolex from the Lower Cambrian Emu Bay Shale of South Australia. Journal of Paleontology 71, 22–32.

Butterfield, D.E.G., 1990. Greenschist-facies metamorphism of the Burgess Shale and its implications for models of fossil formation and preservation. Canadian Journal of Earth Sciences 40, 13–25.

Butterfield, D.E.G., 1995. Secular distribution of Burgess Shale-type preservation. Lethaia 28, 1–13.

Callow, R.H.T., Brasier, M.D., 2009. A solution to Darwin's dilemma of 1859: exceptional preservation in Salter's material from the late Ediacaran Longmyndian Supergroup, England. Journal of the Geological Society, London 166, 1–4.

Calvert, S.E., 1987. Oceanographic controls on the accumulation of organic matter in marine sediments. In: J. Brooks J. & Fleet A.J. eds. Marine Petroleum Source Rocks. Geological Society of London Special Publication, pp. 137–151.

Calvert, S.E., Pedersen, T.F., 1993. Geochemistry of Recent oxic and anoxic marine sediments: Implications for the geological record. Marine Geology 113, 67–88.

Canfield, D.E., Poulton, S.W., Narbonne, G.M., 2007. Late Neoproterozoic deep-ocean oxygenation and the rise of animal life. Science 315, 92–95.

Collins, A.S., Pivaresky, S.A., 2005. Amalgamating eastern Gondwana: The evolution of the Circum-Indian Orogens. Earth-Science Reviews 71, 229–270.

Conway Morris, S., 1986. The community structure of the Middle Cambrian phyllopod bed (Burgess Shale). Palaeontology 29, 423–467.

Conway Morris, S., 1989. Burgess Shale faunas and the Cambrian explosion. Science 246, 339–346.

Conway Morris, S., 1998. The Crucible of Creation. Oxford University Press, Oxford, 242 p.

Conway Morris S., Jenkins R. J. F., 1985. Healed injuries in Early Cambrian trilobites from South Australia. Alcheringa 9, 167–177.

Daily, B., Milnes, A.R., Twidale, C.R., Bourne, J.R., 1979. Geology and Geomorphology. In: Tyler M.J., Twidale C.R. & Ling J.K. eds. Natural History of Kangaroo Island. Royal Society of South Australia, Adelaide, pp.1–38.

Demaison, G., Holck, A.J.J., Jones, R.W., Moore, G.T., 1984. Predictive source bed stratigraphy: a guide to regional petroleum occurrence, North Sea Basin and North American continental margin. In: Proceedings of the 11th World Petroleum Congress, Wiley, New York, pp. 17–29.

Demaison, G.J., Moore, G.T., 1980. Anoxic environments and oil source bed genesis. Organic Geochemistry 2, 9–31.

Dornbos, S.Q., Chen, J.-Y., 2008. Community palaeoecology of the early Cambrian Maotianshan Shale biota: Ecological dominance of priapulid worms. Palaeogeography, Palaeoclimatology, Palaeoecology 258, 200–212.

Dyson, I.A., Gatehouse, C.G., Jago, J.B., 1994. The significance of the sequence boundary at the base of the Early Cambrian Talisker Calc-Siltstone and its relationship to mineralization in the Kanmantoo Trough. Geological Society of Australia Abstracts 37, 92-93.

Fairclough, M.C., 2008. KINGSCOTE SPECIAL map sheet. South Australia. Geological Survey. Geological Atlas 1:250 000 Series, sheet SH 53-16.

Fike, D.A., Grotzinger, J.P., Pratt, L.M., Summons, R.E., 2006. Oxidation of the Ediacaran Ocean. Nature 444, 744–747.

Gaines, R.R., Briggs, D.E.G., Zhao, Y., 2008. Cambrian Burgess Shale-type deposits share a common mode of fossilization. Geology 36, 755–758.

Gaines, R.R., Droser, M.L., 2003. Paleoecology of the familiar trilobite Elrathia kingii: an early exaerobic zone inhabitant. Geology 31, 941–944

Gaines, R.R., Kennedy, M.J., Droser, M.L., 2005. A new hypothesis for organic preservation of Burgess Shale taxa in the Middle Cambrian Wheeler Formation, House Range, Utah. Palaeogeography, Palaeoclimatology, Palaeoecology 220, 193–205.

García-Bellido, D.C., Paterson, J.R., Edgecombe, G.D., Jago, J.B., Gehling, J.G., Lee, M.S.Y., 2009. The bivalved arthropods Isoxys and Tuzoia with soft-part preservation from the Lower Cambrian Emu Bay Shale lagerstätte (Kangaroo Island, Australia). Palaeontology 52, 1221–1241.

Gehling, J.G., 1999. Microbial mats in terminal Proterozoic siliciclastics: Ediacaran death masks. Palaios 14, 40–57.

Gehling, J.G., Jago, J.B., Paterson, J.R., García-Bellido, D.C., Edgecombe, G.D., 2011. The geological context of the lower Cambrian (Series 2) Emu Bay Shale Lagerstätte and adjacent stratigraphic units, Kangaroo Island, South Australia. Australian Journal of Earth Sciences 58, 243-258.

Glaessner, M.F., 1979. Lower Cambrian Crustacea and annelid worms from Kangaroo island, South Australia. Alcheringa 3, 21–31.

Glaessner, M.F., Wade, M., 1966. The late Precambrian fossils from Ediacara, South Australia. Palaeontology 9, 599–628.

Gravestock, D.I., Gatehouse, C.G., 1995. Stansbury Basin. In: Drexel J.F & Preiss W.V. eds. The Geology of South Australia. Volume 2, The Phanerozoic. Geological Survey of South Australia, Bulletin 54, pp. 5–19.

Gum, J.C., 1998. The sedimentology, sequence stratigraphy and mineralization of the Silverton Subgroup, South Australia. PhD thesis, University of South Australia (unpublished).

Gum, J.C., Jago, J.B., Gatehouse, C.G., 1994. Sedimentological constraints on mineralization in the Southern Kanmantoo Trough. Australian Research on Ore Genesis Symposium, Proceedings. Australian Mineral Foundation, Adelaide, pp. 13.1–13.4.

Guo, Q., Shields, G.A., Liu, C., Strauss, H., Zhu, M., Pi, D., Goldberg, T., Yang, X., 2007a. Trace element chemostratigraphy of two Ediacaran–Cambrian successions in South China: Implications for organosedimentary metal enrichment and silicification in the early Cambrian. Palaeogeography, Palaeoclimatology, Palaeoecology 254, 194–216.

Guo, Q., Strauss, H., Liu, C., Goldberg, T., Zhu, M., Pi, D., Heubeck, C., Vernhet, E., Yang, X., Fu, P., 2007b. Carbon isotopic evolution of the terminal Neoproterozoic and early Cambrian: Evidence from the Yangtze Platform, South China. Palaeogeography, Palaeoclimatology, Palaeoecology 254, 140–157.

Hagadorn J. W., 2002. Burgess Shale-type localities: the global picture. In: Bottjer D. J., Etter W., Hagadorn J. W. & Tang C. M. eds. Exceptional Fossil Preservation: A Unique View on the Evolution of Marine Life. Columbia University Press, New York, pp. 91–116.

Hall, P.A, McKirdy, D.M., Halverson, G.P., Turner, B.L., Carson, M.W., Nedin, C., Jago, J.B., Gehling, J.G., Collins, A.S., 2010. The biogeochemical status of the Palaeo-Pacific Ocean: clues from the early Cambrian of South Australia. Geological Society of Australia Abstracts 98, 165–166.

Halverson, G.P., Hurtgen, M.T., Porter, S.M., Collins, A.S., 2009. Neoproterozoic-Cambrian biogeochemical evolution. In: Gaucher C., Sial A.N., Halverson G.P. & Frimmel H.E. eds. Developments in Precambrian Geology 16, Elsevier, pp. 351–365.

Hayes, J.M., Kaplan, I.R., Wedeking, K.W., 1983. Precambrian organic geochemistry - preservation of the record. In: Schopf J.W. ed. Earth's Earliest Biosphere, Its Origin and Evolution. Princeton University Press, New Jersey, pp. 93–134.

Ivantsov, A.Yu., Zhuravlev, A.Yu., Leguta, A.V., Krassilov, V.A., Melnikova, L.M., Ushatinskaya, G.T., 2005. Palaeoecology of the Early Cambrian Sinsk biota from the Siberian Platform. Palaeogeography, Palaeoclimatology, Palaeoecology 220, 167–192.

Jago J. B. & Cooper B. J. 2011. The Emu Bay Shale Lagerstätte: a history of investigations. Australian Journal of Earth Sciences 58, 235-242.

Jago, J.B., Daily, B., Von der Borch, C.C., Cernovskis, A., Saunders, N., 1984. First reported trilobites from the Lower Cambrian Normanville Group, Fleurieu Peninsula, South Australia. Transactions of the Royal Society of South Australia 108, 207–211.

Jago, J.B., Paterson, J.R., Alexander, E.M., Gehling, J.G., 2006. Fossiliferous Cambrian localities on the north coast of Kangaroo Island. In: Jago J.B. & Zang W.L. eds., XI International Conference of the Cambrian Stage Subdivision Working Group. Field Guide. Geological Society of Australia, South Division, Adelaide, pp. 21–24.

Jago, J.B., Zang, W., Sun, X., Brock, G.A., Paterson, G.A., Skovsted, C., 2006. A review of the Cambrian biostratigraphy of South Australia. Palaeoworld 15, 69–88.

James, N.P., Gravestock, D.I.G., 1990. Lower Cambrian shelf and shelf margin buildups, Flinders Ranges, South Australia. Sedimentology 37, 455–480.

Jenkins, R.J.F., 1992. Functional and ecological aspects of Ediacaran assemblages. In: Lipps, J. H., Signor, P. W. eds. Origin and Early Evolution of Metazoa. Plenum, New York, pp. 131–176.

Jenkins, R.J.F., Hasenohr, P., 1989. Trilobites and their trails in a black shale: Early Cambrian of the Fleurieu Peninsula, South Australia. Transactions of the Royal Society of South Australia 113, 195–203.

Jenkins, R.J.F., Nedin, C., 2007. The provenance and palaeobiology of a new multi-vaned, chambered frondose organism from the Ediacaran (later Neoproterozoic) of South Australia. In: Vickers-Rich P. & Komarower P. eds. The Rise and Fall of the Ediacaran Biota. Geological Society, London, Special Publications 286, pp. 195–222.

Jones, B., Manning, D.A.C., 1994. Comparison of geochemical indices used for the interpretation of paleoredox conditions in ancient sediments. Chemical Geology 111, 111–119.

Kelafant J. R., 1987. A reinterpretation of the Burgess Shale paleoenvironment. M.Sc. thesis, George Washington University, Washington, D.C. (unpublished).

Kimura, H., Watanabe, Y., 2001. Ocean anoxia at the Precambrian-Cambrian boundary. Geology 29, 995–998.

Knoll, A.H., Carroll, S.B., 1999. Early animal evolution: emerging views from comparative biology and geology. Science 284, 2129–2137.

Knoll, A.H., Walter, M.R., 1992. Latest Proterozoic stratigraphy and Earth history. Nature 356, 673–677.

Kübler, B., 1968. Evaluation quantitative du métamorphisme par cristallinité de l'illite. Bulletin Centre de Recherche Pau SNPA 2, 385–397.

Landis, C.A., 1971. Graphitization of dispersed carbonaceous material in metamorphic rocks. Contributions to Mineralogy and Petrology 30, 34–45.

Logan, G.R., Summons, R.E. Hayes, J.M., 1997. An isotopic biogeochemical study of Neoproterozoic and Early Cambrian sediments from the Centralian Superbasin, Australia. Geochimica et Cosmochimica Acta 61, 5391–5409.

McKirdy, D., Hall, A., Halverson, G., Nedin, C., Michaelsen B.H., 2010. Biomarker, isotopic and trace element signatures of an early Cambrian Lägerstatte in the Stansbury Basin, South Australia. 15th Australian Organic Geochemistry Conference, Canberra, Abstracts.

McKirdy, D.M., 1971. An organic geochemical study of Australian Cambrian and Precambrian sedimentary rocks. MSc thesis, University of Adelaide (unpublished).

McKirdy, D.M., 1994a. Biomarker geochemistry of the Early Cambrian oil show in Wilkatana-1: implications for oil generation in the Arrowie and Stansbury Basins. PESA Journal 22, 3-17.

McKirdy, D.M., 1994b. Cambrian source rock geochemistry, Stansbury Basin. 3. Thermal maturity of Early Cambrian Mount McDonnell Formation in Investigator-2, northern Kangaroo Island. Report for Canyon (Australia) Pty Limited. South Australia. Department of Primary Industries and Resources. Open file Envelope 8457 R33 (unpublished).

McKirdy, D.M., Kantsler, A.J., Emmett, J.K. Aldridge, A.K., 1984. Hydrocarbon genesis and organic facies in Cambrian carbonates of the eastern Officer Basin, South Australia. In: Palacas J.G. ed. Petroleum Geochemistry and Source Rock Potential of Carbonate Rocks. American Association of Petroleum Geologists Studies in Geology 18, pp. 12–32.

McKirdy, D.M., Powell, T.G., 1974. Metamorphic alteration of carbon isotopic composition in ancient sedimentary organic matter: new evidence from Australia and South Africa. Geology 2, 591–595.

Narbonne, G.M., 2005. The Ediacara biota: Neoproterozoic origin of animals and their ecosystems. Annual Review of Earth and Planetary Sciences 33, 421–442.

Nedin, C., 1995. The palaeontology and palaeoenvironment of the Early Cambrian Emu Bay Shale, Kangaroo Island, South Australia. PhD thesis, University of Adelaide (unpublished).

Nedin, C., 1999. Anomalocaris predation on nonmineralized and mineralized trilobites. Geology 27, 987–990.

Orr, W.G., Briggs, D.E.G., Kearns, S.L., 1998. Cambrian Burgess Shale animals replicated in clay minerals. Science 281, 1173–1175.

Parker, A.J., 1986. Tectonic development and metallogeny of the Kanmantoo trough in South Australia. Ore Geology Reviews 1, 203–212.

Paterson, J.R., Edgecombe, G.D., Garcia-Bellído, D.C., Jago, J.B., Gehling J.G., 2010. Nektaspid arthropods from the lower Cambrian Emu Bay Shale Lagerstätte, South Australia, with a reassessment of lamellipedian relationships. Palaeontology 53, 377–402.

Paterson, J.R., Jago J.B., 2006. New trilobites from the Lower Cambrian Emu Bay Shale Lagerstätte at Big Gully, Kangaroo Island, South Australia. Memoirs of the Association of Australasian Palaeontologists 32, 43–57.

Paterson, J.R., Jago, J.B., Gehling, J.G., Garcia-Bellído, D.C., Edgecombe, G.D., Lee M.S.Y., 2008. Early Cambrian arthropods from the Emu Bay Shale Lagerstätte, South Australia. In: Rábano I., Gozalo R. & Garcia-Bellido D. eds. Advances in Trilobite Research. Insituto Geológico y Minero de España, Madrid, pp. 319–325.

Peat, C.J., 1984. Precambrian microfossils from the Longmyndian of Shropshire. Proceedings of the Geologists' Association 5, 17–22.

Pocock, K.J., 1964. Estaingia, a new trilobite genus from the Lower Cambrian of South Australia. Palaeontology 7, 458–471.

Powell, W., 2003. Greenschist facies metamorphism of the Burgess Shale and its implications for models of fossil formation and preservation. Canadian Journal of Earth Sciences. 40, 13–25.

Powell, W.G., 2009. Comparison of geochemical and distinctive mineralogical features associated with the Kinzers and Burgess Shale formations and their associated units. Palaeogeography, Palaeoclimatology, Palaeoecology 277, 127–140.

Powell, W.G., Johnston, P.A., Collom, C.J., 2003. Geochemical evidence for oxygenated bottom waters during deposition of fossiliferous strata of the Burgess Shale Formation. Palaeogeography, Palaeoclimatology, Palaeoecology 201, 249–268.

Raiswell, R., Berner, R.A., 1987. Organic carbon losses during burial and thermal maturation of normal marine shales. Geology 15, 853-856.

Savrda, C.E., Bottjer, D.J., 1987. The exaerobic zone, a new oxygen-deficient marine biofacies. Nature 327, 54–56.

Seccombe, P.K., Spry, P.G., Both, R.A., Jones, M.T., Schiller, J.C., 1985. Base metal mineralization in the Kanmantoo Group, South Australia: a regional sulfur isotope study. Economic Geology 80, 1824–1841.

Skinner, E.S., 2005. Taphonomy and depositional circumstances of exceptionally preserved fossils from the Kinzers Formation (Cambrian), southeastern Pennsylvania. Palaeogeography, Palaeoclimatology, Palaeoecology 220, 167–192.

Steiner, M., Li, G., Qi, Y., Zhu, M., 2004. Lower Cambrian small shelly fossils of northern Shaanxi (China), and their biostratigraphic importance. Geobios 37, 259–275.

Stewart, W.D., Dixon, O.A., Rust, B.R., 1993. Middle Cambrian carbonate-platform collapse, southeastern Canadian Rocky Mountains. Geology 21, 687–690.

Strauss, H., DesMarais, D.J., Summons, R.E., Hayes, J.M., 1992. Concentrations of organic carbon and maturities and elemental compositions of kerogens. In: Schopf, J.W., Klein, C. eds. The Proterozoic Biosphere: A Multidisciplinary Study. Cambridge University Press, New York, pp. 95–100.

Taylor, S.R., McLennan, S.M., 1985. The Continental Crust – Its Composition and Evolution. Blackwell Scientific, Oxford, 312 p.

Tribovillard, N., Alego, T.J., Lyons, T., Riboulleau, A., 2006. Trace metals as paleoredox and paleoproductivity proxies: An update. Chemical Geology 232, 12–32.

Tucker, M.E., 1989. Carbon isotopes and Precambrian-Cambrian boundary geology, South Australia: ocean basin formation, seawater chemistry and organic evolution. Terra Nova 1, 573–582.

Tyson, R.V., 1995. Sedimentary Organic Matter: Organic Facies and Palynofacies. Chapman & Hall, London, 615 p.

Tyson, R.V., 2001. Sedimentation rate, dilution, preservation and total organic carbon: some results of a modelling study. Organic Geochemistry 32, 333–339.

Vine, J.D., Tourtelot, E.B., 1970. Geochemistry of black shale deposits – a summary report. Economic Geology 65, 253–272.

Weaver C.E., 1961. Clay minerals of the Ouachita structural belt and adjacent foreland. In: Flawn, P.T., Goldstein, A. Jr., King, P.B., Weaver, C.E. eds. The Ouachita System. University of Texas, Bureau of Economic Geology Publication 6120, pp. 147–162.

Williams, L.A., Reimers, C., 1983. Role of bacterial mats in oxygen-deficient marine basins and coastal upwelling regimes: Preliminary report. Geology 11, 267–269.

Zhang, X.L., Liu, W., Zhao, Y.L., 2008. Cambrian Burgess Shale-type Lagerstätten in South China: Distribution and significance. Gondwana Research 14, 255–262.

Zhu, M., Babcock, L.E., Steiner, M., 2005. Fossilization modes in the Chengjiang Lagerstätte (Cambrian of China). Palaeogeography, Palaeoclimatology, Palaeoecology 220, 31–46.

Biomarker and isotopic signatures of an early Cambrian Lagerstätte in the Stansbury Basin, South Australia

P. Anthony Hall[a,*], David M. McKirdy[a,], Galen P. Halverson[a,1], James B. Jago[b] and James G. Gehling[c]

Organic Geochemistry 42 (2011) 1324-1330

[a] Organic Geochemistry in Basin Analysis Group, Centre for Tectonics, Resources & Exploration (TRaX), School of Earth & Environmental Sciences, University of Adelaide, SA 5005, Australia
[b] School of Natural & Built Environments, University of South Australia, Mawson Lakes, SA 5095, Australia
[c] Science Centre, South Australian Museum, Adelaide, SA 5000, Australia
[1] Present address: Department of Earth & Planetary Sciences, McGill University, Montreal, Canada H3A 2A7

STATEMENT OF AUTHORSHIP

Biomarker and isotopic signatures of an early Cambrian Lagerstätte in the Stansbury Basin, South Australia

Philip Anthony Hall (Candidate)

Performed preparation and analysis or oversaw the analysis on all samples, interpreted data, wrote manuscript and acted as corresponding author

I hereby certify that the statement of contribution is accurate

Signed …….*Date*……

David M. McKirdy

Biomarker and isotopic signatures of an early Cambrian Lagerstätte in the Stansbury Basin, South Australia

Statement of contribution (in terms of the conceptualization of the work, its realization and its documentation)

Contributed to planning of article and provided critical evaluation

Certification that the statement of contribution is accurate and permission is given for the inclusion of the paper in the thesis

Signed …….Date…20/06/2012…

Galen P. Halverson

Biomarker and isotopic signatures of an early Cambrian Lagerstätte in the Stansbury Basin, South Australia

Statement of contribution (in terms of the conceptualization of the work, its realization and its documentation)

Contributed to planning of article and provided critical evaluation

Certification that the statement of contribution is accurate and permission is given for the inclusion of the paper in the thesis

Signed …….Date…19/06/2012…

James B. Jago

Biomarker and isotopic signatures of an early Cambrian Lagerstätte in the Stansbury Basin, South Australia

Statement of contribution (in terms of the conceptualization of the work, its realization and its documentation)

Contributed to sample collection and provided critical evaluation

Certification that the statement of contribution is accurate and permission is given for the inclusion of the paper in the thesis

Signed …….Date…20/06/2012…

James G. Gehling

Biomarker and isotopic signatures of an early Cambrian Lagerstätte in the Stansbury Basin, South Australia

Statement of contribution (in terms of the conceptualization of the work, its realization and its documentation)

Contributed to sample collection and provided critical evaluation

Certification that the statement of contribution is accurate and permission is given for the inclusion of the paper in the thesis

Signed …….Date…20/06/2012…

Abstract

The lower Cambrian (Series 2) Emu Bay Shale biota, found at Big Gully on the north coast of Kangaroo Island, South Australia, is by far the richest Burgess Shale-type (BST) fauna in the southern hemisphere. While the trace element geochemistry of the host shale shows it accumulated beneath an *oxic* water column, this appears difficult to reconcile with the exceptional preservation of organs such as gut glands, muscles and eyes in some of its fauna. Micro-scale sealed vessel (MSSV) pyrolysis of kerogen isolated from a solvent-extracted sample of fossiliferous Emu Bay Shale provided independent confirmation of its redox status and also implicated cyanobacteria in the preservation of its fauna. Thermal extraction and pyrolysis each yielded alkanes displaying a low ratio of pristane to phytane (pr/ph = 1) and *n*-alkanes with a marked odd over even predominance in the $<C_{20}$ range. The latter molecular signature is diagnostic of *Gloeocapsomorpha prisca* and is the first indication that mats of this or a similar coccoid cyanobacterium were involved in the taphonomy of a BST deposit. Hopanes (including 2-methylhopanes) are far more abundant than steranes and the shale's bulk organic matter has $\delta^{13}C$ values in the range -32 to -28‰, providing further evidence of the cyanobacterial affinity of its microbial biomass. Thus mat-forming cyanophytes, rather than sulfur-oxidising bacteria, may have played a key role in maintaining a sharp redox boundary at the sediment-water interface during deposition of the Emu Bay Shale Lagerstätte, thereby enabling the survival of soft body parts within its fossil fauna for long enough to permit inorganic replication of their fine detail during late diagenesis.

Key words South Australia, Emu Bay Shale, Lagerstätte, Cambrian, kerogen, biomarker, carbon isotopes, *Gloeocapsomorpha prisca*, cyanobacterial mats.

4.1. Introduction

While fossil assemblages of soft-bodied organisms (Lagerstätten) are rare, they are unusually common in marine sedimentary sequences of early and mid-Cambrian age (Allison and Briggs, 1993). Not surprisingly, their mode of preservation has been the subject of much debate. The Emu Bay Shale biota, found at Big Gully on the north coast of Kangaroo Island (Fig. 1), is by far the richest Burgess Shale-type (BST) fauna in the southern hemisphere (Nedin, 1995; Gehling et al., 2011). Such faunas are characteristically preserved as two-dimensional compression fossils, comprising carbonaceous films on bedding surfaces of the host marine mudstones. The Big Gully assemblage comprises at least 45 taxa, suggesting a habitat very favourable for life. Its preservation is exceptional, with gut remains and other soft parts quite common (e.g. Briggs and Nedin, 1997; García-Bellido et al., 2009; Lee et al., 2011). Predation and scavenging were minimal and the finely laminated texture of the host mudstone attests to a lack of burrowing and bioturbation. Notwithstanding earlier studies suggesting otherwise, Gaines et al. (2008) concluded that conservation of organic tissues, rather than authigenic mineralisation of their more labile components, is the principal taphonomic pathway responsible for BST deposits. Such preservation requires suppression of the early diagenetic processes that normally result in the rapid decay of organic matter at or near the sea floor.

It has long been assumed that the basal ~8 m-thick section of the Emu Bay Shale, which hosts the Lagerstätte, was a sedimentary record of oxygen depletion at the sea floor (Daily et al., 1979; Paterson et al., 2008). This hypothesis remained unchallenged until quite recently when, using the redox-sensitive trace element ratios U/Th, V/Cr and Ni/Co (Jones and Manning, 1994) and V/Sc (Kimura and Watanabe,

2001), McKirdy et al. (2011) demonstrated that the Emu Bay Shale Lagerstätte actually was deposited beneath an *oxic* water column. In this respect it is similar to the archetypical Burgess Shale deposit in British Columbia, Canada (Powell et al., 2003). However, unlike the latter formation, which has undergone lower greenschist facies metamorphism, the Emu Bay Shale is of low enough thermal maturity (late catagenesis; McKirdy *et al*. 2011) to allow preservation of both its primary organic carbon isotopic signatures ($\delta^{13}C_{org}$) and a suite of kerogen-bound biomarker alkanes. Here we present $\delta^{13}C_{org}$ and biomarker data which together indicate that benthic cyanobacterial mats, possibly including *Gloeocapsomorpha prisca*, are likely to have played a key role in maintaining a sharp redox boundary at the sediment-water interface during deposition of the Emu Bay Lagerstätte, thereby aiding the preservation of non-mineralised tissue within its fossil fauna.

4.2. Materials and methods

The kerogen sample analysed in this study was isolated during one of the first organic geochemical investigations of Australian Cambrian and Precambrian sedimentary rocks (McKirdy, 1971). All solvents were AR grade and doubly distilled immediately before use. The additional rock samples (n = 12) intended for further geochemical analysis (McKirdy et al., 2011), including determination of their total organic carbon (TOC) contents and bulk organic carbon isotopic composition ($\delta^{13}C_{org}$), were collected during 2009 from the shoreline and Buck Quarry sites in Big Gully on northern Kangaroo Island (Fig. 1).

NOTE:
This figure/table/image has been removed to comply with copyright regulations.
It is included in the print copy of the thesis held by the University of Adelaide Library.

Fig. 1 Map of the northeastern coast of Kangaroo Island, South Australia, showing (A) Cambrian outcrop and (B) the Big Gully shoreline and Buck Quarry Lagerstätte sites within the Emu Bay Shale (after García-Bellido et al. 2009; reproduced with permission of The Palaeontological Association). 'Smith Bay Shale' between Bald Rock and Hawk Nest is now regarded as an association of fine-grained lithofacies within the lower White Point Conglomerate, while the upper part of this formation has been re-defined as the Marsden Sandstone (Gehling et al., 2011).

4.2.1 Sample preparation

Representative portions (5 g) were broken from freshly exposed interior surfaces of ~2 kg-sized rock specimens (the aforementioned additional rock samples) and then powdered in a pre-cleaned mortar and pestle, in preparation for TOC and $\delta^{13}C_{org}$ analysis.

Using a water-lubricated diamond saw, a solid block (~1 kg) lacking any obvious weathering, fractures or cleavage was cut from the interior of a much larger specimen of fossiliferous Emu Bay Shale, collected in 1967 from the shoreline locality at Big Gully (Fig. 1). After scrubbing with a steel wire brush and rinsing in distilled water, the block was immersed in 20% hydrofluoric acid for sufficient time to achieve a dry weight loss of 5–10%, thoroughly washed in distilled water and air-died. The freshly etched block was crushed with a steel hammer and chips 6–11 mm in diameter retrieved by sieving. The chips were sonicated in benzene/methanol (3:1, 2 x 10 min), dried and finally pulverized to ~200 mesh BSS in the 200 ml chrome steel vessel of a Siebtechnik disc mill (Tema Machinery Ltd). Prior to their use, the crushing implements were rinsed in benzene and a preliminary batch (20-30 g) of rock chips pulverized and discarded.

Powdered shale (0.3 kg; total organic carbon content = 0.37%) was extracted in Soxhlet apparatus with benzene/methanol (4:1) for 114 h, followed by *n*-heptane for a further 102 h. The recovered extractable organic matter (total yield = 6.5 mg/g TOC) was equivalent to bitumen I (Sherman et al., 2007). Demineralisation of an aliquot of the exhaustively extracted shale (50 g), as described in McKirdy and Powell (1974), yielded a kerogen concentrate (266 mg). The kerogen has remained sealed in its original solvent-washed screw-top glass vial (2 ml capacity) and stored in darkness since it was last opened in 1973 to remove an aliquot for stable isotope analysis. The only possible source of contamination is the cap liner. In this case, the expected contaminants would be phthalates, which are not observed in either the thermal extract or the pyrolysate (see below).

4.2.2 Thermal extraction, pyrolysis and GC-MS analysis

Instead of further solvent extraction, we chose to analyse the kerogen using micro-scale sealed vessel (MSSV) thermal extraction and pyrolysis (Hall et al., 1999). The advantage of this approach was that it allowed comparison of the kerogen-occluded bitumen (bitumen II), released in the thermal extraction mode, with the kerogen pyrolysate. For each analysis, kerogen (5 mg) was transferred to a pre-cleaned MSSV glass reactor tube (high purity silica, sealed at one end, with an internal volume of 30–40 μl and bent at approximately 120º in the middle). The tube dead volume was filled with pre-cleaned, 80–120 mesh, glass beads and the tube sealed with a high-temperature propane torch. Samples to undergo investigation by pyrolysis were then transferred to a high precision oven and heated for 24 h at 325ºC. Analyses were undertaken utilising a Quantum MSSV injector fitted to a Hewlett Packard 6890/5973 gas chromatograph-mass spectrometer (GC-MS) system. An HP5-MS capillary column of 25 m length, 0.25 mm ID and 0.25 μdf coating was used for the separations with helium carrier gas at a constant pressure of 60 KPa. Reactor tubes were inserted into the injector heated at 300ºC and taken through a cleaning cycle of the GC by heating from 45 to 300ºC at 15ºC/min before holding at 300ºC for 15 min to remove any contaminants from the exterior of the tubes. This cleaning cycle also served as the thermal desorption stage for non-pyrolysed samples including additional dwell time to extend the overall period to 1 hr. The tubes were then cracked open within the injector, operating in splitless mode for 2 min, with the released analytes cryofocused in the front of the capillary column using a liquid nitrogen bath. GC-MS analysis was conducted, in either full scan or selected ion mode, employing a temperature program of 45 to 300ºC at 6ºC/min, then held isothermal for 17 min. Full scan data were acquired over a range of 40 to 500 amu at approximately 3 scans per sec, whilst

selected ion data was acquired for masses 123, 177, 191, 205, 217, 218, 231, 253 and 259 at a dwell time of 100 ms.

4.2.3 Total organic carbon and stable isotope analyses

Whole-rock samples (~2 g) were submitted to Amdel Limited, Adelaide, for determination of TOC using a Leco Carbon/Sulfur Analyser.

Powdered samples (0.2 g) were digested three times in 10% HCl to remove carbonate, rinsed in deionised water, and dried. The residues were transferred to pre-cleaned 6 x 4 mm tin capsules for combustion in a Carlo Erba EA1500 series II elemental analyser and the produced CO_2 analysed in continuous flow mode on a tandem Fisons Optima IRMS. The acquired data were calibrated against in-house glycine and glutamic acid standards ($\delta^{13}C_{V\text{-}PDB}$ = -31.2, -17.1‰, respectively) and precision and accuracy monitored by regular analyses of an in-house sucrose standard (-25.8‰). Over the course of these analyses, the reproducibility (1s) was ±0.2‰. The resulting $\delta^{13}C_{org}$ measurements are reported relative to the V-PDB standard.

4.3. Results and discussion

4.3.1 Biomarker signatures

The biomarker alkanes identified by GC-MS analysis of the thermal extract and pyrolysate of the Emu Bay Shale kerogen are summarised in Table 1. The *m/z* 57 chromatograms of the two fractions (Fig. 2) reveal a marked predominance of odd-carbon-numbered *n*-alkanes in the $<C_{20}$ range (e.g. OEP at C_{17} ≥2); a low relative abundance of acyclic isoprenoid alkanes (pristane/*n*-heptadecane ≤0.2, phytane/*n*-octadecane ≤0.4) and a low ratio of pristane to phytane (pr/ph ≈ 1.3). Similar

molecular signatures have been widely reported in Ordovician oils, source rocks and oil shales (kukersites) and attributed to the lipid-rich coccoid microorganism *Gloeocapsomorpha prisca* (e.g. Reed et al., 1986; Foster et al., 1986; Hoffmann et al., 1987; Summons and Powell, 1991; Fowler, 1992). While *G. prisca* flourished in sub-equatorial epeiric seas during the Ordovician, it has also been found in Cambrian marine sediments from Canada (Stasiuk and Osadetz, 1990) and elsewhere in South Australia (Michaelsen et al., 1995). During the Cambrian, South Australia was in the tropics (Brock et al., 2000; Jago et al., 2006). A pristane/phytane ratio ~1 is consistent with the existence of a sharp boundary between the oxic water column (indicated by the aforementioned trace element palaeoredox proxies) and non-bioturbated anoxic muds flooring the Emu Bay depocentre (McKirdy et al., 2011).

Although its ecological and biological affinity has been much debated (Fowler, 1992), *G. prisca* is now generally regarded as an obligate marine cyanobacterium (Foster et al., 1989; Glaessner and Foster, 1992) which, according to Stasiuk and Osadetz (1990), may be either planktonic or benthic depending on the stage of its life cycle. Each of the three stages has a distinctive morphology and chemical composition. Kerogen derived from the mat-forming stromatolitic morphotype becomes increasingly aliphatic with increasing thermal maturation (Stasiuk et al., 1993). This pattern is consistent with the survival of the aforementioned normal and isoprenoid alkane fingerprints of a *G. prisca*-like organism in the late catagenetic Emu Bay Shale.

Another characteristic feature of the geolipids derived from *G. prisca* is C_{13}–C_{19} *n*-alkylcyclohexanes with a strong odd-carbon-number preference (Hoffmann et al., 1987; Fowler, 1992). Those present in the Emu Bay Shale, however, extend over a

wider range (C_9–C_{24}) and display little or no odd-over-even predominance. Here the C_{20+} homologues are orphan biomarkers, since they are unlikely to have originated from the fatty acids of cyanobacteria or other bacteria.

Although signal to noise is low in the pyrolysate, 17α-hopanes (C_{27}-C_{32}) and steranes (C_{27}-C_{30}) are present and quantifiable in the thermal extract of the kerogen (Table 1, Fig. 3). Here the high ratio of hopane to cholestane (the dominant homologues) reflects the mainly bacterial and cyanobacterial origin of the organic matter preserved in the Emu Bay Shale Lagerstätte. The presence of 2-methylhopanes could be regarded as further evidence of the contribution of cyanobacteria (Summons et al., 1999) to its microbial biomass. Indeed, cyanobacteria are thought to be the most significant producers of 2-methylhopanoids in the modern environment (Talbot et al., 2008). However, they are not the only modern bacteria capable of synthesizing the precursor 2-methylbacteriohopanepolyols, and not all cyanobacteria make 2-methylhopanoids (Welander et al., 2010).

The dominance of cholestane among the regular steranes may in part reflect the preservation of animal steroids. The C_{28}/C_{29} sterane ratio (0.83) is higher than would normally be expected for a marine shale of Cambrian age (Grantham and Wakefield, 1988). On the other hand, the presence of both 24-*n*- and 24-isopropylcholestane is entirely consistent with the age and depositional environment of the Emu Bay Shale (McCaffrey et al., 1994), especially given that demosponges are part of its fauna (Gehling et al., 2011; McKirdy et al., 2011).

Table 1. Biomarker source and maturity data obtained by GC-MS analysis of the MSSV thermal extract and pyrolysate of kerogen isolated from a sample of solvent-extracted Emu Bay Shale.

Run	Acyclic alkanes					Hopanes			
	OEP		Pr/*n*-C_{17}	Ph/*n*-C_{18}	Pr/Ph	Range	Ts/Tm	29/30	2-MeH/Hop
	n-C_{15}	*n*-C_{17}							
1[a]	1.4	2.1	0.18	0.45	1.2	27–32	0.82	0.79	0.07
2[b]	1.8	3.1	0.06	0.23	1.3	27–30	1.02	1.26	nd
m/z			57				191, 205		

Steranes					Hopane/Sterane
27 %	28 %	29 %	30[c] %	27 Dia/Reg	30 Hop/27 Ster
40	24	29	7	0.75	2.8
nd	nd	nd	nd	2.2	2.1
217, 218					191, 217

OEP = odd/even predominance (Scalan and Smith 1970)
Pr/Ph = pristane/phytane
Ts/Tm = 18α-22,29,30-trisnorneohopane/17α-22,29,30-trisnorhopane
29/30 = 30-norhopane/hopane
2-MeH/Hop = 2α-methylhopane/hopane
27 = 5α,14β,17β-cholestane 20R+20S; 28 = 5α,14β,17β-24-methylcholestane 20R+20S;
29 = 5α,14β,17β-24-ethylcholestane 20R+20S; 30 = 5α,14β,17β-24-propylcholestane 20R+20S
27 Dia/Reg = diacholestane/cholestane
30 Hop/27 Ster = hopane/cholestane
nd = not determined (signal/noise ratio <10:1 in mass chromatogram)
[a] 300ºC for 1 h (equivalent to bitumen II: Sherman et al. 2007)
[b] 325ºC for 24 h (kerogen pyrolysate)
[c] both 24-*n*-propyl and 24-isopropyl

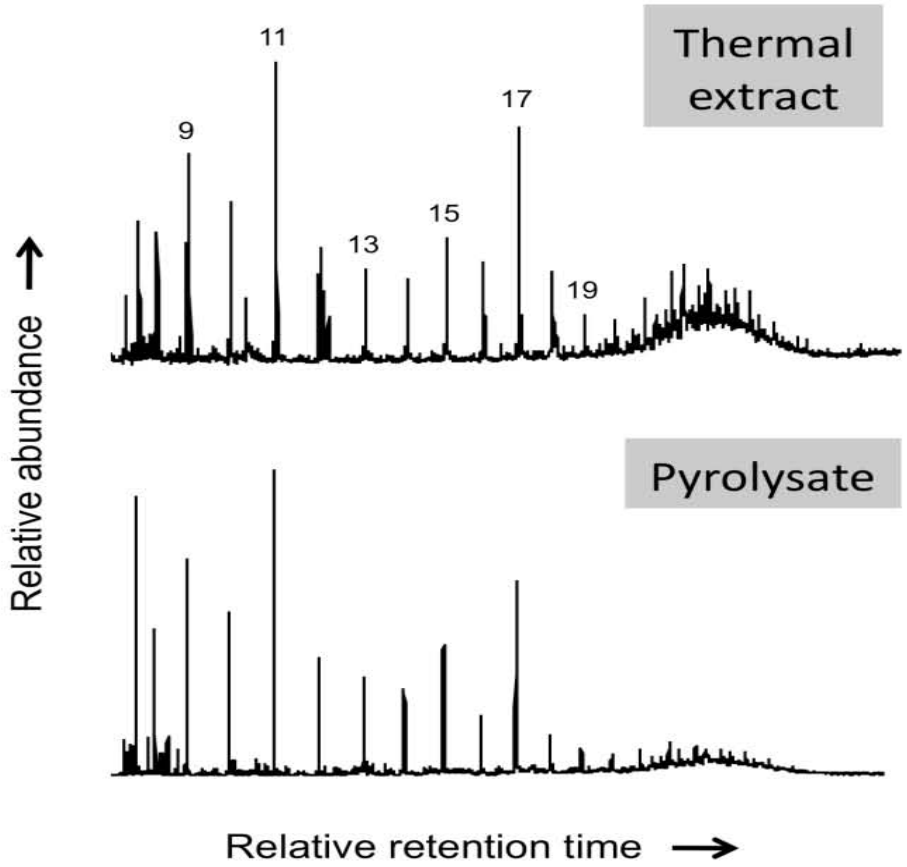

Fig. 2 Mass chromatograms (*m/z* 57) of MSSV thermal extract and pyrolysate of kerogen isolated from solvent-extracted Emu Bay Shale. Numbers indicate chain length of corresponding *n*-alkanes.

Interestingly, the *n*-alkane distribution of the bitumen I extracted from the Emu Bay Shale prior to acid digestion (range = C_{13}–C_{23}; maximum = C_{15}; OEP = 1.1 at C_{15}, 0.97 at C_{17}, 1.1 at C_{19}: McKirdy, 1971) exhibited no sign of the characteristic *G. prisca* signature. Notwithstanding the low porosity (≤15%) and permeability (≤0.1 md) of the original specimen, and the removal of potentially weathered surfaces before crushing, these free hydrocarbons appear to have been contaminated by short-chained *n*-alkanes in the soil organic matter washing down Big Gully to the shore platform (Fig. 1) over thousands of years. Such *n*-alkanes originate from the roots and

leaves of C_4 grasses (Kuhn et al., 2010). Their marked *even-carbon-number predominance* is capable of obscuring the primary *n*-alkane signature of the basal Emu Bay Shale; or, in the case of nearby coastal outcrops on Kangaroo Island of an older Cambrian Series 2 unit (viz. the Mount MacDonnell Formation), overwhelming it (McKirdy and Padley, 1993).

Based on its kerogen H/C = 0.48 and Weaver index of illite crystallinity = 3.8, the Emu Bay Shale at Big Gully has a rank equivalent to ~1.5% vitrinite reflectance (VR: McKirdy et al., 2011). Hitherto, a rock sample of such thermal maturity would perhaps have been regarded as an unlikely repository for indigenous biomarker hydrocarbons such as hopanes and steranes. Nevertheless, recent studies have demonstrated the ability of these biomarkers to survive intact in highly mature Precambrian shales (Sherman et al., 2007). The fact that the diagnostic *n*-alkane signature of *G. prisca* survives in the Emu Bay Shale is less surprising. The same signature is easily recognisable in supermature Ordovician crude oil from the Amadeus Basin, central Australia (heptane value = 35, isoheptane value = 7; methylphenanthrene index = 1.24, calculated VR = 1.15%: Jackson et al., 1984; McKirdy et al., 1986). The two maturity parameters, Ts/Tm and diacholestane/cholestane (Table 1), are lower than expected in the thermal extract. This may be attributed to two separate factors. First, in kerogen-occluded hydrocarbons (bitumen II), both biomarker ratios are commonly less than in the co-existing free hydrocarbons (bitumen I: Nabbefeld et al., 2010). Second, the oxic (high Eh) depositional setting of the Emu Bay Shale also may have suppressed Ts/Tm (e.g. Moldowan et al., 1986).

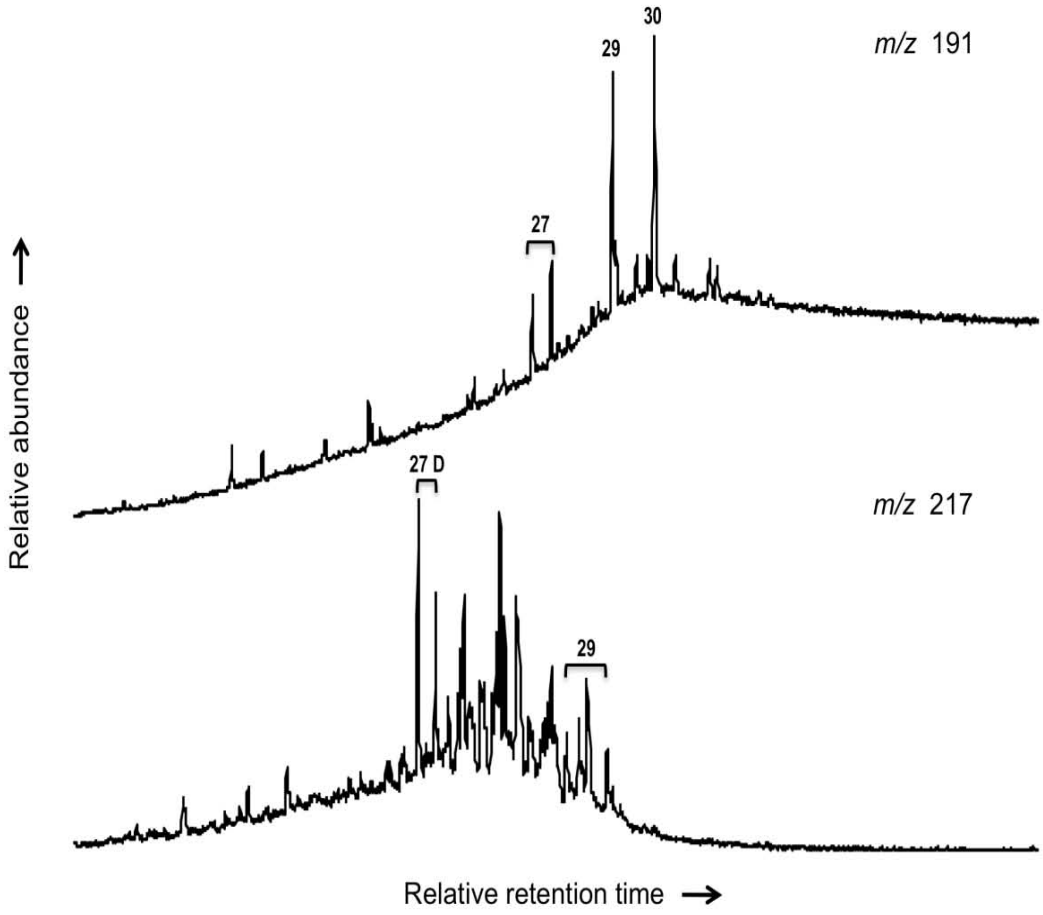

Fig. 3 Mass chromatograms showing the distributions of hopanes (*m/z* 191) and steranes (*m/z* 217) in the thermal extract of an Emu Bay Shale kerogen. Selected homologues identified by their respective carbon number; 27D = diacholestane epimers.

Given its unusually long storage (>40 years), the question of whether the kerogen isolated the Emu Bay Shale underwent significant alteration prior to its thermal extraction and pyrolysis needs to be addressed. According to Vandenbroucke and Largeau (2007), spontaneous oxidation of kerogen isolates can be extensive even when, as in this instance, they have been stored in closed vials. Such oxidative alteration was experimentally demonstrated for two kerogens, one Type II (Salmon et

al., 2000) and the other Type III (Faure et al., 1999), isolated from *thermally immature* marine shales. In both, the alteration led to preferential depletion of unsaturated and higher molecular weight moieties, including C_{20+} *n*-alkanes and hopanoids. The higher rank of the Emu Bay Shale (late catagenesis) means that its kerogen will be more refractory, making it less susceptible to such molecular alteration. The associated bitumen II may be somewhat more reactive, just as asphaltenes isolated from crude oils stored for 40 years are more reactive than those from related but more recently produced oils (Lehne et al., 2009). Significantly, however, open-system pyrolysis GC-FID of the respective asphaltene fractions revealed very little difference in their compositions. Had some loss of hopanoids occurred during storage of the Emu Bay kerogen, this perhaps would explain why the hopane/sterane ratios are not higher than observed (Table 1), while any accompanying neoformation of short-chain homologues may have distorted the distributions of $<C_{20}$ *n*-alkanes (Fig. 2).

4.3.2 Carbon isotopic signatures

Representative TOC and $\delta^{13}C_{org}$ values of the Emu Bay Shale Lagerstätte (after McKirdy et al., 2011) are plotted in Fig. 4, along with those of other lower Cambrian (Series 2) shales from South China and limestones from elsewhere in South Australia.

The Emu Bay shales (TOC <0.6%, $\delta^{13}C_{org}$ = -32 to -28‰) overlap the carbonates which are all shallow water deposits and, in the case of the Wilkawillina and Andamooka Limestones (Arrowie Basin), also demonstrably stromatolitic (James and Gravestock, 1990; McKirdy, 1994). Those from the Ouldburra Formation (Officer Basin) have previously been shown to contain biomarker alkanes attributable to cyanobacteria (McKirdy et al., 1984; Logan et al., 1997), as well as telalginite derived

from *G. prisca* (Kamali, 1995; Michaelsen et al., 1995). Moreover, the $\delta^{13}C_{org}$ signatures of mat-forming coccoid cyanobacteria preserved in Silurian cherts from Poland (Bauersachs et al., 2009) are indistinguishable from those of the Emu Bay Shale Lagerstätte. By implication, the sediments that gave rise to the organically lean Emu Bay Shale accumulated within the photic zone and were host to benthic cyanobacteria.

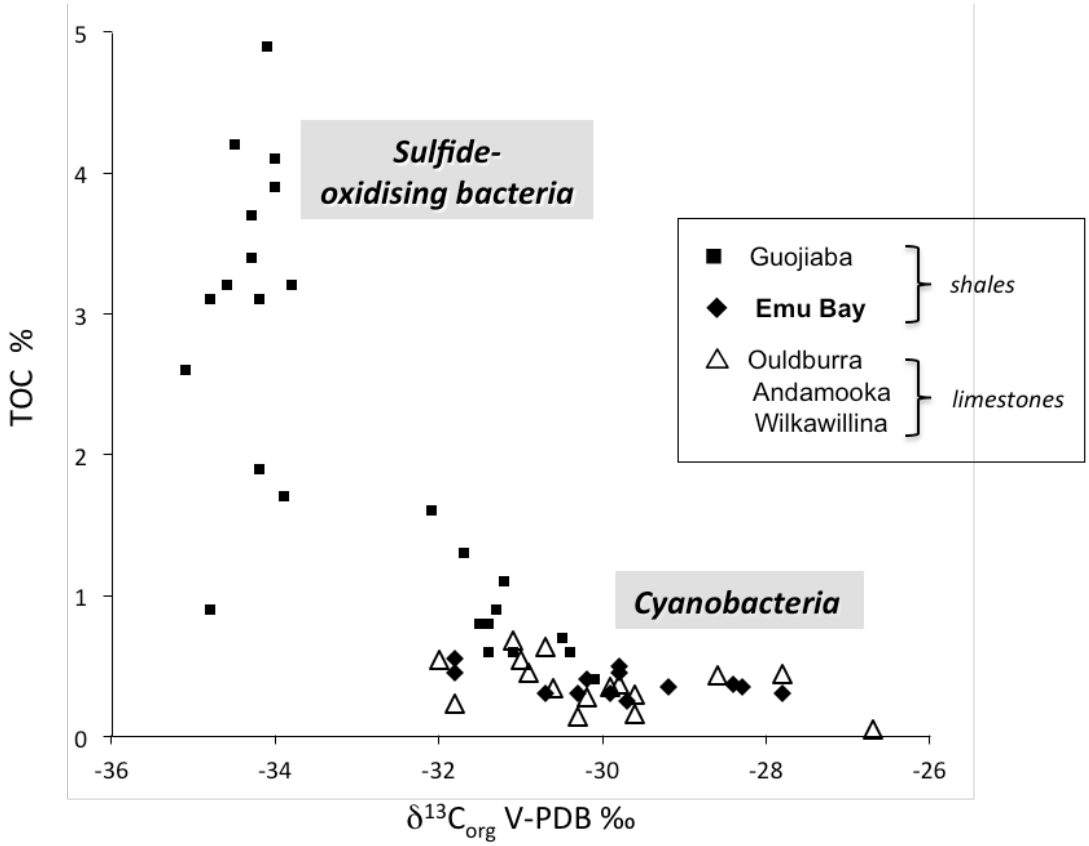

Fig. 4 Relationship between bulk isotopic composition and concentration of organic carbon in shales from unmetamorphosed lower Cambrian (Series 2) units: Emu Bay Shale, Stansbury Basin, South Australia (McKirdy et al., 2011); Wilkawillina and Andamooka Limestones, Arrowie Basin, South Australia (McKirdy, 1994); Ouldburra Formation, Officer Basin, South Australia (McKirdy et al., 1984; Logan et al., 1997) and Guojiaba Formation, Shatan, Yangtze Platform, South China (Guo et al., 2007).

In contrast, the black shales of the Guojiaba Formation (Yangtze Platform) were deposited in an anoxic sulfidic setting (Guo et al., 2007). Accordingly, for the most part they are much richer in dispersed organic matter (up to 5% TOC), which in turn is extremely depleted in ^{13}C ($\delta^{13}C_{org}$ = -36 to -30‰, while $\delta^{13}C_{carb}$ - $\delta^{13}C_{org}$ = 30–33‰) as befits sediments to which sulfate reducers (anaerobic heterotrophs) and sulfur oxidisers (chemoautrophs) contributed bacterial biomass (Hayes et al., 1999; Logan et al., 1999). The latter include mat-forming species (e.g. the modern *Beggiatoa* sp.: Williams and Reimers, 1983), which arguably helped maintain a sharp redox boundary at the sediment-water interface during deposition of the Burgess Shale Lagerstätte (Powell et al., 2003). In the case of the Emu Bay Shale Lagerstätte, however, this role was evidently played by mat-forming cyanobacteria (McKirdy et al., 2011), including *G. prisca* or a similar species. Pancost et al. (1988) report an analogous situation in the Ordovician Platteville Formation, Iowa. Here *G. prisca* deposited a layer of refractory sheath material (possibly comprising resorcinolic lipids: Blokker et al., 2001), thereby limiting diffusion of oxygen and sulfate from the oxic bottom waters into the underlying sediment. Likewise, during deposition of the terminal Proterozoic Rawnsley Quartzite in northern South Australia, microbial mats sealed the sandy substrate of the oxygenated habitat of the classic Ediacara fauna, below fair-weather wave base, facilitating preservation of these soft-bodied, unmineralised metazoans as moulds (Gehling, 1999; Gehling et al., 2005).

4.4. Conclusions

Our identification of the characteristic *n*-alkane signature of *G. prisca* among other biomarker hydrocarbons in bitumen II from the fossiliferous Emu Bay Shale is the first reported evidence for the presence of this or a similar coccoid cyanobacterium in any Cambrian Lagerstätte. Given its demonstrated mat-forming capability in other early Palaeozoic sediments, its likely dual roles in the Emu Bay depocentre, possibly in consort with other benthic cyanobacteria, were 1) to maintain a robust redox boundary at the sediment-water interface, and 2) to mantle the carapaces of recently deceased fauna on the sea floor, thereby extending the preservation of their soft (non-biomineralised) tissue for long enough to allow its inorganic replication during late diagenesis. Furthermore, the presence of cyanobacterial mats implies that the Emu Bay Shale Lagerstätte was deposited in the photic zone. Notwithstanding the long storage time of the kerogen prior to this analysis, it appears to have escaped significant oxidative alteration. MSSV thermal desorption and pyrolysis of kerogen isolated by serial acid digestion of solvent-extracted rock powder is an effective means of accessing indigenous hydrocarbons where, as in this instance, the free hydrocarbons (bitumen I) in the host rock were contaminated by soil-derived lipids.

4.5. Acknowledgements

This study forms part of a project on the Cambrian hydrocarbon potential of the Stansbury and Officer Basins, funded by Primary Industries and Resources South Australia (PIRSA). PAH is in receipt of an Australian Postgraduate Award, while JBJ and JGG acknowledge funding from an Australian Research Council Linkage Grant (LP0774959), and additional financial support from Beach Energy Ltd and the South Australian Museum. Keith Hall (Hall Analytical Laboratories Ltd, Manchester, UK)

generously donated the MSSV pyrolysis kit. Richard Jenkins provided valuable field assistance. Martin Fowler and an anonymous reviewer are thanked for their perceptive comments on the manuscript and helpful suggestions for its improvement. The contributions of PAH, DMMcK and GPH to this paper form TRaX Record #170. Finally, this paper is dedicated to the memory of the late Professor Martin F. Glaessner who, in 1967, suggested to DMMcK that the Emu Bay Shale was worthy of organic geochemical investigation.

4.6. References

Allison, P.A., Briggs, D.E.G., 1993. Exceptional fossil record: Distribution of soft-tissue preservation through the Phanerozoic. Geology 21, 527–530.

Bauersachs, T., Kremer, B., Schouten, S., Sinninghe Damsté, J.S., 2009. A biomarker and $\delta^{15}N$ study of thermally altered Silurian cyanobacterial mats. Organic Geochemistry 40, 149–157.

Blokker, P., Van Bergen, P., Pancost, R., Collinson, M.E., De Leeuw, J.W., Sinninghe Damsté, J.S., 2001. The chemical structure of *Gloeocapsomorpha prisca* microfossils: Implications for their origin. Geochimica et Cosmochimica Acta 65, 885–900.

Briggs, D.E.G., Nedin, C., 1997. The taphonomy and affinities of the problematic fossil *Myoscolex* from the Lower Cambrian Emu Bay Shale of South Australia. Journal of Paleontology 71, 22–32.

Brock, G.A., Engelbretsen, M.J., Jago, J.B., Kruse, P.D., Laurie, J.R., Shergold, J.H., Shi, G.R., Sorauf, J.E., 2000. Palaeobiogeographic affinities of Australian Cambrian faunas. Memoirs of the Australasian Association of Palaeontologists 23, 1–61.

Daily, B., Milnes, A.R., Twidale, C.R., Bourne, J.A., 1979. Geology and Geomorphology. In: Tyler, M.J., Ling, J.K., Twidale, C.R. (Eds.), Natural History of Kangaroo Island. Royal Society of South Australia, Adelaide, pp. 1–38.

Faure, P., Landais, P., Griffault, L., 1999. Behavior of organic matter from Callovian shales during low-temperature air oxidation. Fuel 78, 1515–1525.

Fowler, M.G., 1992. The influence of *Gloecapsomorpha prisca* on the organic geochemistry of oils and organic-rich rocks of Late Ordovician age from Canada. In: Schidlowski, M., Golubic, S., Kimberley, M.K., McKirdy, D.M., Trudinger, P.A. (Eds.), Early Organic Evolution: Implications for Mineral and Energy Resources, Springer, Berlin, pp. 336–356.

Foster C.B., O'Brien, G.W., Watson, S.T., 1986. Hydrocarbon source potential of the Goldwyer Formation, Barbwire Terrace, Canning Basin, Western Australia. Australian Petroleum Exploration Association Journal 26(1), 142–155.

Foster C.B., Reed J.D., Wicander, R., 1989. *Gloecapsomorpha prisca* Zalessky, 1917: A new study. Part 1: Taxonomy, geochemistry, and paleoecology. Geobios 22, 735–759.

Gaines, R.R., Briggs, D.E.G., Zhao, Y., 2008. Cambrian Burgess Shale-type deposits share a common mode of fossilization. Geology 36, 755–758.

García-Bellido, D.C., Paterson, J.R., Edgecombe, G.D., Jago, J.B., Gehling, J.G., Lee, M.S.Y., 2009. The bivalved arthropods *Isoxys* and *Tuzoia* with soft-part preservation from the Lower Cambrian Emu Bay Shale Lagerstätte (Kangaroo Island, Australia). Palaeontology 52, 1221–1241.

Gehling, J.G., 1999. Microbial mats in terminal Proterozoic siliciclastics: Ediacaran death masks. Palaios 14, 40–57.

Gehling, J.G., Droser, M.L., Jensen, S.R., Runnegar, B.N., 2005. Ediacaran organisms: relating form and function. In: Briggs, D.E.G. (Ed.), Evolving Form and Function: Fossils and Development: Proceedings of a symposium honoring Adolf Seilacher for his contributions to paleontology, in celebration of his 80th birthday. Peabody Museum of Natural History, Yale University, New Haven, pp. 43–67.

Gehling, J.G., Jago, J.B., Paterson, J.R., García-Bellido, D.C., Edgecombe, G.D., 2011. The geological context of the lower Cambrian (Series 2) Emu Bay Shale Lagerstätte and adjacent stratigraphic units, Kangaroo Island, South Australia. Australian Journal of Earth Sciences 58, 283–297.

Glaessner, M.F., Foster, C.B., 1992. Paleontology and biogeochemical research: A powerful synergy. In: Schidlowski, M., Golubic, S., Kimberley, M.K., McKirdy, D.M., Trudinger, P.A. (Eds.), Early Organic Evolution: Implications for Mineral and Energy Resources, Springer, Berlin, pp. 193–202.

Grantham, P.J. and Wakefield, L.L., 1988. Variations in the sterane carbon number distributions of marine source rock derived crude oils through geological time. Organic Geochemistry 12, 61–73.

Guo, Q., Strauss, H., Liu, C., Goldberg, T., Zhu, M., Pi, D., Heubeck, C., Vernhet, E., Yang, X., Fu, P., 2007. Carbon isotopic evolution of the terminal Neoproterozoic and early Cambrian: Evidence from the Yangtze Platform, South China. Palaeogeography, Palaeoclimatology, Palaeoecology 254, 140–157.

Hall, P.A., Watson, A.F.R., Garner, G.V., Hall, K., Smith, S., Waterman, D., Horsfield, B., 1999. An investigation of micro-scale sealed vessel thermal extraction-gas chromatography-mass spectrometry (MSSV-GC-MS) and micro-scale sealed vessel pyrolysis-gas chromatography-mass spectrometry applied to a standard reference material of an urban dust/organics. The Science of the Total Environment 235, 269–276.

Hayes, J.M., Strauss, H., Kaufman, A.J., 1999. The abundance of ^{13}C in marine organic matter and isotopic fractionation in the global biogeochemical cycle of carbon during the past 800 Ma. Chemical Geology 161, 103–125.

Hoffmann, C.F., Foster, C.B., Powell, T.G., Summons, R. E., 1987. Hydrocarbon biomarkers from Ordovician sediments and the fossil alga *Gloeocapsomorpha prisca* Zalessky 1917. Geochimica et Cosmochimica Acta 51, 2681–2697.

Jackson, K.S., McKirdy, D.M., Deckelman, J.A., 1984. Hydrocarbon generation in the Amadeus Basin, central Australia. Australian Petroleum Exploration Association Journal 24(1), 42–65.

Jago, J.B., Zang, W.L., Sun, X.W., Brock, G.A., Paterson, J.R., Skovsted, C.R., 2006. A review of the Cambrian biostratigraphy of South Australia. Palaeoworld 15, 406–423.

James, N.P., Gravestock, D.I., 1990. Lower Cambrian shelf and shelf margin buildups, Flinders Ranges, South Australia. Sedimentology 37, 455–480.

Jones, B., Manning, D.A.C., 1994. Comparison of geochemical indices used for the interpretation of paleoredox conditions in ancient sediments. Chemical Geology 111, 111–119.

Kamali, M.R., 1995. Sedimentology and petroleum geochemistry of the Ouldburra Formation, eastern Officer Basin, Australia. Ph.D. thesis, University of Adelaide (unpublished)

Kimura, H., Watanabe, Y., 2001. Ocean anoxia at the Precambrian-Cambrian boundary. Geology 29, 995–998.

Kuhn, T.K., Krull, E.S., Bowater, A., Grice, K., Gleixner, G., 2010. The occurrence of short chain *n*-alkanes with an even over odd predominance in higher plants and soils. Organic Geochemistry 41, 88–95.

Lee, M.S.Y., Jago, J.B., García-Bellido, D.C., Edgecombe, G.D., Gehling, J.G., Paterson, J.R., 2011. Modern optics in exceptionally preserved eyes of Early Cambrian arthropods from Australia. Nature 474, 631–634.

Lehne, E., Dieckmann, V., Horsfield, B., 2010. Comparison of bulk kinetic parameters for asphaltenes from long-time stored and related fresher-produced crude oils. Applied Geochemistry 25, 382–388.

Logan, G.A., Summons, R.E., Hayes, J.M., 1997. An isotopic biogeochemical study of Neoproterozoic and Early Cambrian sediments from the Centralian Superbasin, Australia. Geochimica et Cosmochimica Acta 61, 5391–5409.

Logan, G.A., Calver, C.R., Gorjan, P., Summons, R.E., Hayes, J.M., Walter, M.R., 1999. Terminal Proterozoic mid-shelf benthic microbial mats in the Centralian Superbasin and their environmental significance. Geochimica et Cosmochimica Acta 63, 1345–1358.

McCaffrey, M.A., Moldowan, J.M., Lipton, P.A., Summons, R.E., Peters, K.E., Jeganathan, A. Watt, D.S., 1994. Paleoenvironmental implications of novel C_{30} steranes in Precambrian to Cenozoic age petroleum and bitumen. Geochimica et Cosmochimica Acta 58, 529–532.

McKirdy, D.M. 1971. An organic geochemical study of Australian Precambrian and Cambrian sedimentary rocks. M.Sc. thesis, University of Adelaide (unpublished)

McKirdy, D.M. 1994. Biomarker geochemistry of the Early Cambrian oil show in Wilkatana-1: implications for oil generation in the Arrowie and Stansbury Basins. PESA Journal 22, 3–17.

McKirdy, D.M., Padley, D., 1993. Cambrian source rock geochemistry, Stansbury Basin. 1. Preliminary evaluation of Mount McDonnell Formation in coastal exposures on northern Kangaroo Island. Report for Canyon (Australia) Pty Limited. South Australia. Department of Primary Industries and Resources. Open file envelope 8457 R18 (unpublished).

McKirdy, D.M., Kantsler, A.J., Emmett, J.K., Aldridge, A.K., 1984. Hydrocarbon genesis and organic facies in Cambrian carbonates of the eastern Officer Basin, South Australia. In: Palacas, J.G. (Ed.), Petroleum Geochemistry and Source Rock Potential of Carbonate Rocks. American Association of Petroleum Geologists Studies in Geology 18, pp. 12–32.

McKirdy, D.M., Cox, R.E., O'Leary, T., 1986. Geochemical analysis of oils and condensate from the Amadeus Basin, central Australia. AMDEL Report F6451/86 for Elf Aquitaine Petroleum Australia Pty Limited (unpublished).

McKirdy, D.M., Hall, P.A., Nedin, C., Halverson, G.P., Michaelsen, B.H., Jago, J.B., Gehling, J.G., Jenkins, R.J.F., 2011. Paleoredox status and thermal alteration of the lower Cambrian (Series 2) Emu Bay Shale Lagerstätte, South Australia. Australian Journal of Earth Sciences 58, 311–324.

Michaelsen, B.H., Kamali, M.R., McKirdy, D.M., 1995. Unexpected molecular fossils from Early Cambrian carbonates of the Officer Basin. In: Grimalt, J.O., Dorronsoro, C. (Eds.), Organic Geochemistry: Developments and Applications to Energy, Climate, Environment and Human History. A.I.G.O.A., San Sebastian, Spain, pp. 218–221.

Moldowan, J.M., Sundaraman, P., Schoell, M., 1986. Sensitivity of biomarker properties to depositional environment and/or source input in the Lower Toarcian of S.W. Germany. Organic Geochemistry 10, 915–926.

Nabbefeld, B., Grice, K., Schimmelmann, A., Summons, R.E., Troitzsch, U., Twitchett, R.J., 2010. A comparison of thermal maturity parameters between freely extracted hydrocarbons (Bitumen I) and a second extract (Bitumen II) from within the kerogen matrix of Permian and Triassic sedimentary rocks. Organic Geochemistry 41, 78–87.

Nedin C., 1995. The Emu Bay Shale, a Lower Cambrian fossil Lagerstätten, Kangaroo Island, South Australia. Memoirs of the Australasian Association of Palaeontologists 18, 31–40.

Pancost, R.D., Freeman, K.H., Patzkowsky, M.E., Wavrek, D.A., Collister, J.W., 1998. Molecular indicators of redox and marine photoautotroph composition in the late Middle Ordovician of Iowa, U.S.A. Organic Geochemistry 29, 1649–1662.

Paterson, J.R, Jago, J.B., Gehling, J.G., García-Bellido, D.C., Edgecombe, G.D., Lee, M.S.Y., 2008. Early Cambrian arthropods from the Emu Bay Shale Lagerstätte, South Australia. In: Rábano, I., Gozalo, R. & García-Bellido, D. (Eds.), Advances in Trilobite Research. Cuadernos del Museo Geominero, 9, Instituto Geológico y Minero de España, Madrid, pp. 319–325.

Powell, W.G., Johnston P.A., Collom, C.J., 2003. Geochemical evidence for oxygenated bottom waters during deposition of fossiliferous strata of the Burgess Shale Formation. Palaeogeography, Palaeoclimatology, Palaeoecology 201, 249–268.

Reed, J.D., Illich, H.A., Horsfield, B., 1986. Biochemical evolutionary significance of Ordovician oils and their sources. Organic Geochemistry 10, 347–348.

Salmon, V., Derenne, S., Lallier-Vergès, E., Largeau, C., Beaudoin, B., 2000. Protection of organic matter by mineral matrix in a Cenomanian black shale. Organic Geochemistry 31, 463–474.

Scalan R.S., Smith, J.E., 1970. An improved measure of the odd-to-even predominance in the normal alkanes of sediment extracts and petroleum. Geochimica et Cosmochimica Acta 34, 611–620.

Sherman, L.S., Waldbauer, J.R., Summons, R.E., 2007. Improved methods for isolating and validating indigenous biomarkers in Precambrian rocks. Organic Geochemistry 38, 1987–2000.

Stasiuk, L.D., Osadetz, K.G., 1990. The life cycle and phyletic affinity of *Gloeocapsomorpha prisca* Zalessky 1917 from Ordovician rocks in the Canadian Williston Basin. Geological Survey of Canada Paper 89-1D, 123–137.

Stasiuk, L.D., Kybett, B.D., Bend, S.L., 1993. Reflected light microscopy and micro-FTIR of Upper Ordovician *Gloeocapsomorpha prisca* alginite in relation to paleoenvironment and petroleum generation, Saskatchewan, Canada. Organic Geochemistry 20, 707–719.

Summons, R.E., Powell, T.G., 1991. Petroleum source rocks of the Amadeus Basin. In: Korsch, R.J., Kennard, J.M. (Eds.), Geological and Geophysical Studies in the Amadeus Basin, Central Australia. Bureau of Mineral Resources, Australia, Bulletin 236, 511–524.

Summons, R.E., Jahnke, L.L., Hope, J.M., Logan, G.A., 1999. 2-Methylhopanoids as biomarkers for cyanobacterial oxygenic photosynthesis. Nature 400, 554–547.

Talbot, H.M., Summons, R.E., Jahnke, L.J., Cockell, C.S., Rohmer, M., Farrimond, P., 2008. Cyanobacterial bacteriohopanepolyol signatures from cultures and natural environmental settings. Organic Geochemistry 39, 232–263.

Vandenbroucke, M., Largeau, C., 2007. Kerogen origin, evolution and structure. Organic Geochemistry 38, 719–833.

Welander, P.V., Coleman, M.L., Sessions, A.L., Summons, R.E., Newman, D.K., 2010. Identification of a methylase required for 2-methylhopanoid production and implications for the interpretation of sedimentary hopanes. Proceedings of the National Academy of Sciences USA 107, 8537–8542.

Williams, L.A., Reimers, C., 1983. Role of bacterial mats in oxygen-deficient marine basins and coastal upwelling regimes: Preliminary report. Geology 11, 267–269.

Filling the Australian Cambrian chemostratigraphic gap: Early Cambrian carbon isotopic profiles of three South Australia basins.

P.A. Hall[1*], G.P. Halverson[1,2], A.S. Collins[1], D.M. McKirdy[1] and J.B. Jago[3]

1. Tectonics, Resources and Exploration (TRaX), School of Earth and Environmental Sciences, University of Adelaide, SA 5095
2. Present address: Department of Earth & Planetary Sciences, McGill University, Montreal, Canada H3A 2A7
3. School of Natural and Built Environments, University of South Australia, Mawson Lakes, SA 5005

STATEMENT OF AUTHORSHIP

Filling the Australian Cambrian chemostratigraphic gap: Early Cambrian carbon isotopic profiles of three South Australia basins

Philip Anthony Hall (Candidate)
Performed sample collection, analysis or oversaw the analysis on all samples, interpreted data, wrote manuscript and acted as corresponding author

I hereby certify that the statement of contribution is accurate

Signed …….*Date*……

Galen P. Halverson

Filling the Australian Cambrian chemostratigraphic gap: Early Cambrian carbon isotopic profiles of three South Australia basins

Statement of contribution (in terms of the conceptualization of the work, its realization and its documentation)

Contributed to sample analysis, planning of article and provided critical evaluation

Certification that the statement of contribution is accurate and permission is given for the inclusion of the paper in the thesis

Signed …….Date…19/06/2012…

Alan S. Collins

Filling the Australian Cambrian chemostratigraphic gap: Early Cambrian carbon isotopic profiles of three South Australia basins

Statement of contribution (in terms of the conceptualization of the work, its realization and its documentation)

Contributed to planning of article and provided critical evaluation

Certification that the statement of contribution is accurate and permission is given for the inclusion of the paper in the thesis

Signed …….Date…19/06/2012…

David M. McKirdy

Filling the Australian Cambrian chemostratigraphic gap: Early Cambrian carbon isotopic profiles of three South Australia basins

Statement of contribution (in terms of the conceptualization of the work, its realization and its documentation)

Contributed to planning of article and provided critical evaluation

Certification that the statement of contribution is accurate and permission is given for the inclusion of the paper in the thesis

Signed …….Date…20/06/2012…

James B. Jago

Filling the Australian Cambrian chemostratigraphic gap: Early Cambrian carbon isotopic profiles of three South Australia basins

Statement of contribution (in terms of the conceptualization of the work, its realization and its documentation)

Contributed to planning of article and provided critical evaluation

Certification that the statement of contribution is accurate and permission is given for the inclusion of the paper in the thesis

Signed …….Date…20/06/2012…

Abstract

The Precambrian–Cambrian transition is well documented as a time of major change within the geological record. The biostratigraphic definition of GSSP horizons though the use of cosmopolitan taxa biohorizons is difficult for lower Cambrian deposits where few candidate fossils exist. Instead, an integrated approach comprising chemostratigraphy and/or sequence stratigraphy with the known biostratigraphy greatly increases our ability to make high-resolution correlations. In comparison to the extensively investigated Neoproterozoic or middle and late Cambrian sections, sparse chemostratigraphic data have been published on the early Cambrian of Australia. Here we report new $\delta^{13}C_{carb}$ and $\delta^{18}O_{carb}$ data obtained from drill core and cuttings from three Cambrian basins in South Australian: the Stansbury, the Arrowie and the Officer. In combination with the existing data from early Cambrian carbonates of the Flinders Ranges, these new data permit correlation of South Australian sections with global composite carbon isotope profiles. Specifically, the negative $\delta^{13}C$ ROECE, AECE and SHICE events and the positive $\delta^{13}C$ CARE and MICE events are recognised. This chemostratigraphic interpretation is consistent with the biostratigraphy of the sampled sections. The structure of South Australia's expanded Early Cambrian $\delta^{13}C_{carb}$ profile, in correlation with the global composite, reveals the palaeo-Pacific Ocean varied at several frequencies, implicating multiple processes in the modulation of the marine carbon cycle.

5.1. Introduction

The Precambrian–Cambrian transition is well documented as a time of major change in the Earth system, including the rapid diversification of metazoans and increased oxygenation of the atmosphere and oceans to roughly modern levels (Brazier & Hewitt 1979, Seilacher 1998, Hurtgen et al., 2005; Fike et al., 2006; Halverson et. al 2009; Saltzman et al., 2011), punctuated by episodes of ocean anoxia (Saltzman et al., 2000; Kimura and Watanabe, 2001; Schröder & Grotzinger, 2007, Wotte et al., 2007; Guo et al., 2010, Och et al., 2012). The increase of biomineralising metazoans through this time period (Porter, 2007; Kouchinsky et al., 2012) has allowed robust biostratigraphic correlation regionally, globally and the definition of Global boundary Stratotype Section and Point (GSSP) horizons through the use of cosmopolitan taxa biohorizons, particularily in the middle and late Cambrian (Babcock & Peng, 2007; Babcock et al., 2007; Peng et al., 2009).

However, for problematic sections such as lower Cambrian deposits where few candidate fossils exist and biostratigraphy is notoriously complicated (Tucker, 1989, Babcock & Peng, 2007) and for shallow marine sections with poor biostratigraphic control, an integrated approach comprising chemostratigraphy and, where possible, sequence stratigraphy with the known biostratigraphy greatly improves high-resolution correlation within and between basins (Howley & Jiang, 2010).

The observed carbon isotope composition of unaltered marine carbonates ($\delta^{13}C_{carb}$) precipitated in equilibrium with seawater closely approximates the composition of the dissolved inorganic carbon (DIC) pool of that seawater. These values show secular variation, resulting from a combination of factors including continental weathering, initial isotopic composition of carbon entering the ocean-atmosphere system, primary

productivity, efficiency of organic carbon burial and ocean circulation. Even though the reliability of the carbon isotope proxy applied to ancient carbonate strata has been challenged by a series of recent studies (e.g., Melchin and Holmden, Swart & Kennedy, 2012), it has been widely applied to investigations palaeoenvironmental changes and biological events (Tucker, 1989; Brasier, 1992; Montanez et al., 2000; Buggisch et al., 2003; Zhu et al., 2004; Maloof et al., 2005; Saltzman et al., 2011). The Cambrian displays $\delta^{13}C$ patterns that appear transitional between the Neoproterozoic, marked by long duration and large amplitude fluctations, and the Phanerozoic, distinguished by shorter duration and less extreme anomalies (Halverson et al., 2009; Maloof et al., 2010). Potential explanations for the relatively high frequency fluctuations in the Cambrian $\delta^{13}C$ record include extreme chemical weathering of Gondwana, palaeogeographical configuration, or ecosystem simplicity could have had a significant role in making this interval of geological time more prone to perturbations of the carbon cycle (Woods et al., 2011).

5.2. The Cambrian $\delta^{13}C$ isotope record

The potential of applying secular variations in carbon isotope composition as a tool for both intercontinental stratigraphic correlation and explaining biospheric perturnbations has been highlighted by numerous authors (e.g., Tucker, 1986; Magaritz et al., 1986; Brasier, 1992; Brasier & Sukhov, 1998; Halverson et al., 2005) and has been implemented with a reasonable degree of success in the Cambrian (e.g., Saltzman et al., 1998, 2000; Peng et al 2004; Kouchinshy et al., 2005; Lindsay et al., 2005; Maloof et al., 2005, 2010; Wotte et al., 2007; Guo et al., 2010). The Late Cambrian SPICE $\delta^{13}C$ excursion, which is preserved in a remarkably wide range of depositional and diagenetic settings in a number of sections from North America,

Australia, China, and Kazakhstan (Saltzman et al., 2000), argues for the robust. However, the implementation of isotopic variations through chemostratigraphy is problematic, a number of diagenetic factors may alter or obscure primary signatures; cementation, recrystallisation and late dolomitization as well as alterations through metamorphism (Tucker, 1989; Machel, 1997, 2005; Glumac & Walker, 1998; Railsback et al., 2003; Swart & Kennedy, 2011).

Excursions and shifts in the carbon isotope curve have been shown to correspond with events in sequence stratigraphy, interpreted as indicating the interdependence of sea level and the partition between C_{org} and C_{carb} (Buggisch et al., 2003, Halverson et al., 2009). This interpretation has been questioned because isotopic fluctuations of similar magnitude as those observed in the ancient geological record have been documented in recent Quaternary carbonate platform sediments (Swart, 2008). These are ascribed to the effects of meteoric influences on carbonate shelf environments resulting from eustatic sea level fluctuations rather than secular variation of the global carbon cycle (Swart & Kennedy, 2012; Oehlert et al., 2012) although the application of this model to ancient carbonate platforms is controversial.

The global reproducibility of Cambrian $\delta^{13}C$ excursions has led to the identification and naming of many of these isotopic stages (analogous to the oxygen isotope stages of the Quaternary) such as the Steptoean Positive Carbon Isotope Excursion (SPICE) and Drumian Carbon Isotope Excursion (DICE) (Saltzman et al., 1998, 2000; Babcock et al., 2007; Howley & Jiang, 2010). Following the Fourth International Symposium on the Cambrian System, Zhu et al. (2006), produced a composite $\delta^{13}C$ profile for the Cambrian from available published data (Fig.1). These authors also expanded the existing nomenclature by defining additional acronyms for the

previously unnamed isotopic excursions, linked the chronological position of various Lagerstätten, and highlighted the importance of the $\delta^{13}C$ profile for intra- and inter-continental correlation. The currently defined GSSPs for the Cambrian have all been associated with carbon isotope excursions: the Terreneuvian (Series 1) Fortunian (Stage I) is associated with the BASE negative excursion (Landing et al., 2007), the Series 3 Drumian (Stage VI) is tied to the negative DICE event (Babcock et al 2007); the Furongian (Series IV), Paibian (Series VIII) is linked to the positive SPICE excursion (Peng et al., 2004); and the Series 3 Guzhangian (Stage VII) correlates with an undefined low amplitude negative excursion (Peng et al., 2009). Other prominent biostratigraphical events through the Cambrian are also related to isotopic events; AECE (Archaeocyathid Extinction Carbon isotope Excursion); ROECE excursion (Redlichiid-Olenellid Extinction Carbon isotope Excursion), SHICE (SHIyantou Carbon isotope Excursion corresponding in position to the extinction of many SSF secreting organisms); MICE (MIngxinsi Carbon Isotope Excursion corresponding in position to the radiation of archaeocyathids), ZHUCE (ZHUjiaqing Carbon isotope Excursion corresponding in position to SSF zone 3 on the Yangtze Platform) and CARE (Cambrian Arthropod Radiation isotope Excursion).

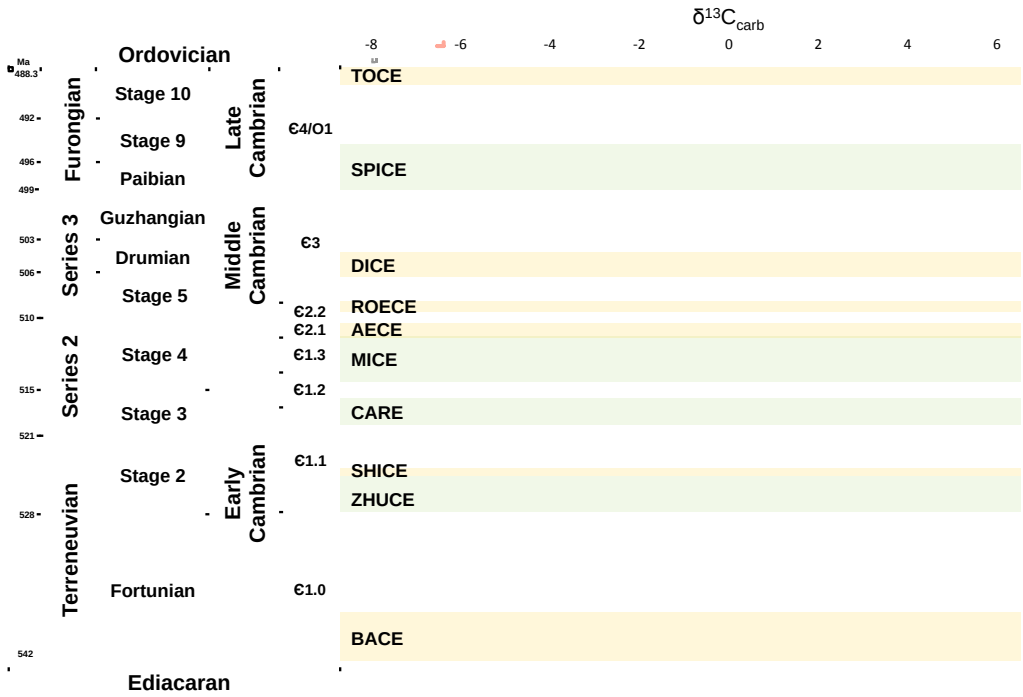

Fig.1 Global carbon isotope composite and excursion events, after Zhu et al. (2006)

5.3. South Australian geochronology

Geochronological constraints for the Cambrian of South Australia is sparse. Two felsic tuffs in the Early Cambrian have been dated by U-Pb Sensitive High Mass Resolution Ion Microprobe (SHRIMP): (i) 522.0±2.1 Ma from the Heatherdale Shale of the Stansbury Basin, about 400m above latest Atdabanian archaeocyathids (Jenkins et al, 2002) and (ii) 522.0±1.8 Ma from the lower Billy Creek Formation in the Arrowie Basin (Gravestock & Shergold, 2001). Both SHRIMP data points, though they are precise, do not correlate well with the biostratigraphic assignment of the host strata as Botoman, with the Atdabanian – Botoman boundary regarded as having an age of 517±1.5Ma (Landing et al., 1998), dates of ≈522Ma correlate with the middle Tommotian (Maloof et al., 2010). Hence, neither date is regarded as reliable

(Paterson, 2005; Jago et al., 2006, 2012). Other less reliable dates include Rb–Sr ages of 524±68 and 660±60 Ma were obtained from the Observatory Hill Formation in Byilkaoora 1 and Cadney Park Member in Byilkaoora 3 (Webb, 1978; Henry and Brewer, 1984, both references from Gravestock et al, 2002) although strontium concentrations may be too high for reliable age determination by the Rb–Sr method (Gravestock et al, 2002). A syn-post kinematic igneous intrusion within the Є2 Kanmantoo Group was dated at 514 ± 3 Ma, using both 207Pb-206Pb single zircon evaporation and U-Pb secondary ion mass spectrometry (Foden et al., 2006), providing some constraint of the upper sequences of the Early Cambrian. Given this scarcity of reliable analytical data, biostratigraphically inferred age constraints are most commonly used, such as the faunal assemblages correlated to the Siberian platform (Daley, 1972), late Atdabanian to late Botoman trilobite zones (Jago et al., 2006) and acritarch assemblages (Zang et al., 2001). However, in higher sections of the Arrowie and Stansbury basins there is little biostratigraphic control whilst almost none exists in the Officer Basin.

Previous studies of the $\delta^{13}C$ profile of Cambrian sequences in Australia are limited. As a consequence of the limited chemostratigraphic and radiometric data, Australian Cambrian strata are poorly correlated with other continents. Lindsay et al. (2005) compiled a comprehensive data set of 996 samples from Middle Cambrian to Ordovician sections in several northern and eastern Australian basins [Fig. 1a]. This study highlighted 3 positive excursions (497.5-495 Ma, 506-503 Ma and 509-506 Ma), between the middle and late Cambrian the youngest of which was correlated with the SPICE event. Tucker (1989) reported 37 $d^{13}C_{carb}$ values across the Tommotian and Atdabanian stages in outcrop samples from the Flinders Ranges, South Australia.

In this study we report new $\delta^{13}C_{carb}$ data from localities in three South Australian basins; the Officer, the Arrowie and the Stansbury (Fig.2). We combine these new data with existing data from carbonate sequences of the Flinders Ranges in order to produce a composite chemostratigraphic section for South Australia that allows global correlation to be made.

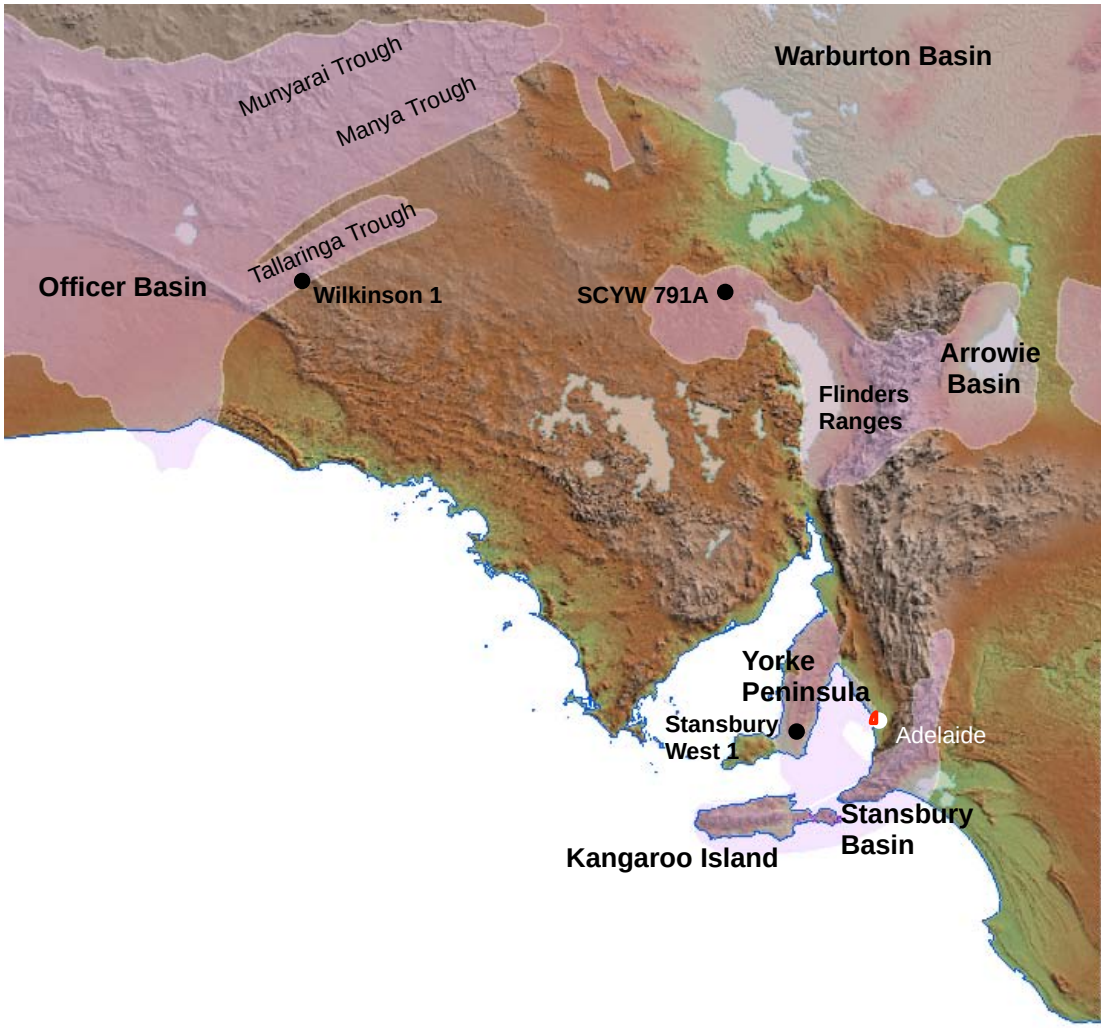

Fig. 2. Location map showing South Australian Cambrian basins (pink) and well sites for the sample set. I think this figure would be better 1) if you redrafted and left off topography, 2) showed where all drill cores intersecting the Early Cambrian are. It becomes, then, a useful resource.

5.4. Geological setting

The early Cambrian successions of South Australia were accumulated at end of an extended period of virtually continuous Neoproterozoic–Cambrian deposition, from approximately 830 Ma to 500 Ma. Cambrian sedimentation occurred in two distinct, but possible interconnected marine basins: the Centralian Superbasin (Officer & Warburton Basins) to the north and west and the Adelaide Fold Belt rift-basin (Stansbury & Arrowie Basins) to the south and east (Fig.2) (Gravestock, 1995; Preiss, 2000). Continental reorganisation culminated with the final assembly of the Gondwanan supercontinent from the remnants of Rodinia during the Cambrian, with both depositional systems linked to this breakup and the amalgamation (Powell et al., 1994; Gravestock, 1995; Preiss, 2000; Lindsay et al., 2002; Collins & Pisarevsky, 2005). Both basins sat in humid, tropical climate at low northern palaeolatitudes on, or connected to, the western margin of the palaeo-Pacific Ocean during the Early Cambrian (Gravestock, 1995; Brock et al., 2000; Li et al., 2008).

The southern basins are renowned for their thick fossiliferous limestones which include peritidal archaeocyathid reefs spanning much of the Early Cambrian (James & Gravestock, 1990, Jago et al., 2006). The South Australian Cambrian was divided into four sequence sets (supersequences), Є1, Є2 (both Early Cambrian), Є3 (Middle Cambrian) and Є4 (Late Cambrian to Ordovician) by Gravestock (1995) with further subdivision into third order sequences Є1.0, Є1.1, Є1.2 & Є1.3 and Є2.1 & Є2.2 within the Early Cambrian sequences (Fig.3) (Gravestock, 1995; Jago et al., 2002b, 2006; Zang et al., 2004).

NOTE:
This figure/table/image has been removed to comply with copyright regulations.
It is included in the print copy of the thesis held by the University of Adelaide Library.

Fig.3. Early to Middle Cambrian stratigraphy of the Officer, Arrowie & Stansbury basins (adapted from Jago et al., 2012).

To the north, the sediments of the Officer Basins were deposited in what was initially an intracratonic sag basin during the Neoproterozoic along with the other contiguous Centralian Superbasin depocentres (Lindsay et al 2002). Later north-south compression (~560 to 550 Ma) during the Petermann Ranges Orogeny resulted in the uplift of the Musgrave Block (Gravestock, 2002), which segmented the Centralian Superbasin and resulted in folding and thrusting over the northern margin of the Officer Basin and flexural subsidence within this basin (Tingate & Duddy 2002). The

Delamerian Orogeny (~515 to 490 Ma) resulted in uplift and halted the Cambrian deposition (Preiss, 1995). This epeiric Cambrian basin was bound to the west by the Yilgarn Block and connected eastward to the open ocean through a series of troughs between the Musgrove Block (north) and Gawler Craton (south). In the northeast the Munyarai and Manya troughs show significant Neoproterozoic to Cambrian sediment fill (up to 10km). The southerly Tallaringa Trough (Fig.2), a 200 km long, 40 km wide depocentre, bound to the northwest by the Nawa Ridge and to the southeast by the Gawler craton, was not part of the ocean seaway but contains the richest oil-prone source rocks in the Officer Basin (Kamali, 1995; Gravestock & Morton, 2002). Near its centre, the trough contains up to 600 m of Cambrian strata and possibly 1600 m of underlying Neoproterozoic sedimentary rocks above magnetic basement (Gravestock, 2002).

The earliest Cambrian sediments were terrestrial throughout the basin, represented by the basal aeolian Relief Sandstone, a formation which continued deposition in the western section of the basin until the end of sequence Є1.3 (late Botoman) with both non-marine and marine units. Evolution of coastal sabkha to shallow marine successions in the eastern section of the basin is demonstrated by the Relief Sandstone being conformably overlain by the evaporitic lower units of the Ouldburra Formation (Gravestock et al., 1995, Morton, 2002). The lower Ouldburra Formation comprise a suite of halite-carbonate-siliciclastic cycles unique in the Cambrian of South Australia, and probably representing the lowstand to early transgressive Є1.1 depositional phases (Gravestock et al., 1995). Deposition of thick transgressive laminated silty carbonate mudstones of sequence Є1.2 ensued. These grade upward into an intercalated laminated carbonate mudstone and red siltstone, with a carbonate breccia marking subaerial exposure representing the top of sequence Є1.2 (Mason,

2001; Morton, 2002). The Є1.3 successions of the upper Ouldburra Formation are characteristically shoaling upwards cycles of red-beds and sabkha carbonates with repeated exposure surfaces in the upper section marking the terminal Є1.3 regression (Gravestock et al., 1995). The Ouldburra Formation is sparsely fossiliferous, with the identified examples being Atdabanian, although trilobites observed in the Manya 3 drill core have been suggest a Botomian age (Morton, 2002). Following this major regression at the end of the Relief–Ouldburra deposition the succeeding Є2 and Є3 units (Observatory Hills Formation to Trainor Hill Sandstone) were formed in non marine environments with alluvial fan to alluvial plain deposits and playa lakes (Morton, 2002).

To the south, the Arrowie and Stansbury basins were developed on the Palaeo-Pacific passive margin along the trailing edge of Gondwana (Preiss, 2000; Jago et al., 2003). By the middle Early Cambrian time, renewed extension resulted in accelerated subsidence. Sequences Є2 and Є3 filled this newly generated accommodation space, the latter ranging up to the middle Cambrian (Gatehouse et al., 1990; Jago et al., 1994; Gravestock, 1995; Jago et al., 2002b). This was the final episode of major crustal thinning within the Adelaide Fold Belt (Preiss, 2000; Foden et al., 2006) prior to the onset of an active margin on the eastern margin of the continent. The encroaching Ross-Delamerian Orogen resulted in the development of a foreland trough in the Stansbury basin (Flöttmann et al., 1998; Preiss, 1995; Jago et al., 2003; Foden et al., 2006).

The Arrowie Basin is situated at the northern end of the fold belt with the Flinders Ranges in the central zone flanked to the west by the Stuart Shelf and east by the Curnamona Province. In the Flinders Ranges a near complete sequence of carbonates

exists from the Tommotian through to the Botoman (Є1.1 to Є1.3). Above the siliclastic sediments of the basal Uratanna Formation the Parachilna Formation comprises interbedded shallow water sandstones, siltstones and subordinate carbonates, whilst the Woodendinna Dolomite and lower Wilkawillina Limestone are mostly shallow water shelf carbonates with oolites, stromatolites, archaeocyathid bioherms and bioclastic limestones (Gravestock & Cowley, 1995). These sequences are interpreted as having been deposited during a transgressive to highstand system during Є1.1 on the passive margin of the palaeo-Pacific Ocean (Tucker, 1989, Gravestock & Cowley, 1995). The overlying Є1.2 sequences, bound at the base by the Flinders Unconformity, consist of a complex succession of shelf (e.g., middle Wilkawillina Limestone) and slope (e,g. Mernmerna Formation)carbonates. This is overlain by the Є1.3 siliciclastics and carbonates deposits: the Bunkers Sandstone, Oraparinna Shale and upper Wilkawillina Limestone (Zang et al., 2007). The Є2.1 siliciclastic Billy Creek Formation unconformably follows with the subsequent, conformable Є2.2 Wirrealpa Limestone containing the youngest archaeocyathid fauna described in Australia (Gravestock, 1984; Kruse 1991; Jago et al., 2006). These sequences pass on into the late Є2.2 to Є3 Lake Frome Group sediments (Gravestock and Cowley, 1995).

The Andamooka Limestone, deposited on the Stuart Shelf is a north western lateral equivalent of the Wilkawillina Limestone (Fig. 2), comprising predominantly shallow marine carbonate deposits. The lower part of the section consists of peritidal oolite, stromatolites and subtidal boundstone with karst surfaces indicating periods of subarial exposure. These lower beds are interpreted as regressive to lowstand deposits but also coincide with a period of regional uplift associated with the Flinders Unconformity (Zang, 2002). The lower unit passes up into burrowed fossil

wackestones in the transgressive to highstand middle part of the section and fenestral spiculitic wackestones in the upper part of the formation rich in archaeocyaths and calcareous sponge-like organisms. Regressive deposits are again observed with peritidal siltstones with mudcracked, fenestral, bioclastic limestone and evaporitic breccia. The lowstand deposits are overlain by prograding bioherm limestones and dolomitised stromatolites evident of a renewed period of transgression (James & Gravestock, 1990, Gravestock & Cowley, 1995). The Andamooka Limestone is abruptly overlain by the Є2.1 Yarrawurta Shale, an correlate of the Billy Creek Formation (Gravestock & Cowley, 1995)

The Stansbury Basin is situated at the southern end of the Adelaide fold belt and crops out in a roughly triangular region bound by the Yorke and Fleurieu Peninsulas and Kangaroo Island, and extending in the subsurface beneath Gulf St Vincent and the Murray Basin across to at least the Victorian border (Gravestock, 1995, Gravestock & Gatehouse, 1995; Flöttmann et al., 1998, Haines et al., 2009). Stable platformal environments are recorded throughout the lowermost parts of the Stansbury Basin in the first of these sequences. Here Є1 comprises predominantly passive margin carbonate shelf-ramp sediments (Gravestock & Gatehouse, 1995; Preiss, 2000; Jago et al., 2003). On the western shelf (Yorke Peninsula) thick successions of carbonates were deposited whilst further to the east (Fleurieu Peninsula) lower carbonate sequences pass up into thick shales. The renewed subsidence during Є2 and Є3 saw the formation of the Kanmantoo Trough in the east with significant (7-8km) of clastic sedimentation, whilst on the western shelf a an attenuated section (~400m) of alternating carbonate and siliciclastic units accumulated.

The shelf sequences of the Yorke Peninsula lie unconformably on crystalline basement of the Gawler Craton. The basal conglomeratic arkose of the Є1.0 Winulta Formation is overlain by stromatolitic and fenestral micritic limestones of the Є1.1 lowstand Kulpara Formation. This is the conformably succeeded by the Parara Limestone, which encompasses the three transgressive sequences of Є1.1, Є1.2 to Є1.3 and includes the Є1.2 Koolywurtie Member. These thick (~400m in the Stansbury West 1 well) carbonates contain numerous fossil assemblages including archaeocyatha, brachiopods and trilobites that range in age from the Atdabanian through the late Botoman (Zhuravlev & Gravestock, 1993; Gravestock & Gatehouse, 1995; Jago et al 2006). The Є1 carbonates are succeeded unconformably by the Minlaton Formation, whose basal conglomerate contains clasts of the underlying limestones. The richly fossiliferous and predominantly nodular lime mudstone of the Ramsay Limestone conformably follows, the base of which forms the boundary between Є2.1 and Є2.2 (Gravestock & Cowley, 1995; Jago et al 2006). Over the transgressive Ramsay Limestone the calcareous sandstones of the Corrodgery Formation and oolitic grainstone/lime mudstone of the Stansbury Limestone show gradual transitions before a sharp contact with the basal Moonan Formation. This non-calcareous shale is conformably overlain by the oolitic Coobowie Limestone. The Ramsay-Coobowie section is interpreted as a transgressive–regressive cycle by Gravestock and Cowley (1995). The intertidal to alluvial stream, feldspathic sandstone and siltstone deposits of the Є3 Yuruga Formation form the top section of Cambrian sediments this westerly section of the Stansbury Basin.

Sedimentation in the Stansbury Basin ceased following the deposition of the Є3, at the onset of the Delamerian Orogeny (Flöttmann et al., 1998; Preiss, 1995, 2000).

5.5. Methodology

5.5.1. Sample location

Drill core sections and cuttings from the Officer, the Arrowie and the Stansbury were sampled (Fig.2) from archives held at the PIRSA Core Library, Glenside, South Australia. A 500m section through the Ouldburra Formation from drill core Wilkinson-1, Officer Basin (PIRSA unit #5438; location Lat: 29°52’02”, Long: 132°33’55”) was sampled at approximately 5m intervals. A 200m section through the Andamooka Formation from drill core SYCW-791A (PEPs; Stuart Creek SCYW 79 001; cited as ‘SCYW1A’ James & Gravestock 1990; location Lat: 30°26'57”, Long: 137°9'50”) was sampled from calcareous (mostly dolomitic) beds. A 700m section through the Parara Limestone (including the Kulpara Formation), Minlaton Formation, Ramsay Limestone, Corrodgery Formation, Stansbury Limestone, Moonan Formation, Coobowie Limestone and Yuruga Formation, from drill core Stansbury West-1, Stansbury Basin (PIRSA unit #21709; location Lat: 34°53'60”, Long: 137°42'51”) was sampled from core chippings at approximately 20ft intervals.

5.5.2. Isotopic analysis

Analysis of the SYCW-791A samples for $\delta^{13}C$ and $\delta^{18}O$ were undertaken simultaneously at the University of Adelaide on a Fisons Optima IRMS with dual inlet isotope ratio mass spectrometer (IRMS) coupled to a Fisons Isocarb carbonate preparation system. Measured data were calibrated against an in-house calcite standard (ANU-P3; $\delta^{13}C_{VPDB}$=2.24‰; $\delta^{18}O_{VPDB}$=-0.30‰) calibrated to VPDB using the international standard NBS19. Total analytical errors (1σ) for $\delta^{13}C$ and $\delta^{18}O$ are estimated at ±0.05‰ and ±0.1‰ based on repeat analyses of standards.

Analysis of 10 samples from the Stansbury West 1 core were undertaken by Nu Instruments Limited, Unit 74 Clywedog Road South, Wrexham, North Wales LL13 9XS UK.

Approximately 600ug of samples was weighed into individual glass vials. The vials were loaded onto the sample carousel of the Nu Instrument NuCarb carbonate system coupled to a Nu Perspective IRMS. The vials were automatically sealed and evacuated prior to addition of 120ul acid with product CO2 transferred cryogenically to a dual inlet. The dual inlet reference gas was balanced to the sample signal prior to a classical dual inlet data acquisition. Standards NBS19 and NBS18 were analysed with the batch for calibration. Sample results were reported with reference to the international standard VPDB and the precision of ±0.03‰ for $\delta^{13}C$ and ±0.05‰ for $\delta^{18}O$ based on repeat analyses of standards.

The remaining analyses were performed at The Godwin Laboratory for Palaeoclimate Research, Department of Earth Sciences, University of Cambridge, Downing Street, Cambridge, CB2 3EQ, UK. Approximately 2 mg of the dried homogenised sample was transferred to exetainer vials and sealed with silicone rubber septa using a screw cap. The samples were flushed with CP grade helium then acidified, left to react for 2hours at 70°C and then analysed using a Thermo Gas Bench preparation system attached to a Thermo MAT 253 mass spectrometer in continuous flow mode. Each run of 30 samples was accompanied by 10 reference carbonates (Carraraz) and 2 control samples (Fletton). Carraraz has been calibrated to VPDB using the international standard NBS19. The results are reported with reference to the international standard VPDB and the precision is better than ±0.08‰ for $\delta^{13}C$ and ±0.1‰ for $\delta^{18}O$.

5.6. Results and discussion

Analytical results for $\delta^{13}C_{carb}$ and $\delta^{18}O_{carb}$ are reported in Tables 1, 2 and 3.

5.6.1 Stansbury Basin

The Stansbury West 1 well penetrated a section of the Cambrian strata dating from Series 1 Stage 2 through to Series 3 Stage 5 of the ICS and IUGS chronological scale (Babcock and Peng, 2007), or the lower to Middle Cambrian sequence sets Є1.1 to Є3 (Jago et al., 2006). The analysed $\delta^{13}C_{carb}$ values vary from -10.8‰ to 1.9‰ with $\delta^{18}O_{carb}$ values of -19.2‰ to -5.0‰ (Table 1, Fig.4) including carbonaceous and dolomitic sandstone and shale intervals. Excluding the non-carbonaceous lithologies the data ranges from -3.5‰ to 1.8‰ and -11.8‰ to -6.1‰ for $\delta^{13}C_{carb}$ and $\delta^{18}O_{carb}$ respectively.

All data with values below -4.0‰ and -12.2‰ for $\delta^{13}C_{carb}$ and $\delta^{18}O_{carb}$ respectively lie within the Yuruga Formation in the upper section of the core at depths between 335m and 579m. This formation has been interpreted as being lowstand tract deposits of intertidal sandflats, subaerial fans and fluvial sands. The $\delta^{13}C_{carb}$ and $\delta^{18}O_{carb}$ data from the Yuruga Formation exhibit a covariance (Fig. 5) indicating the highly negative values displayed in the rather ragged profile at the top of the formation (335–480m) probably reflect a mixed meteoric and marine diagenetic origin for the carbonate cements. The values in the lower section (480–580m) appear to trend more towards marine influences with the basal dolomitic samples corresponding well to the underlying limestones. The shale samples of the Minlaton Formation (835m–920m) become increasingly dolomitic in nature down section and show a similar covariance with $\delta^{13}C_{carb}$ and $\delta^{18}O_{carb}$ becoming more depleted. Although carbonaceous fine

grained sediments such as sandy-mud flats and oolite sand shoals can be representative of a primary marine signature if recrystallisation has not occurred (Tucker, 1989), it is apparent these non-carbonate facies in the Stansbury West 1 core are generally unreliable as indicators of original $\delta^{13}C_{carb}$ values and only data from predominantly carbonate samples are used in the subsequent correlations.

Table 1. $\delta^{13}C_{carb}$ and $\delta^{18}O_{carb}$ values for the Stansbury West 1 drill core cuttings and lithological descriptions.

Stansbury West 1, Stansbury Basin														
Depth (m)	$\delta^{13}C$ (‰)	$\delta^{18}O$ (‰)	Infered Age (Ma)	Formation	Lithology*	Composite	Depth (m)	$\delta^{13}C$ (‰)	$\delta^{18}O$ (‰)	Infered Age (Ma)	Formation	Lithology*	Composite
335	-7.9	-12.7	507.5	Yuruga Formation	SSt/CSt	no	939	-0.6	-6.7	512.5	Parara Limestone	Dol	yes
341	-5.0	-19.2	507.5	Yuruga Formation	SSt	no	945	-0.4	-6.7	512.6	Parara Limestone	Dol	yes
354	-6.2	-14.4	507.6	Yuruga Formation	SSt	no	951	-0.1	-6.2	512.7	Parara Limestone	Lst	yes
360	-4.7	-13.3	507.6	Yuruga Formation	SSt	no	957	-0.9	-8.0	512.7	Parara Limestone	Dol/Sh	yes
366	-10.8	-13.2	507.7	Yuruga Formation	SSt	no	988	-0.6	-8.3	513.1	Parara Limestone	Lst	yes
372	-5.1	-12.8	507.7	Yuruga Formation	SSt	no	1067	0.3	-9.4	514.2	Parara Limestone	Lst	yes
378	-6.5	-14.5	507.8	Yuruga Formation	SSt	no	1073	0.4	-9.6	514.2	Parara Limestone	Lst	yes
378	-5.0	-13.9	507.8	Yuruga Formation	SSt/Sh	no	1079	0.7	-9.0	514.3	Parara Limestone	Lst	yes
384	-5.6	-17.0	507.8	Yuruga Formation	SSt	no	1103	0.3	-9.4	514.6	Parara Limestone	Lst	yes
390	-8.4	-15.4	507.8	Yuruga Formation	SSt	no	1109	0.1	-9.5	514.7	Parara Limestone	Lst	yes
396	-6.1	-14.0	507.9	Yuruga Formation	SSt	no	1116	0.0	-10.2	514.8	Parara Limestone	Lst	yes
402	-5.4	-14.9	507.9	Yuruga Formation	SSt	no	1122	0.1	-9.7	514.9	Parara Limestone	Lst	yes
408	-5.5	-17.8	507.9	Yuruga Formation	SSt	no	1128	0.1	-9.0	514.9	Parara Limestone	Lst	yes
415	-3.0	-15.5	508.0	Yuruga Formation	SSt	no	1134	0.3	-8.5	515.0	Parara Limestone	Lst	yes
421	-3.4	-15.2	508.0	Yuruga Formation	SSt	no	1140	0.0	-8.8	515.1	Parara Limestone	Lst	yes
427	-3.1	-15.7	508.0	Yuruga Formation	SSt	no	1146	-0.3	-9.7	515.2	Parara Limestone	Lst	yes
433	-3.3	-13.0	508.1	Yuruga Formation	SSt	no	1152	-0.3	-8.5	515.3	Parara Limestone	Lst	yes
439	-3.0	-15.7	508.1	Yuruga Formation	SSt	no	1158	-0.2	-9.5	515.3	Parara Limestone	Lst	yes
445	-2.7	-14.5	508.2	Yuruga Formation	SSt	no	1164	0.0	-9.9	515.4	Parara Limestone	Lst	yes
451	-2.4	-14.5	508.2	Yuruga Formation	SSt	no	1170	-0.1	-9.5	515.5	Parara Limestone	Lst	yes
457	-4.4	-15.8	508.2	Yuruga Formation	SSt	no	1177	-0.3	-10.2	515.6	Parara Limestone	Lst	yes
463	-4.4	-18.2	508.3	Yuruga Formation	SSt/Sh	no	1183	-0.5	-10.2	515.7	Parara Limestone	Lst	yes
469	-2.4	-14.2	508.3	Yuruga Formation	SSt	no	1250	-0.4	-11.1	516.5	Parara Limestone	Lst	yes
475	-2.5	-14.5	508.3	Yuruga Formation	SSt	no	1256	0.0	-11.2	516.6	Parara Limestone	Lst	yes
482	-2.3	-12.8	508.4	Yuruga Formation	SSt	no	1268	-0.1	-9.2	516.8	Parara Limestone	Lst	yes
488	-2.4	-13.2	508.4	Yuruga Formation	SSt	no	1274	-0.6	-10.3	516.8	Parara Limestone	Lst	yes
494	-2.6	-13.9	508.5	Yuruga Formation	SSt	no	1280	-0.2	-10.8	516.9	Parara Limestone	Lst	yes
500	-2.7	-13.9	508.5	Yuruga Formation	SSt	no	1286	0.0	-9.4	517.0	Parara Limestone	Lst	yes
506	-2.6	-14.7	508.5	Yuruga Formation	SSt/Sh	no	1292	0.4	-7.3	518.0	Kulpara Formation	Lst/Dol	yes
512	-1.4	-14.2	508.6	Yuruga Formation	SSt/Sh	no	1305	-0.1	-6.5	518.3	Kulpara Formation	Dol	yes
518	-2.0	-15.1	508.6	Yuruga Formation	SSt/Sh	no	1311	-0.1	-6.2	518.5	Kulpara Formation	Dol	yes
524	-3.3	-17.2	508.6	Yuruga Formation	SSt	no	1317	0.0	-6.9	518.7	Kulpara Formation	Dol	yes
536	-2.4	-10.2	508.7	Yuruga Formation	SSt/Sh	no	1323	-0.1	-7.0	518.8	Kulpara Formation	Dol	yes
536	-1.8	-15.4	508.7	Yuruga Formation	SSt/Sh	no	1329	0.1	-6.8	519.0	Kulpara Formation	Dol	yes
543	-0.5	-14.9	508.7	Yuruga Formation	Sh	no	1341	0.2	-6.4	519.4	Kulpara Formation	Dol	yes
549	0.1	-15.0	508.78	Yuruga Formation	Sh	no	1347	0.1	-7.3	519.5	Kulpara Formation	Dol	yes
555	0.7	-13.2	508.82	Yuruga Formation	Sh	no	1359	0.4	-6.9	519.9	Kulpara Formation	Dol	yes
567	1.5	-11.4	508.9	Yuruga Formation	Dol/Sh	yes	1366	0.4	-6.5	520.0	Kulpara Formation	Dol	yes
573	1.8	-11.6	508.9	Yuruga Formation	Dol/Sh	yes	1378	0.1	-6.8	520.4	Kulpara Formation	Dol	yes
579	1.7	-11.8	509.0	Yuruga Formation	Lst	yes	1384	-0.1	-6.2	520.5	Kulpara Formation	Dol	yes
585	0.0	-9.0	509.0	Coobowie Limestone	Lst	yes	1390	-0.4	-6.3	520.7	Kulpara Formation	Dol	yes
591	-1.3	-11.1	509.5	Coobowie Limestone	Lst	yes	1396	-0.9	-7.0	520.9	Kulpara Formation	Dol	yes
597	1.9	-11.1	510.0	Moonan Formation	Sh	no	1402	-0.4	-6.8	521.1	Kulpara Formation	Dol	yes
610	-0.6	-10.1	510.4	Moonan Formation	Sh	no	1414	-0.8	-6.1	521.4	Kulpara Formation	Dol	yes
622	0.0	-8.6	510.9	Stansbury Limestone	Lst	yes	1420	-1.0	-6.1	521.6	Kulpara Formation	Dol	yes
628	0.8	-8.9	510.9	Stansbury Limestone	Lst	yes	1433	-1.2	-6.7	521.9	Kulpara Formation	Dol	yes
634	1.1	-8.6	510.9	Stansbury Limestone	Lst	yes	1439	-1.7	-6.8	522.1	Kulpara Formation	Dol	yes
646	0.7	-8.6	511.0	Stansbury Limestone	Lst	yes	1451	-1.6	-6.7	522.4	Kulpara Formation	Dol	yes
658	-1.3	-8.8	511.1	Stansbury Limestone	Lst/Dol	yes	1457	-1.4	-6.7	522.6	Kulpara Formation	Dol	yes
664	-1.1	-9.2	511.2	Corrodgery Formation	Lst/Dol	yes	1469	-1.7	-6.5	522.9	Kulpara Formation	Dol	yes
671	-1.3	-8.4	511.2	Corrodgery Formation	LSt/SSt/Sh	yes	1475	-1.5	-6.1	523.1	Kulpara Formation	Dol	yes
677	-0.6	-8.1	511.2	Corrodgery Formation	Carb SSt/Sh	yes	1481	-1.6	-6.6	523.3	Kulpara Formation	Dol	yes
683	-0.9	-9.8	511.2	Corrodgery Formation	Carb SSt	yes	1487	-1.7	-6.7	523.4	Kulpara Formation	Dol	yes
689	-1.0	-9.7	511.3	Corrodgery Formation	Carb SSt	yes	1494	-1.8	-6.8	523.6	Kulpara Formation	Dol	yes
695	-1.1	-10.9	511.3	Corrodgery Formation	Carb SSt	yes	1500	-1.9	-6.6	523.8	Kulpara Formation	Dol	yes
707	-1.4	-10.5	511.3	Corrodgery Formation	Carb SSt	yes	1506	-2.2	-6.5	523.9	Kulpara Formation	Dol	yes
713	-0.9	-10.2	511.3	Corrodgery Formation	Carb SSt	yes	1512	-2.6	-6.6	524.1	Kulpara Formation	Dol	yes
719	-2.5	-10.3	511.4	Corrodgery Formation	Carb SSt	yes	1518	-2.8	-7.2	524.3	Kulpara Formation	Dol	yes
732	-3.5	-10.4	511.4	Corrodgery Formation	Carb SSt/Sh	yes	1524	-2.4	-7.1	524.4	Kulpara Formation	Dol	yes
744	-0.7	-7.0	511.5	Ramsay Limestone	Lst	yes	1530	-2.0	-7.2	524.6	Kulpara Formation	Dol	yes
762	0.3	-8.5	511.5	Ramsay Limestone	Lst	yes	1548	-1.6	-7.2	525.1	Kulpara Formation	Dol	yes
768	0.0	-8.5	511.5	Ramsay Limestone	Lst	yes	1554	-2.6	-6.9	525.3	Kulpara Formation	Dol	yes
799	0.4	-6.2	511.6	Ramsay Limestone	Lst/Dol	yes	1567	-1.5	-6.6	525.6	Kulpara Formation	Dol	yes
805	0.2	-8.0	511.6	Ramsay Limestone	Lst	yes	1573	-1.6	-6.4	525.8	Kulpara Formation	Dol	yes
811	-0.1	-8.5	511.7	Ramsay Limestone	LSt/Sh	yes	1585	-1.7	-6.3	526.1	Kulpara Formation	Dol	yes
817	0.2	-6.9	511.7	Ramsay Limestone	Lst/Dol	yes	1591	-1.0	-6.4	526.3	Kulpara Formation	Dol	yes
829	0.4	-7.5	511.7	Ramsay Limestone	Lst/Dol	yes	1615	-1.4	-6.5	527.0	Kulpara Formation	Dol	yes
835	0.2	-5.2	511.7	Minlaton Formation	Sh	no	1622	-1.7	-6.5	527.2	Kulpara Formation	Dol	yes
841	0.4	-5.0	511.8	Minlaton Formation	Sh	no	1634	-1.8	-6.5	527.5	Kulpara Formation	Dol	yes
866	-0.2	-6.9	512.0	Minlaton Formation	Sh	no							
872	-0.4	-8.3	512.0	Minlaton Formation	Sh	no							
878	-1.1	-9.0	512.0	Minlaton Formation	Sh	no							
884	-3.9	-12.2	512.1	Minlaton Formation	Sh	no							
896	-3.2	-11.2	512.2	Minlaton Formation	Sh	no							
902	-3.3	-11.6	512.2	Minlaton Formation	Sh	no							
908	-1.7	-10.1	512.3	Minlaton Formation	Sh	no							
914	-2.7	-10.1	512.3	Minlaton Formation	Sh	no							
920	-1.9	-10.1	512.4	Minlaton Formation	Sh	no							

*Descriptions taken from Watts & Gausden, 1966; Stansbury West 1 Well Completion Report; PIRSA Open File Envelope No:656 OEL24: SSt = Sandstone; CSt = Claystone; Sh = Shale; Lst = Limestone; Dol = Dolomite;

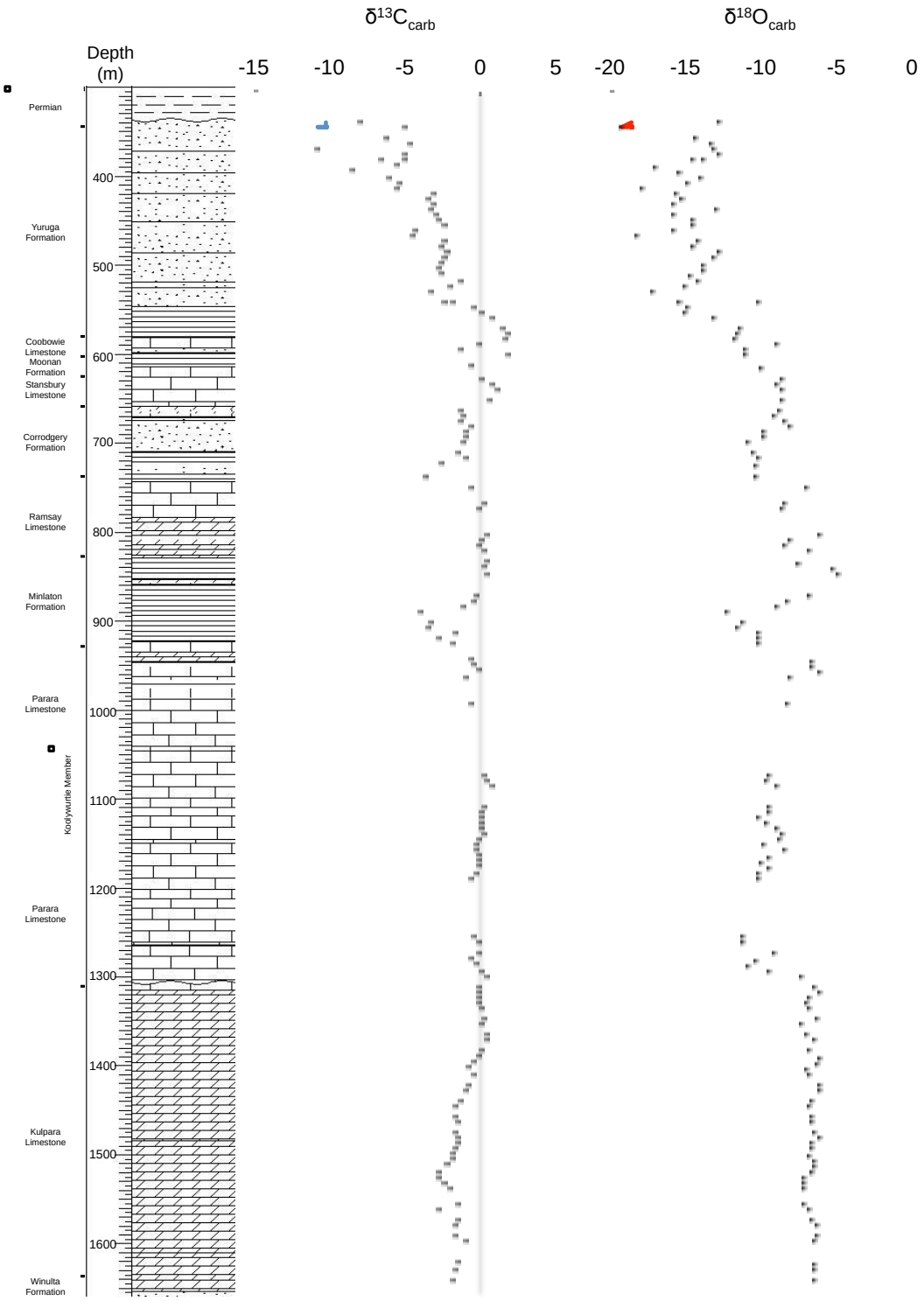

Fig.4. $\delta^{13}C_{carb}$ and $\delta^{18}O_{carb}$ profile of the Stansbury West 1 well cuttings and stratigraphic log (stratigraphic log after Watts & Gausden, 1966).

Whilst the $\delta^{18}O_{carb}$ data does show evidence of diagenetic alteration through depleted values, particularly in the dolomitic facies, the carbonate samples from the core lacks this covariance (Fig.5) suggesting these deposits are more likely to be reflecting a contemporaneous marine $\delta^{13}C_{carb}$ signal. This interpretation is supported by comparison of the $\delta^{18}O_{carb}$ to reported values which show variation within a similar range for carbonates interpreted as being minimally altered with regards to $\delta^{13}C_{carb}$ (e.g. Tucker, 1989; Derry et al., 1994; Saltzman et al., 1998; Zhu et al 2004; Guo et al., 2005; Lindsay et al., 2005; Alvaro et al., 2008; Howley & Jiang, 2010; Hoffmann et al., 2012).

The coeval dolomite sequences in the Arrowie Basin show little sign of alteration in their textural preservation, suggesting an early diagenetic origin for the dolomitization which is commonly associated with the conservation of near original $\delta^{13}C_{carb}$ values (Tucker, 1989). While the analyses were performed on core chips, which do not readily permit petrographic analysis, some small core sections were recovered. The dolomitic beds towards the base of the core are fine to microcrystalline with scatted and isotated small vugs, whilst the limestones higher in the core are generally described as cryptocrystalline with interbedded sedimentrary structures (Watts & Gausden, 1966), analogous to the previously described lower Cambrian dolomites of the Arrowie Basin.

From the base of the core the Kulpara Formation the $\delta^{13}C_{carb}$ isotope profile increases from -1.8‰ to -1.0‰ then falls back, with some small oscillations, to a minimum value of -2.8‰ in the lower third of the formation. The profile then rises to positive values and exhibits a sustained period of enrichment with values of up to 0.4‰. The pronounced negative excursion appears to correlate with the global composite of Zhu

et al. (2006), reflecting the SHICE event (Fig. 1). The 1.8‰ enrichment preceding this SHICE excursion does not compare favourably with the strongly positive ZHUCE event, though as these lowest data points reflect the base of the carbonate sequence the initial depletion observed may be an oscillation on a larger trend similar to that exhibited by the Parachilna section of the Arrowie Basin (Tucker, 1989) (Fig.9). The positive values exhibited subsequent to the negative excursion of the SHICE event may be an expression of the CARE event.

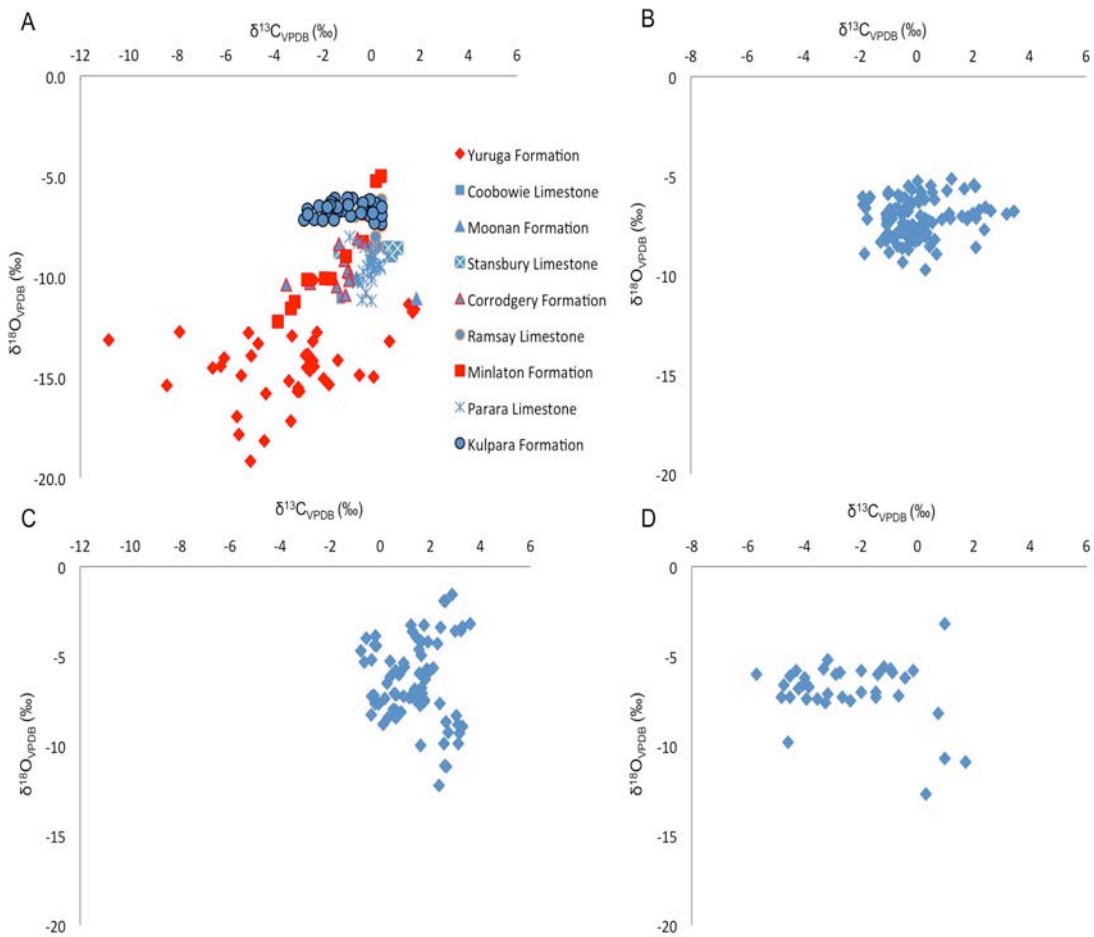

Fig.5. Cross plots for $\delta^{13}C_{carb}$ and $\delta^{18}O_{carb}$; A) Stansbury West 1 (non-carbonaceous clastic sediments coloured red), B) Wilkinson 1, C) SCYW 791A, D) Flinders Ranges (after Tucker, 1989).

Overlying the Flinders Unconformity at the base of the Parara Limestone, the isotope profile reduces from approximately 0‰ to -0.5‰. This is followed by an extended period of enrichement to 0.7‰ before a return to negative values of -0.9‰ in the upper section. Discounting the negative excursion in the siliciclastic Minlaton Formation as a diagenetic alteration as discussed previously, the $\delta^{13}C_{carb}$ profile returns to enriched values of 0.4‰ in the Ramsay Limestone. This resembles the pattern exhibited in the global composite (Zhu et al, 2006) with depleted values followed by a period of enrichment during the MICE event and the subsequent negative AECE excursion (Fig.1). The amplitude of the enrichment is clearly not as pronounced as in the Siberian profile of Kouchinsky et al., (2001) for this MICE event, it is of similar scale to data over this period in the Great Basin, Nevada (Saltzman, 2005). Though the youngest archaeocyatha documented in Australia occur as low diversity assembages within the Wirrealpa Limestone of the Arrowie Basin (Gravestock, 1984), stratigraphically correlated to the Ramsay Limestone (Jago et al., 2012), the last occurrences of archaeocyathids in the Stansbury Basin are from the Parara Limestone (Zhuravlev & Gravestock, 1994), supporting this correlation with the AECE event.

The $\delta^{13}C_{carb}$ profile once again falls from the enriched 0.4‰ values to -0.7‰ up section in the Ramsay Limestone, reducing to a marked depletion towards the basal section of the Corrodgery Formation calcareous sandstones of -3.5‰. Negative values persist through the Corrodgery Formation before rising sharply from -1.3‰ to 1.1‰ in the Stansbury Limestone. The $\delta^{13}C_{carb}$ profile then oscillates from 0‰ at the top of the Stansbury Limestone, through the Moonan Formation shales to -1.3‰ in the Coobowie Limestone and back to 0‰ at the dolomitic base of the red beds of the

Yuruga Formation. This pronounced negative excursion observed in the Corrodgery Formation and top of the Ramsay Limestone possibly represents the ROECE event.

Though the boundary between the Ramsay Limestone and Corrodgery Formation is interpreted as being below the transition between Series 2 and 3 (Jago et al., 2012), over which the prominent negative $\delta^{13}C_{carb}$ ROECE excursion has been documented (Brasier, 1992; Montanez et al., 2000; Zhu et al., 2004; Guo et al., 2010), it does lie within the upper section of Stage 4 consistent with the definition of Zhu et al. (2006). The richly fossiliferous Ramsay Limestone has been correlated with the Wirrealpa Limestone of the Arrowie basin, which contains the trilobite *Redlichia guizhouensis* whilst several specimens of *Pagetia* sp. have been recorded from the Coobowie Limestone (Jago et al., 2006). This suggests the Redlichiid-Olenellid extinction event had occurred before the Coobowie Limestones were deposited. As discussed previously the siliciclastic sequences values may not be wholly reliable for carbon isotope data; however, $\delta^{13}C_{carb}$ and $\delta^{18}O_{carb}$ do not covary in the Corrodgery Formation, and unlike the Yuruga or Moonan Formations, it is described as carbonaceous (Gavestock & Gatehouse, 1995). The biostratigraphic placement coincident with the final Redlichiid occurrences and the magnitude of the depletion being of the same order as the ROECE event adds support to these negative values being valid.

5.6.2 Officer Basin

The Wilkinson 1 drill core penetrated ~500m of early Cambrian carbonates, evaporites and basal clastics of the Ouldburra Formation which range in $\delta^{13}C_{carb}$ and $\delta^{18}O_{carb}$ values from -1.9‰ to 3.4‰ and -9.7‰ to -5.1‰ respectively (Fig.6). The base of the core shows an initial enrichment to 1.2‰ with a subsequent sharp negative excursion to -1.9‰. A significant enrichment is apparent in the $\delta^{13}C_{carb}$ profile with values rising from -1.9‰ steadily to 3.4‰ in the middle section and back to -1.1‰. The $\delta^{18}O_{carb}$ profile is relatively featureless with no covariance to the $\delta^{13}C_{carb}$ profile evident, as is also observed in the $\delta^{13}C_{carb}$ to $\delta^{18}O_{carb}$ cross-plot (Fig.5). Dolomitization in the Ouldburra Formation is predominantly of a replacement nature, with mimic replacement the most widespread; relict patches of original limestone commonly remain (Kamali et al., 1995). Petrographic analysis of samples from the upper carbonate section confirm the presence of high proportions of calcite throughout much of the core (Gatehouse, 1979). The formation is also of relatively low thermal maturity in the Tarraringa Trough, with MPI calculated R_o ~0.6 – 0.7 (Kamali, 1995) indicating thermal alteration of isotopic values is also unlikely. These observations lend support to the interpretation that the $\delta^{13}C_{carb}$ profile represents the original marine signature.

The Ouldburra Formation has limited biostratigraphical constraints, especially in the Wilkinson-1 drill core, where the impoverished Tommotian acritarchs assemblages described by Muir (in Gatehouse, 1979) only confirm a Neoproterozic to mid-Cambrian age. Acritarchs of assemblage Zones 5 (Atdabanian) have been observed from low the sequence in Manya-6, a north-easterly lateral equivalent core to Wilkinson 1 (Zang et al., 2007). Trilobites have also been identified in Manya-6 of

probable Atdabanian age (Jago et al., 2002a). Archaeocyathids of possible Botoman age were described from low (1207m) in Marla-6 (Gravestock & Hibburt, 1991), but reinterpreted by (Gravestock et al., 2002) as calcite pseudomorphs of aragonite fan cements from a reworked bioherm. Trilobite fragments observed in the Marla 3 drill core were assigned to Botoman age on their location within the core being interpreted as part of sequence Є1.3 rather than an actual identification (Dunster, 1987). In light of this poor biostratigraphy the stratigraphic correlation of Gravestock (1995) is applied to the drill core.

Table 2. $\delta^{13}C_{carb}$ and $\delta^{18}O_{carb}$ values for the Ouldburra Formation from Wilkinson 1 drill core.

Wilkinson 1, Officer Basin											
Depth (m)	$\delta^{13}C$ (‰)	$\delta^{18}O$ (‰)	Infered Age (Ma)	Depth (m)	$\delta^{13}C$ (‰)	$\delta^{18}O$ (‰)	Infered Age (Ma)	Depth (m)	$\delta^{13}C$ (‰)	$\delta^{18}O$ (‰)	Infered Age (Ma)
211	-0.9	-7.2	511.5	401	2.0	-5.4	514.6	551	-1.3	-8.3	520.1
216	-0.4	-6.8	511.6	406	1.6	-7.0	514.7	556	0.1	-8.2	520.3
221	-0.2	-7.6	511.7	411	1.7	-5.7	514.8	561	0.4	-7.9	520.5
226	0.2	-5.8	511.7	416	2.0	-6.9	514.8	566	0.7	-8.9	520.7
231	-0.2	-6.3	511.8	421	0.6	-7.4	514.9	569	-0.5	-8.6	520.8
236	0.2	-5.8	511.9	426	1.2	-5.1	515.0	571	-0.3	-6.8	520.9
241	-0.3	-8.1	512.0	431	1.1	-5.7	515.2	573	-0.1	-7.5	521
246	-0.5	-7.0	512.1	436	0.9	-7.2	515.4	578	-0.7	-8.5	521.2
251	0.0	-5.3	512.2	441	0.5	-5.5	515.6	582	-1.0	-6.9	521.4
256	-0.2	-5.7	512.2	446	0.4	-7.3	515.8	586	-0.5	-6.7	521.5
261	-0.3	-5.5	512.3	449	0.0	-8.0	515.9	589	-0.4	-6.1	521.6
266	-1.0	-7.2	512.4	451	0.1	-7.8	516.0	591	-1.0	-6.7	521.7
271	-1.1	-6.9	512.5	456	0.1	-7.6	516.2	596	-1.8	-7.2	521.9
276	-0.6	-6.1	512.6	461	-0.5	-7.4	516.4	601	-1.1	-7.1	522.1
281	-1.1	-8.0	512.6	466	-1.0	-7.3	516.6	606	-1.9	-6.4	522.3
286	-1.0	-7.0	512.7	471	-0.2	-8.1	516.8	611	-0.2	-7.5	522.5
291	-0.8	-6.7	512.8	472	-0.3	-8.0	516.9	616	0.1	-7.6	522.7
296	-1.1	-8.3	512.9	476	0.1	-7.8	517.1	621	-1.7	-6.2	522.9
301	-1.0	-8.8	513.0	478	-0.3	-8.4	517.1	624	-0.7	-6.6	523.0
306	-0.3	-7.5	513.0	481	-1.9	-8.9	517.2	626	-1.0	-8.0	523.1
311	-0.3	-8.7	513.1	486	0.3	-7.2	517.4	632	-0.7	-6.0	523.4
316	0.1	-7.6	513.2	491	0.5	-8.6	517.7	641	-1.0	-5.9	523.7
321	0.1	-7.5	513.3	493	-0.4	-7.5	517.7	646	-0.7	-6.7	523.9
326	0.6	-5.8	513.4	496	0.2	-7.6	517.9	650	-1.0	-5.8	524.1
331	-0.5	-9.4	513.5	500	0.6	-8.2	518.0	656	-0.8	-8.1	524.3
336	1.2	-6.9	513.5	501	0.3	-6.2	518.1	661	-0.8	-8.0	524.5
341	1.8	-7.1	513.6	504	0.0	-8.3	518.2	666	-0.6	-7.8	524.7
346	0.6	-6.2	513.7	506	0.1	-6.1	518.3	671	-0.9	-8.1	524.9
351	3.4	-6.8	513.8	511	0.3	-8.1	518.5	675	-1.8	-6.6	525.1
356	2.2	-6.7	513.9	513	0.3	-7.3	518.6	678	-1.9	-6.1	525.2
361	2.6	-6.8	513.9	516	0.3	-6.2	518.7	681	-0.4	-6.7	525.3
366	3.2	-6.9	514.0	518	0.1	-7.0	518.8	686	-0.3	-7.8	525.5
371	2.1	-5.5	514.1	521	-1.7	-6.1	518.9	691	1.2	-7.2	525.7
376	2.4	-7.7	514.2	526	0.1	-7.8	519.1	696	-1.1	-7.5	525.9
381	2.4	-6.6	514.3	531	0.0	-8.1	519.3	701	0.1	-6.3	526.1
386	2.1	-7.1	514.3	536	-0.6	-7.9	519.5	706	-0.4	-6.7	526.3
391	2.1	-8.6	514.4	541	0.3	-9.7	519.7	710	-0.3	-6.6	526.5
396	1.8	-7.2	514.5	546	-0.2	-8.2	519.9				

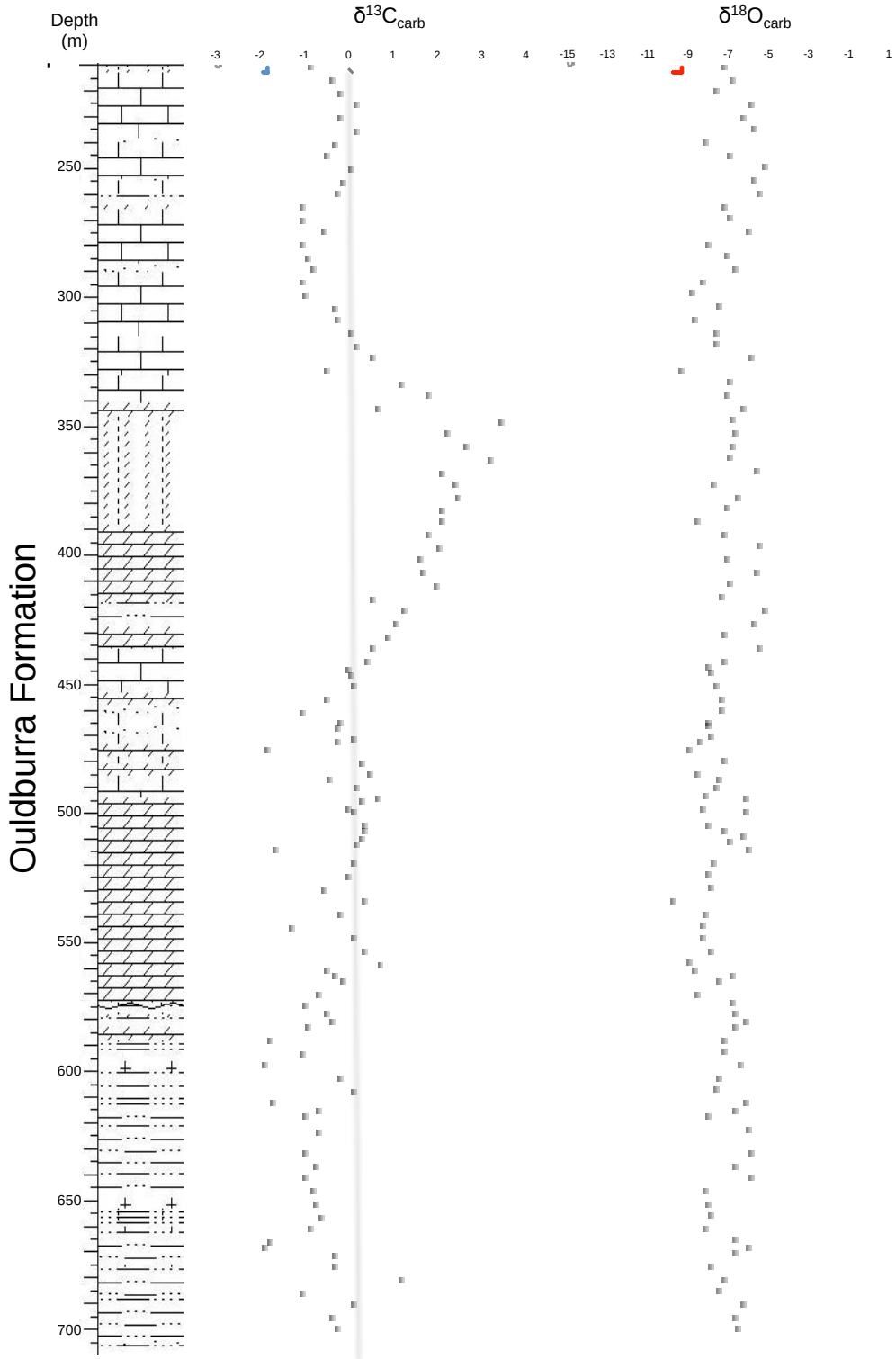

Fig.6. $\delta^{13}C_{carb}$ and $\delta^{18}O_{carb}$ profile of the Wilkinson 1 drill core and stratigraphic log (after Gatehouse, 1979).

The base of the $\delta^{13}C_{carb}$ profile where the lower evaporitic section is ascribed as equivalent to the Kulpara and Parachilna Formations. This corresponds to the culmination of a period of regression that peaked in the Tommotian. The regional uplift that gave rise to the Flinders unconformity to the south and east is correlated as the top of this lower unit (Gravestock, 1995) with the uppermost halite observed at ~575m. The subtidal Є1.2 carbonate sequence is observed as a dolomitic sequence between the halite beds and a siltstone bed with rip-up clasts and clay matrix at ~430m, a position assigned for the Є1.2-Є1.3 boundary. The upper section of the core to the siliciclastic beds at ~210m are assigned to Є1.3, with the inferred age (Table 2) at the top of the $\delta^{13}C_{carb}$ profile taking into account the eroded uppermost section.

The basal depletion from 1.2‰ to -1.9‰ and the enrichment in the upper section of the formation to 3.4‰ (Fig.9) correlate with the SHICE and MICE events respectively on the global composite of Zhu et al. (2006). The middle section of the core shows a rise to predominantly positive values over the period of the CARE excursion, although the magnitude is smaller than that in the Stansbury Basin data. The depletion observed at the top of the section to values <-1‰ are a close fit to those of the AECE excursion in the global composite. The positive ZHUCE event prior to the SHICE is not fully expressed at the base of the section similar to the Stansbury Basin.

5.6.3 Arrowie Basin

In the Andamooka Limestone section of SCYW 791A the $\delta^{13}C_{carb}$ values are predominantly positive, but range from -0.8‰ to 3.6‰ (Table 3, Fig.7). A negative excursion is observed at the base of the formation (-0.8‰), with a gradual rise to short-lived positive (1.7‰) and negative (-0.4‰) excursions in the middle of the section that are followed by a strong positive excursion towards the top of the formation (3.6‰). $\delta^{18}O_{carb}$ values range between -1.6‰ and -12.2‰ with the majority of oscillation observed in the upper section of the core which dampen to values generally between -4‰ and -9‰.

Table 3. $\delta^{13}C_{carb}$ and $\delta^{18}O_{carb}$ values for the Andamooka Limestone from SCYW-791A drill core.

SCYW 791A, Arrowie Basin											
Depth (m)	$\delta^{13}C$ (‰)	$\delta^{18}O$ (‰)	Infered Age (Ma)	Depth (m)	$\delta^{13}C$ (‰)	$\delta^{18}O$ (‰)	Infered Age (Ma)	Depth (m)	$\delta^{13}C$ (‰)	$\delta^{18}O$ (‰)	Infered Age (Ma)
29	1.6	-10.0	513.0	70	1.9	-5.7	516.0	111	1.6	-7.7	519.1
31	3.0	-3.6	513.2	72	1.6	-4.9	516.2	112	1.6	-6.8	519.1
33	2.9	-1.6	513.3	73	1.9	-5.8	516.3	113	1.4	-6.8	519.2
34	3.1	-8.8	513.4	74	1.5	-5.3	516.3	114	1.6	-7.3	519.3
36	3.1	-9.9	513.5	75	1.7	-3.3	516.4	115	1.4	-7.4	519.4
38	3.3	-8.9	513.7	76	1.6	-4.2	516.5	116	1.4	-7.3	519.5
40	3.2	-9.3	513.8	77	1.4	-4.0	516.6	117	0.8	-8.1	519.5
42	3.0	-8.3	514.0	78	1.3	-3.6	516.6	120	0.9	-7.2	519.7
44	2.5	-9.9	514.1	80	1.2	-3.3	516.8	124	0.6	-8.0	520.0
45	2.6	-11.1	514.2	82	0.9	-5.4	517.0	125	0.6	-8.4	520.1
46	2.6	-11.2	514.3	84	1.0	-5.6	517.1	126	0.6	-7.1	520.2
48	2.7	-9.2	514.4	85	-0.3	-7.2	517.2	127	0.5	-8.0	520.2
49	2.6	-8.7	514.5	86	0.2	-7.4	517.2	128	0.6	-8.3	520.3
50	2.5	-1.9	514.6	88	-0.4	-8.3	517.4	129	0.6	-8.4	520.4
51	2.4	-7.6	514.7	91	0.6	-5.8	517.6	130	0.3	-8.5	520.5
53	2.3	-12.2	514.8	95	0.6	-7.1	517.9	133	0.1	-8.8	520.7
54	3.3	-3.4	514.9	98	0.6	-7.1	518.1	137	0.7	-6.0	521.0
55	3.2	-3.6	515.0	99	-0.2	-7.6	518.2	155	0.3	-6.5	522.8
57	3.6	-3.2	515.1	101	0.4	-6.2	518.3	164	-0.6	-4.0	523.7
58	2.6	-1.9	515.2	102	-0.3	-7.2	518.4	166	-0.2	-4.4	523.9
59	1.7	-7.5	515.2	103	-0.1	-7.7	518.5	167	-0.3	-5.2	524.0
60	1.8	-7.4	515.3	105	0.6	-7.2	518.6	169	-0.6	-5.3	524.2
62	2.1	-5.7	515.5	106	1.7	-7.1	518.7	172	-0.8	-4.7	524.5
64	2.4	-3.4	515.6	107	1.2	-7.3	518.8	181	-0.2	-3.9	525.4
65	2.3	-4.3	515.7	108	1.6	-7.2	518.8	185	-0.2	-4.4	525.8
67	1.9	-4.2	515.8	109	1.6	-6.8	518.9	192	0.4	-5.3	526.5
68	1.8	-6.3	515.9	110	1.4	-6.9	519.0				

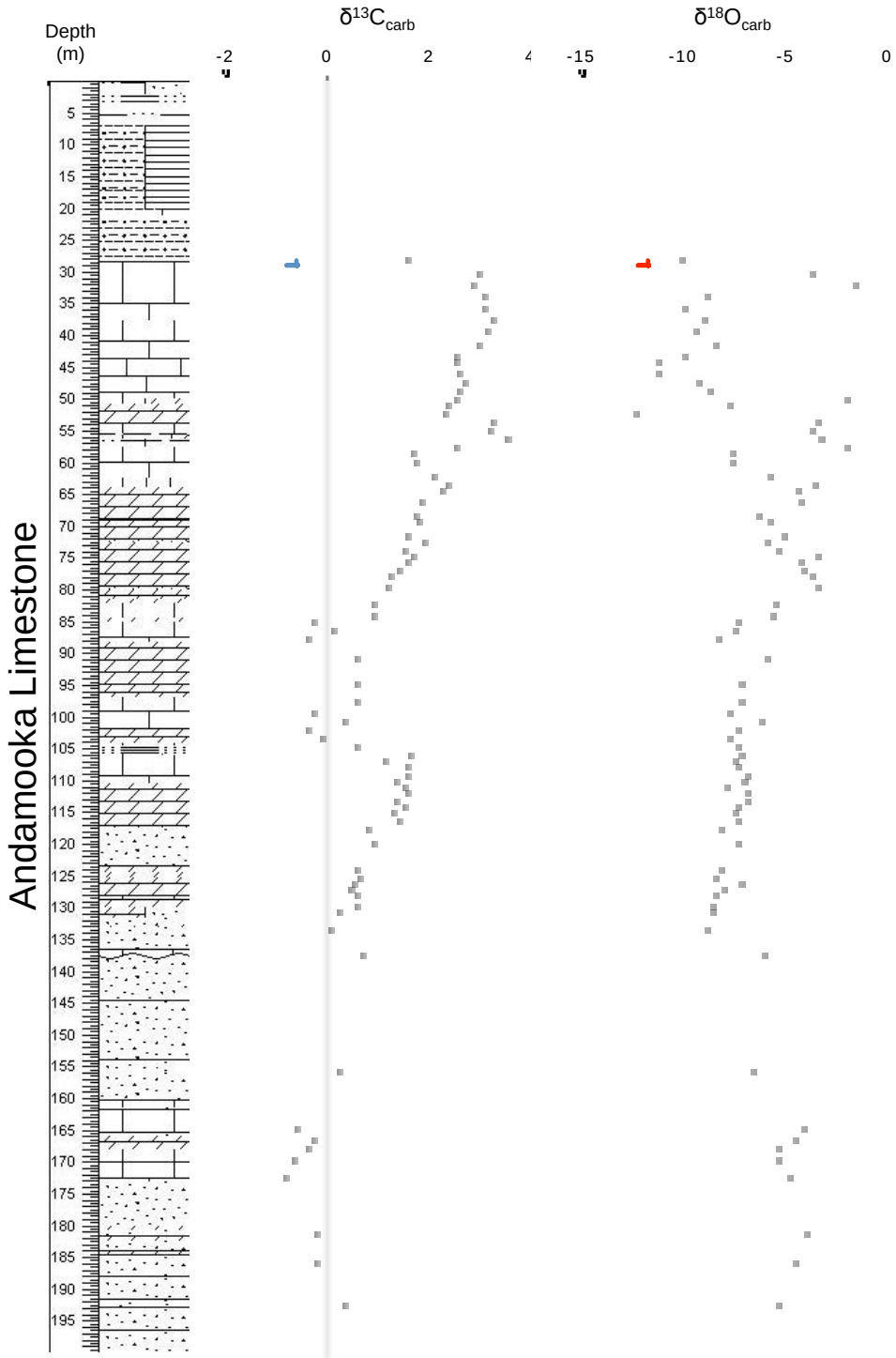

Fig.7. $\delta^{13}C_{carb}$ and $\delta^{18}O_{carb}$ profile of the SCYW 791A drill core and stratigraphic log.

The upper section of the limestone in the core is slightly vuggy indicating some dissolution has occurred which is likely to account for the variation observed in these $\delta^{18}O_{carb}$ values though the original textures are reasonably well preserved suggesting recrystallisation was minimal. This conclusion is consistent with James and Gravestock (1990) who describe the calcite cementation of archaeocyathaid build-ups in the region as partially synsedimentary and partially a shallow burial phenomenon. If percolation with meteoric waters was responsible for the dissolution and recrystallisation it would be expected that the $\delta^{13}C_{carb}$ profile would also show significant depletion (Swart and Kennedy, 2012), which is not apparent. The cross plot of $\delta^{13}C_{carb}$ against $\delta^{18}O_{carb}$ (Fig.5) exhibits no covariance, so though the upper section shows signs of alteration of the more sensitive $\delta^{18}O_{carb}$, as with the Stansbury West 1 and Wilkinson 1 data the $\delta^{13}C_{carb}$ profile is interpreted as reflecting the original marine signal.

The stratigraphic placement of Zang (2002) for the Andamooka Limestone assigns Є1.1A for the lower sequence and Є1.2 for the upper, with the Flinders unconformity splitting the units. The Flinders unconformity is interpreted as a karst surface ~138m depth (Fig. 7), overlain by a thin silicified packstone with green tuffaceous horizons, this is analogous to the position (~140m) of James & Gravestock (1990). Another tuffaceous horizon, a thin bed of approximately 10cm, is observed in the Andamooka core at 88m. We suggest that these tuffs may correlate with the green tuff beds in the upper Wilkawillina Limestone, Parara Limestone and Heatherdale Shale of the Stansbury Basin that are related to the Truro Volcanics (James & Gravestock, 1990; Gravestock & Gatehouse, 1995, Zang, 2002). Above the Flinders unconformity the first archaeocyatha are observed at ~125m depth. These observations correlate with the description and placement of the middle Wilkawillina Limestone, interpreted as

being of lower-mid Botoman age (Zang, 2002, Zang et al., 2007). Casey (2005) described a relatively diverse SSF assemblage from this core which correlate with the upper *Hippopharangites dailyi* (Atdabanian) and lower *Halkieria parva* (mid-Botoman) zones, whilst brachiopod *Eoobolus priscus* and *Karathele yorkensis* of Botoman assemblages were also identified above the Flinders unconformity. This biostratigraphic evidence places the base of the upper Andamooka Limestone slightly lower than in Zang (2002) within the Cambrian Series 2 Stage 3 with the majority of the section in Series 2 Stage 4.

Applying this stratigraphic and biostratigraphic criteria to our $\delta^{13}C_{carb}$ profile the negative excursion at the base of the core occurs in the Cambrian Terreneuvian (Series 1) Stage 2 where the prominent enrichment of the ZHUCE event is followed by the SHICE depletion. The amplitude of the negative excursion in the Andamooka Limestone at ~1.2‰ is not as pronounced as that expressed in lateral equivalent Arrowie Basin section from the Flinders Ranges to the East (Fig.8) or such sections as the Anti-Atlas Margin, Morocco (Maloof et al., 2005). The base of the core is only ~30m below the depletion, and it is unlikely the full extent of the ZHUCE enrichment is observed, especially as the majority of this lowest section is medium sandstone. The enrichment to 1.7‰ seen in the middle of the core section, above the Flinders unconformity, correlates with the CARE event whilst the strong positive excursion higher in the sequence from -0.4‰ to 3.9‰ corresponds to the initiation of the MICE event (Fig.9). The chemostratigraphic interpretation of the upper section of the Andamooka Limestone support extending it into the base of the upper Botoman, a placement beyond the mid-Botoman of Zang (2002).

Table 4. $\delta^{13}C_{carb}$ and $\delta^{18}O_{carb}$ values from the Flinders Ranges (interpreted from Tucker, 1989)

Flinder Ranges, Arrowie Basin							
Wilkawillina Limestone (Wilkawillina Gorge)				Woodendina Dolomite (Parachilna Gorge)			
Depth (m)	$\delta^{13}C$ (‰)	$\delta^{18}O$ (‰)	Infered Age (Ma)	Depth (m)	$\delta^{13}C$ (‰)	$\delta^{18}O$ (‰)	Infered Age (Ma)
41	0.7	-8.2	519.5	228	-3.3	-5.7	522.7
19	1.7	-10.9	520.3	220	-3.2	-7.1	522.8
11	1.0	-10.7	520.6	192	-1.4	-6.0	523.2
6	0.3	-12.7	520.8	188	-2.4	-7.5	523.2
				183	-3.6	-7.4	523.3
Woodendina Dolomite (Fountain Spring)				173	-4.7	-6.6	523.4
Depth (m)	$\delta^{13}C$ (‰)	$\delta^{18}O$ (‰)	Infered Age (Ma)	163	-5.7	-6.0	523.6
120	1.0	-3.2	521.0	141	-4.0	-6.2	523.9
93	-0.1	-5.8	521.4	124	-4.5	-6.1	524.1
74	-0.4	-6.2	521.6	111	-4.2	-6.8	524.3
64	-0.9	-5.9	521.8	106	-4.1	-6.6	524.4
44	-1.0	-5.7	522.1	100	-3.9	-6.7	524.5
32	-1.2	-5.6	522.2	93	-3.9	-7.4	524.5
21	-1.5	-7.0	522.4	88	-4.3	-5.8	524.6
11	-2.0	-5.8	522.5	84	-4.8	-7.3	524.7
10	-2.9	-6.0	522.5				
6	-2.7	-5.9	522.6	Parachilna Formation (Parachilna Gorge)			
3	-3.2	-5.2	522.6	Depth (m)	$\delta^{13}C$ (‰)	$\delta^{18}O$ (‰)	Infered Age (Ma)
				67	-4.6	-9.8	524.9
				61	-4.5	-7.3	525.0
				50	-3.3	-7.6	525.3
				47	-1.5	-7.3	525.4
				40	-2.7	-7.3	525.5
				33	-2.0	-7.0	525.7
				24	-0.7	-7.2	525.9

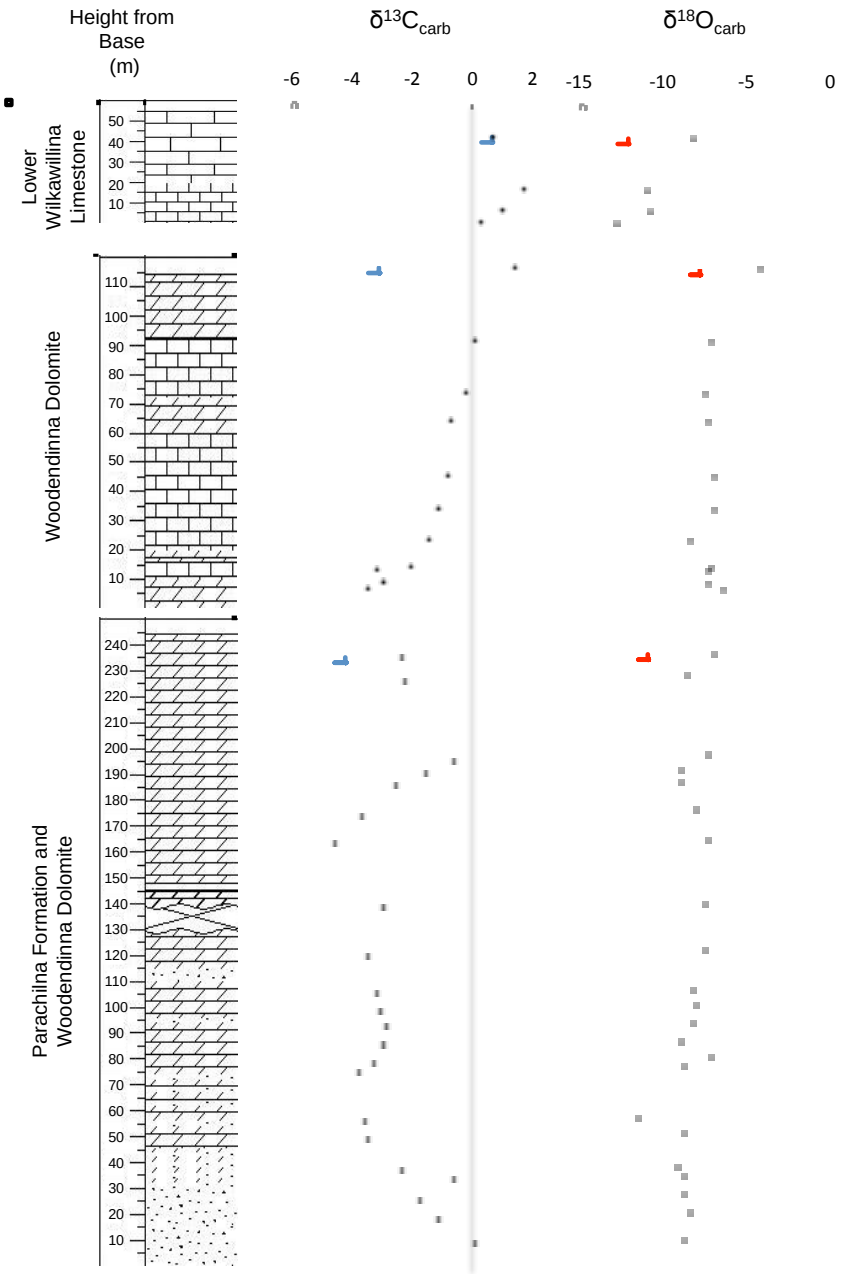

Fig.8. $\delta^{13}C_{carb}$ and $\delta^{18}O_{carb}$ profile of the Flinders Ranges outcrop samples and stratigraphic log (after Tucker, 1989).

5.6.4 Composite $\delta^{13}C_{carb}$ profile of lower Cambrian South Australia.

The individual $\delta^{13}C_{carb}$ profiles for the sequences presented all correlate on a regional scale and show good correspondence with further comparison to the $\delta^{13}C_{carb}$ profile of the Є1.1 sections in the Flinders Ranges (Table 4, Fig. 8) extending this relationship to the previously reported values from Australia (Tucker, 1989). Whilst the lack of strong geochronological constraints for the data is a weakness, correlation with the existing regional interpretation of biostratigraphy and sequence stratigraphy is evident. Combining the data, including that of Tucker (1989) to produce a South Australian composite it is clear they correspond favourably with the global composite of Zhu et al., (2006) for the Cambrian period (Fig. 9).

Whilst the inferred ages do not match exactly, the profile shows depletions and enrichments with similar periods and to amplitudes within the ranges of reported coeval section. The AECE, MICE, CARE and SHICE events are all expressed within the profile with a strong degree of concordance. The ROECE event appears to be below the event period, however, the expression within the South Australian composite does lie in line with the classification given by Zhu et al (2006) i.e., within uppermost part of Stage 4 (uppermost part of Series 2 to lowermost part of Series 3). The minor discrepancy in the inferred position of the ROECE event is easily accounted for by the inherent complications in extrapolation of chronology within this time period and lack of sound radiometric dating in the Australian sections. The chemostratigraphy suggests that the stratigraphic position of the boundary between the Ramsay Limestone and the Corrodgery Formation may lie closer to the Early - Middle Cambrian transition than currently assigned (Jago et al., 2012).

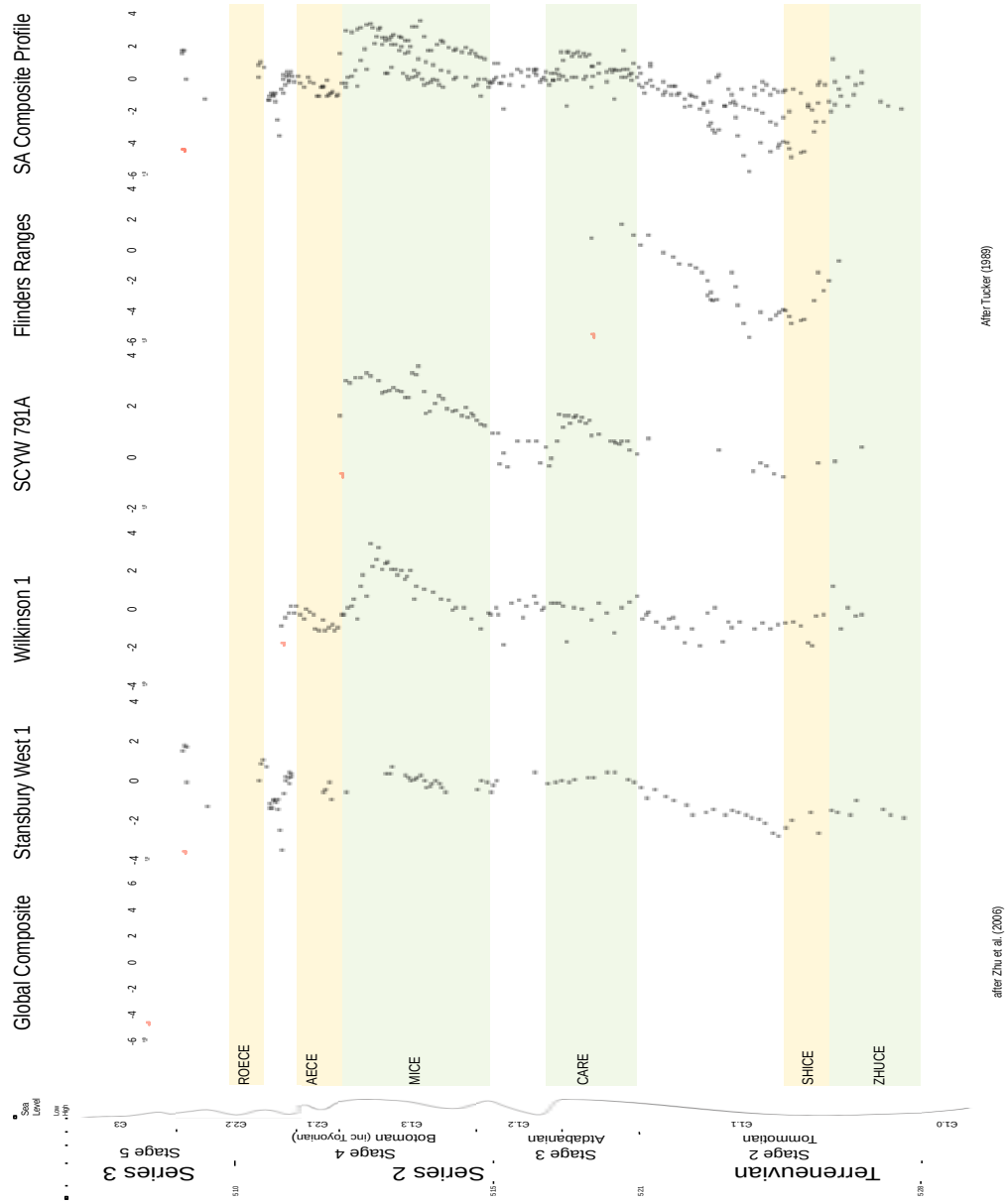

Fig.9. South Australian $\delta^{13}C_{carb}$ composite and individual section profiles with comparison to the global composite (after Zhu et al., 2006). The South Australian (SA) composite is derived from an average of the inferred ages at a 0.1Myr period.

It is clear that further dating of South Australian strata, using an additional technique such as U-Pb isotope dilution–thermal ionization–mass spectrometry (ID-TIMS), would aid in calibrating the data set, refining the inferred ages of the chemostratigraphic data.

There is a distinct correlation between relative sea level and the $\delta^{13}C_{carb}$ profile within the Series 2 epoch (Fig.9). A relationship between eustatic sea level and excursion events has been widely observed from the Proterozoic to Recent (e.g. Joachimski & Buggisch, 1993; Kennedy et al., 1998; Buggisch et al, 2003; Halverson et al., 2002, 2005; Swart & Kennedy, 2012). The explanation for these $\delta^{13}C_{carb}$ perturbations and their link to sea level fluctuations is controversial. Both diagenetic alteration of the exposed carbonate shelf through meteoric interaction (Swart, 2008; Oehlert et al 2012; Swart & Kennedy, 2012) and carbon cycle perturbations (e.g., Buggisch et al, 2003; Halverson et al., 2002, 2005, 2009, 2010; Maloof et al 2005; Saltzman 2011; Caxito et al., 2012; Cremonese et al., 2012; Hoffman et al., 2012) can explain the coincident nature of these expressions. The excursions observed in the profile during the Terreneuvian do not, however, track sea level fluctuations. A number of positive and negative fluctuations are apparent over a protracted period of regression to transgression implying these are independent of sea level and an expression of secular changes within the carbon isotope distribution of the DIC. The global manifestation of these Early Cambrian events implicate multiple mechanisms in the modulation of the Early Cambrian marine carbon cycle, a typical feature of the Cambrian oceans (Maloof et al., 2005). These mechanisms may be associated with fluctuations in oceanic redox, nutrient cycling and the rate of organic matter burial (Halverson et al. 2009) as observed in coeval black shales (e.g., Guo et al., 2007; Lehmann et al., 2007; Powell, 2009; Yu et al., 2009; Cremonese et al., 2012; Och et al., 2012) and expressed locally in the phosphatic Heatherdale Shale and Emu Bay Shale lagerstätte (Hall et al., in press).

This new South Australian data supports the interpreted global composite profile for $\delta^{13}C_{carb}$ compiled by Zhu et al. (2006) from data presented in numerous previous studies. The correspondence of these South Australian units with coeval sections from Siberia (e.g., Keteme, Emyaksin and Pestrotsvet Formations; Basier et al., 1994; Kouchinsky et al., 2001; 2005; 2010), South China (e.g., Kaili and Quinxudong Formations; Guo et al., 2005; 2010; Zhu et al., 2004), Morocco (e.g., Adoudounian and Lie De Vin Formations; Maloof et al., 2005), southern Europe (e.g., Lancara and Lastours Formations; Wotte et al., 2007) and North America (Chisholm, Pioche and lower units in the Great Basin; Montanez et al., 2000; Saltzman et al 2005) strengthen the argument these variation in the $\delta^{13}C_{carb}$ distributions are a secular phenomenon. Hence, global reproduction of similar variations over biostratigraphically constrained intervals demonstrates the utility of the carbon isotopic record for stratigraphic correlation purposes.

5.7. Conclusions

The carbon isotope chemostratigraphy of the South Australian basins shows good correlation regionally and is supported by the sequence stratigraphy and biostratigraphic assignment. Whilst it is apparent additional radiometric dating to the sparse data set available is required in order to calibrate the isotopic profile, comparison to the global chemostratigraphic profile shows a strong degree of concordance. Prominent, globally recognised isotopic excursions are recognised within the South Australian composite; the SHICE, AECE and ROECE depletion events in conjunction with the CARE and MICE enrichments are all correlated. These features allow correlation to be made with Early Cambrian sections from North America, Africa, Asia and Europe.

A relationship is observed between chemostratigraphy and the relative sea level during the Cambrian Stage 2 with the profile mimicking the sea level curve. This may indicate a diagenetic origin for the carbon isotope distribution derived from meteoric interaction with the exposed carbonate shelf during period of regression. Alternatively, eustatic sea level could be the primary causal effect of variation of isotopic distribution within the DIC pool, the initial source of sequestered carbon, through alteration of oceanic redox, nutrient cycling and the rate of organic matter burial which are evidenced within coeval black shale deposits. The Terreneuvian section of the profile lacks this mimicry, though several excursions are evident. This suggest that the carbon isotope profile was independent of eustacy during this period and given the secular nature of these events it seems likely perturbations in the isotopic composition of DIC are exhibited in the profile. The structure of South Australia's expanded Early Cambrian $\delta^{13}C_{carb}$ profile, in correlation with the global composite, reveals the palaeo-Pacific Ocean varied at several frequencies, implicating multiple processes in the modulation of the marine carbon cycle.

5.8. Acknowledgements

This study forms part of a project on the palaeoenvironment, biogeochemistry, chemostratigraphy and aspects of hydrocarbon potential of the Stansbury, Arrowie, Officer and Otway Basins, funded by Primary Industries and Resources South Australia. PAH is in receipt of an Australian Postgraduate Award, while JBJ acknowledges funding from an Australian Research Council Linkage Grant (LP0774959), and additional financial support from Beach Energy Ltd and the South Australian Museum. PAH thanks Keith Hall (Hall Analytical Laboratories Ltd), John Morrison (Nu Instruments Ltd), Andy Mower (IsoScience Pty. Ltd) and Mike Hall

(The Godwin Laboratory, University of Cambridge) for their assistance with the isotopic analyses. The contributions of PAH, DMMcK, GPH and AC to this paper form TRaX Record ###.

5.9. References

Álvaro, J.J., Bauluz, B., Subías, I., Pierre, C., Vizcaïno, D., 2008. Carbon chemostratigraphy of the Cambrian–Ordovician transition in a midlatitude mixed platform, Montagne Noire, France. Geological Society of America Bulletin 120, 962–975.

Babcock L. E., Peng S., 2007. Cambrian chronostratigraphy: Current state and future plans. Palaeogeography, Palaeoclimatology, Palaeoecology 254, 62-66.

Babcock, L.E., Robison, R.A., Rees, M.N., Peng, S.C., Saltzman, M.R., 2007. The Global Stratotype Section and Point (GSSP) of the Drumian Stage (Cambrian) in the Drum Mountains, Utah, USA. Episodes 30, 84-94.

Brasier M. D., Hewitt R. A., 1979. Environmental setting of fossiliferous rocks from the uppermost proterozoic—lower Cambrian of central England. Palaeogeography, Palaeoclimatology, Palaeoecology 27, 35-57.

Brasier M.D., 1992. Towards a carbon isotope stratigraphy of the Cambrian System: potential of the Great Basin succession. In Hailwood, E.A. & Kidd, R.B. (eds) 'High Resolution Stratigraphy'. Geological Society Special Publication, 70, 341-350.

Brasier, M.D., Corfield, R.M., Derry, L.A., Rozanov, A.Yu., Zhuravlev, A.Yu., 1994. Multiple $\delta^{13}C$ excursions spanning the Cambrian explosion to the Botoman crisis in Siberia. Geology 22, 455–458.

Brasier, M.D., Sukhov, S.S., 1998. The falling amplitude of carbon isotopic oscillations through the Lower to Middle Cambrian: northern Siberia data. Canadian Journal of Earth Sciences 35, 353–373.

Brock, G.A., Engelbrestsen M.J., Jago J.B., Kruse P.D., Laurie J.R., Shergold J.H., Shi G.R. and Sorauf, J.E., 2000. Palaeobiogeographic affinities of Australian Cambrian faunas. Association of Australasian Palaeontologists, Memoir 23, 1-61.

Buggisch, W., Keller, M., Lehnert, O., 2003. Carbon isotope record of Late Cambrian to Early Ordovician carbonates of the Argentine Precordillera. Palaeogeography, Palaeoclimatology, Palaeoecology 195, 357–373.

Casey, E., 2005. Faunal diversity and biostratigraphy of Early Cambrian small shelly fossils from the Andamooka Limestone, Stuart Shelf, South Australia. Unpublished Honours Dissertation, Macquarie University, Sydney.

Caxito, F.de A. Halverson, G.P., Uhlein, A., Stevenson, R., Gonçalves Dias, T, Uhlein, G.J., 2012. Marinoan glaciation in east central Brazil, Precambrian Research 200–203, 38-58

Collins A. S., Pisarevsky S. A., 2005. Amalgamating eastern Gondwana: The evolution of the Circum-Indian Orogens. Earth-Science Reviews 71, 229-270.

Cremonese, L., Shields-Zhou, G., Struck, U., Ling, H.-F., Och, L., Chen, X., Li, D., 2012. Marine biogeochemical cycling during the early Cambrian constrained by a nitrogen and organic carbon isotope study of the Xiaotan section, South China. Precambrian Research., doi:10.1016/j.precamres.2011.12.004

Daily, B., 1972. The base of the Cambrian and the first Cambrian faunas. in: Jones, J.B., McGowran, B. (Eds.), Stratigraphic Problems of the Later Precambrian and Early Cambrian. The University of Adelaide Centre for Precambrian Research, 13–41 (Special Paper 1).

Derry, L.A., Brasier, M.D., Corfield, R.M., Rozanov, A.Yu., Zhuravlev, A.Yu., 1994. Sr and C isotopes in Lower Cambrian carbonates from the Siberian craton: a paleoenvironmental record during the 'Cambrian explosion'. Earth and Planetary Sciences Letters 128, 671–681.

Dunster, J.N., 1987. Sedimentology of the Ouldburra Formation (Early Cambrian) northeastern Officer Basin. University of Adelaide. M.Sc. thesis (unpublished).

Fike D.A., Grotzinger J.P., Pratt L.M., Summons R.E., 2006. Oxidation of the Ediacaran Ocean. Nature 444, 744–747.

Flöttmann, T., Haines, P.W., Cockshell C.D., Preiss, W. V., 1998. Reassessment of the seismic stratigraphy of the Early Palaeozoic Stansbury Basin, Gulf St Vincent, South Australia. Australian Journal of Earth Sciences 45, 547-557.

Foden, J.D., Elburg, M. A., Dougherty-Page, J., Burtt, A., 2006. The timing and duration of the Delamerian Orogeny: correlation with the Ross Orogen and implications for Gondwana assembly. Journal of Geology 114, 189–210.

Gatehouse, C.G., 1979. Well completion report, Wilkinson No.1. Department of Mines and Energy Report Book 79/84.

Gatehouse, C.G., Jago, J.B., Cooper, B.J., 1990. Sedimentology and stratigraphy of the Carrickalinga Head Formation (low stand fan to high stand systems tract), Kanmantoo Group, South Australia. Geological Society of Australia Special Publication 16, 351–368.

Glumac, B., Walker, K.R., 1998. A late Cambrian positive carbon-isotope excursion in the southern Appalachians: relation to biostratigraphy, sequence stratigraphy, environments of deposition, and diagenesis. Journal of Sedimentary Research 88, 1212–1222.

Gravestock D.I., 1995. Chapter 7 Early and Middle Palaeozoic. In Drexel J.F., Preiss, W.V. and Parker, A.J., 1995, The Geology of South Australia. Vol. 2, The Phanerozoic. South Australia Geological Survey, Bulletin 54

Gravestock, D. I., Benbow, M.C., Gatehouse, C.G., Krieg, G.W., 1995. Early and Middle Palaeozoic –Eastern Officer Basin.: The geology of South Australia, Volume 2, the Phanerozoic, v. 54: Adelaide, South Australia Geological Society, 35-41.

Gravestock, D. I., Gatehouse, C.G., 1995. Early and Middle Palaeozoic – Stansbury Basin.: The geology of South Australia, Volume 2, the Phanerozoic, v. 54: Adelaide, South Australia Geological Society, 5-20.

Gravestock, D. I., W. M. Cowley, 1995. Early and Middle Palaeozoic -Arrowie Basin.: The geology of South Australia, Volume 2, the Phanerozoic, v. 54: Adelaide, South Australia Geological Society, 20-31.

Gravestock, D.I. Morton J.G.G., 2002. Chapter 8 Source rock distribution and quality. In Morton J.G.G., Drexel, J.F. (Eds.) Petroleum Geology of South Australia Volume 3,http://www.pir.sa.gov.au/petroleum/access_to_data/petroleum_publications/petroleum_geology_of_south_australia/vol_3_-_officer_basin_downsampled

Gravestock, D.I. Morton J.G.G., Zang, W-L., 2002. Chapter 7 Biostratigraphy and correlation. In Morton J.G.G., Drexel, J.F. (Eds.) Petroluem Geology of South Australia Volume 3, http://www.pir.sa.gov.au/petroleum/access_to_data/petroleum_publications/petroleum_geology_of_south_australia/vol_3_-_officer_basin_downsampled

Gravestock, D.I., 1984. Archaeocyatha from lower parts of the Lower Cambrian carbonate sequence in South Australia. Memoir of the Association of Australian Palaeontologists 2, 1-139.

Gravestock, D.I., 2002. Chapter 5 Geological setting and structural history. In Morton J.G.G., Drexel, J.F. (Eds.) Petroleum Geology of South Australia Volume 3, http://www.pir.sa.gov.au/petroleum/access_to_data/petroleum_publications/petroleum_geology_of_south_australia/vol_3_-_officer_basin_downsampled

Gravestock, D.I., Hibburt, J.E., 1991. Sequence stratigraphy of the eastern Officer and Arrowie Basins: a framework for Cambrian oil search. APEA Journal 31, 177–190.

Gravestock, D.I., Shergold, J.H., 2001. Australian Early and Middle Cambrian sequence biostratigraphy with implications for species diversity and correlation. in: Zhuravlev, A.Y., Riding, R. (Eds.), The Ecology of the Cambrian Radiation. Columbia University Press, 105–136.

Guo Q., Shields G.A., Liu C., Strauss H., Zhu M., Pi D., Goldberg T., Yang X., 2007. Trace element chemostratigraphy of two Ediacaran–Cambrian successions in South China: Implications for organosedimentary metal enrichment and silicification in the Early Cambrian. Palaeogeography, Palaeoclimatology, Palaeoecology 254, 194-216.

Guo Q., Strauss H., Liu C., Zhaod Y., Yang X., Peng J., Yang H., 2010. A negative carbon isotope excursion defines the boundary from Cambrian Series 2 to Cambrian Series 3 on the Yangtze Platform, South China. Palaeogeography, Palaeoclimatology, Palaeoecology 285, 143-151.

Guo, Q., Strauss, H., Liu, C., Zhao, Y., Pi, D., Fu, P., Zhu, L., Yuan, J., 2005. Carbon and oxygen isotopic composition of Lower to Middle Cambrian sediments at Taijiang, Guizhou Province, China. Geological Magazine 142, 723–733.

Haines,P.W., Turner, S.P., Foden, J., Jago, J., 2009. Isotopic and geochemical characterization of the Cambrian Kanmantoo Group, South Australia: implications for stratigraphy and provenance. Australian Journal of Earth Sciences 56, 1095-1110.

Hall P.A., McKirdy, D.M., Halverson, G.P., Jago, J.B., Collins, A.S., Carson, M.W., 2012. The biogeochemical status of the Palaeo-Pacific Ocean: clues from the early Cambrian of South Australia. Gondwana Research, submitted manuscript GR-D-12-00258.

Halverson G. P., Wade B. P., Hurtgen M. T., Barovich K. M., 2010. Neoproterozoic Chemostratigraphy. Precambrian Research 182, 239–412.

Halverson G.P., Hurtgen M.T., Porter S.M., Collins A.S., 2009. Chapter 10 Neoproterozoic-Cambrian Biogeochemical Evolution. Developments in Precambrian Geology 16, 351-365.

Halverson, G.P., Hoffman, P.F., Schrag, D.P., Kaufman, J.A., 2002. A major perturbation of the carbon cycle before the Ghaub glaciation (Neoproterozoic) in Namibia: prelude to snowball Earth? Geochemistry, Geophysics, Geosystems 3, doi:10.1029/2001GC000244.

Halverson, G.P., Hoffman, P.F., Schrag, D.P., Maloof, A.C., Rice, A.H., 2005. Towards a Neoproterozoic composite carbon-isotope record. Geological SocIety of American Bulletin 117, 1181–1207.

Hoffman, P.F., Halverson, G.P., Domack, E.W., Maloof, A.C., Swanson-Hysell N.L., Cox, G.M., 2012. Cryogenian glaciations on the southern tropical paleomargin of Laurentia (NE Svalbard and East Greenland), and a primary origin for the upper Russøya (Islay) carbon isotope excursion. Precambrian Research 206– 207, 137– 158.

Howley R. A., Jiang G., 2010. The Cambrian Drumian carbon isotope excursion (DICE) in the Great Basin, western United States. Palaeogeography, Palaeoclimatology, Palaeoecology 296, 138-150.

Hurtgen, M.T., Arthur, M.A., Halverson, G.P., 2005. Neoproterozoic sulfur isotopes, the evolution of microbial sulfur species, and the burial efficiency of sulfide as sedimentary sulfide. Geology 33, 41–44.

Jago J.B., Sun X., Zang W., 2002b. Correlation within early Palaeozoic basins of eastern South Australia. PIRSA Report Book 2002/033.

Jago J.B., Zang W.L, Sun X, Brock G.A., Paterson J.R., Skovsted C.B., 2006, A review of the Cambrian biostratigraphy of South Australia. Palaeoworld 15, 406-423.

Jago, J.B., Dyson, I.A., Gatehouse, C.G., 1994. The nature of the sequence boundary between the Normanville and Kanmantoo Groups on Fleurieu Peninsula, South Australia. Australian Journal of Earth Sciences 41, 445-453.

Jago, J.B., Gum, J.C., Burtt, A.C., Haines, P.W., 2003. Stratigraphy of the Kanmantoo Group: a critical element of the Adelaide Fold Belt and the Palaeo-Pacific plate margin, Eastern Gondwana. Australian Journal of Earth Sciences 50, 343–363.

Jago, J.B., Lin, T.R. & Dunster, J.N., 2002a. A new species of the trilobite *Abadiella* from the Lower Cambrian of the eastern Officer Basin, South Australia. Acta Palaeontologica Sinica 41, 428-433.

James N.P. & Gravestock D.I., 1990, Lower Cambrian shelf and shelf margin buildups, Flinders Ranges, South Australia. Sedimentology 37, 455–480.

Jenkins, R. J.; Cooper, J. C.; and Compston, W. 2002. Age and biostratigraphy of Early Cambrian tuffs from SE Australia and southern China. Journal of the Geological Society of London 159, 645–658.

Joachimski, M.M., Buggisch, W., 1993. Anoxic events in the late Frasnian—Causes of the Frasnian-Famennian faunal crisis? Geology 21, 675-678.

Kamali, M.R., 1995. Sedimentology and Petroleum Geochemistry of the Ouldburra Formation, Eastern Officer Basin, Australia. Unpublished PhD thesis, University of Adelaide.

Kamali, M.R., Lemon, N.M., Apak, S.N., 1995. Porosity generation and reservoir potential of Ouldburra Formation carbonates, Officer Basin, South Australia, APEA Journal 35, 106-120.

Kennedy, M.J., Runnegar, B., Prave, A.R., Hoffmann, K.-H., Arthur, M.A., 1998. Two or four Neoproterozoic glaciations? Geology 26, 1059–1063.

Kimura H., Watanabe Y., 2001. Oceanic anoxia at the Precambrian-cambrian boundary. Geology 29, 995-998.

Kouchinsky, A., Bengtson, S., Missarzhevsky, V. V., Pelechaty, S., Torssander, P. & Val'kov, A. K. 2001. Carbon isotope stratigraphy and the problem of a pre-Tommotian Stage in Siberia. Geological Magazine 138, 387–96.

Kouchinsky, A., Bengtson, S., Runnegar, B., Skovsted, C., Steiner, M., Vendrasco, M., 2012 Chronology of early Cambrian biomineralization. Geological Magazine 149**,** 221–251.

Kouchinsky, A.,Bengtson, S.,Pavlov, V.,Runnegar, B., Val'kov, A. K. & Young, E. 2005. Pre-Tommotian age of the lower Pestrotsvet Formation in the Selinde section on the Siberian platform: carbon isotopic evidence. Geological Magazine 142, 319–25.

Kruse, P.D., 1991. Cyanobacterial-archaeocyathan-radiocyathan bioherms in the Wirrealpa Limestone of South Australia. Canadian Journal of Earth Sciences 28, 601-615.

Landing, E., Bowring, S., Davidek, K., Westrop, S., Geyer, G., Heldmaier, W., 1998. Duration of the Early Cambrian: U-Pb ages of volcanic ashes from Avalon and Gondwana: Canadian Journal of Earth Sciences 35, 329–338.

Landing, E., Peng, S.C., Babcock, L.E., Geyer, G., Moczydlowska-Vidal, M. 2007. Global standard names for the lowermost Cambrian series and stage. Episodes 30, 287-289.

Lehmann, B., Nägler, T.F., Holland, H.D., Wille, M., Mao, J., Pan, J., Dulski, P., 2007. Highly metalliferous carbonaceous shale and early Cambrian seawater. Geology 35, 403–406.

Li Z.X., Bogdanova S.V., Collins A.S., Davidson A., De Waele B., Fitzsimons R.E., Ernst I.C.W., Fuck R.A., Gladkochub D.P., Jacobs J., Karlstrom K.E., Lu S., Natapov L.M., Pease V., Pisarevsky S.A., Thrane K., Vernikovsky V., 2008, Assembly, configuration, and break-up history of Rodinia: A synthesis. Precambrian Research 160, 179-210.

Lindsay J.F., Kruse P.D., Green O.R., Hawkins E., Brasier M.D., Cartlidgee J. and Corfield R.M., 2005, The Neoproterozoic–Cambrian record in Australia: A stable isotope study. Precambrian Research 143, 113-133.

Lindsay, J.F., 2002. Supersequences, superbasins, supercontinents - evidence from the Neoproterozoic basins of Central Australia. Basin Research 14, 204–223.

Machel, H.G., 1997. Recrystallization versus neomorphism, and the concept of ‘significant recrystallization’ in dolomite research. Sedimentary Geology 113, 161–168.

Machel, H.G., 2005. Dolomites. in Selley, R.C., Cocks R., Pilmer. I.R. (Eds.): Encyclopedia of Geology, Elsevier, 79-94

Magartiz M., Holser W.T. and Kirschvink J.L., 1986, Carbon isotope events across the Precambrian/Cambrian boundary on the Siberian Platform. Nature 320, 258-259.

Maloof, A.C., Ramezani, J., Bowring, S.A., Fike, D.A., Porter, S.M., Mazouad, M., 2010. Constraints on early Cambrian carbon cycling from the duration of the Nemakit-Daldynian–Tommotian boundary $\delta^{13}C$ shift, Morocco. Geology 38, 623–626.

Maloof, A.C., Schrag, D.P., Crowley, J.L., & Bowring, S.A., 2005, An expanded record of Early Cambrian carbon cycling from the Anti-Atlas Margin, Morocco; Canadian Journal of Earth Sciences 42, 2195-2216.

Mason, S., 2001. Petroleum generation and expulsion from pressure solution structures in teh Cambrian Ouldburra Formation, Officer Basin. Unpublished Honours Thesis, University of Adelaide.

Montanez I.P., Osleger D.A., Banner J.I., Mack L.E. and Musgrove M., 2000, Evolution of the Sr and C Isotope Composition of Cambrian Oceans. GSA Today, 10, 1-7

Morton J.G.G., 2002 Chapter 6 Lithostratigraphy and Environments of Deposition. In Morton J.G.G., Drexel, J.F. (Eds.) Petroluem Geology of South Australia Volume 3, http://www.pir.sa.gov.au/petroleum/access_to_data/petroleum_publications/petroleum_geology_of_south_australia/vol_3_-_officer_basin_downsampled

Och, L.M., Shields-Zhou, G.A., Poulton, S.W., Manning, C., Thirlwall, M.F., Li, D., Chen, X., Ling, H., Osborn, T., Cremonese, L., 2012. Redox changes in Early Cambrian black shales at Xiaotan section, Yunnan Province, South China. Precambrian Research doi:10.1016/j.precamres.2011.10.005

Oehlert, A.M., Lamb-Wozniak, K.A., Devlin, Q.B., Mackenzie, G.J., Reijmer, J.J.G., Swart, P.K., 2012. The stable carbon isotopic composition of organic material in platform derived sediments: implications for reconstructing the global carbon cycle. Sedimentology 59, 319–335

Paterson, J.R., 2005. Revision of *Discomesites* and *Estaingia* (Trilobita) from the Lower Cambrian Cymbric Vale Formation, western N.S.W.: taxonomic, biostratigraphic and biogeographic implications. Proceedings of the Linnean Society of New South Wales 126, 81–93.

Peng, S., Babcock, L.E., Zuo, J., Lin, H., Zhu, X., Yang, X., Robison, R.A., Qi, Y., Bagnoli, G., Chen, Y. 2009 The Global Boundary Stratotype Section and Point (GSSP) of the Guzhangian Stage (Cambrian) in the Wuling Mountains, Northwestern Hunan, China. Episodes 32, 41-55.

Peng, S.C., Babcock, L.E., Robison, R.A., Lin, H.L., Rees, M.N., Saltzman, M.R., 2004. Global Standard Stratotype-section and Point (GSSP) of the Furongian Series and Paibian Stage (Cambrian). Lethaia 37, 365–379.

Porter, S.M. 2007. Seawater chemistry and early carbonate biomineralization. Science 316, 1302.

Powell W.G., 2009. Comparison of geochemical and distinctive mineralogical features associated with the Kinzers and Burgess Shale formations and their associated units. Palaeogeography, Palaeoclimatology, Palaeoecology 277, 127–140.

Powell, C.M., Preiss, W.V., Gatehouse, C.G., Krapez, B., Li, Z.X., 1994. South Australian record of a Rodinian epi-continental basin and its mid-Neoproterozoic breakup (~700Ma) to form the Palaeo-pacific Ocean. Tectonophysics 237, 113-140.

Preiss, W. V., 2000, The Adelaide Geosyncline of South Australia and its significance in Neoproterozoic continental reconstruction. Precambrian Research 100, 21-63.

Preiss, W.V., 1995. Delamerian Orogeny. In: Drexel J. F., Preiss W. V. (Eds.), The Geology of South Australia, Vol. 2: The Phanerozoic. Geological Survey of South Australia Bulletin 54, 45-60.

Railsback, L.B., Holland, S.M., Hunter, D.M., Jordan, E.M., Díaz, J.R., Crowe, D.E., 2003. Controls on geochemical expression of subaerial exposure in Ordovician limestones from the Nashville Dome, Tennessee, U.S.A. Journal of Sedimentary Research 73, 790–805.

Saltzman M.R., Ripperdan R.L., Brasier M.D., Lohmann K.C., Robinson R.A., Chang W.T., Peng S., Ergaliev E.K. and Runnegar B.R., 2000, A global carbon isotope excursion (SPICE) during the Late Cambrian: relation to trilobite extinctions, organic-matter burial and sea level. Palaeogeography, Palaeoclimatology, Palaeoecology 160, 211–223.

Saltzman, M.R., 2005. Phosphorus, nitrogen, and the redox evolution of the Paleozoic oceans. Geology 33, 573–576.

Saltzman, M.R., Runnegar, B., Lohmann, K.C., 1998. Carbon isotope stratigraphy of Upper Cambrian (Steptoean Stage) sequences of the eastern Great Basin: record of a global oceanographic event. Geological Society of America Bulletin 110, 285–297.

Saltzman, M.R., Young, S.A., Kump, L.R., Gill, B.C., Lyons, T.W., Runnegar, B., 2011 Pulse of atmospheric oxygen during the late Cambrian. Proceedings of the National Academy of Sciences of the United States of America 108, 3876–3881.

Schröder, S., Grotzinger, J.P., 2007. Evidence for anoxia at the Ediacaran-Cambrian boundary: the record of redox-sensitive trace elements and rare earth elements in Oman. Journal of the Geological Society of London 164, 175–187.

Seilacher A., 1998, Patterns of macroevolution: How to be prepared for extinction. Comptes Rendus de l'Académie des Sciences - Series IIA - Earth and Planetary Science 327, 431-440.

Swart, P.K., 2008, Global synchronous changes in the carbon isotopic composition of carbonate sediments unrelated to changes in the global carbon cycle: Proceedings of the National Academy of Sciences of the United States of America 105, 13741–13745.

Swart, P.K., Kennedy, M.J., 2012. Does the global stratigraphic reproducibility of $\delta^{13}C$ in Neoproterozoic carbonates require a marine origin? A Pliocene-Pleistocene comparison. Geology 40, 87–90.

Tingate, P. R., and I. R. Duddy, 2002, The thermal history of the eastern Officer Basin (South Australia): evidence from apatite fission track analysis and organic maturity data: Tectonophysics 349, 251-275.

Tucker M.E., 1986, Carbon isotope excursions in Precambrian/Cambrian boundary beds, Morocco. Nature 319, 48-50.

Tucker M.E., 1989, Carbon isotope and Precambrian-Cambrian boundary geology, South Australia: ocean basin formation, seawater chemistry and organic evolution. Terra Nova.1, 573-582.

Watts T.R., Gausden, J., 1966; Stansbury West 1 Well Completion Report; PIRSA Open File Envelope #656.

Woods, M.A., Wilby, P.R., Leng, M.J., Rushton, A.W.A., Williams, M., 2011 The Furongian (late Cambrian) Steptoean Positive Carbon Isotope Excursion (SPICE) in Avalonia Journal of the Geological Society of London 168, 851–861.

Wotte, T., Álvaro, J.J., Shields, G.A., Brown, B., Brasier, M.D., Veizer, J., 2007. C-, O- and Srisotope stratigraphy across the Lower–Middle Cambrian transition of the Cantabrian Zone (Spain) and the Montagne Noire (France), West Gondwana. Palaeogeography, Palaeoclimatology, Palaeoecology 256, 47–70.

Yu, B.S., Dong, H., Widomb, E., Chen, J, Lin C.S., 2009. Geochemistry of basal Cambrian black shales and cherts from the Northern Tarim Basin, Northwest China: Implications for depositional setting and tectonic history. Journal of Asian Earth Sciences 34, 418–436.

Zang, W-L., 2002. Sequence analysis and petroleum potential in the Arrowie Basin, South Australia. PIRSA Report Book 2002/024.

Zang, W-L., Jago, J.B., Alexander, E.M., Paraschivoiu, E., 2004. A review of basin evolution, sequence analysis and petroleum potential of the frontier Arrowie Basin, South Australia. In: Boult, P.J., Johns, D.R., Lang, S.C. (Eds.), Eastern Australian Basins Symposium II. Petroleum Exploration Society of Australia, Special Publication, 243–256.

Zang, W.-L., Moczydłowska, M. & Jago, J.B., 2007. Early Cambrian acritarch assemblage zones in South Australia and global correlation. Memoirs of the Association of Australasian Palaeontologists 33, 141-177.

Zhu M., Babcock L.E. and Peng S., 2006, Advances in Cambrian Stratigraphy and paleontology: integrating correlation techniques, palaeobiology, taphonomy and paleoenvironmental reconstruction, Palaeoworld, 15, 217–222.

Zhu M., Zhang J., Li G. and Yang A., 2004, Evolution of C isotopes in the Cambrian of China: implications for Cambrian subdivision and trilobite mass extinctions. Geobios 37, 287-301.

Zhuravlev, A.Y., Gravestock, D.I., 1993. Archaeocyaths from Yorke Peninsula, South Australia and archaeocyathan Early Cambrian zonation. Alcheringa 18, 1-54.

Australasian asphaltite strandings revisited: their origin and the effects of weathering and biodegradation on their biomarker and isotopic profiles

P.A Hall[1], D.M. McKirdy[1], K. Grice[2] & D. Edwards[3]

Submitted Manuscript JMPG-D-12-00179
Marine and Petroleum Geology
Elsevier B.V.

1. School of Earth and Environmental Sciences, University of Adelaide, SA 5005, Australia
2. Western Australia Organic and Isotope Geochemistry Centre, The Institute for Geoscience Research, Department of Chemistry, Curtin University of Technology, GPO Box U1987 Perth, WA 6845, Australia
3. Geoscience Australia, GPO Box 378, Canberra, ACT 2601, Australia

STATEMENT OF AUTHORSHIP

Australasian asphaltite strandings revisited: their origin and the effects of weathering and biodegradation on their biomarker and isotopic profiles

Philip Anthony Hall (Candidate)

Performed analysis or oversaw the analysis on all samples, interpreted data, wrote manuscript and acted as corresponding author

I hereby certify that the statement of contribution is accurate

Signed ……..*Date*……

David M. McKirdy

Australasian asphaltite strandings revisited: their origin and the effects of weathering and biodegradation on their biomarker and isotopic profiles

Statement of contribution (in terms of the conceptualization of the work, its realization and its documentation)

Contributed to planning of article and provided critical evaluation

Certification that the statement of contribution is accurate and permission is given for the inclusion of the paper in the thesis

Signed …….Date…20/06/2012…

Kliti Grice

Australasian asphaltite strandings revisited: their origin and the effects of weathering and biodegradation on their biomarker and isotopic profiles

Statement of contribution (in terms of the conceptualization of the work, its realization and its documentation)

Contributed to sample analysis, planning of article and provided critical evaluation

Certification that the statement of contribution is accurate and permission is given for the inclusion of the paper in the thesis

Signed …….Date…27/06/2012…

Dianne Edwards

Australasian asphaltite strandings revisited: their origin and the effects of weathering and biodegradation on their biomarker and isotopic profiles

Statement of contribution (in terms of the conceptualization of the work, its realization and its documentation)

Contributed to sample collection and provided critical evaluation

Certification that the statement of contribution is accurate and permission is given for the inclusion of the paper in the thesis

Signed …….Date…20/06/2012…

Abstract

Asphaltites, long known to strand along the coastline of southern Australia and as distantly as New Zealand and Macquarie Island, are widely regarded as artefacts of submarine oil seepage. Their remarkably uniform composition suggests a common source: marine shale containing sulfur-rich Type II kerogen, probably deposited during an Early Cretaceous oceanic anoxic event (OAE). Suitable hydrocarbon kitchens may exist in the offshore Bight and Otway Basins. Their physical character, including laminations and flow structures, and degree of alteration, which is not the result of biodegradation or extensive water washing, suggest an origin from subsurface tar mats subsequently exposed by the incision of submarine canyons, with the possible formation of asphaltic volcanoes. API gravities of 4–18° impart quasi-neutral buoyancy, implying many asphaltites were submerged drifters prior to stranding, their degree of weathering reflecting, at least in part, the residence time in the marine environment. For any individual asphaltite specimen, this will depend on the proximity of the seafloor seep to the stranding site, an important consideration when attempting to locate their point of origin.

This study investigates the hydrocarbon biomarker signatures and *n*-alkane $\delta^{13}C$ profiles of asphaltite specimens from four localities: Eyre Peninsula (n = 2), Kangaroo Island (n = 4), and the Limestone Coast (n = 3), South Australia and Invercargill, New Zealand (n = 2). Sub-samples of the interior and weathered surface of each specimen were analysed. No distinction could be made between strandings based on their source-dependent molecular and isotopic signatures, confirming their common origin. Comparison of the interior and exterior sub-samples revealed only subtle, though consistent differences. Given their degree of degradation and isotopic variance, these

Australasian asphaltites seem to be products of low intensity seeps in either the eastern Ceduna Sub-basin of the Bight Basin or, more likely, the Morum sub-basin of the Otway Basin.

6.1. Introduction

Reports of bitumen strandings on the coastlines of South Australia, Victoria, Tasmania and Western Australia date from the early 19th Century (Sprigg and Woolley, 1963; Currie et al., 1992; Volkman et al., 1992; McKirdy et al., 1994; Padley, 1995; Edwards et al., 1998 and references therein). The locations of these strandings along Australia's southern margin (Fig. 1), and their greater frequency in southeastern South Australia, western Victoria and southern Tasmania, fuelled early petroleum exploration in the region on the assumption that they were sourced from local submarine seepages (Sprigg, 1986; Volkman et al., 1992; McKirdy, 1994). Accounts describe a variety of oily substances that can be assigned to three categories, each with a different origin: oils (crude and refined), waxy bitumens and asphaltites (McKirdy et al., 1986, 1994; Edwards et al., 1998). While the early reports were of asphaltum strandings, waxy bitumens have become more prevalent since the 1960s (Padley, 1995).

The oils, which typically strand as liquid droplets, are likely anthropogenic inputs arising from local maritime traffic (Padley et al., 1993; Padley, 1995). The waxy bitumens have been assigned to several genetic families, distinguished by subtle but systematic differences in their sulfur content, biomarker and stable isotopic signatures (McKirdy, 1984a,b; McKirdy et al., 1986, 1994; Padley, 1995). Commonly observed as small tar balls (5–120 mm in diameter) they are paraffinic to aromatic-intermediate crude oils with API (American Petroleum Institute) gravities of ~13–38°. Three of

these bitumen families contain biomarkers attributable to tropical angiosperms (dipterocarpaceae) and freshwater algae (notably dinoflagellates and race B of the green alga *Botryococcus braunii*) (McKirdy et al., 1994).

That oils of the same Cenozoic lacustrine source affinity occur in Sumatra suggests that the waxy bitumens originated in Indonesia (McKirdy et al., 1994; Padley, 1995), an interpretation supported by strandings of similar material along the northern (Summons et al., 1992, 1993) and western (Currie et al., 1992) margins of Australia, with long-distance surface transportation on the Southern Equatorial and Leeuwin currents accounting for their widespread dispersal (McKirdy and Horvath, 1976; McGowran et al., 1997; Edwards et al., 1998).

The focus of the present study involves detailed geochemical and isotopic characterisation of asphaltites (i.e. the Family 4 coastal bitumens of McKirdy 1984a, b; McKirdy et al., 1986, 1994). Geochemically quite distinct from the waxy bitumens, these are heavy, sulfur-rich, aromatic-asphaltic crudes (4–18° API; ~4% S; 57–84% asphaltenes) that commonly strand as large, jet-black, ovoid lumps (up to 670 mm across and 7 kg in weight) at the high water mark on medium to high energy, gently sloping sandy beaches (McKirdy et al., 1994; Padley, 1995). Unlike the waxy bitumens, which have positive buoyancy, the Australasian asphaltites are on average slightly denser than seawater and therefore are likely to have resided within the water column prior to stranding.

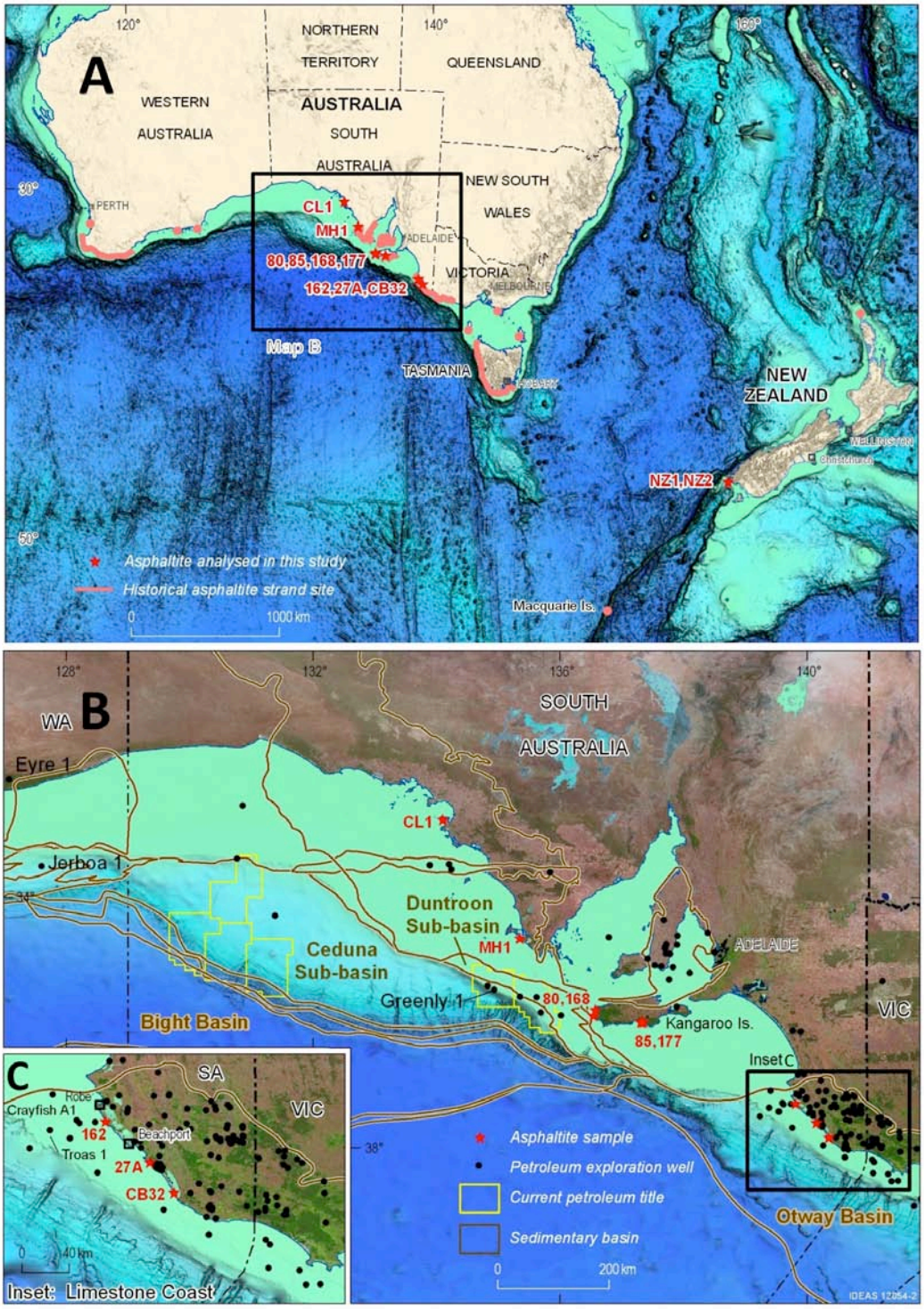

Fig.1 A) location of historically documented asphaltite strandings and samples from this study; B) expanded section for South Australia with sample stranding sites, basin locations and petroleum exploration well sites; C) expanded section for the Limestone Coast, South Australia with sample stranding sites and petroleum exploration well sites.

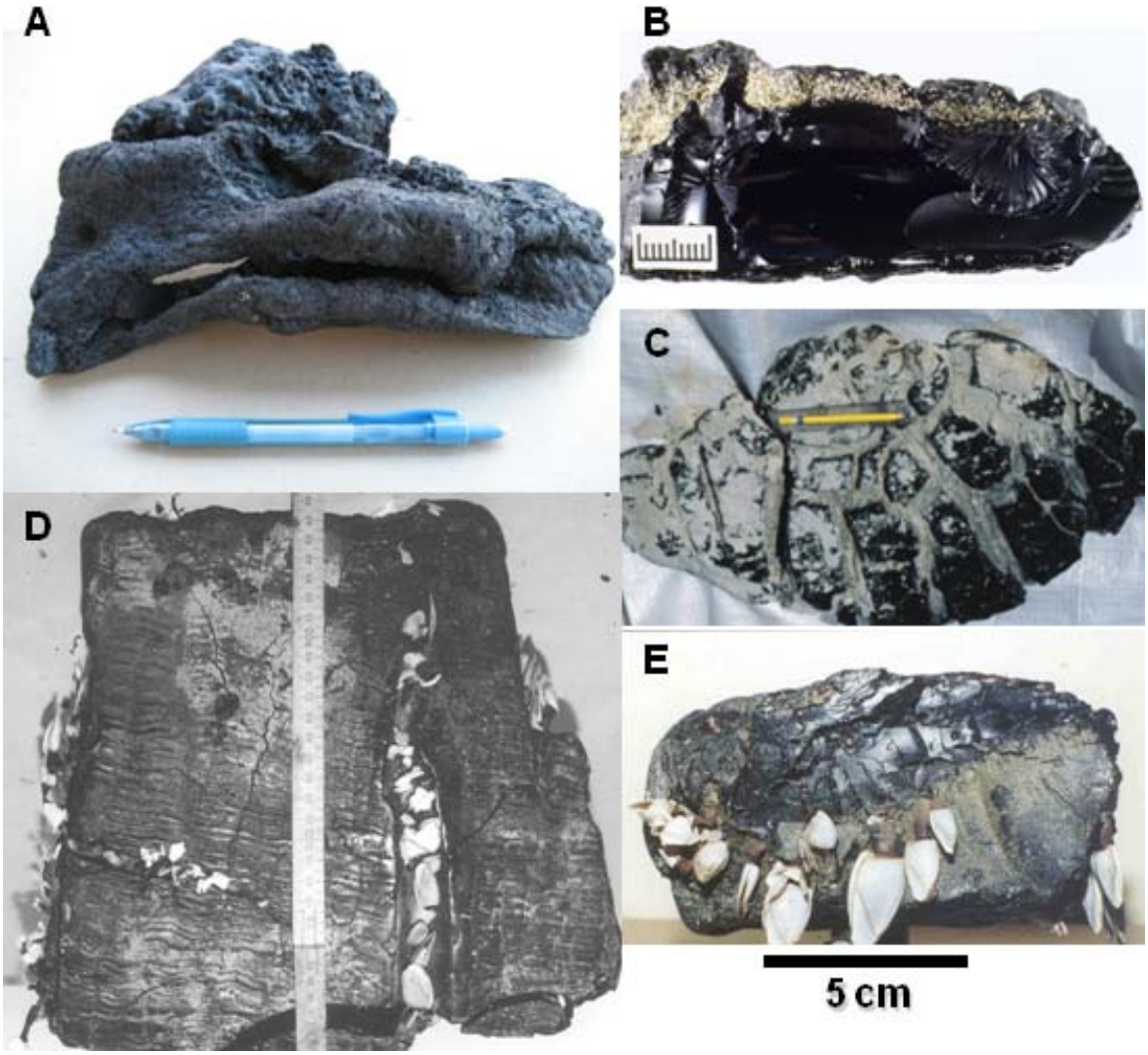

Figure 2. Examples of asphaltite strandings: A) an asphaltite from Port McDonnell (not analysed) with a rolled over edge indicative of viscous flow; B) sample 80, Ravine de Casours, Kangaroo Island, broken open to reveal the conchoidal fracture pattern typical of all asphaltites (scale bar 20 mm); C) sample 177, Bales Bay, Kangaroo Island, a large specimen exhibiting upper surface devolatilization cracks and a characteristic flat ovoid shape (long axis = 75 cm); d) sample NZ1, Invercargill, New Zealand with an unusual internal fabric suggestive of laminar flow, devolatilization cracks and a bivalve colony; e) sample NZ2, Invercargill, New Zealand, also colonised by bivalves. Photographs provided by D. McKirdy (plate A); D. Edwards, nee Padley (plates B and C); and D. Bradley (plates D and E).

The fresh strandings have a strong petroliferous odour (Sprigg and Woolley, 1963; Volkman et al., 1992; Padley, 1995; Edwards et al., 1998). Their upper surface is characteristically traversed by shrinkage cracks and, although the interior is pliable when fresh, they become brittle upon storage and exhibit a conchoidal fracture pattern (Fig. 2). Their stable isotopic and molecular compositions (McKirdy et al., 1986, 1994; Currie et al., 1992; Volkman et al., 1992; Dowling et al., 1995; Padley, 1996; Edwards et al., 1998), including their enrichment in metallo-porphyrins (Boreham et al., 2001; Totterdell et al., 2008), make them unique among Australasian crude oils. Moreover, historic (>100 years ago) and more recent strandings at sites in Western Australia, South Australia, Victoria and Tasmania and even as far afield as New Zealand and Macquarie Island (Fig. 1) are of remarkably similar composition, suggesting that they all originated from the same offshore petroleum system (Padley, 1996; Edwards et al., 1998).

The saturated hydrocarbons of unweathered Australasian asphaltites (Padley, 1995; Edwards et al., 1998) share many of the compositional characteristics of a typical marine crude oil. Their *n*-alkane profile is unimodal (range C_{10}–C_{35+}, maximum at C_{15}/C_{17}) and devoid of odd or even carbon-number predominance. The ratio of pristane to phytane is low (1.1–1.3) generally indicative of anoxic conditions. Their terpane distribution exhibits a dominance of C_{30} αβ hopanes, a Ts/Tm ratio <1 (Ts = C_{27} 18α(H)-22,29,30-trisnorhopane; Tm = C_{27} 17α(H)-22,29,30-trisnorhopane), the presence of both 29,30- and 28,30-bisnorhopanes, and a lack of both 25-norhopanes and land-plant biomarkers (e.g. oleanane and bicadinanes). However, unlike other oils of marine source affinity, their triterpanes do not include 2α- and 3β-methylhopanes. Their regular steranes (C_{27}≥C_{29}>C_{28}>C_{30}) are accompanied by methylsteranes (including dinosterane) and abundant diasteranes (Edwards et al., 1998). Their bulk

hydrocarbon fractions are isotopically light (mean $\delta^{13}C_{sat}$ and $\delta^{13}C_{arom}$ = –30.1 and –29.5‰, respectively) while their *n*-alkane $\delta^{13}C$ *versus* carbon number profiles mostly lie between –31 and –34‰, with the C_{19}–C_{25} homologues being the most depleted in ^{13}C. The abundance of vanadyl relative to nickel porphyrins in these asphaltites is high (≈ 22:1), and their methylphenanthrene indices reveal that they were expelled from their source rock(s) at relatively low thermal maturities (calculated vitrinite reflectance, Rc = 0.5–0.75%).

The source and age-specific biomarkers of these asphaltites indicate an origin from Cretaceous marine shale deposited under anoxic/sulfidic conditions, probably during an oceanic anoxic event (OAE) (McKirdy et al., 1994, Edwards et al., 1998, Boreham et al., 2001). OAEs record profound changes in the climatic and palaeoceanographic state of the planet and represent major perturbations of the global carbon cycle. They correspond to periods of warmer, wetter climate thought to be induced by a rapid influx of CO_2 to the atmosphere causing greenhouse conditions. Increased continental weathering led to high nutrient flow and subsequent high primary productivity in the photic zone. Intense oxygen demand in the water column meant conditions could readily evolve from poorly oxygenated to anoxic and ultimately euxinic, particularly in those oceans and seaways where density stratification was favoured by palaeogeography and significant fluvial input (Jenkyns, 2010). Whether anoxia was prevalent throughout the global oceanic system or confined to these restricted settings is still a matter for conjecture. Nevertheless, examples such as the Tethyan and Atlantic oceans in the Northern Hemisphere are renowned for their extensive organic-rich muds deposited during mid-Cretaceous OAEs. In the Southern Hemisphere the Indian Ocean and contiguous Toolebuc and Blue Whale seaways likewise were sites of restricted circulation. Accordingly, euxinic marine sediments have been identified

in several of the corresponding Australian depocentres, possibly recording the Cenomanian–Turonian OAE2 (Bonarelli Event) and shorter-lived late Albian oceanic anoxic subevent (OAE 1d; Breistrofffer Event) (Edwards et al., 1999; Boreham et al., 2001; Struckmeyer et al., 2001; Pancost et al., 2004; Totterdell et al., 2008; Jenkyns, 2010).

All the Australasian asphaltites lack 25-norhopanes, implying little in-reservoir bacterial alteration (Volkman et al., 1984), and hence may be placed at Level 4 on the degradation scale of Peters and Moldowan (1993) (Edwards et al., 1998). This level of biodegradation also suggests that if they emanate from natural submarine seepage it would be of low intensity (Wenger and Isaksen, 2002), an interpretation consistent with the pattern described for the Australian continental shelf (Logan et al., 2010) and ascribed to low recent burial rates.

The physical properties of the southern margin strandings appear analogous to those of asphaltic mats or volcanoes observed emanating from the sea floor at Chapopote Knoll in the Gulf of Mexico (GOM) as low intensity seeps of heavily biodegraded viscous oil (Brüning et al., 2010; Schubotz et al., 2011). Here surface cracking is due to the *in situ* loss of volatiles and subsequent fragmentation of older more brittle deposits. Flow structures and lamination are evident in cored specimens. Such features have been noted in some Australasian asphaltites, including those analysed in the present study (Fig. 2A, D). Colonisation of the GOM asphalts by benthic mussels, sponges and tubeworms allowed estimation of flow ages, with surface fissures inferred to develop in about a decade. Again, similar occurrences of molluscs and annelids are a feature of some asphaltite strandings in Australia and New Zealand (Padley, 1995; Edwards et al., 1999; Fig. 2E, F). In the GOM the asphalts are, for the

most part, negatively buoyant, although one freshly deposited sample was unexpectedly positively buoyant (>10° API). Boult et al. (2005) proposed seafloor flow seepage of tar as the likely source for the southern Australian asphaltites whereas Logan et al. (2010), expanding upon one of the hypotheses of Edwards et al. (1998), favoured the idea that they were the end result of oil slick mousse stabilising at the ocean surface prior to stranding.

6.2. Possible origins of the asphaltites

The origin of the Australasian asphaltites has long been the subject of debate. As yet, no marine petroleum system has been proven to occur in any of the southern margin petroliferous basins. No reliable correlation of the asphaltites to any oil produced locally on the southern margin of Australia or globally (using the GeoMark™ database, Summons et al., 2001) has been made. Thus the source of these enigmatic hydrocarbons remains in question.

The close proximity of common stranding sites to the locations of former whaling stations raises the possibility of an anthropogenic origin for the asphaltites. According to one early commentator (Wade, 1915 as cited by Padley, 1995) tars used for caulking the wooden boats employed in the industry were buried on beaches, whilst many cargo vessels were lost en-route to supplying the aforementioned stations. These lost cargoes or the erosion of cached barrels during storms would be a viable explanation. However, an investigation of the pine and coal tars recovered from 17th, 18th and 19th century shipwreck sites, and identified as being the common caulking materials brought into the region, showed that they differ significantly in composition from the asphaltites, thus excluding such industrially transported materials as their source (Smart, 1999). On the other hand, the proximity of whaling communities to

sites of regular asphaltite stranding is unlikely to be coincidental as access to a ready supply of high quality pitch, which was an expensive commodity, would have been an attractive benefit to the early settlers. The use of locally sourced caulking materials is confirmed in historical records of the early settlement of southern Australia (e.g. Tolmer, 1882) and distribution of this pitch by the whaling fleet could account for its wide dispersal to other whaling communities (Boult et al., 2005).

Several offshore sedimentary basins along Australia's southern continental margin have been variously evaluated as possible hosts for the asphaltites' parent petroleum system. The first of these is the Stansbury Basin, located immediately west of Adelaide (Fig. 1). Here the potential source rocks are of Cambrian age, with kerogen $\delta^{13}C$ values matching those of the bulk asphaltite hydrocarbons and one of them, the Kulpara Formation, exhibiting a regular C_{27}–C_{29} sterane signature similar to that of the asphaltites (McKirdy et al., 1986). However, other age-specific biomarkers in the asphaltites point to a mid-Cretaceous source (Boreham, 2001).

Younger basins comprising the Australian Southern Rift System do contain sedimentary fill of the required late Mesozoic age (Fig. 3). As Australia separated in an easterly direction from Antarctica, a series of extensional basins formed, viz. the Mentelle, Bight, Otway, Sorell, Bass and Gippsland Basins. The largest of these depocentres is the Bight Basin (Fig. 4), which comprises the Denmark, Bremer, Recherche, Eyre, Ceduna and Duntroon sub-Basins. To the west, in the Mentelle Basin and the Denmark, Bremer and Recherche sub-Basins of the Bight Basin, Cretaceous sediments are either non-marine (fluvial to lacustrine) or non-calcareous shelfal to open marine deposits (Bradshaw et al., 2003; Blevin and Cathro, 2008).

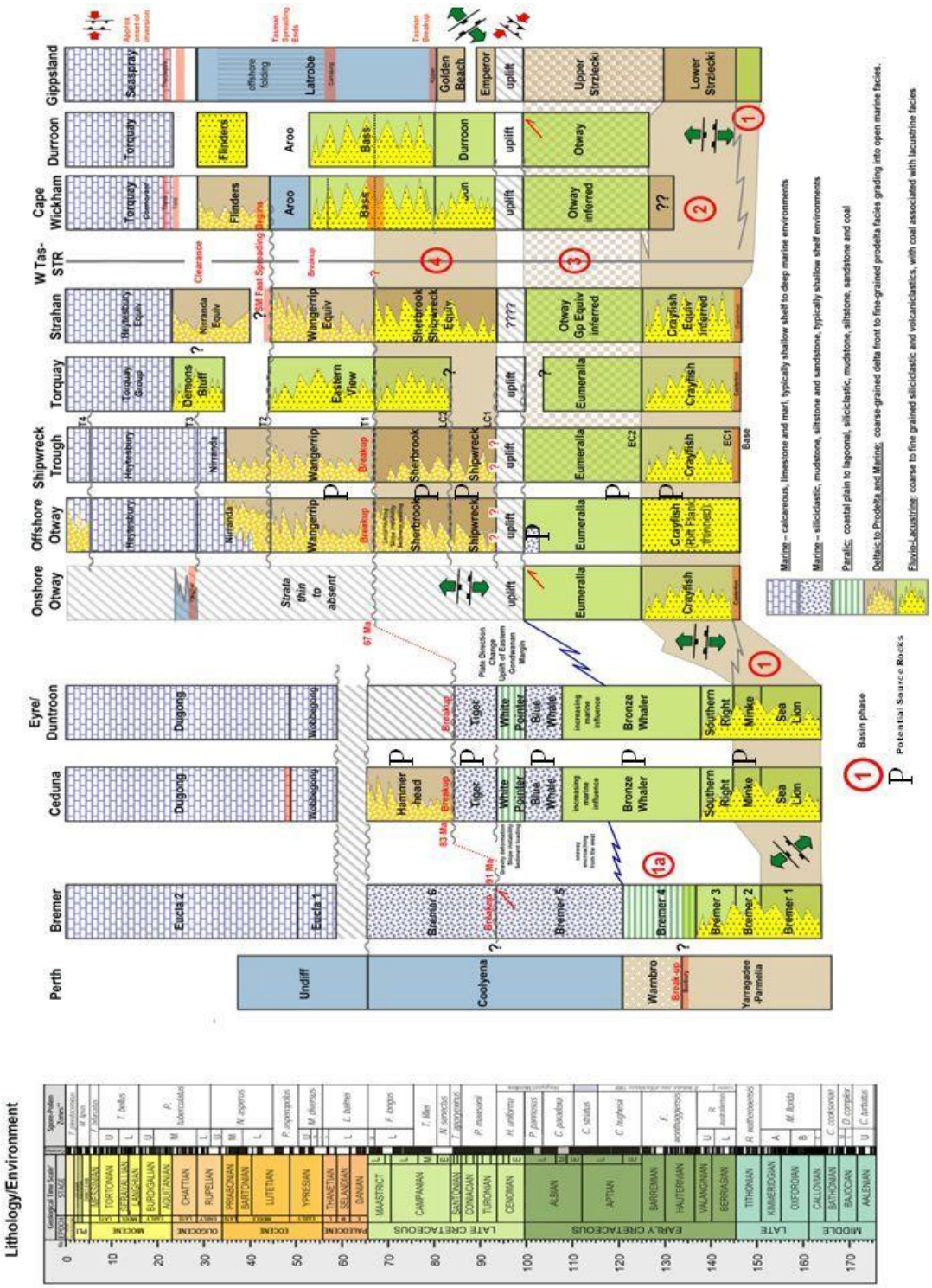

Fig. 3 Stratigraphy of the southern margin basins (after Blevin and Cathro, 2008). Basin phases: 1) mechanical extension; 2) thermal subsidence-1; 3) accelerated subsidence; 4) thermal subsidence-2.

Although no geochemical data are currently available on these sediments, it is unlikely that they could provide a suitable source pod for the asphaltites. Further east, in the Sorell, Bass and Gippsland basins, the Cretaceous lithofacies also are non-marine (Ozimic et al., 1987; Audino et al., 2002a, b; Blevin and Cathro, 2008). Moreover, the hydrocarbons recovered from these basins are derived from terrestrial source rocks and hence have biomarker profiles quite unlike those of the asphaltites (Edwards et al., 1998, 1999).

An important clue to the likely origin of the asphaltites is the striking similarity of their biomarker and isotopic signatures to those of the late Albian Toolebuc Formation in the onshore Eromanga Basin (Boreham et al., 2001). Coeval units deposited along the Blue Whale Seaway, which may well host their enigmatic source facies, form part of the post-rift sag phase succession of the Blue Whale Supersequence in the Eyre and Ceduna sub-basins of the Bight Basin and the Otway Supergroup in the Otway Basin (Boreham et al., 2001, Struckmeyer, 2001; Bradshaw et al., 2003, Totterdell and Struckmeyer, 2004; Boult et al., 2005; Totterdell et al., 2008; Blevin and Cathro, 2008). The Ceduna and Duntroon sub-basins are now the focus of renewed offshore exploration activity. A brief account of the eastern Bight Basin oil shows and potential source rocks follows.

Located along the southern edge of the Madura Shelf in the eastern Bight Basin, the Eyre and Duntroon sub-basins (Fig. 4A) are perched rift basins consisting of Middle Jurassic–Early Cretaceous half graben overlain by a comparatively thin cover of sag phase sediments (Espurt et al., 2009). At Jerboa-1 in the Eyre Sub-basin, organic-rich Blue Whale sediments are geochemically distinct from the asphaltites and the minor oil shows and fluid inclusion oils exhibit a lacustrine source affinity (Edwards et al.,

1999; Ruble et al., 1999; 2001). Here the main potential source rocks are thought to be the earlier syn-rift terrestrial and lacustrine deposits of the Sea Lion and Minke Supersequences (Blevin and Cathro, 2008).

Further east in the Ceduna Sub-basin, oil shows found in Cretaceous sands at Greenly-1 have been assigned to two genetic families (Smith and Donaldson, 1995), one of which has a biomarker distribution indicative of its origin from a calcareous anoxic marine source rock containing a mixture of algal and land-plant organic matter (Edwards et al., 1999). This inferred source facies may be the proximal expression of a deep-water organic facies, located further offshore in the Ceduna Sub-basin (Fig. 4A, B), that lacks terrestrial plant input and therefore qualifies as a potential source of the asphaltites. Further support for this idea is provided by Boreham et al. (2001), whose analysis of an organic-rich mudstone (3.1% TOC) from a thermally immature Blue Whale succession penetrated by the drill hole Eyre-1 in the onshore Bight Basin revealed a close match between its source and age-specific biomarkers and those of the asphaltites.

A subsequent survey of the Ceduna Sub-basin by Geoscience Australia (survey SS01/2007) identified a number of potential areas for natural seepage based on remote sensing observations and collected 259 dredge, core and grab samples primarily from the seaward edge of the Eyre Terrace where canyon formation, slumping and faulting have exposed an interpreted mid-Cretaceous (Albian to Santonian) stratigraphic section (Totterdell et al., 2008).

NOTE:
This figure/table/image has been removed to comply with copyright regulations.
It is included in the print copy of the thesis held by the University of Adelaide Library.

Fig. 4 A) Structural elements map of the eastern Bight Basin; B); Survey areas and location of sampling sites in Geoscience Australia's Bight Basin Sampling and Seepage Survey SS01/2007; C) Modelled present-day maturity zones (% R_o) for the transects marked in yellow on map B (all after Totterdell et al., 2008).

Screening of these specimens identified some as excellent potential source rocks (up to 6.2% TOC and 479 mg HC/g TOC) of late Cenomanian–early Turonian age, albeit thermally immature. Thirty high-graded samples from the Blue Whale, White Pointer and Tiger Super sequences show biomarker distributions closely related to those of the asphaltites. However, subtle but significant differences (viz. Ni>V rather than V>Ni metalloporphyrins and an absence of isorenieratane) indicate that these samples were deposited under more oxic conditions than the asphaltite source (Summons and Powell, 1986; Grice 1996, 1997). Nevertheless, some variation of depositional conditions is to be expected within a given petroleum system and local ‘sweet spots’, such as those indicated by seismic mapping down dip from sampling sites, may be the elusive source zone (Totterdell et al., 2008). These potential source rocks in the western Ceduna Sub-basin presently lie within the gas window or are over-mature, except along the outer edge, with modelling suggesting that any Blue Whale-derived hydrocarbons are likely to be gas accumulations (Fig. 4B, C). In the eastern section of the basin the same sequences are still within the oil generation window; and an active petroleum system has been identified based on information from the aforementioned Greenly-1 well (Edwards et al., 1999; Boult, 2012). Unlike the western section of the sub-basin the shelf-break canyon systems do not appear to expose the Cretaceous section (Boult. 2012). However, there is evidence of hydrocarbon seeps along the margins of the depocentre from sniffer, synthetic aperture radar (SAR) and airborne laser fluorescence (ALF) data, whilst 2D seismic data appear to show pocks, sea floor mounds, upturned reflectors at depth and depressed shallow reflectors within Cenozoic sediments that represent recent or currently active fluid escape features on the shelf (Hillis and Reynolds, 2003; Totterdell et al., 2008; Logan et al., 2010; Boult, 2012).

Within the western Otway Basin, the offshore Morum Sub-basin (Fig. 5A) likewise exhibits good potential to host the asphaltite source facies. The long history and high concentration of asphalt strandings along the adjacent shoreline, as well as the generally larger size of specimens here than at more distant sites, have been regarded as evidence of their local origin (Sprigg and Woolley, 1963; Sprigg, 1986; McKirdy et al., 1994). The apparent temporary increase in strandings following local earthquake activity and the large quantities collected after severe storm events, such as in 1961 when Sprigg and associates retrieved ‘almost half a ton’ south of Kingston, also suggest proximity to the parent petroleum system (Sprigg and Woolley, 1963; McKirdy et al., 1994; Boult et al., 2005).

The Otway Basin displays great similarity to the Bight Basin. A series of grabens and half grabens filled with Jurassic to Early Cretaceous rift sediments are interpreted to exist across most of the basin (Boult and Hibbert, 2002). The rate of rifting slowed during the Barremian to Albian but rapidly increased before the end of the Albian in the northern part of the basin, with extension rate studies suggesting deposition of marine sediments in the Morum Sub-basin corresponding in age to the Albian OAE (Palmowski et al., 2004; Boult et al., 2005). The widespread Cenomanian unconformity mapped in the onshore is predicted not to extend into the Morum Sub-basin, where over 4 km of late Albian to Late Cretaceous sediments are preserved (Boult and Hibbert, 2002). A potential Albian OAE source pod has been interpreted from seismic data (Fig. 5B) along with amplitude anomalies, diapiric structures and possible gas chimneys (Boult et al., 2006).

Fig. 5 A) Outline of Otway Basin with inferred sediment thickness and sub-basin, seismic section 137-03 and Crayfish-A1 well locations; and B) Interpretation of seismic section 137-03, showing the location of the possible upper Albian OAE source pod (after Boult et al., 2005).

These potential source beds appear to be intersected by canyons on the continental slope which cut as deeply as 1.6 km into the stratigraphic section and coincide with SAR anomalies, possibly indicative of light hydrocarbon escape to the sea surface (Fig. 6). Further testimony to the prospectivity of the sub-basin is provided by a previously unrecognised Cretaceous oil show of suboxic marine source affinity in the Crayfish-A1 well (McKirdy et al., 2006), located updip from this inferred hydrocarbon kitchen. Boult et al. (2005) postulated that oil seepage within these canyons or the nearby slope may form asphaltic mats, which are periodically dislodged and transported up the canyons to the shelf on the Bonney Upwelling of the cold, deep-water Flinders Current (Fig. 5). Subsequent interaction of the latter with the easterly coastal current (Middleton and Bye, 2007) could explain the concentration of strandings along the western and northern shores of Kangaroo Island.

In summary, on the basis of our present knowledge of the eastern Bight Basin and the western Otway Basin, both are ideal candidates for the role of sourcing the asphaltites. The west-to-east rifting and subsequent separation of Australia from Antarctica would have created suitable depocentres for their source rocks, the well-documented OAEs of this period of Earth history providing the required depositional conditions implicit in their source and age-specific biomarker signatures. However, in view of the lack of a definitive oil-source correlation, is it possible that further clues to their origin might be derived from the asphaltite strandings themselves?

NOTE:
This figure/table/image has been removed to comply with copyright regulations.
It is included in the print copy of the thesis held by the University of Adelaide Library.

Fig. 6 Bathymetry of the South Australian continental margin with an overlay of surface temperature contours of 3rd March 1995, showing the location of the deep-water Flinders Current, Bonney Upwelling, asphaltite strandings and SAR anomalies (Boult et al., 2005).

In this study we investigate a suite of asphaltites from four widely separated stranding localities: Limestone Coast (n = 3), Kangaroo Island (n = 4), Eyre Peninsula (n = 2) and Invercargill, New Zealand (n = 2). Sub-samples taken from the external weathered surface and 'fresh' interior of each asphaltite specimen were analysed by gas chromatography-mass spectrometry (GC-MS) and compound-specific isotope analysis (CSIA). Comparison of the resulting data allowed 1) oil-oil correlation; and 2) determination of their degree of weathering which, as a function of residence time in the ocean, may be used to better constrain the location(s) of the parent seafloor seepage.

6.3. Materials and methods

6.3.1. Sample suite

The asphaltite samples analysed in this study are listed in Table 1. Those from Kangaroo Island and the Limestone Coast of South Australia were collected during two surveys of coastal bitumen strandings: Department of Mines and Energy Coastal Bitumen Survey, 1983 and a bimonthly survey from 1990 to 1991 (Padley, 1995). The more recent strandings from Eyre Peninsula and Invercargill were collected by Martin Hand and Christine Lawley (University of Adelaide) and Dallas Bradley (Environment Southland, New Zealand).

Table 1 Sample identification, size and weight, location of stranding, year of collection and weathering description.

Sample	Location	Year	Dimensions L:W:D (mm)	Weight (g)	Degree of Weathering
27A	Pether Rock, Canunda N.P., SA	1990	109:85:60	419	Mild
CB 32	Nine Mile Sandhill, Beachport, SA	1983	127:112:49		Moderate
162	German Point, Beachport, SA	1991	328:204:102	2876	Mild
80	Ravine des Casoars, Kangaroo Island, SA	1990	165:100:48	634	Moderate/Heavy
85	Seal Bay, Kangaroo Island, SA	1990		764	Moderate/Heavy
168	West Bay, Kangaroo Island, SA	1990		1944	Mild/Moderate
177	Bales Bay, Kangaroo Island, SA	1991	750:350:40	7000	Mild/Moderate
CL1	Streaky Bay, Eyre Peninsula, SA	2005	138:94:37		Heavy
MH1	S of the Freshmanns, Eyre Peninsula, SA	2005	83:71:26		Mild
NZ1	Invercargill, New Zealand	2002	273:256:87		Moderate
NZ2	Invercargill, New Zealand	2002	116:67:62		Moderate

6.3.2. Isolation of saturated and aromatic hydrocarbons

A portion (150 mg) of the surface and interior of each asphaltite sample was dissolved in a minimum amount of dichloromethane and the asphaltenes precipitated by adding an excess (20 mL) of petroleum ether. Activated copper turnings were then introduced to the solvent flask to remove any associated elemental sulphur. After filtration through glass wool, the asphaltene-free supernatant was rotary evaporated to ~5 ml volume and separated into saturated hydrocarbons, aromatic hydrocarbons and polar compounds by conventional open liquid chromatography on activated silica gel, eluting respectively with petroleum ether, petroleum ether and dichloromethane (40:60), and dichloromethane and methanol (35:65). After removal of the solvent by rotary evaporation, each of the fractions was accurately weighed. The saturated and aromatic hydrocarbon fractions were then redissolved in hexane and stored below –18°C ready for further analysis.

Following their analysis by GC-MS the saturated hydrocarbon fractions were separated into *n*-alkanes and higher molecular weight branched/cyclic alkanes (naphthenes) by urea adduction (following a procedure based on that of Wakeham and Pease, 1992). The samples were evaporated under nitrogen then aliquots of urea, acetone and hexane were added sequentially. Non-adducts were separated by rinsing the urea crystals with hexane. Adducted *n*-alkanes were partitioned into hexane after addition of methanol/H_2O (50:50) to dissolve the urea crystals. The separation procedure was repeated three times to ensure recovery of a highly pure adduct.

6.3.3. GC-MS

Analyses were undertaken utilising a Hewlett Packard 6890/5973 gas chromatograph-mass spectrometer (GC-MS) system at the University of Adelaide. Full scan data on the saturated hydrocarbon fractions were acquired over the range 45–500 Da at ~3 scans sec^{-1}. The GC was fitted with a HP5-MS capillary column (30 m length, 0.25 mm ID and 0.25 μdf coating) and helium was used as the carrier gas at a constant flow rate of 1 ml min^{-1}. A 1 μl-aliquot of sample was injected in split mode with the injector temperature set at 300ºC. The oven temperature was programmed as follows: 50ºC for 1 min, 50–310ºC at 8ºC min^{-1} and 310ºC for 15 min. Full scan data on the aromatic fractions were acquired over the range 50–500 Da at ~3 scans sec^{-1} using a longer column (60 m length, 0.25 mm ID and 0.25 μdf coating) but the same carrier gas, flow rate, injector temperature and sample volume. The sample was injected in pulsed-splitless mode; and the temperature program was 60ºC for 1 min, 60–180ºC at 10ºC min^{-1}, 180–310ºC at 4ºC min^{-1} and 310ºC for 14.5 min.

Selected ion monitoring (SIM) of the saturated hydrocarbon fractions was undertaken using the same column and chromatographic conditions as for full scan analysis of the aromatic fractions, except for a slightly different temperature program, viz. 50ºC for 1 min, 50–150ºC at 10ºC min^{-1}, 150–310ºC at 2.5ºC min^{-1} and 310ºC for 15 min. Data were acquired for masses 123, 177, 191, 205, 217, 218, 231, 253 and 259 at a dwell time of 20 ms.

Individual analytes including biomarkers were identified on the basis of their retention times or mass spectra (Peters and Moldowan, 1993; Peters et al., 2005).

6.3.4. GC-IRMS

Compound-specific isotope analysis (CSIA: $\delta^{13}C$) targeted the most abundant compounds in the urea adduct and non-adduct sub-fractions of the aliphatic hydrocarbon fraction.

A HP6890 gas chromatograph (GC) equipped with a HP6890 autosampler was used in tandem with a Micromass isotope ratio mass spectrometer (IR–MS) for stable carbon isotopic measurements. The GC–IR–MS conditions were those detailed by Dawson et al. (2005). A 60 m x 0.25 mm i.d. x 0.25 μm phase thickness DB-1capillary column was used. In brief, the GC oven was programmed from 50 to 310°C at 3°C min^{-1}, with initial and final hold times of 1 and 20 min, respectively. The carrier gas was He at a flow rate of 1 mL min^{-1}. The $\delta^{13}C$ data were obtained by integrating the ion currents for masses 44, 45 and 46 from the CO_2 formed by oxidation of each chromatographically separated component, after passing through a quartz furnace packed with copper oxide pellets and maintained at 850°C. Monitoring the accuracy and precision of the $\delta^{13}C$ measurements was achieved by analysing a mixture of organic reference compounds with known $\delta^{13}C$ values. Each sample was analysed two or three times and the average $\delta^{13}C$ values and standard deviation reported in per mil (‰) relative to a CO_2 reference gas calibrated to Vienna Peedee Belemnite (VPDB).

6.4. Results and discussion

6.4.1. Oil-oil correlation

For the purposes of oil-oil correlation, the compositions of the inner 'fresh' portion of each asphaltite specimen were compared in order to minimise possible weathering influences. The suite of selected bulk and biomarker ratios employed in the correlation are summarized in Table 2, with representative chromatograms from the GC-MS analyses shown in Fig. 7. The $\delta^{13}C$ values of individual *n*-alkanes, another powerful correlation tool, are summarized in Table 4 and plotted against their respective carbon numbers in Fig. 9.

In terms of their bulk composition, the asphaltites display some variation in the relative proportions of saturated hydrocarbons, aromatic hydrocarbons, polar and asphaltenes, although the relative standard deviation (RSD) is <15%. The saturated hydrocarbon fractions (TIC, Fig. 7A) have a unimodal *n*-alkane distribution ranging from C_{10} to >C_{39}, with a maximum between C_{16} and C_{18} and little odd over even preference (CPI =1.02–1.04). Among the acyclic alkanes, the ratio of pristane (Pr) to phytane (Ph) is uniformly low (range 1.06–1.14) with a RSD of 3%, whilst Pr/*n*-C_{17} and Ph/*n*-C_{18} both have a RSD of 8% (range 0.47–0.58 and 0.40–0.52, respectively).

The terpane distributions of the asphaltites are very similar (*m/z* 191, Fig. 7B), with the majority of the measured parameters exhibiting deviations of <10%. Likewise, the sterane distributions correlate well (*m/z* 217, Fig. 7C) with RSDs for C_{27}:C_{28}:C_{29} ααα 20R and C_{27}:C_{28}:C_{29} αββ 20(R+S) being <5% and <3%, respectively. The tricyclic/pentacyclic terpane ratio is more variable (RSD 15%), probably due to the lower relative abundances of tricyclic homologues, whilst the sterane/terpane values

are within 9% RSD. $\delta^{13}C$ values for the C_{15}–C_{30} *n*-alkanes lie between –33.3 and –36.7‰ and display a reasonable degree of correlation (Fig. 9A). The average variation is ±1.1‰ per homologue, with a maximum of ±1.4‰ for *n*-C_{19}.

The triaromatic steroid distributions (*m/z* 231, Fig. 7D) yield C_{26}:C_{27}:C_{28}:C_{29} values within 6% RSD for all samples. Naphthalene and the methylnaphthalenes are present only at trace levels, with concentrations progressively rising through the dimethyl, trimethyl and tetramethyl naphthalene isomers. The distributions of identifiable polyaromatic hydrocarbons are alike in all samples, although the dibenzothiophenes show greater variation.

The compositional uniformity of the sample suite, evident across such a broad spectrum of parameters, is a clear indication that these asphaltites belong to the same oil family, nothwithstanding their disparate stranding localities. Moreover, their bulk compositions and biomarker distributions are remarkably similar to those previously reported for other stranded southern Australian asphaltites (Currie et al., 1992; Volkman et al., 1992; McKirdy et al., 1994; Padley, 1996; Edwards et al., 1998; Boreham et al., 2001). There is, however, one apparent difference that requires further comment. Their *n*-alkane $\delta^{13}C$ values (Table 4, Fig. 8A) are slightly lighter than those in the existing asphaltite literature (Dowling et al., 1995; Edwards et al., 1998; Boreham et al., 2001). An explanation for this discrepancy is provided in Section 4.3.3.

Table 2 Selected bulk and biomarker parameters of the interior portion of the asphaltite specimens, including their relative standard deviation. See Appendix 1 for peak abbreviations.

	Limestone Coast			Kangaroo Island				Eyre Peninsula		New Zealand		Average	% RSD
	27A	CB-32	162	80	85	168	177	CL1	MH1	NZ1	NZ2		
Bulk Parameters (fullscan)													
Pr/Ph	1.12	1.06	1.10	1.11	1.07	1.14	1.10	1.18	1.12	1.10	1.14	1.11	3%
Pr/nC_{17}	0.50	0.56	0.51	0.48	0.58	0.48	0.47	0.47	0.49	0.47	0.48	0.50	8%
Ph/nC_{18}	0.46	0.48	0.46	0.41	0.52	0.41	0.40	0.41	0.44	0.44	0.43	0.44	8%
OEP	1.02	1.02	1.02	1.04	1.02	1.02	1.03	1.04	1.04	1.04	1.03	1.03	1%
Sats (%)	21.4	19.0	20.0	25.6	21.6	24.4	20.4	24.5	21.6	24.6	23.3	22.4	10%
Aroms (%)	14.1	16.4	13.3	16.2	12.7	13.6	11.4	15.2	12.0	13.1	12.7	13.7	12%
NSO (%)	16.7	15.9	14.2	10.4	14.7	16.3	15.6	18.6	16.5	16.9	19.4	15.9	15%
Asph (%)	47.8	48.7	52.5	47.8	51.0	45.7	52.6	41.7	49.9	45.4	44.6	48.0	7%
Terpanes (m/z 191)													
C_{28}BNH/C_{30}H	0.05	0.06	0.06	0.06	0.06	0.06	0.06	0.05	0.06	0.07	0.05	0.06	8%
C_{29}H/C_{30}H	0.71	0.66	0.71	0.65	0.70	0.72	0.70	0.67	0.70	0.75	0.60	0.69	6%
C_{30}DiaH/C_{30}H	0.09	0.09	0.09	0.09	0.09	0.08	0.09	0.08	0.07	0.07	0.10	0.09	10%
C_{30}Ts/C_{30}H	0.09	0.09	0.09	0.09	0.09	0.09	0.09	0.09	0.08	0.08	0.09	0.09	6%
Gam/C_{31}HR	0.15	0.17	0.18	0.17	0.17	0.17	0.17	0.17	0.17	0.18	0.18	0.17	4%
Ts/(Ts+Tm)	0.40	0.38	0.38	0.39	0.39	0.38	0.39	0.37	0.38	0.40	0.39	0.39	2%
C_{29}Ts/(C_{29}Ts+C_{29}H)	0.22	0.24	0.22	0.24	0.22	0.21	0.23	0.22	0.22	0.20	0.26	0.23	8%
Mor/C_{30}H	0.12	0.13	0.13	0.13	0.13	0.13	0.13	0.13	0.12	0.12	0.13	0.13	4%
C_{32} S/(S+R)	0.59	0.60	0.60	0.60	0.59	0.59	0.60	0.58	0.59	0.59	0.60	0.59	1%
C_{35} Homohopane Index	0.06	0.05	0.06	0.06	0.06	0.06	0.05	0.07	0.06	0.06	0.07	0.06	9%
C_{35}(S+R)/C_{31}(S+R)	0.12	0.10	0.13	0.12	0.12	0.11	0.12	0.15	0.14	0.12	0.15	0.12	12%
C_{35}/C_{34} (S only)	0.59	0.61	0.77	0.69	0.69	0.73	0.72	0.66	0.66	0.53	0.60	0.66	11%
Steranes (m/z 217)													
% C_{27} $\alpha\alpha\alpha$ 20R	35.2	37.3	38.2	38.5	35.0	38.0	38.7	33.7	36.7	36.7	36.7	36.8	4%
% C_{28} $\alpha\alpha\alpha$ 20R	24.5	23.9	24.1	23.8	25.0	23.3	25.1	23.3	23.3	24.3	22.3	23.9	3%
% C_{29} $\alpha\alpha\alpha$ 20R	40.3	38.9	37.6	37.7	40.1	38.7	36.3	43.0	40.1	39.1	40.9	39.3	5%
C_{27} Dia/(Dia+Reg)	0.51	0.48	0.49	0.48	0.53	0.53	0.48	0.48	0.52	0.48	0.55	0.50	5%
C_{29} $\alpha\beta\beta$/($\alpha\alpha\alpha$+$\alpha\beta\beta$)	0.50	0.50	0.51	0.48	0.51	0.52	0.51	0.51	0.52	0.52	0.51	0.51	2%
$\alpha\beta\beta$-Steranes (m/z 218)													
% C_{27} $\alpha\beta\beta$ 20(R+S)	37.7	37.8	38.6	39.3	38.0	38.4	38.4	35.7	37.6	38.9	37.0	37.9	3%
% C_{28} $\alpha\beta\beta$ 20(R+S)	28.1	27.7	27.3	27.8	27.7	27.5	27.4	27.6	27.8	28.0	28.3	27.8	1%
% C_{29} $\alpha\beta\beta$ 20(R+S)	34.2	34.5	34.1	32.9	34.3	34.1	34.2	36.7	34.6	33.1	34.7	34.3	3%
C_{29}/C_{27} $\alpha\beta\beta$ Sterane Ratio	0.91	0.91	0.88	0.84	0.90	0.89	0.89	1.03	0.92	0.85	0.94	0.91	6%
Tricyclic/Pentacyclic Terpanes	0.17	0.14	0.16	0.14	0.15	0.16	0.16	0.10	0.15	0.18	0.13	0.15	15%
Steranes/Terpanes	0.46	0.43	0.44	0.42	0.44	0.47	0.46	0.37	0.43	0.51	0.38	0.44	9%
% Tricyclic Terpanes	10.0	8.73	9.33	8.52	9.16	9.61	9.44	6.62	8.99	10.2	8.30	8.99	11%
% Pentacyclic Terpanes	58.5	61.2	59.9	61.8	60.2	58.3	59.2	66.1	61.2	55.8	64.1	60.6	5%
% Steranes	31.5	30.0	30.8	29.7	30.6	32.1	31.4	27.2	29.8	34.0	27.7	30.4	6%
Triaromatic Steroids (m/z 231)													
% C_{26} Triaromatic Steroids	19.6	19.7	20.1	19.2	19.9	18.8	19.2	21.9	18.5	20.7	19.3	19.7	5%
% C_{27} Triaromatic Steroids	40.9	41.5	41.1	42.4	42.2	42.0	41.7	39.6	42.5	44.4	41.5	41.8	3%
% C_{28} Triaromatic Steroids	32.6	32.3	32.5	32.5	32.0	32.8	33.2	32.0	32.7	28.2	32.2	32.1	4%
% C_{29} Triaromatic Steroids	6.9	6.4	6.3	6.0	6.0	6.3	5.9	6.6	6.4	6.7	7.0	6.4	6%
Polycyclic Aromatic Hydrocarbons (m/z178;184;198;226;252)													
BaP/BbF	2.05	1.97	1.79	1.83	1.70	2.02	1.98	2.24	2.18	1.86	1.82	1.95	9%
P/MP	0.41	0.38	0.41	0.46	0.44	0.42	0.52	0.47	0.50	0.44	0.44	0.44	9%
P/C2P	0.29	0.34	0.38	0.40	0.40	0.38	0.52	0.47	0.50	0.43	0.42	0.41	16%
DBT/MDBT	0.54	0.24	0.30	0.44	0.15	0.40	0.53	0.42	0.56	0.44	0.39	0.40	32%
DBT/C3DBT	0.43	0.11	0.17	0.23	0.02	0.26	0.44	0.28	0.46	0.33	0.29	0.28	51%

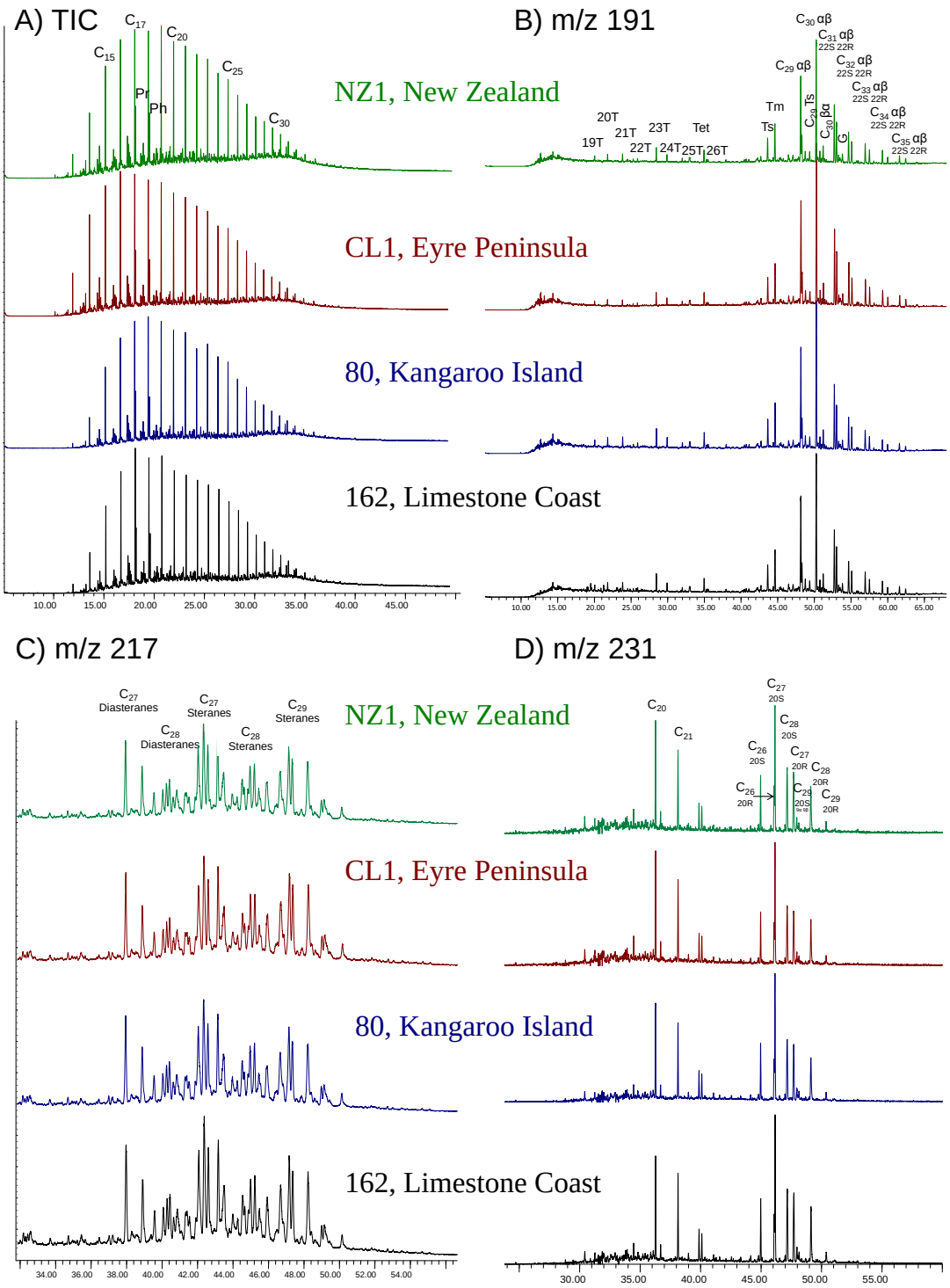

Fig.7 Selected chromatograms of saturated and aromatic hydrocarbons in the interior portion of representative asphaltite specimens from each stranding domain: A) TIC of saturated hydrocarbon fraction; B) *m/z* 191, terpanes; C) *m/z* 217, steranes; and D) *m/z* 231, triaromatic steroids. See Appendix 1 for peak abbreviations.

6.4.2. Origin of the initially discharged asphaltic bitumen

Understanding the genesis of the initially discharged asphaltic bitumen may assist in constraining the source of the southern Australian asphaltite strandings. Undoubtedly, the asphaltites have lost volatile components subsequent to their escape from the subsurface to the sea floor. This loss is likely to have involved both submarine dissolution, as evidenced by the shrinkage cracks on the upper surface of the stranded asphaltite (Fig. 2D), and subaerial evaporation, which accounts for its loss of plasticity observed once removed from the aqueous environment. The difference in distribution of bulk components between the inner and outer portions of the specimens is relatively small, as shown by the combined loss of saturated and aromatic hydrocarbons (average 5%) and the variation in the C_{10}/C_{19} *n*-alkane ratio (average 13%). Thus, it is probable that the major proportion of the light-end loss from the parent crude oil occurred in the subsurface and that the southern Australian asphaltites were discharged into the ocean as semi-solid bitumen.

Solid bitumens are allochthonous, non-disseminated organic matter. According to the classification scheme of Curiale (1986) they may be separated into pre-oil and post-oil products. Whilst pre-oil bitumens are early (immature) expulsion products of rich source rocks that migrate over short distances as very viscous fluids, post-oil bitumens are commonly viewed as remnants of altered oils which have been subjected to severe biodegradation and/or water washing. Other possible origins for post-oil bitumens include thermal maturation of immature oils, residues precipitated along oil migration pathways and deasphalting of reservoired oils by gas (Curiale, 1986; Wilhelms and Larter 1994a, b; Mueller et al., 1995; Mossman and Nagy, 1996; Head et al., 2003). Such bitumens characteristically contain high proportions of NSO-

compounds and asphaltenes relative to saturated and aromatic hydrocarbons. Typical examples are tar sands (e.g. Athabasca tar sands, Canada; Orinoco heavy oil belt, Venezuela), bituminous dykes (e.g. Neuquén Basin, Argentina; Unita Basin, Utah, USA; Seridahli vein, Turkey) and tar mats in both clastic and non-clastic petroleum reservoirs (Wilhelms and Larter 1994a, b; Mueller et al., 1995; Hwang et al., 1998; Cobbold and Rossello, 2003; Head et al., 2003; Peters et al., 2005). Tar mats, which have been described on all scales from microscopic to several tens of metres in thickness, can be defined as zones in petroleum reservoirs where asphaltenes comprise up to 20–60 wt% of an oil's C_{15+} fraction (Wilhelms et al., 1994; Wilhelms and Larter, 1994a, b; Carpentier et al., 2007).

Thermal alteration of reservoired crude oils is one process that can produce heavy oil, in the form of pyrobitumen. However, the ready solubility of the asphaltites in solvents such as dichloromethane distinguishes them from reservoir pyrobitumens, which are only weakly soluble (Wilhelms and Larter, 1994b). Thermal cracking of oil in the reservoir also is known to increase the $\delta^{13}C$ value of the heavier residual crude through the preferential loss of ^{12}C-enriched thermogenic methane (Clayton and Bostick, 1986; Mossman and Nagy, 1996). The asphaltites are isotopically too light ($\delta^{13}C \sim -30‰$: McKirdy et al., 1994; Edwards et al., 1998) to be the result of such a process. Thus, the aforementioned characteristics of the asphaltites preclude in-reservoir thermal alteration from playing a role in their origin.

It is generally acknowledged that the polar (NSO) compounds and asphaltenes in crude oils are resistant to biodegradation, unlike constituents of the saturated and aromatic hydrocarbon fractions which exhibit varying susceptibilities to bacterial attack (Siefert and Moldowan, 1979; Hartman and Hammond, 1981; McKirdy et al.,

1983; Volkman et al., 1983; 1984; Williams et al., 1986; Peters and Moldowan, 1993; Palmer, 1996; Trolio et al., 1999; Grice et al., 2000; Peters et al., 2005; Hallmann et al., 2008; Prince and Walters, 2007). In-reservoir alteration is primarily a product of anaerobic biodegradation, with processes like water washing, phase separation, gravity segregation and gas de-asphalting playing a subordinate role (Palmer et al., 1993; Wilhelms and Larter 1994a, b; Wenger et al., 2001; Larter et al., 2006a, b; Jones et al., 2008). The time-scales involved in such conversions are long, with biodegradation induction times of around 1–2 million years required to perturb an entire light-oil column and 10–20 million years for heavier oils (Larter et al., 2006a).

The southern Australian asphaltites were originally classified by Edwards et al. (1998) as being at Level 4 (or PM4) on the biodegradation scale of Peters and Moldowan (1993), which corresponds to moderate degradation on the scales of Wenger et al. (2002) and Peters et al. (2005). Realising that the existing scales have insufficient resolution to usefully characterize many heavy oil and bitumen occurrences, Larter et al. (2012) proposed a new ‘Manco’ biodegradation scale for solid bitumens classified as ≥PM4. Based on the sequential removal of ‘category’ compound classes according to their susceptibility to bacterial attack, this scale assigns a ranking number that recognises both the degree to which each category has been degraded and its resistance to alteration. The asphaltites analysed in this study have a light Manco number of 431 (vector 310) and a heavy Manco number of 419 (vector 43310000) so that their extents of biodegradation can be expressed as 431, 419 [PM4], or combined to give an ultimate Manco number of 578 (vector 31043310000). It is worth noting that there is no difference in the Manco numbers generated from the inner or outer weathered portions of these asphaltites.

Biodegradation leaves distinctive molecular and isotopic fingerprints in the residual crude oil that reflect both its initial non-degraded composition and the nature and extent of the microbial alteration (Prince and Walters, 2007). Whilst the asphaltites show some signs of degradation, such as significant loss of low-molecular-weight normal and cyclic alkanes, previous investigations (McKirdy et al., 1994; Padley, 1996; Edwards et al., 1998) and the data acquired in this study reveal that they lack 25-norhopanes, which are generally indicative of in-reservoir anaerobic biodegradation (Peters et al., 2005). Moreover, they display no evidence of gas vesicles or gas hydrates, which are commonly observed in the GOM asphaltites (Bruning et al., 2008; Schubotz et al., 2011) where the bacteria responsible for the genesis of the heavy oil produce substantial quantities of methane. Other characteristics, such as their low isoprenoid to *n*-alkane and 20R:20S ααα sterane ratios, their homophopane distributions and their lack of a well-defined unresolvable complex mixture (UCM), all support the conclusion that the asphaltites are not products of biodegradation. Their Manco number vectors also exhibit a clear anomaly. The fractions should show a gradual and progressive removal of components through the categories, but the combined light and heavy asphaltite Manco vector of 31043310000 undoubtedly highlights the involvement of another process in their degradation.

Water washing likewise leaves its own distinctive pattern of alteration in the affected crude oil. Experiments show that this alteration is most apparent in the gasoline and kerosine ranges (C_5–C_{14}) where hydrocarbons with the same carbon number are removed in the following order of decreasing solubility: aromatics > cycloalkanes > branched alkanes > *n*-alkanes (Palmer 1984; Lafargue and Barker, 1988; Kuo, 1994; Lafargue and Thiez, 1996; Palmer, 1996). It is commonly difficult to differentiate the

effects of biodegradation and water washing on the C_{15+} composition because they generally occur in tandem. Nonetheless, abnormally low concentrations of dibenzothiophenes, naphthalenes, phenanthrenes and the C_{20} and C_{21} triaromatic steroids can be indicative of hydrologic alteration, as these species are usually not readily biodegraded (Volkman et al., 1984; Kuo, 1994; Palmer, 1996). The absence from the asphaltites of all hydrocarbons $<C_{10}$ and low-molecular-weight aromatic species such as the alkylbenzenes and naphthalene is consistent with the effects of water washing. However, as noted by Volkman et al. (1992), the southern margin asphaltites do not show signs of extensive water washing since methylated naphthalenes and phenanthrenes would have been less abundant than observed. Dibenzothiophene and its higher homologues are also prominent and the C_{20} and C_{21} triaromatic steroids are present in concentrations similar to those of other triaromatic species (Fig. 6D). Thus, while it is conceivable that this alteration process may have played some minor role in removing their light ends, intensive water washing of these asphaltites is not evident. In any case, laboratory studies have shown that water washing is unlikely to be a viable mechanism for the formation of tar mats (Lafargue and Barker, 1988; Kuo, 1994).

Tar mats, the one remaining option for the genesis of the asphaltites, are common in petroleum reservoirs. The main processes leading to their formation are gas-induced deasphalting, gravity segregation of oil columns, formation water-oil interactions, oil mixing, and secondary/tertiary migration (Wilhelms and Larter, 1994b and references therein). Simply because of the physical constraints on the movement of asphaltene-rich oils, tar mats are located at permeability barriers or phase boundaries (e.g. oil-water contacts).

The biomarker profiles of the asphaltites provide no indication that they are products of in-reservoir mixing of oils of different source affinity; and, as already discussed, water washing is unlikely to have played a part in their formation. Changes in reservoir pressure and temperature will affect asphaltene solubility, with the lowering of either parameter leading to their precipitation. Since petroleum charges in any basin generally move along paths of decreasing pressure and temperature, it would seem inevitable that asphaltenes will be deposited from oils during their migration. Tar mats are most often, but not always, identified in zones of high porosity and lateral permeability, especially along dipping carrier beds where tectonic activity has initiated secondary (and tertiary?) migration (Wilhelms and Larter, 1994b; Carpentier et al., 2007). Where the migration pathway is close to horizontal, asphaltene clusters, aggregating following precipitation, will become concentrated in the rear of the oil stringer and there undergo gravitational settling. Thus, an accumulation of heavy asphaltic bitumen (i.e. a tar mat) is left in the wake of the migrating oil stringer (Wilhelms and Larter, 1994b).

Dissolution of natural gas in reservoired oil is another means by which a significant proportion of its asphaltene fraction can be precipitated (Wilhelms and Larter 1994a; Hwang et al., 1998). For extensive asphaltene deposits to be formed in this way would require gas-invasion of a reservoir that contains oil under-saturated with respect to gas; or, alternatively, an oil pool with an existing gas cap, which subsequently undergoes deeper burial (Wilhelms and Larter, 1994b). Given the nature of the asphaltites' source-rock kerogen (S-rich Type II) and their expulsion in the early oil window (Volkman et al., 1992; Edwards et al., 1998), their hydrocarbon kitchen is highly unlikely to be significantly gas prone. In both the Ceduna Sub-basin and Otway Basin the Cretaceous sequences immediately underlying the inferred Albian

marine source rocks are of deltaic/fluvio-lacustrine and fluvio-lacustrine origin, respectively (Edwards et al., 1999; Blevin and Cathro, 2008). At least in the onshore Otway Basin, these sequences host significant accumulations of gas, whilst the formations in the western Ceduna Sub-basin are modelled as being extensively gas mature. Migrating gas is capable of entraining low concentrations of biomarker hydrocarbons, either derived from their source rocks or solubilised during migration (McKirdy and Chivas, 1992), which would then be mixed with any light reservoired oils they encounter. In this instance, the biomarkers would carry terrestrial signatures. No such signatures have been detected in the asphaltites, although it is possible that such condensate biomarker concentrations are too low to affect the profile of the reservoired oil. Thus, deasphalting through gas charging from more mature, gas-prone underlying sequences is another route to the tar-mat precursors of the asphaltites.

In summary, the original crude oil destined to become stranded asphaltic bitumens is likely to have undergone substantial subsurface alteration prior to its discharge on to the sea floor. Degradation through bacterial removal and/or intensive water washing had no part in their genesis. It is probable the asphaltite originates from tar mats formed along the secondary migration pathway of the main oil charge, or through deasphalting related to gas invasion of the reservoir. The residual viscous material, already low in gasoline-range hydrocarbons, may subsequently have been stripped of the majority of its remaining light-end saturated and aromatic hydrocarbon species by water washing before exposure to the marine environment and a final episode of devolatilization.

The physical characteristics of the asphaltites support this conclusion, with their flow structures and lamination, devolatilization cracks and ovoid shape being strikingly

similar to those of the viscous oil seeps observed in the Gulf of Mexico where bitumen mounds are formed through deasphalting of a low to medium API gravity crude oil at the seafloor. However, for a significant seafloor expression of heavy oil to accumulate, a large volume of lighter hydrocarbons would also need to be released and therefore become noticeable at the ocean surface. Tar balls smaller than the average asphaltite stranding might also commonly escape to the surface and appear similar to the bitumens observed at Coal Oil Point, California. Farwell et al. (2009) estimated sinking rates of 0.4–5 days for 1–10 cm diameter tar droplets from the Coal Oil Point slicks. Therefore, a significant number of strandings in this size range but otherwise matching the Family 4 bitumen profile might be expected along the southern coastline of Australia, which is not the case. Logan et al. (2010) favour an oil slick that formed a stable mousse before stranding as the likely formation mechanism of the asphaltites, but this would clearly not explain their substantial benthic communities nor their flow structures and laminations. Their lack of biodegradation, cited as a reason for the strandings not being sourced from tar mat seepage, can be explained by the common lack of well established bacterial communities in low intensity seeps (Wenger and Isaksen, 2002).

6.4.3. Marine weathering effects: comparison of biomarker distributions from inner and outer portions of stranded asphaltites

Having established that the eleven specimens in our sample suite share a common origin (see Section 4.1), the bulk, biomarker and $\delta^{13}C$ parameters of their ‘fresh’ interiors were compared with those of their ‘weathered’ surfaces (Tables 3 and 4). The observed differences, though commonly subtle due to the bulk of the heavy oil components being both immobile and not very bioavailable, are used in an attempt to

establish their relative degrees of weathering arising from exposure to the marine environment and, by inference, their proximity to the site(s) of seafloor seepage. The obvious lack of a freshly discharged or subsurface example of the bitumen for comparison is a significant complicating factor.

Upon entering the ocean any crude oil is exposed to a combination of weathering processes including biodegradation, water washing, photo-oxidation and evaporation (Munoz et al., 1997; Gagnon et al., 1999; Mezaes and Budzinski, 2002; Mezaes et al., 2002; Wenger and Isaksen, 2002; Peters et al., 2005; Fernandez-Alvarez et al., 2007; Wardlaw et al., 2008; Farwell et al., 2009). These processes, generally acting in concert, can alter the initial concentrations of hydrocarbons in the discharged oil at rates orders of magnitude faster than within the subsurface carrier bed or reservoir, as revealed both by laboratory experiments and field studies of spilled oils and natural seeps (Goodwin et al., 1983; Wardroper et al., 1984; Douglas et al., 1996, 2002; Munoz et al., 1997; Wenger et al., 2001; Wenger and Isaksen, 2002; Peters et al., 2005; Wardlaw et al., 2008).

Photo-oxidation primarily affects the polycyclic aromatic hydrocarbon (PAH) fraction of oils resident within the photic zone of the ocean. By reacting with their aromatic and other unsaturated chemical bonds, ultraviolet light degrades these hydrocarbons. Understandably, the exposed outer surface of asphaltic strandings will be prone to the loss of susceptible species such as benzo(a)pyrene (BaP) (Douglas et al., 2002; Lee, 2003). At the same time water washing will preferentially remove its low-molecular-weight aromatic hydrocarbons (Head et al., 2006), while sub aerial evaporation will potentially result in the loss of all its hydrocarbons with boiling points less than that of *n*-octadecane (Douglas et al., 2002).

Biodegradation, the major pathway for the destruction of hydrocarbons discharged into the ocean (Douglas et al., 1996), is principally mediated by aerobic bacteria, in contrast to the less efficient anaerobes that are largely responsible for such alteration in the subsurface. Susceptibility to bacterial attack decreases as follows: C_5–C_{14} > C_{15+} *n*-alkanes and *iso*alkanes > isoprenoids > low-molecular-weight cycloalkanes and aromatic hydrocarbons > complex cycloalkanes and PAHs. Rates of PAH biodegradation decrease with increasing ring number and alkylation (Volkman et al., 1984; Douglas et al., 1996; Fisher et al., 1998; Trolio et al., 1999). In both subsurface and surface environments there is simultaneous degradation of all hydrocarbons irrespective of molecular weight, and it is simply the lower rates of degradation of the high-molecular-weight and more complex species that causes the illusion of sequential degradation (Head et al., 2006; Wardlaw et al., 2008). There are, however, differences in the rate at which some categories of compounds are removed, related to the bacterial colonies involved in the degradation (Goodwin et al., 1983; Wenger and Isaksen, 2002; Head et al., 2006).

6.4.3.1 Saturated hydrocarbon fraction

Comparison of the saturated hydrocarbon fractions of the paired sub-samples reveals only subtle differences between the interior and exterior of the asphaltites (Table 3). As a proportion of the total sample, saturated hydrocarbons decrease by an average of 16%. This depletion appears to follow a pattern. Thus, in specimens from the Limestone Coast and southern Kangaroo Island the depletion is <10% (with the exception of sample CB-32 in which it is 15.7%). At sites more distant from the Morum Sub-basin, the depletion is generally higher: west coast of Kangaroo Island, 15–32%; Eyre Peninsula, 19–33%; and New Zealand, 17–19%.

Table 3 Percentage difference in selected bulk and molecular parameters between the inner and outer portions of asphaltite specimens. See Appendix 1 for peak abbreviations.

	Limestone Coast			Kangaroo Island				Eyre Peninsula		New Zealand	
	27A	CB-32	162	80	85	168	177	CL1	MH1	NZ1	NZ2
Bulk Composition (fullscan)	Difference inner - outer (%)										
Sats (%)	-9.8	-15.3	-8.9	-31.7	0.9	-14.5	-6.1	-33.3	-18.7	-18.7	-16.7
Aroms (%)	-5.1	-31.0	-12.0	-32.3	-6.5	-23.0	8.4	-30.3	12.5	-3.9	0.8
NSO (%)	1.2	20.8	17.4	44.2	7.8	-21.8	4.4	-14.4	3.0	26.2	6.5
Asph (%)	5.1	6.7	0.9	11.1	-1.2	18.5	-1.0	27.9	3.2	-0.9	4.8
Normal Hydrocarbons (fullscan)											
$C_{10\text{-}19}/C_{30}$	16.3	38.7	27.8	5.0	11.8	2.1	20.7	7.1	8.1	5.7	7.6
Terpanes (m/z 191)											
C_{35} Homohopane Index	-19.2	-5.4	-28.3	-29.4	-23.7	-30.5	-27.2	-40.7	-37.8	-23.1	-38.2
$C_{35}(S+R)/C_{31}(S+R)$	-24.4	-11.5	-33.6	-36.3	-28.4	-23.8	-32.5	-50.7	-45.7	-28.0	-46.8
Steranes (m/z 217)											
% C_{27} $\alpha\alpha\alpha$ 20R	7.5	12.3	-3.9	-0.1	14.2	5.5	-0.6	16.9	3.9	9.9	17.6
% C_{28} $\alpha\alpha\alpha$ 20R	-9.5	-9.1	1.0	-1.3	0.1	4.9	-9.7	-7.0	-6.9	-5.9	0.1
% C_{29} $\alpha\alpha\alpha$ 20R	-1.3	-7.5	3.2	1.0	-14.3	-8.9	6.8	-11.4	0.2	-6.4	-19.0
$\alpha\beta\beta$–Steranes (m/z 218)											
% C_{27} $\alpha\beta\beta$ 20(R+S)	3.9	3.3	-0.2	0.3	3.2	2.9	4.6	8.6	6.8	0.8	11.4
% C_{28} $\alpha\beta\beta$ 20(R+S)	-1.9	-0.6	-2.7	-0.4	-3.1	-1.7	3.4	1.8	-7.3	-0.7	-4.1
% C_{29} $\alpha\beta\beta$ 20(R+S)	-2.8	-3.2	2.3	0.0	-1.2	-2.0	-8.3	-10.6	-2.1	-0.3	-10.1
C29 $\alpha\alpha\alpha$ 20S/20R	9.9	26.6	-9.6	-6.2	8.2	-6.7	-16.8	21.6	6.7	3.5	35.9
C_{29}/C_{27} $\alpha\beta\beta$ Sterane Ratio	-6.7	-6.5	2.5	-0.3	-4.4	-4.9	-12.9	-19.1	-8.9	-1.1	-21.5
Tricyclic/Pentacyclic Terpanes	12.4	19.3	20.4	37.5	21.0	17.4	29.8	59.4	30.5	0.4	32.5
Steranes/Terpanes	9.1	13.2	9.3	19.6	11.4	5.1	17.3	30.6	18.2	-3.6	24.2
% Tricyclic Terpanes	7.6	12.6	14.5	26.1	14.4	13.1	19.5	43.7	20.3	1.6	21.0
% Pentacyclic Terpanes	-4.9	-6.8	-6.0	-11.7	-6.7	-4.3	-10.5	-16.7	-10.3	1.1	-11.7
% Steranes	6.2	9.0	6.3	13.4	7.8	3.4	11.6	21.4	12.4	-2.4	16.9
Triaromatic Steroids (m/z 231)											
% C_{26} Triaromatic Steroids	-1.0	-0.5	-1.8	-0.1	-1.5	0.2	-0.2	-4.1	-0.1	-3.3	-0.7
% C_{27} Triaromatic Steroids	2.0	0.7	1.3	0.3	1.0	0.1	1.1	3.6	0.7	-0.7	1.3
% C_{28} Triaromatic Steroids	-0.9	-0.1	0.2	-0.4	-0.1	-0.1	-1.0	0.3	-0.4	4.2	0.2
% C_{29} Triaromatic Steroids	-0.1	-0.1	0.3	0.3	0.6	-0.2	0.1	0.2	-0.3	-0.1	-0.8
Polycyclic Aromatic Hydrocarbons & Thiophenes (m/z178;184;198;226;252)											
BaP/BbF	-0.5	-4.3	-0.1	-5.0	-1.3	-2.0	-0.4	-15.4	-2.4	-3.0	-4.7
P/MP	-1.9	-12.3	-6.7	1.0	-1.2	-3.8	-1.3	-10.4	0.4	63.1	-10.3
P/C2P	2.3	-18.8	-6.0	-4.4	-1.5	-6.7	-2.0	-12.2	-1.9	90.5	-12.9
DBT/MDBT	12.2	-51.7	-8.1	33.0	-47.9	-12.3	-9.9	-3.0	19.7	-36.1	-32.4
DBT/C3DBT	0.8	-17.2	-0.3	9.0	-10.7	-7.2	-6.0	-2.8	12.0	12.1	-18.4

The affects of water washing and evaporation are most likely to be visible in the distributions of *n*-alkanes. All specimens show an apparent loss of $<C_{20}$ homologues from their outer surface. As expressed in the *n*-alkane ratio $\sum C_{10}–C_{19}/C_{30}$, the extent of this loss ranges from 2 to 39%. Asphaltites from the Limestone Coast and southern Kangaroo Island exhibit the greatest depletion (>10%), suggesting that strandings closest to the Morum Sub-basin undergo significantly more loss of light hydrocarbons. Sample CB-32, collected in 1983, exhibits the largest variation between its interior and exterior, possibly indicating that the difference may be due to

evaporation during storage. However, if so, it might be expected that all the samples collected during the 1990-1991 period would show equivalent *n*-alkane distributions; but this is not the case. These variations in *n*-alkanes may actually be an indication of the residence time in the marine environment and exposure to water washing. A longer exposure may allow equilibration of the lighter hydrocarbons within the sample, which would actually result in less disparity between their interior and exterior distributions. A combination of these two effects is most likely to be at play, with water washing reducing the available light hydrocarbons prior to stranding and subsequent loss through evaporation being less evident in samples with longer marine residencies.

Within several classes of biomarker cycloalkanes, including the steranes and hopanes, certain isomers and homologues are known to be more susceptible to biodegradation than others (Goodwin et al., 1983; McKirdy et al., 1983; Peters et al., 2005). Between the inner and outer portions of the asphaltites there is a general trend of depletion of 20*R* relative to 20*S* ααα steranes (e.g. C_{29} reduces by an average of 7%). However, the C_{27} ααα 20R sterane increases slightly relative to the C_{28} and C_{29} homologues, in contrast to the general C_{27}>C_{28}>C_{29} order of depletion (Peters et al., 2005). These results are consistent with only slight biodegradation of the outer surface of the specimens. It has been shown that aerobic biodegradation of crude oils causes a sequential reduction in the C_{31}–C_{35} homohopanes, increasing with molecular weight. In the asphaltites there is a similar preferential degradation of C_{35} over the $C_{31\text{-}34}$ hopanes (Fig. 8), with the homohopane index decreasing by an average of 28% (range 5–41%). The greatest variation of the latter parameter is observed in the strandings furthest from the Morum Sub-basin, except for sample NZ1. By comparison with the outcomes of laboratory culture experiments (Goodwin et al., 1983), the stranded

asphaltites appear to have had a relatively short exposure to aerobic biodegradation, possibly of the order of ten years. At their outer surfaces, the contribution of hopanoids to the total abundance of terpanes and steranes also diminishes by an average of 5%. Again, it is the specimens further from the Morum Sub-basin that generally sustain the greatest loss of hopanes, though sample NZ1 is once more an outlier.

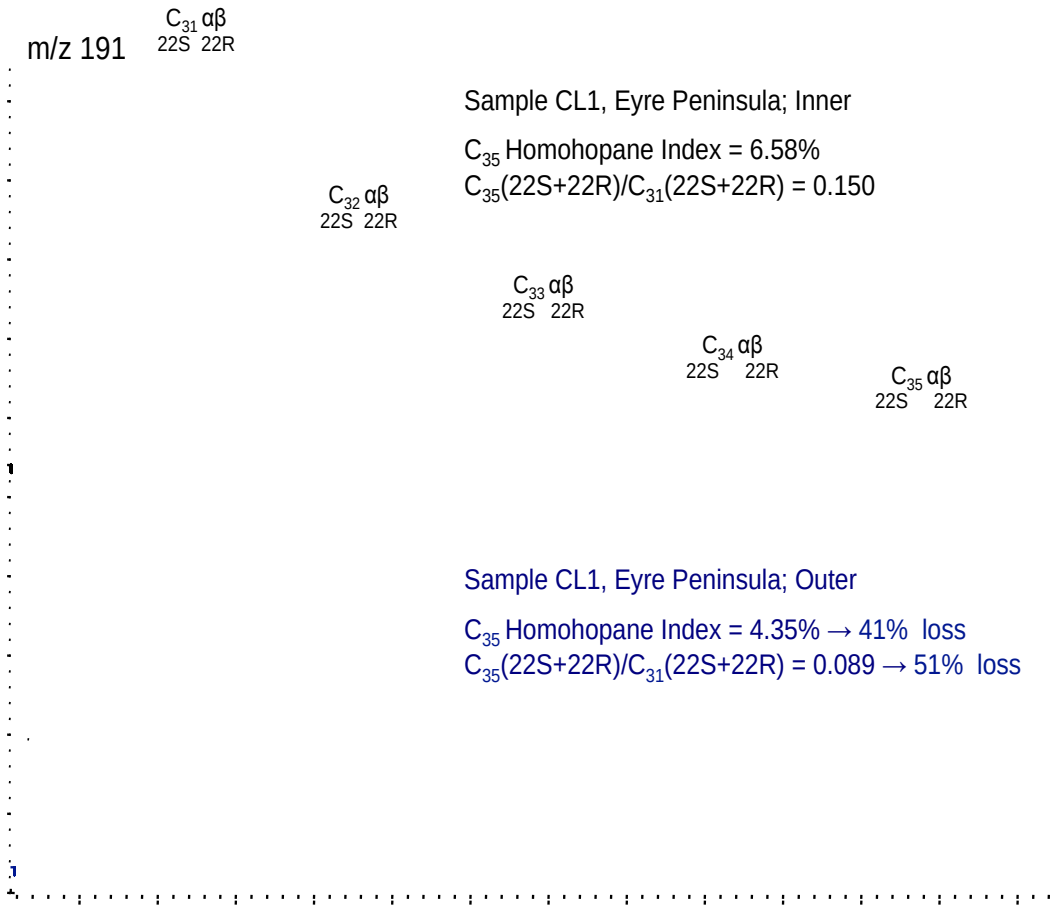

Fig. 8 Partial *m/z* 191 chromatograms of the inner and outer portions of sample CL1, Eyre Peninsula, expanded to highlight their C_{31}–C_{35} 17α,21β(H) homohopane 22S & 22R distributions. See Appendix 1 for peak abbreviations.

There are a number of additional factors that may affect the aforementioned hydrocarbon distributions, such as initial time on the ocean floor before transportation to the shelf, microbial colonisation differences from location to location, and the time beached prior to collection. However, the majority of the parameters based on weathering-susceptible components of the asphaltites concur in showing that the strandings closest to the Morum Sub-basin exhibit less surficial alteration. Sample NZ1 from New Zealand appears anomalous. This specimen has an unusual laminated appearance (Fig. 2E) and the available section was quite thin (<2 cm). If the sample was actually a composite of laminar flows of discharged bitumen then our inner sub-sample may not be sufficiently deep to retain an unweathered profile.

6.4.3.2. Aromatic hydrocarbon fraction

The relative proportions of aromatic hydrocarbons in the exterior of the asphaltite specimens are on average 11% less than in their interior (Table 3). No geographic trend is evident in this depletion, although there does seem to be a correlation with the degree of physical weathering (Table 1). Samples in which the loss of aromatics is >30% (e.g. CB-32, 80 and CL1) appear moderately to heavily weathered, whereas in samples described as less weathered (e.g. 27A, 162 and MH1) the loss is <12.5%. The ‘weathered’ sample 85 (Padley, 1996) from Kangaroo Island, with a decrease of only 7%, does not follow this pattern and both the samples from New Zealand show little difference.

Benzo(a)pyrene (BaP), a UV-sensitive but biodegradation-resistant aromatic species (Lee, 2003), was normalised against the more resistant benzo(b)fluoranthene to assess the extent of its removal from the asphaltites by photo-oxidation. All samples showed a depletion of BaP in the surface portion, with the difference between the inner and

outer portions increasing in the order CL1>80>NZ2>CB-32 >NZ1> MH1>168>85>27A>177>162 (Table 3). This pattern appears to reflect both the physical weathering of the specimens and their geographic distribution. Except for sample 85, the most weathered specimens again show the larger depletion, whilst in the other samples it seems to depend on distance from the Morum Sub-basin. The aqueous solubility of BaP is very low (US EPA TEACH Chemical Summary). Thus, in the short term, water washing will be a secondary factor controlling the rate of BaP removal, but over a longer period it is likely to be an influence. Other compounds such as phenanthrene and dibenzothiophene, normalised against their more stable alkylated homologues, revealed no discernable alteration attributable to photo-oxidation. This may be due to their overlapping vulnerability to biodegradation (Douglas et al., 1996; Haritash and Kaushik, 2009; Wardlaw et al., 2011).

Aromatic compounds are known to be susceptible to photo-oxidation and biodegradation to varying degrees (Volkman 1984; Douglas et al., 1996, 2002; Lee, 2003). Photo-oxidation experiments conducted on crude oils have been shown to deplete their bulk aromatic fractions by up to 40% (Maki et al., 2001), which is probably the major mechanism being observed here. With the majority of the water-soluble, low-molecular-weight aromatic species, such as the BTEX (benzene, toluene, ethyl benzene and xylene isomers) and naphthalenes (Palmer, 1996; Douglas et al., 1996), having probably been removed from the asphaltic bitumens prior to their marine exposure, the consequences of further water washing are likely to be minor and long exposures are probably required to see its effects on their aromatic hydrocarbon fractions. Biodegradation also appears to be relatively minor. Thus, a variety of factors could be influencing the weathering patterns of the aromatic hydrocarbons, with photo-oxidation having the greatest impact.

6.4.3.3. CSIA

The C_{15}–C_{31} *n*-alkanes of the asphaltites are isotopically very light, with $\delta^{13}C$ values falling between –33.3 and –36.9‰ (Table 4). The difference between the values of the same homologue in their inner and outer portions varies systematically according to their geographic location (Fig. 9). Individual *n*-alkanes show >1‰ depletion of ^{13}C in the weathered exterior of the New Zealand and Eyre Peninsula asphaltites, whereas the Limestone Coast specimens deviate by <±0.4‰ and those from Kangaroo Island are generally enriched in ^{13}C by >0.5‰. Analytical precision is ±0.4‰ or better, so the greater difference observed for the Kangaroo Island, Eyre Peninsula and New Zealand strandings must be due to weathering. Unlike the *n*-alkane $\delta^{13}C$ *versus* carbon number profiles previously reported for southern Australian asphaltites (Dowling et al., 1995; Edwards et al., 1998), those of the present sample suite (Fig. 9) are flat (instead of concave upward) and offset to lighter values by ~2‰. While the difference in shape may be due to more intense weathering of the original samples, the latter feature is attributable to the fact that the earlier analyses were performed more than 12 years ago and on a different system.

Isotopic values of petroleum hydrocarbons are deemed to be fairly conservative under the influence of weathering (Sofer 1984; Mezaes et al., 2002; Philp et al., 2002; Schmidt et al, 2004; Jeffery, 2006), so the narrow range of variation per homologue (–2.0 to 1.9‰) is to be expected. During biodegradation, the slightly faster cleavage of ^{12}C–H bonds results in an accumulation of molecules with ^{13}C–H in the remaining substrate (Bouchard et al., 2008; Asif et al., 2009; Hofstetter and Berg, 2010;).

The magnitude of the enrichment decreases with increasing number of carbon atoms, a trend that can partly be explained by the decreasing probability of a ^{13}C atom being

located at the reaction site in the molecule as chain length increases. In laboratory experiments involving abiotic weathering of oil-treated soil microcosms, Hough et al. (2005) showed ^{13}C-depletion for a range of hydrocarbons. Subsequent biotic weathering processes then were observed to return $\delta^{13}C$ to its original values and eventually lead to net enrichment. The factors affecting abiotic degradation of crude oil are unclear. Sofer (1984) highlighted the fact that the C-isotopic composition of crude oils can be altered by water washing and Palmer (1996) cited examples from the Philippines where the saturated hydrocarbon fraction became depleted in ^{13}C, resulting in an isotopically lighter oil.

Hence, it may be as a result of their longer residency in the marine environment that *n*-alkanes in the exterior portions of the Eyre Peninsula and New Zealand asphaltites show such marked depletion in ^{13}C. Specimens from Kangaroo Island (and those from the Limestone Coast) display a slight enrichment which, following the interpretation of Hough et al. (2005), may indicate a shorter period of abiotic alteration prior to biodegradation commencing.

Table 4 Carbon isotopic compositions of individual *n*-alkanes in the outer and inner portions of the asphaltite specimens

n-alkane carbon number	Eyre Peninsula						Kangaroo Island											
	CL1			MH1			80			85			168			177		
	outer (‰)	inner (‰)	diff (‰)	outer (‰)	inner (‰)	diff (‰)	outer (‰)	inner (‰)	diff (‰)	outer (‰)	inner (‰)	diff (‰)	outer (‰)	inner (‰)	diff (‰)	outer (‰)	inner (‰)	diff (‰)
15	-34.7	-34.5	-0.2	-34.7	-34	-0.7	-34.8	-36	1.3	-35.3	-35.8	0.4	-34.7	-34.3	-0.4	-34.7	-34.9	0.2
16	-34.6	-34	-0.5	-34.5	-33.5	-1	-34.3	-35.5	1.3	-34.9	-35.3	0.4	-34.4	-34.2	-0.2	-33.9	-34.3	0.4
17	-34.7	-33.9	-0.8	-34.4	-33.3	-1.1	-34.1	-35.7	1.6	-34.7	-35.2	0.5	-34.3	-34.3	0	-33.5	-34.1	0.6
18	-35	-34.1	-0.9	-34.5	-33.4	-1.1	-34.1	-35.7	1.6	-34.7	-35.2	0.5	-34.2	-34.4	0.2	-33.4	-34.2	0.9
19	-35.4	-34.3	-1.1	-34.7	-33.5	-1.2	-34.2	-36.1	1.9	-34.8	-35.5	0.6	-34.4	-34.8	0.4	-33.7	-34.4	0.8
20	-35.6	-34.4	-1.2	-34.9	-33.7	-1.1	-34.4	-36.2	1.8	-35	-35.5	0.6	-34.5	-35	0.5	-33.4	-34.6	1.2
21	-35.9	-34.8	-1.1	-35.2	-34	-1.3	-34.5	-36.4	1.8	-35.3	-35.9	0.6	-34.7	-35.2	0.5	-33.7	-34.8	1.1
22	-36.3	-34.9	-1.4	-35.3	-33.9	-1.4	-34.6	-36.3	1.7	-34.9	-35.8	0.9	-34.8	-35.3	0.5	-33.8	-34.9	1.1
23	-36.4	-35.1	-1.3	-35.5	-34.2	-1.3	-34.8	-36.7	1.9	-35.3	-36	0.7	-35	-35.7	0.7	-33.6	-34.9	1.3
24	-36.2	-34.9	-1.3	-36	-34	-2	-34.5	-36.1	1.6	-34.9	-35.9	1	-34.8	-35.5	0.7	-34	-35	1
25	-36.9	-35.5	-1.5	-36.1	-34.6	-1.5	-35.1	-36.7	1.5	-35.3	-36.4	1.2	-35.2	-36.4	1.2	-33.7	-35.2	1.5
26		-35.1		-36	-34.2	-1.9	-34.7	-36.1	1.4	-34.9	-35.9	1	-34.8	-35.7	0.9	-33.9	-34.9	1
27		-35.1		-36	-34.4	-1.7	-34.8	-36.6	1.7	-35	-35.9	0.9	-35	-36	0.9	-33.6	-34.9	1.3
28					-34.1		-34.7			-34.8	-35.8	1	-34.8	-35.8	1	-33.7	-35.1	1.3
29							-35.5			-35	-36.1	1.1	-35.3			-33.3	-35.1	1.8
30										-35			-34.8			-34.3	-35.3	1
31													-35.2					

n-alkane carbon number	Limestone Coast									New Zealand					
	27A			CB-32			162			NZ1			NZ2		
	outer (‰)	inner (‰)	diff (‰)	outer (‰)	inner (‰)	diff (‰)	outer (‰)	inner (‰)	diff (‰)	outer (‰)	inner (‰)	diff (‰)	outer (‰)	inner (‰)	diff (‰)
15	-35.4	-35.5	0.2				-34.3	-33.7	-0.6	-35.8	-34.5	-1.3		-34.4	
16	-35	-35	0	-36.6			-34.3	-33.3	-1	-35.3	-34	-1.3	-35.2	-34	-1.2
17	-35	-35.1	0.2	-36.2	-34.7	-1.5	-34.1	-33.4	-0.8	-35.1	-34	-1.2	-35.2	-34.1	-1.1
18	-35.1	-35.5	0.4	-36	-35.2	-0.8	-34.1	-33.3	-0.8	-35.2	-34	-1.2	-35.5	-34.2	-1.3
19	-35.2	-35.4	0.1	-36	-35.4	-0.5	-34.2	-33.7	-0.6	-35.4	-34.1	-1.3	-35.6	-34.4	-1.2
20	-35.4	-35.7	0.3	-36.1	-35.5	-0.6	-34.3	-33.9	-0.5	-35.6	-34.3	-1.3	-35.6	-34.6	-1
21	-35.6	-35.8	0.3	-36.4	-35.9	-0.4	-34.6	-34.1	-0.5	-35.9	-34.5	-1.4	-36	-34.8	-1.2
22	-35.5	-35.9	0.4	-36.4	-36	-0.4	-34.4	-34.1	-0.3	-36	-34.6	-1.4	-36.1	-34.9	-1.1
23	-35.9	-36	0.1	-36.6	-36	-0.6	-34.9	-34.3	-0.6	-36.3	-34.9	-1.4	-35.9	-35	-0.9
24	-35.6	-36.1	0.4	-36.2	-35.7	-0.5	-34.3	-34.2	-0.1	-35.9	-34.7	-1.3	-36.2	-35	-1.2
25	-36	-36.2	0.3	-36.8	-36.5	-0.3	-34.9	-34.6	-0.2	-36.5	-35.3	-1.2	-36.4	-35.1	-1.2
26	-35.4	-36.3	0.8	-36.4	-35.7	-0.7	-34.1	-34.1	0.1	-36.2	-34.8	-1.4		-35.1	
27	-35.5	-36.2	0.6	-36.4	-36.3	-0.1	-34.6	-34.3	-0.2	-36.2	-35	-1.2		-35.1	
28	-35.9	-35.9	0.1	-36.2	-35.5	-0.8	-34.3	-34.1	-0.2	-36	-34.8	-1.3		-35	
29	-35.7			-36.4	-35.2	-1.1	-34.9	-34.9	0	-36.2	-35.6	-0.7		-35.1	
30	-36			-36.2			-34.1	-34.4	0.3	-36.1	-34.9	-1.1		-35.1	
31															

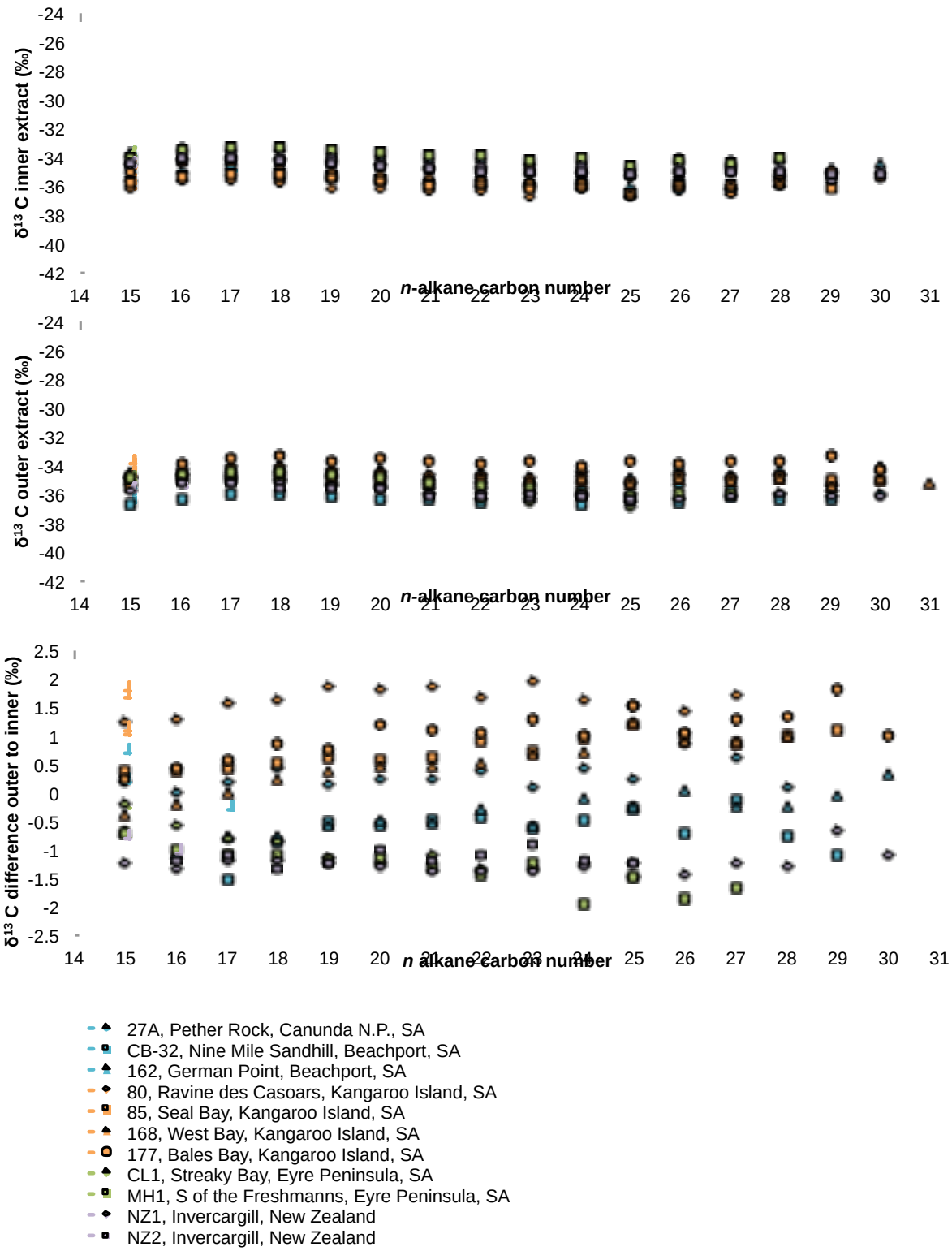

Fig. 9 Plots of *n*-alkane $\delta^{13}C$ versus carbon number for asphaltite specimens: A) inner portion, B) outer portion and C) the difference between inner and outer.

6.4.4. Synthesis

There is strong historical evidence for asphaltites being stranded upon the shores of the western Otway Basin in higher concentration than elsewhere along Australia's southern margin. Moreover, specific sections of the Limestone Coast (viz. Canunda Rocks, Geltwood Beach and Devil's Gap) are identified as loci of asphaltum accumulation (Sprigg and Woolley, 1963). By itself, this is highly suggestive of a local source. The new data presented herein support the hypothesis that these asphaltites are indeed derived from within the Otway Basin. The samples show relatively consistent, if subtle, signs of having had different exposures to the processes of weathering, with those samples deposited on the adjacent beaches of the Limestone Coast and southern Kangaroo Island generally exhibiting the least alteration. Moreover, if the initially discharged bitumen is the product of tar mat formation, as seems likely, then its occurrence at the sea floor would best fit the model proposed by Boult et al. (2005) for the Morum Sub-basin.

The distal sections of the Ceduna palaeo-delta in the central region of the Bight Basin may host significant petroleum resources. Analysis of samples dredged from seepage locations in the western sections of the Ceduna Sub-basin where shelf-break canyons incise the Cretaceous section has revealed that although the local source rocks are immature they are geochemically similar to the asphaltites (Totterdell et al., 2008); and, presumably, further in board they would enter the oil window before becoming gas mature in the basin centre. Thus, while suitable source pods may exist in the Bight Basin, within the deep proximal central Ceduna Sub-basin they are now generating gas. No apparent mechanism exists for the transfer of the asphaltic material from these deep-water westerly zones up onto the shelf, unless buoyancy alone accounts for

all the transportation into the near surface environment. The shallow coastal current will provide no up-canyon fluid flow whilst the Flinders Current, which upwells to the south during the summer, circulates back off the shelf in the western Ceduna Sub-basin (Middleton and Bye, 2007). Thus it seems unlikely that the western Ceduna Sub-basin could source the southern margin asphaltites.

In the eastern Ceduna Sub-basin there is strong evidence of seepage from its petroleum systems onto the shelf. This, and the availability of the Flinders Current transport mechanism during the summer months, is sufficient to make the area a prospective source for the asphaltites. There is anecdotal evidence of asphaltum stranding being common at Sleaford Bay and other localities on southern Eyre Peninsula (Sprigg and Woolley (1963). If an Early Cretaceous source pod had been active, as seems likely from basin modelling (Boult, 2012), and migration of the resulting oil stringer deposited an asphaltic tar mat, the only remaining problem would be migrating it to the surface without contamination. It might reasonably be expected that any oil derived from an OAE-associated, marine shale would mix with the oil and gas known to have migrated from the underlying Borda Formation (as identified at Greenly-1), or entrained hydrocarbons from the overlying Late Cretaceous shallow marine shales and coals of the White Pointer Super sequence and/or the prodelta shales of the Hammerhead Supersequence. All lie on the same fault systems that would provide the principal migration conduit for the seismically interpreted seep features active on the shelf. Shelf-break canyons do not appear to expose the Cretaceous section (Boult, 2012).

The deeply incised canyons of the Morum Sub-basin may allow a pathway for the tar mat to ooze to the surface without contamination from other sequences. A 1.6 km-

deep canyon in the vicinity of a large-scale shelf collapse cuts into the toe-thrust inversion that may contain the inferred upper Albian source rocks (Fig. 5B: Boult et al., 2006). Further east at Troas-1 on the Chama Terrace, the basal Eumeralla Formation of Aptian age has attained maturities of R_o ~0.5–0.7% (Padley, 1996), so the maturation level of R_o ~0.75% required for the Albian shales to be capable of sourcing the asphaltites is not unreasonable. As their generation and expulsion would have occurred quite early in the basin's history (Boult and Hibburt, 2000), the initial oil charge may have been to sub-horizontal carrier beds conducive to tar mat formation. Subsequent structural development of the prominent steeply dipping and inverted faults observed within the sub-basin may then have facilitated the continued migration of the lighter hydrocarbons to reservoirs higher in the sequence, where diapiric structures and gas chimneys have been interpreted (Boult et al., 2005), leaving behind residual tar mats. Later, this heavy bitumen could have been exposed by the erosion of the canyon into the reservoir facies and now be slowly extruding to the sea floor under limited buoyancy from its contact with seawater. This would explain the low amplitude of the seep inferred from the asphaltite's physical characteristics. Loss of the low concentrations of gasoline-range hydrocarbons, evidenced by the shrinkage cracks on the asphaltites, would also explain the SAR anomalies over the canyon (Fig. 6).

The summer upwelling of the Flinders Current is known to focus water flow up the canyon (Middleton and Bye, 2007) and water velocities of 0.1–0.2 m s^{-1} have been measured in shelf-break canyons (Kampf, 2007). Such water flow is more than sufficient to transport asphaltite onto the shelf. Earthquakes, which are common in the region, may exacerbate natural fracturing of the tar mats and dislodge fragments into the water column. They have certainly been noted to temporarily increase the

frequency of coastal bitumen strandings (Sprigg and Woolley, 1963). Once transferred to the shelf the asphaltic bitumen can be distributed to the local coastline or carried westward by the Flinders Current. Alongshore, this current moves past Kangaroo Island and into the Great Australian Bight during periods of upwelling. Its velocity can exceed 50 cm s^{-1} with potential advection estimated at up to 800 km over a three-month period (Middleton and Bye, 2007). This strong current could easily deposit a large quantity of asphaltite along the southern and western shores of Kangaroo Island. The Flinders Current may also drive the distribution further westward along the base of the shelf, thereby explaining the lower frequency but regular distribution of asphaltite strandings in Western Australia. Water flow off the shelf will likewise focus down the canyon and sweep non-buoyant bitumen onto the abyssal plane, where it can be transported to the west. Prevailing southwesterly weather patterns can account for the transport over the narrow shelf where strong storm conditions are often associated with an increase in bitumen stranding, as in May/June 1961 when Sprigg and associates collected 'almost half a ton' in the weeks following the first storm of the winter season (Sprigg and Woolley, 1963). For most of the year the prevailing current across the shelf is actually the easterly coastal current (Middleton and Bye, 2007). This warmer, surface current flows along the full length of the southern margin out past Tasmania towards the Southern Ocean, where it can interact with the prevailing Subantarctic Front of the Antarctic Circumpolar Current system (Rintoul et al., 2001). A study by Bye (1988) showed that drift cards placed in the Antarctic Circumpolar Current eventually stranded on the shores of New Zealand. Therefore the coastal current is a likely mechanism for distribution of asphaltite to the shores of Tasmania, and although further circulation of asphaltic material to New Zealand is less probable, it is far from impossible.

6.5. Conclusions

In investigating the provenance of the asphaltites stranded upon the shores of the southern margin of Australia, and further afield, it seemed appropriate to first reconsider the genesis of such asphaltites. As products of neither severe biodegradation nor extensive water washing, these asphaltites can no longer justifiably be regarded as the weathered remains of floating tar mats. The physical characteristics of the asphaltites provide important clues to their origin. The laminations and flow structures observed in some specimens are similar to those described in the asphaltic volcanoes of the Gulf of Mexico. There, natural seeps of viscous bitumen issuing from the subsurface, similar in expression to volcanic flows, display all the hallmarks of the Australasian asphaltite strandings: devolatilization cracks, large ovoid blocks, benthic bivalve and annelid communities, and the newly described flow characteristics.

The levels of degradation (PM4; Manco 431, 419 [PM4] or ultimate Manco 578 [vector 31043310000]) highlight the fact that the initially generated oil has undergone substantial alteration. Given its arrival at the sea floor in the form of heavy oil, this modification must have occurred in the subsurface. The most likely mechanism is tar mat formation, probably due to deasphalting along a flat lying migration pathway during secondary migration of the main oil stringer.

Geochemical investigation of four previously unanalysed asphaltites from locations in the Bight Basin and New Zealand has shown that these more distant strandings may be correlated with a further seven members of the classic ‘Family 4’ asphaltites from common stranding sites on the Limestone Coast and Kangaroo Island. Comparison of inner, fresher portions of each stranding to the outer, weathered surface section

revealed subtle but relatively consistent variations in a number of degradation-sensitive components. Molecular fossil and compound-specific $\delta^{13}C$ signatures in the saturated hydrocarbons most susceptible to alteration by biodegradation and dissolution suggest that the specimens recovered from the Eyre Peninsula and New Zealand have had longer exposure to weathering in the oceanic realm than those from the Limestone Coast and Kangaroo Island. The corresponding aromatic hydrocarbon distributions of the inner and outer portions differ in a manner consistent with the physical appearance of the strandings.

Within the offshore Bight Basin, the western section of the Ceduna Sub-basin hosts thermally immature organic-rich mudstones with marine biomarker signatures similar (but not identical) to those of the asphaltites, sampled from locations in which shelf-break canyons incise the Cretaceous section. The eastern part of the Ceduna Sub-basin is host to natural seepage and potential source rocks of the required age and thermal maturity, where a possible mode of transportation to the inner shelf is available via the upwelling Flinders Current. Here, however, shelf-break canyons do not appear to expose the Cretaceous section and the seismically interpreted seep features are active on the shelf. The required migration of a viscous tar mat from a highly specific source rock to the sea floor, uncontaminated by the other petroleum systems operating within this sector of the sub-basin, makes this is a less likely scenario.

The Morum Sub-basin is located within the western offshore Otway Basin, adjacent to the Limestone Coast and southern Kangaroo Island where the least weathered asphaltite has stranded. This depocentre has what may be the crucial feature, namely a deep shelf-break canyon that cuts deeply into a toe-thrust inversion interpreted to host

active source rocks of the appropriate Albian age. The associated system of steeply dipping faults provides migration pathways along which light hydrocarbons could have continued their movement to reservoirs higher in the sequence, leaving behind a residual tar mat. This heavy asphaltic bitumen may now be exposed in the floor or walls of the canyon, oozing slowly onto the seafloor where it forms volcano-like structures. Transport of the asphaltite along the canyon and up onto the shelf can be accounted for by the summer upwelling of the deep oceanic Flinders Current, where it may be dispersed by the inshore coastal current or accumulate until washed ashore by winter storm events. Historical distribution patterns support this hypothesis, with the highest concentration of strandings found on the coast closest to the head of the Morum Sub-basin canyons and on Kangaroo Island, which lies westward on the summer route of the Flinders Current. For the remainder of the year the shallow coastal current flows southeastward along the shelf before interacting with the Subantarctic Front of the Antarctic Circumpolar Current system, thereby providing momentum for the carriage of asphaltite further on towards the Victorian and Tasmanian coasts and beyond.

6.6. Acknowledgements

This study forms part of a project on the palaeoenvironment, biogeochemistry, chemostratigraphy and hydrocarbon potential of the Stansbury, Arrowie, Officer and Otway Basins, funded by Primary Industries and Resources South Australia (PIRSA). PAH is in receipt of an Australian Postgraduate Award. We are especially grateful to Dallas Bradley (Environment Southland, New Zealand) for providing the two asphaltites from Invercargill. The contributions of PAH and DMMcK to this paper comprise TRaX Record ???. Stephen Clayton is thanked for technical support for

CSIA at Curtin University. Dr Jennie Totterdell, (Geoscience Australia) and Dr Peter Boult (Bight Petroleum) are thanked for providing information concerning the Bight Basin. Kliti Grice acknowledges the ARC for infrastructure and salary support.

6.7. References

Asif, M., Grice, K., Fazeelat, T., 2009. Assessment of petroleum biodegradation using stable hydrogen isotopes and polycyclic aromatic hydrocarbons Organic Geochemistry 40, 301–311.

Audino, M., Grice, K., Alexander, R, Kagi, R.I., 2002a Macrocyclic alkanes in crude oils from the algaenan of *Botryococcus braunii*. Organic Geochemistry 33, 979–984.

Audino, M., Grice, K., Alexander, R., Kagi R.I., 2002b Macrocyclic alkanes: Markers for the freshwater alga *Botryococcus braunii* in the Gippsland Basin. Australian Petroleum Production and Exploration Association Journal 42, 437–442.

Blevin, J.E., Cathro, D., 2008. Australian Southern Margin Synthesis – GA707 https://www.ga.gov.au/products/servlet/controller?event=GEOCAT_DETAILS&catno=68892

Blevin, J.E., Totterdell, J.M., Logan, G.A., Kennard, J.M., Struckmeyer, H.I.M., Colwell, J.B., 2000. Hydrocarbon prospectively of the Bight Basin—petroleum systems analysis in a frontier basin. Geological Society of Australia, Abstracts 60, 24–29.

Boreham C.J., 2008. Bight Basin marine potential source rocks: a local expression of the Late Cretaceous oceanic anoxic event (OAE2)? In: McKirdy, D.M. (Ed.), Oil, Soil, Water and Wine. 15th Australian Organic Geochemistry Conference, Program and Abstracts, 104–105.

Boreham C.J., Krassay A.A., Totterdell J.M., 2001. Geochemical comparisons between asphaltites on the southern Australian margin and Cretaceous source rock analogues. In: Hill, K.C., Bernecker T. (Eds.), Eastern Australasian Basins Symposium: A refocused energy perspective for the future. Petroleum Exploration Society of Australia, Special Publication, pp. 531–541.

Boult P.J., McKirdy D., Blevin J., Heggeland R., Lang S., Vinall D., 2005. The oil-prone Morum Sub-basin petroleum system, Otway Basin, South Australia. MESA Journal 38, 28–33.

Boult, P.J., Hibburt, J.E., 2002. The Petroleum Geology of South Australia. Volume 1: Otway Basin. 2nd edition. South Australia. Department of Primary Industries and Resources.

Boult. P.J., 2012. Bight Basin Overview. http://www.bightpetroleum.com/bight-basin/overview

Bradshaw, B.E., Rollet, N., Totterdell, J.M., Borissova, I., 2003. A revised structural framework for frontier basins on the southern and south-western Australian continental margin. Geoscience Australia Record 2003/03.

Brüning M., Sahling H., MacDonald I., Ding F., Bohrmann G., 2010. Origin, distribution, and alteration of asphalts at the Chapopote Knoll, southern Gulf of Mexico. Marine and Petroleum Geology 27, 1093–1106.

Carpentier, B., Arab, H., Pluchery, E., Chautru, J.M., 2007. Tar mats and residual oil distribution in a giant oil field offshore Abu Dhabi. Journal of Petroleum Science and Engineering 58, 472–490.

Clayton, J.L., Bostick, N.H., 1986. Temperature effects on kerogen and on molecular and isotopic composition of organic matter in Pierre Shale near an igneous dike. Organic Geochemistry 10, 135-143.

Cobbold, P.R., Rossello, E.A., 2003. Aptian to recent compressional deformation, foothills of the Neuque´n Basin, Argentina. Marine and Petroleum Geology 20, 429–443.

Curiale, J. A., 1986. Origin of solid bitumens, with emphasis on biological marker results. Organic Geochemistry 10, 559-580.

Currie T.J., Alexander R., Kagi R.I., 1992. Coastal bitumens from Western Australia – long distance transport by ocean currents. Organic Geochemistry 18, 595–601.

Dawson, D., Grice, K., Alexander, R., 2005. Effect on maturation on the indigenous δD signatures of individual hydrocarbons in sediments and crude oils from the Perth Basin (Western Australia). Organic Geochemistry 36, 95-104.

Douglas, G.S., Bence, E., Prince, R.C., McMillen, S.J., Butler, E.L., 1996. Environmental stability of selected petroleum hydrocarbon source and weathering ratios. Environmental Science & Technology 30, 2332–2339.

Douglas, G.S., Owens, E.H., Hardenstine, J., Prince, R.C., 2002. The OSSA II Pipeline oil spill: the character and weathering of the spilled oil. Spill Science & Technology Bulletin 7, 135–148.

Dowling, L.M., Boreham, C.J., Hope, J.M., Murray, A.P., Summons, R.E., 1995. Carbon isotopic composition of hydrocarbons in ocean-transported bitumens from the coastline of Australia. Organic Geochemistry 23, 729–737.

Edwards D., McKirdy D.M., Summons R.E., 1998. Enigmatic asphaltites from the southern Australian margin: molecular and carbon isotopic composition. PESA Journal 26, 106–130.

Edwards, D.S., Struckmeyer, H.I.M., Bradshaw, M.T., Skinner, J.E., 1999. Geochemical characteristics of Australia's Southern Margin petroleum systems. Australian Petroleum Production and Exploration Association Journal 39, 297–321.

Espurt, N., Callot, J., Totterdell, J., Struckmeyer, H., Vially, R., 2009. Interactions between continental breakup dynamics and large-scale delta system evolution: Insights from the Cretaceous Ceduna delta system, Bight Basin, Southern Australian margin, Tectonics 28, 1–26.

Farwell, C., Reddy, C.M., Peacock, E., Nelson, R.K., Washburn, L., Valentine, D.L., 2009. Weathering and the fallout plume of heavy oil from strong petroleum seeps near Coal Oil Point, CA. Environmental Science and Technology 43, 3542–3548.

Fernandez-Alvarez, P., Vila, J., Garrido, J.M., Grifoll, M., Feijoo, G., Lema, J.M., 2007. Evaluation of biodiesel as bioremediation agent for the treatment of the shore affected by the heavy oil spill of the Prestige. Journal of Hazardous Material 147, 914–922.

Fisher, S.J., Alexander, R., Kagi, R.I., Oliver, G.A., 1998. Aromatic hydrocarbons as indicators of petroleum biodegradation and multiple accumulation events in north Western Australian oil reservoirs. In: Purcell, P.G., Purcell, R.R., (Eds.), Sedimentary Basins of Western Australia 2, Proceedings of the WA Basins Symposium, Petroleum Exploration Society of Australia, pp. 185–194.

Gagnon, M.M., Grice, K., Kagi, R.I., 1999. Biochemical and chemical parameters for aquatic ecosystem health assessments adapted to the Australian oil and gas industry. Australian Petroleum Production and Exploration Association Journal 39, 584–598.

Goodwin N.S., Park P.J.D., Rawlinson A.P., 1983. Crude oil biodegradation under simulated and natural conditions. In: Björoy, M., (Ed.), Advances in Organic Geochemistry 1981, Wiley, Chichester, pp. 650–658.

Grice, K., Alexander, R., Kagi, R.I., 2000. Diamondoid hydrocarbon ratios as indicators of biodegradation in Australian crude oils. Organic Geochemistry 31, 67–73.

Grice. K., Schaeffer, P., Schwark, L., Maxwell, J.R., 1996. Molecular indicators of the palaeoenvironmental conditions in an immature Permian shale (Kupferschiefer, Lower Rhine Basin, north-west Germany) from free and S-bound lipids. Organic Geochemistry 25, 131–147.

Grice. K., Schaeffer, P., Schwark, L., Maxwell, J.R., 1997. Changes in palaeoenvironmental conditions during deposition of the Permian Kupferschiefer (Lower Rhine Basin, northwest Germany) inferred from molecular and isotopic compositions of biomarker components. Organic Geochemistry 26, 677–690.

Hallmann, C., Schwark, L., Grice, K., 2008. Community dynamics of anaerobic bacteria in deep petroleum reservoirs. Nature Geoscience 1, 588–591.

Hartman, B.H., Hammond, D., 1981. The use of carbon and sulfur isotopes as correlation parameters for the source identification of beach tar in the southern California borderland. Geochimica et Cosmochimica Acta 45, 309–319.

Head I.M., Jones D.M., Röling W.F.M., 2006. Marine microorganisms make a meal of oil. Nature Reviews: Microbiology 4, 173–182.

Head, I.M., Jones, D.M., Larter, S.R., 2003. Biological activity in the deep subsurface and the origin of heavy oil. Nature 426, 344–352.

Hillis, R.D., Reynolds, S.D., 2003. In Situ Stress Field, Fault Reactivation and Seal Integrity in the Bight Basin. South Australia. Department of Primary Industries and Resources. Report Book 2003/2.

Hofstetter, T.B., Berg, M., 2011 Assessing transformation processes of organic contaminants by compound-specific stable isotope analysis. Trends in Analytical Chemistry, 30, 618–627.

Hough, R.L., Whittaker, M., Fallick, A.E., Preston, T, Farmer, J.G., Pollard, S.J.T., 2005. Identifying source correlation parameters for hydrocarbon wastes using compound-specific isotope analysis. Environmental Pollution 143, 489–498.

Hwang, R.J., Teerman, S.C., Carlson, R.M., 1998. Geochemical comparison of reservoir solid bitumens with diverse origins. Organic Geochemistry 29, 505–517.

Jeffery, A.W.A., 2007. Application of stable isotope ratios in spilled oil identification. In: Wang, Z., Stout, S.A. (Eds.), Oil Spill Environmental Forensics: Fingerprinting and Source Identification. Academic Press, Burlington, MA, pp. 207–227.

Jenkyns, H.C., 2010. Geochemistry of oceanic anoxic events. Geochemistry, Geophysics, Geosystems 11, 1–30.

Jones, D.M., Head, I.M., Gray, N.D., Adams, J.J., Rowan, A.K., Aitken, C.M., Bennett, B., Huang, H., Brown, A., Bowler, B.F.J., Oldenburg, T., Erdmann, M., Larter, S.R., 2008. Crude-oil biodegradation via methanogenesis in subsurface petroleum reservoirs. Nature 451, 176–180.

Kuo, L.C., 1994. An experimental study of crude oil alteration in reservoir rocks by water washing. Organic Geochemistry 21, 465–479.

Lafargue, E., Barker, C., 1988. Effect of water washing on crude oil composition. American Association of Petroleum Geologists Bulletin 72, 263–276.

Lafargue, E., Le Thiez, P., 1996. Effect of water washing on light ends compositional heterogeneity. Organic Geochemistry 24, 1141–1150.

Larter, S.R., Gates, I., Adams, J., Bennett, B., Huang, H., Koksalan, T., Fustic, M., 2006a. Reservoir fluid characterization of tar sand and heavy oil reservoirs - impact of fluid heterogeneity on production characteristics. American Association of Petroleum Geologists 2006 Annual Convention – Perfecting the Search – Delivering on Promises, April 9–12. George R. Brown Convention Center, Houston, Texas, USA.

Larter, S.R., Huang, H., Adams, J.J., Bennett, B., Jokanola, O., Oldenburg, T.B.P., Jones, M., Head, I.M., Riediger, C.L., Fowler, M.G., 2006b. The controls on the composition of biodegraded oils in the deep subsurface. Part II – geological controls on subsurface biodegradation fluxes and constraints on reservoir-fluid property prediction. American Association of Petroleum Geologists Bulletin 90, 921–938.

Larter, S.R., Huang, H., Adams, J.J., Bennett, B., Snowdon, L.R., 2012. A practical biodegradation scale for use in reservoir geochemical studies of biodegraded oils. Organic Geochemistry 45, 66–76.

Lee, R.F., 2003. Photo-oxidation and photo-toxicity of crude and refined oils. Spill Science & Technology Bulletin 8, 157–162.

Logan, G.A., Jones, A.T., Kennard, J.M., Ryan, G.J., Rollet, N., 2010. Australian offshore natural hydrocarbon seepage studies, a review and re-evaluation. Marine and Petroleum Geology 27, 26–45.

Mazeas, L., Budzinski H., 2002. Molecular and Stable Carbon Isotopic Source Identification of Oil Residues and Oiled Bird Feathers Sampled along the Atlantic Coast of France after the Erika Oil Spill. Environmental Science & Technology 36, 130–137.

Mazeas, L., Budzinski, H., Raymond N., 2002. Absence of stable carbon isotope fractionation of saturated and polycyclic aromatic hydrocarbons during aerobic bacterial biodegradation. Organic Geochemistry 33, 1259–1272.

McGowran, B., Li, Q., Cann, J., Padley, D., McKirdy, D. M., Shafik, S., 1997. Biogeographic impact of the Leeuwin Current in southern Australia since the late middle Eocene. Palaeogeography, Palaeoclimatology, Palaeoecology 136, 19–40.

McKirdy, D. M., Horvath, Z., 1976. Geochemistry and significance of coastal bitumen from southern and northern Australia. Australian Petroleum Exploration Association Journal 16(1), 123–136.

McKirdy, D.M, Chivas, A.R., 1992. Nonbiodegraded aromatic condensate associated with volcanic supercritical carbon dioxide, Otway Basin: implications for primary migration from terrestrial organic matter. Organic Geochemistry 18, 611–627.

McKirdy, D.M., 1984a. Coastal bitumens and potential source rocks in the western Otway Basin, South Australia and Victoria. AMDEL Report F5840/84 for Australian Aquitaine Petroleum Pty Ltd. and Ultramar Australia Inc.

McKirdy, D.M., 1984b. Coastal bitumen and potential source rocks, Duntroon Basin. South Australia. AMDEL Report F5769/84 for Getty Oil Development Co. Ltd.

McKirdy, D.M., Aldridge, A.K., Ypma, P.J.M., 1983. A geochemical comparison of some crude oils from pre-Ordovician carbonate rocks. In: Björoy, M. (ed.), Advances in Organic Geochemistry 1981, Wiley, Chichester, pp. 99–107.

McKirdy, D.M., Cox, R.E., Volkman, J.K. and Howell, V.J., 1986. Botryococcane in a new class of Australian non-marine crude oils. Nature 320, 57–59.

McKirdy, D.M., Cox, R.E., Volkman, J.K., Howell, V.J., 1986. Biological marker, isotopic and geological studies of lacustrine crude oils in the western Otway Basin, South Australia. in: Fleet, A.J., Kelts, K., Talbot, M.R. (Eds.), Lacustrine Petroleum Source Rocks. Geological Society of London, Special Publication 40, 327.

McKirdy, D.M., Michaelsen, B.H., Yu X., 1996. Thermal maturity and biomarker geochemistry of the Early Cambrian Kulpara Formation, Stansbury Basin. Report for Canyon (Australia) Pty Limited.

McKirdy, D.M., Summons, R.E., Padley, D., Serafini, K.M., Boreham, C.J., Struckmeyer, H.I.M., 1994. Molecular fossils in coastal bitumens from southern Australia: signatures of precursor biota and source rock environments. Organic Geochemistry 21, 265–286.

McKirdy, D.M., Thomas, H.N.M., Boult, P.J., Payenberg, T., Edwards, D., 2006. Southern margin asphaltites: new evidence for their local origin from the northwestern Otway Basin, South Australia. Combined national conference of the Australian Organic Geochemists & Natural Organic Matter Interest Group, Perth, Program and Abstracts, pp. 85–86

Middleton, J.F., Bye, J.A.T., 2007. A review of the shelf-slope circulation along Australia's southern shelves: Cape Leeuwin to Portland. Progress in Oceanography 75, 1–41.

Middleton, J.F., Platov, G., 2003. The mean summertime circulation along Australia's southern shelves: a numerical study. Journal of Physical Oceanography 33, 2270–2287.

Mossman, D., Nagy, B., 1996. Solid bitumens: an assessment of their characteristics, genesis, and role in geological processes. Terra Nova 8, 114–128.

Mueller, E., Philp, R.P., Allen, J., 1995. Geochemical characterization and relationship of oils and solid bitumens from SE Turkey. Journal of Petroleum Geology 18, 289–308.

Munoz, D., Guiliano, M., Doumenq, P., Jacquo, F., Scherreri, P., Mille, G., 1997; Long term evolution of petroleum biomarkers in mangrove soil (Guadeloupe). Marine Pollution Bulletin 34, 868–874.

Ozimic, S., Nicholas, E., Pain, L., 1987. Australian Petroleum Accumulations Report 2: Bass Basin, Tasmania and Victoria. Department of Resources and Energy, Bureau of Mineral Resources, Geology and Geophysics, Canberra.

Padley, D., 1996. Petroleum geochemistry of the Otway Basin and the significance of coastal bitumen strandings on adjacent southern Australian beaches. PhD Thesis, University of Adelaide.

Padley, D., McKirdy, D.M., Murray, A.P., Summons, R.E., 1993. Oil strandings on the beaches of Southern Australia: origins from natural seepage and shipping. In: Øygard, K. (Ed.), Poster Sessions from the 16th International Meeting on Organic Geochemistry 20-24 September 1993, Stavanger, Norway, pp. 660–663.

Palmer, S. E., 1993. Effect of biodegradation and water washing on crude oil composition. In: Engel, M.H., Macko, S.A. (Eds.), Organic Geochemistry, Plenum Press, New York, pp. 511– 533.

Palmer, S.E., 1984. Effect of water washing on C_{15+} hydrocarbon fraction of crude oils from Northwest Palawan, Philippines. American Association of Petroleum Geologists Bulletin 68, 137–149.

Palmowski, D., Hill, K.C., Hoffman, N., 2004. Structural-stratigraphic styles and evolution of the offshore Otway Basin - a structural seismic analysis. In: Boult, P.J., Johns, D.R., Lang, S.C. (Eds.), Eastern Australasian Basins Symposium II, Petroleum Exploration Society of Australia, Special Publication, pp. 75–96.

Pancost, R.D., Crawford, N., Magness, S., Turner, A., Jenkyns, H.C., Maxwell, J.R., 2005. Further evidence for the development of photic-zone euxinic conditions during Mesozoic oceanic anoxic events. Journal of the Geological Society 161, 353–364.

Peters K.E., Walters C.C., Moldowan J.M., 2005. The Biomarker Guide, Volume 2, Biomarkers and Isotopes in Petroleum Systems and Earth History. Cambridge University Press.

Peters, K.E., Moldowan, J.M., 1993. The Biomarker Guide - Interpreting Molecular Fossils in Sediments and Petroleum. Prentice-Hall, New Jersey.

Philp, R.P., Allen, J., Kuder, T, 2002. The use of the isotopic composition of individual compounds for correlating spilled oils and refined products in the environment with suspected sources. Environmental Forensics 3, 341–348

Prince, R.C., Walters, C.C., 2007. Biodegradation of oil and its implications for source identification. In: Wang, Z., Stout, S.A. (Eds.), Oil Spill Environmental Forensics. Academic Press, Burlington, MA, pp. 349–379.

Rintoul, S.R., Hughes, C.W., Olbers, D., 2001. The Antarctic circumpolar current system. In: Ocean Circulation and Climate - Observing and Modeling the Global Ocean. International Geophysics 77, 271–302.

Ruble, T.E., Logan, G.A., Blevin, J.E., Struckmeyer, H.I.M., Ahmed, M., Quezada, R.A., 1999. Geochemistry of Palaeo-oil in Jerboa-1, Eyre Sub-basin, Great Australian Bight. CSIRO Petroleum Confidential Report No. 99-060, 223 p.

Ruble, T.E., Logan, G.A., Blevin, J.E., Struckmeyer, H.I.M., Liu, K., Ahmed, M., Eadington, P.J. and Quezada, R.A., 1999. Geochemistry oand charge history of a palaeo-oil column: Jerboa-1, Eyre Sub-basin, Great Australian Bight. EABS paper TH complete .

Schubotz, F., Lipp, J.S., Elvert, M., Kasten, S., Mollar P.X., Zabel, M., Bohrmann, G., Hinrichs, K., 2011. Petroleum degradation and associated microbial signatures at the Chapopote asphalt volcano, Southern Gulf of Mexico. Geochimica et Cosmochimica Acta 75, 4377–4398.

Seifert, W.K., Moldowan, J.M., 1978. Applications of steranes, terpanes, and monoaromatics to the maturation, migration, and source of crude oils. Geochimica et Cosmochimica Acta 42, 77–95.

Seifert, W.K., Moldowan, J.M., 1979. The effect of biodegradation on steranes and terpanes in crude oils. Geochimica et Cosmochimica Acta 43, 111–126.

Smart, S.M., 1999. Asphaltites from the southern Australian Margin: Submarine oil seeps or maritime artifacts? BSc Honours thesis, National Centre for Petroleum Geology and Geophysics, University of Adelaide (unpublished).

Smith, M.A., Donaldson, I.F., 1995. The hydrocarbon potential of the Duntroon Basin. Australian Petroleum Exploration Association Journal, 35(1), 203–291.

Sofer, Z., 1984. Stable carbon isotope compositions of crude oils: application to source depositional environments and petroleum alteration. American Association of Petroleum Geologists Bulletin 68, 31-49.

Sprigg, R.C., 1986. A history of the search for commercial hydrocarbons in the Otway Basin complex. In: Glenie R.C. (Ed.), Second South-Eastern Australia Oil Exploration Symposium. Petroleum Exploration Society of Australia, Melbourne, pp. 173–200.

Sprigg, R.C., Woolley, J.B., 1963. Coastal bitumen in South Australia with special reference to observations at Geltwood Beach, south-eastern South Australia. Transactions of the Royal Society of South Australia 86, 67–103.

Struckmeyer, H.I.M., Totterdell, J.M., Blevin J.E., Logan, G.A., Boreham, C.J., Deighton, I., Krassay, A.A., Bradshaw, M.T., 2001. Character, maturity and distribution of potential Cretaceous oil source rocks in the Ceduna Sub-basin, Bight Basin, Great Australian Bight. In: Hill, K.C., Bernecker, T. (Eds.) Eastern Australasian Basins Symposium, A refocused energy perspective for the future, Melbourne, 2001. Petroleum Exploration Society of Australia. Special Publication, pp. 543–552.

Summons R.E., Powell T.G., 1986. Chlorobiaceae in Palaeozoic seas - Combined evidence from biological markers, isotopes and geology. Nature 319, 763–765.

Summons, R.E., Bradshaw, J., Burchardt, D.M., Goody, A.K., Murray, A.P., Foster, C.B., 1993. Hydrocarbon composition and origins of coastal bitumens from the Northern Territory, Australia. Petroleum Exploration Society of Australia Journal 21(1), 31–42.

Summons, R.E., Fletcher, P. and Bradshaw, J., 1992. Hydrocarbon composition of stranded bitumen from the Northern territory. BMR Report and Professional Opinion.

Summons, R.E., Logan, G.A., Edwards, D.S., Boreham, C.J., Bradshaw, M.T., Blevin, J.E., Totterdell, J.M., Zumberge, J.E., 2001. Geochemical analogues for Australian coastal asphaltites - search for the source rock. Abstract. American Association of Petroleum Geologists Bulletin, 85 (Supplement).

Tolmer, A., 1882. Boat expedition to Kangaroo Island in pursuit of a gang of desperadoes, headed by Gilkes (in 1844). In: Reminiscences of an Adventurous and Chequered Career at Home and in the Antipodes. Sampson Low, Marston, Searle and Rivington, London, ch. 24.

Totterdell, J., Struckmeyer, H., 2003. Southern Australian Bight Basin holds deepwater potential. Offshore 63, 41–44.

Totterdell, J.M., Blevin, J.E., Struckmeyer, H.I.M., Bradshaw, B.E., Colwell, J.B., Kennard, J.M., 2000. A new sequence framework for the Great Australian Bight: Starting with a clean slate. Australian Petroleum, Production and Exploration Association Journal, 40, 95–117.

Totterdell, J.M., Struckmeyer, H.I.M., Boreham, C.J., Mitchell, C.H., Monteil, E. Bradshaw, B.E., 2008. Mid–Late Cretaceous Organic-Rich Rocks From The Eastern Bight Basin: Implications For Prospectivity. In: Blevin, J.E., Bradshaw, B.E., Uruski, C. (Eds.), Eastern Australasian Basins Symposium III, Petroleum Exploration Society Of Australia, Special Publication, pp. 137–158.

Trolio, R., Grice, K., Fisher, S.J., Alexander, R., Kagi, R.I., 1999. Alkylbiphenyls and alkyldiphenylmethanes as indicators of petroleum biodegradation. Organic Geochemistry 30, 1241–1253.

Volkman J.K., O'Leary T., Summons R.E., Bendall M.R., 1992. Biomarker composition of some asphaltic coastal bitumens from Tasmania, Australia. Organic Geochemistry 18, 669–682.

Volkman, J.K., Alexander, R., Kagi, R.I., Rowland, S.J., Sheppard, P.N., 1984. Biodegradation of aromatic hydrocarbons in crude oils from the Barrow Sub-basin of Western Australia. Organic Geochemistry 6, 619–632.

Wakeham, S.G., Pease, T.K., 1992: Lipid analyses in marine particle and sediment samples: a laboratory handbook. Unpublished manuscript, Skidaway Institute of Oceanography, Savannah, Georgia, U.S.A.

Wardlaw, G.D., Arey, J.S., Reddy, C.M., Nelson, R.K., Ventura, G.T., Valentine, D.L., 2008. Disentangling oil weathering at a marine seep using GCxGC: broad metabolic specificity accompanies subsurface petroleum biodegradation. Environmental Science & Technology 42, 7166–7173.

Wardroper, A.M.K., Hoffman, C.F., Maxwell, J.R., Barwise, A.J.G., Goodwin, N.S., Park, P.J.D., 1984 Crude oil biodegradation under simulated and natural conditions - II. Aromatic steroid hydrocarbons. In: Schenck, P.A., de Leeuw, J.W., Lijmbach, G.W.M. (Eds.), Advances in Organic Geochemistry 1983. Pergamon Press, Oxford, pp. 605–617.

Wenger, L.M., Davis, C.L., Isaksen, G.H., 2001. Multiple controls on petroleum biodegradation and impact in oil quality. Society of Petroleum Engineers Reservoir Evaluation and Engineering 5, 375–383.

Wenger, L.M., Isaksen, G.H., 2002. Control of hydrocarbon seepage intensity on level of biodegradation in sea bottom sediments. Organic Geochemistry 33, 1277–1292.

Wilhelms, A., Carpentier, B., Huc, A.Y., 1994. New methods to detect tar mats in petroleum reservoirs. Journal of Petroleum Science and Engineering 12, 147–155.

Wilhelms, A., Larter, S.R., 1994a. Origin of tar mats in petroleum reservoirs. Part I: Introduction and case studies. Marine and Petroleum Geology 11, 418–441.

Wilhelms, A., Larter, S.R., 1994b. Origin of tar mats in petroleum reservoirs. Part II: Formation mechanisms for tar mats. Marine and Petroleum Geology 11, 442–456.

Appendix 1. Abbreviations for Tables 2 & 3 and Figures7 & 8

Bulk Composition, normal & acyclic hydrocarbons (fullscan)

C_x = normal alkane $C_{carbon\ number}$ e.g. C_{15} = pentadecane ($C_{15}H_{32}$)
Pr = pristine
Ph = phytane
Sats = Saturate Fraction Hydrocarbons
Arom = Aromatic Fraction Hydrocarbons
NSO = Polar Fraction Hydrocarbons
Asph = Asphaltenes
C10-19/C30 = $(\sum nC_{10} : nC_{19})/nC_{30}$

Hopanes (m/z 191)

T = tricyclic terpanes note C_{25} and C_{26} homologues have a chiral centre at C_{22} (R & S)
Tet = C_{24} tetracyclic terpane
Ts = C_{27} 18α(H)-22,29,30-trisnorhopane
Tm = C_{27} 17α(H)-22,29,30-trisnorhopane
C_{28}BNH = C_{28} 17α(H),21β(H)-28,30 bisnorhopane
C_{29}H = C_{29} 17α(H),21β(H)-hopane
C_{30}H = C_{30} 17α(H),21β(H)-hopane
Mor = C_{30} 17β(H),21α(H)-moretane
C_{30}DiaH = C_{30} 17α(H),21β(H)-diahopane
C_{29}Ts = C_{29} 30-norneohopane
C_{30}Ts = C_{30} 30-norneohopane
Gam = Gammacerane
C_{31}HR = C_{31} 17α(H),21β(H)-homohopane (22R)
C_{32} S/(S+R) = C_{32} 17α(H),21β(H)-bishopane (22S)/C_{32} 17α(H),21β(H)-bishopane (22S + 22R)
C_{35}(S+R)/C_{31}(S+R) = C_{35} 17α(H),21β(H)-pentahomohopanes (22S + 22R)/ C_{31} 17α(H),21β(H)-homohopanes(22S + 22R)
C_{35}/C_{34} (S only) = C_{35} 17α(H),21β(H)-pentahomohopane (22S)/ C_{34} 17α(H),21β(H)-tetrahomohopane (22S)
C35 Homohopane Index = C_{35} 17α(H),21β(H)-pentahomohopanes (22S & 22R)/$\sum C_{31}$: C_{35} 17α(H),21β(H)-homohopanes (22S & 22R)

Steranes (m/z 217 & 218)

C_{27} ααα 20R = C_{27} 5α(H),14α(H),17α(H)-sterane (20R)
C_{28} ααα 20R = C_{28} 5α(H),14α(H),17α(H)-sterane (20R)
C_{29} ααα 20R = C_{29} 5α(H),14α(H),17α(H)-sterane (20R)
C_{27} Dia/(Dia+Reg) = C_{27} 13α(H),17α(H) diasteranes (20R + 20S)/(C_{27} 13α(H),17α(H) diasteranes (20R + 20S) + C_{27} 5α(H) steranes (20R + 20S))
C_{29} αββ/(ααα + αββ) = C_{29} 5α(H),14β(H),17β(H)-steranes (20R + 20S)/ (C_{29} 5α(H),14α(H),17α(H)-steranes (20R + 20S) + C_{29} 5α(H),14β(H),17β(H)-steranes (20R + 20S))
C_{27} αββ 20(R+S) = C_{27} 5α(H),14β(H),17β(H)-steranes (20R + 20S)
C_{28} αββ 20(R+S) = C_{28} 5α(H),14β(H),17β(H)-steranes (20R + 20S)
C_{29} αββ 20(R+S) = C_{29} 5α(H),14β(H),17β(H)-steranes (20R + 20S)
C_{29}/C_{27} abb Sterane Ratio = C_{29} 5α(H),14β(H),17β(H)-steranes (20R + 20S)/ C_{27} 5α(H),14β(H),17β(H)-steranes (20R + 20S)

Triaromatic Steroids (m/z 231)

C_{26} Triaromatic Steroids = C_{26} Triaromatic Steroids (20R + 20S)
C_{27} Triaromatic Steroids = C_{27} Triaromatic Steroids (20R + 20S)
C_{28} Triaromatic Steroids = C_{28} Triaromatic Steroids (20R + 20S)
C_{29} Triaromatic Steroids = C_{29} Triaromatic Steroids (20R + 9α20S + 9β20S)

C_{20} = C_{2o} Triaromatic Steroid
C_{21} = C_{21} Triaromatic Steroid
C_{26} 20R = C_{26} Triaromatic Steroid 20R
C_{26} 20S = C_{26} Triaromatic Steroid 20S
C_{27} 20R = C_{27} Triaromatic Steroid 20R
C_{27} 20S = C_{27} Triaromatic Steroid 20S
C_{28} 20R = C_{28} Triaromatic Steroid 20R
C_{28} 20S = C_{28} Triaromatic Steroid 20S
C_{29} 20R = C_{29} Triaromatic Steroid 20R
C_{29} 20S9α = C_{29} Triaromatic Steroid 9α,20S
C_{29} 20S9β = C_{29} Triaromatic Steroid 9β,20S

Polycyclic Aromatic Hydrocarbons (m/z 178, 184, 198, 226, 252)

BaP = Benzo(a)Pyrene
BbF = Benoz(b)Fluoranthene
P = Phenanthrene
MP = Methyl Phenanthrenes
C2P = Ethyl & Dimethyl Phenanthrenes
DBT = Dibenzothiophene
MDBT = Methyl Dibenzothiophenes
C3DBT = Propyl, Methyl-Ethyl & Trimethyl Dibenzothiophenes

Conclusions

Application of mass spectrometric geochemical techniques to investigate palaeoenvironment and chemostratigraphy of Early Cambrian formations from South Australian has provided a number of interesting findings.

The multiproxy approach of using trace element & REE distributions, TOC, bulk isotopic signature and stratigraphic records in conjunction with sedimentological information provides a powerful tool for interpreting palaeoenvironmental conditions. Taken individually each proxy may seem to indicate conflicting accounts of the depositional history, however, when using a multiproxy approach, trends emerge from the information allowing changes towards aerobic or anaerobic environments to be inferred reliably.

The analytical data from the three black shale units under investigation indicate:

1. The prevalent palaeoredox conditions during deposition of the Heatherdale Shale were dysoxic, with evident fluctuations into both fully oxic and anoxic environments. Up section, the formation evolves into progressively more reducing conditions. The Heatherdale Shale exhibits a comparatively pronounced enrichment in U, a possible indication of increased primary productivity.
2. The Talisker Formation similarly becomes more reduced up-section, with indications of possible euxina in the uppermost portion. The interpretations correspond well with the documented sedimentology of the formations. A secular decline in $\delta^{34}S_{pyr}$ observed in the Talisker formation from the correlated Frankton drill hole sections appears to reflect this change in environmental conditions rather than a diagenetic or metamorphic overprint as suggested by previous low resolution analyses. The Talisker Formation

displays a steeper Mo/TOC gradient, again suggesting that it was deposited in more oxygen depleted conditions

3. The Emu Bay Shale conversely demonstrates consistently aerobic interpretations for the redox proxies.

The implication of these findings from the Emu Bay Shale is that oxygen-deficient bottom water were not a pre-requisite for the preservation of its Lagerstätte. In this respect it is similar to the archetypical Burgess Shale Formation in British Columbia.

The absence of burrowing and bioturbation implies the existence of a sharp redox boundary at the sediment-water interface, likely maintained by cyanobacterial mats that also mantled the tests of recently dead fauna.

Biogeochemical identification of the characteristic *n*-alkane signature of *G. prisca* among other biomarker hydrocarbons in bitumen II from the fossiliferous Emu Bay Shale is the first reported evidence for the presence of this or a similar coccoid cyanobacterium in any Cambrian Lagerstätte.

Given its demonstrated mat-forming capability in other early Palaeozoic sediments, its likely dual roles in the Emu Bay depocentre, possibly in consort with other benthic cyanobacteria, were to maintain a robust redox boundary at the sediment-water interface and mantle the carapaces of recently deceased fauna on the sea floor, thereby extending the preservation of their soft (non-biomineralised) tissue for long enough to allow its inorganic replication during late diagenesis.

Below the boundary, anoxic pore water facilitated the preservation of soft tissue, while oxic conditions in the overlying water column diminished the flux of

phytoplanktonic remains to the sea floor, as reflected in the low TOC content of the original sediment.

Furthermore, the presence of cyanobacterial mats implies that the Emu Bay Shale Lagerstätte was deposited in the photic zone.

Notwithstanding the long storage time of the kerogen prior to this analysis, it appears to have escaped significant oxidative alteration. MSSV thermal desorption and pyrolysis of kerogen isolated by serial acid digestion of solvent-extracted rock powder is an effective means of accessing indigenous hydrocarbons where, as in this instance, the free hydrocarbons (bitumen I) in the host rock were contaminated by soil-derived lipids.

The Emu Bay Shale is less thermally altered than the Burgess Shale (which has undergone greenschist facies metamorphism) and less extensively weathered than the Maotianshan Shale (which hosts the Chenjiang biota of South China). Therefore, potentially, it is a more useful source of information on BST preservation than these two classic deposits.

Provenance interpretation using trace and REE data suggests a change in source locality from the late Normanville Group into the Kanmantoo Group. This corroborates previously published detrital zircon interpretations.

Comparison of trace and REE distributions to similar sequences of the Yangtze platform, South China shows striking similarities. This implies similar oceanic seawater chemistry is recorded in the Stansbury Basin and South China black shales. Analogous basinal environments and common provenance may have lead to the seawater trace element chemistry of the Palaeo Pacific & Asian oceans exhibiting a

homogenous nature. It is suggested further geochemical comparison of, as yet unsampled, correlative sections from these basins would be required to prove the significance of this observation.

The carbon isotope chemostratigraphy of the South Australian basins show good correlation regionally, generally supporting the sequence stratigraphy and biostratigraphic assignments. Comparison to the global chemostratigraphic profile shows a strong degree of concordance. Prominent, globally recognised isotopic excursions are recognised within the South Australian composite; the SHICE, AECE and ROECE depletion events in conjunction with the CARE and MICE enrichments are all correlated. These features allow correlation to be made with Early Cambrian sections from North America, Africa, Asia and Europe.

A relationship is observed between chemostratigraphy and the relative sea level during the Cambrian Stage 2 with the profile mimicking the sea level curve. This may indicate a diagenetic origin for the carbon isotope distribution derived from meteoric interaction with the exposed carbonate shelf during period of regression. Alternatively, eustatic sea level could be the primary causal effect of variation of isotopic distribution within the DIC pool, the initial source of sequestered carbon, through alteration of oceanic redox, nutrient cycling and the rate of organic matter burial which are evidenced within coeval black shale deposits.

The Terreneuvian section of the profile does not track sea level fluctuations, though several excursions are evident. This suggest that the carbon isotope profile was independent of eustacy during this period and given the secular nature of these events it seems likely perturbations in the isotopic composition of DIC are exhibited in the profile. The structure of South Australia's expanded Early Cambrian $\delta^{13}C_{carb}$ profile,

in correlation with the global composite, reveals the Palaeo-Pacific Ocean varied at several frequencies, implicating multiple processes in the modulation of the marine carbon cycle.

It is apparent the lack of geochronological constraints within the South Australian basins is a weakness when inferring ages for the lithologies. This is an area where future research would substantially benefit the findings reported in this thesis. A number of tuffaceous horizons are known throughout the Early Cambrian units, some of which are described from the cores investigated within this study, and it is suggested ID-TIMS analysis could provide significant support for the correlations implied herein.

In investigating the possible source location of the asphaltic bitumens stranded upon the shores of the southern margin of Australia, and further afield, it seems appropriate to also reconsider the genesis of the asphaltum. As neither a product biodegradation or extensive water washing, the previous hypothesis that they are the weathered remains of floating tar mats no longer explains physical characteristics exhibited by the asphaltites. Laminations and flow structures observed in specimens allude to an origin more like the asphaltic volcanoes of the Gulf of Mexico. A natural seep of a viscous bitumen from the subsurface, similar in expression to volcanic flows, can be associated with all the hallmarks of the strandings; the devolatilization cracks, large ovoid blocks, benthic communities and these newly described flow characteristics.

The levels of degradation (PM4; Manco 431, 419 [PM4] or ultimate Manco 578 [vector 31043310000]) highlight the initially generated oil has undergone substantial alteration. Given it’s expression at the sea floor is in the form of a heavy oil this modification must have occurred in the subsurface. This can best be explained as a

result of tar mat formation, probably due to deasphalting along a flat lying migration pathway during secondary migration of the main oil stringer.

Geochemical investigation of four previously unanalysed samples from locations in the Bight Basin and New Zealand correlated these more disparate samples to a further seven members of the classic ‘Family 4’ asphaltites from common stranding sites on the Limestone Coast and Kangaroo Island. Comparison of inner, fresher portions of each stranding to the outer, weathered surface section revealed subtle but relatively consistent variations in a number of degradation sensitive components. Molecular fossil distributions and compound specific isotope ratio variations for $\delta^{13}C$ in the saturated fraction hydrocarbons, prone to the effects of biodegradation and dissolution, suggest the samples from the Eyre Peninsula and New Zealand have had longer exposure to weathering in oceanic realm. Aromatic hydrocarbon distribution show a trend corresponding to physical descriptions from the strandings.

The western section Ceduna sub-basin of the Bight Basin is not a plausible host the source of the asphaltites, though the eastern sections cannot be discounted. Reliable evidence of natural seepage and potential source rocks of the correct age within the oil window in this region and a possible transportation mechanism through the upwelling Flinders current bode well. However, migration of a viscous tar mat from a highly specific source to the sea floor, uncontaminated, whilst a number of other petroleum systems are generating within the same system seems improbable.

The Morum sub-basin in the Otway basin has what may be the crucial feature, a deep shelf-break canyon cuts deeply into the toe-thrust inversion interpreted as hosting source rock sediments of the appropriate age and maturation. Likely migration pathways exist through the system of steeply dipping faults where light hydrocarbons

could have continued their movement to reservoirs higher in the sequences to leave a residual tar mat. These heavy asphaltic bitumens may now be exposed by the canyon erosion, oozing slowly onto the seafloor where it forms asphaltite volcano like structures. Transportation of the asphaltum by fluid flow through the canyon, both down from the shelf and more importantly up onto the shelf can be accounted for by the Leeuwin and Flinders oceanic currents. Historical distribution patterns support this hypothesis, with the highest concentration of strandings found on the coast closest to the head of the canyon and on Kangaroo Island, which is next on the westward path of the strong summer upwelling of the Flinders current. The Leeuwin current flows eastward along the shelf for the remainder of the year providing the momentum for the strandings on the Victorian and Tasmanian coasts.

The findings described from the analysis of weathering patterns highlight to potential for this style of investigation. The sample set used herein is small and with an expanded sample suite of freshly stranded specimens it may be possible to further refine the possible source origin. Analysis of a targeted suite of parameters, indentified from this research as being sensitive to weathering, with more sensitive and selective mass spectrometric methodologies will aid these subsequent investigations. Additionally, it is suggested the use of hydrogen isotope analyses may also enhance our ability to differentiate the asphaltum as weathering patterns are subtle and H/D fractionation is known to be environmentally sensitive.

References

Abanda, P.A., Hannigan, R.E., 2006. Effect of diagenesis on trace element partitioning in shales. Chemical Geology 230, 42–59.

Allison, P.A., Briggs, D.E.G., 1993. Exceptional fossil record: Distribution of soft-tissue preservation through the Phanerozoic. Geology 21, 527–530.

Amthor, J.E., Grotzinger, J.P., Schröfer, S., Bowring, S.A., Ramezani, J., Martin, M.W., and Matter, A., 2003, Extinction of Cloudina and Namacalathus at the Precambrian-Cambrian boundary. Geology, v. 31, pp. 431–434.

Babcock L. E., Peng S., 2007. Cambrian chronostratigraphy: Current state and future plans. Palaeogeography, Palaeoclimatology, Palaeoecology 254, 62-66.

Babcock, L.E., 2003. Trilobites in Paleozoic predator–prey systems, and their role in reorganization of early Paleozoic ecosystems. In: Kelley, P.H., Kowalewski, M., Hansen, T.A. (Eds.), Predator–Prey Interactions in the Fossil Record. Kluwer Academic/Plenum Publishers, New York, 55–92.

Babcock, L.E., Rees, M.N., Robison, R.A., Langenburg, E.S., and Peng, S.C., 2004, Potential Global Stratotype-section and Point (GSSP) for a Cambrian stage boundary defined by the first appearance of the trilobite Ptychagnostus atavus, Drum Mountains, Utah, USA. Geobios 37, 149–158.

Babcock, L.E., Robison, R.A., Rees, M.N., Peng, S.C., Saltzman, M.R., 2007. The Global Stratotype Section and Point (GSSP) of the Drumian Stage (Cambrian) in the Drum Mountains, Utah, USA. Episodes 30, 84-94.

Bagnoli, G., Qi, Y-P., Wang, Z-H., 2008. Conodonts from the Global Stratotype section for the base of the Guzhangian Stage (Cambrian) at Luoyixi, Hunan, South China. Palaeoworld 17, 108-114.

Banner, J.L., Hanson, G.N., 1990. Calculation of simultaneous isotopic and trace-element variations during water–rock interaction and with applications to carbonate diagenesis. Geochimica et Cosmochimica Acta 54, 3123–3137.

Bhatia, M.R., Crook, K.A.W., 1986. Trace element characteristics of greywackes and tectonic setting discrimination of sedimentarynbasins. Contributions to Mineralogy and Petrology 92, 181– 193.

Blevin, J..E., Cathro, D., 2008. Australian Southern Margin Synthesis – GA707 https://www.ga.gov.au/products/servlet/controller?event=GEOCAT_DETAILS&catno=68892

Blevin, J.E., Totterdell, J.M., Logan, G.A., Kennard, J.M., Struckmeyer, H.I.M., Colwell, J.B., 2000. Hydrocarbon prospectively of the Bight Basin—petroleum systems analysis in a frontier basin. in: 2nd Sprigg symposium – frontier Basins, frontier ideas, Adelaide, 29–30 June, 2000. geological society of Australia, Abstracts 60, 24–29.

Boreham C.J., 2008. Bight Basin marine potential source rocks: a local expression of the Late Cretaceous oceanic anoxic event (OAE2)? in: McKirdy, D.M. (Ed.) Oil, Soil, Water and Wine. 15th Australian Organic Geochemistry Conference, Program and Abstracts, 104–105.

Boreham C.J., Krassay A.A., Totterdell J.M., 2001. Geochemical comparisons between asphaltites on the southern Australian margin and Cretaceous source rock analogues. in: Hill, K.C., Bernecker T. (Eds.) Eastern Australasian Basins Symposium: A refocused energy perspective for the future. Petroleum Exploration Society of Australia, Special Publication, 531–541.

Boult P.J., McKirdy D., Blevin J., Heggeland R., Lang S., Vinall D., 2005. The oil-prone Morum Sub-basin petroleum system, Otway Basin, South Australia. MESA Journal 38, 28–33.

Boult, P.J., Hibburt, J.E., 2002. The petroleum geology of South Australia. Volume 1: Otway Basin. 2nd edition. South Australia. Department of Primary Industries and Resources. Petroleum Geology of South Australia Series.

Boult. P.J., 2012. Bight Basin Overview. http://www.bightpetroleum.com/bight-basin/overview

Bowring, S.A., Erwin, D.H., 1998. A new look at evolutionary rates in deep time: uniting paleontology and high-precision geochronology. GSA Today 8, 1-8.

Bowring, S.A., Ramezani, J., and Grotzinger, J.P., 2003, High-precision U-Pb geochronology and the Cambrian-Precambrian boundary, in NUNA Conference 2003, New Frontiers in the Fourth Dimension: Generation, Calibration and Application of Geological Timescales, Mont Tremblant, Quebec. Geological Association of Canada.

Bradshaw, B.E., Rollet, N., Totterdell, J.M., Borissova, I., 2003. A revised structural framework for frontier basins on the southern and southwestern Australian continental margin. Geoscience Australia Record 2003/03.

Brasier, M.D., 1992a. Background to the Cambrian explosion. Journal of Geological Society London 149, 585–587.

Brasier M.D., 1992b. Towards a carbon isotope stratigraphy of the Cambrian System: potential of the Great Basin succession. In Hailwood, E.A., Kidd, R.B. (Eds.), High Resolution Stratigraphy. Geological Society Special Publication, 70, 341-350.

Brasier, M.D., Corfield, R.M., Derry, L.A., Rozanov, A.Yu., Zhuravlev, A.Yu., 1994. Multiple δ13C excursions spanning the Cambrian explosion to the Botoman crisis in Siberia. Geology 22, 455–458.

Brasier M.D., Hewitt R.A., 1979. Environmental setting of fossiliferous rocks from the uppermost Proterozoic - lower Cambrian of central England. Palaeogeography, Palaeoclimatology, Palaeoecology 27, 35-57.

Brasier, M., Shields, G., Kuleshov, V., and Zhegallo, E., 1996, Integrated chemo- and biostratigraphic calibration of early animal evolution: Neoproterozoic– Early Cambrian of southwest Mongolia. Geological Magazine 133, 445–485.

Brasier, M.D., Sukhov, S.S., 1998. The falling amplitude of carbon isotopic oscillations through the Lower to Middle Cambrian: northern Siberia data. Canadian Journal of Earth Sciences 35, 353–373.

Brock, G.A., Engelbrestsen M.J., Jago J.B., Kruse P.D., Laurie J.R., Shergold J.H., Shi G.R. and Sorauf, J.E., 2000. Palaeobiogeographic affinities of Australian Cambrian faunas. Association of Australasian Palaeontologists, Memoir 23, 1-61.

Brüning M., Sahling H., MacDonald I., Ding F., Bohrmann G., 2010. Origin, distribution, and alteration of asphalts at the Chapopote Knoll, southern Gulf of Mexico. Marine and Petroleum Geology 27, 1093–1106.

Buggisch, W., Keller, M., Lehnert, O., 2003. Carbon isotope record of Late Cambrian to Early Ordovician carbonates of the Argentine Precordillera. Palaeogeography, Palaeoclimatology, Palaeoecology 195, 357–373.

Calvert, D.E., Pedersen, T.F., 1993. Geochemistry of recent oxic and anoxic marine sediments: implications for the geological record. Marine Geology 113, 67–88.

Canfield, D. E., Farquhar, J., 2009. Animal evolution, bioturbation, and the sulfate concentration of the oceans. Proceedings of the National Academy of Sciences of the United States of America 106, 8123–8127.

Canfield, D. E., Poulton, S. W., Narbonne, G. M., 2007. Late-Neoproterozoic deep-ocean oxygenation and the rise of animal life. Science 315, 92–95.

Canfield, D.E., 1998. A new model for Proterozoic ocean chemistry. Nature 396, 450–453.

Canfield, D.E., 2005. The early history of atmospheric oxygen. Annual Reviews of Earth and Planetary Sciences 33, 1–36.

Canfield, D.E., Olesen, C.A., Raymond, P.C., 2006. Temperature and its control of isotope fractionation by a sulphate-reducing bacterium. Geochimica et Cosmochimica Acta 70, 548-561.

Carson M., 1994. The stratigraphy, sedimentology and thermal history of the Early Cambrian Heatherdale Shale, Fleurieu Peninsula. Unpublished Hons thesis, University of Adelaide.

Collins A. S., Pisarevsky S. A., 2005. Amalgamating eastern Gondwana: The evolution of the Circum-Indian Orogens. Earth-Science Reviews 71, 229-270.

Collins, A.S., Kröner, A., Fitzsimons, I.C.W., Razakamanana, T., 2003. Detrital footprint of the Mozambique ocean: U–Pb SHRIMP and Pb evaporation zircon geochronology of metasedimentary gneisses in eastern Madagascar. Tectonophysics 375, 77–99.

Cooper, J.A., Jenkins, R.J, Compston, W., Williams, I.S., 1992. Ion-probe zircon dating of amid-Early Cambrian tuff in South Australia. Journal of the Geological Society of London 149, 185–192.

Currie T.J., Alexander R., Kagi R.I., 1992. Coastal bitumens from Western Australia – long distance transport from Western Australia, Organic Geochemistry 18, 595–601.

Daily, B., Forbes, B.G., 1969. Notes on the Proterozoic and Cambrian, southern and central Flinders Ranges, South Australia. In: Daily, B. (Ed.), Geological Excursions Handbook. ANZAAS, 49–54.

Daily, B., Milnes A.R., 1971. Stratigraphic notes on Lower Cambrian fossiliferous metasediments between Campbell Creek and Tunkalilla Beach in the type section of the Kanmantoo Group, Fleurieu Peninsula, South Australia. Transactions of the Royal Society of South Australia 95, 199–214.

Daily, B., Milnes A.R., 1973. Stratigraphy, structure and metamorphism of the Kanmantoo Group (Cambrian) in its type section east of Tunkalilla Beach, South Australia. Transactions of the Royal Society of South Australia 97, 199–214.

Daily, B., Milnes, A.R., Twidale, C.R., Bourne, J.A., 1979. Geology and Geomorphology. In: Tyler, M.J., Ling, J.K., Twidale, C.R. (Eds.), Natural History of Kangaroo Island. Royal Society of South Australia, Adelaide, 1–38.

Debrenne F., Gravestock D., 1990. Archaeocyatha from the Sellick Hill Formation and Fork Tree Limestone on Fleurieu Peninsula, South Australia. In: Jago J.B., Moore P.J. (Eds), The evolution of a late Precambrian-early Palaeozoic rift complex: The Adelaide Geosyncline. Geological Society of. Australia, Special. Publication 16, 290-309.

Derry, L.A., Kaufman, A.J., Jacobsen, S., 1992. Sedimentary cycling and environmental change in the Late Proterozoic: evidence from stable and radiogenic isotopes. Geochimica et Cosmochimica Acta 56, 1317–1329.

Dowling, L.M., Boreham, C.J., Hope, J.M., Murray, A.P., Summons, R.E., 1995. Carbon isotopic composition of hydrocarbons in the ocean-transported bitumens from the coastline of Australia. Organic Geochemistry 23, 729–737.

Edwards D., McKirdy D.M., Summons R.E., 1998. Enigmatic asphaltites from the southern Australian margin: molecular and carbon isotopic composition. PESA Journal 26, 106–130.

Edwards, D.S., Struckmeyer, H.I.M., Bradshaw, M.T., Skinner, J.E., 1999. Geochemical characteristics of Australia's Southern Margin petroleum systems. The Australian Petroleum Production and Exploration Association (APPEA) Journal 39, 297-321.

Erwin, D.H., Laflamme, M., Tweedt, S.M. Sperling, E.A., Pisani, D., Peterson, K.J., 2011. The Cambrian conundrum: early divergence and later ecological success in the early history of animals. Science 334, 1091-1097.

Espurt, N., Callot, J., Totterdell, J., Struckmeyer, H., Vially, R., 2009. Interactions between continental breakup dynamics and large-scale delta system evolution: Insights from the Cretaceous Ceduna delta system, Bight Basin, Southern Australian margin, Tectonics 28, 1-26.

Fike D.A., Grotzinger J.P., Pratt L.M., Summons R.E., 2006. Oxidation of the Ediacaran Ocean. Nature 444, 744–747.

Fike, D.A., Grotzinger, J.P., 2008. A paired sulfate-pyrite $\delta^{34}S$ approach to understanding the evolution of the Ediacaran–Cambrian sulfur cycle. Geochimica et Cosmochimica Acta 72, 2636–2648.

Flöttmann, T., Haines, P.W., Cockshell C.D., Preiss, W. V., 1998. Reassessment of the seismic stratigraphy of the Early Palaeozoic Stansbury Basin, Gulf St Vincent, South Australia. Australian Journal of Earth Sciences 45, 547-557.

Flöttmann, T., James, P., 1997. Influence of basin architecture on the style of inversion and fold-thrust belt tectonics - the southern Adelaide Fold-Thrust Belt. South Australia by Journal Of Structural Geology 19, 1093-1110.

Flöttmann, T., James, P.R., Menpes, R., Cesare, P., Twining, M., Fairclough, M., Randabell, J., Marshak, S., 1995. The structure of Kangaroo Island (South Australia): strain and kinematic partitioning during Delamerian basin and platform reactivation. Australian Journal of Earth Sciences 42, 35-49.

Foden, J. D., Turner, S. P., Morrison, R., 1990. The tectonic implications of the Delamerian magmatism in South Australia and western Victoria. In: Jago J. B., Moore, P.S., (Eds.), The evolution of a Late Precambrian–Early Palaeozoic Rift Complex: The Adelaide Geosyncline. Geological Society of Australia Special Publication 16, 483–495.

Foden, J.D., Elburg, M. A., Dougherty-Page, J., Burtt, A., 2006. The timing and duration of the Delamerian Orogeny: correlation with the Ross Orogen and implications for Gondwana assembly. Journal of Geology 114, 189–210.

Foden, J.D., Sandiford, M., Dougherty-Page, J., Williams, I., 1999. The geochemistry and geochronology of the Rathjen Gneiss: implications for the early techtonic evolution of the Delamerian Orogen. Australian Journal of Earth Sciences 46 (3), 377-389.

Gatehouse, C.J., Jago, J.B., Clough, B.J., McCulloch, A.J., 1993. The Early Cambrian volcanics from Red Creek, Eastern Mt Lofty Ranges, South Australia. Transactions of the Royal Society of South Australia 117, 57-66.

Gehling J.G., Jago J.B., Paterson J.R., García-Bellido D.C., Edgecombe G.D., 2011. The geological context of the lower Cambrian (Series 2) Emu Bay Shale Lagerstätte and adjacent stratigraphic units, Kangaroo Island, South Australia. Australian Journal of Earth Sciences 58, 243-257.

Glumac, B., Walker, K.R., 1998. A late Cambrian positive carbon-isotope excursion in the southern Appalachians: relation to biostratigraphy, sequence stratigraphy, environments of deposition, and diagenesis. Journal of Sedimentary Research 88, 1212–1222.

Goldberg, T., Strauss, H., Guo, Q., Liu, C., 2007. Reconstructing marine redox conditions for the early Cambrian Yangtze Platform: Evidence from biogenic sulphur and organic carbon isotopes. Palaeogeography, Palaeoclimatology, Palaeoecology 254, 175–193.

Gorjan, P., Walter, M.R., Swart, R., 2003. Global Neoproterozoic (Sturtian) post-glacial sulfide-sulfur isotope anomaly recognised in Namibia. Journal of African Earth Sciences 36, 89–98

Gradstein, F., Ogg, J.G., Smith, A.G., Bleeker, W., Lourens, L.J., 2004. A new geological time scale, with special reference to Precambrian and Neogene. Episodes 27, 83–99.

Gravestock, D.I., 1984. Archaeocyatha from lower parts of the Lower Cambrian carbonate sequence in South Australia. Memoir of the Association of Australian Palaeontologists 2, 1-139.

Gravestock D.I., 1995. Chapter 7 Early and Middle Palaeozoic. In Drexel J.F., Preiss, W.V. and Parker, A.J., The Geology of South Australia. Vol. 2, The Phanerozoic. South Australia Geological Survey, Bulletin 54

Gravestock, D.I., 2002. Chapter 5 Geological setting and structural history. In Morton J.G.G., Drexel, J.F. (Eds.) Petroluem Geology of South Australia Volume 3, http://www.pir.sa.gov.au/petroleum/access_to_data/petroleum_publications/petroleum_geology_of_south_australia/vol_3_-_officer_basin_downsampled

Gravestock, D. I., Benbow, M.C., Gatehouse, C.G., Krieg, G.W., 1995. Early and Middle Palaeozoic –Eastern Officer Basin. In: Drexel J. F., Preiss W. V. (Eds.), The geology of South Australia, Volume 2, the Phanerozoic, v. 54: Adelaide, South Australia Geological Society, 35-41.

Gravestock, D. I., Gatehouse, C.G., 1995. Early and Middle Palaeozoic – Stansbury Basin. In: Drexel J. F., Preiss W. V. (Eds.), The geology of South Australia, Volume 2, the Phanerozoic, v. 54: Adelaide, South Australia Geological Society, 5-19.

Gravestock, D. I., Cowley, W. M., 1995. Early and Middle Palaeozoic -Arrowie Basin. In: Drexel J. F., Preiss W. V. (Eds.), The geology of South Australia, Volume 2, the Phanerozoic, v. 54: Adelaide, South Australia Geological Society, 20-31.

Gravestock, D.I. Morton J.G.G., 2002. Chapter 8 Source rock distribution and quality. In Morton J.G.G., Drexel, J.F. (Eds.) Petroluem Geology of South Australia Volume 3, http://www.pir.sa.gov.au/petroleum/access_to_data/petroleum_publications/petroleum_geology_of_south_australia/vol_3_-_officer_basin_downsampled

Gravestock, D.I. Morton J.G.G., Zang, W-L., 2002. Chapter 7 Biostratigraphy and correlation. In Morton J.G.G., Drexel, J.F. (Eds.) Petroluem Geology of South Australia Volume 3, http://www.pir.sa.gov.au/petroleum/access_to_data/petroleum_publications/petroleum_geology_of_south_australia/vol_3_-_officer_basin_downsampled

Gravestock, D.I., Shergold, J.H., 2001. Australian Early and Middle Cambrian sequence biostratigraphy with implications for species diversity and correlation. in: Zhuravlev, A.Y., Riding, R. (Eds.), The Ecology of the Cambrian Radiation. Columbia University Press, 105–136.

***Grotzinger, J.P., Bowring, S.A., Saylor, B.Z., and Kaufman, A.J., 1995, Biostratigraphic and geochronologic constraints on early animal evolution. Science 270, 598–604.

Guo Q., Shields G.A., Liu C., Strauss H., Zhu M., Pi D., Goldberg T., Yang X., 2007a. Trace element chemostratigraphy of two Ediacaran–Cambrian successions in South China: Implications for organosedimentary metal enrichment and silicification in the Early Cambrian. Palaeogeography, Palaeoclimatology, Palaeoecology 254, 194-216.

Guo, Q., Strauss, H., Liu, C., Goldberg, T., Zhu, M., Pi, D., Heubeck, C., Vernhet, E., Yang, X., Fu, P., 2007b. Carbon isotopic evolution of the terminal Neoproterozoic and early Cambrian: Evidence from the Yangtze Platform, South China. Palaeogeography, Palaeoclimatology, Palaeoecology 254, 140–157.

Guo Q., Strauss H., Liu C., Zhaod Y., Yang X., Peng J., Yang H., 2010. A negative carbon isotope excursion defines the boundary from Cambrian Series 2 to Cambrian Series 3 on the Yangtze Platform, South China. Palaeogeography, Palaeoclimatology, Palaeoecology 285, 143-151.

Guo, Q., Strauss, H., Liu, C., Zhao, Y., Pi, D., Fu, P., Zhu, L., Yuan, J., 2005. Carbon and oxygen isotopic composition of Lower to Middle Cambrian sediments at Taijiang, Guizhou Province, China. Geological Magazine 142, 723–733.

Haines, P.W. & Flottman, T., 1998, Delamerian Orogeny and potential foreland sedimentation: a review of age and stratigraphic constraints. Australian Journal of Earth Sciences 45, 559-570.

Haines, P.W., Flöttmann, T., Gum, J.C., Jago, J.B., Gatehouse, C.G., 1996. Integrated approach to the reinterpretation of the Cambrian Kanmantoo Group type section, South Australia. Geological Society of Australia Abstracts 41, 77.

Haines, P.W., Jago, J.B., Gum, J.C., 2001. Turbidite deposition in the Cambrian Kanmantoo Group, South Australia. Australian Journal of Earth Sciences 48, 465–478.

Haines,P.W., Turner, S.P., Foden, J., Jago, J., 2009. Isotopic and geochemical characterization of the Cambrian Kanmantoo Group, South Australia: implications for stratigraphy and provenance. Australian Journal of Earth Sciences 56, 1095-1110.

Halverson G. P., Wade B. P., Hurtgen M. T., Barovich K. M., 2010. Neoproterozoic Chemostratigraphy. Precambrian Research 182, 239–412.

Halverson G.P., Hurtgen M.T., Porter S.M., Collins A.S., 2009. Neoproterozoic-Cambrian biogeochemical evolution. In: Gaucher C., Sial A.N., Halverson G.P., Frimmel H.E. (Eds.), Developments in Precambrian Geology 16, 351–365.

Halverson, G. P. and Hurtgen, M. T., 2007. Ediacaran growth of the marine sulfate reservoir. Earth and Planetary Science Letters 263, 32–44.

Halverson, G.P., Hoffman, P.F., Schrag, D.P., Kaufman, J.A., 2002. A major perturbation of the carbon cycle before the Ghaub glaciation (Neoproterozoic) in Namibia: prelude to snowball Earth? Geochemistry, Geophysics, Geosystems 3, doi:10.1029/2001GC000244.

Halverson, G.P., Hoffman, P.F., Schrag, D.P., Maloof, A.C., Rice, A.H., 2005. Towards a Neoproterozoic composite carbon-isotope record. Geological SocIety of American Bulletin 117, 1181–1207.

Hatch J.R., Leventhal J.S., 1992. Relationship between inferred redox potential of the depositional environment and geochemistry of the Upper Pennsylvanian (Missourian) Stark Shale Member of the Dennis Limestone, Wabaunsee County, Kansas, U.S.A. Chemical Geology 99, 1-3, 10, 65-82.

Hayes J.M., Kaplan I.R., Wedeking K.W., 1983. Precambrian organic geochemistry - preservation of the record. In: Schopf J.W. (Ed.), Earth's Earliest Biosphere, Its Origin and Evolution. Princeton University Press, New Jersey, 93–134.

Hayes, J.M., Strauss, H., Kaufman, A.J., 1999. The abundance of ^{13}C in marine organic matter and isotopic fractionation in the global biogeochemical cycle of carbon during the past 800 Ma. Chemical Geology 161, 103–125.

Hillis, R.D. and Reynolds, S.D., 2003. In Situ Stress Field, Fault Reactivation and Seal Integrity in the Bight Basin. South Australia. Department of Primary Industries and Resources. Report Book,.2003/2.

Howley R. A., Jiang G., 2010. The Cambrian Drumian carbon isotope excursion (DICE) in the Great Basin, western United States. Palaeogeography, Palaeoclimatology, Palaeoecology 296, 138-150.

Hurtgen, M.T., Arthur, M.A., Halverson, G.P., 2005. Neoproterozoic sulfur isotopes, the evolution of microbial sulfur species, and the burial efficiency of sulfide as sedimentary sulfide. Geology 33, 41–44.

Hurtgen, M.T., Arthur, M.A., Suits, N.S., Kaufman, A.J., 2002. The sulfur isotopic composition of Neoproterozoic seawater sulfate: implications for a snowball Earth? Earth and Planetary Science Letters 203, 413–430.

Ireland, T.R., Flöttmann T., Fanning, C.M., Gibson, G.M., Preiss, W.V., 1998. Development of the Early Paleozoic Pacific margin of Gondwana from detrital zircon ages across the Delamerian Orogen. Geology 26, 243–246.

Jago, J.B., Daily, B., von der Borch, C.C., Cernovskis, A., Saunders, N., 1984. First reported trilobites from the Lower Cambrian Normanville Group, Fleurieu Peninsula, South Australia. Royal Society of South Australia. Transactions 108, 207-211.

Jago, J.B., Dyson, I.A., Gatehouse, C.G., 1994. The nature of the sequence boundary between the Normanville and Kanmantoo Groups on Fleurieu Peninsula, South Australia. Australian Journal of Earth Sciences 41, 445-453.

Jago, J.B., Gatehouse C.G., 2009. The type section of the Cambrian Backstairs Passage Formation, Kanmantoo Group, South Australia. Transactions of the Royal Society of South Australia 133, 150–163.

Jago, J.B., Gehling, J.G., Paterson, J.R., Brock, G.A. & Zang, W.L., 2012. Cambrian stratigraphy and biostratigraphy and biostratigraphy of the Flinders Ranges and the north coast of Kangaroo Island, South Australia. Episodes 35 (in press)

Jago, J.B., Gum, J.C., Burtt, A.C., Haines, P.W., 2003. Stratigraphy of the Kanmantoo Group: a critical element of the Adelaide Fold Belt and the Palaeo-Pacific plate margin, Eastern Gondwana. Australian Journal of Earth Sciences 50, 343–363.

Jago, J.B., Lin, T.R. & Dunster, J.N., 2002a. A new species of the trilobite Abadiella from the Lower Cambrian of the eastern Officer Basin, South Australia. Acta Palaeontologica Sinica 41, 428-433.

Jago J.B., Sun X., Zang W., 2002b. Correlation within early Palaeozoic basins of eastern South Australia. PIRSA Report Book 2002/033.

Jago, J.B., Zang, W.L., Sun, X.W., Brock, G.A., Paterson, J.R., Skovsted, C.R., 2006. A review of the Cambrian biostratigraphy of South Australia. Palaeoworld 15, 406–423.

James N.P., Gravestock D.I., 1990. Lower Cambrian shelf and shelf margin buildups, Flinders Ranges, South Australia. Sedimentology 37, 455–480.

Jenkins, R. J.; Cooper, J. C.; and Compston, W. 2002. Age and biostratigraphy of Early Cambrian tuffs from SE Australia and southern China. Journal of the Geological Society of London 159, 645–658.

Jenkins, R.J.F., Hasenohr, P., 1989. Trilobites and their trails in a black shale: Early Cambrian of the Fleurieu Peninsula, South Australia. Transactions of the Royal Society of South Australia 113, 195-203.

Jenkyns, H.C., 2010. Geochemistry of oceanic anoxic events. Geochemistry, Geophysics, Geosystems 11, 1-30.

Jiang, S.Y., Zhao, H.X., Chen, Y.Q., Yang, T., Yang, J.H., Ling, H.F., 2007. Trace and rare earth element geochemistry of phosphate nodules from the lower Cambrian black shale sequence in the Mufu Mountain of Nanjing, Jiangsu province, China. Chemical Geology 244, 584–604.

Johnston, D.T., Farquhar, J., Canfield, D.E., 2007. Sulfur isotope insight into microbial sulphate reduction: When microbes meet models. Geochimica et Cosmochimica Acta 71, 3929-3947.

Jones, B., Manning, D.A.C., 1994. Comparison of geochemical indices used for the interpretation of paleoredox conditions in ancient sediments. Chemical Geology 111, 111–119.

Kamali, M.R., 1995. Sedimentology and petroleum geochemistry of the Ouldburra Formation, eastern Officer Basin, Australia. Ph.D. thesis, University of Adelaide (unpublished)

Kelsey, D.E., Wade, B.P., Collins, A.S., Hand, M., Sealing, C.R., Netting, A. 2008. Discovery of a Neoproterozoic basin in the Prydz belt in East Antarctica and its implications for Gondwana assembly and ultrahigh temperature metamorphism. Precambrian Research 161, 3-4, 355-388

Kennedy, M.J., Pevear, D.R., Hill, R.J., 2002. Mineral Surface Control of Organic Carbon in Black Shale. Science 295, 657-660.

Kennedy, M.J., Wagner, T., 2011. Clay mineral continental amplifier for marine carbon sequestration in a greenhouse ocean. Proceedings of the National Academy of Sciences of the United States of America 108, 9776-9781.

Kidder, D.L., Krishnaswamy, R., Mapes, R.H., 2003. Elemental mobility in phosphatic shales during concretion growth and implications for provenance analysis. Chemical Geology 198 (3–4), 335–353.

Kimura H., Watanabe Y., 2001. Oceanic anoxia at the Precambrian-cambrian boundary. Geology 29, 11, 995-998.

Knoll, A., Hayes, J., Kaufman, A., Swett, K., Lambert, I., 1986. Secular variation in carbon isotope ratios from upper Proterozoic successions of Svalbard and east Greenland. Nature 321, 832–837.

Kouchinsky, A., Bengtson, S., Missarzhevsky, V. V., Pelechaty, S., Torssander, P. & Val'kov, A. K. 2001. Carbon isotope stratigraphy and the problem of a pre-Tommotian Stage in Siberia. Geological Magazine 138, 387–96.

Kouchinsky, A., Bengtson, S., Runnegar, B., Skovsted, C., Steiner, M., Vendrasco, M., 2012 Chronology of early Cambrian biomineralization. Geological Magazine 149**,** 221–251.

Kouchinsky, A.,Bengtson, S.,Pavlov, V.,Runnegar, B., Val'kov, A. K. & Young, E. 2005. Pre-Tommotian age of the lower Pestrotsvet Formation in the Selinde section on the Siberian platform: carbon isotopic evidence. Geological Magazine 142, 319–25.

Kruse, P.D., 1991. Cyanobacterial-archaeocyathan-radiocyathan bioherms in the Wirrealpa Limestone of South Australia. Canadian Journal of Earth Sciences 28, 601-615.

Landing, E., Bowring, S.A., Davidek, K., Westrop, S.R., Geyer, G., Heldmaier, W., 1998, Duration of the Early Cambrian: U-Pb ages of volcanic ashes from Avalon and Gondwana. Canadian Journal of Earth Sciences 35, 329–338.

Landing, E., Peng, S.C., Babcock, L.E., Geyer, G., Moczydlowska-Vidal, M. 2007. Global standard names for the lowermost Cambrian series and stage. Episodes 30, 287-289.

Lehmann, B., Nägler, T.F., Holland, H.D., Wille, M., Mao, J., Pan, J., Dulski, P., 2007. Highly metalliferous carbonaceous shale and early Cambrian seawater. Geology 35, 403–406.

Li Z.X., Bogdanova S.V., Collins A.S., Davidson A., De Waele B., Fitzsimons R.E., Ernst I.C.W., Fuck R.A., Gladkochub D.P., Jacobs J., Karlstrom K.E., Lu S., Natapov L.M., Pease V., Pisarevsky S.A., Thrane K., Vernikovsky V., 2008, Assembly, configuration, and break-up history of Rodinia: A synthesis. Precambrian Research 160, 179-210.

Lindsay J.F., Kruse P.D., Green O.R., Hawkins E., Brasier M.D., Cartlidgee J., Corfield R.M., 2005. The Neoproterozoic–Cambrian record in Australia: A stable isotope study. Precambrian Research 15, 113-133.

Lindsay, J.F., 2002. Supersequences, superbasins, supercontinents - evidence from the Neoproterozoic basins of Central Australia. Basin Research 14, 204–223.

Logan, G.A., Jones, A.T., Kennard, J.M., Ryan, G.J., Rollet, N., 2010. Australian offshore natural hydrocarbon seepage studies, a review and re-evaluation. Marine and Petroleum Geology 27, 26–45.

Machel, H.G., 1997. Recrystallization versus neomorphism, and the concept of 'significant recrystallization' in dolomite research. Sedimentary Geology 113, 161–168.

Machel, H.G., 2005. Dolomites. in Selley, R.C., Cocks R., Pilmer. I.R. (Eds.): Encyclopedia of Geology, Elsevier, 79-94

Magartiz M., Holser W.T. and Kirschvink J.L., 1986, Carbon isotope events across the Precambrian/Cambrian boundary on the Siberian Platform. Nature 320, 258-259.

Maloof, A.C., Porter, S.M., Moore, J.L., Dudas, F.O., Bowring, S.A., Higgins, J.A., Fike, D.A., Eddy, M.P., 2010a. The earliest Cambrian record of animals and ocean geochemical change. Geological Society of America Bulletin 122, 1731–1774.

Maloof, A.C., Ramezani, J., Bowring, S.A.,, Fike, D.A.,, Porter, S.M.,, Mazouad, M., 2010b. Constraints on early Cambrian carbon cycling from the duration of the Nemakit-Daldynian–Tommotian boundary δ13C shift, Morocco. Geology 38; 623–626.

Maloof, A.C., Schrag, D.P., Crowley, J.L., & Bowring, S.A., 2005, An expanded record of Early Cambrian carbon cycling from the Anti-Atlas Margin, Morocco; Canadian Journal of Earth Sciences 42, 2195-2216.

Mancktelow, N.S., 1990. The structure of the southern Adelaide Fold Belt, South Australia. In: Jago, J.B., Moore, P.S. (Eds.), The Evolution of a late Precambrian-Early Palaeozoic Rift Complex: The Adelaide Geosyncline, Geological Society of Australia Special Publication 16, 369-395

Mason, S., 2001. Petroleum generation and expulsion from pressure solution structures in teh Cambrian Ouldburra Formation, Officer Basin. Unpublished Honours Thesis, University of Adelaide.

McGowran, B., Li, Q., Cann, J., Padley, D., McKirdy, D. M., Shafik, S., 1997. Biogeographic impact of the Leeuwin Current in southern Australia since the late middle Eocene. Palaeogeography, Palaeoclimatology, Palaeoecology 136, 19-40.

McKirdy, D.M., 1984a. Coastal bitumens and potential source rocks in the western Otway Basin, South Australia and Victoria. AMDEL Report F5840/84 for Australian Aquitaine Petroleum Pty Ltd. and Ultramar Australia Inc.

McKirdy, D.M., 1984b. Coastal bitumen and potential source rocks, Duntroon Basin. South Australia. AMDEL Report F5769/84 for Getty Oil Development Co. Ltd,

McKirdy, D.M. 1994. Biomarker geochemistry of the Early Cambrian oil show in Wilkatana-1: implications for oil generation in the Arrowie and Stansbury Basins. PESA Journal 22, 3–17.

McKirdy, D.M., Burgess, J.M., Lemon, N.M., Yu, X., Cooper, A.M., Gostin, V.A., Jenkins, R.J.F., Both, R.A., 2001. A chemostratigraphic overview of the late Cryogenian interglacial sequence in the Adelaide Fold-Thrust Belt, South Australia. Precambrian Research 106, 149-186.

McKirdy, D.M., Cox, R.E., O'Leary, T., 1986. Geochemical analysis of oils and condensate from the Amadeus Basin, central Australia. AMDEL Report F6451/86 for Elf Aquitaine Petroleum Australia Pty Limited (unpublished).

McKirdy, D.M., Hall, P.A., Nedin C., Halverson, G.P., Michaelsen, B.H., Jago, J.B., Gehling, J.G., Jenkins, R.J.F., 2011. Palaeoredox status and thermal alteration of the lower Cambrian (Series 2) Emu Bay Shale Lagerstätte, South Australia. Australian Journal of Earth Sciences 58, 259-272.

McKirdy, D. M., Horvath, Z., 1976. Geochemistry and significance of coastal bitumen from southern and northern Australia. Australian Petroleum Exploration Association Journal 16, 123 136.

McKirdy, D.M., Michaelsen, B.H., Yu, X., 1996. Thermal maturity and biomarker geochemistry of the Early Cambrian Kulpara Formation, Stansbury Basin. Report for Canyon (Australia) Pty Ltd. (unpublished).

McKirdy D.M., Powell T.G., 1974. Metamorphic alteration of carbon isotopic composition in ancient sedimentary organic matter: new evidence from Australia and South Africa. Geology 2, 591–595.

McKirdy, D.M., Summons, R.E., Padley, D., Serafini, K.M., Boreham, C.J., Struckmeyer, H.I.M., 1994. Molecular fossils in coastal bitumens from southern Australia: signatures of precursor biota and source rock environments. Organic Geochemistry 21, 265–286.

McLennan S. M., Taylor S. R., 1987. Crustal evolution: Comments on 'The Archean-Proterozoic transition: Evidence from the geochemistry of metasedimentary rocks from Guyana And Montana" By A.K. Gibbs, C.W. Montgomery, P.A. O'day and E.A. Erslev. Geochimica et Cosmochimica Acta 52, 785-787.

Mclennan, S.M., 1989. Rare earth elements in sedimentary rocks: Influence of provenance and sedimentary processes. Reviews in Mineralogy and Geochemistry.21, 169–200.

Meert J.G., Lieberman B.S., 2008. The Neoproterozoic assembly of Gondwana and its relationship to the Ediacaran–Cambrian radiation. Gondwana Research 14, 1-2, 5-21.

Melchin, M.J., Holmden, C., 2006. Carbon isotope chemostratigraphy in Arctic Canada: Sea-level forcing of carbonate platform weathering and implications for Hirnantian global correlation. *Palaeogeography, palaeoclimatology, palaeoecology* 234, 186-200.

Montanez I.P., Osleger D.A., Banner J.I., Mack L.E. and Musgrove M., 2000, Evolution of the Sr and C Isotope Composition of Cambrian Oceans. GSA Today, 10, 1-7

Morton J.G.G., 2002 Chapter 6 Lithostratigraphy and Environments of Deposition. In Morton J.G.G., Drexel, J.F. (Eds.) Petroluem Geology of South Australia Volume 3, http://www.pir.sa.gov.au/petroleum/access_to_data/petroleum_publications/petroleum_geology_of_south_australia/vol_3_-_officer_basin_downsampled

Muruyama, S., Santosh, M., 2008. Models on Snowball Earth and Cambrian explosion: a synopsis. Gondwana Research 14, 22-32.

Myrow, P.M., Hughes, N.C., Goodge, J.W., Fanning, C.M., Williams I.S., Peng, S., Bhargava, O.N., Parcha, S.K., Pogue, K.R., 2010. Extraordinary transport and mixing of sediment across Himalayan central Gondwana during the Cambrian–Ordovician. Geological Society of America Bulletin 122; 1660–1670.

Naqvi, S.M., Uday Raj, B., Subba Rao, D.V., Manikyamba, C., Nirmal Charan, S., Balaram, V., Srinivasa Sarma, D., 2002. Geology and geochemistry of arenite–quartzwacke from the Late Archaean Sandur schist belt - implications for provenance and accretion processes. Precambrian research 114 (3-4), 177-197

Nedin C., 1995a. The Emu Bay Shale, a Lower Cambrian fossil Lagerstätten, Kangaroo Island, South Australia. Memoirs of the Australasian Association of Palaeontologists 18, 31–40.

Nedin C., 1995b. The palaeontology and palaeoenvironment of the Early Cambrian Emu Bay Shale, Kangaroo Island,. South Australia. Unpublished PhD thesis, University of Adelaide.

Och, L.M., Shields-Zhou, G.A., 2012. The Neoproterozoic oxygenation event: Environmental perturbations and biogeochemical cycling. Earth-Science Reviews 110, 26–57.

Och, L.M., Shields-Zhou, G.A., Poulton, S.W., Manning, C., Thirlwall, M.F., Li, D., Chen, X., Ling, H., Osborn, T., Cremonese, L., 2012. Redox changes in Early Cambrian black shales at Xiaotan section, Yunnan Province, South China. Precambrian Research doi:10.1016/j.precamres.2011.10.005

Oehlert, A.M., Lamb-Wozniak, K.A., Devlin, Q.B., Mackenzie, G.J., Reijmer, J.J.G., Swart, P.K., 2012. The stable carbon isotopic composition of organic material in platform derived sediments: implications for reconstructing the global carbon cycle. Sedimentology 59, 319–335

Ogg, J.G., Ogg, G. & Gradstein, F.M., 2008. The concise Geologic Time Scale. Cambridge University Press, Cambridge, 177p.

Ozimic, S., Nicholas, E., Pain, L., 1987. Australian Petroleum Accumulations Report 2 Bass Basin, Tasmania and Victoria. Department of Resources and Energy Bureau of Mineral Resources, Geology and Geophysics

Padley, D., 1996. Petroleum geochemistry of the Otway Basin and the significance of coastal bitumen strandings on adjacent southern Australian beaches. PhD Thesis, University of Adelaide.

Padley, D., McKirdy, D.M., Murray, A.P., Summons, R.E., 1993. Oil strandings on the beaches of Southern Australia: origins from natural seepage and shipping. in: Øygard, K. (Ed.) Poster Sessions from the 16th International Meeting on Organic Geochemistry 20-24 September 1993, Stavanger, Norway, 660-663.

Palmowski, D., Hill, K.C., Hoffman, N., 2004. Structural-stratigraphic styles and evolution of the offshore Otway Basin - a structural seismic analysis. in: Boult, P.J.,

Johns, D.R., Lang, S.C. (Eds.) Eastern Australasian Basins Symposium II, Petroleum Exploration Society of Australia, Special Publication, 75-96.

Pancost, R.D., Crawford, N., Magness, S., Turner, A., Jenkyns, H.C., Maxwell, J.R., 2005. Further evidence for the development of photic-zone euxinic conditions during Mesozoic oceanic anoxic events. Journal of the Geological Society 161, 353-364.

Paterson, J.R, Jago, J.B., Gehling, J.G., García-Bellido, D.C., Edgecombe, G.D., Lee, M.S.Y., 2008. Early Cambrian arthropods from the Emu Bay Shale Lagerstätte, South Australia. In: Rábano, I., Gozalo, R. & García-Bellido, D. (Eds.), Advances in Trilobite Research. Cuadernos del Museo Geominero, 9, Instituto Geológico y Minero de España, Madrid, pp. 319–325.

Paterson, J.R., 2005. Revision of *Discomesites* and *Estaingia* (Trilobita) from the Lower Cambrian Cymbric Vale Formation, western N.S.W.: taxonomic, biostratigraphic and biogeographic implications. Proceedings of the Linnean Society of New South Wales 126, 81–93.

Peng, S.C., Babcock, L.E., Robison, R.A., Lin, H.L., Rees, M.N., Saltzman, M.R., 2004. Global Standard Stratotype-section and Point (GSSP) of the Furongian Series and Paibian Stage (Cambrian). Lethaia 37, 365–379.

Peng, S.C., Babcock, L.E., Zuo, J.X, Lin, H.L., Zhu, X.J.,Yang, X.F., Robison, R.A., Qi, Y.P., Bagnoli, G., 2006. Proposed GSSP for the base of Cambrian Stage 7, coinciding with the first appearance of *Lejopyge laevigata*, Hunan, China. Palaeoworld, 15: 367-383.

Peng, S., Babcock, L.E., Zuo, J., Lin, H., Zhu, X., Yang, X., Robison, R.A., Qi, Y., Bagnoli, G., Chen, Y. 2009 The Global Boundary Stratotype Section and Point (GSSP) of the Guzhangian Stage (Cambrian) in the Wuling Mountains, Northwestern Hunan, China. Episodes 32, 41-55.

Peters K.E., Walters C.C., Moldowan J.M., 2005. The Biomarker Guide, Volume 2, Biomarkers and Isotopes in Petroleum Systems and Earth History. Cambridge University Press.

Peters, K.E., Moldowan, J.M., 1993. The Biomarker Guide - Interpreting Molecular Fossils in Sediments and Petroleum. Prentice-Hall, New Jersey.

Pi, D.H., Liub, C.Q., Shields-Zhou, G.A., Jianga, S.Y., 2011. Trace and rare earth element geochemistry of black shale and kerogen in the early Cambrian Niutitang Formation in Guizhou province, South China: Constraints for redox environments and origin of metal enrichments. Precambrian Research. doi:10.1016/j.precamres.2011.07.004

Piper, D.Z., Calvert, S.E., 2009. A marine biogeochemical perspective on black shale deposition. Earth-Science Reviews 95, 63–96.

Porter, S.M. 2007. Seawater chemistry and early carbonate biomineralization. Science 316, 1302.

Powell W.G., 2009. Comparison of geochemical and distinctive mineralogical features associated with the Kinzers and Burgess Shale formations and their associated units. Palaeogeography, Palaeoclimatology, Palaeoecology 277, 127–140.

Powell W.G., Johnston P.A., Collom C.J., 2003. Geochemical evidence for oxygenated bottom waters during deposition of fossiliferous strata of the Burgess Shale Formation. Palaeogeography, Palaeoclimatology, Palaeoecology 201, 249-268.

Powell, C.M., Preiss, W.V., Gatehouse, C.G., Krapez, B., Li, Z.X., 1994. South Australian record of a Rodinian epi-continental basin and its mid-Neoproterozoic breakup (~700Ma) to form the Palaeo-pacific Ocean. Tectonophysics 237, 113-140.

Preiss, W.V., 1995. Delamerian Orogeny. In: Drexel J. F., Preiss W. V. (Eds.), The Geology of South Australia, Vol. 2: The Phanerozoic. Geological Survey of South Australia Bulletin 54, 45-60.

Preiss, W.V., 2000. The Adelaide Geosyncline of South Australia and its significance in Neoproterozoic continental reconstructions. Precambrian Research 100, 21–63.

Railsback, L.B., Holland, S.M., Hunter, D.M., Jordan, E.M., Díaz, J.R., Crowe, D.E., 2003. Controls on geochemical expression of subaerial exposure in Ordovician limestones from the Nashville Dome, Tennessee, U.S.A. Journal of Sedimentary Research 73, 790–805.

Saltzman M.R., Ripperdan R.L., Brasier M.D., Lohmann K.C., Robinson R.A., Chang W.T., Peng S., Ergaliev E.K. and Runnegar B.R., 2000, A global carbon isotope excursion (SPICE) during the Late Cambrian: relation to trilobite extinctions, organic-matter burial and sea level. Palaeogeography, Palaeoclimatology, Palaeoecology 160, 211–223.

Saltzman, M.R., 2005. Phosphorus, nitrogen, and the redox evolution of the Paleozoic oceans. Geology 33, 573–576.

Saltzman, M.R., Runnegar, B., Lohmann, K.C., 1998. Carbon isotope stratigraphy of Upper Cambrian (Steptoean Stage) sequences of the eastern Great Basin: record of a global oceanographic event. Geological Society of America Bulletin 110, 285–297.

Saltzman, M.R., Young, S.A., Kump, L.R., Gill, B.C., Lyons, T.W., Runnegar, B., 2011 Pulse of atmospheric oxygen during the late Cambrian. Proceedings of the National Academy of Sciences of the United States of America 108, 3876–3881.

Schröder, S., Grotzinger, J.P., 2007. Evidence for anoxia at the Ediacaran-Cambrian boundary: the record of redox-sensitive trace elements and rare earth elements in Oman. Journal of the Geological Society of London 164, 175–187.

Scott, C., Lyons, T.W., Bekker, A., Shen, Y., Poulton, S.W., Chu, X., Anbar, A.D., 2008. Tracing the stepwise oxygenation of the Proterozoic ocean. Nature 452, 456–459.

Seilacher A., 1998, Patterns of macroevolution: How to be prepared for extinction. Comptes Rendus de l'Académie des Sciences - Series IIA - Earth and Planetary Science 327, 431-440.

Shergold, J.H., Cooper, R.A., 2004. The Cambrian Period. In Gradstein, F., Ogg, J., Smith, A. (Eds.), A Geologic Time Scale 2004. Cambridge University Press, Cambridge, 147-164.

Shields, G., Kimura, H., Yang, J., Gammon, P., 2004. Sulphur isotopic evolution of Neoproterozoic–Cambrian seawater: new francolite-bound sulphate $\delta^{34}S$ data and critical appraisal of the existing record. Chemical Geology 204, 163–182.

Shields, G., Stille, P., 2001. Diagenetic constrains on the use of cerium anomalies as palaeoseawater proxies: an isotopic and REE study of Cambrian phosphorites. Chemical Geology 175, 29–48.

Shields, G., Strauss, H., Howe, S.S., Siegmund, H., 1999. Sulphur isotope compositions of sedimentary phosphorites from the basal Cambrian of China: implications for Neoproterozoic-Cambrian biogeochemical cycling. Journal of the Geological Society 156, 943-955.

Smart, S.M., 1999. Asphaltites from the southern Australian Margin: Submarine oil seeps or maritime artefacts? University of Adelaide. National Centre for Petroleum Geology and Geophysics. BSc Honours thesis (unpublished).

Sprigg, R.C., 1986. A history of the search for commercial hydrocarbons in the Otway Basin complex. in: Glenie R.C. (Ed.) Second South-Eastern Australia Oil Exploration Symposium. Petroleum Exploration Society of Australia, Melbourne, 173-200.

Sprigg, R.C., Woolley, J.B., 1963. Coastal bitumen in South Australia with special reference to observations at Geltwood beach, south-eastern South Australia. Transactions of the Royal Society of South Australia 86, 67-103.

Squire, R.J., Campbell, I.H., Allen, C.M., Wilson, C.J.L., 2006. Did the Transgondwanan Supermountain trigger the explosive radiation of animals on Earth. Earth and Planetary Science Letters 250, 116–113.

Strauss, H., 2002. The isotopic composition of Precambrian sulphides-seawater chemistry and biological evolution. Special Publications International Association of Sedimentologists 33, 67–105.

Struckmeyer, H.I.M., Totterdell, J.M., Blevin J.E., Logan, G.A., Boreham, C.J., Deighton, I., Krassay, A.A., Bradshaw, M.T., 2001. Character, maturity and distribution of potential Cretaceous oil source rocks in the Ceduna Sub-basin, Bight Basin, Great Australian Bight. in: Hill, K.C., Bernecker, T. (Eds.) Eastern Australasian Basins Symposium, A refocused energy perspective for the future, Melbourne, 2001. Petroleum Exploration Society of Australia. Special Publication, 543-552.

Summons, R.E., Bradshaw, J., Burchardt, D.M., Goody, A.K., Murray, A.P., Foster, C.B., 1993. Hydrocarbon composition and origins of coastal bitumens from the Northern Territory, Australia. Petroleum Exploration Society of Australia Journal 21, 31-42.

Summons, R.E., Logan, G.A., Edwards, D.S., Boreham, C.J., Bradshaw, M.T., Blevin, J.E., Totterdell, J.M., Zumberge, J.E., 2001. Geochemical analogues for Australian coastal asphaltites - search for the source rock. Abstract. American Association of Petroleum Geologists Bulletin, 85 (Supplement).

Suto, A., 2011. Structure of the Kangaroo Island Fleurieu Peninsula Shear Zone and the Provenance of its host sediments- The Kanmantoo Group- South Eastern Australia. Unpublished Hons thesis, University of Adelaide.

Swart, P.K., 2008, Global synchronous changes in the carbon isotopic composition of carbonate sediments unrelated to changes in the global carbon cycle: Proceedings of the National Academy of Sciences of the United States of America 105, 13741–13745.

Swart, P.K., Kennedy, M.J., 2012. Does the global stratigraphic reproducibility of $\delta^{13}C$ in Neoproterozoic carbonates require a marine origin? A Pliocene-Pleistocene comparison. Geology 40, 87–90.

Taylor, S.R., McLennan, S.M., 1985. The Continental Crust: its Composition and Evolution. Blackwell Scientific Publications. Geoscience texts.

Thomson, B. P., 1969. The Kanmantoo Group and Early Palaeozoic Tectonics. In: Parkin L. W. (Ed.), Handbook of South Australian Geology, Geological Survey of South Australia, 97–108

Thomson, J., Jarvis, I., Green, D.R.H., Green, D., Clayton, T., 1998. Mobility and immobility of redox-sensitive elements in deep-sea turbidites during shallow burial. Geochimica et Cosmochimica Acta 62, 643–656.

Tingate, P.R., Duddy, I.R., 2002, The thermal history of the eastern Officer Basin (South Australia): evidence from apatite fission track analysis and organic maturity data: Tectonophysics 349, 251-275.

Totterdell, J., Struckmeyer, H., 2003. Southern Australian Bight basin holds deepwater potential. Offshore 63, 41-44.

Totterdell, J.M., Blevin, J.E., Struckmeyer, H.I.M., Bradshaw, B.E., Colwell, J.B., Kennard, J.M., 2000. A New Sequence Framework For The Great Australian Bight: Starting With A Clean Slate. The APPEA Journal, 40, 95–117.

Totterdell, J.M., Struckmeyer, H.I.M., Boreham, C.J., Mitchell, C.H., Monteil, E. Bradshaw, B.E., 2008. Mid–Late Cretaceous Organic-Rich Rocks From The Eastern Bight Basin: Implications For Prospectivity. in: Blevin, J.E., Bradshaw, B.E., Uruski, C. (Eds.) Eastern Australasian Basins Symposium III, Petroleum Exploration Society Of Australia, Special Publication, 137–158.

Tribovillard, N., Algeo, T.J., Lyons, T., Riboulleau, A., 2006. Trace metals as paleoredox and paleoproductivity proxies: an update. Chemical Geology 232, 12–32.

Tribovillard, N., Riboulleau, A., Lyons, T., Baudin, F., 2004. Enhanced trapping of molybdenum by sulfurized organic matter of marine origin as recorded by various Mesozoic formations. Chemical Geology 213, 385–401.

Tucker M.E., 1986, Carbon isotope excursions in Precambrian/Cambrian boundary beds, Morocco. Nature 319, 48-50.

Tucker M.E., 1989, Carbon isotope and Precambrian-Cambrian boundary geology, South Australia: ocean basin formation, seawater chemistry and organic evolution. Terra Nova.1, 573-582.

Turner B., 1994. Cambrian black shales in the Karinya Syncline: stratigraphic distribution, sedimentology and kerogen composition. Unpublished Hons thesis, University of Adelaide.

Turner, S.P., Adams, C.J., Flöttmann, T., Foden, J.D., 1993. Geochemical and geochronological constraints on the Glenelg River Complex, Western Victoria. Austrailian Journal of Earth Sciences 40, 275-292.

Turner, S.P., Haines, P.W., Foster, D., Powell, R., Sandiford, M., Offler, R., 2009. Did the Delamerian Orogeny Start in the Neoproterozoic? The Journal of Geology 117, 575–583.

Veevers, J.J., Belousova, E.A., Saeed, A., Sircombe, K., Cooper, A.F., Read, S.R., 2006. Pan-Gondwanaland detrital zircons from Australia analysed for Hf-isotopes and trace elements reflect an ice-coveredAntarctic provenance of 700-500 Ma age, TDM of 2.0—1.0 Ga, and alkaline affinity. Earth-Science Reviews 76, 135–174.

Volkman J.K., O'Leary T., Summons R.E., Bendall M.R., 1992. Biomarker composition of some asphaltic coastal bitumens from Tasmania, Australia, Organic Geochemistry 18, 669–682.

Webb, G.E., Kamber, B.S., 2000. Rare earth elements in Holocene reefal microbialites: a new shallow seawater proxy. Geochimica et Cosmochimica Acta, 64, 1557-1565.

Wenger, L.M., Isaksen, G.H., 2002. Control of hydrocarbon seepage intensity on level of biodegradation in sea bottom sediments. Organic Geochemistry 33, 1277–1292.

Wilde, P., Lyons, T.W., Quinby-Hunt, M.S., 2004. Organic carbon proxies in black shales: molybdenum. Chemical Geology 206, 167–176.

Wombacher, F., Munker, C., 2000. Pb, Nd, and Sr isotopes and REE systematic of Cambrian sediments from New Zealand: implications for the reconstruction of the Early Palaeozoic Gondwana margin along Australia and Antarctica. Journal of Geology 108, 663-686.

Woods, M.A., Wilby, P.R., Leng, M.J., Rushton, A.W.A., Williams, M., 2011 The Furongian (late Cambrian) Steptoean Positive Carbon Isotope Excursion (SPICE) in Avalonia Journal of the Geological Society of London 168, 851–861.

Wotte, T., Álvaro, J.J., Shields, G.A., Brown, B., Brasier, M.D., Veizer, J., 2007. C-, O- and Srisotope stratigraphy across the Lower–Middle Cambrian transition of the Cantabrian Zone (Spain) and the Montagne Noire (France), West Gondwana. Palaeogeography, Palaeoclimatology, Palaeoecology 256, 47–70.

Wu, N., Farquhar, J., Strauss, H., Kim, S., Canfield, D.E., 2010. Evaluating the S-isotope fractionation associated with Phanerozoic pyrite burial. Geochimica et Cosmochimica Acta 74, 2053–2071.

Xie, S., Wu, Y., Gao, S., Liu, X., Zhou, L., Zhao, L., Hu, Z., 2011. Sr–Nd isotopic and geochemical constraints on provenance of late Paleozoic to early cretaceous sedimentary rocks in the Western Hills of Beijing, North China: Implications for the uplift of the northern North China Craton. Sedimentary Geology, doi:10.1016/j.sedgeo.2011.12.005

Yan X., Kerrich R., Hendry M.J., 2000. Trace element geochemistry of a thick till and clay-rich aquitard sequence, Saskatchewan, Canada. Chemical Geology 164, 930-120.

Yan, Y., Xia, B., Lin, G., Carter, A., Hu, X., Cui, X., Liu, B., Yan, P., Song, Z., 2007. Geochemical and Nd isotope composition of detrital sediments on the north margin of the South China Sea: provenance and tectonic implications. Sedimentology 54, 1-17.

Yu, B.S., Dong, H., Widomb, E., Chen, J, Lin C.S., 2009. Geochemistry of basal Cambrian black shales and cherts from the Northern Tarim Basin, Northwest China: Implications for depositional setting and tectonic history. Journal of Asian Earth Sciences 34, 418–436.

Zang, W.-L., Moczydłowska, M. & Jago, J.B., 2007. Early Cambrian acritarch assemblage zones in South Australia and global correlation. Memoirs of the Association of Australasian Palaeontologists 33, 141-177.

Zang, W-L., 2002. Sequence analysis and petroleum potential in the Arrowie Basin, South Australia. PIRSA Report Book 2002/024.

Zang, W-L., Jago, J.B., Alexander, E.M., Paraschivoiu, E., 2004. A review of basin evolution, sequence analysis and petroleum potential of the frontier Arrowie Basin, South Australia. In: Boult, P.J., Johns, D.R., Lang, S.C. (Eds.), Eastern Australian Basins Symposium II. Petroleum Exploration Society of Australia, Special Publication, 243–256.

Zhao, Y., Zheng, Y., Chen, F., 2009. Trace element and strontium isotope constraints on sedimentary environment of Ediacaran carbonates in southern Anhui, South China. Chemical Geology 265, 345–362.

Zhou, C.M., Jiang, S.Y., 2009. Palaeoceanographic redox environments for the lower Cambrian Hetang Formation in South China: Evidence from pyrite framboids, redox-sensitive trace elements, and sponge biota occurrence. Palaeogeography, Palaeoclimatology, Palaeoecology 271, 279–286.

Zhu M., Babcock L.E. and Peng S., 2006, Advances in Cambrian Stratigraphy and paleontology: integrating correlation techniques, palaeobiology, taphonomy and paleoenvironmental reconstruction, Palaeoworld, 15, 217–222.

Zhu M., Zhang J., Li G. and Yang A., 2004, Evolution of C isotopes in the Cambrian of China: implications for Cambrian subdivision and trilobite mass extinctions. Geobios 37, 287-301.

Zhuravlev, A.Y., Gravestock, D.I., 1993. Archaeocyaths from Yorke Peninsula, South Australia and archaeocyathan Early Cambrian zonation. Alcheringa 18, 1-54.

ELEMENTAL, ISOTOPIC AND MOLECULAR SIGNATURES OF EARLY CAMBRIAN MARINE SEDIMENTS AND A PHANTOM PETROLEUM SYSTEM IN SOUTH AUSTRALIA

Volume 2 - Appendices

By

Philip Anthony Hall

M.Phil. Environmental and Geographical Sciences, Manchester Metropolitan University, U.K.
B.Sc. Hons. Geology and Petroleum Geology, University of Aberdeen, U.K.

Thesis submitted for the degree of

Doctor of Philosophy

Geology and Geophysics
School of Earth and Environmental Science
Faculty of Science
University of Adelaide

2012

Appendix I

Standard Operating Procedures

1. ICP-MS Acid Digestion

1.1. Chemicals

- Double distilled conc HCl
- Double distilled conc HNO_3
- Conc HF
- Double distilled 6M HCl
- Double distilled 3.5M HNO_3
- Double distilled 0.5M HNO_3
- 10% H_2O_2 solution

1.2. Glassware and other consumables

- 20ml Teflon beakers and caps (acid cleaned)
- 2ml eppindorf centrifuge vials (acid cleaned)
- 5ml Teflon vials and caps (acid cleaned)
- Adjustable pipette 20-200ul and PTFE tips
- Adjustable pipette 100-1000ul and PTFE tips
- Adjustable pipette 1ml-5ml and PTFE tips
- Hotplate (80°C)
- Hotplate (140°C)
- Centrifuge (13K/min)
- Disposable gloves

1.3. Sample Preparation.

1) Weigh approx 15mg of powdered sample into Teflon beaker, note weight

2) Add 1ml conc HCl

3) Add 200ul conc HNO_3

4) Add 500ul HF (use double set of disposable gloves)

5) Cap tightly and loosen by 10th turn to allow gas expansion

6) Place on hotplate (80°C) for minimum 12hr (generally overnight)

7) Uncap sample and add 500ul conc HNO_3 and leave to dry down on hotplate

8) After approximately 3hr add 500ul conc HNO_3 (repeat again if time)

9) Leave on hotplate until dry

10) Add about 0.5 mL HNO3 and 2.0 mL of 10% H2O2 leave overnight at room temp

11) Place samples on the 80C hot plate for 6 to 9 hours

12) Transfer to the 140 C hot plate over night.

13) Uncap them and let them dry down on 140°C hotplate.

14) Add 1.5 mL of 6 M HCl to each of the samples and place back on the hot plate (80°C) for a 2hr minimum period.

15) Pour the solution into a 2ml eppindorf centrifuge tube and centrifuge at 13k/min for 5 min

16) Transfer 100 uL into a 5ml telfon vial then dry down the samples at 80C (probably adding a drop or 2 of about 3.5 M HNO3 as they are drying down).

17) Redissolve in 1.5ml of 2% HNO3 (0.5M) ready for analysis by ICP-MS (final conc is equivalent to 67ug shale/ml).

2. Urea Adduction

(modified after Wakeham, S.G. and Pease, T.K. (1992): Lipid analyses in marine particle and sediment samples: a laboratory handbook. Unpublished manuscript, Skidaway Institute of Oceanography, Savannah, Georgia, U.S.A.)

1. Chemicals, consumables, and preparation steps

1.1. Chemicals

- Cold-saturated urea (CH_4N_2O) solution (see below for preparation details)
- n-hexane (highest purity for, chromatography)
- Acetone (highest purity, for chromatography)
- Methanol (highest purity, for chromatography)
- deionised water extracted with dichloromethane (DCM)
- Dichloromethane (DCM) for initial rinsing of the syringes
- High purity nitrogen (N_2) for blowing down solvents

1.2. Glassware and other consumables

- Per sample 5× 4ml-vials with PTFE-lined screw cap, baked out at ≥ 400°C for ≥ 6 hours (or thoroughly rinsed with DCM):
  - 1st vial: for the saturated hydrocarbon fraction of the sample at the beginning of the procedure
  - 2nd vial: for the sub-fraction of non-adducts
  - 3rd vial: for the sub-fraction of adducts during the 1st round of urea adduction
  - 4th vial: for the sub-fraction of adducts during the 2nd round of urea adduction
  - 5th vial: for the sub-fraction of adducts during the 3rd, i.e. last, round of urea adduction
- Rack or other setup to securely hold the 4 ml vials, preventing them from tipping over and loosing the valuable samples
- Large quantity of Pasteur pipettes, baked out in a muffle furnace at ≥ 400°C for ≥ 6 hours
- Rack or other setup (e.g. rolled pieces of aluminium foil) to temporarily deposit the Pasteur pipettes in between individual steps of the urea adduction procedure (intended to prevent the pipette tip to touch any “dirty” surface)
- 4× calibrated 1000 µl (1 ml) syringes, one for each of the 4 main chemicals/solvents used in the urea adduction procedure, i.e. the urea solution, n-hexane, acetone, and the DCM-extracted deionised water. Each syringe should be (a) cleaned before use by rinsing it 3× with DCM and then 3× with the chemical/solvent it will be used for and (b) labelled with the name of the chemical/solvent it will take up)

- Nitrogen (N_2) blowdown sample concentrator (with ≥ 6 sample positions; optionally including temperature controllable heater)
- Refrigerator/freezer, that can be set to a temperature of ≤ -4°C

1.3. Preparation of cold-saturated urea (CH_4N_2O) solution

A larger quantity of the cold-saturated urea (CH_4N_2O) solution can be prepared in advance, e.g. in a 200 or 500 ml flask, and be stored over longer times. The solvent for the urea is methanol.

Prepare the solution in a fume hood, use nitrile or other suitable gloves, and avoid inhaling any dusts of the crystalline urea

1) Add urea (crystalline from) to a glass flask (with a ground glass stopper), e.g. with a volume of 200 ml, until an approximately 1 cm thick layer covers the bottom of the flask.
2) Add methanol to the flask until reaching the normal, maximal filling level for the flask in use (i.e. not to the very top of the neck).
3) Close the flask with its ground glass stopper and shake the closed flask well (keep holding the stopper firmly in place), to facilitate the dissolution of the urea in the methanol. In case all of the urea already dissolves as a result of the shaking, more urea needs to be added to the flask and shaken until a clearly visible bottom layer of undissolved (i.e. crystalline) urea remains in the flask. However, usually the shaking will not lead to a complete dissolution of all of the initially added urea.
4) Place the flask with this urea solution (and its bottom layer of undissolved urea) in an oven or drying cabinet for at least 1 hour at 50°C
5) If the solution then still exhibits a clearly visible bottom layer of undissolved (i.e. crystalline) urea (thickness of layer at least several mm), place the flask in a fume hood and let it cool down to room temperature (the cooling may even lead to an increase in the thickness of the bottom urea layer). The urea solution is then cold-saturated and ready to use.

   If, however, no clearly visible bottom layer of undissolved (i.e. crystalline) urea is present after the heating at 50°C, more crystalline urea needs to be added to the solution, and steps (3) and (4) have to be repeated, until a clearly visible bottom layer of undissolved (i.e. crystalline) urea (at least several mm) remains after heating and cooling down. Only then is the solution cold-saturated, which is a requirement for a successful urea adduction procedure.

2. Urea adduction procedure

<u>Do all of the following steps, except step (5), in a fume hood</u>

1) Add an aliquot (e.g. ¼, ½, ¾, or all) of the fraction of aliphatic (i.e. saturated) hydrocarbons, which was previously obtained from your sample by means of silica-gel column chromatography and is now dissolved in n-hexane, to a clean and dry 4 ml vial (with PTFE-lined screw cap) by using a calibrated 1000 µl (1 ml) syringe (or, in case of very small aliquot volumes, a smaller calibrated syringe). Use a rack or other suitable setup to securely hold the vial and to prevent it from tipping over and loosing your valuable sample (do this also with all other vials in the further course of the urea adduction procedure!)
2) Use the nitrogen (N_2) blowdown sample concentrator to **<u>completely</u>** evaporate the hexane solvent of the sample (i.e. blow down to dryness).
   If your nitrogen blowdown sample concentrator is equipped with a temperature controllable heater, you can set the temperature to 27-28°C, i.e. slightly above normal room temperature, to accelerate the evaporation process. This is however not a requirement and thus optional.
3) Add the following chemicals/solvents **<u>exactly in the below given sequence</u>** to your sample in the 4 ml vial, using for each of these chemicals/solvents a rinsed and calibrated 1000 µl (1 ml) syringe:
   (i) 200 µl cold-saturated urea solution
   (ii) 200 µl acetone (highest purity for, chromatography)
   (iii) 200 µl n-hexane (highest purity for, chromatography).
   After the addition of the n-hexane, a white precipitate of urea crystals should form and be visible in the vial. The urea-adductable compounds (adducts: all normal and isoalkanes), which were contained in your aliphatic (i.e. saturated) hydrocarbons fraction, are now incorporated and trapped inside the crystal lattices of the precipitated urea crystals. The non-adductable compounds (non-adducts: branched and cyclic alkanes), which were contained in your aliphatic hydrocarbons fraction, remain in solution and are thus contained in the solvent mixture in the vial.
4) Close the vial tightly with its PTFE-lined screw cap and shake the vial to further facilitate precipitation of urea crystals and thus adduction of the normal and isoalkanes.
5) Place the vial in a fridge at -4°C (or lower temperature) for 30 minutes.

6) Remove the vial from the fridge after 30 minutes and use the nitrogen (N_2) blowdown sample concentrator to **completely** evaporate the solvents from the vial (i.e. blow down to dryness).
7) For each sample you work, have 1 clean (i.e. baked out) Pasteur pipette ready now, placed on the pipette rack or self-made setup (e.g. rolled pieces of aluminium foil).
8) Open the vial, add 500 µl of n-hexane to the vial (using the designated n-hexane1000 µl syringe), close the vial again tightly with its PTFE-lined screw cap, and shake it well to ensure that the urea precipitate and all inner walls of the vial are rinsed thoroughly with the n-hexane.

   The n-hexane will thereby dissolve and take up the non-adductable compounds (non-adducts).
9) Transfer all of the non-adducts-containing n-hexane with a clean (i.e. baked out) Pasteur pipette into the 4 ml vial, which you have labelled during the preparations for the urea adduction procedure with the sample number, the identifier "non-adducts", and any further potentially important details.

   Steps 8) and 9) now have to be repeated 2 more times, in order to maximise the extraction of the non-adducts from the vial with the urea precipitate.

   Altogether, there are thus 3 rinses, each with 500 µl of n-hexane, of the vial containing the urea precipitate. After these 3 rinses and the transfer of the thereby extracted non-adducts into the designated non-adducts 4 ml vial, the latter contains a total volume of 1500 µl, i.e. 1.5 ml, of non-adducts-containing n-hexane.
10) Use the nitrogen (N_2) blowdown sample concentrator to **completely** evaporate the hexane solvent from the non-adducts-containing vial (i.e. blow down to dryness). If your nitrogen blowdown sample concentrator is equipped with a temperature controllable heater, you can set the temperature to 27-28°C, i.e. slightly above normal room temperature, to accelerate the evaporation process. This is however not a requirement and thus optional.

The separation and purification of the sub-fraction of non-adducts from your initial aliphatic (i.e. saturated) hydrocarbon fraction is now already finished. Redissolve the now dried non-adducts fraction in 1 ml of hexane, transfer this solution into a GC autosampler vial using a clean calibrated 1 ml syringe, and store it in a fridge at ≤ 4°C.

It might be necessary to concentrate the obtained non-adducts fraction, i.e. to decrease its volume in the GC autosampler vial (now 1 ml), prior to GC-FID, GC-MS, and/or GC-IRMS analyses, in order to obtain compound concentrations, which exceed the detection limit of the respective type of analyses. This applies particularly to compound-specific isotope analyses by means of GC-IRMS, which may require a significant decrease in solvent volume in the autosampler vial down to > 100 µl (!!). In this case, micro vial inserts or limited volume vials have to be used.

11) Add 500 µl of methanol (highest purity, for chromatography) and 500 µl of deionised water (pre-extracted with dichloromethane) to the vial with the urea precipitate using the 2 clean calibrated 1000 µl syringes designated for these solvents, close the vial tightly with its PTFE-lined screw cap, and shake it well. This will cause the redissolution of the urea precipitate. The urea-adductable compounds (adducts) bound in the urea crystal lattice will thus be dissolved by and taken up into the methanol/water mixture.

12) Open the vial containing the redissolved adducts (methanol/water mixture), add 1000 µl of n-hexane, close the vial again tightly with its PTFE-lined screw cap, and shake it well. Wait until the n-hexane has separated completely from the methanol/water mixture, i.e. until a clear and sharp interface between these 2 phases is visible. The hexane phase now sits on top of the methanol/water phase.

    This step will facilitate the extraction of the adducts compounds from the methanol/water mixture (phase at bottom of vial) into the n-hexane phase (upper phase in vial).

13) Transfer the adducts-containing n-hexane phase with a clean (i.e. baked out) Pasteur pipette into the 4 ml vial, which you have labelled during the preparations for the urea adduction procedure with the sample number, the identifier “adducts - 1st round of urea adduction”, and any further potentially important details.

    !During take up of the hexane phase into the pipette, take care to not aspirate anything of the methanol/water phase. You can only achieve this by leaving a very thin layer of the hexane phase in the vial!

Steps 12) and 13) now have to be repeated 2 more times, in order to ensure the complete extraction of the adducts compounds from the methanol/water phase (and the thin layer of hexane left in the vial; see above).

Altogether, there are thus 3 rinses, each with 1000 µl of n-hexane, of the methanol/water mixture. After these 3 rinses and the transfer of the thereby extracted adducts into the designated adducts 4 ml vial, the latter contains a total volume of 3000 µl, i.e. 3 ml, of adducts-containing n-hexane.

14) Use the nitrogen (N_2) blowdown sample concentrator to **completely** evaporate the hexane solvent from the adducts-containing vial (i.e. blow down to dryness).

If your nitrogen blowdown sample concentrator is equipped with a temperature controllable heater, you can set the temperature to 27-28°C, i.e. slightly above normal room temperature, to accelerate the evaporation process. This is however not a requirement and thus optional.

!However, the now obtained sub-fraction of adducts usually still contains very small residual quantities of non-adducts, which almost inevitably escaped the pipetting in step 9) and should be removed in order to obtain a highly pure adducts sub-fraction. This is especially of importance for later compound-specific isotope analyses by GC-IRMS!

Hence, the steps 2) to 14) have to be repeated 2 more times now.

The separation and purification of the sub-fraction of adducts from your initial aliphatic (i.e. saturated) hydrocarbon fraction is then finished. Redissolve the now dried final adducts fraction in 1 ml of hexane, transfer this solution into a GC autosampler vial using a clean calibrated 1 ml syringe, and store it in a fridge at ≤ 4°C.

!It might be necessary to concentrate the obtained adducts fraction, i.e. to decrease its volume in the GC autosampler vial (now 1 ml), prior to GC-FID, GC-MS, and/or GC-IRMS analyses, in order to obtain compound concentrations, which exceed the detection limit of the respective type of analyses. This applies particularly to compound-specific isotope analyses by means of GC-IRMS, which may require a significant decrease in solvent volume in the autosampler vial down to > 100 µl (!!). In this case, micro vial inserts or limited volume vials have to be used!

Appendix II

Supporting Data: The biogeochemical status of the Palaeo-Pacific Ocean: clues from the early Cambrian of South Australia

TOC, $\delta^{13}C_{org}$, $\delta^{34}S_{pyr}$ and trace element concentrations for the Talisker Formation

Sample	Formation	Locality	Depth	TOC	$\delta^{13}C_{org}$	$\delta^{34}S$	Weighed	Li	Be	B	Sc	V	Co	Ni	Cu	Zn	Ga	Ge
			(m)	(%)	(‰)	(‰)	(mg)	(ug/g)	(ug/g)	(ug/g)	(ug/g)	(ug/g)	(ug/g)	(ug/g)	(ug/g)	(ug/g)	(ug/g)	(ug/g)
F1 (1)	Talisker	Frankton 1	125	1.9	-21.43	-9.56	16.6	47.35	4.08	45.40	14.88	358.15	21.05	87.33	64.75	174.76	27.27	3.42
F1 (2)	Talisker	Frankton 1	121	1.28	-19.21	-11.03	17.2	46.49	3.55	36.76	15.18	180.35	30.55	87.54	73.70	181.01	28.79	4.11
F1 (3)	Talisker	Frankton 1	118	0.92	-17.07	-10.99	14.7	42.76	3.55	36.20	14.30	240.13	43.06	83.13	39.09	522.45	26.81	2.89
F1 (4)	Talisker	Frankton 1	85	1.09	-15.19	-11.50	13.2	48.87	4.40	38.19	14.61	485.78	19.46	83.92	56.66	241.52	32.20	3.30
F1 (5)	Talisker	Frankton 1	80	0.93	-13.69	-7.26	14.2	37.87	3.73	51.02	15.26	270.21	31.96	60.44	76.43	131.22	28.59	3.16
F1 (6)	Talisker	Frankton 1	75	0.96	-14.33	-7.83	14	31.70	3.14	28.48	11.92	217.04	27.39	52.40	29.67	38.57	24.96	2.87
F1 (7)	Talisker	Frankton 1	68	1.15	-14.63	-8.97	13	46.72	3.84	40.01	14.71	139.57	26.27	42.81	45.48	164.78	30.96	3.07
F1 (8)	Talisker	Frankton 1	60	0.94	-12.84		16	33.62	2.49	24.84	4.43	97.61	23.16	58.49	94.30	111.63	21.96	2.52
F1 (9)	Talisker	Frankton 1	16	0.36	-16.53		16.2	29.79	2.83	3.32	8.64	85.69	13.11	35.48	2.26	72.68	25.78	2.55
F1 (10)	Talisker	Frankton 1	5	0.41	-18.49		15.6	42.34	3.47	10.41	12.27	107.86	17.88	48.84	6.25	113.07	28.11	3.56
F2 (1)	Talisker	Frankton 2	103	1.39	-23.14	-2.18	13.1	39.33	3.07	20.07	13.30	459.75	39.02	84.99	87.76	94.18	24.86	2.50
F2 (2)	Talisker	Frankton 2	96	1.33	-23.33	-0.98	14.9	44.76	3.98	20.68	14.65	490.10	42.41	98.95	115.69	140.05	33.99	2.99
F2 (3)	Talisker	Frankton 2	85	1.24	-19.36	-2.22	14.5	44.19	3.19	44.09	14.99	271.97	22.61	64.98	48.51	78.22	28.40	2.94
F2 (4)	Talisker	Frankton 2	78	1.12	-15.91	2.02	14.7	37.78	2.80	20.16	13.34	218.09	20.97	40.92	37.24	71.34	25.02	2.55
F2 (5)	Talisker	Frankton 2	75	1.18	-16.26	1.33	16	52.34	4.34	22.82	15.81	181.69	27.66	50.87	53.76	95.65	42.45	3.20
F2 (6)	Talisker	Frankton 2	72	0.93	-15.91	1.57	15.6	44.84	2.99	8.53	14.90	128.99	19.59	44.55	56.39	112.67	28.47	2.70
F2 (7)	Talisker	Frankton 2	52	1.36	-16.29	8.41	13.5	41.57	3.73	5.56	10.59	147.66	26.29	41.92	40.76	340.40	34.03	2.49
F2 (8)	Talisker	Frankton 2	45	1.03	-17.08	0.26	15.7	45.00	3.53	7.56	12.46	201.76	26.10	52.43	46.57	516.77	32.81	2.82
F2 (9)	Talisker	Frankton 2	42	1.11	-16.62	9.79	13	39.33	3.72	7.89	8.44	205.07	15.12	38.08	47.59	738.71	30.60	2.19
F2 (10)	Talisker	Frankton 2	32	1.03	-16.04		15.1	40.82	3.07	8.21	11.28	148.30	12.34	35.03	34.74	438.73	27.88	2.17
K1	Talisker	The Gap		1.06	-24.71		13.9	28.77	3.28	26.17	15.62	364.53	0.31	4.30	11.97	16.05	29.82	0.86
K2	Talisker	The Gap		0.79	-24.33		16	29.98	3.50	29.67	17.28	395.26	0.60	17.67	49.02	19.86	32.10	1.49
K3	Talisker	The Gap		0.9	-24.47		14.3	32.52	3.42	28.16	19.70	455.93	0.58	6.56	29.75	14.32	31.35	1.49
K4	Talisker	The Gap		1.28	-14.79		13.8	26.36	3.11	23.60	16.84	389.31	0.53	23.13	18.83	31.12	26.73	1.51
K5	Talisker	The Gap		1.18	-24.62		14.1	25.88	3.01	9.94	13.77	418.99	0.55	18.60	18.22	45.26	29.10	2.30
K6	Talisker	The Gap		1.24	-24.48		14	25.74	2.87	10.68	13.92	288.91	0.32	14.50	8.52	20.84	27.13	1.08
K7	Talisker	The Gap		1.44	-26.42		14.2	23.57	2.79	13.15	16.82	396.95	0.77	6.43	133.68	21.91	28.32	1.42
K8	Talisker	The Gap		1.04	-24.68		14.6	26.55	2.92	13.98	13.52	489.28	0.28	2.60	9.95	18.10	28.28	0.50
K9	Talisker	The Gap		1.18	-24.16		14	24.46	2.84	10.87	15.32	434.95	0.34	8.14	18.05	29.73	26.58	0.73

TOC, $\delta^{13}C_{org}$, $\delta^{34}S_{pyr}$ and trace element concentrations for the Talisker Formation (cont).

Sample	Formation	Locality	As (ug/g)	Se (ug/g)	Rb (ug/g)	Y (ug/g)	Nb (ug/g)	Mo (ug/g)	Cd (ug/g)	Sn [1] (ug/g)	Sn [2] (ug/g)	Sn [3] (ug/g)	Cs (ug/g)	La (ug/g)	Ce (ug/g)	Pr (ug/g)	Nd (ug/g)	Sm (ug/g)
F1 (1)	Talisker	Frankton 1	14.85	2.68	172.89	16.05	9.21	32.68	0.24	2.86	2.95	3.29	5.85	39.62	81.01	8.97	33.46	6.56
F1 (2)	Talisker	Frankton 1	5.38	2.91	161.60	14.39	9.36	13.98	1.32	2.79	2.85	3.19	5.41	60.96	118.74	13.05	48.11	8.54
F1 (3)	Talisker	Frankton 1	3.85	2.15	162.42	13.17	8.92	18.39	1.09	2.77	2.78	3.12	5.32	30.70	65.08	7.08	26.51	5.13
F1 (4)	Talisker	Frankton 1	1.88	2.70	175.14	13.23	8.94	10.35	1.11	3.39	2.97	2.92	7.11	45.44	89.60	9.85	37.46	6.88
F1 (5)	Talisker	Frankton 1	22.40	1.76	178.80	14.56	9.93	14.71	0.59	3.38	3.51	3.76	6.36	49.07	95.84	10.39	38.60	6.98
F1 (6)	Talisker	Frankton 1	1.57	2.02	106.61	13.26	9.76	20.63	0.13	2.77	3.17	3.23	4.75	37.11	76.92	8.49	32.15	6.07
F1 (7)	Talisker	Frankton 1	2.32	1.57	162.32	15.32	6.73	7.96	0.38	4.63	4.47	4.84	6.43	47.93	95.50	10.23	38.05	6.98
F1 (8)	Talisker	Frankton 1	42.47	1.38	46.69	24.75	2.11	3.14	0.23	2.11	2.17	2.38	5.33	26.44	62.00	7.09	28.19	6.24
F1 (9)	Talisker	Frankton 1	9.74	0.18	139.21	10.12	12.81	0.99	0.08	2.48	2.57	2.83	3.77	34.71	70.36	7.87	29.87	5.57
F1 (10)	Talisker	Frankton 1	8.35	0.24	198.63	9.91	16.21	1.06	0.09	3.26	3.30	3.59	5.70	51.99	104.29	11.22	41.52	7.06
F2 (1)	Talisker	Frankton 2	10.59	4.16	144.60	14.19	9.85	14.16	0.46	2.64	2.67	3.01	5.77	39.20	78.81	8.45	31.75	5.93
F2 (2)	Talisker	Frankton 2	3.66	3.05	149.98	18.00	10.24	19.22	1.53	3.62	2.97	2.43	5.67	51.02	101.85	10.67	40.10	7.39
F2 (3)	Talisker	Frankton 2	3.89	1.98	178.98	15.35	10.77	8.41	0.17	3.18	3.30	3.59	8.43	46.63	90.86	9.86	36.99	6.90
F2 (4)	Talisker	Frankton 2	20.04	1.45	149.55	18.86	9.12	4.30	0.28	2.69	2.74	3.03	6.54	42.30	83.65	8.95	33.53	6.23
F2 (5)	Talisker	Frankton 2	4.76	0.88	183.55	18.15	5.62	13.86	0.27	4.05	2.92	1.95	9.92	49.26	96.46	10.58	39.86	7.24
F2 (6)	Talisker	Frankton 2	51.75	1.10	173.85	16.47	9.31	1.19	0.23	2.90	3.03	3.30	9.94	42.84	82.72	8.93	33.16	6.02
F2 (7)	Talisker	Frankton 2	2.58	1.39	120.18	12.48	9.88	5.59	3.32	3.16	2.75	2.50	8.05	31.83	69.67	7.59	28.68	5.43
F2 (8)	Talisker	Frankton 2	1.93	1.46	128.45	13.49	8.90	14.61	5.28	3.16	2.78	2.69	7.00	39.40	79.91	8.79	33.06	6.05
F2 (9)	Talisker	Frankton 2	3.39	0.62	85.16	11.80	6.82	8.96	9.90	2.76	2.07	1.78	5.70	26.90	59.74	6.31	24.07	4.42
F2 (10)	Talisker	Frankton 2	1.73	0.47	161.74	13.86	4.64	1.26	4.05	2.53	1.98	1.86	11.19	32.73	64.55	6.93	26.06	4.85
K1	Talisker	The Gap	5.08	1.21	122.08	9.92	10.09	9.68	0.05	4.20	3.40	3.26	3.96	21.27	37.53	3.62	12.18	2.50
K2	Talisker	The Gap	61.92	3.64	124.31	9.63	13.38	19.53	0.05	5.91	5.61	5.85	4.05	30.86	47.70	4.28	13.74	2.53
K3	Talisker	The Gap	33.37	5.39	140.85	10.55	15.12	42.48	0.06	4.29	4.42	4.90	4.62	34.63	58.05	4.95	15.32	2.88
K4	Talisker	The Gap	17.78	2.89	120.58	10.72	13.09	29.34	0.06	3.55	3.69	4.18	3.91	38.33	58.73	5.94	20.17	3.60
K5	Talisker	The Gap	54.23	4.70	122.49	9.37	10.03	17.42	0.06	3.26	3.43	3.76	4.42	35.99	58.68	5.85	19.75	3.41
K6	Talisker	The Gap	42.19	0.88	120.31	10.38	9.99	6.76	0.04	4.72	4.80	6.16	4.03	28.22	53.49	4.60	15.74	3.10
K7	Talisker	The Gap	49.77	6.30	112.02	9.49	11.89	41.63	0.06	5.07	5.19	5.76	3.88	19.49	36.76	3.22	11.06	2.35
K8	Talisker	The Gap	11.18	1.16	123.08	7.22	11.86	9.61	0.06	3.24	3.43	3.73	4.42	10.28	22.92	1.85	6.30	1.46
K9	Talisker	The Gap	31.91	2.77	110.87	8.52	10.48	18.80	0.06	4.41	4.51	4.96	3.94	19.53	27.72	2.43	7.91	1.64

TOC, $\delta^{13}C_{org}$, $\delta^{34}S_{pyr}$ and trace element concentrations for the Talisker Formation (cont).

Sample	Formation	Locality	Eu (ug/g)	Gd (ug/g)	Tb (ug/g)	Dy (ug/g)	Ho (ug/g)	Er (ug/g)	Tm (ug/g)	Yb (ug/g)	Lu (ug/g)	Ta (ug/g)	Re (ug/g)	Au (ug/g)	Tl (ug/g)	206 Pb (ug/g)	207 Pb (ug/g)	208 Pb (ug/g)	Th (ug/g)	U (ug/g)
F1 (1)	Talisker	Frankton 1	1.46	5.87	0.85	3.83	0.79	1.95	0.38	2.01	0.41	1.11	0.13	43.80	1.93	101.89	104.32	99.53	18.25	7.98
F1 (2)	Talisker	Frankton 1	1.65	7.11	0.81	3.67	0.62	1.70	0.24	1.68	0.25	0.88	0.01	22.98	1.75	82.31	85.98	82.40	24.27	4.22
F1 (3)	Talisker	Frankton 1	1.06	4.65	0.59	3.02	0.55	1.53	0.23	1.54	0.24	0.75	0.01	11.18	1.72	43.27	44.14	41.30	16.03	4.52
F1 (4)	Talisker	Frankton 1	1.25	6.02	0.72	3.40	0.58	1.56	0.23	1.63	0.27	0.95	0.03	8.84	1.53	15.85	14.76	15.08	19.98	7.19
F1 (5)	Talisker	Frankton 1	1.28	6.15	0.75	3.66	0.62	1.63	0.23	1.73	0.28	0.83	0.01	16.39	1.35	68.86	69.02	63.93	19.76	6.69
F1 (6)	Talisker	Frankton 1	1.17	5.43	0.68	3.56	0.63	1.71	0.26	1.77	0.26	0.87	0.01	4.84	1.18	29.24	28.57	28.69	13.47	7.70
F1 (7)	Talisker	Frankton 1	1.29	6.15	0.74	3.68	0.64	1.77	0.25	1.82	0.27	0.48	0.01	4.98	1.19	67.75	68.77	63.64	20.12	7.35
F1 (8)	Talisker	Frankton 1	1.52	6.94	1.11	6.88	1.33	3.59	0.48	2.95	0.39	0.08	0.01	2.85	0.93	33.89	32.59	31.96	3.39	9.49
F1 (9)	Talisker	Frankton 1	1.16	4.85	0.58	2.77	0.46	1.17	0.16	1.06	0.16	0.95	N.D,	2.77	0.87	13.37	13.01	13.32	11.52	3.45
F1 (10)	Talisker	Frankton 1	1.41	5.60	0.60	2.61	0.41	1.09	0.15	1.05	0.15	1.26	0.00	4.24	1.11	22.07	22.10	22.16	17.86	4.26
F2 (1)	Talisker	Frankton 2	1.09	5.37	0.67	3.19	0.59	1.67	0.25	1.79	0.28	1.12	0.02	9.70	1.59	79.05	87.50	80.20	16.68	4.74
F2 (2)	Talisker	Frankton 2	1.33	6.67	0.80	4.06	0.73	2.11	0.32	2.28	0.34	0.75	0.02	11.72	1.84	58.30	59.92	55.65	21.50	5.98
F2 (3)	Talisker	Frankton 2	1.19	6.09	0.75	3.75	0.65	1.74	0.26	1.86	0.27	0.77	0.02	3.87	1.88	33.61	32.76	33.29	19.90	4.99
F2 (4)	Talisker	Frankton 2	1.12	5.87	0.76	4.04	0.75	2.12	0.32	2.34	0.34	0.67	0.00	2.54	1.48	35.31	35.68	34.81	15.19	3.53
F2 (5)	Talisker	Frankton 2	1.31	6.61	0.81	4.13	0.74	2.06	0.30	2.05	0.30	0.28	0.01	2.06	1.92	43.70	45.03	42.04	18.83	4.95
F2 (6)	Talisker	Frankton 2	1.16	5.49	0.68	3.55	0.65	1.75	0.26	1.87	0.28	0.62	0.01	4.34	1.73	20.94	20.72	20.86	17.30	4.14
F2 (7)	Talisker	Frankton 2	1.05	4.97	0.65	3.39	0.62	1.71	0.25	1.69	0.26	0.54	0.00	1.64	2.00	92.23	95.39	90.96	10.06	4.95
F2 (8)	Talisker	Frankton 2	1.07	5.32	0.65	3.39	0.59	1.71	0.25	1.76	0.27	0.56	0.01	1.09	1.67	97.08	99.59	96.10	13.33	4.71
F2 (9)	Talisker	Frankton 2	0.85	4.00	0.55	2.83	0.55	1.50	0.22	1.56	0.23	0.36	0.01	1.07	1.24	88.22	92.22	87.48	7.94	4.60
F2 (10)	Talisker	Frankton 2	0.92	4.44	0.57	2.90	0.52	1.44	0.22	1.57	0.24	0.21	0.01	0.61	1.52	54.52	55.80	51.60	11.86	3.62
K1	Talisker	The Gap	0.60	2.63	0.38	2.25	0.42	1.24	0.18	1.35	0.19	0.67	0.00	1.27	1.46	82.72	87.52	82.08	11.39	3.17
K2	Talisker	The Gap	0.60	2.68	0.38	2.21	0.40	1.19	0.18	1.32	0.19	0.96	0.00	2.65	1.59	155.78	161.58	154.47	20.20	2.91
K3	Talisker	The Gap	0.69	2.92	0.43	2.49	0.47	1.33	0.20	1.49	0.22	1.15	0.00	1.96	1.79	186.96	193.17	185.94	17.86	3.84
K4	Talisker	The Gap	0.84	3.64	0.48	2.66	0.47	1.32	0.20	1.34	0.19	0.92	0.01	2.01	1.53	161.77	168.10	159.65	13.99	4.55
K5	Talisker	The Gap	0.76	3.37	0.45	2.53	0.44	1.29	0.19	1.35	0.19	0.70	0.02	2.33	1.63	182.01	187.17	180.53	16.38	4.58
K6	Talisker	The Gap	0.68	3.15	0.44	2.48	0.46	1.29	0.18	1.36	0.19	0.81	N.D.	0.75	1.61	170.20	176.66	170.02	12.52	6.49
K7	Talisker	The Gap	0.62	2.62	0.40	2.34	0.42	1.20	0.18	1.34	0.19	0.81	0.01	1.03	1.53	58.82	60.64	56.02	16.27	3.22
K8	Talisker	The Gap	0.50	1.80	0.29	1.86	0.36	1.07	0.18	1.40	0.21	0.85	0.00	2.99	1.69	70.32	73.32	67.11	11.40	2.80
K9	Talisker	The Gap	0.47	1.89	0.31	1.84	0.35	1.05	0.17	1.22	0.18	0.76	0.00	1.48	1.41	92.20	95.01	90.59	13.28	1.80

TOC, $\delta^{13}C_{org}$, $\delta^{34}S_{pyr}$ and trace element concentrations for the Heatherdale Shale, Mount Lofty ranges.

Sample	Formation	Locality	Height (m)	TOC (%)	$\delta^{13}C_{org}$ (‰)	$\delta^{34}S$ (‰)	Weighed (mg)	Li (ug/g)	Be (ug/g)	B (ug/g)	Sc (ug/g)	V (ug/g)	Co (ug/g)	Ni (ug/g)	Cu (ug/g)	Zn (ug/g)	Ga (ug/g)	Ge (ug/g)	As (ug/g)
N22	Heatherdale	Red Creek North Fork	84	0.65	-13.02		15.6	17.62	2.76	15.86	9.10	84.75	4.42	24.52	32.74	39.91	25.41	2.23	2.15
N28	Heatherdale	Red Creek North Fork	125	0.81	-16.64		15.6	19.08	2.70	7.32	12.60	200.01	4.72	22.55	47.00	40.99	25.93	2.74	5.19
N44	Heatherdale	Red Creek North Fork	268	0.44	-15.87		15	43.01	3.44	5.43	13.72	120.04	4.73	22.50	21.63	102.41	30.56	3.24	4.89
N46	Heatherdale	Red Creek North Fork	272	0.73	-15.41		15.2	60.32	4.14	19.20	18.82	184.55	11.67	33.90	44.89	93.70	42.06	2.86	2.95
N47	Heatherdale	Red Creek North Fork	274	0.69	-16.02		15.8	56.16	4.16	20.33	20.00	179.43	9.01	28.98	51.09	107.84	38.60	2.68	2.46
N48	Heatherdale	Red Creek North Fork	278	0.57	-15.86		14.8	48.25	3.46	10.17	10.92	140.98	10.83	50.83	36.82	121.71	32.95	1.85	2.62
N49	Heatherdale	Red Creek North Fork	284	0.82	-15.90		13.6	37.21	3.35	10.35	14.04	157.74	10.16	35.23	49.56	57.96	31.04	2.74	4.95
S5	Heatherdale	Red Creek South Fork	125	0.55	-11.10		15	7.31	1.45	25.30	9.54	165.52	21.59	35.46	72.75	20.01	18.20	2.47	1.25
S16	Heatherdale	Red Creek South Fork	165	0.74	-12.15		15.8	14.57	2.24	9.31	9.64	203.72	11.82	35.96	62.85	116.68	21.26	1.81	2.81
S17	Heatherdale	Red Creek South Fork	172	0.59	-11.21		16.3	12.80	2.20	13.66	11.91	113.55	6.27	17.80	31.46	39.51	20.95	1.44	5.14
S23	Heatherdale	Red Creek South Fork	208	0.42	-10.97		15.6	13.01	2.09	10.02	12.09	101.58	13.43	40.92	39.62	23.84	19.39	2.36	1.43
S26	Heatherdale	Red Creek South Fork	232	1.12	-14.92		15.2	16.83	2.86	5.28	13.49	367.62	15.27	66.31	109.78	49.12	23.84	2.79	31.03
S30	Heatherdale	Red Creek South Fork	250	0.23	-11.48		14.9	60.22	4.98	17.43	23.30	169.37	27.19	56.73	17.62	141.26	48.06	4.01	29.87
S31	Heatherdale	Red Creek South Fork	256	0.21	-15.47		14.8	55.65	4.80	17.72	23.68	179.83	18.17	57.28	25.96	125.34	43.24	3.92	11.32
S32	Heatherdale	Red Creek South Fork	258	0.25	-19.53		14.7	50.58	4.62	25.02	23.90	189.01	13.16	40.24	1.48	74.08	43.29	3.66	6.26
S37	Heatherdale	Red Creek South Fork	288	0.57	-10.00		15.2	27.10	2.79	12.40	15.06	110.28	11.14	21.74	23.90	100.86	24.77	3.54	4.41
S38	Heatherdale	Red Creek South Fork	295	1.06	-11.93		15.8	31.04	3.49	42.06	14.95	181.80	11.48	61.99	67.24	63.16	29.42	2.99	1.90
S39	Heatherdale	Red Creek South Fork	297	0.32	-15.03		16.4	57.76	4.32	62.23	22.45	173.02	24.62	48.70	39.33	113.63	40.97	3.57	31.55
SQ2	Heatherdale	Sedan Hill Quarry		1.56	-19.02		15	14.49	2.27	27.44	16.63	669.13	0.48	13.18	23.29	52.44	28.62	0.55	19.59
SQ3	Heatherdale	Sedan Hill Quarry		1.24	-18.51		15.4	22.25	3.84	31.42	15.03	530.96	0.47	11.86	23.09	42.73	26.67	1.45	3.59
SQ5	Heatherdale	Sedan Hill Quarry		0.92	-18.83		15.4	22.78	2.39	24.69	13.55	222.06	1.13	18.58	38.53	47.12	23.98	1.24	17.96

TOC, $\delta^{13}C_{org}$, $\delta^{34}S_{pyr}$ and trace element concentrations for the Heatherdale Shale, Mount Lofty ranges.

Sample	Formation	Locality	Se (ug/g)	Rb (ug/g)	Y (ug/g)	Nb (ug/g)	Mo (ug/g)	Cd (ug/g)	Sn [1] (ug/g)	Sn [2] (ug/g)	Sn [3] (ug/g)	Cs (ug/g)	La (ug/g)	Ce (ug/g)	Pr (ug/g)	Nd (ug/g)	Sm (ug/g)	Eu (ug/g)
N22	Heatherdale	Red Creek North Fork	0.25	100.05	15.93	15.66	2.03	0.36	2.31	1.80	1.49	3.59	36.80	65.05	7.32	27.14	4.99	1.04
N28	Heatherdale	Red Creek North Fork	1.15	134.73	12.12	14.42	5.56	0.08	2.88	2.83	3.02	4.01	45.39	84.91	9.48	35.32	6.41	1.31
N44	Heatherdale	Red Creek North Fork	0.49	167.31	17.79	22.90	1.18	0.07	3.53	3.52	3.72	8.72	51.08	102.38	11.69	45.27	8.92	1.42
N46	Heatherdale	Red Creek North Fork	2.41	206.73	13.38	4.97	2.19	0.08	3.93	3.57	3.54	8.02	40.96	78.56	8.79	32.78	5.99	1.08
N47	Heatherdale	Red Creek North Fork	3.71	208.36	13.70	6.02	0.85	0.06	3.83	4.02	4.16	9.60	28.01	65.86	8.15	30.54	5.88	1.12
N48	Heatherdale	Red Creek North Fork	1.01	89.61	5.09	7.76	1.36	0.06	3.46	3.59	3.76	6.97	18.34	34.52	4.63	17.76	3.40	0.75
N49	Heatherdale	Red Creek North Fork	2.61	166.68	13.83	10.74	3.31	0.11	3.93	3.57	3.33	5.75	46.77	86.61	9.68	35.88	6.46	1.19
S5	Heatherdale	Red Creek South Fork	0.96	34.47	11.79	27.88	6.61	0.17	1.27	1.31	1.42	1.33	31.06	63.46	7.04	26.42	4.77	1.44
S16	Heatherdale	Red Creek South Fork	1.15	54.50	10.15	7.46	5.21	1.02	3.31	3.48	3.68	2.86	18.55	39.32	4.73	18.39	3.58	0.81
S17	Heatherdale	Red Creek South Fork	0.47	109.12	10.54	12.03	1.68	0.15	2.26	2.39	2.60	2.40	13.65	28.03	3.17	12.19	2.44	0.62
S23	Heatherdale	Red Creek South Fork	0.59	59.37	13.09	13.08	1.49	0.13	1.59	1.61	1.74	1.47	26.82	56.10	6.30	24.48	4.78	1.20
S26	Heatherdale	Red Creek South Fork	2.45	128.07	12.76	4.95	14.65	0.29	4.58	4.77	5.31	1.98	40.08	80.29	8.81	33.35	6.13	1.16
S30	Heatherdale	Red Creek South Fork	0.24	220.25	16.41	18.81	0.25	0.23	5.90	5.62	5.49	7.15	56.97	112.44	12.47	46.46	8.21	1.50
S31	Heatherdale	Red Creek South Fork	0.28	221.91	15.83	18.01	0.24	0.07	4.85	5.16	5.54	4.39	54.93	107.19	11.81	44.10	7.76	1.52
S32	Heatherdale	Red Creek South Fork	0.25	227.54	13.78	19.30	0.22	0.04	5.33	5.49	6.11	6.06	56.53	112.56	12.52	45.58	7.67	1.33
S37	Heatherdale	Red Creek South Fork	0.43	178.50	16.53	18.27	0.46	0.35	5.19	4.56	4.78	9.34	37.70	80.50	8.63	31.18	5.89	1.13
S38	Heatherdale	Red Creek South Fork	1.05	173.56	13.32	15.45	5.03	0.18	3.70	3.89	4.14	15.94	42.59	84.25	9.16	33.91	6.13	1.06
S39	Heatherdale	Red Creek South Fork	0.24	200.63	15.06	16.73	0.26	0.05	4.26	4.49	4.92	4.98	50.40	98.85	10.93	40.75	7.19	1.32
SQ2	Heatherdale	Sedan Hill Quarry	1.71	82.12	11.23	5.48	11.24	0.10	6.26	6.54	7.30	1.51	10.20	17.37	1.73	6.18	1.32	0.32
SQ3	Heatherdale	Sedan Hill Quarry	1.39	143.17	11.39	3.21	13.07	0.05	5.09	5.31	5.84	2.47	24.83	52.70	5.79	22.44	4.24	0.90
SQ5	Heatherdale	Sedan Hill Quarry	1.48	116.20	13.63	4.51	14.61	0.07	4.20	4.23	4.77	5.14	24.07	43.59	4.16	15.30	3.14	0.70

TOC, $\delta^{13}C_{org}$, $\delta^{34}S_{pyr}$ and trace element concentrations for the Heatherdale Shale, Mount Lofty ranges.

Sample	Formation	Locality	Gd (ug/g)	Tb (ug/g)	Dy (ug/g)	Ho (ug/g)	Er (ug/g)	Tm (ug/g)	Yb (ug/g)	Lu (ug/g)	Ta (ug/g)	Re (ug/g)	Au (ug/g)	Tl (ug/g)	206 Pb (ug/g)	207 Pb (ug/g)	208 Pb (ug/g)	Th (ug/g)	U (ug/g)
N22	Heatherdale	Red Creek North Fork	4.69	0.60	3.16	0.60	1.71	0.25	1.83	0.26	0.75	0.00	1.49	0.64	15.11	14.92	15.00	12.00	3.54
N28	Heatherdale	Red Creek North Fork	5.49	0.63	2.87	0.49	1.45	0.22	1.65	0.24	0.79	0.00	0.92	0.78	14.29	13.48	13.97	14.15	3.58
N44	Heatherdale	Red Creek North Fork	7.41	0.86	4.02	0.72	2.03	0.30	2.19	0.34	0.64	0.00	0.58	0.94	12.67	12.51	12.83	14.10	2.63
N46	Heatherdale	Red Creek North Fork	5.13	0.64	3.03	0.53	1.48	0.22	1.65	0.24	0.36	0.00	0.68	1.09	13.80	13.02	13.51	20.27	3.66
N47	Heatherdale	Red Creek North Fork	5.26	0.67	3.31	0.56	1.57	0.24	1.74	0.26	0.43	0.01	0.91	1.15	42.66	43.56	40.43	18.08	3.97
N48	Heatherdale	Red Creek North Fork	2.91	0.37	1.88	0.33	0.95	0.15	1.04	0.16	0.53	0.00	1.17	0.95	18.63	18.53	18.81	5.58	2.75
N49	Heatherdale	Red Creek North Fork	5.82	0.69	3.18	0.55	1.52	0.22	1.55	0.23	0.65	N.D.	1.36	0.90	12.20	11.77	12.20	15.92	4.07
S5	Heatherdale	Red Creek South Fork	4.48	0.54	2.68	0.48	1.41	0.21	1.50	0.23	1.68	0.00	2.54	0.37	9.11	7.73	8.02	9.94	5.86
S16	Heatherdale	Red Creek South Fork	3.46	0.48	2.55	0.46	1.32	0.19	1.42	0.23	0.45	0.00	0.67	0.64	16.93	16.52	16.83	6.62	3.41
S17	Heatherdale	Red Creek South Fork	2.48	0.35	2.07	0.41	1.22	0.19	1.41	0.20	0.88	0.00	0.90	0.61	7.81	7.10	7.56	11.89	2.77
S23	Heatherdale	Red Creek South Fork	4.34	0.53	2.69	0.49	1.43	0.20	1.48	0.22	0.63	0.00	0.43	0.22	4.70	4.01	4.35	11.14	2.52
S26	Heatherdale	Red Creek South Fork	5.20	0.63	2.98	0.50	1.37	0.20	1.38	0.20	0.31	0.00	0.60	0.49	14.42	11.28	11.61	14.47	7.60
S30	Heatherdale	Red Creek South Fork	7.06	0.84	3.93	0.67	1.86	0.27	1.86	0.27	1.42	0.00	1.48	0.97	24.90	24.13	24.88	20.99	3.53
S31	Heatherdale	Red Creek South Fork	6.60	0.77	3.73	0.67	1.80	0.26	1.89	0.27	1.29	0.00	1.43	0.97	17.96	17.46	17.98	20.66	3.04
S32	Heatherdale	Red Creek South Fork	6.43	0.74	3.45	0.58	1.61	0.23	1.61	0.24	1.39	0.00	1.31	1.00	8.05	7.20	7.91	20.78	3.29
S37	Heatherdale	Red Creek South Fork	4.59	0.63	3.18	0.60	1.73	0.27	1.87	0.30	1.72	0.00	0.05	0.87	14.54	12.88	13.82	20.32	5.27
S38	Heatherdale	Red Creek South Fork	5.20	0.65	3.20	0.56	1.51	0.21	1.49	0.23	1.55	0.03	2.28	1.04	12.45	11.24	11.75	18.04	6.13
S39	Heatherdale	Red Creek South Fork	6.18	0.74	3.48	0.62	1.77	0.26	1.85	0.28	1.25	0.00	5.73	0.77	7.33	6.45	7.27	21.02	3.95
SQ2	Heatherdale	Sedan Hill Quarry	1.49	0.27	1.97	0.41	1.26	0.21	1.55	0.23	0.39	0.01	0.54	0.40	5.39	4.27	4.51	13.25	3.78
SQ3	Heatherdale	Sedan Hill Quarry	4.07	0.48	2.28	0.40	1.19	0.18	1.39	0.21	0.26	0.01	0.62	0.86	23.74	22.51	22.59	12.39	5.68
SQ5	Heatherdale	Sedan Hill Quarry	3.27	0.46	2.66	0.53	1.55	0.24	1.68	0.24	0.40	0.01	0.57	1.04	31.95	31.28	30.96	12.42	9.52

TOC, $\delta^{13}C_{org}$, $\delta^{34}S_{pyr}$ and trace element concentrations for the Heatherdale Shale, Fleurieu Peninsula.

Sample	Formation	Locality	Height (m)	TOC (%)	$\delta^{13}C_{org}$ (‰)	$\delta^{34}S$ (‰)	Weighed (mg)	Li (ug/g)	Be (ug/g)	B (ug/g)	Sc (ug/g)	V (ug/g)	Co (ug/g)	Ni (ug/g)	Cu (ug/g)	Zn (ug/g)
C3	Heatherdale Shale (lower)	Carrickalinga Head Creek	1	1.66	-30.99		14.8	27.79	1.73	2.76	8.38	250.07	5.47	24.44	26.82	71.28
C5	Heatherdale Shale (lower)	Carrickalinga Head Creek	5	0.63	-30.88		15.6	19.55	1.23	6.23	6.57	109.39	2.90	13.48	22.42	75.88
C6	Heatherdale Shale (lower)	Carrickalinga Head Creek	9.5	0.55	-31.28		16.6	8.99	0.83	2.49	2.82	55.12	2.73	4.57	9.35	47.97
C7	Heatherdale Shale (lower)	Carrickalinga Head Creek	10	0.77	-31.19		15	34.46	3.06	12.94	15.19	119.51	3.66	19.14	54.49	66.66
C8	Heatherdale Shale (lower)	Carrickalinga Head Creek	10.5	0.55	-32		16.2	9.05	0.81	0.68	2.69	56.78	2.89	4.21	8.80	38.10
C9	Heatherdale Shale (lower)	Carrickalinga Head Creek	12	0.77	-31.71		15.9	9.94	0.88	0.69	3.11	65.39	2.76	5.75	10.72	38.97
C10	Heatherdale Shale (lower)	Carrickalinga Head Creek	13.5	0.47	-31.69		15.2	10.95	1.06	0.41	2.92	52.53	2.28	3.50	7.64	33.78
C10A	Heatherdale Shale (lower)	Carrickalinga Head Creek	13.5	0.52	-31.43		14.5	25.30	1.71	3.48	8.06	220.42	6.50	25.47	29.18	80.69
C11	Heatherdale Shale (lower)	Carrickalinga Head Creek	17	0.40	-31.81		15.9	9.45	0.84	N.D.	2.49	34.72	3.02	4.21	10.80	57.24
C15	Heatherdale Shale (lower)	Carrickalinga Head Cove	59.5	0.46	-32.7		14.2	13.91	1.02	0.91	3.24	45.80	2.71	6.75	14.21	93.69
C16	Heatherdale Shale (lower)	Carrickalinga Head Cove	59	1.07	-29.33		16.4	29.47	2.24	10.25	9.51	143.07	12.40	44.87	29.17	344.08
C17	Heatherdale Shale (lower)	Carrickalinga Head Cove	57.5	1.75	-27.33		15.5	39.48	2.50	8.49	12.02	323.78	6.86	30.67	55.83	80.77
C18A	Heatherdale Shale (lower)	Carrickalinga Head Cove	57	1.16	-31.57		15.4	29.70	1.84	5.63	8.71	107.49	5.64	19.13	43.07	63.14
C18C	Heatherdale Shale (lower)	Carrickalinga Head Cove	57	0.56	-32.39		14.6	17.67	0.82	0.07	3.75	41.99	3.17	6.55	41.62	31.09
C19A	Heatherdale Shale (lower)	Carrickalinga Head Cove	55	0.72	-31.97	10.1	15.2	14.78	1.07	0.14	4.21	65.28	2.38	4.30	10.46	53.82
C19B	Heatherdale Shale (lower)	Carrickalinga Head Cove	55	2.14	-32.28		14.9	36.65	2.35	4.20	10.70	697.33	6.88	44.62	54.10	104.73
C20	Heatherdale Shale (lower)	Carrickalinga Head Cove	50	0.25	-32.36		15.8	10.57	1.13	N.D.	3.42	43.32	1.56	3.37	13.14	48.08
C23	Heatherdale Shale (lower)	Carrickalinga Head Cove	41	0.24	-31.34		14.4	9.64	0.90	0.17	3.23	49.98	5.56	11.22	7.50	84.57
C27	Heatherdale Shale (lower)	Carrickalinga Head Cove	25	1.05	-30.86		16	26.67	1.48	3.57	6.95	77.49	2.45	10.04	11.57	40.65
C28	Heatherdale Shale (lower)	Carrickalinga Head Cove	24	0.19	-29.55		15.4	12.61	0.78	0.07	3.24	22.20	1.69	N.D.	9.07	55.10
C29	Heatherdale Shale (lower)	Carrickalinga Head Cove	22	1.16	-30.43		14.8	36.46	1.72	1.36	9.01	68.83	4.30	15.36	16.26	51.10
C31	Heatherdale Shale (lower)	Carrickalinga Head Cove	9	0.21	-30.51		16.4	13.46	0.70	N.D.	3.25	18.59	2.39	N.D.	12.78	15.44
M3	Heatherdale Shale (lower)	Myponga Beach		0.37	-32.11		14.6	35.91	2.02	3.61	10.38	126.60	14.76	38.98	29.66	186.00
S12	Heatherdale Shale (upper)	Sellick Hill		0.83	-30.49		16.1	37.30	2.58	5.83	12.77	158.96	4.11	24.16	50.49	74.06
S13	Heatherdale Shale (upper)	Sellick Hill		1.09	-31.7	7.79	16.7	41.45	1.72	10.70	8.14	279.77	3.98	27.74	31.64	97.51
S14	Heatherdale Shale (upper)	Sellick Hill		0.73	-31.24	11.2	14.6	46.20	2.84	13.97	13.39	176.00	4.38	32.26	66.93	104.80
S17	Heatherdale Shale (upper)	Sellick Hill	2	1.62	-31	-2.68	15.4	32.67	2.18	3.82	11.16	303.51	7.90	21.83	46.73	79.72
S18	Heatherdale Shale (upper)	Sellick Hill	2.5	1.60	-30.95	-3.00	16.7	39.69	2.46	5.52	12.91	208.56	8.94	32.62	60.27	119.78
S20	Heatherdale Shale (upper)	Sellick Hill	4.5	1.85	-31.22		15.9	37.97	2.55	17.70	12.82	1034.40	13.92	70.77	125.23	126.68
S21	Heatherdale Shale (upper)	Sellick Hill	6	2.03	-30.92		14.7	18.87	2.05	3.93	12.15	143.90	6.43	11.72	50.37	119.02
S22	Heatherdale Shale (upper)	Sellick Hill	7	1.99	-30.89		14.7	24.18	2.96	7.24	15.23	827.59	4.34	18.95	28.49	105.44
S23	Heatherdale Shale (upper)	Sellick Hill	9.5	2.03	-31.22		16.2	32.26	2.46	10.77	12.39	728.05	3.80	28.21	65.42	119.85
S24	Heatherdale Shale (upper)	Sellick Hill	11.5	2.22	-31.41		15.6	30.99	2.88	7.71	14.59	704.97	4.03	25.82	38.81	98.89
S25	Heatherdale Shale (upper)	Sellick Hill	15	1.94	-31.29		15.5	31.56	2.59	6.13	13.72	879.74	3.81	27.35	47.49	103.07
S27	Heatherdale Shale (upper)	Sellick Hill	21	1.57	-30.79	6.36	14.9	33.42	2.54	12.98	14.08	280.49	2.19	12.17	44.28	63.87
S28	Heatherdale Shale (upper)	Sellick Hill	24.5	2.28	-31.26		16.3	20.56	2.66	6.50	15.34	283.99	4.63	17.66	55.68	74.78
S30	Heatherdale Shale (upper)	Sellick Hill	26.5	2.57	-31.15		15.5	27.87	2.98	6.62	14.55	352.27	8.79	24.34	60.83	74.04
S32	Heatherdale Shale (upper)	Sellick Hill	29	0.91	-31.1		16.1	38.61	2.13	11.19	8.46	79.75	9.07	30.20	47.54	84.09
S33	Heatherdale Shale (upper)	Sellick Hill	40	2.11	-31.13		16.5	25.09	2.86	5.71	14.45	492.56	4.53	19.64	50.58	92.66
S35	Heatherdale Shale (upper)	Sellick Hill	43.5	2.05	-31.45		15.3	26.13	2.59	5.94	14.54	475.71	6.43	28.94	37.20	81.62
S37	Heatherdale Shale (upper)	Sellick Hill	47.5	1.18	-31.73		16.5	16.75	1.00	1.33	5.25	254.25	5.16	13.45	17.16	64.40
S39	Heatherdale Shale (upper)	Sellick Hill	54.5	2.33	-31.15		14.5	24.12	3.05	11.62	15.69	424.47	1.13	4.04	48.33	40.57

TOC, $\delta^{13}C_{org}$, $\delta^{34}S_{pyr}$ and trace element concentrations for the Heatherdale Shale, Fleurieu Peninsula.

Sample	Formation	Locality	Ga (ug/g)	Ge (ug/g)	As (ug/g)	Se (ug/g)	Rb (ug/g)	Y (ug/g)	Nb (ug/g)	Mo (ug/g)	Cd (ug/g)	Sn [1] (ug/g)	Sn [2] (ug/g)	Sn [3] (ug/g)	Cs (ug/g)	La (ug/g)	Ce (ug/g)	Pr (ug/g)	Nd (ug/g)	Sm (ug/g)
C3	Heatherdale Shale (lower)	Carrickalinga Head Creek	12.40	2.58	15.42	1.60	98.02	25.34	7.79	6.66	0.69	2.76	2.39	2.22	5.80	30.34	62.82	7.18	26.64	4.90
C5	Heatherdale Shale (lower)	Carrickalinga Head Creek	9.19	2.06	12.46	0.38	70.85	23.05	5.86	6.04	1.84	2.29	1.94	2.13	3.33	25.33	49.05	5.87	21.70	4.28
C6	Heatherdale Shale (lower)	Carrickalinga Head Creek	3.40	1.37	5.69	0.58	23.42	20.08	2.39	2.39	1.95	2.46	2.12	2.27	2.01	16.35	29.72	3.77	13.79	3.04
C7	Heatherdale Shale (lower)	Carrickalinga Head Creek	24.48	3.95	13.04	0.87	173.37	31.32	15.69	1.90	0.22	5.13	4.57	4.92	10.56	57.83	116.26	12.57	44.62	8.01
C8	Heatherdale Shale (lower)	Carrickalinga Head Creek	3.53	1.30	5.94	0.56	24.07	20.72	2.42	2.42	3.90	0.84	0.74	0.78	1.91	16.61	30.35	3.82	14.62	2.94
C9	Heatherdale Shale (lower)	Carrickalinga Head Creek	4.55	1.58	6.24	0.39	32.16	28.61	3.02	3.73	0.88	1.17	0.99	1.04	2.43	29.47	43.82	4.82	17.90	3.36
C10	Heatherdale Shale (lower)	Carrickalinga Head Creek	4.42	1.25	4.95	0.32	30.62	18.44	2.85	1.02	1.82	0.94	0.91	0.89	2.48	16.32	28.89	3.69	13.62	2.80
C10A	Heatherdale Shale (lower)	Carrickalinga Head Creek	11.88	2.89	17.09	0.90	91.62	33.21	7.37	7.50	1.51	2.81	2.35	2.56	5.47	34.80	70.96	8.13	29.73	5.83
C11	Heatherdale Shale (lower)	Carrickalinga Head Creek	3.85	1.09	5.97	0.26	26.14	12.52	2.54	3.25	1.74	0.76	0.69	0.73	1.98	13.46	24.29	2.87	10.93	2.16
C15	Heatherdale Shale (lower)	Carrickalinga Head Cove	5.12	1.17	8.48	0.38	39.12	18.43	3.28	0.64	1.08	1.06	0.95	1.00	2.88	15.56	26.09	3.15	11.37	2.29
C16	Heatherdale Shale (lower)	Carrickalinga Head Cove	15.25	2.55	22.51	0.96	123.27	23.15	9.79	2.72	0.39	3.25	3.08	3.19	9.23	31.24	63.50	6.65	23.74	4.40
C17	Heatherdale Shale (lower)	Carrickalinga Head Cove	18.99	2.93	24.58	2.69	151.26	26.51	11.70	4.10	0.09	3.83	3.49	3.67	10.27	37.40	74.32	7.83	27.70	5.19
C18A	Heatherdale Shale (lower)	Carrickalinga Head Cove	13.95	2.32	8.65	1.67	112.24	24.69	8.79	1.70	0.22	3.16	2.77	2.94	7.89	30.63	59.53	6.59	23.33	4.45
C18C	Heatherdale Shale (lower)	Carrickalinga Head Cove	4.55	2.38	14.41	1.21	30.26	47.50	2.86	1.78	3.67	0.77	0.63	0.73	2.48	35.13	57.93	6.97	26.28	5.25
C19A	Heatherdale Shale (lower)	Carrickalinga Head Cove	6.03	1.61	7.97	1.03	47.39	25.74	3.96	4.20	0.42	1.24	1.07	1.08	2.90	22.48	41.01	4.72	17.47	3.48
C19B	Heatherdale Shale (lower)	Carrickalinga Head Cove	16.85	3.09	26.34	3.29	137.36	26.92	11.83	15.86	0.40	3.31	3.01	3.19	9.24	36.02	75.84	8.33	29.96	5.77
C20	Heatherdale Shale (lower)	Carrickalinga Head Cove	4.99	1.64	27.60	0.79	38.63	32.03	3.13	0.41	3.77	0.84	0.79	0.88	2.97	29.81	46.50	5.17	18.92	3.67
C23	Heatherdale Shale (lower)	Carrickalinga Head Cove	3.77	1.36	4.92	0.20	27.96	21.37	2.46	1.22	1.64	0.79	0.65	0.76	2.49	16.28	30.40	3.99	15.57	3.22
C27	Heatherdale Shale (lower)	Carrickalinga Head Cove	11.94	2.88	8.22	1.51	87.18	30.96	6.89	2.11	0.25	5.32	4.86	5.12	4.46	35.48	76.83	8.62	32.34	6.33
C28	Heatherdale Shale (lower)	Carrickalinga Head Cove	4.84	1.35	5.61	1.61	35.87	13.62	3.32	1.72	0.88	2.25	2.14	2.26	2.76	18.19	30.33	3.61	12.85	2.47
C29	Heatherdale Shale (lower)	Carrickalinga Head Cove	14.54	2.42	8.53	0.65	109.90	21.22	9.38	1.82	0.20	2.98	2.64	2.86	6.02	28.05	54.05	6.49	23.21	4.55
C31	Heatherdale Shale (lower)	Carrickalinga Head Cove	4.64	1.32	2.17	0.18	37.09	14.11	3.43	0.06	0.07	1.72	1.54	1.65	2.24	17.21	29.09	3.80	13.63	2.73
M3	Heatherdale Shale (lower)	Myponga Beach	13.63	2.58	12.70	0.59	117.82	25.37	9.56	4.51	1.78	2.70	2.43	2.44	5.34	30.85	59.18	7.01	25.17	4.76
S12	Heatherdale Shale (upper)	Sellick Hill	20.68	3.24	10.94	0.57	150.16	24.73	19.13	1.89	0.99	3.82	3.40	3.59	10.13	43.19	86.37	9.14	32.20	5.79
S13	Heatherdale Shale (upper)	Sellick Hill	14.62	2.23	10.54	0.61	104.90	19.32	12.05	3.47	0.58	3.89	3.34	3.64	5.80	29.67	62.68	6.39	22.36	4.14
S14	Heatherdale Shale (upper)	Sellick Hill	22.05	3.63	14.37	0.86	158.24	29.93	16.06	2.47	0.58	4.19	3.82	4.16	10.99	49.25	99.56	10.39	36.42	6.89
S17	Heatherdale Shale (upper)	Sellick Hill	18.35	3.09	18.88	3.30	132.56	21.30	11.69	5.04	0.18	3.24	2.96	3.05	8.25	37.96	79.82	8.42	30.01	5.51
S18	Heatherdale Shale (upper)	Sellick Hill	20.32	3.47	17.86	2.56	143.35	24.18	13.33	4.00	0.45	3.95	3.48	3.73	8.87	42.25	90.49	9.38	33.00	5.87
S20	Heatherdale Shale (upper)	Sellick Hill	20.75	3.53	43.09	6.52	153.30	22.84	13.64	24.42	0.87	4.10	3.57	3.88	9.78	39.13	84.82	9.35	33.13	6.04
S21	Heatherdale Shale (upper)	Sellick Hill	20.52	3.18	70.64	4.67	140.40	21.41	14.95	44.35	0.66	4.35	3.75	4.03	8.37	41.61	86.57	9.18	31.85	5.73
S22	Heatherdale Shale (upper)	Sellick Hill	24.50	3.27	49.68	7.73	188.70	26.41	18.54	15.56	0.40	5.25	4.67	5.11	10.60	52.00	106.77	11.25	38.67	6.76
S23	Heatherdale Shale (upper)	Sellick Hill	20.70	3.03	32.76	4.78	155.84	21.71	14.18	16.56	0.28	3.62	3.27	3.54	9.69	39.90	82.11	8.75	30.37	5.47
S24	Heatherdale Shale (upper)	Sellick Hill	24.18	3.39	29.26	3.67	179.30	22.45	16.08	15.76	0.30	4.87	4.41	4.58	11.36	49.25	101.33	10.66	36.34	6.22
S25	Heatherdale Shale (upper)	Sellick Hill	22.58	3.36	31.45	3.33	169.94	24.90	16.43	18.85	0.34	5.38	4.75	5.09	11.12	47.07	97.61	10.41	35.94	6.47
S27	Heatherdale Shale (upper)	Sellick Hill	23.44	3.25	17.39	3.05	168.21	26.32	15.73	3.53	0.15	4.57	4.06	4.39	9.58	46.59	94.56	9.85	33.92	6.28
S28	Heatherdale Shale (upper)	Sellick Hill	24.29	3.99	32.78	4.33	181.47	26.38	16.48	19.99	0.40	4.55	4.07	4.45	9.82	54.71	117.81	12.43	42.65	7.49
S30	Heatherdale Shale (upper)	Sellick Hill	23.26	3.87	33.08	3.51	166.15	26.87	14.50	19.82	0.90	4.44	3.80	4.17	9.73	48.61	101.54	10.94	38.37	6.95
S32	Heatherdale Shale (upper)	Sellick Hill	13.82	3.20	7.43	0.98	91.65	33.06	9.08	1.96	5.73	2.72	2.35	2.58	6.27	33.55	68.17	7.73	28.41	5.67
S33	Heatherdale Shale (upper)	Sellick Hill	24.26	4.59	37.29	6.58	171.99	37.70	14.99	12.76	0.22	4.25	3.83	3.93	9.96	56.34	126.21	13.87	51.24	9.89
S35	Heatherdale Shale (upper)	Sellick Hill	23.21	3.73	28.59	2.86	167.22	27.86	14.51	11.37	0.16	4.16	3.66	3.80	9.64	49.73	105.44	11.26	40.00	7.53
S37	Heatherdale Shale (upper)	Sellick Hill	8.26	2.08	12.37	0.93	63.42	22.15	5.49	5.46	0.93	1.30	1.07	1.22	3.99	21.92	40.53	4.92	18.29	3.60
S39	Heatherdale Shale (upper)	Sellick Hill	25.88	3.75	12.44	1.07	190.75	30.65	15.84	5.17	0.10	5.53	4.84	5.29	10.63	56.97	118.37	12.60	44.72	8.64

TOC, $\delta^{13}C_{org}$, $\delta^{34}S_{pyr}$ and trace element concentrations for the Heatherdale Shale, Fleurieu Peninsula.

Sample	Formation	Locality	Eu (ug/g)	Gd (ug/g)	Tb (ug/g)	Dy (ug/g)	Ho (ug/g)	Er (ug/g)	Tm (ug/g)	Yb (ug/g)	Lu (ug/g)	Ta (ug/g)	Re (ug/g)	Au (ug/g)	Tl (ug/g)	206 Pb (ug/g)	207 Pb (ug/g)	208 Pb (ug/g)	Th (ug/g)	U (ug/g)
C3	Heatherdale Shale (lower)	Carrickalinga Head Creek	0.97	4.48	0.63	3.90	0.76	2.27	0.28	2.05	0.27	1.13	0.00	N.D.	0.93	19.06	16.50	17.48	9.79	6.22
C5	Heatherdale Shale (lower)	Carrickalinga Head Creek	1.01	4.12	0.65	3.55	0.74	2.00	0.29	1.69	0.28	0.84	0.01	0.52	0.85	23.14	20.50	21.03	8.24	7.39
C6	Heatherdale Shale (lower)	Carrickalinga Head Creek	1.18	3.09	0.47	2.77	0.57	1.61	0.22	1.33	0.20	0.26	0.01	0.22	0.44	13.07	11.19	11.63	3.08	4.45
C7	Heatherdale Shale (lower)	Carrickalinga Head Creek	1.75	7.09	0.98	5.32	1.09	3.13	0.46	3.00	0.46	1.72	0.03	0.19	1.42	24.40	22.90	24.02	21.43	6.93
C8	Heatherdale Shale (lower)	Carrickalinga Head Creek	0.91	3.00	0.47	2.75	0.57	1.62	0.21	1.34	0.19	0.28	0.01	0.12	0.33	16.75	14.56	14.78	3.02	4.49
C9	Heatherdale Shale (lower)	Carrickalinga Head Creek	1.01	3.69	0.53	3.19	0.67	1.95	0.26	1.57	0.24	0.37	0.01	0.09	0.40	12.76	10.84	11.07	3.72	5.10
C10	Heatherdale Shale (lower)	Carrickalinga Head Creek	0.90	2.85	0.42	2.36	0.49	1.32	0.18	1.10	0.16	0.30	0.01	0.08	0.31	9.74	8.49	8.74	3.35	3.04
C10A	Heatherdale Shale (lower)	Carrickalinga Head Creek	1.19	5.63	0.84	5.04	1.03	2.93	0.42	2.51	0.38	0.93	0.01	0.09	1.35	25.66	22.74	23.24	9.58	7.63
C11	Heatherdale Shale (lower)	Carrickalinga Head Creek	0.76	2.05	0.31	1.73	0.34	0.94	0.13	0.78	0.12	0.26	0.02	0.05	0.26	14.02	12.56	12.70	3.09	3.57
C15	Heatherdale Shale (lower)	Carrickalinga Head Cove	0.83	2.45	0.38	2.31	0.50	1.37	0.21	1.21	0.19	0.29	0.01	0.03	0.26	6.96	6.37	6.50	3.99	2.59
C16	Heatherdale Shale (lower)	Carrickalinga Head Cove	0.91	4.00	0.60	3.50	0.76	2.22	0.33	2.21	0.32	1.02	0.01	0.05	0.85	18.96	17.64	18.29	12.56	4.21
C17	Heatherdale Shale (lower)	Carrickalinga Head Cove	1.06	4.52	0.67	4.00	0.85	2.52	0.39	2.52	0.38	1.10	0.02	0.04	1.08	19.91	18.06	18.78	15.71	5.89
C18A	Heatherdale Shale (lower)	Carrickalinga Head Cove	0.88	4.08	0.60	3.60	0.76	2.34	0.33	2.16	0.32	0.88	0.01	0.04	0.74	12.59	11.34	11.99	12.37	3.83
C18C	Heatherdale Shale (lower)	Carrickalinga Head Cove	1.45	6.03	0.90	5.57	1.19	3.46	0.44	2.75	0.41	0.26	0.01	0.03	0.28	12.13	10.58	10.79	3.65	5.01
C19A	Heatherdale Shale (lower)	Carrickalinga Head Cove	0.83	3.46	0.54	3.33	0.71	2.08	0.30	1.84	0.26	0.42	0.01	0.02	0.33	14.90	9.33	9.33	4.48	20.28
C19B	Heatherdale Shale (lower)	Carrickalinga Head Cove	1.10	5.04	0.72	4.22	0.87	2.50	0.38	2.34	0.33	1.25	0.03	0.05	1.22	29.07	26.14	26.72	14.11	8.29
C20	Heatherdale Shale (lower)	Carrickalinga Head Cove	1.07	3.97	0.63	3.80	0.85	2.50	0.35	2.15	0.33	0.33	0.01	0.03	0.25	10.64	9.63	9.88	3.72	2.98
C23	Heatherdale Shale (lower)	Carrickalinga Head Cove	0.98	3.33	0.48	2.77	0.58	1.56	0.22	1.28	0.19	0.23	0.01	0.03	0.27	12.56	11.05	11.28	2.96	3.26
C27	Heatherdale Shale (lower)	Carrickalinga Head Cove	1.12	5.77	0.84	4.69	0.92	2.54	0.34	2.06	0.28	0.81	0.02	0.02	0.59	12.14	10.30	10.61	8.51	5.21
C28	Heatherdale Shale (lower)	Carrickalinga Head Cove	0.67	2.24	0.33	1.88	0.39	1.07	0.15	0.93	0.13	0.34	0.00	0.02	0.22	10.98	10.48	10.75	3.71	1.72
C29	Heatherdale Shale (lower)	Carrickalinga Head Cove	0.87	4.08	0.58	3.38	0.66	1.89	0.27	1.74	0.26	1.16	0.01	0.04	0.70	13.69	12.16	12.84	10.36	3.39
C31	Heatherdale Shale (lower)	Carrickalinga Head Cove	0.60	2.42	0.38	2.09	0.42	1.12	0.15	0.96	0.14	0.31	0.00	0.01	0.17	5.27	4.82	4.96	3.26	1.41
M3	Heatherdale Shale (lower)	Myponga Beach	0.93	4.14	0.63	3.89	0.82	2.46	0.36	2.33	0.34	1.19	0.02	0.21	0.90	23.94	22.32	22.99	11.02	3.58
S12	Heatherdale Shale (upper)	Sellick Hill	1.38	4.74	0.66	3.77	0.79	2.42	0.37	2.40	0.37	1.35	0.02	0.10	1.76	22.68	21.21	21.92	15.64	6.41
S13	Heatherdale Shale (upper)	Sellick Hill	0.84	3.53	0.48	2.85	0.61	1.88	0.29	1.97	0.29	0.86	0.03	0.07	0.94	22.59	20.81	21.49	11.85	5.94
S14	Heatherdale Shale (upper)	Sellick Hill	1.52	5.90	0.80	4.59	0.92	2.66	0.38	2.55	0.37	1.27	0.01	0.07	1.61	24.91	23.15	23.75	17.47	6.11
S17	Heatherdale Shale (upper)	Sellick Hill	0.97	4.57	0.61	3.46	0.70	2.00	0.31	1.94	0.29	0.83	0.02	0.05	1.30	20.95	19.30	19.77	13.95	5.86
S18	Heatherdale Shale (upper)	Sellick Hill	1.12	5.09	0.69	3.89	0.81	2.35	0.35	2.29	0.34	1.31	0.01	0.05	1.35	22.69	20.78	21.49	15.84	6.72
S20	Heatherdale Shale (upper)	Sellick Hill	1.07	5.03	0.71	3.99	0.79	2.41	0.35	2.27	0.36	1.24	0.02	0.06	2.44	45.25	42.58	43.37	15.93	10.59
S21	Heatherdale Shale (upper)	Sellick Hill	0.92	4.40	0.62	3.60	0.75	2.39	0.38	2.54	0.41	0.87	0.02	0.05	1.79	78.66	74.57	76.11	16.81	12.11
S22	Heatherdale Shale (upper)	Sellick Hill	1.38	5.36	0.72	4.19	0.89	2.73	0.42	2.80	0.42	1.53	0.04	0.04	1.74	40.96	38.21	39.11	20.54	9.34
S23	Heatherdale Shale (upper)	Sellick Hill	1.17	4.51	0.62	3.67	0.75	2.22	0.33	2.19	0.35	1.48	0.02	0.05	1.57	33.06	30.55	31.26	16.94	8.11
S24	Heatherdale Shale (upper)	Sellick Hill	1.26	4.90	0.65	3.71	0.77	2.33	0.37	2.45	0.39	1.65	0.02	0.05	1.77	39.75	37.54	38.16	19.81	8.03
S25	Heatherdale Shale (upper)	Sellick Hill	1.32	5.34	0.72	4.07	0.84	2.52	0.38	2.50	0.37	1.65	0.02	0.06	2.68	40.46	36.86	37.65	18.25	10.98
S27	Heatherdale Shale (upper)	Sellick Hill	1.44	5.09	0.70	4.04	0.84	2.47	0.39	2.50	0.39	1.57	0.02	0.04	1.38	25.94	24.48	24.76	17.71	6.41
S28	Heatherdale Shale (upper)	Sellick Hill	1.28	5.72	0.75	4.20	0.86	2.61	0.39	2.77	0.42	1.05	0.02	0.03	1.79	51.77	48.17	48.91	20.94	11.49
S30	Heatherdale Shale (upper)	Sellick Hill	1.18	5.67	0.78	4.46	0.92	2.75	0.42	2.81	0.43	1.18	0.02	0.05	1.90	51.18	46.81	47.36	18.72	13.97
S32	Heatherdale Shale (upper)	Sellick Hill	1.59	5.33	0.79	4.48	0.96	2.66	0.38	2.30	0.36	1.01	0.01	0.04	0.93	14.36	13.03	13.46	11.54	3.52
S33	Heatherdale Shale (upper)	Sellick Hill	2.07	8.72	1.16	6.38	1.22	3.44	0.48	3.02	0.44	1.50	0.03	0.03	1.71	46.96	42.98	43.91	19.50	11.10
S35	Heatherdale Shale (upper)	Sellick Hill	1.49	6.28	0.88	4.82	0.95	2.77	0.41	2.71	0.39	1.57	0.03	0.05	1.20	40.73	37.86	38.83	18.51	7.63
S37	Heatherdale Shale (upper)	Sellick Hill	0.84	3.55	0.53	3.02	0.63	1.75	0.25	1.46	0.22	0.66	0.01	0.02	0.98	20.65	18.27	18.83	6.32	5.81
S39	Heatherdale Shale (upper)	Sellick Hill	1.74	7.10	0.93	5.16	1.02	2.87	0.44	2.87	0.43	1.49	0.03	0.04	1.37	35.14	32.22	33.12	19.47	8.74

TOC, $\delta^{13}C_{org}$, $\delta^{34}S_{pyr}$ and trace element concentrations for the Emu Bay Shale, Average Shales & Chondrite

Sample	Formation	Locality	Height (m)	TOC (%)	$\delta^{13}C_{org}$ (‰)	$\delta^{34}S$ (‰)	Weighed (mg)	Li (ug/g)	Be (ug/g)	B (ug/g)	Sc (ug/g)	V (ug/g)	Co (ug/g)	Ni (ug/g)	Cu (ug/g)	Zn (ug/g)	Ga (ug/g)	Ge (ug/g)
EB09S0.1	Emu Bay Shale	Big Gully	0.1	0.35	-29.2		15.6	81.61	5.44	24.72	17.59	141.85	11.63	29.74	79.93	32927.33	32.27	5.17
EB09S0.9	Emu Bay Shale	Big Gully	0.9	0.30	-30.7		17.0	75.48	3.85	11.35	15.85	105.30	10.03	31.50	40.59	2224.64	26.09	4.12
EB09S2.8	Emu Bay Shale	Big Gully	2.8	0.25	-29.7		16.6	85.10	4.31	8.70	17.14	118.67	14.01	33.94	42.49	740.49	28.20	4.20
EB09S4.0	Emu Bay Shale	Big Gully	4	0.30	-27.8		15.4	65.86	2.90	6.15	13.65	90.61	10.35	23.58	33.89	60.06	21.44	3.65
EB09S5.0	Emu Bay Shale	Big Gully	5	0.50	-29.8		16.0	78.02	3.31	21.00	14.87	99.47	10.91	28.26	38.56	112.35	24.70	3.85
EB09S6.0	Emu Bay Shale	Big Gully	6	0.45	-29.8		15.5	77.26	3.65	18.57	15.63	110.75	13.23	32.94	54.10	110.03	26.37	3.87
EB09S7.0	Emu Bay Shale	Big Gully	7	0.40	-30.2		14.8	80.46	3.39	18.64	17.68	119.48	13.13	37.91	54.46	110.97	28.66	4.15
EB09S7.1	Emu Bay Shale	Big Gully	7.1	0.35	-28.3		15.5	72.03	3.18	17.01	9.65	109.05	8.51	16.73	31.48	115.41	24.09	2.14
EB09S7.6	Emu Bay Shale	Big Gully	7.6	0.30	-29.9		15.7	87.84	3.66	11.95	16.55	108.53	17.06	37.26	34.25	72.54	27.94	3.65
EB09S	Emu Bay Shale	Big Gully		0.45	-31.8		17.0	71.97	3.56	12.15	16.24	133.42	9.53	32.29	81.94	867.59	27.68	3.48
EBQ1	Emu Bay Shale	Buck Quarry	5-6	0.30	-30.3		15.9	66.42	3.40	10.90	15.66	112.68	10.38	33.73	74.63	78.44	25.43	3.56
EBQ2	Emu Bay Shale	Buck Quarry	5-6	0.55	-31.8		15.0	69.39	3.15	8.71	15.33	113.86	10.46	30.71	75.16	568.54	26.63	3.56
Average shale	after Guo et al 2007a										10	99		56	39	76	16	
Average shale	Yan et al 2000										16	150	23	55	50	85		
PAAS	Taylor & Mclennan 1985										10	99		56	39	76	16	
chondrite	Taylor & Mclennan 1985																	

Sample	Formation	Locality	As (ug/g)	Se (ug/g)	Rb (ug/g)	Y (ug/g)	Nb (ug/g)	Mo (ug/g)	Cd (ug/g)	Sn [1] (ug/g)	Sn [2] (ug/g)	Sn [3] (ug/g)	Cs (ug/g)	La (ug/g)	Ce (ug/g)	Pr (ug/g)	Nd (ug/g)	Sm (ug/g)
EB09S0.1	Emu Bay Shale	Big Gully	76.41	1.23	246.42	41.12	15.98	2.27	67.90	4.89	4.20	4.09	17.38	53.35	117.08	13.53	51.13	10.43
EB09S0.9	Emu Bay Shale	Big Gully	27.73	1.12	217.19	28.41	15.23	0.41	7.33	4.69	4.09	3.92	15.00	45.56	88.58	10.30	37.36	6.78
EB09S2.8	Emu Bay Shale	Big Gully	32.19	0.36	238.72	25.54	15.04	3.17	1.67	5.39	4.47	4.42	21.60	42.22	89.17	10.06	36.77	6.95
EB09S4.0	Emu Bay Shale	Big Gully	74.79	0.65	198.20	24.91	13.29	0.58	0.46	3.76	3.37	3.22	16.22	38.89	82.09	8.86	31.73	5.96
EB09S5.0	Emu Bay Shale	Big Gully	49.81	1.00	213.98	25.43	13.85	0.45	0.37	4.05	3.38	3.20	15.71	39.68	81.46	9.42	34.23	6.43
EB09S6.0	Emu Bay Shale	Big Gully	43.57	0.72	232.35	25.11	14.56	0.90	0.55	5.32	4.71	4.42	21.59	40.03	85.51	9.22	33.44	6.17
EB09S7.0	Emu Bay Shale	Big Gully	17.45	0.54	241.66	26.76	13.85	2.06	0.40	5.39	4.66	4.27	20.33	42.41	90.17	10.14	37.10	6.78
EB09S7.1	Emu Bay Shale	Big Gully	11.70	N.D.	138.19	15.19	8.71	0.18	0.30	4.63	2.68	N.D.	14.36	23.86	50.14	5.50	19.60	3.78
EB09S7.6	Emu Bay Shale	Big Gully	23.90	0.44	233.24	22.62	14.84	0.58	0.17	5.38	4.78	4.44	18.87	36.03	72.27	8.32	30.32	5.77
EB09S	Emu Bay Shale	Big Gully	33.42	0.55	208.34	26.26	13.35	1.35	1.36	4.64	3.89	3.82	16.90	36.41	68.94	8.64	31.14	5.89
EBQ1	Emu Bay Shale	Buck Quarry	15.03	0.48	225.80	22.43	14.47	0.29	0.18	4.52	4.25	4.01	19.28	38.21	65.14	8.43	29.76	5.37
EBQ2	Emu Bay Shale	Buck Quarry	23.04	0.42	204.85	24.31	11.83	0.62	0.66	4.13	3.70	3.49	18.16	33.60	70.32	8.90	33.62	6.54
Average shale	after Guo et al 2007a		1.5		108		14	3	0.23	4			3.7					
Average shale	Yan et al 2000				160	27	19						15	38.0	80	8.9	32	5.6
PAAS	Taylor & Mclennan 1985		1.5		108		14	1	0.23	4			3.7					
chondrite	Taylor & Mclennan 1985													0.367	0.957	0.137	0.711	0.231

TOC, $\delta^{13}C_{org}$, $\delta^{34}S_{pyr}$ and trace element concentrations for the Emu Bay Shale, Average Shales & Chondrite

Sample	Formation	Locality	Eu (ug/g)	Gd (ug/g)	Tb (ug/g)	Dy (ug/g)	Ho (ug/g)	Er (ug/g)	Tm (ug/g)	Yb (ug/g)	Lu (ug/g)	Ta (ug/g)	Re (ug/g)	Au (ug/g)	Tl (ug/g)	206 Pb (ug/g)	207 Pb (ug/g)	208 Pb (ug/g)	Th (ug/g)	U (ug/g)
EB09S0.1	Emu Bay Shale	Big Gully	2.18	10.10	1.40	7.69	1.41	3.73	0.48	3.17	0.43	3.73	N.D.	0.03	1.47	4905.75	4705.06	4972.81	21.10	4.51
EB09S0.9	Emu Bay Shale	Big Gully	1.26	6.21	0.87	5.11	0.99	2.90	0.39	2.72	0.38	2.30	N.D.	0.01	1.03	364.26	349.88	365.73	19.00	3.31
EB09S2.8	Emu Bay Shale	Big Gully	1.21	5.88	0.83	4.89	0.93	2.74	0.36	2.51	0.35	2.19	0.00	N.D.	1.42	35.98	33.76	36.33	20.53	4.10
EB09S4.0	Emu Bay Shale	Big Gully	1.12	5.38	0.73	4.58	0.87	2.59	0.34	2.44	0.33	2.04	N.D.	N.D.	1.40	35.02	33.24	35.48	16.81	3.50
EB09S5.0	Emu Bay Shale	Big Gully	1.16	5.75	0.77	4.62	0.90	2.63	0.35	2.45	0.34	2.06	N.D.	N.D.	1.10	36.07	34.13	36.44	17.79	3.49
EB09S6.0	Emu Bay Shale	Big Gully	1.16	5.51	0.78	4.62	0.86	2.59	0.34	2.43	0.33	2.06	N.D.	N.D.	1.50	38.32	36.64	38.94	19.04	3.89
EB09S7.0	Emu Bay Shale	Big Gully	1.25	6.22	0.84	4.91	0.94	2.71	0.36	2.58	0.36	4.70	N.D.	N.D.	1.24	20.99	19.53	21.16	19.70	3.95
EB09S7.1	Emu Bay Shale	Big Gully	0.68	3.40	0.44	2.75	0.51	1.53	0.18	1.50	0.18	1.22	N.D.	N.D.	0.78	N.D.	N.D.	N.D.	11.27	2.45
EB09S7.6	Emu Bay Shale	Big Gully	1.12	5.07	0.67	4.20	0.79	2.26	0.30	2.11	0.29	2.26	N.D.	N.D.	1.24	36.22	34.00	36.42	17.37	3.94
EB09S	Emu Bay Shale	Big Gully	1.19	5.43	0.75	4.65	0.90	2.61	0.34	2.49	0.35	2.05	N.D.	N.D.	1.04	26.03	24.56	26.20	17.43	3.02
EBQ1	Emu Bay Shale	Buck Quarry	1.03	4.69	0.63	4.00	0.77	2.28	0.30	2.21	0.31	1.81	N.D.	N.D.	1.12	37.37	36.40	38.08	17.37	3.79
EBQ2	Emu Bay Shale	Buck Quarry	1.21	5.70	0.75	4.48	0.81	2.37	0.31	2.06	0.28	1.71	N.D.	N.D.	0.98	21.52	20.07	21.50	16.75	2.63
Average shale	after Guo et al 2007a															18			9.2	3
Average shale	Yan et al 2000		1.1	4.7	0.77	4.4	1	2.9	0.4	2.8	0.43					20			14.6	3.1
PAAS	Taylor & Mclennan 1985																			
chondrite	Taylor & Mclennan 1985		0.087	0.306	0.058	0.381	0.0851	0.249	0.0356	0.248	0.0381									

Appendix III

Supporting Data: Biomarker and isotopic signatures of an early Cambrian Lagerstätte in the Stansbury Basin, South Australia

Thermal Extraction of Whole Rock Emu Bay Shale Sample EBQ1

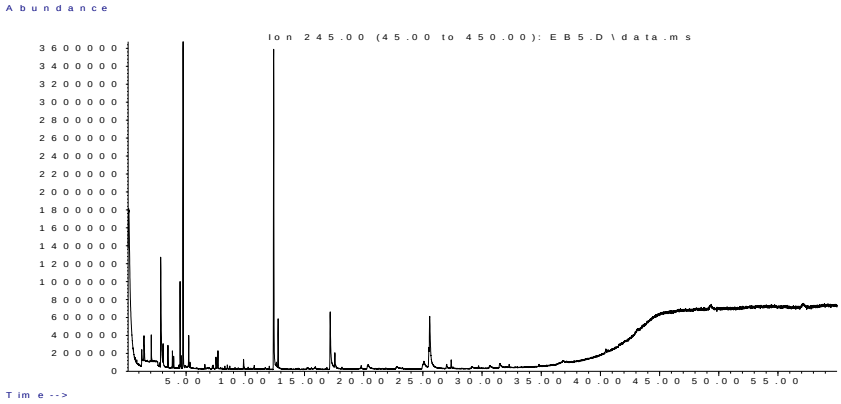

Fullscan chromatogram, prominent peaks at RT ~5min & ~12min are m&p Xylene isomers (observed as 1 peak through coelution) and naphthalene respectively.

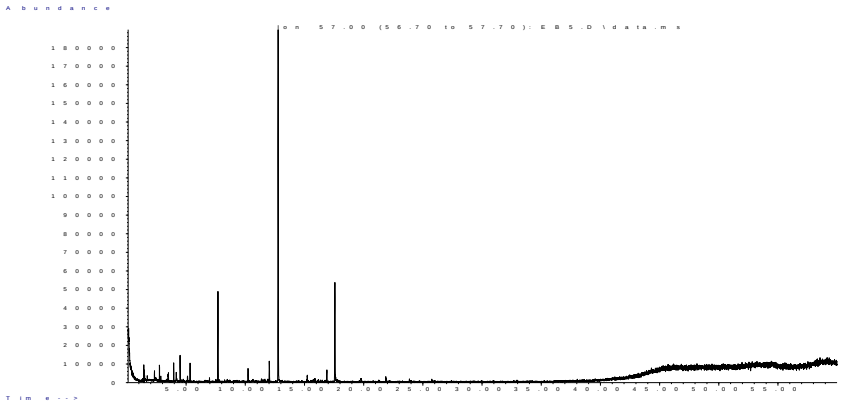

Ion chromatogram 57Da exhibiting strong even over odd preference for nC_{10} to nC_{14} – this unusual profile is a signature of burnt higher plant material and indicative of contamination of the EBS. Library spectral identifications follow.

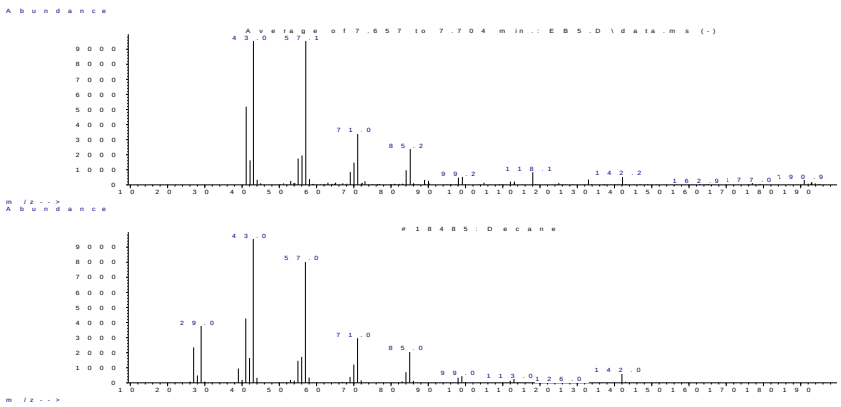

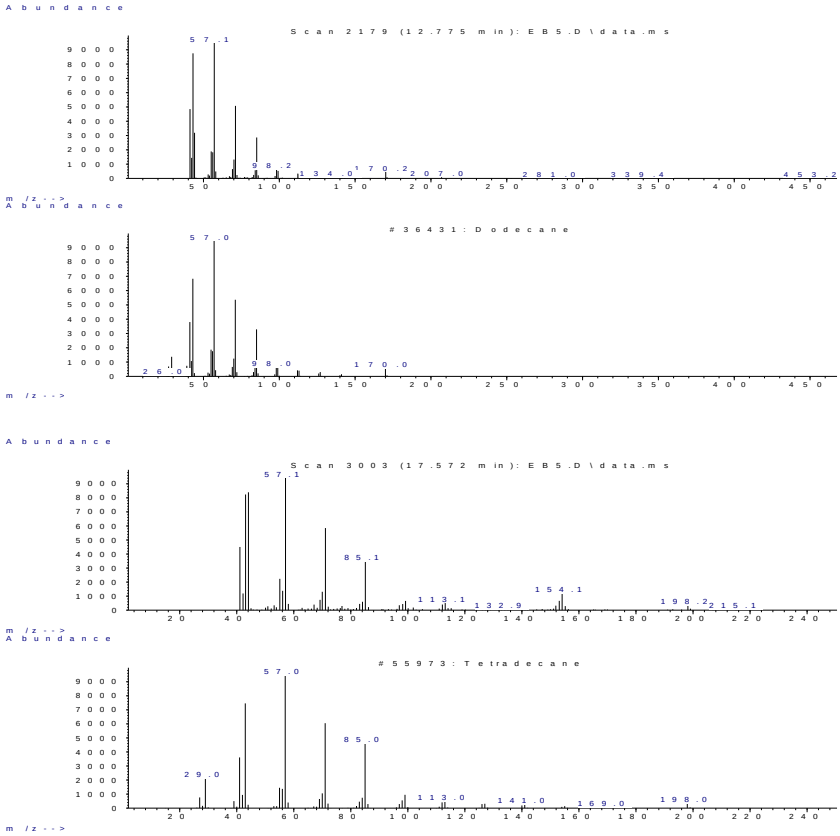

Benzene, Toluene & Xylenes

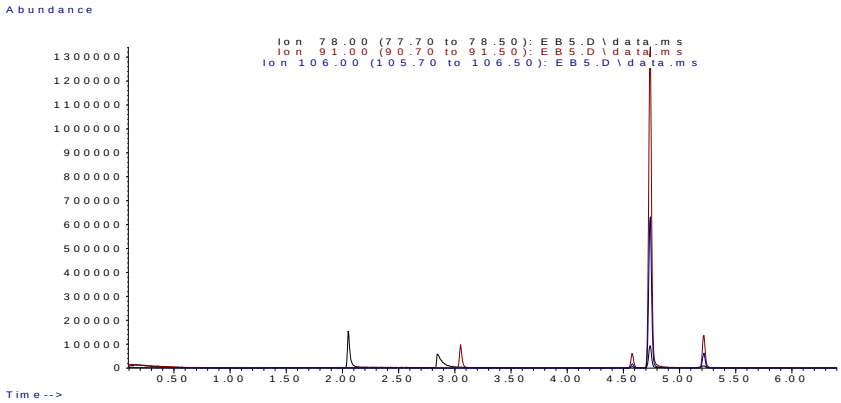

Combined ion chromatograms for 78, 91 & 106Da showing benzene (2min), toluene (3.1min) & ethyl benzene (4.6min) and the xylenes isomers (m&p 4.7min; o 5.2min). Library spectral identifications follow.

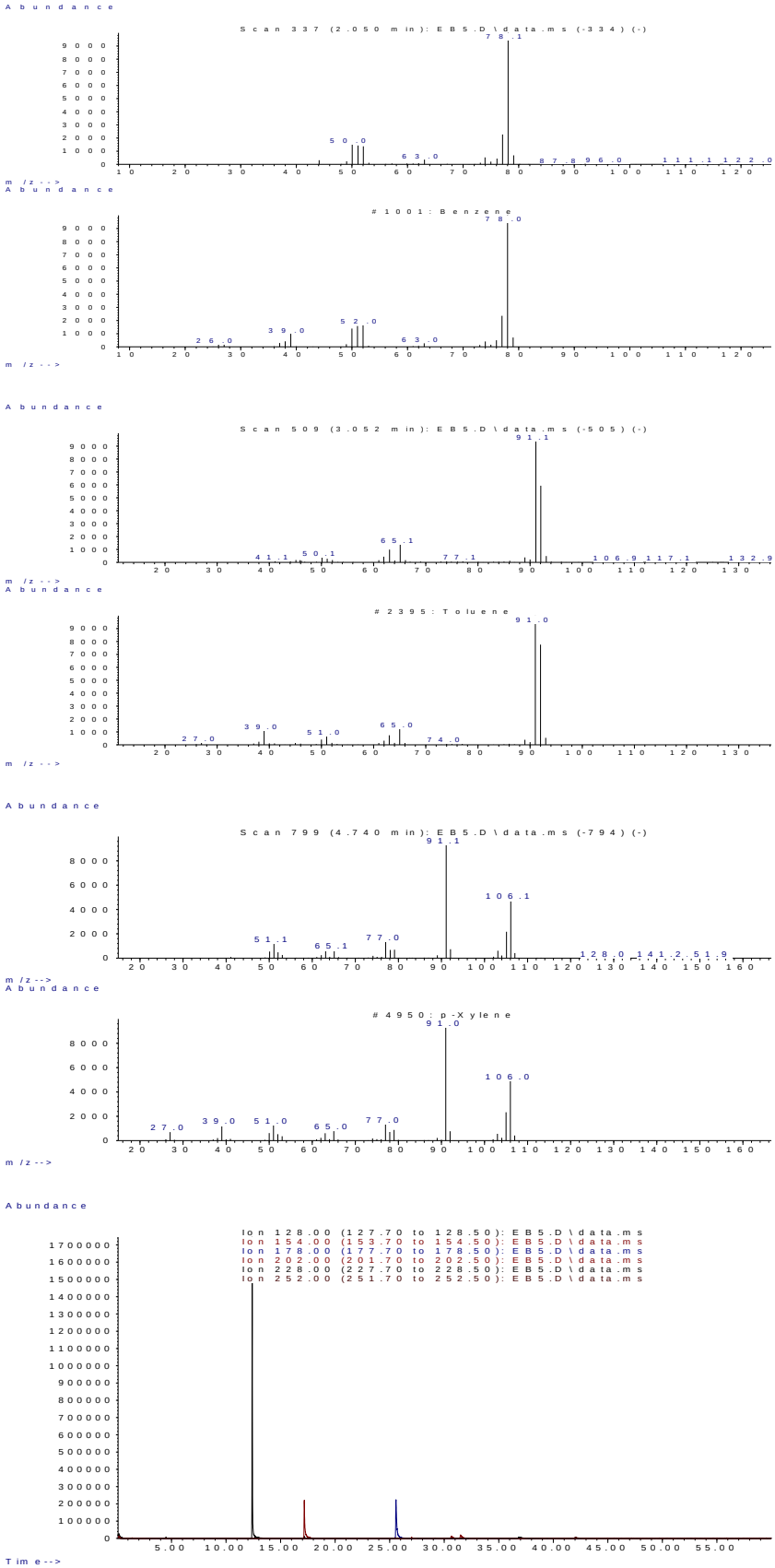

Combined ion chromatograms for 128, 154, 178,202, 228 & 252 showing a range of polycyclic aromatic hydrocarbons. These components are typical of burnt organic matter. Example library spectral identifications follow.

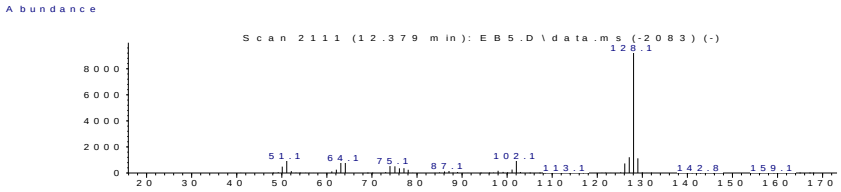
Abundance
Scan 2111 (12.379 min): EB5.D\data.ms (-2083) (-)
128.1
51.1
64.1
75.1
87.1
102.1
113.1
142.8
159.1
m/z-->

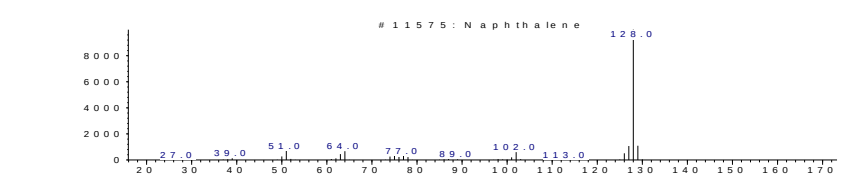
Abundance
#11575: Naphthalene
128.0
27.0
39.0
51.0
64.0
77.0
89.0
102.0
113.0
m/z-->

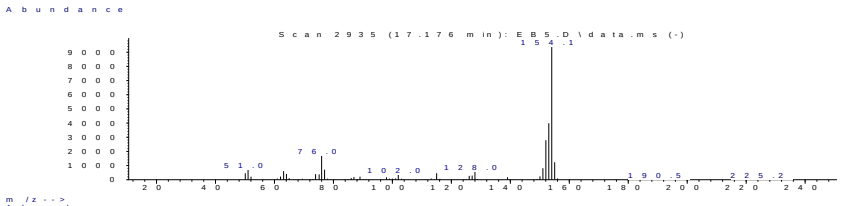
Abundance
Scan 2935 (17.176 min): EB5.D\data.ms (-)
154.1
76.0
51.0
102.0
128.0
190.5
225.2
m/z-->

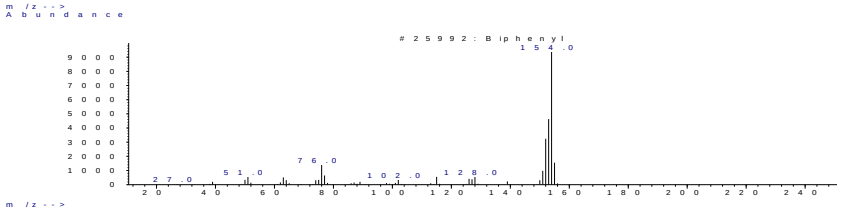
Abundance
#25992: Biphenyl
154.0
76.0
27.0
51.0
102.0
128.0
m/z-->

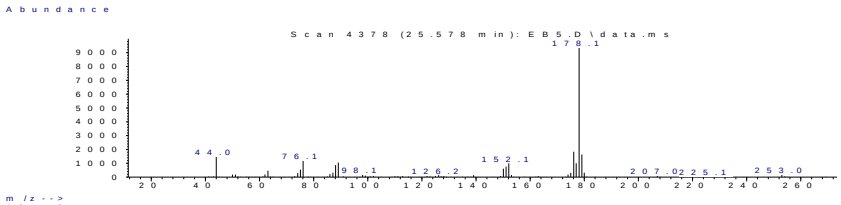
Abundance
Scan 4378 (25.578 min): EB5.D\data.ms
178.1
44.0
76.1
98.1
126.2
152.1
207.0
225.1
253.0
m/z-->

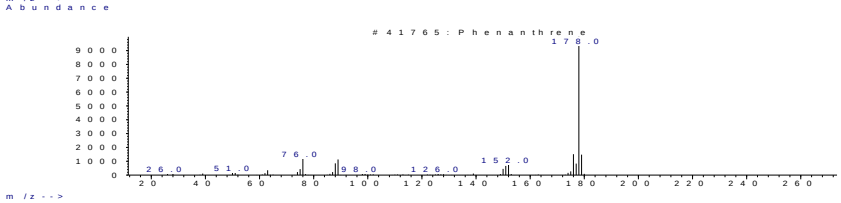
Abundance
#41765: Phenanthrene
178.0
26.0
51.0
76.0
98.0
126.0
152.0
m/z-->

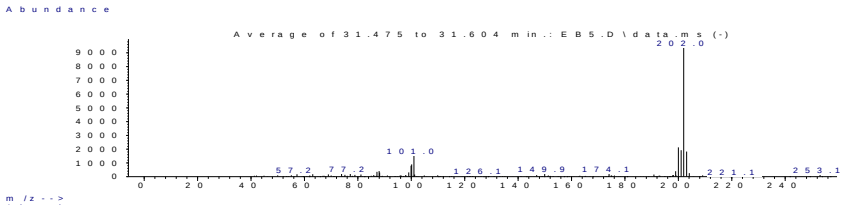
Abundance
Average of 31.475 to 31.604 min.: EB5.D\data.ms (-)
202.0
101.0
57.2
77.2
126.1
149.9
174.1
221.1
253.1
m/z-->

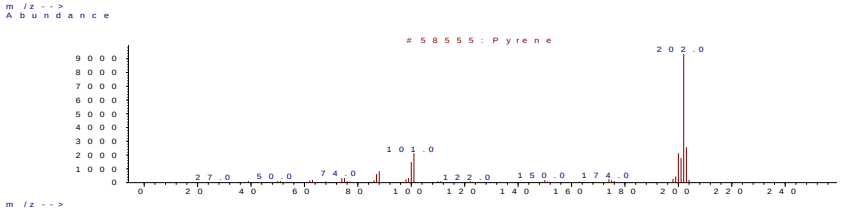
Abundance
#58555: Pyrene
202.0
101.0
27.0
50.0
74.0
122.0
150.0
174.0
m/z-->

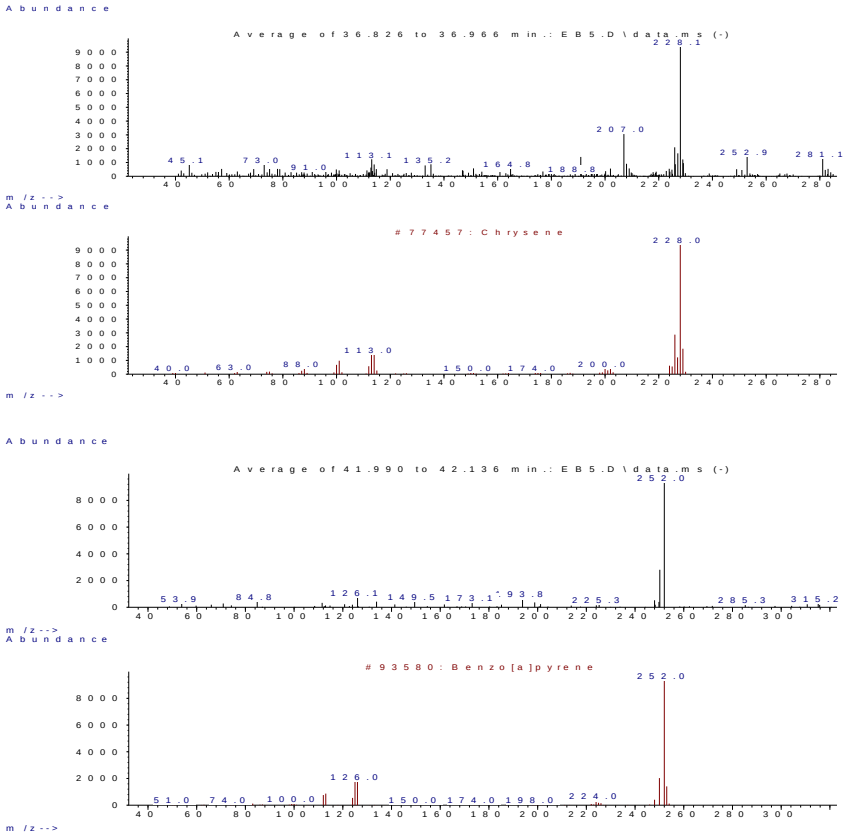
Abundance
Average of 36.826 to 36.966 min.: EB5.D\data.ms (-)
228.1
207.0
252.9
281.1
45.1
73.0
91.0
113.1
135.2
164.8
188.8
m/z-->
Abundance
77457: Chrysene
228.0
40.0
63.0
88.0
113.0
150.0
174.0
200.0
m/z-->
Abundance
Average of 41.990 to 42.136 min.: EB5.D\data.ms (-)
252.0
53.9
84.8
126.1
149.5
173.1
193.8
225.3
285.3
315.2
m/z-->
Abundance
93580: Benzo[a]pyrene
252.0
126.0
51.0
74.0
100.0
150.0
174.0
198.0
224.0
m/z-->

Emu Bay Shale Isolated Kerogen Analyses

Thermal Extract			MSSV Pyrolysis		
Compound Name	RT (min)	Area	Compound Name	RT (min)	Area
nC17	23.709	790477	nC17	23.697	2462942
Pr	23.813	139118	Pr	23.801	148567
nC18	25.601	262381	nC18	25.589	503382
Ph	25.764	116868	Ph	25.756	116047
	Pr/Ph	1.2		Pr/Ph	1.3
	Pr/nC17	0.2		Pr/nC17	0.1
	Ph/nC18	0.4		Ph/nC18	0.2
Odd Over Even Preference (OEP)					
nC13	15.092	251927	nC13	15.090	1355173
nC14	17.421	254512	nC14	17.415	1029284
nC15	19.633	377250	nC15	19.624	1629865
nC16	21.729	350656	nC16	21.712	878059
nC17	23.709	778512	nC17	23.697	2537151
nC18	25.601	267361	nC18	25.589	516730
nC19	27.4	160372	nC19	27.377	329564
	OEP (15:19)	1.36		OEP (15:19)	1.79
	OEP (13:17)	2.11		OEP (13:17)	3.08
Terpanes					
Ts	41.88	45915	Ts	41.835	11954
Tm	42.361	55036	Tm	42.333	11719
C29 H	43.953	140132	C29 H	43.933	17514
C29 Ts	44.036	38908	C29 Ts	44.024	3428
C30	45.039	176741	C30	45.044	13855
	h29/h30	0.79		h29/h30	1.26
	Ts/(Ts+Tm)	0.45		Ts/(Ts+Tm)	0.50
	Ts/Tm	0.83		Ts/Tm	1.02
Steranes (m/z217)					
27DbaS	38.921	30198	27DbaS	38.875	10130
27DbaR	39.368	16692	27DbaR	39.331	4330
28DbaSA	40.04	11883	28DbaSA	40.003	2624
28DbaSB	40.114	15577	28DbaSB	40.069	4094
28DbaRA	40.546	15418	28DbaRA	40.492	1475
28DbaRB	40.546	9369	28DbaRB	40.592	1252
27aaS	40.952	11168	27aaS	40.923	863
27bbR+29DbaS	41.043	28816	27bbR+29DbaS	40.99	3857
27bbS	41.167	13128	27bbS	41.131	1963
27aaR	41.474	21244	27aaR	41.479	1749
28aaS	42.303	6421	28aaS	42.308	309
28bbR	42.378	6807	28bbR	42.383	56
28bbS	42.469	9676	28bbS	42.432	84
28aaR	42.768	12258	28aaR	42.764	217
29aaS	43.091	9393	29aaS	43.096	160
29bbR	43.298	13135	29bbR	43.353	633
29bbS	43.298	13387	29bbS	43.353	633
29aaR	43.821	10164	29aaR	43.842	118
30bbR&S	45.039	1861	30bbR&S		
Steranes (m/z218)					
27bbR 218	41.06	23678	27bbR 218	41.031	2183
27bbS 218	41.159	18153	27bbS 218	41.122	1567
28bbR 218	42.303	15234	28bbR 218	42.324	877
28bbS 218	42.386	9411	28bbS 218	42.366	244
29bbR 218	43.298	17322	29bbR 218	43.278	331
29bbS 218	43.365	13478	29bbS 218	43.377	357
30bbR&S 218	45.039	6893	30bbR&S 218		
	C30H/C27St	0.68		C30H/C27St	2.13
	C27D/C27Reg	0.78		C27D/C27Reg	2.22

Thermal Extraction of Emu Bay Shale Kerogen

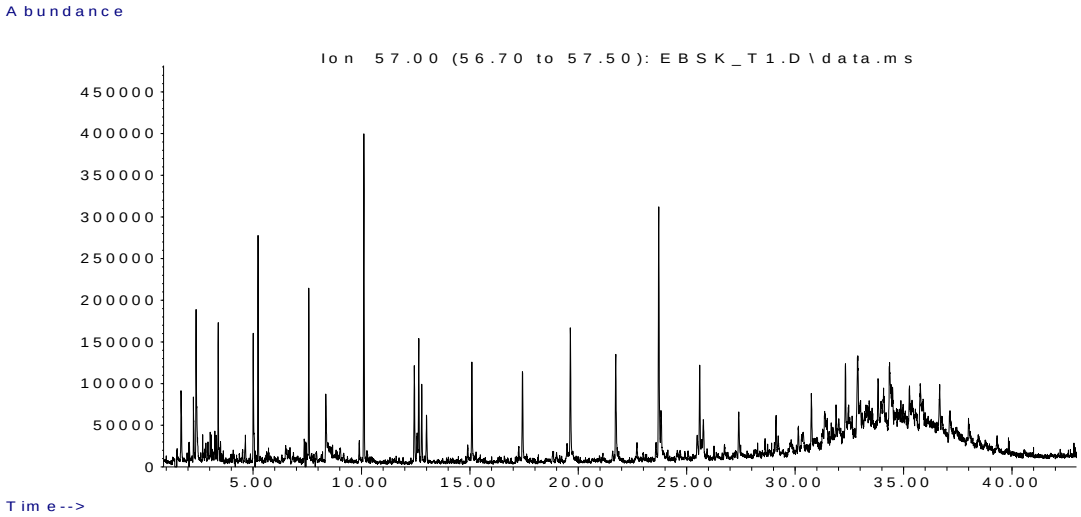

Ion chromatogram 57Da exhibiting strong odd over even preference for nC_9 to nC_{25} in contrast to the even over odd preference of the whole rock. Undecane (10.1min) and heptadecane (23.7min) are prominent, the isoprenoids pristine and phytane are also observed at 23.8min & 25.8min respectively. Library spectral identifications follow.

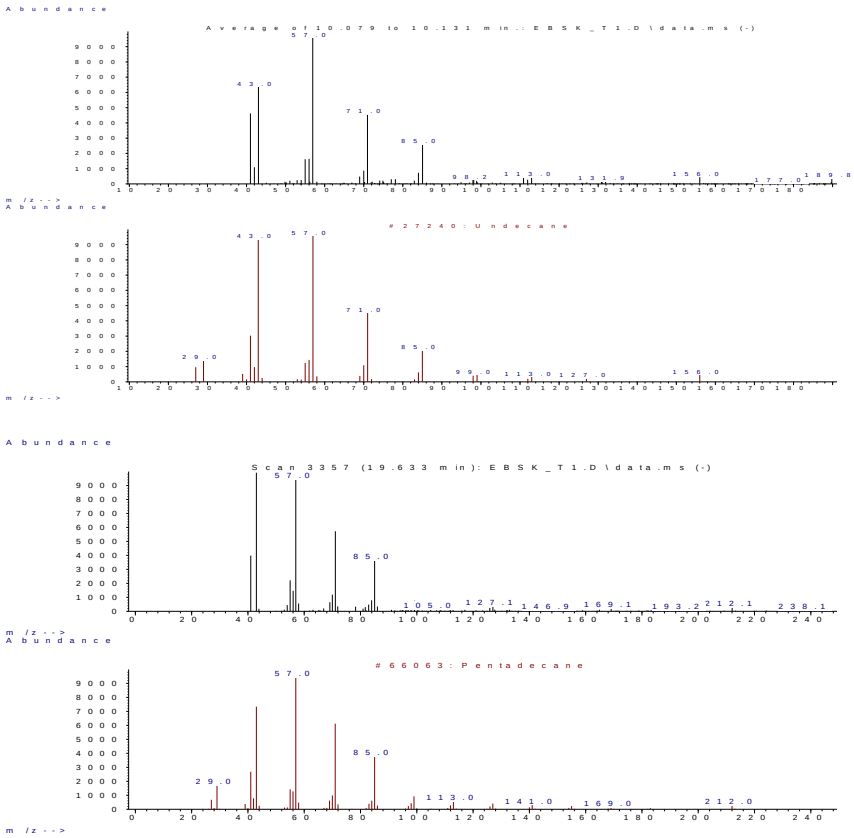

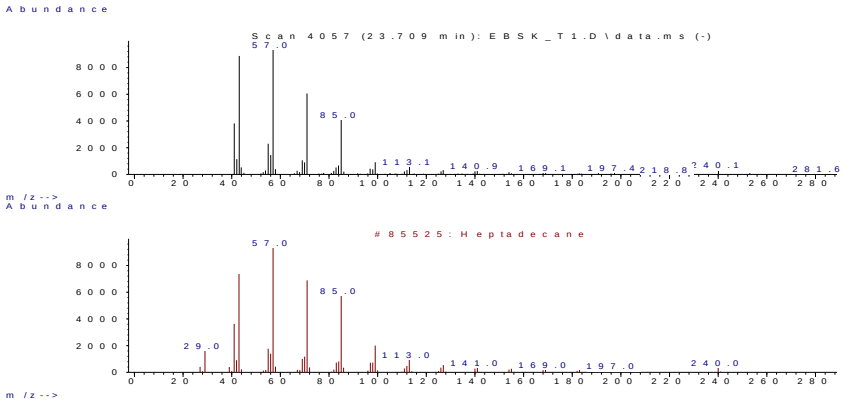

Biomarker Chromatograms; 191, 217 & 218Da

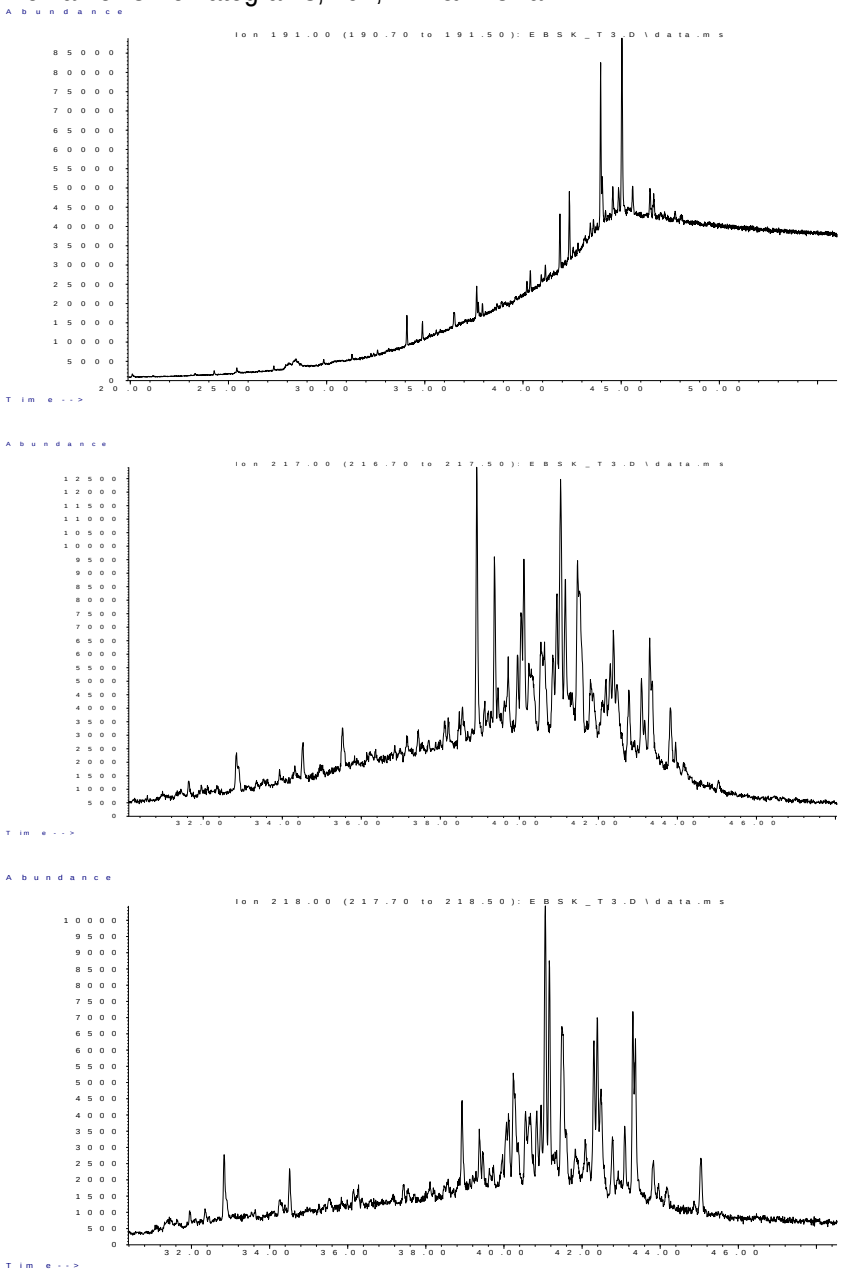

MSSV Pyrolysis Extraction of Emu Bay Shale Kerogen

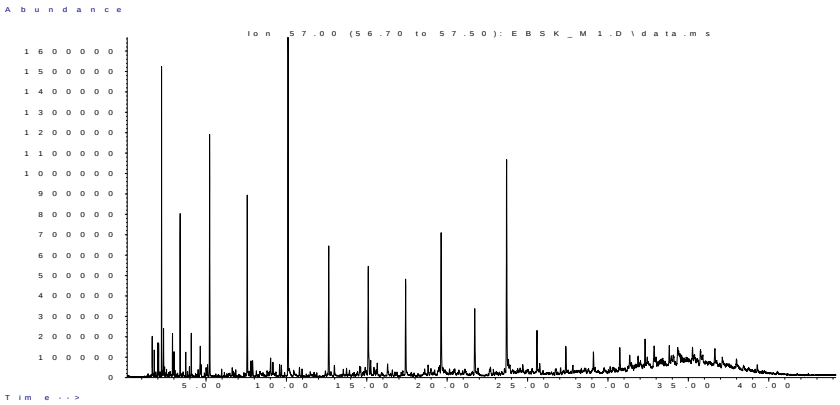

Ion chromatogram 57Da exhibiting strong odd over even preference for nC_7 to nC_{25}. Undecane (10.1min) and heptadecane (23.7min) are prominent, the isoprenoids pristine and phytane are also observed at 23.8min & 25.8min respectively. Library spectral identifications follow.

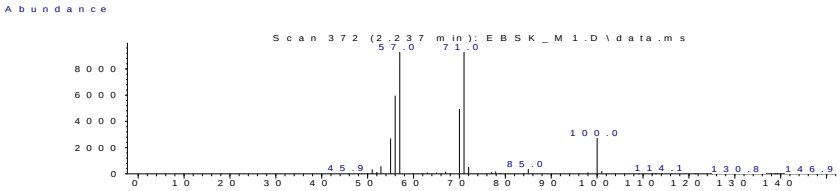

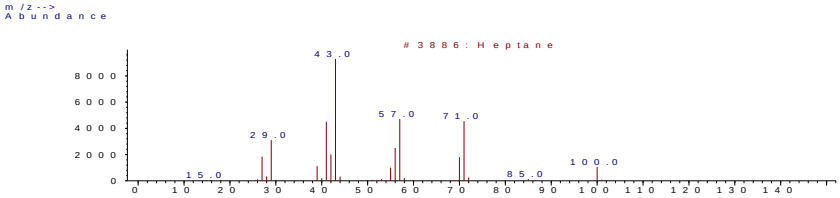

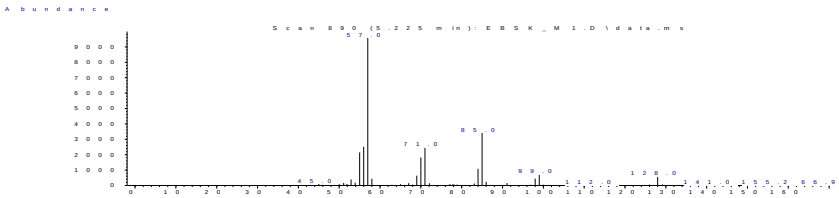

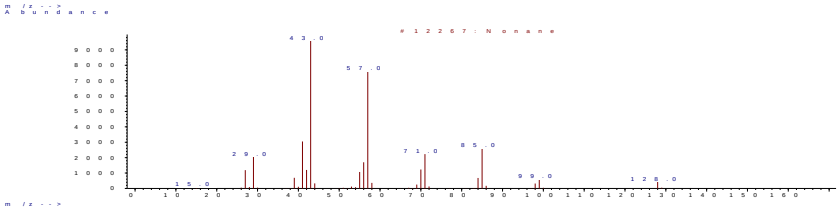

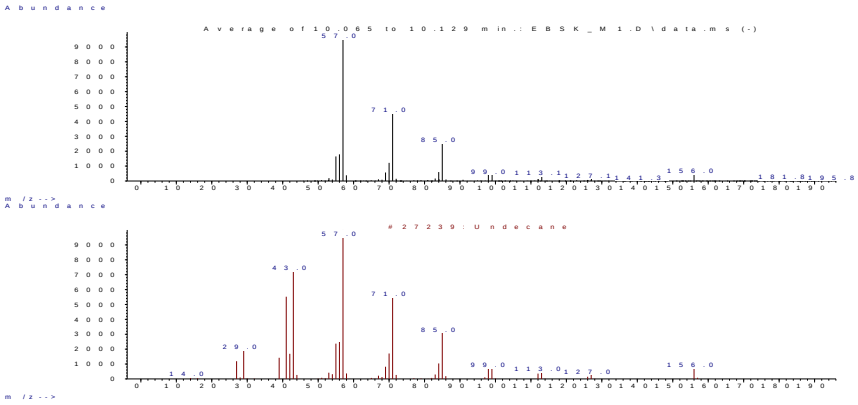

Biomarker Chromatograms; 191, 217 & 218Da

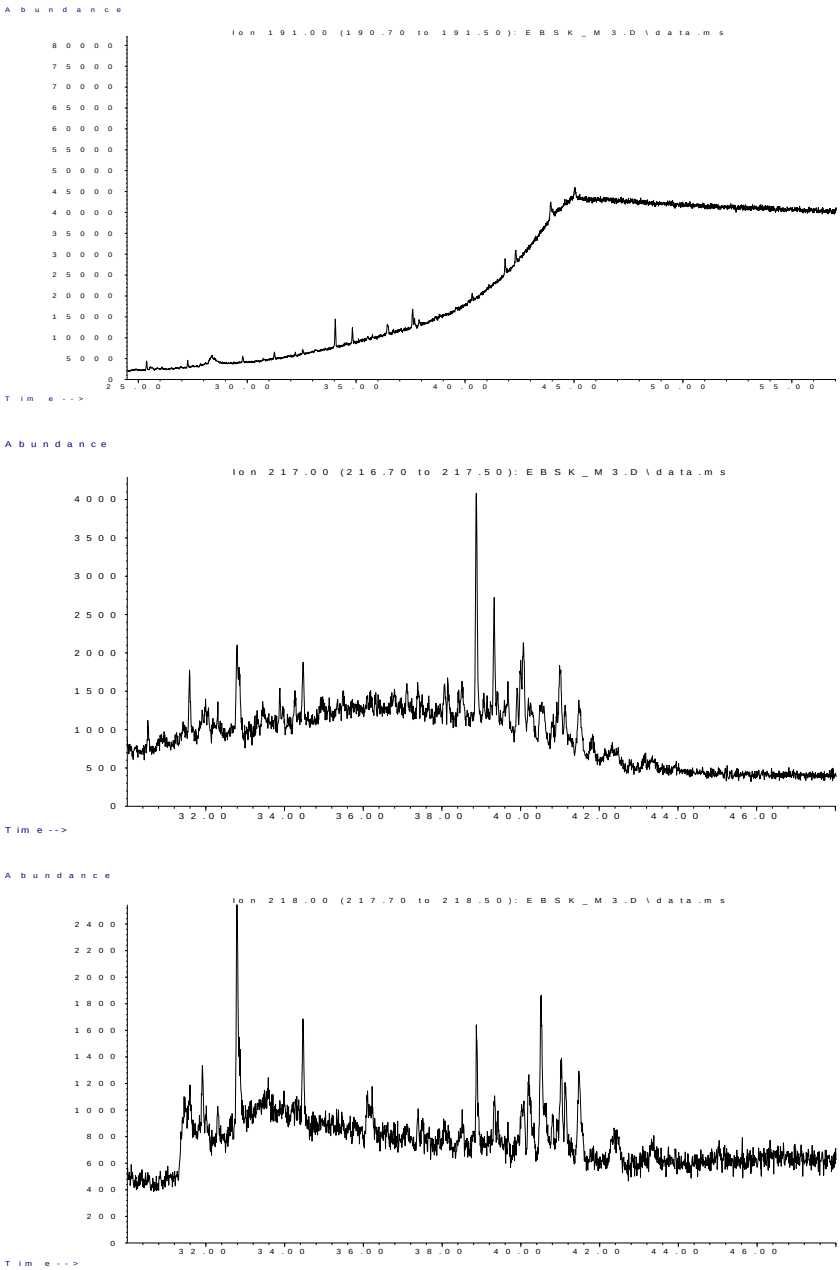

Appendix IV

Supporting Data: Filling the Australian Cambrian chemostratigraphic gap: Early Cambrian carbon isotopic profiles of three South Australia basins.

Inferred Ages Stansbury West 1

Stansbury West 1, Stansbury Basin

Depth (m)	$\delta^{13}C$ (‰)	$\delta^{18}O$ (‰)	Infered Age (Ma)	Formation	Lithology*	Composite	Depth (m)	$\delta^{13}C$ (‰)	$\delta^{18}O$ (‰)	Infered Age (Ma)	Formation	Lithology*	Composite	Depth (m)	$\delta^{13}C$ (‰)	$\delta^{18}O$ (‰)	Infered Age (Ma)	Formation	Lithology*	Composite
335	-7.9	-12.7	507.5	Yuruga Formation	SSt/CSt	no	664	-1.1	-9.2	511.2	Corrodgery Formation	Lst/Dol	yes	1177	-0.3	-10.2	515.6	Parara Limestone	Lst	yes
341	-5.0	-19.2	507.5	Yuruga Formation	SSt	no	671	-1.3	-8.4	511.2	Corrodgery Formation	LSt/SSt/Sh	yes	1183	-0.5	-10.2	515.7	Parara Limestone	Lst	yes
354	-6.2	-14.4	507.6	Yuruga Formation	SSt	no	677	-0.6	-8.1	511.2	Corrodgery Formation	Carb SSt/Sh	yes	1250	-0.4	-11.1	516.5	Parara Limestone	Lst	yes
360	-4.7	-13.3	507.6	Yuruga Formation	SSt	no	683	-0.9	-9.8	511.2	Corrodgery Formation	Carb SSt	yes	1256	0.0	-11.2	516.6	Parara Limestone	Lst	yes
366	-10.8	-13.2	507.7	Yuruga Formation	SSt	no	689	-1.0	-9.7	511.3	Corrodgery Formation	Carb SSt	yes	1268	-0.1	-9.2	516.8	Parara Limestone	Lst	yes
372	-5.1	-12.8	507.7	Yuruga Formation	SSt	no	695	-1.1	-10.9	511.3	Corrodgery Formation	Carb SSt	yes	1274	-0.6	-10.3	516.8	Parara Limestone	Lst	yes
378	-6.5	-14.5	507.8	Yuruga Formation	SSt	no	707	-1.4	-10.5	511.3	Corrodgery Formation	Carb SSt	yes	1280	-0.2	-10.8	516.9	Parara Limestone	Lst	yes
378	-5.0	-13.9	507.8	Yuruga Formation	SSt/Sh	no	713	-0.9	-10.2	511.3	Corrodgery Formation	Carb SSt	yes	1286	0.0	-9.4	517.0	Parara Limestone	Lst	yes
384	-5.6	-17.0	507.8	Yuruga Formation	SSt	no	719	-2.5	-10.3	511.4	Corrodgery Formation	Carb SSt	yes	1292	0.4	-7.3	518.0	Kulpara Formation	Lst/Dol	yes
390	-8.4	-15.4	507.8	Yuruga Formation	SSt	no	732	-3.5	-10.4	511.4	Corrodgery Formation	Carb SSt/Sh	yes	1305	-0.1	-6.5	518.3	Kulpara Formation	Dol	yes
396	-6.1	-14.0	507.9	Yuruga Formation	SSt	no	744	-0.7	-7.0	511.5	Ramsay Limestone	Lst	yes	1311	-0.1	-6.2	518.5	Kulpara Formation	Dol	yes
402	-5.4	-14.9	507.9	Yuruga Formation	SSt	no	762	0.3	-8.5	511.5	Ramsay Limestone	Lst	yes	1317	0.0	-6.9	518.7	Kulpara Formation	Dol	yes
408	-5.5	-17.8	507.9	Yuruga Formation	SSt	no	768	0.0	-8.5	511.5	Ramsay Limestone	Lst	yes	1323	-0.1	-7.0	518.8	Kulpara Formation	Dol	yes
415	-3.0	-15.5	508.0	Yuruga Formation	SSt	no	799	0.4	-6.2	511.6	Ramsay Limestone	Lst/Dol	yes	1329	0.1	-6.8	519.0	Kulpara Formation	Dol	yes
421	-3.4	-15.2	508.0	Yuruga Formation	SSt	no	805	0.2	-8.0	511.6	Ramsay Limestone	Lst	yes	1341	0.2	-6.4	519.4	Kulpara Formation	Dol	yes
427	-3.1	-15.7	508.0	Yuruga Formation	SSt	no	811	-0.1	-8.5	511.7	Ramsay Limestone	LSt/Sh	yes	1347	0.1	-7.3	519.5	Kulpara Formation	Dol	yes
433	-3.3	-13.0	508.1	Yuruga Formation	SSt	no	817	0.2	-6.9	511.7	Ramsay Limestone	Lst/Dol	yes	1359	0.4	-6.9	519.9	Kulpara Formation	Dol	yes
439	-3.0	-15.7	508.1	Yuruga Formation	SSt	no	829	0.4	-7.5	511.7	Ramsay Limestone	Lst/Dol	yes	1366	0.4	-6.5	520.0	Kulpara Formation	Dol	yes
445	-2.7	-14.5	508.2	Yuruga Formation	SSt	no	835	0.2	-5.2	511.7	Minlaton Formation	Sh	no	1378	0.1	-6.8	520.4	Kulpara Formation	Dol	yes
451	-2.4	-14.5	508.2	Yuruga Formation	SSt	no	841	0.4	-5.0	511.8	Minlaton Formation	Sh	no	1384	-0.1	-6.2	520.5	Kulpara Formation	Dol	yes
457	-4.4	-15.8	508.2	Yuruga Formation	SSt	no	866	-0.2	-6.9	512.0	Minlaton Formation	Sh	no	1390	-0.4	-6.3	520.7	Kulpara Formation	Dol	yes
463	-4.4	-18.2	508.3	Yuruga Formation	SSt/Sh	no	872	-0.4	-8.3	512.0	Minlaton Formation	Sh	no	1396	-0.9	-7.0	520.9	Kulpara Formation	Dol	yes
469	-2.4	-14.2	508.3	Yuruga Formation	SSt	no	878	-1.1	-9.0	512.0	Minlaton Formation	Sh	no	1402	-0.4	-6.8	521.1	Kulpara Formation	Dol	yes
475	-2.5	-14.5	508.3	Yuruga Formation	SSt	no	884	-3.9	-12.2	512.1	Minlaton Formation	Sh	no	1414	-0.8	-6.1	521.4	Kulpara Formation	Dol	yes
482	-2.3	-12.8	508.4	Yuruga Formation	SSt	no	896	-3.2	-11.2	512.2	Minlaton Formation	Sh	no	1420	-1.0	-6.1	521.6	Kulpara Formation	Dol	yes
488	-2.4	-13.2	508.4	Yuruga Formation	SSt	no	902	-3.3	-11.6	512.2	Minlaton Formation	Sh	no	1433	-1.2	-6.7	521.9	Kulpara Formation	Dol	yes
494	-2.6	-13.9	508.5	Yuruga Formation	SSt	no	908	-1.7	-10.1	512.3	Minlaton Formation	Sh	no	1439	-1.7	-6.8	522.1	Kulpara Formation	Dol	yes
500	-2.7	-13.9	508.5	Yuruga Formation	SSt	no	914	-2.7	-10.1	512.3	Minlaton Formation	Sh	no	1451	-1.6	-6.7	522.4	Kulpara Formation	Dol	yes
506	-2.6	-14.7	508.5	Yuruga Formation	SSt/Sh	no	920	-1.9	-10.1	512.4	Minlaton Formation	Sh	no	1457	-1.4	-6.7	522.6	Kulpara Formation	Dol	yes
512	-1.4	-14.2	508.6	Yuruga Formation	SSt/Sh	no	939	-0.6	-6.7	512.5	Parara Limestone	Dol	yes	1469	-1.7	-6.5	522.9	Kulpara Formation	Dol	yes
518	-2.0	-15.1	508.6	Yuruga Formation	SSt/Sh	no	945	-0.4	-6.7	512.6	Parara Limestone	Dol	yes	1475	-1.5	-6.1	523.1	Kulpara Formation	Dol	yes
524	-3.3	-17.2	508.6	Yuruga Formation	SSt	no	951	-0.1	-6.2	512.7	Parara Limestone	Lst	yes	1481	-1.6	-6.6	523.3	Kulpara Formation	Dol	yes
536	-2.4	-10.2	508.7	Yuruga Formation	SSt/Sh	no	957	-0.9	-8.0	512.7	Parara Limestone	Dol/Sh	yes	1487	-1.7	-6.7	523.4	Kulpara Formation	Dol	yes
536	-1.8	-15.4	508.7	Yuruga Formation	SSt/Sh	no	988	-0.6	-8.3	513.1	Parara Limestone	Lst	yes	1494	-1.8	-6.8	523.6	Kulpara Formation	Dol	yes
543	-0.5	-14.9	508.7	Yuruga Formation	Sh	no	1067	0.3	-9.4	514.2	Parara Limestone	Lst	yes	1500	-1.9	-6.6	523.8	Kulpara Formation	Dol	yes
549	0.1	-15.0	508.78	Yuruga Formation	Sh	no	1073	0.4	-9.6	514.2	Parara Limestone	Lst	yes	1506	-2.2	-6.5	523.9	Kulpara Formation	Dol	yes
555	0.7	-13.2	508.82	Yuruga Formation	Sh	no	1079	0.7	-9.0	514.3	Parara Limestone	Lst	yes	1512	-2.6	-6.6	524.1	Kulpara Formation	Dol	yes
567	1.5	-11.4	508.9	Yuruga Formation	Dol/Sh	yes	1103	0.3	-9.4	514.6	Parara Limestone	Lst	yes	1518	-2.8	-7.2	524.3	Kulpara Formation	Dol	yes
573	1.8	-11.6	508.9	Yuruga Formation	Dol/Sh	yes	1109	0.1	-9.5	514.7	Parara Limestone	Lst	yes	1524	-2.4	-7.1	524.4	Kulpara Formation	Dol	yes
579	1.7	-11.8	509.0	Yuruga Formation	Lst	yes	1116	0.0	-10.2	514.8	Parara Limestone	Lst	yes	1530	-2.0	-7.2	524.6	Kulpara Formation	Dol	yes
585	0.0	-9.0	509.0	Coobowie Limestone	Lst	yes	1122	0.1	-9.7	514.9	Parara Limestone	Lst	yes	1548	-1.6	-7.2	525.1	Kulpara Formation	Dol	yes
591	-1.3	-11.1	509.5	Coobowie Limestone	Lst	yes	1128	0.1	-9.0	514.9	Parara Limestone	Lst	yes	1554	-2.6	-6.9	525.3	Kulpara Formation	Dol	yes
597	1.9	-11.1	510.0	Moonan Formation	Sh	no	1134	0.3	-8.5	515.0	Parara Limestone	Lst	yes	1567	-1.5	-6.6	525.6	Kulpara Formation	Dol	yes
610	-0.6	-10.1	510.4	Moonan Formation	Sh	no	1140	0.0	-8.8	515.1	Parara Limestone	Lst	yes	1573	-1.6	-6.4	525.8	Kulpara Formation	Dol	yes
622	0.0	-8.6	510.9	Stansbury Limestone	Lst	yes	1146	-0.3	-9.7	515.2	Parara Limestone	Lst	yes	1585	-1.7	-6.3	526.1	Kulpara Formation	Dol	yes
628	0.8	-8.9	510.9	Stansbury Limestone	Lst	yes	1152	-0.3	-8.5	515.3	Parara Limestone	Lst	yes	1591	-1.0	-6.4	526.3	Kulpara Formation	Dol	yes
634	1.1	-8.6	510.9	Stansbury Limestone	Lst	yes	1158	-0.2	-9.5	515.3	Parara Limestone	Lst	yes	1615	-1.4	-6.5	527.0	Kulpara Formation	Dol	yes
646	0.7	-8.6	511.0	Stansbury Limestone	Lst	yes	1164	0.0	-9.9	515.4	Parara Limestone	Lst	yes	1622	-1.7	-6.5	527.2	Kulpara Formation	Dol	yes
658	-1.3	-8.8	511.1	Stansbury Limestone	Lst/Dol	yes	1170	-0.1	-9.5	515.5	Parara Limestone	Lst	yes	1634	-1.8	-6.5	527.5	Kulpara Formation	Dol	yes

*Descriptions taken from Watts & Gausden, 1966; Stansbury West 1 Well Completion Report; PIRSA Open File Envelope No:656 OEL24: SSt = Sandstone; CSt = Claystone; Sh = Shale; Lst = Limestone; Dol = Dolomite; Carb = Carbonaceous

Inferred Ages Wilkinson 1

Wilkinson 1, Officer Basin								
Depth (m)	$\delta^{13}C$ (‰)	$\delta^{18}O$ (‰)	Depth (m)	$\delta^{13}C$ (‰)	$\delta^{18}O$ (‰)	Depth (m)	$\delta^{13}C$ (‰)	$\delta^{18}O$ (‰)
211	-0.9	-7.2	401	2.0	-5.4	551	-1.3	-8.3
216	-0.4	-6.8	406	1.6	-7.0	556	0.1	-8.2
221	-0.2	-7.6	411	1.7	-5.7	561	0.4	-7.9
226	0.2	-5.8	416	2.0	-6.9	566	0.7	-8.9
231	-0.2	-6.3	421	0.6	-7.4	569	-0.5	-8.6
236	0.2	-5.8	426	1.2	-5.1	571	-0.3	-6.8
241	-0.3	-8.1	431	1.1	-5.7	573	-0.1	-7.5
246	-0.5	-7.0	436	0.9	-7.2	578	-0.7	-8.5
251	0.0	-5.3	441	0.5	-5.5	582	-1.0	-6.9
256	-0.2	-5.7	446	0.4	-7.3	586	-0.5	-6.7
261	-0.3	-5.5	449	0.0	-8.0	589	-0.4	-6.1
266	-1.0	-7.2	451	0.1	-7.8	591	-1.0	-6.7
271	-1.1	-6.9	456	0.1	-7.6	596	-1.8	-7.2
276	-0.6	-6.1	461	-0.5	-7.4	601	-1.1	-7.1
281	-1.1	-8.0	466	-1.0	-7.3	606	-1.9	-6.4
286	-1.0	-7.0	471	-0.2	-8.1	611	-0.2	-7.5
291	-0.8	-6.7	472	-0.3	-8.0	616	0.1	-7.6
296	-1.1	-8.3	476	0.1	-7.8	621	-1.7	-6.2
301	-1.0	-8.8	478	-0.3	-8.4	624	-0.7	-6.6
306	-0.3	-7.5	481	-1.9	-8.9	626	-1.0	-8.0
311	-0.3	-8.7	486	0.3	-7.2	632	-0.7	-6.0
316	0.1	-7.6	491	0.5	-8.6	641	-1.0	-5.9
321	0.1	-7.5	493	-0.4	-7.5	646	-0.7	-6.7
326	0.6	-5.8	496	0.2	-7.6	650	-1.0	-5.8
331	-0.5	-9.4	500	0.6	-8.2	656	-0.8	-8.1
336	1.2	-6.9	501	0.3	-6.2	661	-0.8	-8.0
341	1.8	-7.1	504	0.0	-8.3	666	-0.6	-7.8
346	0.6	-6.2	506	0.1	-6.1	671	-0.9	-8.1
351	3.4	-6.8	511	0.3	-8.1	675	-1.8	-6.6
356	2.2	-6.7	513	0.3	-7.3	678	-1.9	-6.1
361	2.6	-6.8	516	0.3	-6.2	681	-0.4	-6.7
366	3.2	-6.9	518	0.1	-7.0	686	-0.3	-7.8
371	2.1	-5.5	521	-1.7	-6.1	691	1.2	-7.2
376	2.4	-7.7	526	0.1	-7.8	696	-1.1	-7.5
381	2.4	-6.6	531	0.0	-8.1	701	0.1	-6.3
386	2.1	-7.1	536	-0.6	-7.9	706	-0.4	-6.7
391	2.1	-8.6	541	0.3	-9.7	710	-0.3	-6.6
396	1.8	-7.2	546	-0.2	-8.2			

Inferred Ages SCYW 791A

SCYW 791A, Arrowie Basin											
Depth (m)	$\delta^{13}C$ (‰)	$\delta^{18}O$ (‰)	Infered Age (Ma)	Depth (m)	$\delta^{13}C$ (‰)	$\delta^{18}O$ (‰)	Infered Age (Ma)	Depth (m)	$\delta^{13}C$ (‰)	$\delta^{18}O$ (‰)	Infered Age (Ma)
29	1.6	-10.0	513.0	70	1.9	-5.7	516.0	111	1.6	-7.7	519.1
31	3.0	-3.6	513.2	72	1.6	-4.9	516.2	112	1.6	-6.8	519.1
33	2.9	-1.6	513.3	73	1.9	-5.8	516.3	113	1.4	-6.8	519.2
34	3.1	-8.8	513.4	74	1.5	-5.3	516.3	114	1.6	-7.3	519.3
36	3.1	-9.9	513.5	75	1.7	-3.3	516.4	115	1.4	-7.4	519.4
38	3.3	-8.9	513.7	76	1.6	-4.2	516.5	116	1.4	-7.3	519.5
40	3.2	-9.3	513.8	77	1.4	-4.0	516.6	117	0.8	-8.1	519.5
42	3.0	-8.3	514.0	78	1.3	-3.6	516.6	120	0.9	-7.2	519.7
44	2.5	-9.9	514.1	80	1.2	-3.3	516.8	124	0.6	-8.0	520.0
45	2.6	-11.1	514.2	82	0.9	-5.4	517.0	125	0.6	-8.4	520.1
46	2.6	-11.2	514.3	84	1.0	-5.6	517.1	126	0.6	-7.1	520.2
48	2.7	-9.2	514.4	85	-0.3	-7.2	517.2	127	0.5	-8.0	520.2
49	2.6	-8.7	514.5	86	0.2	-7.4	517.2	128	0.6	-8.3	520.3
50	2.5	-1.9	514.6	88	-0.4	-8.3	517.4	129	0.6	-8.4	520.4
51	2.4	-7.6	514.7	91	0.6	-5.8	517.6	130	0.3	-8.5	520.5
53	2.3	-12.2	514.8	95	0.6	-7.1	517.9	133	0.1	-8.8	520.7
54	3.3	-3.4	514.9	98	0.6	-7.1	518.1	137	0.7	-6.0	521.0
55	3.2	-3.6	515.0	99	-0.2	-7.6	518.2	155	0.3	-6.5	522.8
57	3.6	-3.2	515.1	101	0.4	-6.2	518.3	164	-0.6	-4.0	523.7
58	2.6	-1.9	515.2	102	-0.3	-7.2	518.4	166	-0.2	-4.4	523.9
59	1.7	-7.5	515.2	103	-0.1	-7.7	518.5	167	-0.3	-5.2	524.0
60	1.8	-7.4	515.3	105	0.6	-7.2	518.6	169	-0.6	-5.3	524.2
62	2.1	-5.7	515.5	106	1.7	-7.1	518.7	172	-0.8	-4.7	524.5
64	2.4	-3.4	515.6	107	1.2	-7.3	518.8	181	-0.2	-3.9	525.4
65	2.3	-4.3	515.7	108	1.6	-7.2	518.8	185	-0.2	-4.4	525.8
67	1.9	-4.2	515.8	109	1.6	-6.8	518.9	192	0.4	-5.3	526.5
68	1.8	-6.3	515.9	110	1.4	-6.9	519.0				

Inferred Ages Flinders Ranges

Flinder Ranges, Arrowie Basin

Wilkawillina Limestone (Wilkawillina Gorge)

Depth (m)	$\delta^{13}C$ (‰)	$\delta^{18}O$ (‰)	Infered Age (Ma)
41	0.7	-8.2	519.5
19	1.7	-10.9	520.3
11	1.0	-10.7	520.6
6	0.3	-12.7	520.8

Woodendina Dolomite (Fountain Spring)

Depth (m)	$\delta^{13}C$ (‰)	$\delta^{18}O$ (‰)	Infered Age (Ma)
120	1.0	-3.2	521.0
93	-0.1	-5.8	521.4
74	-0.4	-6.2	521.6
64	-0.9	-5.9	521.8
44	-1.0	-5.7	522.1
32	-1.2	-5.6	522.2
21	-1.5	-7.0	522.4
11	-2.0	-5.8	522.5
10	-2.9	-6.0	522.5
6	-2.7	-5.9	522.6
3	-3.2	-5.2	522.6

Woodendina Dolomite (Parachilna Gorge)

Depth (m)	$\delta^{13}C$ (‰)	$\delta^{18}O$ (‰)	Infered Age (Ma)
228	-3.3	-5.7	522.7
220	-3.2	-7.1	522.8
192	-1.4	-6.0	523.2
188	-2.4	-7.5	523.2
183	-3.6	-7.4	523.3
173	-4.7	-6.6	523.4
163	-5.7	-6.0	523.6
141	-4.0	-6.2	523.9
124	-4.5	-6.1	524.1
111	-4.2	-6.8	524.3
106	-4.1	-6.6	524.4
100	-3.9	-6.7	524.5
93	-3.9	-7.4	524.5
88	-4.3	-5.8	524.6
84	-4.8	-7.3	524.7

Parachilna Formation (Parachilna Gorge)

Depth (m)	$\delta^{13}C$ (‰)	$\delta^{18}O$ (‰)	Infered Age (Ma)
67	-4.6	-9.8	524.9
61	-4.5	-7.3	525.0
50	-3.3	-7.6	525.3
47	-1.5	-7.3	525.4
40	-2.7	-7.3	525.5
33	-2.0	-7.0	525.7
24	-0.7	-7.2	525.9

Appendix V; Supporting Data for Australasian asphaltite strandings revisited: the effects of weathering and biodegradation on their biomarker profiles

Bulk Composition, normal & acyclic hydrocarbons (fullscan)

C_x = normal alkane $C_{carbion\ number}$ e.g. C_{15} = pentadecane ($C_{15}H_{32}$)
Pr = pristine
Ph = phytane
Sats = Saturate Fraction Hydrocarbons
Arom = Aromatic Fraction Hydrocarbons
NSO = Polar Fraction Hydrocarbons
Asph = Asphaltenes
C10-19/C30 = $(\sum nC_{10} : nC_{19})/nC_{30}$

Hopanes (m/z 191)

T = tricyclic terpanes note C_{25} and C_{26} homologues have a chiral centre at C_{22} (R & S)
Tet = C_{24} tetracyclic terpane
Ts = C_{27} 18α(H)-22,29,30-trisnorhopane
Tm = C_{27} 17α(H)-22,29,30-trisnorhopane
C_{28}BNH = C_{28} 17α(H),21β(H)-28,30 bisnorhopane
C_{29}H = C_{29} 17α(H),21β(H)-hopane
C_{30}H = C_{30} 17α(H),21β(H)-hopane
Mor = C_{30} 17β(H),21α(H)-moretane
C_{30}DiaH = C_{30} 17α(H),21β(H)-diahopane
C_{29}Ts = C_{29} 30-norneohopane
C_{30}Ts = C_{30} 30-norneohopane
Gam = Gammacerane
C_{31}HR = C_{31} 17α(H),21β(H)-homohopane (22R)
C_{32} S/(S+R) = C_{32} 17α(H),21β(H)-bishopane (22S)/C_{32} 17α(H),21β(H)-bishopane (22S + 22R)
C_{35}(S+R)/C_{31}(S+R) = C_{35} 17α(H),21β(H)-pentahomohopanes (22S + 22R)/ C_{31} 17α(H),21β(H)-homohopanes (22S + 22R)
C_{35}/C_{34} (S only) = C_{35} 17α(H),21β(H)-pentahomohopane (22S)/ C_{34} 17α(H),21β(H)-tetrahomohopane (22S)
C35 Homohopane Index = C_{35} 17α(H),21β(H)-pentahomohopanes (22S & 22R)/$\sum C_{31}$: C_{35} 17α(H),21β(H)-homohopanes (22S & 22R)

Steranes (m/z 217 & 218)

C_{27} ααα 20R = C_{27} 5α(H),14α(H),17α(H)-sterane (20R)
C_{28} ααα 20R = C_{28} 5α(H),14α(H),17α(H)-sterane (20R)
C_{29} ααα 20R = C_{29} 5α(H),14α(H),17α(H)-sterane (20R)
C_{27} Dia/(Dia+Reg) = C_{27} 13α(H),17α(H) diasteranes (20R + 20S)/(C_{27} 13α(H),17α(H) diasteranes (20R + 20S) + C_{27} 5α(H) steranes (20R + 20S))
C_{29} αββ/(ααα + αββ) = C_{29} 5α(H),14β(H),17β(H)-steranes (20R + 20S)/ (C_{29} 5α(H),14α(H),17α(H)-steranes (20R + 20S) + C_{29} 5α(H),14β(H),17β(H)-steranes (20R + 20S))
C_{27} αββ 20(R+S) = C_{27} 5α(H),14β(H),17β(H)-steranes (20R + 20S)
C_{28} αββ 20(R+S) = C_{28} 5α(H),14β(H),17β(H)-steranes (20R + 20S)
C_{29} αββ 20(R+S) = C_{29} 5α(H),14β(H),17β(H)-steranes (20R + 20S)
C_{29}/C_{27} abb Sterane Ratio = C_{29} 5α(H),14β(H),17β(H)-steranes (20R + 20S)/ C_{27} 5α(H),14β(H),17β(H)-steranes (20R + 20S)

Triaromatic Steroids (m/z231)

C_{26} Triaromatic Steroids = C_{26} Triaromatic Steroids (20R + 20S)
C_{27} Triaromatic Steroids = C_{27} Triaromatic Steroids (20R + 20S)
C_{28} Triaromatic Steroids = C_{28} Triaromatic Steroids (20R + 20S)
C_{29} Triaromatic Steroids = C_{29} Triaromatic Steroids (20R + 9α20S + 9β20S)

C_{20} = C_{2o} Triaromatic Steroid
C_{21} = C_{21} Triaromatic Steroid
C_{26} 20R = C_{26} Triaromatic Steroid 20R
C_{26} 20S = C_{26} Triaromatic Steroid 20S
C_{27} 20R = C_{27} Triaromatic Steroid 20R
C_{27} 20S = C_{27} Triaromatic Steroid 20S
C_{28} 20R = C_{28} Triaromatic Steroid 20R
C_{28} 20S = C_{28} Triaromatic Steroid 20S
C_{29} 20R = C_{29} Triaromatic Steroid 20R
C_{29} 20S9α = C_{29} Triaromatic Steroid 9α,20S
C_{29} 20S9β = C_{29} Triaromatic Steroid 9β,20S

Polycyclic Aromatic Hydrcarbons (m/z 178, 184, 198, 226, 252)

BaP = Benzo(a)Pyrene
BbF = Benoz(b)Fluoranthene
P = Phenanthrene
MP = Methyl Phenanthrenes
C2P = Ethyl & Dimethyl Phenanthrenes
DBT = Dibenzothiophene
MDBT = Methyl Dibenzothiophenes
C3DBT = Propyl, Methyl-Ethyl & Trimethyl Dibenzothiophenes

Bulk Geochemistry

Limestone Coast

Bulk Parameters (fullscan)	27A				CB32				162			
	outer	inner	diff	% diff	outer	inner	diff	% diff	outer	inner	diff	% diff
Sats (%)	19.4	21.4	-2.00	-9.80%	16.3	19	-2.70	-15.30%	18.3	20	-1.70	-8.88%
Aroms (%)	13.4	14.1	-0.70	-5.09%	12	16.4	-4.40	-30.99%	11.8	13.3	-1.50	-11.95%
NSO (%)	16.9	16.7	0.20	1.19%	19.6	15.9	3.70	20.85%	16.9	14.2	2.70	17.36%
Asph (%)	50.3	47.8	2.50	5.10%	52.1	48.7	3.40	6.75%	53	52.5	0.50	0.95%

Kangaroo Island

Bulk Parameters (fullscan)	80				85				168				177			
	outer	inner	diff	% diff	outer	inner	diff	% diff	outer	inner	diff	% diff	outer	inner	diff	% diff
Sats (%)	18.6	25.6	-7.00	-31.67%	21.8	21.6	0.20	0.9%	21.1	24.4	-3.30	-14.51%	19.2	20.4	-1.20	-6.06%
Aroms (%)	11.7	16.2	-4.50	-32.26%	11.9	12.7	-0.80	-6.5%	10.8	13.6	-2.80	-22.95%	12.4	11.4	1.00	8.40%
NSO (%)	16.3	10.4	5.90	44.19%	15.9	14.7	1.20	7.8%	13.1	16.3	-3.20	-21.77%	16.3	15.6	0.70	4.39%
Asph (%)	53.4	47.8	5.60	11.07%	50.4	51	-0.60	-1.2%	55	45.7	9.30	18.47%	52.1	52.6	-0.50	-0.96%

Eyre Peninsula

Bulk Parameters (fullscan)	cl1				mh1			
	outer	inner	diff	% diff	outer	inner	diff	% diff
Sats (%)	17.5	24.5	-7.00	-33.33%	17.9	21.6	-3.70	-18.73%
Aroms (%)	11.2	15.2	-4.00	-30.30%	13.6	12.0	1.60	12.50%
NSO (%)	16.1	18.6	-2.50	-14.41%	17.0	16.5	0.50	2.99%
Asph (%)	55.2	41.7	13.50	27.86%	51.5	49.9	1.60	3.16%

New Zealand

Bulk Parameters (fullscan)	nz1				nz2			
	outer	inner	diff	% diff	outer	inner	diff	% diff
Sats (%)	20.4	24.6	-4.20	-18.67%	19.7	23.3	-3.60	-16.74%
Aroms (%)	12.6	13.1	-0.50	-3.89%	12.8	12.7	0.10	0.78%
NSO (%)	22.0	16.9	5.10	26.22%	20.7	19.4	1.30	6.48%
Asph (%)	45.0	45.4	-0.40	-0.88%	46.8	44.6	2.20	4.81%

GC-MS Bulk Interpretive Ratios, Peak Areas and Chromatograms.

Limestone Coast

Pristane & Phytane Ratios						
	27A		CB32		162	
	outer	inner	outer	inner	outer	inner
Pr	1811172	930609	969835	754431	1864817	708170
Ph	1631400	776423	1035236	662731	1917235	606899
Pr/Ph	1.11	1.20	0.94	1.14	0.97	1.17
Pr/C17	0.48	0.50	0.49	0.56	0.49	0.51
Ph/C18	0.46	0.46	0.43	0.48	0.48	0.46

Weathering Ratio, C10-15/C16-20						
	27A		CB32		162	
	outer	inner	outer	inner	outer	inner
C10	166	69	4768	506	3279	1140
C11	791	385	6894	769	3943	1218
C12	3003	1719	1019	178	1851	818
C13	45042	35277	4251	3754	31224	19548
C14	254783	144819	26491	30607	151818	81221
C15	574086	272107	110767	104096	392417	178052
C16	727339	333967	233523	188843	616632	233135
C17	754715	344085	387513	246812	758431	257248
C18	716515	327922	475588	261446	783385	245954
C19	660182	300817	491963	255390	746814	232810
C20	650411	299101	511697	261792	742571	226394
c30	202931	80080	170907	65658	231798	60027
C10:19/C30	18.413	21.993	10.197	16.638	15.055	20.843
diff	16.3%		38.7%		27.8%	

Odd Even Preference (inner)			
	27A	CB32	162
C21	270467	237735	207313
C22	242651	213480	186143
C23	229173	203974	177333
C24	209446	185281	164871
C25	196646	172814	156145
	1.02	1.02	1.02

Kangaroo Island

Pristane & Phytane Ratios

	80		85		168		177	
	outer	inner	outer	inner	outer	inner	outer	inner
Pr	2508855	739681	1512680	682582	3117077	900440	1662602	1133057
Ph	2302435	622553	1317822	607970	3093045	753635	1520129	936358
Pr/Ph	1.09	1.19	1.15	1.12	1.01	1.19	1.09	1.21
Pr/C17	0.45	0.48	0.58	0.58	0.42	0.48	0.46	0.47
Ph/C18	0.42	0.41	0.49	0.52	0.40	0.41	0.44	0.41

Weathering Ratio, C10-15/C16-20

	80		85		168		177	
	outer	inner	outer	inner	outer	inner	outer	inner
C10	1209	64	2842	290	340	0	5725	913
C11	1796	119	2713	365	567	0	6538	1798
C12	2968	393	3590	3620	6289	4365	3391	1650
C13	50102	11779	47966	30562	121651	68983	40908	16142
C14	289660	76817	180176	89603	382711	191314	244139	69291
C15	692005	193059	336652	151964	642844	292457	759464	177645
C16	993015	265486	458657	192720	763451	334980	1202617	249882
C17	1097910	289728	515130	213525	806561	347978	1459117	279335
C18	1061156	285819	524954	215739	801589	339534	1512041	272766
C19	1013602	263752	505665	204337	757697	318830	1421317	254940
C20	995292	256342	509829	210490	741446	317752	1410837	249436
c30	257258	65138	172070	64902	198433	86073	374487	59104
C10:19/C30	20.226	21.293	14.984	16.991	21.588	22.056	17.772	22.407
diff	5.0%		11.8%		2.1%		20.7%	

Odd Even Preference (inner)

	80	85	168	177
C21	236883	183956	289204	221705
C22	213428	167232	264875	198867
C23	207383	157933	249931	186705
C24	184272	145681	225689	166228
C25	167840	143891	211311	158923
OEP	1.04	1.02	1.02	1.03

Eyre Peninsula

Pristane & Phytane Ratios				
	cl1		mh1	
	outer	inner	outer	inner
Pr	1662602	1133057	2543529	950724
Ph	1520129	936358	2290361	795880
Pr/Ph	1.09	1.21	1.11	1.19
Pr/C17	0.46	0.47	0.48	0.49
Ph/C18	0.44	0.41	0.46	0.44

Weathering Ratio, C10-15/C16-20				
	cl1		mh1	
	outer	inner	outer	inner
C10	1952	67	3314	70
C11	3240	52	4003	196
C12	4353	16388	6554	1477
C13	98281	151312	85009	24343
C14	363636	331473	358315	116199
C15	614899	445385	794579	263605
C16	697750	455584	1000464	337233
C17	710185	448783	1043737	357177
C18	680060	419704	980769	337904
C19	617877	386504	902806	310147
C20	612316	383303	917345	316976
c30	137755	89567	260304	80737
C10:19/C30	27.529	29.645	19.898	21.655
diff	7.1%		8.1%	

Odd Even Preference (inner)		
	cl1	mh1
C21	343627	282880
C22	301772	248673
C23	290268	239914
C24	256380	213311
C25	238616	198230
OEP	1.04	1.04

New Zealand

Pristane & Phytane Ratios				
	nz1		nz2	
	outer	inner	outer	inner
Pr	1870694	1190412	1600928	576268
Ph	1735655	1007914	1323912	472344
Pr/Ph	1.08	1.18	1.21	1.22
Pr/C17	0.44	0.47	0.47	0.48
Ph/C18	0.42	0.44	0.41	0.43

Weathering Ratio, C10-15/C16-20				
	nz1		nz2	
	outer	inner	outer	inner
C10	2633	55	1789	113
C11	4664	355	2642	53
C12	8429	13207	49530	1838
C13	103915	79222	268114	51905
C14	314069	204360	509984	151078
C15	609313	354186	680121	220637
C16	770300	433670	681401	228130
C17	836208	458817	675849	220794
C18	807026	442514	631423	208556
C19	742752	415558	582967	188985
C20	739553	410581	583363	188954
c30	195385	105370	159387	45872
C10:19/C30	21.492	22.795	25.622	27.731
diff	5.7%		7.6%	

Odd Even Preference (inner)		
	nz1	nz2
C21	367671	170078
C22	324566	153187
C23	311980	146383
C24	276580	132267
C25	260197	124375
OEP	1.04	1.03

Sample 27 Inner Saturate Chromatograms; Fullscan and Hydrocarbons

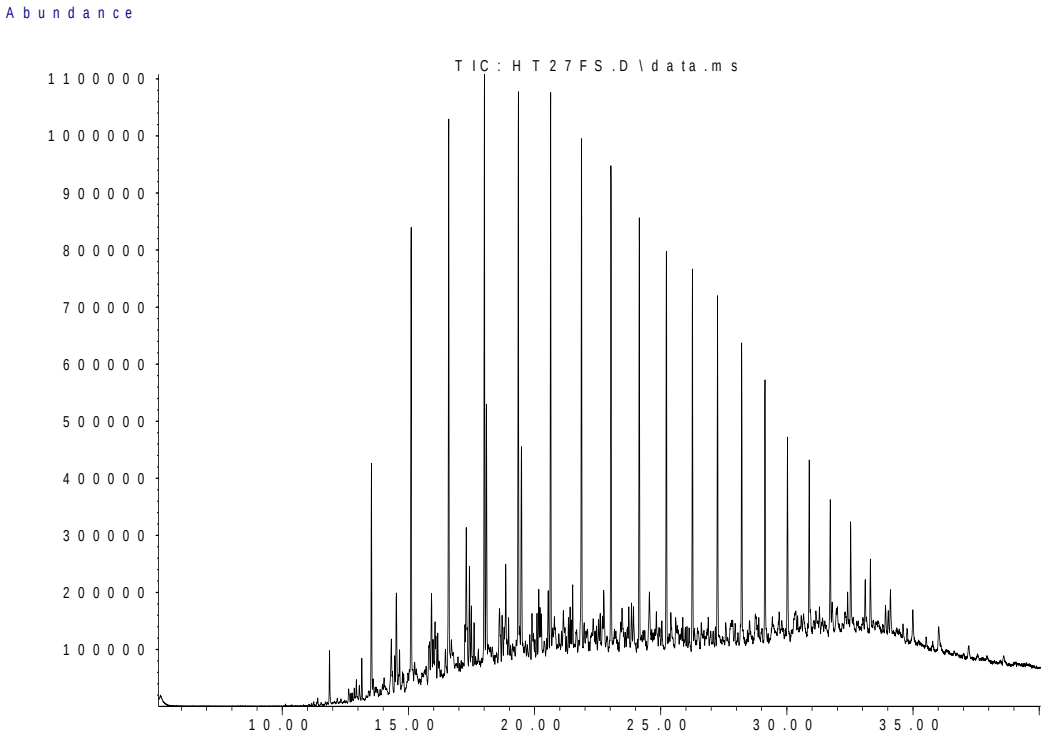

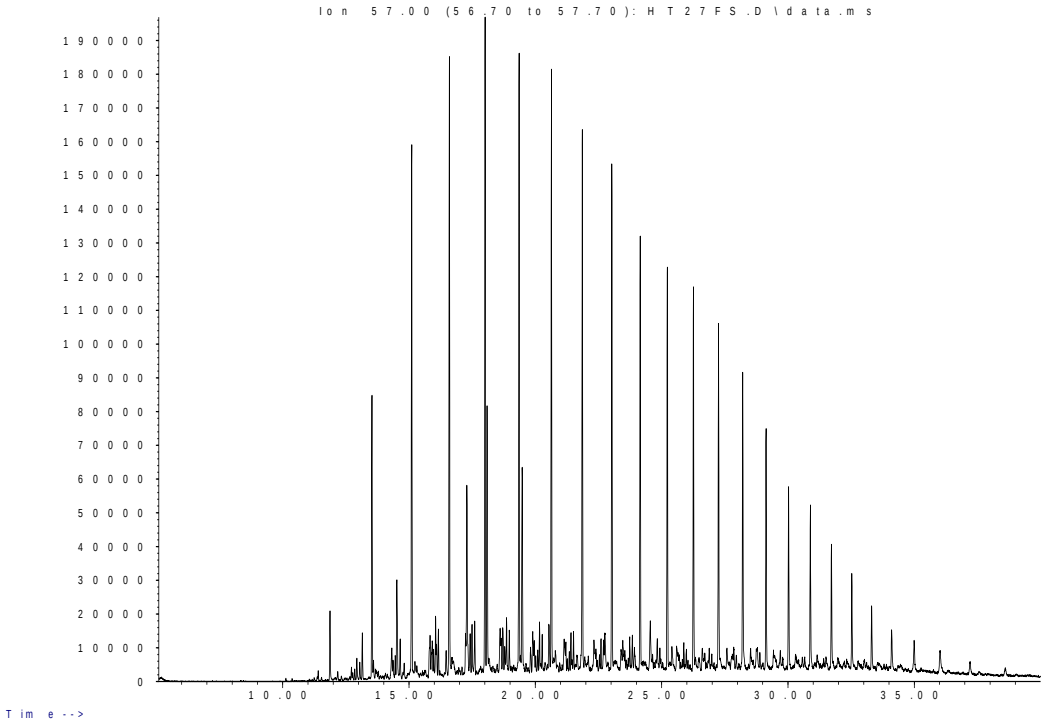

Sample 27 Outer Saturate Chromatograms; Fullscan and Hydrocarbons

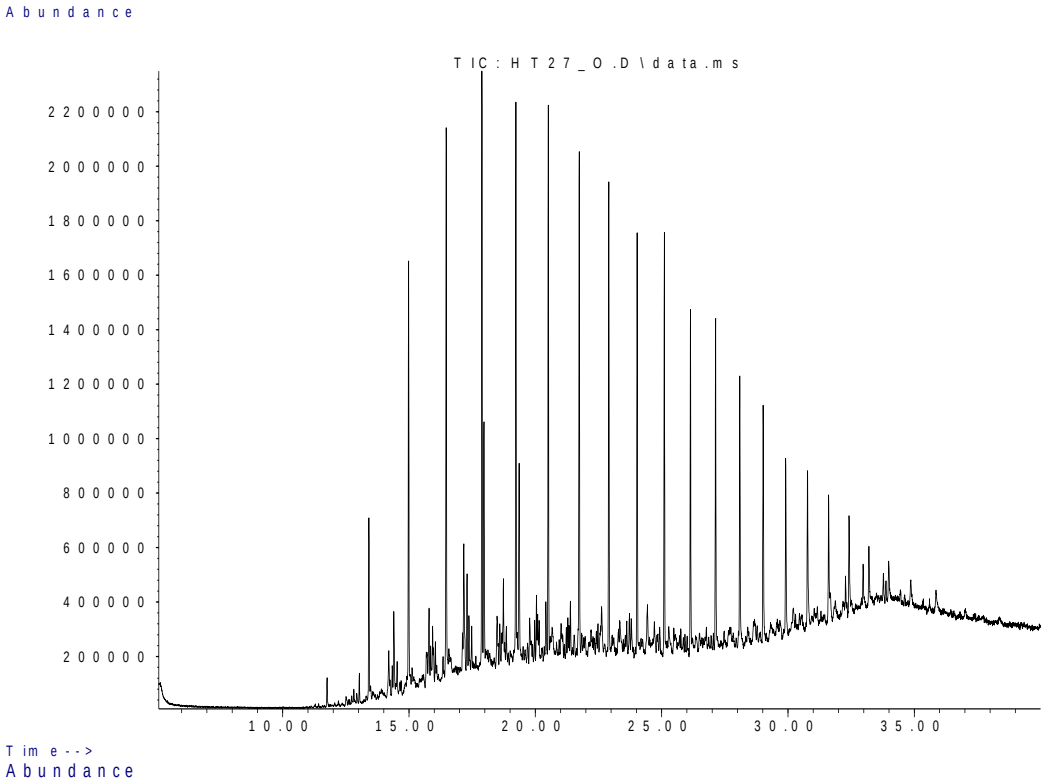

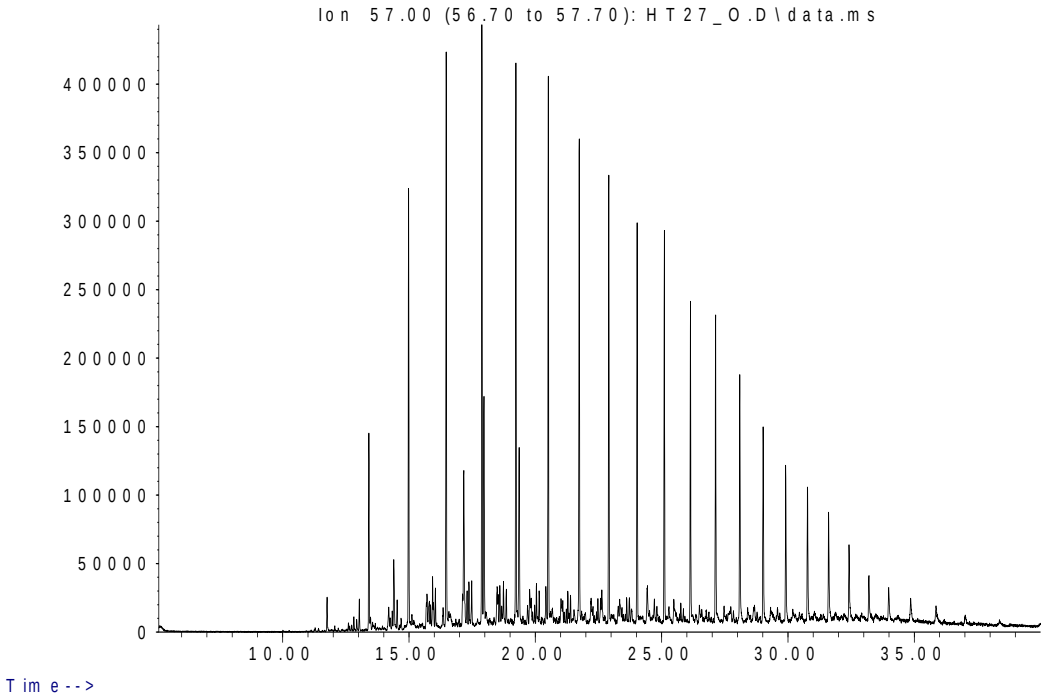

Sample 32 Inner Saturate Chromatograms; Fullscan and Hydrocarbons

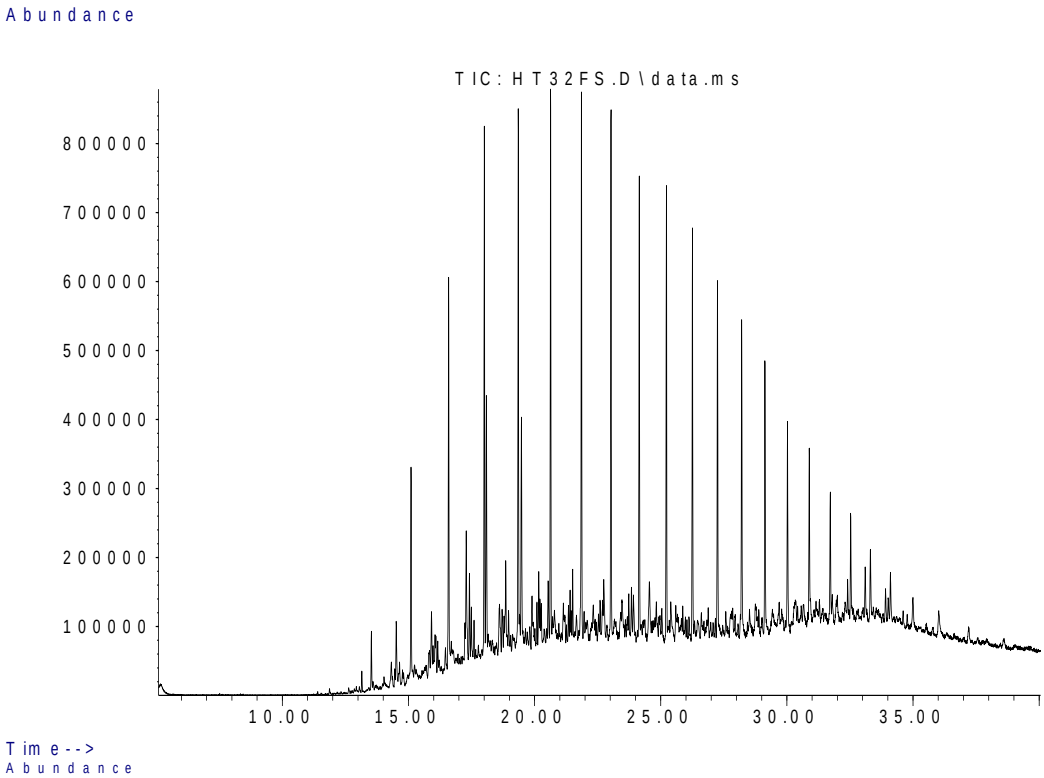

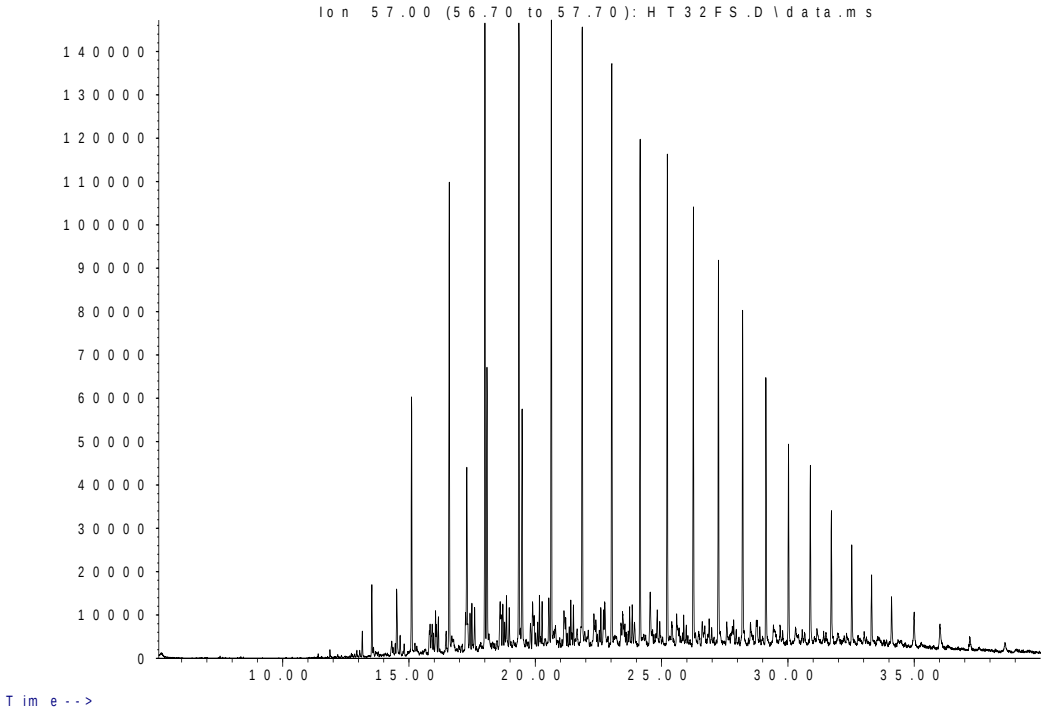

Sample 32 Outer Saturate Chromatograms; Fullscan and Hydrocarbons

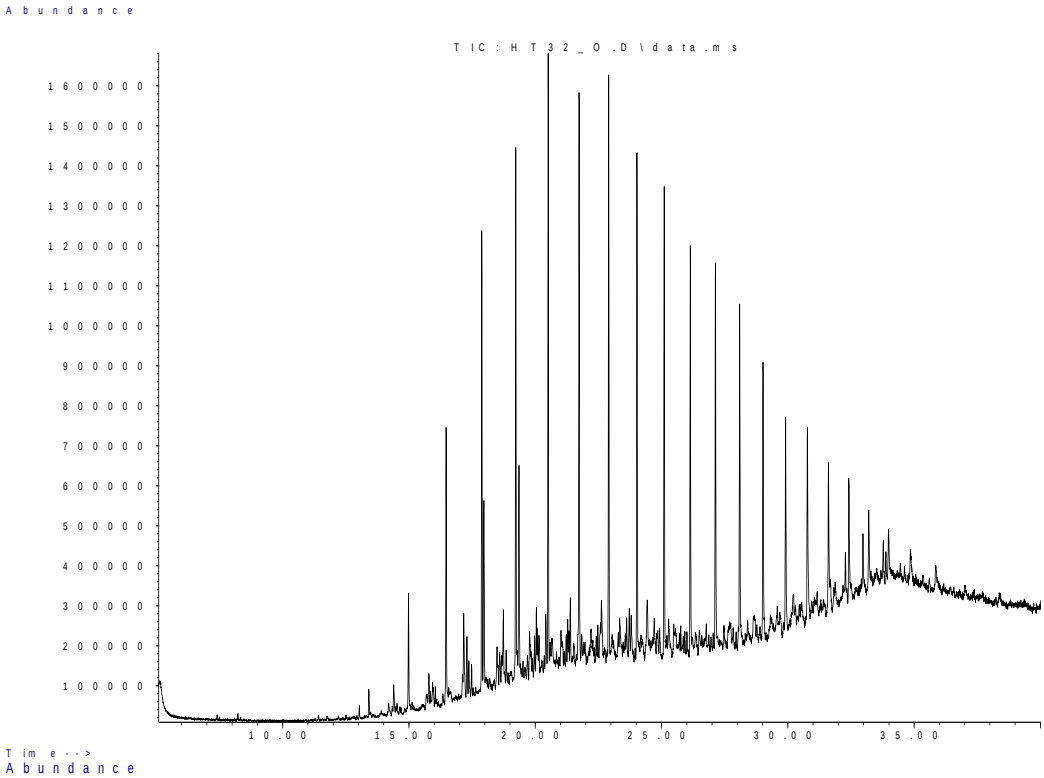

Sample 162 Inner Saturate Chromatograms; Fullscan and Hydrocarbons

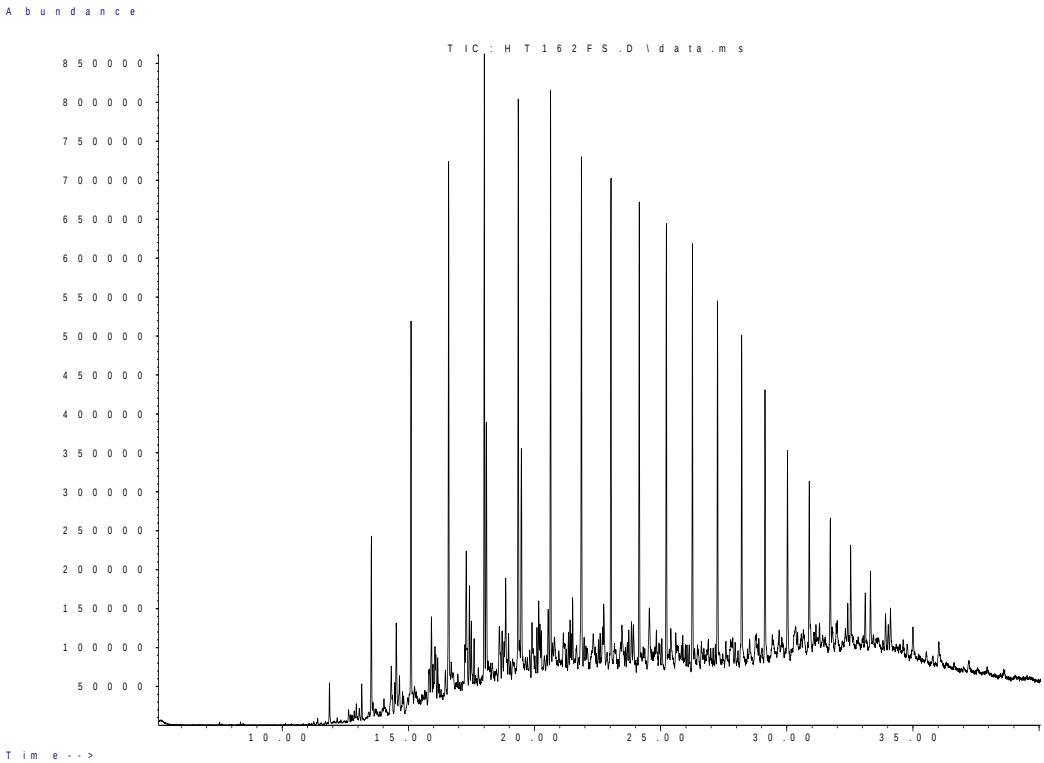

Sample 162 Outer Saturate Chromatograms; Fullscan and Hydrocarbons

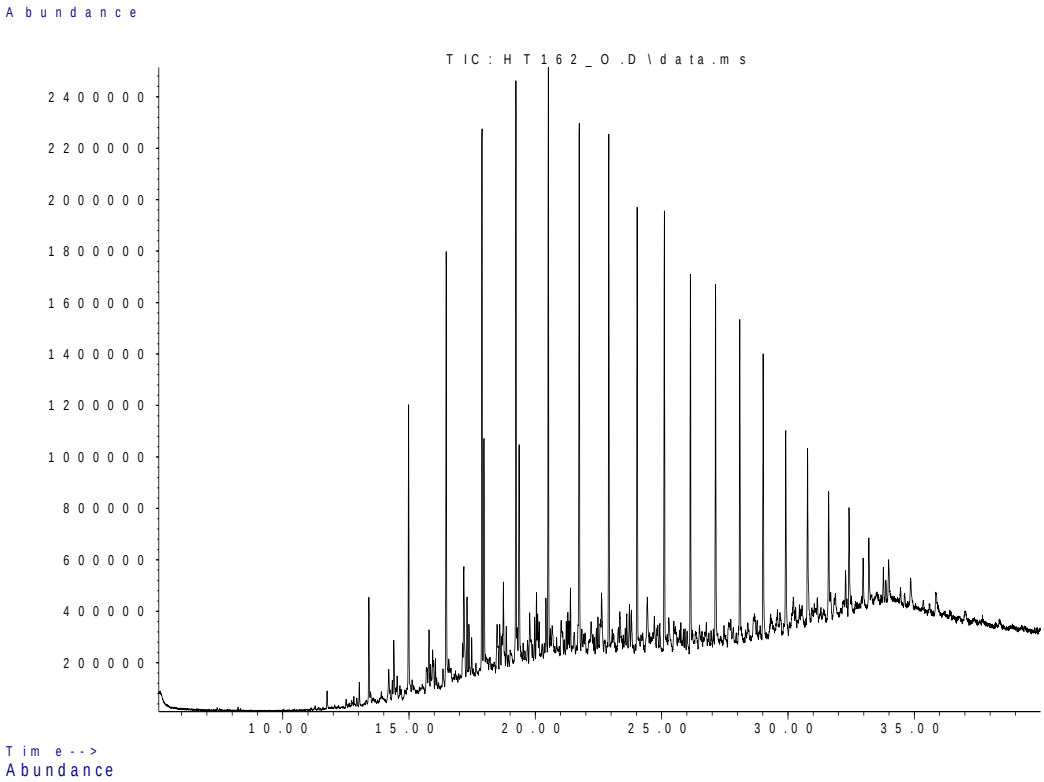

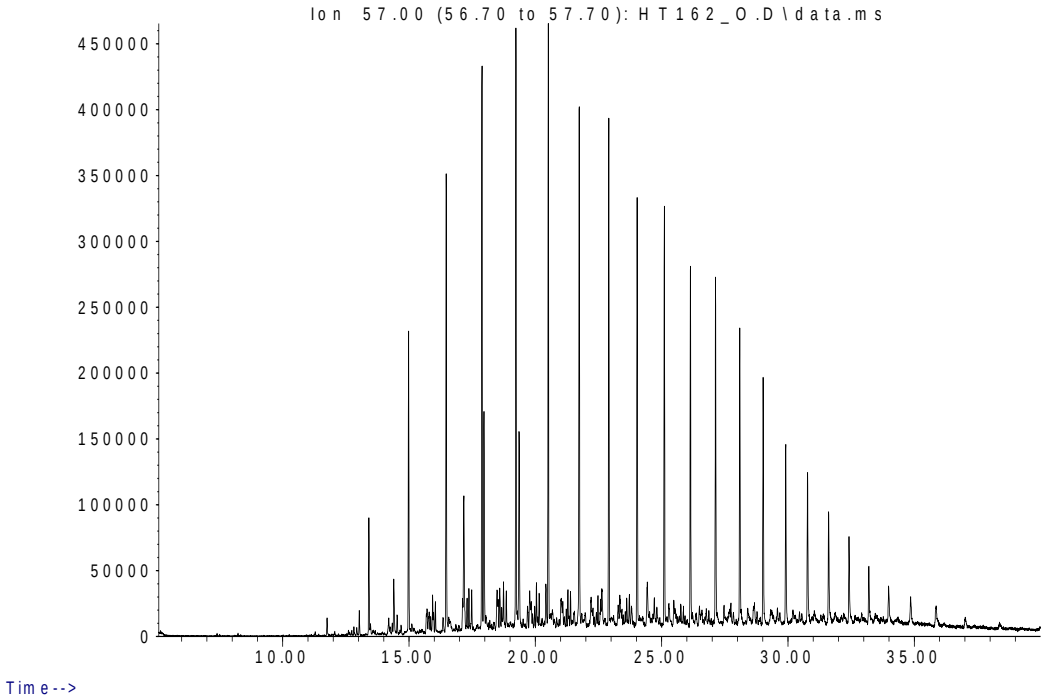

Sample 80 Inner Saturate Chromatograms; Fullscan and Hydrocarbons

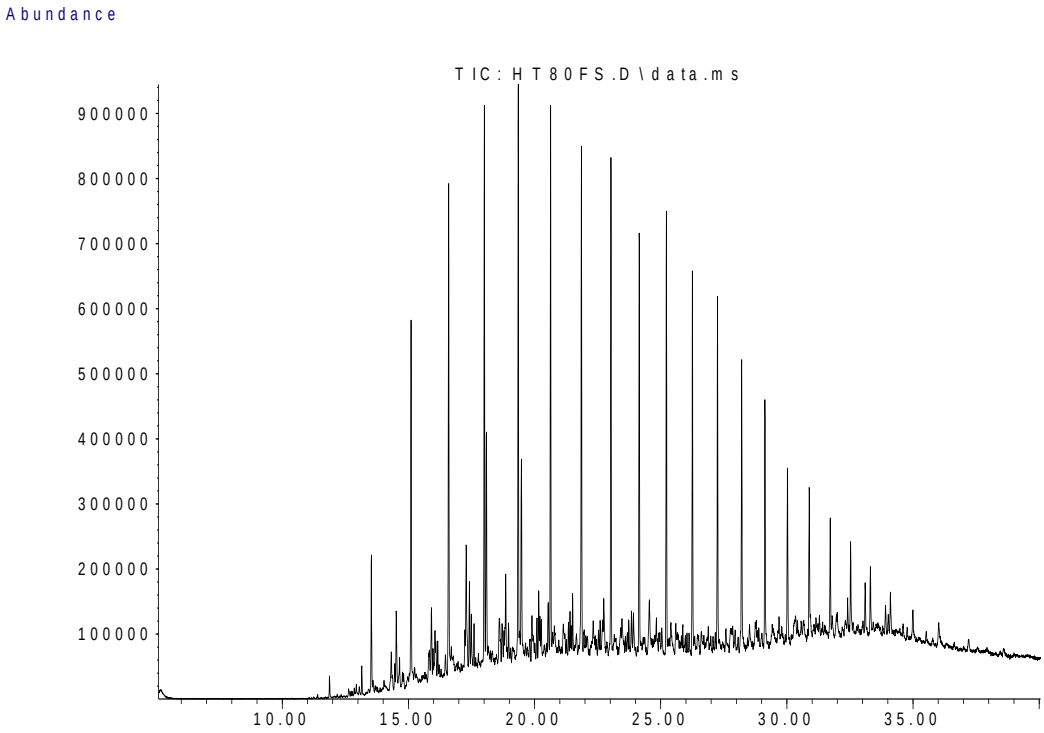

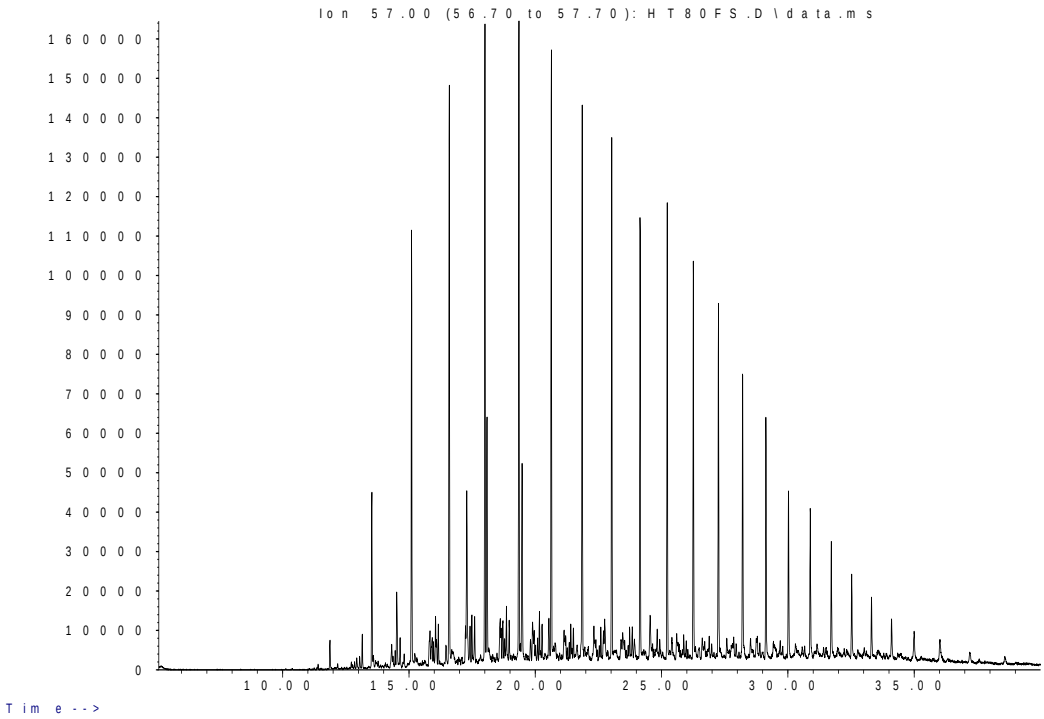

Sample 80 Outer Saturate Chromatograms; Fullscan and Hydrocarbons

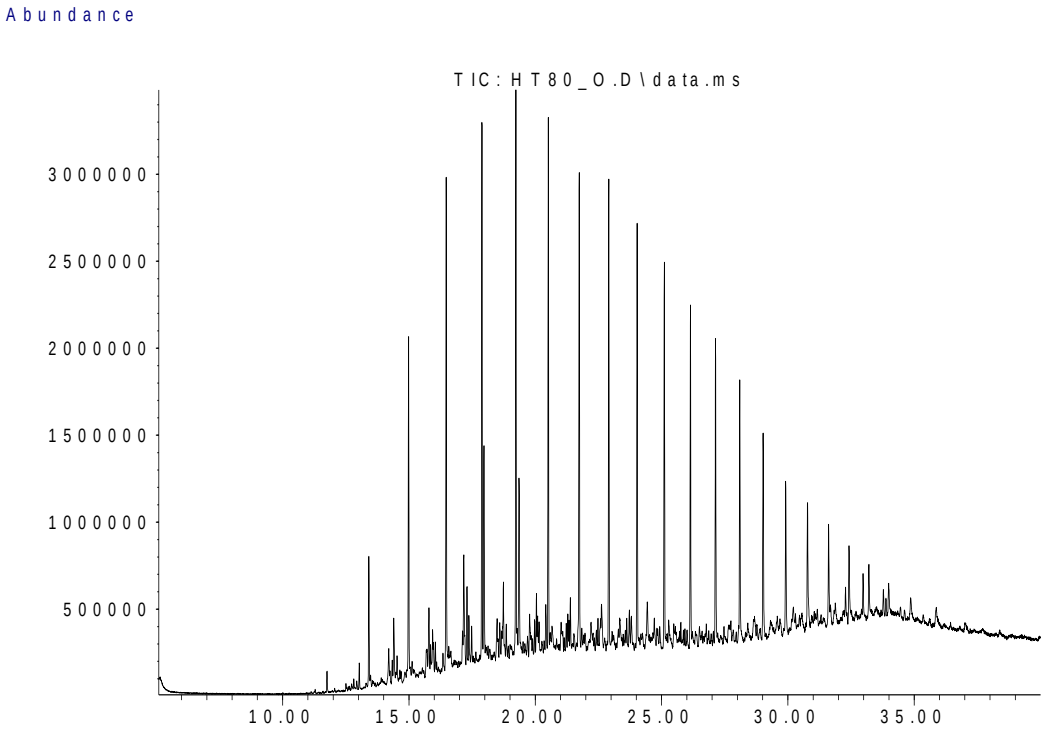

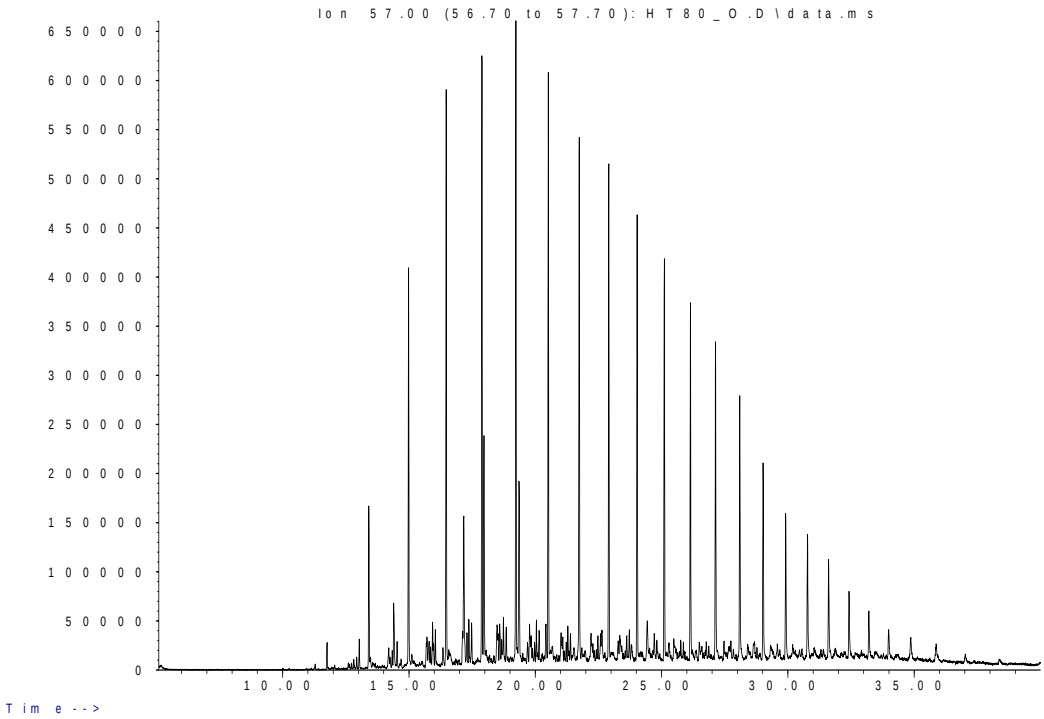

Sample 85 Inner Saturate Chromatograms; Fullscan and Hydrocarbons

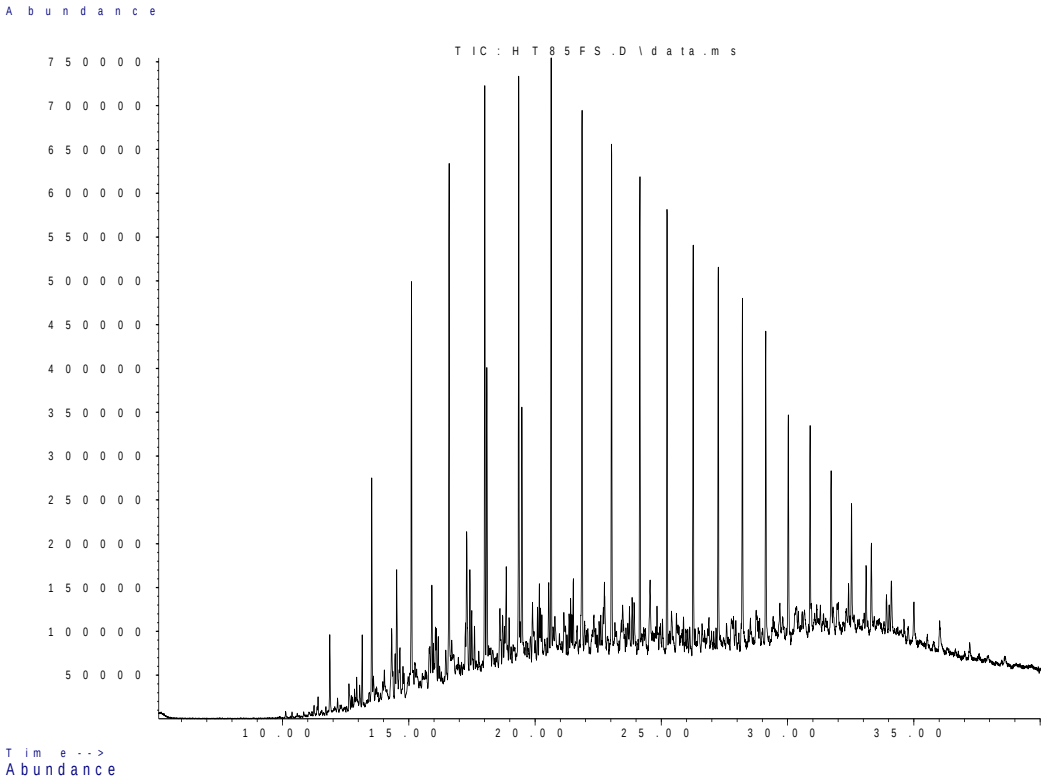

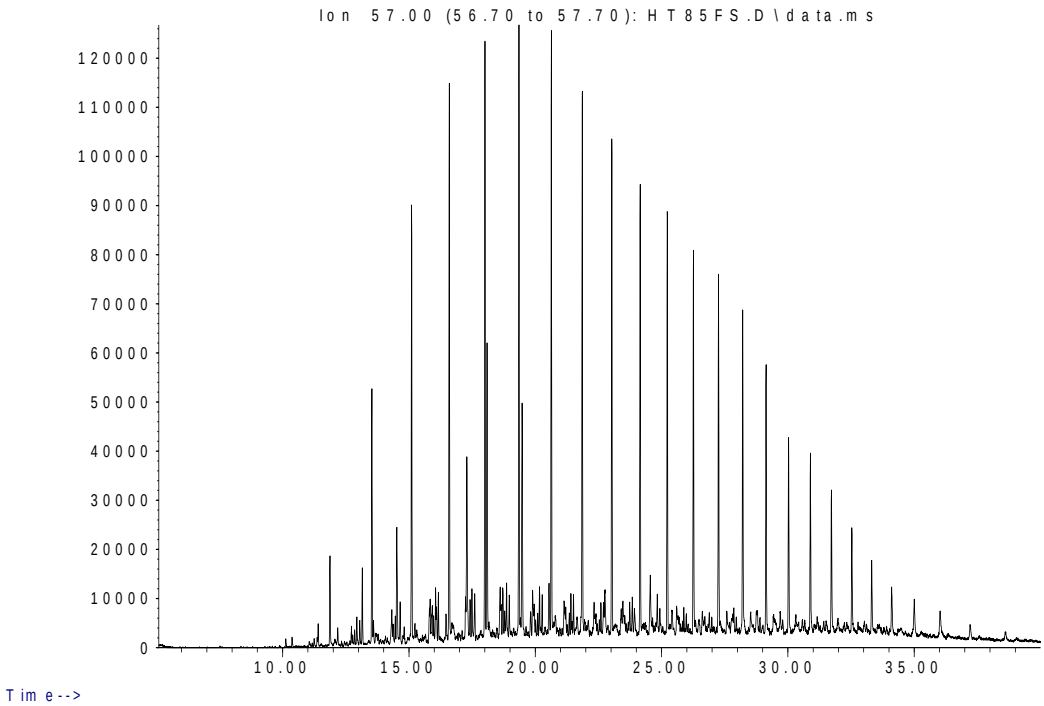

Sample 85 Outer Saturate Chromatograms; Fullscan and Hydrocarbons

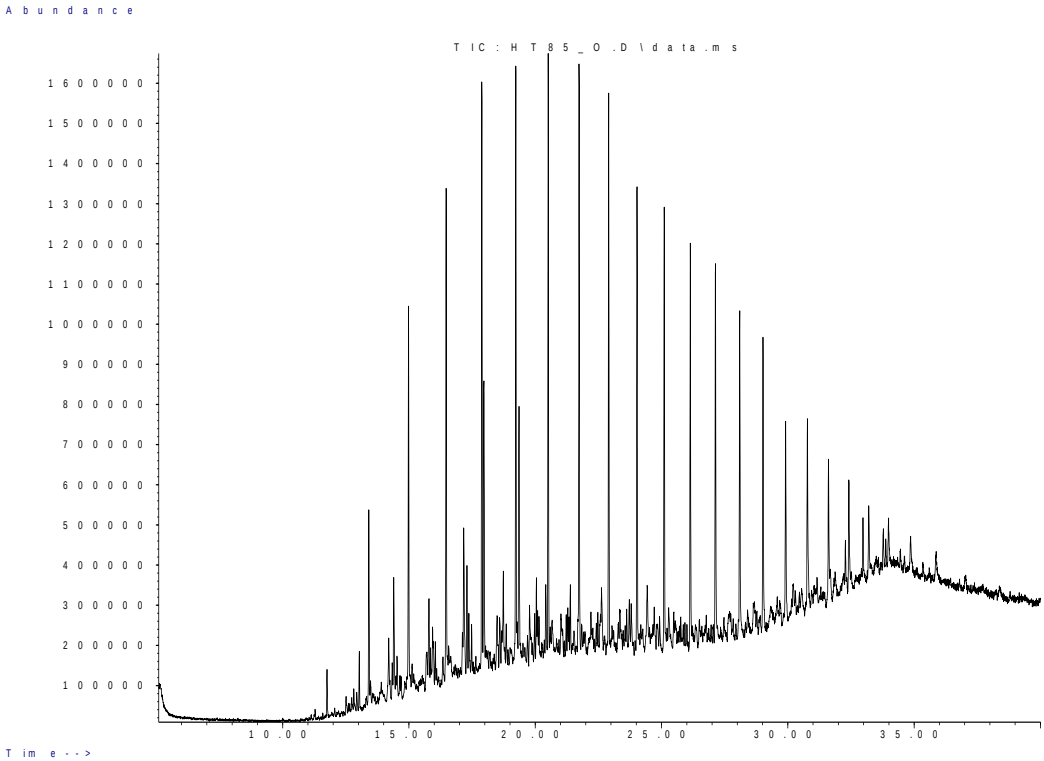

Sample 168 Inner Saturate Chromatograms; Fullscan and Hydrocarbons

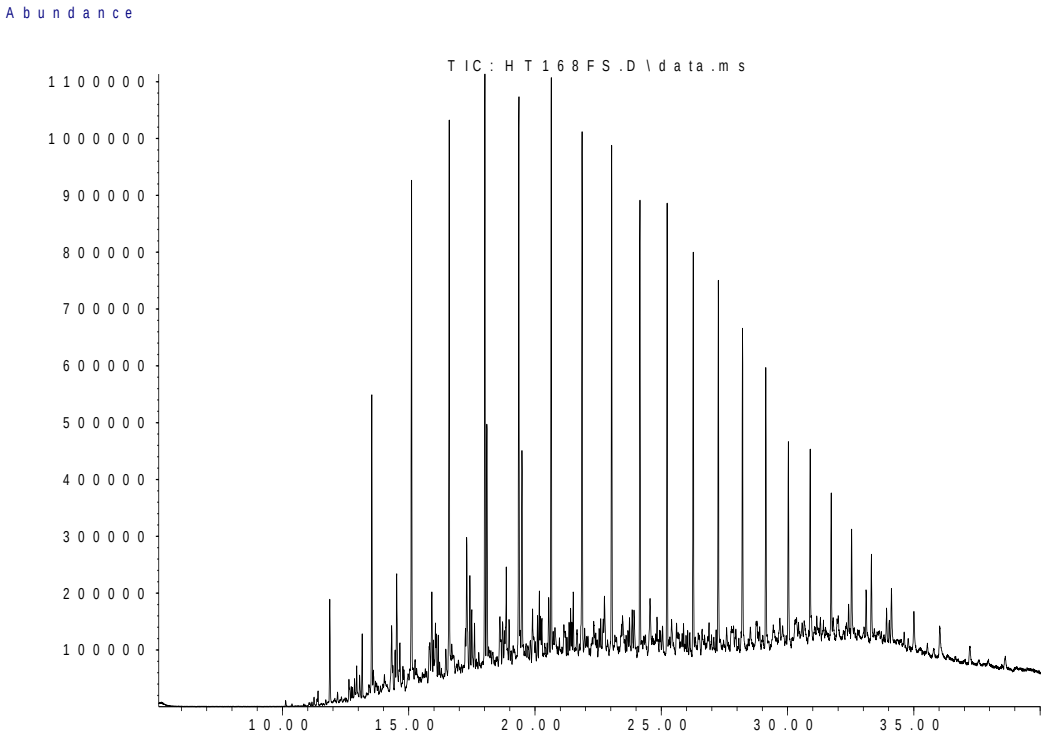

Sample 168 Outer Saturate Chromatograms; Fullscan and Hydrocarbons

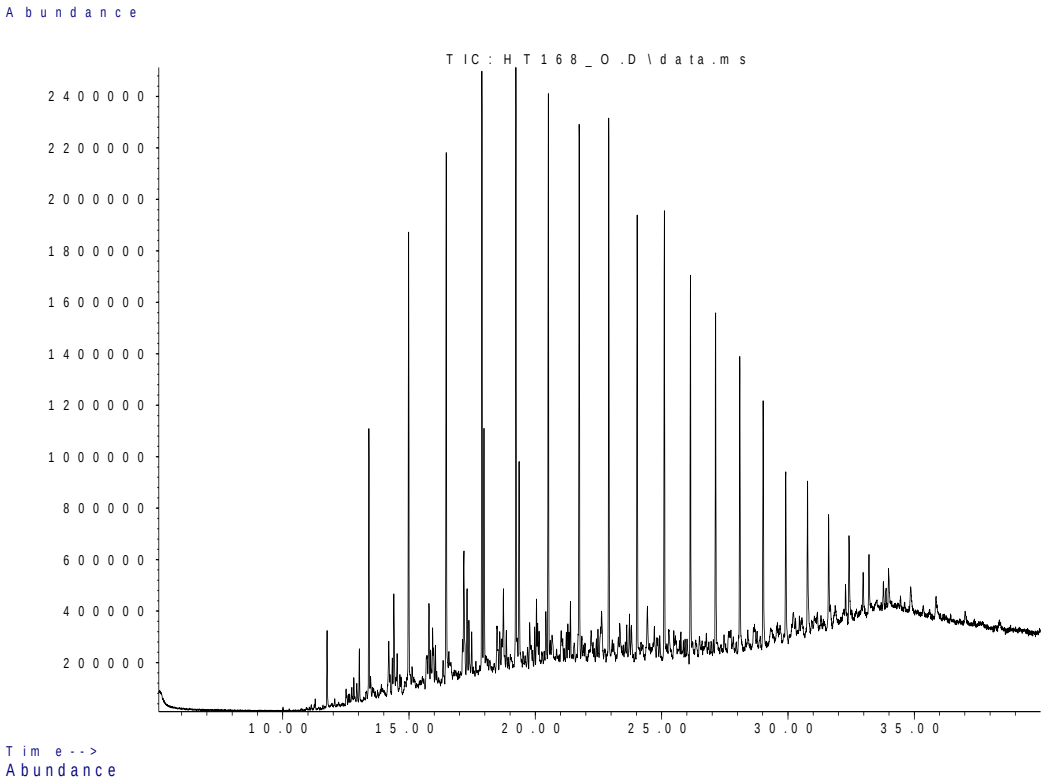

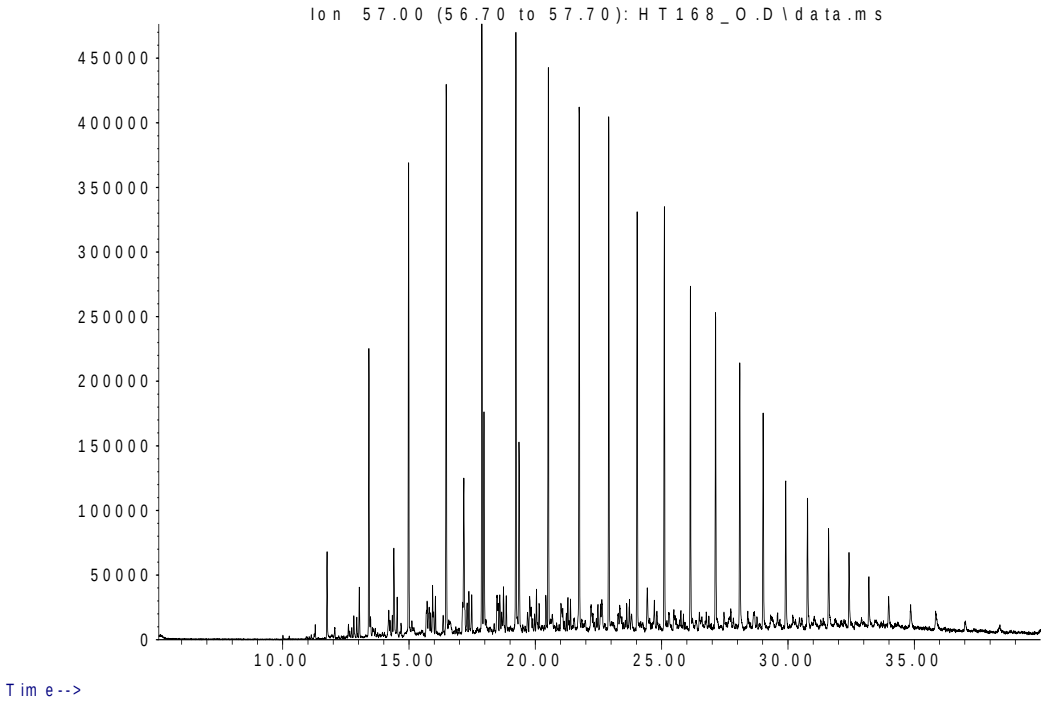

Sample 177 Inner Saturate Chromatograms; Fullscan and Hydrocarbons

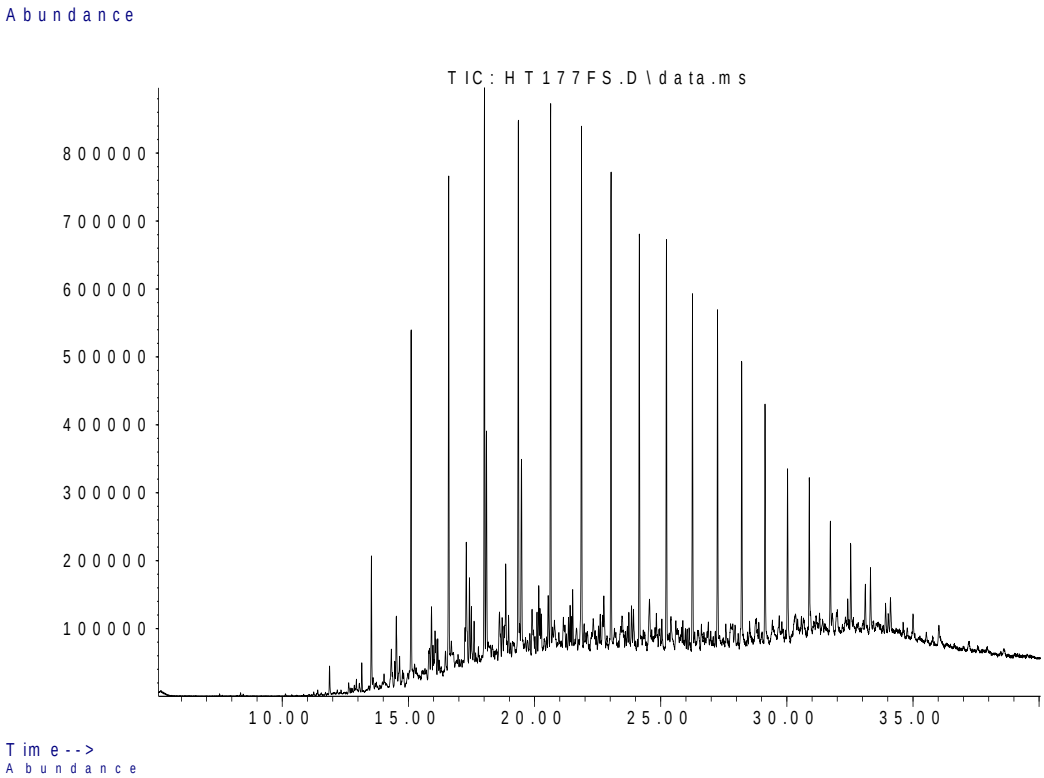

Sample 177 Outer Saturate Chromatograms; Fullscan and Hydrocarbons

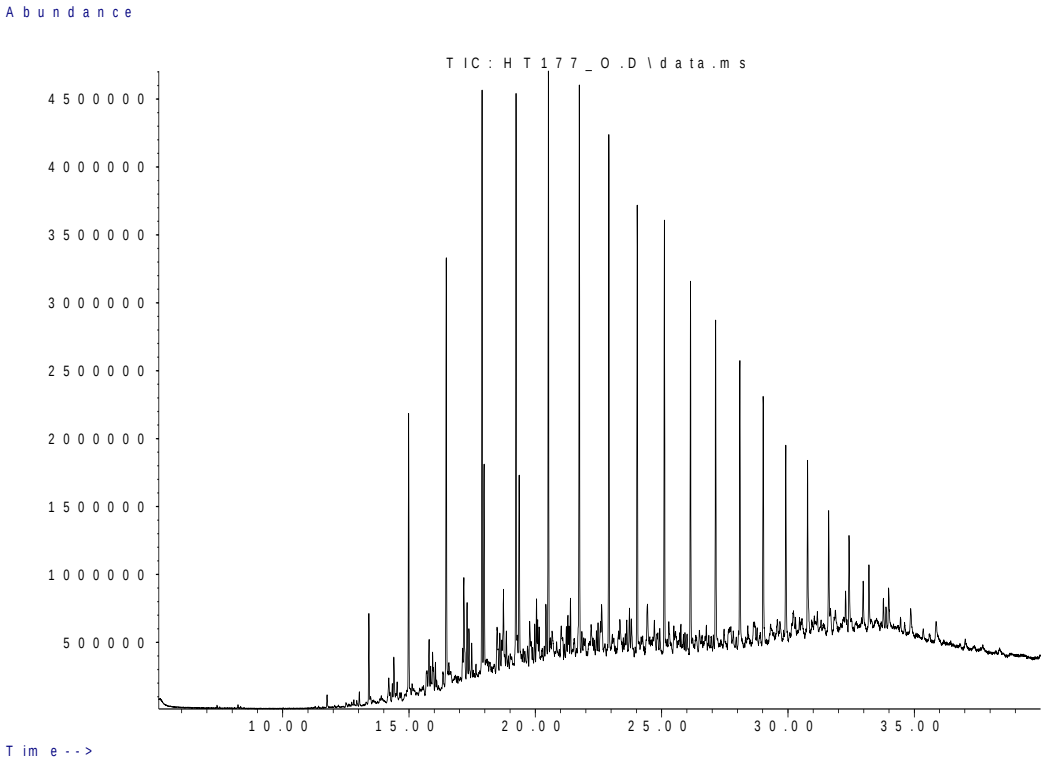

Sample CL1 Inner Saturate Chromatograms; Fullscan and Hydrocarbons

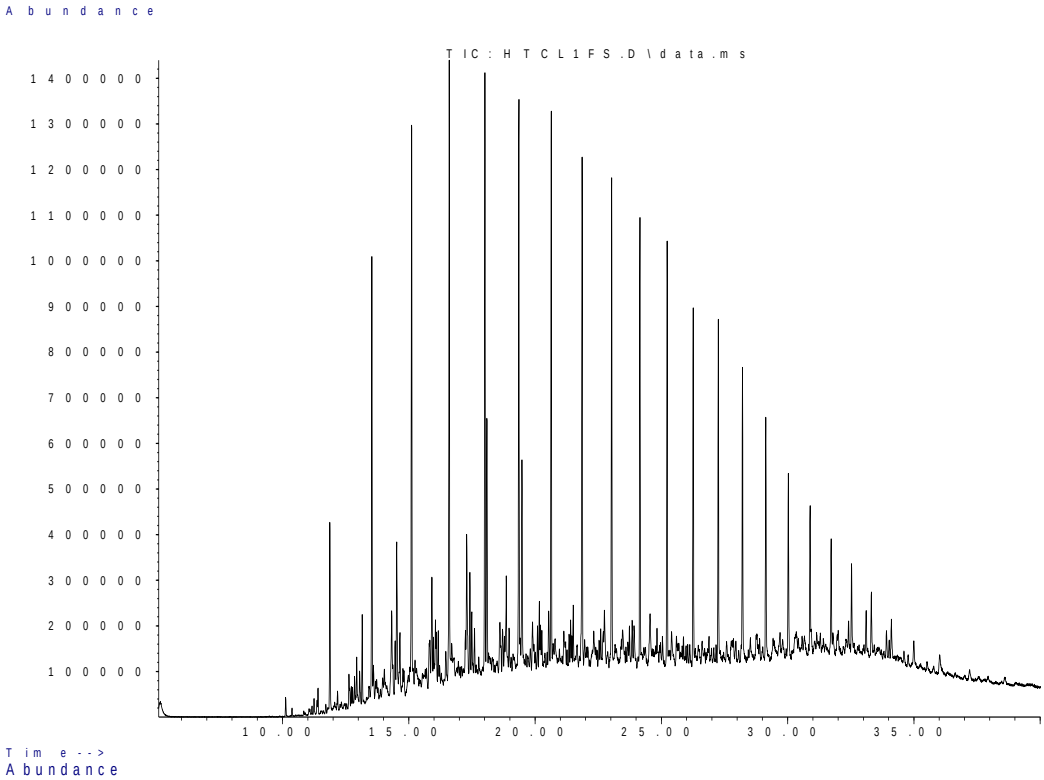

Sample CL1 Outer Saturate Chromatograms; Fullscan and Hydrocarbons

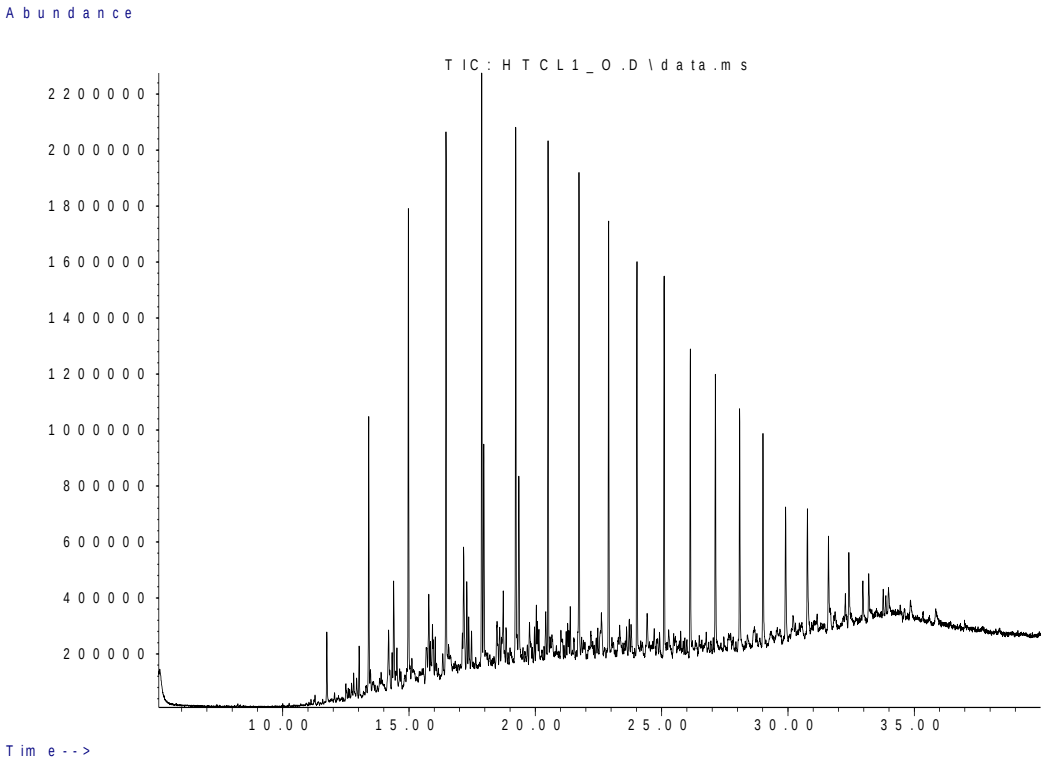

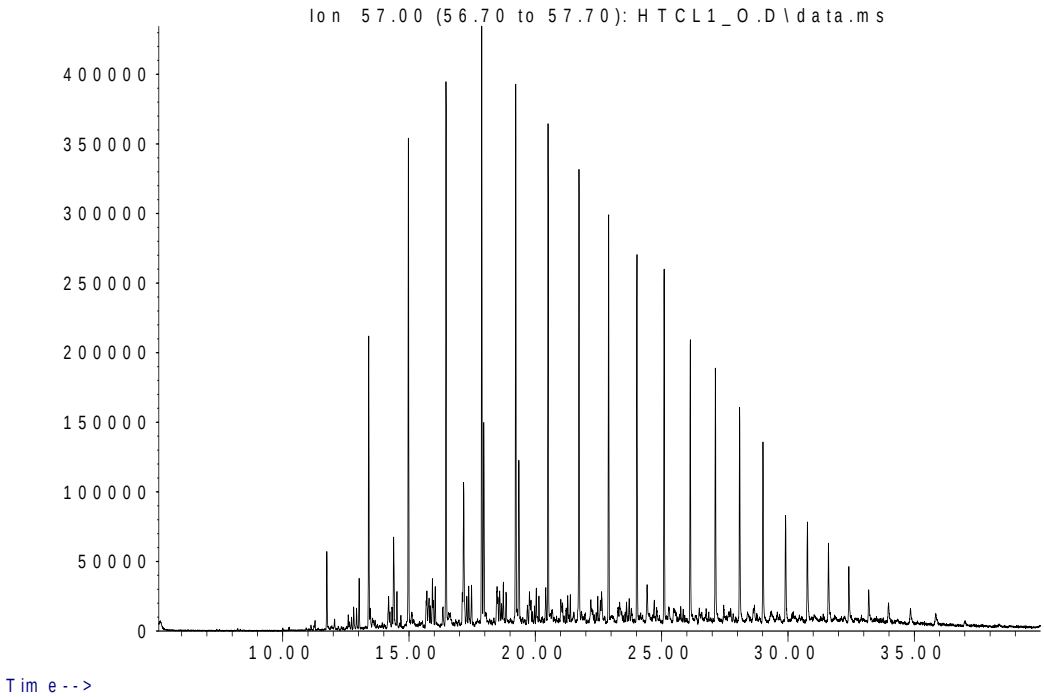

Sample MH1 Inner Saturate Chromatograms; Fullscan and Hydrocarbons

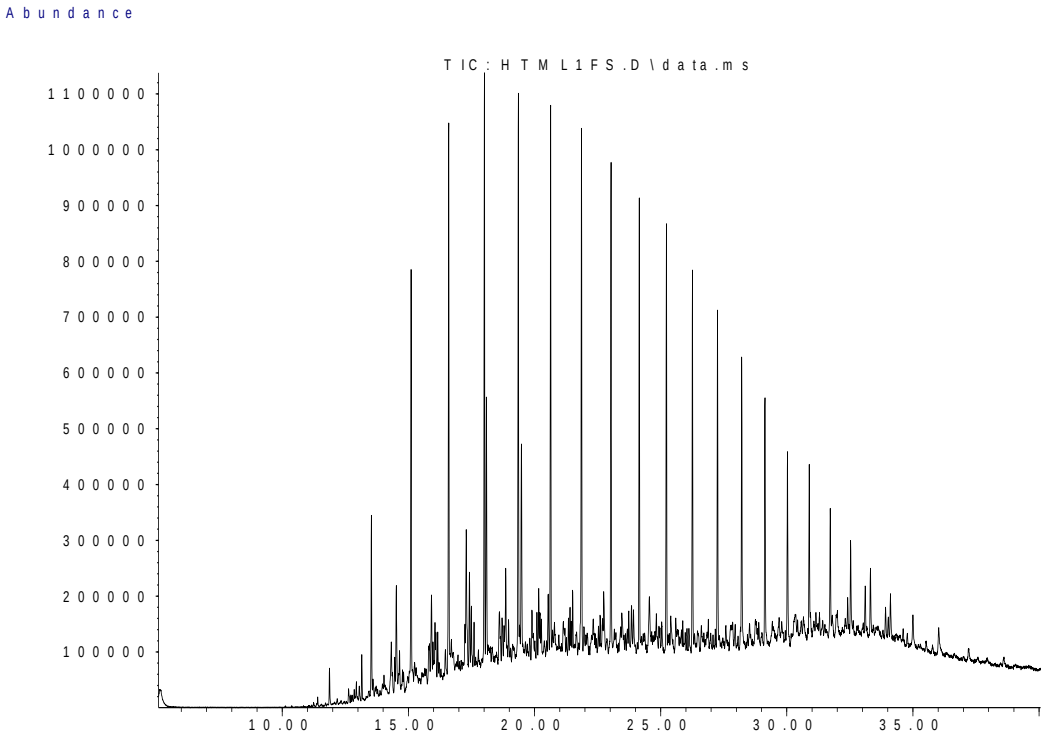

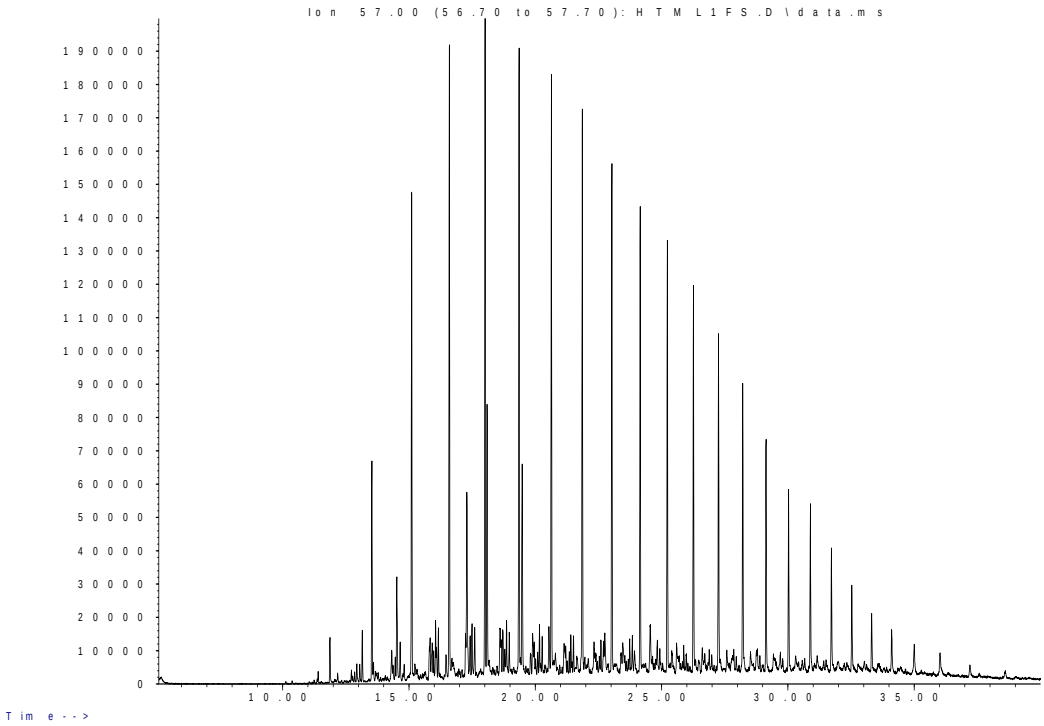

Sample MH1 Outer Saturate Chromatograms; Fullscan and Hydrocarbons

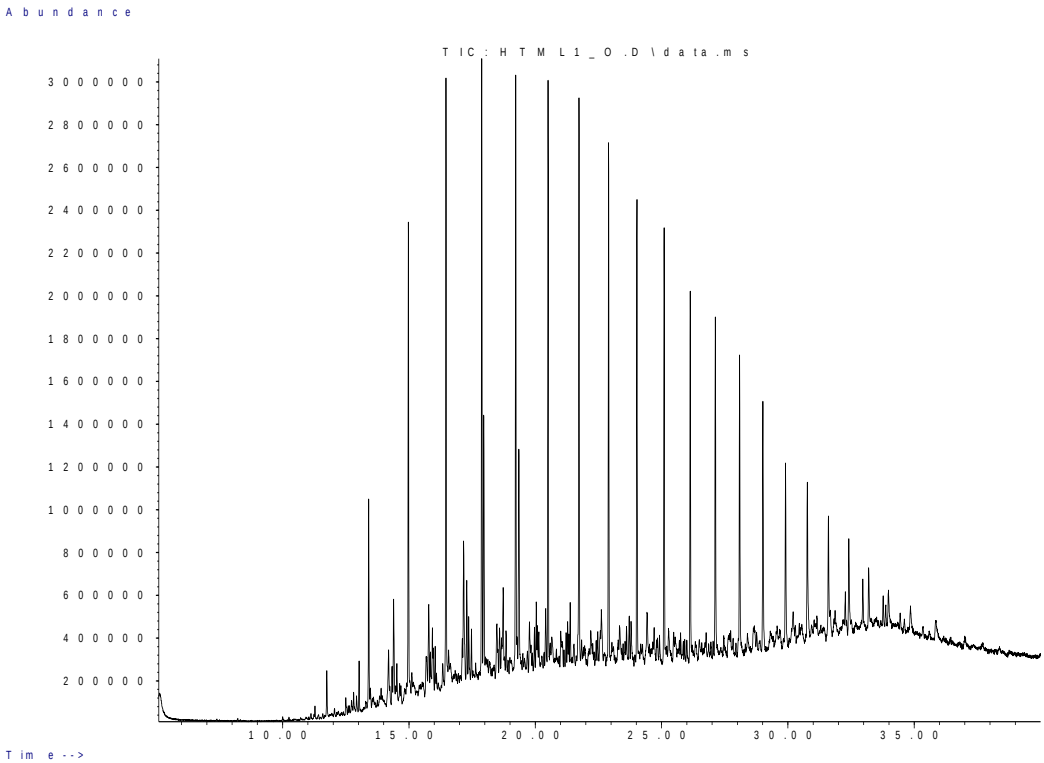

Sample NZ1 Inner Saturate Chromatograms; Fullscan and Hydrocarbons

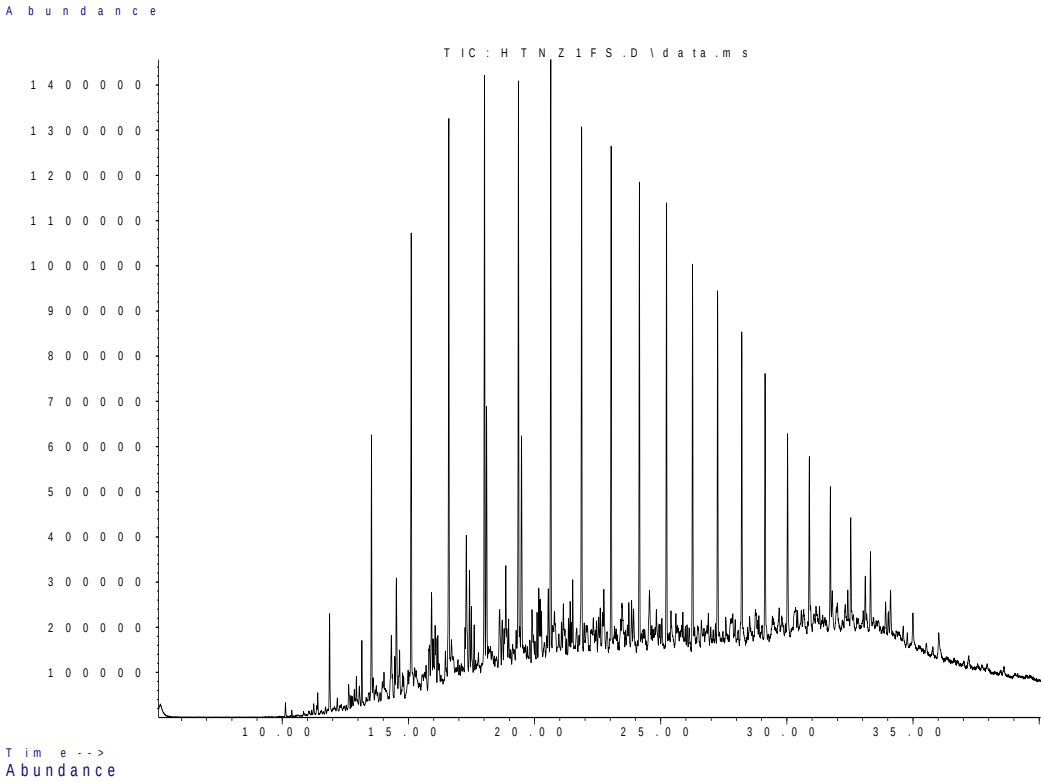

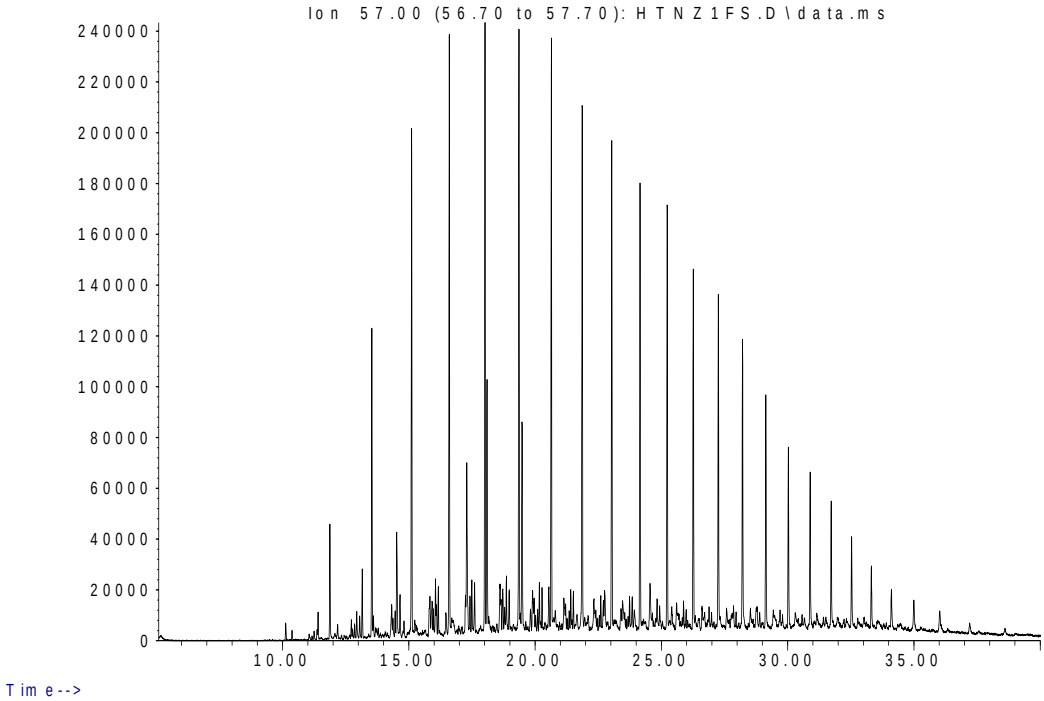

Sample NZ1 Outer Saturate Chromatograms; Fullscan and Hydrocarbons

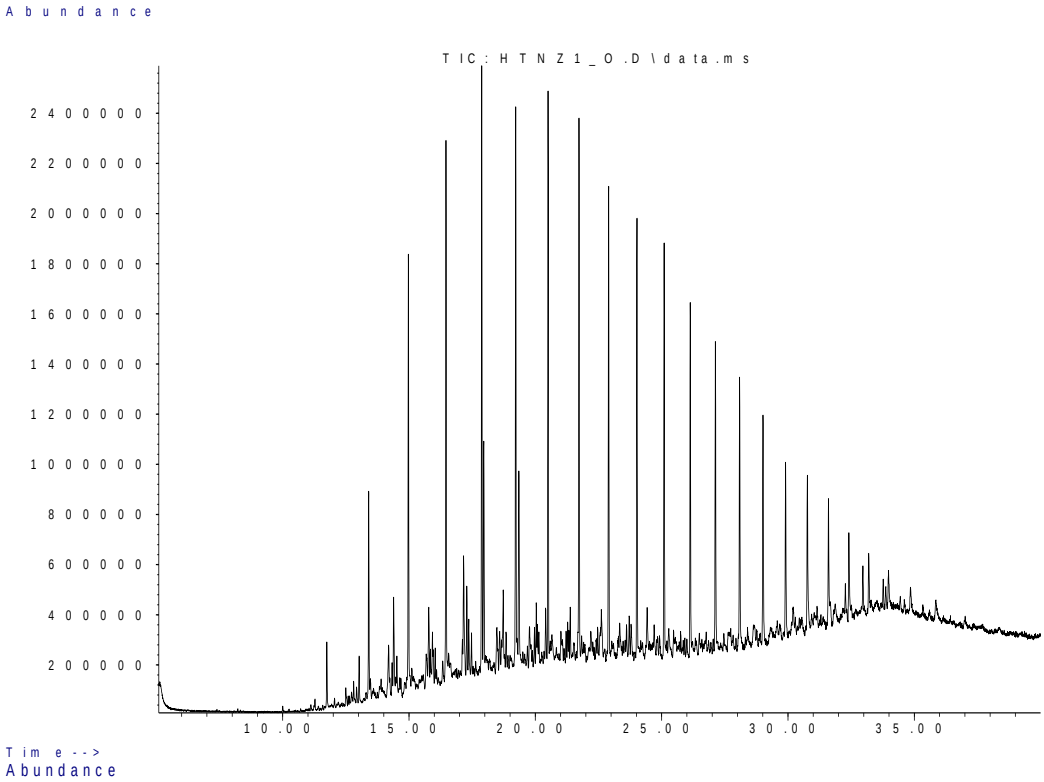

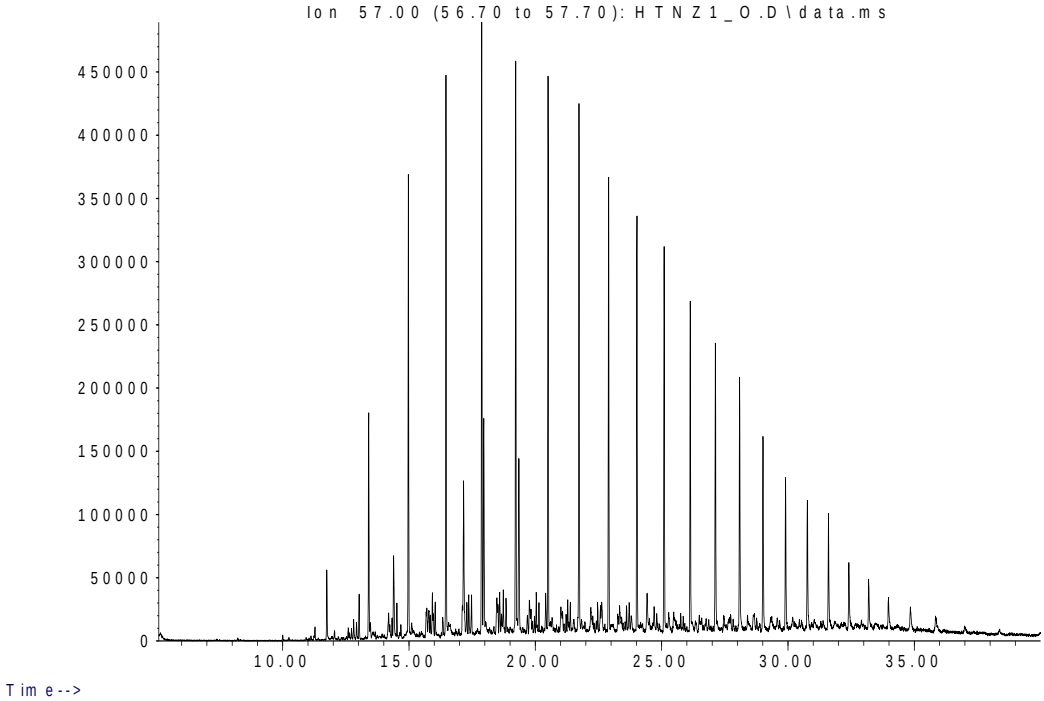

Sample NZ2 Inner Saturate Chromatograms; Fullscan and Hydrocarbons

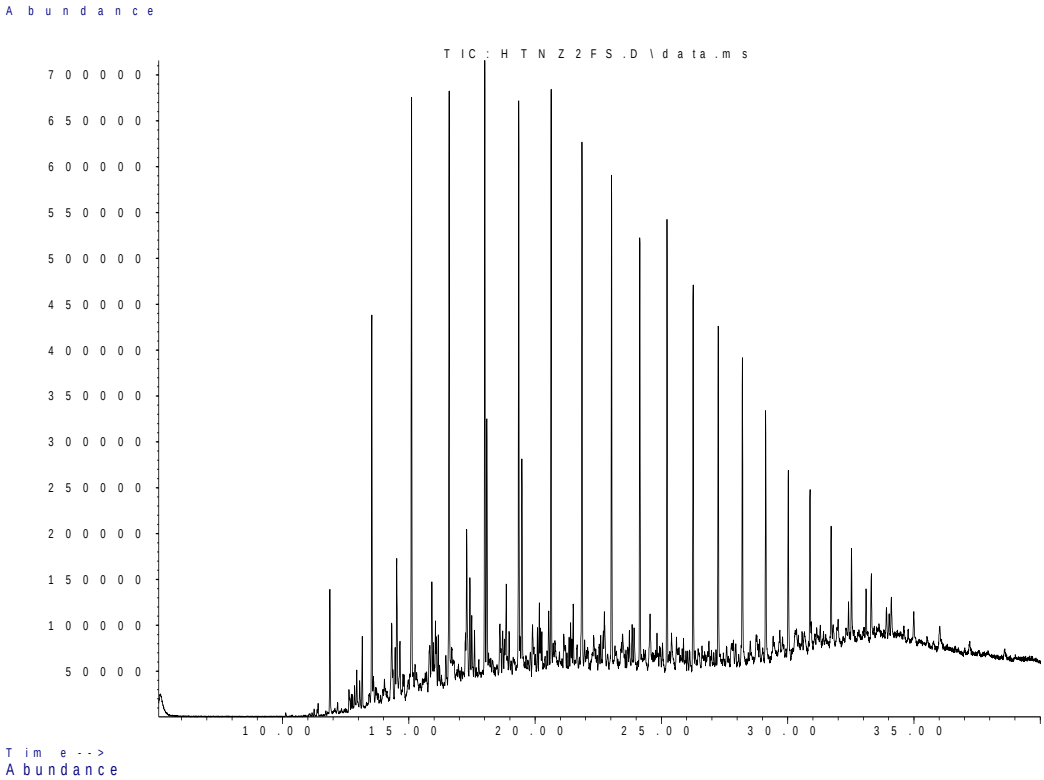

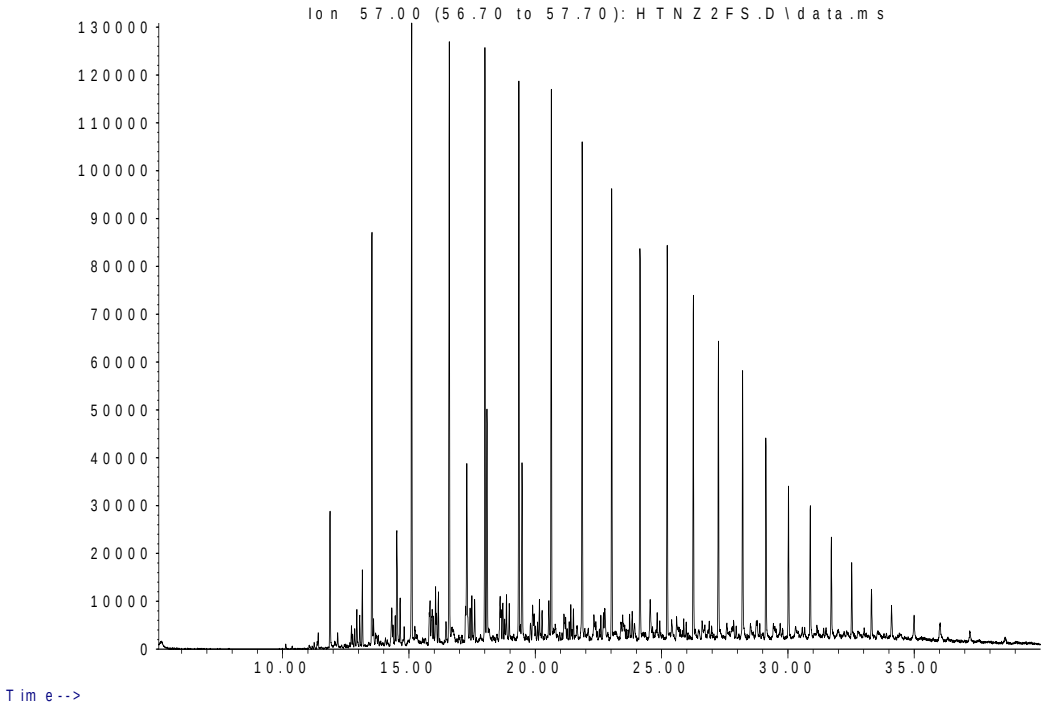

Sample NZ2 Outer Saturate Chromatograms; Fullscan and Hydrocarbons

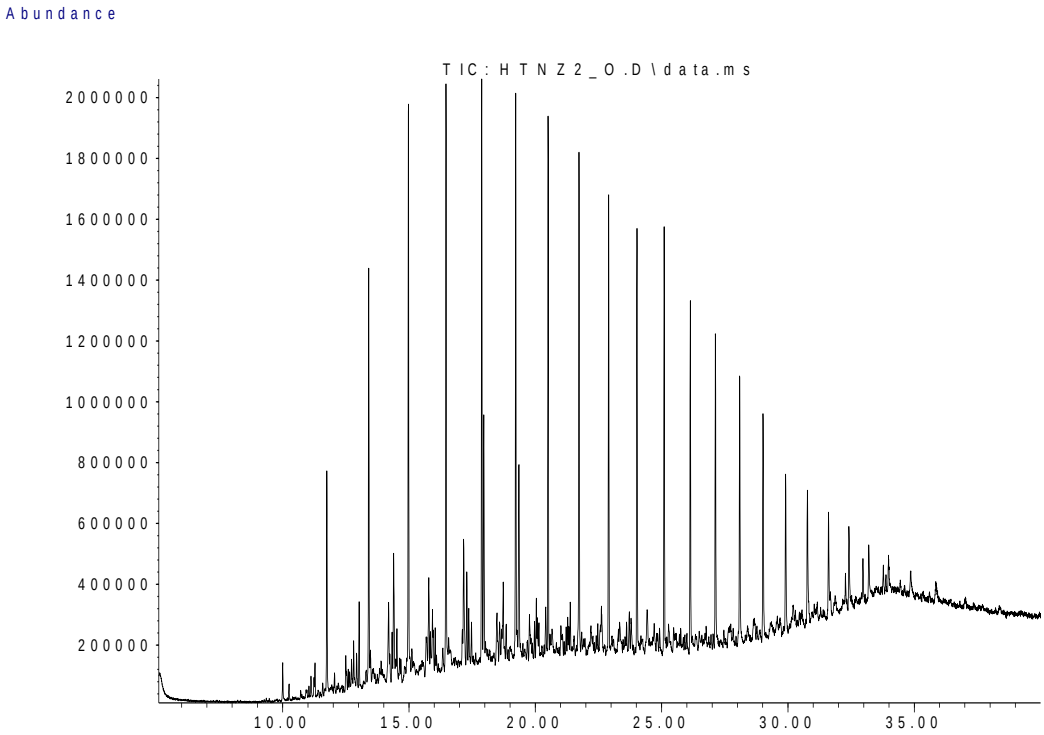

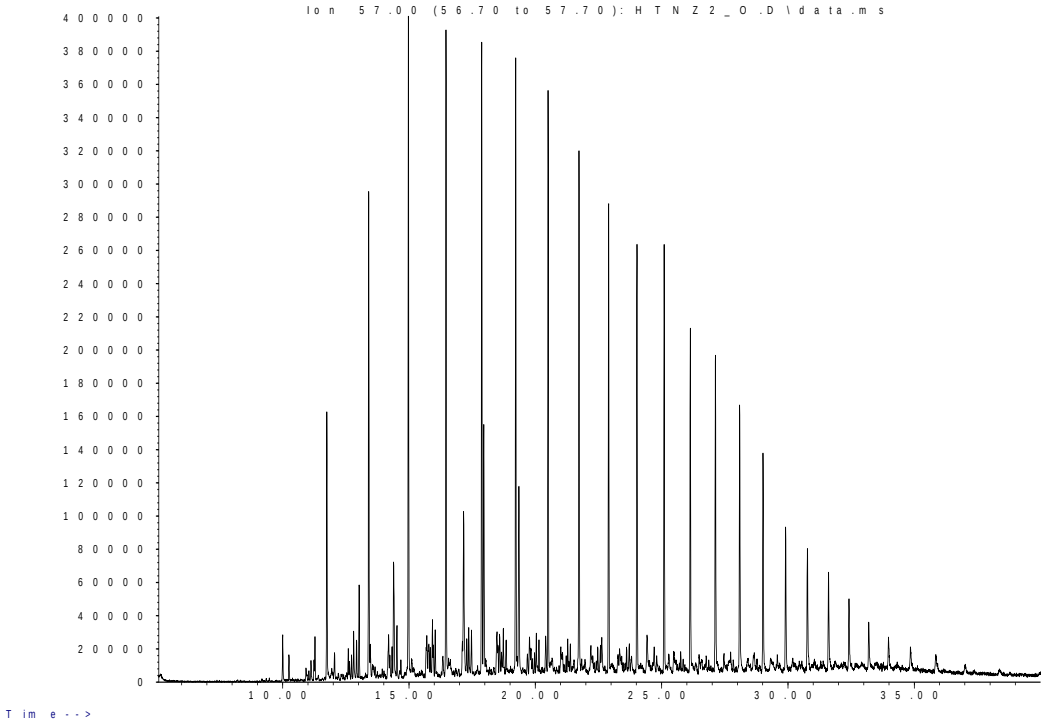

GC-MS Saturate Biomarker Interpretive Ratios, Peak Areas and Chromatograms.

Limestone Coast

Terpanes (m/z 191)	27A				CB32				162			
	outer	inner	diff	% diff	outer	inner	diff	% diff	outer	inner	diff	% diff
C19t/C23t	0.24	0.21	0.02	10.94%	0.29	0.28	0.01	3.59%	0.34	0.29	0.05	14.79%
C22t/C21t	0.38	0.38	0.00	0.76%	0.45	0.43	0.02	4.39%	0.42	0.50	-0.07	-16.06%
C22t/C24t	0.32	0.45	-0.13	-33.84%	0.39	0.47	-0.08	-18.57%	0.40	0.47	-0.07	-15.20%
C24t/C23t	0.45	0.43	0.02	5.10%	0.59	0.53	0.06	11.24%	0.60	0.61	-0.01	-2.22%
C26t/C25t	0.77	0.69	0.08	10.58%	0.82	0.82	0.00	-0.31%	0.81	0.86	-0.05	-5.53%
C24Tet/C23t	0.58	0.74	-0.16	-23.80%	0.82	0.90	-0.08	-9.14%	0.89	0.96	-0.07	-7.42%
C24Tet/C26t	1.66	2.09	-0.43	-22.96%	1.98	1.98	0.00	-0.07%	2.09	2.10	0.00	-0.24%
C23t/C30H	0.16	0.14	0.02	16.20%	0.13	0.10	0.03	22.47%	0.13	0.11	0.03	22.27%
C24Tet/C30H	0.10	0.10	-0.01	-7.68%	0.11	0.09	0.01	13.40%	0.12	0.10	0.02	14.91%
C28BNH/C30H	0.05	0.05	0.00	-1.77%	0.06	0.06	0.00	-6.86%	0.05	0.06	-0.01	-22.07%
C29H/C30H	0.76	0.71	0.06	7.85%	0.72	0.66	0.06	8.04%	0.72	0.71	0.01	2.08%
C30DiaH/C30H	0.07	0.09	-0.02	-21.29%	0.09	0.09	0.00	-0.64%	0.07	0.09	-0.02	-25.89%
C30Ts/C30H	0.07	0.09	-0.02	-26.36%	0.08	0.09	0.00	-5.76%	0.08	0.09	-0.01	-8.84%
Gam/C30H	0.04	0.05	-0.01	-23.79%	0.05	0.05	0.00	-7.94%	0.05	0.05	-0.01	-12.20%
Gam/C31HR	0.13	0.15	-0.03	-19.12%	0.17	0.17	0.00	-2.00%	0.16	0.18	-0.01	-6.48%
C35HS/C34HS	0.51	0.59	-0.08	-14.77%	0.58	0.61	-0.04	-6.00%	0.59	0.67	-0.09	-13.97%
Ts/(Ts+Tm)	0.39	0.40	-0.01	-1.50%	0.39	0.38	0.01	1.33%	0.39	0.38	0.01	1.48%
C29Ts/(C29Ts+C29H)	0.19	0.22	-0.03	-15.86%	0.22	0.24	-0.02	-6.55%	0.22	0.22	0.00	-2.11%
Mor/C30H	0.12	0.12	-0.01	-7.72%	0.12	0.13	-0.01	-7.79%	0.12	0.13	-0.01	-6.49%
C32 S/(S+R)	0.60	0.59	0.00	0.81%	0.59	0.60	-0.01	-1.12%	0.59	0.60	-0.01	-1.45%
C35 Homohopane Index	0.05	0.06	-0.01	-19.22%	0.04	0.05	0.00	-5.41%	0.04	0.06	-0.01	-28.28%
C35/C31	0.10	0.12	-0.03	-24.38%	0.09	0.10	-0.01	-11.51%	0.08	0.12	-0.03	-33.55%
C35/C34 (S only)	0.57	0.59	-0.02	-3.32%	0.55	0.61	-0.07	-11.50%	0.59	0.69	-0.11	-16.46%
Steranes (m/z 217)												
% C27 ααα 20R	38	35	2.74	7.49%	42	37	4.90	12.33%	37	38	-1.46	-3.89%
% C28 ααα 20R	22	25	-2.23	-9.52%	22	24	-2.07	-9.08%	24	24	0.25	1.02%
% C29 ααα 20R	40	40	-0.51	-1.28%	36	39	-2.82	-7.53%	39	38	1.21	3.17%
C27 Dia/(Dia+Reg)	0.47	0.51	-0.04	-7.31%	0.51	0.48	0.03	6.01%	0.54	0.49	0.05	10.48%
(C21+C22)/(C27+C28+C29)	0.14	0.13	0.01	9.80%	0.16	0.13	0.04	24.49%	0.17	0.14	0.03	16.32%
C29 αββ/(ααα+αββ)	0.52	0.50	0.02	3.92%	0.51	0.50	0.01	2.65%	0.56	0.51	0.05	9.12%
C29 ααα 20S/20R	0.84	0.76	0.08	9.87%	0.99	0.76	0.23	26.60%	0.66	0.72	-0.07	-9.61%
C29 ααα 20S/(S+R)	0.46	0.43	0.02	5.50%	0.50	0.43	0.07	14.31%	0.40	0.42	-0.02	-5.69%
αββ-Steranes (m/z 218)												
% C27 αββ 20(R+S)	39	38	1.49	3.88%	39	38	1.25	3.27%	39	39	-0.07	-0.19%
% C28 αββ 20(R+S)	28	28	-0.53	-1.92%	28	28	-0.17	-0.62%	27	27	-0.73	-2.72%
% C29 αββ 20(R+S)	33	34	-0.95	-2.83%	33	35	-1.08	-3.19%	35	34	0.81	2.34%
C29/C27 αββ Sterane Ratio	0.85	0.91	-0.06	-6.70%	0.86	0.91	-0.06	-6.45%	0.91	0.88	0.02	2.53%
Tricyclic/Pentacyclic Terpanes	0.19	0.17	0.02	12.42%	0.17	0.14	0.03	19.34%	0.19	0.16	0.04	20.44%
Steranes/Terpanes	0.50	0.46	0.04	9.11%	0.49	0.43	0.06	13.17%	0.49	0.44	0.04	9.30%
% Tricyclic Terpanes	10.80	10.02	0.79	7.55%	9.90	8.73	1.17	12.60%	10.79	9.33	1.46	14.51%
% Pentacyclic Terpanes	55.69	58.48	-2.79	-4.88%	57.21	61.23	-4.02	-6.78%	56.42	59.90	-3.48	-5.98%
% Steranes	33.50	31.50	2.00	6.15%	32.88	30.04	2.84	9.04%	32.78	30.77	2.02	6.35%

Kangaroo Island

Terpanes (m/z 191)	80				85				168				177			
	outer	inner	diff	% diff	outer	inner	diff	% diff	outer	inner	diff	% diff	outer	inner	diff	% diff
C19t/C23t	0.35	0.28	0.06	20.19%	0.33	0.27	0.06	20.2%	0.31	0.27	0.04	12.38%	0.33	0.28	0.05	16.86%
C22t/C21t	0.47	0.49	-0.02	-3.73%	0.43	0.56	-0.13	-27.1%	0.46	0.48	-0.02	-3.51%	0.34	0.55	-0.21	-46.96%
C22t/C24t	0.47	0.42	0.05	11.73%	0.45	0.50	-0.05	-11.2%	0.42	0.46	-0.03	-7.54%	0.36	0.50	-0.13	-31.15%
C24t/C23t	0.57	0.60	-0.03	-5.81%	0.57	0.57	0.00	-0.7%	0.59	0.60	-0.01	-1.31%	0.56	0.57	-0.01	-1.56%
C26t/C25t	0.75	0.80	-0.06	-7.20%	0.79	0.72	0.07	8.7%	0.74	0.72	0.02	2.19%	0.61	0.73	-0.13	-18.86%
C24Tet/C23t	0.92	0.96	-0.04	-3.85%	0.81	0.94	-0.13	-14.5%	0.88	0.94	-0.06	-6.04%	0.86	0.98	-0.12	-13.37%
C24Tet/C26t	2.09	2.02	0.07	3.64%	1.94	2.18	-0.24	-11.7%	1.95	2.07	-0.12	-6.00%	2.35	2.37	-0.01	-0.53%
C23t/C30H	0.14	0.10	0.04	32.97%	0.13	0.11	0.03	21.2%	0.14	0.11	0.02	17.81%	0.15	0.11	0.04	31.19%
C24Tet/C30H	0.13	0.09	0.03	29.21%	0.11	0.10	0.01	6.8%	0.12	0.11	0.01	11.81%	0.13	0.11	0.02	18.01%
C28BNH/C30H	0.06	0.06	0.00	0.89%	0.05	0.06	0.00	-8.5%	0.07	0.06	0.01	8.63%	0.06	0.06	0.00	-6.98%
C29H/C30H	0.73	0.65	0.07	10.65%	0.70	0.70	0.00	-0.1%	0.72	0.72	0.00	0.59%	0.74	0.70	0.03	4.65%
C30DiaH/C30H	0.08	0.09	-0.01	-16.34%	0.09	0.09	0.00	0.9%	0.09	0.08	0.01	8.63%	0.07	0.09	-0.02	-23.75%
C30Ts/C30H	0.08	0.09	-0.01	-9.33%	0.09	0.09	0.00	-4.7%	0.08	0.09	-0.01	-8.70%	0.07	0.09	-0.02	-20.90%
Gam/C30H	0.05	0.05	-0.01	-13.79%	0.05	0.05	-0.01	-17.0%	0.05	0.05	0.00	-7.65%	0.05	0.05	0.00	-5.45%
Gam/C31HR	0.16	0.17	-0.01	-3.69%	0.15	0.17	-0.02	-12.8%	0.17	0.17	-0.01	-3.41%	0.17	0.17	0.01	3.96%
C35HS/C34HS	0.64	0.77	-0.13	-17.93%	0.60	0.68	-0.07	-11.6%	0.65	0.71	-0.07	-9.66%	0.59	0.73	-0.14	-21.32%
Ts/(Ts+Tm)	0.39	0.39	0.00	0.07%	0.39	0.39	0.00	0.3%	0.40	0.38	0.02	5.35%	0.38	0.39	-0.01	-1.84%
C29Ts//(C29Ts+C29H)	0.22	0.24	-0.03	-11.35%	0.23	0.22	0.01	4.7%	0.22	0.21	0.02	7.19%	0.20	0.23	-0.03	-12.00%
Mor/C30H	0.12	0.13	-0.01	-7.09%	0.11	0.13	-0.02	-15.2%	0.12	0.13	-0.01	-5.23%	0.12	0.13	-0.02	-12.82%
C32 S/(S+R)	0.59	0.60	-0.01	-1.52%	0.61	0.59	0.01	2.2%	0.61	0.59	0.02	3.27%	0.59	0.60	-0.01	-2.19%
C35 Homohopane Index	0.04	0.06	-0.01	-29.41%	0.04	0.06	-0.01	-23.7%	0.04	0.06	-0.02	-30.49%	0.04	0.05	-0.01	-27.22%
C35/C31	0.09	0.13	-0.04	-36.33%	0.09	0.12	-0.03	-28.4%	0.09	0.11	-0.02	-23.78%	0.08	0.12	-0.03	-32.55%
C35/C34 (S only)	0.64	0.77	-0.13	-17.93%	0.60	0.69	-0.09	-14.4%	0.65	0.73	-0.08	-12.03%	0.59	0.72	-0.14	-20.79%
Steranes (m/z 217)																
% C27 ααα 20R	38	38	-0.06	-0.15%	40	35	5.33	14.2%	40	38	2.14	5.47%	38	39	-0.21	-0.56%
% C28 ααα 20R	24	24	-0.32	-1.34%	25	25	0.02	0.1%	24	23	1.16	4.88%	23	25	-2.33	-9.75%
% C29 ααα 20R	38	38	0.37	0.99%	35	40	-5.35	-14.3%	35	39	-3.30	-8.92%	39	36	2.55	6.78%
C27 Dia/(Dia+Reg)	0.54	0.48	0.07	12.95%	0.49	0.53	-0.04	-7.6%	0.53	0.53	0.00	0.50%	0.55	0.48	0.07	13.05%
(C21+C22)/(C27+C28+C29)	0.16	0.13	0.03	19.60%	0.15	0.13	0.02	14.4%	0.17	0.15	0.02	11.66%	0.19	0.14	0.05	27.91%
C29 αββ/(ααα+αββ)	0.53	0.48	0.05	9.79%	0.54	0.51	0.03	5.0%	0.56	0.52	0.04	6.96%	0.53	0.51	0.02	3.27%
C29 ααα 20S/20R	0.71	0.75	-0.05	-6.21%	0.78	0.72	0.06	8.2%	0.69	0.74	-0.05	-6.69%	0.65	0.77	-0.12	-16.83%
C29 ααα 20S/(S+R)	0.41	0.43	-0.02	-3.59%	0.44	0.42	0.02	4.7%	0.41	0.42	-0.02	-3.91%	0.40	0.44	-0.04	-9.85%
αββ-Steranes (m/z 218)																
% C27 αββ 20(R+S)	39	39	0.12	0.31%	39	38	1.25	3.2%	40	38	1.14	2.92%	40	38	1.79	4.57%
% C28 αββ 20(R+S)	28	28	-0.11	-0.41%	27	28	-0.85	-3.1%	27	28	-0.46	-1.70%	28	27	0.95	3.40%
% C29 αββ 20(R+S)	33	33	-0.01	-0.03%	34	34	-0.41	-1.2%	33	34	-0.67	-2.00%	31	34	-2.74	-8.34%
C29/C27 αββ Sterane Ratio	0.84	0.84	0.00	-0.34%	0.86	0.90	-0.04	-4.4%	0.84	0.89	-0.04	-4.91%	0.78	0.89	-0.11	-12.89%
Tricyclic/Pentacyclic Terpanes	0.20	0.14	0.06	37.50%	0.19	0.15	0.04	21.0%	0.20	0.16	0.03	17.35%	0.22	0.16	0.06	29.83%
Steranes/Terpanes	0.51	0.42	0.09	19.60%	0.49	0.44	0.05	11.4%	0.50	0.47	0.02	5.07%	0.54	0.46	0.09	17.35%
% Tricyclic Terpanes	11.08	8.52	2.56	26.09%	10.58	9.16	1.42	14.4%	10.95	9.61	1.34	13.07%	11.47	9.44	2.04	19.50%
% Pentacyclic Terpanes	54.94	61.76	-6.82	-11.69%	56.31	60.21	-3.90	-6.7%	55.83	58.29	-2.46	-4.31%	53.31	59.21	-5.90	-10.48%
% Steranes	33.99	29.72	4.26	13.38%	33.11	30.63	2.48	7.8%	33.21	32.10	1.12	3.42%	35.22	31.36	3.86	11.59%

Eyre Peninsula

Terpanes (m/z 191)	cl1				mh1			
	outer	inner	diff	% diff	outer	inner	diff	% diff
C19t/C23t	0.32	0.27	0.05	18.61%	0.35	0.31	0.04	12.72%
C22t/C21t	0.47	0.63	-0.16	-29.41%	0.43	0.43	0.00	0.27%
C22t/C24t	0.46	0.39	0.07	15.76%	0.42	0.45	-0.02	-5.23%
C24t/C23t	0.52	0.59	-0.07	-13.07%	0.57	0.61	-0.04	-6.81%
C26t/C25t	0.86	0.72	0.13	17.10%	0.78	0.66	0.12	16.64%
C24Tet/C23t	0.87	1.11	-0.24	-24.26%	0.85	0.96	-0.11	-12.25%
C24Tet/C26t	2.26	2.41	-0.15	-6.32%	1.87	2.11	-0.24	-11.95%
C23t/C30H	0.14	0.07	0.07	69.32%	0.14	0.10	0.04	32.68%
C24Tet/C30H	0.12	0.07	0.05	47.04%	0.12	0.09	0.02	20.64%
C28BNH/C30H	0.05	0.05	-0.01	-17.40%	0.06	0.06	0.00	-8.16%
C29H/C30H	0.70	0.67	0.03	4.72%	0.73	0.70	0.03	3.98%
C30DiaH/C30H	0.06	0.08	-0.02	-22.32%	0.07	0.07	0.00	-6.30%
C30Ts/C30H	0.09	0.09	0.00	-4.67%	0.08	0.08	0.00	-6.07%
Gam/C30H	0.05	0.06	-0.01	-19.94%	0.05	0.06	-0.01	-12.81%
Gam/C31HR	0.16	0.17	-0.01	-7.41%	0.17	0.17	-0.01	-3.57%
C35HS/C34HS	0.57	0.61	-0.04	-5.96%	0.59	0.64	-0.05	-8.83%
Ts/(Ts+Tm)	0.39	0.37	0.01	3.72%	0.38	0.38	0.00	-0.02%
C29Ts/(C29Ts+C29H)	0.23	0.22	0.01	2.45%	0.21	0.22	0.00	-1.34%
Mor/C30H	0.13	0.13	0.00	-2.97%	0.12	0.12	0.00	-0.64%
C32 S/(S+R)	0.59	0.58	0.01	1.63%	0.59	0.59	0.00	0.66%
C35 Homohopane Index	0.04	0.07	-0.02	-40.7%	0.04	0.06	-0.02	-37.83%
C35/C31	0.09	0.15	-0.06	-50.7%	0.09	0.14	-0.05	-45.70%
C35/C34 (S only)	0.57	0.66	-0.09	-14.74%	0.59	0.66	-0.07	-10.68%
Steranes (m/z 217)								
% C27 $\alpha\alpha\alpha$ 20R	40	34	6.23	16.93%	38	37	1.46	3.89%
% C28 $\alpha\alpha\alpha$ 20R	22	23	-1.59	-7.05%	22	23	-1.55	-6.90%
% C29 $\alpha\alpha\alpha$ 20R	38	43	-4.64	-11.40%	40	40	0.10	0.24%
C27 Dia/(Dia+Reg)	0.52	0.48	0.04	8.72%	0.54	0.52	0.03	5.04%
(C21+C22)/(C27+C28+C29)	0.16	0.09	0.07	58.87%	0.17	0.13	0.03	21.66%
C29 $\alpha\beta\beta/(\alpha\alpha\alpha+\alpha\beta\beta)$	0.51	0.51	0.00	0.26%	0.50	0.52	-0.02	-3.33%
C29 $\alpha\alpha\alpha$ 20S/20R	0.81	0.65	0.16	21.56%	0.76	0.71	0.05	6.72%
C29 $\alpha\alpha\alpha$ 20S/(S+R)	0.45	0.39	0.05	12.53%	0.43	0.41	0.02	3.88%
$\alpha\beta\beta$-Steranes (m/z 218)								
% C27 $\alpha\beta\beta$ 20(R+S)	39	36	3.19	8.56%	40	38	2.66	6.85%
% C28 $\alpha\beta\beta$ 20(R+S)	28	28	0.51	1.84%	26	28	-1.95	-7.25%
% C29 $\alpha\beta\beta$ 20(R+S)	33	37	-3.71	-10.63%	34	35	-0.72	-2.09%
C29/C27 $\alpha\beta\beta$ Sterane Ratio	0.85	1.03	-0.18	-19.15%	0.84	0.92	-0.08	-8.94%
Tricyclic/Pentacyclic Terpanes	0.18	0.10	0.08	59.38%	0.20	0.15	0.05	30.47%
Steranes/Terpanes	0.51	0.37	0.14	30.59%	0.51	0.43	0.09	18.21%
% Tricyclic Terpanes	10.32	6.62	3.70	43.73%	11.02	8.99	2.03	20.33%
% Pentacyclic Terpanes	55.93	66.15	-10.22	-16.74%	55.18	61.18	-5.99	-10.30%
% Steranes	33.75	27.24	6.52	21.37%	33.79	29.84	3.96	12.44%

New Zealand

Terpanes (m/z 191)	nz1				nz2			
	outer	inner	diff	% diff	outer	inner	diff	% diff
C19t/C23t	0.32	0.21	0.12	44.43%	0.34	0.31	0.02	6.88%
C22t/C21t	0.46	0.29	0.16	43.43%	0.41	0.52	-0.12	-25.13%
C22t/C24t	0.40	0.30	0.10	28.98%	0.40	0.48	-0.07	-16.04%
C24t/C23t	0.55	0.56	-0.01	-1.99%	0.55	0.57	-0.02	-3.45%
C26t/C25t	0.75	0.60	0.15	22.57%	0.78	0.92	-0.14	-16.77%
C24Tet/C23t	0.87	0.68	0.18	23.72%	0.86	0.97	-0.12	-12.97%
C24Tet/C26t	2.13	1.97	0.16	7.82%	2.11	2.29	-0.18	-8.14%
C23t/C30H	0.13	0.15	-0.02	-12.40%	0.13	0.09	0.04	33.79%
C24Tet/C30H	0.12	0.10	0.01	11.40%	0.11	0.09	0.02	21.05%
C28BNH/C30H	0.06	0.07	-0.01	-18.51%	0.05	0.05	0.00	-10.08%
C29H/C30H	0.72	0.75	-0.03	-4.03%	0.70	0.60	0.11	16.75%
C30DiaH/C30H	0.09	0.07	0.02	24.75%	0.09	0.10	-0.01	-6.51%
C30Ts/C30H	0.08	0.08	0.01	10.90%	0.08	0.09	-0.01	-9.93%
Gam/C30H	0.05	0.05	-0.01	-10.99%	0.05	0.06	-0.01	-19.68%
Gam/C31HR	0.16	0.18	-0.02	-8.89%	0.16	0.18	-0.01	-7.14%
C35HS/C34HS	0.50	0.53	-0.03	-5.68%	0.52	0.61	-0.09	-16.12%
Ts/(Ts+Tm)	0.39	0.40	-0.02	-4.46%	0.38	0.39	0.00	-0.93%
C29Ts/(C29Ts+C29H)	0.22	0.20	0.02	9.31%	0.23	0.26	-0.04	-15.50%
Mor/C30H	0.12	0.12	0.01	5.05%	0.12	0.13	-0.01	-7.14%
C32 S/(S+R)	0.59	0.59	0.00	-0.15%	0.60	0.60	0.00	0.10%
C35 Homohopane Index	0.04	0.06	-0.01	-23.10%	0.04	0.07	-0.02	-38.22%
C35/C31	0.09	0.12	-0.03	-27.97%	0.09	0.15	-0.06	-46.83%
C35/C34 (S only)	0.50	0.53	-0.03	-5.68%	0.52	0.60	-0.08	-14.94%
Steranes (m/z 217)								
% C27 $\alpha\alpha\alpha$ 20R	40	37	3.82	9.90%	44	37	7.08	17.58%
% C28 $\alpha\alpha\alpha$ 20R	23	24	-1.39	-5.92%	22	22	0.03	0.14%
% C29 $\alpha\alpha\alpha$ 20R	37	39	-2.43	-6.41%	34	41	-7.12	-19.04%
C27 Dia/(Dia+Reg)	0.51	0.48	0.03	5.62%	0.49	0.55	-0.06	-11.72%
(C21+C22)/(C27+C28+C29)	0.17	0.14	0.03	19.74%	0.16	0.13	0.03	20.94%
C29 $\alpha\beta\beta/(\alpha\alpha\alpha+\alpha\beta\beta)$	0.52	0.52	0.00	-0.43%	0.52	0.51	0.01	2.54%
C29 $\alpha\alpha\alpha$ 20S/20R	0.91	0.88	0.03	3.54%	1.04	0.73	0.32	35.87%
C29 $\alpha\alpha\alpha$ 20S/(S+R)	0.48	0.47	0.01	1.87%	0.51	0.42	0.09	19.31%
$\alpha\beta\beta$-Steranes (m/z 218)								
% C27 $\alpha\beta\beta$ 20(R+S)	39	39	0.29	0.75%	41	37	4.48	11.41%
% C28 $\alpha\beta\beta$ 20(R+S)	28	28	-0.19	-0.67%	27	28	-1.13	-4.07%
% C29 $\alpha\beta\beta$ 20(R+S)	33	33	-0.11	-0.32%	31	35	-3.35	-10.15%
C29/C27 $\alpha\beta\beta$ Sterane Ratio	0.84	0.85	-0.01	-1.07%	0.75	0.94	-0.18	-21.50%
Tricyclic/Pentacyclic Terpanes	0.18	0.18	0.00	0.43%	0.18	0.13	0.05	32.48%
Steranes/Terpanes	0.50	0.51	-0.02	-3.61%	0.49	0.38	0.11	24.20%
% Tricyclic Terpanes	10.35	10.19	0.16	1.58%	10.25	8.30	1.95	21.00%
% Pentacyclic Terpanes	56.47	55.82	0.64	1.15%	56.99	64.05	-7.07	-11.67%
% Steranes	33.18	33.99	-0.81	-2.40%	32.77	27.65	5.12	16.94%

Sample 27 Inner

Bulk Properties

Saturate (%)	21.4
Aromatics (%)	14.1
Resin (%)	16.7
Asphaltene (%)	47.8

Whole Oil/Extract GC

Pristane/Phytane	1.12
Pristane/n-C17	0.50
Phytane/n-C18	0.46

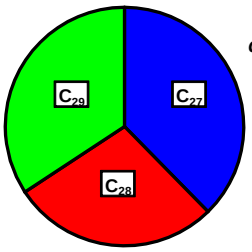

C_{27}-C_{28}-C_{29} αββ Steranes

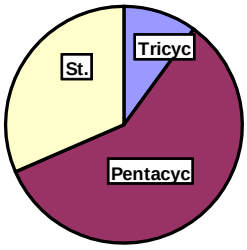

Tricyclic, Pentacyclic Terpanes & Steranes

Saturate Biomarker Interpretive Ratios

Interpretive Ratios	By Area
Terpanes (m/z 191)	
C19t/C23t	0.21
C22t/C21t	0.38
C22t/C24t	0.45
C24t/C23t	0.43
C26t/C25t	0.69
C24Tet/C23t	0.74
C24Tet/C26t	2.09
C23t/C30H	0.14
C24Tet/C30H	0.10
C28BNH/C30H	0.05
25-Nor/C30H	0.02
C29H/C30H	0.71
C30DiaH/C30H	0.09
Ole/C30H	0.00
C30Ts/C30H	0.09
Gam/C30H	0.05
Gam/C31HR	0.15
C35HS/C34HS	0.59
C35 Homohopane Index	0.06
Ts/(Ts+Tm)	0.40
C29Ts/(C29Ts+C29H)	0.22
Mor/C30H	0.12
C32 S/(S+R)	0.59
Steranes (m/z 217)	
% C27 ααα 20R	35.2
% C28 ααα 20R	24.5
% C29 ααα 20R	40.3
C27 Dia/(Dia+Reg)	0.51
(C21+C22)/(C27+C28+C29)	0.13
C29 αββ/(ααα+αββ)	0.50
C29 ααα 20S/20R	0.76
C29 ααα 20S/(S+R)	0.43
αββ−Steranes (m/z 218)	
% C27 αββ 20(R+S)	37.7
% C28 αββ 20(R+S)	28.1
% C29 αββ 20(R+S)	34.2
C29/C27 αββ Sterane Ratio	0.91
C27 Dia/Ster	0.59
Tricyclic/Pentacyclic Terpanes	0.17
Steranes/Terpanes	0.46
% Tricyclic Terpanes	10.0
% Pentacyclic Terpanes	58.5
% Steranes	31.5

Sample 27 Inner

Saturate Biomarker Integration Results (Terpanes)				
Ion	**Peak Label**	**Compound Name**	**R.Time (min.)**	**Peak Area**
191	C19t	C19 tricyclic diterpane	20.078	14482
191	C20t	C20 tricyclic diterpane	21.834	25203
191	C21t	C21 tricyclic diterpane	23.882	34587
191	C22t	C22 tricyclic terpane	25.93	13096
191	C23t	C23 tricyclic terpane	28.497	67802
191	C24t	C24 tricyclic terpane	29.955	29257
191	C25tS	C25 tricyclic terpane (S)	33.008	17851
191	C25tR	C25 tricyclic terpane (R)	33.008	16846
191	C24T	C24 tetracyclic terpane (TET)	34.995	49946
191	C26tS	C26 tricyclic terpane (S)	35.33	10143
191	C26tR	C26 tricyclic terpane (R)	35.524	13759
191	C28tS	C28 extended tricyclic terpane (S)	40.766	21161
191	C28tR	C28 extended tricyclic terpane (R)	41.101	10102
191	C29tS	C29 extended tricyclic terpane (S)	42.229	7607
191	C29tR	C29 extended tricyclic terpane (R)	42.748	22499
191	C30tS	C30 extended tricyclic terpane (S)	45.452	9597
191	C30tR	C30 extended tricyclic terpane (R)	45.806	10911
191	Ts	Ts 18a(H)-trisnorhopane	43.669	97727
191	Tm	Tm 17a(H)-trisnorhopane	44.669	149621
191	C28BNH	C28 17a18a21b(H)-bisnorhopane	47.109	26454
191	Nor25H	C29 Nor-25-hopane	47.75	11448
191	C29H	C29 Tm 17a(H)21b(H)-norhopane	48.18	342230
191	C29Ts	C29 Ts 18a(H)-norneohopane	48.331	95738
191	C30DiaH	C30 17a(H)-diahopane	48.784	44627
191	Normor	C29 normoretane	49.383	39232
191	a-Ole	a-oleanane	50.03	87
191	b-Ole	b-oleanane	50.03	87
191	C30H	C30 17a(H)-hopane	50.28	484296
191	C30Ts	17a(H)-30-nor-29-homohopane	50.775	42301
191	Mor	C30 moretane	51.228	60193
191	C31HS	C31 22S 17a(H) homohopane	52.743	209027
191	C31HR	C31 22R 17a(H) homohopane	53.045	148005
191	Gam	gammacerane	53.319	22464
191	C32HS	C32 22S 17a(H) bishomohopane	54.687	113935
191	C32HR	C32 22R 17a(H) bishomohopane	55.103	78164
191	C33HS	C33 22S 17a(H) trishomohopane	56.938	68431
191	C33HR	C33 22R 17a(H) trishomohopane	57.514	45428
191	C34HS	C34 22S 17a(H) extended hopane	59.288	43408
191	C34HR	C34 22R 17a(H) extended hopane	59.987	21646
191	C35HS	C35 22S 17a(H) extended hopane	61.61	25431
191	C35HR	C35 22R 17a(H) extended hopane	62.45	18391

Sample 27 Inner

Saturate Biomarker Integration Results (Steranes)				
Ion	**Peak Label**	**Compound Name**	**R.Time (min.)**	**Peak Area**
217	S21	C21 sterane	26.28	69748
217	S22	C22 sterane	29.15	37399
217	27DbaS	C27 ba 20S diacholestane	37.99	87356
217	27DbaR	C27 ba 20R diacholestane	38.92	60961
217	28DbaSA	C28 ba 20S diasterane a	40.30	28595
217	28DbaSB	C28 ba 20S diasterane b	40.47	38135
217	28DbaRA	C28 ba 20R diasterane a	41.34	25113
217	28DbaRB	C28 ba 20R diasterane b	41.34	15015
217	27aaS	C27 aa 20S cholestane	42.09	70302
217	27bbR	C27 bb 20R cholestane	42.39	115571
217	27bbS	C27 bb 20S cholestane	42.63	61336
217	27aaR	C27 aa 20R cholestane	43.19	74287
217	28aaS	C28 aa 20S ergostane	44.57	41157
217	28bbR	C28 bb 20R ergostane	45.01	44125
217	28bbS	C28 bb 20S ergostane	45.25	62095
217	28aaR	C28 aa 20R ergostane	45.96	51689
217	29aaS	C29 aa 20S stigmastane	46.72	64243
217	29bbR	C29 bb 20R stigmastane	47.19	72963
217	29bbS	C29 bb 20S stigmastane	47.38	73922
217	29aaR	C29 aa 20R stigmastane	48.25	84896
218	27bbR	C27 bb 20R cholestane	42.38	128455
218	27bbS	C27 bb 20S cholestane	42.63	91550
218	28bbR	C28 bb 20R ergostane	45.01	83100
218	28bbS	C28 bb 20S ergostane	45.25	80986
218	29bbR	C29 bb 20R stigmastane	47.20	105869
218	29bbS	C29 bb 20S stigmastane	47.38	94182
259	27DbaS	C27 ba 20S diacholestane	38.00	14579
259	27DbaR	C27 ba 20R diacholestane	38.93	10757
259	28DbaSA	C28 ba 20S diaergostane a	40.29	5258
259	28DbaSB	C28 ba 20S diaergostane b	40.46	5364
259	28DbaRA	C28 ba 20R diaergostane a	41.32	4495
259	28DbaRB	C28 ba 20R diaergostane b	41.43	2980
259	29DbaS	C29 ba 20S diastigmastane	42.40	11833
259	29DbaR	C29 ba 20R diastigmastane	43.99	2240
259	30TP1	C30 Terpane	47.89	2225
259	30TP2	C30 Terpane	48.18	2030

Sample 27 Inner Saturate Chromatograms; Terpanes

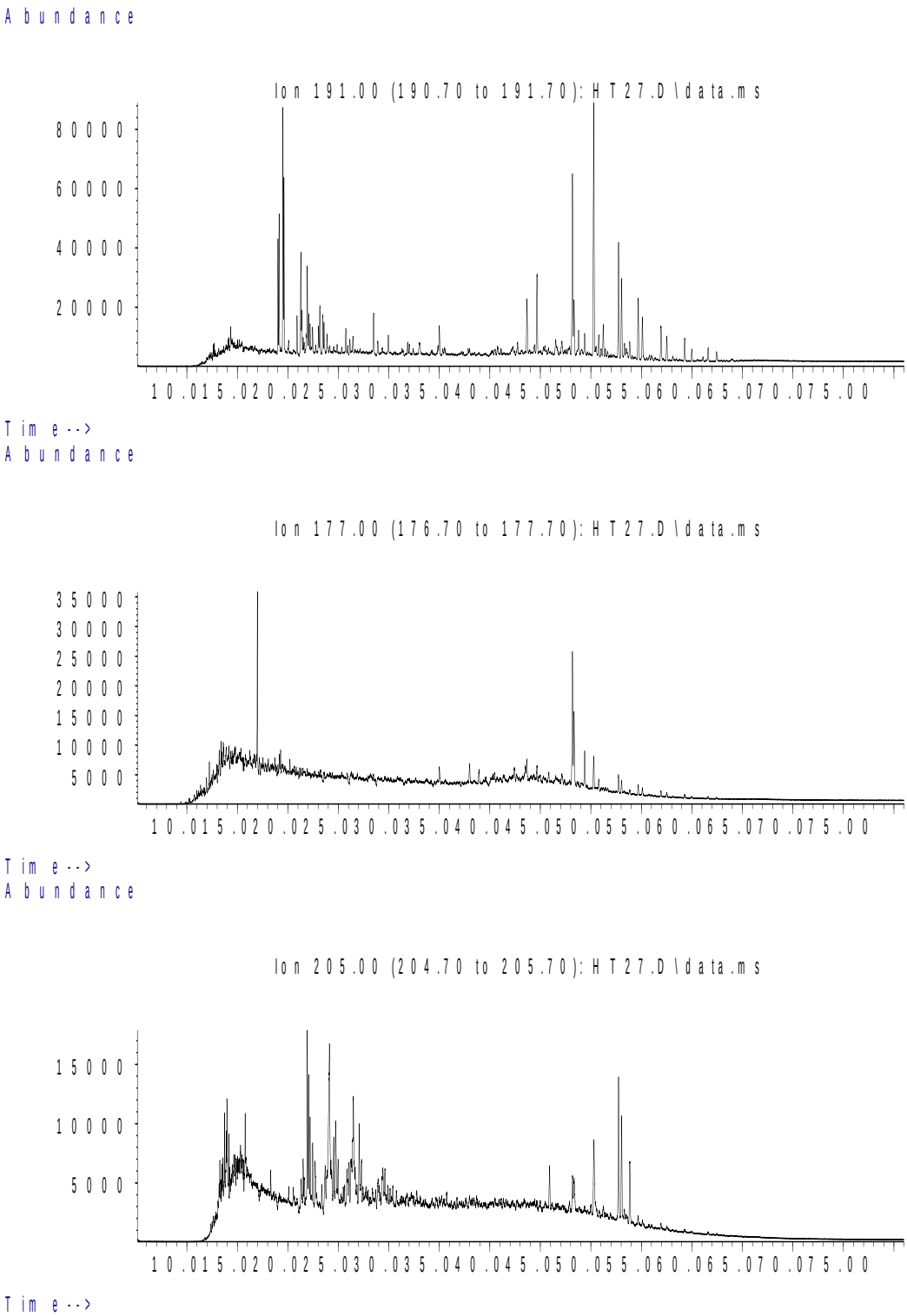

Sample 27 Inner Saturate Chromatograms; Steranes & Steroids

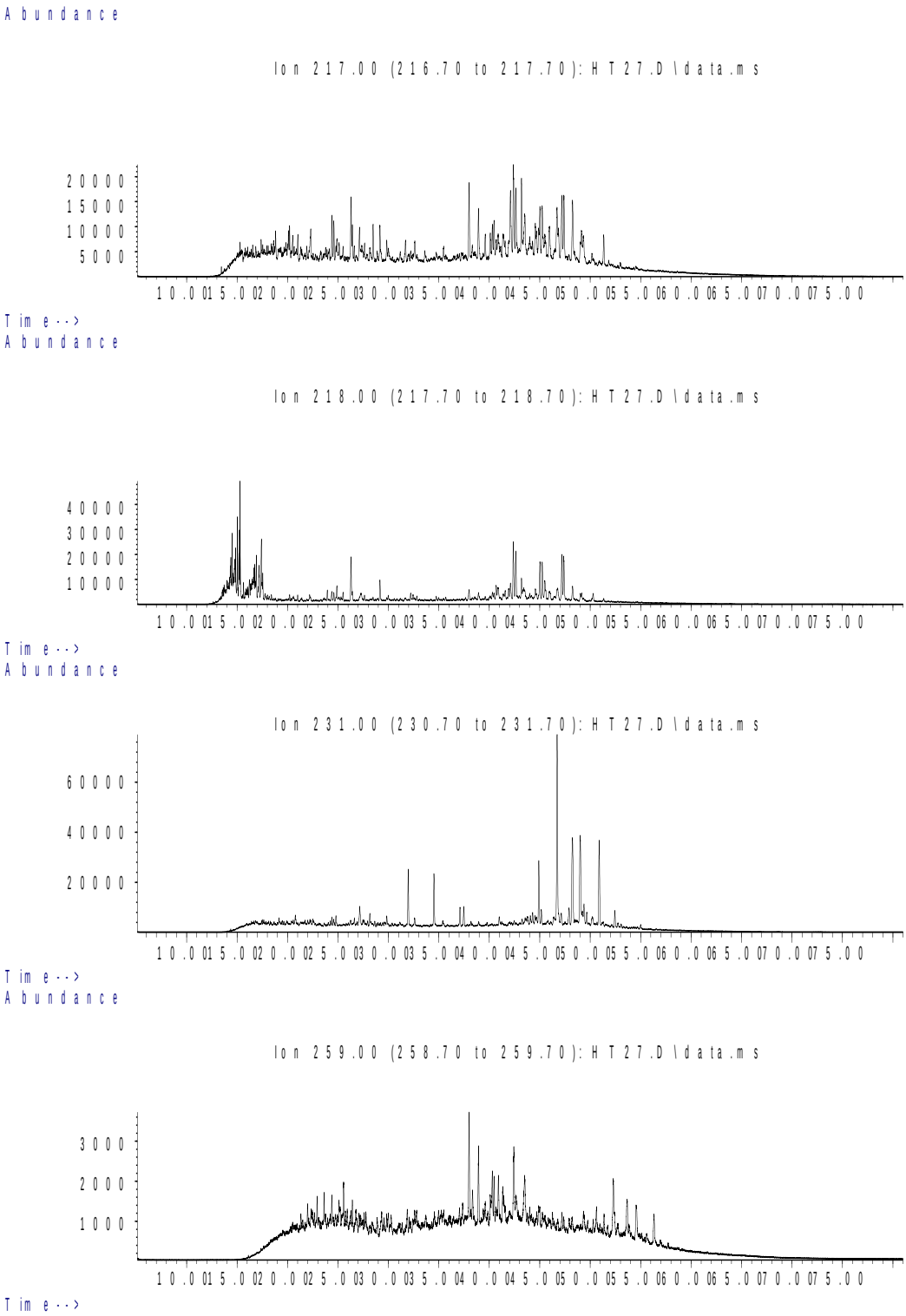

Sample 27 Outer

Bulk Properties

Saturate (%)	19.4
Aromatics (%)	13.4
Resin (%)	16.9
Asphaltene (%)	50.3

Whole Oil/Extract GC

Pristane/n-C17	1.11
Phytane/n-C18	0.48
Pristane/Phytane	0.46

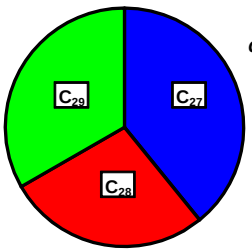

C_{27}-C_{28}-C_{29} αββ Steranes

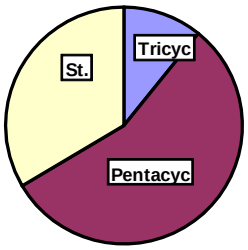

Tricyclic, Pentacyclic Terpanes & Steranes

Saturate Biomarker Interpretive Ratios

Interpretive Ratios	By Area
Terpanes (m/z 191)	
C19t/C23t	0.24
C22t/C21t	0.38
C22t/C24t	0.32
C24t/C23t	0.45
C26t/C25t	0.77
C24Tet/C23t	0.58
C24Tet/C26t	1.66
C23t/C30H	0.16
C24Tet/C30H	0.10
C28BNH/C30H	0.05
25-Nor/C30H	0.02
C29H/C30H	0.76
C30DiaH/C30H	0.07
Ole/C30H	0.01
C30Ts/C30H	0.07
Gam/C30H	0.04
Gam/C31HR	0.13
C35HS/C34HS	0.51
C35 Homohopane Index	0.04
Ts/(Ts+Tm)	0.39
C29Ts/(C29Ts+C29H)	0.19
Mor/C30H	0.12
C32 S/(S+R)	0.60
Steranes (m/z 217)	
% C27 ααα 20R	38.0
% C28 ααα 20R	22.3
% C29 ααα 20R	39.7
C27 Dia/(Dia+Reg)	0.47
(C21+C22)/(C27+C28+C29)	0.14
C29 αββ/(ααα+αββ)	0.52
C29 ααα 20S/20R	0.84
C29 ααα 20S/(S+R)	0.46
αββ−Steranes (m/z 218)	
% C27 αββ 20(R+S)	39.2
% C28 αββ 20(R+S)	27.6
% C29 αββ 20(R+S)	33.3
C29/C27 αββ Sterane Ratio	0.85
C27 Dia/Ster	0.54
Tricyclic/Pentacyclic Terpanes	0.19
Steranes/Terpanes	0.50
% Tricyclic Terpanes	10.8
% Pentacyclic Terpanes	55.7
% Steranes	33.5

Sample 27 Outer

Saturate Biomarker Integration Results (Terpanes)				
Ion	**Peak Label**	**Compound Name**	**R.Time (min.)**	**Peak Area**
191	C19t	C19 tricyclic diterpane	20.078	24181
191	C20t	C20 tricyclic diterpane	21.834	66251
191	C21t	C21 tricyclic diterpane	23.882	38412
191	C22t	C22 tricyclic terpane	25.93	14655
191	C23t	C23 tricyclic terpane	28.497	101471
191	C24t	C24 tricyclic terpane	29.955	46077
191	C25tS	C25 tricyclic terpane (S)	33.008	23251
191	C25tR	C25 tricyclic terpane (R)	33.008	23058
191	C24T	C24 tetracyclic terpane (TET)	34.995	58848
191	C26tS	C26 tricyclic terpane (S)	35.33	15028
191	C26tR	C26 tricyclic terpane (R)	35.524	20438
191	C28tS	C28 extended tricyclic terpane (S)	40.766	14758
191	C28tR	C28 extended tricyclic terpane (R)	41.101	14301
191	C29tS	C29 extended tricyclic terpane (S)	42.229	9612
191	C29tR	C29 extended tricyclic terpane (R)	42.748	21732
191	C30tS	C30 extended tricyclic terpane (S)	45.452	10291
191	C30tR	C30 extended tricyclic terpane (R)	45.806	12247
191	Ts	Ts 18a(H)-trisnorhopane	43.669	126151
191	Tm	Tm 17a(H)-trisnorhopane	44.669	197963
191	C28BNH	C28 17a18a21b(H)-bisnorhopane	47.109	33069
191	Nor25H	C29 Nor-25-hopane	47.75	11570
191	C29H	C29 Tm 17a(H)21b(H)-norhopane	48.18	471008
191	C29Ts	C29 Ts 18a(H)-norneohopane	48.331	107962
191	C30DiaH	C30 17a(H)-diahopane	48.784	45856
191	Normor	C29 normoretane	49.383	46921
191	a-Ole	a-oleanane	50.03	1961
191	b-Ole	b-oleanane	50.03	1284
191	C30H	C30 17a(H)-hopane	50.28	616183
191	C30Ts	17a(H)-30-nor-29-homohopane	50.775	41287
191	Mor	C30 moretane	51.228	70895
191	C31HS	C31 22S 17a(H) homohopane	52.743	244197
191	C31HR	C31 22R 17a(H) homohopane	53.045	179614
191	Gam	gammacerane	53.319	22504
191	C32HS	C32 22S 17a(H) bishomohopane	54.687	128548
191	C32HR	C32 22R 17a(H) bishomohopane	55.103	86447
191	C33HS	C33 22S 17a(H) trishomohopane	56.938	72351
191	C33HR	C33 22R 17a(H) trishomohopane	57.514	48939
191	C34HS	C34 22S 17a(H) extended hopane	59.288	42211
191	C34HR	C34 22R 17a(H) extended hopane	59.987	20880
191	C35HS	C35 22S 17a(H) extended hopane	61.61	21329
191	C35HR	C35 22R 17a(H) extended hopane	62.45	13915

Sample 27 Outer

Saturate Biomarker Integration Results (Steranes)				
Ion	**Peak Label**	**Compound Name**	**R.Time (min.)**	**Peak Area**
217	S21	C21 sterane	25.91	102899
217	S22	C22 sterane	28.74	56200
217	27DbaS	C27 ba 20S diacholestane	37.54	124343
217	27DbaR	C27 ba 20R diacholestane	38.48	78186
217	28DbaSA	C28 ba 20S diasterane a	39.64	36185
217	28DbaSB	C28 ba 20S diasterane b	39.85	43222
217	28DbaRA	C28 ba 20R diasterane a	40.89	28485
217	28DbaRB	C28 ba 20R diasterane b	41.12	27207
217	27aaS	C27 aa 20S cholestane	41.62	130977
217	27bbR	C27 bb 20R cholestane	41.93	161733
217	27bbS	C27 bb 20S cholestane	42.17	83357
217	27aaR	C27 aa 20R cholestane	42.71	96799
217	28aaS	C28 aa 20S ergostane	44.10	52800
217	28bbR	C28 bb 20R ergostane	44.55	63478
217	28bbS	C28 bb 20S ergostane	44.79	68973
217	28aaR	C28 aa 20R ergostane	45.48	56814
217	29aaS	C29 aa 20S stigmastane	46.23	84640
217	29bbR	C29 bb 20R stigmastane	46.74	92998
217	29bbS	C29 bb 20S stigmastane	46.93	105296
217	29aaR	C29 aa 20R stigmastane	47.80	101335
218	27bbR	C27 bb 20R cholestane	41.93	175966
218	27bbS	C27 bb 20S cholestane	42.17	138930
218	28bbR	C28 bb 20R ergostane	44.55	112419
218	28bbS	C28 bb 20S ergostane	44.79	109213
218	29bbR	C29 bb 20R stigmastane	46.74	126473
218	29bbS	C29 bb 20S stigmastane	46.93	141299
259	27DbaS	C27 ba 20S diacholestane	37.55	79342
259	27DbaR	C27 ba 20R diacholestane	38.48	59708
259	28DbaSA	C28 ba 20S diaergostane a	39.84	24141
259	28DbaSB	C28 ba 20S diaergostane b	40.03	32504
259	28DbaRA	C28 ba 20R diaergostane a	40.89	23582
259	28DbaRB	C28 ba 20R diaergostane b	41.12	9182
259	29DbaS	C29 ba 20S diastigmastane	41.98	53480
259	29DbaR	C29 ba 20R diastigmastane	43.55	11733
259	30TP1	C30 Terpane	47.44	10702
259	30TP2	C30 Terpane	47.72	5929

Sample 27 Outer Saturate Chromatograms; Terpanes

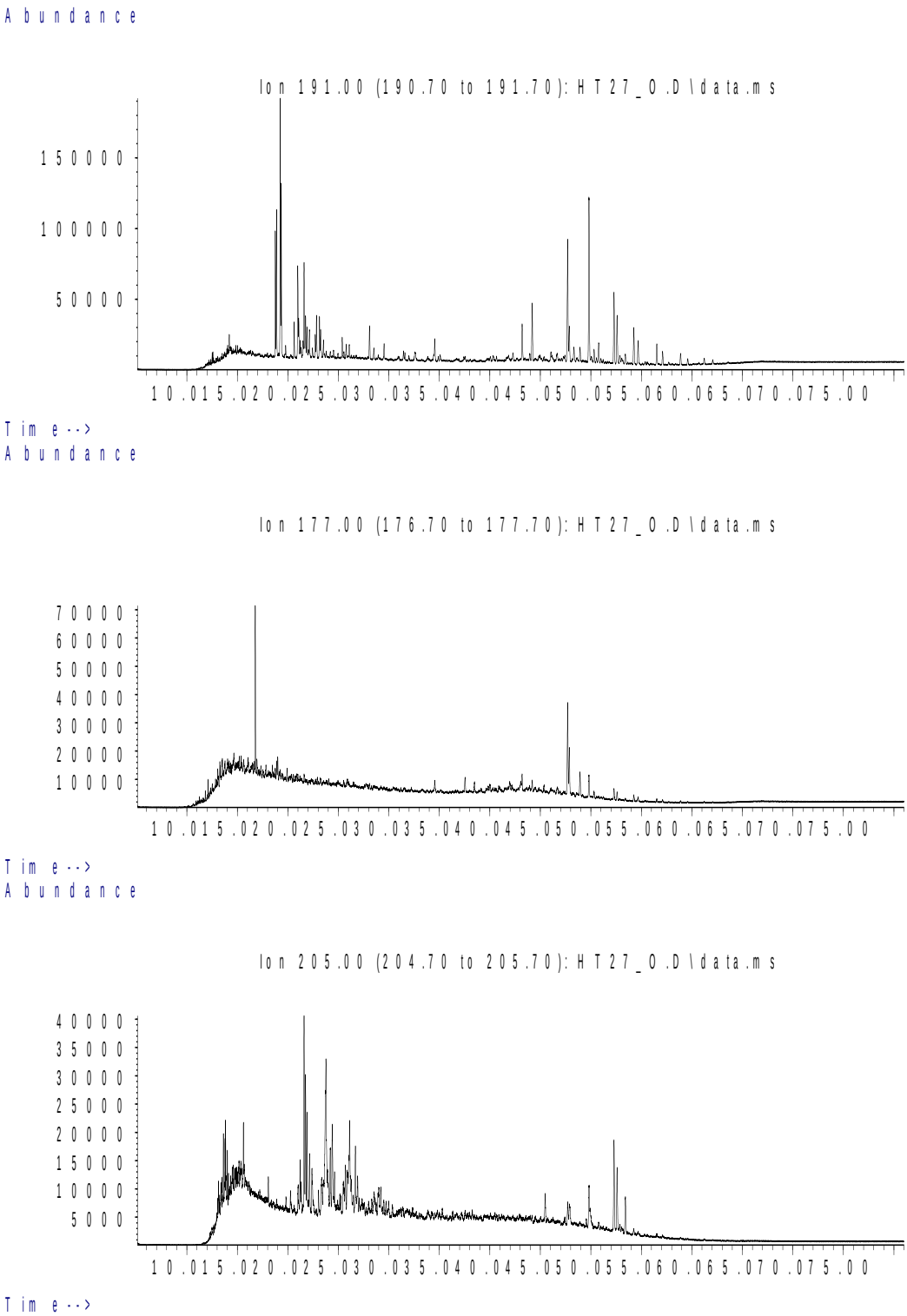

Sample 27 Outer Saturate Chromatograms; Steranes & Steroids

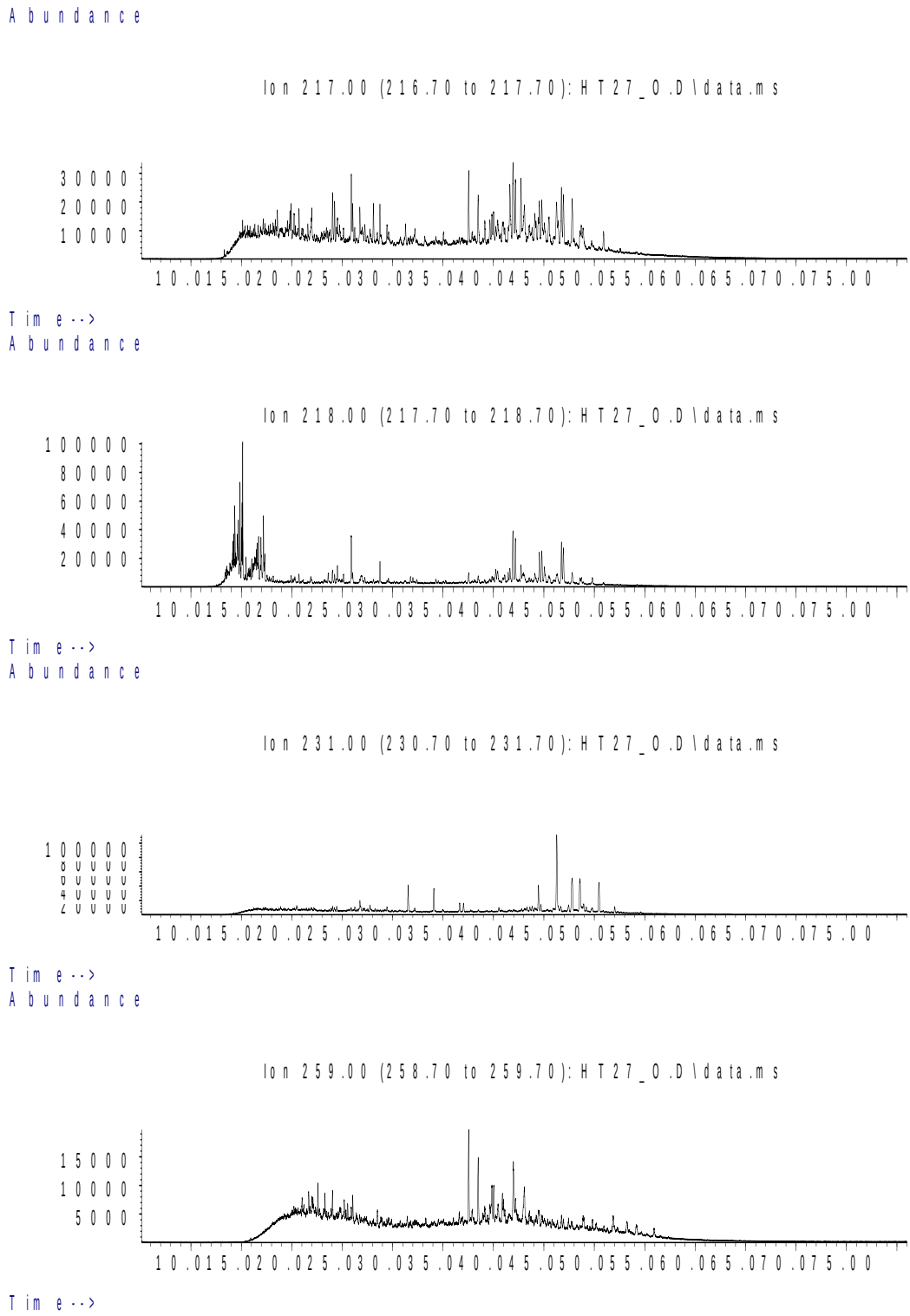

Aromatic Biomarker Integration Results				
Ion	Peak Label	Compound Name	R.Time (min.)	Peak Area
178	P	Phenantrene	22.946	3153539
184	DBT	Dibenzothiophene	22.376	2158299
192	C1P iso 1	Methyl Phenanthrene Isomer	25.258	1375685
192	C1P iso 2	Methyl Phenanthrene Isomer	25.387	1727188
192	C1P iso 3	Methyl Phenanthrene Isomer	25.781	2659433
192	C1P iso 4	Methyl Phenanthrene Isomer	25.911	1998289
192	C1P sum	Methyl Phenanthrene Isomers (summed)		7760595
198	4 MDBT	4 Methyldibenzothiophene	24.833	1037272
198	2+3 MDBT	2 & 3 Methyldibenzothiophene	24.403	1714473
198	1 MDBT	1 Methyldibenzothiophene	25.283	1209649
206	C2P iso 1	Ethyl/Dimethyl Phenanthrene Isomer	27.558	660405
206	C2P iso 2	Ethyl/Dimethyl Phenanthrene Isomer	27.719	757121
206	C2P iso 3	Ethyl/Dimethyl Phenanthrene Isomer	27.838	473590
206	C2P iso 4	Ethyl/Dimethyl Phenanthrene Isomer	28.108	3358153
206	C2P iso 5	Ethyl/Dimethyl Phenanthrene Isomer	28.279	1763234
206	C2P iso 6	Ethyl/Dimethyl Phenanthrene Isomer	28.393	1524061
206	C2P iso 7	Ethyl/Dimethyl Phenanthrene Isomer	28.543	545813
206	C2P iso 8	Ethyl/Dimethyl Phenanthrene Isomer	28.59	898554
206	C2P iso 9	Ethyl/Dimethyl Phenanthrene Isomer	28.942	525833
206	C2P iso 10	Ethyl/Dimethyl Phenanthrene Isomer	29.279	474553
206	C2P sum	Ethyl/Dimethyl Phenanthrene Isomers (summed)		10981317
226	C4P sum	C4 Phenanthrene Isomers (summed)		5020555
252	dbf	benzo(b)fluoranthene	42.706	41576
252	bap	benzo(a)pyrene	44.064	84934

Sample 32 Inner

Bulk Properties

Saturate (%)	19.0
Aromatics (%)	16.4
Resin (%)	15.9
Asphaltene (%)	48.7

Whole Oil/Extract GC

Pristane/Phytane	1.06
Pristane/n-C17	0.56
Phytane/n-C18	0.48

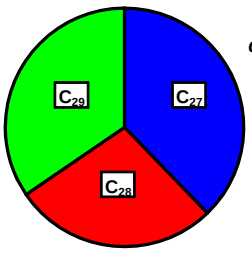

C_{27}-C_{28}-C_{29} αββ Steranes

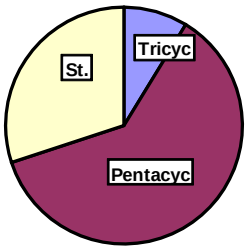

Tricyclic, Pentacyclic Terpanes & Steranes

Saturate Biomarker Interpretive Ratios

Interpretive Ratios	By Area
Terpanes (m/z 191)	
C19t/C23t	0.28
C22t/C21t	0.43
C22t/C24t	0.47
C24t/C23t	0.53
C26t/C25t	0.82
C24Tet/C23t	0.90
C24Tet/C26t	1.98
C23t/C30H	0.10
C24Tet/C30H	0.09
C28BNH/C30H	0.06
25-Nor/C30H	0.03
C29H/C30H	0.66
C30DiaH/C30H	0.09
Ole/C30H	0.00
C30Ts/C30H	0.09
Gam/C30H	0.05
Gam/C31HR	0.17
C35HS/C34HS	0.61
C35 Homohopane Index	0.06
Ts/(Ts+Tm)	0.38
C29Ts/(C29Ts+C29H)	0.24
Mor/C30H	0.13
C32 S/(S+R)	0.60
Steranes (m/z 217)	
% C27 ααα 20R	37.3
% C28 ααα 20R	23.9
% C29 ααα 20R	38.9
C27 Dia/(Dia+Reg)	0.48
(C21+C22)/(C27+C28+C29)	0.13
C29 αββ/(ααα+αββ)	0.50
C29 ααα 20S/20R	0.76
C29 ααα 20S/(S+R)	0.43
αββ−Steranes (m/z 218)	
% C27 αββ 20(R+S)	37.8
% C28 αββ 20(R+S)	27.7
% C29 αββ 20(R+S)	34.5
C29/C27 αββ Sterane Ratio	0.91
C27 Dia/Ster	0.55
Tricyclic/Pentacyclic Terpanes	0.14
Steranes/Terpanes	0.43
% Tricyclic Terpanes	8.7
% Pentacyclic Terpanes	61.2
% Steranes	30.0

Sample 32 Inner

Saturate Biomarker Integration Results (Terpanes)				
Ion	**Peak Label**	**Compound Name**	**R.Time (min.)**	**Peak Area**
191	C19t	C19 tricyclic diterpane	20.05	13165
191	C20t	C20 tricyclic diterpane	21.81	16974
191	C21t	C21 tricyclic diterpane	23.85	26467
191	C22t	C22 tricyclic terpane	25.90	11501
191	C23t	C23 tricyclic terpane	28.46	46618
191	C24t	C24 tricyclic terpane	29.92	24582
191	C25tS	C25 tricyclic terpane (S)	32.99	11954
191	C25tR	C25 tricyclic terpane (R)	32.99	14083
191	C24T	C24 tetracyclic terpane (TET)	34.96	42135
191	C26tS	C26 tricyclic terpane (S)	35.30	8389
191	C26tR	C26 tricyclic terpane (R)	35.49	12903
191	C28tS	C28 extended tricyclic terpane (S)	40.72	9911
191	C28tR	C28 extended tricyclic terpane (R)	41.07	8620
191	C29tS	C29 extended tricyclic terpane (S)	42.26	7277
191	C29tR	C29 extended tricyclic terpane (R)	42.73	20184
191	C30tS	C30 extended tricyclic terpane (S)	45.43	8603
191	C30tR	C30 extended tricyclic terpane (R)	45.77	10214
191	Ts	Ts 18a(H)-trisnorhopane	43.64	82886
191	Tm	Tm 17a(H)-trisnorhopane	44.64	134519
191	C28BNH	C28 17a18a21b(H)-bisnorhopane	47.11	28297
191	Nor25H	C29 Nor-25-hopane	47.73	12323
191	C29H	C29 Tm 17a(H)21b(H)-norhopane	48.14	299039
191	C29Ts	C29 Ts 18a(H)-norneohopane	48.31	93958
191	C30DiaH	C30 17a(H)-diahopane	48.77	39654
191	Normor	C29 normoretane	49.36	35327
191	a-Ole	a-oleanane	0.00	0
191	b-Ole	b-oleanane	0.00	0
191	C30H	C30 17a(H)-hopane	50.27	450900
191	C30Ts	17a(H)-30-nor-29-homohopane	50.75	39342
191	Mor	C30 moretane	51.21	59931
191	C31HS	C31 22S 17a(H) homohopane	52.72	202179
191	C31HR	C31 22R 17a(H) homohopane	53.02	143218
191	Gam	gammacerane	53.30	24176
191	C32HS	C32 22S 17a(H) bishomohopane	54.67	112440
191	C32HR	C32 22R 17a(H) bishomohopane	55.09	74893
191	C33HS	C33 22S 17a(H) trishomohopane	56.93	70182
191	C33HR	C33 22R 17a(H) trishomohopane	57.51	45690
191	C34HS	C34 22S 17a(H) extended hopane	59.28	43189
191	C34HR	C34 22R 17a(H) extended hopane	59.98	22643
191	C35HS	C35 22S 17a(H) extended hopane	61.61	26481
191	C35HR	C35 22R 17a(H) extended hopane	62.44	18094

Sample 32 Inner

Saturate Biomarker Integration Results (Steranes)				
Ion	**Peak Label**	**Compound Name**	**R.Time (min.)**	**Peak Area**
217	S21	C21 sterane	26.27	57393
217	S22	C22 sterane	29.12	30995
217	27DbaS	C27 ba 20S diacholestane	37.96	72294
217	27DbaR	C27 ba 20R diacholestane	38.90	54980
217	28DbaSA	C28 ba 20S diasterane a	40.27	25783
217	28DbaSB	C28 ba 20S diasterane b	40.43	35594
217	28DbaRA	C28 ba 20R diasterane a	41.33	19268
217	28DbaRB	C28 ba 20R diasterane b	41.33	14965
217	27aaS	C27 aa 20S cholestane	42.05	69469
217	27bbR	C27 bb 20R cholestane	42.36	103671
217	27bbS	C27 bb 20S cholestane	42.60	55128
217	27aaR	C27 aa 20R cholestane	43.15	67100
217	28aaS	C28 aa 20S ergostane	44.53	33860
217	28bbR	C28 bb 20R ergostane	44.97	35196
217	28bbS	C28 bb 20S ergostane	45.23	45228
217	28aaR	C28 aa 20R ergostane	45.91	43024
217	29aaS	C29 aa 20S stigmastane	46.68	53023
217	29bbR	C29 bb 20R stigmastane	47.17	63881
217	29bbS	C29 bb 20S stigmastane	47.36	59475
217	29aaR	C29 aa 20R stigmastane	48.23	69994
218	27bbR	C27 bb 20R cholestane	42.36	113662
218	27bbS	C27 bb 20S cholestane	42.60	83074
218	28bbR	C28 bb 20R ergostane	44.99	72593
218	28bbS	C28 bb 20S ergostane	45.23	71617
218	29bbR	C29 bb 20R stigmastane	47.17	93060
218	29bbS	C29 bb 20S stigmastane	47.36	86733
259	27DbaS	C27 ba 20S diacholestane	37.96	12061
259	27DbaR	C27 ba 20R diacholestane	38.89	8725
259	28DbaSA	C28 ba 20S diaergostane a	40.27	4187
259	28DbaSB	C28 ba 20S diaergostane b	40.45	4891
259	28DbaRA	C28 ba 20R diaergostane a	41.31	3830
259	28DbaRB	C28 ba 20R diaergostane b	41.41	2420
259	29DbaS	C29 ba 20S diastigmastane	42.40	10597
259	29DbaR	C29 ba 20R diastigmastane	43.97	1703
259	30TP1	C30 Terpane	47.86	1682
259	30TP2	C30 Terpane	48.17	1397

Sample 32 Inner Saturate Chromatograms; Terpanes

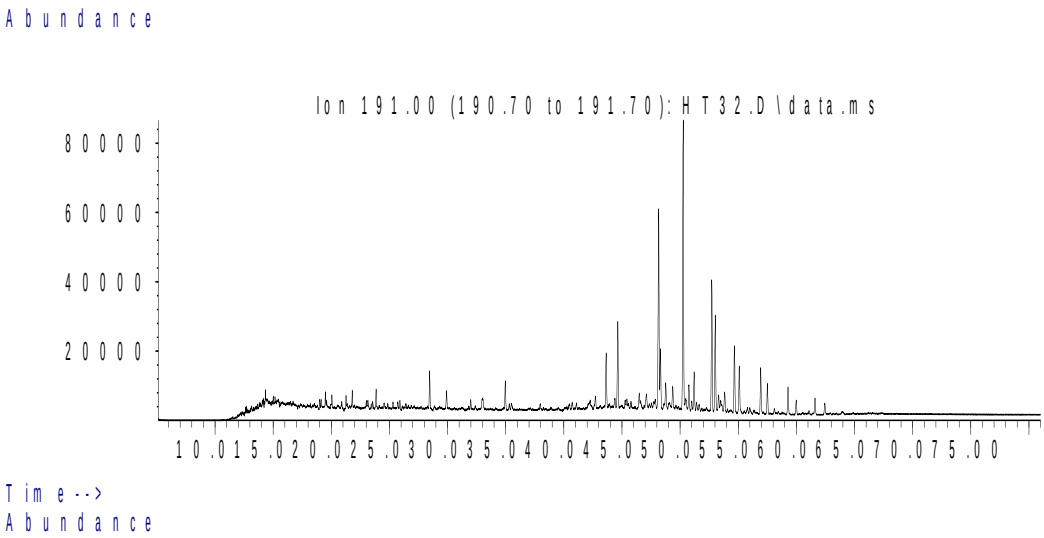

Sample 32 Inner Saturate Chromatograms; Steranes & Steroids

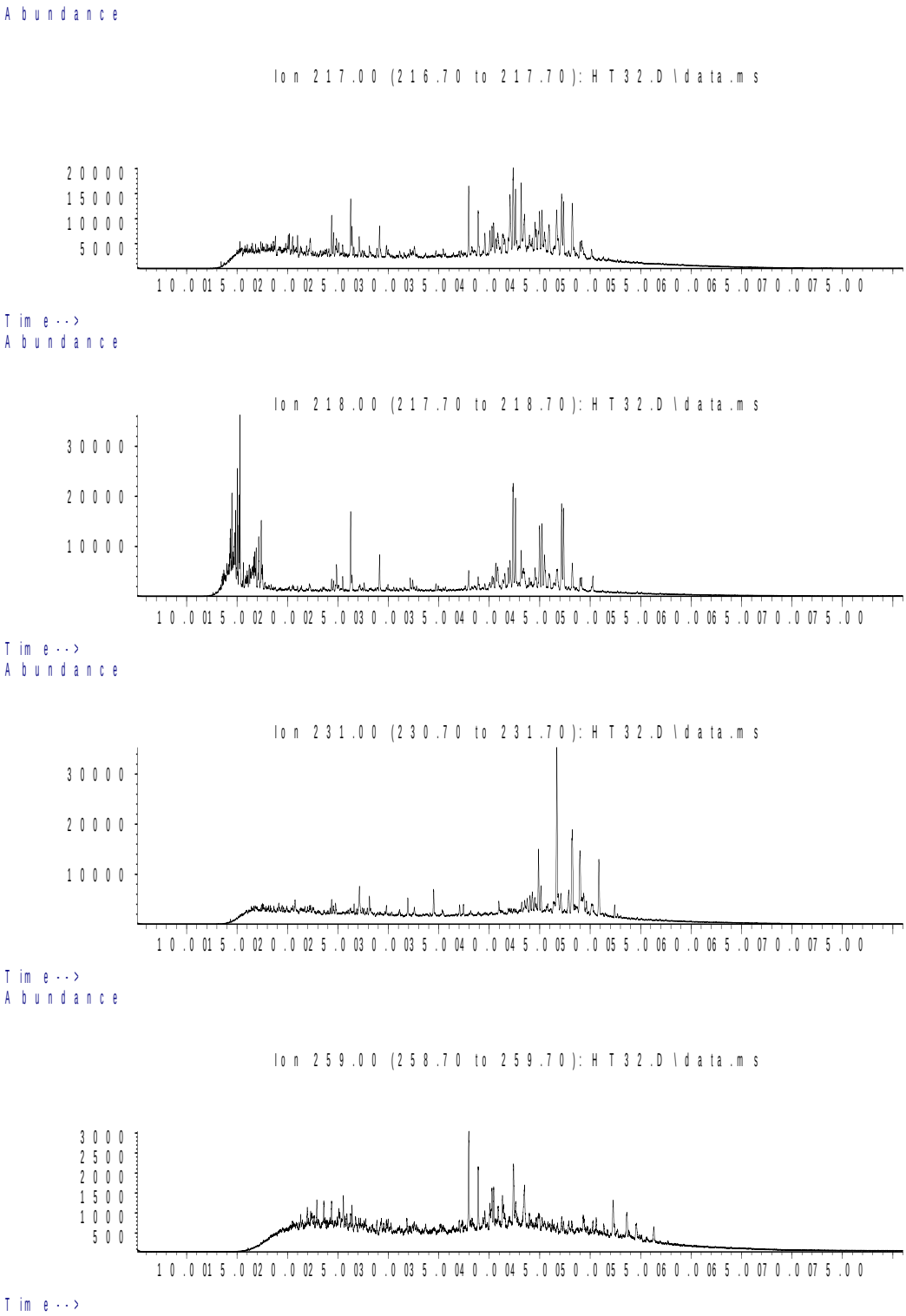

Sample 32 Outer

Bulk Properties

Saturate (%)	16.3
Aromatics (%)	12.0
Resin (%)	19.6
Asphaltene (%)	52.1

Whole Oil/Extract GC

Pristane/Phytane	0.94
Pristane/n-C17	0.49
Phytane/n-C18	0.43

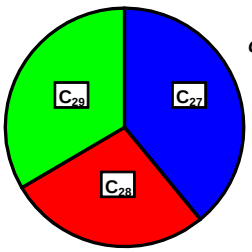

C_{27}-C_{28}-C_{29} αββ Steranes

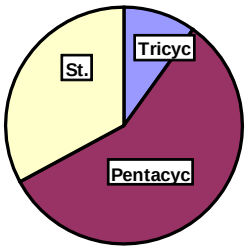

Tricyclic, Pentacyclic Terpanes & Steranes

Saturate Biomarker Interpretive Ratios

Interpretive Ratios	By Area
Terpanes (m/z 191)	
C19t/C23t	0.29
C22t/C21t	0.45
C22t/C24t	0.39
C24t/C23t	0.59
C26t/C25t	0.82
C24Tet/C23t	0.82
C24Tet/C26t	1.98
C23t/C30H	0.13
C24Tet/C30H	0.11
C28BNH/C30H	0.06
25-Nor/C30H	0.03
C29H/C30H	0.72
C30DiaH/C30H	0.09
Ole/C30H	0.01
C30Ts/C30H	0.08
Gam/C30H	0.05
Gam/C31HR	0.17
C35HS/C34HS	0.58
C35 Homohopane Index	0.05
Ts/(Ts+Tm)	0.39
C29Ts/(C29Ts+C29H)	0.22
Mor/C30H	0.12
C32 S/(S+R)	0.59
Steranes (m/z 217)	
% C27 ααα 20R	42.1
% C28 ααα 20R	21.8
% C29 ααα 20R	36.0
C27 Dia/(Dia+Reg)	0.51
(C21+C22)/(C27+C28+C29)	0.16
C29 αββ/(ααα+αββ)	0.51
C29 ααα 20S/20R	0.99
C29 ααα 20S/(S+R)	0.50
αββ−Steranes (m/z 218)	
% C27 αββ 20(R+S)	39.0
% C28 αββ 20(R+S)	27.5
% C29 αββ 20(R+S)	33.4
C29/C27 αββ Sterane Ratio	0.86
C27 Dia/Ster	0.60
Tricyclic/Pentacyclic Terpanes	0.17
Steranes/Terpanes	0.49
% Tricyclic Terpanes	9.9
% Pentacyclic Terpanes	57.2
% Steranes	32.9

Sample 32 Outer

Saturate Biomarker Integration Results (Terpanes)				
Ion	**Peak Label**	**Compound Name**	**R.Time (min.)**	**Peak Area**
191	C19t	C19 tricyclic diterpane	19.77	22283
191	C20t	C20 tricyclic diterpane	21.49	25921
191	C21t	C21 tricyclic diterpane	23.50	38419
191	C22t	C22 tricyclic terpane	25.54	17444
191	C23t	C23 tricyclic terpane	28.08	76121
191	C24t	C24 tricyclic terpane	29.51	44918
191	C25tS	C25 tricyclic terpane (S)	32.55	22037
191	C25tR	C25 tricyclic terpane (R)	32.55	16911
191	C24T	C24 tetracyclic terpane (TET)	34.53	62788
191	C26tS	C26 tricyclic terpane (S)	34.89	13618
191	C26tR	C26 tricyclic terpane (R)	35.08	18133
191	C28tS	C28 extended tricyclic terpane (S)	40.03	17746
191	C28tR	C28 extended tricyclic terpane (R)	40.64	11508
191	C29tS	C29 extended tricyclic terpane (S)	41.83	11862
191	C29tR	C29 extended tricyclic terpane (R)	42.27	26596
191	C30tS	C30 extended tricyclic terpane (S)	44.96	11402
191	C30tR	C30 extended tricyclic terpane (R)	45.32	12793
191	Ts	Ts 18a(H)-trisnorhopane	43.18	119047
191	Tm	Tm 17a(H)-trisnorhopane	44.17	189075
191	C28BNH	C28 17a18a21b(H)-bisnorhopane	46.66	34425
191	Nor25H	C29 Nor-25-hopane	47.42	19243
191	C29H	C29 Tm 17a(H)21b(H)-norhopane	47.68	422272
191	C29Ts	C29 Ts 18a(H)-norneohopane	47.85	121831
191	C30DiaH	C30 17a(H)-diahopane	48.32	51338
191	Normor	C29 normoretane	48.91	44351
191	a-Ole	a-oleanane	49.54	2975
191	b-Ole	b-oleanane	49.54	2975
191	C30H	C30 17a(H)-hopane	49.80	587528
191	C30Ts	17a(H)-30-nor-29-homohopane	50.31	48391
191	Mor	C30 moretane	50.77	72234
191	C31HS	C31 22S 17a(H) homohopane	52.28	245732
191	C31HR	C31 22R 17a(H) homohopane	52.58	175838
191	Gam	gammacerane	52.86	29096
191	C32HS	C32 22S 17a(H) bishomohopane	54.24	126878
191	C32HR	C32 22R 17a(H) bishomohopane	54.67	86891
191	C33HS	C33 22S 17a(H) trishomohopane	56.51	74344
191	C33HR	C33 22R 17a(H) trishomohopane	57.10	49238
191	C34HS	C34 22S 17a(H) extended hopane	58.87	37946
191	C34HR	C34 22R 17a(H) extended hopane	59.58	22482
191	C35HS	C35 22S 17a(H) extended hopane	61.21	21912
191	C35HR	C35 22R 17a(H) extended hopane	62.06	16797

Sample 32 Outer

Saturate Biomarker Integration Results (Steranes)				
Ion	**Peak Label**	**Compound Name**	**R.Time (min.)**	**Peak Area**
217	S21	C21 sterane	25.88	99998
217	S22	C22 sterane	28.73	60601
217	27DbaS	C27 ba 20S diacholestane	37.52	116845
217	27DbaR	C27 ba 20R diacholestane	38.46	87317
217	28DbaSA	C28 ba 20S diasterane a	39.63	42763
217	28DbaSB	C28 ba 20S diasterane b	39.84	40792
217	28DbaRA	C28 ba 20R diasterane a	40.89	31718
217	28DbaRB	C28 ba 20R diasterane b	41.09	22949
217	27aaS	C27 aa 20S cholestane	41.60	97757
217	27bbR	C27 bb 20R cholestane	41.92	160524
217	27bbS	C27 bb 20S cholestane	42.16	80744
217	27aaR	C27 aa 20R cholestane	42.71	96605
217	28aaS	C28 aa 20S ergostane	44.09	48400
217	28bbR	C28 bb 20R ergostane	44.52	58634
217	28bbS	C28 bb 20S ergostane	44.79	62013
217	28aaR	C28 aa 20R ergostane	45.47	49993
217	29aaS	C29 aa 20S stigmastane	46.22	81770
217	29bbR	C29 bb 20R stigmastane	46.73	94599
217	29bbS	C29 bb 20S stigmastane	46.92	79345
217	29aaR	C29 aa 20R stigmastane	47.79	82602
218	27bbR	C27 bb 20R cholestane	41.91	174821
218	27bbS	C27 bb 20S cholestane	42.16	128426
218	28bbR	C28 bb 20R ergostane	44.53	107240
218	28bbS	C28 bb 20S ergostane	44.79	106569
218	29bbR	C29 bb 20R stigmastane	46.73	135908
218	29bbS	C29 bb 20S stigmastane	46.92	123897
259	27DbaS	C27 ba 20S diacholestane	37.53	76746
259	27DbaR	C27 ba 20R diacholestane	38.46	51177
259	28DbaSA	C28 ba 20S diaergostane a	39.84	23401
259	28DbaSB	C28 ba 20S diaergostane b	40.01	31107
259	28DbaRA	C28 ba 20R diaergostane a	40.86	23346
259	28DbaRB	C28 ba 20R diaergostane b	41.11	9694
259	29DbaS	C29 ba 20S diastigmastane	41.96	62611
259	29DbaR	C29 ba 20R diastigmastane	43.54	9879
259	30TP1	C30 Terpane	47.41	8465
259	30TP2	C30 Terpane	47.72	7979

Sample 32 Outer Saturate Chromatograms; Terpanes

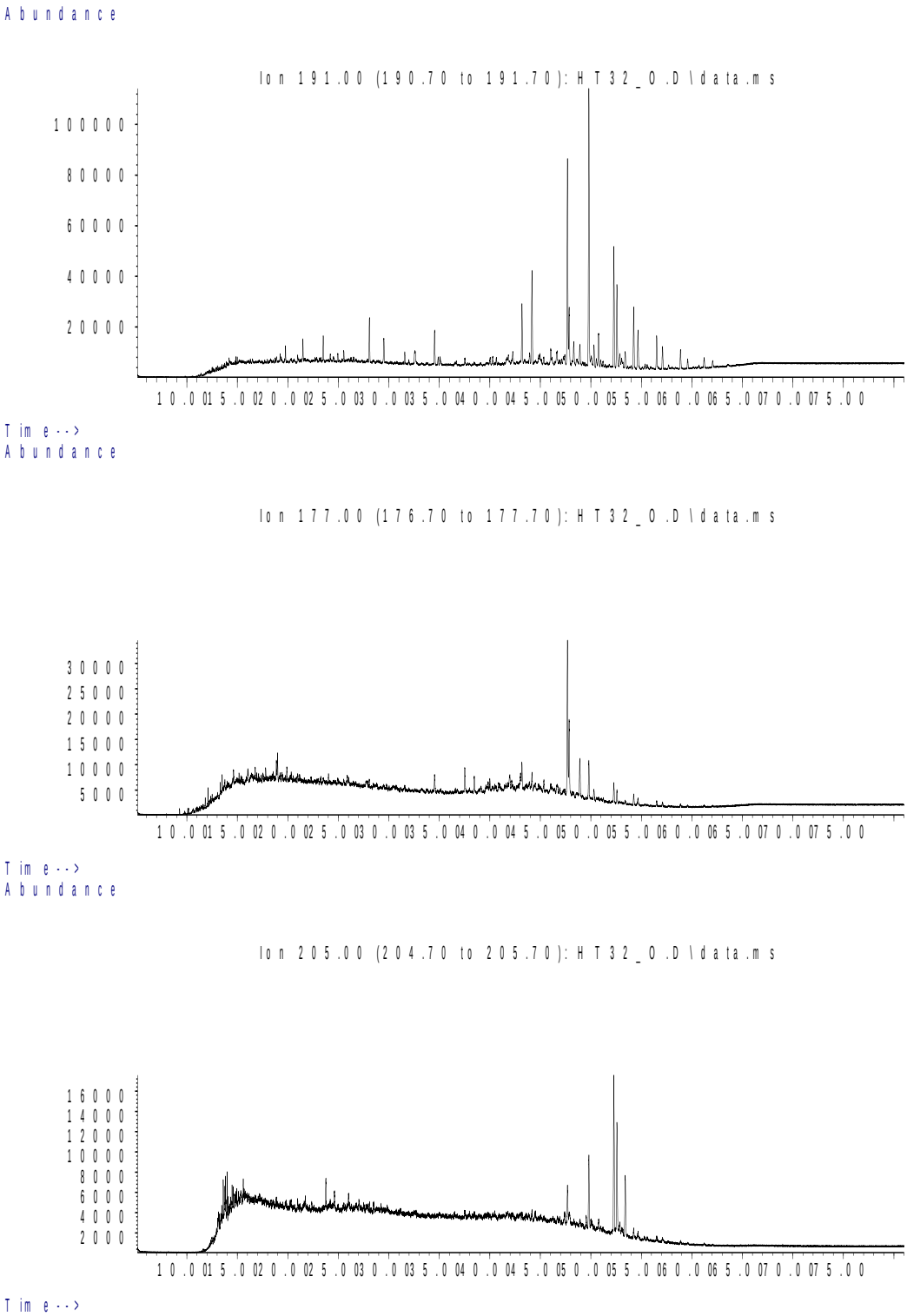

Sample 32 Outer Saturate Chromatograms; Steranes & Steroids

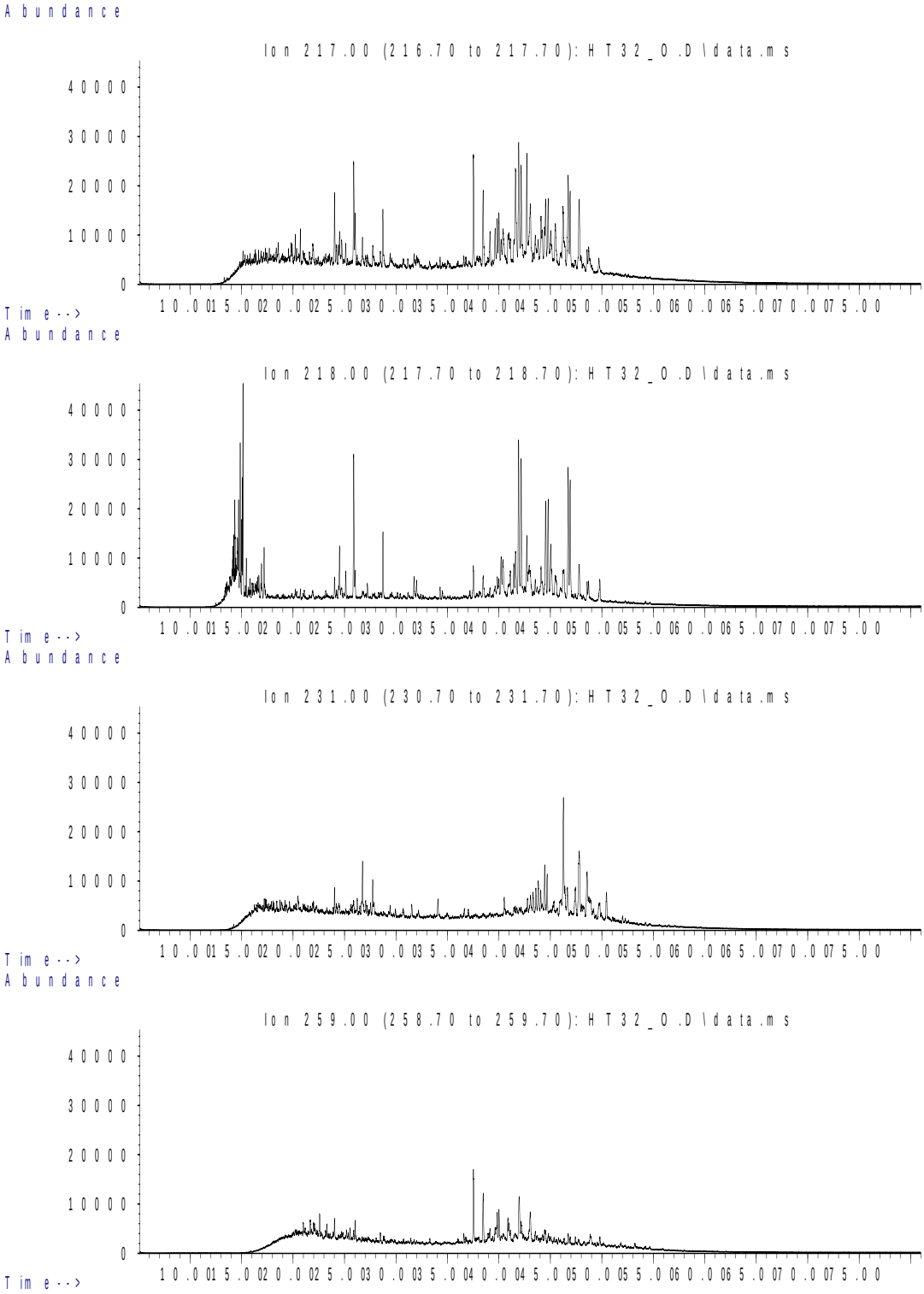

Sample 162 Inner

Bulk Properties

Saturate (%)	20.0
Aromatics (%)	13.3
Resin (%)	14.2
Asphaltene (%)	52.5

Whole Oil/Extract GC

Pristane/Phytane	1.10
Pristane/n-C17	0.51
Phytane/n-C18	0.46

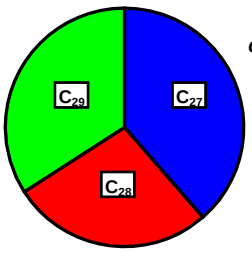

C_{27}-C_{28}-C_{29} αββ Steranes

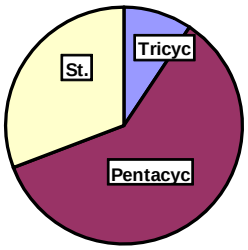

Tricyclic, Pentacyclic Terpanes & Steranes

Saturate Biomarker Interpretive Ratios

Interpretive Ratios	By Area
Terpanes (m/z 191)	
C19t/C23t	0.29
C22t/C21t	0.50
C22t/C24t	0.47
C24t/C23t	0.61
C26t/C25t	0.86
C24Tet/C23t	0.96
C24Tet/C26t	2.10
C23t/C30H	0.11
C24Tet/C30H	0.10
C28BNH/C30H	0.06
25-Nor/C30H	0.02
C29H/C30H	0.71
C30DiaH/C30H	0.09
Ole/C30H	0.00
C30Ts/C30H	0.09
Gam/C30H	0.05
Gam/C31HR	0.18
C35HS/C34HS	0.67
C35 Homohopane Index	0.05
Ts/(Ts+Tm)	0.38
C29Ts/(C29Ts+C29H)	0.22
Mor/C30H	0.13
C32 S/(S+R)	0.60
Steranes (m/z 217)	
% C27 ααα 20R	38.2
% C28 ααα 20R	24.1
% C29 ααα 20R	37.6
C27 Dia/(Dia+Reg)	0.49
(C21+C22)/(C27+C28+C29)	0.14
C29 αββ/(ααα+αββ)	0.51
C29 ααα 20S/20R	0.72
C29 ααα 20S/(S+R)	0.42
αββ−Steranes (m/z 218)	
% C27 αββ 20(R+S)	38.6
% C28 αββ 20(R+S)	27.3
% C29 αββ 20(R+S)	34.1
C29/C27 αββ Sterane Ratio	0.88
C27 Dia/Ster	0.55
Tricyclic/Pentacyclic Terpanes	0.16
Steranes/Terpanes	0.44
% Tricyclic Terpanes	9.3
% Pentacyclic Terpanes	59.9
% Steranes	30.8

Sample 162 Inner

Saturate Biomarker Integration Results (Terpanes)				
Ion	**Peak Label**	**Compound Name**	**R.Time (min.)**	**Peak Area**
191	C19t	C19 tricyclic diterpane	20.06	15612
191	C20t	C20 tricyclic diterpane	21.82	23172
191	C21t	C21 tricyclic diterpane	23.87	30513
191	C22t	C22 tricyclic terpane	25.91	15167
191	C23t	C23 tricyclic terpane	28.48	52952
191	C24t	C24 tricyclic terpane	29.93	32350
191	C25tS	C25 tricyclic terpane (S)	32.98	15708
191	C25tR	C25 tricyclic terpane (R)	32.98	12571
191	C24T	C24 tetracyclic terpane (TET)	34.99	50814
191	C26tS	C26 tricyclic terpane (S)	35.33	10321
191	C26tR	C26 tricyclic terpane (R)	35.52	13879
191	C28tS	C28 extended tricyclic terpane (S)	40.73	13550
191	C28tR	C28 extended tricyclic terpane (R)	41.10	11647
191	C29tS	C29 extended tricyclic terpane (S)	42.27	7337
191	C29tR	C29 extended tricyclic terpane (R)	42.73	21947
191	C30tS	C30 extended tricyclic terpane (S)	45.43	10252
191	C30tR	C30 extended tricyclic terpane (R)	45.79	10946
191	Ts	Ts 18a(H)-trisnorhopane	43.65	95620
191	Tm	Tm 17a(H)-trisnorhopane	44.66	153067
191	C28BNH	C28 17a18a21b(H)-bisnorhopane	47.11	30915
191	Nor25H	C29 Nor-25-hopane	47.74	11452
191	C29H	C29 Tm 17a(H)21b(H)-norhopane	48.16	351536
191	C29Ts	C29 Ts 18a(H)-norneohopane	48.32	101526
191	C30DiaH	C30 17a(H)-diahopane	48.77	43947
191	Normor	C29 normoretane	49.36	34784
191	a-Ole	a-oleanane	50.04	274
191	b-Ole	b-oleanane	50.04	274
191	C30H	C30 17a(H)-hopane	50.28	496025
191	C30Ts	17a(H)-30-nor-29-homohopane	50.77	44874
191	Mor	C30 moretane	51.22	63708
191	C31HS	C31 22S 17a(H) homohopane	52.72	215187
191	C31HR	C31 22R 17a(H) homohopane	53.03	153854
191	Gam	gammacerane	53.31	27045
191	C32HS	C32 22S 17a(H) bishomohopane	54.67	115926
191	C32HR	C32 22R 17a(H) bishomohopane	55.08	77516
191	C33HS	C33 22S 17a(H) trishomohopane	56.92	71521
191	C33HR	C33 22R 17a(H) trishomohopane	57.50	46434
191	C34HS	C34 22S 17a(H) extended hopane	59.27	37696
191	C34HR	C34 22R 17a(H) extended hopane	59.98	22060
191	C35HS	C35 22S 17a(H) extended hopane	61.59	25404
191	C35HR	C35 22R 17a(H) extended hopane	62.43	17409

Sample 162 Inner

Saturate Biomarker Integration Results (Steranes)				
Ion	**Peak Label**	**Compound Name**	**R.Time (min.)**	**Peak Area**
217	S21	C21 sterane	26.28	69235
217	S22	C22 sterane	29.13	41315
217	27DbaS	C27 ba 20S diacholestane	37.97	85412
217	27DbaR	C27 ba 20R diacholestane	38.90	59363
217	28DbaSA	C28 ba 20S diasterane a	40.29	29727
217	28DbaSB	C28 ba 20S diasterane b	40.45	41212
217	28DbaRA	C28 ba 20R diasterane a	41.34	23285
217	28DbaRB	C28 ba 20R diasterane b	41.34	15022
217	27aaS	C27 aa 20S cholestane	42.08	76452
217	27bbR	C27 bb 20R cholestane	42.38	119709
217	27bbS	C27 bb 20S cholestane	42.61	62773
217	27aaR	C27 aa 20R cholestane	43.17	76985
217	28aaS	C28 aa 20S ergostane	44.55	40694
217	28bbR	C28 bb 20R ergostane	45.00	47342
217	28bbS	C28 bb 20S ergostane	45.23	46328
217	28aaR	C28 aa 20R ergostane	45.93	48578
217	29aaS	C29 aa 20S stigmastane	46.69	54865
217	29bbR	C29 bb 20R stigmastane	47.17	72875
217	29bbS	C29 bb 20S stigmastane	47.37	62538
217	29aaR	C29 aa 20R stigmastane	48.23	75754
218	27bbR	C27 bb 20R cholestane	42.36	131000
218	27bbS	C27 bb 20S cholestane	42.61	94840
218	28bbR	C28 bb 20R ergostane	45.00	80881
218	28bbS	C28 bb 20S ergostane	45.22	78961
218	29bbR	C29 bb 20R stigmastane	47.17	104503
218	29bbS	C29 bb 20S stigmastane	47.37	94990
259	27DbaS	C27 ba 20S diacholestane	37.97	13263
259	27DbaR	C27 ba 20R diacholestane	38.91	8768
259	28DbaSA	C28 ba 20S diaergostane a	40.29	3811
259	28DbaSB	C28 ba 20S diaergostane b	40.46	5343
259	28DbaRA	C28 ba 20R diaergostane a	41.31	4261
259	28DbaRB	C28 ba 20R diaergostane b	41.42	1356
259	29DbaS	C29 ba 20S diastigmastane	42.41	11855
259	29DbaR	C29 ba 20R diastigmastane	43.98	1745
259	30TP1	C30 Terpane	47.89	1625
259	30TP2	C30 Terpane	48.17	1431

Sample 162 Inner Saturate Chromatograms; Terpanes

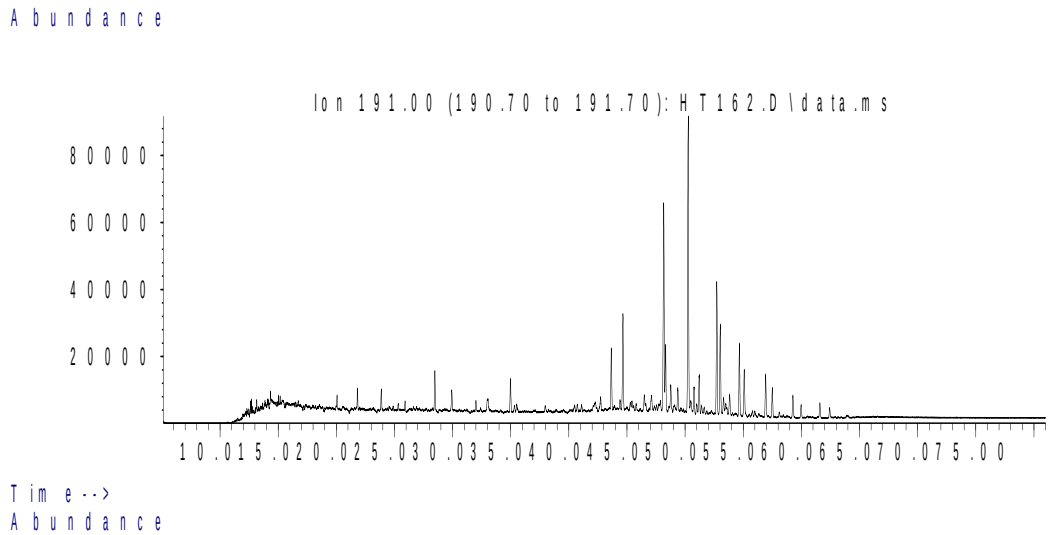

Sample 162 Inner Saturate Chromatograms; Steranes & Steroids

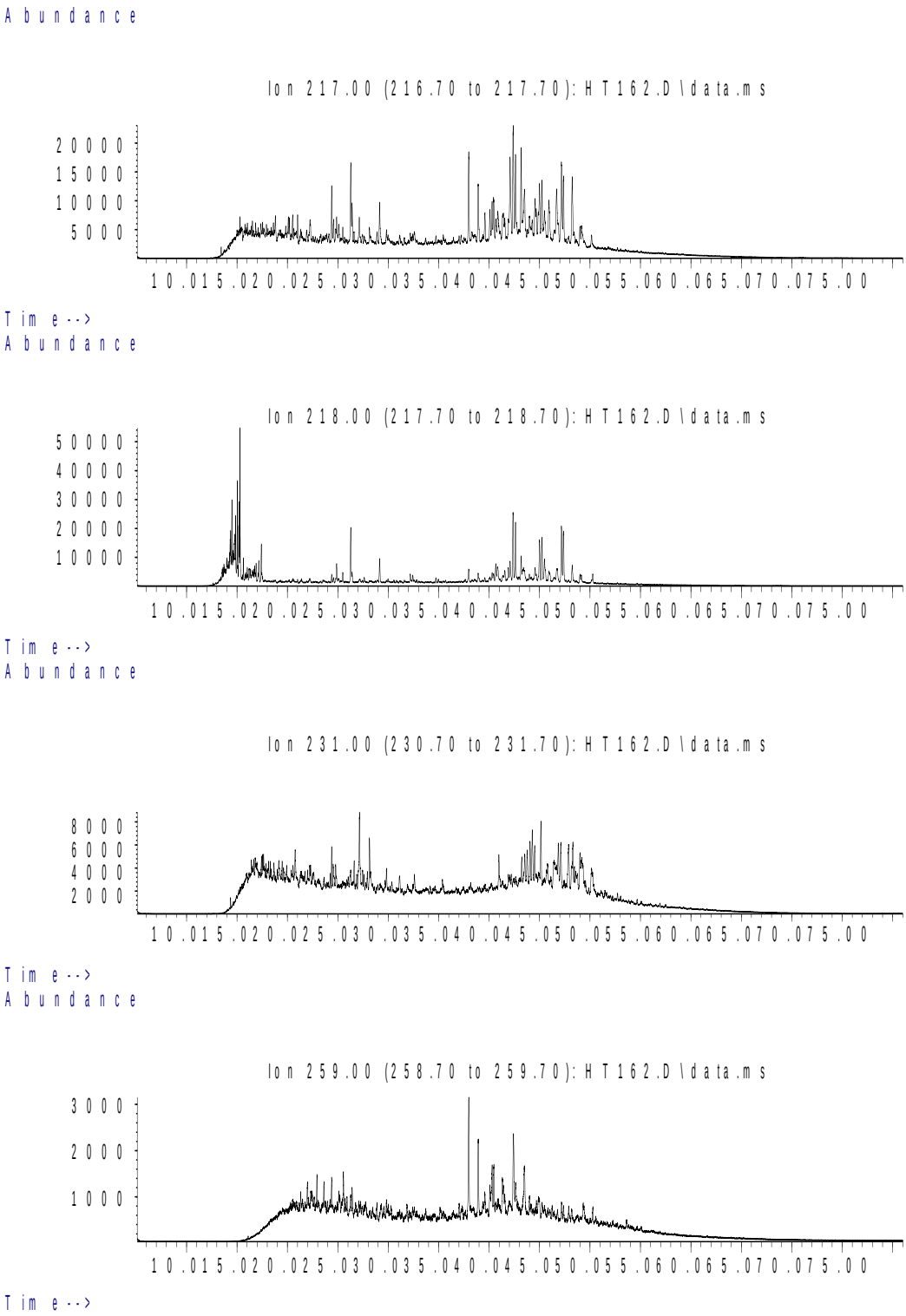

Sample 162 Outer

Bulk Properties

Saturate (%)	18.3
Aromatics (%)	11.8
Resin (%)	16.9
Asphaltene (%)	53.0

Whole Oil/Extract GC

Pristane/Phytane	0.97
Pristane/n-C17	0.49
Phytane/n-C18	0.48

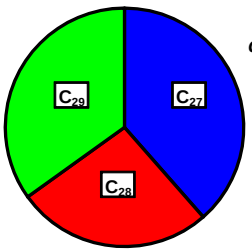

C_{27}-C_{28}-C_{29} αββ Steranes

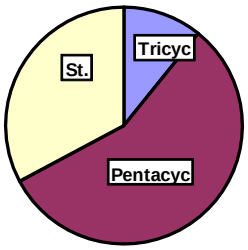

Tricyclic, Pentacyclic Terpanes & Steranes

Saturate Biomarker Interpretive Ratios

Interpretive Ratios	By Area
Terpanes (m/z 191)	
C19t/C23t	0.34
C22t/C21t	0.42
C22t/C24t	0.40
C24t/C23t	0.60
C26t/C25t	0.81
C24Tet/C23t	0.89
C24Tet/C26t	2.09
C23t/C30H	0.13
C24Tet/C30H	0.12
C28BNH/C30H	0.05
25-Nor/C30H	0.03
C29H/C30H	0.72
C30DiaH/C30H	0.07
Ole/C30H	0.00
C30Ts/C30H	0.08
Gam/C30H	0.05
Gam/C31HR	0.16
C35HS/C34HS	0.59
C35 Homohopane Index	0.04
Ts/(Ts+Tm)	0.39
C29Ts/(C29Ts+C29H)	0.22
Mor/C30H	0.12
C32 S/(S+R)	0.59
Steranes (m/z 217)	
% C27 ααα 20R	36.8
% C28 ααα 20R	24.4
% C29 ααα 20R	38.8
C27 Dia/(Dia+Reg)	0.54
(C21+C22)/(C27+C28+C29)	0.17
C29 αββ/(ααα+αββ)	0.56
C29 ααα 20S/20R	0.66
C29 ααα 20S/(S+R)	0.40
αββ−Steranes (m/z 218)	
% C27 αββ 20(R+S)	38.5
% C28 αββ 20(R+S)	26.6
% C29 αββ 20(R+S)	34.9
C29/C27 αββ Sterane Ratio	0.91
C27 Dia/Ster	0.63
Tricyclic/Pentacyclic Terpanes	0.19
Steranes/Terpanes	0.49
% Tricyclic Terpanes	10.8
% Pentacyclic Terpanes	56.4
% Steranes	32.8

Sample 162 Outer

Saturate Biomarker Integration Results (Terpanes)				
Ion	**Peak Label**	**Compound Name**	**R.Time (min.)**	**Peak Area**
191	C19t	C19 tricyclic diterpane	19.8	35484
191	C20t	C20 tricyclic diterpane	21.5	49082
191	C21t	C21 tricyclic diterpane	23.5	58996
191	C22t	C22 tricyclic terpane	25.6	24965
191	C23t	C23 tricyclic terpane	28.1	103775
191	C24t	C24 tricyclic terpane	29.5	62005
191	C25tS	C25 tricyclic terpane (S)	32.6	26966
191	C25tR	C25 tricyclic terpane (R)	32.6	27544
191	C24T	C24 tetracyclic terpane (TET)	34.6	92460
191	C26tS	C26 tricyclic terpane (S)	34.9	19956
191	C26tR	C26 tricyclic terpane (R)	35.1	24182
191	C28tS	C28 extended tricyclic terpane (S)	40.0	16964
191	C28tR	C28 extended tricyclic terpane (R)	40.7	22579
191	C29tS	C29 extended tricyclic terpane (S)	41.9	15871
191	C29tR	C29 extended tricyclic terpane (R)	42.3	35293
191	C30tS	C30 extended tricyclic terpane (S)	45.0	13168
191	C30tR	C30 extended tricyclic terpane (R)	45.4	19776
191	Ts	Ts 18a(H)-trisnorhopane	43.2	163885
191	Tm	Tm 17a(H)-trisnorhopane	44.2	256083
191	C28BNH	C28 17a18a21b(H)-bisnorhopane	46.7	38816
191	Nor25H	C29 Nor-25-hopane	47.4	22384
191	C29H	C29 Tm 17a(H)21b(H)-norhopane	47.7	562434
191	C29Ts	C29 Ts 18a(H)-norneohopane	47.9	158083
191	C30DiaH	C30 17a(H)-diahopane	48.3	53079
191	Normor	C29 normoretane	48.9	59835
191	a-Ole	a-oleanane	49.5	832
191	b-Ole	b-oleanane	49.5	832
191	C30H	C30 17a(H)-hopane	49.8	777302
191	C30Ts	17a(H)-30-nor-29-homohopane	50.3	64367
191	Mor	C30 moretane	50.8	93563
191	C31HS	C31 22S 17a(H) homohopane	52.3	316838
191	C31HR	C31 22R 17a(H) homohopane	52.6	227667
191	Gam	gammacerane	52.9	37508
191	C32HS	C32 22S 17a(H) bishomohopane	54.2	165180
191	C32HR	C32 22R 17a(H) bishomohopane	54.7	114487
191	C33HS	C33 22S 17a(H) trishomohopane	56.5	96312
191	C33HR	C33 22R 17a(H) trishomohopane	57.1	62904
191	C34HS	C34 22S 17a(H) extended hopane	58.9	46168
191	C34HR	C34 22R 17a(H) extended hopane	59.6	28609
191	C35HS	C35 22S 17a(H) extended hopane	61.2	27051
191	C35HR	C35 22R 17a(H) extended hopane	62.1	18822

Sample 162 Outer

Saturate Biomarker Integration Results (Steranes)				
Ion	**Peak Label**	**Compound Name**	**R.Time (min.)**	**Peak Area**
217	S21	C21 sterane	25.91	143337
217	S22	C22 sterane	28.74	74718
217	27DbaS	C27 ba 20S diacholestane	37.54	158537
217	27DbaR	C27 ba 20R diacholestane	38.49	111538
217	28DbaSA	C28 ba 20S diasterane a	39.64	42481
217	28DbaSB	C28 ba 20S diasterane b	39.85	51778
217	28DbaRA	C28 ba 20R diasterane a	40.89	45363
217	28DbaRB	C28 ba 20R diasterane b	41.13	28954
217	27aaS	C27 aa 20S cholestane	41.62	114673
217	27bbR	C27 bb 20R cholestane	41.95	219586
217	27bbS	C27 bb 20S cholestane	42.18	107648
217	27aaR	C27 aa 20R cholestane	42.73	116177
217	28aaS	C28 aa 20S ergostane	44.10	60070
217	28bbR	C28 bb 20R ergostane	44.56	74905
217	28bbS	C28 bb 20S ergostane	44.80	84726
217	28aaR	C28 aa 20R ergostane	45.47	77000
217	29aaS	C29 aa 20S stigmastane	46.25	80709
217	29bbR	C29 bb 20R stigmastane	46.74	155738
217	29bbS	C29 bb 20S stigmastane	46.93	100673
217	29aaR	C29 aa 20R stigmastane	47.80	122688
218	27bbR	C27 bb 20R cholestane	41.91	233648
218	27bbS	C27 bb 20S cholestane	42.18	168288
218	28bbR	C28 bb 20R ergostane	44.56	132591
218	28bbS	C28 bb 20S ergostane	44.79	144780
218	29bbR	C29 bb 20R stigmastane	46.73	192954
218	29bbS	C29 bb 20S stigmastane	46.94	171196
259	27DbaS	C27 ba 20S diacholestane	37.55	100522
259	27DbaR	C27 ba 20R diacholestane	38.49	65697
259	28DbaSA	C28 ba 20S diaergostane a	39.86	31661
259	28DbaSB	C28 ba 20S diaergostane b	40.04	35395
259	28DbaRA	C28 ba 20R diaergostane a	40.89	30065
259	28DbaRB	C28 ba 20R diaergostane b	41.13	13019
259	29DbaS	C29 ba 20S diastigmastane	41.98	76604
259	29DbaR	C29 ba 20R diastigmastane	43.56	12882
259	30TP1	C30 Terpane	47.43	8736
259	30TP2	C30 Terpane	47.71	11157

Sample 162 Outer Saturate Chromatograms; Terpanes

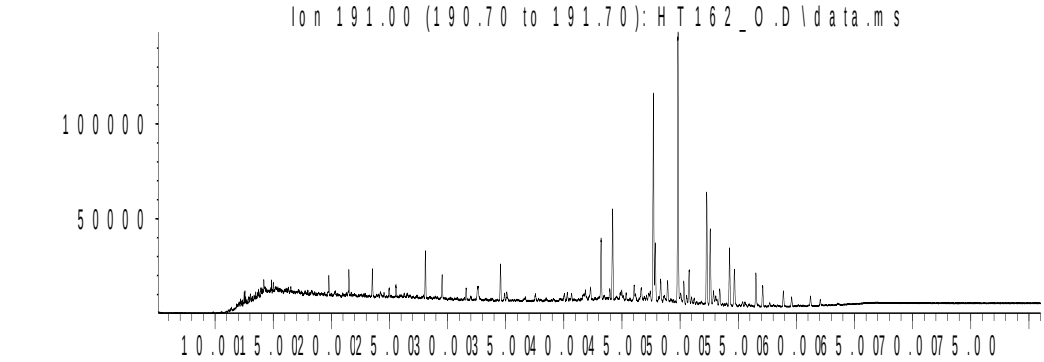

Sample 162 Outer Saturate Chromatograms; Steranes & Steroids

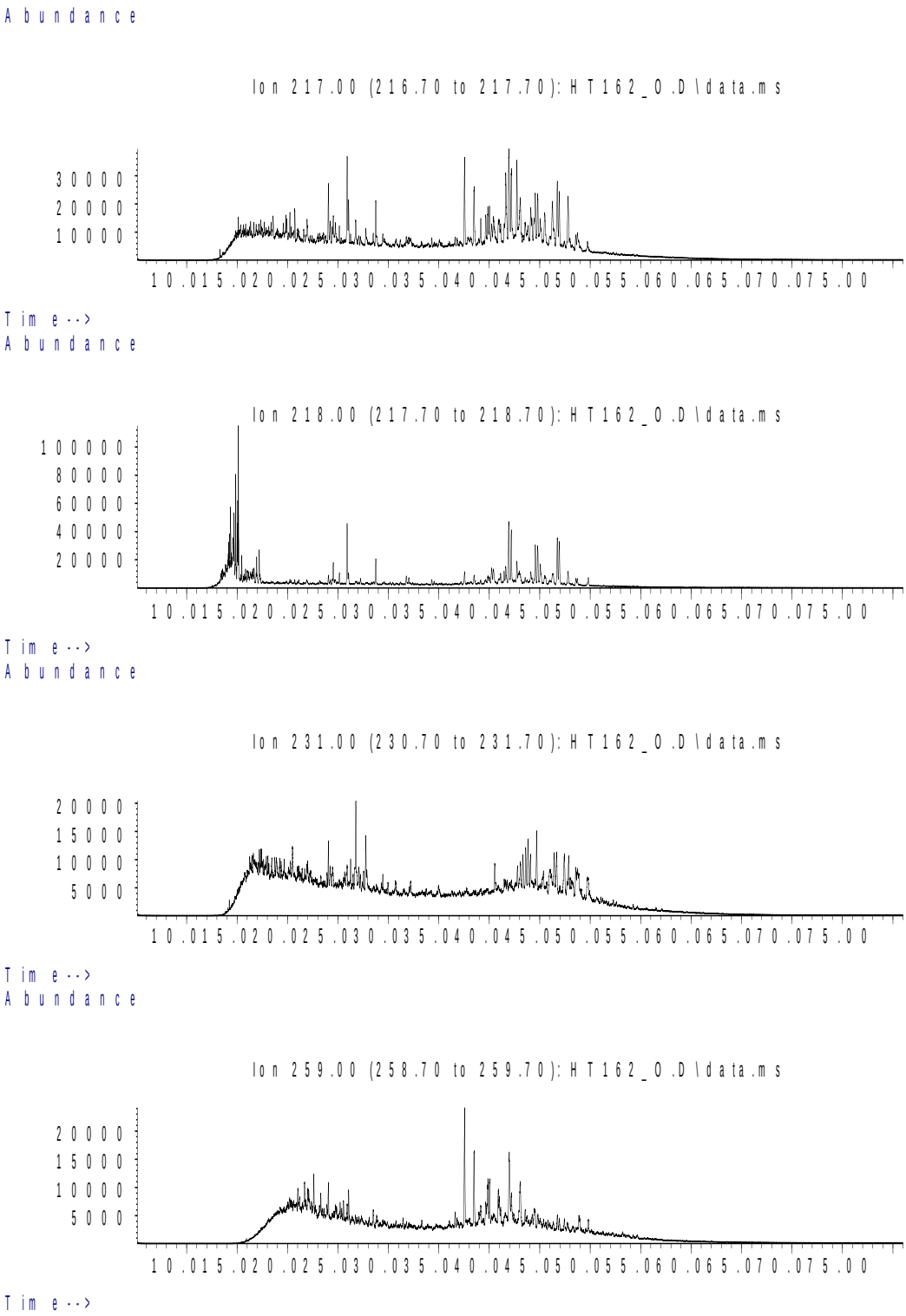

Sample 80 Inner

Bulk Properties

Saturate (%)	25.6
Aromatics (%)	16.2
Resin (%)	10.4
Asphaltene (%)	47.8

Whole Oil/Extract GC

Pristane/Phytane	1.11
Pristane/n-C17	0.48
Phytane/n-C18	0.41

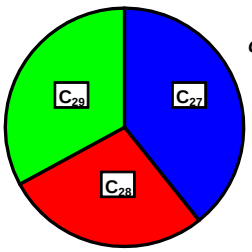

C_{27}-C_{28}-C_{29} αββ Steranes

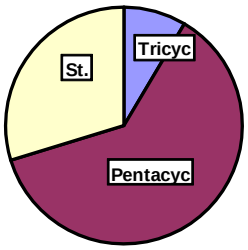

Tricyclic, Pentacyclic Terpanes & Steranes

Saturate Biomarker Interpretive Ratios

Interpretive Ratios	By Area
Terpanes (m/z 191)	
C19t/C23t	0.28
C22t/C21t	0.49
C22t/C24t	0.42
C24t/C23t	0.60
C26t/C25t	0.80
C24Tet/C23t	0.96
C24Tet/C26t	2.02
C23t/C30H	0.10
C24Tet/C30H	0.09
C28BNH/C30H	0.06
25-Nor/C30H	0.03
C29H/C30H	0.65
C30DiaH/C30H	0.09
Ole/C30H	0.01
C30Ts/C30H	0.09
Gam/C30H	0.05
Gam/C31HR	0.17
C35HS/C34HS	0.77
C35 Homohopane Index	0.06
Ts/(Ts+Tm)	0.39
C29Ts/(C29Ts+C29H)	0.24
Mor/C30H	0.13
C32 S/(S+R)	0.60
Steranes (m/z 217)	
% C27 ααα 20R	38.5
% C28 ααα 20R	23.8
% C29 ααα 20R	37.7
C27 Dia/(Dia+Reg)	0.48
(C21+C22)/(C27+C28+C29)	0.13
C29 αββ/(ααα+αββ)	0.48
C29 ααα 20S/20R	0.75
C29 ααα 20S/(S+R)	0.43
αββ−Steranes (m/z 218)	
% C27 αββ 20(R+S)	39.3
% C28 αββ 20(R+S)	27.8
% C29 αββ 20(R+S)	32.9
C29/C27 αββ Sterane Ratio	0.84
C27 Dia/Ster	0.54
Tricyclic/Pentacyclic Terpanes	0.14
Steranes/Terpanes	0.42
% Tricyclic Terpanes	8.5
% Pentacyclic Terpanes	61.8
% Steranes	29.7

Sample 80 Inner

Saturate Biomarker Integration Results (Terpanes)				
Ion	**Peak Label**	**Compound Name**	**R.Time (min.)**	**Peak Area**
191	C19t	C19 tricyclic diterpane	20.05	11997
191	C20t	C20 tricyclic diterpane	21.80	17509
191	C21t	C21 tricyclic diterpane	23.85	21918
191	C22t	C22 tricyclic terpane	25.89	10678
191	C23t	C23 tricyclic terpane	28.45	42212
191	C24t	C24 tricyclic terpane	29.90	25419
191	C25tS	C25 tricyclic terpane (S)	32.98	15135
191	C25tR	C25 tricyclic terpane (R)	32.98	9877
191	C24T	C24 tetracyclic terpane (TET)	34.95	40579
191	C26tS	C26 tricyclic terpane (S)	35.29	7970
191	C26tR	C26 tricyclic terpane (R)	35.48	12143
191	C28tS	C28 extended tricyclic terpane (S)	40.69	9852
191	C28tR	C28 extended tricyclic terpane (R)	41.07	9226
191	C29tS	C29 extended tricyclic terpane (S)	42.24	6021
191	C29tR	C29 extended tricyclic terpane (R)	42.69	16553
191	C30tS	C30 extended tricyclic terpane (S)	45.40	7723
191	C30tR	C30 extended tricyclic terpane (R)	45.77	10269
191	Ts	Ts 18a(H)-trisnorhopane	43.62	82820
191	Tm	Tm 17a(H)-trisnorhopane	44.62	131559
191	C28BNH	C28 17a18a21b(H)-bisnorhopane	47.10	25337
191	Nor25H	C29 Nor-25-hopane	47.86	10955
191	C29H	C29 Tm 17a(H)21b(H)-norhopane	48.14	283698
191	C29Ts	C29 Ts 18a(H)-norneohopane	48.29	91175
191	C30DiaH	C30 17a(H)-diahopane	48.74	41120
191	Normor	C29 normoretane	49.36	32689
191	a-Ole	a-oleanane	49.98	2211
191	b-Ole	b-oleanane	49.98	2211
191	C30H	C30 17a(H)-hopane	50.25	434492
191	C30Ts	17a(H)-30-nor-29-homohopane	50.74	40462
191	Mor	C30 moretane	51.20	57280
191	C31HS	C31 22S 17a(H) homohopane	52.71	199758
191	C31HR	C31 22R 17a(H) homohopane	53.01	139047
191	Gam	gammacerane	53.30	23689
191	C32HS	C32 22S 17a(H) bishomohopane	54.66	108805
191	C32HR	C32 22R 17a(H) bishomohopane	55.08	72653
191	C33HS	C33 22S 17a(H) trishomohopane	56.93	69391
191	C33HR	C33 22R 17a(H) trishomohopane	57.49	45425
191	C34HS	C34 22S 17a(H) extended hopane	59.27	34381
191	C34HR	C34 22R 17a(H) extended hopane	59.97	22095
191	C35HS	C35 22S 17a(H) extended hopane	61.60	26416
191	C35HR	C35 22R 17a(H) extended hopane	62.44	16252

Sample 80 Inner

Saturate Biomarker Integration Results (Steranes)				
Ion	**Peak Label**	**Compound Name**	**R.Time (min.)**	**Peak Area**
217	S21	C21 sterane	26.25	54115
217	S22	C22 sterane	29.12	34163
217	27DbaS	C27 ba 20S diacholestane	37.95	69749
217	27DbaR	C27 ba 20R diacholestane	38.88	52785
217	28DbaSA	C28 ba 20S diasterane a	40.25	24792
217	28DbaSB	C28 ba 20S diasterane b	40.41	34663
217	28DbaRA	C28 ba 20R diasterane a	41.31	19349
217	28DbaRB	C28 ba 20R diasterane b	41.31	12636
217	27aaS	C27 aa 20S cholestane	42.05	71074
217	27bbR	C27 bb 20R cholestane	42.35	102509
217	27bbS	C27 bb 20S cholestane	42.59	52684
217	27aaR	C27 aa 20R cholestane	43.15	63977
217	28aaS	C28 aa 20S ergostane	44.53	35432
217	28bbR	C28 bb 20R ergostane	44.96	40334
217	28bbS	C28 bb 20S ergostane	45.22	38757
217	28aaR	C28 aa 20R ergostane	45.90	39666
217	29aaS	C29 aa 20S stigmastane	46.67	47076
217	29bbR	C29 bb 20R stigmastane	47.16	61328
217	29bbS	C29 bb 20S stigmastane	47.34	41881
217	29aaR	C29 aa 20R stigmastane	48.23	62741
218	27bbR	C27 bb 20R cholestane	42.33	111486
218	27bbS	C27 bb 20S cholestane	42.58	81475
218	28bbR	C28 bb 20R ergostane	44.97	68823
218	28bbS	C28 bb 20S ergostane	45.22	67945
218	29bbR	C29 bb 20R stigmastane	47.16	89507
218	29bbS	C29 bb 20S stigmastane	47.34	72236
259	27DbaS	C27 ba 20S diacholestane	37.95	11200
259	27DbaR	C27 ba 20R diacholestane	38.88	8324
259	28DbaSA	C28 ba 20S diaergostane a	40.25	3800
259	28DbaSB	C28 ba 20S diaergostane b	40.44	4745
259	28DbaRA	C28 ba 20R diaergostane a	41.29	3809
259	28DbaRB	C28 ba 20R diaergostane b	41.40	1499
259	29DbaS	C29 ba 20S diastigmastane	42.39	9757
259	29DbaR	C29 ba 20R diastigmastane	43.98	1750
259	30TP1	C30 Terpane	47.86	1559
259	30TP2	C30 Terpane	48.17	1542

Sample 80 Inner Saturate Chromatograms; Terpanes

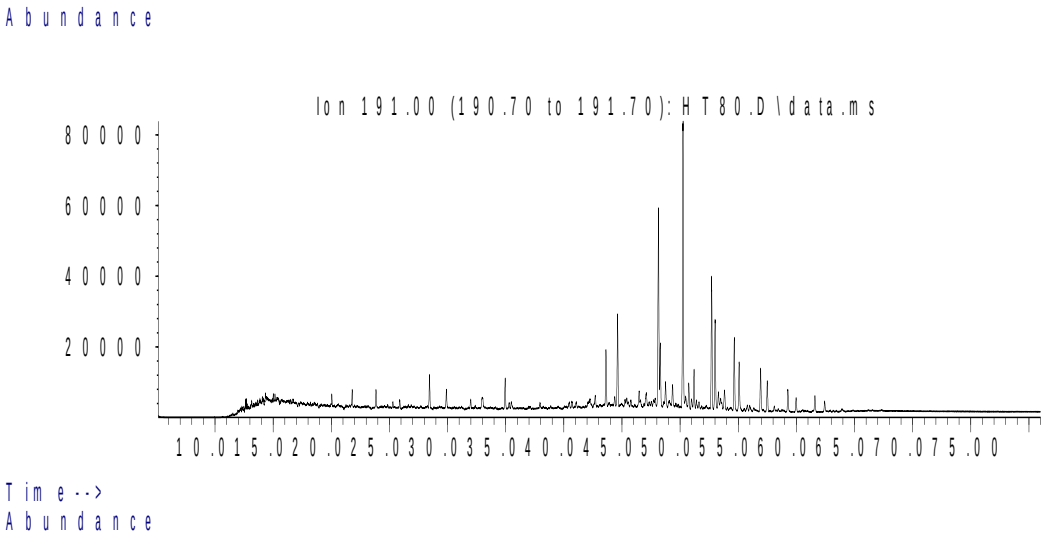

Sample 80 Inner Saturate Chromatograms; Steranes & Steroids

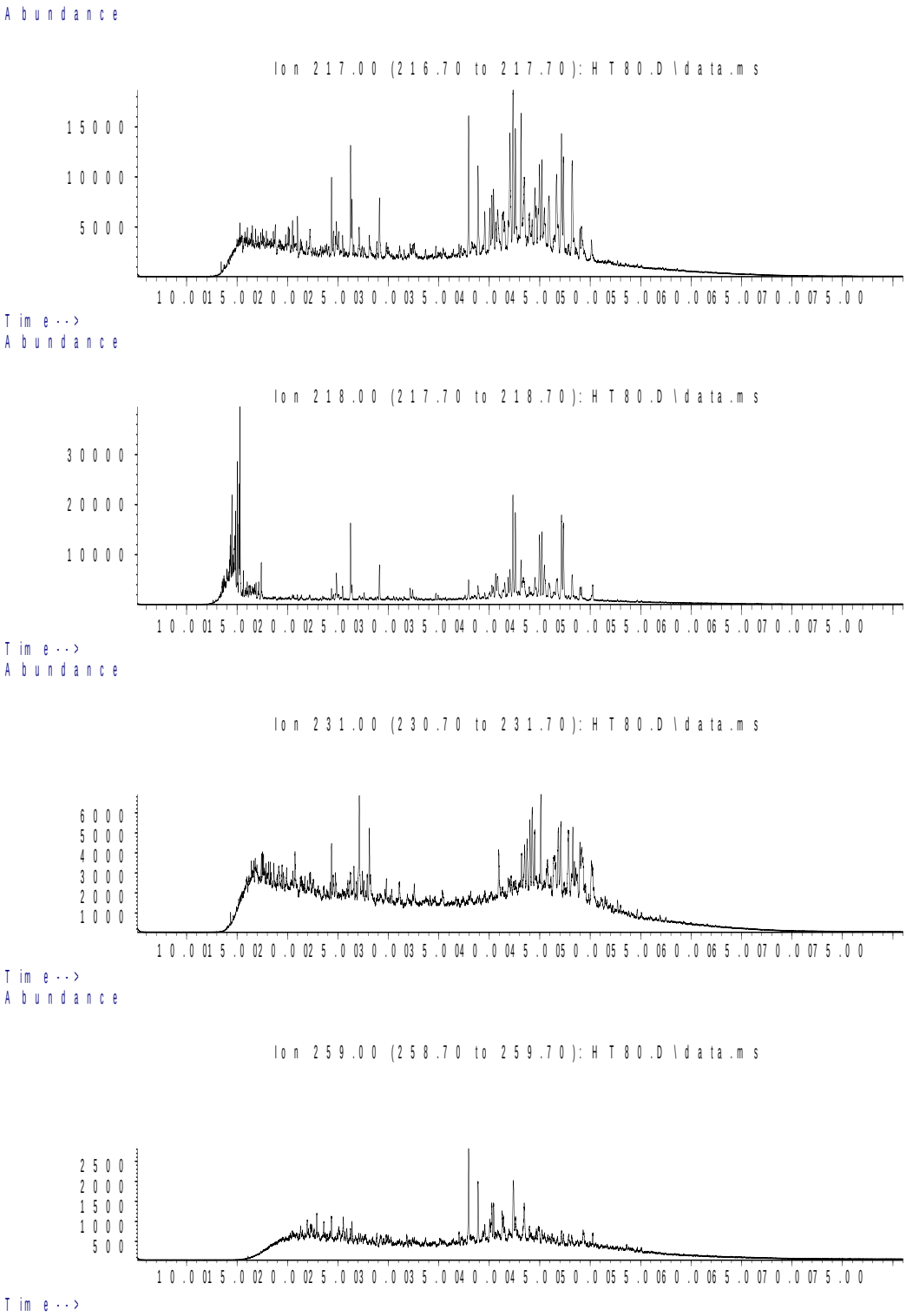

Sample 80 Outer

Bulk Properties

Saturate (%)	18.6
Aromatics (%)	11.7
Resin (%)	16.3
Asphaltene (%)	53.4

Whole Oil/Extract GC

Pristane/Phytane	1.09
Pristane/n-C17	0.45
Phytane/n-C18	0.42

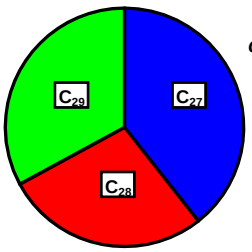

C_{27}-C_{28}-C_{29} αββ Steranes

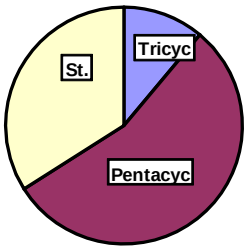

Tricyclic, Pentacyclic Terpanes & Steranes

Saturate Biomarker Interpretive Ratios

Interpretive Ratios	By Area
Terpanes (m/z 191)	
C19t/C23t	0.35
C22t/C21t	0.47
C22t/C24t	0.47
C24t/C23t	0.57
C26t/C25t	0.75
C24Tet/C23t	0.92
C24Tet/C26t	2.09
C23t/C30H	0.14
C24Tet/C30H	0.13
C28BNH/C30H	0.06
25-Nor/C30H	0.02
C29H/C30H	0.73
C30DiaH/C30H	0.08
Ole/C30H	0.00
C30Ts/C30H	0.08
Gam/C30H	0.05
Gam/C31HR	0.16
C35HS/C34HS	0.64
C35 Homohopane Index	0.04
Ts/(Ts+Tm)	0.39
C29Ts/(C29Ts+C29H)	0.22
Mor/C30H	0.12
C32 S/(S+R)	0.59
Steranes (m/z 217)	
% C27 ααα 20R	38.4
% C28 ααα 20R	23.5
% C29 ααα 20R	38.1
C27 Dia/(Dia+Reg)	0.54
(C21+C22)/(C27+C28+C29)	0.16
C29 αββ/(ααα+αββ)	0.53
C29 ααα 20S/20R	0.71
C29 ααα 20S/(S+R)	0.41
αββ−Steranes (m/z 218)	
% C27 αββ 20(R+S)	39.4
% C28 αββ 20(R+S)	27.7
% C29 αββ 20(R+S)	32.9
C29/C27 αββ Sterane Ratio	0.84
C27 Dia/Ster	0.65
Tricyclic/Pentacyclic Terpanes	0.20
Steranes/Terpanes	0.51
% Tricyclic Terpanes	11.1
% Pentacyclic Terpanes	54.9
% Steranes	34.0

Sample 80 Outer

Saturate Biomarker Integration Results (Terpanes)				
Ion	**Peak Label**	**Compound Name**	**R.Time (min.)**	**Peak Area**
191	C19t	C19 tricyclic diterpane	19.80	41248
191	C20t	C20 tricyclic diterpane	21.53	56746
191	C21t	C21 tricyclic diterpane	23.56	67779
191	C22t	C22 tricyclic terpane	25.58	31812
191	C23t	C23 tricyclic terpane	28.11	118517
191	C24t	C24 tricyclic terpane	29.55	67340
191	C25tS	C25 tricyclic terpane (S)	32.59	36721
191	C25tR	C25 tricyclic terpane (R)	32.59	33294
191	C24T	C24 tetracyclic terpane (TET)	34.57	109625
191	C26tS	C26 tricyclic terpane (S)	34.92	23180
191	C26tR	C26 tricyclic terpane (R)	35.12	29211
191	C28tS	C28 extended tricyclic terpane (S)	40.06	28943
191	C28tR	C28 extended tricyclic terpane (R)	40.69	25735
191	C29tS	C29 extended tricyclic terpane (S)	41.87	16285
191	C29tR	C29 extended tricyclic terpane (R)	42.30	38748
191	C30tS	C30 extended tricyclic terpane (S)	44.99	17973
191	C30tR	C30 extended tricyclic terpane (R)	45.37	25207
191	Ts	Ts 18a(H)-trisnorhopane	43.21	182602
191	Tm	Tm 17a(H)-trisnorhopane	44.21	289732
191	C28BNH	C28 17a18a21b(H)-bisnorhopane	46.66	51461
191	Nor25H	C29 Nor-25-hopane	47.31	18258
191	C29H	C29 Tm 17a(H)21b(H)-norhopane	47.72	635292
191	C29Ts	C29 Ts 18a(H)-norneohopane	47.88	176169
191	C30DiaH	C30 17a(H)-diahopane	48.33	70268
191	Normor	C29 normoretane	48.94	61065
191	a-Ole	a-oleanane	49.54	1633
191	b-Ole	b-oleanane	49.54	1633
191	C30H	C30 17a(H)-hopane	49.83	874620
191	C30Ts	17a(H)-30-nor-29-homohopane	50.34	74192
191	Mor	C30 moretane	50.77	107406
191	C31HS	C31 22S 17a(H) homohopane	52.30	355878
191	C31HR	C31 22R 17a(H) homohopane	52.60	252961
191	Gam	gammacerane	52.89	41534
191	C32HS	C32 22S 17a(H) bishomohopane	54.26	183275
191	C32HR	C32 22R 17a(H) bishomohopane	54.68	127050
191	C33HS	C33 22S 17a(H) trishomohopane	56.53	103479
191	C33HR	C33 22R 17a(H) trishomohopane	57.10	69309
191	C34HS	C34 22S 17a(H) extended hopane	58.89	49683
191	C34HR	C34 22R 17a(H) extended hopane	59.59	30539
191	C35HS	C35 22S 17a(H) extended hopane	61.21	31891
191	C35HR	C35 22R 17a(H) extended hopane	62.06	20845

Sample 80 Outer

Saturate Biomarker Integration Results (Steranes)				
Ion	**Peak Label**	**Compound Name**	**R.Time (min.)**	**Peak Area**
217	S21	C21 sterane	25.94	166201
217	S22	C22 sterane	28.77	89364
217	27DbaS	C27 ba 20S diacholestane	37.57	195082
217	27DbaR	C27 ba 20R diacholestane	38.51	133801
217	28DbaSA	C28 ba 20S diasterane a	39.66	72354
217	28DbaSB	C28 ba 20S diasterane b	39.87	60189
217	28DbaRA	C28 ba 20R diasterane a	40.91	46031
217	28DbaRB	C28 ba 20R diasterane b	41.13	31107
217	27aaS	C27 aa 20S cholestane	41.65	128286
217	27bbR	C27 bb 20R cholestane	41.95	243001
217	27bbS	C27 bb 20S cholestane	42.20	128280
217	27aaR	C27 aa 20R cholestane	42.74	150101
217	28aaS	C28 aa 20S ergostane	44.12	82387
217	28bbR	C28 bb 20R ergostane	44.56	90756
217	28bbS	C28 bb 20S ergostane	44.82	103587
217	28aaR	C28 aa 20R ergostane	45.50	91958
217	29aaS	C29 aa 20S stigmastane	46.27	104978
217	29bbR	C29 bb 20R stigmastane	46.76	180800
217	29bbS	C29 bb 20S stigmastane	46.93	110535
217	29aaR	C29 aa 20R stigmastane	47.83	148875
218	27bbR	C27 bb 20R cholestane	41.95	272942
218	27bbS	C27 bb 20S cholestane	42.19	203805
218	28bbR	C28 bb 20R ergostane	44.57	171910
218	28bbS	C28 bb 20S ergostane	44.82	163575
218	29bbR	C29 bb 20R stigmastane	46.75	225282
218	29bbS	C29 bb 20S stigmastane	46.94	172983
259	27DbaS	C27 ba 20S diacholestane	37.56	128286
259	27DbaR	C27 ba 20R diacholestane	38.50	83563
259	28DbaSA	C28 ba 20S diaergostane a	39.87	37350
259	28DbaSB	C28 ba 20S diaergostane b	40.05	47040
259	28DbaRA	C28 ba 20R diaergostane a	40.91	35873
259	28DbaRB	C28 ba 20R diaergostane b	41.13	14174
259	29DbaS	C29 ba 20S diastigmastane	41.99	86752
259	29DbaR	C29 ba 20R diastigmastane	43.57	17823
259	30TP1	C30 Terpane	47.45	13047
259	30TP2	C30 Terpane	47.75	11140

Sample 80 Outer Saturate Chromatograms; Terpanes

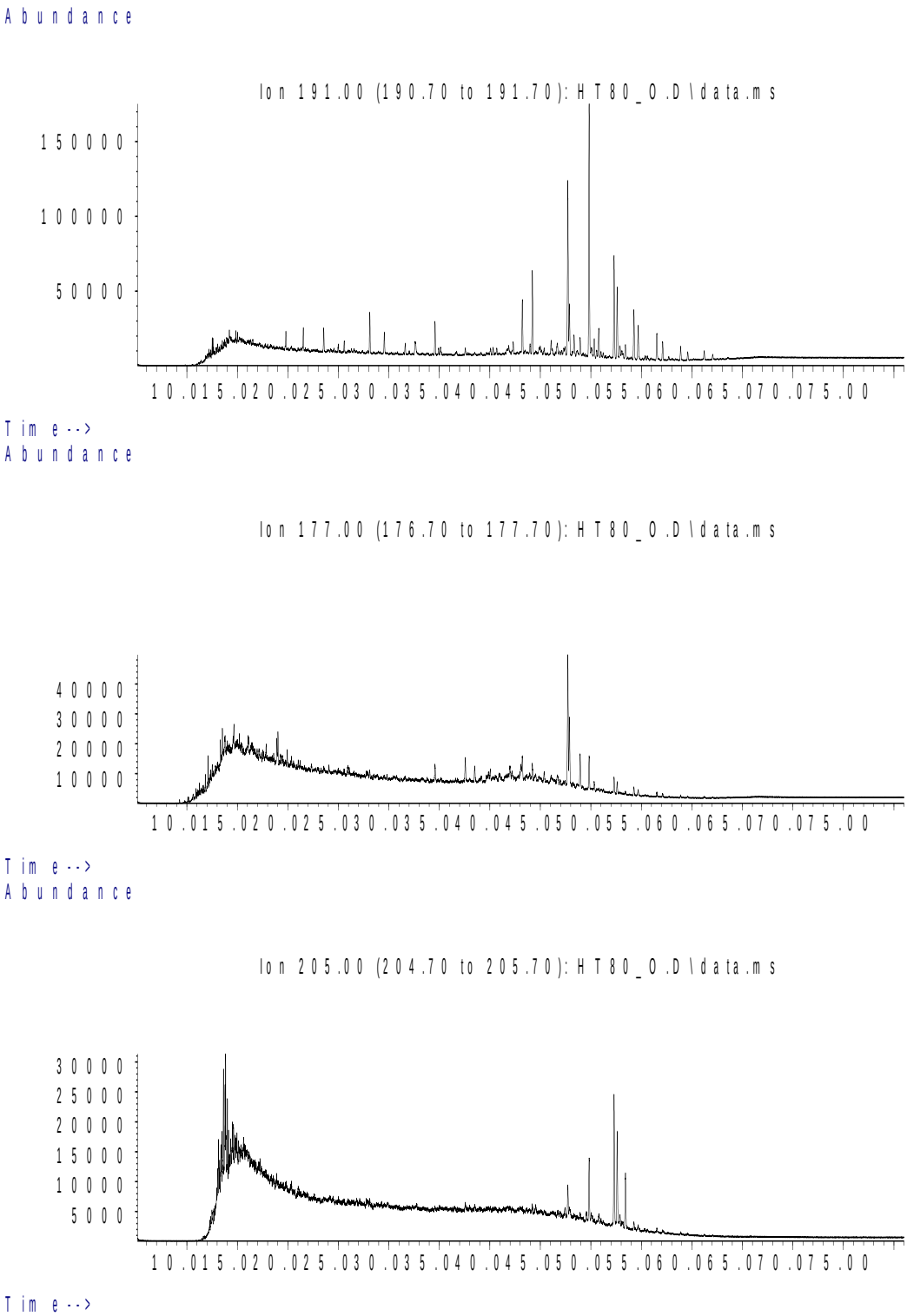

Sample 80 Outer Saturate Chromatograms; Steranes & Steroids

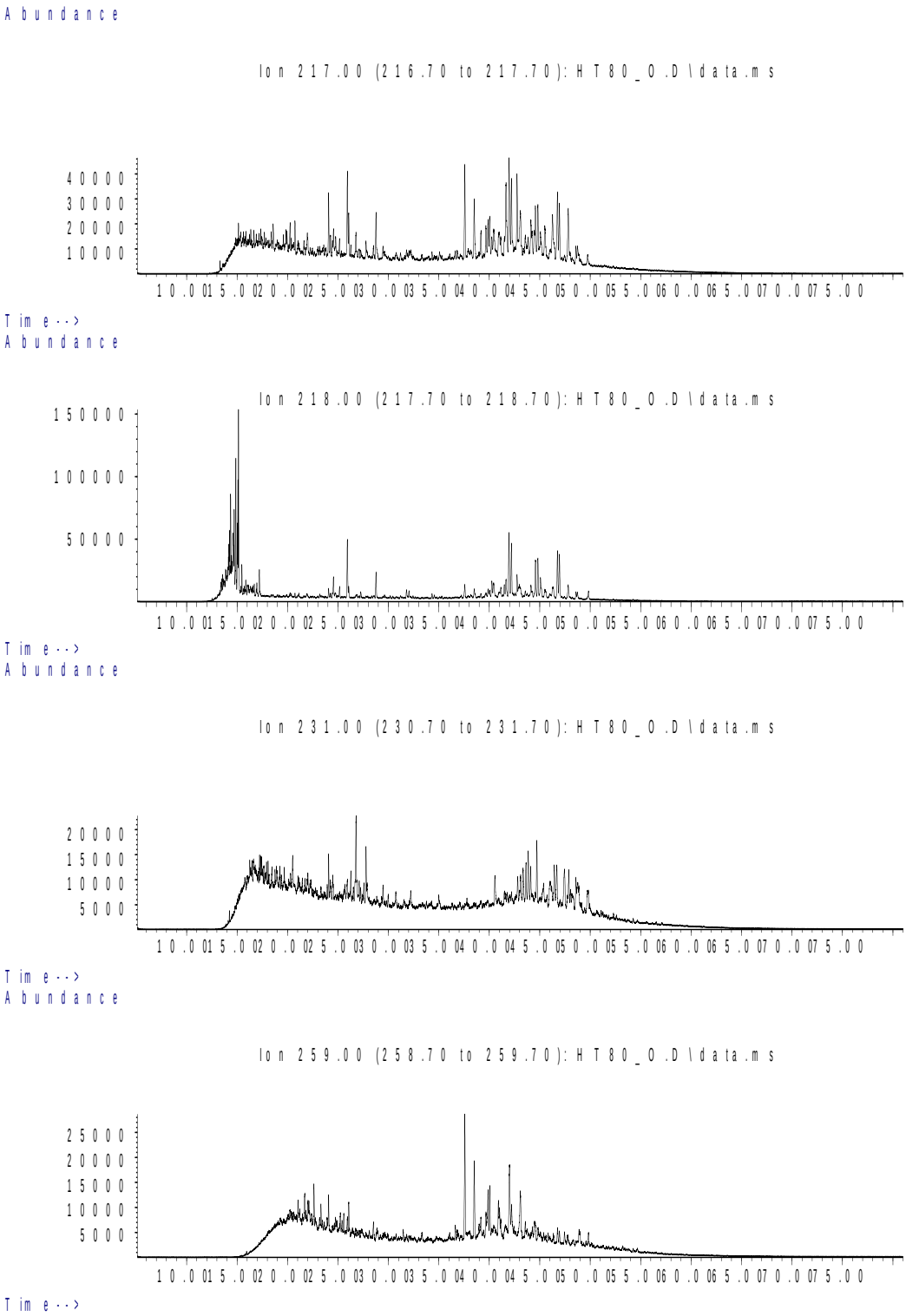

Sample 85 Inner

Bulk Properties

Saturate (%)	21.6
Aromatics (%)	12.7
Resin (%)	14.7
Asphaltene (%)	51.0

Whole Oil/Extract GC

Pristane/Phytane	1.07
Pristane/n-C17	0.58
Phytane/n-C18	0.52

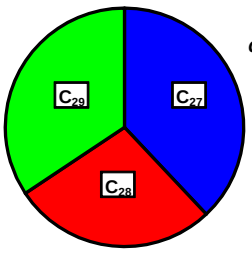

C_{27}-C_{28}-C_{29} αββ Steranes

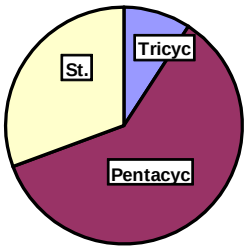

Tricyclic, Pentacyclic Terpanes & Steranes

Saturate Biomarker Interpretive Ratios

Interpretive Ratios	By Area
Terpanes (m/z 191)	
C19t/C23t	0.27
C22t/C21t	0.56
C22t/C24t	0.50
C24t/C23t	0.57
C26t/C25t	0.72
C24Tet/C23t	0.94
C24Tet/C26t	2.18
C23t/C30H	0.11
C24Tet/C30H	0.10
C28BNH/C30H	0.06
25-Nor/C30H	0.03
C29H/C30H	0.70
C30DiaH/C30H	0.09
Ole/C30H	0.00
C30Ts/C30H	0.09
Gam/C30H	0.05
Gam/C31HR	0.17
C35HS/C34HS	0.68
C35 Homohopane Index	0.06
Ts/(Ts+Tm)	0.39
C29Ts/(C29Ts+C29H)	0.22
Mor/C30H	0.13
C32 S/(S+R)	0.59
Steranes (m/z 217)	
% C27 ααα 20R	35.0
% C28 ααα 20R	25.0
% C29 ααα 20R	40.1
C27 Dia/(Dia+Reg)	0.53
(C21+C22)/(C27+C28+C29)	0.13
C29 αββ/(ααα+αββ)	0.51
C29 ααα 20S/20R	0.72
C29 ααα 20S/(S+R)	0.42
αββ−Steranes (m/z 218)	
% C27 αββ 20(R+S)	38.0
% C28 αββ 20(R+S)	27.7
% C29 αββ 20(R+S)	34.3
C29/C27 αββ Sterane Ratio	0.90
C27 Dia/Ster	0.62
Tricyclic/Pentacyclic Terpanes	0.15
Steranes/Terpanes	0.44
% Tricyclic Terpanes	9.2
% Pentacyclic Terpanes	60.2
% Steranes	30.6

Sample 85 Inner

Saturate Biomarker Integration Results (Terpanes)				
Ion	**Peak Label**	**Compound Name**	**R.Time (min.)**	**Peak Area**
191	C19t	C19 tricyclic diterpane	20.054	13503
191	C20t	C20 tricyclic diterpane	21.814	21388
191	C21t	C21 tricyclic diterpane	23.857	25346
191	C22t	C22 tricyclic terpane	25.905	14252
191	C23t	C23 tricyclic terpane	28.468	50248
191	C24t	C24 tricyclic terpane	29.921	28594
191	C25tS	C25 tricyclic terpane (S)	32.979	16531
191	C25tR	C25 tricyclic terpane (R)	32.979	13565
191	C24T	C24 tetracyclic terpane (TET)	34.971	47280
191	C26tS	C26 tricyclic terpane (S)	35.301	10169
191	C26tR	C26 tricyclic terpane (R)	35.499	11567
191	C28tS	C28 extended tricyclic terpane (S)	40.714	12120
191	C28tR	C28 extended tricyclic terpane (R)	41.091	10429
191	C29tS	C29 extended tricyclic terpane (S)	42.266	6716
191	C29tR	C29 extended tricyclic terpane (R)	42.719	21093
191	C30tS	C30 extended tricyclic terpane (S)	45.414	9184
191	C30tR	C30 extended tricyclic terpane (R)	45.758	11480
191	Ts	Ts 18a(H)-trisnorhopane	43.639	91721
191	Tm	Tm 17a(H)-trisnorhopane	44.645	144091
191	C28BNH	C28 17a18a21b(H)-bisnorhopane	47.108	27790
191	Nor25H	C29 Nor-25-hopane	47.877	13461
191	C29H	C29 Tm 17a(H)21b(H)-norhopane	48.155	329451
191	C29Ts	C29 Ts 18a(H)-norneohopane	48.311	93073
191	C30DiaH	C30 17a(H)-diahopane	48.764	43859
191	Normor	C29 normoretane	49.373	33900
191	a-Ole	a-oleanane	49.982	487
191	b-Ole	b-oleanane	49.982	487
191	C30H	C30 17a(H)-hopane	50.27	469025
191	C30Ts	17a(H)-30-nor-29-homohopane	50.765	42365
191	Mor	C30 moretane	51.213	60213
191	C31HS	C31 22S 17a(H) homohopane	52.719	203773
191	C31HR	C31 22R 17a(H) homohopane	53.021	146253
191	Gam	gammacerane	53.313	25464
191	C32HS	C32 22S 17a(H) bishomohopane	54.672	111186
191	C32HR	C32 22R 17a(H) bishomohopane	55.088	76237
191	C33HS	C33 22S 17a(H) trishomohopane	56.923	68421
191	C33HR	C33 22R 17a(H) trishomohopane	57.509	44680
191	C34HS	C34 22S 17a(H) extended hopane	59.278	36354
191	C34HR	C34 22R 17a(H) extended hopane	59.977	21655
191	C35HS	C35 22S 17a(H) extended hopane	61.605	24549
191	C35HR	C35 22R 17a(H) extended hopane	62.435	16748

Sample 85 Inner

Saturate Biomarker Integration Results (Steranes)				
Ion	**Peak Label**	**Compound Name**	**R.Time (min.)**	**Peak Area**
217	S21	C21 sterane	26.26	64318
217	S22	C22 sterane	29.13	33292
217	27DbaS	C27 ba 20S diacholestane	37.97	82913
217	27DbaR	C27 ba 20R diacholestane	38.91	60226
217	28DbaSA	C28 ba 20S diasterane a	40.28	27108
217	28DbaSB	C28 ba 20S diasterane b	40.43	38211
217	28DbaRA	C28 ba 20R diasterane a	41.31	22673
217	28DbaRB	C28 ba 20R diasterane b	41.31	15115
217	27aaS	C27 aa 20S cholestane	42.07	64329
217	27bbR	C27 bb 20R cholestane	42.38	113868
217	27bbS	C27 bb 20S cholestane	42.61	56458
217	27aaR	C27 aa 20R cholestane	43.15	64248
217	28aaS	C28 aa 20S ergostane	44.54	37246
217	28bbR	C28 bb 20R ergostane	44.99	46738
217	28bbS	C28 bb 20S ergostane	45.23	49801
217	28aaR	C28 aa 20R ergostane	45.91	45831
217	29aaS	C29 aa 20S stigmastane	46.69	52615
217	29bbR	C29 bb 20R stigmastane	47.16	75543
217	29bbS	C29 bb 20S stigmastane	47.35	56894
217	29aaR	C29 aa 20R stigmastane	48.24	73573
218	27bbR	C27 bb 20R cholestane	42.36	121859
218	27bbS	C27 bb 20S cholestane	42.61	88724
218	28bbR	C28 bb 20R ergostane	44.99	77720
218	28bbS	C28 bb 20S ergostane	45.23	75747
218	29bbR	C29 bb 20R stigmastane	47.16	102396
218	29bbS	C29 bb 20S stigmastane	47.36	87988
259	27DbaS	C27 ba 20S diacholestane	37.97	13673
259	27DbaR	C27 ba 20R diacholestane	38.91	9450
259	28DbaSA	C28 ba 20S diaergostane a	40.28	3810
259	28DbaSB	C28 ba 20S diaergostane b	40.44	4400
259	28DbaRA	C28 ba 20R diaergostane a	41.31	4218
259	28DbaRB	C28 ba 20R diaergostane b	41.41	1694
259	29DbaS	C29 ba 20S diastigmastane	42.41	11728
259	29DbaR	C29 ba 20R diastigmastane	43.98	2212
259	30TP1	C30 Terpane	47.88	1450
259	30TP2	C30 Terpane	48.17	1389

Sample 85 Inner Saturate Chromatograms; Terpanes

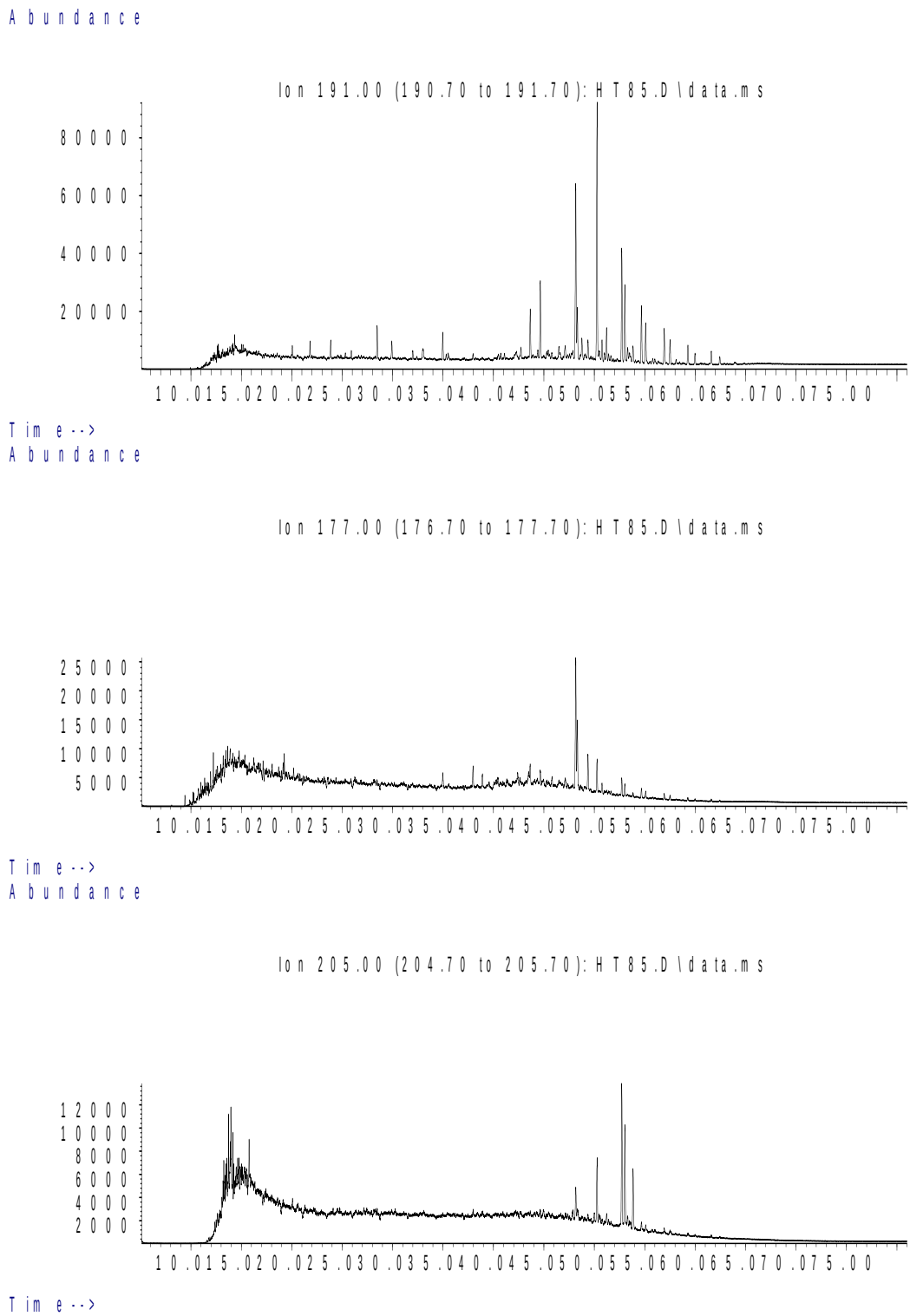

Sample 85 Inner Saturate Chromatograms; Steranes & Steroids

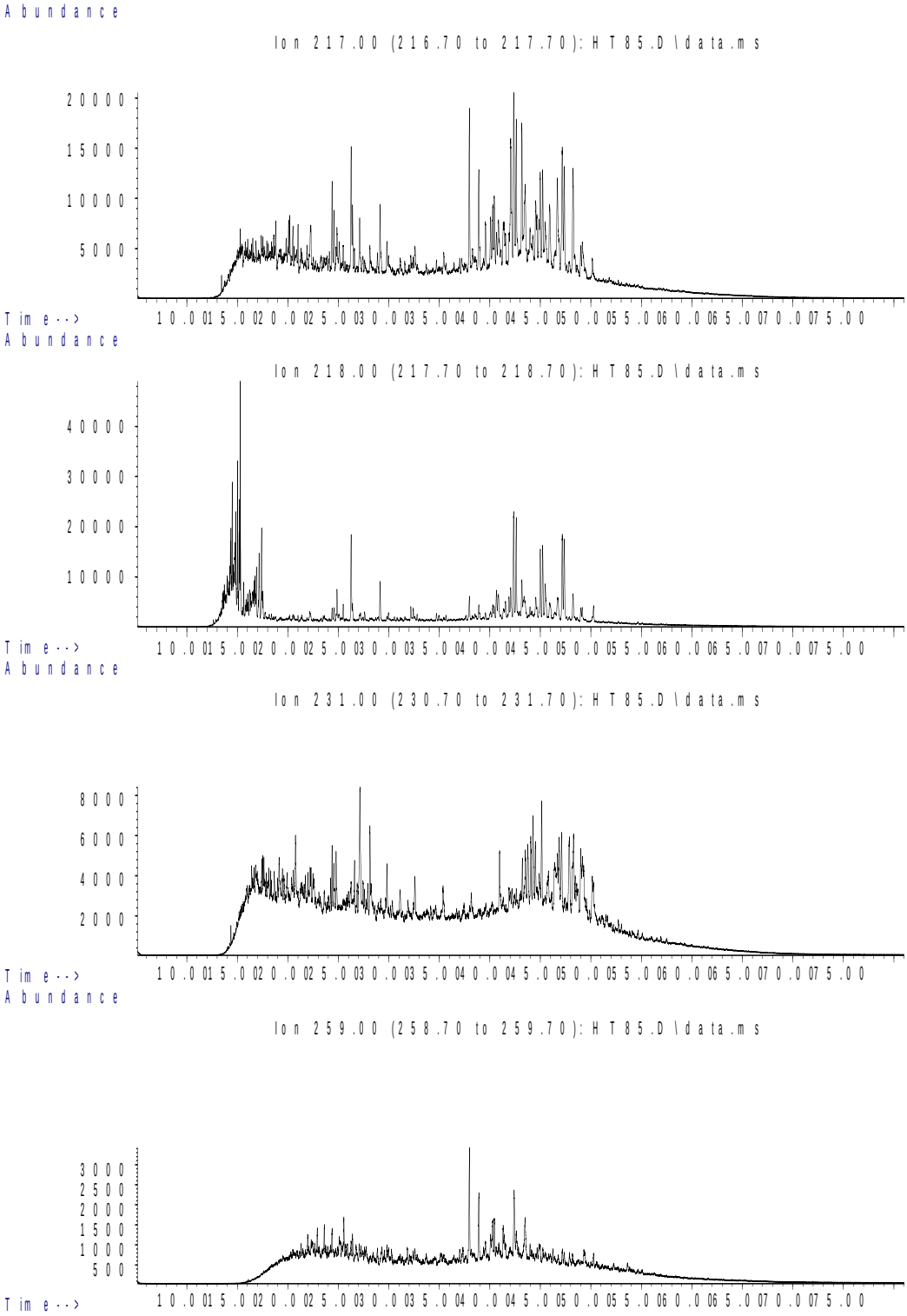

Sample 85 Outer

Bulk Properties

Saturate (%)	21.8
Aromatics (%)	11.9
Resin (%)	15.9
Asphaltene (%)	50.4

Whole Oil/Extract GC

Pristane/Phytane	1.15
Pristane/n-C17	0.58
Phytane/n-C18	0.49

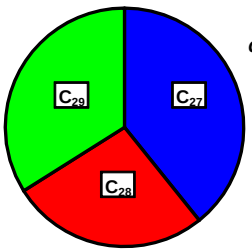

C_{27}-C_{28}-C_{29} αββ Steranes

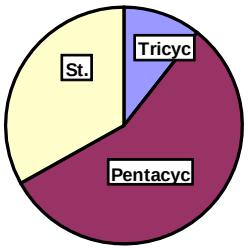

Tricyclic, Pentacyclic Terpanes & Steranes

Saturate Biomarker Interpretive Ratios

Interpretive Ratios	By Area
Terpanes (m/z 191)	
C19t/C23t	0.33
C22t/C21t	0.43
C22t/C24t	0.45
C24t/C23t	0.57
C26t/C25t	0.79
C24Tet/C23t	0.81
C24Tet/C26t	1.94
C23t/C30H	0.13
C24Tet/C30H	0.11
C28BNH/C30H	0.05
25-Nor/C30H	0.02
C29H/C30H	0.70
C30DiaH/C30H	0.09
Ole/C30H	0.00
C30Ts/C30H	0.09
Gam/C30H	0.05
Gam/C31HR	0.15
C35HS/C34HS	0.60
C35 Homohopane Index	0.04
Ts/(Ts+Tm)	0.39
C29Ts/(C29Ts+C29H)	0.23
Mor/C30H	0.11
C32 S/(S+R)	0.61
Steranes (m/z 217)	
% C27 ααα 20R	40.3
% C28 ααα 20R	25.0
% C29 ααα 20R	34.7
C27 Dia/(Dia+Reg)	0.49
(C21+C22)/(C27+C28+C29)	0.15
C29 αββ/(ααα+αββ)	0.54
C29 ααα 20S/20R	0.78
C29 ααα 20S/(S+R)	0.44
αββ−Steranes (m/z 218)	
% C27 αββ 20(R+S)	39.2
% C28 αββ 20(R+S)	26.8
% C29 αββ 20(R+S)	33.9
C29/C27 αββ Sterane Ratio	0.86
C27 Dia/Ster	0.56
Tricyclic/Pentacyclic Terpanes	0.19
Steranes/Terpanes	0.49
% Tricyclic Terpanes	10.6
% Pentacyclic Terpanes	56.3
% Steranes	33.1

Sample 85 Outer

Saturate Biomarker Integration Results (Terpanes)				
Ion	**Peak Label**	**Compound Name**	**R.Time (min.)**	**Peak Area**
191	C19t	C19 tricyclic diterpane	19.77	26406
191	C20t	C20 tricyclic diterpane	21.50	37678
191	C21t	C21 tricyclic diterpane	23.51	47209
191	C22t	C22 tricyclic terpane	25.54	20205
191	C23t	C23 tricyclic terpane	28.08	80249
191	C24t	C24 tricyclic terpane	29.51	45345
191	C25tS	C25 tricyclic terpane (S)	32.55	20897
191	C25tR	C25 tricyclic terpane (R)	32.55	21927
191	C24T	C24 tetracyclic terpane (TET)	34.53	65305
191	C26tS	C26 tricyclic terpane (S)	34.87	14487
191	C26tR	C26 tricyclic terpane (R)	35.08	19255
191	C28tS	C28 extended tricyclic terpane (S)	40.01	14939
191	C28tR	C28 extended tricyclic terpane (R)	40.63	13691
191	C29tS	C29 extended tricyclic terpane (S)	41.84	12855
191	C29tR	C29 extended tricyclic terpane (R)	42.29	29561
191	C30tS	C30 extended tricyclic terpane (S)	44.97	13225
191	C30tR	C30 extended tricyclic terpane (R)	45.34	16041
191	Ts	Ts 18a(H)-trisnorhopane	43.18	123487
191	Tm	Tm 17a(H)-trisnorhopane	44.17	192966
191	C28BNH	C28 17a18a21b(H)-bisnorhopane	46.67	32942
191	Nor25H	C29 Nor-25-hopane	47.40	11631
191	C29H	C29 Tm 17a(H)21b(H)-norhopane	47.69	424483
191	C29Ts	C29 Ts 18a(H)-norneohopane	47.85	127500
191	C30DiaH	C30 17a(H)-diahopane	48.32	57099
191	Normor	C29 normoretane	48.91	40492
191	a-Ole	a-oleanane	49.53	978
191	b-Ole	b-oleanane	49.53	978
191	C30H	C30 17a(H)-hopane	49.79	605187
191	C30Ts	17a(H)-30-nor-29-homohopane	50.31	52177
191	Mor	C30 moretane	50.76	66690
191	C31HS	C31 22S 17a(H) homohopane	52.28	255327
191	C31HR	C31 22R 17a(H) homohopane	52.58	180838
191	Gam	gammacerane	52.87	27706
191	C32HS	C32 22S 17a(H) bishomohopane	54.24	135883
191	C32HR	C32 22R 17a(H) bishomohopane	54.67	88093
191	C33HS	C33 22S 17a(H) trishomohopane	56.51	79377
191	C33HR	C33 22R 17a(H) trishomohopane	57.09	51281
191	C34HS	C34 22S 17a(H) extended hopane	58.88	40561
191	C34HR	C34 22R 17a(H) extended hopane	59.59	22366
191	C35HS	C35 22S 17a(H) extended hopane	61.21	24376
191	C35HR	C35 22R 17a(H) extended hopane	62.05	14792

Sample 85 Outer

Saturate Biomarker Integration Results (Steranes)				
Ion	**Peak Label**	**Compound Name**	**R.Time (min.)**	**Peak Area**
217	S21	C21 sterane	25.89	104695
217	S22	C22 sterane	28.73	56406
217	27DbaS	C27 ba 20S diacholestane	37.53	121708
217	27DbaR	C27 ba 20R diacholestane	38.46	90549
217	28DbaSA	C28 ba 20S diasterane a	39.63	44747
217	28DbaSB	C28 ba 20S diasterane b	39.84	40556
217	28DbaRA	C28 ba 20R diasterane a	40.89	27288
217	28DbaRB	C28 ba 20R diasterane b	41.10	23104
217	27aaS	C27 aa 20S cholestane	41.61	121859
217	27bbR	C27 bb 20R cholestane	41.92	166425
217	27bbS	C27 bb 20S cholestane	42.16	87537
217	27aaR	C27 aa 20R cholestane	42.71	100742
217	28aaS	C28 aa 20S ergostane	44.09	55362
217	28bbR	C28 bb 20R ergostane	44.54	61716
217	28bbS	C28 bb 20S ergostane	44.78	63210
217	28aaR	C28 aa 20R ergostane	45.48	62419
217	29aaS	C29 aa 20S stigmastane	46.24	67345
217	29bbR	C29 bb 20R stigmastane	46.73	94473
217	29bbS	C29 bb 20S stigmastane	46.91	85208
217	29aaR	C29 aa 20R stigmastane	47.79	86746
218	27bbR	C27 bb 20R cholestane	41.91	180210
218	27bbS	C27 bb 20S cholestane	42.15	138937
218	28bbR	C28 bb 20R ergostane	44.54	111156
218	28bbS	C28 bb 20S ergostane	44.79	107132
218	29bbR	C29 bb 20R stigmastane	46.73	142108
218	29bbS	C29 bb 20S stigmastane	46.91	133918
259	27DbaS	C27 ba 20S diacholestane	37.53	80689
259	27DbaR	C27 ba 20R diacholestane	38.46	57298
259	28DbaSA	C28 ba 20S diaergostane a	39.83	24775
259	28DbaSB	C28 ba 20S diaergostane b	40.01	32176
259	28DbaRA	C28 ba 20R diaergostane a	40.87	22009
259	28DbaRB	C28 ba 20R diaergostane b	41.12	9285
259	29DbaS	C29 ba 20S diastigmastane	41.96	56767
259	29DbaR	C29 ba 20R diastigmastane	43.52	10426
259	30TP1	C30 Terpane	47.42	6944
259	30TP2	C30 Terpane	47.70	6336

Sample 85 Outer Saturate Chromatograms; Terpanes

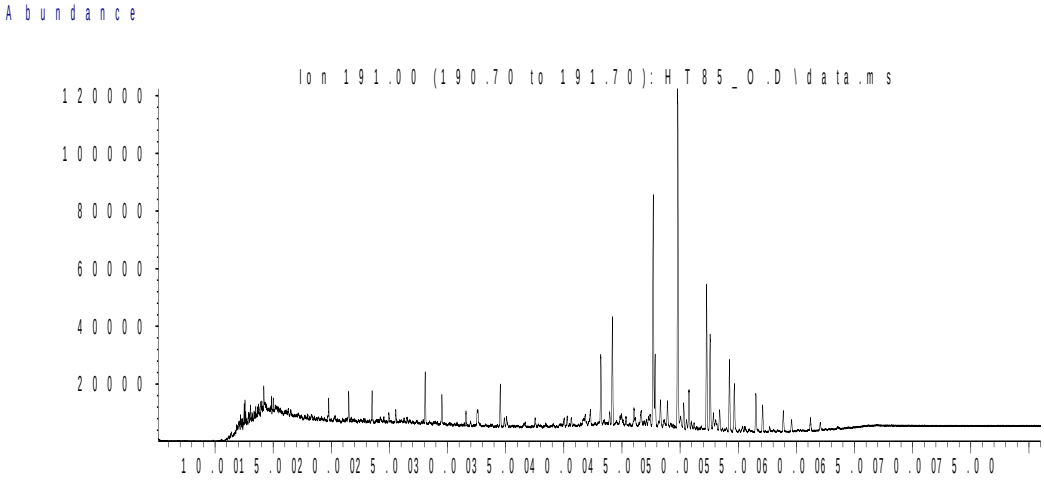

Sample 85 Outer Saturate Chromatograms; Steranes & Steroids

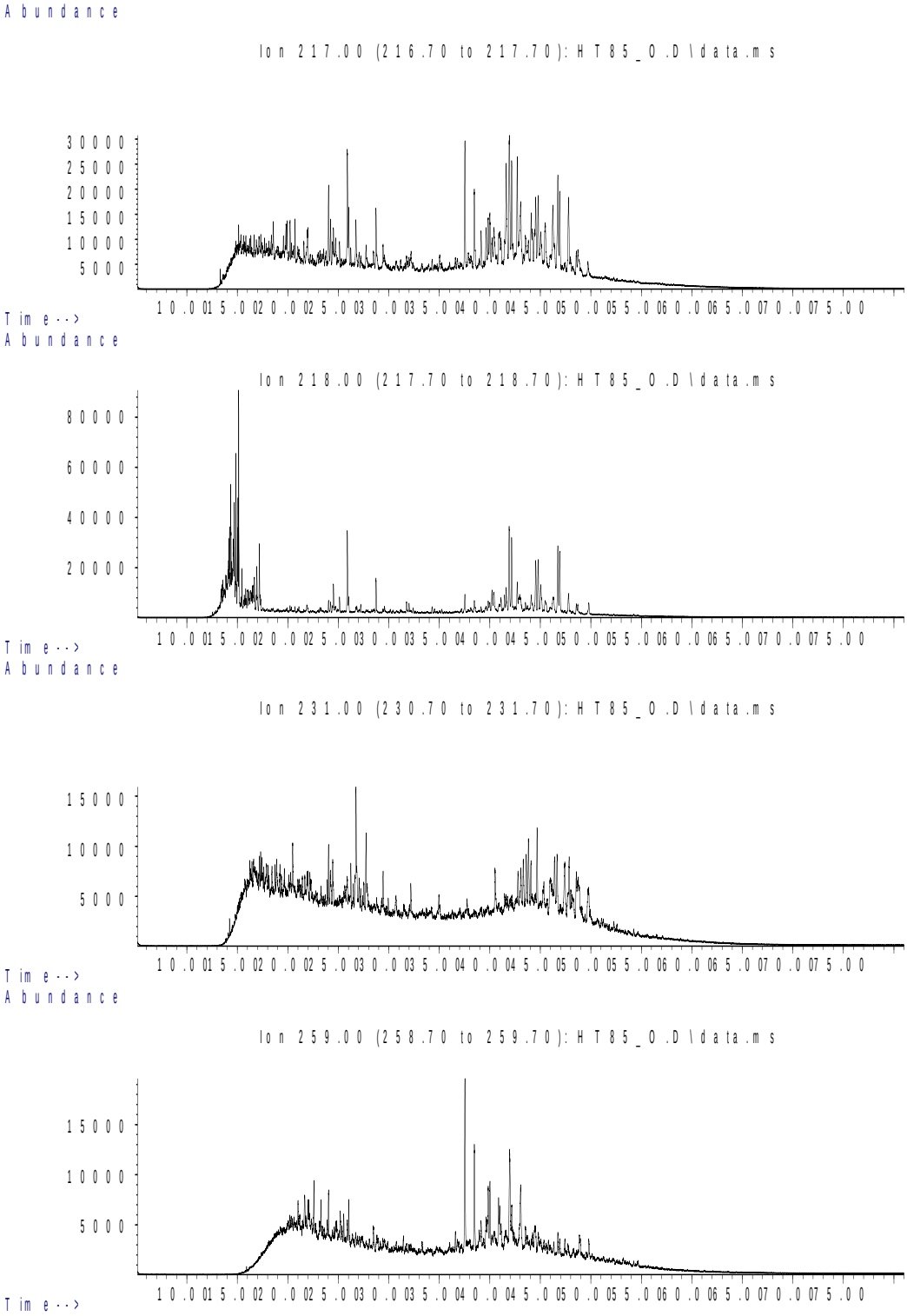

Sample 168 Inner

Bulk Properties

Saturate (%)	24.4
Aromatics (%)	13.6
Resin (%)	16.3
Asphaltene (%)	45.7

Whole Oil/Extract GC

Pristane/Phytane	1.14
Pristane/n-C17	0.48
Phytane/n-C18	0.41

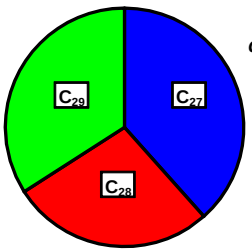

C_{27}-C_{28}-C_{29} αββ Steranes

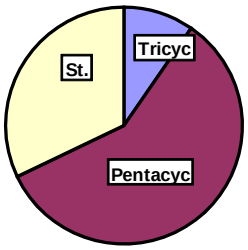

Tricyclic, Pentacyclic Terpanes & Steranes

Saturate Biomarker Interpretive Ratios

Interpretive Ratios	By Area
Terpanes (m/z 191)	
C19t/C23t	0.27
C22t/C21t	0.48
C22t/C24t	0.46
C24t/C23t	0.60
C26t/C25t	0.72
C24Tet/C23t	0.94
C24Tet/C26t	2.07
C23t/C30H	0.11
C24Tet/C30H	0.11
C28BNH/C30H	0.06
25-Nor/C30H	0.02
C29H/C30H	0.72
C30DiaH/C30H	0.08
Ole/C30H	0.00
C30Ts/C30H	0.09
Gam/C30H	0.05
Gam/C31HR	0.17
C35HS/C34HS	0.71
C35 Homohopane Index	0.05
Ts/(Ts+Tm)	0.38
C29Ts/(C29Ts+C29H)	0.21
Mor/C30H	0.13
C32 S/(S+R)	0.59
Steranes (m/z 217)	
% C27 ααα 20R	38.0
% C28 ααα 20R	23.3
% C29 ααα 20R	38.7
C27 Dia/(Dia+Reg)	0.53
(C21+C22)/(C27+C28+C29)	0.15
C29 αββ/(ααα+αββ)	0.52
C29 ααα 20S/20R	0.74
C29 ααα 20S/(S+R)	0.42
αββ−Steranes (m/z 218)	
% C27 αββ 20(R+S)	38.4
% C28 αββ 20(R+S)	27.5
% C29 αββ 20(R+S)	34.1
C29/C27 αββ Sterane Ratio	0.89
C27 Dia/Ster	0.63
Tricyclic/Pentacyclic Terpanes	0.16
Steranes/Terpanes	0.47
% Tricyclic Terpanes	9.6
% Pentacyclic Terpanes	58.3
% Steranes	32.1

Sample 168 Inner

Saturate Biomarker Integration Results (Terpanes)				
Ion	**Peak Label**	**Compound Name**	**R.Time (min.)**	**Peak Area**
191	C19t	C19 tricyclic diterpane	20.08	16017
191	C20t	C20 tricyclic diterpane	21.84	25776
191	C21t	C21 tricyclic diterpane	23.89	33575
191	C22t	C22 tricyclic terpane	25.93	16076
191	C23t	C23 tricyclic terpane	28.50	59268
191	C24t	C24 tricyclic terpane	29.95	35269
191	C25tS	C25 tricyclic terpane (S)	33.02	15122
191	C25tR	C25 tricyclic terpane (R)	33.02	22086
191	C24T	C24 tetracyclic terpane (TET)	35.01	55687
191	C26tS	C26 tricyclic terpane (S)	35.34	11636
191	C26tR	C26 tricyclic terpane (R)	35.53	15301
191	C28tS	C28 extended tricyclic terpane (S)	40.75	14219
191	C28tR	C28 extended tricyclic terpane (R)	41.11	12161
191	C29tS	C29 extended tricyclic terpane (S)	42.29	5706
191	C29tR	C29 extended tricyclic terpane (R)	42.75	20351
191	C30tS	C30 extended tricyclic terpane (S)	45.45	8934
191	C30tR	C30 extended tricyclic terpane (R)	45.80	14013
191	Ts	Ts 18a(H)-trisnorhopane	43.68	101246
191	Tm	Tm 17a(H)-trisnorhopane	44.67	164598
191	C28BNH	C28 17a18a21b(H)-bisnorhopane	47.13	31175
191	Nor25H	C29 Nor-25-hopane	47.75	12151
191	C29H	C29 Tm 17a(H)21b(H)-norhopane	48.17	370128
191	C29Ts	C29 Ts 18a(H)-norneohopane	48.32	96508
191	C30DiaH	C30 17a(H)-diahopane	48.78	40782
191	Normor	C29 normoretane	49.39	37708
191	a-Ole	a-oleanane	50.00	1141
191	b-Ole	b-oleanane	50.00	1141
191	C30H	C30 17a(H)-hopane	50.28	516443
191	C30Ts	17a(H)-30-nor-29-homohopane	50.78	46737
191	Mor	C30 moretane	51.23	65889
191	C31HS	C31 22S 17a(H) homohopane	52.73	220372
191	C31HR	C31 22R 17a(H) homohopane	53.04	159491
191	Gam	gammacerane	53.31	27411
191	C32HS	C32 22S 17a(H) bishomohopane	54.67	116503
191	C32HR	C32 22R 17a(H) bishomohopane	55.10	81809
191	C33HS	C33 22S 17a(H) trishomohopane	56.92	72018
191	C33HR	C33 22R 17a(H) trishomohopane	57.50	47109
191	C34HS	C34 22S 17a(H) extended hopane	59.28	36293
191	C34HR	C34 22R 17a(H) extended hopane	59.98	22428
191	C35HS	C35 22S 17a(H) extended hopane	61.59	25817
191	C35HR	C35 22R 17a(H) extended hopane	62.43	17100

Sample 168 Inner

Saturate Biomarker Integration Results (Steranes)				
Ion	**Peak Label**	**Compound Name**	**R.Time (min.)**	**Peak Area**
217	S21	C21 sterane	26.295	80988
217	S22	C22 sterane	29.173	46711
217	27DbaS	C27 ba 20S diacholestane	38.002	99510
217	27DbaR	C27 ba 20R diacholestane	38.941	70781
217	28DbaSA	C28 ba 20S diasterane a	40.31	31827
217	28DbaSB	C28 ba 20S diasterane b	40.466	44223
217	28DbaRA	C28 ba 20R diasterane a	41.339	29053
217	28DbaRB	C28 ba 20R diasterane b	41.339	13407
217	27aaS	C27 aa 20S cholestane	42.089	68780
217	27bbR	C27 bb 20R cholestane	42.391	130125
217	27bbS	C27 bb 20S cholestane	42.641	66902
217	27aaR	C27 aa 20R cholestane	43.198	83337
217	28aaS	C28 aa 20S ergostane	44.567	45078
217	28bbR	C28 bb 20R ergostane	45.005	50283
217	28bbS	C28 bb 20S ergostane	45.246	54828
217	28aaR	C28 aa 20R ergostane	45.93	51002
217	29aaS	C29 aa 20S stigmastane	46.69	62491
217	29bbR	C29 bb 20R stigmastane	47.186	94129
217	29bbS	C29 bb 20S stigmastane	47.379	64778
217	29aaR	C29 aa 20R stigmastane	48.252	84745
218	27bbR	C27 bb 20R cholestane	42.391	141516
218	27bbS	C27 bb 20S cholestane	42.632	101669
218	28bbR	C28 bb 20R ergostane	45.01	89690
218	28bbS	C28 bb 20S ergostane	45.251	84615
218	29bbR	C29 bb 20R stigmastane	47.19	117636
218	29bbS	C29 bb 20S stigmastane	47.384	98045
259	27DbaS	C27 ba 20S diacholestane	38.002	16792
259	27DbaR	C27 ba 20R diacholestane	38.937	10626
259	28DbaSA	C28 ba 20S diaergostane a	40.31	5000
259	28DbaSB	C28 ba 20S diaergostane b	40.475	5668
259	28DbaRA	C28 ba 20R diaergostane a	41.339	4518
259	28DbaRB	C28 ba 20R diaergostane b	41.424	1614
259	29DbaS	C29 ba 20S diastigmastane	42.424	11285
259	29DbaR	C29 ba 20R diastigmastane	44	2335
259	30TP1	C30 Terpane	47.893	1527
259	30TP2	C30 Terpane	48.191	1383

Sample 168 Inner Saturate Chromatograms; Terpanes

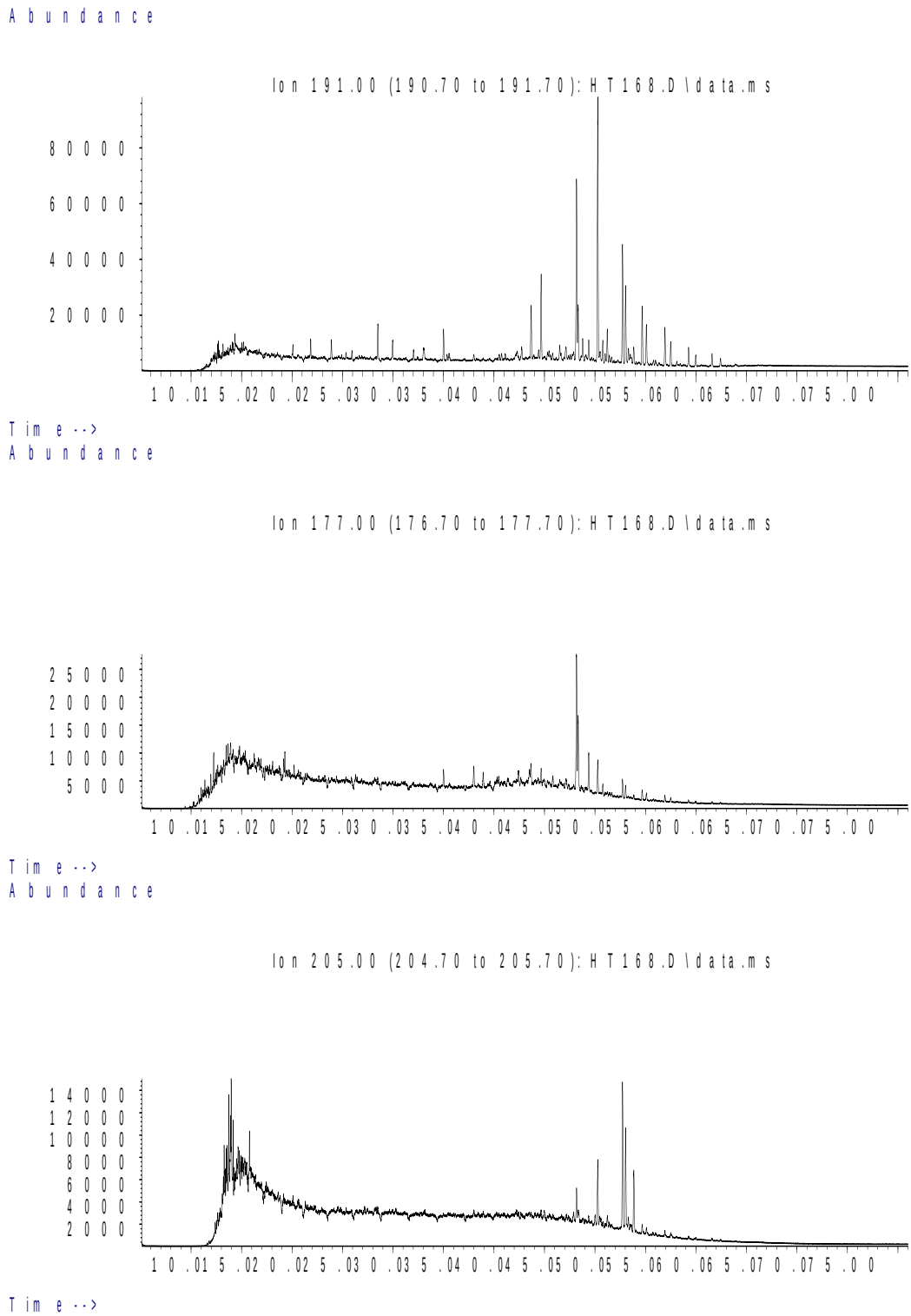

Sample 168 Inner Saturate Chromatograms; Steranes & Steroids

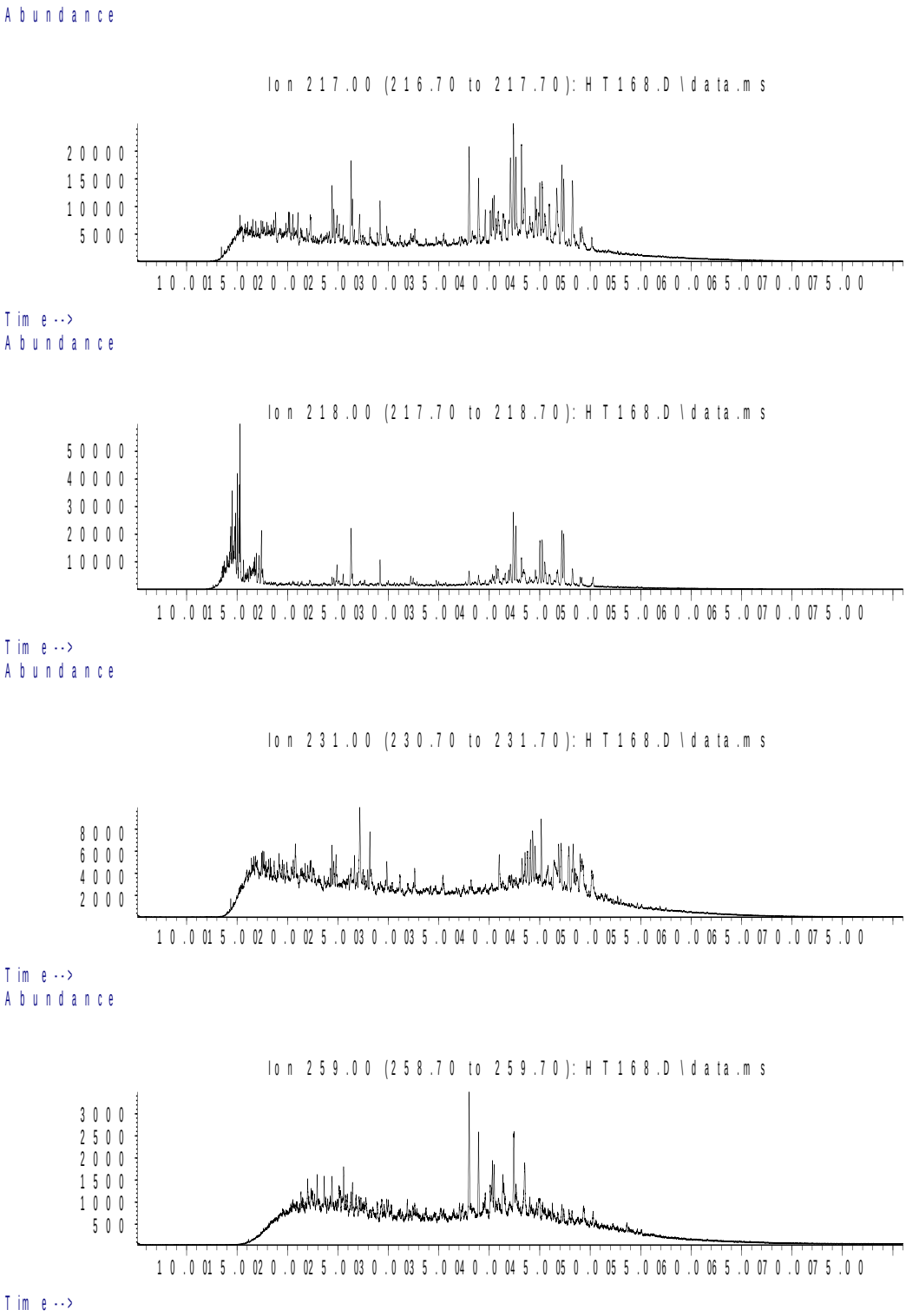

Sample 168 Outer

Bulk Properties

Saturate (%)	21.1
Aromatics (%)	10.8
Resin (%)	13.1
Asphaltene (%)	55.0

Whole Oil/Extract GC

Pristane/Phytane	1.05
Pristane/n-C17	0.46
Phytane/n-C18	0.44

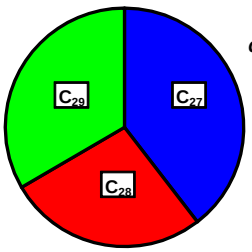

C_{27}-C_{28}-C_{29} αββ Steranes

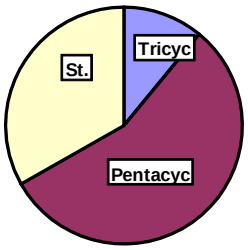

Tricyclic, Pentacyclic Terpanes & Steranes

Saturate Biomarker Interpretive Ratios

Interpretive Ratios	By Area
Terpanes (m/z 191)	
C19t/C23t	0.31
C22t/C21t	0.46
C22t/C24t	0.42
C24t/C23t	0.59
C26t/C25t	0.74
C24Tet/C23t	0.88
C24Tet/C26t	1.95
C23t/C30H	0.14
C24Tet/C30H	0.12
C28BNH/C30H	0.07
25-Nor/C30H	0.04
C29H/C30H	0.72
C30DiaH/C30H	0.09
Ole/C30H	0.01
C30Ts/C30H	0.08
Gam/C30H	0.05
Gam/C31HR	0.17
C35HS/C34HS	0.65
C35 Homohopane Index	0.04
Ts/(Ts+Tm)	0.40
C29Ts/(C29Ts+C29H)	0.22
Mor/C30H	0.12
C32 S/(S+R)	0.61
Steranes (m/z 217)	
% C27 ααα 20R	40.2
% C28 ααα 20R	24.4
% C29 ααα 20R	35.4
C27 Dia/(Dia+Reg)	0.53
(C21+C22)/(C27+C28+C29)	0.17
C29 αββ/(ααα+αββ)	0.56
C29 ααα 20S/20R	0.69
C29 ααα 20S/(S+R)	0.41
αββ−Steranes (m/z 218)	
% C27 αββ 20(R+S)	39.5
% C28 αββ 20(R+S)	27.1
% C29 αββ 20(R+S)	33.4
C29/C27 αββ Sterane Ratio	0.84
C27 Dia/Ster	0.63
Tricyclic/Pentacyclic Terpanes	0.20
Steranes/Terpanes	0.50
% Tricyclic Terpanes	11.0
% Pentacyclic Terpanes	55.8
% Steranes	33.2

Sample 168 Outer

Saturate Biomarker Integration Results (Terpanes)				
Ion	**Peak Label**	**Compound Name**	**R.Time (min.)**	**Peak Area**
191	C19t	C19 tricyclic diterpane	19.78	28554
191	C20t	C20 tricyclic diterpane	21.51	42253
191	C21t	C21 tricyclic diterpane	23.53	50126
191	C22t	C22 tricyclic terpane	25.54	23173
191	C23t	C23 tricyclic terpane	28.08	93341
191	C24t	C24 tricyclic terpane	29.52	54824
191	C25tS	C25 tricyclic terpane (S)	32.57	32264
191	C25tR	C25 tricyclic terpane (R)	32.57	25045
191	C24T	C24 tetracyclic terpane (TET)	34.54	82563
191	C26tS	C26 tricyclic terpane (S)	34.89	18825
191	C26tR	C26 tricyclic terpane (R)	35.09	23585
191	C28tS	C28 extended tricyclic terpane (S)	40.03	24818
191	C28tR	C28 extended tricyclic terpane (R)	40.65	15149
191	C29tS	C29 extended tricyclic terpane (S)	41.84	13626
191	C29tR	C29 extended tricyclic terpane (R)	42.28	31706
191	C30tS	C30 extended tricyclic terpane (S)	44.96	8829
191	C30tR	C30 extended tricyclic terpane (R)	45.36	18740
191	Ts	Ts 18a(H)-trisnorhopane	43.19	141954
191	Tm	Tm 17a(H)-trisnorhopane	44.18	211348
191	C28BNH	C28 17a18a21b(H)-bisnorhopane	46.66	44771
191	Nor25H	C29 Nor-25-hopane	47.40	24449
191	C29H	C29 Tm 17a(H)21b(H)-norhopane	47.69	490480
191	C29Ts	C29 Ts 18a(H)-norneohopane	47.86	140160
191	C30DiaH	C30 17a(H)-diahopane	48.32	58571
191	Normor	C29 normoretane	48.92	48651
191	a-Ole	a-oleanane	49.55	2625
191	b-Ole	b-oleanane	49.55	2625
191	C30H	C30 17a(H)-hopane	49.81	680323
191	C30Ts	17a(H)-30-nor-29-homohopane	50.31	56435
191	Mor	C30 moretane	50.77	82372
191	C31HS	C31 22S 17a(H) homohopane	52.28	281656
191	C31HR	C31 22R 17a(H) homohopane	52.58	201383
191	Gam	gammacerane	52.87	33450
191	C32HS	C32 22S 17a(H) bishomohopane	54.25	148127
191	C32HR	C32 22R 17a(H) bishomohopane	54.66	95895
191	C33HS	C33 22S 17a(H) trishomohopane	56.52	85489
191	C33HR	C33 22R 17a(H) trishomohopane	57.09	55547
191	C34HS	C34 22S 17a(H) extended hopane	58.88	40425
191	C34HR	C34 22R 17a(H) extended hopane	59.59	24479
191	C35HS	C35 22S 17a(H) extended hopane	61.21	26107
191	C35HR	C35 22R 17a(H) extended hopane	62.05	16614

Sample 168 Outer

Saturate Biomarker Integration Results (Steranes)				
Ion	**Peak Label**	**Compound Name**	**R.Time (min.)**	**Peak Area**
217	S21	C21 sterane	25.91	132024
217	S22	C22 sterane	28.74	65784
217	27DbaS	C27 ba 20S diacholestane	37.54	144381
217	27DbaR	C27 ba 20R diacholestane	38.47	106369
217	28DbaSA	C28 ba 20S diasterane a	39.64	50867
217	28DbaSB	C28 ba 20S diasterane b	39.84	45950
217	28DbaRA	C28 ba 20R diasterane a	40.88	26688
217	28DbaRB	C28 ba 20R diasterane b	41.12	28277
217	27aaS	C27 aa 20S cholestane	41.63	106923
217	27bbR	C27 bb 20R cholestane	41.92	195169
217	27bbS	C27 bb 20S cholestane	42.17	99604
217	27aaR	C27 aa 20R cholestane	42.72	114700
217	28aaS	C28 aa 20S ergostane	44.08	61348
217	28bbR	C28 bb 20R ergostane	44.54	71740
217	28bbS	C28 bb 20S ergostane	44.78	76462
217	28aaR	C28 aa 20R ergostane	45.47	69784
217	29aaS	C29 aa 20S stigmastane	46.24	69653
217	29bbR	C29 bb 20R stigmastane	46.73	118428
217	29bbS	C29 bb 20S stigmastane	46.93	95702
217	29aaR	C29 aa 20R stigmastane	47.79	100996
218	27bbR	C27 bb 20R cholestane	41.92	212642
218	27bbS	C27 bb 20S cholestane	42.17	159016
218	28bbR	C28 bb 20R ergostane	44.55	125897
218	28bbS	C28 bb 20S ergostane	44.78	128476
218	29bbR	C29 bb 20R stigmastane	46.73	164896
218	29bbS	C29 bb 20S stigmastane	46.92	148918
259	27DbaS	C27 ba 20S diacholestane	37.54	95266
259	27DbaR	C27 ba 20R diacholestane	38.47	63247
259	28DbaSA	C28 ba 20S diaergostane a	39.84	25175
259	28DbaSB	C28 ba 20S diaergostane b	40.02	37452
259	28DbaRA	C28 ba 20R diaergostane a	40.88	26743
259	28DbaRB	C28 ba 20R diaergostane b	41.11	7459
259	29DbaS	C29 ba 20S diastigmastane	41.97	75725
259	29DbaR	C29 ba 20R diastigmastane	43.55	13861
259	30TP1	C30 Terpane	47.42	7520
259	30TP2	C30 Terpane	47.71	7560

Sample 168 Outer Saturate Chromatograms; Terpanes

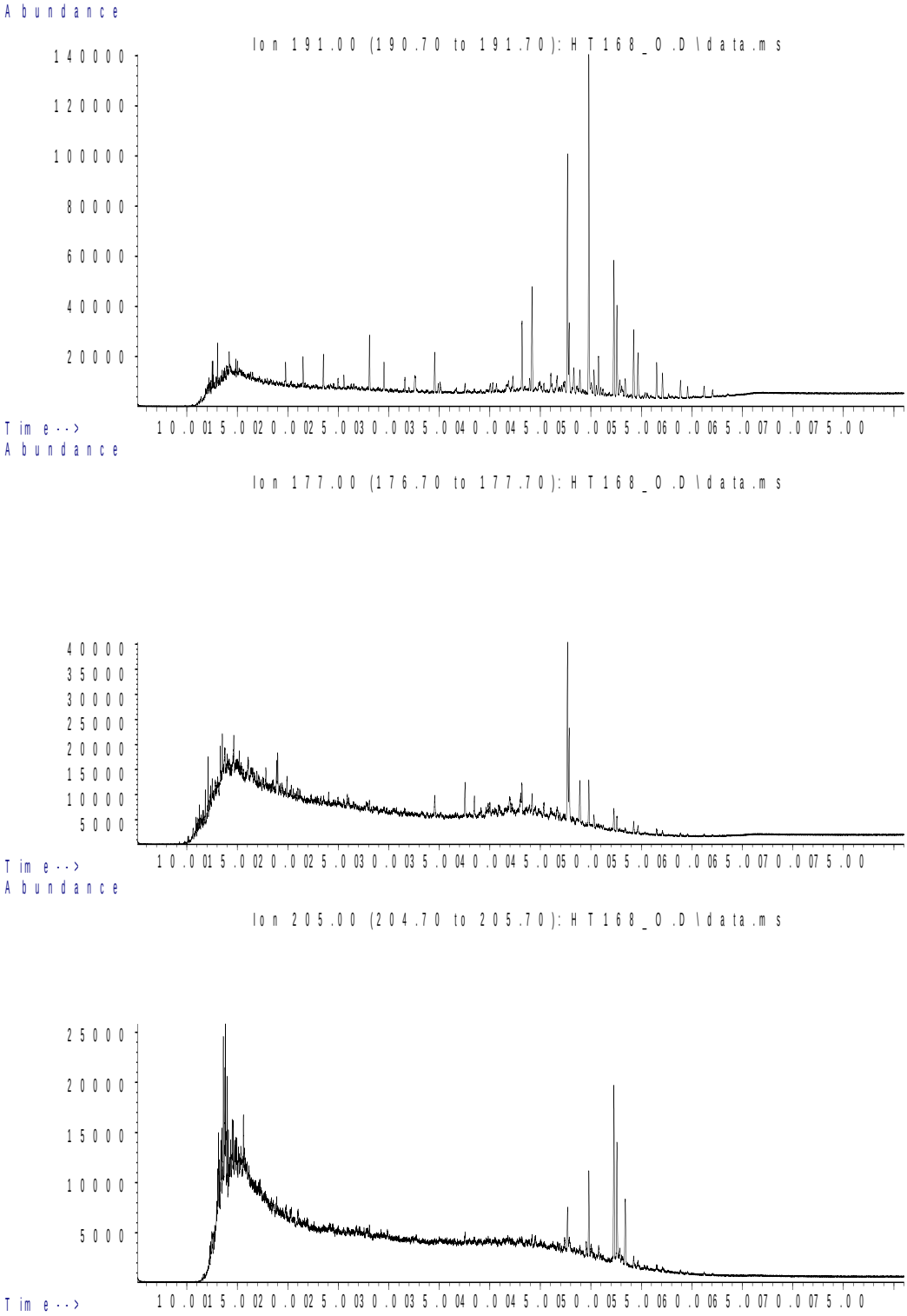

Sample 168 Outer Saturate Chromatograms; Steranes & Steroids

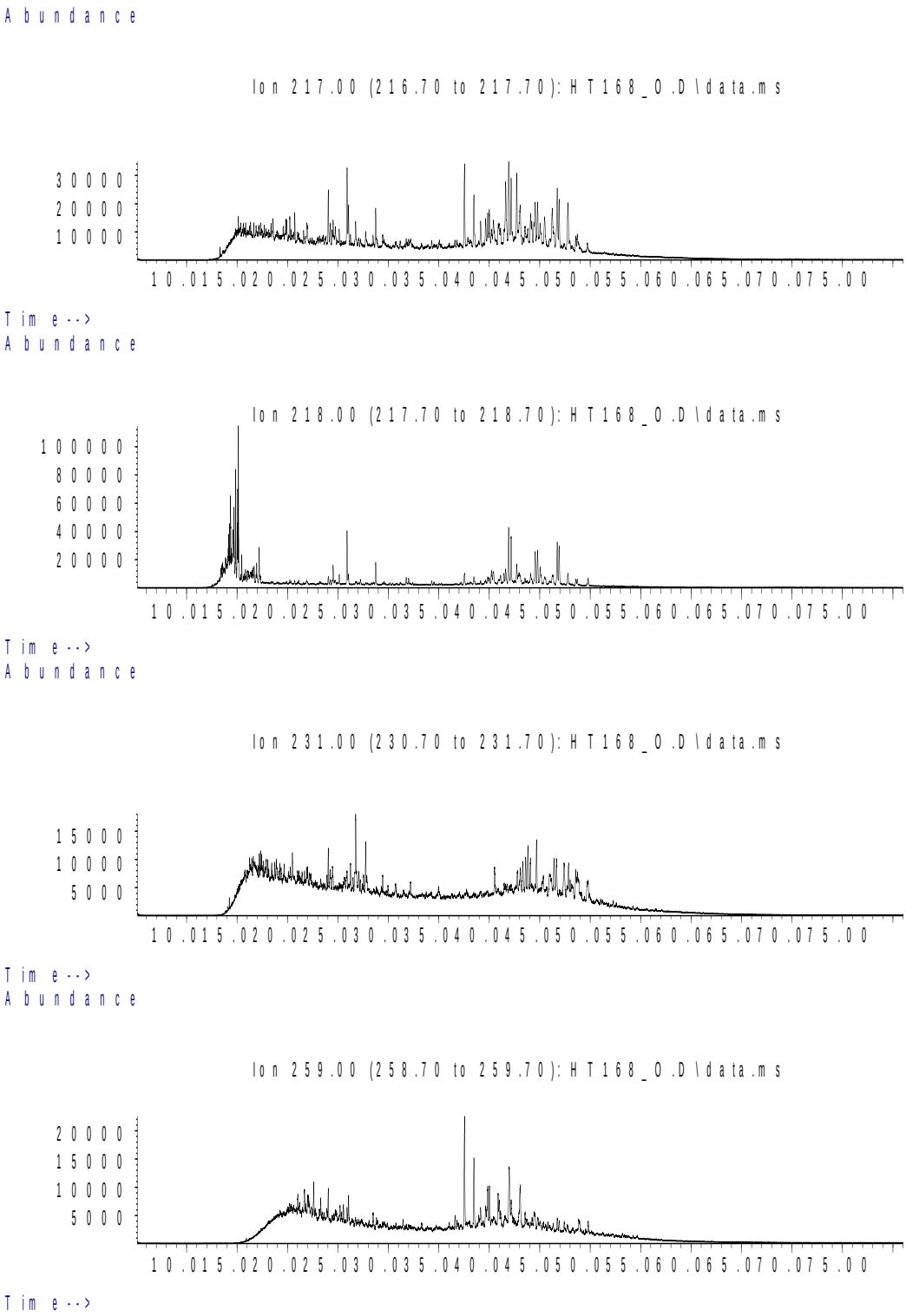

Sample 177 Inner

Bulk Properties

Saturate (%)	20.4
Aromatics (%)	11.4
Resin (%)	15.6
Asphaltene (%)	52.6

Whole Oil/Extract GC

Pristane/Phytane	1.10
Pristane/n-C17	0.47
Phytane/n-C18	0.40

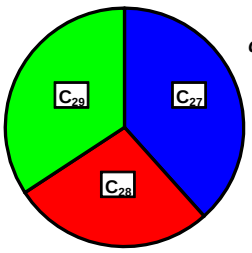

C_{27}-C_{28}-C_{29} αββ Steranes

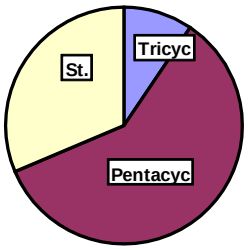

Tricyclic, Pentacyclic Terpanes & Steranes

Saturate Biomarker Interpretive Ratios

Interpretive Ratios	By Area
Terpanes (m/z 191)	
C19t/C23t	0.28
C22t/C21t	0.55
C22t/C24t	0.50
C24t/C23t	0.57
C26t/C25t	0.73
C24Tet/C23t	0.98
C24Tet/C26t	2.37
C23t/C30H	0.11
C24Tet/C30H	0.11
C28BNH/C30H	0.06
25-Nor/C30H	0.02
C29H/C30H	0.70
C30DiaH/C30H	0.09
Ole/C30H	0.01
C30Ts/C30H	0.09
Gam/C30H	0.05
Gam/C31HR	0.17
C35HS/C34HS	0.73
C35 Homohopane Index	0.05
Ts/(Ts+Tm)	0.39
C29Ts/(C29Ts+C29H)	0.23
Mor/C30H	0.13
C32 S/(S+R)	0.60
Steranes (m/z 217)	
% C27 ααα 20R	38.7
% C28 ααα 20R	25.1
% C29 ααα 20R	36.3
C27 Dia/(Dia+Reg)	0.48
(C21+C22)/(C27+C28+C29)	0.14
C29 αββ/(ααα+αββ)	0.51
C29 ααα 20S/20R	0.77
C29 ααα 20S/(S+R)	0.44
αββ−Steranes (m/z 218)	
% C27 αββ 20(R+S)	38.4
% C28 αββ 20(R+S)	27.4
% C29 αββ 20(R+S)	34.2
C29/C27 αββ Sterane Ratio	0.89
C27 Dia/Ster	0.55
Tricyclic/Pentacyclic Terpanes	0.16
Steranes/Terpanes	0.46
% Tricyclic Terpanes	9.4
% Pentacyclic Terpanes	59.2
% Steranes	31.4

Sample 177 Inner

Saturate Biomarker Integration Results (Terpanes)				
Ion	**Peak Label**	**Compound Name**	**R.Time (min.)**	**Peak Area**
191	C19t	C19 tricyclic diterpane	20.056	13838
191	C20t	C20 tricyclic diterpane	21.816	20616
191	C21t	C21 tricyclic diterpane	23.873	25660
191	C22t	C22 tricyclic terpane	25.912	14226
191	C23t	C23 tricyclic terpane	28.465	50260
191	C24t	C24 tricyclic terpane	29.928	28510
191	C25tS	C25 tricyclic terpane (S)	32.981	10535
191	C25tR	C25 tricyclic terpane (R)	32.981	17917
191	C24T	C24 tetracyclic terpane (TET)	34.982	49241
191	C26tS	C26 tricyclic terpane (S)	35.307	8416
191	C26tR	C26 tricyclic terpane (R)	35.492	12386
191	C28tS	C28 extended tricyclic terpane (S)	40.687	11981
191	C28tR	C28 extended tricyclic terpane (R)	41.084	10173
191	C29tS	C29 extended tricyclic terpane (S)	42.282	8362
191	C29tR	C29 extended tricyclic terpane (R)	42.73	23071
191	C30tS	C30 extended tricyclic terpane (S)	45.406	8468
191	C30tR	C30 extended tricyclic terpane (R)	45.765	10619
191	Ts	Ts 18a(H)-trisnorhopane	43.655	89740
191	Tm	Tm 17a(H)-trisnorhopane	44.637	142330
191	C28BNH	C28 17a18a21b(H)-bisnorhopane	47.105	28329
191	Nor25H	C29 Nor-25-hopane	47.827	10170
191	C29H	C29 Tm 17a(H)21b(H)-norhopane	48.148	314420
191	C29Ts	C29 Ts 18a(H)-norneohopane	48.299	93997
191	C30DiaH	C30 17a(H)-diahopane	48.761	40909
191	Normor	C29 normoretane	49.356	35416
191	a-Ole	a-oleanane	49.984	1387
191	b-Ole	b-oleanane	49.984	1387
191	C30H	C30 17a(H)-hopane	50.253	446103
191	C30Ts	17a(H)-30-nor-29-homohopane	50.748	40580
191	Mor	C30 moretane	51.187	58673
191	C31HS	C31 22S 17a(H) homohopane	52.711	196634
191	C31HR	C31 22R 17a(H) homohopane	53.004	139536
191	Gam	gammacerane	53.296	23255
191	C32HS	C32 22S 17a(H) bishomohopane	54.66	104928
191	C32HR	C32 22R 17a(H) bishomohopane	55.071	69711
191	C33HS	C33 22S 17a(H) trishomohopane	56.911	64693
191	C33HR	C33 22R 17a(H) trishomohopane	57.482	42315
191	C34HS	C34 22S 17a(H) extended hopane	59.261	31879
191	C34HR	C34 22R 17a(H) extended hopane	59.964	19894
191	C35HS	C35 22S 17a(H) extended hopane	61.583	23160
191	C35HR	C35 22R 17a(H) extended hopane	62.423	15428

Sample 177 Inner

Saturate Biomarker Integration Results (Steranes)				
Ion	**Peak Label**	**Compound Name**	**R.Time (min.)**	**Peak Area**
217	S21	C21 sterane	26.28	65871
217	S22	C22 sterane	29.13	37158
217	27DbaS	C27 ba 20S diacholestane	37.97	79664
217	27DbaR	C27 ba 20R diacholestane	38.90	60109
217	28DbaSA	C28 ba 20S diasterane a	40.27	28205
217	28DbaSB	C28 ba 20S diasterane b	40.43	38905
217	28DbaRA	C28 ba 20R diasterane a	41.32	21109
217	28DbaRB	C28 ba 20R diasterane b	41.32	12108
217	27aaS	C27 aa 20S cholestane	42.06	79083
217	27bbR	C27 bb 20R cholestane	42.37	113311
217	27bbS	C27 bb 20S cholestane	42.60	56644
217	27aaR	C27 aa 20R cholestane	43.16	71396
217	28aaS	C28 aa 20S ergostane	44.52	38321
217	28bbR	C28 bb 20R ergostane	44.99	43590
217	28bbS	C28 bb 20S ergostane	45.22	42669
217	28aaR	C28 aa 20R ergostane	45.91	46281
217	29aaS	C29 aa 20S stigmastane	46.66	51793
217	29bbR	C29 bb 20R stigmastane	47.17	65426
217	29bbS	C29 bb 20S stigmastane	47.36	59173
217	29aaR	C29 aa 20R stigmastane	48.22	66931
218	27bbR	C27 bb 20R cholestane	42.35	121744
218	27bbS	C27 bb 20S cholestane	42.60	88453
218	28bbR	C28 bb 20R ergostane	44.99	76025
218	28bbS	C28 bb 20S ergostane	45.22	74089
218	29bbR	C29 bb 20R stigmastane	47.16	97087
218	29bbS	C29 bb 20S stigmastane	47.36	90398
259	27DbaS	C27 ba 20S diacholestane	37.97	12173
259	27DbaR	C27 ba 20R diacholestane	38.90	8926
259	28DbaSA	C28 ba 20S diaergostane a	40.27	3813
259	28DbaSB	C28 ba 20S diaergostane b	40.46	4688
259	28DbaRA	C28 ba 20R diaergostane a	41.31	3494
259	28DbaRB	C28 ba 20R diaergostane b	41.41	1391
259	29DbaS	C29 ba 20S diastigmastane	42.38	8918
259	29DbaR	C29 ba 20R diastigmastane	43.98	2198
259	30TP1	C30 Terpane	47.87	1311
259	30TP2	C30 Terpane	48.16	1381

Sample 177 Inner Saturate Chromatograms; Terpanes

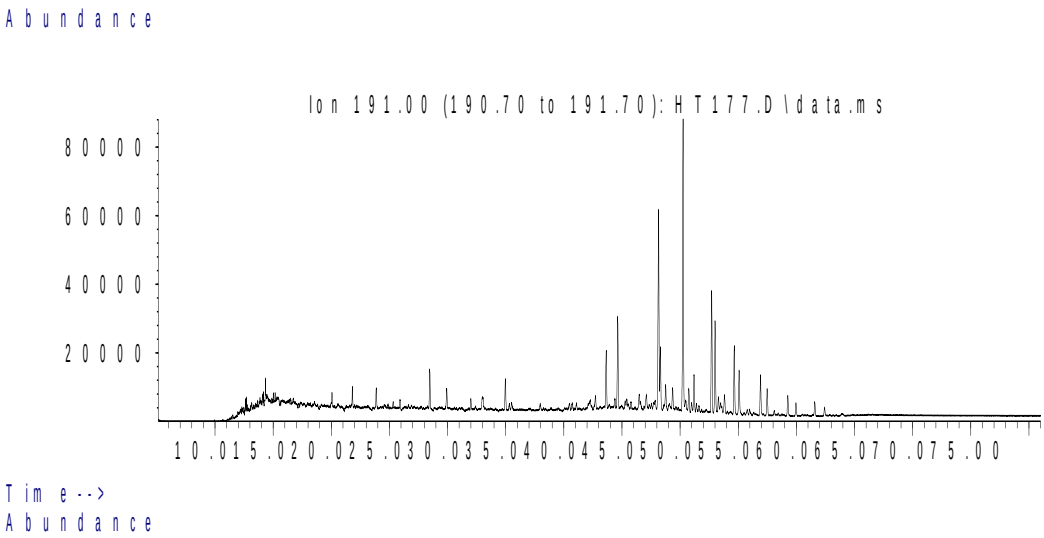

Sample 177 Inner Saturate Chromatograms; Steranes & Steroids

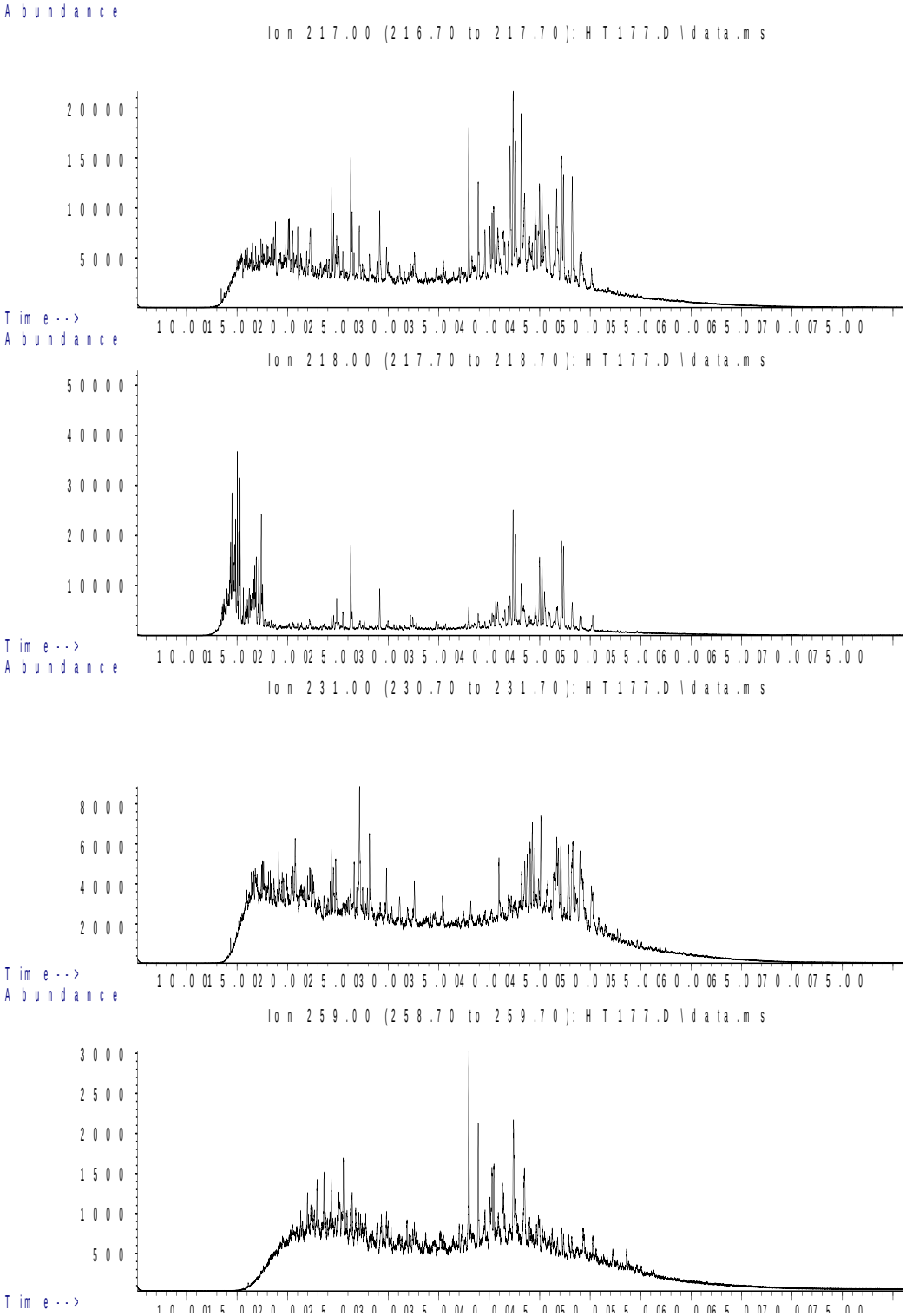

Sample 177 Outer

Bulk Properties

Saturate (%)	19.2
Aromatics (%)	12.4
Resin (%)	16.3
Asphaltene (%)	52.1

Whole Oil/Extract GC

Pristane/Phytane	1.01
Pristane/n-C17	0.42
Phytane/n-C18	0.40

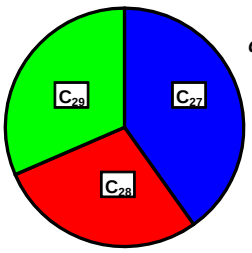

C_{27}-C_{28}-C_{29} αββ Steranes

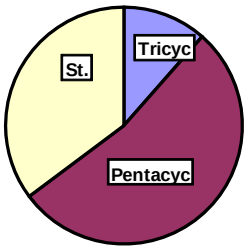

Tricyclic, Pentacyclic Terpanes & Steranes

Saturate Biomarker Interpretive Ratios

Interpretive Ratios	By Area
Terpanes (m/z 191)	
C19t/C23t	0.33
C22t/C21t	0.34
C22t/C24t	0.36
C24t/C23t	0.56
C26t/C25t	0.61
C24Tet/C23t	0.86
C24Tet/C26t	2.35
C23t/C30H	0.15
C24Tet/C30H	0.13
C28BNH/C30H	0.06
25-Nor/C30H	0.03
C29H/C30H	0.74
C30DiaH/C30H	0.07
Ole/C30H	0.01
C30Ts/C30H	0.07
Gam/C30H	0.05
Gam/C31HR	0.17
C35HS/C34HS	0.59
C35 Homohopane Index	0.04
Ts/(Ts+Tm)	0.38
C29Ts/(C29Ts+C29H)	0.20
Mor/C30H	0.12
C32 S/(S+R)	0.59
Steranes (m/z 217)	
% C27 ααα 20R	38.5
% C28 ααα 20R	22.7
% C29 ααα 20R	38.8
C27 Dia/(Dia+Reg)	0.55
(C21+C22)/(C27+C28+C29)	0.19
C29 αββ/(ααα+αββ)	0.53
C29 ααα 20S/20R	0.65
C29 ααα 20S/(S+R)	0.40
αββ−Steranes (m/z 218)	
% C27 αββ 20(R+S)	40.2
% C28 αββ 20(R+S)	28.4
% C29 αββ 20(R+S)	31.5
C29/C27 αββ Sterane Ratio	0.78
C27 Dia/Ster	0.67
Tricyclic/Pentacyclic Terpanes	0.22
Steranes/Terpanes	0.54
% Tricyclic Terpanes	11.5
% Pentacyclic Terpanes	53.3
% Steranes	35.2

Sample 177 Outer

Saturate Biomarker Integration Results (Terpanes)				
Ion	**Peak Label**	**Compound Name**	**R.Time (min.)**	**Peak Area**
191	C19t	C19 tricyclic diterpane	19.82	53544
191	C20t	C20 tricyclic diterpane	21.56	89379
191	C21t	C21 tricyclic diterpane	23.58	97306
191	C22t	C22 tricyclic terpane	25.62	33429
191	C23t	C23 tricyclic terpane	28.14	164230
191	C24t	C24 tricyclic terpane	29.59	91716
191	C25tS	C25 tricyclic terpane (S)	32.64	59072
191	C25tR	C25 tricyclic terpane (R)	32.64	39709
191	C24T	C24 tetracyclic terpane (TET)	34.60	140735
191	C26tS	C26 tricyclic terpane (S)	34.97	23929
191	C26tR	C26 tricyclic terpane (R)	35.15	35843
191	C28tS	C28 extended tricyclic terpane (S)	40.09	28481
191	C28tR	C28 extended tricyclic terpane (R)	40.70	24615
191	C29tS	C29 extended tricyclic terpane (S)	41.90	14849
191	C29tR	C29 extended tricyclic terpane (R)	42.35	44417
191	C30tS	C30 extended tricyclic terpane (S)	45.03	20682
191	C30tR	C30 extended tricyclic terpane (R)	45.39	30589
191	Ts	Ts 18a(H)-trisnorhopane	43.25	223766
191	Tm	Tm 17a(H)-trisnorhopane	44.25	365643
191	C28BNH	C28 17a18a21b(H)-bisnorhopane	46.70	63028
191	Nor25H	C29 Nor-25-hopane	47.47	34307
191	C29H	C29 Tm 17a(H)21b(H)-norhopane	47.74	785896
191	C29Ts	C29 Ts 18a(H)-norneohopane	47.91	201523
191	C30DiaH	C30 17a(H)-diahopane	48.36	76879
191	Normor	C29 normoretane	48.96	80021
191	a-Ole	a-oleanane	49.57	2849
191	b-Ole	b-oleanane	49.57	2849
191	C30H	C30 17a(H)-hopane	49.84	1064324
191	C30Ts	17a(H)-30-nor-29-homohopane	50.35	78499
191	Mor	C30 moretane	50.80	123123
191	C31HS	C31 22S 17a(H) homohopane	52.32	423316
191	C31HR	C31 22R 17a(H) homohopane	52.61	303000
191	Gam	gammacerane	52.90	52537
191	C32HS	C32 22S 17a(H) bishomohopane	54.26	216798
191	C32HR	C32 22R 17a(H) bishomohopane	54.69	152018
191	C33HS	C33 22S 17a(H) trishomohopane	56.53	123445
191	C33HR	C33 22R 17a(H) trishomohopane	57.11	79373
191	C34HS	C34 22S 17a(H) extended hopane	58.88	63025
191	C34HR	C34 22R 17a(H) extended hopane	59.59	34965
191	C35HS	C35 22S 17a(H) extended hopane	61.21	36965
191	C35HR	C35 22R 17a(H) extended hopane	62.07	23503

Sample 177 Outer

Saturate Biomarker Integration Results (Steranes)				
Ion	**Peak Label**	**Compound Name**	**R.Time (min.)**	**Peak Area**
217	S21	C21 sterane	25.97	244807
217	S22	C22 sterane	28.80	122209
217	27DbaS	C27 ba 20S diacholestane	37.61	259264
217	27DbaR	C27 ba 20R diacholestane	38.54	168228
217	28DbaSA	C28 ba 20S diasterane a	39.69	90878
217	28DbaSB	C28 ba 20S diasterane b	39.90	85639
217	28DbaRA	C28 ba 20R diasterane a	40.95	59054
217	28DbaRB	C28 ba 20R diasterane b	41.16	40506
217	27aaS	C27 aa 20S cholestane	41.68	157126
217	27bbR	C27 bb 20R cholestane	41.99	316627
217	27bbS	C27 bb 20S cholestane	42.23	162366
217	27aaR	C27 aa 20R cholestane	42.78	194377
217	28aaS	C28 aa 20S ergostane	44.14	101729
217	28bbR	C28 bb 20R ergostane	44.59	108477
217	28bbS	C28 bb 20S ergostane	44.84	131570
217	28aaR	C28 aa 20R ergostane	45.53	114927
217	29aaS	C29 aa 20S stigmastane	46.27	128197
217	29bbR	C29 bb 20R stigmastane	46.79	234325
217	29bbS	C29 bb 20S stigmastane	46.96	130044
217	29aaR	C29 aa 20R stigmastane	47.83	196100
218	27bbR	C27 bb 20R cholestane	41.98	339868
218	27bbS	C27 bb 20S cholestane	42.23	256488
218	28bbR	C28 bb 20R ergostane	44.60	212331
218	28bbS	C28 bb 20S ergostane	44.84	208629
218	29bbR	C29 bb 20R stigmastane	46.79	274748
218	29bbS	C29 bb 20S stigmastane	46.96	192743
259	27DbaS	C27 ba 20S diacholestane	37.61	164400
259	27DbaR	C27 ba 20R diacholestane	38.55	107511
259	28DbaSA	C28 ba 20S diaergostane a	39.90	48427
259	28DbaSB	C28 ba 20S diaergostane b	40.08	50362
259	28DbaRA	C28 ba 20R diaergostane a	40.93	47447
259	28DbaRB	C28 ba 20R diaergostane b	41.16	16448
259	29DbaS	C29 ba 20S diastigmastane	42.00	123726
259	29DbaR	C29 ba 20R diastigmastane	43.59	21534
259	30TP1	C30 Terpane	47.47	15591
259	30TP2	C30 Terpane	47.75	14553

Sample 177 Outer Saturate Chromatograms; Terpanes

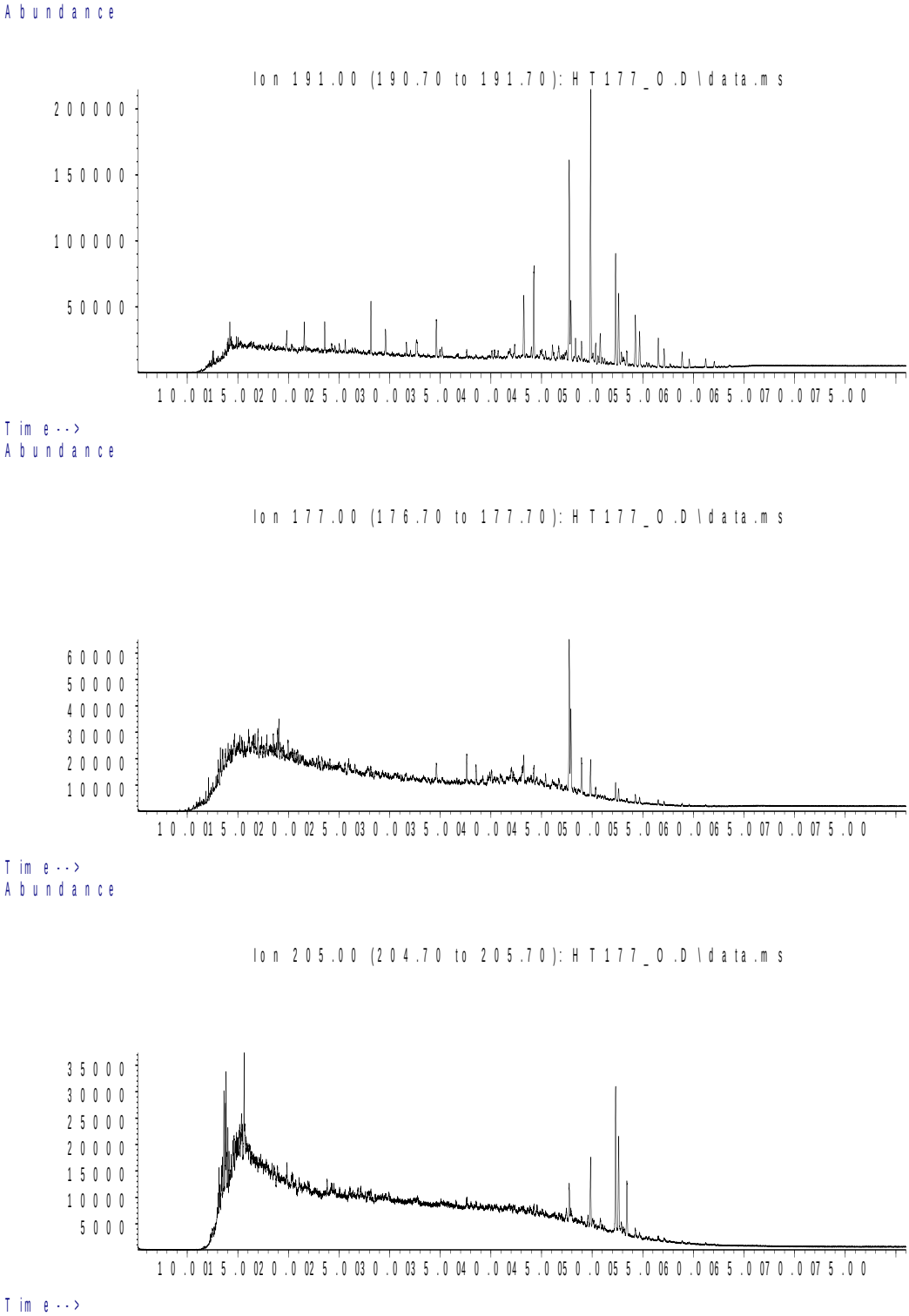

Sample 177 Outer Saturate Chromatograms; Steranes & Steroids

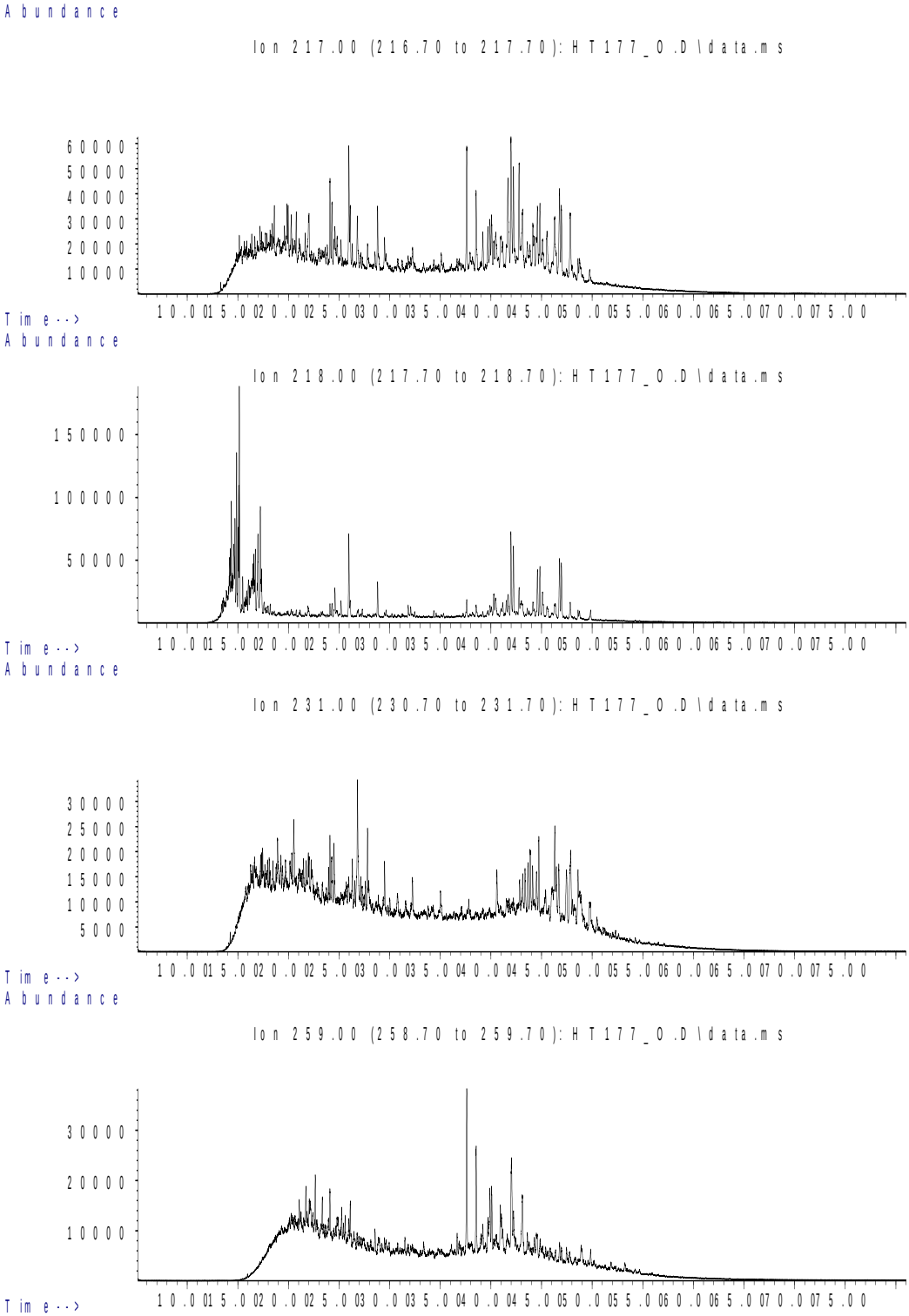

Sample CL1 Inner

Bulk Properties

Saturate (%)	24.5
Aromatics (%)	15.2
Resin (%)	18.6
Asphaltene (%)	41.7

Whole Oil/Extract GC

Pristane/Phytane	1.18
Pristane/n-C17	0.47
Phytane/n-C18	0.41

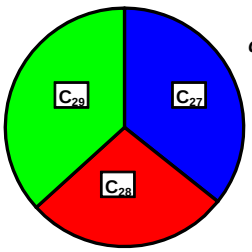

C_{27}-C_{28}-C_{29} αββ Steranes

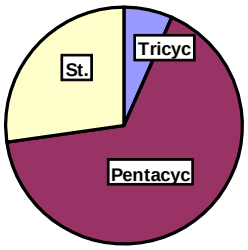

Tricyclic, Pentacyclic Terpanes & Steranes

Saturate Biomarker Interpretive Ratios

Interpretive Ratios	By Area
Terpanes (m/z 191)	
C19t/C23t	0.27
C22t/C21t	0.63
C22t/C24t	0.39
C24t/C23t	0.59
C26t/C25t	0.72
C24Tet/C23t	1.11
C24Tet/C26t	2.41
C23t/C30H	0.07
C24Tet/C30H	0.07
C28BNH/C30H	0.05
25-Nor/C30H	0.03
C29H/C30H	0.67
C30DiaH/C30H	0.08
Ole/C30H	0.00
C30Ts/C30H	0.09
Gam/C30H	0.06
Gam/C31HR	0.17
C35HS/C34HS	0.61
C35 Homohopane Index	0.06
Ts/(Ts+Tm)	0.37
C29Ts/(C29Ts+C29H)	0.22
Mor/C30H	0.13
C32 S/(S+R)	0.58
Steranes (m/z 217)	
% C27 ααα 20R	33.7
% C28 ααα 20R	23.3
% C29 ααα 20R	43.0
C27 Dia/(Dia+Reg)	0.48
(C21+C22)/(C27+C28+C29)	0.09
C29 αββ/(ααα+αββ)	0.51
C29 ααα 20S/20R	0.65
C29 ααα 20S/(S+R)	0.39
αββ−Steranes (m/z 218)	
% C27 αββ 20(R+S)	35.7
% C28 αββ 20(R+S)	27.6
% C29 αββ 20(R+S)	36.7
C29/C27 αββ Sterane Ratio	1.03
C27 Dia/Ster	0.53
Tricyclic/Pentacyclic Terpanes	0.10
Steranes/Terpanes	0.37
% Tricyclic Terpanes	6.6
% Pentacyclic Terpanes	66.1
% Steranes	27.2

Sample CL1 Inner

Saturate Biomarker Integration Results (Terpanes)				
Ion	**Peak Label**	**Compound Name**	**R.Time (min.)**	**Peak Area**
191	C19t	C19 tricyclic diterpane	20.037	9403
191	C20t	C20 tricyclic diterpane	21.783	12792
191	C21t	C21 tricyclic diterpane	23.822	12885
191	C22t	C22 tricyclic terpane	25.87	8161
191	C23t	C23 tricyclic terpane	28.432	35220
191	C24t	C24 tricyclic terpane	29.895	20930
191	C25tS	C25 tricyclic terpane (S)	32.967	11562
191	C25tR	C25 tricyclic terpane (R)	32.967	10964
191	C24T	C24 tetracyclic terpane (TET)	34.963	39121
191	C26tS	C26 tricyclic terpane (S)	35.298	7194
191	C26tR	C26 tricyclic terpane (R)	35.487	9063
191	C28tS	C28 extended tricyclic terpane (S)	40.711	11447
191	C28tR	C28 extended tricyclic terpane (R)	41.089	8929
191	C29tS	C29 extended tricyclic terpane (S)	42.348	7526
191	C29tR	C29 extended tricyclic terpane (R)	42.717	20080
191	C30tS	C30 extended tricyclic terpane (S)	45.43	8183
191	C30tR	C30 extended tricyclic terpane (R)	45.793	11386
191	Ts	Ts 18a(H)-trisnorhopane	43.646	81840
191	Tm	Tm 17a(H)-trisnorhopane	44.642	136971
191	C28BNH	C28 17a18a21b(H)-bisnorhopane	47.124	28536
191	Nor25H	C29 Nor-25-hopane	47.893	13635
191	C29H	C29 Tm 17a(H)21b(H)-norhopane	48.167	356167
191	C29Ts	C29 Ts 18a(H)-norneohopane	48.318	101056
191	C30DiaH	C30 17a(H)-diahopane	48.79	41915
191	Normor	C29 normoretane	49.37	37652
191	a-Ole	a-oleanane	50.007	167
191	b-Ole	b-oleanane	50.007	167
191	C30H	C30 17a(H)-hopane	50.295	532383
191	C30Ts	17a(H)-30-nor-29-homohopane	50.781	48081
191	Mor	C30 moretane	51.225	70526
191	C31HS	C31 22S 17a(H) homohopane	52.754	245537
191	C31HR	C31 22R 17a(H) homohopane	53.046	180575
191	Gam	gammacerane	53.334	31109
191	C32HS	C32 22S 17a(H) bishomohopane	54.708	141420
191	C32HR	C32 22R 17a(H) bishomohopane	55.123	100953
191	C33HS	C33 22S 17a(H) trishomohopane	56.959	90443
191	C33HR	C33 22R 17a(H) trishomohopane	57.525	60412
191	C34HS	C34 22S 17a(H) extended hopane	59.309	55269
191	C34HR	C34 22R 17a(H) extended hopane	60.007	31245
191	C35HS	C35 22S 17a(H) extended hopane	61.64	33438
191	C35HR	C35 22R 17a(H) extended hopane	62.47	27549

Sample CL1 Inner

Saturate Biomarker Integration Results (Steranes)				
Ion	**Peak Label**	**Compound Name**	**R.Time (min.)**	**Peak Area**
217	S21	C21 sterane	26.22	37500
217	S22	C22 sterane	29.10	25515
217	27DbaS	C27 ba 20S diacholestane	37.96	67741
217	27DbaR	C27 ba 20R diacholestane	38.89	50677
217	28DbaSA	C28 ba 20S diasterane a	40.26	24749
217	28DbaSB	C28 ba 20S diasterane b	40.43	30367
217	28DbaRA	C28 ba 20R diasterane a	41.30	17986
217	28DbaRB	C28 ba 20R diasterane b	41.30	14893
217	27aaS	C27 aa 20S cholestane	42.06	62926
217	27bbR	C27 bb 20R cholestane	42.36	101304
217	27bbS	C27 bb 20S cholestane	42.61	54468
217	27aaR	C27 aa 20R cholestane	43.16	65301
217	28aaS	C28 aa 20S ergostane	44.53	35822
217	28bbR	C28 bb 20R ergostane	44.98	44155
217	28bbS	C28 bb 20S ergostane	45.24	47033
217	28aaR	C28 aa 20R ergostane	45.93	45177
217	29aaS	C29 aa 20S stigmastane	46.69	54320
217	29bbR	C29 bb 20R stigmastane	47.19	87432
217	29bbS	C29 bb 20S stigmastane	47.37	56719
217	29aaR	C29 aa 20R stigmastane	48.24	83503
218	27bbR	C27 bb 20R cholestane	42.35	110772
218	27bbS	C27 bb 20S cholestane	42.59	81282
218	28bbR	C28 bb 20R ergostane	44.98	74288
218	28bbS	C28 bb 20S ergostane	45.24	74217
218	29bbR	C29 bb 20R stigmastane	47.19	108844
218	29bbS	C29 bb 20S stigmastane	47.37	88751
259	27DbaS	C27 ba 20S diacholestane	37.96	11929
259	27DbaR	C27 ba 20R diacholestane	38.89	8694
259	28DbaSA	C28 ba 20S diaergostane a	40.26	4003
259	28DbaSB	C28 ba 20S diaergostane b	40.44	4768
259	28DbaRA	C28 ba 20R diaergostane a	41.30	3960
259	28DbaRB	C28 ba 20R diaergostane b	41.42	1794
259	29DbaS	C29 ba 20S diastigmastane	42.41	11750
259	29DbaR	C29 ba 20R diastigmastane	43.99	2264
259	30TP1	C30 Terpane	47.90	1541
259	30TP2	C30 Terpane	48.21	2023

Sample CL1 Inner Saturate Chromatograms; Terpanes

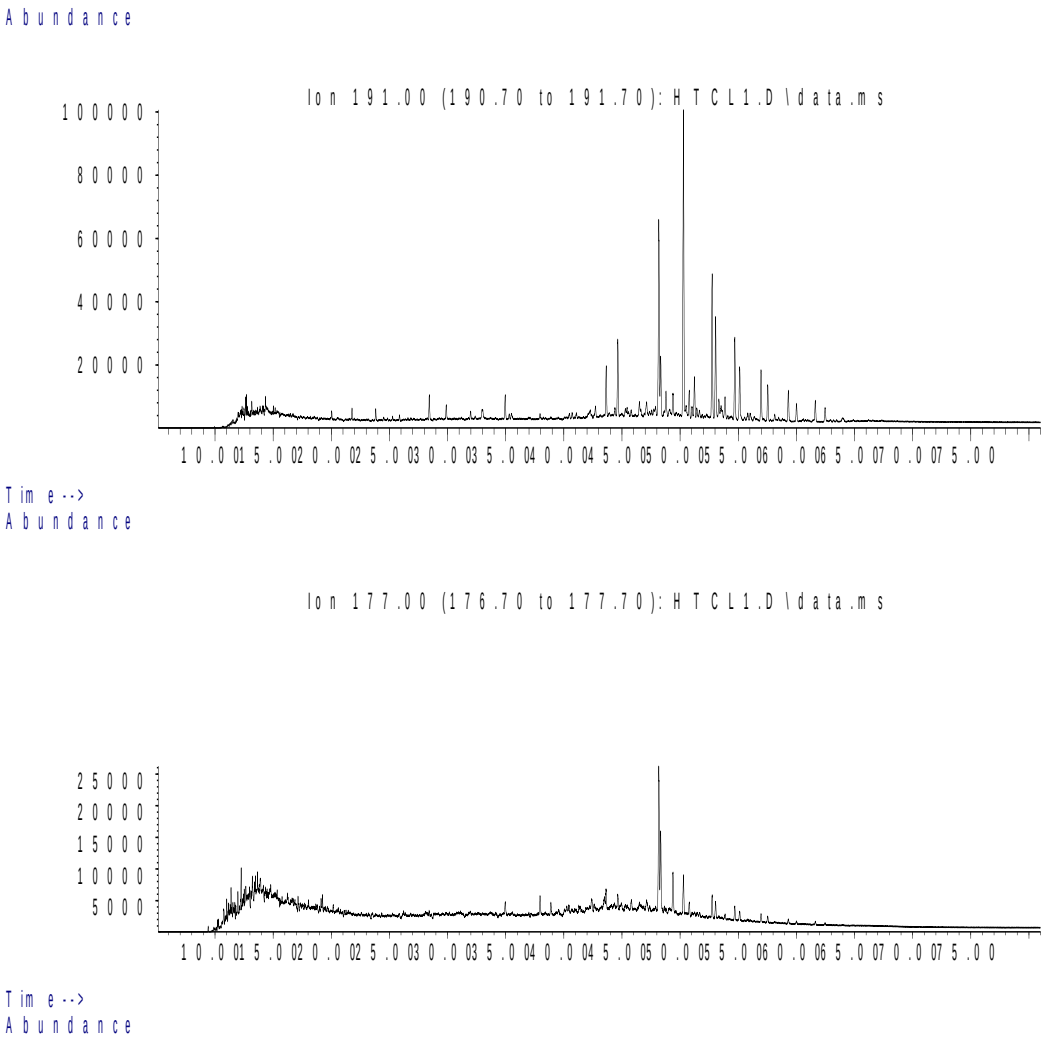

Sample CL1 Inner Saturate Chromatograms; Steranes & Steroids

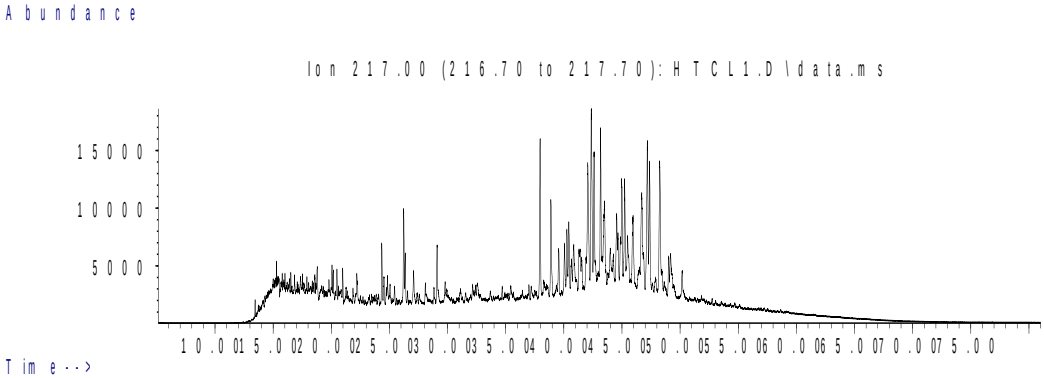

Sample CL1 Outer

Bulk Properties

Saturate (%)	17.5
Aromatics (%)	11.2
Resin (%)	16.1
Asphaltene (%)	55.2

Whole Oil/Extract GC

Pristane/Phytane	1.09
Pristane/n-C17	0.46
Phytane/n-C18	0.44

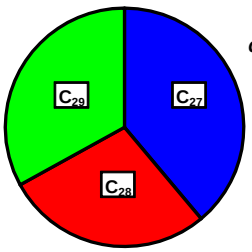

C_{27}-C_{28}-C_{29} αββ Steranes

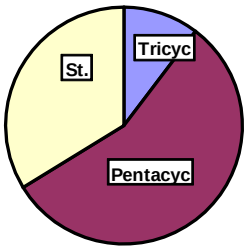

Tricyclic, Pentacyclic Terpanes & Steranes

Saturate Biomarker Interpretive Ratios

Interpretive Ratios	By Area
Terpanes (m/z 191)	
C19t/C23t	0.32
C22t/C21t	0.47
C22t/C24t	0.46
C24t/C23t	0.52
C26t/C25t	0.86
C24Tet/C23t	0.87
C24Tet/C26t	2.26
C23t/C30H	0.14
C24Tet/C30H	0.12
C28BNH/C30H	0.05
25-Nor/C30H	0.03
C29H/C30H	0.70
C30DiaH/C30H	0.06
Ole/C30H	0.00
C30Ts/C30H	0.09
Gam/C30H	0.05
Gam/C31HR	0.16
C35HS/C34HS	0.57
C35 Homohopane Index	0.04
Ts/(Ts+Tm)	0.39
C29Ts/(C29Ts+C29H)	0.23
Mor/C30H	0.13
C32 S/(S+R)	0.59
Steranes (m/z 217)	
% C27 ααα 20R	39.9
% C28 ααα 20R	21.7
% C29 ααα 20R	38.4
C27 Dia/(Dia+Reg)	0.52
(C21+C22)/(C27+C28+C29)	0.16
C29 αββ/(ααα+αββ)	0.51
C29 ααα 20S/20R	0.81
C29 ααα 20S/(S+R)	0.45
αββ−Steranes (m/z 218)	
% C27 αββ 20(R+S)	38.9
% C28 αββ 20(R+S)	28.1
% C29 αββ 20(R+S)	33.0
C29/C27 αββ Sterane Ratio	0.85
C27 Dia/Ster	0.62
Tricyclic/Pentacyclic Terpanes	0.18
Steranes/Terpanes	0.51
% Tricyclic Terpanes	10.3
% Pentacyclic Terpanes	55.9
% Steranes	33.8

Sample CL1 Outer

Saturate Biomarker Integration Results (Terpanes)				
Ion	**Peak Label**	**Compound Name**	**R.Time (min.)**	**Peak Area**
191	C19t	C19 tricyclic diterpane	19.78	25590
191	C20t	C20 tricyclic diterpane	21.51	34699
191	C21t	C21 tricyclic diterpane	23.52	40200
191	C22t	C22 tricyclic terpane	25.55	18933
191	C23t	C23 tricyclic terpane	28.09	79533
191	C24t	C24 tricyclic terpane	29.53	41464
191	C25tS	C25 tricyclic terpane (S)	32.57	19758
191	C25tR	C25 tricyclic terpane (R)	32.57	16016
191	C24T	C24 tetracyclic terpane (TET)	34.55	69228
191	C26tS	C26 tricyclic terpane (S)	34.89	14256
191	C26tR	C26 tricyclic terpane (R)	35.08	16391
191	C28tS	C28 extended tricyclic terpane (S)	40.05	15982
191	C28tR	C28 extended tricyclic terpane (R)	40.66	15191
191	C29tS	C29 extended tricyclic terpane (S)	41.85	12048
191	C29tR	C29 extended tricyclic terpane (R)	42.30	26554
191	C30tS	C30 extended tricyclic terpane (S)	44.99	12025
191	C30tR	C30 extended tricyclic terpane (R)	45.36	15712
191	Ts	Ts 18a(H)-trisnorhopane	43.20	120196
191	Tm	Tm 17a(H)-trisnorhopane	44.20	189437
191	C28BNH	C28 17a18a21b(H)-bisnorhopane	46.65	26261
191	Nor25H	C29 Nor-25-hopane	47.43	19870
191	C29H	C29 Tm 17a(H)21b(H)-norhopane	47.70	409125
191	C29Ts	C29 Ts 18a(H)-norneohopane	47.86	119805
191	C30DiaH	C30 17a(H)-diahopane	48.32	36703
191	Normor	C29 normoretane	48.92	43265
191	a-Ole	a-oleanane	49.57	374
191	b-Ole	b-oleanane	49.57	374
191	C30H	C30 17a(H)-hopane	49.82	583328
191	C30Ts	17a(H)-30-nor-29-homohopane	50.31	50279
191	Mor	C30 moretane	50.78	75012
191	C31HS	C31 22S 17a(H) homohopane	52.29	247663
191	C31HR	C31 22R 17a(H) homohopane	52.60	174430
191	Gam	gammacerane	52.88	27904
191	C32HS	C32 22S 17a(H) bishomohopane	54.25	128099
191	C32HR	C32 22R 17a(H) bishomohopane	54.68	87892
191	C33HS	C33 22S 17a(H) trishomohopane	56.53	75116
191	C33HR	C33 22R 17a(H) trishomohopane	57.10	50145
191	C34HS	C34 22S 17a(H) extended hopane	58.88	40753
191	C34HR	C34 22R 17a(H) extended hopane	59.60	22622
191	C35HS	C35 22S 17a(H) extended hopane	61.23	23228
191	C35HR	C35 22R 17a(H) extended hopane	62.05	13960

Sample CL1 Outer

Saturate Biomarker Integration Results (Steranes)				
Ion	**Peak Label**	**Compound Name**	**R.Time (min.)**	**Peak Area**
217	S21	C21 sterane	25.91	107890
217	S22	C22 sterane	28.74	55183
217	27DbaS	C27 ba 20S diacholestane	37.54	122123
217	27DbaR	C27 ba 20R diacholestane	38.48	89023
217	28DbaSA	C28 ba 20S diasterane a	39.65	38355
217	28DbaSB	C28 ba 20S diasterane b	39.84	39561
217	28DbaRA	C28 ba 20R diasterane a	40.90	34646
217	28DbaRB	C28 ba 20R diasterane b	41.12	20286
217	27aaS	C27 aa 20S cholestane	41.63	88906
217	27bbR	C27 bb 20R cholestane	41.93	150157
217	27bbS	C27 bb 20S cholestane	42.18	85994
217	27aaR	C27 aa 20R cholestane	42.72	102988
217	28aaS	C28 aa 20S ergostane	44.12	55187
217	28bbR	C28 bb 20R ergostane	44.56	62295
217	28bbS	C28 bb 20S ergostane	44.80	72183
217	28aaR	C28 aa 20R ergostane	45.47	56034
217	29aaS	C29 aa 20S stigmastane	46.24	80084
217	29bbR	C29 bb 20R stigmastane	46.74	112781
217	29bbS	C29 bb 20S stigmastane	46.93	75670
217	29aaR	C29 aa 20R stigmastane	47.80	99154
218	27bbR	C27 bb 20R cholestane	41.92	176181
218	27bbS	C27 bb 20S cholestane	42.18	131328
218	28bbR	C28 bb 20R ergostane	44.56	112562
218	28bbS	C28 bb 20S ergostane	44.80	109759
218	29bbR	C29 bb 20R stigmastane	46.74	144907
218	29bbS	C29 bb 20S stigmastane	46.93	116185
259	27DbaS	C27 ba 20S diacholestane	37.54	80279
259	27DbaR	C27 ba 20R diacholestane	38.49	51083
259	28DbaSA	C28 ba 20S diaergostane a	39.84	24033
259	28DbaSB	C28 ba 20S diaergostane b	40.01	32330
259	28DbaRA	C28 ba 20R diaergostane a	40.88	22022
259	28DbaRB	C28 ba 20R diaergostane b	41.12	9798
259	29DbaS	C29 ba 20S diastigmastane	41.97	66090
259	29DbaR	C29 ba 20R diastigmastane	43.54	10666
259	30TP1	C30 Terpane	47.43	8723
259	30TP2	C30 Terpane	47.71	7353

Sample CL1 Outer Saturate Chromatograms; Terpanes

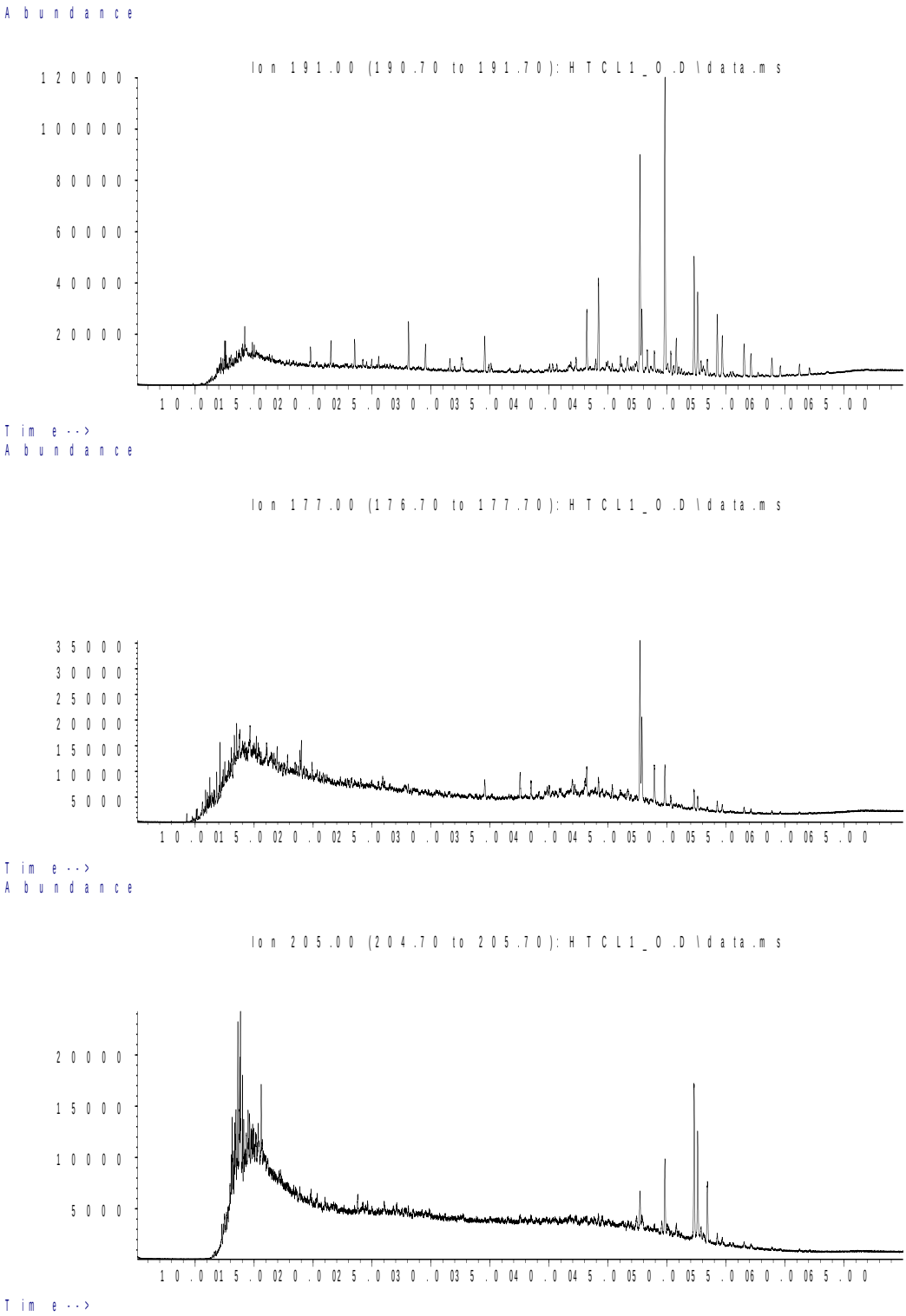

Sample CL1 Outer Saturate Chromatograms; Steranes & Steroids

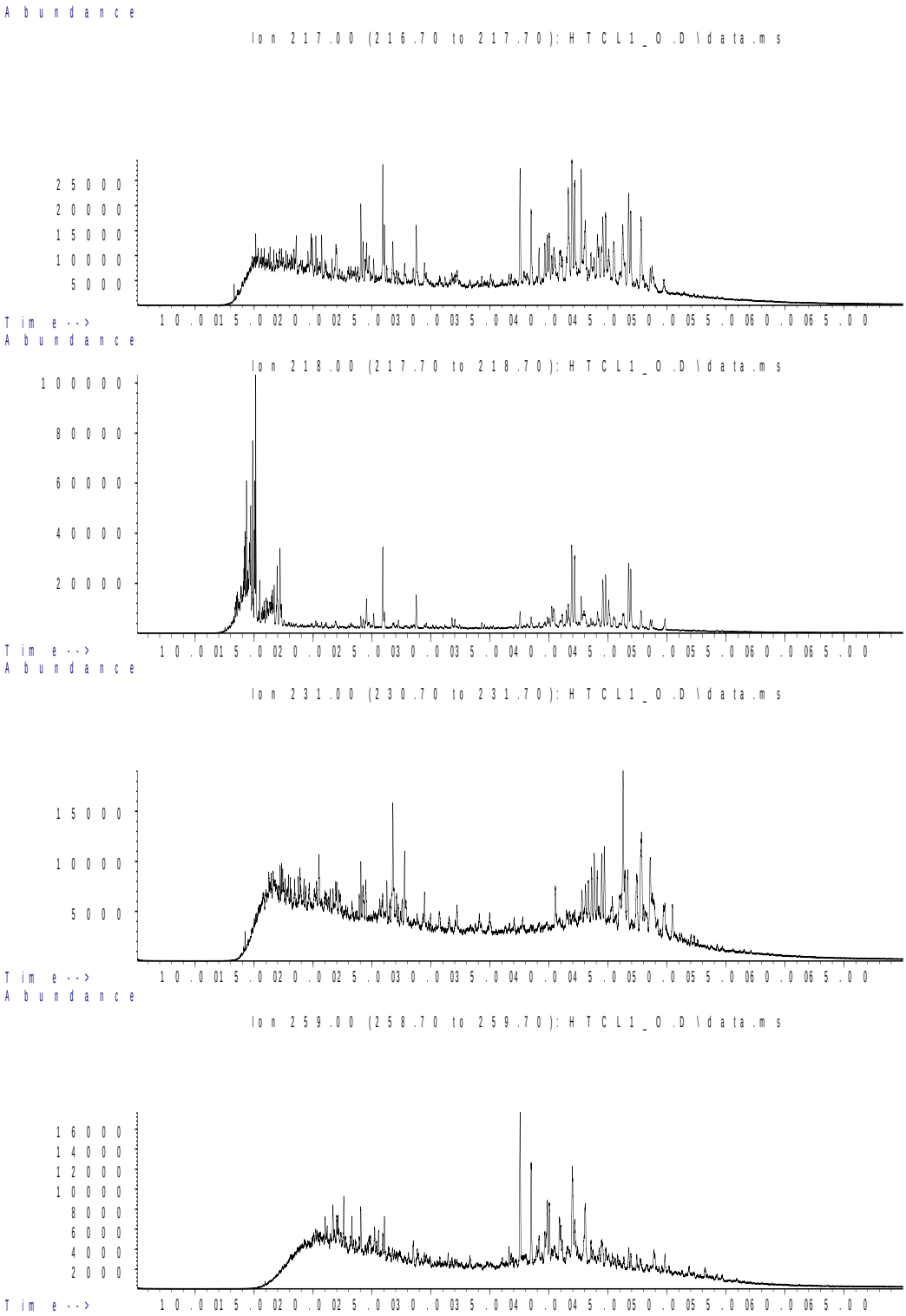

Sample MH1 Inner

Bulk Properties

Saturate (%)	21.6
Aromatics (%)	12.0
Resin (%)	16.5
Asphaltene (%)	49.9

Whole Oil/Extract GC

Pristane/Phytane	1.12
Pristane/n-C17	0.49
Phytane/n-C18	0.44

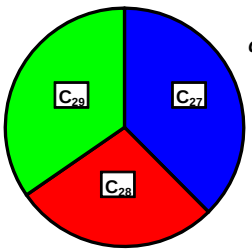

C_{27}-C_{28}-C_{29} αββ Steranes

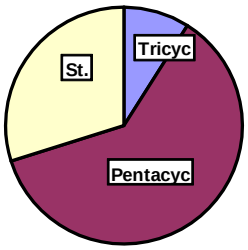

Tricyclic, Pentacyclic Terpanes & Steranes

Saturate Biomarker Interpretive Ratios

Interpretive Ratios	By Area
Terpanes (m/z 191)	
C19t/C23t	0.31
C22t/C21t	0.43
C22t/C24t	0.45
C24t/C23t	0.61
C26t/C25t	0.66
C24Tet/C23t	0.96
C24Tet/C26t	2.11
C23t/C30H	0.10
C24Tet/C30H	0.09
C28BNH/C30H	0.06
25-Nor/C30H	0.02
C29H/C30H	0.70
C30DiaH/C30H	0.07
Ole/C30H	0.00
C30Ts/C30H	0.08
Gam/C30H	0.06
Gam/C31HR	0.17
C35HS/C34HS	0.64
C35 Homohopane Index	0.07
Ts/(Ts+Tm)	0.38
C29Ts/(C29Ts+C29H)	0.22
Mor/C30H	0.12
C32 S/(S+R)	0.59
Steranes (m/z 217)	
% C27 ααα 20R	36.7
% C28 ααα 20R	23.3
% C29 ααα 20R	40.1
C27 Dia/(Dia+Reg)	0.52
(C21+C22)/(C27+C28+C29)	0.13
C29 αββ/(ααα+αββ)	0.52
C29 ααα 20S/20R	0.71
C29 ααα 20S/(S+R)	0.41
αββ−Steranes (m/z 218)	
% C27 αββ 20(R+S)	37.6
% C28 αββ 20(R+S)	27.8
% C29 αββ 20(R+S)	34.6
C29/C27 αββ Sterane Ratio	0.92
C27 Dia/Ster	0.59
Tricyclic/Pentacyclic Terpanes	0.15
Steranes/Terpanes	0.43
% Tricyclic Terpanes	9.0
% Pentacyclic Terpanes	61.2
% Steranes	29.8

Sample MH1 Inner

Saturate Biomarker Integration Results (Terpanes)				
Ion	**Peak Label**	**Compound Name**	**R.Time (min.)**	**Peak Area**
191	C19t	C19 tricyclic diterpane	20.08	16436
191	C20t	C20 tricyclic diterpane	21.83	23001
191	C21t	C21 tricyclic diterpane	23.89	33612
191	C22t	C22 tricyclic terpane	25.92	14546
191	C23t	C23 tricyclic terpane	28.50	53252
191	C24t	C24 tricyclic terpane	29.96	32654
191	C25tS	C25 tricyclic terpane (S)	33.02	17940
191	C25tR	C25 tricyclic terpane (R)	33.02	18864
191	C24T	C24 tetracyclic terpane (TET)	35.01	51077
191	C26tS	C26 tricyclic terpane (S)	35.34	10417
191	C26tR	C26 tricyclic terpane (R)	35.55	13769
191	C28tS	C28 extended tricyclic terpane (S)	40.76	13539
191	C28tR	C28 extended tricyclic terpane (R)	41.12	10780
191	C29tS	C29 extended tricyclic terpane (S)	42.30	7759
191	C29tR	C29 extended tricyclic terpane (R)	42.76	22594
191	C30tS	C30 extended tricyclic terpane (S)	45.46	10586
191	C30tR	C30 extended tricyclic terpane (R)	45.82	11970
191	Ts	Ts 18a(H)-trisnorhopane	43.69	97041
191	Tm	Tm 17a(H)-trisnorhopane	44.67	158329
191	C28BNH	C28 17a18a21b(H)-bisnorhopane	47.15	33372
191	Nor25H	C29 Nor-25-hopane	47.91	13616
191	C29H	C29 Tm 17a(H)21b(H)-norhopane	48.19	381982
191	C29Ts	C29 Ts 18a(H)-norneohopane	48.35	105249
191	C30DiaH	C30 17a(H)-diahopane	48.80	40664
191	Normor	C29 normoretane	49.41	39035
191	a-Ole	a-oleanane	50.02	930
191	b-Ole	b-oleanane	50.02	930
191	C30H	C30 17a(H)-hopane	50.31	545147
191	C30Ts	17a(H)-30-nor-29-homohopane	50.80	46203
191	Mor	C30 moretane	51.25	66946
191	C31HS	C31 22S 17a(H) homohopane	52.75	238348
191	C31HR	C31 22R 17a(H) homohopane	53.07	174087
191	Gam	gammacerane	53.35	30060
191	C32HS	C32 22S 17a(H) bishomohopane	54.71	132278
191	C32HR	C32 22R 17a(H) bishomohopane	55.12	93219
191	C33HS	C33 22S 17a(H) trishomohopane	56.97	83182
191	C33HR	C33 22R 17a(H) trishomohopane	57.53	55126
191	C34HS	C34 22S 17a(H) extended hopane	59.31	49831
191	C34HR	C34 22R 17a(H) extended hopane	60.01	27100
191	C35HS	C35 22S 17a(H) extended hopane	61.62	32105
191	C35HR	C35 22R 17a(H) extended hopane	62.47	24454

Sample MH1 Inner

Saturate Biomarker Integration Results (Steranes)				
Ion	**Peak Label**	**Compound Name**	**R.Time (min.)**	**Peak Area**
217	S21	C21 sterane	26.30	70282
217	S22	C22 sterane	29.17	39929
217	27DbaS	C27 ba 20S diacholestane	38.01	91532
217	27DbaR	C27 ba 20R diacholestane	38.94	62820
217	28DbaSA	C28 ba 20S diasterane a	40.31	30761
217	28DbaSB	C28 ba 20S diasterane b	40.47	32494
217	28DbaRA	C28 ba 20R diasterane a	41.35	26504
217	28DbaRB	C28 ba 20R diasterane b	41.35	19818
217	27aaS	C27 aa 20S cholestane	42.12	65654
217	27bbR	C27 bb 20R cholestane	42.40	121583
217	27bbS	C27 bb 20S cholestane	42.65	66194
217	27aaR	C27 aa 20R cholestane	43.20	79403
217	28aaS	C28 aa 20S ergostane	44.57	43183
217	28bbR	C28 bb 20R ergostane	45.03	48696
217	28bbS	C28 bb 20S ergostane	45.26	48330
217	28aaR	C28 aa 20R ergostane	45.95	50362
217	29aaS	C29 aa 20S stigmastane	46.72	61425
217	29bbR	C29 bb 20R stigmastane	47.21	100217
217	29bbS	C29 bb 20S stigmastane	47.40	58404
217	29aaR	C29 aa 20R stigmastane	48.26	86697
218	27bbR	C27 bb 20R cholestane	42.39	133797
218	27bbS	C27 bb 20S cholestane	42.64	97680
218	28bbR	C28 bb 20R ergostane	45.04	87609
218	28bbS	C28 bb 20S ergostane	45.26	83963
218	29bbR	C29 bb 20R stigmastane	47.21	121572
218	29bbS	C29 bb 20S stigmastane	47.40	91651
259	27DbaS	C27 ba 20S diacholestane	38.01	18366
259	27DbaR	C27 ba 20R diacholestane	38.94	11707
259	28DbaSA	C28 ba 20S diaergostane a	40.31	5605
259	28DbaSB	C28 ba 20S diaergostane b	40.47	5269
259	28DbaRA	C28 ba 20R diaergostane a	41.35	5188
259	28DbaRB	C28 ba 20R diaergostane b	41.44	2399
259	29DbaS	C29 ba 20S diastigmastane	42.43	12585
259	29DbaR	C29 ba 20R diastigmastane	44.00	2578
259	30TP1	C30 Terpane	47.92	1814
259	30TP2	C30 Terpane	48.20	1720

Sample MH1 Inner Saturate Chromatograms; Terpanes

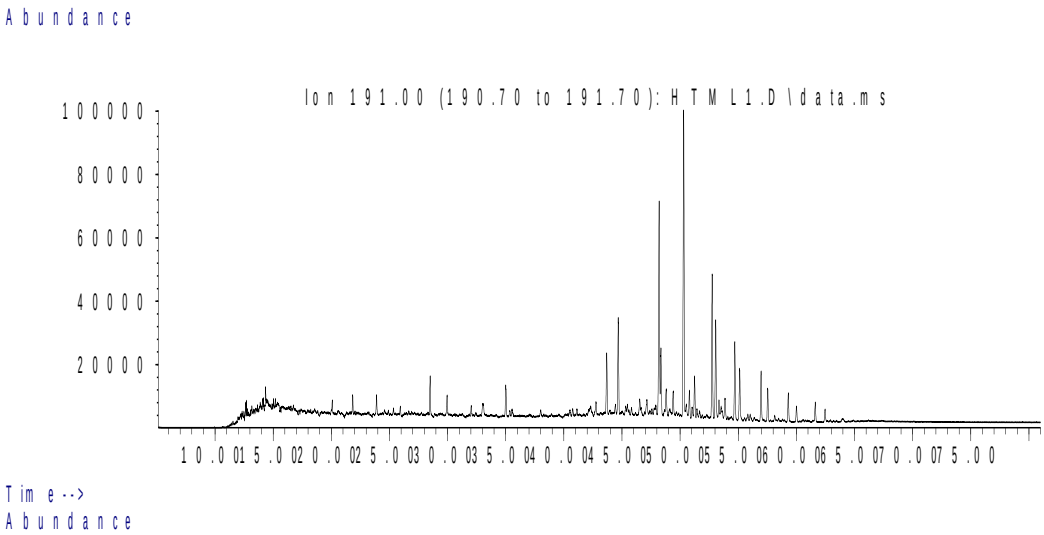

Sample MH1 Inner Saturate Chromatograms; Steranes & Steroids

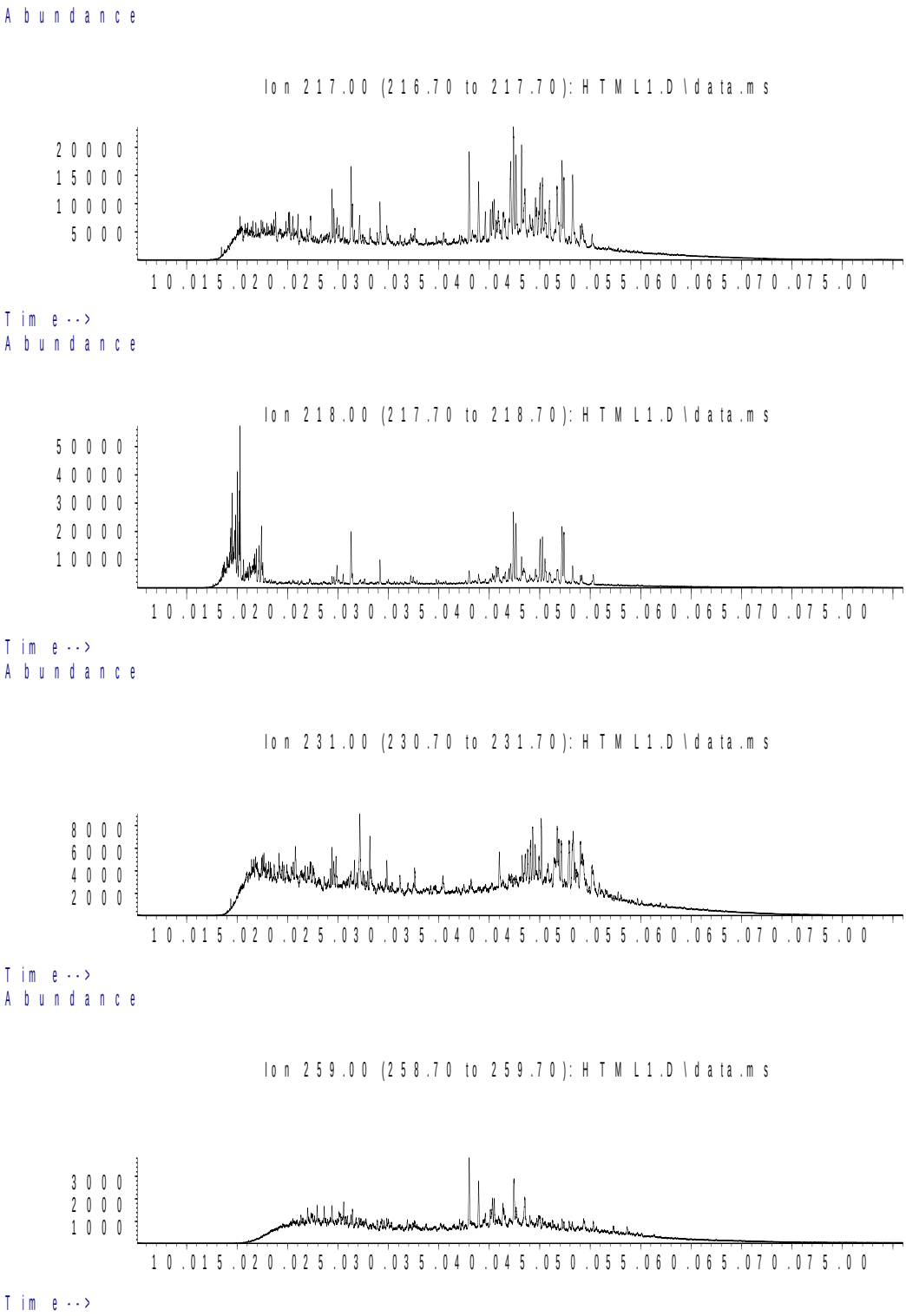

Sample MH1 Outer

Bulk Properties

Saturate (%)	17.9
Aromatics (%)	13.6
Resin (%)	17.0
Asphaltene (%)	51.5

Whole Oil/Extract GC

Pristane/Phytane	1.11
Pristane/n-C17	0.48
Phytane/n-C18	0.46

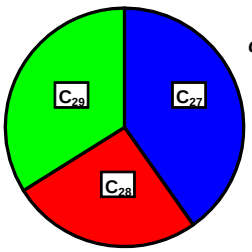

C_{27}-C_{28}-C_{29} αββ Steranes

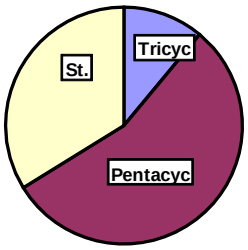

Tricyclic, Pentacyclic Terpanes & Steranes

Saturate Biomarker Interpretive Ratios

Interpretive Ratios	By Area
Terpanes (m/z 191)	
C19t/C23t	0.35
C22t/C21t	0.43
C22t/C24t	0.42
C24t/C23t	0.57
C26t/C25t	0.78
C24Tet/C23t	0.85
C24Tet/C26t	1.87
C23t/C30H	0.14
C24Tet/C30H	0.12
C28BNH/C30H	0.06
25-Nor/C30H	0.03
C29H/C30H	0.73
C30DiaH/C30H	0.07
Ole/C30H	0.00
C30Ts/C30H	0.08
Gam/C30H	0.05
Gam/C31HR	0.17
C35HS/C34HS	0.59
C35 Homohopane Index	0.06
Ts/(Ts+Tm)	0.38
C29Ts/(C29Ts+C29H)	0.21
Mor/C30H	0.12
C32 S/(S+R)	0.59
Steranes (m/z 217)	
% C27 ααα 20R	38.1
% C28 ααα 20R	21.7
% C29 ααα 20R	40.1
C27 Dia/(Dia+Reg)	0.54
(C21+C22)/(C27+C28+C29)	0.17
C29 αββ/(ααα+αββ)	0.50
C29 ααα 20S/20R	0.76
C29 ααα 20S/(S+R)	0.43
αββ−Steranes (m/z 218)	
% C27 αββ 20(R+S)	40.2
% C28 αββ 20(R+S)	25.9
% C29 αββ 20(R+S)	33.9
C29/C27 αββ Sterane Ratio	0.84
C27 Dia/Ster	0.66
Tricyclic/Pentacyclic Terpanes	0.20
Steranes/Terpanes	0.51
% Tricyclic Terpanes	11.0
% Pentacyclic Terpanes	55.2
% Steranes	33.8

Sample MH1 Outer

Saturate Biomarker Integration Results (Terpanes)				
Ion	**Peak Label**	**Compound Name**	**R.Time (min.)**	**Peak Area**
191	C19t	C19 tricyclic diterpane	19.81	36237
191	C20t	C20 tricyclic diterpane	21.54	48711
191	C21t	C21 tricyclic diterpane	23.54	57684
191	C22t	C22 tricyclic terpane	25.58	25031
191	C23t	C23 tricyclic terpane	28.12	103361
191	C24t	C24 tricyclic terpane	29.57	59207
191	C25tS	C25 tricyclic terpane (S)	32.60	24951
191	C25tR	C25 tricyclic terpane (R)	32.60	35335
191	C24T	C24 tetracyclic terpane (TET)	34.58	87699
191	C26tS	C26 tricyclic terpane (S)	34.94	20614
191	C26tR	C26 tricyclic terpane (R)	35.11	26193
191	C28tS	C28 extended tricyclic terpane (S)	40.07	24459
191	C28tR	C28 extended tricyclic terpane (R)	40.70	20879
191	C29tS	C29 extended tricyclic terpane (S)	41.88	15418
191	C29tR	C29 extended tricyclic terpane (R)	42.32	36755
191	C30tS	C30 extended tricyclic terpane (S)	45.00	14582
191	C30tR	C30 extended tricyclic terpane (R)	45.39	23026
191	Ts	Ts 18a(H)-trisnorhopane	43.23	152463
191	Tm	Tm 17a(H)-trisnorhopane	44.22	248851
191	C28BNH	C28 17a18a21b(H)-bisnorhopane	46.69	42930
191	Nor25H	C29 Nor-25-hopane	47.31	19359
191	C29H	C29 Tm 17a(H)21b(H)-norhopane	47.72	554837
191	C29Ts	C29 Ts 18a(H)-norneohopane	47.88	150294
191	C30DiaH	C30 17a(H)-diahopane	48.35	53290
191	Normor	C29 normoretane	48.94	55997
191	a-Ole	a-oleanane	49.56	1160
191	b-Ole	b-oleanane	49.56	1160
191	C30H	C30 17a(H)-hopane	49.84	760912
191	C30Ts	17a(H)-30-nor-29-homohopane	50.34	60692
191	Mor	C30 moretane	50.80	92843
191	C31HS	C31 22S 17a(H) homohopane	52.31	307661
191	C31HR	C31 22R 17a(H) homohopane	52.60	221505
191	Gam	gammacerane	52.89	36908
191	C32HS	C32 22S 17a(H) bishomohopane	54.26	160178
191	C32HR	C32 22R 17a(H) bishomohopane	54.68	111087
191	C33HS	C33 22S 17a(H) trishomohopane	56.53	92037
191	C33HR	C33 22R 17a(H) trishomohopane	57.12	62414
191	C34HS	C34 22S 17a(H) extended hopane	58.89	45372
191	C34HR	C34 22R 17a(H) extended hopane	59.60	27527
191	C35HS	C35 22S 17a(H) extended hopane	61.23	26759
191	C35HR	C35 22R 17a(H) extended hopane	62.08	18774

Sample MH1 Outer

Saturate Biomarker Integration Results (Steranes)				
Ion	**Peak Label**	**Compound Name**	**R.Time (min.)**	**Peak Area**
217	S21	C21 sterane	25.93	146801
217	S22	C22 sterane	28.77	76426
217	27DbaS	C27 ba 20S diacholestane	37.57	169133
217	27DbaR	C27 ba 20R diacholestane	38.50	118777
217	28DbaSA	C28 ba 20S diasterane a	39.66	45849
217	28DbaSB	C28 ba 20S diasterane b	39.88	55000
217	28DbaRA	C28 ba 20R diasterane a	40.92	29363
217	28DbaRB	C28 ba 20R diasterane b	41.15	29827
217	27aaS	C27 aa 20S cholestane	41.67	115837
217	27bbR	C27 bb 20R cholestane	41.96	209175
217	27bbS	C27 bb 20S cholestane	42.20	112089
217	27aaR	C27 aa 20R cholestane	42.75	127273
217	28aaS	C28 aa 20S ergostane	44.13	68952
217	28bbR	C28 bb 20R ergostane	44.57	85785
217	28bbS	C28 bb 20S ergostane	44.81	90055
217	28aaR	C28 aa 20R ergostane	45.49	72458
217	29aaS	C29 aa 20S stigmastane	46.28	101523
217	29bbR	C29 bb 20R stigmastane	46.75	140056
217	29bbS	C29 bb 20S stigmastane	46.96	95593
217	29aaR	C29 aa 20R stigmastane	47.82	133974
218	27bbR	C27 bb 20R cholestane	41.95	234536
218	27bbS	C27 bb 20S cholestane	42.19	170927
218	28bbR	C28 bb 20R ergostane	44.57	118396
218	28bbS	C28 bb 20S ergostane	44.82	142596
218	29bbR	C29 bb 20R stigmastane	46.77	194272
218	29bbS	C29 bb 20S stigmastane	46.96	147269
259	27DbaS	C27 ba 20S diacholestane	37.57	111755
259	27DbaR	C27 ba 20R diacholestane	38.51	72083
259	28DbaSA	C28 ba 20S diaergostane a	39.88	30697
259	28DbaSB	C28 ba 20S diaergostane b	40.06	37344
259	28DbaRA	C28 ba 20R diaergostane a	40.90	27603
259	28DbaRB	C28 ba 20R diaergostane b	41.14	11165
259	29DbaS	C29 ba 20S diastigmastane	42.00	88985
259	29DbaR	C29 ba 20R diastigmastane	43.59	14246
259	30TP1	C30 Terpane	47.46	9545
259	30TP2	C30 Terpane	47.74	10530

Sample MH1 Outer Saturate Chromatograms; Terpanes

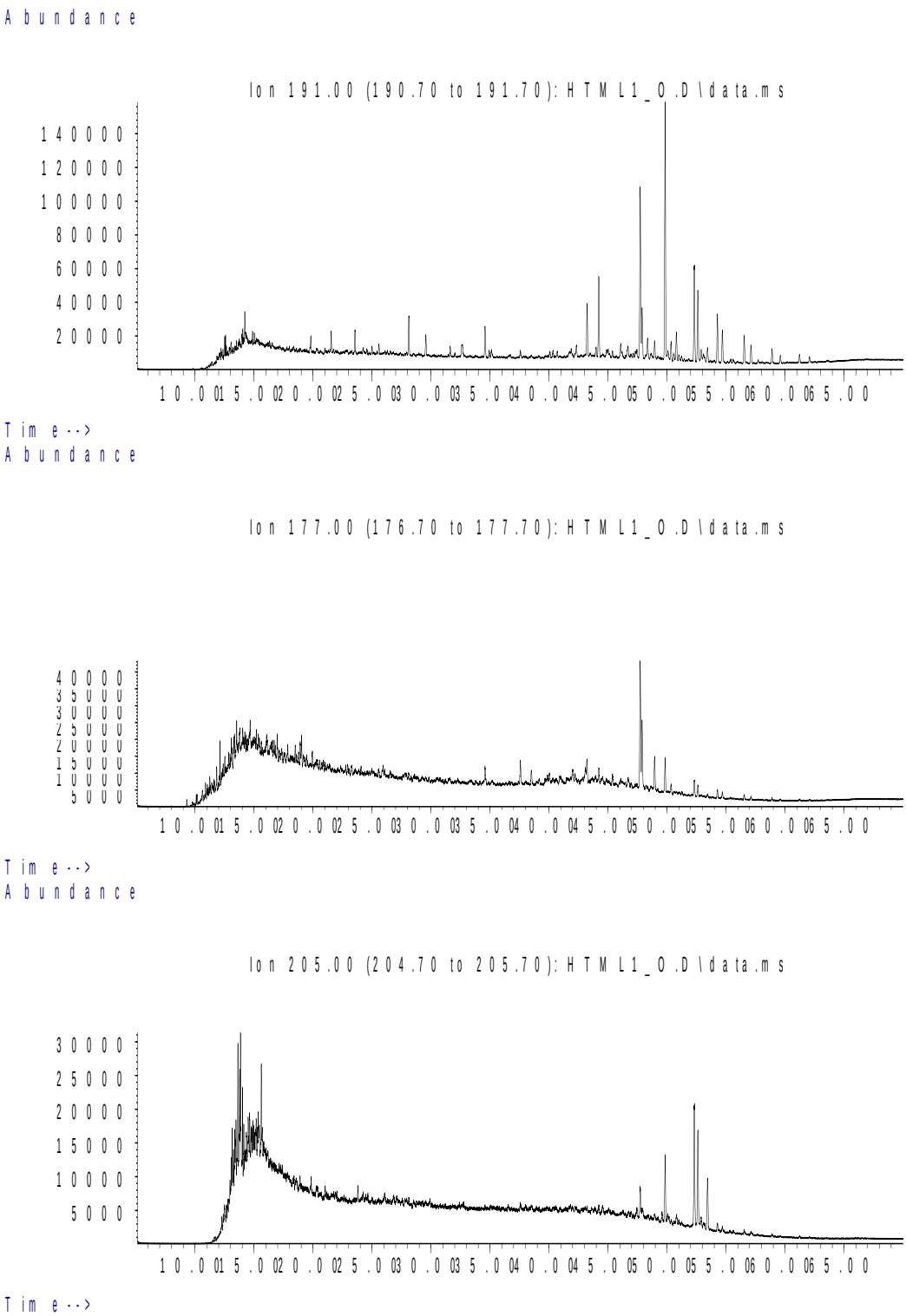

Sample MH1 Outer Saturate Chromatograms; Steranes & Steroids

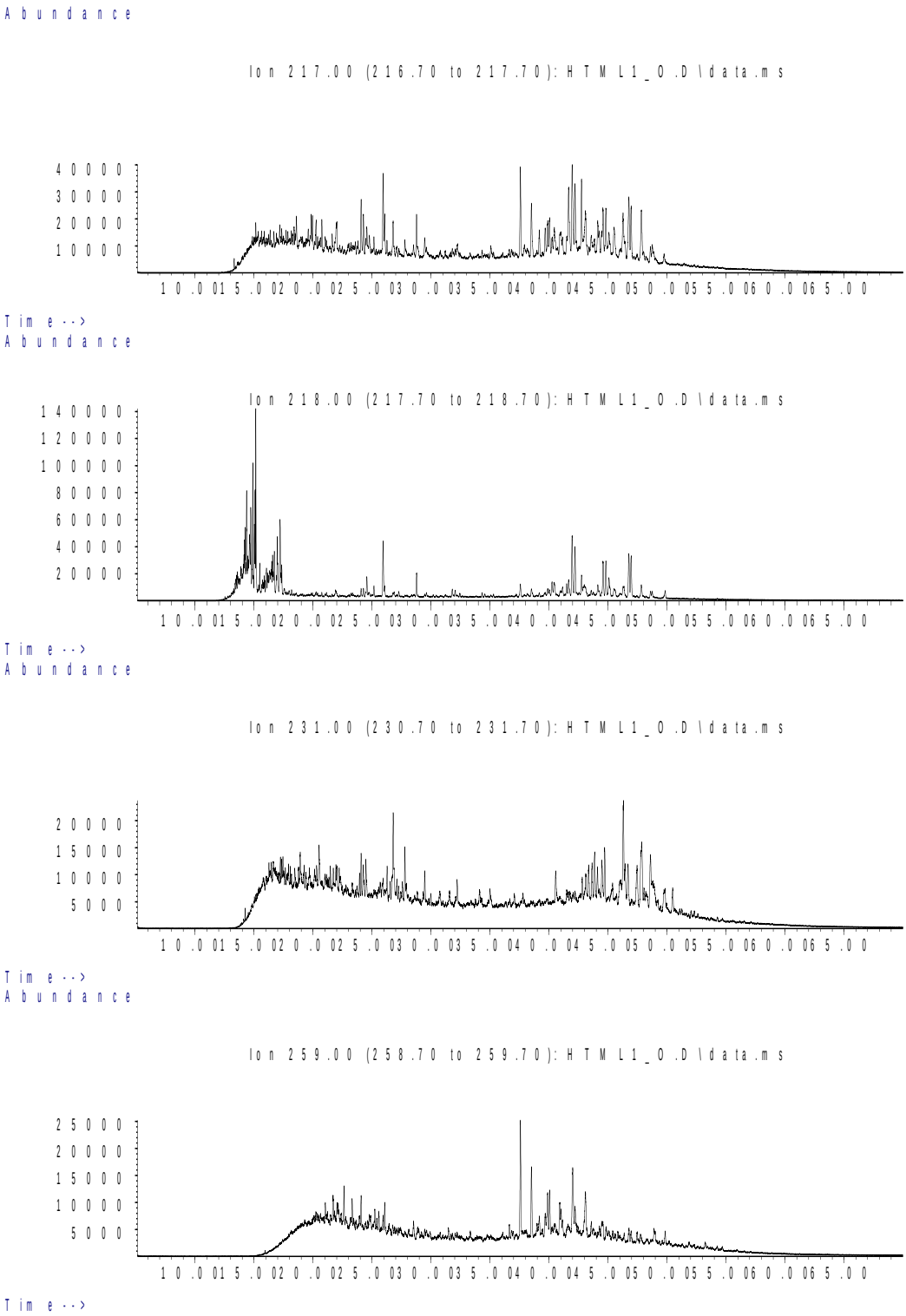

Sample NZ1 Inner

Bulk Properties

Saturate (%)	24.6
Aromatics (%)	13.1
Resin (%)	16.9
Asphaltene (%)	45.4

Whole Oil/Extract GC

Pristane/Phytane	1.10
Pristane/n-C17	0.47
Phytane/n-C18	0.44

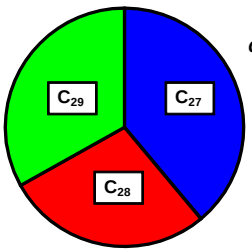

C_{27}-C_{28}-C_{29} αββ Steranes

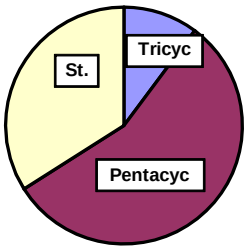

Tricyclic, Pentacyclic Terpanes & Steranes

Saturate Biomarker Interpretive Ratios

Interpretive Ratios	By Area
Terpanes (m/z 191)	
C19t/C23t	0.21
C22t/C21t	0.29
C22t/C24t	0.30
C24t/C23t	0.56
C26t/C25t	0.60
C24Tet/C23t	0.68
C24Tet/C26t	1.97
C23t/C30H	0.15
C24Tet/C30H	0.10
C28BNH/C30H	0.07
25-Nor/C30H	0.03
C29H/C30H	0.75
C30DiaH/C30H	0.07
Ole/C30H	0.00
C30Ts/C30H	0.08
Gam/C30H	0.05
Gam/C31HR	0.18
C35HS/C34HS	0.53
C35 Homohopane Index	0.07
Ts/(Ts+Tm)	0.40
C29Ts/(C29Ts+C29H)	0.20
Mor/C30H	0.12
C32 S/(S+R)	0.59
Steranes (m/z 217)	
% C27 ααα 20R	36.7
% C28 ααα 20R	24.3
% C29 ααα 20R	39.1
C27 Dia/(Dia+Reg)	0.48
(C21+C22)/(C27+C28+C29)	0.14
C29 αββ/(ααα+αββ)	0.52
C29 ααα 20S/20R	0.88
C29 ααα 20S/(S+R)	0.47
αββ−Steranes (m/z 218)	
% C27 αββ 20(R+S)	38.9
% C28 αββ 20(R+S)	28.0
% C29 αββ 20(R+S)	33.1
C29/C27 αββ Sterane Ratio	0.85
C27 Dia/Ster	0.57
Tricyclic/Pentacyclic Terpanes	0.18
Steranes/Terpanes	0.51
% Tricyclic Terpanes	10.2
% Pentacyclic Terpanes	55.8
% Steranes	34.0

Sample NZ1 Inner

Saturate Biomarker Integration Results (Terpanes)				
Ion	**Peak Label**	**Compound Name**	**R.Time (min.)**	**Peak Area**
191	C19t	C19 tricyclic diterpane	20.06	16296
191	C20t	C20 tricyclic diterpane	21.84	14515
191	C21t	C21 tricyclic diterpane	23.98	45104
191	C22t	C22 tricyclic terpane	26.00	13305
191	C23t	C23 tricyclic terpane	28.57	78832
191	C24t	C24 tricyclic terpane	30.03	44134
191	C25tS	C25 tricyclic terpane (S)	32.98	24805
191	C25tR	C25 tricyclic terpane (R)	33.10	20734
191	C24T	C24 tetracyclic terpane (TET)	35.08	53843
191	C26tS	C26 tricyclic terpane (S)	35.44	11813
191	C26tR	C26 tricyclic terpane (R)	35.62	15490
191	C28tS	C28 extended tricyclic terpane (S)	40.88	26076
191	C28tR	C28 extended tricyclic terpane (R)	41.18	12816
191	C29tS	C29 extended tricyclic terpane (S)	42.28	7787
191	C29tR	C29 extended tricyclic terpane (R)	42.82	25009
191	C30tS	C30 extended tricyclic terpane (S)	45.52	10928
191	C30tR	C30 extended tricyclic terpane (R)	45.86	10707
191	Ts	Ts 18a(H)-trisnorhopane	43.75	119100
191	Tm	Tm 17a(H)-trisnorhopane	44.75	175128
191	C28BNH	C28 17a18a21b(H)-bisnorhopane	47.20	34519
191	Nor25H	C29 Nor-25-hopane	47.80	16241
191	C29H	C29 Tm 17a(H)21b(H)-norhopane	48.24	389746
191	C29Ts	C29 Ts 18a(H)-norneohopane	48.40	100432
191	C30DiaH	C30 17a(H)-diahopane	48.84	38451
191	Normor	C29 normoretane	49.44	44107
191	a-Ole	a-oleanane	50.02	225
191	b-Ole	b-oleanane	50.02	225
191	C30H	C30 17a(H)-hopane	50.34	521045
191	C30Ts	17a(H)-30-nor-29-homohopane	50.84	39257
191	Mor	C30 moretane	51.28	61255
191	C31HS	C31 22S 17a(H) homohopane	52.78	215764
191	C31HR	C31 22R 17a(H) homohopane	53.09	155338
191	Gam	gammacerane	53.36	27881
191	C32HS	C32 22S 17a(H) bishomohopane	54.71	118533
191	C32HR	C32 22R 17a(H) bishomohopane	55.13	81568
191	C33HS	C33 22S 17a(H) trishomohopane	56.97	69889
191	C33HR	C33 22R 17a(H) trishomohopane	57.55	44456
191	C34HS	C34 22S 17a(H) extended hopane	59.31	47388
191	C34HR	C34 22R 17a(H) extended hopane	60.01	22018
191	C35HS	C35 22S 17a(H) extended hopane	61.62	25171
191	C35HR	C35 22R 17a(H) extended hopane	62.46	20304

Sample NZ1 Inner

Saturate Biomarker Integration Results (Steranes)				
Ion	**Peak Label**	**Compound Name**	**R.Time (min.)**	**Peak Area**
217	S21	C21 sterane	26.38	88656
217	S22	C22 sterane	29.25	47910
217	27DbaS	C27 ba 20S diacholestane	38.07	108758
217	27DbaR	C27 ba 20R diacholestane	39.02	71939
217	28DbaSA	C28 ba 20S diasterane a	40.18	22937
217	28DbaSB	C28 ba 20S diasterane b	40.54	42170
217	28DbaRA	C28 ba 20R diasterane a	41.43	27585
217	28DbaRB	C28 ba 20R diasterane b	41.43	28436
217	27aaS	C27 aa 20S cholestane	42.18	105282
217	27bbR	C27 bb 20R cholestane	42.47	134313
217	27bbS	C27 bb 20S cholestane	42.72	70591
217	27aaR	C27 aa 20R cholestane	43.27	89656
217	28aaS	C28 aa 20S ergostane	44.62	42965
217	28bbR	C28 bb 20R ergostane	45.06	52882
217	28bbS	C28 bb 20S ergostane	45.32	77028
217	28aaR	C28 aa 20R ergostane	46.02	59290
217	29aaS	C29 aa 20S stigmastane	46.77	83604
217	29bbR	C29 bb 20R stigmastane	47.26	102285
217	29bbS	C29 bb 20S stigmastane	47.46	90103
217	29aaR	C29 aa 20R stigmastane	48.31	95497
218	27bbR	C27 bb 20R cholestane	42.46	148028
218	27bbS	C27 bb 20S cholestane	42.71	110671
218	28bbR	C28 bb 20R ergostane	45.08	92541
218	28bbS	C28 bb 20S ergostane	45.33	93443
218	29bbR	C29 bb 20R stigmastane	47.26	119443
218	29bbS	C29 bb 20S stigmastane	47.44	100582
259	27DbaS	C27 ba 20S diacholestane	38.08	19567
259	27DbaR	C27 ba 20R diacholestane	39.01	14074
259	28DbaSA	C28 ba 20S diaergostane a	40.38	8426
259	28DbaSB	C28 ba 20S diaergostane b	40.56	6157
259	28DbaRA	C28 ba 20R diaergostane a	41.30	6664
259	28DbaRB	C28 ba 20R diaergostane b	41.41	3714
259	29DbaS	C29 ba 20S diastigmastane	42.49	15674
259	29DbaR	C29 ba 20R diastigmastane	44.08	2826
259	30TP1	C30 Terpane	47.95	2476
259	30TP2	C30 Terpane	48.25	2097

Sample NZ1 Inner Saturate Chromatograms; Terpanes

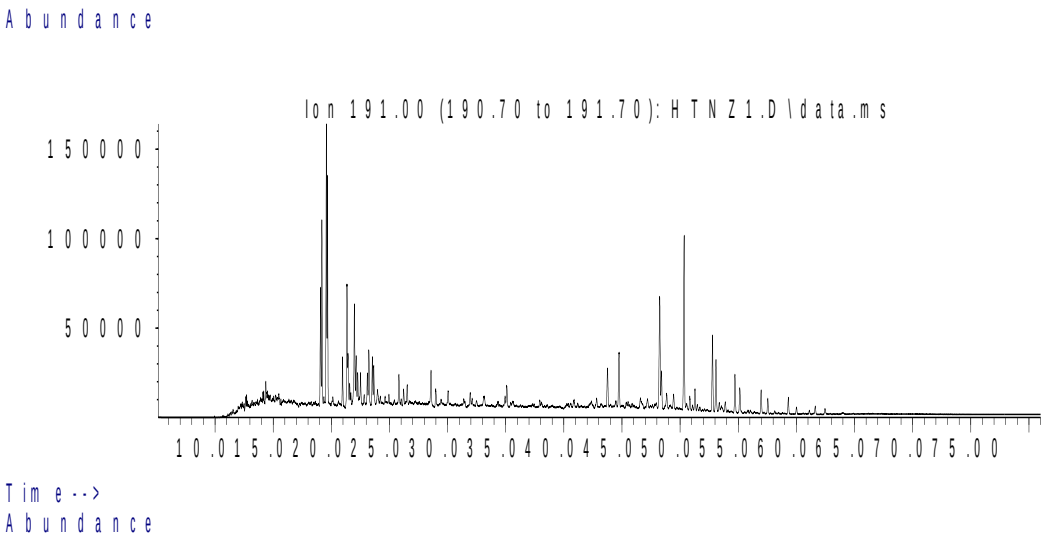

Sample NZ1 Inner Saturate Chromatograms; Steranes & Steroids

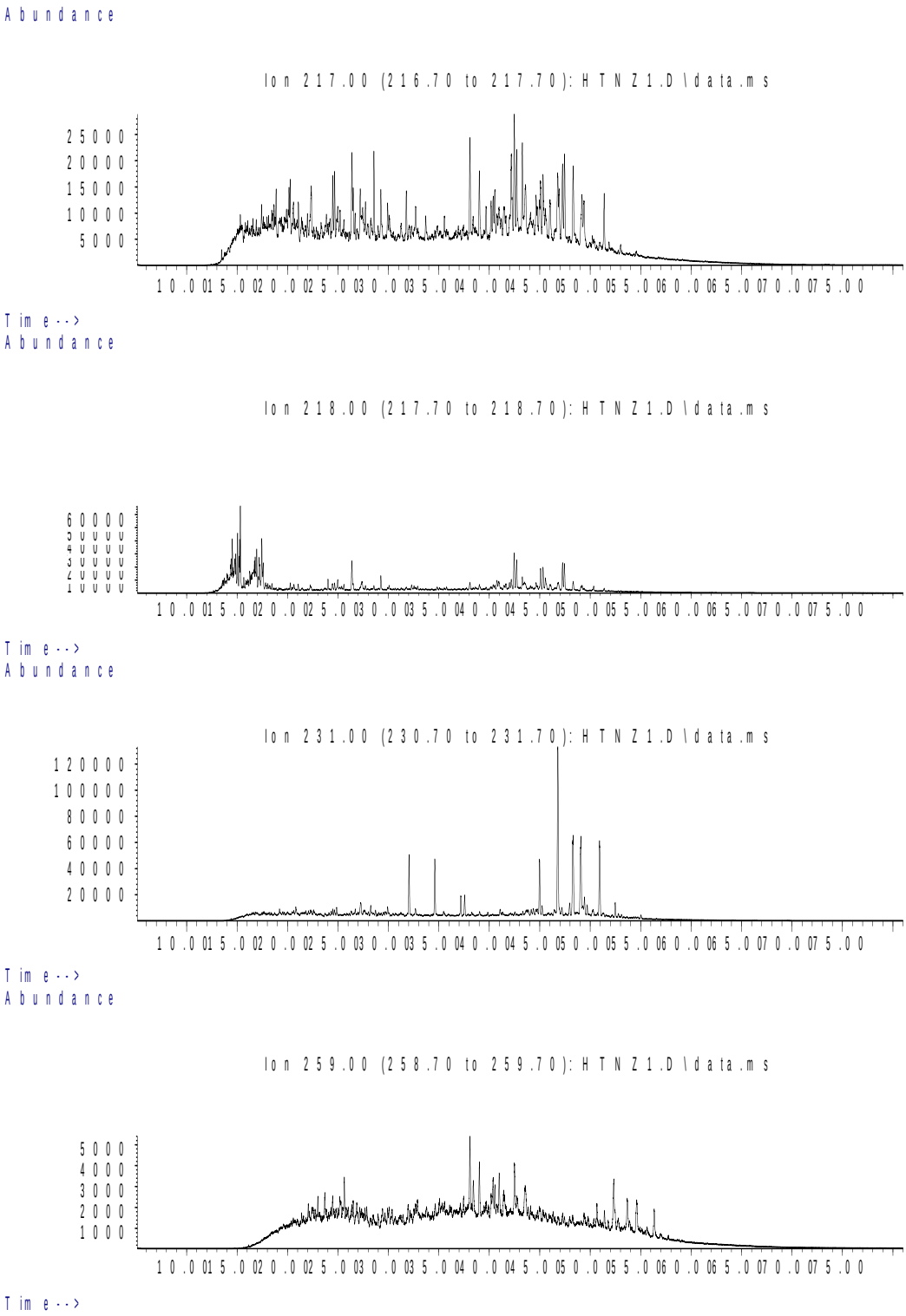

Sample NZ1 Outer

Bulk Properties

Saturate (%)	20.4
Aromatics (%)	12.6
Resin (%)	22.0
Asphaltene (%)	45.0

Whole Oil/Extract GC

Pristane/Phytane	1.08
Pristane/n-C17	0.44
Phytane/n-C18	0.42

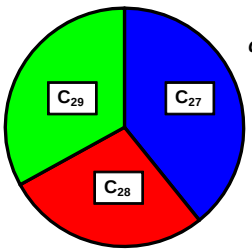

C_{27}-C_{28}-C_{29} αββ Steranes

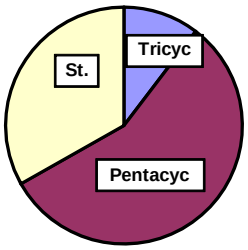

Tricyclic, Pentacyclic Terpanes & Steranes

Saturate Biomarker Interpretive Ratios

Interpretive Ratios	By Area
Terpanes (m/z 191)	
C19t/C23t	0.32
C22t/C21t	0.46
C22t/C24t	0.40
C24t/C23t	0.55
C26t/C25t	0.75
C24Tet/C23t	0.87
C24Tet/C26t	2.13
C23t/C30H	0.13
C24Tet/C30H	0.12
C28BNH/C30H	0.06
25-Nor/C30H	0.02
C29H/C30H	0.72
C30DiaH/C30H	0.09
Ole/C30H	0.00
C30Ts/C30H	0.08
Gam/C30H	0.05
Gam/C31HR	0.16
C35HS/C34HS	0.50
C35 Homohopane Index	0.06
Ts/(Ts+Tm)	0.39
C29Ts/(C29Ts+C29H)	0.22
Mor/C30H	0.12
C32 S/(S+R)	0.59
Steranes (m/z 217)	
% C27 ααα 20R	40.5
% C28 ααα 20R	22.9
% C29 ααα 20R	36.6
C27 Dia/(Dia+Reg)	0.51
(C21+C22)/(C27+C28+C29)	0.17
C29 αββ/(ααα+αββ)	0.52
C29 ααα 20S/20R	0.91
C29 ααα 20S/(S+R)	0.48
αββ−Steranes (m/z 218)	
% C27 αββ 20(R+S)	39.2
% C28 αββ 20(R+S)	27.8
% C29 αββ 20(R+S)	33.0
C29/C27 αββ Sterane Ratio	0.84
C27 Dia/Ster	0.60
Tricyclic/Pentacyclic Terpanes	0.18
Steranes/Terpanes	0.50
% Tricyclic Terpanes	10.4
% Pentacyclic Terpanes	56.5
% Steranes	33.2

Sample NZ1 Outer

Saturate Biomarker Integration Results (Terpanes)				
Ion	**Peak Label**	**Compound Name**	**R.Time (min.)**	**Peak Area**
191	C19t	C19 tricyclic diterpane	19.79	29650
191	C20t	C20 tricyclic diterpane	21.52	40114
191	C21t	C21 tricyclic diterpane	23.54	44093
191	C22t	C22 tricyclic terpane	25.57	20222
191	C23t	C23 tricyclic terpane	28.10	91286
191	C24t	C24 tricyclic terpane	29.54	50099
191	C25tS	C25 tricyclic terpane (S)	32.59	23025
191	C25tR	C25 tricyclic terpane (R)	32.59	26312
191	C24T	C24 tetracyclic terpane (TET)	34.56	79126
191	C26tS	C26 tricyclic terpane (S)	34.91	15368
191	C26tR	C26 tricyclic terpane (R)	35.10	21737
191	C28tS	C28 extended tricyclic terpane (S)	40.06	23711
191	C28tR	C28 extended tricyclic terpane (R)	40.67	16602
191	C29tS	C29 extended tricyclic terpane (S)	41.86	13743
191	C29tR	C29 extended tricyclic terpane (R)	42.30	24916
191	C30tS	C30 extended tricyclic terpane (S)	44.99	13144
191	C30tR	C30 extended tricyclic terpane (R)	45.36	17803
191	Ts	Ts 18a(H)-trisnorhopane	43.21	140340
191	Tm	Tm 17a(H)-trisnorhopane	44.20	222163
191	C28BNH	C28 17a18a21b(H)-bisnorhopane	46.67	37592
191	Nor25H	C29 Nor-25-hopane	47.30	16068
191	C29H	C29 Tm 17a(H)21b(H)-norhopane	47.71	490820
191	C29Ts	C29 Ts 18a(H)-norneohopane	47.88	142403
191	C30DiaH	C30 17a(H)-diahopane	48.33	64654
191	Normor	C29 normoretane	48.93	49026
191	a-Ole	a-oleanane	49.56	933
191	b-Ole	b-oleanane	49.56	933
191	C30H	C30 17a(H)-hopane	49.83	683150
191	C30Ts	17a(H)-30-nor-29-homohopane	50.33	57404
191	Mor	C30 moretane	50.79	84469
191	C31HS	C31 22S 17a(H) homohopane	52.30	282777
191	C31HR	C31 22R 17a(H) homohopane	52.61	199424
191	Gam	gammacerane	52.90	32746
191	C32HS	C32 22S 17a(H) bishomohopane	54.26	145200
191	C32HR	C32 22R 17a(H) bishomohopane	54.68	100294
191	C33HS	C33 22S 17a(H) trishomohopane	56.54	82733
191	C33HR	C33 22R 17a(H) trishomohopane	57.11	55442
191	C34HS	C34 22S 17a(H) extended hopane	58.88	48590
191	C34HR	C34 22R 17a(H) extended hopane	59.60	24672
191	C35HS	C35 22S 17a(H) extended hopane	61.22	24383
191	C35HR	C35 22R 17a(H) extended hopane	62.06	19445

Sample NZ1 Outer

Saturate Biomarker Integration Results (Steranes)				
Ion	**Peak Label**	**Compound Name**	**R.Time (min.)**	**Peak Area**
217	S21	C21 sterane	25.91	126978
217	S22	C22 sterane	28.75	67979
217	27DbaS	C27 ba 20S diacholestane	37.56	139395
217	27DbaR	C27 ba 20R diacholestane	38.50	104626
217	28DbaSA	C28 ba 20S diasterane a	39.66	46071
217	28DbaSB	C28 ba 20S diasterane b	39.87	47055
217	28DbaRA	C28 ba 20R diasterane a	40.89	36129
217	28DbaRB	C28 ba 20R diasterane b	41.25	23012
217	27aaS	C27 aa 20S cholestane	41.64	126379
217	27bbR	C27 bb 20R cholestane	41.94	190651
217	27bbS	C27 bb 20S cholestane	42.18	97237
217	27aaR	C27 aa 20R cholestane	42.74	109140
217	28aaS	C28 aa 20S ergostane	44.11	59664
217	28bbR	C28 bb 20R ergostane	44.56	64398
217	28bbS	C28 bb 20S ergostane	44.80	77309
217	28aaR	C28 aa 20R ergostane	45.48	61610
217	29aaS	C29 aa 20S stigmastane	46.25	89556
217	29bbR	C29 bb 20R stigmastane	46.76	104322
217	29bbS	C29 bb 20S stigmastane	46.94	96162
217	29aaR	C29 aa 20R stigmastane	47.80	98740
218	27bbR	C27 bb 20R cholestane	41.94	202842
218	27bbS	C27 bb 20S cholestane	42.18	152857
218	28bbR	C28 bb 20R ergostane	44.57	127797
218	28bbS	C28 bb 20S ergostane	44.80	124308
218	29bbR	C29 bb 20R stigmastane	46.76	155353
218	29bbS	C29 bb 20S stigmastane	46.94	143949
259	27DbaS	C27 ba 20S diacholestane	37.55	91575
259	27DbaR	C27 ba 20R diacholestane	38.50	63017
259	28DbaSA	C28 ba 20S diaergostane a	39.87	27485
259	28DbaSB	C28 ba 20S diaergostane b	40.03	36552
259	28DbaRA	C28 ba 20R diaergostane a	40.88	27603
259	28DbaRB	C28 ba 20R diaergostane b	41.14	10069
259	29DbaS	C29 ba 20S diastigmastane	41.98	67059
259	29DbaR	C29 ba 20R diastigmastane	43.56	13468
259	30TP1	C30 Terpane	47.45	7856
259	30TP2	C30 Terpane	47.71	7840

Sample NZ1 Outer Saturate Chromatograms; Terpanes

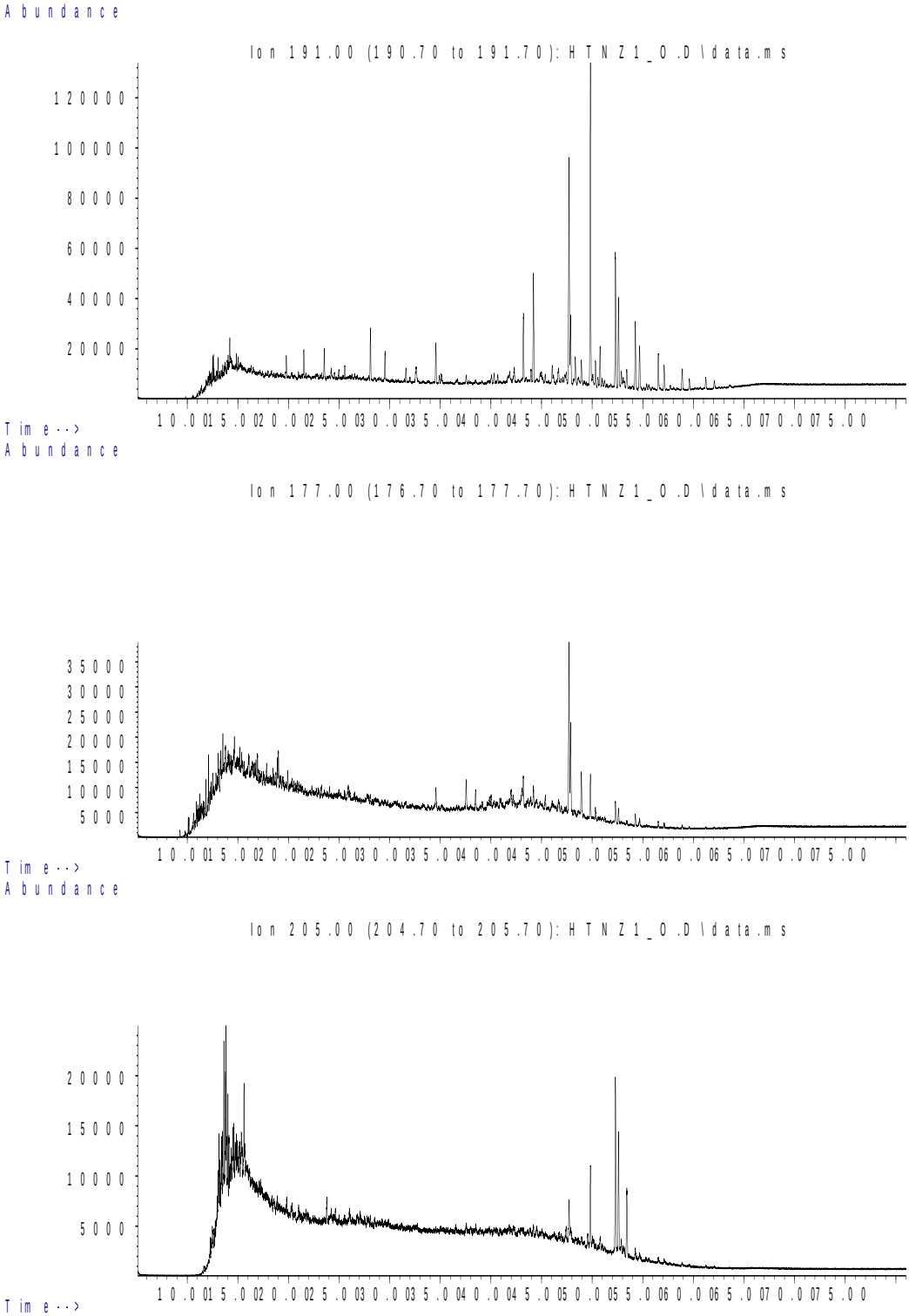

Sample NZ1 Outer Saturate Chromatograms; Steranes & Steroids

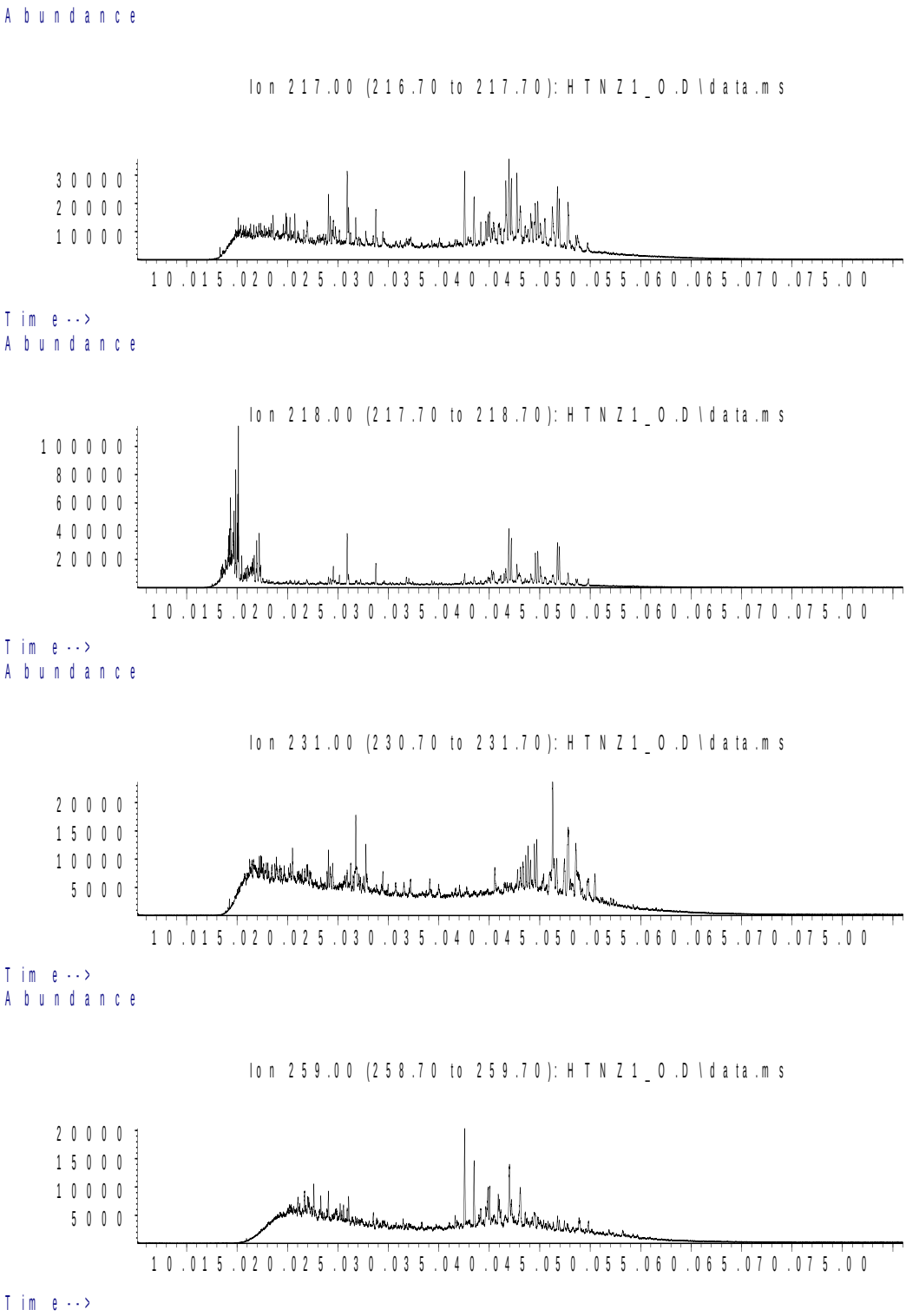

Sample NZ2 Inner

Bulk Properties

Saturate (%)	23.3
Aromatics (%)	12.7
Resin (%)	19.4
Asphaltene (%)	44.6

Whole Oil/Extract GC

Pristane/Phytane	1.14
Pristane/n-C17	0.48
Phytane/n-C18	0.43

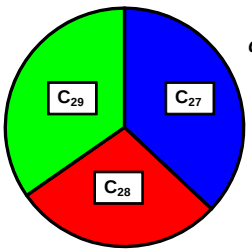

C_{27}-C_{28}-C_{29} αββ Steranes

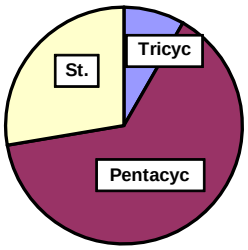

Tricyclic, Pentacyclic Terpanes & Steranes

Saturate Biomarker Interpretive Ratios

Interpretive Ratios	By Area
Terpanes (m/z 191)	
C19t/C23t	0.31
C22t/C21t	0.52
C22t/C24t	0.48
C24t/C23t	0.57
C26t/C25t	0.92
C24Tet/C23t	0.97
C24Tet/C26t	2.29
C23t/C30H	0.09
C24Tet/C30H	0.09
C28BNH/C30H	0.05
25-Nor/C30H	0.03
C29H/C30H	0.60
C30DiaH/C30H	0.10
Ole/C30H	0.00
C30Ts/C30H	0.09
Gam/C30H	0.06
Gam/C31HR	0.18
C35HS/C34HS	0.61
C35 Homohopane Index	0.08
Ts/(Ts+Tm)	0.39
C29Ts/(C29Ts+C29H)	0.26
Mor/C30H	0.13
C32 S/(S+R)	0.60
Steranes (m/z 217)	
% C27 ααα 20R	36.7
% C28 ααα 20R	22.3
% C29 ααα 20R	40.9
C27 Dia/(Dia+Reg)	0.55
(C21+C22)/(C27+C28+C29)	0.13
C29 αββ/(ααα+αββ)	0.51
C29 ααα 20S/20R	0.73
C29 ααα 20S/(S+R)	0.42
αββ−Steranes (m/z 218)	
% C27 αββ 20(R+S)	37.0
% C28 αββ 20(R+S)	28.3
% C29 αββ 20(R+S)	34.7
C29/C27 αββ Sterane Ratio	0.94
C27 Dia/Ster	0.66
Tricyclic/Pentacyclic Terpanes	0.13
Steranes/Terpanes	0.38
% Tricyclic Terpanes	8.3
% Pentacyclic Terpanes	64.1
% Steranes	27.7

Sample NZ2 Inner

Saturate Biomarker Integration Results (Terpanes)				
Ion	**Peak Label**	**Compound Name**	**R.Time (min.)**	**Peak Area**
191	C19t	C19 tricyclic diterpane	20.05	11397
191	C20t	C20 tricyclic diterpane	21.79	16054
191	C21t	C21 tricyclic diterpane	23.84	18639
191	C22t	C22 tricyclic terpane	25.88	9759
191	C23t	C23 tricyclic terpane	28.44	36290
191	C24t	C24 tricyclic terpane	29.89	20521
191	C25tS	C25 tricyclic terpane (S)	32.95	9412
191	C25tR	C25 tricyclic terpane (R)	32.95	7369
191	C24T	C24 tetracyclic terpane (TET)	34.94	35356
191	C26tS	C26 tricyclic terpane (S)	35.28	7282
191	C26tR	C26 tricyclic terpane (R)	35.48	8153
191	C28tS	C28 extended tricyclic terpane (S)	40.71	9425
191	C28tR	C28 extended tricyclic terpane (R)	41.06	7763
191	C29tS	C29 extended tricyclic terpane (S)	42.29	4906
191	C29tR	C29 extended tricyclic terpane (R)	42.70	15990
191	C30tS	C30 extended tricyclic terpane (S)	45.41	8507
191	C30tR	C30 extended tricyclic terpane (R)	45.76	9609
191	Ts	Ts 18a(H)-trisnorhopane	43.63	72485
191	Tm	Tm 17a(H)-trisnorhopane	44.62	115786
191	C28BNH	C28 17a18a21b(H)-bisnorhopane	47.09	20460
191	Nor25H	C29 Nor-25-hopane	47.86	11270
191	C29H	C29 Tm 17a(H)21b(H)-norhopane	48.13	236126
191	C29Ts	C29 Ts 18a(H)-norneohopane	48.29	84502
191	C30DiaH	C30 17a(H)-diahopane	48.75	38206
191	Normor	C29 normoretane	49.36	30173
191	a-Ole	a-oleanane	50.00	734
191	b-Ole	b-oleanane	50.00	734
191	C30H	C30 17a(H)-hopane	50.26	396332
191	C30Ts	17a(H)-30-nor-29-homohopane	50.75	36959
191	Mor	C30 moretane	51.21	52221
191	C31HS	C31 22S 17a(H) homohopane	52.72	184551
191	C31HR	C31 22R 17a(H) homohopane	53.02	130752
191	Gam	gammacerane	53.31	22906
191	C32HS	C32 22S 17a(H) bishomohopane	54.67	102143
191	C32HR	C32 22R 17a(H) bishomohopane	55.09	67866
191	C33HS	C33 22S 17a(H) trishomohopane	56.93	66073
191	C33HR	C33 22R 17a(H) trishomohopane	57.51	43810
191	C34HS	C34 22S 17a(H) extended hopane	59.29	42828
191	C34HR	C34 22R 17a(H) extended hopane	59.99	21469
191	C35HS	C35 22S 17a(H) extended hopane	61.61	25946
191	C35HR	C35 22R 17a(H) extended hopane	62.46	20533

Sample NZ2 Inner

Saturate Biomarker Integration Results (Steranes)				
Ion	**Peak Label**	**Compound Name**	**R.Time (min.)**	**Peak Area**
217	S21	C21 sterane	26.238	42224
217	S22	C22 sterane	29.102	25746
217	27DbaS	C27 ba 20S diacholestane	37.941	58988
217	27DbaR	C27 ba 20R diacholestane	38.87	46226
217	28DbaSA	C28 ba 20S diasterane a	40.244	22147
217	28DbaSB	C28 ba 20S diasterane b	40.409	28197
217	28DbaRA	C28 ba 20R diasterane a	41.301	18034
217	28DbaRB	C28 ba 20R diasterane b	41.461	13538
217	27aaS	C27 aa 20S cholestane	42.042	34263
217	27bbR	C27 bb 20R cholestane	42.334	79172
217	27bbS	C27 bb 20S cholestane	42.584	41949
217	27aaR	C27 aa 20R cholestane	43.136	51223
217	28aaS	C28 aa 20S ergostane	44.51	25186
217	28bbR	C28 bb 20R ergostane	44.967	36216
217	28bbS	C28 bb 20S ergostane	45.208	34229
217	28aaR	C28 aa 20R ergostane	45.902	31127
217	29aaS	C29 aa 20S stigmastane	46.661	41474
217	29bbR	C29 bb 20R stigmastane	47.143	51521
217	29bbS	C29 bb 20S stigmastane	47.336	49271
217	29aaR	C29 aa 20R stigmastane	48.205	57040
218	27bbR	C27 bb 20R cholestane	42.334	87261
218	27bbS	C27 bb 20S cholestane	42.584	70213
218	28bbR	C28 bb 20R ergostane	44.972	61200
218	28bbS	C28 bb 20S ergostane	45.208	59351
218	29bbR	C29 bb 20R stigmastane	47.143	69783
218	29bbS	C29 bb 20S stigmastane	47.336	77729
259	27DbaS	C27 ba 20S diacholestane	37.941	10435
259	27DbaR	C27 ba 20R diacholestane	38.885	7413
259	28DbaSA	C28 ba 20S diaergostane a	40.244	3595
259	28DbaSB	C28 ba 20S diaergostane b	40.414	4272
259	28DbaRA	C28 ba 20R diaergostane a	41.287	2981
259	28DbaRB	C28 ba 20R diaergostane b	41.504	1386
259	29DbaS	C29 ba 20S diastigmastane	42.377	7848
259	29DbaR	C29 ba 20R diastigmastane	43.953	1426
259	30TP1	C30 Terpane	47.86	1729
259	30TP2	C30 Terpane	48.157	1234

Sample NZ2 Inner Saturate Chromatograms; Terpanes

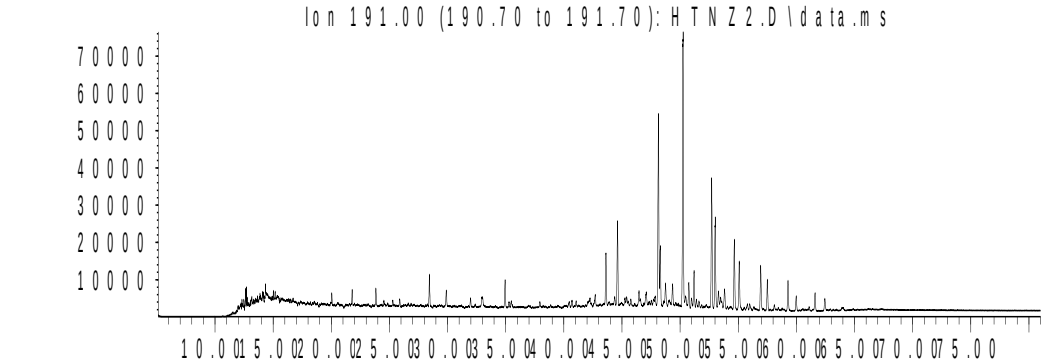

Sample NZ2 Inner Saturate Chromatograms; Steranes & Steroids

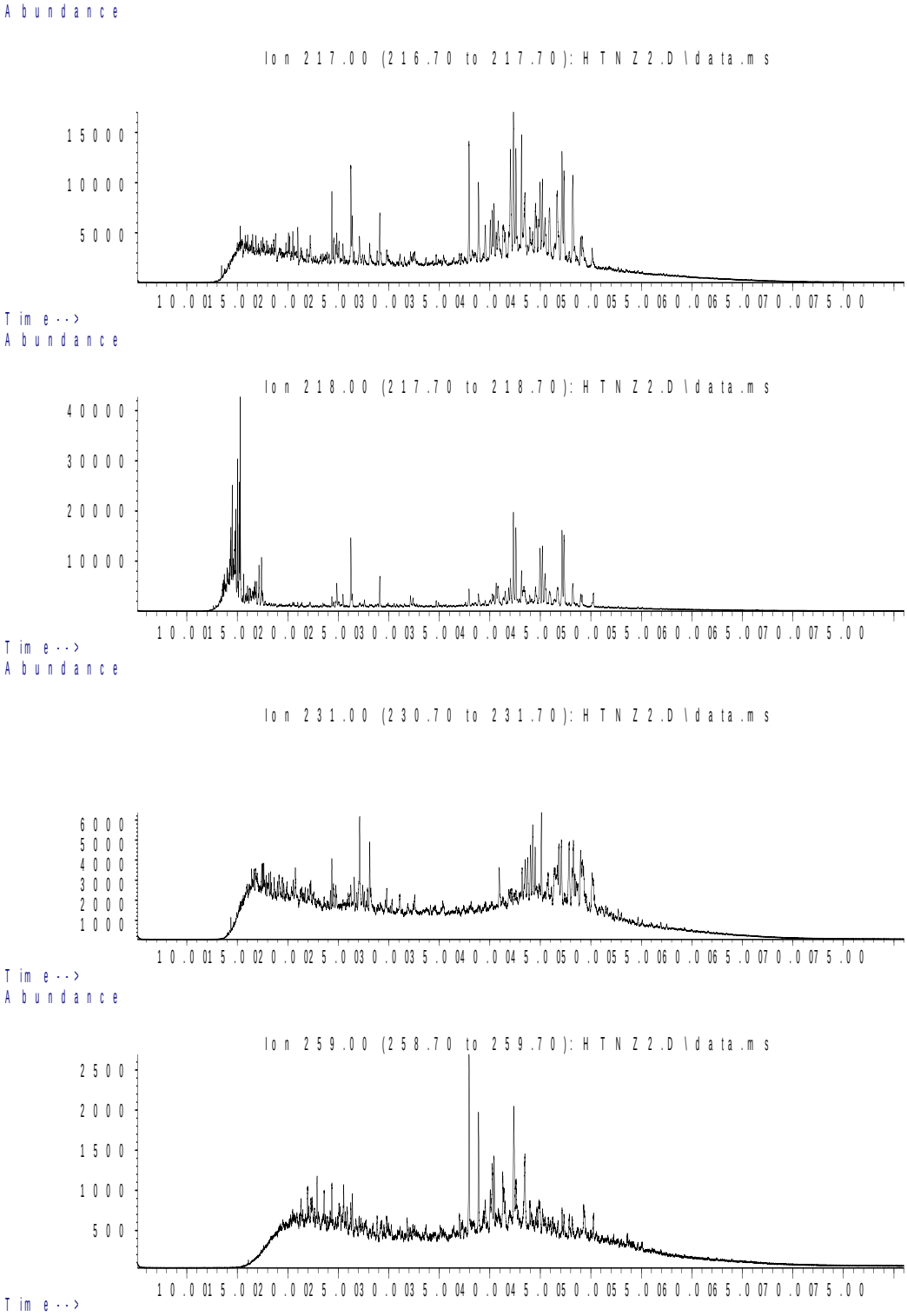

Sample NZ2 Outer

Bulk Properties

Saturate (%)	19.7
Aromatics (%)	12.8
Resin (%)	20.7
Asphaltene (%)	46.8

Whole Oil/Extract GC

Pristane/Phytane	1.21
Pristane/n-C17	0.47
Phytane/n-C18	0.41

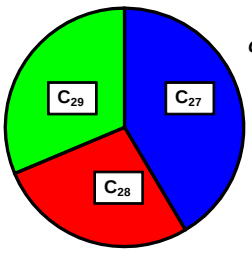

C_{27}-C_{28}-C_{29} αββ Steranes

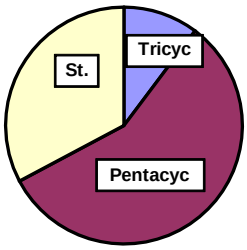

Tricyclic, Pentacyclic Terpanes & Steranes

Saturate Biomarker Interpretive Ratios

Interpretive Ratios	By Area
Terpanes (m/z 191)	
C19t/C23t	0.34
C22t/C21t	0.41
C22t/C24t	0.40
C24t/C23t	0.55
C26t/C25t	0.78
C24Tet/C23t	0.86
C24Tet/C26t	2.11
C23t/C30H	0.13
C24Tet/C30H	0.11
C28BNH/C30H	0.05
25-Nor/C30H	0.02
C29H/C30H	0.70
C30DiaH/C30H	0.09
Ole/C30H	0.01
C30Ts/C30H	0.08
Gam/C30H	0.05
Gam/C31HR	0.16
C35HS/C34HS	0.52
C35 Homohopane Index	0.06
Ts/(Ts+Tm)	0.38
C29Ts/(C29Ts+C29H)	0.23
Mor/C30H	0.12
C32 S/(S+R)	0.60
Steranes (m/z 217)	
% C27 ααα 20R	43.8
% C28 ααα 20R	22.4
% C29 ααα 20R	33.8
C27 Dia/(Dia+Reg)	0.49
(C21+C22)/(C27+C28+C29)	0.16
C29 αββ/(ααα+αββ)	0.52
C29 ααα 20S/20R	1.04
C29 ααα 20S/(S+R)	0.51
αββ−Steranes (m/z 218)	
% C27 αββ 20(R+S)	41.5
% C28 αββ 20(R+S)	27.2
% C29 αββ 20(R+S)	31.3
C29/C27 αββ Sterane Ratio	0.75
C27 Dia/Ster	0.57
Tricyclic/Pentacyclic Terpanes	0.18
Steranes/Terpanes	0.49
% Tricyclic Terpanes	10.2
% Pentacyclic Terpanes	57.0
% Steranes	32.8

Sample NZ2 Outer

Saturate Biomarker Integration Results (Terpanes)				
Ion	**Peak Label**	**Compound Name**	**R.Time (min.)**	**Peak Area**
191	C19t	C19 tricyclic diterpane	19.78	24748
191	C20t	C20 tricyclic diterpane	21.51	32166
191	C21t	C21 tricyclic diterpane	23.52	40015
191	C22t	C22 tricyclic terpane	25.55	16273
191	C23t	C23 tricyclic terpane	28.08	73562
191	C24t	C24 tricyclic terpane	29.52	40186
191	C25tS	C25 tricyclic terpane (S)	32.56	18229
191	C25tR	C25 tricyclic terpane (R)	32.56	20110
191	C24T	C24 tetracyclic terpane (TET)	34.54	62937
191	C26tS	C26 tricyclic terpane (S)	34.89	12501
191	C26tR	C26 tricyclic terpane (R)	35.07	17306
191	C28tS	C28 extended tricyclic terpane (S)	40.03	14760
191	C28tR	C28 extended tricyclic terpane (R)	40.66	13256
191	C29tS	C29 extended tricyclic terpane (S)	41.84	11135
191	C29tR	C29 extended tricyclic terpane (R)	42.29	27349
191	C30tS	C30 extended tricyclic terpane (S)	44.96	8659
191	C30tR	C30 extended tricyclic terpane (R)	45.35	15018
191	Ts	Ts 18a(H)-trisnorhopane	43.19	112575
191	Tm	Tm 17a(H)-trisnorhopane	44.18	182557
191	C28BNH	C28 17a18a21b(H)-bisnorhopane	46.65	26654
191	Nor25H	C29 Nor-25-hopane	47.28	12080
191	C29H	C29 Tm 17a(H)21b(H)-norhopane	47.69	402476
191	C29Ts	C29 Ts 18a(H)-norneohopane	47.86	117280
191	C30DiaH	C30 17a(H)-diahopane	48.32	51584
191	Normor	C29 normoretane	48.92	41075
191	a-Ole	a-oleanane	49.54	1926
191	b-Ole	b-oleanane	49.54	1926
191	C30H	C30 17a(H)-hopane	49.82	571134
191	C30Ts	17a(H)-30-nor-29-homohopane	50.31	48219
191	Mor	C30 moretane	50.77	70067
191	C31HS	C31 22S 17a(H) homohopane	52.29	237076
191	C31HR	C31 22R 17a(H) homohopane	52.59	166121
191	Gam	gammacerane	52.88	27095
191	C32HS	C32 22S 17a(H) bishomohopane	54.25	125013
191	C32HR	C32 22R 17a(H) bishomohopane	54.67	82856
191	C33HS	C33 22S 17a(H) trishomohopane	56.51	70668
191	C33HR	C33 22R 17a(H) trishomohopane	57.10	46127
191	C34HS	C34 22S 17a(H) extended hopane	58.88	40678
191	C34HR	C34 22R 17a(H) extended hopane	59.59	20500
191	C35HS	C35 22S 17a(H) extended hopane	61.22	20968
191	C35HR	C35 22R 17a(H) extended hopane	62.06	16260

Sample NZ2 Outer

Saturate Biomarker Integration Results (Steranes)				
Ion	**Peak Label**	**Compound Name**	**R.Time (min.)**	**Peak Area**
217	S21	C21 sterane	25.90	100471
217	S22	C22 sterane	28.73	50612
217	27DbaS	C27 ba 20S diacholestane	37.53	111098
217	27DbaR	C27 ba 20R diacholestane	38.47	81081
217	28DbaSA	C28 ba 20S diasterane a	39.64	38504
217	28DbaSB	C28 ba 20S diasterane b	39.85	38962
217	28DbaRA	C28 ba 20R diasterane a	40.87	29060
217	28DbaRB	C28 ba 20R diasterane b	41.11	24092
217	27aaS	C27 aa 20S cholestane	41.61	105214
217	27bbR	C27 bb 20R cholestane	41.93	156335
217	27bbS	C27 bb 20S cholestane	42.16	76775
217	27aaR	C27 aa 20R cholestane	42.71	94286
217	28aaS	C28 aa 20S ergostane	44.09	49852
217	28bbR	C28 bb 20R ergostane	44.54	57820
217	28bbS	C28 bb 20S ergostane	44.79	62243
217	28aaR	C28 aa 20R ergostane	45.46	48102
217	29aaS	C29 aa 20S stigmastane	46.24	75986
217	29bbR	C29 bb 20R stigmastane	46.73	96097
217	29bbS	C29 bb 20S stigmastane	46.92	64193
217	29aaR	C29 aa 20R stigmastane	47.79	72718
218	27bbR	C27 bb 20R cholestane	41.92	171508
218	27bbS	C27 bb 20S cholestane	42.16	129104
218	28bbR	C28 bb 20R ergostane	44.54	92878
218	28bbS	C28 bb 20S ergostane	44.79	104229
218	29bbR	C29 bb 20R stigmastane	46.74	127175
218	29bbS	C29 bb 20S stigmastane	46.91	99762
259	27DbaS	C27 ba 20S diacholestane	37.53	74575
259	27DbaR	C27 ba 20R diacholestane	38.47	51836
259	28DbaSA	C28 ba 20S diaergostane a	39.84	19073
259	28DbaSB	C28 ba 20S diaergostane b	40.01	30396
259	28DbaRA	C28 ba 20R diaergostane a	40.88	22338
259	28DbaRB	C28 ba 20R diaergostane b	41.11	10219
259	29DbaS	C29 ba 20S diastigmastane	41.96	51779
259	29DbaR	C29 ba 20R diastigmastane	43.54	9865
259	30TP1	C30 Terpane	47.43	7573
259	30TP2	C30 Terpane	47.71	6209

Sample NZ2 Outer Saturate Chromatograms; Terpanes

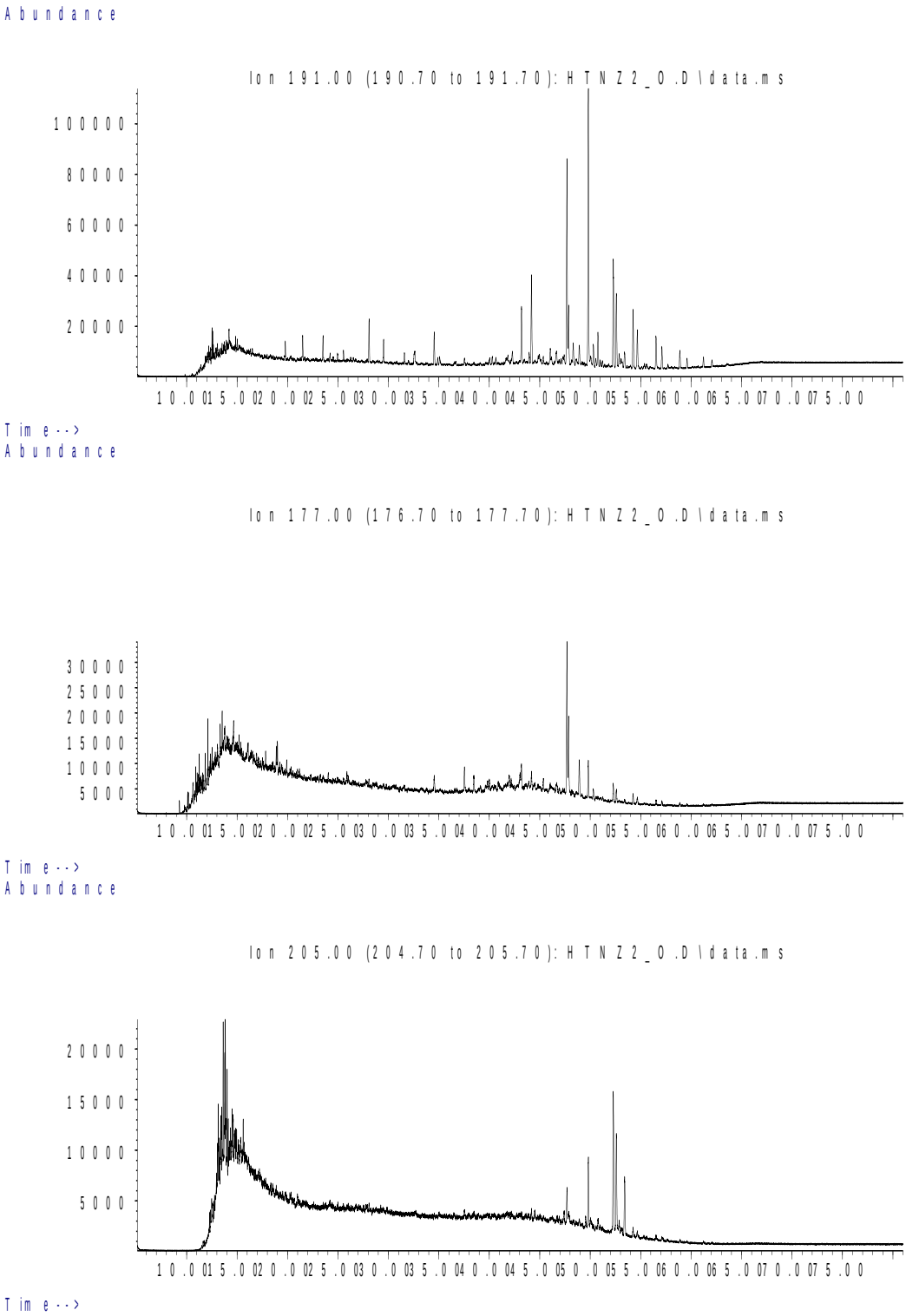

Sample NZ2 Outer Saturate Chromatograms; Steranes & Steroids

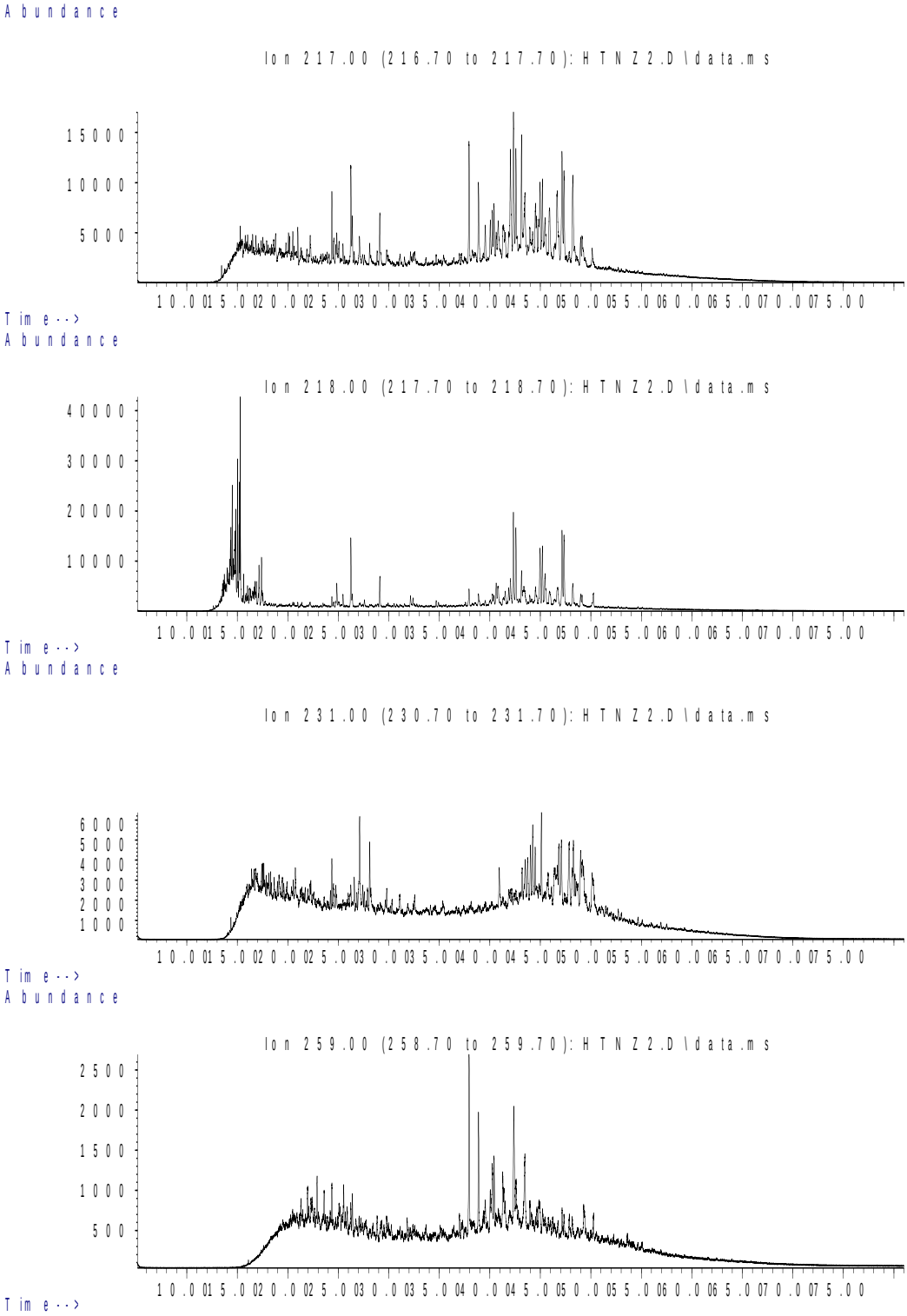

GC-MS Saturate Biomarker Interpretive Ratios, Peak Areas and Chromatograms.

Limestone Coast

Triamromatic Steriods	27A				CB32				162			
	outer	inner	diff	% diff	outer	inner	diff	% diff	outer	inner	diff	% diff
C26	19.6	18.5	-1.0	-5%	19.7	19.3	-0.5	-2%	20.1	18.3	-1.8	-10%
C27	40.9	42.9	2.0	5%	41.5	42.2	0.7	2%	41.1	42.3	1.3	3%
C28	32.6	31.7	-0.9	-3%	32.3	32.2	-0.1	0%	32.5	32.7	0.2	1%
C29	6.9	6.8	-0.1	-1%	6.4	6.3	-0.1	-1%	6.3	6.6	0.3	5%
Thiophenes												
DBT/MDBT	0.48	0.54	0.06	11%	0.41	0.24	-0.17	-41%	0.32	0.30	-0.03	-8%
DBT/C3 DBT	0.42	0.43	0.01	2%	0.28	0.11	-0.17	-61%	0.17	0.17	0.00	-2%
PAHs												
P/C1P	0.41	0.41	-0.01	-2%	0.43	0.38	-0.05	-12%	0.44	0.41	-0.03	-6%
P/C2P	0.28	0.29	0.01	2%	0.41	0.34	-0.07	-17%	0.40	0.38	-0.02	-6%
BaP/BbF	2.05	2.04	-0.01	-0.5%	1.97	1.89	-0.08	-4.3%	1.79	1.79	0.00	-0.1%

Kangaroo Island

Triamromatic Steriods	80				85				168				177			
	outer	inner	diff	% diff	outer	inner	diff	% diff	outer	inner	diff	% diff	outer	inner	diff	% diff
C26	19.2	19.1	-0.1	-1%	19.9	18.3	-1.5	-8%	18.8	19.1	0.2	1%	19.2	19.0	-0.2	-1%
C27	42.4	42.7	0.3	1%	42.2	43.2	1.0	2%	42.0	42.1	0.1	0%	41.7	42.9	1.1	3%
C28	32.5	32.0	-0.4	-1%	32.0	31.8	-0.1	0%	32.8	32.7	-0.1	0%	33.2	32.2	-1.0	-3%
C29	6.0	6.2	0.3	5%	6.0	6.6	0.6	11%	6.3	6.2	-0.2	-3%	5.9	6.0	0.1	2%
Thiophenes																
DBT/MDBT	0.31	0.44	0.12	28%	0.25	0.15	-0.10	-39%	0.45	0.40	-0.05	-12%	0.58	0.53	-0.06	-9%
DBT/C3 DBT	0.14	0.23	0.09	39%	0.13	0.02	-0.11	-82%	0.33	0.26	-0.07	-22%	0.50	0.44	-0.06	-12%
PAHs																
P/C1P	0.46	0.46	0.00	1%	0.44	0.44	-0.01	-1%	0.43	0.42	-0.02	-4%	0.52	0.52	-0.01	-1%
P/C2P	0.42	0.40	-0.02	-4%	0.40	0.40	-0.01	-1%	0.40	0.38	-0.03	-6%	0.53	0.52	-0.01	-2%
BaP/BbF	1.83	1.74	-0.09	-5.0%	1.70	1.68	-0.02	-1.3%	2.02	1.98	-0.04	-2.0%	1.98	1.97	-0.01	-0.4%

Eyre Peninsula

Triamromatic Steriods	cl1				mh1			
	outer	inner	diff	% diff	outer	inner	diff	% diff
C26	21.9	17.8	-4.1	-23%	18.5	18.4	-0.1	0%
C27	39.6	43.2	3.6	9%	42.5	43.2	0.7	2%
C28	32.0	32.3	0.3	1%	32.7	32.3	-0.4	-1%
C29	6.6	6.8	0.2	2%	6.4	6.1	-0.3	-5%
Thiophenes								
DBT/MDBT	0.43	0.42	-0.01	-3%	0.46	0.56	0.10	18%
DBT/C3 DBT	0.31	0.28	-0.03	-9%	0.34	0.46	0.12	26%
PAHs								
P/C1P	0.53	0.47	-0.05	-10%	0.50	0.50	0.00	0%
P/C2P	0.53	0.47	-0.06	-12%	0.51	0.50	-0.01	-2%
BaP/BbF	2.24	1.90	-0.35	-15.4%	2.18	2.13	-0.05	-2.4%

New Zealand

Triamromatic Steriods	nz1				nz2			
	outer	inner	diff	% diff	outer	inner	diff	% diff
C26	20.7	17.4	-3.3	-19%	19.3	18.6	-0.7	-4%
C27	44.4	43.6	-0.7	-2%	41.5	42.8	1.3	3%
C28	28.2	32.4	4.2	15%	32.2	32.3	0.2	0%
C29	6.7	6.6	-0.1	-2%	7.0	6.2	-0.8	-12%
Thiophenes								
DBT/MDBT	0.68	0.44	-0.25	-36%	0.54	0.39	-0.15	-28%
DBT/C3 DBT	0.21	0.33	0.12	37%	0.47	0.29	-0.18	-39%
PAHs								
P/C1P	0.16	0.44	0.28	63%	0.49	0.44	-0.05	-10%
P/C2P	0.04	0.43	0.39	90%	0.48	0.42	-0.06	-12%
BaP/BbF	1.86	1.81	-0.06	-3.0%	1.82	1.74	-0.09	-4.7%

Sample 27 Inner

Aromatic Biomarker Integration Results				
Ion	Peak Label	Compound Name	R.Time (min.)	Peak Area
178	P	Phenantrene	22.951	4427577
184	DBT	Dibenzothiophene	22.381	3227888
192	C1P iso 1	Methyl Phenanthrene Isomer	25.262	1903445
192	C1P iso 2	Methyl Phenanthrene Isomer	25.392	2377527
192	C1P iso 3	Methyl Phenanthrene Isomer	25.786	3648090
192	C1P iso 4	Methyl Phenanthrene Isomer	25.91	2764054
192	C1P sum	Methyl Phenanthrene Isomers (summed)		10693116
198	4 MDBT	4 Methyldibenzothiophene	24.412	2429304
198	2+3 MDBT	2 & 3 Methyldibenzothiophene	24.412	2427207
198	1 MDBT	1 Methyldibenzothiophene	25.288	1835784
206	C2P iso 1	Ethyl/Dimethyl Phenanthrene Isomer	27.573	986846
206	C2P iso 2	Ethyl/Dimethyl Phenanthrene Isomer	27.724	1085600
206	C2P iso 3	Ethyl/Dimethyl Phenanthrene Isomer	27.853	674743
206	C2P iso 4	Ethyl/Dimethyl Phenanthrene Isomer	28.118	4811451
206	C2P iso 5	Ethyl/Dimethyl Phenanthrene Isomer	28.289	2594261
206	C2P iso 6	Ethyl/Dimethyl Phenanthrene Isomer	28.403	2179551
206	C2P iso 7	Ethyl/Dimethyl Phenanthrene Isomer	28.548	687064
206	C2P iso 8	Ethyl/Dimethyl Phenanthrene Isomer	28.594	1364256
206	C2P iso 9	Ethyl/Dimethyl Phenanthrene Isomer	28.952	738498
206	C2P iso 10	Ethyl/Dimethyl Phenanthrene Isomer	29.278	659362
206	C2P sum	Ethyl/Dimethyl Phenanthrene Isomers (summed)		15781632
226	C3DBT sum	C3 Dibenzothiophene Isomers (summed)		7645358
252	dbf	benzo(b)fluoranthene	42.705	55554
252	bap	benzo(a)pyrene	44.073	114110

Sample 27 Inner Aromatic Chromatograms; Naphthalenes

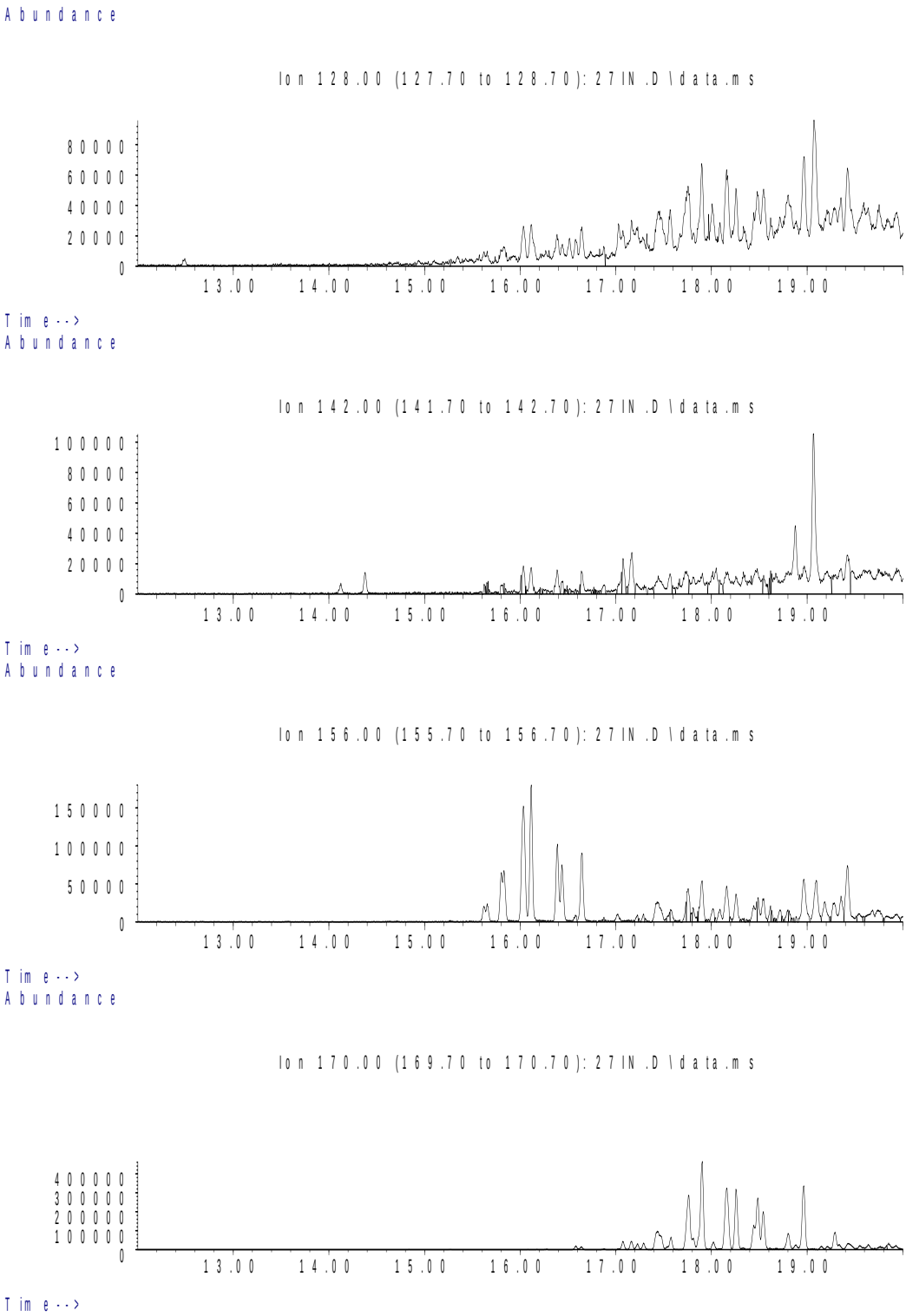

Sample 27 Inner Aromatic Chromatograms; Phenanthrenes

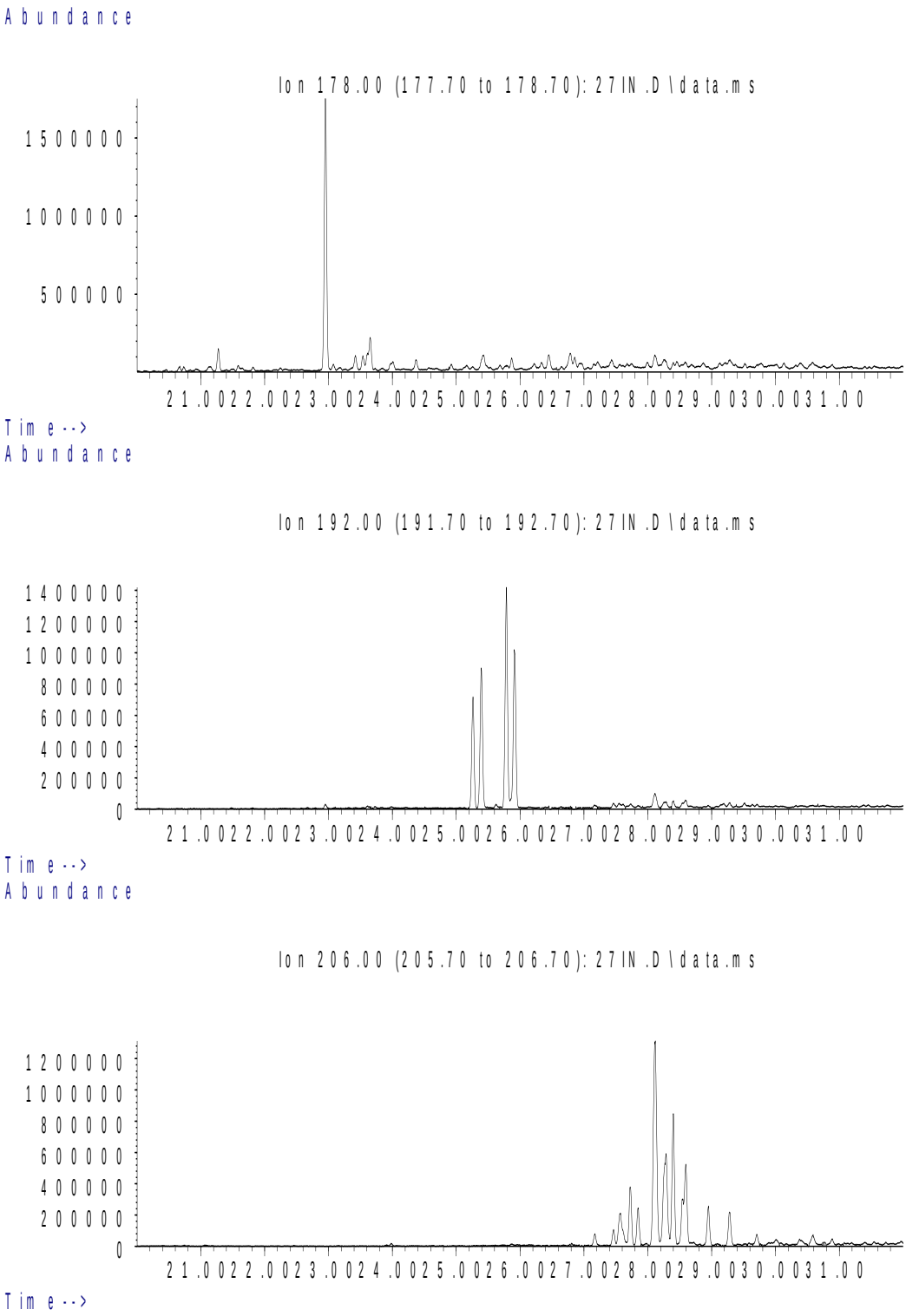

Sample 27 Inner Aromatic Chromatograms; Thiophenes & PAHs

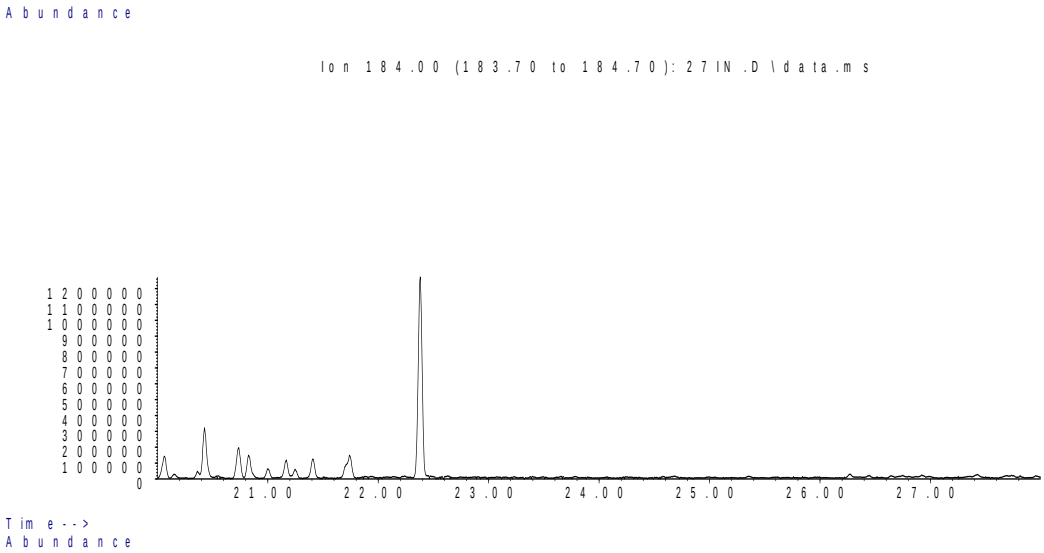

Sample 27 Outer

Aromatic Biomarker Integration Results				
Ion	Peak Label	Compound Name	R.Time (min.)	Peak Area
178	P	Phenantrene	22.946	3153539
184	DBT	Dibenzothiophene	22.376	2158299
192	C1P iso 1	Methyl Phenanthrene Isomer	25.258	1375685
192	C1P iso 2	Methyl Phenanthrene Isomer	25.387	1727188
192	C1P iso 3	Methyl Phenanthrene Isomer	25.781	2659433
192	C1P iso 4	Methyl Phenanthrene Isomer	25.911	1998289
192	C1P sum	Methyl Phenanthrene Isomers (summed)		7760595
198	4 MDBT	4 Methyldibenzothiophene	24.833	1037272
198	2+3 MDBT	2 & 3 Methyldibenzothiophene	24.403	1714473
198	1 MDBT	1 Methyldibenzothiophene	25.283	1209649
206	C2P iso 1	Ethyl/Dimethyl Phenanthrene Isomer	27.558	660405
206	C2P iso 2	Ethyl/Dimethyl Phenanthrene Isomer	27.719	757121
206	C2P iso 3	Ethyl/Dimethyl Phenanthrene Isomer	27.838	473590
206	C2P iso 4	Ethyl/Dimethyl Phenanthrene Isomer	28.108	3358153
206	C2P iso 5	Ethyl/Dimethyl Phenanthrene Isomer	28.279	1763234
206	C2P iso 6	Ethyl/Dimethyl Phenanthrene Isomer	28.393	1524061
206	C2P iso 7	Ethyl/Dimethyl Phenanthrene Isomer	28.543	545813
206	C2P iso 8	Ethyl/Dimethyl Phenanthrene Isomer	28.59	898554
206	C2P iso 9	Ethyl/Dimethyl Phenanthrene Isomer	28.942	525833
206	C2P iso 10	Ethyl/Dimethyl Phenanthrene Isomer	29.279	474553
206	C2P sum	Ethyl/Dimethyl Phenanthrene Isomers (summed)		10981317
226	C3DBT sum	C3 Dibenzothiophene Isomers (summed)		5020555
252	dbf	benzo(b)fluoranthene	42.706	41576
252	bap	benzo(a)pyrene	44.064	84934

Sample 27 Outer Aromatic Chromatograms; Naphthalenes

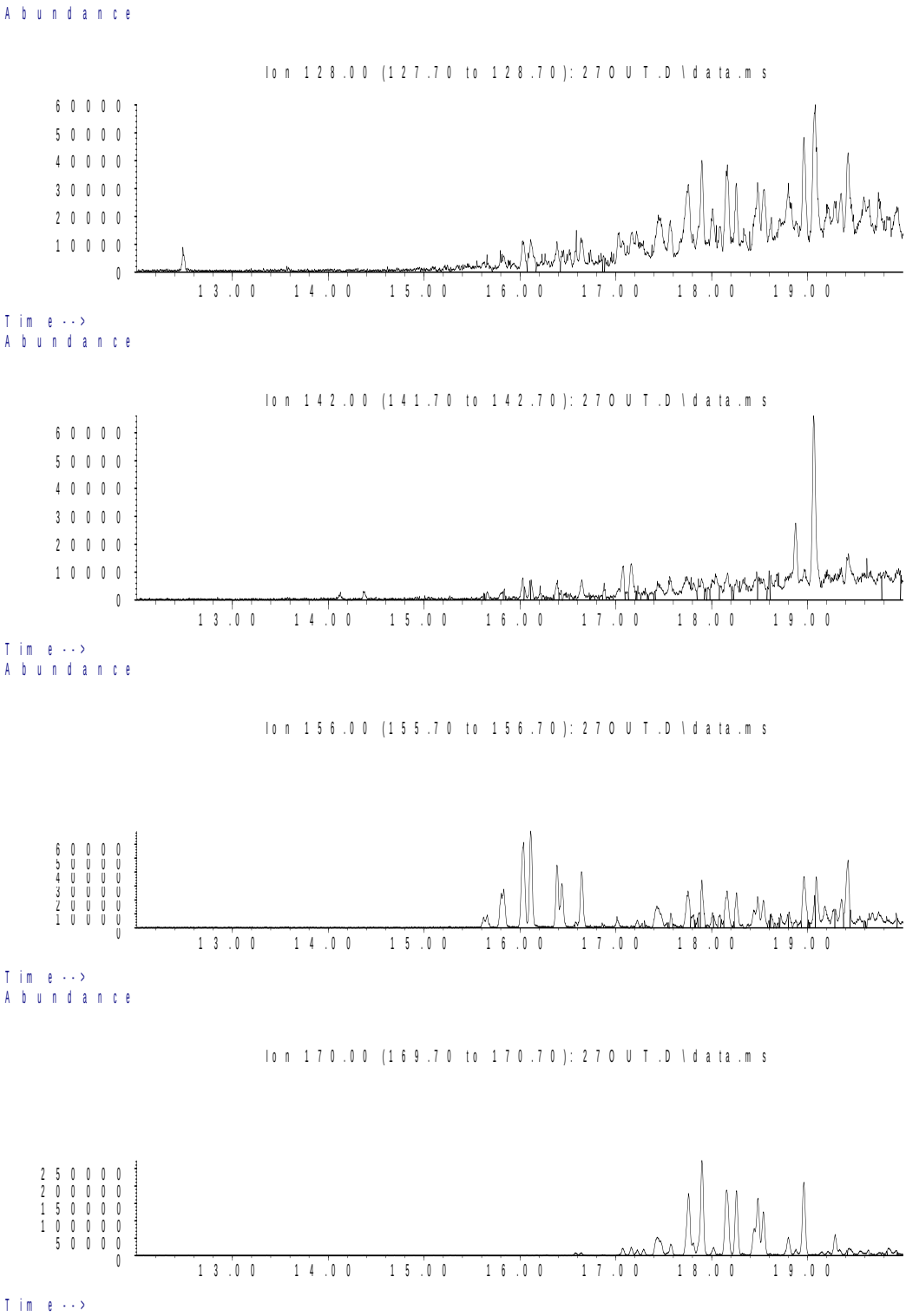

Sample 27 Outer Aromatic Chromatograms; Phenanthrenes

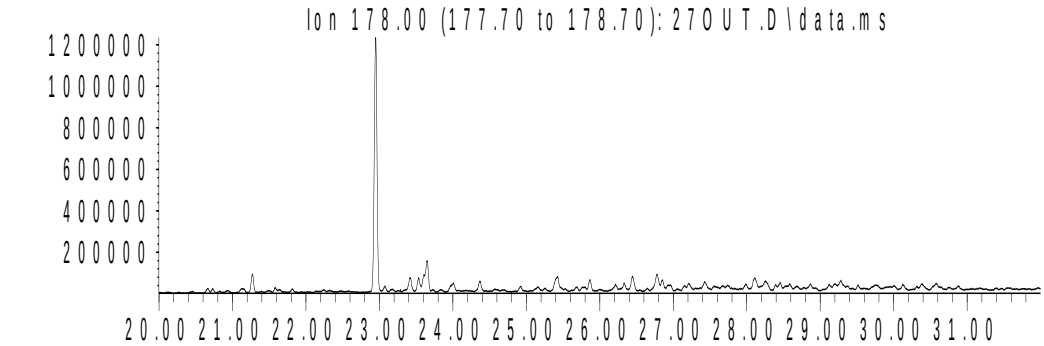

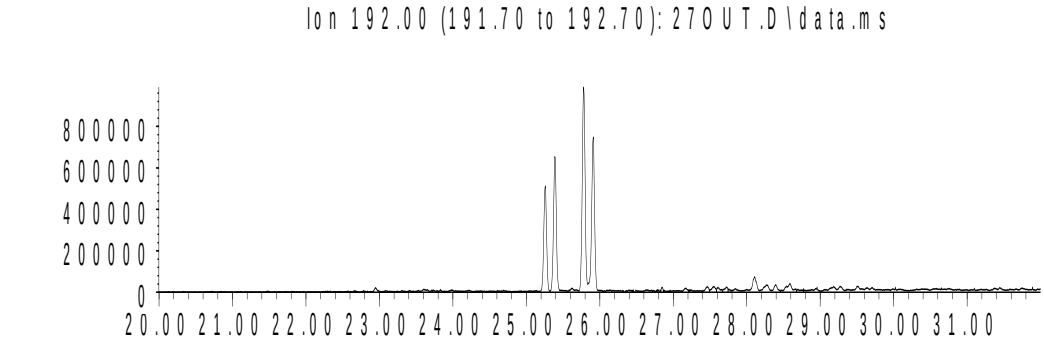

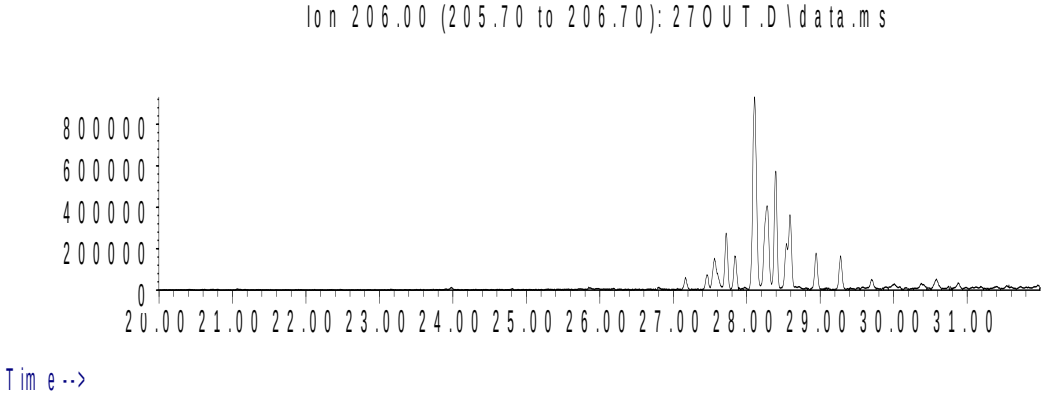

Sample 27 Outer Aromatic Chromatograms; Thiophenes & PAHs

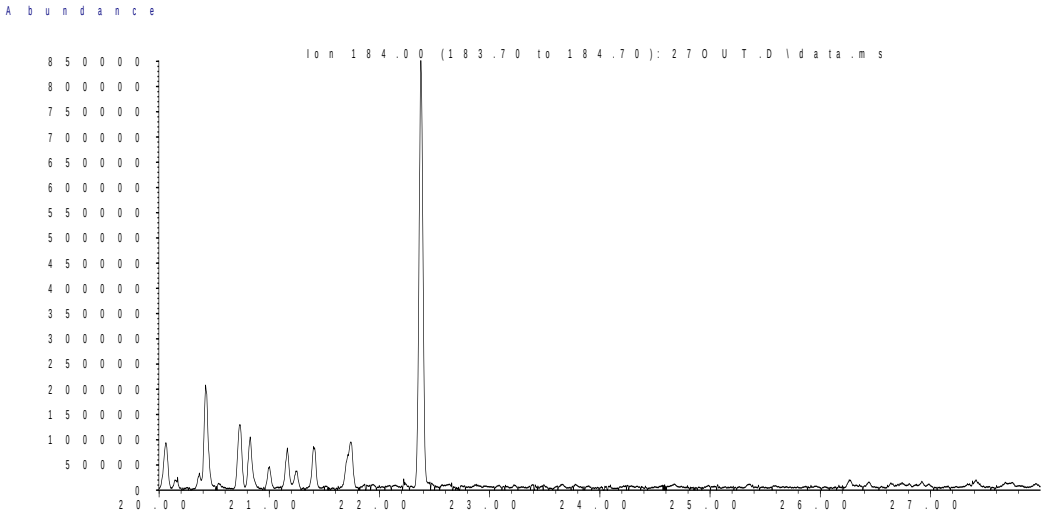

Sample 32 Inner

Aromatic Biomarker Integration Results				
Ion	Peak Label	Compound Name	R.Time (min.)	Peak Area
178	P	Phenantrene	22.957	9147527
184	DBT	Dibenzothiophene	22.382	4696099
192	C1P iso 1	Methyl Phenanthrene Isomer	25.263	3718380
192	C1P iso 2	Methyl Phenanthrene Isomer	25.398	4664390
192	C1P iso 3	Methyl Phenanthrene Isomer	25.792	7577800
192	C1P iso 4	Methyl Phenanthrene Isomer	25.916	5405795
192	C1P sum	Methyl Phenanthrene Isomers (summed)		21366365
198	4 MDBT	4 Methyldibenzothiophene	24.408	4947916
198	2+3 MDBT	2 & 3 Methyldibenzothiophene	24.833	2983339
198	1 MDBT	1 Methyldibenzothiophene	25.289	3400102
206	C2P iso 1	Ethyl/Dimethyl Phenanthrene Isomer	27.564	1632277
206	C2P iso 2	Ethyl/Dimethyl Phenanthrene Isomer	27.73	1486349
206	C2P iso 3	Ethyl/Dimethyl Phenanthrene Isomer	27.844	964267
206	C2P iso 4	Ethyl/Dimethyl Phenanthrene Isomer	28.113	7120740
206	C2P iso 5	Ethyl/Dimethyl Phenanthrene Isomer	28.29	3751021
206	C2P iso 6	Ethyl/Dimethyl Phenanthrene Isomer	28.404	2917764
206	C2P iso 7	Ethyl/Dimethyl Phenanthrene Isomer	28.544	896205
206	C2P iso 8	Ethyl/Dimethyl Phenanthrene Isomer	28.601	1733593
206	C2P iso 9	Ethyl/Dimethyl Phenanthrene Isomer	28.948	940951
206	C2P iso 10	Ethyl/Dimethyl Phenanthrene Isomer	29.285	721698
206	C2P sum	Ethyl/Dimethyl Phenanthrene Isomers (summed)		22164865
226	C3DBT sum	C3 Dibenzothiophene Isomers (summed)		16594004
252	dbf	benzo(b)fluoranthene	42.712	60605
252	bap	benzo(a)pyrene	44.074	119506

Sample 32 Inner Aromatic Chromatograms; Naphthalenes

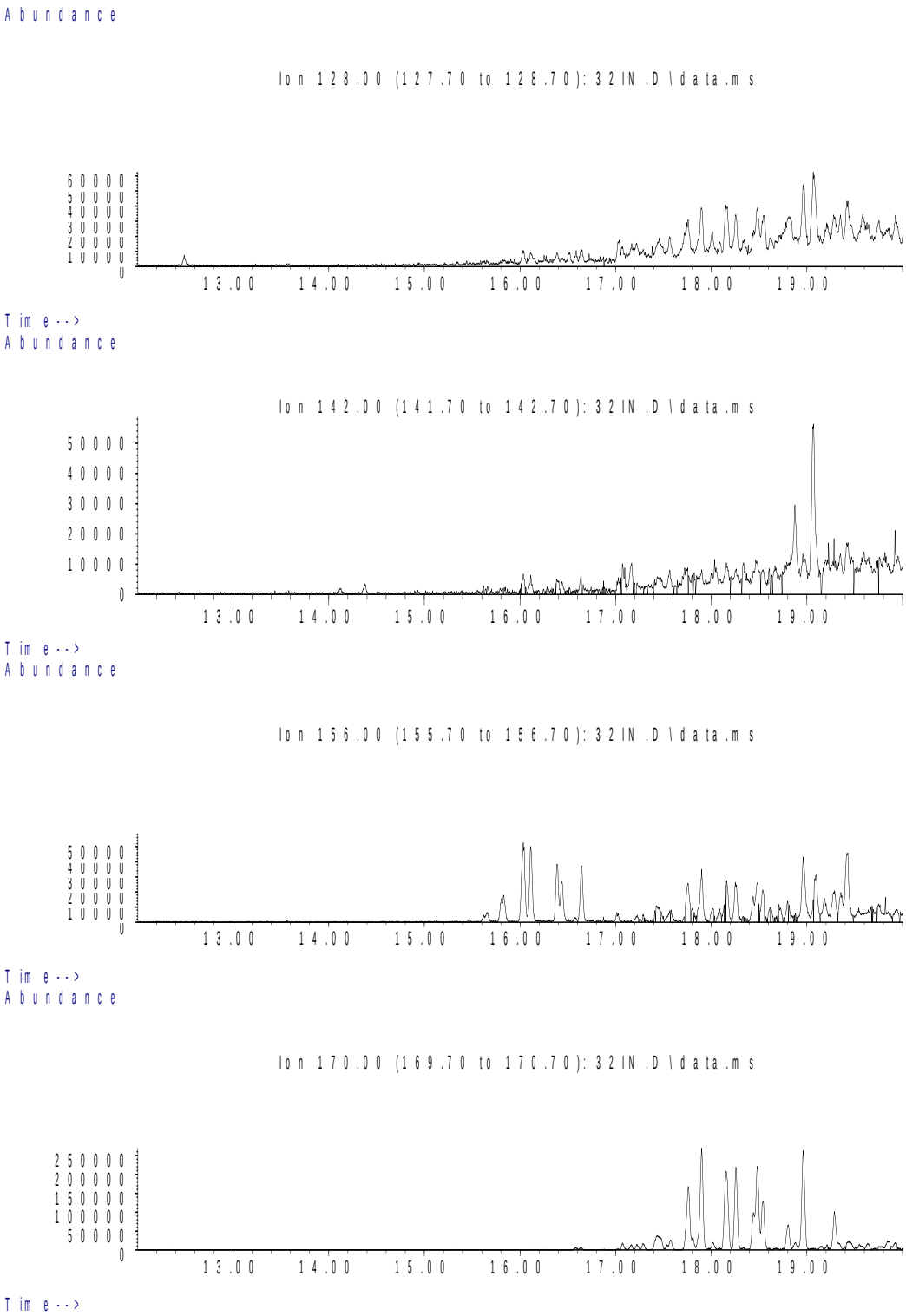

Sample 32 Inner Aromatic Chromatograms; Phenanthrenes

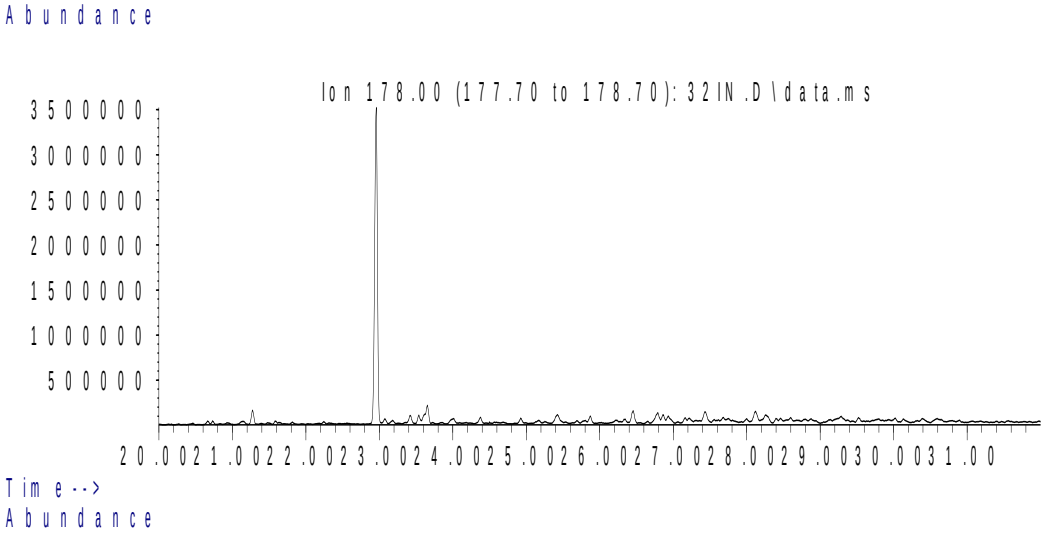

Sample 32 Inner Aromatic Chromatograms; Thiophenes & PAHs

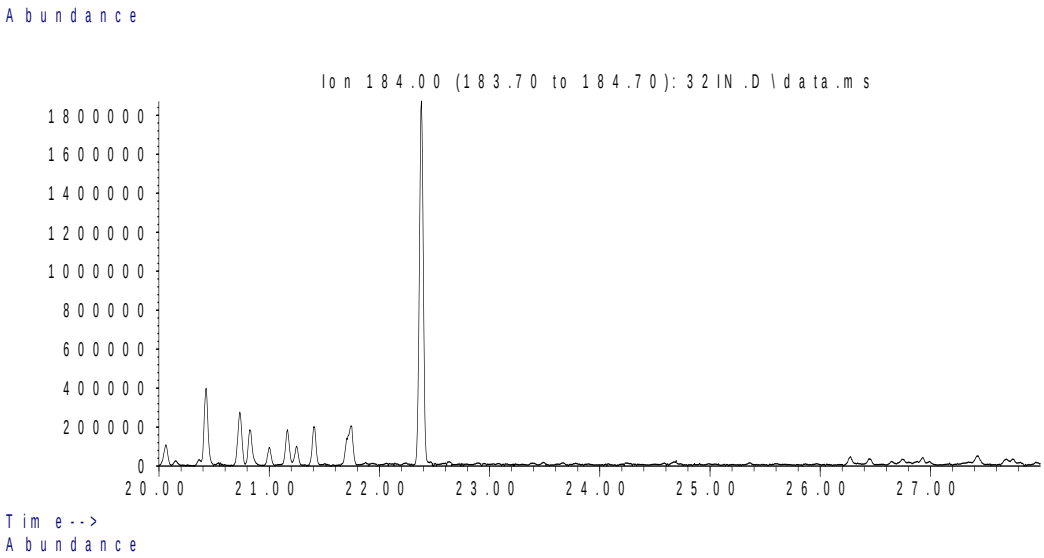

Sample 32 Outer

Aromatic Biomarker Integration Results				
Ion	Peak Label	Compound Name	R.Time (min.)	Peak Area
178	P	Phenantrene	22.95	5097167
184	DBT	Dibenzothiophene	22.375	1118371
192	C1P iso 1	Methyl Phenanthrene Isomer	25.256	2300420
192	C1P iso 2	Methyl Phenanthrene Isomer	25.391	2970317
192	C1P iso 3	Methyl Phenanthrene Isomer	25.779	4761842
192	C1P iso 4	Methyl Phenanthrene Isomer	25.914	3437200
192	C1P sum	Methyl Phenanthrene Isomers (summed)		13469779
198	4 MDBT	4 Methyldibenzothiophene	24.406	2269787
198	2+3 MDBT	2 & 3 Methyldibenzothiophene	24.831	1167323
198	1 MDBT	1 Methyldibenzothiophene	25.282	1145144
206	C2P iso 1	Ethyl/Dimethyl Phenanthrene Isomer	27.557	1126211
206	C2P iso 2	Ethyl/Dimethyl Phenanthrene Isomer	27.717	1004984
206	C2P iso 3	Ethyl/Dimethyl Phenanthrene Isomer	27.847	621824
206	C2P iso 4	Ethyl/Dimethyl Phenanthrene Isomer	28.111	4778223
206	C2P iso 5	Ethyl/Dimethyl Phenanthrene Isomer	28.282	2461548
206	C2P iso 6	Ethyl/Dimethyl Phenanthrene Isomer	28.396	1969415
206	C2P iso 7	Ethyl/Dimethyl Phenanthrene Isomer	28.541	590433
206	C2P iso 8	Ethyl/Dimethyl Phenanthrene Isomer	28.593	1199497
206	C2P iso 9	Ethyl/Dimethyl Phenanthrene Isomer	28.946	664814
206	C2P iso 10	Ethyl/Dimethyl Phenanthrene Isomer	29.272	493715
206	C2P sum	Ethyl/Dimethyl Phenanthrene Isomers (summed)		14910664
226	C3DBT sum	C3 Dibenzothiophene Isomers (summed)		10118727
252	dbf	benzo(b)fluoranthene	42.709	41289
252	bap	benzo(a)pyrene	44.072	77932

Sample 32 Outer Aromatic Chromatograms; Naphthalenes

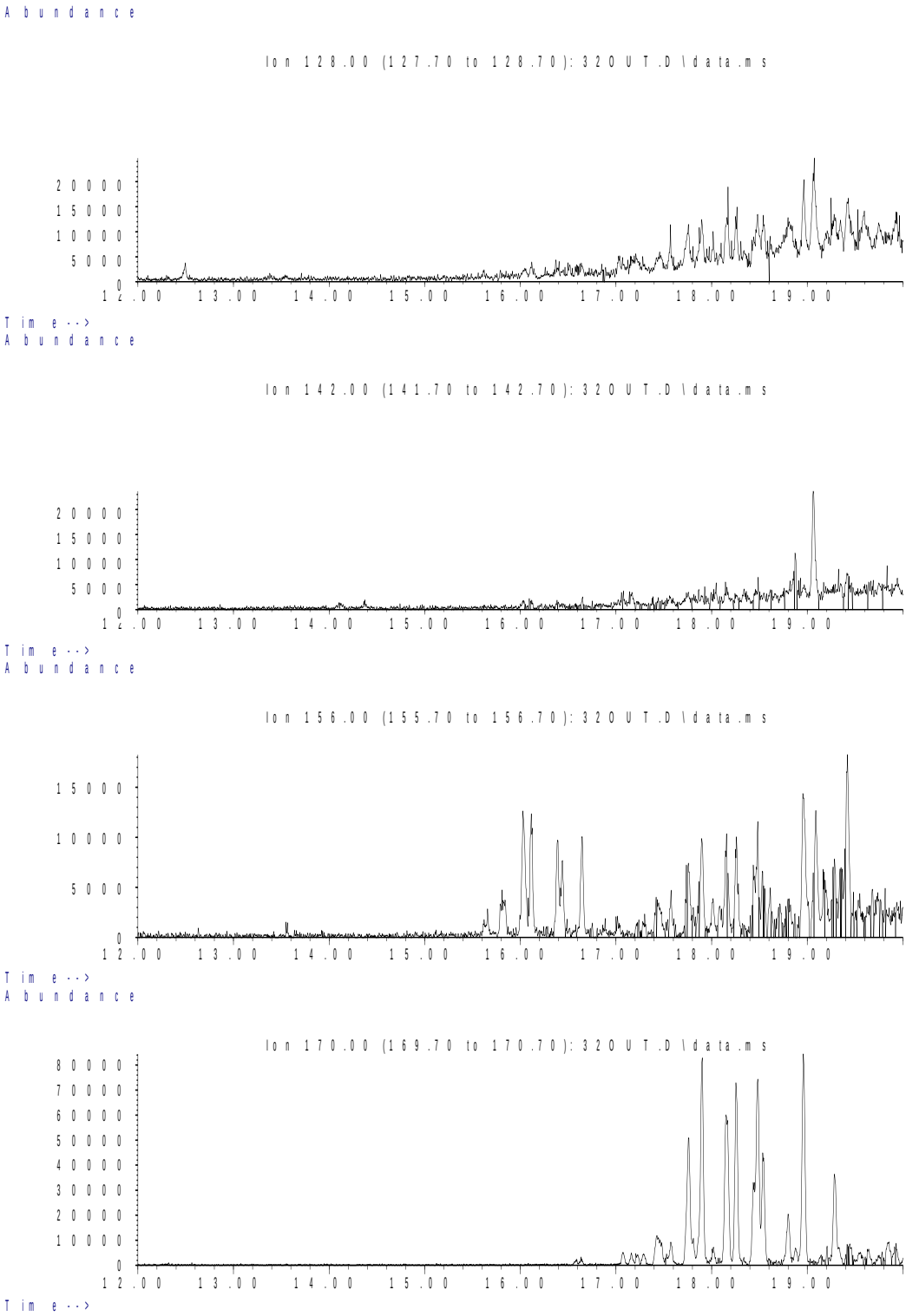

Sample 32 Outer Aromatic Chromatograms; Phenanthrenes

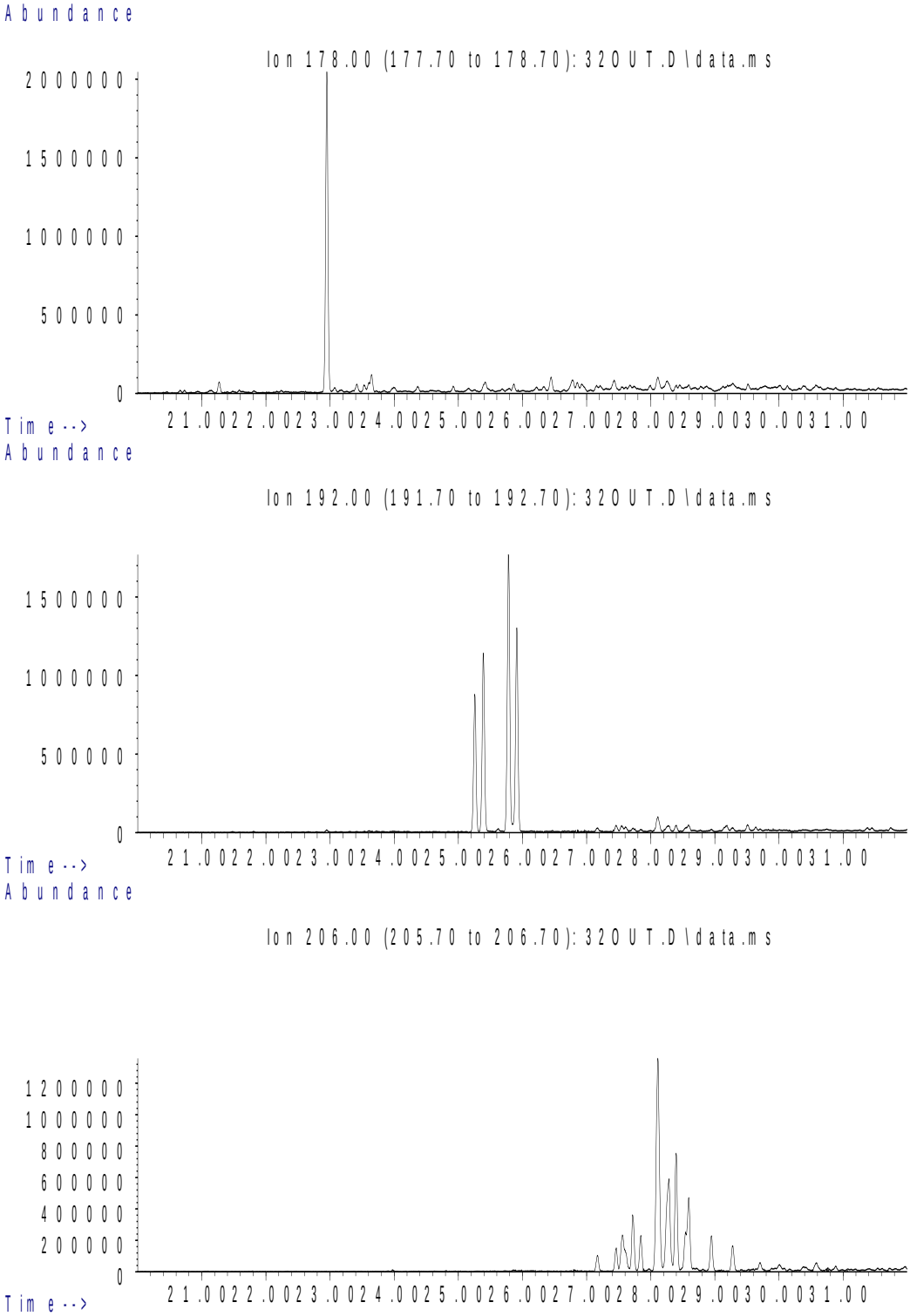

Sample 32 Outer Aromatic Chromatograms; Thiophenes & PAHs

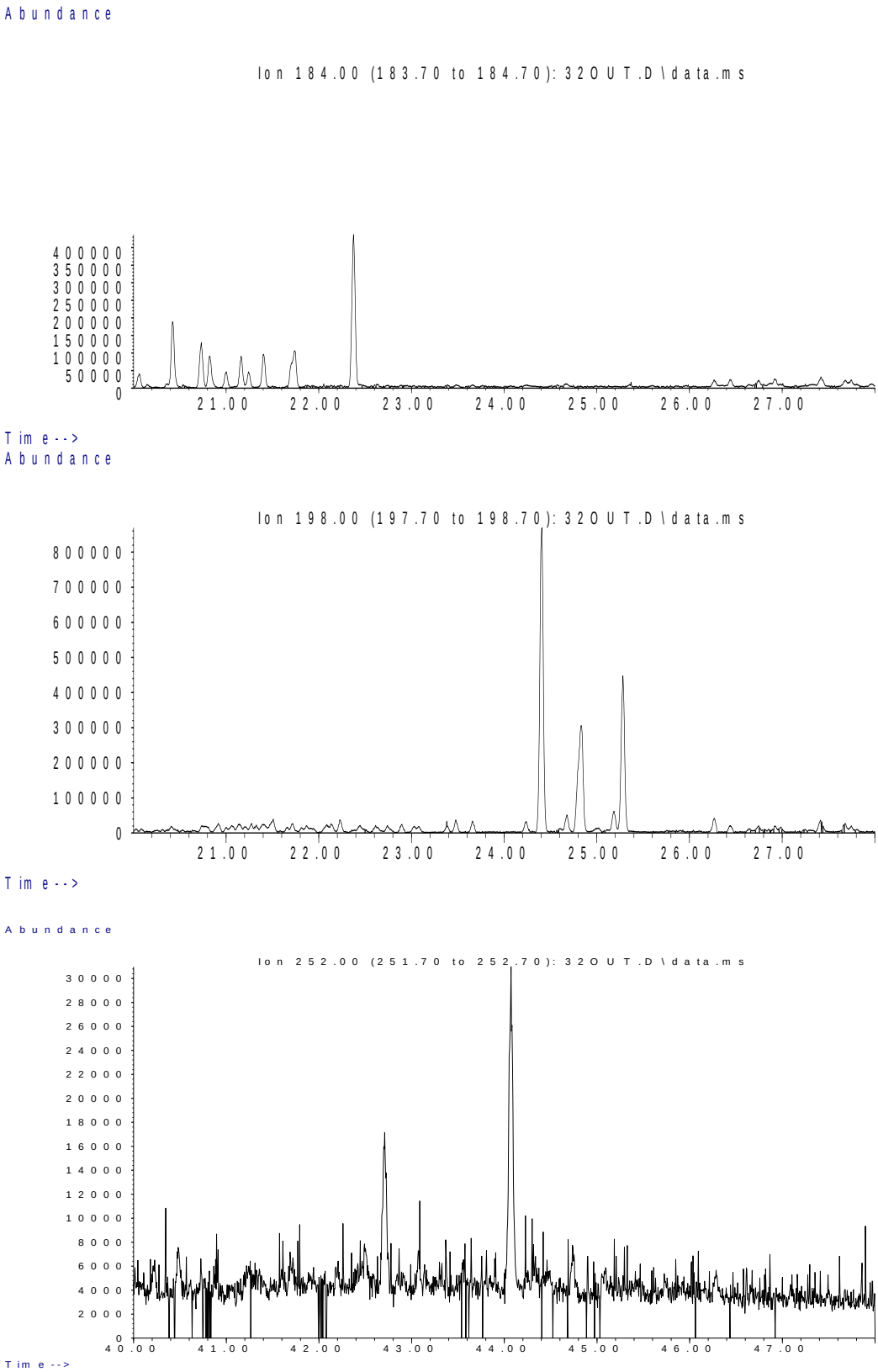

Sample 162 Inner

Aromatic Biomarker Integration Results				
Ion	Peak Label	Compound Name	R.Time (min.)	Peak Area
178	P	Phenantrene	22.949	9909653
184	DBT	Dibenzothiophene	22.373	3235888
192	C1P iso 1	Methyl Phenanthrene Isomer	25.255	3830806
192	C1P iso 2	Methyl Phenanthrene Isomer	25.389	4874468
192	C1P iso 3	Methyl Phenanthrene Isomer	25.783	8008707
192	C1P iso 4	Methyl Phenanthrene Isomer	25.913	5758585
192	C1P sum	Methyl Phenanthrene Isomers (summed)		22472566
198	4 MDBT	4 Methyldibenzothiophene	24.405	4831208
198	2+3 MDBT	2 & 3 Methyldibenzothiophene	24.835	2524036
198	1 MDBT	1 Methyldibenzothiophene	25.286	2674104
206	C2P iso 1	Ethyl/Dimethyl Phenanthrene Isomer	27.555	1837476
206	C2P iso 2	Ethyl/Dimethyl Phenanthrene Isomer	27.721	1625778
206	C2P iso 3	Ethyl/Dimethyl Phenanthrene Isomer	27.846	1002573
206	C2P iso 4	Ethyl/Dimethyl Phenanthrene Isomer	28.115	7841987
206	C2P iso 5	Ethyl/Dimethyl Phenanthrene Isomer	28.281	4114315
206	C2P iso 6	Ethyl/Dimethyl Phenanthrene Isomer	28.395	3284850
206	C2P iso 7	Ethyl/Dimethyl Phenanthrene Isomer	28.54	957163
206	C2P iso 8	Ethyl/Dimethyl Phenanthrene Isomer	28.592	2020966
206	C2P iso 9	Ethyl/Dimethyl Phenanthrene Isomer	28.944	1092345
206	C2P iso 10	Ethyl/Dimethyl Phenanthrene Isomer	29.276	836690
206	C2P sum	Ethyl/Dimethyl Phenanthrene Isomers (summed)		24614143
226	C3DBT sum	C3 Dibenzothiophene Isomers (summed)		18800116
252	dbf	benzo(b)fluoranthene	42.708	116607
252	bap	benzo(a)pyrene	44.071	209120

Sample 162 Inner Aromatic Chromatograms; Naphthalenes

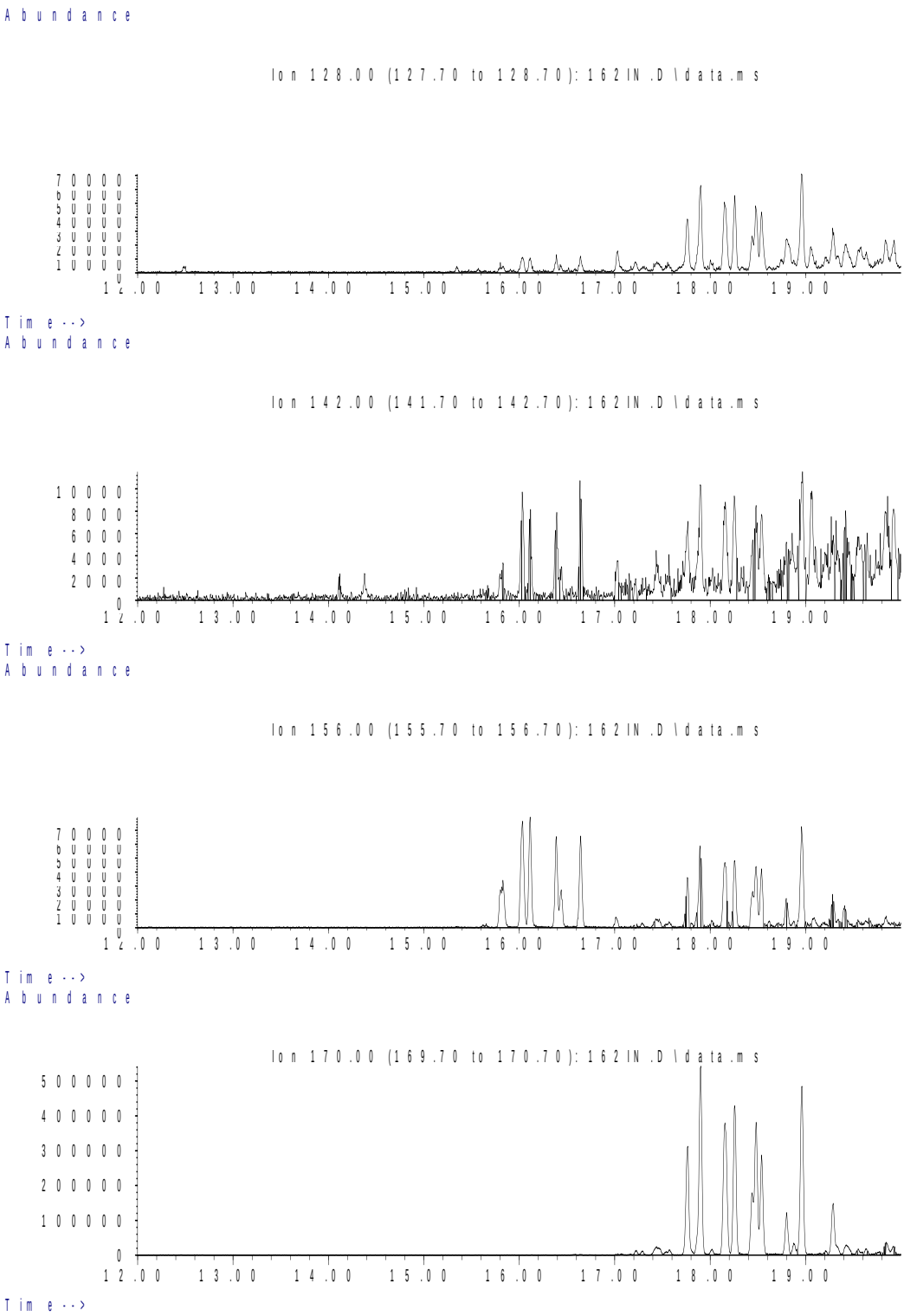

Sample 162 Inner Aromatic Chromatograms; Phenanthrenes

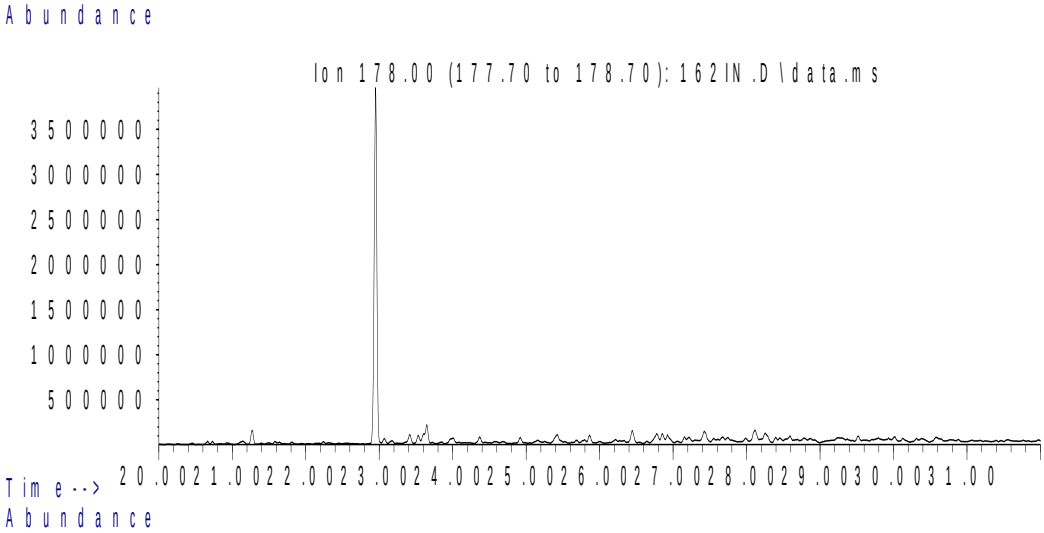

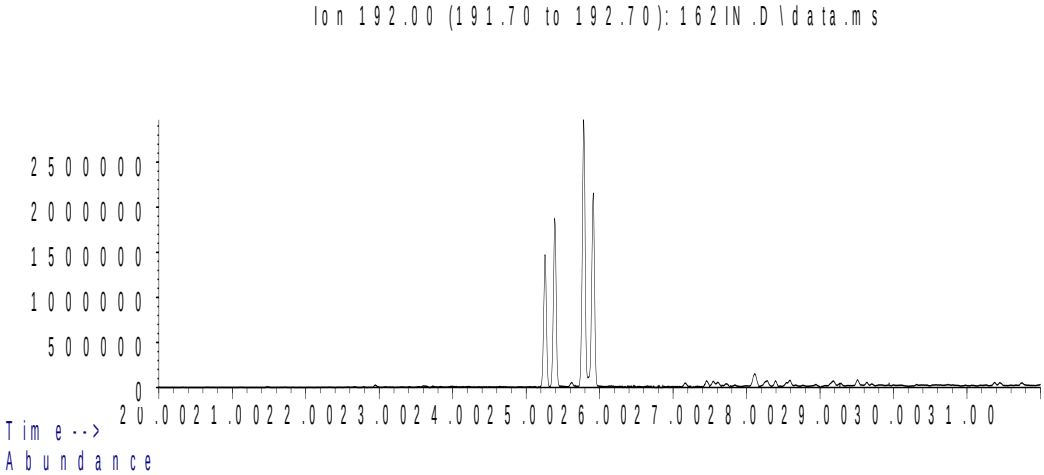

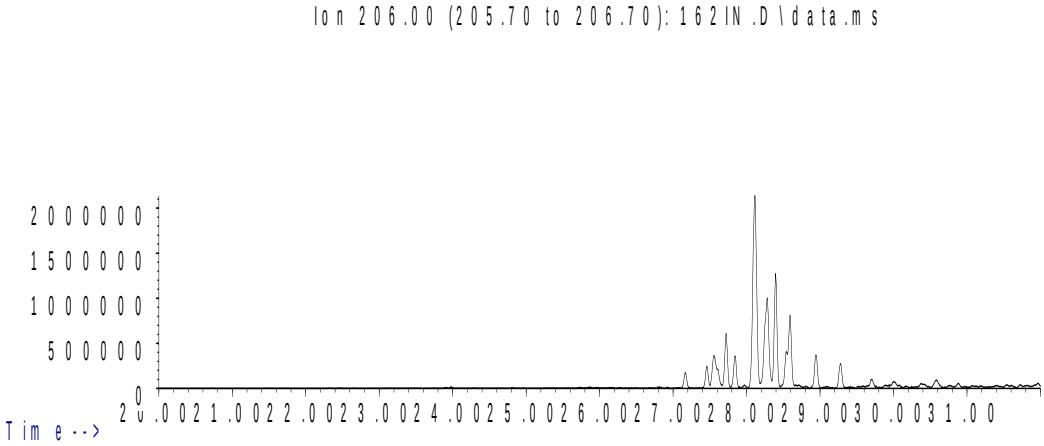

Sample 162 Inner Aromatic Chromatograms; Thiophenes & PAHs

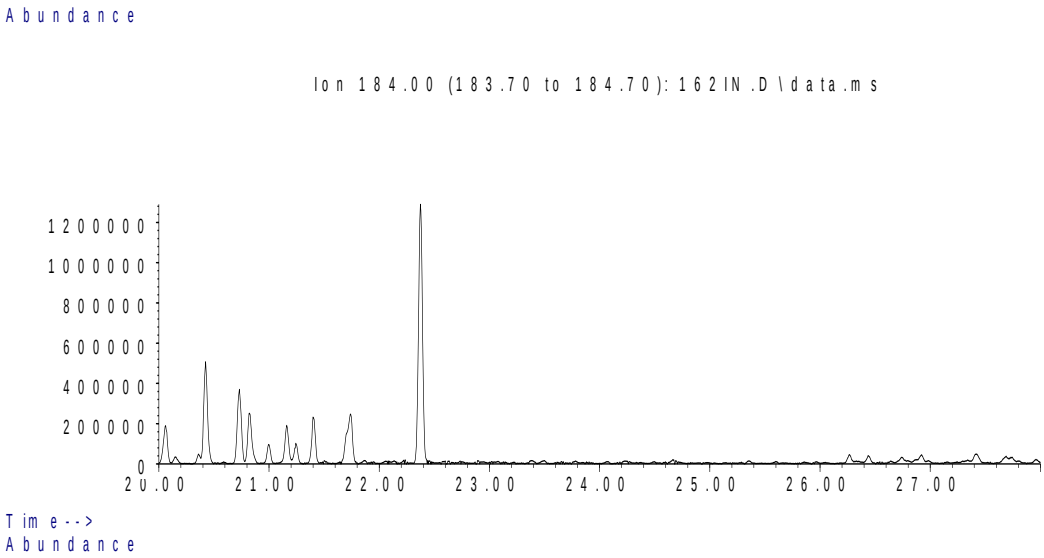

Sample 162 Outer

Aromatic Biomarker Integration Results				
Ion	Peak Label	Compound Name	R.Time (min.)	Peak Area
178	P	Phenantrene	22.957	6189405
184	DBT	Dibenzothiophene	22.381	2241122
192	C1P iso 1	Methyl Phenanthrene Isomer	25.268	2576006
192	C1P iso 2	Methyl Phenanthrene Isomer	25.397	3248119
192	C1P iso 3	Methyl Phenanthrene Isomer	25.791	5383180
192	C1P iso 4	Methyl Phenanthrene Isomer	25.921	3797895
192	C1P sum	Methyl Phenanthrene Isomers (summed)		15005200
198	4 MDBT	4 Methyldibenzothiophene	24.413	3580620
198	2+3 MDBT	2 & 3 Methyldibenzothiophene	24.838	1886121
198	1 MDBT	1 Methyldibenzothiophene	25.294	2067388
206	C2P iso 1	Ethyl/Dimethyl Phenanthrene Isomer	27.564	1228683
206	C2P iso 2	Ethyl/Dimethyl Phenanthrene Isomer	27.729	1063783
206	C2P iso 3	Ethyl/Dimethyl Phenanthrene Isomer	27.849	644896
206	C2P iso 4	Ethyl/Dimethyl Phenanthrene Isomer	28.113	5253969
206	C2P iso 5	Ethyl/Dimethyl Phenanthrene Isomer	28.289	2721462
206	C2P iso 6	Ethyl/Dimethyl Phenanthrene Isomer	28.403	2183257
206	C2P iso 7	Ethyl/Dimethyl Phenanthrene Isomer	28.548	649902
206	C2P iso 8	Ethyl/Dimethyl Phenanthrene Isomer	28.595	1325369
206	C2P iso 9	Ethyl/Dimethyl Phenanthrene Isomer	28.952	712472
206	C2P iso 10	Ethyl/Dimethyl Phenanthrene Isomer	29.284	546271
206	C2P sum	Ethyl/Dimethyl Phenanthrene Isomers (summed)		16330064
226	C3DBT sum	C3 Dibenzothiophene Isomers (summed)		13221764
252	dbf	benzo(b)fluoranthene	42.701	65893
252	bap	benzo(a)pyrene	44.079	118100

Sample 162 Outer Aromatic Chromatograms; Naphthalenes

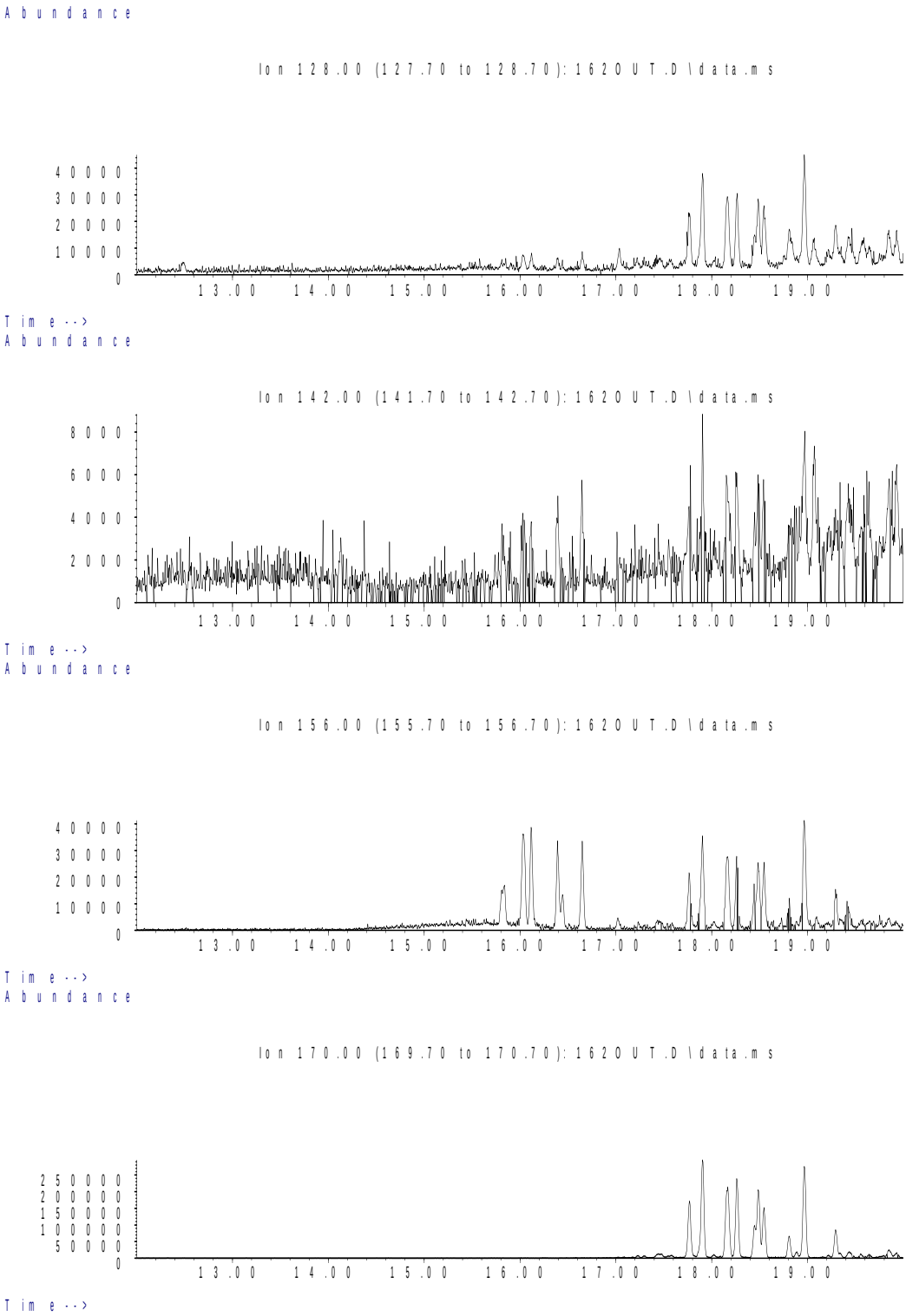

Sample 162 Outer Aromatic Chromatograms; Phenanthrenes

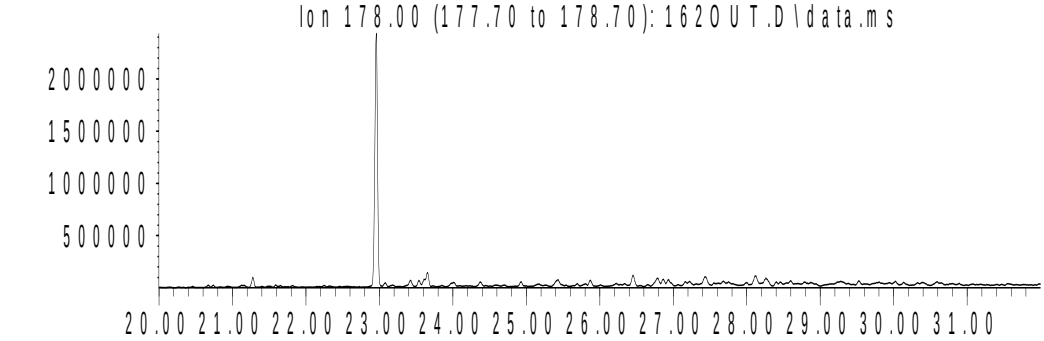

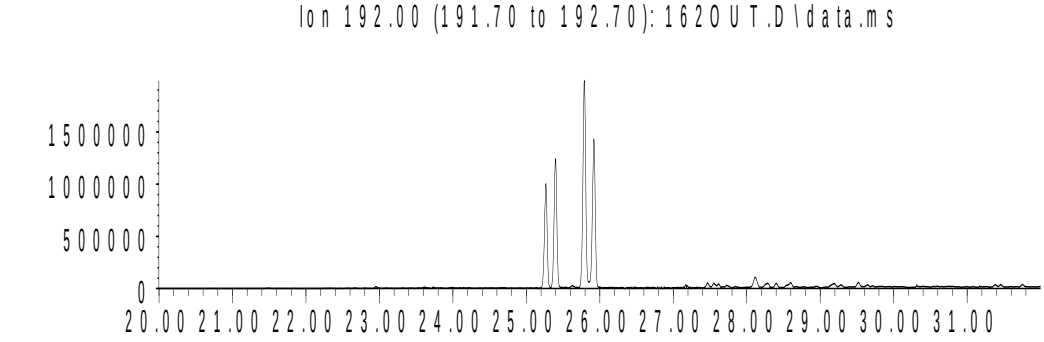

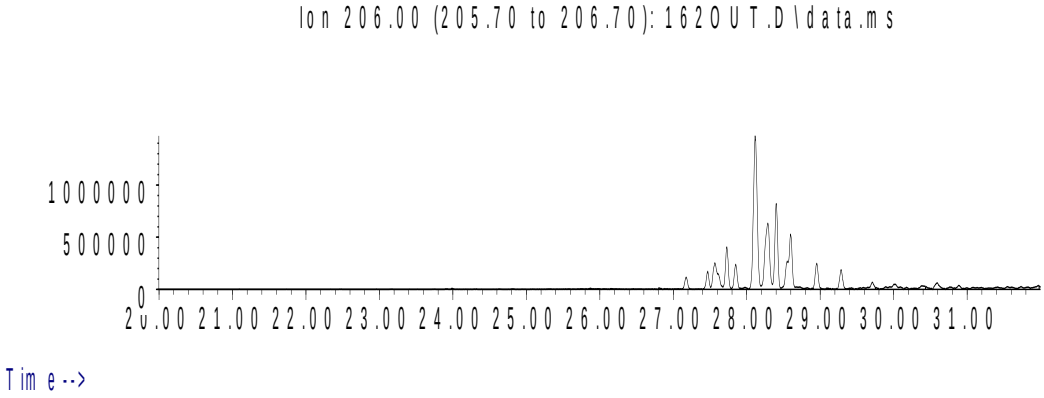

Sample 162 Outer Aromatic Chromatograms; Thiophenes & PAHs

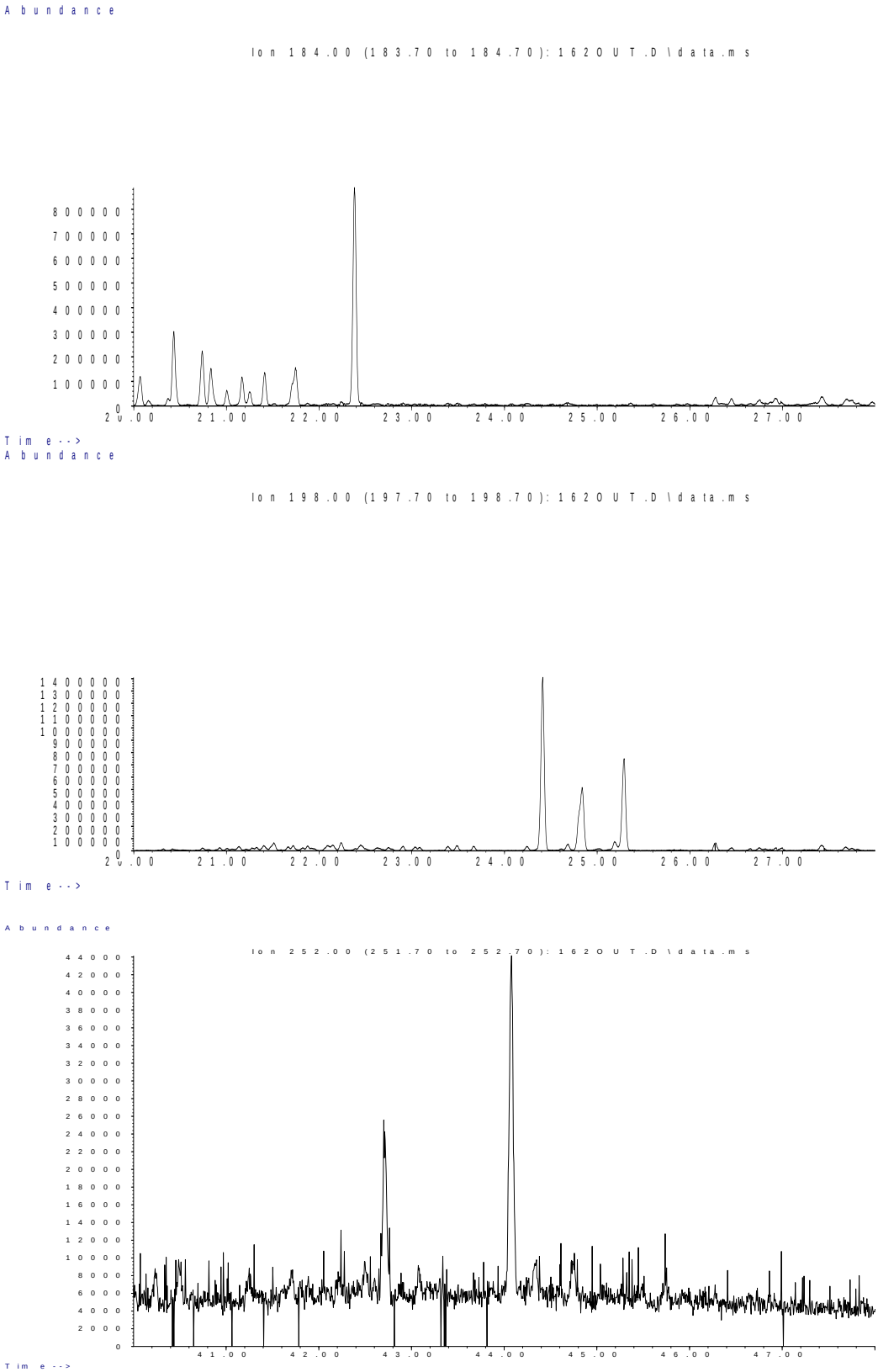

Sample 80 Inner

Aromatic Biomarker Integration Results				
Ion	Peak Label	Compound Name	R.Time (min.)	Peak Area
178	P	Phenantrene	22.945	8453814
184	DBT	Dibenzothiophene	22.37	1934244
192	C1P iso 1	Methyl Phenanthrene Isomer	25.251	3178278
192	C1P iso 2	Methyl Phenanthrene Isomer	25.381	4074496
192	C1P iso 3	Methyl Phenanthrene Isomer	25.775	6520958
192	C1P iso 4	Methyl Phenanthrene Isomer	25.904	4707836
192	C1P sum	Methyl Phenanthrene Isomers (summed)		18481568
198	4 MDBT	4 Methyldibenzothiophene	24.396	3071006
198	2+3 MDBT	2 & 3 Methyldibenzothiophene	24.826	1531899
198	1 MDBT	1 Methyldibenzothiophene	25.272	1588917
206	C2P iso 1	Ethyl/Dimethyl Phenanthrene Isomer	27.552	1504796
206	C2P iso 2	Ethyl/Dimethyl Phenanthrene Isomer	27.718	1333573
206	C2P iso 3	Ethyl/Dimethyl Phenanthrene Isomer	27.832	818963
206	C2P iso 4	Ethyl/Dimethyl Phenanthrene Isomer	28.096	6421788
206	C2P iso 5	Ethyl/Dimethyl Phenanthrene Isomer	28.278	3258135
206	C2P iso 6	Ethyl/Dimethyl Phenanthrene Isomer	28.387	2718527
206	C2P iso 7	Ethyl/Dimethyl Phenanthrene Isomer	28.532	633104
206	C2P iso 8	Ethyl/Dimethyl Phenanthrene Isomer	28.583	1670371
206	C2P iso 9	Ethyl/Dimethyl Phenanthrene Isomer	28.936	908885
206	C2P iso 10	Ethyl/Dimethyl Phenanthrene Isomer	29.273	706014
206	C2P sum	Ethyl/Dimethyl Phenanthrene Isomers (summed)		19974156
226	C3DBT sum	C3 Dibenzothiophene Isomers (summed)		13703813
252	dbf	benzo(b)fluoranthene	42.689	100760
252	bap	benzo(a)pyrene	44.057	184888

Sample 80 Inner Aromatic Chromatograms; Naphthalenes

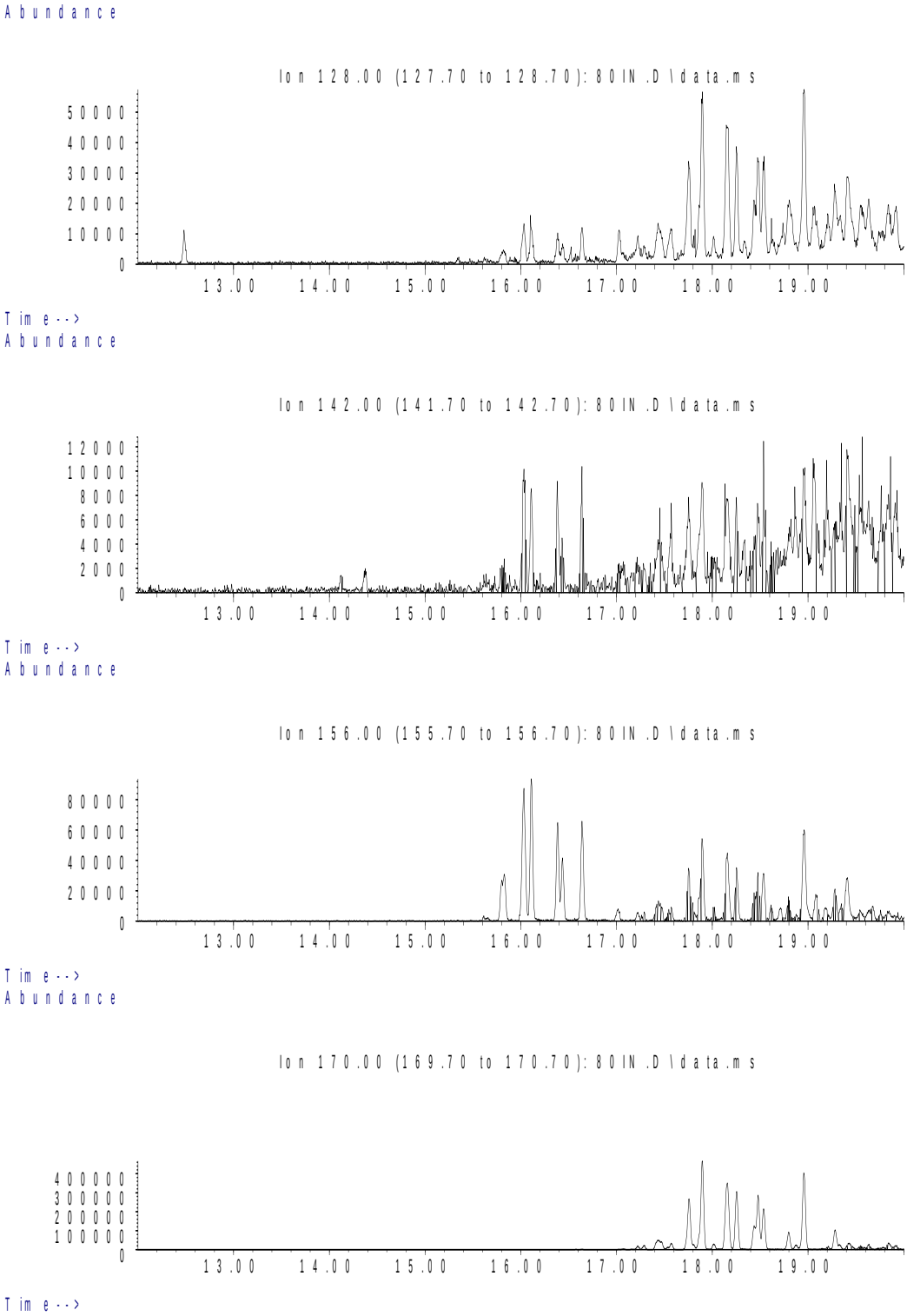

Sample 80 Inner Aromatic Chromatograms; Phenanthrenes

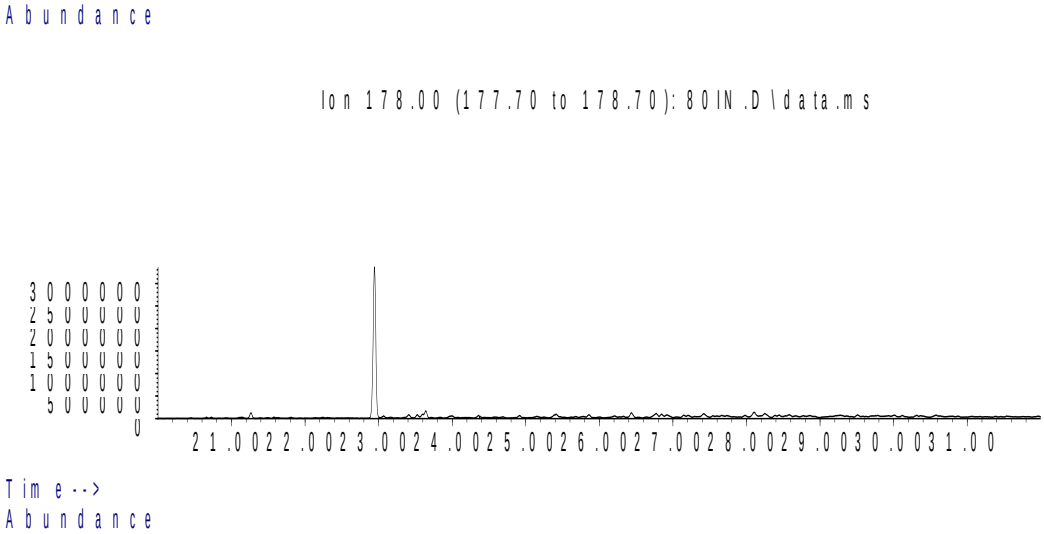

Sample 80 Inner Aromatic Chromatograms; Thiophenes & PAHs

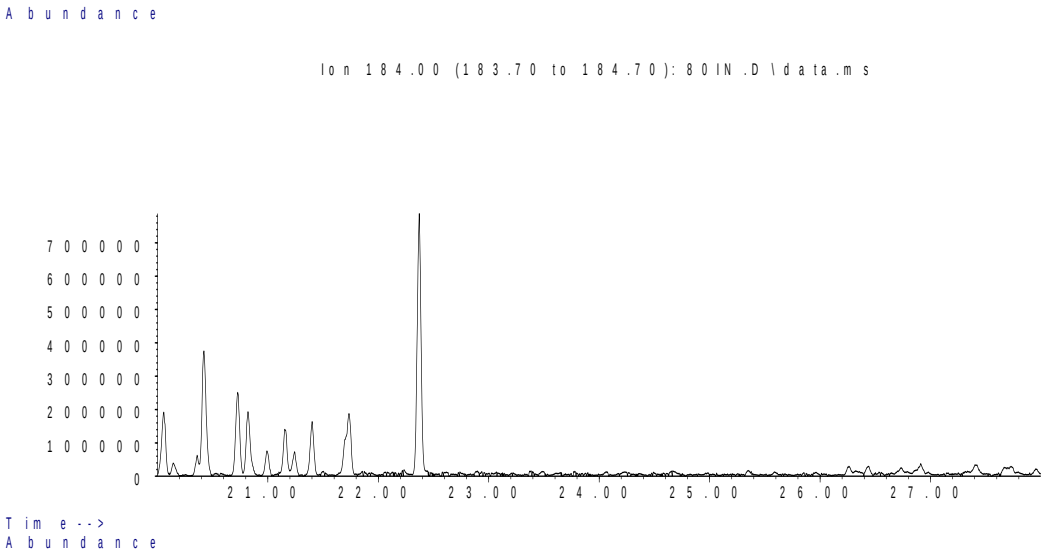

Sample 80 Outer

Aromatic Biomarker Integration Results				
Ion	Peak Label	Compound Name	R.Time (min.)	Peak Area
178	P	Phenantrene	22.951	10056606
184	DBT	Dibenzothiophene	22.376	4402437
192	C1P iso 1	Methyl Phenanthrene Isomer	25.257	3733863
192	C1P iso 2	Methyl Phenanthrene Isomer	25.387	4699907
192	C1P iso 3	Methyl Phenanthrene Isomer	25.786	7626789
192	C1P iso 4	Methyl Phenanthrene Isomer	25.91	5715134
192	C1P sum	Methyl Phenanthrene Isomers (summed)		21775693
198	4 MDBT	4 Methyldibenzothiophene	24.407	4837643
198	2+3 MDBT	2 & 3 Methyldibenzothiophene	24.832	2501361
198	1 MDBT	1 Methyldibenzothiophene	25.278	2757266
206	C2P iso 1	Ethyl/Dimethyl Phenanthrene Isomer	27.558	1848964
206	C2P iso 2	Ethyl/Dimethyl Phenanthrene Isomer	27.719	1615853
206	C2P iso 3	Ethyl/Dimethyl Phenanthrene Isomer	27.838	1014154
206	C2P iso 4	Ethyl/Dimethyl Phenanthrene Isomer	28.107	7772913
206	C2P iso 5	Ethyl/Dimethyl Phenanthrene Isomer	28.278	4068244
206	C2P iso 6	Ethyl/Dimethyl Phenanthrene Isomer	28.398	3394157
206	C2P iso 7	Ethyl/Dimethyl Phenanthrene Isomer	28.543	1165768
206	C2P iso 8	Ethyl/Dimethyl Phenanthrene Isomer	28.589	2017660
206	C2P iso 9	Ethyl/Dimethyl Phenanthrene Isomer	28.942	1097935
206	C2P iso 10	Ethyl/Dimethyl Phenanthrene Isomer	29.273	836579
206	C2P sum	Ethyl/Dimethyl Phenanthrene Isomers (summed)		24832227
226	C3DBT sum	C3 Dibenzothiophene Isomers (summed)		19017716
252	dbf	benzo(b)fluoranthene	42.705	128281
252	bap	benzo(a)pyrene	44.063	223682

Sample 80 Outer Aromatic Chromatograms; Naphthalenes

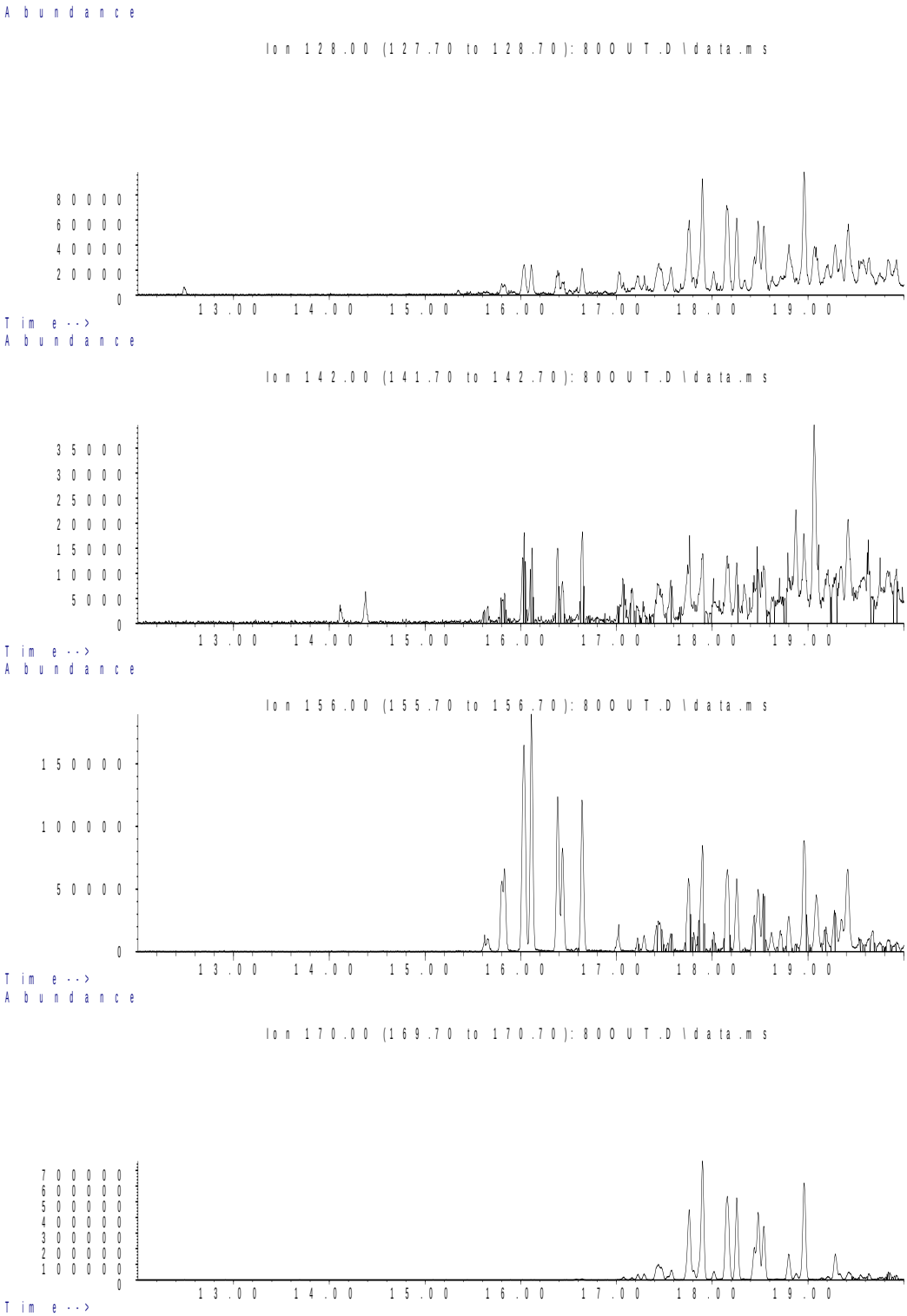

Sample 80 Outer Aromatic Chromatograms; Phenanthrenes

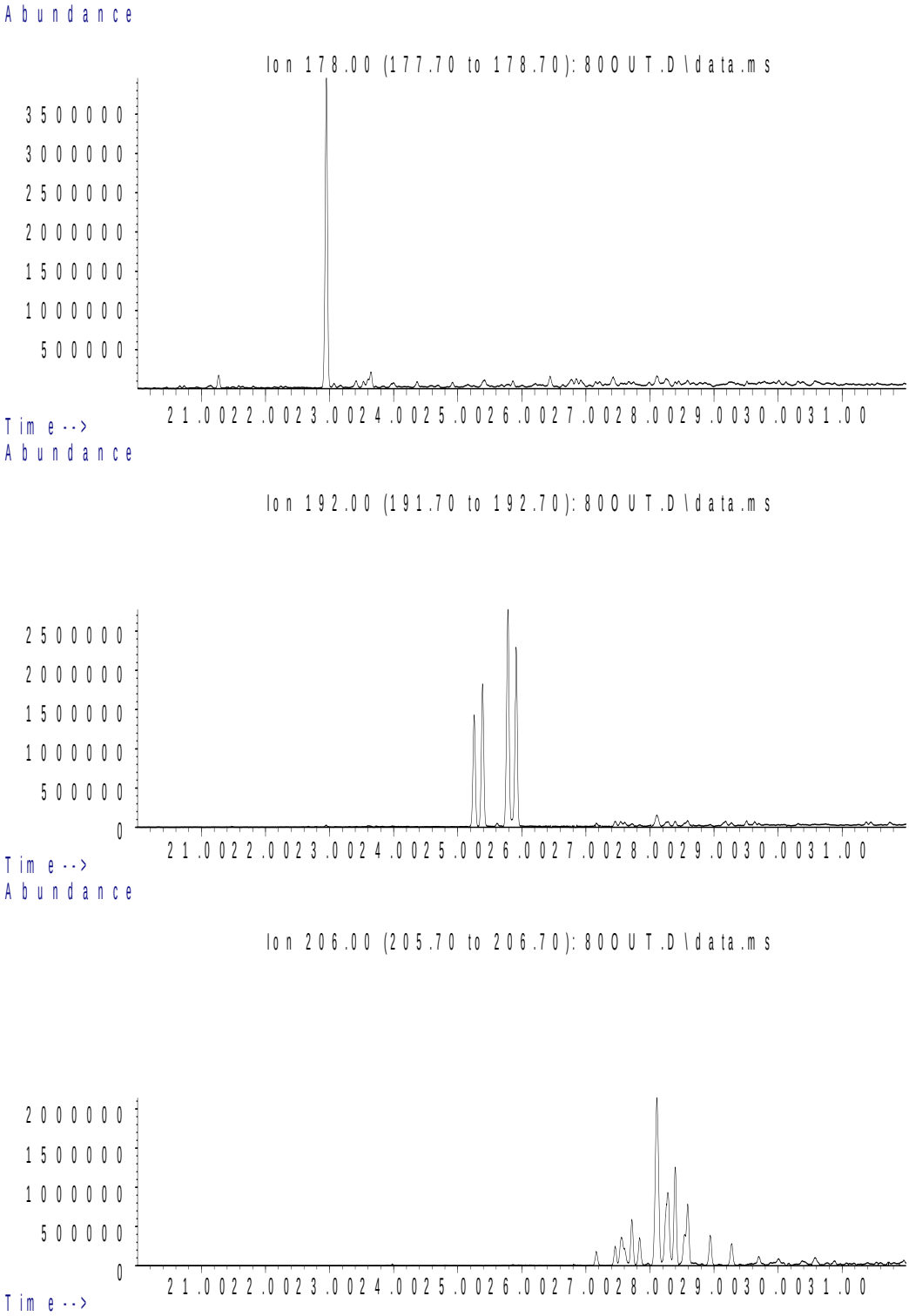

Sample 80 Outer Aromatic Chromatograms; Thiophenes & PAHs

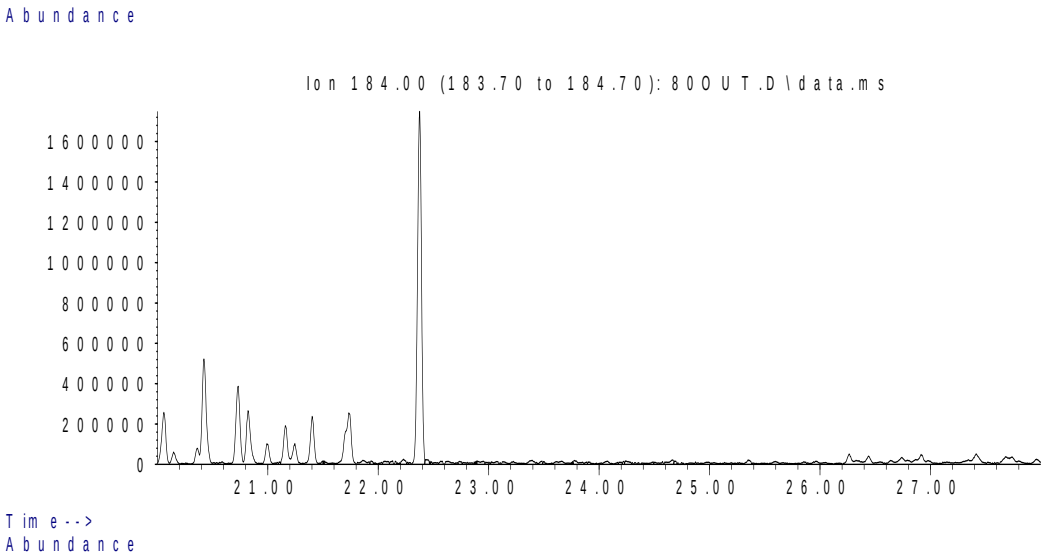

Sample 85 Inner

Aromatic Biomarker Integration Results				
Ion	Peak Label	Compound Name	R.Time (min.)	Peak Area
178	P	Phenantrene	22.948	9083889
184	DBT	Dibenzothiophene	22.373	2170890
192	C1P iso 1	Methyl Phenanthrene Isomer	25.254	3483199
192	C1P iso 2	Methyl Phenanthrene Isomer	25.384	4356664
192	C1P iso 3	Methyl Phenanthrene Isomer	25.778	7390798
192	C1P iso 4	Methyl Phenanthrene Isomer	25.907	5221120
192	C1P sum	Methyl Phenanthrene Isomers (summed)		20451781
198	4 MDBT	4 Methyldibenzothiophene	24.399	3968196
198	2+3 MDBT	2 & 3 Methyldibenzothiophene	24.824	2282342
198	1 MDBT	1 Methyldibenzothiophene	25.28	2365858
206	C2P iso 1	Ethyl/Dimethyl Phenanthrene Isomer	27.555	1678747
206	C2P iso 2	Ethyl/Dimethyl Phenanthrene Isomer	27.721	1488234
206	C2P iso 3	Ethyl/Dimethyl Phenanthrene Isomer	27.835	931086
206	C2P iso 4	Ethyl/Dimethyl Phenanthrene Isomer	28.099	7146782
206	C2P iso 5	Ethyl/Dimethyl Phenanthrene Isomer	28.276	3719070
206	C2P iso 6	Ethyl/Dimethyl Phenanthrene Isomer	28.39	3125090
206	C2P iso 7	Ethyl/Dimethyl Phenanthrene Isomer	28.54	847389
206	C2P iso 8	Ethyl/Dimethyl Phenanthrene Isomer	28.586	1837671
206	C2P iso 9	Ethyl/Dimethyl Phenanthrene Isomer	28.939	995303
206	C2P iso 10	Ethyl/Dimethyl Phenanthrene Isomer	29.271	759449
206	C2P sum	Ethyl/Dimethyl Phenanthrene Isomers (summed)		22528821
226	C3DBT sum	C3 Dibenzothiophene Isomers (summed)		16781552
252	dbf	benzo(b)fluoranthene	42.703	102595
252	bap	benzo(a)pyrene	44.055	174632

Sample 85 Inner Aromatic Chromatograms; Naphthalenes

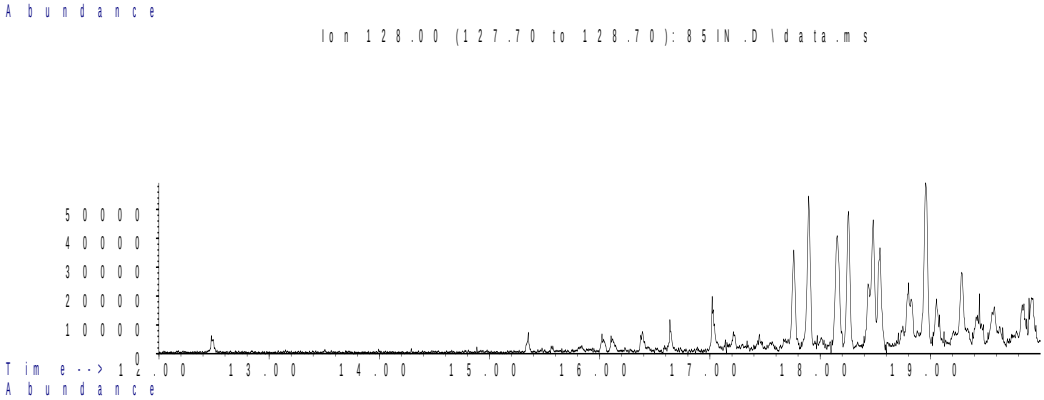

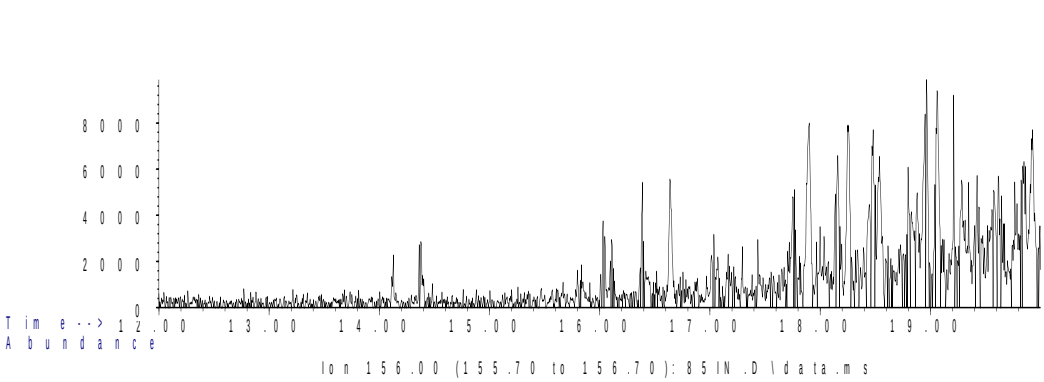

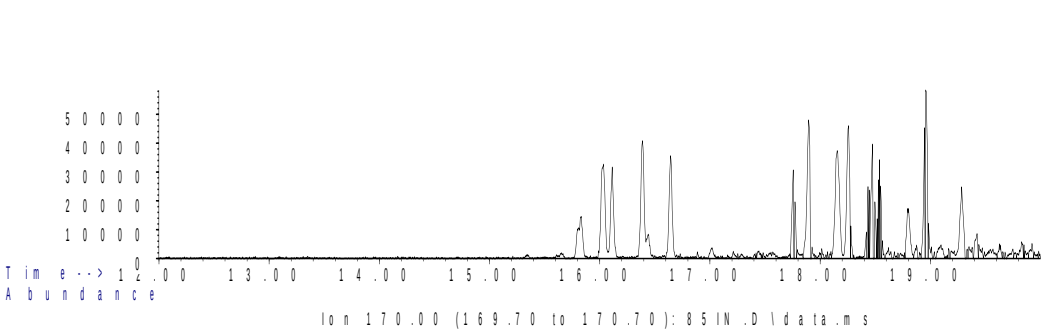

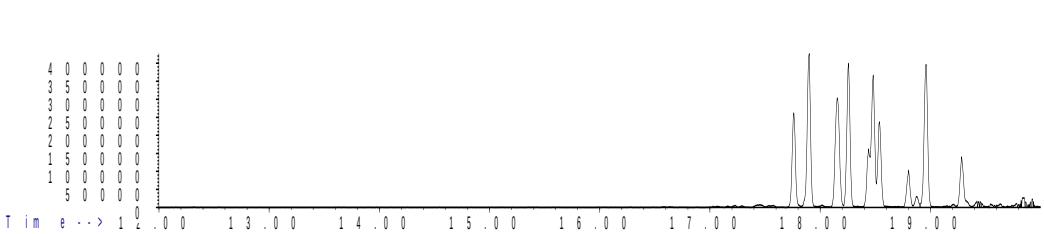

Sample 85 Inner Aromatic Chromatograms; Phenanthrenes

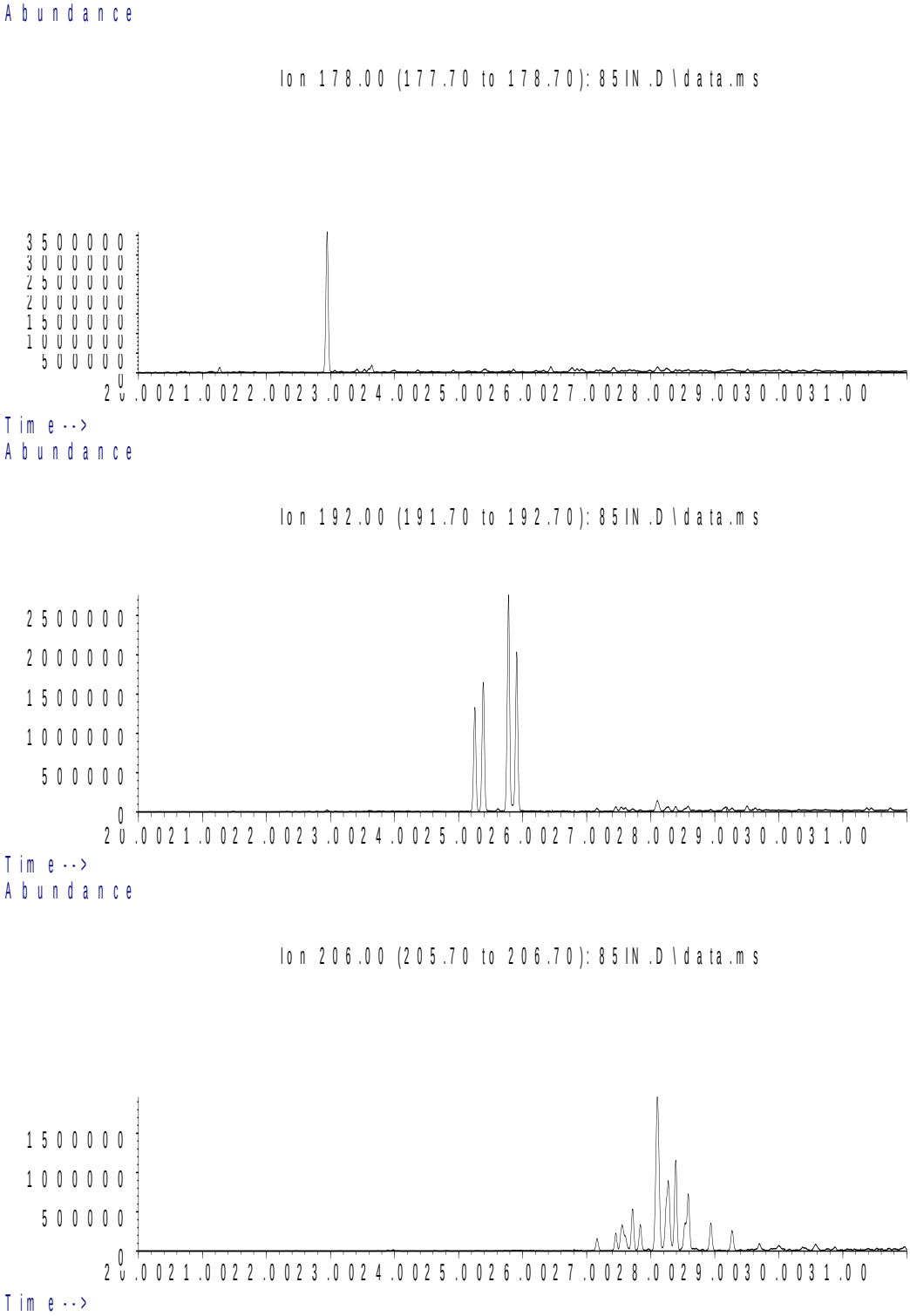

Sample 85 Inner Aromatic Chromatograms; Thiophenes & PAHs

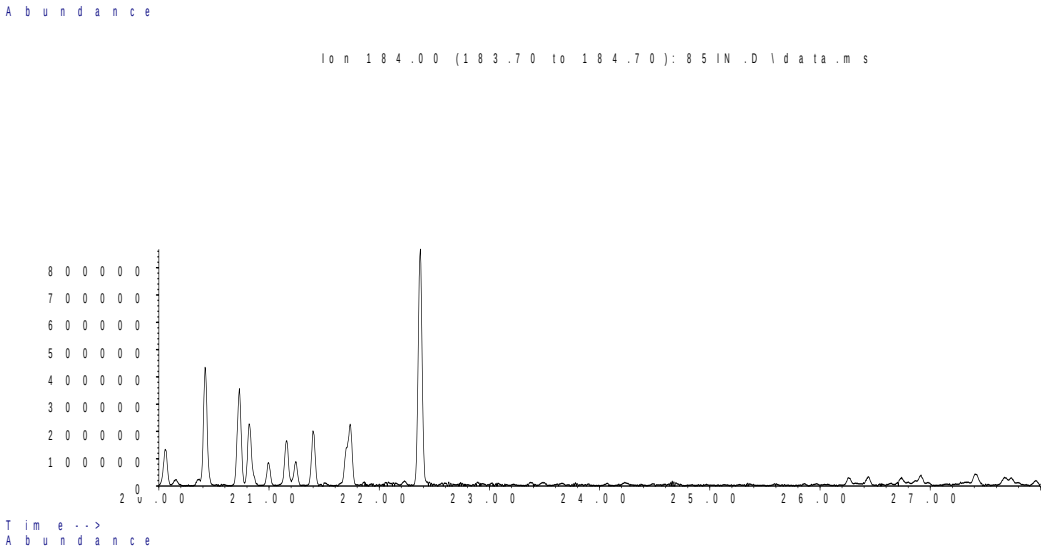

Sample 85 Outer

Aromatic Biomarker Integration Results				
Ion	Peak Label	Compound Name	R.Time (min.)	Peak Area
178	P	Phenantrene	22.948	6206973
184	DBT	Dibenzothiophene	22.373	242548
192	C1P iso 1	Methyl Phenanthrene Isomer	25.254	2397593
192	C1P iso 2	Methyl Phenanthrene Isomer	25.389	3004480
192	C1P iso 3	Methyl Phenanthrene Isomer	25.778	5090807
192	C1P iso 4	Methyl Phenanthrene Isomer	25.907	3649240
192	C1P sum	Methyl Phenanthrene Isomers (summed)		14142120
198	4 MDBT	4 Methyldibenzothiophene	24.399	929839
198	2+3 MDBT	2 & 3 Methyldibenzothiophene	24.829	348497
198	1 MDBT	1 Methyldibenzothiophene	25.275	289944
206	C2P iso 1	Ethyl/Dimethyl Phenanthrene Isomer	27.555	1140180
206	C2P iso 2	Ethyl/Dimethyl Phenanthrene Isomer	27.716	1016770
206	C2P iso 3	Ethyl/Dimethyl Phenanthrene Isomer	27.84	633356
206	C2P iso 4	Ethyl/Dimethyl Phenanthrene Isomer	28.099	4903537
206	C2P iso 5	Ethyl/Dimethyl Phenanthrene Isomer	28.276	2583334
206	C2P iso 6	Ethyl/Dimethyl Phenanthrene Isomer	28.39	2145867
206	C2P iso 7	Ethyl/Dimethyl Phenanthrene Isomer	28.535	558844
206	C2P iso 8	Ethyl/Dimethyl Phenanthrene Isomer	28.586	1323660
206	C2P iso 9	Ethyl/Dimethyl Phenanthrene Isomer	28.939	751886
206	C2P iso 10	Ethyl/Dimethyl Phenanthrene Isomer	29.271	562247
206	C2P sum	Ethyl/Dimethyl Phenanthrene Isomers (summed)		15619681
226	C3DBT sum	C3 Dibenzothiophene Isomers (summed)		10630972
252	dbf	benzo(b)fluoranthene	42.697	114258
252	bap	benzo(a)pyrene	44.066	192000

Sample 85 Outer Aromatic Chromatograms; Naphthalenes

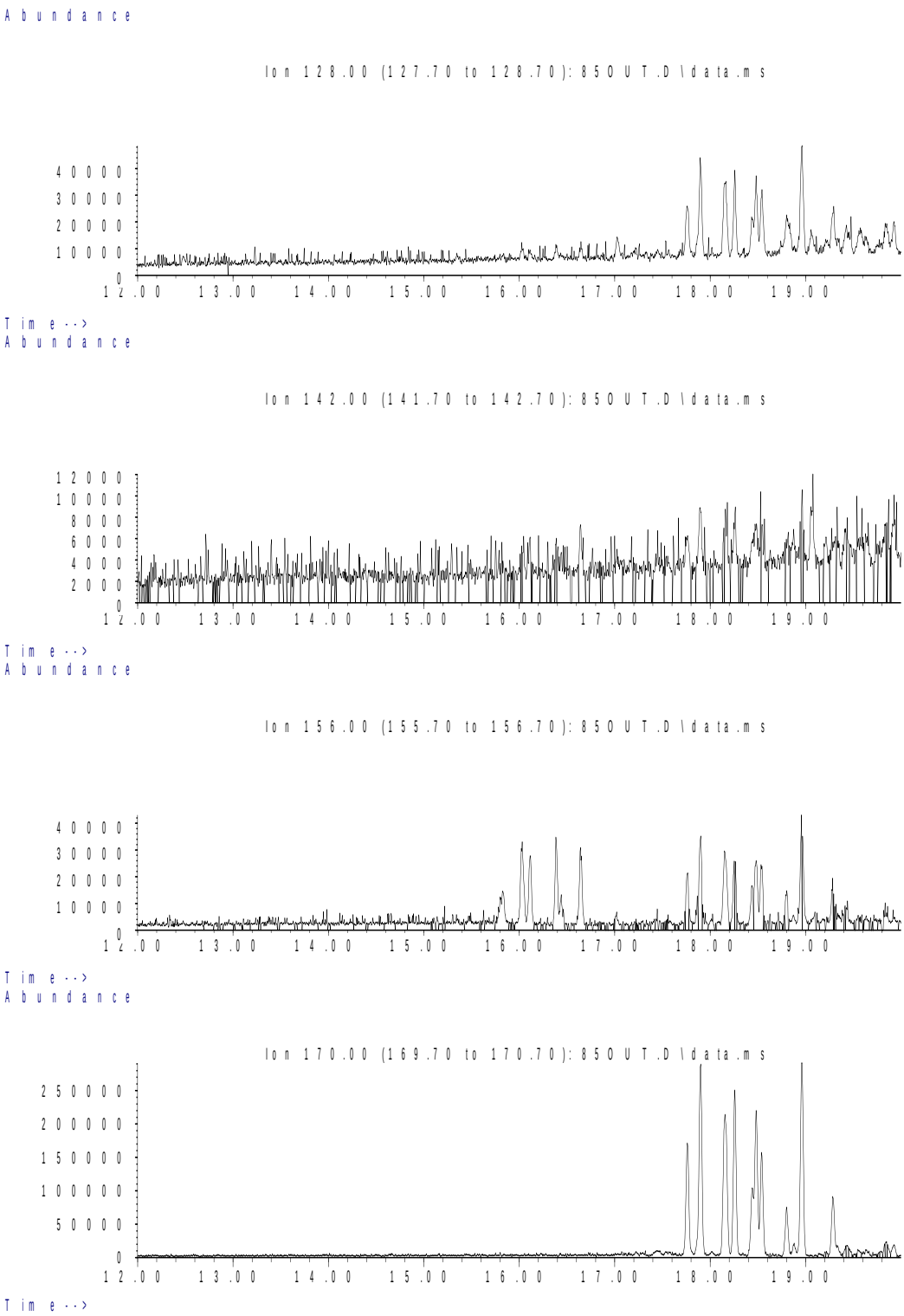

Sample 85 Outer Aromatic Chromatograms; Phenanthrenes

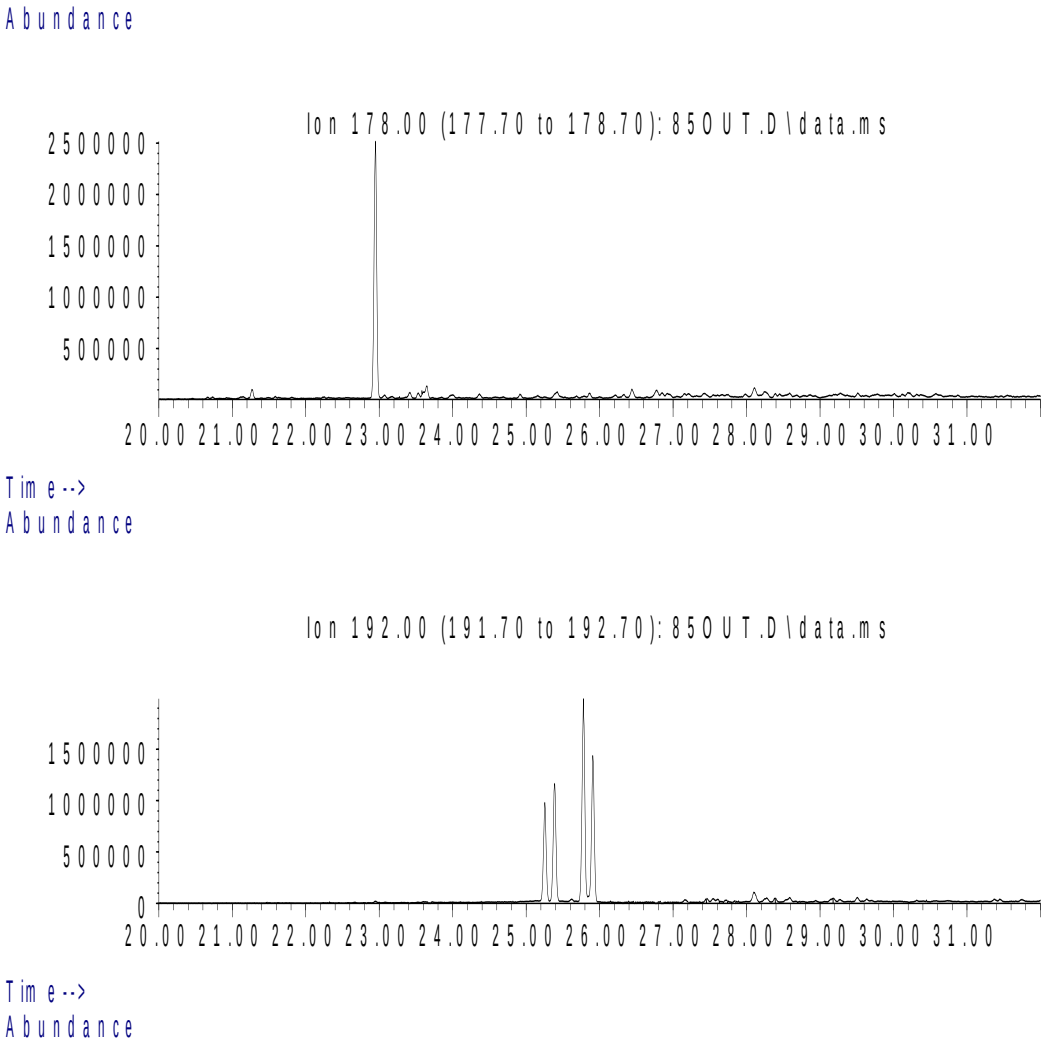

Sample 85 Outer Aromatic Chromatograms; Thiophenes & PAHs

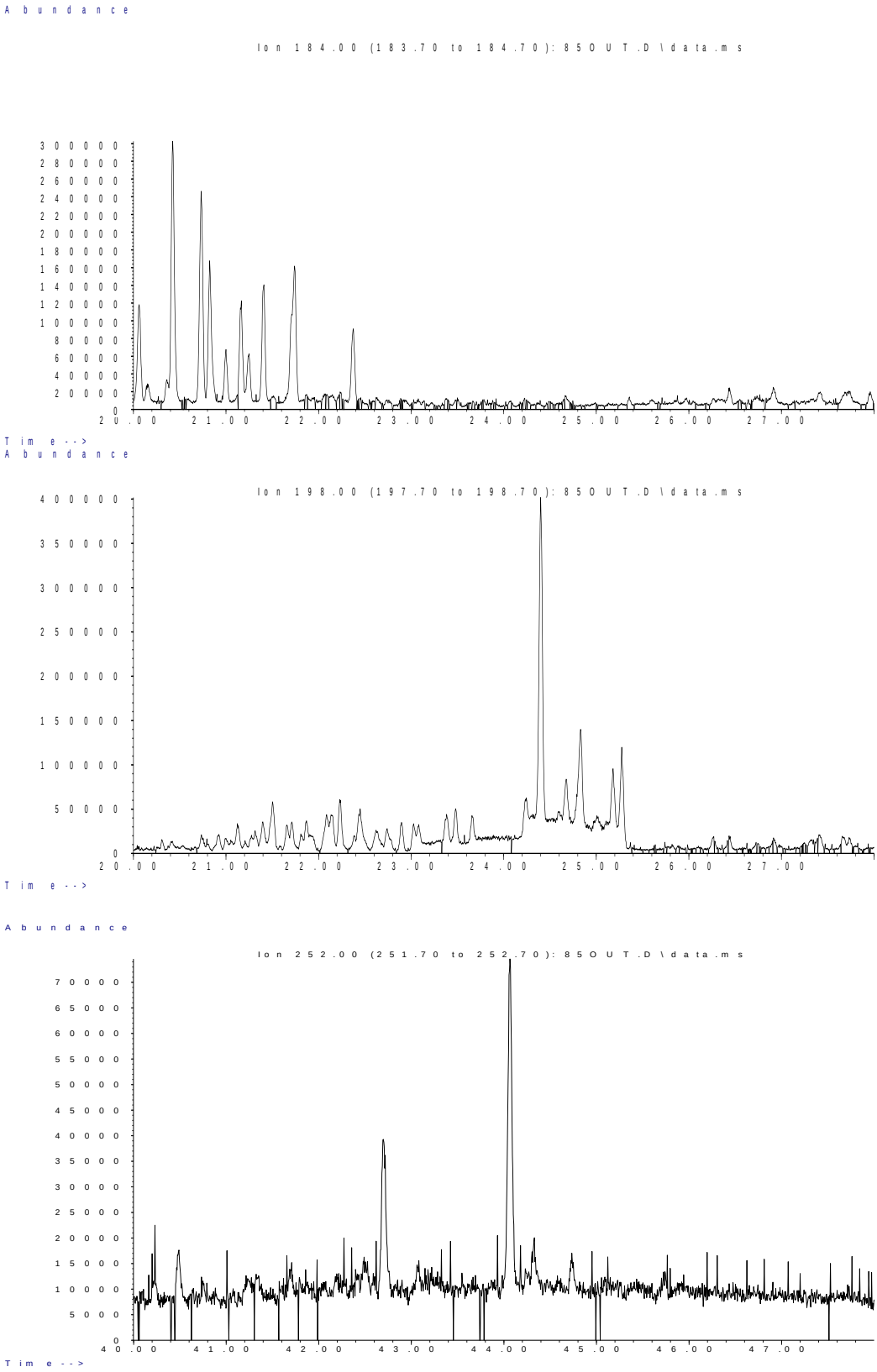

Sample 168 Inner

Aromatic Biomarker Integration Results				
Ion	Peak Label	Compound Name	R.Time (min.)	Peak Area
178	P	Phenantrene	22.952	9138270
184	DBT	Dibenzothiophene	22.382	6468384
192	C1P iso 1	Methyl Phenanthrene Isomer	25.269	3640395
192	C1P iso 2	Methyl Phenanthrene Isomer	25.398	4585960
192	C1P iso 3	Methyl Phenanthrene Isomer	25.787	7507863
192	C1P iso 4	Methyl Phenanthrene Isomer	25.917	5307646
192	C1P sum	Methyl Phenanthrene Isomers (summed)		21041864
198	4 MDBT	4 Methyldibenzothiophene	24.414	6280653
198	2+3 MDBT	2 & 3 Methyldibenzothiophene	24.834	3667786
198	1 MDBT	1 Methyldibenzothiophene	25.29	4288205
206	C2P iso 1	Ethyl/Dimethyl Phenanthrene Isomer	27.565	1726982
206	C2P iso 2	Ethyl/Dimethyl Phenanthrene Isomer	27.73	1523234
206	C2P iso 3	Ethyl/Dimethyl Phenanthrene Isomer	27.85	945681
206	C2P iso 4	Ethyl/Dimethyl Phenanthrene Isomer	28.119	7192561
206	C2P iso 5	Ethyl/Dimethyl Phenanthrene Isomer	28.285	3739959
206	C2P iso 6	Ethyl/Dimethyl Phenanthrene Isomer	28.399	3010481
206	C2P iso 7	Ethyl/Dimethyl Phenanthrene Isomer	28.549	806314
206	C2P iso 8	Ethyl/Dimethyl Phenanthrene Isomer	28.601	1883796
206	C2P iso 9	Ethyl/Dimethyl Phenanthrene Isomer	28.953	988588
206	C2P iso 10	Ethyl/Dimethyl Phenanthrene Isomer	29.28	769255
206	C2P sum	Ethyl/Dimethyl Phenanthrene Isomers (summed)		22586851
226	C3DBT sum	C3 Dibenzothiophene Isomers (summed)		19431588
252	dbf	benzo(b)fluoranthene	42.707	74961
252	bap	benzo(a)pyrene	44.080	151646

Sample 168 Inner Aromatic Chromatograms; Naphthalenes

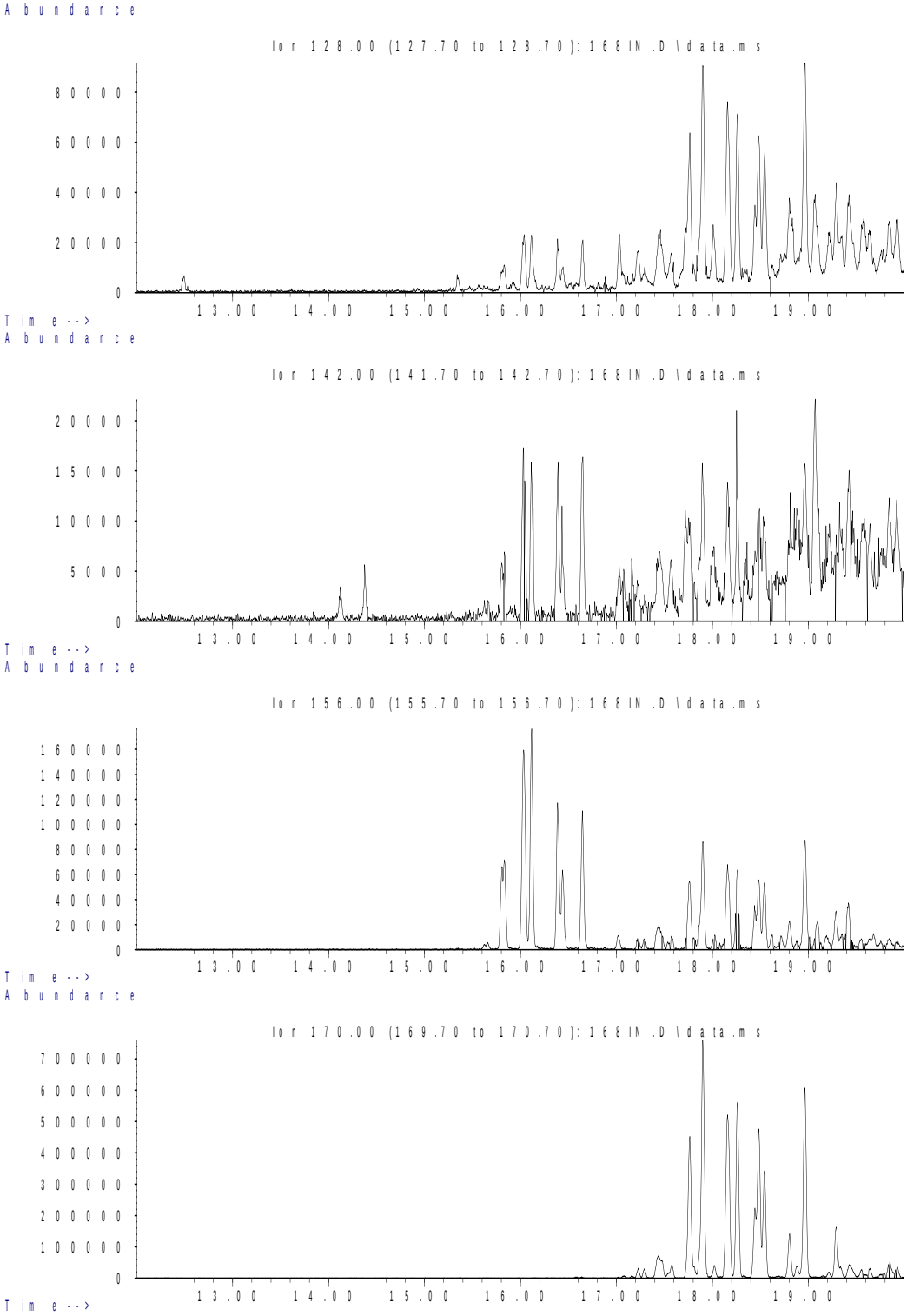

Sample 168 Inner Aromatic Chromatograms; Phenanthrenes

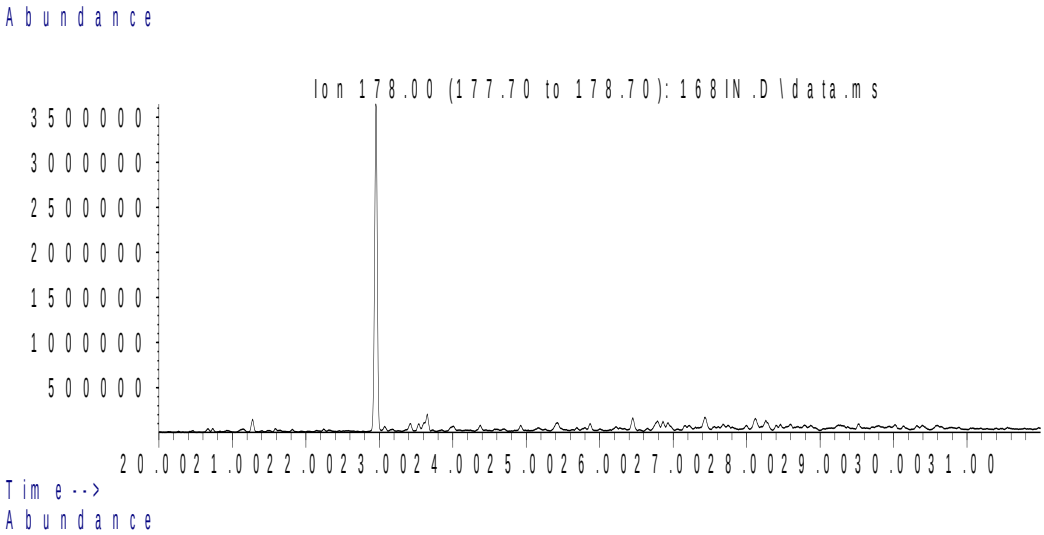

Sample 168 Inner Aromatic Chromatograms; Thiophenes & PAHs

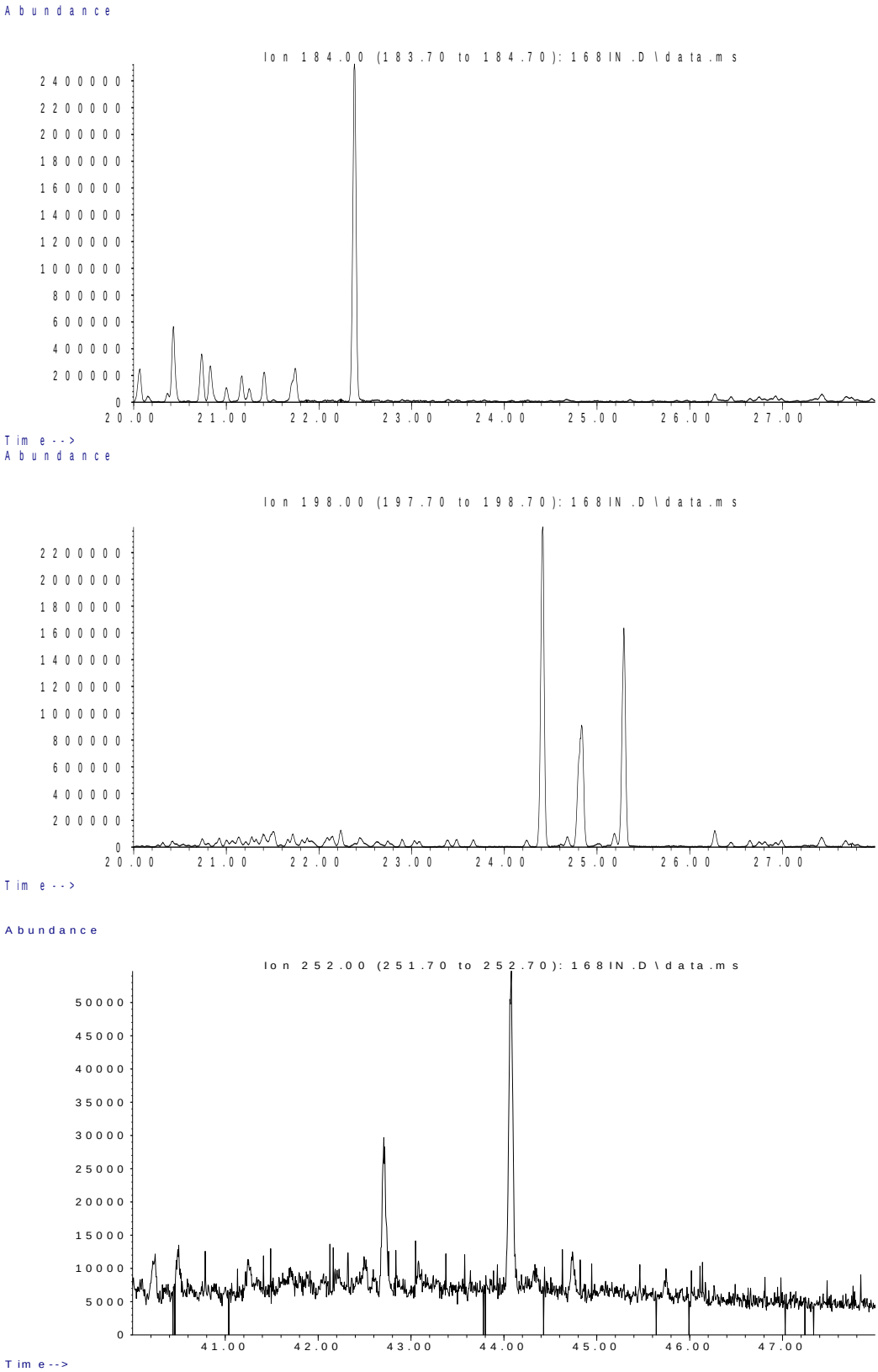

Sample 168 Outer

Aromatic Biomarker Integration Results				
Ion	Peak Label	Compound Name	R.Time (min.)	Peak Area
178	P	Phenantrene	22.951	5545654
184	DBT	Dibenzothiophene	22.381	3178049
192	C1P iso 1	Methyl Phenanthrene Isomer	25.262	2282167
192	C1P iso 2	Methyl Phenanthrene Isomer	25.391	2904739
192	C1P iso 3	Methyl Phenanthrene Isomer	25.78	4696865
192	C1P iso 4	Methyl Phenanthrene Isomer	25.91	3379337
192	C1P sum	Methyl Phenanthrene Isomers (summed)		13263108
198	4 MDBT	4 Methyldibenzothiophene	24.412	3588093
198	2+3 MDBT	2 & 3 Methyldibenzothiophene	24.832	1975663
198	1 MDBT	1 Methyldibenzothiophene	25.283	2349860
206	C2P iso 1	Ethyl/Dimethyl Phenanthrene Isomer	27.557	1123002
206	C2P iso 2	Ethyl/Dimethyl Phenanthrene Isomer	27.718	985693
206	C2P iso 3	Ethyl/Dimethyl Phenanthrene Isomer	27.842	598417
206	C2P iso 4	Ethyl/Dimethyl Phenanthrene Isomer	28.107	4631413
206	C2P iso 5	Ethyl/Dimethyl Phenanthrene Isomer	28.278	2414776
206	C2P iso 6	Ethyl/Dimethyl Phenanthrene Isomer	28.397	2025419
206	C2P iso 7	Ethyl/Dimethyl Phenanthrene Isomer	28.542	510211
206	C2P iso 8	Ethyl/Dimethyl Phenanthrene Isomer	28.589	1225304
206	C2P iso 9	Ethyl/Dimethyl Phenanthrene Isomer	28.941	653000
206	C2P iso 10	Ethyl/Dimethyl Phenanthrene Isomer	29.273	490805
206	C2P sum	Ethyl/Dimethyl Phenanthrene Isomers (summed)		14658040
226	C3DBT sum	C3 Dibenzothiophene Isomers (summed)		12165883
252	dbf	benzo(b)fluoranthene	42.710	48100
252	bap	benzo(a)pyrene	44.063	95355

Sample 168 Outer Aromatic Chromatograms; Naphthalenes

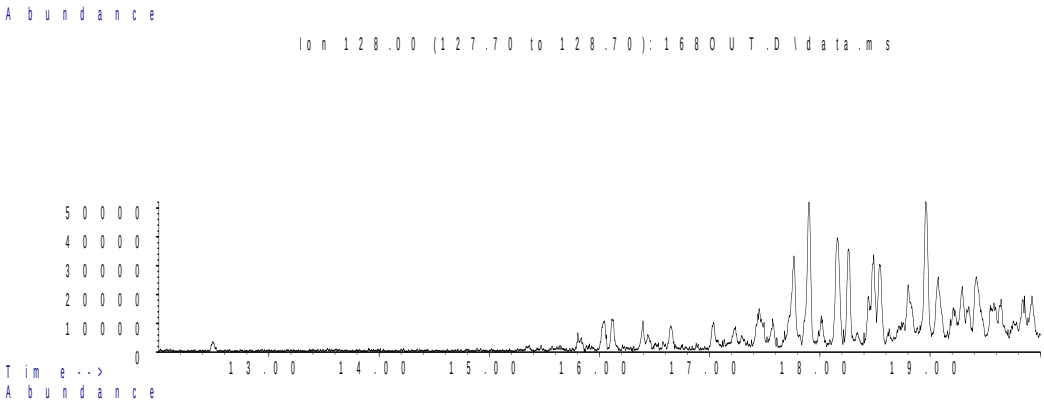

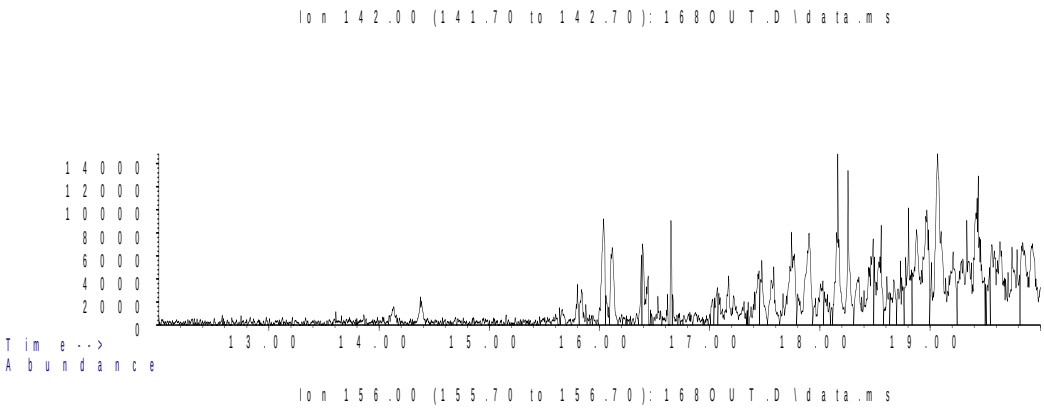

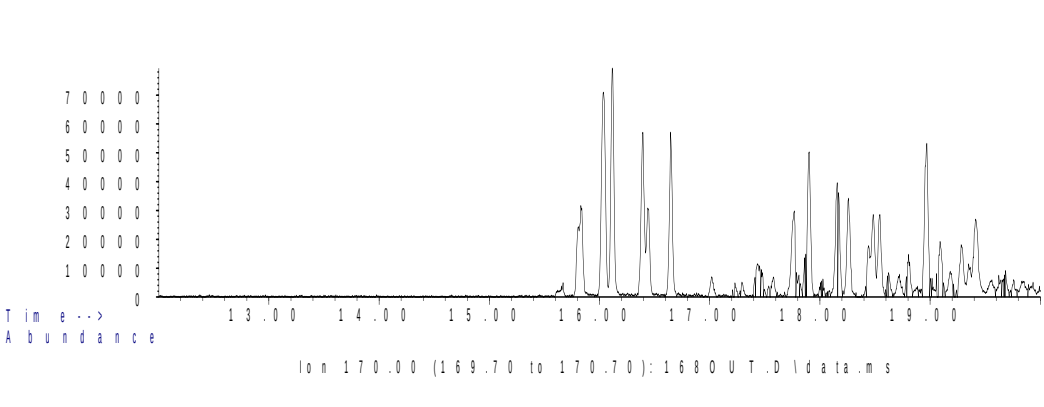

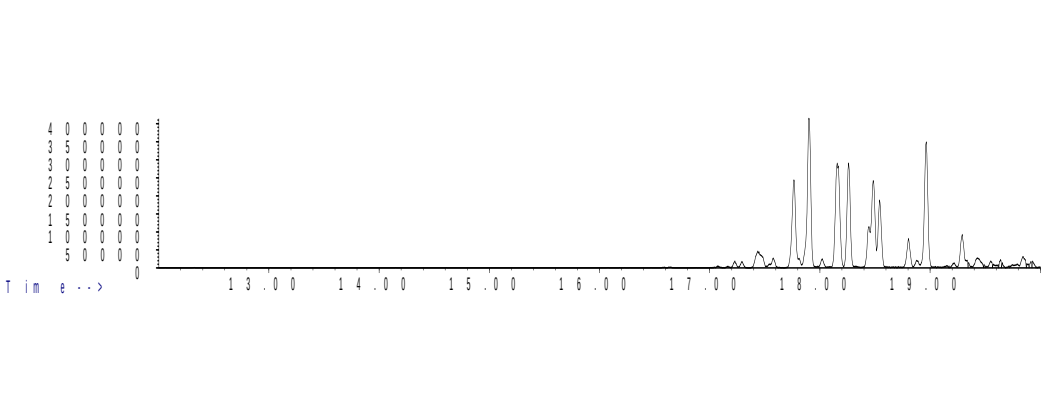

Sample 168 Outer Aromatic Chromatograms; Phenanthrenes

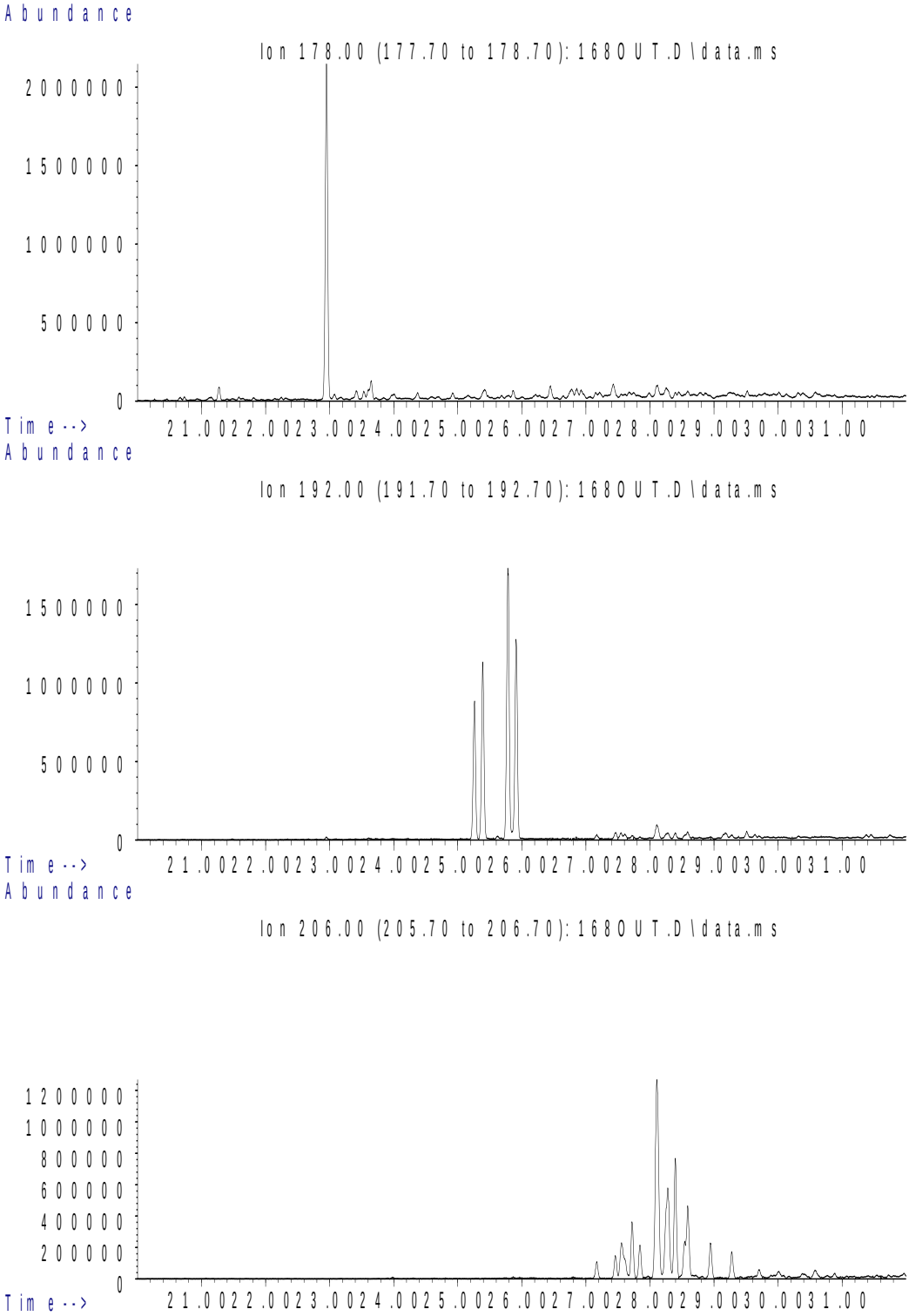

Sample 168 Outer Aromatic Chromatograms; Thiophenes & PAHs

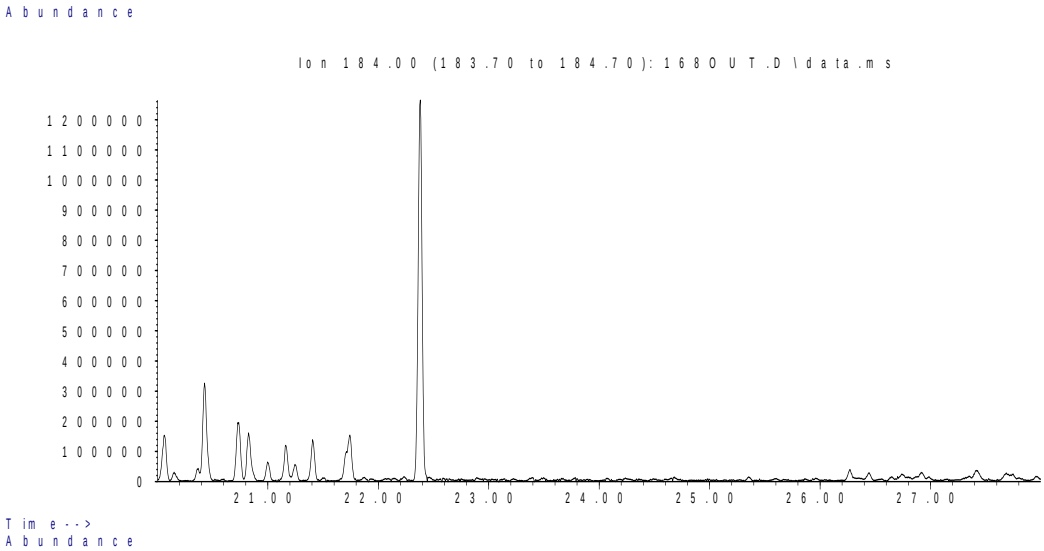

Sample 177 Inner

Aromatic Biomarker Integration Results				
Ion	Peak Label	Compound Name	R.Time (min.)	Peak Area
178	P	Phenantrene	22.96	12516852
184	DBT	Dibenzothiophene	22.385	10649277
192	C1P iso 1	Methyl Phenanthrene Isomer	25.266	4153869
192	C1P iso 2	Methyl Phenanthrene Isomer	25.401	5164639
192	C1P iso 3	Methyl Phenanthrene Isomer	25.794	8580053
192	C1P iso 4	Methyl Phenanthrene Isomer	25.919	5992715
192	C1P sum	Methyl Phenanthrene Isomers (summed)		23891276
198	4 MDBT	4 Methyldibenzothiophene	24.416	7653312
198	2+3 MDBT	2 & 3 Methyldibenzothiophene	24.841	4828342
198	1 MDBT	1 Methyldibenzothiophene	25.292	5733247
206	C2P iso 1	Ethyl/Dimethyl Phenanthrene Isomer	27.562	1772912
206	C2P iso 2	Ethyl/Dimethyl Phenanthrene Isomer	27.727	1542875
206	C2P iso 3	Ethyl/Dimethyl Phenanthrene Isomer	27.847	923519
206	C2P iso 4	Ethyl/Dimethyl Phenanthrene Isomer	28.116	7581851
206	C2P iso 5	Ethyl/Dimethyl Phenanthrene Isomer	28.297	4028945
206	C2P iso 6	Ethyl/Dimethyl Phenanthrene Isomer	28.401	3159659
206	C2P iso 7	Ethyl/Dimethyl Phenanthrene Isomer	28.551	1021005
206	C2P iso 8	Ethyl/Dimethyl Phenanthrene Isomer	28.598	1953795
206	C2P iso 9	Ethyl/Dimethyl Phenanthrene Isomer	28.95	1018814
206	C2P iso 10	Ethyl/Dimethyl Phenanthrene Isomer	29.287	776095
206	C2P sum	Ethyl/Dimethyl Phenanthrene Isomers (summed)		23779470
226	C3DBT sum	C3 Dibenzothiophene Isomers (summed)		21161138
252	dbf	benzo(b)fluoranthene	42.714	71523
252	bap	benzo(a)pyrene	44.072	141539

Sample 177 Inner Aromatic Chromatograms; Naphthalenes

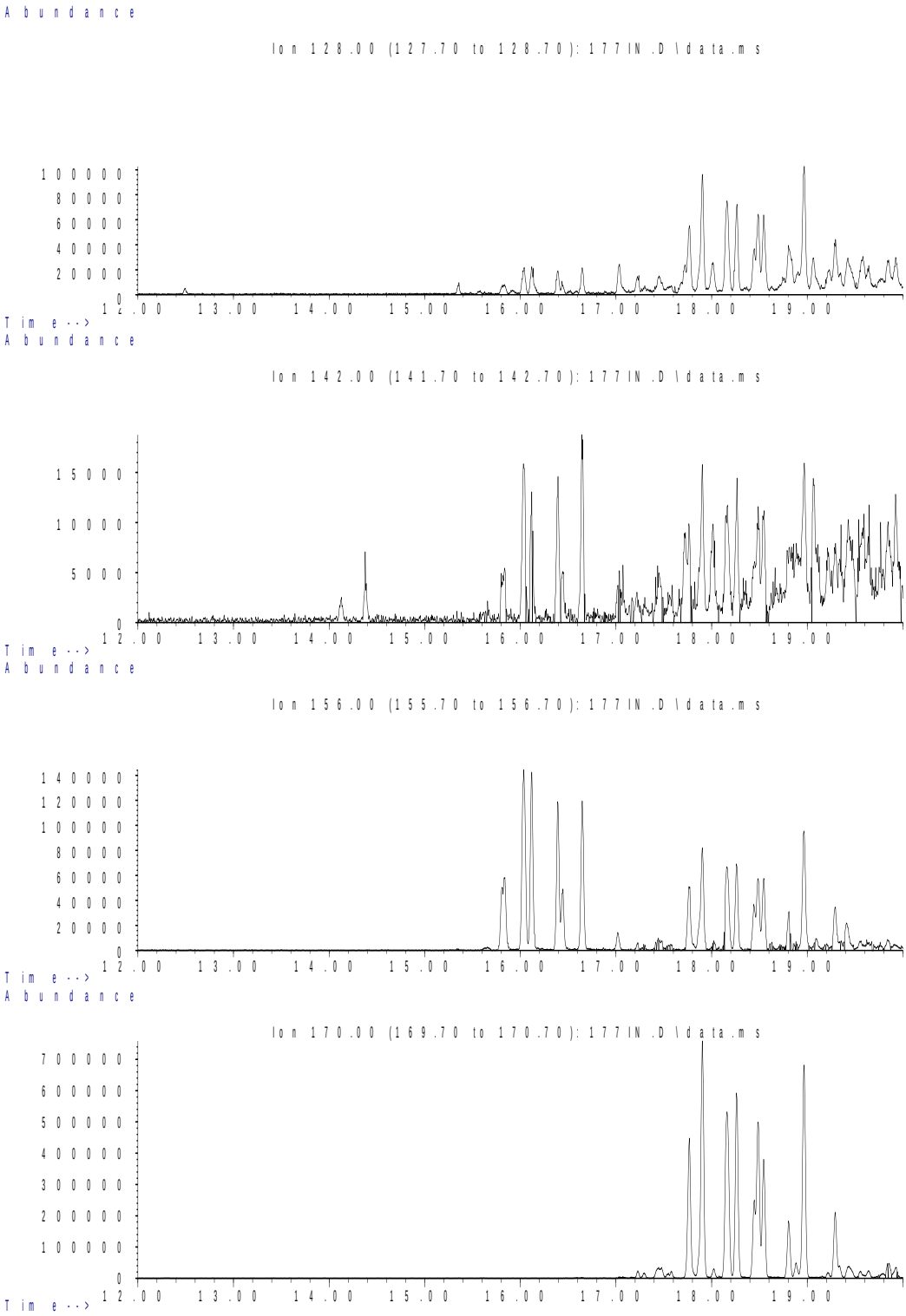

Sample 177 Inner Aromatic Chromatograms; Phenanthrenes

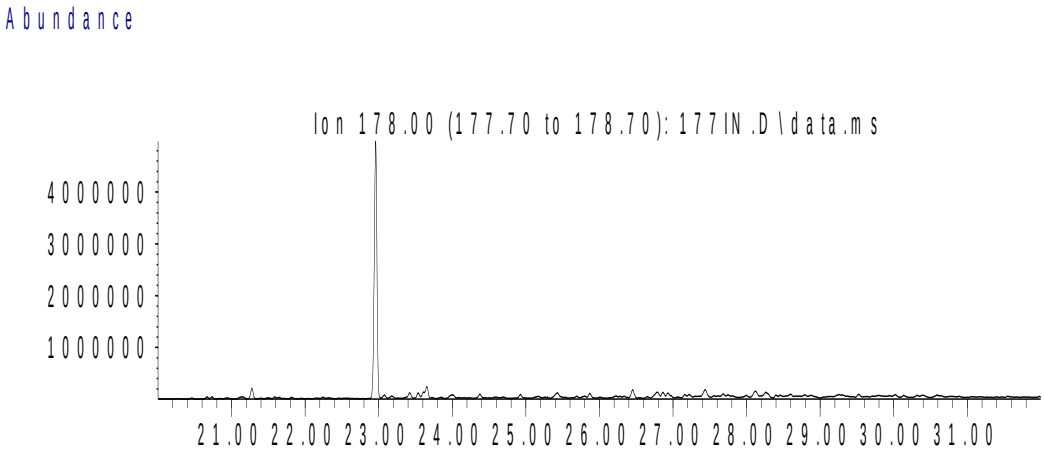

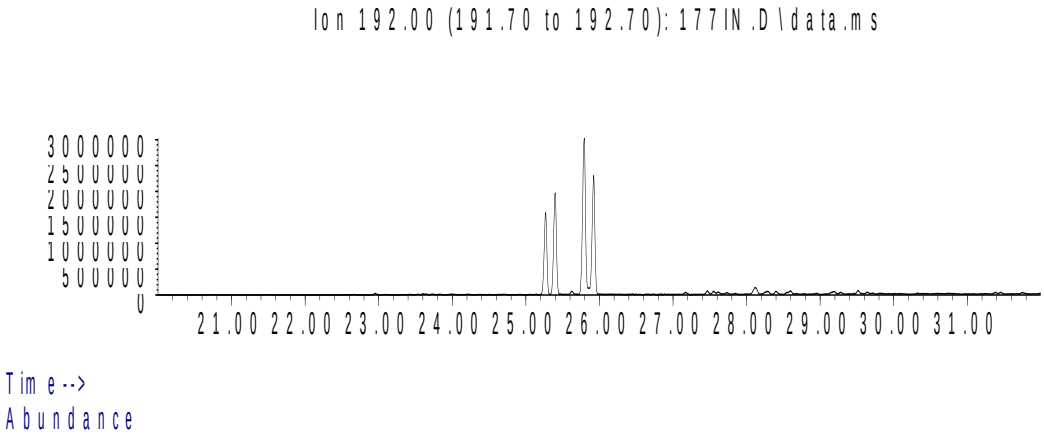

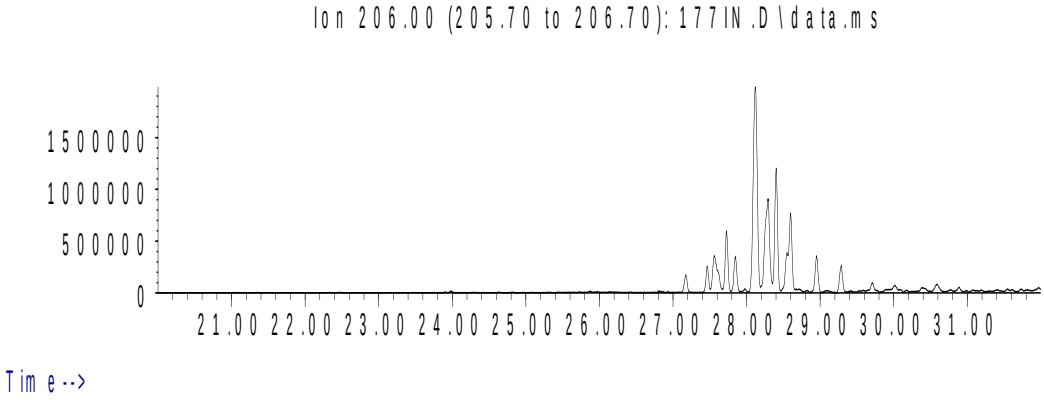

Sample 177 Inner Aromatic Chromatograms; Thiophenes & PAHs

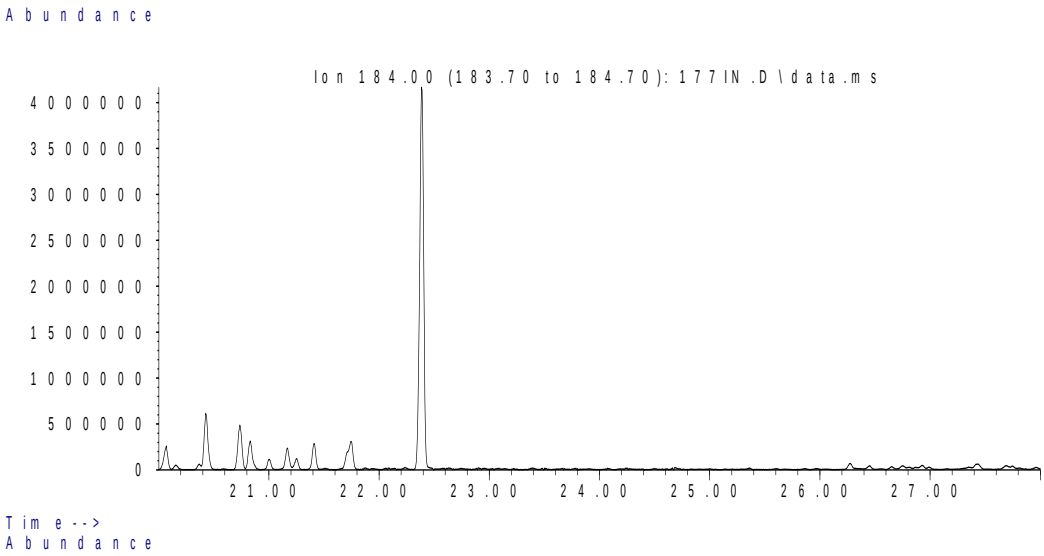

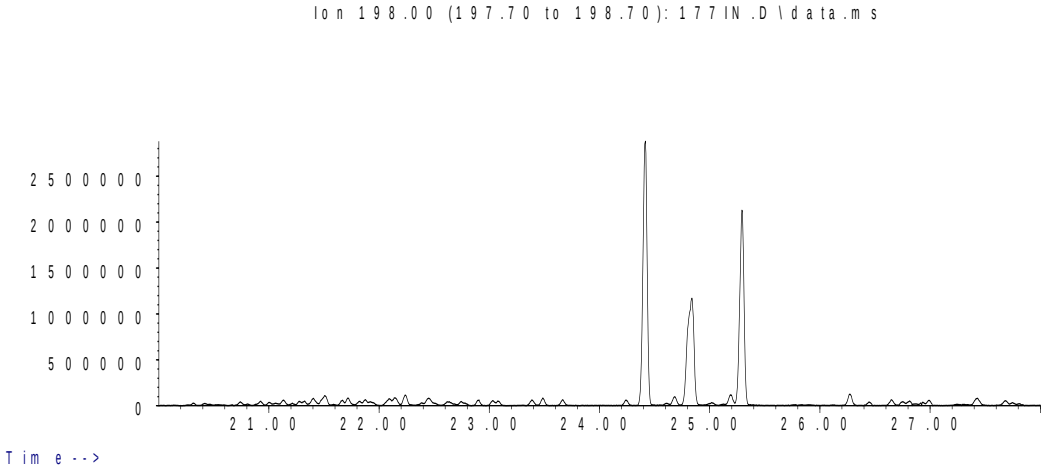

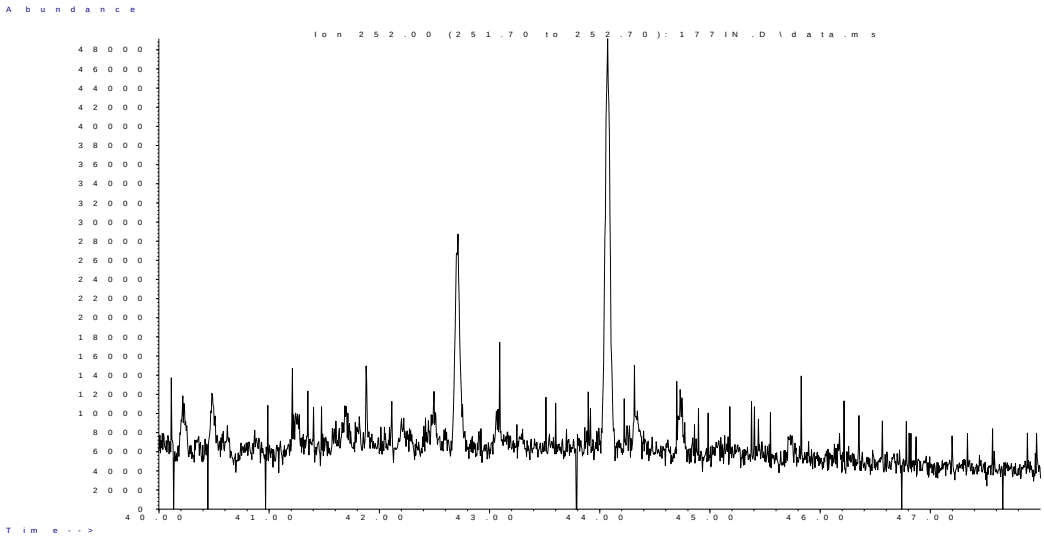

Sample 177 Outer

Aromatic Biomarker Integration Results				
Ion	Peak Label	Compound Name	R.Time (min.)	Peak Area
178	P	Phenantrene	22.961	14555845
184	DBT	Dibenzothiophene	22.386	10708677
192	C1P iso 1	Methyl Phenanthrene Isomer	25.273	4918560
192	C1P iso 2	Methyl Phenanthrene Isomer	25.402	6164128
192	C1P iso 3	Methyl Phenanthrene Isomer	25.796	9933946
192	C1P iso 4	Methyl Phenanthrene Isomer	25.926	7122877
192	C1P sum	Methyl Phenanthrene Isomers (summed)		28139511
198	4 MDBT	4 Methyldibenzothiophene	24.418	8325335
198	2+3 MDBT	2 & 3 Methyldibenzothiophene	24.842	5503501
198	1 MDBT	1 Methyldibenzothiophene	25.293	6396158
206	C2P iso 1	Ethyl/Dimethyl Phenanthrene Isomer	27.568	2169156
206	C2P iso 2	Ethyl/Dimethyl Phenanthrene Isomer	27.729	1908405
206	C2P iso 3	Ethyl/Dimethyl Phenanthrene Isomer	27.848	1176774
206	C2P iso 4	Ethyl/Dimethyl Phenanthrene Isomer	28.123	8973481
206	C2P iso 5	Ethyl/Dimethyl Phenanthrene Isomer	28.294	4739565
206	C2P iso 6	Ethyl/Dimethyl Phenanthrene Isomer	28.408	3721179
206	C2P iso 7	Ethyl/Dimethyl Phenanthrene Isomer	28.558	1079805
206	C2P iso 8	Ethyl/Dimethyl Phenanthrene Isomer	28.6	2316751
206	C2P iso 9	Ethyl/Dimethyl Phenanthrene Isomer	28.952	1215987
206	C2P iso 10	Ethyl/Dimethyl Phenanthrene Isomer	29.284	919244
206	C2P sum	Ethyl/Dimethyl Phenanthrene Isomers (summed)		28220347
226	C3DBT sum	C3 Dibenzothiophene Isomers (summed)		24135820
252	dbf	benzo(b)fluoranthene	42.710	80229
252	bap	benzo(a)pyrene	44.073	158209

Sample 177 Outer Aromatic Chromatograms; Naphthalenes

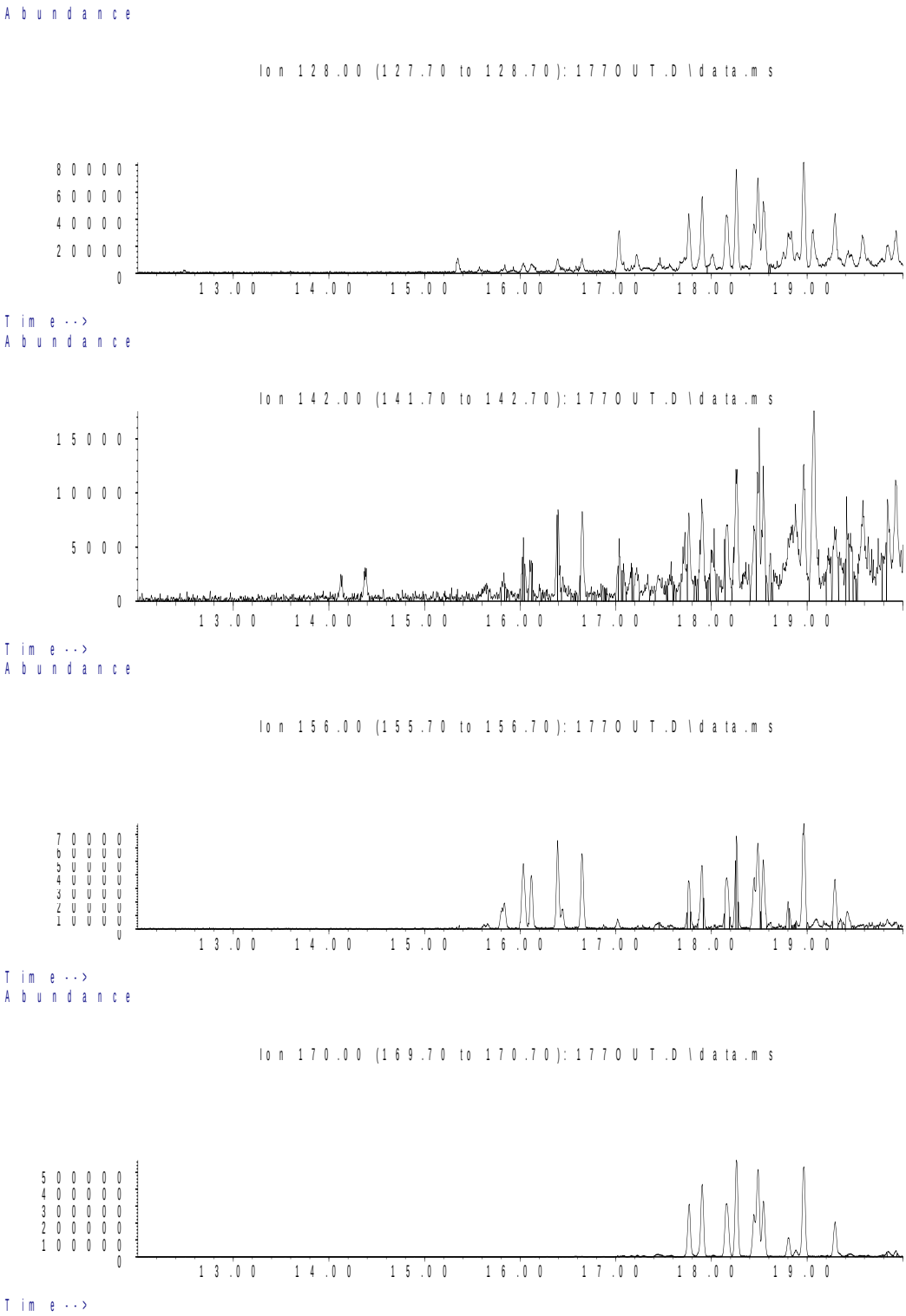

Sample 177 Outer Aromatic Chromatograms; Phenanthrenes

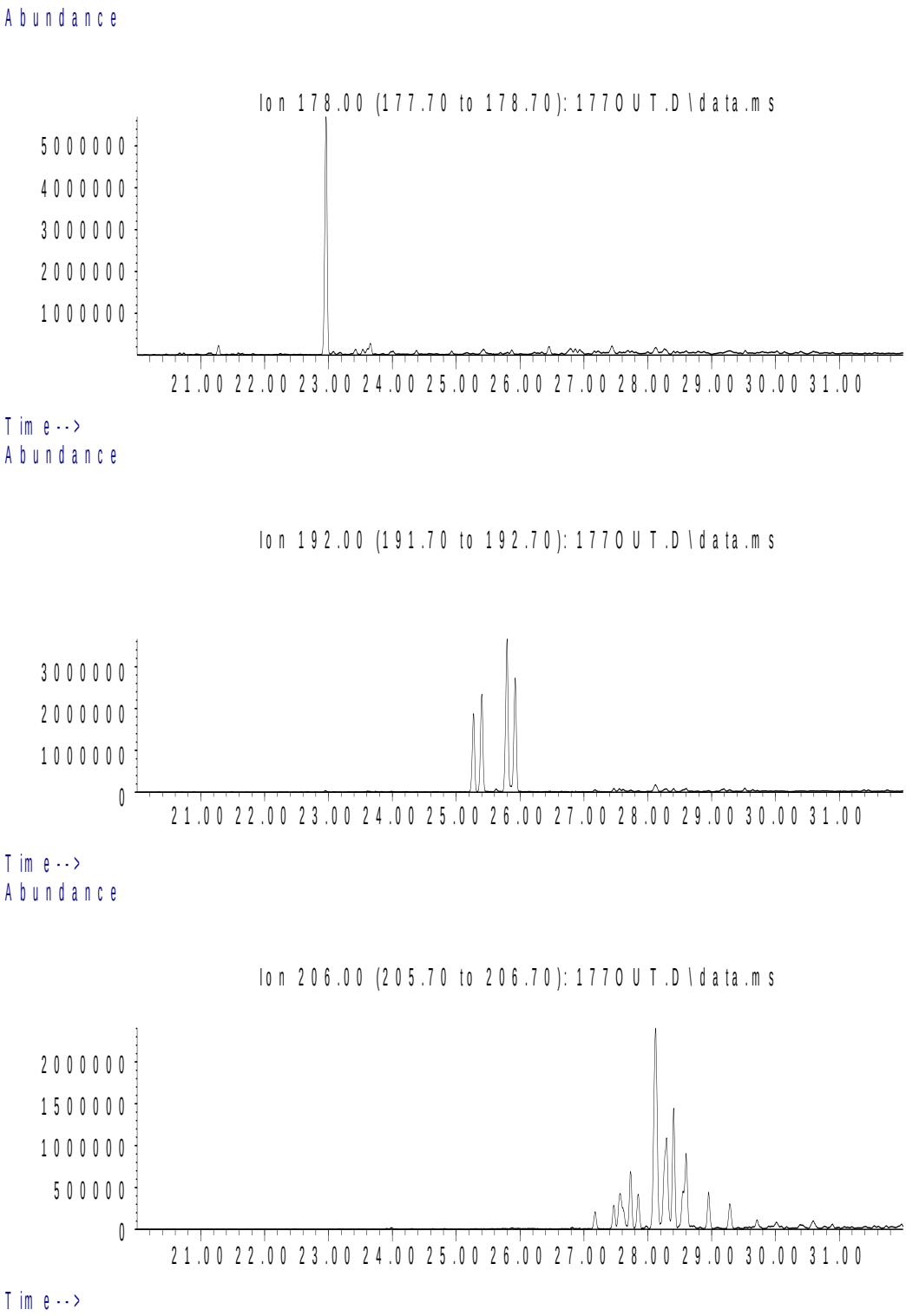

Sample 177 Outer Aromatic Chromatograms; Thiophenes & PAHs

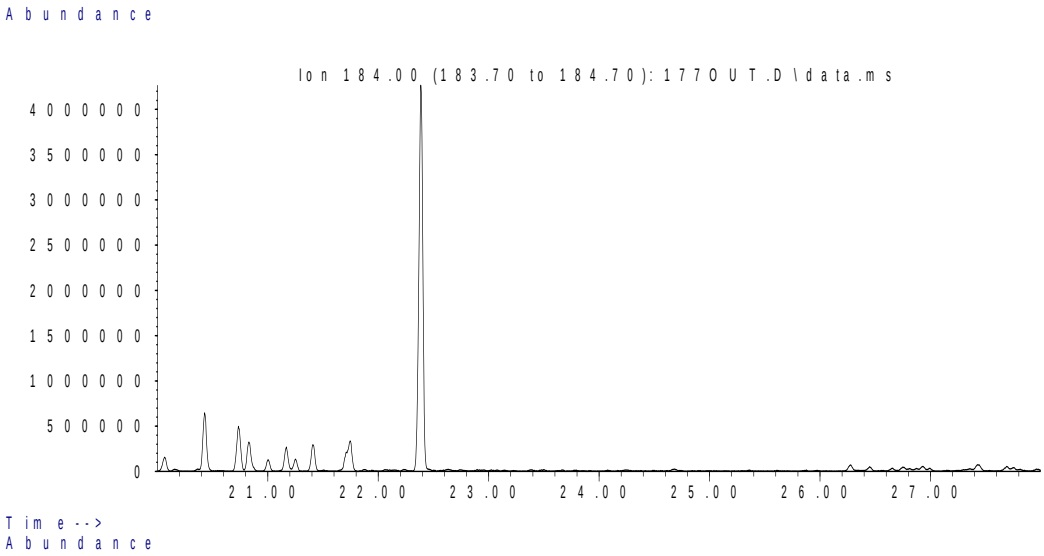

Sample CL1 Inner

Aromatic Biomarker Integration Results				
Ion	Peak Label	Compound Name	R.Time (min.)	Peak Area
178	P	Phenantrene	22.956	10102689
184	DBT	Dibenzothiophene	22.381	4754700
192	C1P iso 1	Methyl Phenanthrene Isomer	25.262	3334562
192	C1P iso 2	Methyl Phenanthrene Isomer	25.397	4242690
192	C1P iso 3	Methyl Phenanthrene Isomer	25.786	6780887
192	C1P iso 4	Methyl Phenanthrene Isomer	25.915	4848034
192	C1P sum	Methyl Phenanthrene Isomers (summed)		19206173
198	4 MDBT	4 Methyldibenzothiophene	24.407	4827113
198	2+3 MDBT	2 & 3 Methyldibenzothiophene	24.832	2960730
198	1 MDBT	1 Methyldibenzothiophene	25.288	3265758
206	C2P iso 1	Ethyl/Dimethyl Phenanthrene Isomer	27.563	1415246
206	C2P iso 2	Ethyl/Dimethyl Phenanthrene Isomer	27.729	1297790
206	C2P iso 3	Ethyl/Dimethyl Phenanthrene Isomer	27.843	809093
206	C2P iso 4	Ethyl/Dimethyl Phenanthrene Isomer	28.112	6158116
206	C2P iso 5	Ethyl/Dimethyl Phenanthrene Isomer	28.278	3305030
206	C2P iso 6	Ethyl/Dimethyl Phenanthrene Isomer	28.397	2486921
206	C2P iso 7	Ethyl/Dimethyl Phenanthrene Isomer	28.543	688840
206	C2P iso 8	Ethyl/Dimethyl Phenanthrene Isomer	28.594	1526186
206	C2P iso 9	Ethyl/Dimethyl Phenanthrene Isomer	28.952	838181
206	C2P iso 10	Ethyl/Dimethyl Phenanthrene Isomer	29.278	626622
206	C2P sum	Ethyl/Dimethyl Phenanthrene Isomers (summed)		19152025
226	C3DBT sum	C3 Dibenzothiophene Isomers (summed)		15403387
252	dbf	benzo(b)fluoranthene	42.716	44975
252	bap	benzo(a)pyrene	44.073	100940

Sample CL1 Inner Aromatic Chromatograms; Naphthalenes

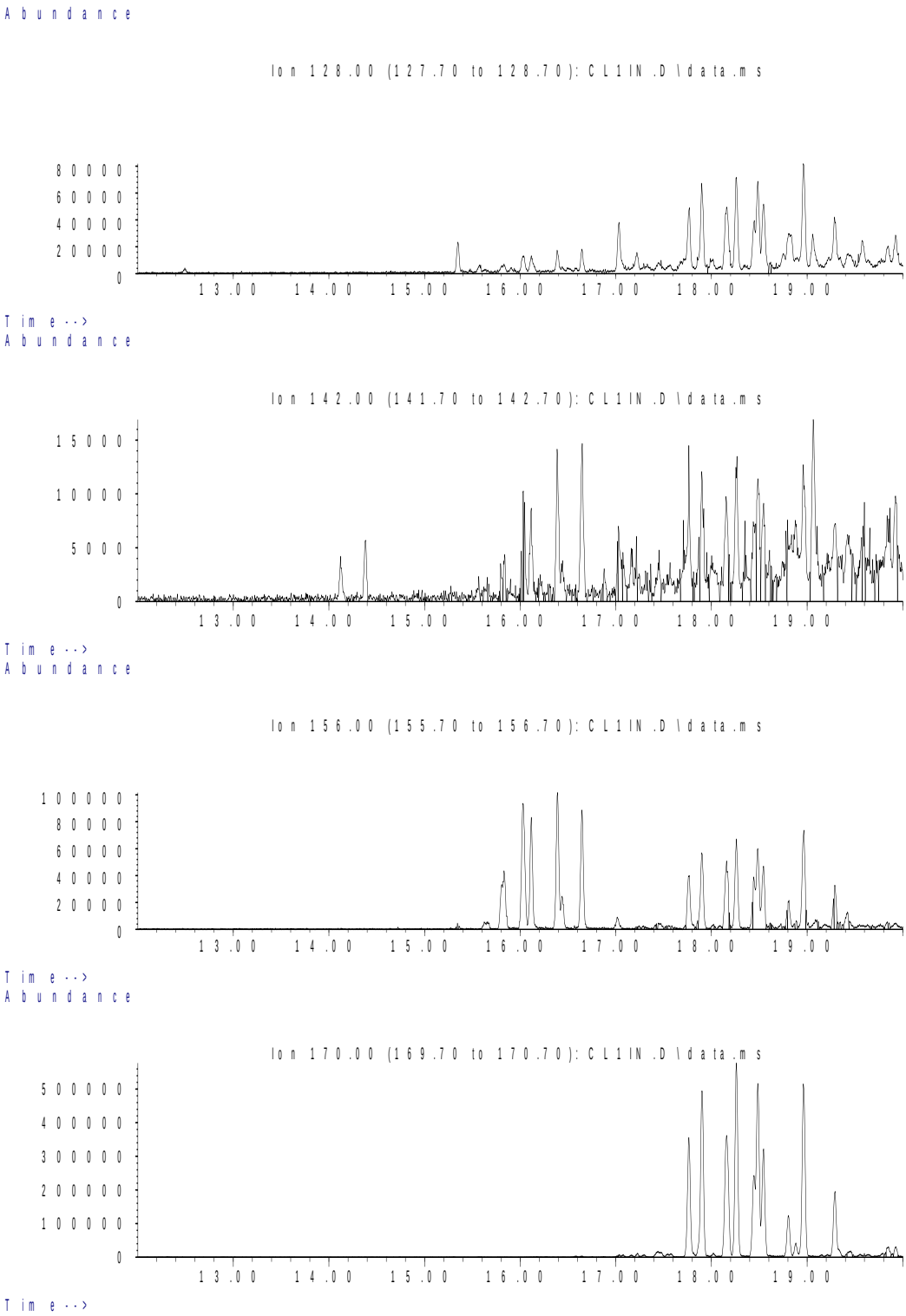

Sample CL1 Inner Aromatic Chromatograms; Phenanthrenes

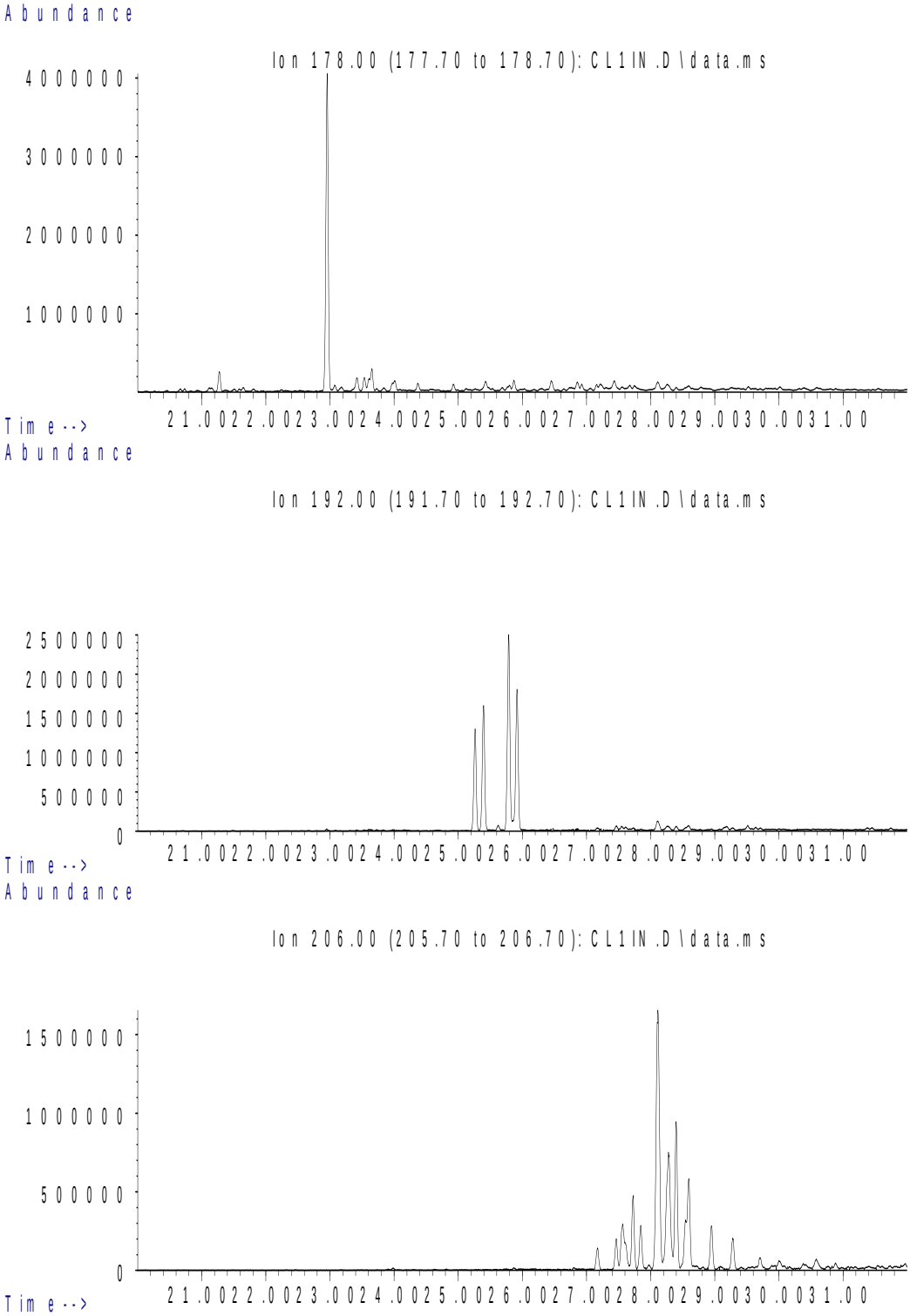

Sample CL1 Inner Aromatic Chromatograms; Thiophenes & PAHs

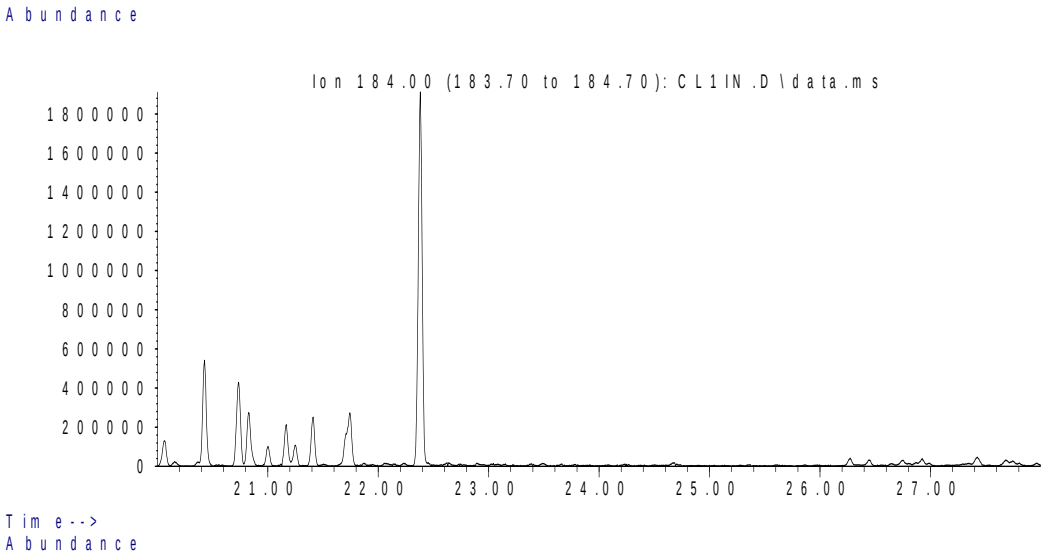

SampleCL1 Outer

Aromatic Biomarker Integration Results				
Ion	Peak Label	Compound Name	R.Time (min.)	Peak Area
178	P	Phenantrene	22.95	6031169
184	DBT	Dibenzothiophene	22.374	2768619
192	C1P iso 1	Methyl Phenanthrene Isomer	25.256	2217085
192	C1P iso 2	Methyl Phenanthrene Isomer	25.39	2761937
192	C1P iso 3	Methyl Phenanthrene Isomer	25.779	4531993
192	C1P iso 4	Methyl Phenanthrene Isomer	25.909	3214502
192	C1P sum	Methyl Phenanthrene Isomers (summed)		12725517
198	4 MDBT	4 Methyldibenzothiophene	24.406	2966175
198	2+3 MDBT	2 & 3 Methyldibenzothiophene	24.831	1719344
198	1 MDBT	1 Methyldibenzothiophene	25.282	1949518
206	C2P iso 1	Ethyl/Dimethyl Phenanthrene Isomer	27.551	985349
206	C2P iso 2	Ethyl/Dimethyl Phenanthrene Isomer	27.717	890748
206	C2P iso 3	Ethyl/Dimethyl Phenanthrene Isomer	27.836	543889
206	C2P iso 4	Ethyl/Dimethyl Phenanthrene Isomer	28.106	4100482
206	C2P iso 5	Ethyl/Dimethyl Phenanthrene Isomer	28.277	2159409
206	C2P iso 6	Ethyl/Dimethyl Phenanthrene Isomer	28.391	1701864
206	C2P iso 7	Ethyl/Dimethyl Phenanthrene Isomer	28.541	498584
206	C2P iso 8	Ethyl/Dimethyl Phenanthrene Isomer	28.588	1053068
206	C2P iso 9	Ethyl/Dimethyl Phenanthrene Isomer	28.94	565210
206	C2P iso 10	Ethyl/Dimethyl Phenanthrene Isomer	29.277	420610
206	C2P sum	Ethyl/Dimethyl Phenanthrene Isomers (summed)		12919213
226	C3DBT sum	C3 Dibenzothiophene Isomers (summed)		9877003
252	dbf	benzo(b)fluoranthene	42.714	35031
252	bap	benzo(a)pyrene	44.062	66479

Sample CL1 Outer Aromatic Chromatograms; Naphthalenes

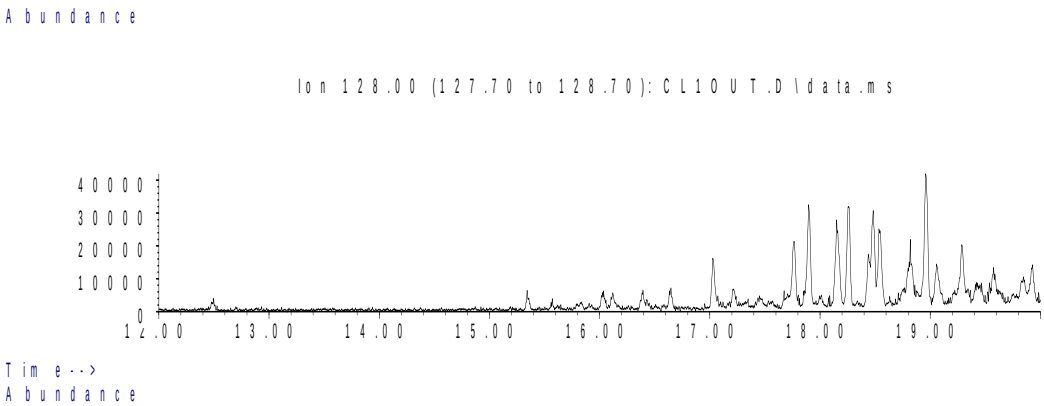

SampleCL1 Outer Aromatic Chromatograms; Phenanthrenes

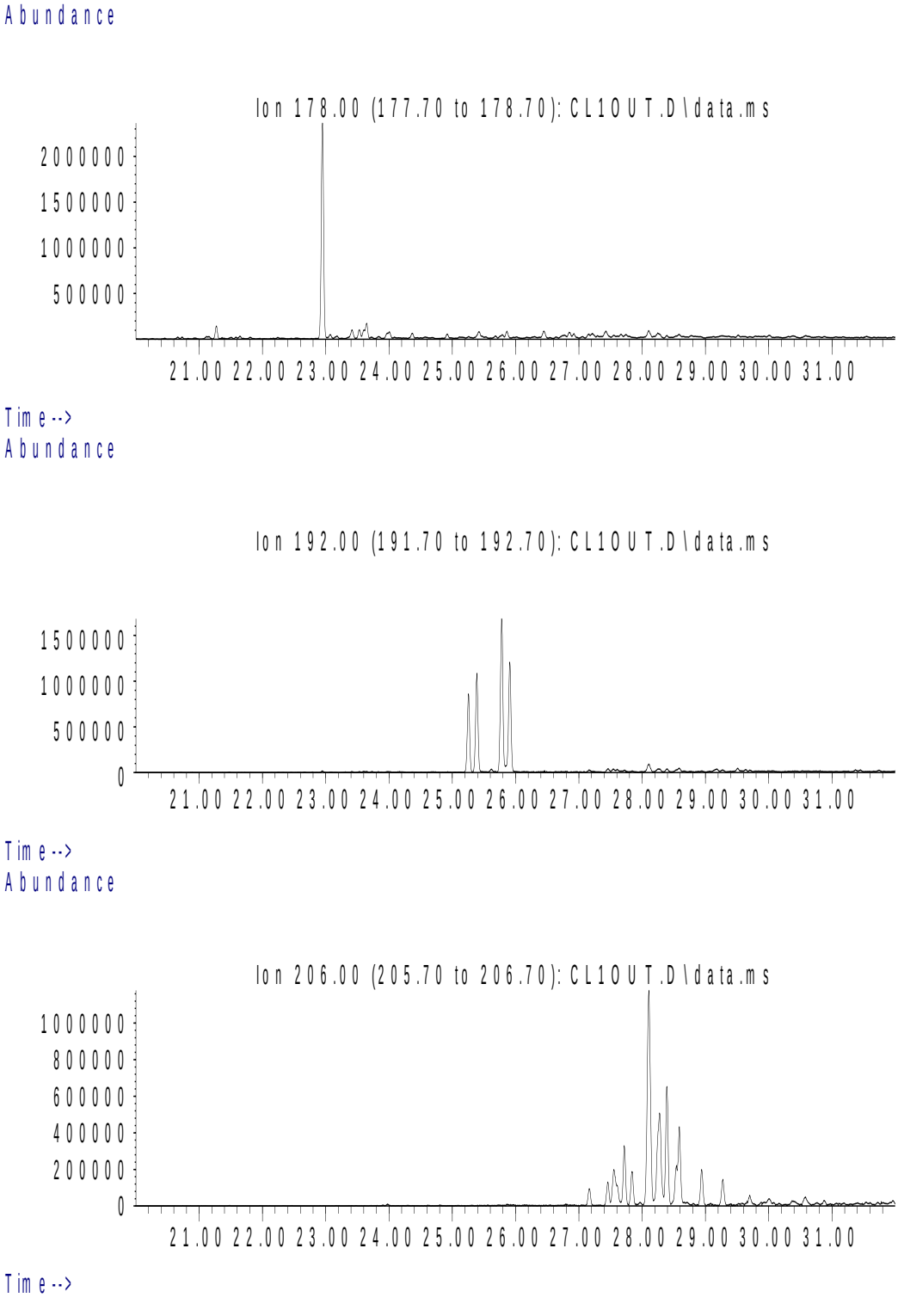

SampleCL1 Outer Aromatic Chromatograms; Thiophenes & PAHs

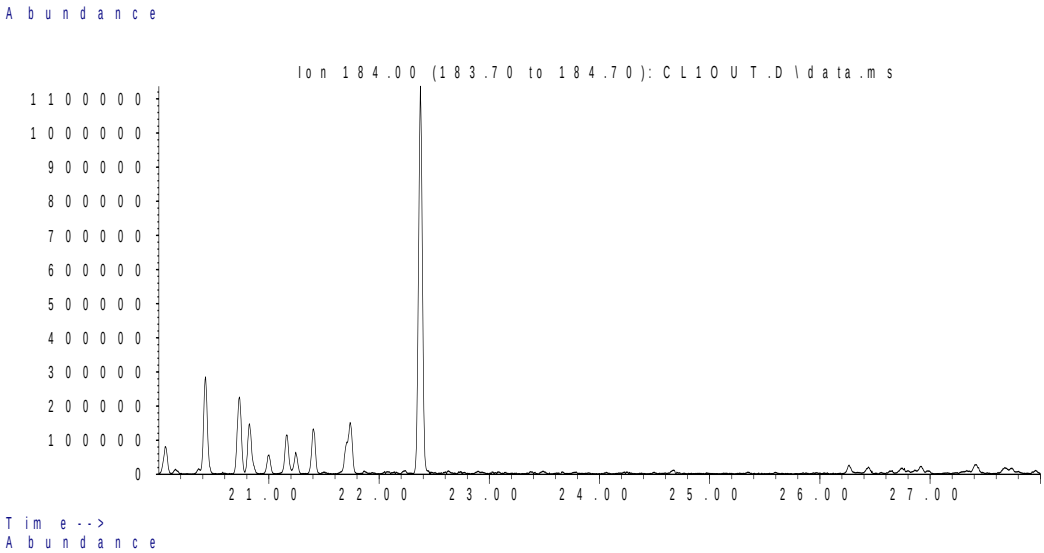

Sample MH1 Inner

Aromatic Biomarker Integration Results				
Ion	Peak Label	Compound Name	R.Time (min.)	Peak Area
178	P	Phenantrene	22.954	9414540
184	DBT	Dibenzothiophene	22.378	5155123
192	C1P iso 1	Methyl Phenanthrene Isomer	25.26	3270669
192	C1P iso 2	Methyl Phenanthrene Isomer	25.394	4125409
192	C1P iso 3	Methyl Phenanthrene Isomer	25.783	6661170
192	C1P iso 4	Methyl Phenanthrene Isomer	25.913	4716524
192	C1P sum	Methyl Phenanthrene Isomers (summed)		18773772
198	4 MDBT	4 Methyldibenzothiophene	24.41	4991897
198	2+3 MDBT	2 & 3 Methyldibenzothiophene	24.835	2950107
198	1 MDBT	1 Methyldibenzothiophene	25.286	3262324
206	C2P iso 1	Ethyl/Dimethyl Phenanthrene Isomer	27.555	1400649
206	C2P iso 2	Ethyl/Dimethyl Phenanthrene Isomer	27.721	1219283
206	C2P iso 3	Ethyl/Dimethyl Phenanthrene Isomer	27.846	713904
206	C2P iso 4	Ethyl/Dimethyl Phenanthrene Isomer	28.105	5923271
206	C2P iso 5	Ethyl/Dimethyl Phenanthrene Isomer	28.286	3080846
206	C2P iso 6	Ethyl/Dimethyl Phenanthrene Isomer	28.395	2489980
206	C2P iso 7	Ethyl/Dimethyl Phenanthrene Isomer	28.54	636549
206	C2P iso 8	Ethyl/Dimethyl Phenanthrene Isomer	28.592	1507423
206	C2P iso 9	Ethyl/Dimethyl Phenanthrene Isomer	28.949	829549
206	C2P iso 10	Ethyl/Dimethyl Phenanthrene Isomer	29.276	626048
206	C2P sum	Ethyl/Dimethyl Phenanthrene Isomers (summed)		18427502
226	C3DBT sum	C3 Dibenzothiophene Isomers (summed)		14955092
252	dbf	benzo(b)fluoranthene	42.708	48703
252	bap	benzo(a)pyrene	44.066	106304

Sample MH1 Inner Aromatic Chromatograms; Naphthalenes

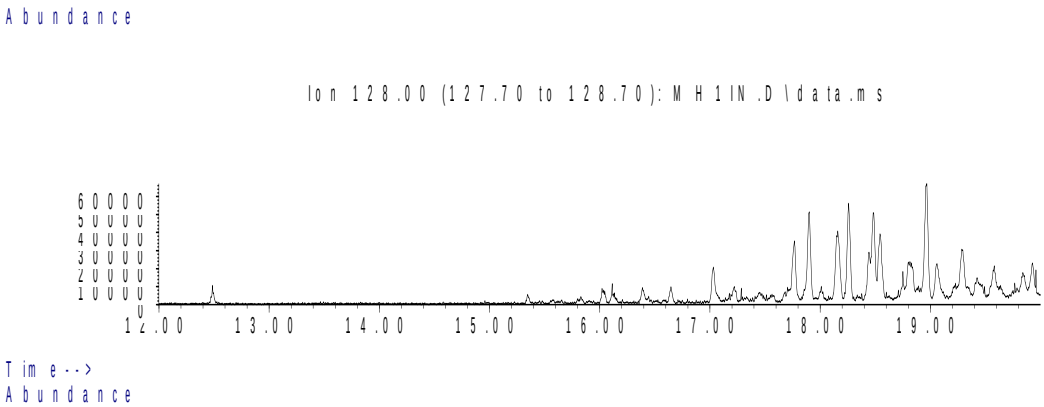

Sample MH1 Inner Aromatic Chromatograms; Phenanthrenes

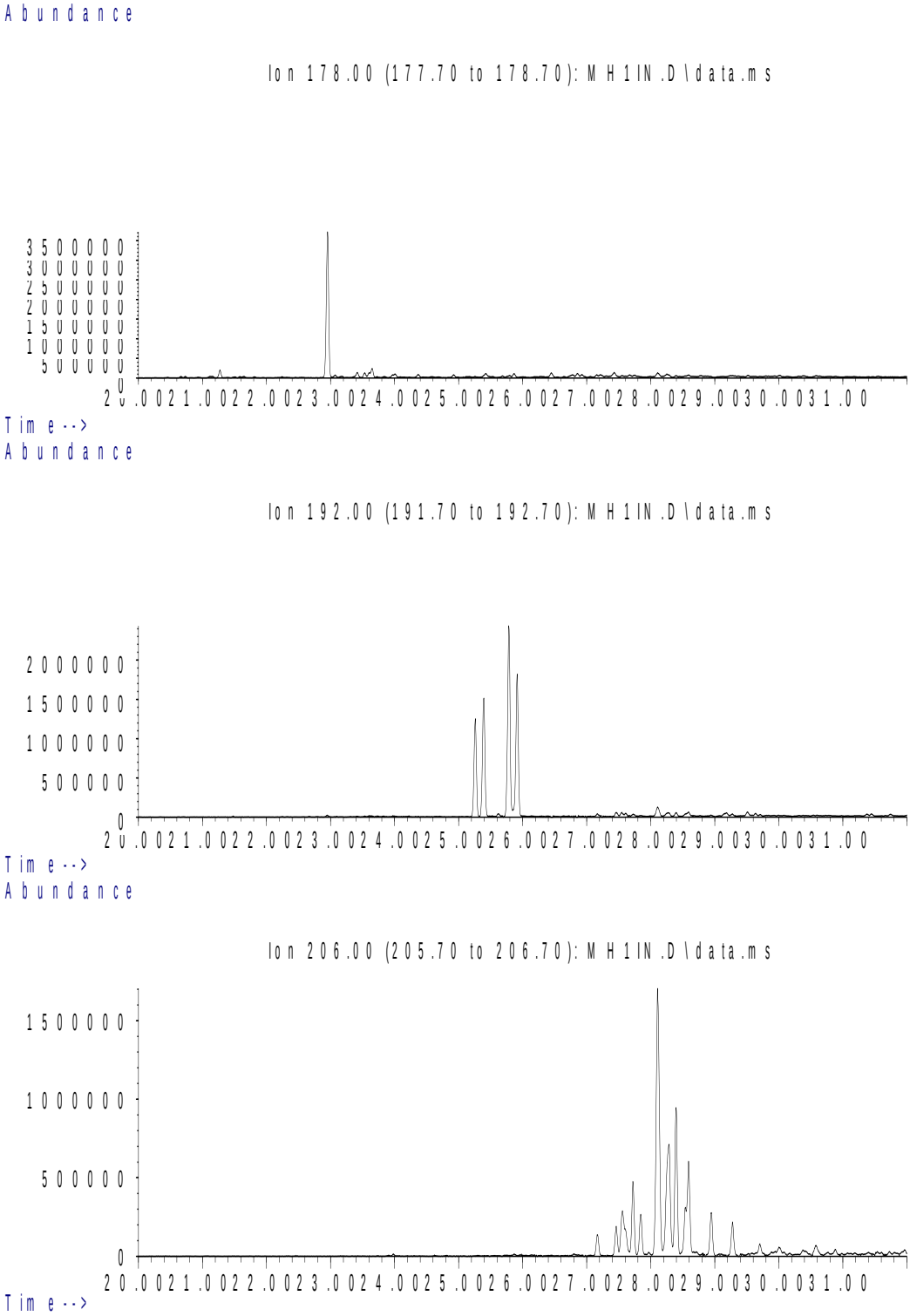

Sample MH1 Inner Aromatic Chromatograms; Thiophenes & PAHs

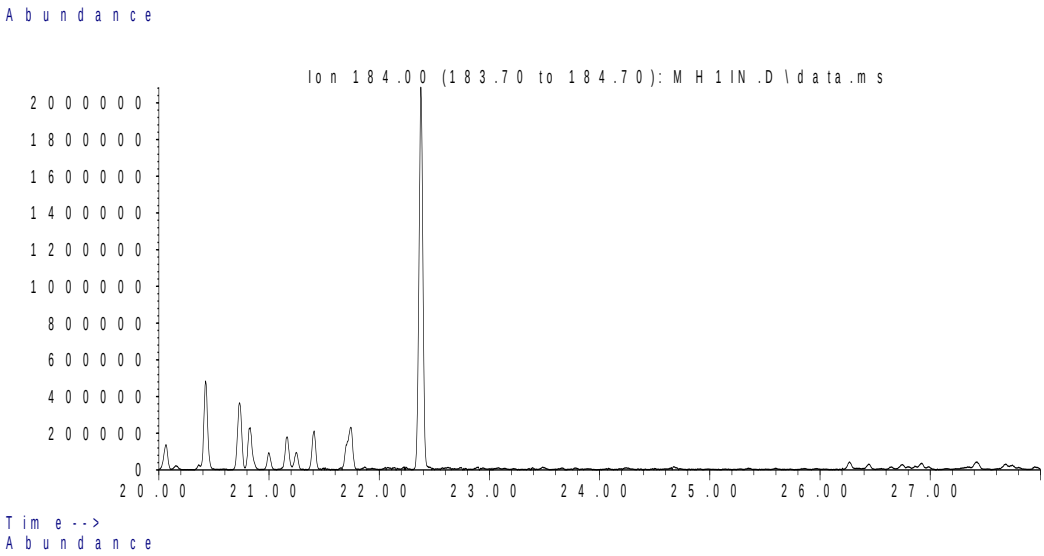

Sample MH1 Outer

Aromatic Biomarker Integration Results				
Ion	Peak Label	Compound Name	R.Time (min.)	Peak Area
178	P	Phenantrene	22.957	10459551
184	DBT	Dibenzothiophene	22.381	8374033
192	C1P iso 1	Methyl Phenanthrene Isomer	25.263	3646831
192	C1P iso 2	Methyl Phenanthrene Isomer	25.392	4577489
192	C1P iso 3	Methyl Phenanthrene Isomer	25.786	7298853
192	C1P iso 4	Methyl Phenanthrene Isomer	25.916	5245330
192	C1P sum	Methyl Phenanthrene Isomers (summed)		20768503
198	4 MDBT	4 Methyldibenzothiophene	24.413	6320618
198	2+3 MDBT	2 & 3 Methyldibenzothiophene	24.833	3984840
198	1 MDBT	1 Methyldibenzothiophene	25.289	4632912
206	C2P iso 1	Ethyl/Dimethyl Phenanthrene Isomer	27.564	1615151
206	C2P iso 2	Ethyl/Dimethyl Phenanthrene Isomer	27.724	1428569
206	C2P iso 3	Ethyl/Dimethyl Phenanthrene Isomer	27.843	893946
206	C2P iso 4	Ethyl/Dimethyl Phenanthrene Isomer	28.118	6624372
206	C2P iso 5	Ethyl/Dimethyl Phenanthrene Isomer	28.284	3475121
206	C2P iso 6	Ethyl/Dimethyl Phenanthrene Isomer	28.398	2737582
206	C2P iso 7	Ethyl/Dimethyl Phenanthrene Isomer	28.548	824988
206	C2P iso 8	Ethyl/Dimethyl Phenanthrene Isomer	28.595	1655260
206	C2P iso 9	Ethyl/Dimethyl Phenanthrene Isomer	28.947	902485
206	C2P iso 10	Ethyl/Dimethyl Phenanthrene Isomer	29.284	710811
206	C2P sum	Ethyl/Dimethyl Phenanthrene Isomers (summed)		20868285
226	C3DBT sum	C3 Dibenzothiophene Isomers (summed)		18016550
252	dbf	benzo(b)fluoranthene	42.711	51857
252	bap	benzo(a)pyrene	44.069	110420

Sample MH1 Outer Aromatic Chromatograms; Naphthalenes

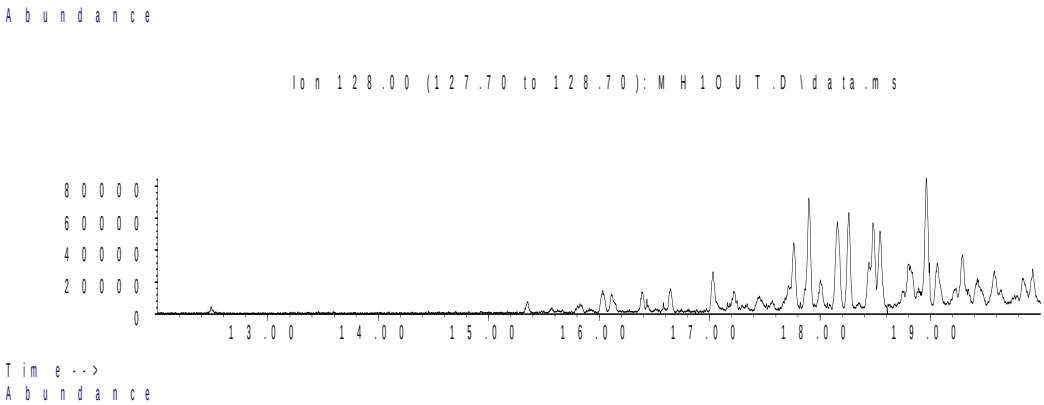

Sample MH1 Outer Aromatic Chromatograms; Phenanthrenes

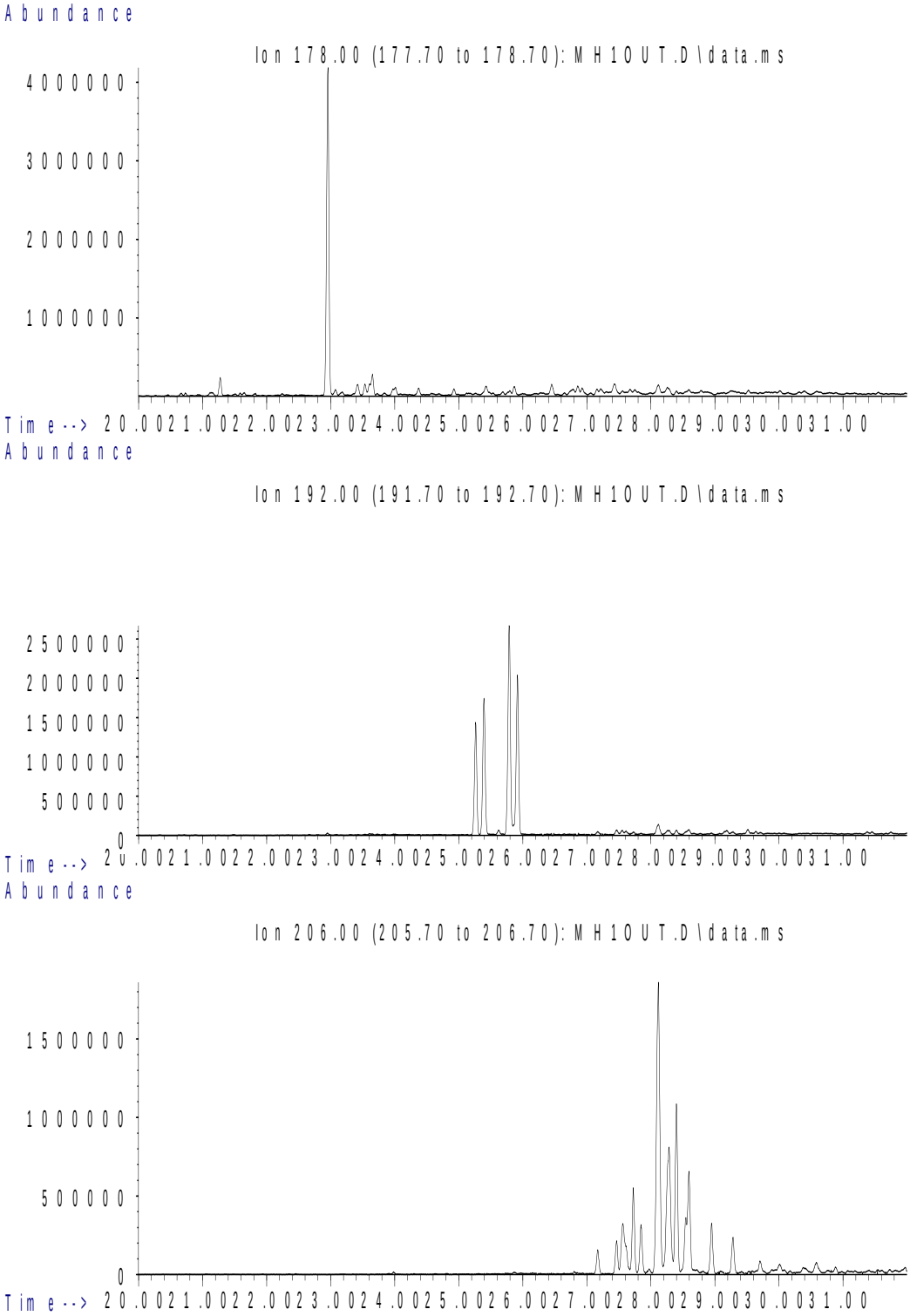

Sample MH1 Outer Aromatic Chromatograms; Thiophenes & PAHs

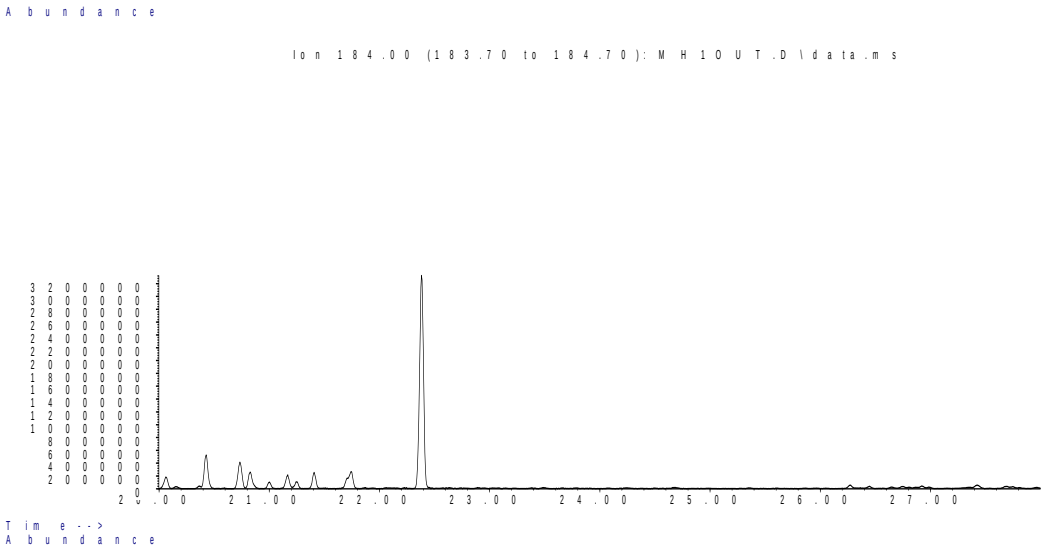

Sample NZ1 Inner

Aromatic Biomarker Integration Results				
Ion	Peak Label	Compound Name	R.Time (min.)	Peak Area
178	P	Phenantrene	22.948	586486
184	DBT	Dibenzothiophene	22.378	519434
192	C1P iso 1	Methyl Phenanthrene Isomer	25.254	582636
192	C1P iso 2	Methyl Phenanthrene Isomer	25.384	852130
192	C1P iso 3	Methyl Phenanthrene Isomer	25.772	1090570
192	C1P iso 4	Methyl Phenanthrene Isomer	25.907	1062169
192	C1P sum	Methyl Phenanthrene Isomers (summed)		3587505
198	4 MDBT	4 Methyldibenzothiophene	24.399	336355
198	2+3 MDBT	2 & 3 Methyldibenzothiophene	24.824	240119
198	1 MDBT	1 Methyldibenzothiophene	24.824	181984
206	C2P iso 1	Ethyl/Dimethyl Phenanthrene Isomer	27.565	475465
206	C2P iso 2	Ethyl/Dimethyl Phenanthrene Isomer	27.721	988341
206	C2P iso 3	Ethyl/Dimethyl Phenanthrene Isomer	27.84	641514
206	C2P iso 4	Ethyl/Dimethyl Phenanthrene Isomer	28.104	4101895
206	C2P iso 5	Ethyl/Dimethyl Phenanthrene Isomer	28.27	2250122
206	C2P iso 6	Ethyl/Dimethyl Phenanthrene Isomer	28.395	2150018
206	C2P iso 7	Ethyl/Dimethyl Phenanthrene Isomer	28.535	830519
206	C2P iso 8	Ethyl/Dimethyl Phenanthrene Isomer	28.586	1291561
206	C2P iso 9	Ethyl/Dimethyl Phenanthrene Isomer	28.939	735480
206	C2P iso 10	Ethyl/Dimethyl Phenanthrene Isomer	29.27	756851
206	C2P sum	Ethyl/Dimethyl Phenanthrene Isomers (summed)		14221766
226	C3DBT sum	C3 Dibenzothiophene Isomers (summed)		2531103
252	dbf	benzo(b)fluoranthene	42.708	68699
252	bap	benzo(a)pyrene	44.065	138771

Sample NZ1 Inner Aromatic Chromatograms; Naphthalenes

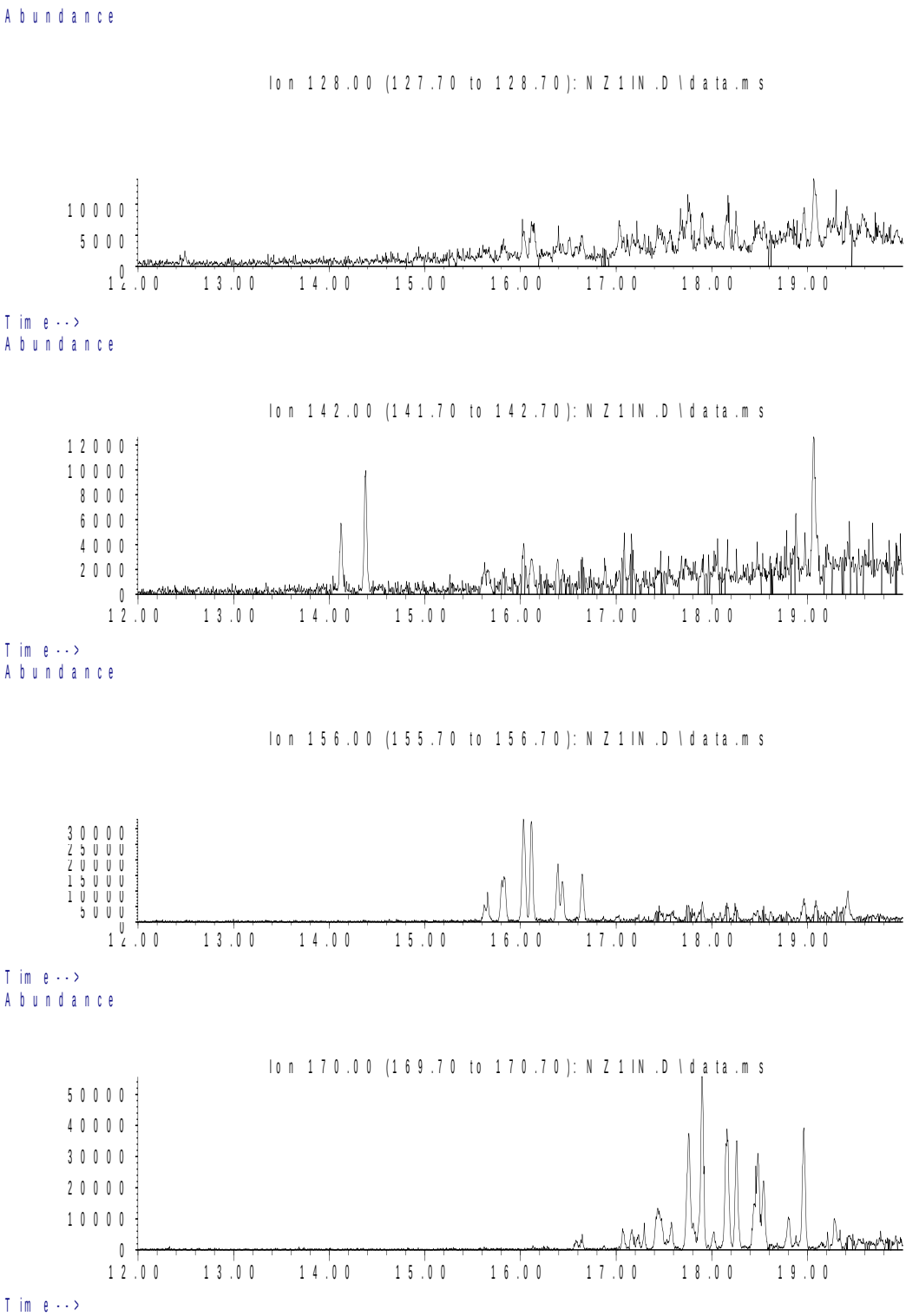

Sample NZ1 Inner Aromatic Chromatograms; Phenanthrenes

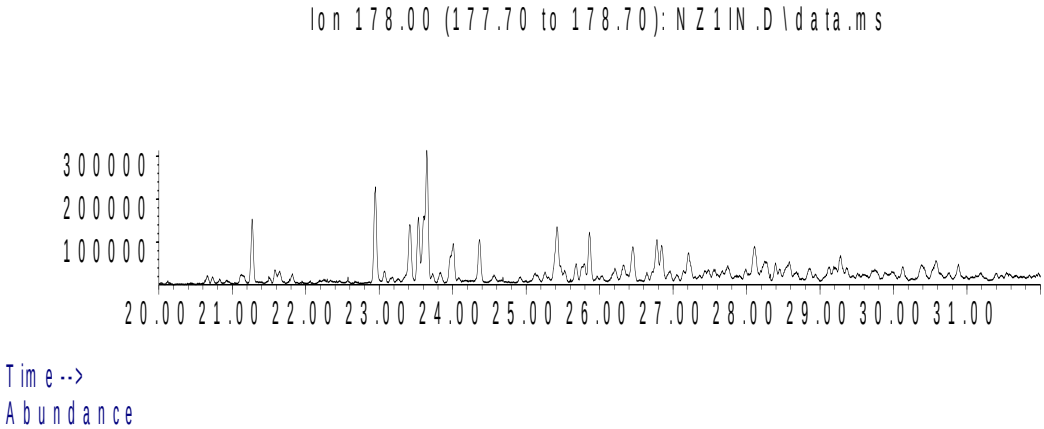

Sample NZ1 Inner Aromatic Chromatograms; Thiophenes & PAHs

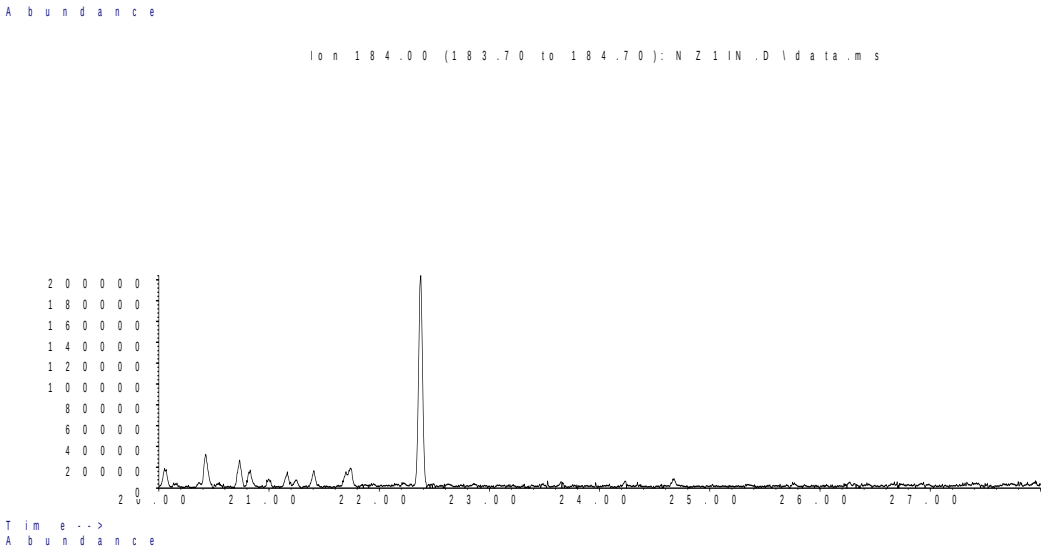

Sample NZ1 Outer

Aromatic Biomarker Integration Results				
Ion	Peak Label	Compound Name	R.Time (min.)	Peak Area
178	P	Phenantrene	22.952	6253407
184	DBT	Dibenzothiophene	22.377	4067012
192	C1P iso 1	Methyl Phenanthrene Isomer	25.253	2405827
192	C1P iso 2	Methyl Phenanthrene Isomer	25.388	3124942
192	C1P iso 3	Methyl Phenanthrene Isomer	25.782	4979737
192	C1P iso 4	Methyl Phenanthrene Isomer	25.911	3595511
192	C1P sum	Methyl Phenanthrene Isomers (summed)		14106017
198	4 MDBT	4 Methyldibenzothiophene	24.408	3979090
198	2+3 MDBT	2 & 3 Methyldibenzothiophene	24.828	2488270
198	1 MDBT	1 Methyldibenzothiophene	25.279	2827942
206	C2P iso 1	Ethyl/Dimethyl Phenanthrene Isomer	27.559	1095863
206	C2P iso 2	Ethyl/Dimethyl Phenanthrene Isomer	27.72	959396
206	C2P iso 3	Ethyl/Dimethyl Phenanthrene Isomer	27.839	575130
206	C2P iso 4	Ethyl/Dimethyl Phenanthrene Isomer	28.108	4677590
206	C2P iso 5	Ethyl/Dimethyl Phenanthrene Isomer	28.279	2398852
206	C2P iso 6	Ethyl/Dimethyl Phenanthrene Isomer	28.393	1939428
206	C2P iso 7	Ethyl/Dimethyl Phenanthrene Isomer	28.533	528176
206	C2P iso 8	Ethyl/Dimethyl Phenanthrene Isomer	28.585	1144552
206	C2P iso 9	Ethyl/Dimethyl Phenanthrene Isomer	28.943	650165
206	C2P iso 10	Ethyl/Dimethyl Phenanthrene Isomer	29.269	475237
206	C2P sum	Ethyl/Dimethyl Phenanthrene Isomers (summed)		14444389
226	C3DBT sum	C3 Dibenzothiophene Isomers (summed)		12476075
252	dbf	benzo(b)fluoranthene	42.706	39887
252	bap	benzo(a)pyrene	44.069	72018

Sample NZ1 Outer Aromatic Chromatograms; Naphthalenes

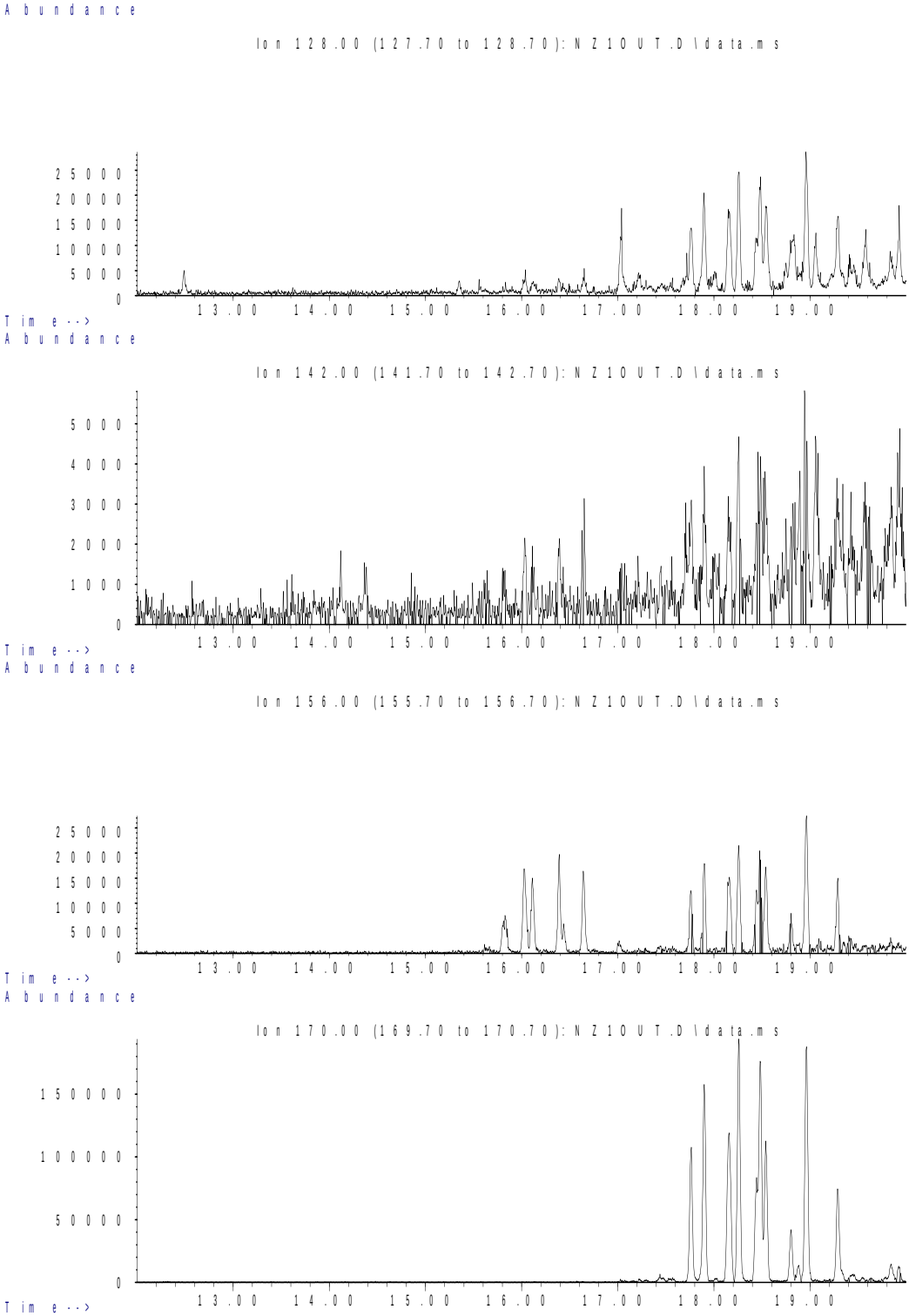

Sample NZ1 Outer Aromatic Chromatograms; Phenanthrenes

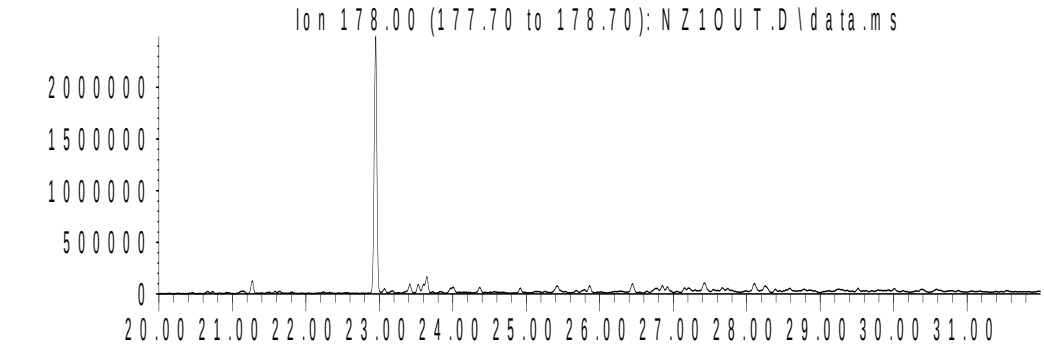

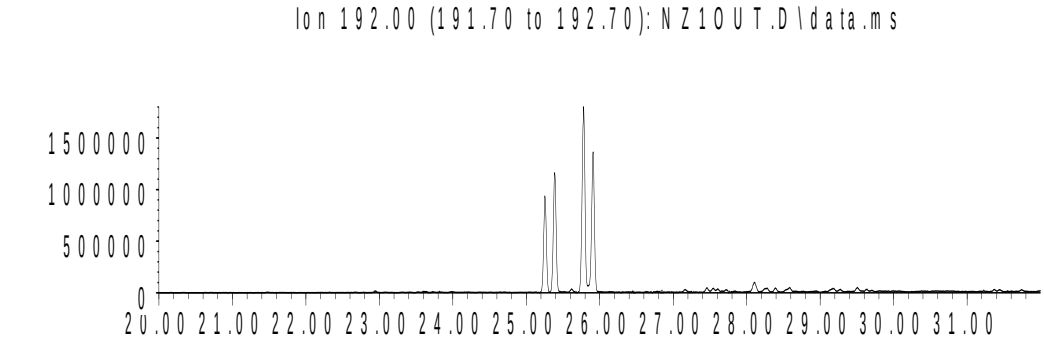

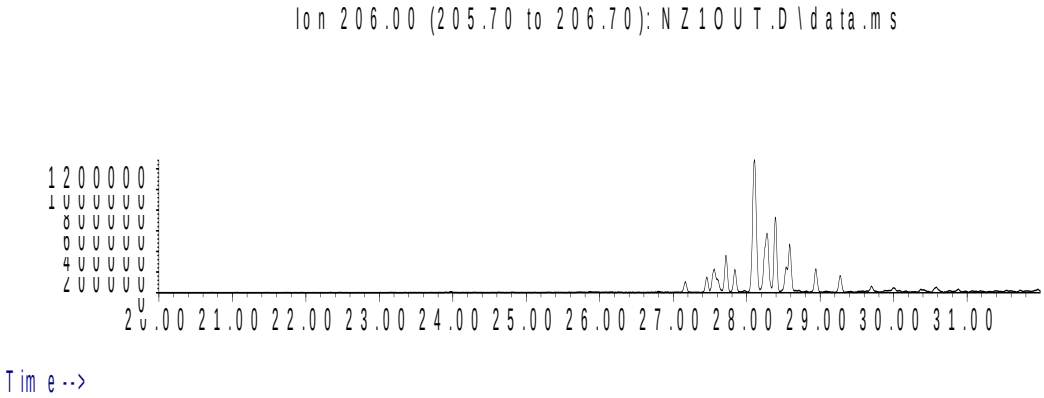

Sample NZ1 Outer Aromatic Chromatograms; Thiophenes & PAHs

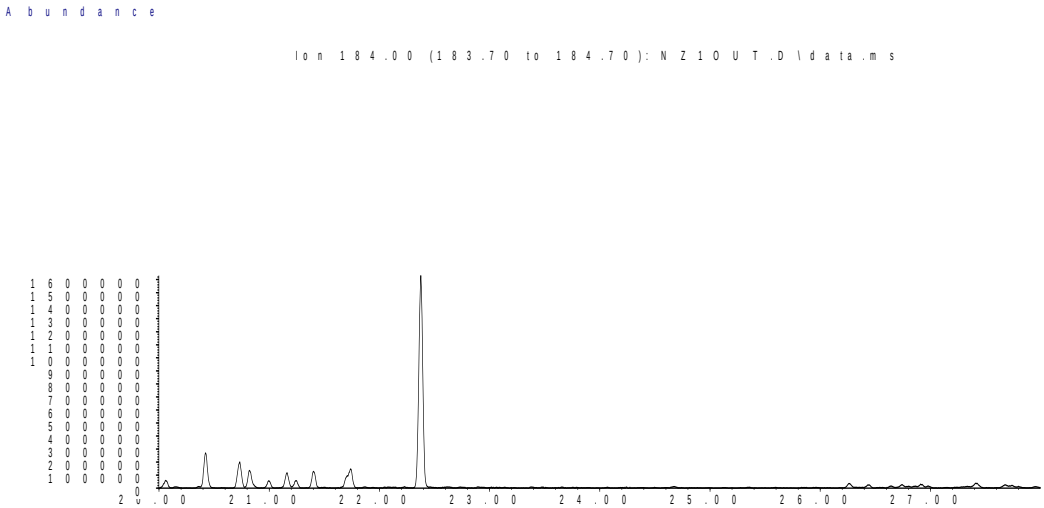

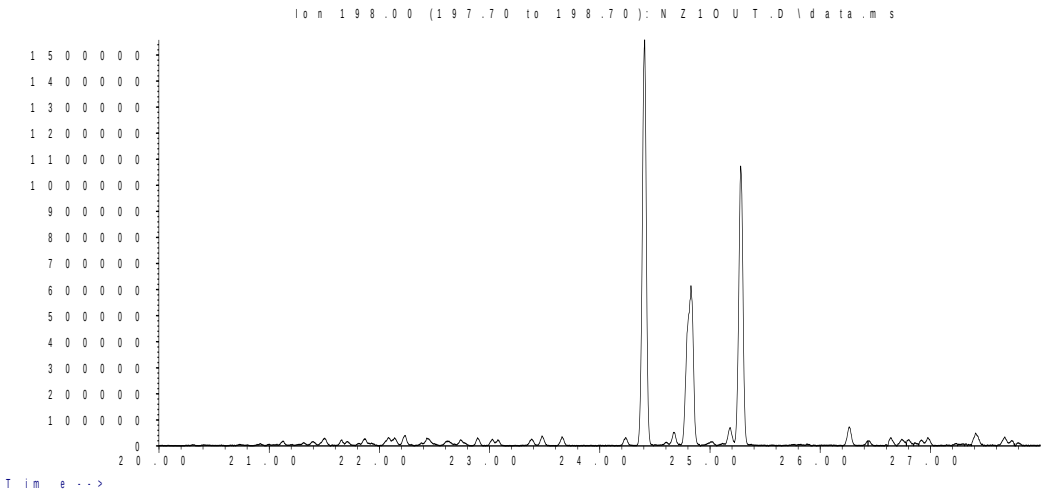

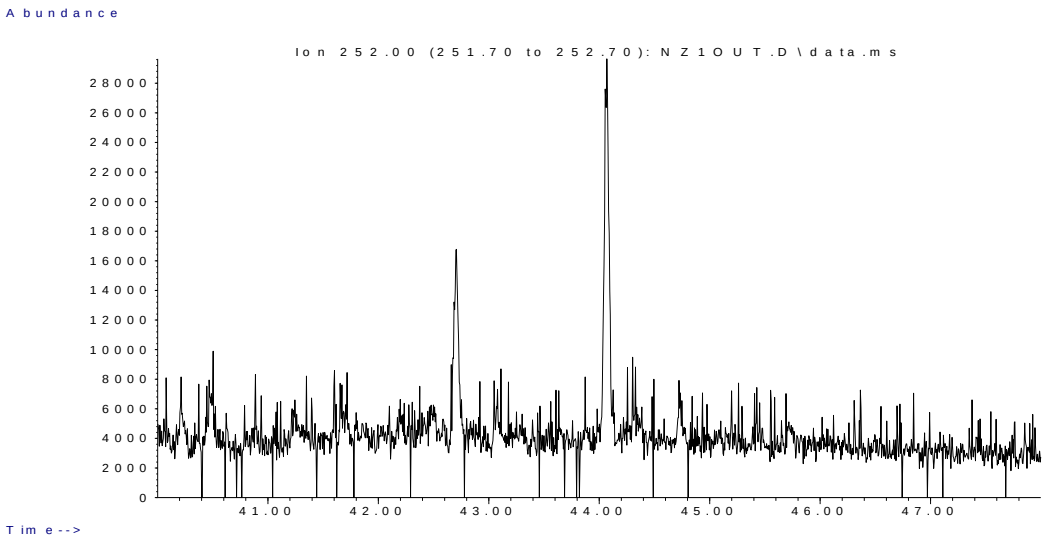

Sample NZ2 Inner

Aromatic Biomarker Integration Results				
Ion	Peak Label	Compound Name	R.Time (min.)	Peak Area
178	P	Phenantrene	22.951	7146690
184	DBT	Dibenzothiophene	22.381	6305592
192	C1P iso 1	Methyl Phenanthrene Isomer	25.257	2541618
192	C1P iso 2	Methyl Phenanthrene Isomer	25.387	3222242
192	C1P iso 3	Methyl Phenanthrene Isomer	25.786	5224280
192	C1P iso 4	Methyl Phenanthrene Isomer	25.91	3714411
192	C1P sum	Methyl Phenanthrene Isomers (summed)		14702551
198	4 MDBT	4 Methyldibenzothiophene	24.407	5063971
198	2+3 MDBT	2 & 3 Methyldibenzothiophene	24.832	3077556
198	1 MDBT	1 Methyldibenzothiophene	25.283	3635125
206	C2P iso 1	Ethyl/Dimethyl Phenanthrene Isomer	27.558	1172097
206	C2P iso 2	Ethyl/Dimethyl Phenanthrene Isomer	27.719	1005285
206	C2P iso 3	Ethyl/Dimethyl Phenanthrene Isomer	27.843	617598
206	C2P iso 4	Ethyl/Dimethyl Phenanthrene Isomer	28.107	4719112
206	C2P iso 5	Ethyl/Dimethyl Phenanthrene Isomer	28.278	2477911
206	C2P iso 6	Ethyl/Dimethyl Phenanthrene Isomer	28.392	1979740
206	C2P iso 7	Ethyl/Dimethyl Phenanthrene Isomer	28.537	574707
206	C2P iso 8	Ethyl/Dimethyl Phenanthrene Isomer	28.589	1202329
206	C2P iso 9	Ethyl/Dimethyl Phenanthrene Isomer	28.941	641756
206	C2P iso 10	Ethyl/Dimethyl Phenanthrene Isomer	29.273	494293
206	C2P sum	Ethyl/Dimethyl Phenanthrene Isomers (summed)		14884828
226	C3DBT sum	C3 Dibenzothiophene Isomers (summed)		13419419
252	dbf	benzo(b)fluoranthene	42.700	34415
252	bap	benzo(a)pyrene	44.068	68266

Sample NZ2 Inner Aromatic Chromatograms; Naphthalenes

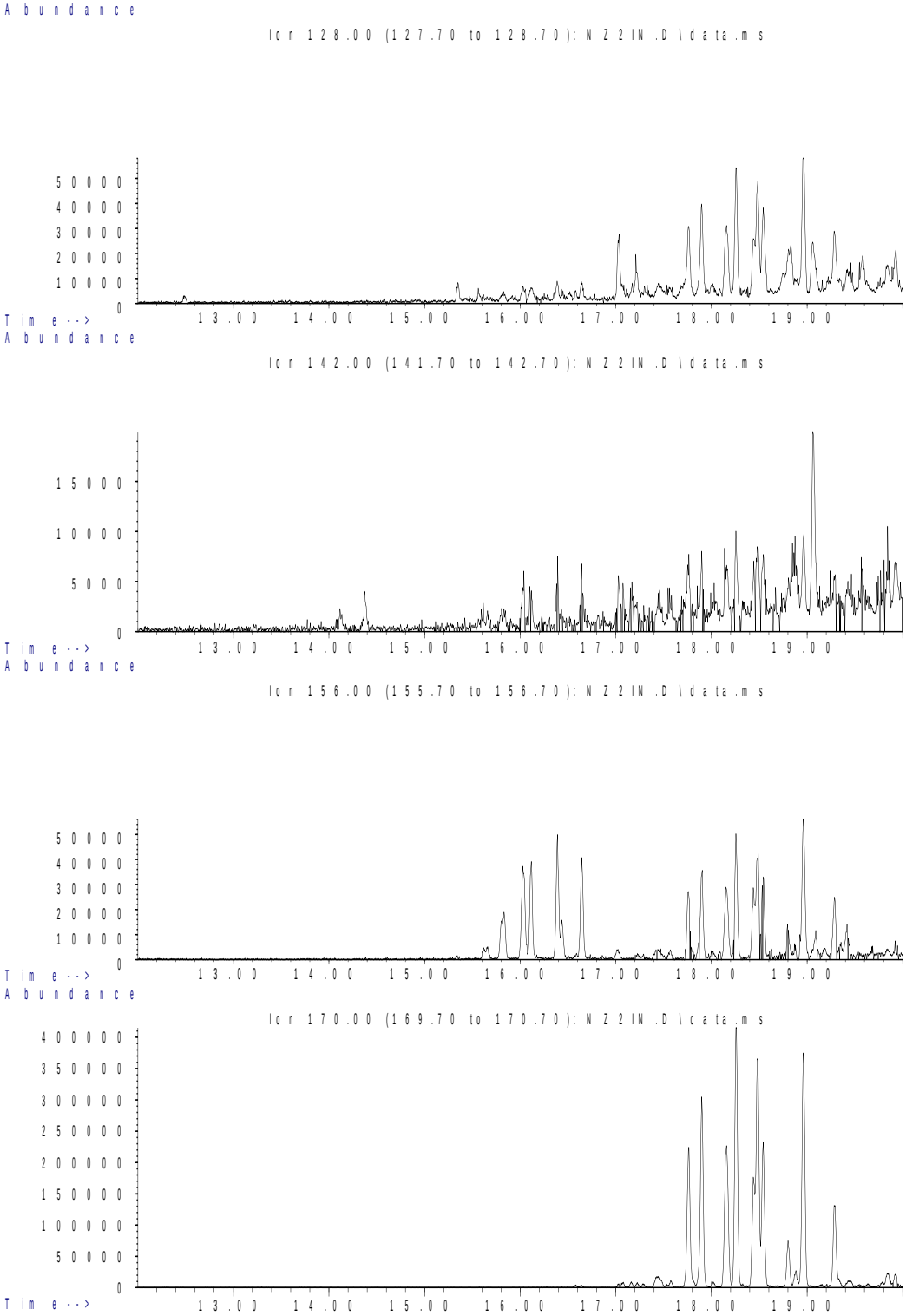

Sample NZ2 Inner Aromatic Chromatograms; Phenanthrenes

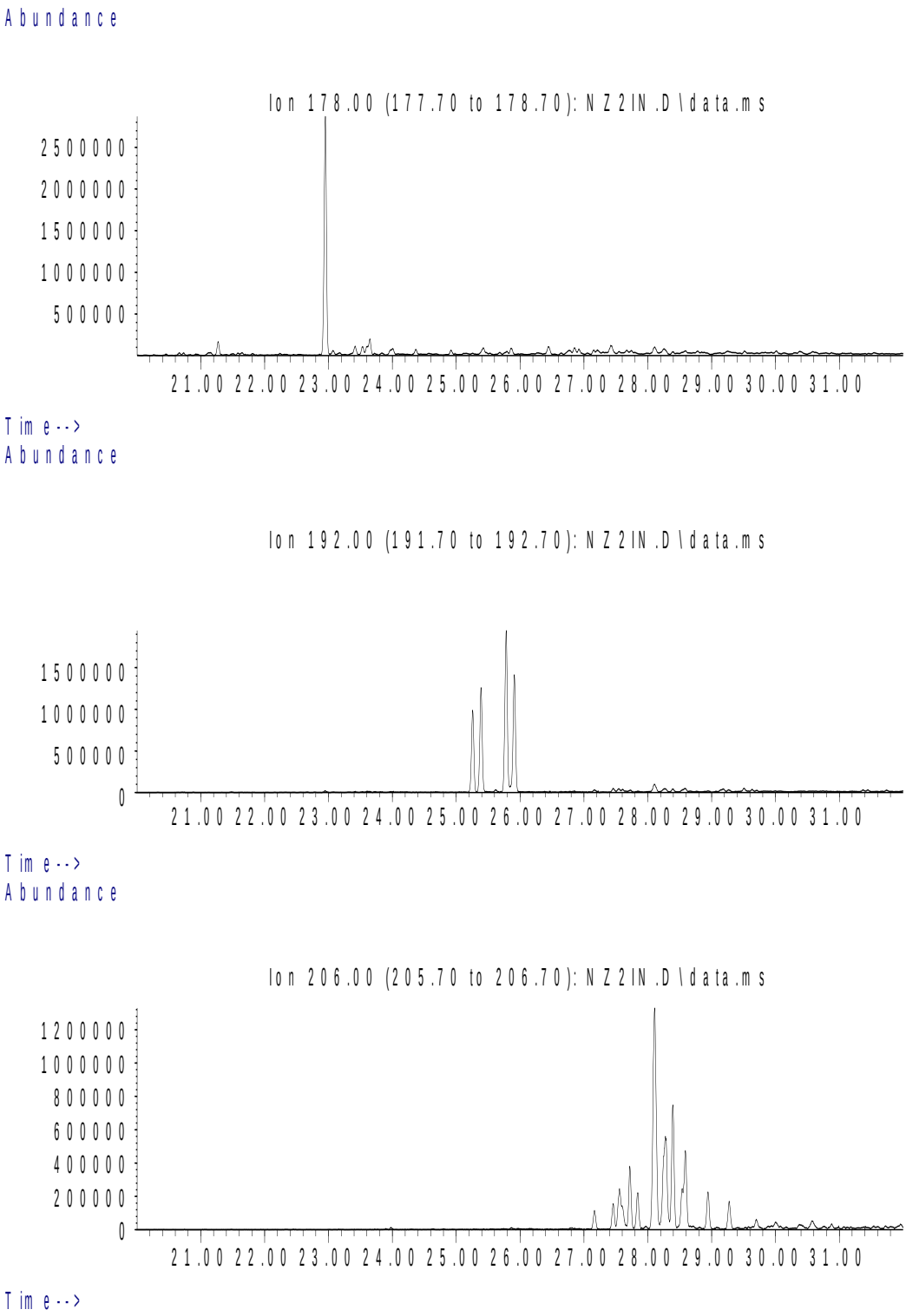

Sample NZ2 Inner Aromatic Chromatograms; Thiophenes & PAHs

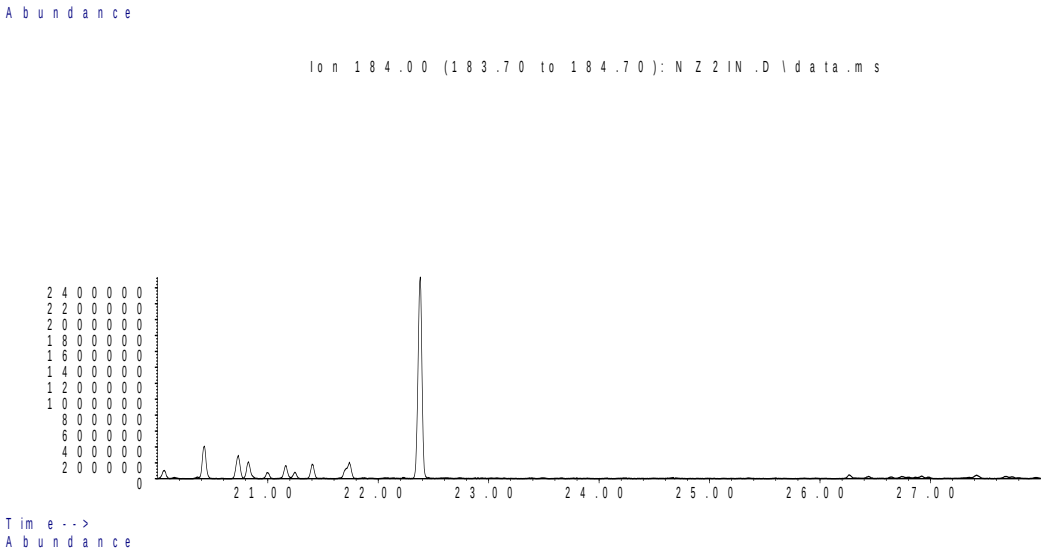

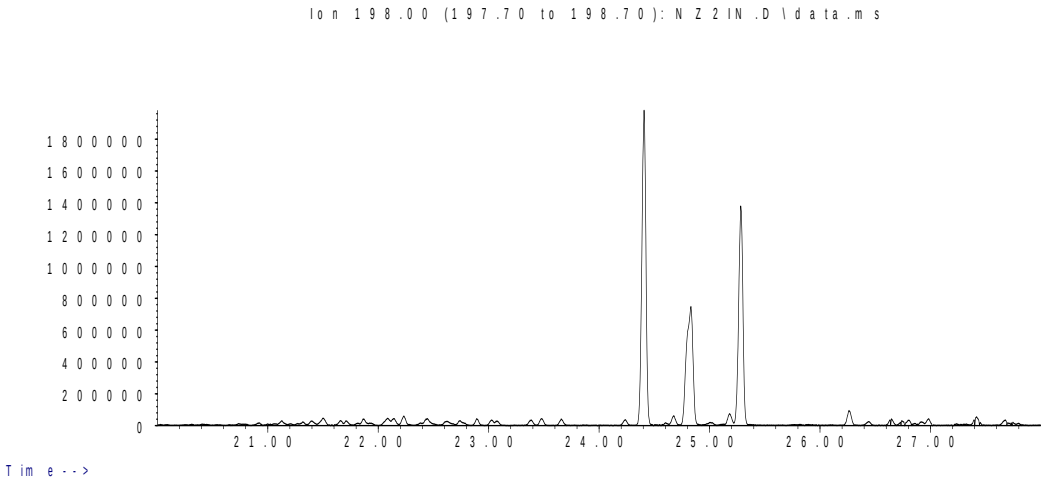

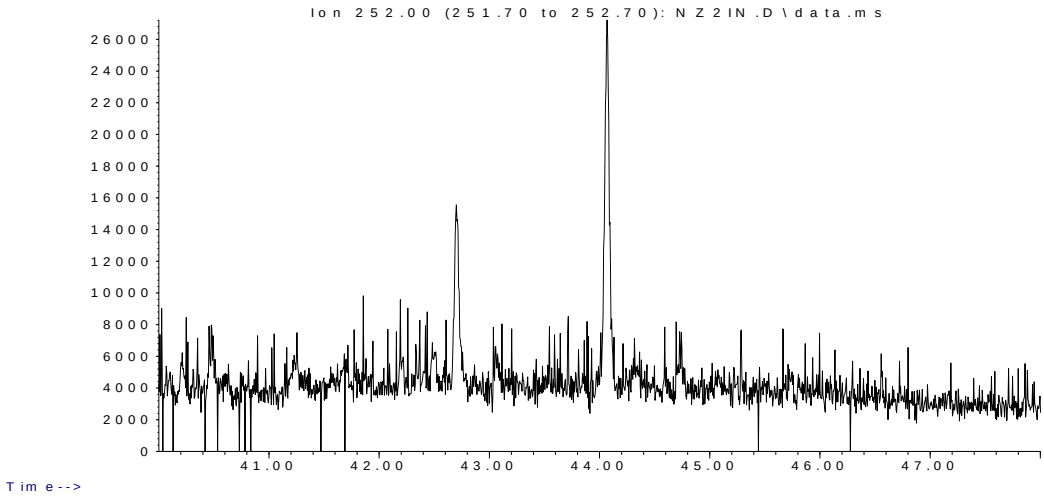

Sample NZ2 Outer

Aromatic Biomarker Integration Results				
Ion	Peak Label	Compound Name	R.Time (min.)	Peak Area
178	P	Phenantrene	22.946	4420098
184	DBT	Dibenzothiophene	22.376	2562652
192	C1P iso 1	Methyl Phenanthrene Isomer	25.258	1745461
192	C1P iso 2	Methyl Phenanthrene Isomer	25.387	2240813
192	C1P iso 3	Methyl Phenanthrene Isomer	25.776	3547725
192	C1P iso 4	Methyl Phenanthrene Isomer	25.905	2549178
192	C1P sum	Methyl Phenanthrene Isomers (summed)		10083177
198	4 MDBT	4 Methyldibenzothiophene	24.402	2942313
198	2+3 MDBT	2 & 3 Methyldibenzothiophene	24.827	1747650
198	1 MDBT	1 Methyldibenzothiophene	25.283	1949174
206	C2P iso 1	Ethyl/Dimethyl Phenanthrene Isomer	27.558	807980
206	C2P iso 2	Ethyl/Dimethyl Phenanthrene Isomer	27.719	719782
206	C2P iso 3	Ethyl/Dimethyl Phenanthrene Isomer	27.838	448061
206	C2P iso 4	Ethyl/Dimethyl Phenanthrene Isomer	28.103	3306783
206	C2P iso 5	Ethyl/Dimethyl Phenanthrene Isomer	28.268	1721348
206	C2P iso 6	Ethyl/Dimethyl Phenanthrene Isomer	28.388	1375516
206	C2P iso 7	Ethyl/Dimethyl Phenanthrene Isomer	28.538	414725
206	C2P iso 8	Ethyl/Dimethyl Phenanthrene Isomer	28.584	882121
206	C2P iso 9	Ethyl/Dimethyl Phenanthrene Isomer	28.942	459760
206	C2P iso 10	Ethyl/Dimethyl Phenanthrene Isomer	29.274	340589
206	C2P sum	Ethyl/Dimethyl Phenanthrene Isomers (summed)		10476665
226	C3DBT sum	C3 Dibenzothiophene Isomers (summed)		8965081
252	dbf	benzo(b)fluoranthene	42.716	28891
252	bap	benzo(a)pyrene	44.058	49254

Sample NZ2 Inner Aromatic Chromatograms; Naphthalenes

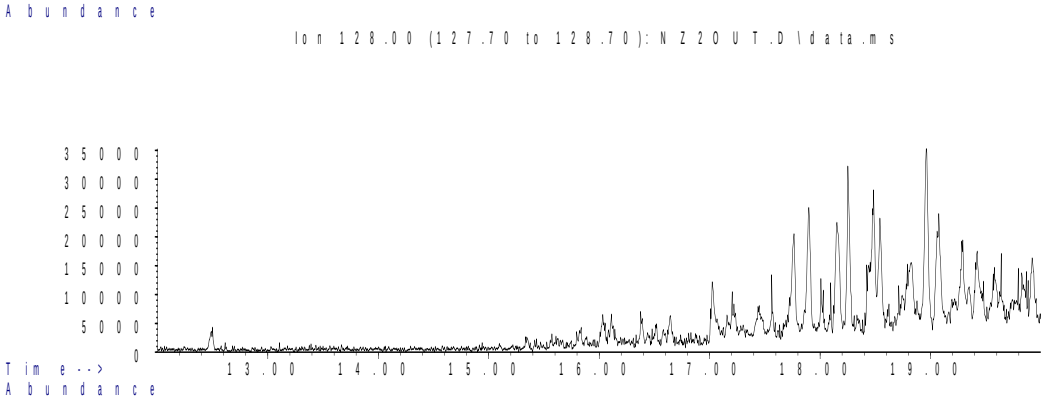

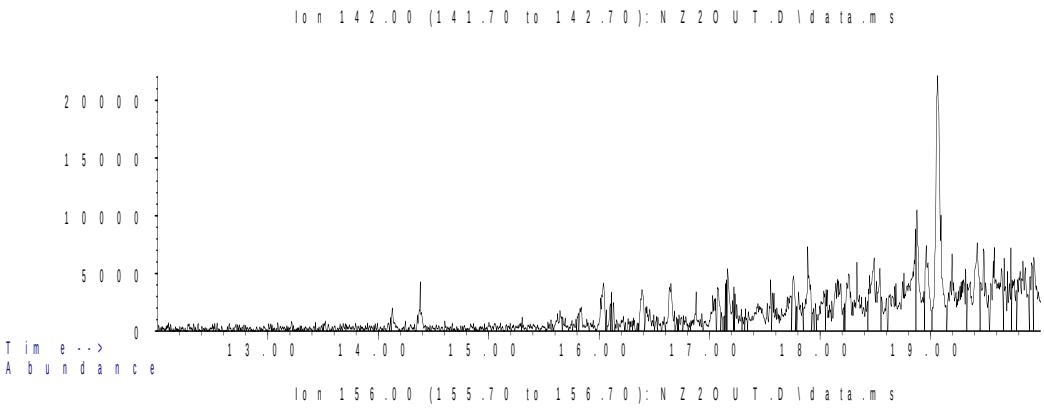

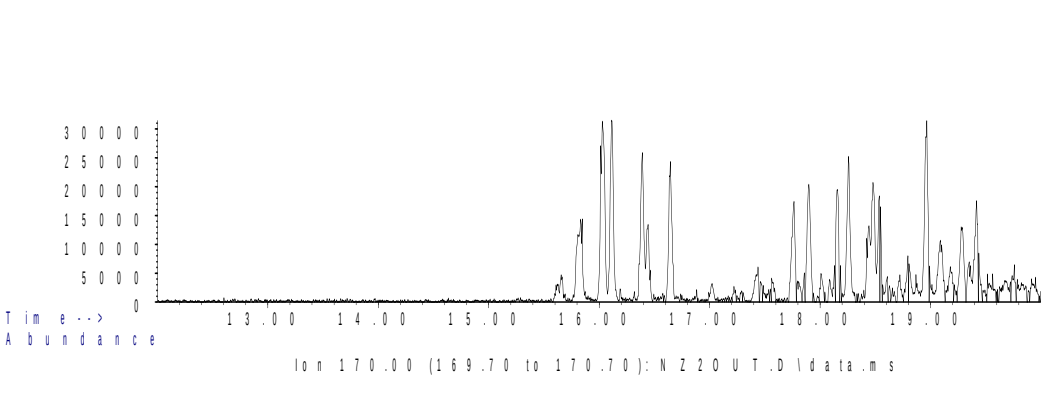

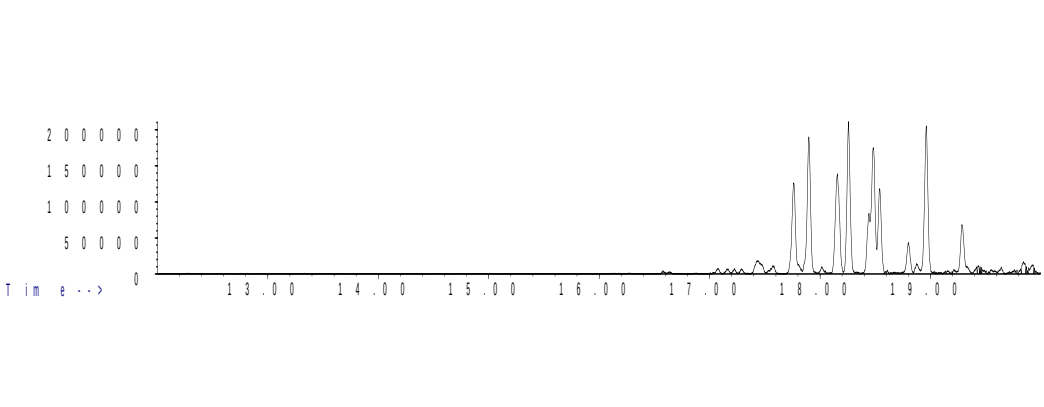

Sample NZ2 Outer Aromatic Chromatograms; Phenanthrenes

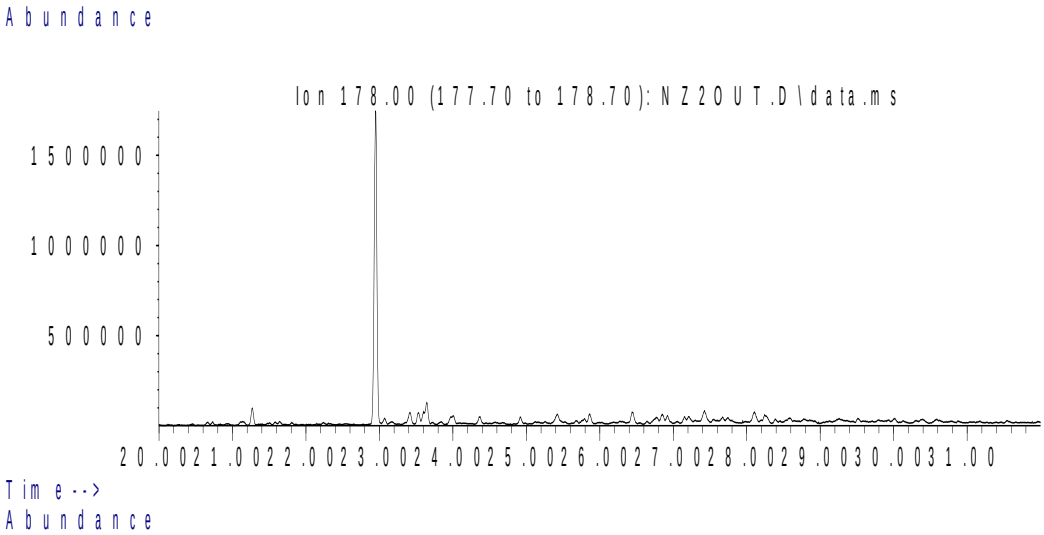

Sample NZ2 Outer Aromatic Chromatograms; Thiophenes & PAHs

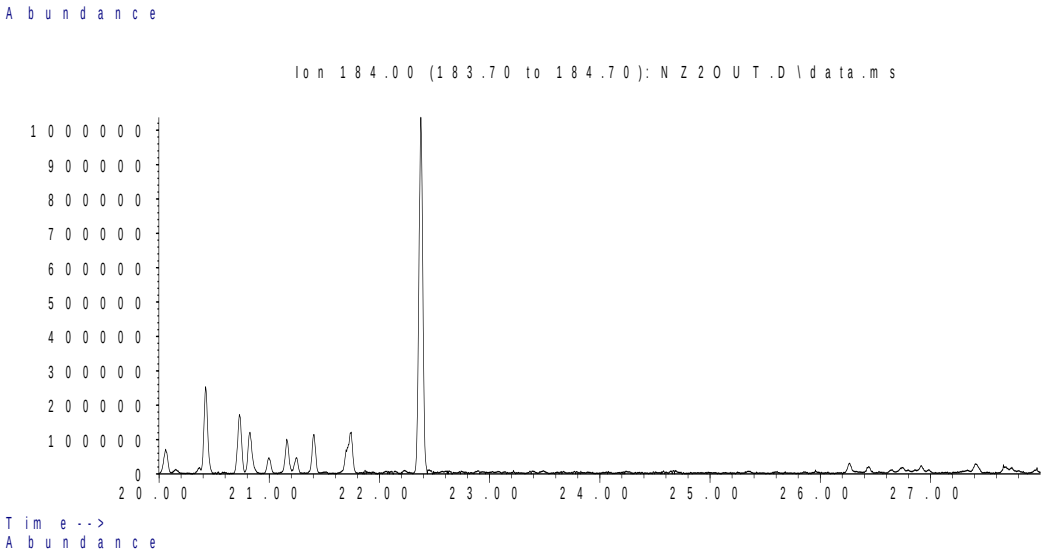

MANCO Scale Interpretation

Larter et al 2012, A practical biodegradation scale for use in reservoir geochemical studies of biodegraded oils.
Organic Geochemistry 45 (2012) 66–76

Light Manco

Category	0	1	2		
Vector	3	1	0		
MN1	3	5	0	L MN1 =	8

	categories	scale - 1	MN1	$\log_5$(MN1)		
MN2	3	999	8	1.29	L MN2 =	431

Heavy Manco

Category	0	1	2	3	4	5	6	7		
Vector	4	3	3	1	0	0	0	0		
MN1	4	15	75	125	0	0	0	0	MN1 =	219

	categories	scale - 1	MN1	$\log_5$(MN1)		
MN2	8	999	219	3.35	MN2 =	419

Ultimate Manco

Category	0	1	2	3	4	5	6	7	8	9	10		
Vector	3	1	0	4	3	3	1	0	0	0	0		
MN1	3	5	0	500	1875	9375	15625	0	0	0	0	MN1 =	27383

	categories	scale - 1	MN1	$\log_5$(MN1)		
MN2	11	999	27383	6.35	MN2 =	578

Australian Earth Sciences Convention; Canberra, 4-8th July, 2010

Abstract & Oral Presentation

Hall, P.A., McKirdy, D.M., Halverson, G.P., Turner, B.L., Carson, M.W., Nedin, C., Jago, J.B., Gehling, J.G. & Collins, A.S. (2010). `The biogeochemical status of the Palaeo-Pacific Ocean: clues from the early Cambrian of South Australia' in *Australian Earth Sciences Convention (AESC) 2010, Earth systems: change, sustainability, vulnerability. The 20th Australian Geological Convention, Geological Society of Australia*, Canberra, Australian Capital Territory. July 4-8 July, pp. 165-166.

NOTE:
This publication is included on pages 269-270 in the print copy of the thesis held in the University of Adelaide Library.

16th Australian Organic Geochemistry Conference; Canberra, 7-10th December, 2010

Abstract & Oral Presentation

Australian Organic Geochemistry Conference 2010, Canberra – Program and Abstracts

Australasian asphaltite strandings revisited: the effects of weathering and biodegradation on biomarker profiles

Tony Hall and David McKirdy

Organic Geochemistry in Basin Analysis Group, Centre for Tectonics, Resources and Exploration (TRaX), School of Earth and Environmental Sciences, University of Adelaide, SA 5005 (email: philip.a.hall@adelaide.edu.au)

Asphaltic bitumens, long known to strand along the coastline of southern Australia and as far afield as New Zealand and Macquarie Island (Padley, 1995), are now widely regarded as artefacts of submarine oil seepage. Their biomarker and isotopic compositions are remarkably uniform (Currie *et al*., 1992; Volkman *et al*., 1992; McKirdy *et al*., 1994; Edwards *et al*., 1998) suggesting that they represent a single oil family expelled from a marine shale containing S-rich Type II kerogen, probably deposited during a Cretaceous oceanic anoxic event (Boreham *et al*., 2001). While no such anoxic/sulphidic lithofacies of appropriate thermal maturity has yet been intersected by drilling, suitable hydrocarbon kitchens may exist in the offshore Otway Basin (Boult *et al*., 2005) and Bight Basin (Boreham, 2008). With low API gravities (4-18°) many of the stranded asphaltites are heavier than seawater, implying that for much of their time in the ocean they were bottom drifters. Their degree of weathering (including biodegradation) will reflect, at least in part, the duration of their exposure to the marine environment. For any individual asphaltite specimen, this in turn will depend on the proximity of the seafloor seep to the stranding site, an important consideration when attempting to locate the oil kitchen in which it was generated.

In this study we determined the alkane biomarker profiles of asphaltite specimens from four localities: Eyre Peninsula (n = 2), Kangaroo Island (n = 4), and the Limestone Coast (n = 3) in South Australia and Invercargill, New Zealand (n = 2). Saturates fractions prepared from sub-samples of the interior and the outer, weathered surface of each specimen were analysed by GC-MS operating in full scan and SIM modes. Some 43 biomarker ratios were calculated. The interior portions exhibit similar distributions of isoprenoid alkanes, terpanes and steranes (standard deviation for individual ratios commonly <10%). No distinction could be made between the Australian and New Zealand strandings implying a common source, despite their widely separated localities.

All the asphaltites lack 25-norhopanes and may be characterised as only moderately biodegraded. Comparison of the interior and weathered surface of each specimen likewise revealed only minor differences. Depletion of n-alkanes was apparent only in the $<C_{14}$ range; and all specimens displayed a minor decrease (~5%) in the contribution of hopanoids to the relative abundances of tricyclic terpanes, pentacyclic triterpanes and steranes. There is a preferential degradation of C_{35} over C_{31}-C_{34} hopanes, with the homohopane index decreasing (as expected: Peters *et al*., 2005) by an average of 28%.

The general trend evident in the sterane distributions is for depletion of 20R relative to 20S ααα isomers (avg. 7%), again as expected (McKirdy *et al*., 1983). Moreover, the C_{27} ααα 20R sterane increases relative to the C_{28} and C_{29} homologues, with C_{28} showing the greatest depletion (avg. 5%). Collectively, these results suggest that the stranded asphaltites have had a relatively short exposure to the processes of aerobic biodegradation, possibly in the order of 10 years by comparison with the outcomes of laboratory culture experiments undertaken by Goodwin *et al*. (1983). Finally, given their degree of degradation, these Australasian asphaltites seem likely to be products of low intensity seeps (Wenger and Isaksen, 2002), with those from the Limestone Coast and Kangaroo Island being less weathered than those from Eyre Peninsula and New Zealand.

REFERENCES

Boreham, C.J., 2008. Bight Basin marine potential source rocks: a local expression of the Late Cretaceous oceanic anoxic event (OAE2)? In *Oil, Soil, Water and Wine* (ed. D.M. McKirdy). 15th Australian Organic Geochemistry Conference, Program and Abstracts, pp. 104–105.

Boreham, C.J., Krassay, A.A. and Totterdell, J.M., 2001. Geochemical comparisons between asphaltites on the southern Australian margin and Cretaceous source rock analogues. In *Eastern Australasian Basins Symposium: A refocused energy perspective for the future* (eds. K.C. Hill and T. Bernecker). Petroleum Exploration Society of Australia, Special Publication, pp. 531–541.

Boult, P., McKirdy, D., Blevin, J., Heggeland, R., Lang, S. and Vinall, D., 2005. The oil-prone Morum Sub-basin petroleum system, Otway Basin, South Australia. *MESA J.* **38**, 28–33.

Currie, T.J., Alexander, R. and Kagi, R.I., 1992. Coastal bitumens from Western Australia – long distance transport from Western Australia, *Org. Geochem.* **18**, 595–601.

Edwards, D., McKirdy, D.M. and Summons, R.E., 1998. Enigmatic asphaltites from the southern Australian margin: molecular and carbon isotopic composition. *PESA J.* **26**, 106–130.

Goodwin, N.S., Park, P.J.D and Rawlinson, A.P., 1983. Crude oil biodegradation under simulated and natural conditions. In *Advances in Organic Geochemistry 1981* (eds. M. Bjoroy *et al*.). Wiley, Chichester, pp. 650–658.

McKirdy, D.M., Aldridge, A.K. and Ypma, P.J.M., 1983. A geochemical comparison of some crude oils from pre-Ordovician carbonate rocks. In *Advances in Organic Geochemistry 1981* (eds. M. Bjoroy *et al*.), Wiley, Chichester, pp. 99–107.

McKirdy, D.M., Summons, R.E., Padley, D., Serafini, K.M., Boreham, C.J. and Struckmeyer, H.I.M., 1994. Molecular fossils in coastal bitumens from southern Australia: signatures of precursor biota and source rock environments. *Org. Geochem*. **21**, 265–286.

Padley, D., 1995. Petroleum geochemistry of the Otway Basin and the significance of coastal bitumen strandings on adjacent southern Australian beaches. PhD Thesis, University of Adelaide.

Peters, K.E., Walters, C.C. and Moldowan, J.M., 2005. *The Biomarker Guide, Volume 2, Biomarkers and Isotopes in Petroleum Systems and Earth History.* Cambridge University Press.

Volkman, J.K., O'Leary, T., Summons, R.E. and Bendall, M.R., 1992. Biomarker composition of some asphaltic coastal bitumens from Tasmania, Australia, *Org. Geochem.* **18**, 669–682.

Wenger, L.M. and Isaksen, G.H., 2002. Control of hydrocarbon seepage intensity on level of biodegradation in sea bottom sediments. *Org. Geochem*. **33**, 1277–1292.

16th Australian Organic Geochemistry Conference; Canberra, 7-10th December, 2010

Abstract & Oral Presentation

Australian Organic Geochemistry Conference 2010, Canberra – Program and Abstracts

Biomarker, isotopic and trace element signatures of an early Cambrian Lagerstätte in the Stansbury Basin, South Australia

David McKirdy[1], Tony Hall[1], Galen Halverson[1,4], Chris Nedin[2] and Bernd Michaelsen[3]

[1] *Organic Geochemistry in Basin Analysis Group, Centre for Tectonics, Resources & Exploration (TRaX), School of Earth & Environmental Sciences, University of Adelaide, SA 5005 (email: david.mckirdy@adelaide.edu.au)*
[2] *Department of Innovation, Industry, Science & Research, Canberra, ACT 2601*
[3] *Geological Survey of South Australia, Primary Industries & Resources SA, Adelaide, SA 5000*
[4] *Present address: Department of Earth & Planetary Sciences, McGill University, Montreal, Canada H3A 2A7*

While fossil assemblages of soft-bodied organisms (Lagerstätten) are rare, they are unusually common in marine sedimentary sequences of early and mid-Cambrian age (Allison and Briggs, 1993). Not surprisingly, their mode of preservation has been the subject of much debate. The Emu Bay Shale biota, found at Big Gully on the north coast of Kangaroo Island, is by far the best Burgess Shale-type (BST) fauna in the southern hemisphere (Nedin, 1995). Such fauna are characteristically preserved as two-dimensional compression fossils, comprising carbonaceous films on bedding surfaces of the host marine mudstones. The Big Gully assemblage comprises at least 45 taxa, suggesting a habitat very favourable for life. Its preservation is exceptional, with gut remains and other soft parts quite common. Predation and scavenging were minimal and the finely laminated texture of the host mudstone attests to a lack of burrowing and bioturbation. Notwithstanding earlier studies suggesting otherwise, Gaines *et al*. (2008) concluded that conservation of organic tissues, rather than authigenic mineralisation of their more labile components, is the principal taphonomic pathway responsible for BST deposits. Insofar as such preservation requires suppression of the early diagenetic processes that normally result in the rapid decay of organic matter at or near the sea floor, the oxicity of the bottom waters, below which the Emu Bay Shale accumulated, becomes critically important. Here we determine the palaeo-redox status of the fossiliferous basal portion of the formation using total organic carbon (TOC) concentrations, isotopic signatures ($\delta^{13}C_{org}$) and biomarker alkanes, in combination with selected trace element proxies. We also establish its degree of thermal alteration as a datum for use in taphonomic comparisons with other Cambrian Lagerstätten.

Oxygen-depleted bottom waters favour the preservation of sedimentary organic matter. The greater the depletion, the higher the TOC content of the underlying sediment, although enhanced productivity in the photic zone can also lead to the same outcome. Assuming a normal level of primary planktonic productivity across its inner-shelf depocentre, the Emu Bay Shale appears to contain insufficient organic

matter (TOC = 0.25–0.55%) to have accumulated under stable anoxic conditions. Even allowing for the inevitable loss of organic carbon during the oil- and gas-generation phases of thermal maturation, to a present rank equivalent to ~1.5% vitrinite reflectance (kerogen H/C = 0.48; Weaver index of illite crystallinity = 3.8), its *original* TOC content is likely to have been <1%. Like organic matter, certain trace metals also are commonly enriched in modern muds and ancient black shales that were deposited in anoxic marine settings (Calvert and Pedersen, 1993). A series of elemental ratios have been devised in which one metal (the numerator) is redox sensitive, while the other (denominator) is essentially independent of Eh. Of these U/Th, V/Cr and Ni/Co (Jones and Manning, 1994) and V/Sc (Kimura and Watanabe, 2001) have proved to be the most reliable and, when measured in the Emu Bay Shale, confirm that it was deposited beneath an *oxic* water column. In this respect it is similar to the archetypical Burgess Shale Formation (Powell *et al*., 2003).

Micro-scale sealed vessel (MSSV) pyrolysis of kerogen isolated from a solvent-extracted sample of the Emu Bay Shale provided independent confirmation of its redox status. The thermal extract (300°C for 1 h; equivalent to bitumen II) and kerogen pyrolysis (325°C for 24 h) both yielded alkanes displaying a low ratio of pristane to phytane (pr/ph = 1.2, sub-oxic) and *n*-alkanes with a marked OEP in the $<C_{20}$ range. The latter feature is diagnostic of *Gloecapsomorpha prisca* (Foster *et al*., 1989) and is the first indication that mats of this colonial cyanobacterium were involved in the taphonomy of a BST deposit. Its $\delta^{13}C_{org}$ values (-28 to -32‰) are consistent with the contribution of cyanobacterial biomass to the kerogen.

REFERENCES

Allison, P.A. and Briggs, D.E.G., 1993. Exceptional fossil record: Distribution of soft-tissue preservation through the Phanerozoic. *Geology* **21**, 527–530.

Calvert, S.E. and Pedersen, T.F., 1993. Geochemistry of Recent oxic and anoxic marine sediments: Implications for the geological record. *Mar. Geol.* **113**, 67–88.

Foster, C.B., Reed, J.D. and Wicander, R., 1989. *Gloecapsomorpha prisca* Zalessky, 1917: a restudy, part 1; Taxonomy, geochemistry, and paleoecology. *Geobios* **22**, 735–759.

Gaines, R.R., Briggs, D.E.G. and Zhao, Y. 2008. Cambrian Burgess Shale-type deposits share a common mode of fossilization. *Geology* **36**, 755–758.

Jones, B. and Manning, D.A.C., 1994. Comparison of geochemical indices used for the interpretation of paleoredox conditions in ancient sediments. *Chem. Geol.* **111**, 111–119.

Kimura, H. and Watanabe, Y., 2001. Ocean anoxia at the Precambrian-Cambrian boundary. *Geology* **29**, 995–998.

Nedin, C., 1995, The Emu Bay Shale, a Lower Cambrian fossil Lagerstätten, Kangaroo Island, South Australia. *Mem. Australas. Assoc. Palaeontol.* **18**, 31–40.

Powell, W.G., Johnston, P.A. and Collom, C.J., 2003. Geochemical evidence for oxygenated bottom waters during deposition of fossiliferous strata of the Burgess Shale Formation. *Palaeogeogr. Palaeoclimatol. Palaeoecol.* **201**, 249–268.

McKirdy, D.M., Hall, P.A., Nedin C., Halverson, G.P., Michaelsen, B.H., Jago, J.B., Gehling, J.G. & Jenkins, R.J.F. (2011). Palaeoredox status and thermal alteration of the lower Cambrian (Series 2) Emu Bay Shale Lagerstätte, South Australia.
Australian Journal of Earth Sciences, v. 58 (3), pp. 259-272.

NOTE:
This publication is included on pages 275-288 in the print copy of the thesis held in the University of Adelaide Library.

It is also available online to authorised users at:

http://dx.doi.org/10.1080/08120099.2011.557439

Hall, P.A., McKirdy, D.M., Halverson, G.P., Jago, J.B. & Gehling, J.G. (2011). Biomarker and isotopic signatures of an early Cambrian Lagerstätte in the Stansbury Basin, South Australia. *Organic Geochemistry, v. 42 (11), pp. 1324-1330.*

NOTE:
This publication is included on pages 289-295 in the print copy of the thesis held in the University of Adelaide Library.

It is also available online to authorised users at:

http://dx.doi.org/10.1016/j.orggeochem.2011.09.003

Garciano, L.O., Tran, N.H., Kannangara, G.S.K., Milev, A.S., Wilson, M.A., McKirdy, D.M., & Hall, P.A. (2012). Pyrolysis of a Naturally Dried Botryococcus braunii Residue.
Energy & Fuels, v. 26 (6), pp. 3874-3881

NOTE:
This publication is included on pages 297-304 in the print copy of the thesis held in the University of Adelaide Library.

It is also available online to authorised users at:

http://dx.doi.org/10.1021/ef300451s

34th International Geological Congress; Brisbane, 5-10th August, 2012
Abstract & Poster Presentation

The biogeochemical status of the Palaeo-Pacific Ocean: clues from the early Cambrian of South Australia

P.A. Hall[1], D.M. McKirdy[1], G.P. Halverson[1,3], B.L. Turner[1,4], M.W. Carson[1,5], J.B. Jago[2], and A.S. Collins[1]
1. School of Earth and Environmental Sciences, University of Adelaide, SA 5005
E-mail: philip.a.hall@adelaide.edu.au
2. School of Natural and Built Environments, University of South Australia, Mawson Lakes, SA 5005
3. Present address: Department of Earth & Planetary Sciences, McGill University, Montreal, Canada H3A 2A7
4. Present address: 93 Thiessen Crescent, Miena, TAS 7030
5. Present address: BHP Billiton Iron Ore, 225 St Georges Terrace, Perth, WA 6000

Abstract

The Ediacaran-Cambrian transition was a time of profound reorganisation of the biosphere, coinciding with the final breakup of Rodinia, assembly of Gondwana and increasing atmospheric and oceanic oxygenation. The early Cambrian marine sediments of the Stansbury Basins, South Australia, were deposited at low northern palaeolatitudes on the western margin of the emerging Pacific Ocean. Here we report results of a multi-pronged investigation employing trace and REE abundances, TOC and stable isotopes (C, S) from three formations; Heatherdale Shale, Emu Bay Shale and Talisker Formation (sequences Є1.2 to Є2.2).

TOCs range from ≤0.5%, to 1.9% and 2.6% in the Emu Bay Shale, Talisker Formation and Heatherdale Shale respectively. Covariance is demonstrated between trace elements and organic matter, with comparative uranium enrichment in the Heatherdale Shale implying increased primary productivity. REE concentrations typically exhibited LREE enrichment with HREE & Yttrium depletion. Provenance appears to evolve through the late Normanville sediments into the Kanmantoo Group, corroborating published detrital zircon interpretations.

A multiproxy approach in conjunction with sedimentological information provides a powerful tool for interpreting palaeoenvironmental conditions. Prevalent palaeoredox conditions of the Heatherdale Shale and Talisker Formation were dysoxic, evolving progressively more reducing natures up section, the latter exhibiting a secular decline in $\delta^{34}S_{pyr}$ (10‰ to -11‰). The Emu Bay Shale conversely demonstrates consistently aerobic interpretations for the redox proxies. Comparison of trace element and REE distributions to similar sequences of the Yangtze platform, South China shows striking similarities, implying seawater trace element chemistry of the Palaeo Pacific & Asian oceans was homogenous.

Eastern Australian Basins Symposium IV; Brisbane, 11-14th September, 2012

Extended Abstract & Oral Presentation

Australasian asphaltite strandings revisited: their origin and the effects of weathering and biodegradation on their biomarker and isotopic profiles

P.A Hall[1], D.M. McKirdy[1], K. Grice[2] & D. Edwards[3]

1. School of Earth and Environmental Sciences, University of Adelaide, SA 5005, Australia
E-mail: tony.hall@adelaide.edu.au
2. Western Australia Organic and Isotope Geochemistry Centre, The Institute for Geoscience Research, Department of Chemistry, Curtin University of Technology, GPO Box U1987 Perth, WA 6845, Australia
3. Geoscience Australia, GPO Box 378, Canberra, ACT 2601, Australia

Abstract

Reports of bitumen strandings on the coastlines of South Australia, Victoria, Tasmania and Western Australia date from the early 19th Century (Sprigg and Woolley, 1963; Currie et al., 1992; Volkman et al., 1992; McKirdy et al., 1994; Padley, 1995; Edwards et al., 1998 and references therein). The locations of these strandings along Australia's southern margin (Fig. 1), and their greater frequency in southeastern South Australia, western Victoria and southern Tasmania, fuelled early petroleum exploration in the region on the assumption that they were sourced from local submarine seepages (Sprigg, 1986; Volkman et al., 1992; McKirdy et al., 1994). Accounts describe a variety of oily substances that can be assigned to three categories, each with a different origin: oils (crude and refined), waxy bitumens and asphaltites (McKirdy et al., 1986, 1994; Padley, 1995; Edwards et al., 1998).

The focus of the present study involves detailed molecular and isotopic characterisation of the asphaltites (i.e. the Family 4 costal bitumens of McKirdy et al., 1986, 1994). Geochemically quite distinct from the waxy bitumens, these are heavy, sulfur-rich, aromatic-asphaltic crudes (4–18° API; ~4% S; 57–84% asphaltenes) that commonly strand as large jet-black ovoid lumps (up to 670 mm across and 7 kg in weight) at the high water mark on medium to high energy, gently sloping sandy beaches (McKirdy et al., 1994; Padley, 1995). Unlike the waxy bitumens, which have positive buoyancy, the Australasian asphaltites are on average slightly denser than seawater and therefore are likely to have resided mostly within the water column prior to stranding. The fresh strandings have a strong petroliferous odour (Sprigg and Woolley, 1963; Volkman et al., 1992; Padley, 1995; Edwards et al., 1998). Their upper surface is characteristically traversed by shrinkage cracks and, although the interior is pliable when fresh, they become brittle upon storage and exhibit a conchoidal fracture pattern (Fig. 2). Their stable isotopic and molecular compositions (McKirdy et al., 1986, 1994; Currie et al., 1992; Volkman et al., 1992; Dowling et al., 1995; Padley, 1995; Edwards et al., 1998), including their enrichment in metallo-porphyrins (Boreham et al., 2001; Totterdell et al., 2008), make them unique among Australasian crude oils. Moreover, historic (>100 years ago) and more recent strandings at sites in Western Australia, South Australia, Victoria and Tasmania and

even as far afield as New Zealand and Macquarie Island (Fig. 1) are of remarkably similar composition, suggesting that they all originated from the same offshore petroleum system (Padley, 1995; Edwards et al., 1998).

The source and age-specific biomarkers of these asphaltites indicate they are derived from a Cretaceous marine shale deposited under anoxic/sulphidic conditions, probably during an oceanic anoxic event (OAE) (McKirdy et al., 1994, Edwards et al., 1998, Boreham et al., 2001). In the Southern Hemisphere the Indian Ocean and contiguous Toolebuc and Blue Whale Seaways were sites of restricted circulation. Accordingly, euxinic marine sediments have been identified in several of the corresponding Australian depocentres, possibly recording the Cenomanian–Turonian OAE2 (Bonarelli Event) and shorter-lived late Albian oceanic anoxic subevent (OAE 1d; Breistrofffer Event) (Edwards et al., 1999; Boreham et al., 2001; Struckmeyer et al., 2001; Pancost et al., 2005; Totterdell et al., 2008; Jenkyns, 2010).

The origin of the Australasian asphaltites has long been the subject of debate. No reliable correlation of the asphaltites to any oil produced locally on the southern margin of Australia or globally (using the GeoMark™ database, Summons et al., 2001) has been made. Thus the source of these enigmatic hydrocarbons remains in question.

The close proximity of common stranding sites to the locations of former whaling stations raises the possibility of an anthropogenic origin for the asphaltites. However, the common caulking materials recovered from shipwreck sites differ significantly in composition from the asphaltites (Smart, 1999).

An important clue to the likely origin of the asphaltites is the striking similarity of their biomarker and isotopic signatures to those of the late Albian Toolebuc Formation in the onshore Eromanga Basin (Boreham et al., 2001). Coeval units deposited along the Blue Whale Seaway, which may well host their enigmatic source facies, form part of the post-rift sag phase succession of the Blue Whale Supersequence in the Eyre and Ceduna sub-basins of the Bight Basin and the Otway Supergroup in the Otway Basin (Boreham et al., 2001, Struckmeyer et al., 2001; Bradshaw et al., 2003, Totterdell and Struckmeyer, 2003; Boult et al., 2005; Totterdell et al., 2008; Blevin and Cathro, 2008; Boreham, 2008). However, in view of the lack of a definitive oil-source correlation, is it possible that further clues to their origin might be derived from the asphaltite strandings themselves?

In this study we investigate a suite of asphaltites from four widely separated stranding localities: Limestone Coast (n = 3), Kangaroo Island (n = 4), Eyre Peninsula (n = 2) and Invercargill, New Zealand (n = 2) (Table 1). Sub-samples taken from the external weathered surface and ‘fresh’ interior of each asphaltite specimen were analysed by gas chromatography-mass spectrometry (GC-MS) and compound-specific isotope analysis (CSIA). Comparison of the resulting data allowed 1) oil-oil correlation; and 2) determination of their degree of weathering which, as a function of residence time in the ocean, may be used to better constrain the location(s) of the parent seafloor seepage.

In investigating the provenance of the asphaltites stranded upon the shores of the southern margin of Australia, and further afield, it seemed appropriate to first reconsider the genesis of such asphaltites. The physical characteristics of the

Australasian asphaltites provide additional clues to their origin. Laminations and flow structures observed in some specimens (Fig. 2A, D) are similar to those described in the asphaltic volcanoes of the Gulf of Mexico (Brüning et al., 2010; Schubotz et al., 2011) wherein surface cracking is also observed due to the *in situ* loss of volatiles. In fact, these submarine seeps of viscous bitumen display all the hallmarks of the Australasian asphaltite strandings: devolatilization cracks, large ovoid blocks, benthic bivalve and annelid communities, and the newly described flow characteristics.

Undoubtedly, the asphaltites have lost volatile components subsequent to their escape from the subsurface to the sea floor. This loss is likely to have involved both submarine dissolution, as evidenced by the shrinkage cracks on the upper surface of the stranded asphaltite (Fig. 2D), and subaerial evaporation, which accounts for its loss of plasticity observed once removed from the aqueous environment. The difference in distribution of bulk components between the inner and outer portions of the specimens is relatively small, as shown by the combined loss of saturated and aromatic hydrocarbons (average 5%) and the variation in the C_{10-19}/C_{30} *n*-alkane ratio (average 13%). Thus, it is probable that most of the light-end loss from the parent crude oil occurred in the subsurface and that the asphaltites were discharged into the ocean as semi-solid bitumen. All the Australasian asphaltites lack 25-norhopanes, implying little in-reservoir bacterial alteration (Volkman et al., 1984). The levels of degradation, classified by Edwards et al. (1998) as being at Level 4 (or PM4) on the biodegradation scale of Peters and Moldowan (1993), which corresponds to moderate degradation on the scales of Wenger et al. (2001) and Peters et al. (2005), are calculated to be Manco 431, 419 [PM4] or ultimate Manco 578 [vector 31043310000] on the recently published scale of Larter et al. (2012), which highlights the fact that the initially generated oil has undergone substantial alteration. However, degradation through bacterial removal and/or intensive water washing had no part in their genesis. The level of biodegradation also suggests that if they emanate from natural submarine seepage it would be of low intensity (Wenger and Isaksen, 2002), an interpretation consistent with the pattern described for the Australian continental shelf (Logan et al., 2010) and ascribed to low recent burial rates. Given its arrival at the sea floor in the form of heavy oil, this modification must have occurred in the subsurface. The most likely mechanism is tar mat formation, due either to deasphalting of the main oil stringer along a flat-lying secondary migration pathway or subsequent invasion of an oil-bearing reservoir by gas from a more mature hydrocarbon kitchen.

Geochemical investigation of the inner ‘fresh’ portion of four previously unanalysed asphaltites from locations in the Bight Basin and New Zealand has shown that these more distant strandings may be correlated with a further seven members of the classic ‘Family 4’ asphaltites from common stranding sites on the Limestone Coast and Kangaroo Island. The compositional uniformity of the sample suite, evident across a broad spectrum of parameters, with representative chromatograms from the GC-MS analyses shown in Fig.3, is a clear indication that these asphaltites belong to the same oil family, nothwithstanding their disparate stranding localities. Moreover, their bulk composition and biomarker distributions are remarkably similar to those previously reported for other stranded southern Australian asphaltites (Currie et al., 1992; Volkman et al., 1992; McKirdy et al., 1994; Padley, 1996; Edwards et al., 1998; Boreham et al., 2001).

Comparison of inner, fresher portions of each stranding to the outer, weathered surface section revealed subtle but relatively consistent variations in a number of degradation-sensitive components. Molecular fossil and compound-specific $\delta^{13}C$ signatures (Fig.4) in the saturated hydrocarbons most susceptible to alteration by biodegradation and dissolution suggest that the specimens recovered from the Eyre Peninsula and New Zealand have had longer exposure to weathering in the oceanic realm than those from the Limestone Coast and Kangaroo Island. The corresponding aromatic hydrocarbon distributions of the inner and outer portions differ in a manner consistent with the physical appearance of the strandings.

Within the offshore Bight Basin, the western section of the Ceduna Sub-basin hosts thermally immature organic-rich mudstones with marine biomarker signatures similar (but not identical) to those of the asphaltites (Totterdell et al., 2008), sampled from locations in which shelf-break canyons incise the Cretaceous section. The eastern part of the Ceduna Sub-basin is host to natural seepage and potential source rocks of the required age and thermal maturity (Boult, 2012), where a possible mode of transportation to the inner shelf is available via the upwelling Flinders Current (Middleton and Bye, 2007). However, shelf-break canyons do not appear to expose the Cretaceous section and the seismically interpreted seep features are active on the shelf (Boult, 2012). Migration of a viscous tar mat from a highly specific source rock to the sea floor of the shelf, uncontaminated by the other petroleum systems operating within this sector of the sub-basin, makes this is a less likely (though viable) scenario.

The Morum Sub-basin is located within the western offshore Otway Basin, adjacent to the Limestone Coast and southern Kangaroo Island where the least weathered asphaltite strands. This depocentre has what may be the crucial feature, namely a deep shelf-break canyon that cuts deeply into a toe-thrust inversion interpreted to host active source rocks of the appropriate Albian age (Boult et al., 2005). The associated system of steeply dipping faults provides migration pathways along which light hydrocarbons could have continued their movement to reservoirs higher in the sequence, leaving behind a residual tar mat. This heavy asphaltic bitumen may now be exposed in the floor or walls of the canyon, oozing slowly onto the seafloor to form volcano-like structures. Transport of the asphaltite along the canyon and up onto the shelf can be accounted for by the summer upwelling of the deep oceanic Flinders Current (Middleton and Bye, 2007), where it may be dispersed by the inshore coastal current or accumulate until being washed ashore by winter storm events. Historical distribution patterns support this hypothesis, with the highest concentration of strandings found on the coast closest to the head of the Morum Sub-basin canyons and on Kangaroo Island, which lies westward on the summer route of the Flinders Current. For the remainder of the year the shallow coastal current flows southeastward along the shelf before interacting with the Subantarctic Front of the Antarctic Circumpolar Current system (Rintoul et al., 2001; Middleton and Bye, 2007), thereby providing momentum for the carriage of asphaltite further on towards the Victorian and Tasmanian coasts and beyond.

6. Acknowledgements

This study was funded in part by Primary Industries and Resources South Australia (PIRSA). PAH is in receipt of an Australian Postgraduate Award. We are especially grateful to Dallas Bradley (Environment Southland, New Zealand) for providing the two asphaltites from Invercargill. The contributions of PAH and DMMcK to this

paper comprise TRaX Record 232. Stephen Clayton is thanked for technical support for CSIA at Curtin University. Kliti Grice acknowledges the ARC for infrastructure and salary support.

7. References

BLEVIN, J.E. and CATHRO, D., 2008. Australian Southern Margin Synthesis – GA707 https://www.ga.gov.au/products/servlet/controller?event=GEOCAT_DETAILS&catno=68892

BOREHAM, C.J., KRASSAY, A.A. and TOTTERDELL, J.M., 2001. Geochemical comparisons between asphaltites on the southern Australian margin and Cretaceous source rock analogues. In: HILL, K.C. and BERNECKER, T. (Eds.), Eastern Australasian Basins Symposium: A refocused energy perspective for the future. PESA, Special Publication, pp. 531–541.

BOREHAM, C.J., 2008. Bight Basin marine potential source rocks: a local expression of the Late Cretaceous oceanic anoxic event (OAE2)? In: MCKIRDY, D.M. (ED.), Oil, Soil, Water and Wine. 15th Australian Organic Geochemistry Conference, Program and Abstracts, 104–105.

BOULT, P.J., MCKIRDY, D., BLEVIN, J., HEGGELAND, R., LANG, S. and VINALL, D., 2005. The oil-prone Morum Sub-basin petroleum system, Otway Basin, South Australia. MESA Journal 38, 28–33.

BOULT, P.J., 2012. Bight Basin Overview. http://www.bightpetroleum.com/bight-basin/overview

BRADSHAW, B.E., ROLLET, N., TOTTERDELL, J.M. and BORISSOVA, I., 2003. A revised structural framework for frontier basins on the southern and south-western Australian continental margin. Geoscience Australia Record 2003/03.

BRÜNING, M., SAHLING, H., MACDONALD, I., DING, F. and BOHRMANN, G., 2010. Origin, distribution, and alteration of asphalts at the Chapopote Knoll, southern Gulf of Mexico. Marine and Petroleum Geology 27, 1093–1106.

CURRIE, T.J., ALEXANDER, R. and KAGI, R.I., 1992. Coastal bitumens from Western Australia – long distance transport by ocean currents. Organic Geochemistry 18, 595–601.

DOWLING, L.M., BOREHAM, C.J., HOPE, J.M., MURRAY, A.P. and SUMMONS, R.E., 1995. Carbon isotopic composition of hydrocarbons in ocean-transported bitumens from the coastline of Australia. Organic Geochemistry 23, 729–737.

EDWARDS, D., MCKIRDY, D.M. and SUMMONS, R.E., 1998. Enigmatic asphaltites from the southern Australian margin: molecular and carbon isotopic composition. PESA Journal 26, 106–130.

EDWARDS, D.S., STRUCKMEYER, H.I.M., BRADSHAW, M.T. and SKINNER, J.E., 1999. Geochemical characteristics of Australia's Southern Margin petroleum systems. APPEAJournal 39, 297–321.

JENKYNS, H.C., 2010. Geochemistry of oceanic anoxic events. Geochemistry, Geophysics, Geosystems 11, 1–30.

LARTER, S.R., HUANG, H., ADAMS, J.J., BENNETT, B. and SNOWDON, L.R., 2012. A practical biodegradation scale for use in reservoir geochemical studies of biodegraded oils. Organic Geochemistry 45, 66–76.

LOGAN, G.A., JONES, A.T., KENNARD, J.M., RYAN, G.J. and ROLLET, N., 2010. Australian offshore natural hydrocarbon seepage studies, a review and re-evaluation. Marine and Petroleum Geology 27, 26–45.

MCKIRDY, D.M., COX, R.E., VOLKMAN, J.K. and HOWELL, V.J., 1986. Botryococcane in a new class of Australian non-marine crude oils. Nature 320, 57–59.

MCKIRDY, D.M., SUMMONS, R.E., PADLEY, D., SERAFINI, K.M., BOREHAM, C.J. and STRUCKMEYER, H.I.M., 1994. Molecular fossils in coastal bitumens from southern Australia: signatures of precursor biota and source rock environments. Organic Geochemistry 21, 265–286.

MIDDLETON, J.F. and BYE, J.A.T., 2007. A review of the shelf-slope circulation along Australia’s southern shelves: Cape Leeuwin to Portland. Progress in Oceanography 75, 1–41.

PADLEY, D., 1995. Petroleum geochemistry of the Otway Basin and the significance of coastal bitumen strandings on adjacent southern Australian beaches. PhD Thesis, University of Adelaide.

PANCOST, R.D., CRAWFORD, N., MAGNESS, S., TURNER, A., JENKYNS, H.C. and MAXWELL, J.R., 2005. Further evidence for the development of photic-zone euxinic conditions during Mesozoic oceanic anoxic events. Journal of the Geological Society 161, 353–364.

PETERS, K.E. and MOLDOWAN, J.M., 1993. The Biomarker Guide - Interpreting Molecular Fossils in Sediments and Petroleum. Prentice-Hall, New Jersey.

PETERS, K.E., WALTERS, C.C. and MOLDOWAN, J.M., 2005. The Biomarker Guide, Volume 2, Biomarkers and Isotopes in Petroleum Systems and Earth History. Cambridge University Press.

RINTOUL, S.R., HUGHES, C.W. and OLBERS, D., 2001. The Antarctic circumpolar current system. In: Siedler, G., Church, J., Gould, J. (Eds.), Ocean Circulation and Climate: Observing and Modelling the Global Ocean. Academic, San Diego, pp. 271–302.

SCHUBOTZ, F., LIPP, J.S., ELVERT, M., KASTEN, S., MOLLAR, P.X., ZABEL, M., BOHRMANN, G. and HINRICHS, K., 2011. Petroleum degradation and

associated microbial signatures at the Chapopote asphalt volcano, Southern Gulf of Mexico. Geochimica et Cosmochimica Acta 75, 4377–4398.

SMART, S.M., 1999. Asphaltites from the southern Australian Margin: Submarine oil seeps or maritime artifacts? BSc Honours thesis, National Centre for Petroleum Geology and Geophysics, University of Adelaide (unpublished).

SPRIGG, R.C. and WOOLLEY, J.B., 1963. Coastal bitumen in South Australia with special reference to observations at Geltwood Beach, south-eastern South Australia. Transactions of the Royal Society of South Australia 86, 67–103.

SPRIGG, R.C., 1986. A history of the search for commercial hydrocarbons in the Otway Basin complex. In: GLENIE R.C. (Ed.), Second South-Eastern Australia Oil Exploration Symposium. PESA, Melbourne, pp. 173–200.

STRUCKMEYER, H.I.M., TOTTERDELL, J.M., BLEVIN, J.E., LOGAN, G.A., BOREHAM, C.J., DEIGHTON, I., KRASSAY, A.A. and BRADSHAW, M.T., 2001. Character, maturity and distribution of potential Cretaceous oil source rocks in the Ceduna Sub-basin, Bight Basin, Great Australian Bight. In: HILL, K.C. and BERNECKER, T. (Eds.) Eastern Australasian Basins Symposium, A refocused energy perspective for the future, Melbourne, 2001. PESA. Special Publication, pp. 543–552.

SUMMONS, R.E., LOGAN, G.A., EDWARDS, D.S., BOREHAM, C.J., BRADSHAW, M.T., BLEVIN, J.E., TOTTERDELL, J.M. and ZUMBERGE, J.E., 2001. Geochemical analogues for Australian coastal asphaltites - search for the source rock. Abstract. AAPG Bulletin, 85 (Supplement).

TOTTERDELL, J.M. and STRUCKMEYER, H.I.M., 2003. Southern Australian Bight Basin holds deepwater potential. Offshore 63, 41–44.

TOTTERDELL, J.M., STRUCKMEYER, H.I.M., BOREHAM, C.J., MITCHELL, C.H., MONTEIL, E. and BRADSHAW, B.E., 2008. Mid–Late Cretaceous Organic-Rich Rocks From The Eastern Bight Basin: Implications For Prospectivity. In: BLEVIN, J.E., BRADSHAW, B.E. and URUSKI, C. (Eds.), Eastern Australasian Basins Symposium III, PESA, Special Publication, pp. 137–158.

VOLKMAN, J.K., ALEXANDER, R., KAGI, R.I., ROWLAND, S.J. and SHEPPARD, P.N., 1984. Biodegradation of aromatic hydrocarbons in crude oils from the Barrow Sub-basin of Western Australia. Organic Geochemistry 6, 619–632.

VOLKMAN, J.K., O'LEARY, T., SUMMONS, R.E. and BENDALL, M.R., 1992. Biomarker composition of some asphaltic coastal bitumens from Tasmania, Australia. Organic Geochemistry 18, 669–682.

WENGER, L.M., DAVIS, C.L. and ISAKSEN, G.H., 2001. Multiple controls on petroleum biodegradation and impact in oil quality. Society of Petroleum Engineers Reservoir Evaluation and Engineering 5, 375–383.

WENGER, L.M. and ISAKSEN, G.H., 2002. Control of hydrocarbon seepage intensity on level of biodegradation in sea bottom sediments. Organic Geochemistry 33, 1277–1292.

Table and figure captions

Table 1. Sample identification, size and weight, location of stranding, year of collection and weathering description.

Figure 1. Location of historically documented asphaltite strandings and samples analysed in this study (after Edwards et al., 1998).

Figure 2. Examples of asphaltite strandings: A) an asphaltite from Port McDonnell (not analysed) with a rolled over edge indicative of viscous flow; B) sample 80, Ravine de Casours, Kangaroo Island, broken open to reveal the conchoidal fracture pattern typical of all asphaltites (scale bar 20 mm); C) sample 177, Bales Bay, Kangaroo Island, a large specimen exhibiting upper surface devolatilization cracks and a characteristic flat ovoid shape (long axis = 75 cm); d) sample NZ1, Invercargill, New Zealand with an unusual internal fabric suggestive of laminar flow, devolatilization cracks and a bivalve colony; e) sample NZ2, Invercargill, New Zealand, also colonised by bivalves. Photographs provided by D. McKirdy (plate A); D. Edwards, nee Padley (plates B and C); and D. Bradley (plates D and E).

Figure 3. Selected chromatograms of saturated and aromatic hydrocarbons in the interior portion of representative asphaltite specimens from each stranding domain: A) TIC of saturated hydrocarbon fraction; B) *m/z* 191, terpanes; C) *m/z* 217, steranes; and D) *m/z* 231, triaromatic steroids. See Appendix 1 for key to peak identifications.

Figure 4. Plots of *n*-alkane $\delta^{13}C$ versus carbon number for asphaltite specimens, showing the difference between their inner and outer portions.

Table 1

Sample	Location	Year	Dimensions L:W:D (mm)	Weight (g)	Degree of Weathering
27A	Pether Rock, Canunda N.P., SA	1990	109:85:60	419	Mild
CB 32	Nine Mile Sandhill, Beachport, SA	1983	127:112:49		Moderate
162	German Point, Beachport, SA	1991	328:204:102	2876	Mild
80	Ravine des Casoars, Kangaroo Island, SA	1990	165:100:48	634	Moderate/Heavy
85	Seal Bay, Kangaroo Island, SA	1990		764	Moderate/Heavy
168	West Bay, Kangaroo Island, SA	1990		1944	Mild/Moderate
177	Bales Bay, Kangaroo Island, SA	1991	750:350:40	7000	Mild/Moderate
CL1	Streaky Bay, Eyre Peninsula, SA	2005	138:94:37		Heavy
MH1	S of the Freshmanns, Eyre Peninsula, SA	2005	83:71:26		Mild
NZ1	Invercargill, New Zealand	2002	273:256:87		Moderate
NZ2	Invercargill, New Zealand	2002	116:67:62		Moderate

Figure 1

NOTE:
This figure/table/image has been removed to comply with copyright regulations.
It is included in the print copy of the thesis held by the University of Adelaide Library.

Figure 2

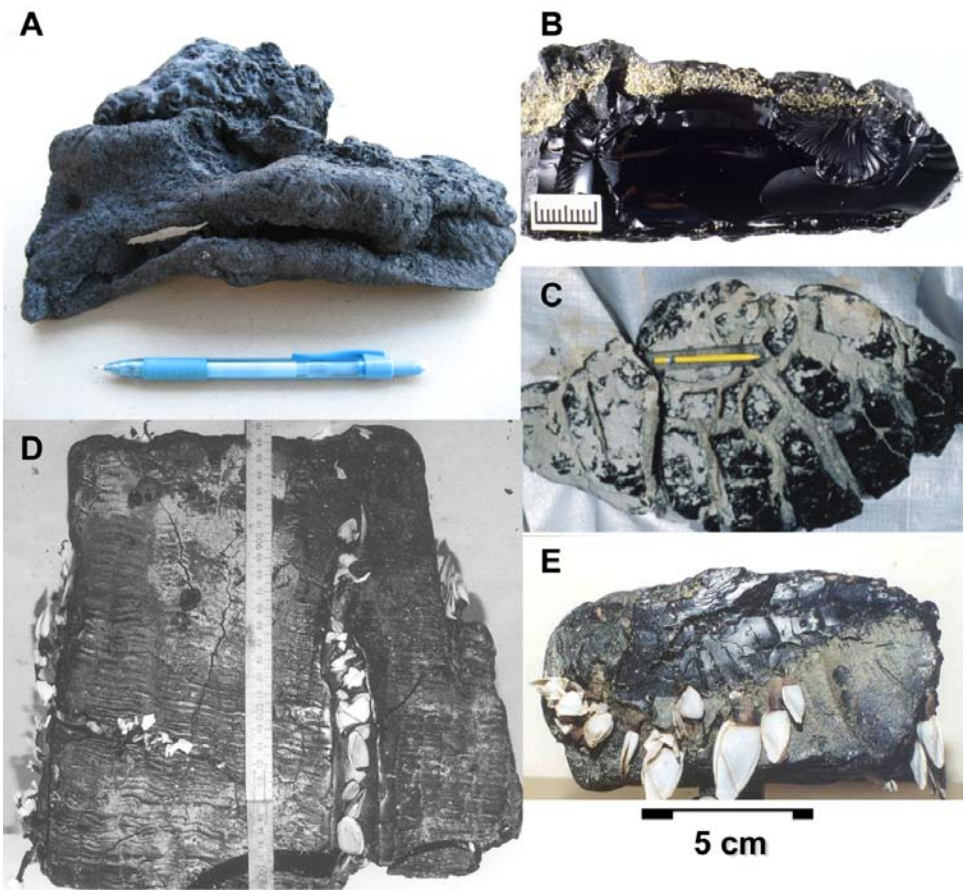

Figure 3

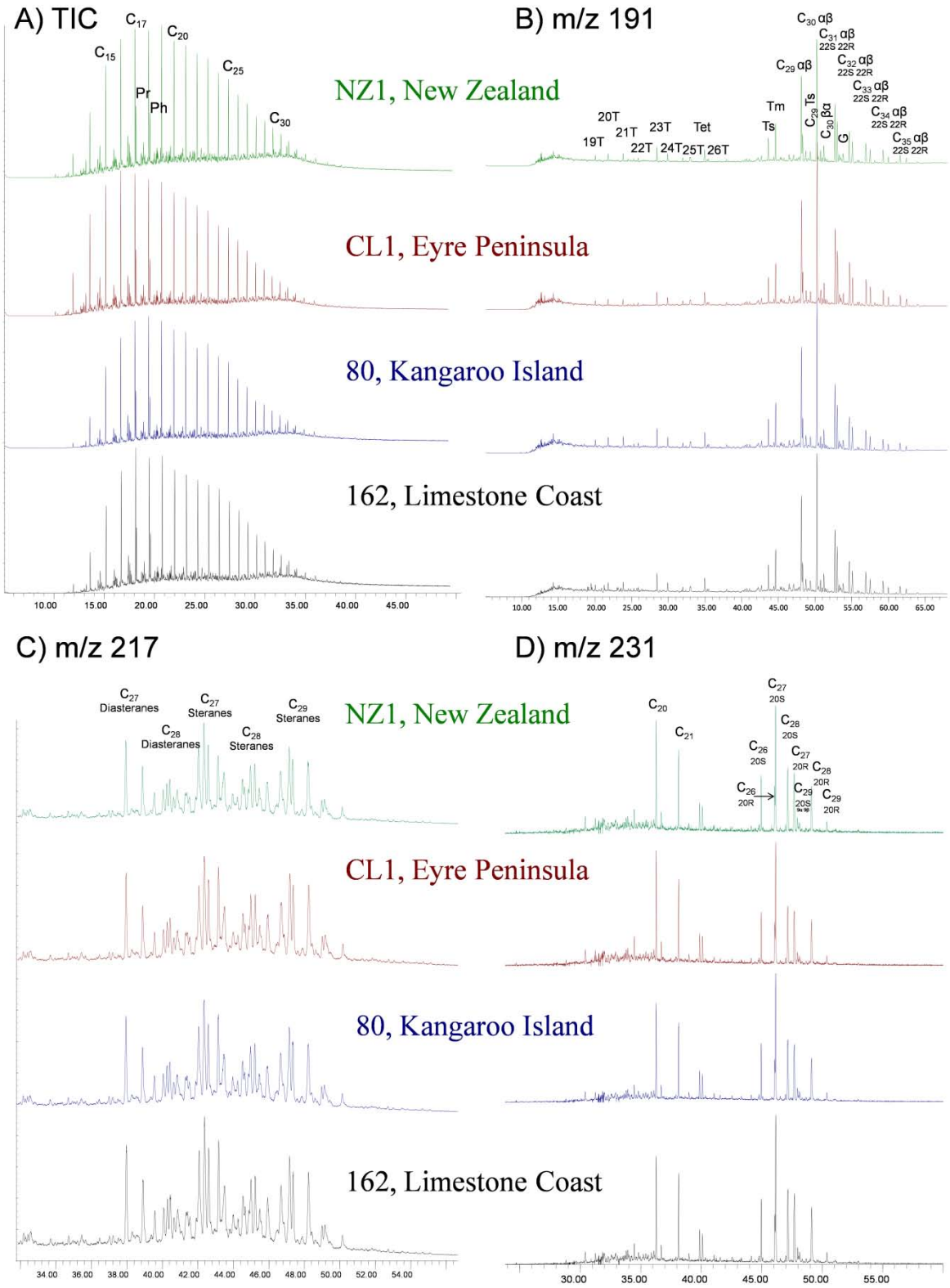
A) TIC
B) m/z 191
C) m/z 217
D) m/z 231
NZ1, New Zealand
CL1, Eyre Peninsula
80, Kangaroo Island
162, Limestone Coast
C15
C17
C20
C25
C30
Pr
Ph
19T
20T
21T
22T
23T
24T
25T
26T
Tet
Tm
Ts
C29 αβ
C29 Ts
C30 βα
G
C30 αβ
C31 αβ 22S 22R
C32 αβ 22S 22R
C33 αβ 22S 22R
C34 αβ 22S 22R
C35 αβ 22S 22R
C27 Diasteranes
C28 Diasteranes
C27 Steranes
C28 Steranes
C29 Steranes
C20
C21
C26 20R
C26 20S
C27 20S
C27 20R
C28 20S
C28 20R
C29 20S
C29 20R

Figure 4

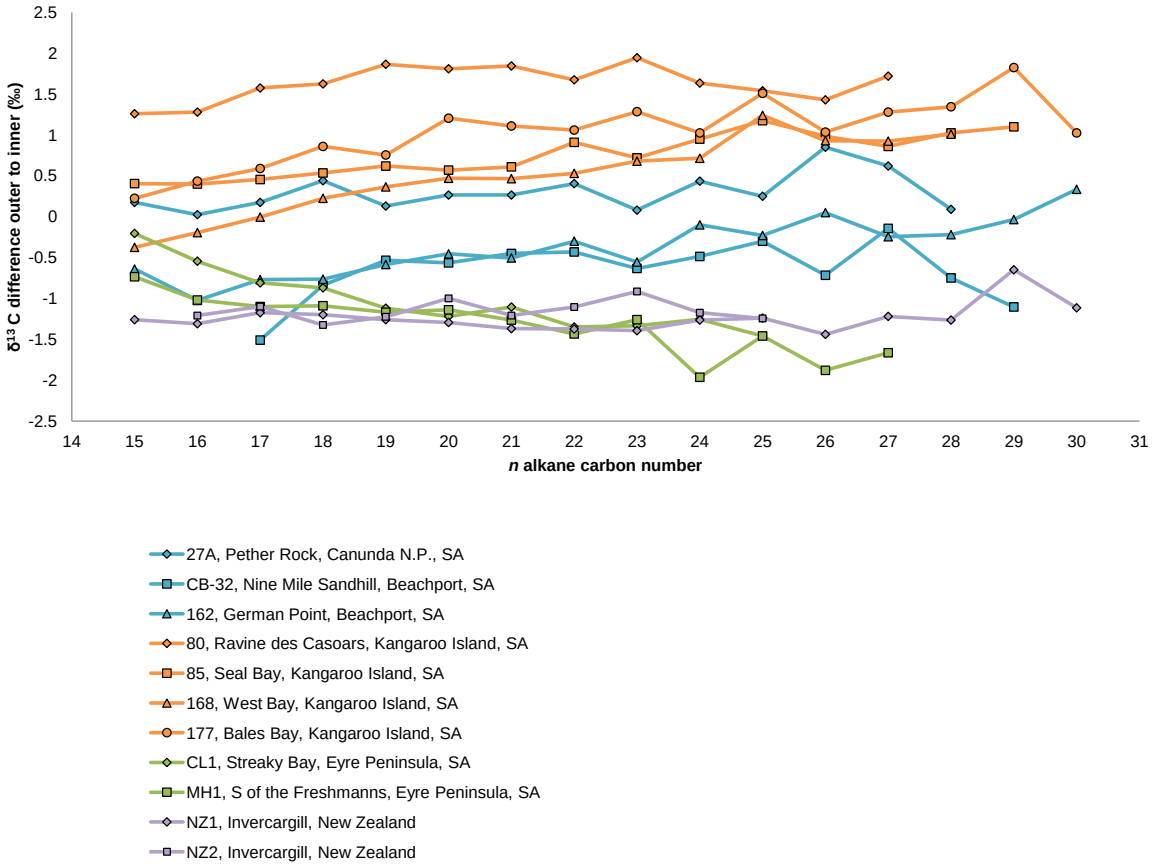
2.5
2
1.5
1
0.5
0
-0.5
-1
-1.5
-2
-2.5
δ13C difference outer to inner (‰)
14
15
16
17
18
19
20
21
22
23
24
25
26
27
28
29
30
31
n alkane carbon number
27A, Pether Rock, Canunda N.P., SA
CB-32, Nine Mile Sandhill, Beachport, SA
162, German Point, Beachport, SA
80, Ravine des Casoars, Kangaroo Island, SA
85, Seal Bay, Kangaroo Island, SA
168, West Bay, Kangaroo Island, SA
177, Bales Bay, Kangaroo Island, SA
CL1, Streaky Bay, Eyre Peninsula, SA
MH1, S of the Freshmanns, Eyre Peninsula, SA
NZ1, Invercargill, New Zealand
NZ2, Invercargill, New Zealand

Appendix 1. Abbreviations for Fig. 3.

Bulk Composition, normal & acyclic hydrocarbons (fullscan)

C_x = normal alkane $C_{carbon\ number}$ e.g. C_{15} = pentadecane ($C_{15}H_{32}$)
Pr = pristine
Ph = phytane

Hopanes (m/z 191)

T = tricyclic terpanes note C_{25} and C_{26} homologues have a chiral centre at C_{22} (R & S)
Tet = C_{24} tetracyclic terpane
Ts = C_{27} 18α(H)-22,29,30-trisnorhopane
Tm = C_{27} 17α(H)-22,29,30-trisnorhopane
C_{29} αβ = C_{29} 17α(H),21β(H)-hopane
C_{29}Ts = C_{29} 30-norneohopane
C_{30} αβ = C_{30} 17α(H),21β(H)-hopane
C_{30} βα = C_{30} 17β(H),21α(H)-hopane
C_{xx}αβ = C_{xx} 17α(H),21β(H)-homohopane (xx = carbon number i.e. 31 through 35)
G = Gammacerane

Steranes (m/z 217 & 218)

C_{27} Steranes = C_{27} 5α(H) steranes (20R + 20S)
C_{28} Steranes = C_{28} 5α(H) steranes (20R + 20S)
C_{29} Steranes = C_{29} 5α(H) steranes (20R + 20S)
C_{27} Diasteranes = C_{27} 13α(H),17α(H) diasteranes (20R + 20S)
C_{28} Diasteranes = C_{28} 13α(H),17α(H) diasteranes (20R + 20S)

Triaromatic Steroids (m/z231)

C_{20} = C_{2o} Triaromatic Steroid
C_{21} = C_{21} Triaromatic Steroid
C_{26} 20R = C_{26} Triaromatic Steroid 20R
C_{26} 20S = C_{26} Triaromatic Steroid 20S
C_{27} 20R = C_{27} Triaromatic Steroid 20R
C_{27} 20S = C_{27} Triaromatic Steroid 20S
C_{28} 20R = C_{28} Triaromatic Steroid 20R
C_{28} 20S = C_{28} Triaromatic Steroid 20S
C_{29} 20R = C_{29} Triaromatic Steroid 20R
C_{29} 20S9α = C_{29} Triaromatic Steroid 9α,20S
C_{29} 20S9β = C_{29} Triaromatic Steroid 9β,20S